Number 7 Volume 22 1958

P11

BULLETIN

of the

Academy of Sciences of the USSR

- Physical Series -

(Izvestiia Akademii Nauk SSSR)
(Seriia fizicheskaia)

Reproduction rights reserved

by

Columbia Technical Translations
5 Vermont Avenue
White Plain, New York

Single Issues
$20

Annual Subscription
$215

Lithoprinted in U.S.A.
EDWARDS BROTHERS, INC.
Ann Arbor, Michigan

Transactions

of the

Eighth All-Union Conference on Nuclear Spectroscopy

(Continued from Vol.22, No.2; to be continued in Vol.22, No.8)

INTERNAL CONVERSION - A Review

- M. A. Listengarten

Measurement of the internal conversion coefficients (hereinafter ICC) of γ-rays is an extensively used procedure for investigation of nuclear radiation and determination of the spins and parities of nuclear levels.

In the present article we shall review recent contributions to the subject and consider to what extent the theory of internal conversion is in agreement with experiment and to what degree both theory and experiment are in need of improvement.

It has been shown by a number of investigators (Refs.1-3 and others) that in the case of conversion of magnetic dipole radiation on the K and L_I shells the ICC calculated by Sliv[4] taking into account the distribution of charges and currents over a nucleus of finite size are in appreciably better agreement with experiment than the coefficients of Rose et al[5], calculated for a point nucleus (the error in Rose's ICC attains as much as 50% for heavy nuclei). There is also an appreciable difference (20-30%) between the coefficients of Sliv and Rose in the region of heaviest nuclei ($Z > 85$) for conversion of M2 and M3 transitions.

For other multipole orders the difference between the tables of Sliv and Rose is considerably smaller (if we disregard the obvious errors in Rose's tables, as for example, for E3 conversion on the L_{III} shell). These differences do not appreciably exceed the limits of error of both tables.

The corrections for finite nuclear size, taken into account in the work of Sliv, amount essentially to elimination of the physically meaningless infinite series in the expressions for the multipole potentials and in the electron wave functions which arise in a number of cases if the nucleus is assumed to be a point one, that is, in Sliv's calculations of ICC there were used corrected wave functions and potentials corresponding to a finite distribution of charges and currents in the nucleus.

As a rule, taking into account finer details of nuclear structure should not introduce any appreciable changes in the ICC. This is evident if only from the fact that at the energies under consideration the de Broglie electron wavelength is much greater than the dimensions of the nucleus and the effects connected with their interaction are in general insensitive to the form of the nuclear potential of the transition. Recently, however, Church & Weneser[6] showed that there may nevertheless be certain anomalous cases when the structure of the nucleus may prove to be an important factor where the magnitude of the ICC is concerned.

In order to determine under what conditions there may appear corrections to the ICC dependent on the details of the nuclear structure, let us consider the expression for the ICC:

$$\mathrm{ICC} = \left| \frac{U_e}{U_\gamma} \right|^2, \tag{1}$$

where U_e and U_γ are the matrix elements for the emission of a conversion electron and a γ-ray by the excited nucleus. In the case, for example, of a magnetic 2^l-pole

$$U_e = \int_0^\infty \psi_f^* \vec{\alpha} \mathbf{A}_l \psi_i d\tau \ , \tag{2}$$

where ψ_f and ψ_i are the wave functions of the final and initial states of the electron, $\vec{\alpha}$ is the Dirac matrix and $\mathbf{A}_l$ is the vector potential of the magnetic 2^l-pole. For a nucleus of finite size, U_e must be represented in the form of a

sum of two terms:

$$U_e = \int_0^{R_0} A_{\text{int.}} + \int_{R_0}^{\infty} A_{\text{ext.}}, \tag{3}$$

where R_0 is the nuclear radius.

The expressions for the vector potential inside and outside the currents giving rise to it are well known (see, for example, Ref.7). They differ in that $A_{\text{ext.}}$ contains only one term with a Hankel function (first kind), whereas $A_{\text{int.}}$ contains two terms with Hankel and Bessel functions, respectively. An important characteristic of $\int A_{\text{ext.}}$ is that it is proportional to U_γ:

$$\int A_{\text{ext.}} = a \cdot U_\gamma, \tag{4}$$

where a does not depend on the nuclear wave functions (but a does depend on the integration limits). In the case of a point nucleus, when there is no first term in (3), the integral over the nucleus is reduced in dividing

$$\frac{U_e}{U_\gamma} = a \qquad (R_0 = 0), \tag{5}$$

and the ICC proves to be a characteristic of the nuclear transition, entirely free of the influence of nuclear structure. In the case of a nucleus of finite size the integral over the nucleus is reduced only in the second term

$$\text{ICC} = \left| \frac{\int_0^{R_0} A_{\text{int.}}}{U_\gamma} + a' \right|^2 = \left| \frac{M_e}{U_\gamma} + a' \right|^2. \tag{6}$$

The numerator of the first fraction in (6) - the intranuclear matrix element M_e - represents the contribution to conversion due to interaction of the electron with nuclear currents during the time the electron is within the nucleus. This intranuclear matrix element is always taken into account in the calculations of Sliv et al.[4] Specifically, it was assumed in compiling the tables that the nuclear currents of the transition are on the nuclear surface. Calculations showed that the intranuclear matrix element is small - of the order of 2-3% relative to the leading extranuclear term in (3).

It was shown[4] that different assumptions regarding the nuclear currents and charges - from surface to volume distributions - result in variations of only 1.5-2% in the magnitude of the ICC, even for the heaviest nuclei. This point is also noted by Church & Weneser[6] and hence the term "new matrix element" used by them for M_e is not entirely justified. What is new in the work of Church & Weneser is something different, namely, they call attention to the fact that U_γ and M_e may lead to different selection rules for radiative transitions and for conversion transitions determined by the region of the nucleus. If the γ-transition is forbidden, U_γ in the denominator of (6) is strongly attenuated or may even be close to zero, while at the same time the numerator M_e, which has a different integrand, may have the usual value. Then the fraction M_e/U_γ will be large and may even exceed the second leading term in the expression for the ICC. In this case it is essential that the selection rules forbidding U_γ put little or no restriction on the value of the intranuclear matrix element M_e. This is a rigorous requirement; usually in the first approximation the selection rules will be the same for M_e and U_γ.

Inasmuch as the intranuclear conversion matrix element M_e is relatively small, for the contribution for M_e, which is dependent on the details of the

nuclear structure, to be noticeable and measurable experimentally, one must have a very large decrease of the denominator U_γ, i.e., a very high degree of forbiddenness of the radiative transition.

Thus our principal deduction is that the fine details of nuclear structure can have a noticeable influence on the ICC only when the corresponding γ-transition has a high degree of forbiddenness. For transitions having a normal lifetime, all the earlier inferences[4] regarding the independence of the ICC of nuclear structure (within the limits of 1-2%) remain in force. Thus the attempts of certain authors to attribute the divergence between the experimental and theoretical values of ICC to the influence of nuclear structure regardless of whether the given transition is allowed or forbidden are erroneous.

The physical significance of such intranuclear conversion is analogous to that underlying $0 \rightarrow 0$ transitions: a radiative transition is forbidden, while a conversion transition occurring due to penetration of an electron into the nucleus is allowed. The details of nuclear structure under these conditions have a strong influence on the probability of the conversion transition.

Structural corrections in the ICC of the order of 15-20% may be expected when the transition is hindered by a factor of at least 10^3.

The deviations from Sliv's ICC may be to either side, depending on the sign of M_e and the remaining principal part of the matrix element in (3) or (6). For different subshells the magnitude of the deviations, depending on the nuclear model, may be very different, but it may be expected, consistent with the length of time the electron spends in the nucleus, that the greatest deviations will be for the K and L_I coefficients and the smallest for the L_{III} coefficients. The magnitude of the structural correction should presumably be the greater, the stronger the inhibition of the γ-transition (other conditions being equal).

With decrease of Z, the role of the region of the nucleus in the ICC decreases and hence the degree of forbiddenness of the γ-radiation necessary for obtaining a noticeable effect of nuclear structure must rapidly increase.

The structural correction may change sharply for neighboring nuclei and even for different transitions in the same nucleus.

Another important point is the following: for the appearance of structural corrections to the ICC, forbiddenness of the γ-radiation alone is not sufficient. A further necessary condition is that the inhibition must have little or no influence on the nonradiative transitions determined by the region of the nucleus. If the inhibition applies in equal degree to both the radiative and nonradiative transition, both the denominator and numerator in the M_e/U_γ correction term decrease by the same factor and the structural correction becomes insignificant even with a very high degree of forbiddenness. This is the case, for example, when the transition is inhibited by the K selection rule (K is the projection of the total angular momentum on the nuclear symmetry axis). This fact has been noted by Nilsson & Rasmussen[8]. Thus a normal (or almost normal) value of the ICC is observed for the 316 kev transition in Pu^{239} despite the 10^9 retardation and for the 89 kev transition in Hf^{178} despite the $2 \cdot 10^{14}$-fold reduced probability, and only for the 57.6 kev transition in Hf^{180} with an inhibition of 10^{15} is there observed an anomaly in the ICC (see Table 1).[8] At the same time for transitions in which the U_γ inhibition is due to other factors (for example, forbiddenness with respect to the asymptotic quantum numbers N, n_z, Σ, Λ, etc.) the matrix element M_e may be allowed and then one can attempt to interpret certain ICC as dependent on the details of the nuclear structure even with inhibitions of the order of 10^5. Nilsson & Rasmussen cite a number of such cases (Table 2).

Table 1

K-forbidden M1 and E1 transitions in deformed nuclei

Nucleus	E_γ, kev	$F = \frac{\tau_{exp}}{\tau_{sing.part.}}$	Multipole order	Remarks
Pu^{239}	210	10^4	M1	α_K normal
	228	$5 \cdot 10^4$	M1	
	278	$6 \cdot 10^4$	M1	
Tu^{169}	178	$5 \cdot 10^5$	M1	
	199	$5 \cdot 10^5$	M1	
Re^{183}	382	$2 \cdot 10^2$	E1	
Pu^{239}	316	10^9	E1	
	334	10^9	E1	
Hf^{178}	88,9	$2 \cdot 10^{14}$	E1	α_K normal (within 20%)
Hf^{180}	57,6	10^{15}	E1	α_{L_I} anomalously large

Table 2

E1 and M1 transitions interpreted by Nilsson & Rasmussen[8] as anomalous (of the total number of 18 transitions in deformed nuclei forbidden with respect to asymptotic quantum numbers)

Nucleus	E_γ, kev	F	Multi-pole order	Remarks
Np^{237}	267	$5{,}5 \cdot 10^8$	E1	α_K (possible); exceeds theoretical by a factor of 10
W^{182}	152	?	E1	K/L = 2.8; theoretical 8.3
Ta^{181}	482	$3 \cdot 10^6$	M1	α_K exceeds theoretical 2–10 times
Pa^{231}	84	$3 \cdot 10^6$	E1	$\alpha_{L_I}, \alpha_{L_{II}}$ exceed theoretical 20 times; $\alpha_{L_{III}}$ normal
Pu^{239}	106	$5 \cdot 10^5$	E1	α_{L_I} exceeds theoretical by 1.5 times
Np^{237}	60	$3 \cdot 10^5$	E1	$\alpha_{L_{II}}$ " " " 2.5 "; α_{L_I} " " " 1.5 "; $\alpha_{L_{II}}$ " " " 4 "
Np^{237}	26	$3 \cdot 10^5$	E1	$\alpha_{L_{III}}$ normal; α_L exceeds theoretical 2 times.

We must note, however, that not all the cases cited by Nilsson & Rasmussen are necessarily authentic. Thus, for example, in the case of the 267 kev transition in Np^{237} all the anomalies can readily be explained by some admixture of M2; from a comparison of the experimental coefficients α_K and α_{L_I} with the theoretical values, it becomes apparent that the fraction of M2 is the same in both cases.[9] Where the 482 kev transition in Ta^{181} is concerned, the difference between the ratios M1/E2 obtained from the ICC and from angular correlation has been noted earlier by several investigators. But inasmuch as the fraction of M1 is small (3-5%), a change of only 10% in the experimental value of α_K corresponds to a factor of three difference in the partial (M1) value of α_K. If the proportion of M1 is taken from angular correlation[10,11], then the theoretical α_K must be $19 \cdot 10^{-4}$, whereas recent measurements give values of $(23 \pm 2) \cdot 10^{-4}$ (Snyder & Frankel[10]) and $21 \cdot 10^{-4}$ (Sunyar reported in Ref.11). The difference is not large; hence there can be some doubt regarding the existence of this anomaly. In the case of the 152 kev transition in W^{182}, Nilsson & Rasmussen base their citation on one unpublished measurement which is in need of verification.

In the case of the Pa^{231} 84 kev, Pu^{239} 106 kev and Np^{237} 60 & 26 kev transitions, the observed anomalies cannot be explained by an admixture of M2. While in the case of Pa^{231} Nilsson & Rasmussen give only one reference to an unpublished

investigation and for Pu^{239} cite only one measurement[12], for the transitions in Np^{237} the anomalous values of the ICC were obtained from a number of authors (Refs.9,13,14) who are essentially in agreement. It may be that in this case the anomaly is really due to influence of the nuclear structure on the ICC. Another interesting suggestion was put forward by Rosenblum & Valadares[14]: inasmuch as E1 is strongly forbidden and one can hardly expect magnetic quadrupole radiation to be important, here possibly we have competition between E1, M2 and E3 conversion. The increase in conversion on the L_{II} shell can partially be explained by an admixture of E3.

To characterize the magnitude of the structural effect Church & Weneser introduced the dimensionless parameter λ; it shows by what factor the additional term (the fraction M_e/U_γ) in (6) in any given case differs from the term taken into account by Sliv in the surface current model. This parameter can be determined from experiment

$$\lambda = 1 - \frac{\left(\frac{\alpha_{K\,exp.}}{\alpha_{K\,theo}}\right)^2 - 1}{C(Z,\ E_\gamma)},$$

where $C(Z, E_\gamma)$ is a coefficient that has been tabulated by Church & Weneser[6] for M1 (the Table in Ref.1 contains a numerical error: the tabular values of $C(Z, E_\gamma)$ should be multiplied by $\sqrt{2/3}$). So far, however, attempts to construct a quantitative theory giving the ICC corrections for strongly forbidden transitions on the basis of a specific nuclear model[8,15] have failed to yield significant results.

Thus the influence of the structure of the nucleus on the ICC to an extent greater than 1.5-2% is possible in principle, but in reality this effect should occur very rarely and only when certain conditions regarding the character of the γ-transition are rigorously satisfied. In fact, that the influence actually exists cannot be regarded as definitively proved; the present hypothesis still stands in need of thorough experimental verification.

Another important physical approximation made in calculating ICC was the method of taking into account screening of the nuclear charge by atomic electrons. The potential used is assumed to be that for statistical distribution of electrons in the Thomas-Fermi-Dirac model. The calculations of Rose differ slightly from those of Sliv in that in the latter the exchange term[16] is taken into account individually for each electron state.

For heavy atoms the statistical model is a good approximation and hence its use can lead only to minor errors. However, for light nuclei ($Z \lesssim 30$) and low energies ($E_\gamma \lesssim 50$ kev), calculations of the ICC by the same method may lead to errors of up to 10-15%. For $Z \approx 40$ and $E_\gamma \approx 70$-80% the tables already appear to be fairly accurate, but we are not yet able to affirm that the theory here is in complete agreement with experiment for the simple reason that we do not as yet have sufficient accurate experimental data in this region.

It would obviously be desirable to have a further investigation of the possible influence on the ICC of the statistical approximation in taking into account screening in the case of low energy transitions in light nuclei.

Let us see to what extent the theoretical and experimental ICC agree for some groups of nuclei.

There is a large number of even-even nuclei in which the ground and first excited states are 0+ and 2+. In these nuclei the transition between these states is pure E2.

Such transitions are very convenient for checking the validity of ICC theory, for admixtures of higher multipoles are entirely excluded. Further, inasmuch as among these transitions there are no forbidden ones, the possibility of

structural effects on the ICC is precluded. Finally, for not very large Z there are no transitions with a low γ-ray energy, which excludes errors in taking screening into account. Cases where the ICC on the K shell has been measured are listed in Table 3.

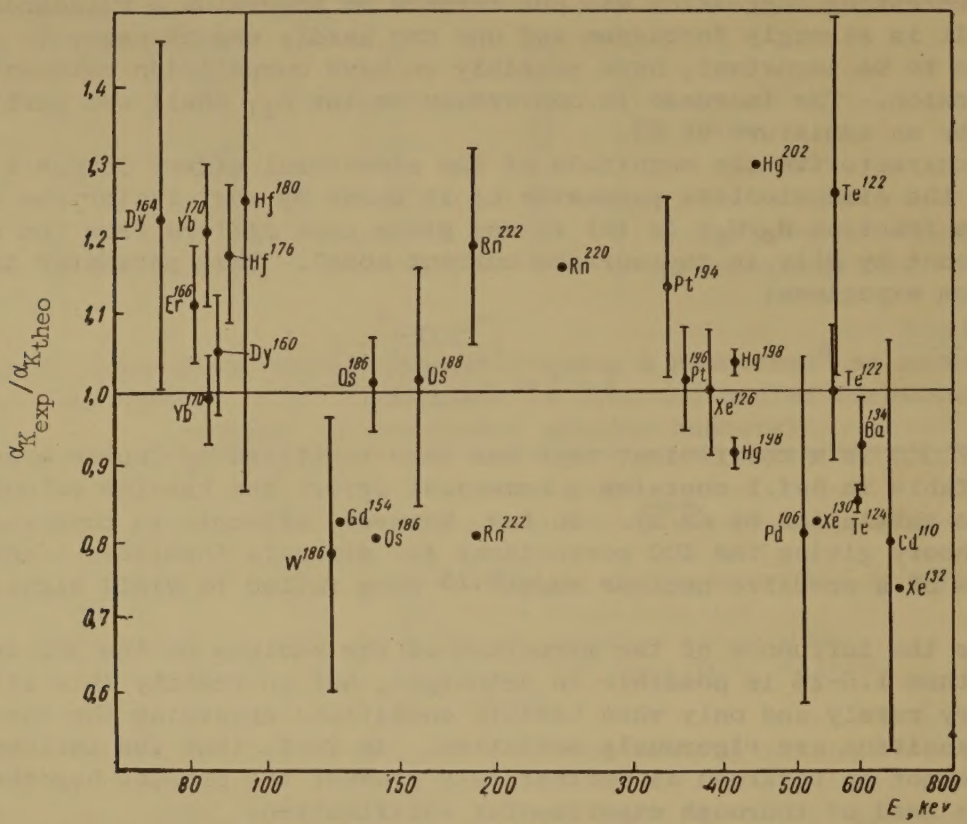

Fig.1. Ratio of experimental to theoretical values of K shell conversion coefficients for pure E2 (2+→0+) transitions with energies of 70 to 800 kev.

The experimental to theoretical ratios of α_K are plotted in Fig.1. The theoretical ICC values are taken from Sliv. Inasmuch as the effect of finite nuclear size is relatively unimportant for E2, these values differ only slightly (1-1.5%) from those of Rose et al.

The ICC of the 80 kev transition in Er^{166}, 84.1 kev in Yb^{170} and 89 kev in Hf^{176}, which exceed the theoretical values by 13-23%, were again measured in 1957 by McGowan & Stelson[21], who called attention to a certain discrepancy between theory and experiment in the case of low-lying E2 transitions. At energies higher than 100 kev, as may be seen from Fig.1, the deviations of $\alpha_{K\ exp}/\alpha_{K\ theo}$ occur with about equal frequency to both sides of unity. It should be noted that according to McGowan & Stelson, only for Yb^{170} is the deviation more than twice the experimental error and that in the same year (1957) Houtermans[26] obtained an experimental value of α_K for Yb^{170} in agreement with theory. From the standpoint of theory a 20% deviation of experimental ICC values from the theoretical ones for pure E2 transitions is wholly inexplicable. Approximations in taking into account shielding cannot yield a correction of this magnitude for α_K (if this were the case then for $\alpha_{L_{III}}$ the magnitude of the error would be ~200%, which is not at all the case - see Table 4).

Table 3

K shell conversion coefficients for pure E2 (2+→0+) transitions with energies from 70 to 800 kev

Nucleus	E_γ, kev	$\alpha_{K_{exp}}$	Ref.	$\alpha_{K_{theo}}$	$\alpha_{K_{exp}}/\alpha_{K_{theo}}$
Dy^{164}	72,8	$2,7 \pm 0,5$	[17]	2,20	$1,23 \pm 0,23$
Er^{166}	80,0	$1,9 \pm 0,3$	[18]	1,65	$1,15 \pm 0,16$
		$1,9 \pm 0,2$	[19]		$1,15 \pm 0,11$
		1,9	[20]		1,15
		$1,85 \pm 0,13$	[21]		$1,12 \pm 0,08$
Yb^{170}	84,1	$1,5 \pm 0,2$	[18]	1,36	$1,10 \pm 0,13$
		$1,60 \pm 0,15$	[22]		$1,18 \pm 0,10$
		$1,56 \pm 0,15$	[23]		$1,15 \pm 0,10$
		1,6	[24]		1,18
		$1,69 \pm 0,02$	[25]		$1,24 \pm 0,03$
		$1,65 \pm 0,12$	[21]		$1,21 \pm 0,09$
		$1,34 \pm 0,08$	[26]		$0,99 \pm 0,06$
Dy^{160}	86,2	$1,65 \pm 0,2$	[18]	1,57	$1,05 \pm 0,08$
		1,6	[27]		1,02
		1,5	[28]		0,96
Hf^{176}	89,0	1,3	[18]	1,12	1,16
		$1,32 \pm 0,11$	[21]		$1,18 \pm 0,09$
Hf^{180}	93,3	$1,3 \pm 0,4$	[29]	1,04	$1,25 \pm 0,38$
W^{186}	122,9	$0,45 \pm 0,10$	[30]	0,58	$0,78 \pm 0,18$
Gd^{154}	123	0,54	[31]	0,653	0,83
Os^{186}	137,2	$0,37 \pm 0,08$	[30]	0,446	$0,83 \pm 0,17$
		$0,35 \pm 0,10$	[32]		$0,78 \pm 0,20$
		$0,45 \pm 0,03$	[33]		$1,01 \pm 0,06$
		0,36	[34]		0,81
Os^{188}	155	$0,40 \pm 0,05$	[33]	0,323	$1,24 \pm 0,16$
		$0,32 \pm 0,05$	[35]*		$1,02 \pm 0,15$
Rn^{222}	188	0,15	[36]	0,185	0,81
		$0,22 \pm 0,02$	[37]		$1,19 \pm 0,12$
Rn^{220}	241	0,13	[38]	0,111	1,17
Pt^{194}	328	$(5,6 \pm 0,6) \cdot 10^{-2}$	[39]	$4,9 \cdot 10^{-2}$	$1,14 \pm 0,12$
Pt^{196}	354	$(4,2 \pm 0,3) \cdot 10^{-2}$	[40]	$4,12 \cdot 10^{-2}$	$1,02 \pm 0,07$
Xe^{126}	385	$(1,6 \pm 0,2) \cdot 10^{-2}$	[41]	$1,65 \cdot 10^{-2}$	$1,00 \pm 0,08$
		$1,7 \cdot 10^{-2}$	[42]		1,03
Hg^{198}	411	$(3,18 \pm 0,03) \cdot 10^{-2}$	[43]	$3,04 \cdot 10^{-2}$	$1,04 \pm 0,01$
		$2,5 \cdot 10^{-2}$	[44]		0,82
		$(2,82 \pm 0,05) \cdot 10^{-2}$	[45]		$0,92 \pm 0,02$
Hg^{202}	439	$3,4 \cdot 10^{-2}$	[46]	$2,63 \cdot 10^{-2}$	1,30
Pd^{106}	511	$(3,5 \pm 1,0) \cdot 10^{-3}$	[47]	$4,9 \cdot 10^{-3}$	$0,82 \pm 0,23$
		$3 \cdot 10^{-3}$	[48]		0,61
Xe^{130}	528	$5,5 \cdot 10^{-3}$	[49]	$6,6 \cdot 10^{-3}$	0,83
Te^{122}	556	$(5,2 \pm 0,4) \cdot 10^{-3}$	[50]	$5,20 \cdot 10^{-3}$	$1,00 \pm 0,08$
		$(6,6 \pm 1,7) \cdot 10^{-3}$	[51]		$1,26 \pm 0,26$
		$5,2 \cdot 10^{-3}$	[52]		1,00
Te^{124}	603	$3,4 \cdot 10^{-3}$	[53]	$4,18 \cdot 10^{-3}$	0,81
		$(3,63 \pm 0,04) \cdot 10^{-3}$	[54]		$0,86 \pm 0,01$
Ba^{134}	605	$(4,7 \pm 0,3) \cdot 10^{-3}$	[55]	$5,07 \cdot 10^{-3}$	$0,93 \pm 0,06$
		$(4,6 \pm 0,4) \cdot 10^{-3}$ **	[56 & 57]		$0,91 \pm 0,08$
Cd^{110}	656	$(2,2 \pm 0,8) \cdot 10^{-3}$	[51]	$2,74 \cdot 10^{-3}$	$0,80 \pm 0,29$
Xe^{132}	657	$2,7 \cdot 10^{-3}$	[58]	$3,67 \cdot 10^{-3}$	0,74

*Weighted mean from Ref. 35

**Computed from α_{tot} from Ref. 56 and K/(L + M) from Ref. 57

Table 4

Ratios of K and L shell conversion coefficients for pure E2 (2+→0+) transitions with energies from 70 to 250 kev

Nucleus	E_γ, kev	$K : L_1 : L_2 : L_3$ (experiment)	$K : L_1 : L_2 : L_3$ (theoret. according to Sliv)	$\frac{(K/L_3)\text{exp}}{(K/L_3)\text{theo}}$	$\frac{(L_1/L_3)\text{exp}}{(L_1/L_3)\text{theo}}$	$\frac{(L_2/L_3)\text{exp}}{(L_2/L_3)\text{theo}}$	$\frac{(K/L_3)\text{exp}}{(K/L_3)\text{theo}}$	$\frac{(L_1/L_2)\text{exp}}{(L_1/L_2)\text{theo}}$	$\frac{(L_1/K)\text{exp}}{(L_1/K)\text{theo}}$
Er^{166}	79,8	(0,77 ± 0,08) : : (0,84 ± 0,08) : 1,00 [59]*	0,80 : 0,08 : 0,95 : 1,00	0,96 ± 0,10	—	0,81* ± 0,08	—	—	—
Er^{166}	80,0	0,73 : <0,10 : 0,72 : 1,00 [60,61]**	0,82 : 0,08 : 0,96 : 1,00	0,89	<1,28	0,75	1,17	<1,7	<1,43
		1,22 : <0,10 : 0,72 : 1,00 [62,61]**		1,49	—	—	2,0	—	<0,83
Yb^{172}	84,1	(0,59 ± 0,06) : 0,10 : 0,83 : 1,00 [63,61]**	0,74 : 0,08 : 0,98 : 1,00	0,80 ± 0,08	1,33	0,84	0,95 ± 0,10	1,57	1,60 ± 0,16
		0,8 : 1,0 [64]*				0,75*			
Dy^{160}	86,2	1,22 0,2 : 1,1 : 1,00 [27,65]**	1,29 : 0,12 : 0,92 : 1,00	0,95	1,67	1,20	0,78	1,39	1,8
Hf^{178}	89,0	0,24 — : 0,71 : 1,00 [66]	0,68 : 0,08 : 1,04 : 1,00	0,35	—	0,68	0,51	—	—
Hf^{180}	93,3	(1,15 ± 0,35) : (1,4 ± 0,3) : 1,0 [29]*	0,81 : 0,09 : 1,06 : 1,00	1,42 ± 0,42	—	1,22* ± 0,26	1,17* ± 0,25	—	—
W^{186}	100,9	1,11 : 0,10 : 1,07 : 1,00 [67]	0,84 : 0,09 : 1,11 : 1,00	1,32	1,06	0,97	1,37	1,09	0,8
Sm^{152}	122	(4,38 ± 0,10) : (0,46 ± 0,01) : (1,03 ± 0,02) : 1,00 [68]	4,38 : 0,41 : 0,99 : 1,00	1,00 ± 0,02	1,13 ± 0,02	1,04 ± 0,02	0,96 ± 0,02	1,09 ± 0,02	1,12 ± 0,03
Gd^{154}	123	(3,77 ± 0,08) : (0,41 ± 0,01) : (1,09 ± 0,03) : 1,00 [68]	3,77 : 0,36 : 0,99 : 1,00	1,00 ± 0,02	1,13 ± 0,03	1,10 ± 0,03	0,91 ± 0,02	1,03 ± 0,02	1,12 ± 0,03
Os^{186}	137	(1,53 ± 0,07) : — : 1,24 : 1,00 [69,70]**	1,65 : 0,18 : 1,27 : 1,00	—	—	0,93 ± 0,04	0,95 ± 0,04	—	—
Os^{188}	155	(2,13 ± 0,40) : (0,3 ± 0,2) : (1,4 ±0,1) : 1,00 [33]	2,21 : 0,25 : 1,34 : 1,09	0,96 ± 0,18	1,20 ± 0,80	1,05 ± 0,08	0,93 ± 0,20	1,15 ± 0,80	1,23 ± 0,82
		(2,47 ± 0,13) : (0,3 ± 0,2) : (1,4 ± 0,1) : 1,00 [69,71]**		1,12 ± 0,06	—	—	1,07 ± 0,06	—	1,08 ± 0,72
Os^{192}	206	4,58 : (0,71 ± 0,01) : (1,64 ± 0,02) : 1,00 [71,72]**	4,32 : 0,51 : 1,53 : 1,00	1,06	1,38 ± 0,02	1,07 ± 0,02	0,99	1,30 ± 0,02	1,30

* $(L_1 + L_2)/L_3$. **K/L from the first Ref., $L_1 : L_2 : L_3$ from the second Ref.

The concluding remark of McGowan & Stelson[21] regarding the possible influence of nuclear structure is entirely baseless inasmuch as all such transitions from rotational levels are not only not forbidden but are on the contrary usually speeded-up (favored). Hence despite the obvious care with which McGowan & Stelson carried out their experiments and reduced their data, it must be concluded that a systematic error crept into their work. It would be highly desirable to have further careful measurements of the ICC of pure E2 transitions in the full range of lowlying rotational levels of even-even nuclei.

In Table 4 we have collected the available data on $L_I : L_{II} : L_{III}$ for pure E2 (2+→0+) transitions of energies from 70 to 250 kev. We also give the K/L_{III} values for the same transitions. Sliv's coefficients of conversion on the L shells (Ref.73) differ little in the given range of Z and energies from the ICC of Rose for electric quadrupole transitions.

We have also plotted the ratios of the experimental to theoretical values of K/L_{III}, L_{II}/L_{III} and L_I/L_{III} in Fig.2. It will be seen that in most cases these ratios are close to unity, i.e., that theory is in good agreement with experiment. For K/L_{III} and L_{II}/L_{III} the deviations from unity are equally frequent to the side of lower and higher values of the ratio and, except for Os^{192}, virtually do not exceed the limits of error.

All the L_I/L_{III} and L_I/L_{II} and almost all the L_I/K ratios proved to be greater than unity; that is, the experimental values of α_{L_I} are consistently higher than the theoretical. However, inasmuch as the deviation is small, while conversion on the L_I shell in this region of Z and E_γ is appreciably weaker than on the L_{II} and L_{III} subshells and is consequently more difficult to measure accurately, it may be assumed that the deviation is primarily the result of experimental errors.

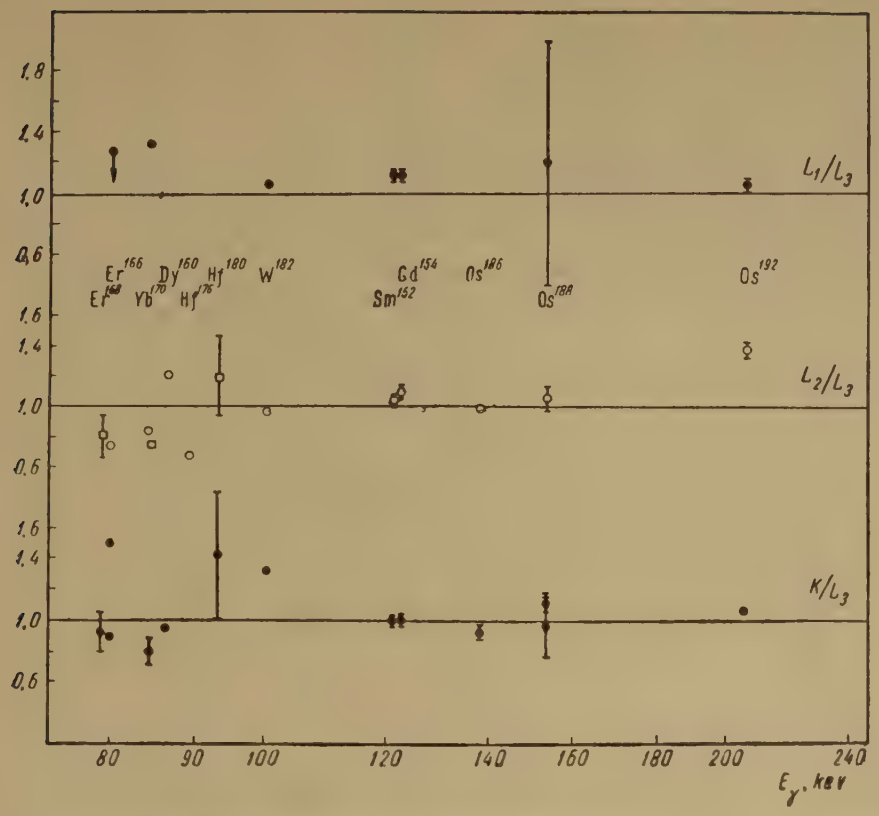

Fig.2. Ratios of experimental to theoretical values of K/L_{III}, L_I/L_{III} (•), L_{II}/L_{III} (o) and $(L_I + L)/L_{III}$ (□) for pure E2 (2+→0+) transitions with energies from 70 to 250 kev.

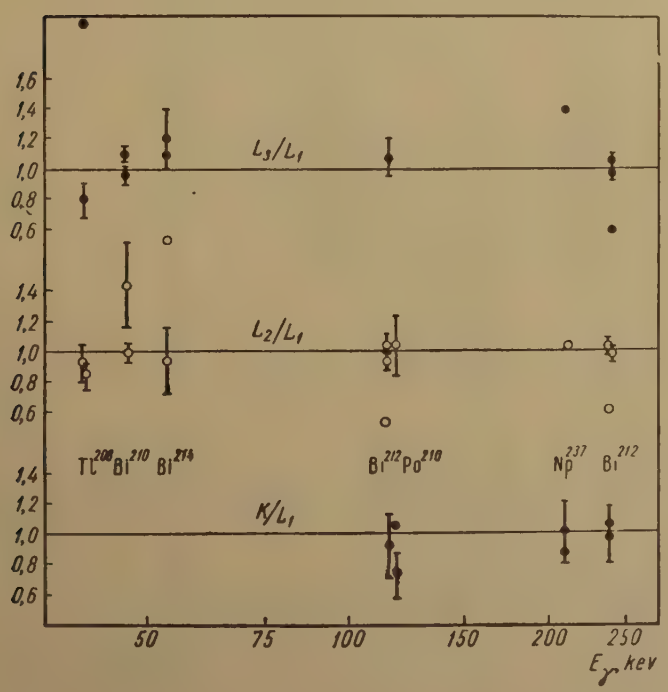

In Table 5 we have collected data on some transitions in heavy nuclei that as regards $L_I:L_{II}:L_{III}$ may be regarded as pure M1 transitions. The experimental to theoretical ratios of the K/L_I, L_{II}/L_I and L_{III}/L_I values for these transitions are plotted in Fig.3.

The corrections for finite nuclear size are largest for the L_I shell, where they amount to 30% for Z = 85. Calculations[73] show that as a result of taking into

←Fig.3. Ratios of experimental to theoretical values of K/L_I, L_{III}/L_I (•) and L_{II}/L_I (o) for conversion transitions of energies between 40 and 250 kev which as regards $L_I:L_{II}:L_{III}$, may be regarded as pure M1.

Table 5

Data on the K and L shell conversion coefficient ratios for transitions with energies from 40 to 250 kev which on the basis of the relative L subshell conversion coefficients may be regarded as pure M1 transitions

Nucleus	E_γ, kev	$(K/L)_{exp}$	$K : L_1 : L_2 : L_3$ (experiment.)	Ref.	$(K/L)_{theo}$	$K : L_1 : L_2 : L_3$ (theoret. according to Sliv)	$\frac{(K/L_1)exp}{(K/L_1)theo}$	$\frac{(L_2/L_1)exp}{(L_2/L_1)theo}$	$\frac{(L_3/L_1)exp}{(L_3/L_1)theo}$
Tl^{208}	40	—	—	[1,74]	—	— 100 : 10,8 : 1,00	—	$0,92 \pm 0,13$	2
			$100 : (10 \pm 1,4) : 2$	[75,76]			—	$0,85 \pm 0,05$	$0,8 \pm 0,1$
			$100 : (9,2 \pm 0,4) : (0,8 \pm 0,1)$						
Bi^{210}	46,6	—	—	[77]		— 100 : 10,6 : 0,90	—	$1,44 \pm 0,29$	$0,96 \pm 0,06$
			$100 : (15 \pm 3) : (0,86 \pm 0,05)$	[78]			—	$1,00 \pm 0,02$	$1,07 \pm 0,05$
			$100 : (10,5 \pm 0,5) : (1,00 \pm 0,05)$	[76]			—	$1,02 \pm 0,04$	$1,03 \pm 0,05$
			$100 : (10,6 \pm 0,2) : (0,96 \pm 0,05]$						
Bi^{214}	53	—	—	[79]		— 100 : 10,7 : 0,90	—	$0,94 \pm 0,23$	$1,20 \pm 0,20$
			$100 : (10 \pm 2,5) : (1,1 \pm 0,2)$	[80]			—	1,78	1,1
			$100 : 19 : 1$						
Bi^{212}	115	5 ± 1			5,47	612 : 100 : 10,9 : 0,81	$0,92 \pm 0,20$*	—	—
				[1,74]			—	0,55	—
			$100 : 6 : —$	[81]			—	$1,03 \pm 0,08$	<2,4
			$100 : (12 \pm 1) : <2$	[76]			—	$0,95 + 0,03$	$1,1 \pm 0,1$
			$100 : (10,4 \pm 0,3) : (0,88 \pm 0,10)$					—	—
Po^{210}	117	5,8		[82]	5,42	605 : 100 : 11,0 : 0,78	1,07*		
		4	$(440 \pm 90) : 100 : (11,4 \pm 2,2) : —$	[83]		533 : 100 : 12,7 : 0,50	$0,73 \pm 0,15$	$1,04 \pm 0,20$	—
			$480 : 100 : —$	[84]	4,88		0,88	—	—
Np^{237}	208		$(570 \pm 110) : 100 : 13 : 0,7$	[9]			$1,03 \pm 0,20$	1,02	1,4
Bi^{212}	238	$5,5 \pm 2$		[85]	5,50	610 : 100 : 10,6 : 0,75	$1,00 \pm 0,18$*	—	—
				[1,74]			—	0,60	0,60
			$100 : 6,4 : 0,45$	[86]			—	$1,02 \pm 0,01$	$1,06 \pm 0,03$
			$100 : (10,8 \pm 0,1) : (0,8 \pm 0,02)$	[87]			1,08	$1,09 \pm 0,03$	$0,88 \pm 0,06$
			$663 : 100 : (11,6 \pm 0,3) : (0,66 \pm 0,04)$	[76]				$0,98 \pm 0,03$	$0,99 \pm 0,06$
		5,9	$100 : (10,4 \pm 0,3) : (0,74 \pm 0,04)$						

*Based on the theoretical value of $L_1/(L_2 + L_3)$.

account finite nuclear size, $\alpha_{L_{II}}$ is decreased by only about 10% for Z = 85, while $\alpha_{L_{III}}$ remains virtually unchanged.

In connection with experimental substantiations of corrections to the L_I conversion coefficients, some authors[1,88] have also found a large correction for $\alpha_{L_{II}}$, i.e., a correction of the same magnitude as for α_{L_I} or even greater (up to 60%). In Fig.3 we show the two points - $(L_{II}/L_I)_{exp}/(L_{II}/L_I)_{theo} \approx 0.6$ - for the 115 and 238 kev transitions in Bi^{212} that gave rise to this inference of a large correction for $\alpha_{L_{II}}$. It will be seen from the figure, however, that these data diverge appreciably from the results of most measurements.

The most accurate measurements (see, for example, Kel'man et al[86]) show that Sliv's ICC are in good agreement with the experimental values and that no appreciable corrections for $\alpha_{L_{II}}$ are required.

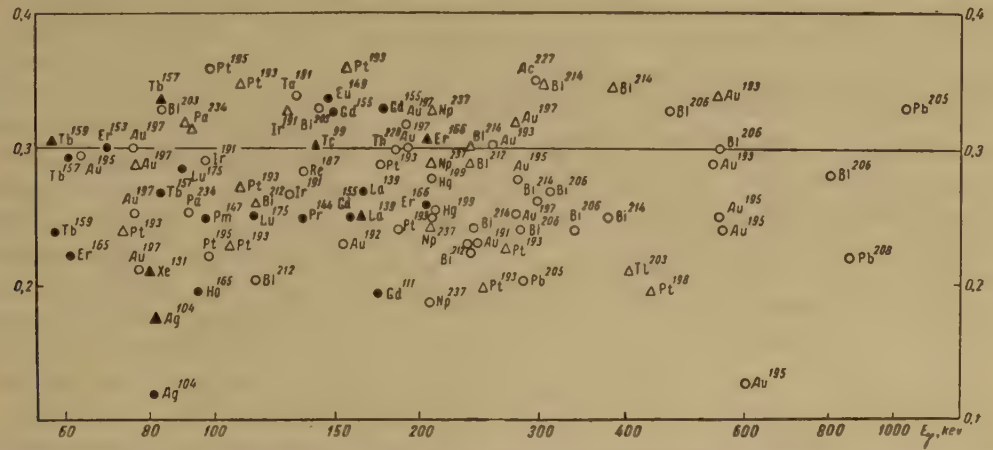

Fig.4. Values of M/L (circles) and (M + N)/L (triangles) for M1 transitions of 50 to 1250 kev energy. Solid circles and triangles - Z ⩽ 73; open circles and triangles - Z ⩾ 74.

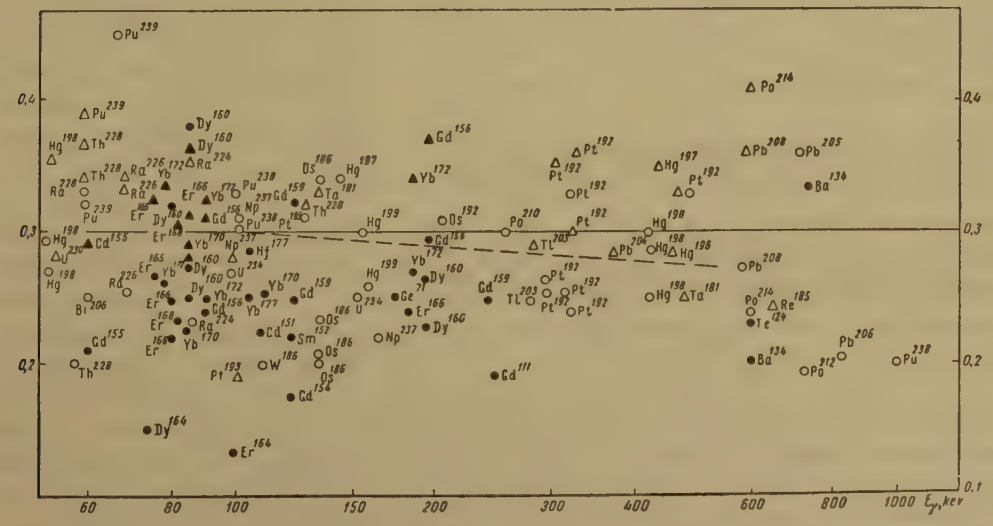

Fig.5. Values of M/L (circles) and (M + N)/L (triangles) for E2 transitions of 50 to 1250 kev energy. Solid circles and triangles - Z ⩽ 73; open circles and triangles - Z ⩾ 74.

The above mentioned errors[1,88] undoubtedly arose owing to the difficulties encountered in graphic resolution of the close strong L_I and weak L_{II} lines or in determining the relative intensities of these lines in case of photographic recording. The possibility that there was an error involved (i.e., that the

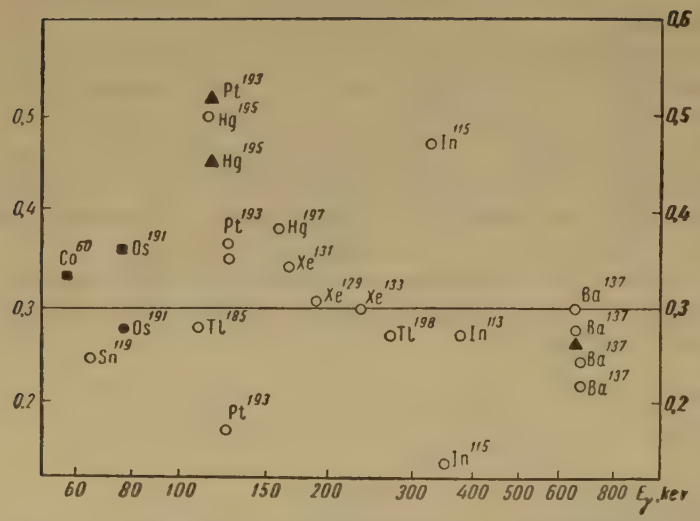

Fig.6. Values of M/L for M3 (●) and M4 (○) transitions of 50 to 1000 kev energy and values of (M + N)/L for M3 (■) and M4 (▲) transitions.

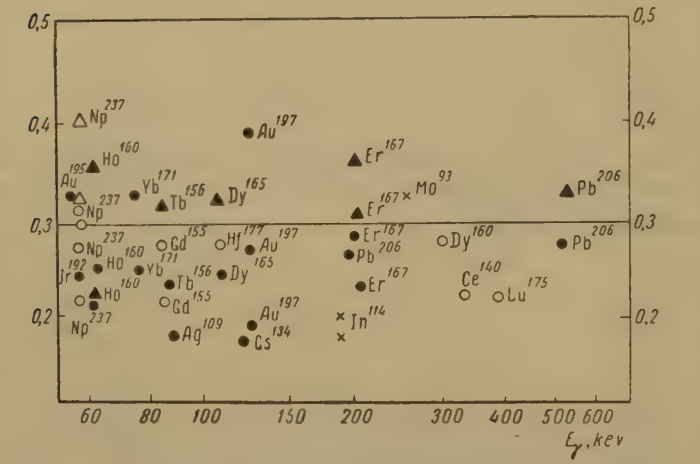

Fig.7. Values of M/L (circles and crosses) and (M + N)/L (triangles) for E1 (open circles and triangles), E3 (solid circles and triangles), and E4 (crosses) transitions.

experimental value of L_{II}/L_I was an overestimate) was noted by Wapstra & Nijgh[1]; nevertheless the assumption that the theoretical value of αL_{II} requires a large correction appears to have been widely accepted. Thus, for example, when Rasmussen et al[9] in 1957 did not find the need for a 50% correction in the value of αL_{II} for the pure M1 208 kev transition in Np^{237}, they considered this to be a new anomaly in the ICC and tentatively attributed it to the Church & Weneser effect.

Finally, let us review the available data on the M/L ratio. Recently, Rose (the work is referred to in Ref.9,14,78 & 89) calculated the M shell conversion coefficients. However, these calculations, which were carried out without taking screening into account, as regards absolute value diverge from experiment by a factor of 1.5-2 and are suitable only for determining the ratios of conversion on the M subshells. At present, therefore, one can only use empirical values of M/L.

Figs.4,5,6 & 7 show the values of M/L and (M + N)/L for E1, E2, E3, E4, M1, M3 and M4 transitions.[90] For mixed transitions (for example, M1 + E2) the M/L ratio is plotted for the multipole order accounting for more than 50% of the mixture. Unfortunately, many investigators fail to specify precisely which ratio they measured and hence many of the M/L ratios are actually (M + N)/L. This naturally hampers analysis of the data.

It will be seen from the figures that the ratio M/L is very weakly dependent on the energy, nuclear charge and multipole order and that in all cases it equals about 0.3. This, at first glance, strange result may be explained by the fact that conversion on the M_{IV} and M_V subshells is small, while conversion on the M_I, M_{II} and M_{III} subshells depends on all the previously enumerated factors in the same way as conversion on the L_I, L_{II} and L_{III} subshells and that consequently the M/L ratio remains constant. For energies less than 50 kev, however, this is no longer the case. In view of the large scatter of the data, we have so far not been able to note any consistent regularities and accordingly have not plotted the data for $E_\gamma < 50$ kev in the figures. For E2 and M1 ($E_\gamma > 50$ kev), one can deduce more accurate values, i.e., $M/L \approx 0.25$ and $(M + N)/L \approx 0.31$.

As regards (N + O)/M, we have even fewer data and for the most part these are even less reliable. In general, however, the values of this ratio fall between 0.2 and 0.4.

In conclusion, it should be noted that in many cases measurements of ICC are rather inaccurate and often contradictory. Thus, for example, for the 74.7 kev transition in Dy^{161} we find a value of 1.30 for K/L reported by Cork et al[91] and a value of ~7 reported by Smith et al[92]. Both series of measurements were made in 1956. For the 337 kev transition in In^{115} Antonova[93] reports a value of 2.2±0.3 for L/M, whereas Varma & Mandeville give > 10 for this ratio[94] (see Fig.6). Other examples of large divergences are not lacking in the literature.

Moreover it must be noted that until now ICC have been measured for less than 10% of the known γ-transitions.

In cases when the ICC has been measured with reasonable accuracy, it is found that the theoretical ICC of Sliv, calculated taking into account the finite nuclear size, are generally in satisfactory agreement with experiment. At the same time there is reason to assume that for strongly forbidden transitions there may be cases when the ICC may depend significantly on finer details of nuclear structure. The effect - if it exists at all and definitive proof is still lacking - is undoubtedly rare and peculiar to individual nuclei.

The author desires to express his gratitude to L.A.Sliv for making available some results of his calculations of L shell conversion coefficients prior to publication, for supplying reprint copies of Refs.8,45 and 89 and for discussion of the present review.

References

1. A.Wapstra & G.Nijgh, Nucl.Phys., 1, 245 (1956).
2. F.McGowan & P.Stelson, Phys.Rev., 103, 1133 (1956).
3. E.M.Krisiuk, G.D.Latyshev, M.A.Listengarten, L.A.Ostretsov & A.G.Sergeev, Izv.AN SSSR, Ser.fiz., 20, 363 (1956). (Trans.Bulletin 20, No.3, 332.)
4. L.A.Sliv, Zhur.eksp.i teor.fiz., 21, 770 (1951); L.A.Sliv & M.A.Listengarten, Zhur.eksp.i teor.fiz., 22, 29 (1952); L.A.Sliv & I.M.Band, Tablitsy koeffitsientov vnutrennei konversii γ-izlucheniia (Tables of internal conversion coefficients) Part 1, M.-L., 1956.
5. M.Rose, G.Goertzel, B.Spinard, J.Harr & P.Strong, Phys.Rev., 83, 79 (1951); M.Rose, in Beta- and Gamma-Ray Spectroscopy, edited by K.Siegbahn, Amsterdam, 1955.
6. E.Church & J.Weneser, Phys.Rev., 104, 1382 (1956).
7. V.B.Berestetskii, A.Z.Dolginov & K.A.Ter-Martirosian, Zhur.eksp.i teor. fiz., 20, 527 (1950).
8. S.Nilsson & J.Rasmussen, Nucl.Phys., 5, 617 (1958).
9. J.O.Rasmussen, F.L.Canavan & J.M.Hollander, Phys.Rev., 107, 141 (1957).
10. E.Snyder & S.Frankel, Phys.Rev., 106, 755 (1957).
11. P.Stelson & F.McGowan, Phys.Rev., 105, 1346 (1957).
12. D.Engelkemeier & L.Magnusson, Phys.Rev., 99, 135 (1955).
13. J.Milsted, S.Rosenblum & M.Valadares, C.R.Acad.Sci., 239, 259, 700 (1954); T.F.Turner, Philos.Mag., 46, 687 (1955); N.Jaffe, T.Passel, C.Braun & I.Perlman, Phys.Rev., 97, 142 (1955); S.A.Baranov & K.N.Shliagin, Reports presented at International Conference on the Peaceful Uses of Atomic Energy, 1955.
14. S.Rosenblum & M.Valadares, J.phys.et radium, 18, 609 (1957).
15. L.Kisslinger, Bull.Amer.Phys.Soc., 2, 358 (1957); A.S.Reiner, Nucl.Phys., 5, 544 (1958).
16. J.Reitz, Phys.Rev., 77, 10 (1950).
17. H.Brown & R.Becker, Phys.Rev., 96, 1372 (1954).

18. F.McGowan, Phys.Rev., 85, 151 (1952).
19. A.Sunyar, Phys.Rev., 93, 1345 (1954).
20. R.L.Graham, J.L.Wolfson & M.Clark, Phys.Rev., 98, 1173 (1955).
21. F.McGowan & P.Stelson, Phys.Rev., 107, 1674 (1957).
22. R.Graham, J.Wolfson & R.Bell, Canad.J.Phys., 30, 459 (1952).
23. K.Linden & N.Starfelt, Arkiv Fys., 7, 109 (1954).
24. N.Jaffe, Nucl.Sci.Abstrs., 9, No.24B, (1955).
25. A.Bisi, E.Germagnoli & L.Zappa, Nuovo Cimento, 3, 1007 (1956).
26. H.Houtermans, Z.Phys., 149, 215 (1957).
27. O.Nathan, Nucl.Phys., 4, 125 (1957).
28. M.Clark & J.Knowles, Bull.Amer.Phys.Soc., 2, 231 (1957).
29. V.S.Gvozdev, L.I.Rusinov & Iu.L.Khazov, Abstracts of reports presented at the Eighth Conference on Nuclear Spectroscopy, M.-L., 1958.
30. R.M.Steffen, Phys.Rev., 82, 827 (1951).
31. J.Juliano & F.Stephens, Phys.Rev., 108, 341 (1957).
32. F.Metzger & R.Hill, Phys.Rev., 82, 646 (1951).
33. M.Johns, C.McMullen, I.Williams & S.Nablo, Canad.J.Phys., 34, 69 (1956).
34. F.Porter, M.Freedman, T.Novey & F.Wagner, Phys.Rev., 103, 921 (1956).
35. V.R.Potnis, Phys.Rev., 104, 722 (1956).
36. R.Roy & M.Goes, C.R.Acad.Sci., 238, 469 (1954).
37. M.Juric & D.Stanojević, Bull.Inst.Nucl.Sci.Boris Kidric, 5, 15 (1956).
38. S.Rosenblum, M.Valadares & M.Guillot, J.phys.et radium, 15, 129 (1954).
39. M.Thieme & E.Bleuler, Phys.Rev., 102, 195 (1956).
40. M.Thieme & E.Bleuler, Phys.Rev., 101, 1031 (1956).
41. N.Marty, H.Langevin & P.Huber, J.phys.et radium., 14, 662 (1953); C.R. Acad.Sci., 236, 1153 (1953).
42. L.Koerts, P.Macklin, B.Farelly, R.Van Lieshout & C.Wu, Phys.Rev., 98, 1230 (1955).
43. L.Simons, Phys.REv., 86, 570 (1952).
44. D.Connors, W.Miller & B.Waldman, Phys.Rev., 102, 1584 (1956).
45. A.Wapstra, Proceedings Rehovoth Conference on Nuclear Structure. - Amsterdam, 1958.
46. P.Kramers, H.Hamers & G.Meijer, Physica, 22, 208 (1956).
47. D.E.Alburger, Phys.Rev., 88, 339 (1952).
48. W.Bendel, Phys.Rev., 90, 880 (1952).
49. R.S.Caird & A.C.Mitchell, Phys.Rev., 94, 412 (1954).
50. M.J.Glaubman, Phys.Rev., 98, 645 (1955).
51. R.Rohr & R.Birkhof, Phys.Rev., 98, 1266 (1955).
52. B.Farrelly, L.Koerts, N.Benczer, R.Lieshout & C.Wu, Phys.Rev., 99, 1440 (1955).
53. L.Langer, N.Lazar & R.Moffat, Phys.Rev., 91, 338, 485 (1953).
54. D.Hutchinson & M.Wiedenbeck, Phys.Rev., 88, 699 (1952).
55. G.Bertolini, M.Bettoni & E.Lazzarini, Nuovo Cimento, 2, 273 (1955).
56. Z.O'Friel & A.Weber, Phys.Rev., 101, 1076 (1956).
57. G.Keister, E.Lee & F.Schmidt, Phys.Rev., 97, 451 (1955).
58. H.Finston & W.Bernstein, Phys.Rev., 96, 71 (1954).
59. K.Ia.Gromov, B.S.Dzhelepov & B.K.Preobrazhenskii, Izv.AN SSSR, Ser. fiz., 21, 918 (1957). (Trans.Bulletin, 21, No.9, 920.)
60. R.L.Graham, J.L.Wolfson & M.A.Clark, Nucl.Sci.Abstr., 9, No.24 B, 96 (1955).
61. J.Mihelich, Phys.Rev., 87, 646 (1952).
62. K.Ia.Gromov, B.S.Dzhelepov, V.G.Dmitriev, V.A.Morozov, L.K.Peker & B.K.Preobrazhenskii, Abstracts of reports presented at the Eighth Conference on Nuclear Spectroscopy, M.-L., 1958.

63. P.Gray, Phys.Rev., 101, 1306 (1956).
64. Iu.G.Bobrov, K.Ia.Gromov, B.S.Dzhelepov & B.K.Preobrazhenskii, Izv. AN SSSR, Ser.fiz., 21, 940 (1957). (Trans.Bulletin 21, No.7, 942.)
65. E.P.Grigor'ev, B.S.Dzhelepov, A.V.Zolotavin, B.Kratsik, B.K.Preobrazhenskii & I.S.Ianchevskaia, Doklady AN SSSR, 117, 53 (1957).
66. J.Mihelich & E.Church, Phys.Rev., 85, 690 (1952).
67. J.Murray, P.Snelgrove, P.Marmier & J.Dumond, Phys.Rev., 97, 1007 (1956).
68. V.M.Kel'man, V.A.Romanov, R.Ia.Meskhvarishvili & V.A.Kol'tsov, Zhur. eksp.i teor.fiz., 32, 39 (1957); Nucl.Phys., 2, 395 (1956).
69. K.Nielsen & O.Nielsen, Nucl.Phys., 5, 319 (1958).
70. J.Swann & R.Hill, Phys.Rev., 91, 424 (1953).
71. L.Baggerly, P.Marmier, F.Boehm & J.Dumond, Phys.Rev., 100, 1364 (1955).
72. V.M.Kel'man, R.Ia. Metskhvarishvili, V.A.Romanov & V.V.Tuchkevich, Zhur. eksp.teor.fiz., 33, 588 (1957); Nucl.Phys., 4, 240 (1957).
73. L.A.Sliv & I.M.Band, Tablitsy koeffitsientov vnutrennei konversii γ-izlucheniia (Tables of internal conversion coefficients) Part 2, L shell, M.1958.
74. K.Siegbahn & T.Gerholm, in Beta- and Gamma-Ray Spectroscopy, edited by Siegbahn, Amsterdam, 1955.
75. A.Zhernovoi, E.Krisiuk, G.Latyshev, A.Remennyi, A.Sergeev & V.Fadeev, Zhur.eksp.i teor.fiz., 32, 682 (1957). (Trans.JETP - Soviet Phys.)
76. A.G.Sergeev, Transactions of the Eighth Conference on Nuclear Spectroscopy, L., 1958.
77. B.S.Dzhelepov, A.A.Bashilov & L.S.Chervinskaia, Izv.AN SSSR, Ser.fiz., 17, 428 (1953).
78. M.Frilley & M.Valadares, J.phys.et.radium, 18, 468 (1957).
79. K.Nielsen, O.Nielsen & M.Wagonner, Nucl.Phys., 2, 476 (1956).
80. M.Mladenovic & H.Slätis, Arkiv Fys., 8, 65 (1954).
81. E.M.Krisyouk, A.V.Sergeev, G.D.Latyshev & V.D.Vorobyev, Nucl.Phys., 4, 579 (1957).
82. R.Hoff, Nucl.Sci.Abstr., 9, 24 B, 119 (1955).
83. J.Mihelich, A.Schardt & E.Segrè, Phys.Rev., 95, 1508 (1954).
84. F.Wagner, M.Friedman, D.Engelkemeier & J.Huizenga, Phys.Rev., 89, 502 (1953).
85. O.B.Nielsen, Dan.Mat.-Fys.Medd., 30, 11 (1955).
86. V.M.Kel'man, V.A.Romanov & R.Ia.Metskhvarishvili, Doklady AN SSSR, 103, 577 (1956).
87. V.Vorob'ev, K.Il'in, T.Kol'chinskaia, G.Latyshev, A.Sergeev, Iu.Trofimov, & V.Fadeev, Izv.AN SSSR, Ser.fiz., 21, 954 (1957). (Trans.Bulletin, 21, No.7, 956.)
88. E.Sokolovski, K.Edvarson & K.Siegbahn, Nucl.Phys., 1, 160 (1956).
89. R.Cressman & R.Wilkinson, in Proceedings of the Rehovoth Conference on Nuclear Structure, Amsterdam, 1958.
90. Data taken primarily from Nuclear Science Abstract, 24 B, 7 (1953), 8 (1954), 9 (1955), 10 (1956); 11, 1-20 (1957); J.M.Hollander, I.Perlman & G.T. Seaborg, Revs.Mod.Phys., 28, 469 (1953).
91. J.Cork, M.Brice, L.Schmid & R.Helmer, Phys.Rev., 104, 481 (1956).
92. W.Smith, J.Hamilton, R.Robinson & L.Langer, Phys.Rev., 104, 1020 (1956).
93. A.Antonova, Izv.AN SSSR, Ser.fiz., 20, 896 (1956). (Trans.Bulletin 20, No.8, 814.)
94. J.Varma & C.Mandeville, Phys.Rev., 97, 977 (1955).

CONVERSION ELECTRONS FROM Yb^{169}

- K.Ia.Gromov, B.S.Dzhelepov & B.K.Preobrazhenskii

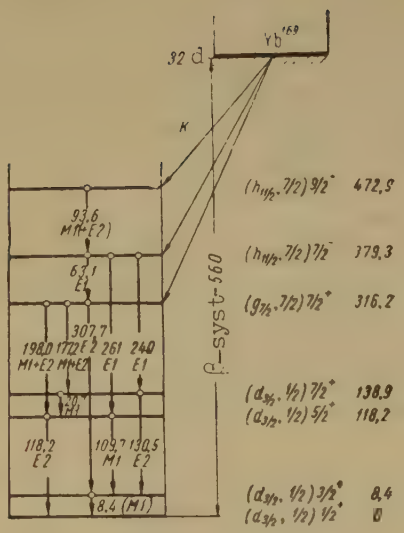

Fig.1. Decay scheme for Yb^{169}.

Ytterbium^{169}, capturing atomic electrons, transforms to Tm^{169}. The radiation accompanying the decay of Yb^{169} has been investigated a number of times.[1-4]

As a result of investigation of γ-γ coincidences[2], precision measurements of the γ-transition energies[4] and determination of the relative γ-ray and conversion electron intensities[1-4] there has been elaborated the decay scheme shown in Fig.1. In all the investigations referred to, the γ-ray and conversion electron measurements were made on Yb^{169} samples prepared by neutron irradiation of stable ytterbium.

We investigated the conversion electron spectrum of Yb^{169} obtained by spallation of tantalum.[5] The ytterbium (lactate) sample obtained as a result of chromatographic separation was evaporated onto a 0.005 x 1.0 x 6 mm aluminum strip which was used as the source in studying the conversion electron spectrum in a Ketron type[6] magnetic spectrometer. The resolution of this instrument in our experiments was 0.6%.

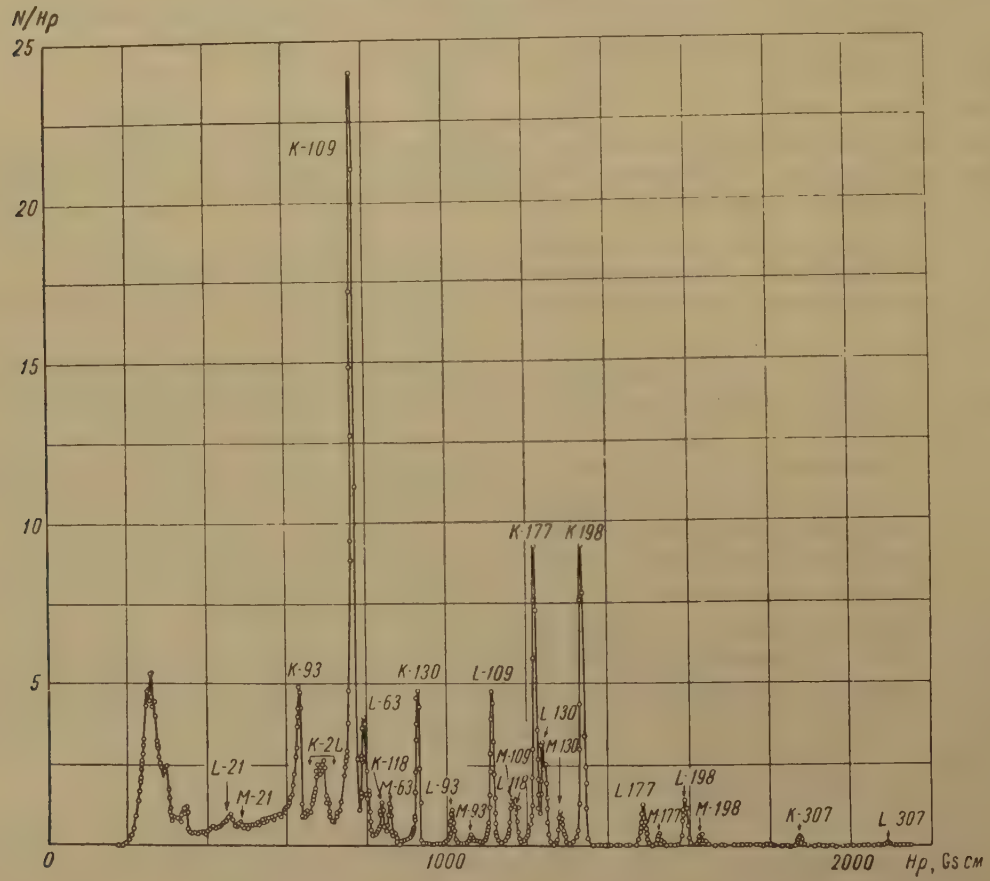

Fig.2. Conversion electron spectrum of Yb^{169}.

Table 1

Results of experimental investigation of conversion electrons from Yb^{169}

No.	E_e, kev	$H\rho$, Gs·cm	Relative intensity	Identification	E_γ, kev
1	5,47±0,06	250	—	L-Auger	
2	5,94±0,02	261	—	L-Auger	
3	6,30±0,02	268,5	—	(*M*-8,4)	
4	7,70±0,02	297	—	(*N*-8,4)	
5	10,42±0,06	346	—	*L*-21	
6	18,22±0,14	459	—	*M*-21	
7	20,16±0,12	507,5	—	*N*-21	
8	33,86±0,05	631	136±12	*K*-93	93,2±0,3
9	35,35±0,05	645	—	—	
10	38,88±0,15	673	—	—	
11	40,23±0,13	690	—	—	
12	41,40±0,10	700	—	—	
13	49,93±0,17	772	348±12	*K*-109	109,3±0,3
14	52,70±0,07	794	76±6	L_I-63	62,7±0,3
15	54,11±0,14	805	76±6	L_{III}-63	
16	58,38±0,12	838	17,2±1,4	*K*-118	117,71±0,25
17	60,38±0,28	853	16,8±1,2	*M*-63	
18	62,20±0,13	866	3,6±1,2	*N*-63	
19	70,71±0,07	927,5	59±2	*K*-130	
20	83,08±0,25	1011	14,2±1,2	L_I-93	
21	91,00±0,29	1062	2,8±0,2	*M*-93	
22	92,6	1072	0,5±0,1	*N*-93	
23	99,19±0,06	1113	51,6±1,0	*L*-109	
24	107,05±0,21	1160	30,6±1,5	*M*-109	
25	108,05±0,30	1166	30,6±1,5	*L*-118,N-109	
26	109,14±0,02	1173	30,6±1,5		
27	117,50±0,05	1221	92±5	*K*-177	
28	120,69±0,05	1239	44±3	L_{II}-130	
29	121,53±0,05	1244	44±3	L_{III}-130	
30	128,22±0,16	1281	11,6±1,6	*M*-130	
31	129,75±0,20	1290	5,5±0,5	*N*-130	
32	138,41±0,13	1337	100	*K*-198	
33	167,08±0,20	1487	13,5±2,1	L_{II}-177	
34	168,1 ±0,20	1492	13,5±2,1	L_{III}-177	
35	174,72±0,10	1525	3,2±0,4	*M*-177	
36	176,6 ±0,2	1535	1,4±0,4	*N*-177	
37	188,07±0,10	1591	19±2	L_{II}-198	
38	189,0 ±0,2	1596	19±2	L_{III}-198	
39	195,7 ±0,3	1625	3,4±0,4	*M*-198	
40	197,6 ±0,3	1638	1,4±0,2	*N*-198	
41	201,8 ±0,2	1658	0,4±0,1	*K*-261	
42	248,70±0,05	1875	4,1±0,1	*K*-308	308,03
43	249,9 ±0,1	1881	4,1±0,1	*K*-309	309,23
44	298,48±0,13	2094	1,2±0,1	*L*-308	
45	306,07±0,10	2127	0,3±0,1	*M*-308	

The tantalum target was bombarded with protons for about three months. The chromatographic separation was carried out one week after the end of bombardment and the measurements were begun two weeks later.

The recorded conversion electron spectrum is shown in Fig.2. Repeat measurements of the spectrum carried out twice at intervals of about a month showed that the appearance of the spectrum did not change with time and that the intensity of the conversion lines fell off with a period of about 32 days. Thus all the observed conversion lines could safely be attributed to Yb^{169}.

The results of our measurements are listed in Table 1.

63 kev transition

We attributed the 52.70, 54.11, 60.38 and 62.20 kev conversion lines (Fig. 3) to a 62.7 ± 0.3 kev γ-transition, identifying them as the $(L_I + L_{II})$, L_{III}, M and N lines respectively. The ratio of intensities of the L internal conversion lines, $(L_I + L_{II})/L_{III}$, is in best agreement with the theoretical value of this ratio for an E1 transition (Table 2).

93 kev transition

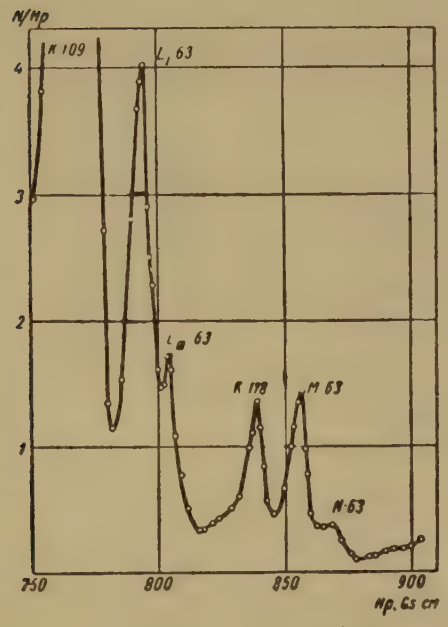

Fig.3. Section of Yb^{169} conversion electron spectrum: lines due to conversion of the 62.7 kev γ-transition.

We ascribed the 33.86 (K), 83.08 (L_I), 91.00 (M) and 92.6 kev (N) electron lines to a 93 kev transition. From the difference K - M (57.14 ± ± 0.34 kev), we unambiguously established that the transition occurs in the Tm nucleus (Z = 69). On the basis of the K line, the energy of the transition is found to be 93.2 ± 0.3 kev. The 83.08 kev peak agrees exactly with the position of the L_I subshell internal conversion line for a transition of this energy. This substantiates our identification of the 83.08 kev line. Consideration of the theoretical L subshell conversion coefficients for a transition of 93.2 kev energy shows that conversion occurs primarily on the L_I subshell only for E1, M1 and M2 type transitions. The experimental value of the ratio of intensities of the K and L conversion lines for this transition is 9.6. This ratio does not agree with any of the theoretical values but is closest to the theoretical K/L ratios for M1 and E1 transitions (Table 2).

Table 2

Comparison of the experimental and theoretical line intensity ratios in the conversion spectrum of Yb^{169}

Transition energy, kev	Ratio	Experimental value	Theoretical values					
			E1	E2	E3	M1	M2	M3
63	$(L_I+L_{II})/L_{III}$	2,9	2,9	1,1	0,24	0,01	3,8	1,3
93	K/L	9,6	6,9	0,97	0,12	5,7	3,2	0,85
109	K/L	6,7	7,0	1,1	0,15	5,7	3,5	1,2
118	K/L	1	6,4	1,4	0,17	5,5	3,8	1,2
130	K/L	1,3	6	1,6	0,23	5,2	3,9	1,5
	$(L_I+L_{II})/L_{III}$	1	4,3	1,2	2,3	115	5,7	1,3
177	K/L	6,8	6,8	2,5	0,57	5,2	4,4	2,1
	$(L_I+L_{II})/L_{III}$	1,5	7,4	1,5	2,4	135	9,0	2,5
198	K/L	5,4	6,9	2,5	0,81	5,5	4,9	2,5
	$(L_I+L_{II})/L_{III}$	2,2	7,2	2,2	1,9	135	10	3,0
308	K/L	3,4	6,8	4,0	1,6	6,3	5,8	3,5

109 kev transition

We attributed the 49.94 (K), 99.19 (L) and 107.05 kev (M) electron lines to a γ-transition of 109 kev. From the fact that the difference K - M equals 57.1 ± 0.4 kev, we infer that this transition occurs in the thullium nucleus. From the energy of the K line, we obtain a value of 109.3 ± 0.3 kev for the precise energy of the γ-transition. The energy of the L line (99.19 kev) and its shape allow us to infer that L conversion of this transition occurs primarily on the L_I subshell. The experimental value of K/L is closest to the theoretical ones for M1 or E1 (Table 2). Preferential conversion on the L_I subshell ($L_I/(L_{II} + L_{III}) = 10$) is characteristic of M1 type transitions (for E1 we would have $L_I/(L_{II} + L_{III}) = 1.8$).

118 kev transition

We do not have sufficient clear data to affirm the existence of a transition of this energy (the K line is discernible, but the L line is not resolved from the neighboring lines), but other authors[4] report the existence of the γ-transition. It may be assumed therefore that the conversion line at 53.38 kev is the K line of this transition. If we assume that this γ-transition occurs in the thullium nucleus, its energy comes out to be 117.71 ± 0.25 kev. The L shell conversion line of a 117.7 kev transition should have an energy of about 108 kev, i.e., should be located between the M and N lines of the 109 kev γ-transition. In this region there actually are several unresolved electron lines. Probably these are the M and N lines of the 109 kev transition and the L line of the 117.7 kev transition. Inasmuch as the lines have not been resolved, we cannot determine the intensity of the L line. However, on the basis of the experimentally established fact that the intensity of conversion on the M and N subshells usually amounts to 25-40% relative to the intensity of L conversion, we can evaluate the intensity of the M and N conversion lines of the 109 kev transition. In the relative units utilized in Table 1, this intensity is ~15; hence the L-117.7 intensity is also ~15, i.e., the K/L ratio for the 117.7 kev transition is approximately unity.

Comparison of this value with the theoretical one (Table 2) enables us to limit the possible multipole orders of the 117.7 kev transition to E2 and M3. The M line of this transition, whose energy must be about 115.4 kev, is indiscernible against the background of the intense 117.5 kev (K-177) line.

130 kev transition

We associated the 70.71 (K), 120.69 ($L_I + L_{II}$), 121.53 (L_{III}), 128.22 (M) and 129.75 kev (N) lines with a 130 kev transition. The difference K - M = = 57.51 ± 0.20 kev; consequently, this transition occurs in the thullium nucleus. From the position of the K line we obtain a value of 130.04 ± 0.2 kev for the energy of this transition. It follows from this energy value that the 120.69 and 121.53 kev lines are the ($L_I + L_{II}$) and L_{III} lines, respectively. Comparison of the experimental and theoretical values of K/L and $(L_I + L_{II})/L_{III}$ shows that this transition is either E2 or M3 (Table 2). It should be noted that the (L_I + + L_{II}) peak is located closer to the energy position of the L_{III} line, which is characteristic of an E2 transition (in the case of M3 the peak should be closer to the nominal position of the L_I line).

177 kev transition

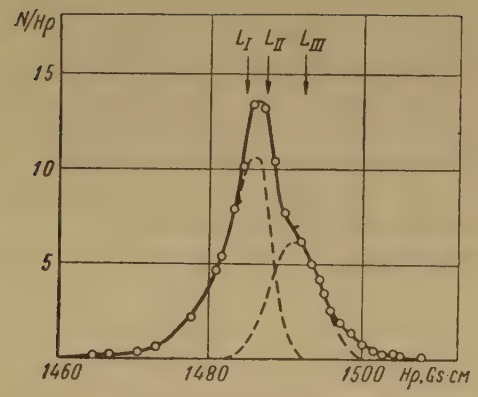

Fig.4. Section of Yb^{169} conversion spectrum: L lines of the 177.2 kev γ-transition.

We associated the 117.50 (K), 167.08 (L_I + L_{II}), 168.1 (L_{III}), 174.72 (M) and 176.6 kev (N) lines with a transition of 177 kev energy. From the difference K - M, which is 52.20 ± 0.15 kev, it may be inferred that the transition occurs in a nucleus with Z = 69. Consequently, the transition energy on the basis of the K line position is 176.83 ± 0.3 kev. Assuming this energy value, we can identify the lines at 167.08 and 168.1 kev as the (L_I + L_{II}) and L_{III} conversion lines; from the position of the 167.08 kev line peak it may be inferred that conversion occurs primarily on the L_{II} subshell.

From a comparison of the experimental and theoretical values of K/L and (L_I + L_{II})/L_{III} (Table 2 & Fig.4) we cannot unambiguously select between Mi and E2 for this transition. Probably in this case we have a mixture of M1 + E2.

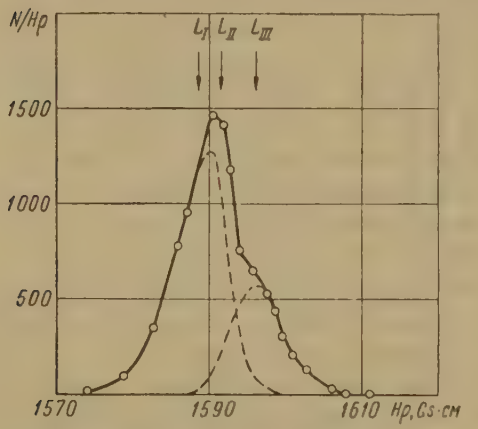

Fig.5. Section of the Yb^{169} conversion spectrum: L lines of the 198.0 kev γ-transition.

198 kev transition

We attributed the 138.41 (K), 188.07 (L_I + L_{II}), 189.0 (L_{III}), 195.7 (M) and 197.06 kev (N) electron lines to a 198 kev γ-transaction. From the fact that K - M = 57.3 ± 0.4 kev we infer that the transition occurs in the thullium nucleus. From the K line we obtain a value of 197.74 ± 0.4 kev for the transition energy. Assuming this value, the lines at 188.07 and 189.0 kev may be identified as the (L_I + L_{II}) and L_{III} conversion lines; the position of the (L_I + L_{II}) peak indicates that conversion occurs primarily on the L_{II} subshell.

We cannot make an unambiguous choice between Mi and E2 through comparison of the experimental and theoretical values of K/L and (L_I + L_{II})/L_{III} (Table 1 & Fig.5). Probably the 198 kev transition is a mixture of M1 + E2.

261 kev transition

The line at 201.8 kev may be attributed to a 261 kev transition. Assuming this to be the K conversion line, we obtained an energy value of 261.1 ± 0.5 kev for this transition.

308 kev transition

The 248.7 (K), 298.48 (L) and 306.07 kev (M) electron lines may be attributed to a transition of 308 kev energy. The shape of the 248.7 kev line (Fig. 6) is distinctive; it must be assumed that there exists a close unresolved line of 249.9 ± 0.1 kev energy. This line might be identified as the L line of the 261 kev transition. In this case, however, the order of this transition would be quadrupole or higher (K/L = 0.4). Against this identification there is also

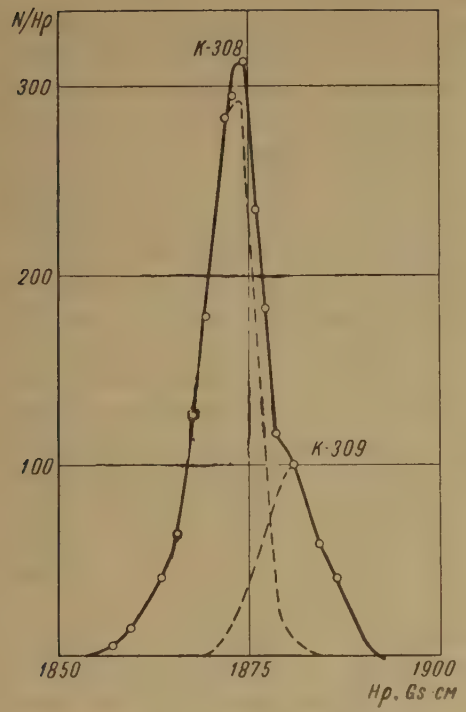

Fig.6. Section of Yb^{169} conversion spectrum: K line of the 308 kev γ-transition.

the fact that the M line of the 261 kev transition is not discernible, although if this identification were true it should be quite noticeable. We feel it more plausible to identify this line as the K line of a 309.2 kev transition. This identification is not inconsistent with the shape of the 298.48 and 306.07 kev lines, if they are assumed to be the joint L and M peaks associated with 308.03 and 309.23 kev γ-transition.

Inasmuch as it is impossible to separate the L lines of these transitions, we cannot determine the K/L ratios for them. The ratio of the total intensities of the K and L lines of these transitions is 3.4. This value is close to the theoretical ratios for E2 and M3 transitions (Table 4).

Discussion

The above are the principal experimental results of our investigation of the conversion electron spectrum of Yb^{169}. With a view to refining the data on the multipolarity of the γ-transitions we can compare the relative conversion line intensities obtained in the present investigation with the relative intensities of the γ-rays according to the data of DuMond's group[4]. For calculating the conversion coefficients we assumed that the 130.5 kev transition is E2. Our assumption is based on the facts that the existence of a rotational band based on the ground state of Tm^{169} is proved beyond doubt[4] and that a 130.5 kev transition in this band must be of the E2 type. Furthermore, the multipole order of the 130.5 kev transition is established on the basis of the K/L and $(L_I - L_{II})/L_{III}$ ratios with greater certainty than for the other transitions.

In column 2 of Table 3 we give the relative γ-ray intensities according to DuMond[4]. In columns 3 & 4 we give the relative intensities of the K and L conversion lines according to our data in the same units as for the γ-ray intensities (α_K for the 130.5 kev transition was taken equal to the theoretical value of 0.56). In columns 6 & 7 we give the experimenta values of the internal conversion coefficients α_K and α_L calculated as the ratios of the intensities of the K and L lines and the intensities of the corresponding γ-rays. In the remaining columns we list the theoretical conversion coefficients for transitions of different multipole orders.

Comparison of the experimental and theoretical values of the internal conversion coefficients leads us to the following conclusions.

1. The calculated value of α_L for the 130.5 kev transition is in good agreement with the theoretical value for E2 which again substantiates our assignment above.

2. The experimental value of α_K indicates that the 118.2 kev transition is pure E2.

3. Comparison of the experimental and theoretical values of α_L shows that the 63.1 kev transition is pure E1. This substantiates the assignment made above on the basis of the $(L_I + L_{II})/L_{III}$ ratio.

Table 3

Transition data for Yb^{169}

DuMond[4] data		Our data				α_K theo.						α_L theo.						I_{tot}	Multipole order assignments
E_γ, kev	I_γ	I_K	I_L	α_K	α_L	*E*1	*E*2	*E*3	*M*1	*M*2	*M*3	*E*1	*E*2	*E*3	*M*1	*M*2	*M*3		
1	2	3	4	5	6	7	8	9	10	11	12	13	14	15	16	17	18	19	20
8,42	—																	(94)	(*M*1)
20,75	—																	(12)	(*M*1)
63,12	65	49	10,9	—	0,17	0,75	—	—	—	—	—	0,14	6,8	190	1,6	4,8	1580	95	*E*1
93,60	4,4	19,5	2,0	4,5	0,45	0,29	0,99	2,9	2,4	19,5	85	0,042	1,02	20,4	0,42	6,0	100	20	*M*1
109,78	22	49,7	7,4	2,2	0,34	0,24	0,87	2,6	2,0	15,9	73	0,034	0,81	14	0,35	4,5	61	60	*M*1 (+10% *E*2)
118,20	2,6	2,5	—	0,96	1	0,19	0,76	2,4	1,7	13	52	0,029	0,53	1,07	0,31	3,4	44	5,7	*E*2
130,53	15	(8,4)	6,3	—	0,42	—	0,56	—	—	—	—	0,023	0,36	6,8	0,23	2,2	25	23	*E*2
177,24	31	13,3	1,9	0,43	0,06	0,063	0,24	0,74	0,46	2,8	12	0,0093	0,096	1,1	0,089	0,64	5,7	33	*M*1+*E*2 (*E*2>20%)
197,97	51	14,3	2,7	0,28	0,053	0,046	0,17	0,52	0,35	1,95	9,8	0,0067	0,067	0,55	0,063	0,40	3,1	51	*M*1+*E*2 (*E*2>20%)
240,4	1	—	—	—	—	—	—	—	—	—	—	—	—	—	—	—	—	1	(*E*1)
261,0	8	0,057	—	0,007	—	0,023	0,076	0,23	0,14	0,78	2,8	0,003	0,025	0,17	0,029	0,14	0,84	6	*E*1
307,7 309,2	18	0,59	0,043	0,033	0,0024	0,015	0,049	0,15	0,12	0,46	1,5	0,0022	0,0135	0,087	0,019	0,078	0,42	14	*E*2

4. The experimental values of α_K and α_L for the 93.6 kev transition are in closest agreement with the theoretical values for M1. One can find no mixture that will give complete agreement for the experimental and theoretical values of both α_K and α_L. Admittedly, the experimental value of α_K for this transition (4.5) is almost two times greater than the theoretical value (2.4) for an M1 transition. This may be explained by inaccuracy in determining the intensity of the K-93.6 line. It should be borne in mind that this electron line has the lowest energy of all the lines for which we have given relative intensities.

5. The experimental values of the conversion coefficients for the 109.78 kev transition are in good agreement with the theoretical ones for M1. Any admixture of E2, apparently, does not exceed 10%.

6. As was noted above, where the 177 and 198 kev transitions are concerned one cannot make a choice between M1 and E2 on the basis of the K and L conversion intensity ratio. The values of the internal conversion coefficients listed in Table 3 are close to the theoretical ones for M1 transitions. It may, however, be asserted that the admixture of E2 in these transitions is not less than 20%. The principal argument in favor of this assertion is the shape of the total L conversion lines, indicating predominance of conversion on the L_{III} subshell.

7. The experimental value of the K shell conversion coefficient for the 261.0 kev transition indicates that it is E1.

8. We hypothesized the existence of a 309.2 kev γ-transition. This transition has not been detected in observation of γ-rays. Hence the intensity of the 307.7 kev γ-rays given in DuMond's work must be regarded as the total intensity of the 307.7 and 309.2 kev γ-rays. In Table 3 we give the values of α_K and α_L calculated as $\frac{I_{K\text{-}307,7} + I_{K\text{-}309,2}}{I_{\gamma\text{-}307,7} + I_{\gamma\text{-}309,2}}$ and $\frac{I_{L\text{-}307,7} + I_{L\text{-}309,2}}{I_{\gamma\text{-}307,7} + I_{\gamma\text{-}307,7}}$, respectively. The listed values are closest to the theoretical ones for E2. It is possible that both the 309.2 and 307.7 kev transitions are of the E2 type.

9. In column 19 of Table 3 we have listed the total intensities of the various γ-transitions referred to the total intensity of Yb^{169} decay, taken as 100. The intensity of the γ-transitions is proportional to the intensity of the γ-rays multiplied by $(1 + \alpha_{tot})$. For the total conversion coefficient, α_{tot}, we took the sum of the experimental K and L shell conversion coefficients. In cases where experimental coefficients were lacking we used the theoretical values.

Our data on the conversion electrons from Yb^{169} substantiate the decay scheme proposed by Johannson[2] and the DuMond group[4] and reproduced in Fig.1. There is a minor disagreement between our data and those of DuMond regarding the multipolarity of the 177 and 198 kev transitions. According to DuMond, the admixture of E2 in these transitions does not exceed 20%, whereas according to our data the admixture of E2 cannot be less than 20%. Our data show that the 261 kev transition is really E2, as was hypothesized by DuMond and his co-workers. The suggested existence of a 309.2 kev γ-transition requires verification.

Appendix

Verification of the energy calibration of the instrument

In the present investigation, as in the work of Refs.7,8 & 9, the conversion line energies were determined by means of the calibration curve established for our instrument. The instrument was calibrated in 1951-1952 by P.P.Zarubin[6] with reference to the well known A, Bb, B F and X conversion lines of Th(B+C+C'++C''). The calibration uncertainty did not exceed 0.2%. However, comparison of our data on conversion line energies with the data of other authors showed sys-

tematic divergences attaining ~1% at an energy of about 50 kev. In view of this, the conversion line energies obtained from the instrument calibration curve were corrected in the work of Refs.7-9 by the method indicated therein to take into account the said deviations. The precision measurements of the Yb^{169} γ-transition energies carried out by the DuMond group by means of a curved crystal γ-spectrometer[4] offered an excellent opportunity for checking the calibartion curve of our instrument through comparison of our conversion line energy values with the γ-ray data of DuMond.

On the basis of these data we plotted the calibration curve corrections shown in Fig.7. As may be seen from the figure, in the region from 130 to 300 kev our energy values agree within the limits of the calibration uncertainty with those of DuMond's group. In the region below 130 kev there is a systematic deviation between our values and those of DuMond. It is possible that the deviations are connected not with incorrect calibration of the instrument but with the finite thickness of the source. In view of the fact that all the sources which we used in investigating the conversion electron spectra of neutron-deficient isotopes of rare earths were prepared by an identical procedure, there is reason to assume that the thickness of the sources was approximately the same. Hence in the future we plan to use the curve of Fig.7 for refining our conversion electron energy values. We assume that the 1951-1952 calibration is essentially correct in the range of energies above 130 kev. Up to 300 kev this is substantiated by the curve in Fig.7. For checking the calibration in the region above 300 kev we used the absolute values of the magnetic field intensity in the homogeneous region of the magnet gap in our instrument as measured by the method of proton resonance. Comparison of the field strengths obtained from the calibration curve with the values ascertained by the proton resonance procedure indicates that the calibration of the instrument in this energy region is essentially correct.

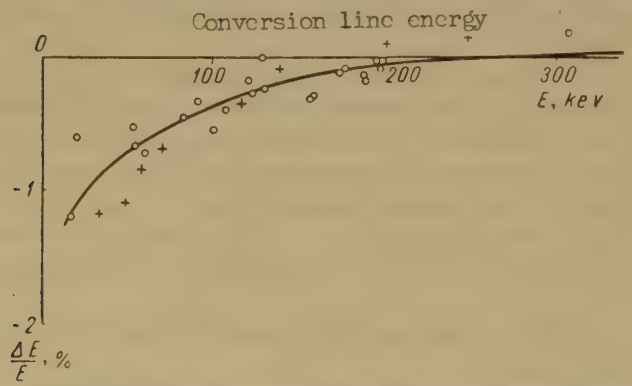

Fig.7. Verification of the energy calibration curve for our spectrometer: + - data of Ref.4; o - our data.

"V.G.Khlopin" Radium Institute
Academy of Sciences of the USSR

References

1. S.Martin, J.Jensen, F.Hughes & R.Nichols, Phys.Rev., 82, 579 (1951).
2. S.Johansson, Phys.Rev., 100, 835 (1955).
3. J.Cork, M.Brice, O.Martin, L.Schmid & R.Helmer, Phys.Rev.,101,1042 (1956).
4. E.Hatch, F.Boehm, P.Marmier & J.DuMond, Phys.Rev., 104, 745 (1956).
5. B.K.Preobrazhenskii, O.M.Lilova, A.N.Dobronravova & E.D.Teterin, Zhur. neorg.khim. (Journal,Inorganic Chemistry), 1, 2294 (1956).
6. P.P.Zarubin, Izv.AN SSSR, Ser.fiz.,18,563 (1954). (Trans.Bull.18,No.5,244.
7. K.Ia.Gromov, B.S.Dzhelepov & B.K.Preobrazhenskii, Izv.AN SSSR, Ser.fiz., 21,918 (1957). (Trans.Bull.21, No.7, 920.)
8. Iu.G.Bobrov, E.Ia.Gromov, B.S.Dzhelepov & B.K.Preobrazhenskii, Izv.AN SSSR, Ser.fiz., 21, 940 (1957). (Trans.Bull.21, No.7, 942.)
9. K.Ia.Gromov, B.S.Dzhelepov, A.G.Dmitriev & B.K.Preobrazhenskii, Izv.AN SSSR, Ser.fiz., 21, 1573 (1957). (Trans.Bull.21, No.12, 1562.)

LEVEL DIAGRAM OF Tl^{208}

- A.G.Sergeev, E.M.Krisiuk, G.D.Latyshev, V.D.Vorob'ev & T.I.Kol'chinskaia

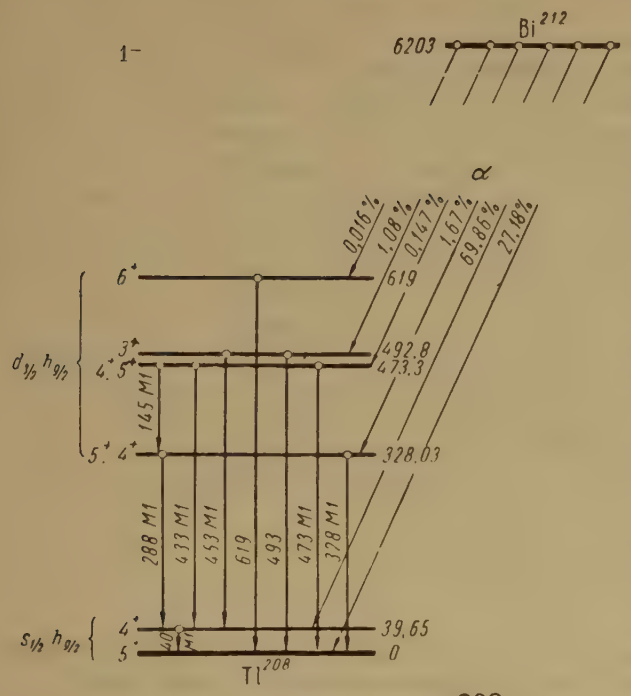

Level diagram of Tl^{208}

The sequence of Tl^{208} levels, evinced in α-decay of Bi^{212}, has been established in studies[1,2] of the α-spectrum fine structure (see figure). A spin assignment of 5+ for the ground state of Tl^{208} follows from the work of Krisiuk et al[3]. According to Horton's[4] investigation of α-γ angular correlation, the spin of the first excited level (40 kev) of Tl^{208} is 4+. Nielsen[5] on the basis of the determined multipole orders of the γ-transitions assigned the following spins and parities to the excited levels of Tl^{208}: 328 kev - 4+, 5+; 473 kev - 4+, 5+; 493 kev - 3+.

On the basis of an investigation of the internal conversion spectrum of a radiothorium active deposit we[6-8] determined the multipole orders of the γ-transitions pertaining to the $Bi^{212} \rightarrow Tl^{208}$ decay (Table 1). The multipole orders were determined from the absolute conversion coefficients and in three cases substantiated by the ratios of the K and L conversion probabilities. The multipole order of the 40 kev transition was determined from the ratios $L_I:L_{II}:L_{III}$. The absolute conversion coefficients were calculated using the data of Rytz[1] on α-group intensities. The multipole orders determined in this manner substantiate the spin assignments for the excited levels of Tl^{208} given by Nielsen[5].

Table 1

Multipole orders of γ-transitions

E_γ, kev	Shell	Percent per decay		Multipole order
		I_e	I	
	L_I	44,6		
	L_{II}	4,7		$M1$
	L_{III}	0,41		
39,85	M	12,0	68,5	
	N	3,0		
	O	0,65		
144,9	K	0,036	0,05	$M1$
288,18	K	0,26	1,04	$M1$
	L	0,05		
328,02	K	0,083	0,43	$M1$
	L	0,013		
433,6	K	0,005	0,048	$M1$
452,98	K	0,09	1,05	$M1$
	L	0,02		
473,0	K	0,012	0,14	$M1$
493,2	K	0,007	0,36	

In order to verify and revise the spin assignments for the excited levels of Tl^{208}, we calculated the relative intensities of the α-transitions taking into account the angular momentum carried off in each case (Table 2).

Table 2

Relative intensities of α-transitions

Level	Spin	Angular momentum of α-particle	Relative intensities		
			Exper.	Theo. $l = 0$*	Theo. $l \neq 0$**
0	5	5	1	1	1
40	4	3 & 5	2,6	0,67	3,4—0,67
328	4	3 & 5	0,06	0,034	0,18—0,034
	5	5			0,034
473	4	3 & 5			0,04—0,007
	5	5	0,0055	0,007	0,007
493	3	3	0,04	0,005	0,03
619	5	5			0,0014
	6	5 & 7	0,0006	0,0014	0,0014—0,0002
	7	7			0,0002

*Calculation according to Ref.9.
**Table 3 in Ref.4 used in the calculation.

It will be seen from Table 2 that taking into account the angular momentum of the α-particles leads to appreciably better agreement with experiment. It will be noted that there is excellent agreement of the calculated relative probabilities with the experimental values for the α-transitions to the 0, 40 and 493 kev levels, the spins of which have been established unambiguously. This allows of determining the spins of the other levels for which no definite assignments have been made. It will be evident from Table 2 that the most probable assignment for the 619 kev level is 6+. This is substantiated by the fact that in the conversion spectrum[10,11] there is observed a transition from the 619 level to the ground state (5+), whereas there is no detectable transition from the 619 kev level to the 40 kev level (4+).

Where the 328 and 473 kev levels are concerned, the best agreement with the experimental α-group intensities is obtained with the assignments 4+ and 5+, respectively. With these spins, however, the absence of a γ-transition between the 493 and 328 kev levels is inexplicable. If these assignments were correct, this transition should be M1 and a rather strong line should appear in the conversion spectrum; no such line was observed however. The absence of such a transition can be explained if we assign a spin of 5+ to the 328 kev level, inasmuch as in this case the transition will be E2 and hence will have so low an intensity as to be unnoticeable in the conversion spectrum.

Pryce[12] interpreted the 0 and 40 kev levels as a doublet originating as a result of splitting of the $s_{1/2}\, g_{9/2}$ configuration. This configuration is in agreement with the experimentally established spins of these levels. The 328, 473, 493 and 619 kev levels are explained by splitting of the $d_{5/2}\, g_{9/2}$ configuration. The splitting yields a quadruplet with spins 3+, 4+, 5+ and 6+. Assignments of 3+ and 6+ for the 493 and 619 kev levels are consistent with this configuration. At present we cannot determine which of the two remaining levels (328 and 473 kev) has spin 4+ and which 5+.

Faculty of Physics,
"V.N.Obratsov" Leningrad Institute of Railroad Transport Engineers

References

1. A.Rytz, Compt.Rend., 233, 790 (1951).
2. G.H.Briggs, Revs.Mod.Phys., 26, 1 (1954).
3. E.M.Krisiuk, A.G.Sergeev, G.D.Latyshev, K.I.Il'in & V.I.Fadeev, Zhur. eksp.i teor.fiz., 33, 1144 (1957).
4. J.W.Horton, Phys.Rev., 101, 717 (1956).
5. O.B.Nielsen, Kgl.Danske vied.selskab. Mat-fys.medd., 30, 11 (1955).
6. A.I.Zhernovoi, E.M.Krisiuk, G.D.Latyshev, A.S.Remennyi, A.G.Sergeev & V.I.Fadeev, Zhur.eksp.i teor.fiz., 32, 682 (1957). (Trans. JETP - Soviet Phys.)
7. V.D.Vorob'ev, K.I.Il'in, T.I.Kol'chinskaia, G.D.Latyshev, A.G.Sergeev, Iu.F.Trofimov & V.I.Fadeev, Izv.AN SSSR, Ser.fiz., 21, 954 (1957). (Trans. Bulletin 21, No.7, 956.)
8. E.M.Krisiuk, A.D.Vitman, V.D.Vorob'ev, G.D.Latyshev & A.G.Sergeev, Izv. AN SSSR, Ser.fiz., 20, 877 (1956). (Trans. Bulletin 20, No.8, 797.)
9. E.Fermi, Nuclear Physics (Cited in Russ.trans., 1951.)
10. C.Ellis, Proc.Roy.Soc.A138, 318 (1932).
11. J.Surugue, Ann.Phys.8, 484 (1937).
12. M.H.L.Pryce, Proc.Phys.Soc.A65, 773 (1952).

β-SPECTRA OF THE SHORT-LIVED ISOTOPES Al^{28} AND F^{17}

- S.S.Vasil'ev & L.Ia.Shavtvalov

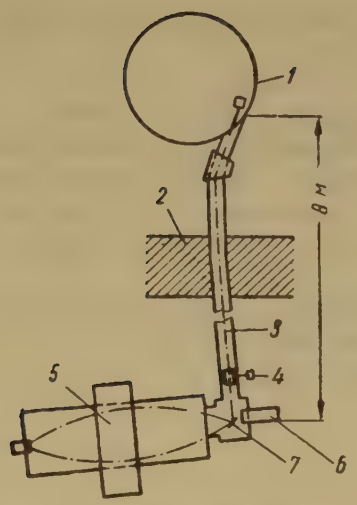

Fig.1. Experimental arrangement: 1) cyclotron, 2) shield, 3) deuteron beam, 4) beam catcher (Faraday cylinder), 5) β-spectrometer, 6) FEU-S photomultiplier, 7) target.

The present work was devoted to an investigation of the β- and γ-radiations of short-lived isotopes[1-14] by means of a magnetic lens β-spectrometer and a scintillation γ-spectrometer. The isotopes were obtained by bombardment of the appropriate targets with 4 Mev deuterons, accelerated in the NIIaF MGU (Scientific Research Institute of Nuclear Physics at Moscow State University) and extracted into the β-spectrometer 5 (Fig.1). The deuterons first passed through an opening in the beam catcher 4, coupled to an integrator recording the relative intensity of the beam 3. Investigation of the β-spectra of the target 7, located at one of the focal points of the β-spectrometer, was carried out with continuous irradiation of the target. With this arrangement one can work with isotopes having extremely short lives. This experimental arrangement proved to be feasible by virtue of location of the β-spectrometer far outside the shield 2 and introduction of additional shielding for reducing the β-counter background.

One of the short-lived isotopes investigated was Al^{28} obtained by the (d,p) reaction. In most previous investigations[15-21] the energy of the β- and γ-radiations from Al^{28} was determined by the absorption method. The β-spectrum of Al^{28} obtained in our experiments is shown in Fig.2; the Fermi-Kurie plot is reproduced in Fig.3. The end-point energy of the β-spectrum is 2820 ± 50 kev. It will be noted that our Fermi-Kurie plot is linear, in contrast to the plot given by Motz & Alburger[16]. These investigators obtained an appreciable deviation from a straight line beginning with 1700 kev. According to Olsen & O'Kelley[19], the β-spectrum of Al^{28} has an allowed shape up to about 500 kev. In the range of lower energies, in the work of Olsen & O'Kelley, there was superimposed on the Al^{28} spectrum the β-spectrum of Mg^{28}, inasmuch as the Al^{28} was obtained as a result of decay of Mg^{28}, which has a half-life of 21.2 hours.

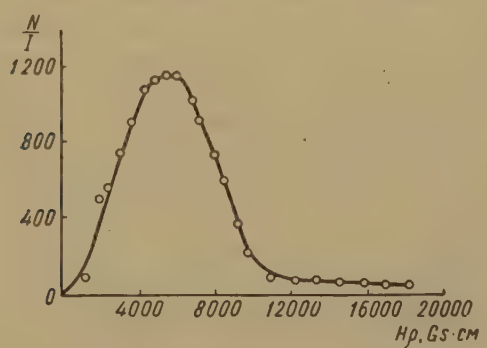

Fig.2. β-spectrum of Al^{28}.

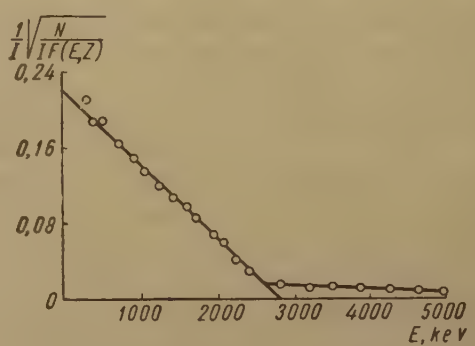

Fig.3. Al^{28} Fermi-Kurie plot.

The half-life, evaluated from our measurements of the intensity in the 1100 kev region of the β-spectrum, was found to be 2.1 ± 0.2 min. The half-life, determined from the γ-rays by means of the scintillation spectrometer, proved to be

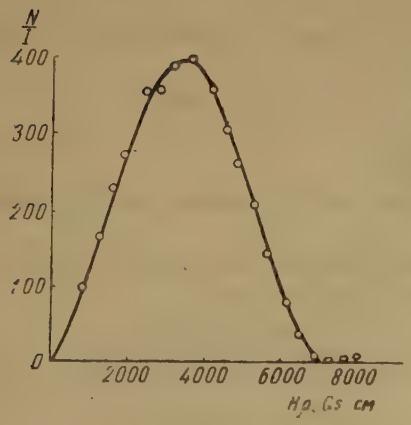

Fig.4. β-spectrum of F^{17}.

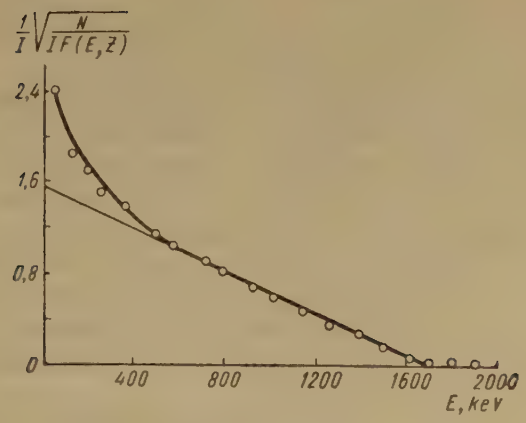

Fig.5. F^{17} Fermi-Kurie plot.

2.2 ± 0.1 min. The agreement of the period as determined from the β- and γ-rays can be taken as an indication that the observed γ-rays accompany the above mentioned β-decay of Al^{28}.

It will be seen from Figs.2 & 3 that there may also be a low intensity β-spectrum with an end-point energy of ~6 Mev. Evaluation of the half-life corresponding to this component, carried out on the β-spectrometer (at 3.2 Mev) yielded a value of 25 ± 20 sec. The source of this β-spectrum has not been ascertained.

F^{17} has been studied by a number of investigators.[22-25] We investigated the β-spectrum of F^{17} obtained by the (d,n) reaction on oxygen; the spectrum is shown in Fig.4; the Fermi-Kurie plot in Fig.5. The end-point energy is 1700 ± ± 15 kev. There is a noticeable deviation from linearity below ~600 kev. Deviation from a straight line has also been observed by Wong.[22]

The half-life of F^{17} as measured by means of the β-spectrometer (at 800 kev) was found to be 71 ± 5 sec. The measurements with the scintillation spectrometer failed to disclose any γ-rays from the target after cessation of deuteron bombardment.

We desire to thank B.M.Makuni and Z.I.Tikhomirova for help in the work and the cyclotron crew, particularly G.V.Kosheliaev, A.A.Danilov and V.P.Khlapov, for their assistance.

Scientific Research Institute of Nuclear Physics,
Moscow State University

References

1. A.A.Reut, S.M.Korenchenko, V.V.Iur'ev & B.M.Pontekorvo, Doklady AN SSSR, 102, 723 (1955).
2. P.A.Iampol'skii, O.I.Leipunskii, M.Ia.Gen & A.M.Tikhomirov, Izv.AN SSSR, Ser.fiz., 19, 338 (1955). (Trans.Bulletin 19, No.3, 312.)
3. J.D.Gow & L.W.Alvarez, Phys.Rev., 94, 365 (1954).
4. W.M.Martin & S.W.Breckon, Canad.J.Phys., 30, 643 (1952).
5. H.Tyren & P.A.Tove, Phys.Rev., 96, 773 (1954).
6. R.M.Kline & D.Zaffarano, Phys.Rev., 96, 1620 (1954).
7. H.Roderick, O.Lönsjö & W.E.Meyerhof, Phys.Rev., 97, 97 (1955).
8. W.F.Hornyak, C.B.Dougherty & T.Lauritsen, Phys.Rev., 74, 1727 (1948).

9. W.A.Hut, R.M.Kline & D.J.Zaffarano, Phys.Rev., A, 96, 611 (1954).
10. S.D.Softky, Phys.Rev., 98, 736 (1955).
11. N.W.Glass & J.R.Richardson, Phys.Rev., 98, 1251 (1955).
12. L.W.Alvarez, Phys.Rev., 75, 1815 (1949).
13. H.Morinaga, Phys.Rev., 100, 431 (1955).
14. O.I.Leipunskii, V.V.Miller, A.M.Morozov & P.A.Iampol'skii, Doklady AN SSSR, 109, 5, 935 (1956).
15. A.J.Alichanow, A.J.Alichanian & B.S.Dzhelepov, Nature, 133, 871 (1934).
16. H.T.Motz & D.E.Alburger, Phys.Rev. 86, 165 (1952).
17. R.K.Sheline & N.R.Johnson, Phys.Rev., 90, 325 (1953).
18. R.K.Sheline, N.R.Johnson, P.R.Bell, R.C.Davis & F.K.McGowan, Phys.Rev., 94, 1642 (1954).
19. J.L.Olsen & G.D.O'Kelley, Phys.Rev., 93, 1125 (1954).
20. Th.Mayer-Kuckuk, Z.Naturforsch. a, 9, 338 (1954).
21. J.Nahmias, phys.et radium, 15, 568 (1954).
22. C.Wong, Phys.Rev., 92, 529 (1953); Ibid., 95, 765 (1954).
23. L.Koester, Z.Naturforsch. a, 9, 104 (1954).
24. V.Perez-Mendez & P.Lindenfeld, Phys.Rev., 80, 1097 (1950).
25. J.B.Warren, K.A.Lauric, D.B.James & K.C.Erdman, Canadian J.Phys., 32, 563 (1954).

CONVERSION ELECTRON COINCIDENCES IN $Tb^{155} \rightarrow Gd^{155}$ DECAY

- B.S.Dzhelepov, B.K.Preobrazhenskii & V.A.Sergienko

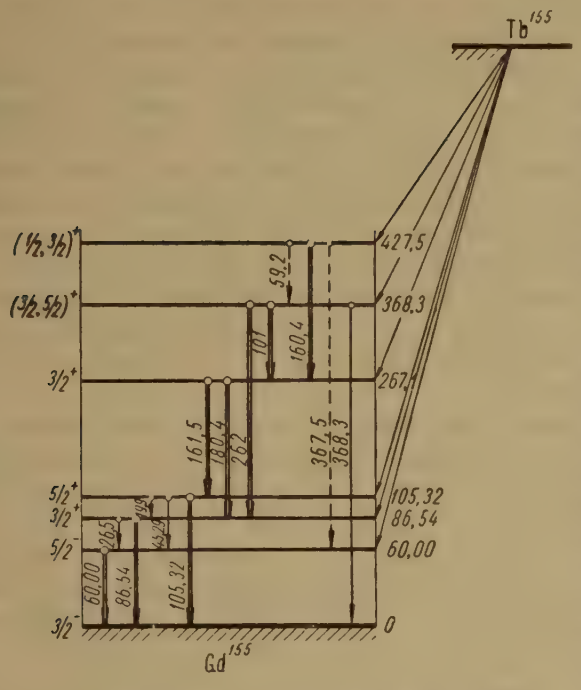

Fig.1. Transition scheme for Gd^{155}.

We investigated coincidences between conversion electrons formed in the decay of Tb^{155} to Cd^{155}. The Tb^{155} was obtained by bombardment of a tantalum target with 660 Mev protons for several hours. The terbium was separated chromatographically some 20-30 hours after irradiation.

The coincidence measurements were carried out on the twin magnetic lens β-spectrometer[1] at Leningrad State University. The activity was deposited on thin lightly aluminized collodion films; the diameter of the sources did not exceed 5 mm. The measurements of $e^- - e^-$ coincidences were started several days after separation of the fraction, when most of the short-lived part of the terbium fraction had disintegrated and the Dy had transformed to Tb. At first we investigated coincidences between conversion electrons forming in the decay of Tb^{155} separated from the Tb fraction and then the electron coincidences in the decay of Tb^{155} formed from Dy.

Terbium[155] ($T \approx 5.6$ days) was first separated by Ward et al[2] from the radioactive cascade $Ho^{155} \xrightarrow{EC} Dy^{155} \xrightarrow{EC} Tb^{155}$ which occurs in proton bombardment of Dy^{155}. The disintegration of Tb^{155} occurs through capture of K and L electrons and leads to the formation of Gd^{155}.

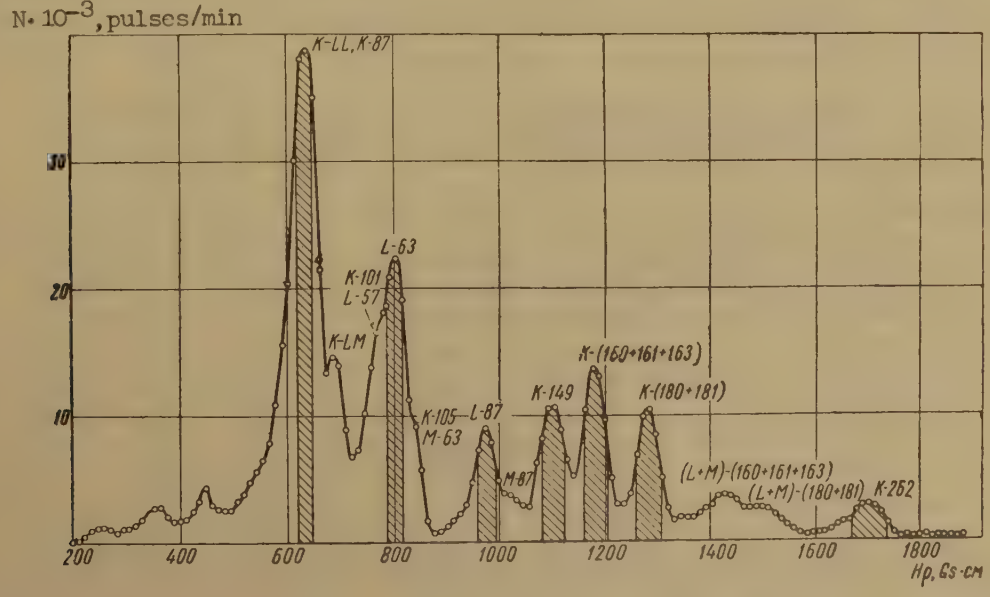

Fig.2. Spectrum of terbium fraction conversion lines having a period of ~5 days recorded in one-half the twin spectrometer.

The transition scheme for Gd^{155}, constructed on the basis of investigations of the $Tb^{155} \rightarrow Gd^{155}$ and $Eu^{155} \rightarrow Gd^{155}$ decays[5], is shown in Fig.1. As illustrated, the scheme does not include the following transitions observed in the decay of Tb^{155}: 31.6, 63, 148.8, 163.4, 181.6, 221.2, 239.7 and 350.8 kev.[2,4] In addition, in the decay of Tb accumulated from Dy^{155} there was observed a 57 kev transition, and in a terbium fraction[4] (from proton bombarded Ta) there were observed transitions having energies of 89 and 199 kev. Although these transitions are characterized by a period of about 5 days, they apparently pertain to other Tb isotopes. A distinctive feature of the decay scheme is the large number of very close doublets and even triplets; they obviously hamper interpretation of the decay scheme.

The spectrum of the ~5 day conversion electrons from the terbium fraction, recorded in one-half the twin spectrometer is shown in Fig.2. There are clearly evident conversion lines associated with γ-transitions of 87, 149, 161, 180 and 262 kev energy and a group of lines that may be attributed to transitions having energies of 57-63 kev and 101-105 kev. No lines due to γ-transitions of other energies were observed in the conversion electron spectrum of the mixture of Tb isotopes obtained from the dysprosium fraction.

The coincidences between the conversion electrons from Tb^{155} were investigated in the following manner: one half the spectrometer was adjusted to detect the K or L electrons from a given γ-transition, while the other half was adjusted to record the K or L line of another transition. Inasmuch as the Tb^{155} was deposited on a very thin film, the energy loss and electron scattering in it had virtually no effect on the shape of the spectrum and the counting rates at the line peaks by the spectrometer on the backing side. The electron energy intervals encompassed by the spectrometer are indicated by the hatched columns in Fig.2; it will be seen that in the hard part of the spectrum the interval was equal approximately to the half-width of the conversion lines. The number of true coincidences at the line peaks differed, varying from 24 to 228 pulses per hour at counting rates in the individual channels from $13 \cdot 10^3$ to $77 \cdot 10^3$ counts per minute; the ratio N_{true}/N_{cha}, where N_{true} is the number of true and N_{cha} is the number of chance coincidences, varied from 1.3 to 25.

We detected coincidences for seven different line combinations. The results of the coincidence experiments are summarized in the accompanying table and are shown in Figs.3 & 4.

Results of measurements of coincidences between conversion electrons in $Tb^{155} \rightarrow Gd^{155}$ decay

Line detected by first spectrometer (thru backing)	Counting rate at peak, $N_1 - N_{bkgd} \cdot 10^{-3}$ counts/min	Line detected by second spectrometer	Counting rate at peak, $N_2 - N_{bkgd}$ 10^{-3} cnts/min	No. of coincidences per hour		
				Obs.	Chance	True
L-63	77	*K*-262	13.0	123	22	101
K-(160+161+163)	30	*L*-63	48	210	8	202
K-149	18.5	*K*-(160+161+163)	21	48	8	40
K-(180+181)	36	*L*-87	34.5	240	12	228
		M-87	15	160	13	147
		K-149	36	42	18	24
		K-(160+161+163)	41	100	18	82

Analysis of the Coincidence Data

1. Coincidences between L-63 and K-262 electrons

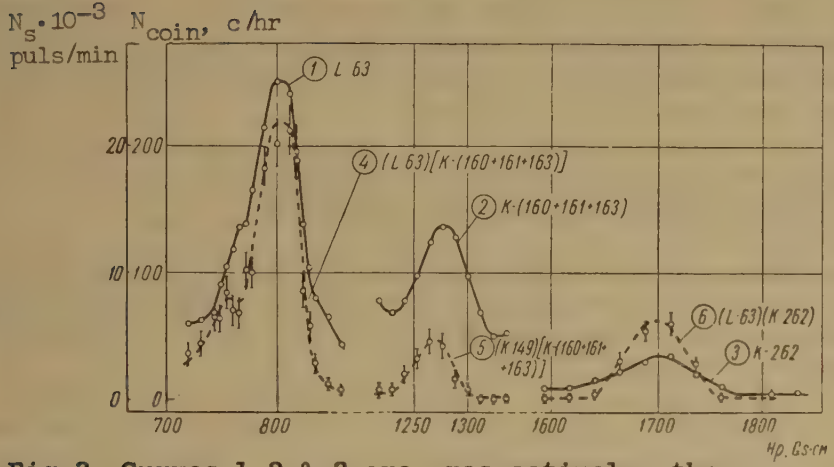

Fig.3. Curves 1,2 & 3 are, respectively, the L-63, K-(160+161+163) and K-262 conversion lines recorded in one half the twin spectrometer. Curves 4,5 & 6 are, respectively, the coincidence spectra of [K-(160+161+163)] — (L063), (K-149) — — [K-(160+161+163)] and (L-63) — (K-262) electrons. The electrons of the lines listed first in each case passed through the source backing. The intensity of all the lines has been corrected for decay (~5 days).

The experimental coincidence curve is shown in Fig. 3 (curve 6). The line we have designated as L-63 probably actually consists of L-60.00, K-101 and K-105.32; possibly it also includes the L electrons from the 57 and 63 kev transitions observed in the work of Ref.3, but not detected in the investigations of Refs.2,4 & 5. According to the scheme of Fig.1 no (K-262—(K-101) and (K-262) — —(K-105.32) coincidences should be observed, but (K-262) — (L-60) coincidences, although weakened by branching at the 86.54 kev level, should be observed.

In our experiments the total number of (L-63) — —(K-262) coincidences amounted to 123 per hour: of these 22 were chance and 101 were true coincidences. Thus the fact that there are coincidences between the L-63 and K-262 electrons cannot be doubted. In our opinion these coincidences are associated primarily with the existence of a 60 and 262 kev γ-transition cascade in the Gd^{155} nucleus.

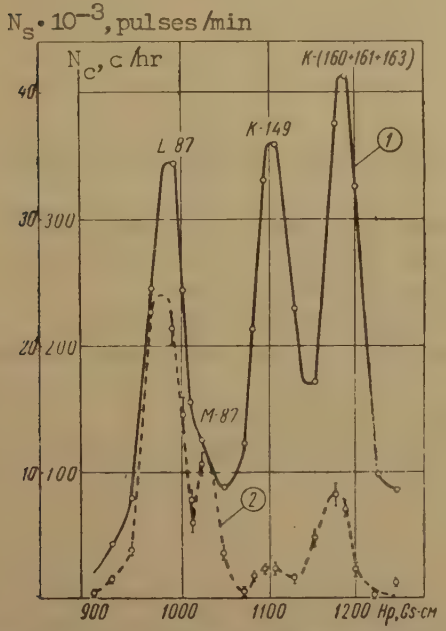

Fig.4. Coincidence spectrum of the K-180 line electrons with the electrons of the L-87, K-149 and K-(160+162) lines: 1) section of conversion electron spectrum recorded in one half the twin spectrometer; 2) coincidence spectrum.

2. Coincidences between L-63 and K-(160+161+163) electrons

That there are coincidences between these electrons cannot be doubted. This is evident from the table and the experimental coincidence curve 4 shown in Fig.3. The possible combinations that might be comprised in these coincidences are the following: (L-60.00) — (K-160.4), (L-60.00) — (K-161.5), (K-101) — (K-161.5), (K-105.32) — (K-161.5) and (K-105.32) — (K-160.4) (Fig.1).

The existence of such cascades is also substantiated by the complex character of the coincidence spectrum of K electrons from the 160+

+161+163 kev transitions with the electrons of the given line.

3. Coincidences between K-149 and K-(160+161+163) electrons (curve 5,Fig.3)

The reported 148.8 and 163.4 kev transitions have not yet been fitted into the decay scheme for Tb^{155}—Gd^{155}. The (K-149)—[K-(160+161+163)] coincidences may be associated with a 148.4 and 163.4 kev γ-transition cascade. Knowledge of the existence of these coincidences should be of help in fitting these transitions into the decay scheme.

4. Coincidences between K-(180+181.4) electrons and (L + M)-87, K-149 and K-(160+161+163) electrons.

The experimental coincidence curve is shown in Fig.4. The existence of [K-(180+181.4)] — [(L + M)-87] and [K-(180+181.4)] — [K-(160+161+163)] coincidences cannot be questioned; the existence of the [K-(180+181.4)] —(K-149) coincidences, however, can only be tentatively assumed.

According to the decay scheme pictured in Fig.1, there should be observed (K-180)—(L-87) and (K-180)—(K-160.4) coincidences. We infer that the observed [K-(180+181.4)] —(L-87) and [K-(180+181.4)] — [K-(160+161+163)] coincidences are connected with the existence of 180 & 87 kev and 180 & 160 kev γ-transition cascades. The small number of [K-(180+181.4)] —(K-149) coincidences may be attributed to coincidences between the 181.4 and 149 kev transitions that have not been fitted into the decay scheme shown in Fig.1.

We have indicated the inferred γ-transition cascades in the decay of Tb^{155} to Gd^{155} by heavy double lines in Fig.1.

Comparison of the coincidence counting rates for different combinations may serve as a valuable criterion in checking the decay scheme.[6] However, for Tb^{155} we do not as yet have an intensity-balanced decay scheme.

Scientific Research Physical Institute,
Leningrad State University

References

1. V.Sergienko, Izv.AN SSSR, Ser.fiz., 22, 198 (1958). (Trans.Bulletin 22, No.2, 195.)

2. T.Ward, K.P.Jacob & J.W.Mihelich, Bull.Amer.Phys.Soc., 2, 259 (1957).

3. B.S.Dzhelepov, B.K.Preobrazhenskii, I.M.Rogachev & P.A.Tishkin, Izv. AN SSSR, Ser.fiz., 22, 126 (1958). (Trans.Bulletin 22, No.2, 125.)

4. N.M.Anton'eva, A.A.Bashilov, B.S.Dzhelepov & B.K.Preobrazhenskii, Program (Abstracts) of the Eighth All-Union Conference on Nuclear Spectroscopy, M.-L, 1958.

5. F.Boehn & E.N.Hatch, Bull.Amer.Phys.Soc., 2, 231 (1957).

6. B.S.Dzhelepov, B.K.Preobrazhenskii & V.A.Sergienko, Present issue of the Bulletin, p.789.

COINCIDENCES BETWEEN CONVERSION ELECTRONS IN THE DECAY OF Lu^{173}. REFINEMENT OF THE $Lu^{173} \rightarrow Yb^{173}$ DECAY SCHEME

- B.S.Dzhelepov, B.K.Preobrazhenskii & V.A.Sergienko

Introduction

We used the Leningrad State University twin magnetic lens spectrometer[1] to investigate coincidences between some of the conversion transitions in Yb^{173}, forming in the decay of ~170 day Lu^{173}. The data obtained proved useful in revising the decay scheme for $Lu^{173} \rightarrow Yb^{173}$.

The available data on this decay has been summarized in Refs.2 & 3.

Recently Gorodinskii et al[4] established a fact that is important for identification of this lutetium isotope; they found that the γ-spectrum of 170-day Lu from the lutetium fraction (separated from proton-bombarded Ta) is identical with the spectrum of 170-day Lu forming from Hf. Inasmuch as Hf^{174} is stable, the identity of the spectra eliminates the possibility that the lutetium fraction activity may belong to Lu^{174} and proves that the observed lines must be attributed to Lu^{173}.

1. Experimental data

We received the Lu^{173} source approximately one year after chromatographic separation of the lutetium fraction from a tantalum target irradiated with 660 Mev protons; by this time activity of the short-lived Lu isotopes had died out completely.

The Lu^{173} was deposited on a narrow strip of 5μ thick aluminum foil.

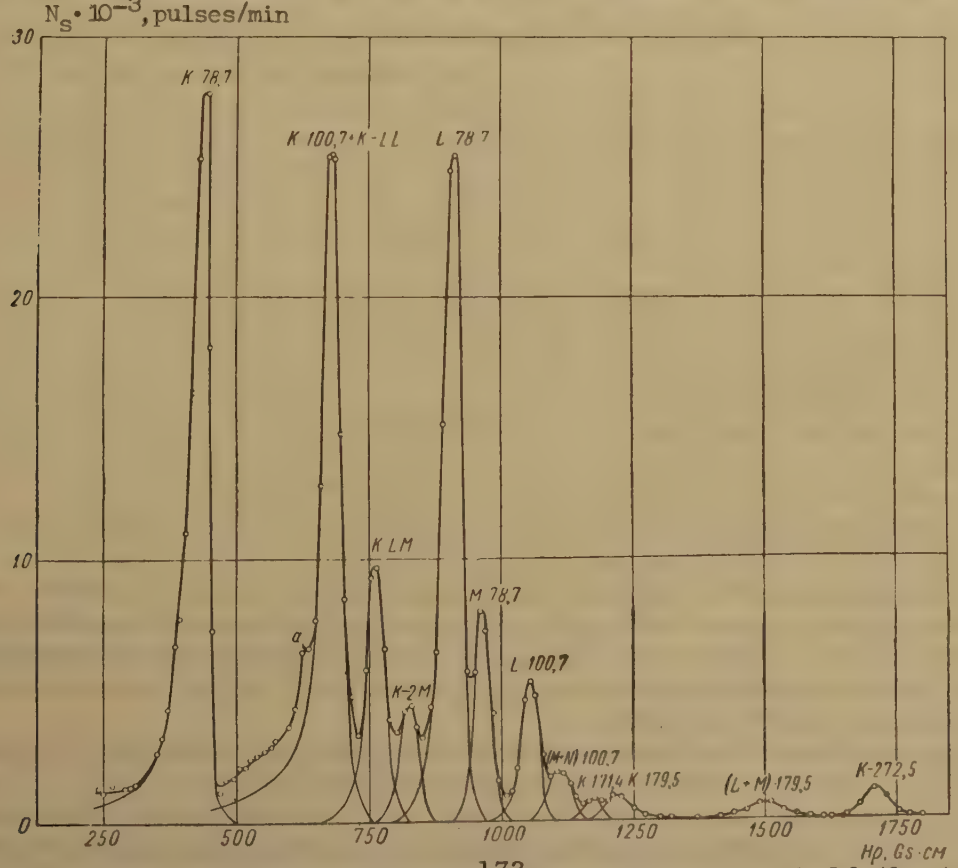

Fig.1. Conversion electron spectrum of Lu^{173} recorded on one half the twin spectrometer.

Bobrov et al[2] detected 20 lines in the conversion spectrum of 170-day Lu. They definitely established the existence of transitions with energies of 78.7, 100.7, 179.5 and 272.5 kev. Further, they tentatively inferred the existence of a 171.7 kev transition (line "c" in Table 2 of Ref.2) for which they detected only the K line.

In our spectrometers, which have an inferior resolution, some details of the conversion spectra are not evinced, but its general appearance agrees with that given in Ref.2 as regards both the location of the lines and their relative intensities (except for the K-78.7 and K-LM lines which appeared relatively weaker in our experiment). The conversion electron spectrum recorded by means of the lens facing the activity side of the source (i.e., not the backing) is shown in Fig.1.

Inasmuch as the active material was applied to a relatively thick backing, the low energy conversion electrons were strongly scattered and absorbed in the backing. As a rule the spectrometer viewing the backing side of the source was set to detect the faster electrons in each cascade. In determining the existence of a cascade, scattering in the foil per se is unimportant; one must simply compare only data pertaining to detection "through the backing" of one and the same line (values grouped by the braces in Table 1).

Table 1

Coincidences between conversion electrons emitted in $Lu^{173} \rightarrow Yb^{173}$ decay

Line detected by first spectrometer (thru the foil)	Counting rate at peak, $N_1 - N_{bkgd} \cdot 10^{-3}$ counts/min	Line detected by second spectrometer	Counting rate at peak, $N_2 - N_{bkgd} \cdot 10^{-3}$ counts/min	Coincidences per hour		
				Total	Chan.	True
L-78,7	16	*K*-100,7+*K*—*LL*	26	283	8	275
		K—*LM*	8	47	5	42
		K-78,7	29,5	29	8	21
		L-78,7	27,5	13	6	7
K-272,5	1,3	*K*-78,7	29,5	17	2	15
		L-78,7	27,5	14	3	11
		K-100,7+*K*—*LL*	26	15	2	13
		K—*LM*	8	10	1	9
		L-100,7	5	1	1	0
K-171,4	0,75	*K*-78,7	29,5	9	1	8
		K-100,7+*K*—*LL*	26	58	1	57
		K—*LM*	8	6	0	6
K-100,7+*K*—*LL*	3,0	*a*	6,5	39	1	38
		K-100,7+*K*—*LL*	26	42	6	36
K—*LM*	1,0	*a*	7,5	28	1	27
		K-100,7+*K*—*LL*	25	20	1	19

Note: Line a, according to Bobrov et al[2], has an electron energy of 34.1±0.2 kev.

Scattering in the backing actually plays a certain positive role: it must smooth out the angular anisotropy of ejection of cascade conversion electrons; the same may be said of the influence of the geometry of defining the electrons by two lenses (our spectrometers have different angles between the directions of emergence (154° and 180°).

The results of our measurements are given in Table 1 and Figs.2,3 & 4. Let us analyze the results listed in Table 1.

1. There can be no doubt regarding the existence of (78.7)—(100.7) coincidences. The experimental curve characterizing the coincidence of L-78.7 electrons with K-100 + K-LL and K-LM electrons is shown in Fig.2.

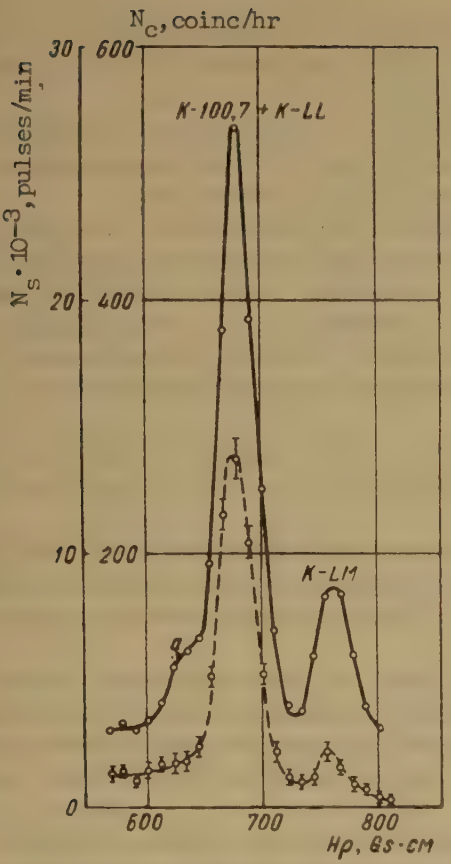

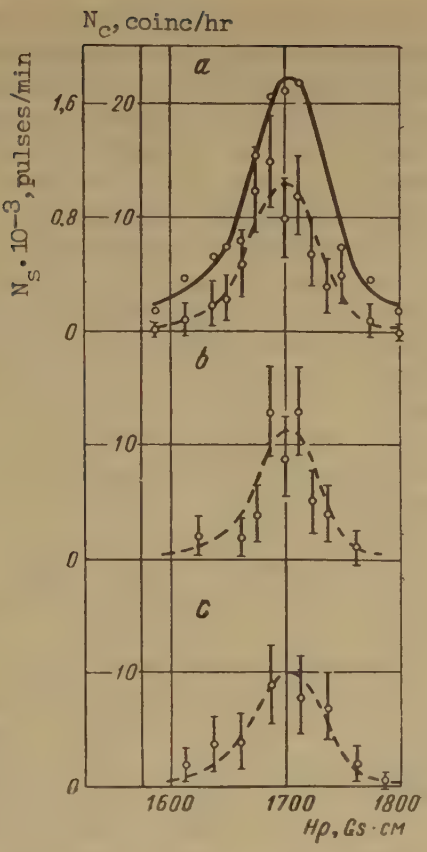

Fig.2. Coincidences between the (L-78.7)—(K-100.7 + K-LL) and (L-78.7)—(K-LM) electrons. Upper curves - appearance of the K-100.7 + K-LL and K-LM lines as recorded by a single (half twin) spectrometer.

Fig.3. Coincidences between conversion electrons: a - (K-272.5)—(K-78.7), b - (K-272.5)—(K-100.7 + K-LL), c - (K-272.5)—(K-LM). Solid line in a - the K-272.5 line as recorded by one spectrometer.

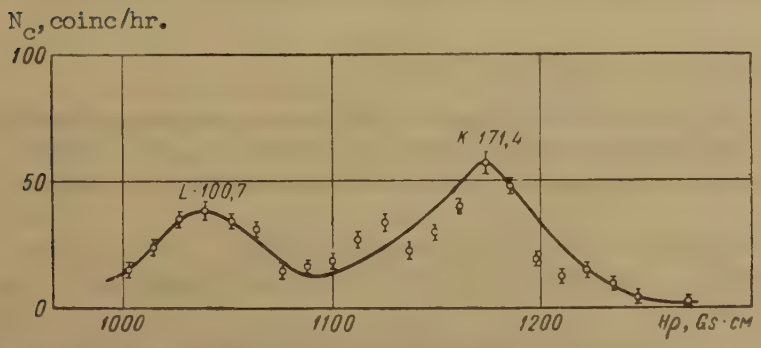

Fig.4. Coincidences between electrons: (K-100.7 + K-LL)—(L-100.7) and (K-100.7 + + K-LL)—(K-171.4).

In order to prove the existence of (L-78.7)—(K-100.7) coincidence we must know the composition of the K-100.7 + K-LL line. This question is examined in detail in Section 4, where we show that the K-LL electrons amount to twice the intensity of the K-LM group and that the K-100.7 fraction amounts to 1/3 the intensity of the (K-100.7 + K-LL) line.

The K-LL and K-LM Auger electrons must participate in equal portions in all the coincidences, hence of the 275 coincidences per hour, the K-LL electron fraction accounts for 84 and the K-100.7 fraction accounts for 191 coincidences per hour.

Thus the existence of (K-78.7)—(K-100.7) coincidences cannot be questioned; the quantitative aspects of the matter will be examined below.

2. The small number of (L-78.7)—(K-78.7) and (L-78.7)—(L-78.7) coincidences indicates the degree of admixture of K-100.7 + K-LL in the K-78.7 line and of K-MM electrons in the L-78.7 line.

3. It will be evident that (K-272.5)—(K-78.7) coincidences also exist.

The 272.5 kev transition is in cascade with the 78.7 kev transition. This is clearly evident from the data of Table 1 and Fig.3 (curve a).

The fact that these coincidences are present indicates that the decay scheme for Lu^{173} given in Refs.2 & 3 is in need of revision: in this scheme the 272.5 kev transition is plotted as terminating at the ground level of Yb^{173}, inasmuch as in the initial experiments of Gorodinskii & Pokrovskii no coincidences were detected between the 272.5 kev γ-rays and any other γ-rays. More recently, however, the existence of (γ-272.5)—(γ-78.7) coincidences was reported by the same authors[8].

4. There obviously occur (K-272.5)—(K-LM) coincidences (curve c in Fig.3).

5. Apparently there are no (K-272.5)—(K-100.7) or (K-272.5)—(L-100.7) coincidences.

Table 1 and Fig.3 (curve b) clearly indicate coincidences involving the K--272.5 and K-100.7 + K-LL lines. In order to determine with what electrons the K-272.5 electrons are in coincidence, we must take into account the composition of the K-100.7 + K-LL line.

Assuming, as was done above, that there must be twice as many (K-272.5)——(K-LL) coincidences as (K-272.5)—(K-LM) coincidences, we find that there should be 18 such coincidences per hour. In the experiment we observed only 13 coincidences per hour! Thus there is no remainder left for the K-100.7 line, although this line is comparatively strong.

It is also evident from Table 1 that there are no (K-272.5)—(L-100.7) coincidences. We infer therefore that the 272.5 and 100.7 kev γ-transitions are not in cascade.

6. Apparently (K-171.4)—(K-78.7) coincidences exist, but in a very small amount. In contrast, there are five times more (K-171.4)—(K-100.7 + K-LL) coincidences (Fig.4), although the K-100.7 + K-LL line has about the same intensity as the K-78.7 line.

The admixture of Auger electrons in the K-100.7 line leads to the appearance of a small number of (K-100.7 + K-LL)—(L-100.7) coincidences.

2. Revised decay scheme for Lu^{173}

In view of the fact that the K-272.5 electrons yield coincidences with the K-78.7 and L-78.7 electrons but no coincidences with the K-100.7 and L-100.7 electrons, we can make certain modifications in the Lu^{173} decay scheme shown in Ref.2.

The new decay scheme we propose for Lu^{173} is shown in Fig.5. In it the 272.5 kev transition goes to the E_1 = 78.7 kev level. Thus we introduce a new level E_3 = 272.5 + 78.7 = 351.2 kev.

It is interesting to note that the difference $E_3 - E_2$ = 351.2 - 179.5 = 171.7 kev is almost exactly equal to the transition energy that we get if we take the "c" line found by Bobrov et al[2] and shown in our Fig.1 as the K line of a γ-transition, i.e., a transition of 171.4 kev energy.

Gorodinskii et al[4] report that in a repeat investigation of the Lu^{173} γ-spectrum on a scintillation spectrometer they detected a weak line in the 350 kev region. Apparently this is a cross-over transition from the 351.2 kev level to the ground level of Yb^{173}.

These two facts strongly support the decay scheme shown in Fig.5.

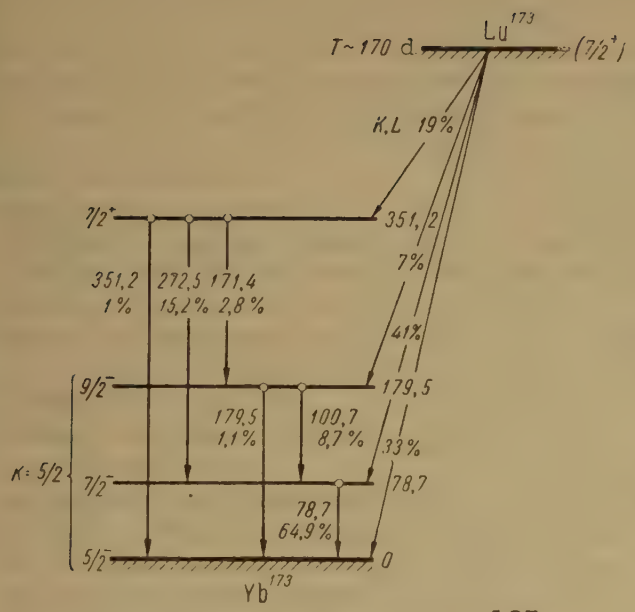

Fig.5. New decay scheme for Lu^{137}.

The 351.2 kev level is not comprised in the ground state rotational band, but is, apparently, a single particle level (vibrational levels in this region lie higher).

3. Characteristics of the excited states of Yb^{173}

The ground state of Yb^{173} and its first two excited states (E_1 = 78.7 and E_2 = 179.5 kev) form a rotational band and have the spins and parities 5/2-, 7/2- and 9/2-. The spin assignments follow directly from the data of Ref.2; the parities from the level sequence of Nilsson.

Now we must determine the characteristics of the third level lying at the 351.2 kev.

It was shown in Ref.2 that the 272.5 kev transition is E1. Inasmuch as it has been established that this transition goes to a 7/2- level, the assignment for the 251.3 kev level must be 5/2+, 7/2+ or 9/2+. To choose between these possibilities one can utilize a) the fact that there exists a cross-over transition to the ground level and b) the ratio of intensities of the K-272.5 and K--171.4 kev conversion lines.

Inasmuch as the Yb^{173} 351.2 kev level is apparently a single particle one, for comparing the intensities we can have recourse to the Weisskopf-Moszkowski formulas for the probability of single particle transitions.[5] Table 2 clearly shows that the 5/2+ assignment is definitely excluded by the K-171.4/K-272.5 ratio and the 9/2+ assignment by the $I_{\gamma\text{-}351.2}/I_{\gamma\text{-}272.5}$ ratio; therefore only the 7/2+ assignment remains. This deduction remains in force even if we assume the possibility of a three orders of magnitude deviation from theory.

Table 2

Determination of the assignment for the 351.2 kev level of Yb^{173} (the theoretical values are calculated on the basis of the single particle model)

Indicative characteristics	Experimental value	Assignments		
		5/2+	7/2+	9/2+
Multipole orders		$E1/E1$	$E1/E1$	$(E3+M2)/E1$
$\frac{I_{\gamma\text{-}351,2}}{I_{\gamma\text{-}272,5}}$	0,06	2,0	2,0	$2\cdot10^{-11}\div2\cdot10^{-7}$
Multipole orders		$(E3+M2)/E1$	$E1/E1$	$E1/E1$
$\frac{K\text{-}171,4}{K\text{-}272,5}$	0,84	$5\cdot10^{-12}$—10^{-6}	0,0 5	0,075

4. Revision of the relative transition probabilities in the decay of Lu^{173}

The relative probabilities of some transitions have already been determined in the work of Bobrov et al.[2] Now, however, on the basis of Refs.3 & 4 we can introduce certain refinements. The additional and revised values are listed in Table 3.

Table 3

Relative intensities of different transitions in the decay of Lu^{173} (the intensity of the 78.7 kev γ-rays is taken as 1.00 and this transition is assumed to be M1)

Transition energy, kev	Relative intensities				
		Electrons			transition as a whole
	γ-rays	*K*	*L*	*M*	
78,7	1,00	5,8	1,1	0,3	8,2
100,7	0,51	0,38	0,17	0,04	1,1
171,4	0,32	0,028	—	—	0,35
179,5	0,10	0,028	0,014	—	0,14
272 5	1,87	0,033	0,033	—	1,94
351,2	0,11	0,013	—	—	0,12
K—LL	16,2	—	0,78	—	17,4
K—LM		—	0,39	—	
K—MX		—	—	0,05	

Note: As shown in the text, in these units the intensity of K capture is 11.1, that of L capture is 1.6 and the total number of captures is 12.7.

To convert to percent of disintegrations, all the figures in Table 3 must be multiplied by 7.9 (100 : 12.7 ≈ 7.9); the converted percentages are shown in Fig.5.

Table 3 was compiled in the following manner.

1. The intensity of the 78.7 kev γ-rays was taken as 1.00. The relative intensities of the other γ-rays were taken according to the indications of Ref.3. The relative intensity of the 171.4 + 179.5 kev doublet was divided between the components so that there would obtain for the 179.5 kev transition a conversion coefficient corresponding to a pure E2 transition.

2. It was assumed that the 78.7 kev transition is pure M1. Hence for the K-78.7 probability, we assumed the value following from the conversion - 5.8 in the units of Table 3.

Actually the 78.7 kev transition may be a mixture of M1 + E2 rather than pure M1. It was shown in Ref.2 that the admixture of E2 cannot exceed 10%. Such an admixture would reduce α_K to 5.2, i.e., would reduce all the numbers of electrons in Table 3 by 10%, which would have virtually no effect on all our deductions.

3. The relative intensity values for all the other conversion lines have been taken directly from the experimental data of Bobrov et al[2].

4. The relative intensity of the K-LM Auger line merits particular attention inasmuch as it was used for evaluating the relative intensity of the K-100.7 line.

In the work of Ref.2 the K-LM line was observed to be very wide and as a result its intensity came out so high that the integral intensity of the K-100.7 + + K-LL combination had no "reserve" (after subtraction of K-100.7) for the K-LL line, which should be twice as strong as the K-LM line. Hence the intensity ratio

$$\frac{\text{(K-100.7 + K-LL)}}{\text{K-LM}} = 1.37$$

is either incorrect or is connected with some extraneous line augmenting the K-LM line. In our measurements this ratio was found to be approximately 3, but the accuracy is relatively low in view of the poor resolution of the lines. Nevertheless below we shall use this ratio.

5. To determine the intensity of the K-100.7 line, we must first determine the magnitude of the ratio (K-LL)/(K-LM).

Table 4

Data of different investigators on the ratio $\rho = \frac{K - LX}{K - LL}$

Z	ρ	Ref.	Z	ρ	Ref.
26	0,20±0,01	[6]	49	0,42±0,10	[8]
29	0,3 ±0,02	[7]	49	0,417	[12]
43	0,48±0,06	[8]	57—58	0,32	[13]
47	0,493	[9]	84	0,52	[14]
47	0,73	[10]	84	0,64	[15]
47	0,71	[11]			

The K-LL and K-LX (here X = M, N, etc.) Auger electrons originate in competing processes that do not depend on how the vacancies in the K shell are formed. The intensity ratio ρ = = (K-LX)/(K-LL) should be a function of Z only.

The scanty experimental data available at present are listed in Table 4.

There are no data in Table 4 for Z = 70, but in view of the weak dependence of ρ on Z, we can take the average of the values of Z = 49 and Z = 84 and assume that ρ = 0.5 ± 0.1 for Z = 70.

Thus we take (K-LL)/(K-LM) = 2 and, consequently, get K-100.7 = (K-100.72 + + K-LL)/3 = 0.38 in the units of Table 3 ($I_{\gamma-78.7} = 1.00$).

6. Analysis of the data pertaining to the 100.7 kev transition shows certain inconsistencies. It is difficult to see how one can reconcile the following four facts:

a) the value of the L shell conversion coefficient given by the experimental data (Table 3), namely, $\alpha_L = 0.17/0.51 = 0.33$ lies outside the range of α_L values for E2 and M1 transitions (1.09 and 0.47, respectively);

b) the K shell conversion coefficient following from the data of Table 3, $\alpha_K = 0.38/0.51 = 0.75$, lies outside the range of α_K values for E2 and M1 transitions (1.0 and 2.88, respectively);

c) at the same time the conversion ratio K/L = 0.38/0.17 = 2.23 lies between the values for E2 and M1 (0.91 and 6.1, respectively) and indicates a 50% E2 + 50% M1 mixture;

d) the composition of the mixture can be determined independently by means of the formulas for the relative probability of competing transitions between retational levels with $I_0 = 5/2$ (see, for example, Ref.16):

$$\frac{E2}{E1} = \frac{\lambda}{5.88 - \lambda},$$

where λ is the intensity ratio of the $E_2 \rightarrow E_0$ and $E_2 \rightarrow E_1$ γ-transitions. Substituting $\lambda = 0.1/0.52 = 0.2$, we obtain the composition 4% E2 + 96% M1.

The conflicting data on α_K, α_L and K/L can be reconciled in two cases:

a) if we assume that the relative intensity of the 100.7 γ-rays is 2.3 times lower than indicated by the experiments of Gorodinskii et al[3], or

b) if we assume that the relative intensities of the K-100.7 and L-100.7 lines are 2.3 times greater than indicated in the table.

Yet it is difficult to envisage the source of so great an error. The K-78.7 line, the softest line in the conversion spectrum, could have been weakened due to absorption in the counter window, but this would lead to a reduction rather than an increase of all the electron intensities listed in Table 3. The presence of some hitherto unsuspected electron line in the region of the K-LM Auger line would lead us to the necessity of reducing the relative intensities attributed to the Auger electrons and consequently would increase the intensity of the K-100.7 line; the intensity of the L-100.7 line, however, would remain unchanged, i.e., contradiction (a) above would remain.

The 78.7 kev transition, which we assumed to be pure M1, is actually probably a mixture of M1 + E2, but the possible admixture of E2 is, first, small, and second, acts in the opposite direction, i.e., aggravates the discrepancy.

In both cases, the values of α_K, α_L and K/L would lead to an approximately equal proportion of E2 and M1 in the composition of the 100.7 kev transition. But the composition following from the theoretical formula still remains entirely different: either 4% E2 + 96% M1 if we modify the intensity of the conversion lines or 10% E2 + 90% M1 if we modify the intensity of the γ-rays. We note that in all other odd rare earth nuclei with a rotational structure, except Hf^{177}, the fraction of M1 varies from 72 to 99%.[16]

7. The situation as regards the 171.4 kev transition is satisfactory. According to the decay scheme (Fig.5) this is a transition between 7/2+ and 9/2- levels, i.e., an E1 transition. The conversion coefficient α_K for such a transition should be 0.079; experiment gives 0.088. The L shell conversion coefficient should be $1.18 \cdot 10^{-2}$; consequently, the L-171.4 kev line should have an intensity of 0.0038 in the units of Table 3, i.e., be four times weaker than the neighboring L-179.5 line. Lines with an intensity less than 0.01 were not detected in the experiments of Ref.2.

8. For the 179.5 kev transition the γ-ray intensity was selected so that α_K would be equal to the theoretical value for E2. The ratio K/L = 2.0 differs little from the theoretical value for E2, namely, K/L = 1.7.

9. The intensity of the K-MX Auger line was taken equal to 12% of the intensity of the K-LM line (average value for the data cited in Ref.8).

10. The intensity of the K x-rays was calculated from the total intensity of the K series Auger electrons on the assumption that the K fluorescence yield for Z = 70 is 93% (this is based on the summary of the experimental data given in Ref.8).

11. The total intensity of the K series transitions, which is equal to 17.4 (in the units in which $I_{\gamma-78.7} = 1.00$), is connected both with K capture and with filling of the K shell after conversion on it. Inasmuch as the sum of the relative intensities of the K lines for all transitions is 6.3, the intensity for K capture is 11.1 units (Table 3).

12. The ratio of capture probabilities for electrons from the L and K shells for allowed transitions is

$$\frac{|\psi_L|^2}{|\psi_K|^2} \cdot \frac{(\varepsilon - E_L)^2}{(\varepsilon - E_K)^2},$$

where $|\psi_L|^2$ and $|\psi_K|^2$ are the squares of the moduli of the L and K electron wave functions, ε is the disintegration energy and E_K and E_L are the electron binding energies in the K shell and the L_1 subshell, respectively. If the nuclear mass difference before and after capture of an electron is large as compared with E_K and E_L, the second factor is approximately equal to unity and the ratio of K to L capture probabilities is determined by the first factor which depends wholly on the structure of the atom. This factor calculated by Rose & Jackson[17] and for Z = 70 equals 0.135.

Gorodinskii et al[4] report that they detected weak lines having energies of 570 ± 15 and 630 ± 15 kev (with intensities of 0.08 and 0.14 relative to $I_{\gamma-272.5}$) in the γ-spectrum of Lu^{173}. If this is true, the Lu^{173}-Yb^{173} mass difference is > 630 kev.

If the disintegration energy is very high, then L/K = 0.135; at an energy of 700 kev, L/K for decay to different levels varies from 1.60 to 1.87. In addition, the ratio L/K may depend on the degree of forbiddenness. We assume L/K = 0.15; we note that a variation of 10-20% in the value of L/K should have virtually no effect on our further deductions. The L capture probability in the units of Table 3 then proves to be 1.6.

13. The total number of disintegrations in the units of Table 3 comes out to be 12.7 and consequently this unit itself equals 7.9% disintegrations.

14. Conversion from the relative units of Table 3 to absolute units is generally realized through the Auger electrons. There is a considerable uncertainty, however, in the measurements of their relative intensity and their yield (~7%) is not accurately known. Hence the decay percentages for each branch indicated in the decay scheme of Fig.5 comprise an uncertainty of the order of 30%.

Table 3 shows that there should be many x-rays in the decay of Lu^{173} - 16 times more than 78.7 kev γ-rays. Direct comparison of the intensities of these two lines is very important for verification of Table 3 and our further deductions.

5. Relative intensities of capture to different levels of Yb^{173}

Using the intensities listed in Table 3, we can determine the fraction of capture events to each level of Yb^{173}. This has been done in Table 5. The figures for the percent capture to each level must be regarded with circumspection, however, inasmuch as they depend on the Auger effect yield.

Table 5

Balance of intensities for different Yb^{173} levels formed in the decay of Lu^{173}

Level energy kev	Departing	Arriving
351,2	Transition 171,4 kev — 2,8% » 272,5 » — 15,3% » 351,2 » — 1,0% Total: 19,1%	Capture — 19,1%
179,5	Transition 100,7 kev — 8,7% » 179,5 » — 1,1% Total: 9,8%	Transition 171,4 kev — 2,8% Capture — 7,0% Total: 9,8%
78,7	Transition 78,7 kev — 64,5%	Transition 100,6 kev — 8,7% » 272,5 » — 15,3% Capture —40,5% Total: 64,5%
0	—	Transition 78,7 kev — 64,5% » 179,5 » — 1,1% » 351,2 » — 1,0% Capture — 33,4% Total: 100,0%

In comparing the relative probabilities of formation of different excited states of Yb^{173} in the decay of Lu^{173}, we cannot but note the high probability for formation of the highly excited 351.2 kev state (7/2+) of Yb. This can readily be explained: according to Nilsson[18] the ground state of $_{70}Lu^{173}_{103}$ is determined by the 103rd neutron and is characterized by 7/2+.

Recently Ward et al[19], who investigated the $Hf^{173} \rightarrow Lu^{173}$ decay process, came to the same conclusion, namely, that the spin of the Lu^{173} ground state is 7/2.

Thus the spin assignments for the ground state of Lu^{173} and the 351.2 kev level of Yb^{173} agree; consequently, the transition between them must be allowed.

Transitions to all the other lower-lying levels of Yb^{173} are parity-forbidden. It is interesting to note that among these transitions, the one having the highest probability is the transition to the level with 7/2-.

If capture to the 351.2 kev level of Yb^{173} is allowed, the ft value for this transition should be $\sim 10^5$. The partial time, however, is very large, namely, 170 days$\cdot(100/\eta)$, where η is the percent decays to this level; this percentage must be close to 10-20% inasmuch as this is the total intensity of the 272.5 and 171.4 kev transitions. Consequently, $t \approx (7\text{-}15)\cdot 10^7$ whence $f \approx 10^{-3}$.

In the case of K capture, so small an f_K value means that the disintegration energy is very close to the K shell binding energy (energetically "almost forbidden" K capture), i.e., about 60 kev. This is inconsistent with the existence of hard γ-rays of 570 and 630 kev energy.

If the data of Gorodinskii et al[4] regarding the existence of these hard γ-rays and, consequently, the large Lu^{173} - Yb^{173} mass difference should be substantiated, then f_K will prove to be large. We will then have the question of why there is such a large value of ft for an allowed 7/2+→7/2+ transition.

Table 6

ft Values for decay of Lu^{173} to different levels of Yb^{173}

ft values for K-capture to the indicated Yb^{173} levels, kev	Assumed Lu^{173}-Yb^{173} mass difference	
	1000 kev	2000 kev
351.2	$3.6\cdot10^8$	$2.6\cdot10^9$
179.5	$1.6\cdot10^9$	$8.6\cdot10^9$
78.7	$3.6\cdot10^8$	$1.7\cdot10^9$
0	$5.4\cdot10^8$	$2.3\cdot10^9$

The values of ft for transitions to other levels of Yb^{173} also depend on the Lu^{173} - Yb^{173} mass difference. The ft values calculated for mass differences of 1000 and 2000 kev are listed in Table 6.

6. Quantitative analysis of e^--e^- coincidences in Lu^{173} decay

For quantitative comparison of the coincidence counting rates with one and the same current in the magnetic lens of the spectrometer viewing the backing side of the source and different currents in the other spectrometer, one must have an adequately developed decay scheme; that is, the decay scheme must include the probabilities for all possible modes of transformation of the initial nucleus to the final one. By way of illustration let us consider the simple scheme shown in Fig.6. All the transitions γ_1, γ_2 and γ_3 are in cascade and yield γ-γ coincidences. But in the illustrated scheme γ_2 always follows γ_1 (if we neglect conversion), while γ_3 sometimes follows γ_1 and sometimes occurs directly after a capture event K_2. Hence for quantitative comparison of the γ_1-γ_2, γ_1-γ_3 and γ_2-γ_3 coincidence rates we must know the ratio K_1:K_2 and the conversion coefficients for all the transitions. Analogous considerations obviously apply to coincidence between the conversion electrons.

In the absence of continuous electron and positron spectra, the number of "effective" coincidences per disintegration caused by «1i» electrons (type i electrons from the «1» transition) and «nj» electrons (type j electrons from the «n» transition) is given by

$$\frac{N_{nj}^{1i}}{N} = (\omega_1 \varepsilon_{1i} P_1 \alpha'_{1i})\, \delta_{nj}^{1i}\, (\omega_2 \varepsilon_{nj} P_n \alpha'_{nj})\, \varepsilon. \qquad (1)$$

Here N_{nj}^{1i} is the observed number of coincidences per unit time, N is the number of disintegrations per unit time, ω_1 and ω_2 are the solid angles of the first and second spectrometers, ε_{1i} and ε_{nj} are the efficiencies of the first and second spectrometer counters for detecting the given conversion electrons, ε is the efficiency in recording coincidences, P_1 and P_n are the probabilities of the

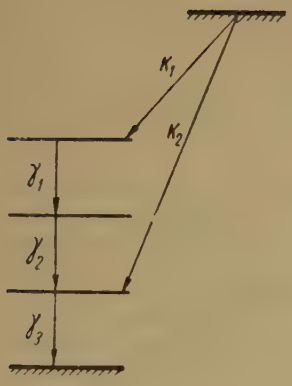

Fig.6.

«1» and «n» transitions expressed in fractions of the total number of decays, α'_{1i} and α'_{nj} are the probabilities of formation of a conversion electron of the given type (i or j) referred to one «1» or «n» type transition, for example,

$$\alpha'_L = \frac{\alpha_L}{1 + \alpha_K + \alpha_L + \alpha_M + \dots},$$

where α_K, $\alpha_L \dots$ are the conversion coefficients, $P_n\alpha'_{nj}$ is the number of conversion electrons of type nj per disintegration, $(\omega_1\varepsilon_{1j}P_1\alpha_{1i})$ and $(\omega_2\varepsilon_{nj}P_n\alpha'_{nj})$ are the counting rates (per one decay/sec) in the right and left spectrometers adjusted to detect the $1i$ and nj conversion lines and δ^{1i}_{nj} is the ratio of the number of type «n» transitions in cascade with the «1» type transitions to the total number of «n» transitions. This quantity is always less than unity and approaches this limit only when the transition probabilities become equal; if the transitions are not in cascade, δ equals zero.

Measuring the conversion electron spectra on single spectrometers, we readily find $\omega_1\varepsilon_{1i}P_1\alpha'_{1i}$ and $\omega_2\varepsilon_{nj}P_n\alpha'_{nj}$, but we can draw no deductions regarding the unexpected coincidence rate as long as we do not know δ^{1i}_{nj}.

Eq.(1) can be rewritten as

$$\frac{N^{1i}_{nj}}{N} = \omega_1\varepsilon_{1i}\omega_2\varepsilon_{nj}x^{1i}_{nj}\cdot\varepsilon,$$

where $x^{1i}_{nj} = P_1\alpha'_{1i}\delta^{1i}_{nj}P_n\alpha'_{nj}$ is the probability (per decay) of simultaneous appearance of $1i$ and nj electrons.

As was noted above, it is meaningful to compare coincidence rates only for pairs when one of the spectrometers is always adjusted to detect one and the same line and the other is shifted in sequence to the peaks of the other lines. In this case the $\omega_1\cdot\varepsilon_{1i}\cdot\omega_2$ will cancel out in the coincidence counting rate ratios and only the $\varepsilon_{nj}x^{1i}_{nj}\varepsilon$ will remain. Beginning with an electron energy of 40 kev, ε_{nj} and ε are virtually independent of the energy and hence their variation can be disregarded, but the values of x^{1i}_{nj} must be taken from the decay scheme.

Fig.7 shows the decay scheme for Lu^{173} in which we have plotted the various decay branches and indicated the relative probabilities thereof; we have also indicated the relative intensities of the K-LM Auger electrons. The intensities of the K-LL electrons are two times higher, while those of the K-MX electrons are 8 times lower. In elaborating the scheme, it was assumed that the Lu^{173} - Yb^{173} mass difference is about 700 kev ($L/K \approx 0.15$). We used the data of Fig. 7 to calculate x^{1i}_{nj} and the corresponding coincidence rates; these are juxtaposed in Table 7 with the experimental rates.

Examining the data of Table 7 we note the following:

1. The experimental data differ from the calculated coincidence values by a factor of 7-9 when the K-78.7 line is involved in the measurements. The appreciable divergence between the experimental and calculated data in this case may be connected with the fact that the K-78.7 line, being the softest line in the conversion spectrum, is "underdetected" in recording coincidences (ε low).

2. In all coincidences not involving the K-78.7 line, the experimental and calculated data agree within ±25%.

V.Bunakov and A.Miakusheva, students at Leningrad State University, participated in the coincidence measurements and reduction of the experimental data.

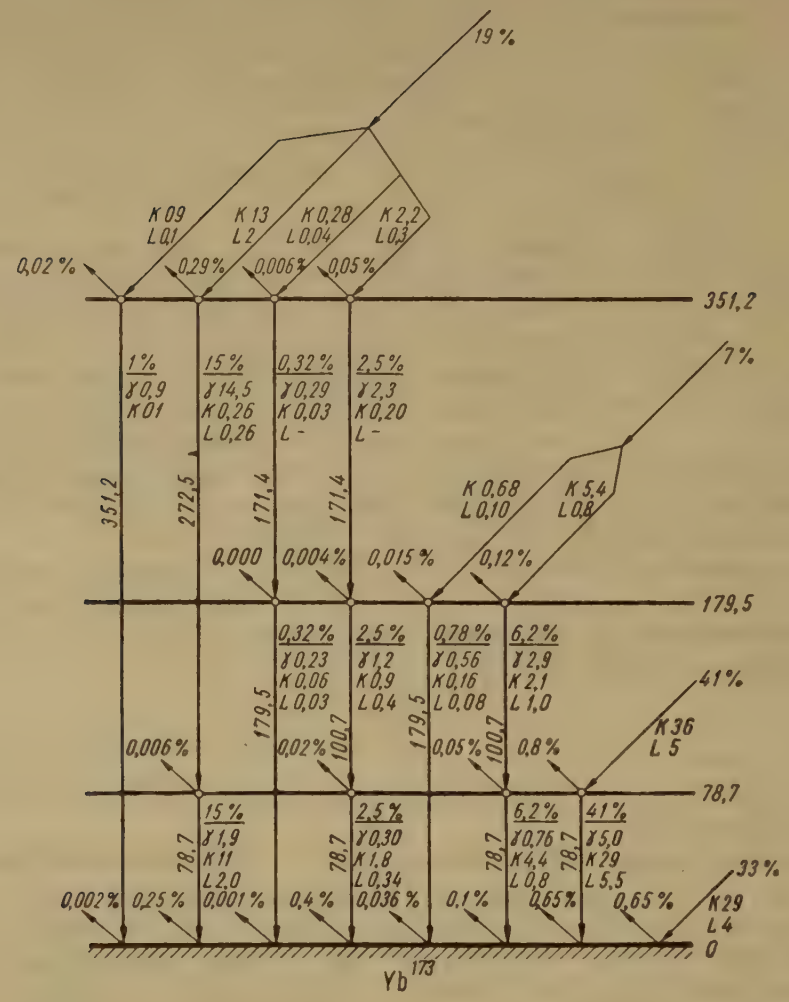

Fig.7. Relative intensities of different $Lu^{173} \rightarrow Yb^{173}$ decay branches. All figures are in percent of the number of disintegrations. Arrows pointing upward to the left indicate Auger electrons; the figures near them pertain to K-LM electrons.

Table 7

Comparison of experimental and calculated coincidence rates

Coincidences	Exper.	Calc. basis scheme of Fig.7
$(L\text{-}78,7)(K\text{-}100,7+K\text{—}LL)$: $:(L\ 78,7)(K-LM)$	6,5 : 1	4 : 1
$(K\text{-}272,5)(K\text{-}78,7)$: $:(K\text{-}2\ 2,5)(K\text{-}100,7+K\text{—}LL)$: $:(K\text{-}272,5)(K-LM)$	1,7 : 1,4 : 1	12 : 2 : 1
$(K\text{-}171,4)(K\text{-}\ 8,7)$: $:(K\text{-}171,4)(K\text{-}100,7+K-LL)$: $:(K\text{-}171,4)(K\text{—}LM)$	1,1 : 7,6 : 1	10 : 7 : 1

We desire to express our gratitude to A.N.Murin, G.M.Gorodinskii and V.N. Pokrovskii for communicating the results of their investigation of the Lu γ-spectrum prior to publication.

Scientific Research Physical Institute,
"A.A.Zhdanov" Leningrad State University

References

1. V.Sergienko, Izv.AN SSSR, Ser.fiz., 22, 198 (1958). (Trans. Bulletin 22, No.2, 195.)
2. D.Bobrov, K.Gromov, B.Dzhelepov & B.K.Preobrazhenskii, Izv.AN SSSR, Ser. fiz., 21, 940 (1957). (Trans. Bulletin, 21, No.7, 942.)
3. G.Gorodinskii, A.Murin, V.Pokrovskii & B.Preobrazhenskii, Izv.AN SSSR, Ser.fiz., 21, 1004 (1957). (Trans. Bulletin, 21, No.7, 1005.)
4. G.Gorodinskii, A.Murin, V.Pokrovskii & B.Preobrazhenskii, Abstracts of reports presented at the Eighth Conference on Nuclear Spectroscopy,M.-L.,1958.
5. S.Moszkowski, in Beta- and Gamma-Ray Spectroscopy, edited by K.Siegbahn, Amsterdam, 1955.
6. J.Bellicard & A.Moussa, J.phys.et radium, 18, 115 (1957).
7. J.Bellicard, A.Moussa & S.Haynes, Nucl.Phys., 3, 307 (1957).
8. J.Laberrique-Frolow & P.Radvany, J.phys.et radium, 17, 944 (1956).
9. O.Huber, F.Humbel, H.Schneider & A.deShalit, Helv.phys.acta, 25, 3 (1952).
10. J.Laberrique-Frolow & P.Radvanyi, Compt.rend., 242, 901 (1956).
11. F.Johnson & J.Foster, Canad.J.Phys., 31, 469 (1953).
12. G.Harrison, R.Crawford & I.Hopkins, Phys.Rev., 100, 841 (1955).
13. K.Gromov, B.Dzhelepov, A.Dmitriev & B.Preobrazhenskii, Izv.AN SSSR, Ser. fiz, 22, 153 (1958). (Trans.Bulletin 22, No.2, 151.)
14. A.Zhernovoi, E.Krisiuk, G.Latyshev, A.Remennyi, A.Sergeev & V.Fadeev, Zhur.eksp.i teor.fiz, 32, 682 (1957). (Trans.JETP - Soviet Phys.)
15. M.Mladjenovic & H.Slätis, Arkiv fys., 9, 41 (1955).
16. N.Heydenburg & G.Temnver, Phys.Rev., 104, 981 (1957).
17. M.Rose & J.Jackson, Phys.Rev., 76, 1540 (1949).
18. S.Nilsson, Kgl.Danske, 29, 16 (1955).
19. T.Ward, J.Mihelich, T.Handley & B.Harmatz, Bull.Amer.Phys.Soc., 2,341 (1957).

MASS NUMBERS OF NEUTRON-DEFICIENT TERBIUM ISOTOPES

- V.I.Baranovskii, A.N.Murin, V.N.Pokrovskii & I.A.Iutlandov

At present there is information in the literature on neutron-deficient Tb isotopes with mass number from 158 (the only stable terbium isotope has A = 159) to 149. For convenience of reference, the principal data of different investigators have been summarized in the accompanying table. In addition to the half-lives and types of decay, we list the "degree of certainty" of the isotopic assignments after Seaborg[4]: A - mass number certain, B - mass number probable and D - mass number not well established (Z in all cases certain). It should be noted that on the basis of the recent investigation of Ward et al[6], Tb^{155} can be put in class B.

Mass number	Refs.1,2 & 3; these are listed in Seaborg's (1953) table[4]			More recent data
	Class	Type of decay	$T_{1/2}$	Ref.5
149*	A	α,K(?)	4.1 hours	
151*	B	α,K(?)	19 hours	α with $T_{1/2}$ ~19 hrs not detected
152				< 10 min. or > 5 yrs.
153*	B	K	5.1 days	
154	B	K,β+	1.2 hours	K,β+(?) 7.5 hrs; 17.5 hrs.
155	D(B)	K	190 days	< 10 min or > 5 yrs. {K, 5.6 days - Ref.6}
156	B	K,β+	5 hours	K 5.2 days**; Isom., β- 5.5 hrs.
157	B	K	4.7 days	< 10 min*** or > 25 yrs
158				< 10 min or > 5 yrs.

*Isotopes investigated in the present study.

**These data have been substantiated in the work of Refs.7-9.

***A similar value for the period of Tb^{157} was obtained in Ref.10.

It will be seen that there are a number of disagreements between the results of different investigators. These discrepancies probably stem primarily from the method of preparing the isotopes by reactions of the (α,xn) or (p,xn) type, where x, the number of outgoing neutrons, is not always reliably known.

In our work the neutron deficient Tb isotopes were obtained together with other rare earth nuclides by spallation of tantalum under bombardment with 660 Mev protons.[11,12] In view of the fact that chromatographic (ion exchange) techniques[13,14] were used for the separation, we could be certain of the atomic number of the investigated isotopes.

Earlier it was found[11,12] that there were present in the terbium fraction isotopes with the following half-lives: ~20 hours (according to the tabular data either Tb^{151} or Tb^{154}); ~5 days (Tb^{153}, Tb^{155}, & Tb^{156}) and ~3 days (this period

had not been observed earlier in Tb).*

We could detect only traces of Tb^{149} (~4 hours) inasmuch as an interval of at least 15 hours always elapsed between the irradiation in the Joint Institute for Nuclear Research synchrocyclotron and the measurements on the scintillation spectrometer in Leningrad.

In order to verify the mass numbers of the Tb isotopes present in the investigated fraction, we attempted to establish the genetic relationships by means of repeated chromatographic separation of the daughter elements and investigation thereof. This procedure allows of establishing both the mass number of the parent isotope (when the daughter is known) and its half-life (inasmuch as the amount of separated out daughter isotope with equal time intervals between successive separations is proportional to $e^{-\lambda t}$, where λ is the decay constant of the parent nuclide). In this manner we could investigate the Tb isotopes with A = 149, 151 and 153 inasmuch as the corresponding radioactive Gd (Z = 64) isotopes are known; the other isotopes of Tb in decaying transform into stable Gd isotopes.

The separation of the daughter nuclides from Tb was carried out four times with an interval of 3 days between separations (4 days passed between the third and fourth separations). Gd was obtained in all four separations; this fraction contained two isotopes: Gd^{153} (present in all cases) and Gd^{151} (observed in the first two separations). No other daughter elements (for example, Eu, which would correspond to α-decay of Tb) were present in noticeable amounts.

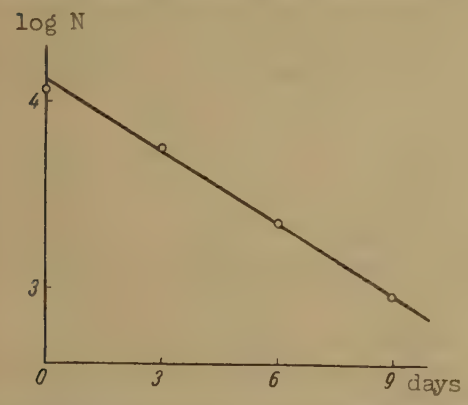

Determination of the period of Tb^{153}. $T_{1/2}$ = 2.4 ± 0.2 days.

Gd^{153} is a thoroughly investigated isotope with a reliably established decay scheme. Its presence in the separated out decay product was firmly established both from the period and the γ-spectrum. The amounts of Gd^{153} in the successive separations were compared on the basis of the relative intensities of the distinct 100 kev line in the γ-spectrum of Gd (the measurements were made on a scintillation spectrometer).

The amounts of Gd^{153} obtained in the successive separations with appropriate corrections for losses in the ion exchange process are plotted against time in the accompanying figure. The last point is also adjusted for the longer interval between the third and fourth separations.

It will be seen that the points fit a straight line corresponding to a period of 2.4 ± 0.2 days for the parent nuclide. Thus the existence of Tb^{153} with a period of 2.4 days may be considered firmly established. The most noticeable feature in the γ-spectrum of Tb^{153} is a group of lines in the 205 and 210 kev region. (The complexity of the γ-spectrum of the Tb fraction, which contained several isotopes, hampered more detailed analysis.) The intensity of this group of γ-lines in the spectrum of the Tb fraction fell off with a period of ~ 2.7 days. This somewhat longer period is to be explained, in our opinion, by the fact that there are also present in this energy region comparatively weak γ-lines pertaining to longer-lived isotopes, for example, Tb^{155}. [6]

The second of the daughter isotopes - Gd^{151} - observed by us has been less thoroughly investigated than Gd^{153}. As regards certainty of assignment, Gd^{151}

---

*The possible presence of a nuclide with a period of ~8 days was noted in Ref.12; further careful investigation, however, failed to substantiate this.

may be put in class B; according to our data its period is 120-150 days and its spectrum consists of lines at 154 and 247 kev (Seaborg's table lists $T_{1/2}$ = 150 days and a 265 kev γ-ray). Comparing the amounts of Gd^{151} in successive separations on the basis of the intensity of the 154 kev γ-line, we obtained a value of 18 ± 2 hrs for the period of the parent nuclide. This agrees with the 19 hour period given for Tb^{151} in Seaborg's table.[4]

The fact that we established a genetic relationship between Tb^{151} and Gd^{151} (not observed earlier) gives reason to assert that the mass number assignments for these isotopes are more reliable than hitherto assumed. Inasmuch as the performed experiments could not establish the presence (or absence) of Tb^{154} in the terbium fraction, we cannot be certain to which of these isotopes (or their mixture) the 270 kev (probably a group) and 345 kev γ-lines, observed earlier[12], belong. From the fact that the daughter elements do not include Eu, we infer that the fraction of α-decay (with respect to electron capture) for Tb^{151} does not exceed 1%. (The lower bound given in Seaborg's table is $4 \cdot 10^{-3}$%.)

Experimental investigation of the short-lived products of the spallation reaction on Ta enabled us to establish a genetic relationship between Tb^{149} and Gd^{149}. Inasmuch as the mass number assignment for Tb^{149} is certain, in view of the existence of this relationship one can consider the said A value for Gd^{149} as reliable; the properties of this isotope have been described earlier.[12]

We desire to thank B.K.Preobrazhenskii and V.N.Mel'nikov for assistance in the chromatographic separations and N.Bushuev for help in carrying out the measurements.

"V.G.Khlopin" Radium Institute,
Academy of Sciences of the USSR

References

1. G.Wilkinson & H.G.Hicks, Phys.Rev., 79, 815 (1950).
2. J.O.Rasmussen, F.L.Reynolds, S.G.Thompson & A.Ghiorso, Phys.Rev., 80, 475 (1950).
3. J.O.Rasmussen, S.G.Thompson & A.Chiorso, Phys.Rev., 89, 33 (1953).
4. J.Hollander, I.Perlman & G.Seaborg, (Tables of Isotopes) Revs.Mod.Phys., 25, 469 (1953). (Cited in Russian trans., M., 1956.)
5. T.H.Handley & W.S.Lion, Phys.Rev., 99, 1415 (1955).
6. T.Ward, K.P.Jacob, J.W.Mihelich, B.Harmatz & T.H.Handley, Bull.Amer. Phys.Soc., Ser.II, 2, 259 (1957).
7. L.T.Dillman, R.W.Henry, N.B.Gove & R.A.Becker, Bull.Amer.Phys.Soc., Ser.II, 2, 341 (1957).
8. R.W.Henry, L.T.Dillman, N.B.Gove & R.A.Becker, Bull.Amer.Phys.Soc., Ser.II, 2, 341 (1957).
9. J.W.Mihelich & B.Harmatz, Phys.Rev., 106, 1232 (1957).
10. T.H.Handley & E.L.Olson, Phys.Rev., 90, 500 (1957).
11. G.M.Gorodinskii, A.N.Murin, V.N.Pokrovskii, B.K.Preobrazhenskii & N.E. Titov, Doklady AN SSSR, 112, 405 (1957).
12. G.M.Gorodinskii, A.N.Murin, V.N.Pokrovskii & B.K.Preobrazhenskii, Izv. AN SSSR, Ser.fiz., 21, 1624 (1957). (Trans.Bulletin 21, No.12, 1611.)
13. B.K.Preobrazhenskii, O.M.Lilova, A.N.Dobranravova & E.D.Teterin, Zhur. neorg.khim. (Journ.Inorganic Chemistry), 1, 2294 (1956).
14. B.K.Preobrazhenskii, A.V.Kaliamin & O.M.Lilova, ibid., 2, 1164 (1957).
15. B.S.Dzhelepov & L.K.Peker, Skhemy raspada radioaktivnykh izotopov (Decay schemes of radioactive isotopes). M., 1957.

MASS NUMBERS OF 52-DAY GADOLINIUM AND 4.3-DAY EUROPIUM ISOTOPES

- G.M.Gorodinskii, A.N.Murin & V.N.Pokrovskii

The γ-spectrum of the gadolinium fraction obtained by spallation of tantalum was investigated on a scintillation γ-spectrometer and a scintillation γ-γ coincidence set-up. The scintillation equipment and experimental procedure have been described in Ref.1. Earlier[2,3] we established the existence of the new radioactive series,

$$64^{Gd} \xrightarrow[(52\pm10)\,days]{E} 63^{Eu} \xrightarrow[(4.3\pm0.6)\,days]{E} 62^{Sm}, \qquad (1)$$

and investigated the γ-spectra of the isotopes involved. It was not feasible to investigate the 52-day Gd in pure form inasmuch as the following isotopes were also present in the gadolinium fraction:

Gd^{149} - $T_{1/2}$ = 9 days (E_γ = 150, 300, 347 & 520 kev);
Gd^{151} - $T_{1/2}$ = 150 " (E_γ = 154 & 247 kev);
Gd^{153} - $T_{1/2}$ = 230 " (E_γ = 70 & 100 kev).

Approximately one month after irradiation (Fig.1) the intensity of the 115 kev line of 52-day of Gd becomes equal to the intensity of the 150 kev line of 9-day Gd^{149}. Some 2-3 months after irradiation, when the Gd^{149} activity has died down to negligible proportions, there begin to appear γ-lines of energies of 100 kev (Gd^{153}) and 154 kev (Gd^{151}), the intensities of which are commensurate with the intensity of the 115 kev line.

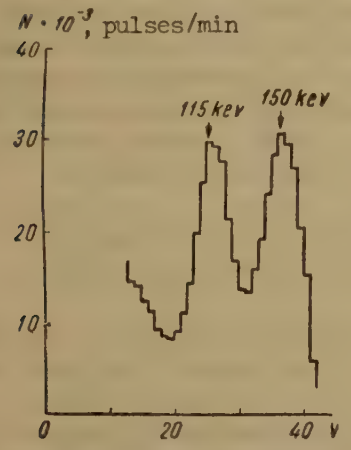

Fig.1. γ-spectrum of Gd fraction separated from Eu. Spectrum obtained one month after irradiation. The 115 kev line decays with a period of 52 days. The 150 kev line is due primarily to the decay of Gd^{149}.

In order to determine the content of 52-day Gd in the gadolinium fraction we measured the energy of the γ-line in the 115 kev region. The center of gravity of this line gradually shifted to the low energy side and in 6-8 month old sources its peak appeared at 100 kev in the energy scale. This means that there was appreciably less 52-day Gd (E_γ = 115 kev) than Gd^{153} in the gadolinium fraction.

A month old Gd source was investigated in the γ-γ coincidence set-up. The heavy solid line in Fig.2 shows the coincidence spectrum of 52-day Gd obtained under conditions when the "stationary" channel of the γ-spectrometer was gated to detect the energy interval shown by the hatched area under the Gd γ-spectrum, which is given by the light solid line in the figure. The 115 kev peak in the coincidence spectrum, as we noted in Ref.3, is explained by the presence of the γ-ray cascade with an energy close to 115 kev. The peak at ~150 kev indicates that 52-day Gd in decaying also emits 150 kev γ-rays, which coincide in time with the 115 kev cascade. It was not feasible to resolve fully the 150 kev (52-day Gd) line in the spectrum of the gadolinium fraction in view of the presence of γ-rays of close energy belonging to other Gd isotopes.

Anton'eva et al[4] report that in the conversion electron spectrum of gadolinium with a period of ~50 days they detected lines corresponding to a γ-transition of 155 kev energy, which is in good agreement with our data deriving from the coincidence spectrum.

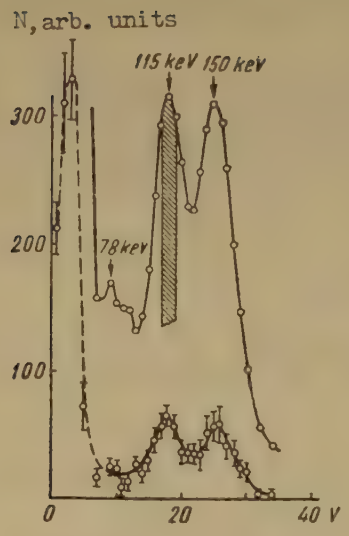

Fig.2. γ-spectrum (light solid line) and coincidence spectrum (heavy solid line) of 52-day Gd. The hatched section of the spectrum is the interval detected by the "stationary" channel of the γ-γ coincidence set-up.

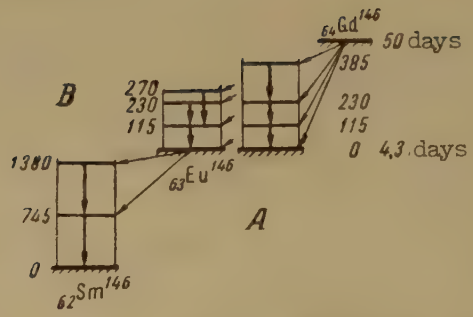

Fig.3. A - Decay scheme for 52-day Gd (two versions); B - decay scheme for 4.3-day Eu.

Thus the γ-spectrum of 52-day Gd consists of two γ-lines having energies close to 115 kev and a 150 kev γ-line; apparently all these γ-rays are emitted in coincidence.

Fig.3 shows the tentative decay scheme for ~50-day Gd (including the additional data given above for the 150 kev line) and the decay scheme for 4.3-day Eu proposed in Ref.6. The period of our intermediate nucleus (4.3 days) agrees within the limits of the experimental error with the period given by Hoff et al[5] for Eu^{145}: 5 ± 1 days. Hence at the first stage of the investigation we were inclined to assign the mass number 145 to the isotopes of the radioactive series in question. Upon further investigation and consideration, however, it occurred to us that this coincidence of the periods may be fortuitous. One can advance the following arguments against the A = 145 assignment:

1. We carried out a special experiment aimed at detecting Sm^{145} which should have formed from the 4.3-day Eu if this had A = 145. The experiment yielded negative results: no Sm^{145} was detected.

2. Hoff et al[5] report that Eu^{145} emits 200 kev conversion electrons; consequently, it must also emit 260 kev γ-rays. According to our data there were no γ-lines of less than 636 kev energy in the spectrum of the 4.3-day europium separated from the Gd activity. This divergence can readily be explained if we admit that the Eu isotope investigated by us and the Eu^{145} discovered by Hoff et al are different isotopes.

3. In the europium fraction investigated by A.A.Bashilov* there were detected conversion lines in the 100 kev region, whose intensity fell off with a period of about 5 days.**

---

*We take this occasion to thank A.A.Bashilov for communicating his results.

**We also investigated the spectrum of the europium fraction but failed to detect a γ-line corresponding to ~100 kev conversion electrons. This presumably can be explained by the presence of Eu^{147} which emits 120 and 200 kev γ-rays. The γ-line in question, which is probably of low intensity, could readily escape detection against the background of the 120 kev Eu^{147} γ-line.

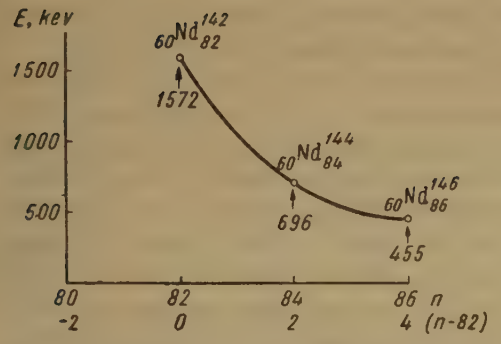

Fig.4. Energy of the first excited level of even-even neodymium nuclei as a function of the number of neutrons.

The above in conjunction with our data suggests that there exist at least two neutron-deficient europium isotopes with close periods; presumably one of these is the isotope investigated by Hoff et al[5]. Thus the close agreement of the half-lives, the indication upon which we based our A = 145 assignment, is no longer convincing.

We can attempt to determine the mass number of the isotopes through comparison of their γ-spectra with the γ-spectra of thoroughly investigated nuclides. To this end we can utilize the following established experimental facts:

1. Odd-odd isotopes of heavy nuclei tenerally have a first excited state about 100 kev above the ground state (see, for example, Ref.6).

2. Nuclei with A $<$ 150 have a spherical equilibrium shape. Collective excited states of spherical even-even nuclei are of the vibrational type. The energy of the first vibrational level in such nuclei increases as the number of neutrons approaches the magic number 82 (closed neutron shell). A typical example is furnished by the odd-odd Nd isotopes with mass numbers 142, 144 and 146. The curve of Fig.4 shows the variation of the first excited level energy of neodynium isotopes as a function of the number of neutrons outside the filled shell.

Now let us see what mass number can be assigned to the isotopes composing our series, Gd→Eu→Sm, so as not to come into conflict with the extant experimental data on neutron-deficient isotopes. Of the known Eu isotopes, that with mass number 144 has too short a half-life. Let us tentatively assume that the mass number assignment made by Hoff et al for Eu^{146} (degree of certainty - class C) is mistaken and that this mass number belongs to the isotopes of our radioactive series.

Let us tabulate the series in accordance with the old and new assumptions regarding the mass number:

Initial assumption: A = 145	New assumption: A = 146	Period	Level energies, kev
$_{64}Gd^{145}_{81}$ even-odd	$_{64}Gd^{146}_{82}$ even-even	52 *days*	---
$_{63}Eu^{145}_{82}$ odd-even	$_{63}Eu^{146}_{83}$ odd-even	4.3 *days*	115;230
$_{62}Sm^{145}_{83}$ even-odd	$_{62}Sm^{146}_{84}$ even-even	---	745;1380
1. All nuclei either even-odd or odd-even.	1. Initial and final nuclei - even-even; intermediate nucleus - odd-odd.		
2. Eu has a closed neutron shell and hence must have a first vibrational level at about 1500 kev.	2. Gd has a closed neutron shell (82 n); the following nuclei have 1 & 2 neutrons outside the closed shell.		

Examining our two columns, we note that in the case of the new assignment (A = 146), the Eu nucleus which has comparatively low-lying first excited states, is odd-odd, while the Sm nucleus, which has two levels with a high excitation energy (745 and 1380 kev) proves to be even-even. Thus the observed level energies are consistent with the values that whould be expected for the excited states of an odd-odd (Eu^{146}) and an even-even nuclide (Sm^{146}). This is particularly clearly evident in the case of Sm. With the new A assignment the samarium nucleus has two neutrons outside the filled shell. Hence it may be expected that the energy of the first vibrational level will be close to the energy of the similar level in Nd^{144}, which also has two excess neutrons and an even number of protons. This is actually the case, specifically, we have E_γ = 696 kev for Nd^{144} and E_γ = 745 kev for Sm^{146}. Thus we can now establish the mass number of the isotopes under study with reasonable certainty and write the formula for the discovered radioactive series as

$$_{64}Gd^{146} \xrightarrow[T_{\frac{1}{2}} \approx 50 \text{ days}]{E} {}_{63}Eu^{146} \xrightarrow[T_{\frac{1}{2}} \approx 4.3 \text{ days}]{E} {}_{62}Sm^{146}.$$

We desire to thank L.A.Peker for valuable discussions and A.V.Kaliamin for assistance in the work.

"V.G.Khlopin" Radium Institute,
Academy of Sciences of the USSR

References

1. G.M.Gorodinskii, A.N.Murin, V.N.Pokrovskii & B.K.Preobrazhenskii, Izv. AN SSSR, Ser.fiz., 21, 1004 (1957). (Trans.Bulletin 21, No.7, 1005.)

2. G.M.Gorodinskii, A.N.Murin, V.N.Pokrovskii, B.K.Preobrazhenskii & N.E.Titov, Doklady AN SSSR, 112, 405 (1957).

3. G.M.Gorodinskii, A.N.Murin, V.N.Pokrovskii & B.K.Preobrazhenskii, Izv.AN SSSR, Ser.fiz., 21, 1624 (1957). (Trans.Bulletin 21, No.12, 1611.)

4. N.M.Anton'eva, A.A.Bashilov, B.S.Dzhelepov & B.K.Preobrazhenskii, Izv.AN SSSR, Ser.fiz., 22, 135 (1958). (Trans.Bulletin 22, No.2, 134.)

5. R.Hoff, J.O.Rasmussen & S.G.Thompson, Phys.Ref., 83, 1068 (1951).

6. B.S.Dzhelepov & L.K.Peker, Skhemy raspada radioaktivnykh isotopov (Decay schemes of radioactive isotopes), M.-L., 1957.

MASS NUMBERS OF NEUTRON-DEFICIENT Dy ISOTOPES

- A.N.Dobronravova, L.M.Krizhanskii, A.N.Murin & V.N.Pokrovskii

Until recently only two neutron-deficient isotopes of dysprosium (Z = 66) were known[1]: Dy^{159} (134 days) and Dy^{157} (8.2 hours). There were also indications[1] that there exist short-lived α-active Dy isotopes with A < 153.

We studied neutron-deficient isotopes in the work described in Refs.2-4. Investigating the Dy fraction and the genetic relationship of the Dy isotopes with their daughter elements (Tb and Gd), we came to the conclusion[4] that there were present in the Dy fraction isotopes with A = 159, 157, 155 & 153.

To check this we undertook a direct determination of the mass of the Dy isotopes forming in the spallation reaction on Ta. To this end we separated the Dy fraction in a mass spectrometer and recorded the γ-spectra of the separated isotopes by means of a scintillation spectrometer.

For the separation we used a commercial type MS-2 mass spectrometer in which the slits were widened somewhat to enhance the transmission (we used an ion source operating on the principle of surface ionization) and installed a platinum coated tungsten source filament. The recording was carried out by means of a photographic attachment[5] with collection on a photographic plate; in calibrating the instrument we used the stable isotopes Eu^{151}, Eu^{153}, Dy^{161}, Dy^{162}, Dy^{163} & Dy^{164}. In the actual separation, the Dy isotopes were collected on foil mounted in the position of the photographic plate. This foil was then cut into strips, one for each mass (the separation between neighboring masses was ~1.5 mm).

The source prepared in this manner were investigated on a scintillation γ-spectrometer with a 30 x 20 mm NaI(Tl) crystal. In this manner we definitely established the existence of radioactive Dy isotopes with A = 159, 157, 155 & 153 and possibly 151. The weak activity of the Dy^{159} sample and the very weak activity of Dy^{151} precluded carrying out further measurements on these. From the integral activity count and the recorded γ-spectra of the separated Dy^{157}, Dy^{155} and Dy^{153} isotopes we can infer the following.

Dy^{157}. The period is 8.5 ± 0.5 hours; no daughter activity apparent. The γ-spectrum consists of an 80 (weak) and a 325 kev line.

Dy^{155}. Period - 9 ± 2 hours; a daughter activity with a period of ~5 days was observed (Tb^{155} - Refs.4 & 6). The γ-spectrum consists of an 80 (doubtful) and a 227 kev line.

Dy^{153}. Period - 7 ± 3 hours; a daughter activity with a period of ~2 days was observed (Tb^{153} - Ref.7). The γ-spectrum comprises a line at 80 kev.

Recently there have appeared two investigations,[8,9] the results of which are not in conflict with the data of Ref.4 and the present note. Toth & Rasmussen[9] report that Dy^{153} (5 hours) emits 3.48 Mev α-particles. The half-life of Dy^{155} according to Toth & Rasmussen is 10 hours (see above), while according to Mihelich, Harmatz & Handley[8] it is 20 hours. The difference is probably due to errors in determining the periods of the very weak Dy^{155} sources used by Mihelich et al.

"V.G.Khlopin" Radium Institute,
Academy of Sciences of the USSR

References

1. J.Hollander, I.Perlman & G.Seaborg (Table of Isotopes), Rev.Mod.Phys., 25, 469 (1953). (Cited in Russian trans., M., 1956.)

2. G.M.Gorodinskii, A.N.Murin, V.N.Pokrovskii, B.K.Preobrazhenskii & N.E.Titov, Doklady, AN SSSR, 112, 405 (1957).

3. G.M.Gorodinskii, A.N.Murin, B.N.Pokrovskii & B.K.Preobrazhenskii. Izv. AN SSSR, Ser.fiz., 21, 1004 (1957). (Trans.Bulletin 21, No.7, 1005.)

4. G.M.Gorodinskii, A.N.Murin, V.N.Pokrovskii & B.K.Preobrazhenskii, Izv. AN SSSR, 21, 1624 (1957). (Trans.Bulletin 21, No.12, 1611.)

5. G.R.Rik, L.M.Krizhanskii & A.N.Dobronravova, PTE (Instruments & Experimental Techniques), 2, 90 (1956).

6. T.J.Ward, K.P.Jacob, J.W.Mihelich, B.Harmatz & T.H.Handley, Bull. Amer.Phys.Soc., Ser.II, 2, 259 (1957).

7. V.I.Baranovskii, A.N.Murin, V.N.Pokrovskii & Iutlandov, Present issue of the Bulletin, p.802.

8. J.W.Mihelich, B.Harmatz & T.H.Handley, Phys.Rev., 108, 989 (1957).

9. K.S.Toth, J.O.Rasmussen, Bull.Amer.Phys.Soc., Ser.II, 2, 386 (1957).

NEW NEUTRON-DEFICIENT RARE EARTH ISOTOPES. LUTETIUM ISOTOPE WITH MASS NUMBER 167.

- P.M.Aron, A.V.Kaliamin, A.N.Murin & V.A.Iakovlev

As a result of bombardment of tantalum with 660 Mev protons in the Joint Institute for Nuclear Research synchrocyclotron there were formed neutron-deficient isotopes of the rare earths, including some that were previously unknown.[1-5] In the chromatographically separated lutetium fraction we discovered a radioactive nuclide with a period of 55 ± 3 min.

This value for the period was obtained through resolution of the curve characterizing the growth and decay in intensity of a γ-line of ~100 kev energy, observed by means of a scintillation γ-spectrometer. The same line was observed in the spectrum of ytterbium chromatographically separated from the lutetium fraction 7 hours after the initial separation of the rare earth elements. The intensity of this line in the spectrum of the ytterbium fraction fell off with a period of 18 min. Both the γ-ray energy and the period agree within the limits of the experimental error with the tabular data for Yb^{167} ($T_{1/2}$ = 18 min; E = 118 kev).

In the spectrum of the thulium fraction separated simultaneously with the ytterbium from the lutetium fraction we observed the γ-lines characteristic of Tm^{167}. The intensity of the bright 207 kev γ-line fell off with a period of ~10 days (the tabular value for the period of Tm^{167} is 9.6 days). Thus we have unquestionable evidence of the existence of a hitherto unknown lutetium isotope, namely Lu^{167}:

$$Lu^{167} \xrightarrow[T = 55\ min]{E} Yb^{167} \xrightarrow[T = 18\ min]{E} Tm^{167} \xrightarrow[T = 9.6\ min]{E} Er^{167}\ (stable).$$

In addition to the above mentioned ~100 kev line we observed γ-lines having energies of ~170 and ~240 kev in the spectrum of the initially separated lutetium fraction. The ~170 kev line was also observed in the spectrum of the daughter ytterbium and its intensity (second after the intensity of the ~100 kev line) was found to fall off with a period close to that of Yb^{167}. The ~240 kev line was not observed in the ytterbium spectrum and hence must be attributed to Lu^{167}.

We desire to express our gratitude to V.P.Dzhelepov, Director of the Laboratory of Nuclear Problems of the Joint Institute for Nuclear Research, the crew of the Institute synchrocyclotron and B.K.Preobrazhenskii for his help in the initial search experiments.

"V.G.Khlopin" Radium Institute,
Academy of Sciences of the USSR

References

1. G.M.Gorodinskii, A.N.Murin, V.N.Pokrovskii & B.K.Preobrazhenskii, Doklady AN SSSR, 112, No.3, 405 (1957).

2. G.M.Gorodinskii, A.N.Murin, V.N.Pokrovskii & B.K.Preobrazhenskii, Izv. AN SSSR, Ser.fiz., 21, 1004 (1957). (Trans.Bulletin 21, No.7, 1005); 21, 1624 (1957), (Trans.Bulletin, 21, No.12, 1611.)

3. B.K.Preobrazhenskii, A.M.Lilova, A.N.Dobronravova & E.D.Teterin, Zhur. neorg.khim. (Jour.Inorganic Chemistry), 1, 2294 (1956).

4. B.K.Preobrazhenskii, A.V.Kaliamin & O.M.Lilova, ibid., 2, 1164 (1957).

5. J.Hollander, I.Perlman & G.Seaborg, (Table of Isotopes) Revs.Mod.Phys., 25, 469 (1953). (Cited in Russian trans., M. 1956.)

LUTETIUM ISOTOPE WITH MASS NUMBER 173

- G.M.Gorodinskii, A.N.Murin, V.N.Pokrovskii & B.K.Preobrazhenskii

Among the rare earth nuclides obtained by the spallation reaction on Ta, we discovered a long-lived Lu isotope with a period of ~200 days to which we assigned mass number A = 173.[1] Inasmuch as the indicated period differs from the value given for Lu^{173} in Seaborg's table[2] and is close to the period given for Lu^{174} (165 days), we undertook a separation of Lu from Hf for the purpose of verifying the above mass number assignment.

The dissolved tantalum target, 10 hours after bombardment with 660 Mev protons, was purified of the rare earths by precipitation with lanthanum. Several days after this the lutetium formed by decay of Hf was separated from the mother liquor by the usual procedure.

The γ-spectrum of the lutetium separated from the Hf and of the lutetium obtained by ion exchange separation from the radioactive rare earths were studied several months after separation when the activity of the short-lived Lu isotopes had died out. Prior to measurements, where necessary, we repurified the lutetium sources to remove Yb^{169} (32 days) forming as a result of disintegration of Lu^{169} (2 days).

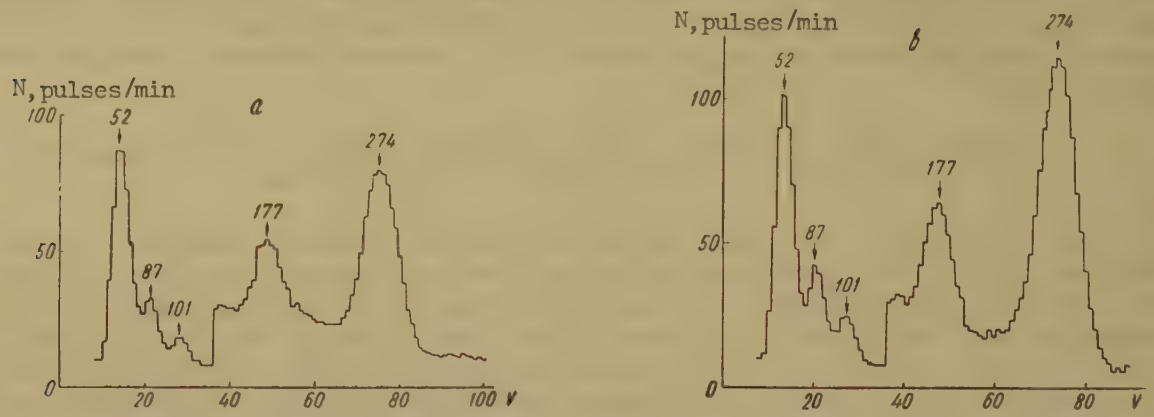

Fig.1. γ-spectrum of ~200-day Lu: a) Lu separated from the rare earths formed by spallation of tantalum; b) Lu separated from Hf. The horizontal scale is laid off in values of the discriminator bias.

Fig.1 shows the experimental γ-spectra of the long-lived Lu activity separated from the rare earths formed in spallation of tantalum (a) and of the Lu activity formed in the decay of Hf (b). Both spectra were recorded automatically on the same set-up. The discontinuity in the spectra corresponds to a change in the recording scale. It will be obvious from a comparison of figures a and b that both spectra have γ-lines of equal energies and close intensities. It should be noted that owing to the low activity of the Lu from Hf its spectrum is characterized by relatively lower statistical accuracy. It will be seen from a comparison of the spectra that at least the major portion of the activity of long-lived Lu is due to one and the same isotope with $T_{1/2} \approx 200$ days. Examination of Seaborg's Table of Isotopes[2] shows that the only Lu isotope remaining in the material separated from the Hf is Lu^{173}. Thus our earlier identification has been confirmed.

In a further study of the high energy part of the Lu^{173} γ-spectrum we detected γ-lines having energies of 345, 570 and 630 kev.* The relative intensi-

---

*At present we are only tentatively attributing the 570 and 630 kev lines to Lu^{173}.

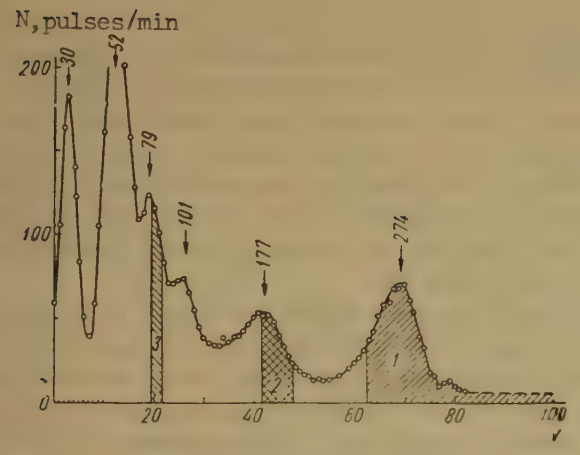

Fig.2. γ-spectrum of Lu^{173} recorded by the "stationary" channel of the coincidence set-up. The three hatched sections identify the settings of the "stationary" channel in investigating coincidences.

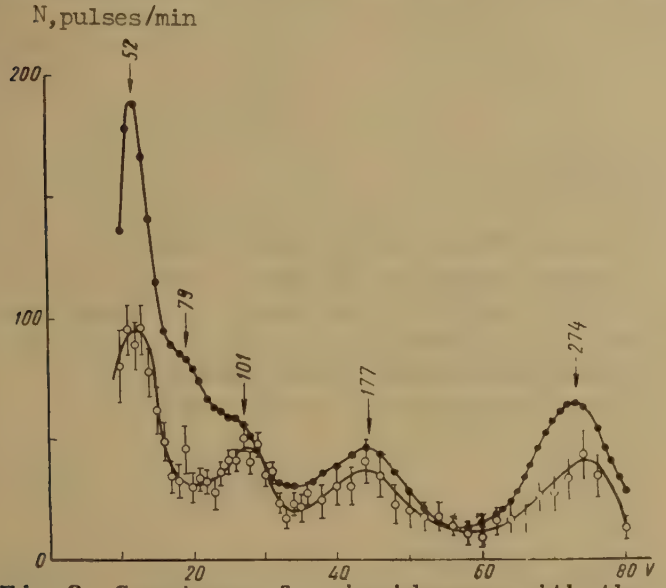

Fig.3. Spectrum of coincidences with the 79 kev γ-rays.

ties of the γ-lines of Lu^{173} are characterized by the following ratios:

$\gamma_{79}:\gamma_{101}:\gamma_{175}:\gamma_{274}:\gamma_{345}:\gamma_{570}:\gamma_{630}$ = 1 : 0.52 : 0.425 : 1.85 : 0.0113 : 0.15 : : 0.26.

The energy of the 175 ± 2 kev line differs appreciably from the energy of the 179.2 kev γ-rays identified from the conversion electron spectrum by Bobrov et al[3]. The same investigators detected the K line of a 171.2 kev transition (designated as line "c" in Ref.3), whence it follows that the 175 ± 2 kev line is the sum of lines with energies of 171 and 179 kev and comparable intensities ($\gamma_{171}:\gamma_{179}$ = 0.31:0.11).

In the first γ-γ coincidence experiments[1] it was established that all the γ-rays (77, 101, 175 and 274 kev) coincide in time with the emission of x-radiation, that the 79 and 101 kev γ-rays yield coincidences and, finally, that no coincidences are observed between the 175 and 274 kev γ-rays.

For purposes of further investigation of the γ-radiation from Lu^{173}, we carried out the following experiments. We studied in turn the coincidences of the 274, 175 and 79 kev γ-rays with the other radiations from Lu^{173}. The three hatched areas in the spectrum shown in Fig.2 correspond to the successive settings of the "stationary" channel of the coincidence set-up.

In investigating the coincidences of the 79 kev γ-rays with the other gammas, the x-ray radiation was attenuated by a factor of ~10 by means of a 0.3 mm thick lead absorber.

By way of illustration the spectrum of coincidences of the 79 kev γ-rays with the other γ-rays of Lu^{173} is shown in Fig.3. The upper curve is the spectrum recorded by the "scanning" channel simultaneously with the coincidence spectrum represented by the lower curve. We note that the energy resolution of the crystals and photomultipliers used in the coincidence circuit is inferior to the resolution of the single crystal γ-spectrometer; this explains the more "diffuse" appearance of the γ-spectrum (compare with Fig.1).

The results of the coincidence experiments may be summarized as follows.

The 79 kev γ-rays yield coincidences with the 101, 175 and 274 kev γ-rays; the 175 kev γ-line yields coincidences with the 101 kev line and self coincidences substantiating its composite character. Control experiments on coincidences of the 274 kev γ-rays with the other γ-rays substantiate the above.

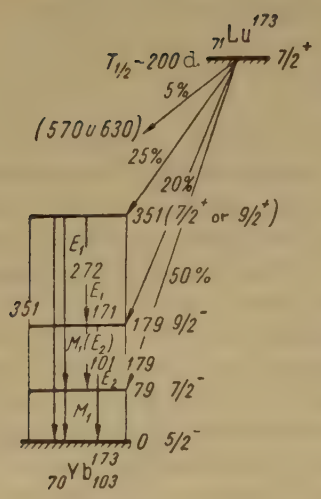

Fig.4. Decay scheme for Lu^{173}.

On the basis of joint discussions of the results obtained by Bobrov et al[3] and ourselves, we propose the decay scheme for Lu^{173} shown in Fig.4. We note that the indicated level populations represent the relative probabilities of transitions to the respective excited states. In view of the weak activity of our source it was impossible to establish the locations of the 570 and 630 kev transitions. Their relative abundances are less than 5%.

Using the decay scheme shown in Fig.4 and knowing the parameters of our γ-γ coincidence set-up, we calculated the relative probabilities for coincidences of the different γ-rays from Lu^{173}. The results of these calculations proved in satisfactory agreement with the experimental data.

In conclusion we desire to express our deep gratitude to the staff of the Laboratory of Nuclear Problems of the Joint Institute for Nuclear Research for assistance in the study and to K.Ia.Gromov and B.S.Dzhelepov for their interest in the work and discussion of their and our data.

"V.G.Khlopin" Radium Institute
Adacemy of Sciences of the USSR

References

1. G.M.Gorodinskii, A.N.Murin, V.N.Pokrovskii & B.K.Preobrazhenskii, Izv. AN SSSR, Ser.fiz., 21, 1004 (1957). (Trans. Bulletin 21, No.7, 1005.)

2. J.Hollander, I.Perlman & G.Seaborg (Tables of Isotopes) Revs.Mod.Phys., 25, 469 (1953). (Cited in Russian trans., M., 1956.)

3. Iu.G.Bobrov, K.Ia.Gromov, B.S.Dzhelepov & B.K.Preobrazhenskii, Izv. AN SSSR, Ser.fiz., 21, 940 (1957). (Trans.Bulletin 21, No.7, 942.)

RELATIVE INTENSITIES OF γ-TRANSITIONS IN Ho^{160}

- E.P.Grigor'ev, B.S.Dzhelepov & A.V.Zolotavin

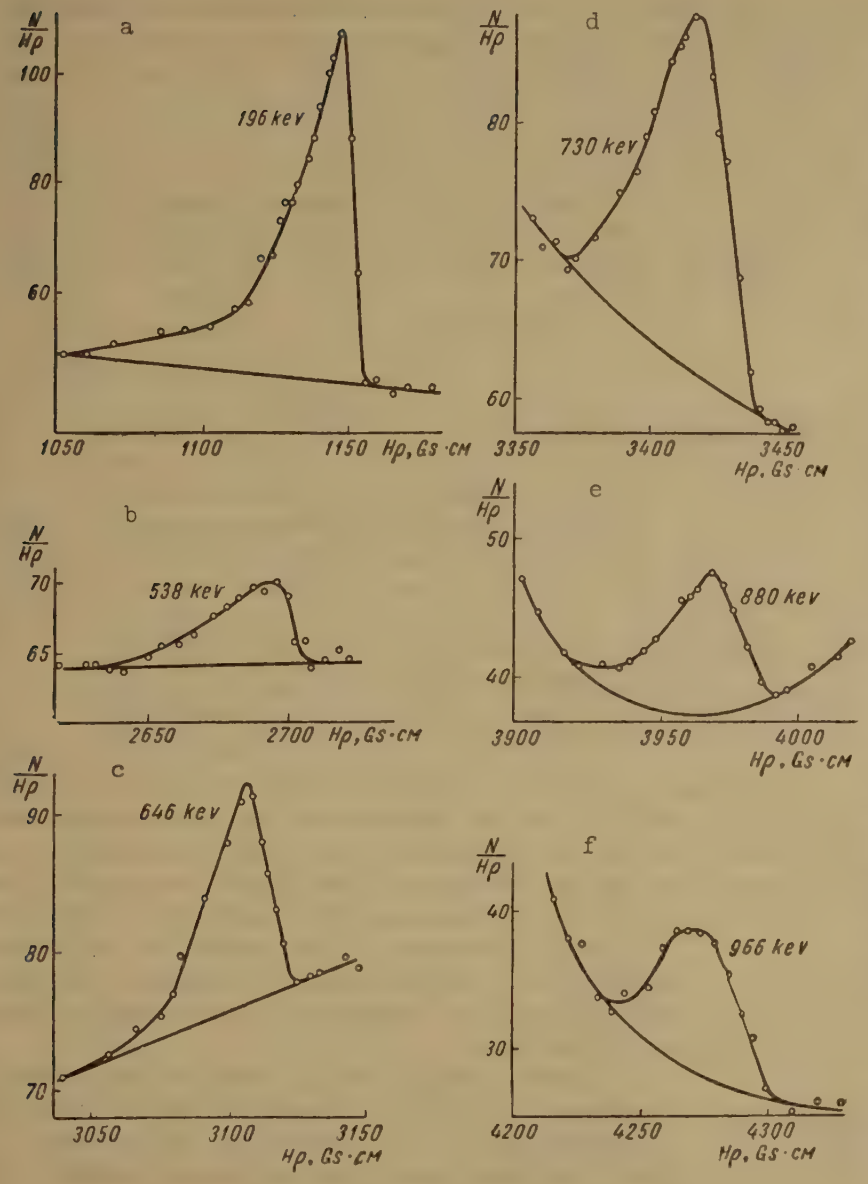

Fig.1. Photopeaks from the γ-rays of Ho^{160}. The 196 kev line was obtained with the 2.9 mg/cm^2 Bi target; the others with the 14.9 mg/cm^2 thick Bi target. The background under the lines is due to Compton recoils and conversion electrons penetrating the backing and the target.

Earlier we investigated the conversion electron and β^+-spectrum of Ho^{160} obtained by irradiation of a tantalum target with 660 Mev protons.[1,2] The comparatively strong activity of the source enabled us to investigate the relative intensities of the strongest γ-transitions on the same double-focusing β-spectrometer. To this end we twice (two different sources) studied the photoelectron spectrum of the Ho^{160} γ-rays, using a 4 mg/cm^2 thorium target (radiator) and 14.9±0.1 and 2.9±0.1 bismuth targets (Fig.1). The thick target was used for investigating the high energy lines; the 196 kev transition was investigated with the thinner target. Accurate knowledge of the thickness of the bismuth radiators enabled us to determine the ratios between the intensities of the 196 kev and harder γ-lines. The same source was used in these measurements (with bismuth targets of different thickness).

The target was made in the form of a semi-cylinder 3 mm in diameter; the source in the form of a narrow strip was mounted along the cylinder axis. The source thickness was of the order of a few micrograms per cm^2; a 0.2 mm thick layer of aluminum, onto which the target was cemented, served to absorb or attenuate the conversion lines. There was no noticeable absorption of the γ-rays in the target backing or in the source itself; the correction for absorption of photoelectrons in the target amounted to 5% for the 196 kev line.

As a result of the experiments there were determined the energies and intensities of the six strongest γ-transitions. The data are listed in Table 1.

Table 1

Energies and relative intensities of the strongest γ-transitions in Ho^{160}

No.	Bi target		Th target		Average values	
	$h\nu$, kev	I_γ	$h\nu$, kev	I_γ	$h\nu$, kev	I_γ
1	196,4	41			196,4	41±4
2	538,2	9,1	538,1	12,5	538,2	11±2
3	646,0	41,5	645,6	41,5	645,8	41,5±4
4	730,0	100	728,7	100	729,4	100
5	879,3	51			879,3	51±5
6	965,1	71			965,1	71±7

Table 2

Conversion coefficients and multipole orders of Ho^{160} transitions

No.	Transition, kev	I_γ	I_{e^-}	$\alpha_K \cdot 10^4$			Multipole order
				experimental	theoretical		
					$E2$	$M1$	
1	196,4	41,0±4	100±5		169,0		$E2$
2	538,2	10,8±2	2,25±0,15	14±6	10,2	20,9	$E2+M1$, $E2$
3	645,8	41,5±4	5,25±0,3	8,8±2,7	6,66	13,3	$E2+M1$, $E2$
4	729,4	100±5	6,9±0,4	4,8±1,2	5,04	9,89	$E2$
5	879,3	51±5	3,52±0,2	4,8±1,5	3,4	6,3	$E2+M1$, $E2$
6	965,1	71±7	3,9±0,3	3,8±1,2	2,8	5,0	$E2+M1$, $E2$

On the basis of the determined relative γ-rays intensities and the earlier data on the conversion spectrum of Ho^{160}, we can determine the conversion coefficients and the multipole orders of the transitions if we bear in mind that the 196 kev transition occurs between 4+ and 2+ levels of the first rotational band of Dy^{160}. Assuming the conversion coefficient of this transition to be equal to the theoretical one for electric quadrupole radiation, we obtain the conversion coefficients listed in Table 2.

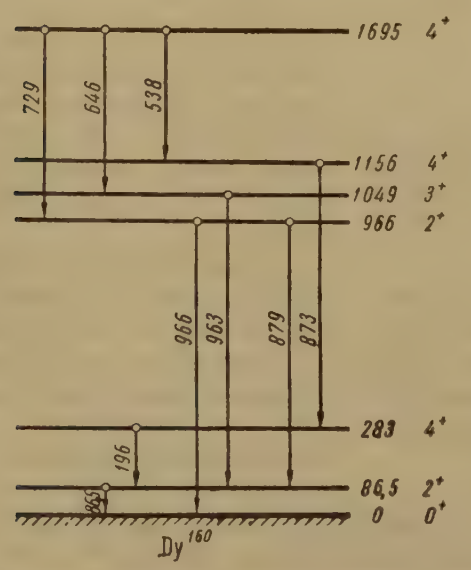

Fig.2. Diagram of the most densely populated levels of Dy^{160}.

These results fully confirm the level diagram for Dy^{160} proposed in Ref.2 and reproduced in Fig.2. The even (+) parity of the 1695 kev level has now been proved; the 4 spin assignment appears highly probable. In this case the 729 kev transition is E2, while the 646 and 538 kev transitions are either a mixture of E2 + M1 or E2; more accurate data are necessary to determine the proportions of the mixture. The 879 and 966 kev lines are complex[1] and one cannot speak of their multipole order; but since the characteristics of the levels between which these transitions occur are known, the choice of assignments is limited to E2, M1 or E2 + M1. The high energy component of the 963-966 kev doublet is pure E2 and, consequently,

the multipole order of the 963 kev transition must be either M1 or E2 + M1. Regarding the 873 and 879 kev transitions, at present we can only say that both are probably E2 + M1.

In the light of the above results we can evaluate the correctness of the balance of intensities in the decay of Ho^{160} drawn up in Ref.2; there we used the conversion line intensities and from the theoretical conversion coefficients for the inferred multipole orders determined the transition intensities. The present photoelectron spectrum measurements substantiate the intensities evaluated for the 538, 646, 873 + 879 and 963 kev transitions and show that there was a divergence of up to 30-40% as regards the intensity of the 730 kev transition.

We take this opportunity to thank the personnel of the Joint Institute for Nuclear Research and the Radium Institute for irradiation of the tantalum target and preparing the pure erbium and holmium sources.

Scientific Research Physical Institute,
Leningrad State University

References

1. E.P.Grigor'ev, B.S.Dzhelepov, A.V.Zolotavin, B.Kratsik, B.K.Preobrazhenskii & I.S.Ianchevskaia, Doklady AN SSSR, 117, 53 (1957).

2. E.P.Grigor'ev, B.S.Dzhelepov, A.V.Zolotavin, O.E.Kraft, B.Kratsik & L.K.Peker, Izv.AN SSSR, Ser.fiz., 22, 101 (1958). (Trans.Bulletin, 22, No.2, 99.)

3. M.A.Abroian, E.P.Grigor'ev & A.V.Zolotavin, Izv.AN SSSR, Ser.fiz., 20, 289 (1956). (Trans.Bulletin, 20, No.3, 271.)

4. M.P.Avotina, E.P.Grigor'ev, A.V.Zolotavin & B.Kratsik, Doklady AN SSSR, 119, 1127 (1958).

INVESTIGATION OF THE LOWER EXCITED LEVELS OF Th^{230} BY OBSERVING α-e_K COINCIDENCES

- A.P.Komar, G.A.Korolev & G.E.Kocharov

Recent years have seen increasing use of ionization chambers with a grid. The principal advantage of ionization chambers is their large acceptance angle, which allows of investigating weak α-lines, investigation of which on magnetic spectrometers is virtually impossible. In a number of cases the grid ionization chamber technique[1-3] has been used for investigating the fine structure of α-spectra.

We designed an apparatus for detecting α-e_K coincidences. The instrument consists of a pulse ionization chamber inside which is a proportional counter for detecting conversion electrons. We used this equipment for investigating coincidences between the α-spectrum of U^{234} and conversion electrons.

Description of the equipment

The pulse ionization chamber with the proportional counter is shown in Fig.

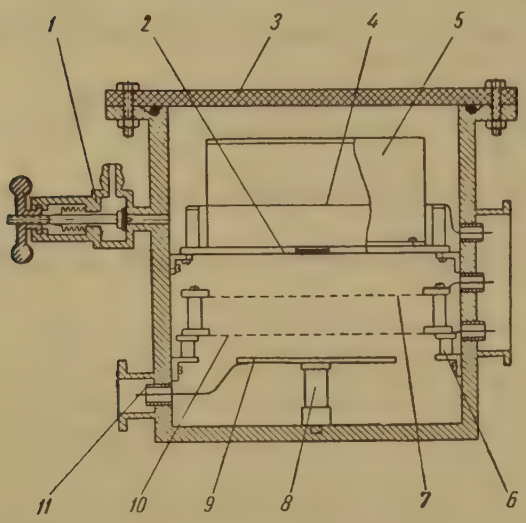

Fig.1. Ionization chamber with proportional counter: 1 - valve, 2 - electrode with source foil, 3 - plexiglass cover, 4 - proportional counter filament, 5 - cylindrical counter cathode, 6- insulator, 7 - first grid, 8 - insulator, 9 - collecting electrode, 10 - second grid, 11 - insulator.

The α-particle source is mounted on the high voltage electrode. The first grid 7 is intended for investigation of the angular distribution of particles, for example, investigation of α-e_K directional correlation and also for the introduction of electric collimation. The second grid 10 shields the collecting electrode from the influence of positive ions. The grids were prepared by spot welding of 0.1 mm diameter nichrome wire to a stainless steel ring. The separation between wires is 1.5 mm in the first grid and 3 mm in the second grid.

The distance between the high voltage electrode and the first grid is 50 mm; the distance between the grids is 20 mm; distance between the second grid and the collecting electrode is 15 mm. The "noneffectiveness" parameter of the two grids was determined experimentally; the determined value agreed with the calculated one[4].

We used a semicylindrical proportional counter with a cylinder diameter of 100 mm; the filament diameter was 0.012 mm. The experimentally determined evaluation of the gas amplification coefficient k as a function of the applied voltage is shown in Fig.2.

The particle source was a thin (<40 $\mu g/cm^2$) film of the active material 20 mm in diameter. The film source had good mechanical strength and uniform distribution of the active material. The distribution was checked radiographically. The technique of preparing such film sources is described in Ref.5. The chamber was evacuated to 10^{-4} mm Hg and filled with argon through a sodium purifier.

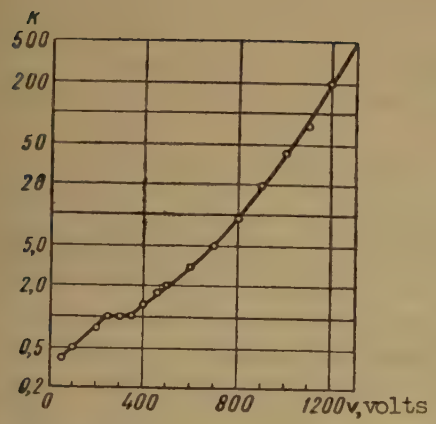

Fig.2. Variation of the gas amplification coefficient k as a function of the voltage on the 0.012 mm diameter filament at a pressure of 1.3 atoms. Cylinder diameter - 100 mm.

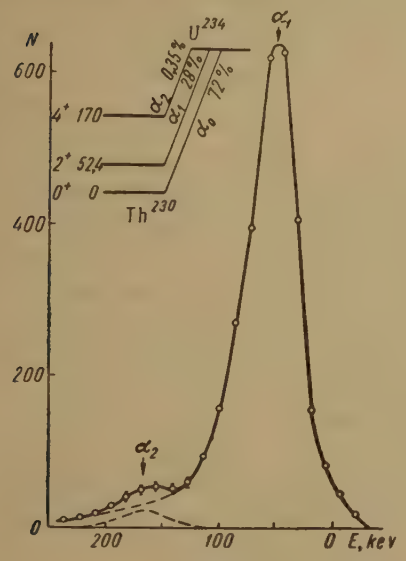

Fig.3. α-spectrum of U^{234}. Upper left - diagram of $U^{234} \rightarrow Th^{230}$ α-transitions.

The associated electronic equipment includes a preamplifier with a low noise level and has provision for suppressing the background of chance α-α coincidences. The instability of the electronic equipment over a period of 24 hours proved to be less than 0.2%.

α-particle spectrum of U^{234}

Investigation of the second excited level of Th^{230} by direct investigation of U^{234} α-particle spectrum was virtually impossible in practice due to the presence of the principal group of U^{235} α-particles which have an energy almost equal to that of the α_2 group, corresponding to the transition to the second level of Th^{230}. When the α-e_K technique is used, however, the principal group of U^{235} particles should not be detected.

The recorded spectrum is shown in Fig.3. As may have been expected, the principal α-particle groups of U^{234} and U^{235} do not appear. The α_2 group corresponds to a transition to the 2+ level of the daughter nucleus. This α-particle group has been investigated by Bochagov et al[2], Gol'din et al[7] and Valladas[8]. Analysis of the spectral curve allows of determining the intensity of the transition to the 4+ level. This intensity is found to be 0.35±0.15% (the intensity of the α_1 group is assumed to be known). The energy of the 4+ level is 170 kev, as follows from the unified nuclear model. According to Seaborg's table[9], the γ-spectrum of U^{234} contains 53 and 118 kev lines with intensities of 1 and 0.4. It may be assumed that the 53 kev γ-rays correspond to the transition from the 2+ to the ground level, while the 118 kev γ-rays correspond to the transitions from the 4+ level to the 2+ one. The cross-over transition from the 4+ level to the ground level has not been observed, although it is not necessarily precluded.

Using the theoretical values of the K and L shell conversion coefficients[10,11] and taking the experimental value for the ratio $N_{\gamma\text{-}53}/N_{\gamma\text{-}118} = 2.5$, we can calculate the intensity of the transition to the 4+ level. This calculated intensity agrees with the experimentally determined value of 0.35 %.

Valladas[8] investigated coincidences of U^{234} α-particles with x-rays. The value for the intensity of the transition to the 4+ level obtained by Valladas is 0.3%. Thus our data agree with those of Valladas within the limits of the experimental error.

We desire to express our indebtedness to B.A.Bochangov and S.N.Nikolaev for valuable advice on the experimental procedure and the electronic equipment.

Physical-Technical Institute,
Academy of Sciences of the USSR

References

1. D.W.Engelkemeir & L.B.Magnusson, Rev.Sci.Instr., 26, 295 (1955).
2. B.A.Bochagov, A.P.Komar, G.E.Kocharov, Zhur.eksp.i teor.fiz., 32, No.5, 1257 (1957). (Trans. JETP - Soviet Phys.)
3. S.A.Baranov, A.G.Zelenkov & Iu.F.Rodionov, Izv.AN SSSR, Ser.fiz., 21, 913 (1957). (Trans.Bulletin 21, No.7, 915.)
4. O.Bunemann, T.E.Cranshaw & J.Harvey, Can.J.Res., 27, 191 (1949).
5. G.A.Korolev & G.E.Kocharov, PTE (Instruments & Experimental Techniques), No.2 (1958).
6. B.A.Bochagov, G.E.Kocharov & G.F.Kirshin, PTE, 6 (1957).
7. L.L.Gol'din, E.F.Tret'iakov & G.I.Novikova,Reports presented at the 1-5 July 1955 meeting of the USSR Acad. of Sciences on Peaceful Uses of Atomic Energy.
8. G.Valladas, Dissertation, Paris, 1955.
9. J.Hollander, I.Perlman & G.Seaborg, (Tables of Isotopes) Revs.Mod.Phys, 25, 469 (1953). (Cited in Russian trans., M., 1956.)
10. L.A.Sliv & I.M.Band, Tablitsy koeffitsientov vnutrennei konversii gamma-izlucheniia (Tables of internal conversion coefficients) M.-L., 1956.
11. L.A.Sliv, Report presented at the Eighth All-Union Conference on Nuclear Spectroscopy, 1958.

INVESTIGATION OF Cs^{134} BY THE COINCIDENCE METHOD

- Iu.A.Aleksandrov

Introduction

Although there have been numerous investigations[1-11] of the decay of cesium 134 we cannot as yet unambiguously establish its decay scheme.

There can be little doubt regarding the existence of the following cascade transitions: 797-605, 605-570, 797-605-570, 605-1370 and 802-1170 kev. In the work of Ref.9, carried out by means of a fast-slow coincidence set-up, there was also observed a 605-460 kev cascade, the existence of which, however, is open to question inasmuch as in the spectrum reproduced in the report there is considerable statistical scatter and a large interfering admixture of coincidences with the 797 kev γ-rays.*

β-γ coincidences were studied in the work of Refs.10 & 11. It was found that the 605 and 797 kev γ-rays and a fraction of the γ-rays with energies of 563 and 570 kev yield coincidences with the hard component of the β-spectrum. In Ref.1 it is noted that there are coincidences between the 1370 kev γ-rays and the soft β-spectrum component.

The presence of hard γ-rays in the decay of Cs^{134} has been noted in Refs. 12 & 13. It was found that there exist γ-rays of energies 1640, 1750, 1870, 1960 and 2030 kev with intensities of the order of 10^{-6} photons per decay.

We undertook further investigation of the γ-γ and β-γ coincidences for the purpose of refining the decay scheme.

Apparatus and results

The measurements were carried out by means of scintillation spectrometers connected into a coincidence circuit with a resolving time of $2 \cdot 10^{-7}$ sec.

Each of the scintillation spectrometers consisted of an FEU-S photomultiplier and a 15 mm thick NaI(Tl) crystal. The relative half-width of the Zn^{65} γ-line was 8%. The stability of operation of the spectrometers was investigated with reference to the position of the Zn^{65} photopeak. After warm-up, the drift of the Zn^{65} photopeak with constant loading of the spectrometer did not exceed 0.5% over 20 hours continuous operation.

For detecting the β-spectrum we used an FEU-19M photomultiplier coupled to a tolane crystal 3 mm thick. The detecting efficiency of the tolane crystal as regards Cs^{134} γ-rays was 5%. The β-spectrometer was calibrated in energy with reference to the Hg^{203} conversion line.

For investigating the hard part of the Cs^{134} γ-spectrum we used a scintillation counter with a 15 mm thick NaI(Tl) crystal coupled to an FEU-11 photomultiplier. A lead absorber 10 cm thick was installed between the sources and the crystal. The activity of the source was approximately 500 millicurie.

We investigated the spectra of coincidences with the 605, 797, 1170 and 1370 kev γ-rays. The coincidence spectra were resolved into individual components on the basis of careful investigation of the shapes of the Hg^{203} 279 kev, Cs^{137} 660 kev and Zn^{65} 1120 kev lines recorded under the same experimental conditions.

---

*Stewart et al, listed under Ref.9, make no mention of 605-460 kev correlation. In general, the reference as listed in the original report appear to be thoroughly mixed up. We have corrected them only to the extent of attempting to correlate the authors with the proper Phys.Rev. volume and page numbers. Translation editor.

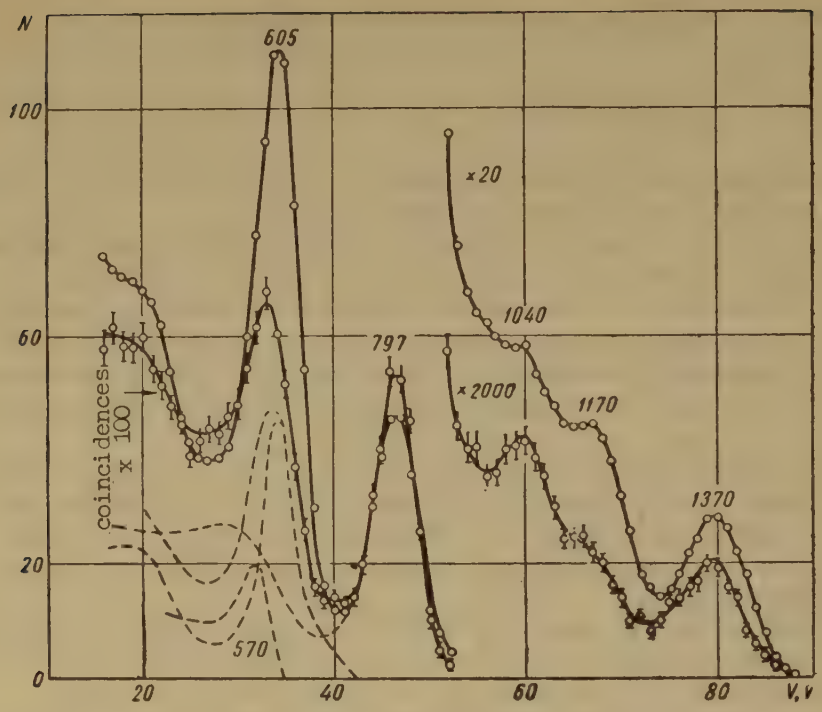

Fig.1. Spectrum of coincidences with the 605 kev γ-rays; ΔE_{set} = 570-700 kev.

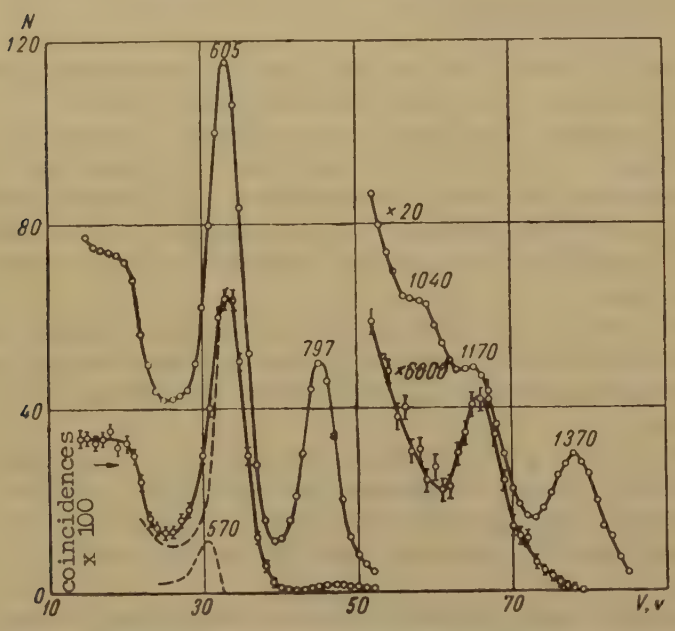

Fig.2. Spectrum of coincidences with the 797 kev γ-rays; ΔE_{set} = 740-870 kev.

Our measurements substantiate the existence of the 605-797, 605-1370, 605--570, 797-570 and 1170--802 (797) kev cascade transitions. Our results also indicate the existence of the following cascades: 605-1040 and 1170-475 kev.

The coincidence spectra and the corresponding sections of the single-spectrometer γ-ray spectrum are shown in Figs.1-4. The 570 and 475 kev photopeaks corresponding to the 570-605, 570-797 and 475--1170 kev cascades were obtained by resolution of the coincidence spectrum into individual components. The presence of interfering coincidences in the 400 to 600 kev region in Figs.1 & 3 is explained by the fact that in addition to the given photopeak part of the Compton distribution in the other γ-lines entered the "stationary" channel at the given setting.

We did not detect the 605-475 kev cascade mentioned in Ref.9. A search for the 475-1370 kev transition cascade, whose existence has been inferred by other authors, failed to yield positive results. According to our evaluations, the relative intensity of this presumed cascade cannot exceed 0.5%. For evaluating the relative intensities of the cascade transitions we used the data of Foster & Wiggins[6] on the relative intensities of Cs^{134} γ-rays.

The relative intensities of the cascade transitions according to our evaluations are the following:

605-797 kev	100%	797-570	10%
605-570	10%	1170-802(797)	3%
605-1370	3%	1170-475	2%
605-1040	3%		

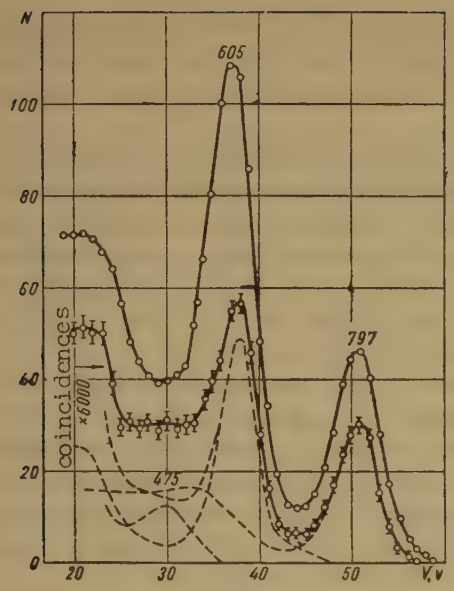

Fig.3

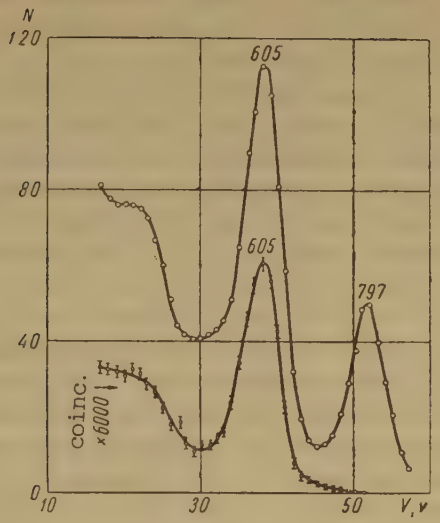

Fig.4

Fig.3. Spectrum of coincidences with the 1170 kev γ-rays; ΔE_{set} = 1150-1250 kev.
Fig.4. Spectrum of coincidences with the 1370 kev γ-rays; ΔE_{set} = 1300-1440 kev.

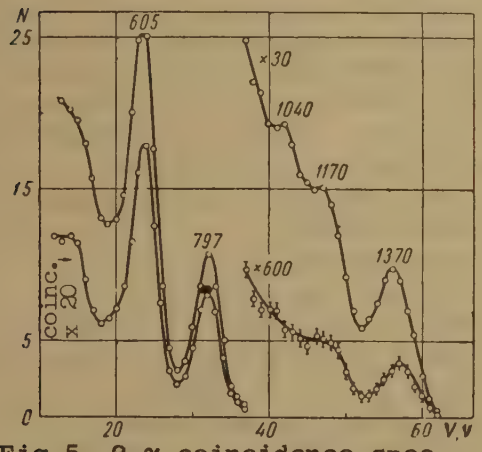

Fig.5. β-γ coincidence spectrum; ΔE^{β}_{set} = 360-660 kev.

In investigating β-γ coincidences, we discriminated the 360 to 660 kev section of the β-spectrum. In this case the γ-radiation background amounted to about 5%. It was subtracted accordingly in reducing the results.

From analysis of the coincidence spectrum, shown in Fig.5, it is evident that the hard part of the β-spectrum yields more coincidences with the 797 kev than with the 605 kev γ-rays, which is in agreement with the results of Keister, Lee & Schmidt[10]. It was found that part (30-50%) of the 1370 kev γ-rays are in coincidence with the hard part of the β-spectrum. These coincidences cannot be explained by the γ-background or by summation of the scintillations in the crystal inasmuch as the thickness of the crystal and the solid angle subtended by the source are too small.

If we take the intensity of the coincidences of the hard part of the β-spectrum with the 797 kev line as 100%, then the intensity of the coincidences with the 605 kev γ-rays is of the order of 90% and the intensity of the coincidences with the 1370 kev γ-rays is of the order of 2%.

We also investigated the high energy region of the Cs^{134} γ-spectrum. We observed photopeaks from γ-rays of 1640, 1750, 1870, 1960 and 2040 kev energy. The intensity of all these γ-rays is of the order of 10^{-6} photons per disintegration. In order to make sure that these γ-rays were not due to some impurity in the Cs^{134} source, the spectrum was investigated two times with an interval of one year between measurements. No changes in the relative intensities of the γ-lines were observed.

All our experimental data on β-γ coincidences and the hard part of the Cs^{134} γ-spectrum are consistent with the decay scheme proposed by Foster & Wiggins[6]

with the addition of the high energy γ-transitions[13]. The only disagreement is for the 475 kev γ-transition which, according to our data, should be located between the 1644 and 1168 kev levels rather than between the 1870 and 1368 kev levels, as shown in Ref.6.

From the results of our β-γ coincidence measurements it may be inferred that part of the 1370 kev γ-transitions goes to the ground state of Ba^{134}. The spin and parity of the 1370 kev level are 3-. In this case the 1370 kev γ-transition must be E3, whereas according to the data of many authors this γ-transition should be either E1 or E2. This difficulty can be obviated if we assume that the spin and parity of the 1370 kev level are either 1- or 2-, but then the probability of the β-transition from the ground state of Cs^{134} with spin 4+ to the 1370 kev level will be too low. The presence of 1370-605 kev γ-γ coincidences leads us to infer that there exists a second 1370 kev or a second 605 kev γ-transition. The first alternative is more acceptable inasmuch as there are reported to be coincidences between the 1370 kev γ-rays and the soft part of the β-spectrum, although it must be admitted that the presence of these coincidences can also be explained by the existence of a second γ-transition of 605 kev energy.

In conclusion I desire to thank S.V.Golenetskii who was of great assistance in carrying out the investigation.

Leningrad State University

References

1. L.G.Elliot & R.E.Bell, Phys.Rev., 72, 979 (1947).
2. E.R.Brady & M.Deutsch, Phys.Rev., 78, 558 (1950).
3. J.R.Beyster & M.L.Wiedenbeck, Phys.Rev., 79, 411 (1950); M.A.Waggoner, M.L.Moon & A.Roberts, Phys.Rev., 80, 420 (1950) .
4. M.Kloepper, E.S.Lennox & M.L.Wiedenbeck, Phys.Rev., 88, 695 (1952).
5. D.C.Lu & M.L.Wiedenbeck, Phys.Rev., 94, 501 (1954).
6. H.H.Foster & J.S.Wiggins, Nuovo Cim., 2, 854 (1955).
7. A.E.Everett & M.J.Glaubman, Phys.Rev., 100, 955 (1955).
8. Girish, Chandra, Proc.of Indian Academy of Science, 44, 194 (1956).
9. M.G.Stewart, R.P.Scharenberg & M.L.Wiedenbeck, Phys.Rev., 99, 691 (1955).
10. G.L.Keister, E.B.Lee & F.H.Schmidt, Phys.Rev., 97, 451 (1955).
11. L.Bertolini, M.Bettoni & E.Lazzarini, Nuovo Cim., 2, 273 (1955).
12. E.I.Firsov & A.A.Bashilov, Izv.AN SSSR, Ser.fiz., 21, 1633 (1957). (Trans.Bulletin 21, No.12, 1619.)
13. R.G.Fluharty & M.Deutsch, Phys.Rev., 76, 182 (1949).

RADIATION FROM As^{74}

- E.P.Grigor'ev, B.S.Dzhelepov, A.V.Zolotavin, V.Ia.Mishin, V.P.Prikhodtseva, Iu.V.Khol'nov and G.E.Shchukin

In December 1957 we were able to obtain a radiochemically pure sample of As^{74} (~4 millicurie) with a good specific activity. The principal features of the decay of As^{74} being fairly well known, we undertook our investigation primarily for the purpose of verifying and refining the different characteristics of this decay.

1. Source

The As^{74} was prepared by bombardment of germanium with 10.8 Mev deuterons. After separation of the germanium in the form of $GeCl_4$, the arsenic was purified by the procedure described by Green & Kafalas[1], converted to AsH_3 and then deposited as a speculum layer on a quartz tube. The source for the β-measurements was further sublimated onto an aluminum foil (10 μ) from which a 25 x 1 mm strip was cut. To provide for complete absorption of the positrons and full transmission of the annihilation radiation, the source for the γ-measurements was encapsulated in copper.

2. Investigation of the β^+- and β^--spectra

The measurements were carried out on a double focusing β-spectrometer with a resolution $\Delta H\rho/H\rho = 0.4\%$. The β^+- and β^--spectra of As^{74} consists of two components each (Figs.1 & 2). The energies and relative intensities of the components are listed in Table 1.

Table 1

Energies and relative intensities of the As^{74} β^+- and β^--spectra

Spectrum components	Our data		Mei et al[3]		Johansson et al[4]	
	$E_{e.p.}$, kev	Relative intensity	$E_{e.p.}$, kev	Relative intensity	$E_{e.p.}$, kev	Relative intensity
β_1^+	1510±15	24±5	—	—	1530	19
β_2^+	910±10	180±10	960	95	920	160
β_1^-	1355±10	122±10	1450	89	1360	104
β_2^-	720±15	100	820	100	690	100

In order to resolve the β-spectra into components one must know the shape of the respective high energy components. Fig.2 shows that the high energy components are closest to the unique shape ($\Delta I = 2$, yes): the Kurie plot is most nearly rectilinear if one takes into account the correction factor for unique transitions[5]. In this case the experimental points fall on a straight line within the limits of the experimental error, while without the correction factor, C_{uniq}, the deviation from a straight line is appreciable. Johansson et al[4] established only that the β^- component is of the uniquely forbidden shape. One cannot unambiguously classify the β_1^+- and β_1^--transitions as unique solely on the basis of the shape of the spectra. There is, however, another stronger argument: the product $ft(W_0^2-1)$ calculated according to the data shown in the decay scheme (Fig.5) equals $0.8\cdot10^{10}$ for β_1^+ and $0.5\cdot10^{10}$ for β_1^-. For most unique transitions this product lies in the range from $0.5\cdot10^{-10}$ to $1.8\cdot10^{-10}$, despite the considerable diversity of the disintegration energies W_0.[6] Assuming that these transi-

tions are uniquely forbidden, we must infer that the spin and parity of the ground state of As^{74} are 2-.

The Kurie plots for the soft components of both spectra, obtained after subtraction of the unique spectra, proved to be linear. The upward deviation of the experimental points in the region under 300 kev (Fig.2) is explained by the relatively large thickness of the source. This effect has been observed in investigating other isotopes, for example, P^{32}, with the same source thickness.

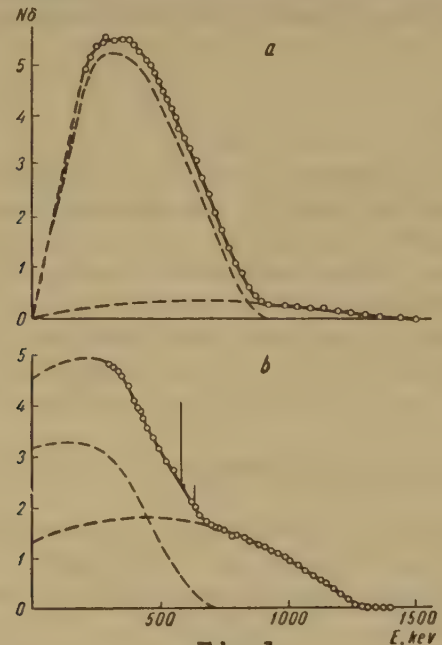

Fig.1

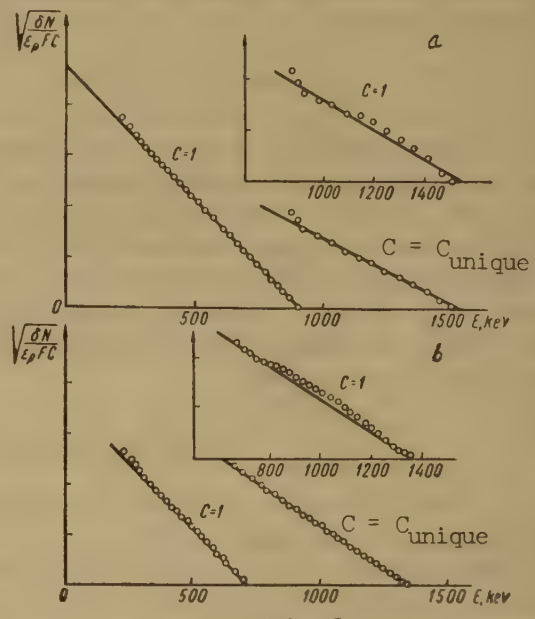

Fig.2

Fig.1. a) Positron spectrum of As^{74}; b) electron spectrum of As^{74}.
Fig.2. Kurie plot for As^{74}; a) positron spectrum, b) electron spectrum. The inserts show the Kurie plots of the hard components without the unique correction. The size of the circle points indicates the experimental uncertainty.

3. Conversion Electrons

Table 2
Energies and relative intensities of As^{74} conversion lines

Conversion line	Intensity of line referred to that of the β_2-spectrum taken as 100	Relative line intensity
K-596	0.48±0.04	1.00
$(L+M)$-596	0.06±0.01	0.12
K-635	0.137±0.014	0.28

The K and L + M conversion lines associated with the 596 and 635 kev γ-transitions stand out clearly against the β-spectrum background (Fig.3). The data pertaining to these lines are listed in Table 2.

The transition energies were determined most accurately, apparently, in the work of Johansson et al[4]: 596.3 ± 1.10 and 635.2 ± 1.0 kev; accordingly, below we shall use these energy values. The energies determined in our experiments differ from the cited values by 0.2%. From the relative intensity of the K-635 line and the soft component of the β^--spectrum, we obtain for the K conversion coefficient

$$\alpha_K = (1.37 \pm 0.14)\cdot 10^{-3}.$$

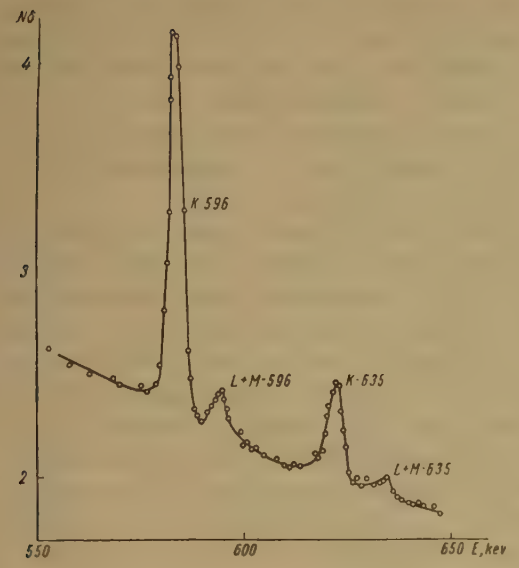

Fig.3. Conversion lines associated with the 596 and 635 kev γ-transitions.

This value is close to the theoretical one[7] for E2 type transitions, namely, $\alpha_K = 1.30 \cdot 10^{-3}$. Thus there can be no doubt that we are dealing with a 2+→0+ type transition common to even-even nuclei.

The situation is somewhat more complicated as regards the 596 kev transition associated with the positron branch, inasmuch as for determining α_K in this case one must know the K branching ratio. We shall return to this question in Section 6 below.

4. Gamma-Rays

The γ-ray spectrum of As^{74} was investigated by observing recoil electrons on two different Ritron[8,9] type spectrometers. The instrument with the higher resolution was used for measuring the relative intensities of three γ-lines: annihilation, 596 and 635 kev. The lines are shown in Fig.4; pertinent data are listed in Table 3. The 596 and 635 kev lines could not be fully separated, but the resolution of the spectrum into components was carried out on the basis of the shape of the thoroughly studied annihilation and 603 kev lines of Sb^{124}.

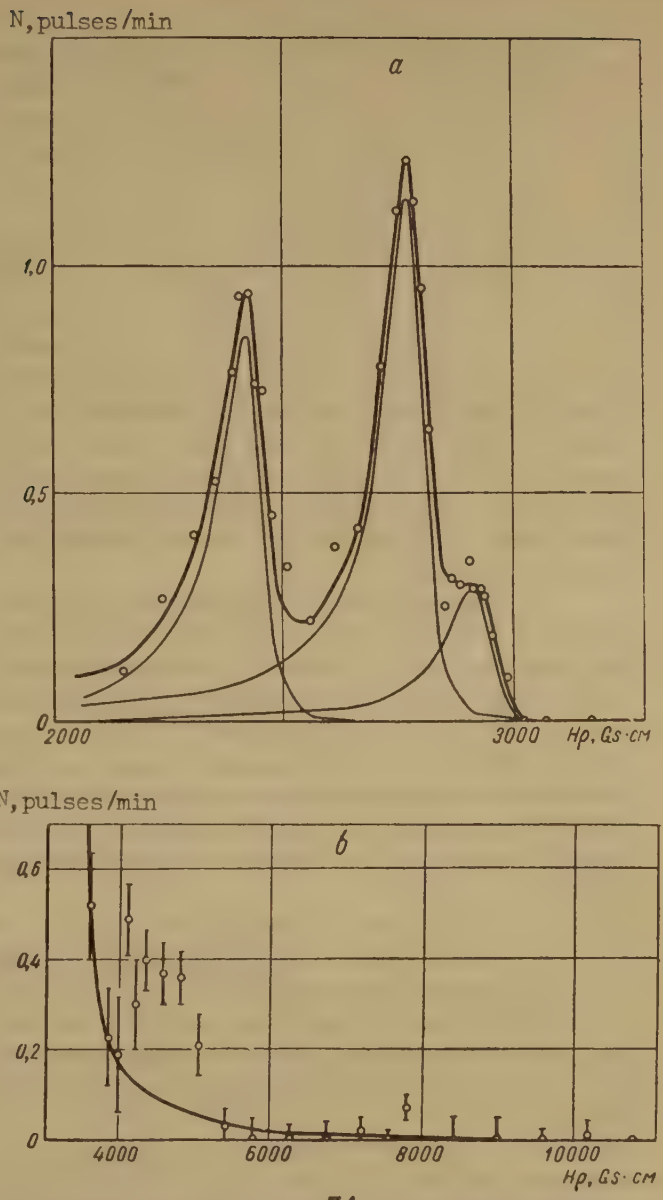

Fig.4. γ-spectrum of As^{74}: a) soft section of the spectrum obtained on a Ritron spectrometer under ordinary conditions; b) hard section of the spectrum obtained on a Ritron with an enhanced transmission factor.

The Ritron spectrometer with poorer resolution but with ~100-fold increased transmission was used to search for the harder γ-lines in the radiation from As^{74};

Table 3

Relative intensities of As^{74} γ-rays

$h\nu$, kev	Our data	Johansson et al[4]
511	4.06±0.12	—
596	4.22±0.12	4
635	1	1
1200	0.018±0.005	—
>1200	<0.004	—

in view of the $As^{74} \rightarrow Gd^{74}$ disintegration energy one may expect to find excited levels of Ge^{74} up to 2500 kev. Actually, there was observed a definite rise in the counting rate above the smooth background, due to the softer γ-rays, in the 1200 kev region (Fig.4,b). The intensity of this line is approximately 1/220 that of the annihilation line.

A line of this energy has not hitherto been observed in the decay of As^{74}, but in 1955 Sinclair[10] reported that incident to bombardment of Ge with fast (4.4 Mev) neutrons there is excited a γ-line of 1230±50 kev energy. In 1957 he published revised confirmatory data: the γ-rays have an energy of 1230±19 kev; the excitation occurs in Ge^{74} and the excitation probability is 17 times lower than for the 596.3 kev level. Soon thereafter (1958) Eichler et al[12] reported that they observed γ-lines with the following energies in the decay of Ge^{74}: 600, 860, 1100, 1500, 1900 and 2300 kev. It is reasonable to assume that Sinclair, Eichler et al and we observed the same transition with an energy of about 1200 kev.

In neighboring even-even nuclei the second excited level is usually located 2.0-2.2 times higher than the first level (for example, Zn^{65}, Se^{76}, Kr^{82} and Kr^{84}). In view of this, there is a good probability that the second level of Ge^{74} has an energy of ~1200 kev which is almost twice the energy of the first level (596.3 kev). If this is the case, it may be hypothesized that there may also exist a transition from this second level to the first one, a transition having an energy of about 600 kev and forming a doublet with the 596 kev γ-rays. However, the ~1200 kev level is weakly excited both in the decay As^{74} and in neutron excitation. There is no mention of doublet structure of the 596 kev line in the literature.

5. Branching in the As^{74} Decay Scheme

The decay scheme for As^{74} is shown in Fig.5. Our problem is to determine the values of a, b, c, d, e, f and g ($a+b+c+d+e+f+g = 100\%$).

We have the following equations deriving directly from our experimental data:

$$e : d : f : g = (24 \pm 5) : (180 \pm 10) : (122 \pm 10) : 100 \qquad (1)$$

(ratios of the β-spectra intensities - Table 1), and

$$2(d+e) : (b+d) : g : a = (4.06 \pm 0.12) : (4.22 \pm 0.12) : 1 : (0.018 \pm 0.005) \qquad (2)$$

(ratios of the γ-line intensities - data of Table 3; we are tentatively assuming here that the 1200 kev γ-transition is the only mode of de-excitation of this level).

These equations are not entirely independent: it follows from (1) that $2(d+e):g$ = 4.08±0.22, while from (2) we have $2(d+e):g$ = 4.06±0.12.

The deduced values are in good agreement and we can average them, but nevertheless, one of our equalities disappears, and thus we have only six equations for determining seven unknowns. It will be noted, however, that c, the probability of capture to the ground state of Ge^{74}, is not comprised in any one of the experimental equations. Neither we, nor apparently anyone else, has

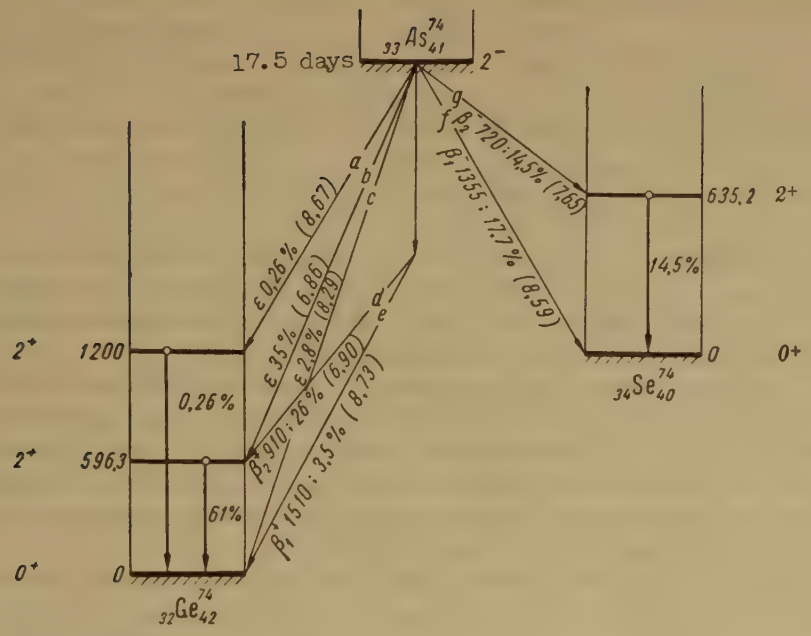

Fig.5. Decay scheme for As^{74}.

measured any parameters connected with capture to the ground level of Ge^{74}. Such parameters might be:

a) the ratio of intensities of the x-rays to any γ-ray,

b) the ratio of the intensities of the Auger electrons to any conversion line or

c) the fraction of x-ray quanta yielding coincidences with the 596.3 kev γ-rays.

We can get around the quandary by using theoretical value of K/β^+ for the decay of As^{74} to the Ge^{74} ground state. Fortunately, this transition is a unique one and hence the ratio can be calculated unambiguously inasmuch as the matrix element involved drops out.

L.N.Zyrianova informed us that for the transition in question

$$\frac{K + L_I + L_{II}}{\beta^+} = \frac{c}{g} = 0.797.$$

Adding this equation to those listed above we can readily solve the entire set of equations and as a result we obtain

$$a = (0.26 \pm 0.07)\ \%, \qquad e = (3.5 \pm 0{,}7)\ \%,$$
$$b = (35 \pm 3)\ \%, \qquad f = (17.7 \pm 1.5)\ \%,$$
$$c = (2{,}8 \pm 0{,}5)\ \%, \qquad g = (14.5 \pm 0.4)\ \%.$$
$$d = (26.4 \pm 1{,}6)\ \%,$$

These are the values we have inserted in Fig.5.

6. Remarks Concerning Individual Levels

A. Conversion of the Ge^{74} 596.3 kev transition

Conversion coefficient α_K for the 596.3 kev transition can be determined in two ways:

a) from the intensity ratios of the 596.3 kev and 635.2 kev γ-rays and the

corresponding conversion lines

$$\alpha_{K\text{-}596} = \alpha_{K\text{-}635} \cdot \frac{N_{K\text{-}596}}{N_{K\text{-}635}} \cdot \frac{N_{\gamma\text{-}635}}{N_{\gamma\text{-}596}} = 1.30 \cdot 10^{-3} \cdot \frac{0.49 \pm 0.04}{0.137 \pm 0.014} \cdot \frac{1}{4.22 \pm 0.12} =$$
$$= (1.10 \pm 0.15) \cdot 10^{-3};$$

b) from the ratio of two experimentally determined values:

$$\alpha_{K\text{-}596} = \frac{N_{K\text{-}596}}{N_{\beta^-\text{-}720}} \cdot \frac{N_{\gamma\text{-}635}}{N_{\gamma\text{-}596}} = \frac{(0.48 \pm 0.04)\, 10^{-2}}{4.22 \pm 0.12} = (1.14 \pm 0.10)\, 10^{-3}.$$

The two methods are not entirely independent: in both use is made of the ratio $N_{\gamma\text{-}635} / N_{\gamma\text{-}596}$; in the former case, however, use is made of the ratio of the areas under the two conversion lines, while in the latter case use is made of the areas under the lines and the continuous spectrum.

The two values are in good agreement with each other but not with the theoretical conversion coefficient for E2 transitions: $\alpha_K = 1.43 \cdot 10^{-3}$.

The reason for this divergence is not clear. A small admixture of the hypothetical 604 kev transition, which could be M1, does not alter the situation inasmuch as the conversion coefficient for M1 type transitions is $1.02 \cdot 10^{-3}$, i.e., differs little from α_K for E2 ($1.43 \cdot 10^{-3}$).

Utilizing the data of Table 2 and setting M/L equal to 0.2, we obtain for this transition

$$K/L = 9.6 \pm 2.1.$$

This value is in good agreement with the theoretical one for E2 transitions, namely, K/L = 9.4; it is also not inconsistent with the theoretical value for M1, namely, K/L = 10.

B. Value of K/β^+ for the decay of As^{74} to the 596.3 kev level of Ge^{74}

Above, in Section 5, we found

$$\frac{N_{\varepsilon\text{-}910}}{N_{\beta^+\text{-}910}} = \frac{35 \pm 3}{26.4 \pm 1.6} = 1.32 \pm 0.14.$$

Taking L/K = 0.10, we obtain

$$\frac{K}{\beta^+} = 1.20 \pm 0.14.$$

For allowed transitions of this energy[5,13]

$$\frac{K}{\beta^+} = \frac{f_k}{f^+} = \frac{1.66}{1.37} = 1.21.$$

For a first forbidden 2→2+ transition the value of K/β^+ can differ slightly from that given above. In any case we can conclude that the K/β^+ ratio for this transition is normal.

C. 1200 kev level of Ge^{74}

In evaluating the intensity of the As^{74}→1200 kev Ge^{74} transition, it was assumed that emission of the 1200 kev γ-rays is the only form of de-excitation of this level. As noted above, however, it is possible that there also exists a γ-transition of energy 1200 - 596 = 604 kev, which has not been observed because it is masked by the 596 kev γ-transition. The 1200 kev level in Ge^{74} is probably a second vibrational one. The possible assignments for a second vibrational level in general are 0+, 2+ and 4+; the 0+ assignment, however, is pre-

cluded inasmuch as there is a γ-transition to a level with 0+. Let us consider the two remaining alternatives.

If the spin of this level is 2+, we can attempt to determine the ratio of the 2+→2+ and 2+→0+ transition intensities by analogy with the neighboring nuclei inasmuch as Deliagin & Shpinel'[14] have shown that this ratio changes gradually in going from nucleus to nucleus. In Zn^{66} and Ge^{72} it equals 2; in Se^{76} it equals 1.12. If we take an average value of 1.5, then we must increase by a factor of 2.5 (to 0.65%) the fraction of As^{74} decays to the 1200 kev level of Ge^{74}. The ratio of intensities of the hypothetical "604" and observed 596 kev γ-lines should be 0.39:61 = 1:150. With this intensity ratio the "604" line could hardly be detected (even from γ-γ "self-coincidences").

If the assignment for the 1200 kev level is 4+, the ratio of intensities of the 604 and 1200 kev levels should be much greater - the Weisskopf-Moszkowski single-particle formulas yield a value of $2\cdot10^7$ - and in this case the 1200 kev line would be so faint as to be virtually undetectable (as in the case of Mg^{24}, Ti^{46}, Ti^{48}, Cr^{52}, Ni^{60}, Ge^{72} and similar nuclides).

Thus it would appear that we should give preference to the 2+ assignment.

β^+-decay of As^{76} to such a level must be of the 2-→2+ type, i.e., first forbidden and in addition hindered with respect to the quantum number (the 1200 kev level is a two-quantum vibrational one). In the analogous case of As^{76}→1210 kev Se^{76}, the value of log ft is 8.5. A not dissimilar situation obtains in our case:

$$E_{e.p.} = 320 \text{ kev}; \quad E_0 = 0.625;$$

$$\frac{f_k}{f^+} = 50; \quad \prod = \frac{0{,}65\,\%}{50} = 12\cdot10^{-3}\,\%;$$

$$f^+ = \Phi(E_0)\,S(E_0) = 0.053\cdot0{,}289 = 1{,}5\cdot10^{-2} \quad \text{and} \quad \lg f^+t = 8.2.$$

Thus no inconsistencies arise.

D. Hard γ-rays and the β^--branch

The second excited level of Se^{74} probably lies near 1300 kev and is characterized by 2+. It may be excited in the decay of As^{74}, but the probability of such excitation is very low: with log ft = 8.8 and $E_{e.p.}$ = 50 kev, the excitation probability is ~10^{-4}%.

E. Competition of β^+- and β^--decay of As^{74}

The decays of As^{74} to the Ge^{74} and Se^{74} ground levels should be equally forbidden and the products $(W_0^2-1)ft$ should in the first approximation be equal. In the second approximation this product characterizes the nuclear structure: it should be smaller for the transition that brings the nucleus closer to a closed shell.[15]

In our case, as a result of the decay $_{33}As^{74}_{41} \rightarrow {}_{34}Se^{74}_{40}$ there is obtained a nucleus with a closed 40 neutron subshell. And we actually find that for this transition the product $(W_0^2-1)ft$ is smaller by a factor of 1.65 (the respective values being $0.47\cdot10^{10}$ and $0.78\cdot10^{10}$) and ft is smaller by a factor of 1.38 ($3.9\cdot10^8$ and $5.4\cdot10^8$) than for the transition to the Ge ground state. A similar situation obtains for transitions to the first excited (2+) states of Ge^{74} and Se^{74}: ft in this case is smaller by a factor of 5.6.

We take this occasion to thank B.M.Isaev, I.P.Selinov, E.E.Baroni, E.N.Khoprov and their collective for assistance in the work.

References

1. M.Green & J.Kafalas, J.Chem.Phys., 22, 760 (1954).
2. A.V.Zolotavin, Izv.AN SSSR, Ser.fiz., 18, 127 (1954).
3. J.Mei, A.Mitchell & C.Huddleston, Phys.Rev., 79, 19 (1950).
4. S.Johansson, J.Couchois & K.Siegbahn, Phys.Rev., 82, 275 (1951).
5. B.Dzhelepov & L.Zyrianova, Izv.AN SSSR, Ser.fiz., Vol.20 A nonexistent page is given in the Russian; no such Ref. in Vol.20. Translator.
6. F.Shull & E.Feenberg, Phys.Rev., 75, 1768 (1949).
7. L.A.Sliv & I.M.Band, Tablitsy koeffitsientov vnutrennei konversii gamma-izlucheniia (Tables of internal conversion coefficients), M.-L., 1956.
8. B.S.Dzhelepov, N.N.Zhukovskii & Iu.V.Khol'nov, Izv.AN SSSR, Ser.fiz., 18, 599 (1954). (Trans.Bulletin, 18, No.5, 285.)
9. B.S.Dzhelepov, B.K.Preobrazhenskii, Iu.V.Khol'nov & G.E.Shchukin, Report presented at the Eighth All-Union Conference on Nuclear Spectroscopy, 1958.
10. R.Sinclair, Phys.Rev., 99, 621 (1955).
11. R.Sinclair, Phys.Rev., 107, 1306 (1957).
12. E.Eichler, N.Johnson & G.O'Kelley, Bul.Amer.Phys.Soc., 3, 62 (1958).
13. I.M.Band, L.N.Zyrianov & Tsin Chen-Zhui, Izv.AN SSSR, Ser.fiz., 20, 1387 (1956). (Trans.Bulletin 20, No.12a, 1269.)
14. N.N.Deliagin & V.S.Shpinel', Zhur.eksp.i teor.fiz., 32, 373 (1957). (Trans.Soviet Phys. - JETP.)
15. B.S.Dzhelepov & L.K.Peker, Doklady AN SSSR, 106, 626 (1956).

GAMMA-SPECTRUM OF Lu^{171}

- A. I. Lebedev, A. N. Silant'ev & I. A. Iutlandov

Among the nuclides formed as a result of bombardment of tantalum with fast protons are radioactive Lu isotopes. The presence of radioactive Lu isotopes with a period of about 8 days in the spallation product has been reported by Nevirk & Seaborg[1] and the Preobrazhenskii group[2]. The observed activity was ascribed to Lu^{171} or Lu^{172}. In the investigation of Ref.3 there were detected γ-lines of ~180, 730 and 1100 kev energy in the spectrum of the ~8 day activity. The study of Ref.4 was concerned with the conversion electron spectrum of ~8 day Lu; there were observed conversion electrons corresponding to 75.8, 90.6 and 181.7 kev γ-rays. The Preobrazhenskii group also studied[5] the conversion electron spectrum of Lu separated from Hf, originally produced by the spallation reaction on tantalum. The authors attribute the observed conversion electrons, corresponding to γ-rays of 26.7, 65, 75.8 and 90.6 kev energy, to Lu^{171}. Finally, the group investigated[6] coincidences between the conversion electrons formed in the decay of Lu^{171} and deduced the existence of 75.8 & 90.6 kev and 75.6 & 181.7 kev γ-cascades.

The Lu^{171} activity investigated in the present work was obtained as a result of bombardment of a tantalum target with fast protons. The rare earth elements were first separated from the tantalum target chemically and then the lutetium was separated from the rare earth elements by the ion exchange procedure.

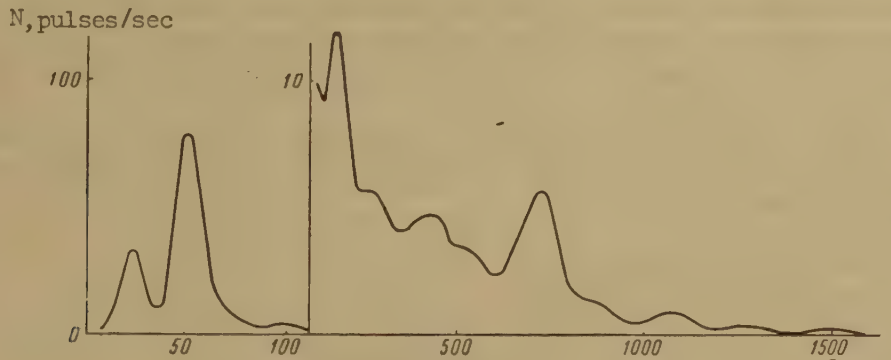

γ-spectrum of Lu^{171}

The principal activity in the source material obtained belonged to $Lu^{169,170}$. In decaying Lu^{169} converts to Yb^{169}, which in turn with a period of ~30 days decays to Tm^{169}. The period of $Lu^{169,170}$ is about 2 days. To separate the lutetium from these isotopes, the material was stored for about a month and then chromatographically purified to remove the Yb. The produce obtained in this manner contained primarily only Lu decaying with a period of about 8 days. No appreciable amounts of any other radioactive material with a different period were present in the source. The γ-spectrum was investigated by means of a scintillation spectrometer. The recorded spectrum was resolved into components by the procedure described by Maeder et al[7]. The experimental spectrum is shown in the accompanying figure; the energies and relative intensities of the γ-lines are listed in the table. The 1250 and 1500 kev γ-lines lie in the region of low sensitivity of our instrument, hence we could not evaluate their relative intensities.

The 450 and 550 kev γ-lines lie in the region of the Compton tail associated with the strong 650 and 730 kev γ-lines; hence the listed energies and intensities of the 450 and 550 kev γ-rays are only approximate. The 75 kev γ-line is located on the side of the strong characteristic radiation line. To evaluate the relative intensity of this line the spectrum was recorded through a 1.2 g/cm^2

Energies and relative intensities of γ- and x-rays from Lu^{171}

Energy, kev			Relative intensity
Refs.2,3	Refs.4,5	Our data	
—	26.7	20	30
—	—	52	180
—	65	75	16
—	75.8		
—	90.6	90	2
180	181	180	7
300	—	270	4
480	—	450	9
—	—	550	9
—	—	650	100
730	—	730	
900	906	860	17
980	964	—	—
1100	—	1050	24
—	—	1250	—
—	—	1500	—

copper absorber; as a result the relative intensities of these lines became comparable, which made it feasible to resolve the total line into components.

Two peaks were obtained in recording the soft part of the γ-ray spectrum by means of the scintillation γ-spectrometer: a principal peak corresponding to the energy of the incident γ-rays and a secondary, side peak shifted to the low energy side relative to the principal one. The peak due to the 20 kev γ-line is superimposed on the side peak due to 52 x-rays. In order to separate these peaks we recorded the γ-ray spectrum through a copper absorber 0.4 g/cm^2 thick. Such an absorber completely stops the 20 kev γ-rays but only partially absorbs the 52 kev x-radiation.

The multipole order assignments deduced in Refs.4 & 5 for the 75.8, 90.6 and 181.7 kev γ-transitions are E2, E2 and a mixture of M1 + E2 or E2 + M3, respectively. Taking the values of the internal coefficients from Refs.8 & 9 and the relative conversion electron intensities from Ref.4, we can calculate the relative intensities of the corresponding γ-rays. The relative intensities of the 65 + 75.8, 90.6 and 181.7 kev γ-rays evaluated in this manner proved to be in good agreement with our experimental values.

We desire to thank G.V.Gorshkov, in whose laboratory the present work was performed, for his interest and valuable advice and A.N.Murin for making available the lutetium source.

"V.G.Khlopin" Radium Institute,
Academy of Sciences of the USSR

References

1. W.Nevirk & G.Seaborg, Phys.Rev., 97, 1092 (1955).

2. G.Gorodinskii, A.Murin, V.Pokrovskii, B.Preobrazhenskii & N.Titov, Doklady AN SSSR, 112, 405 (1957).

3. G.Gorodinskii, A.Murin, V.Pokrovskii & B.Preobrazhenskii, Izv.AN SSSR, Ser.fia., 21, 1004 (1957). (Trans.Bulletin 21, No.7, 1005.)

4. Iu.Bobrov, K.Gromov, B.Dzhelepov & B.Preobrazhenskii, Izv.AN SSSR, Ser.fiz., 21, 940 (1957). (Trans.Bulletin 21, No.7, 942.)

5. K.Gromov, B.Dzhelepov, A.Dmitriev & B.Preobrazhenskii, Izv.AN SSSR, Ser.fiz., 21, 1573 (1957). (Trans.Bulletin 21, No.12, 1562.)

6. B.Dzhelepov, B.Preobrazhenskii & V.Sergienko, Program and Abstracts - Eighth All-Union Conference on Nuclear Spectroscopy, M.-L., 1958.

7. D.Maeder, R.Müller & V.Wintersteiger, Helv.phys.acta., 27, 3 (1954).

8. L.Sliv & I.Band, Tablitsa koeffitsientov vnutrennei konversii gamma-izlucheniia (Table of internal conversion coefficients)., M.-L., 1956.

9. D.Granitsyna, Koeffitsienty vnutrennei konversii na L_I-L_{II}- i L_{III}--podobolochkakh (L_I, L_{II} and L_{III} subshell conversion coefficients), M.-L., 1957.

NEW DATA ON THE RELATIVE INTENSITIES OF THE γ-LINES OF RaC IN EQUILIBRIUM WITH ITS DECAY PRODUCTS

- B.S.Dzhelepov, N.N.Zhukovskii, I.F.Uchevatkin & S.A.Shestopalova

Introduction

Investigations show that the γ-spectrum of radium C is extremely complicated. One cannot explain the entire distribution of experimental points solely by the earlier known and clearly discernible new γ-lines recorded for this activity. Resolution of the spectrum obtained in our previous measurements[1] brought out the existence of a number of new low intensity lines.

For the purpose of verifying and revising the data of Ref.1 on the relative intensities of RaC γ-rays, we again investigated its spectrum on the Radium Institute Elotron[2]. The instrument was converted to the separate vacuum regime: the spectrometer chamber was pumped continuously, while the counters were filled with a mixture of 60% argon and 40% methane at a total pressure of 100 mm Hg. This lowered the background and enhanced the resolution of the instrument. Under these new conditions, the width of the Compton lines at helf-heights is 3.0% at 400 kev and 1.5% in the energy region from 1500 kev up. The source was 2 grams of radium in the form of $RaBr_2$. The size and shape of the source were the same as in Ref. 1 (stack of angled ampoules partially filled with $RaBr_2$).

Results

The experimental spectrum is shown in Fig.1. The solid points give the background, i.e., the number of counts with the target out of the beam. The experimental background points fall so that they can readily be replaced by two straight lines; these were fitted by the method of least squares. After subtraction of the background, the spectral curve was resolved into standard shape components. The standard line shape was determined on the basis of measurements of the following single lines: Au^{198} 411.8 kev, Cs^{137} 661.6 kev, Co^{60} 1171.5 and 1331.6 kev, Na^{24} 1367.9 and 2753.5 kev and ThC" 2614.3 kev.

The resolution procedure employed was the same as in Ref.1, namely, the more intense 352.0, 609.3, 768.7, 934.8, 1120.4, 1378.2, 1509.3, 1764.4 and 2204.2 kev lines were used as the energy references. The energy values were taken from the work of Mladjenovic & Slätis[3]. As regards the weak lines, when their position coincided with that given by Mladjenovic & Slätis, we retained this value as the most accurate one. In the absence of coincidence, the energy was determined with reference to our calibration curve, i.e., with reference to the above listed lines. The component intensities were evaluated and adjusted so as to assure best consistence with the distribution of experimental points.

The results of resolution of the different sections of the spectrum are shown in Figs.2,3 & 4. Fig.2 shows the section of the spectrum from ~150 to 630 kev. This is the first time the spectrum below the 609 kev line has been investigated by observing recoil electrons. In addition to the well-known 241.9, 295.2 and 352.0 kev lines of radium B, one can readily distinguish the "excess" of recoil electrons near the 295.5 kev line. The resolution shows that this excess has a maximum near 285 kev. In Ref.3, among the unidentified lines are lines Nos.43,44,45,46,59,60 & 62. If they are assumed to be the K and L conversion electron lines of RaC, then we obtain 273.2, 273.9, 277.6 and 281.5 kev for the γ-line energies. Probably these lines in conjunction are responsible for the noted "excess".

It will be seen from Fig.2 that between the intense 352 and 609 kev lines there is a series of closely spaced less intense γ-lines. Some of these can be

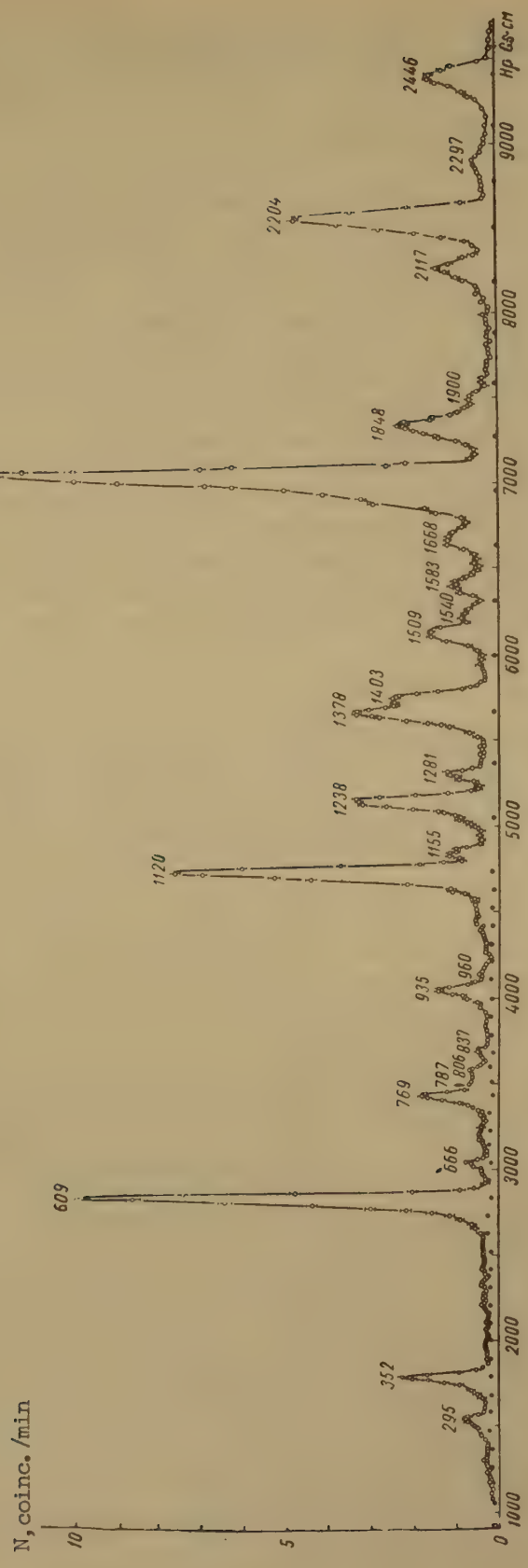

Fig.1. Experimental γ-spectrum of RaC in equilibrium with its decay products. Solid points - background.

found among the unidentified lines listed by Mladjenovic & Slätis; these are lines Nos.68,70,77,78 & 79. If we identify them as being due to the K conversion electrons from radium C, we obtain energy values of 386.8, 388.9, 466.7, 471.2 and 484.6 kev for the corresponding γ-lines; some of these coincide with those observed by us and shown in Fig.2.

The resolution in the section of the spectrum extending from 630 to 1810 kev is shown in Fig.3. In Ref.1 we made an attempt to explain the excess of recoil electrons between the 609.3 and 768.7 kev lines by the presence of lines having energies of 652.4, 660.9 and 703.2 kev and noted a rise in the region of 720 kev. In Fig.3 in this region one can clearly discern a line of 666 ± 7 kev energy and find evidence for lines at 703.2 and 721 ± 7 kev. In the present investigation we did not detect the 652.4 kev line. After plotting of the above mentioned lines there becomes evident a small excess of recoil electrons in the vicinity of 740 kev. On the high energy side of the 768.7 kev line there are three lines with energies of 787.1, 806.3 and 837 ± 5 kev. In the investigation of Ref.1 in this region we observed excess which was attributed to 787.1, 806.3 and 821.3 kev lines on the basis of identification of the lines found by Mladjenovic & Slätis. Our new curve substantiates the existence of the first two lines, but the third line apparently

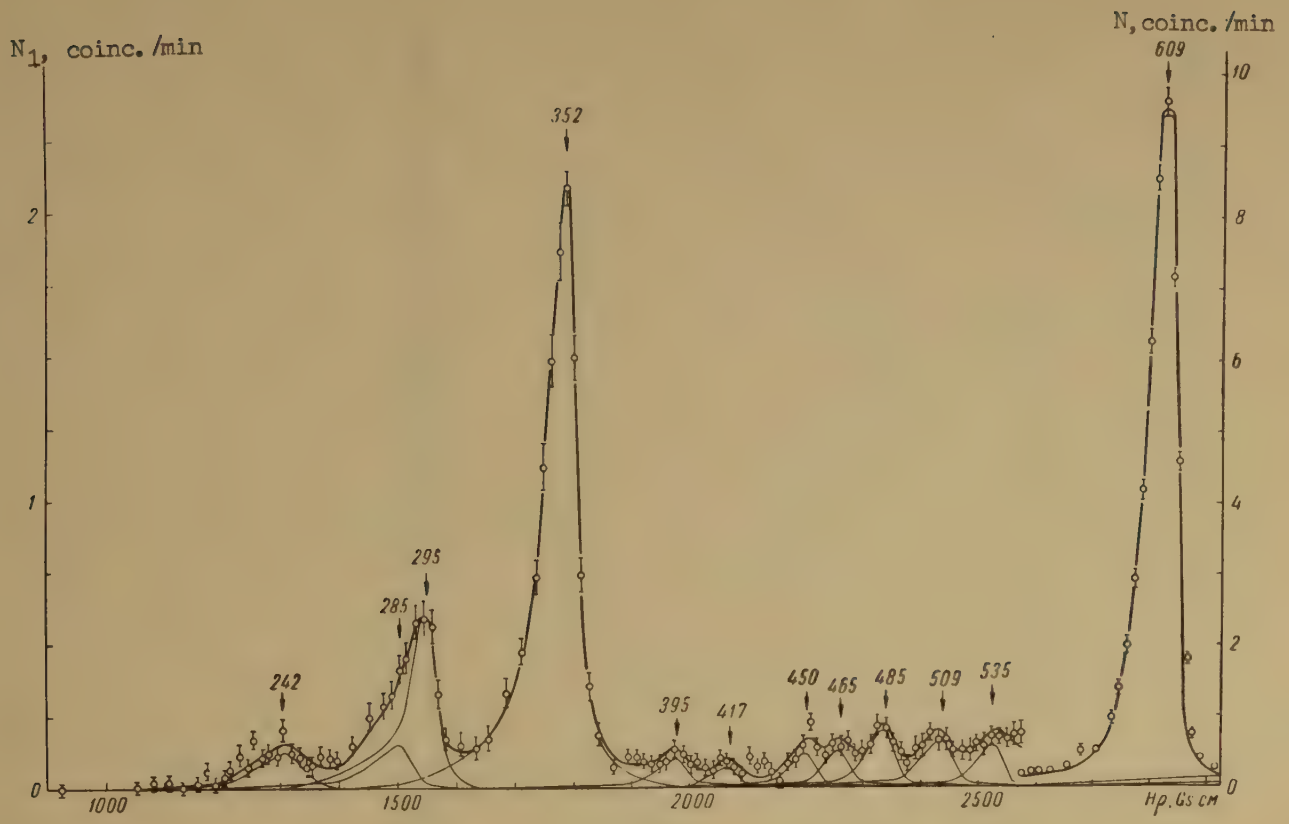

Fig.2. Resolution of the 150 to 630 kev section of the Ra γ-spectrum. N_1 - number of coincidences per minute with background subtracted.

has an appreciably higher energy than originally estimated.

In Ref.1 we drew attention to recoil electron excesses in the 840-890 and 960-1040 kev regions. In these regions we discovered new γ-lines with energies of 885 ± 10, 960 ± 5 and 1050 ± 10 kev.

In Fig.3 there is also clearly evident a line having an energy of 1541 ± 5 kev which so far has not been detected by observation of conversion electrons.

In this investigation we did not notice any broadening of the 1764.4 kev line and consequently have no further evidence for the 1783.8 and 1790.7 kev lines mentioned in Ref.1.

Fig.4 shows the section of the spectrum from 1780 to 2530 kev. The peak at the position of the well known 1848.5 kev line differs in shape from the standard line: it is somewhat wider and has a flatter slope on the high energy side. After allowing for the maximum possible intensity of the 1848.5 kev line, we found an excess of electrons with a maximum at about 1860 kev. We believe that this excess can be explained by the presence of an 1862.3 kev line[1]. The existence of the 1900 kev γ-line detected in Ref.1 was substantiated in the present investigation. In the region of 2016.7 and 2090 kev there is an excess of recoil electrons; as regards intensity, however, it is about 3 times lower than indicated in Ref.1.

The 2446 ± 10 kev line proved to be somewhat wider than the standard line. The excess on the low energy side after plotting of the greatest possible intensity of the 2446 kev line has a maximum in the vicinity of 2410 kev and an area approximately 10 times smaller than under the 2446 kev line.

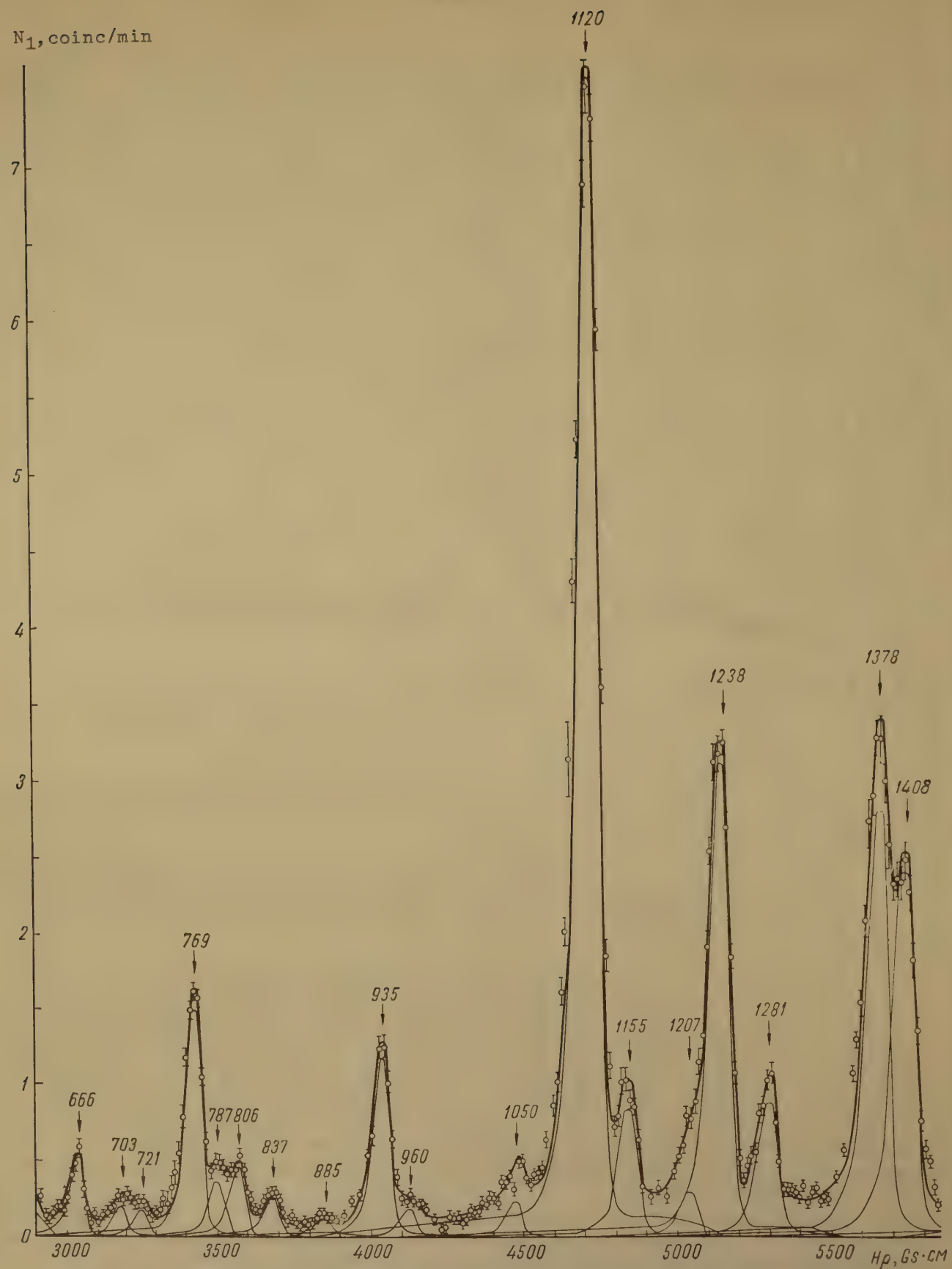

Fig. 3a. Resolution of the 630 to 1810 kev section of the Ra γ-spectrum (low energy portion).

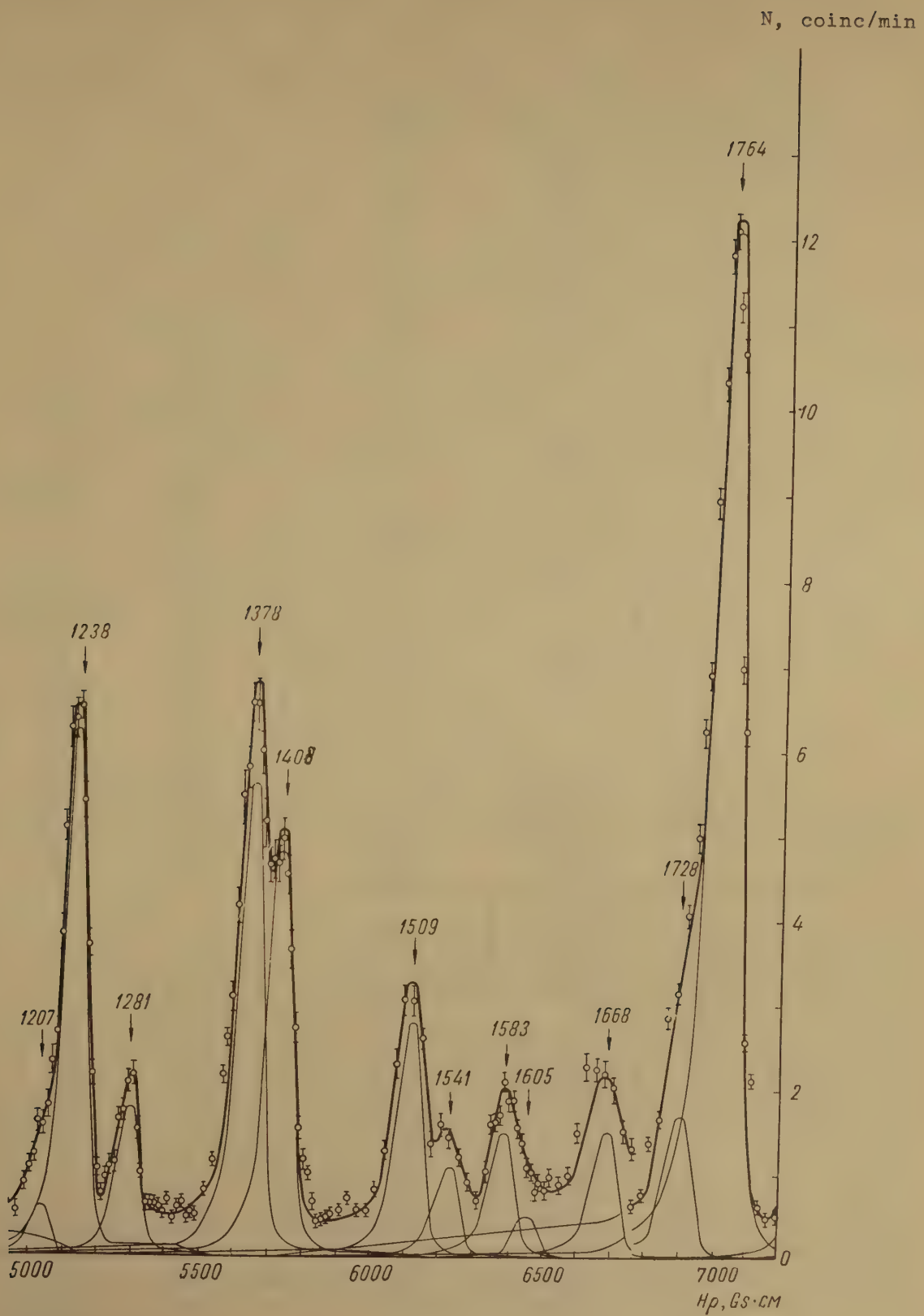

Fig. 3b. Resolution of the 630 to 1810 kev section of the Ra γ-spectrum (high energy portion).

Energies and relative intensities of the γ-lines in the spectrum of radium in equilibrium with its decay products (200 to 2500 kev region)

Line No.	E_γ, kev (Ref. 3)	Relative intensities	E_γ, kev
		Dzhelepov et al[1]	Our data
1*	239,6	—	
2	241,9	—	2,0 242
3	258,8	—	
*	273,2	—	
5*	273,9	—	
6*	277,6	—	1,0 285±10
7*	281,5	—	
8	295,2	—	
9*	304,0	—	3,6 295
10*	348,5	—	
11	352,0	—	7,18 352
12*	386,8	—	
13*	388,9	—	~0,24 ~395
14	—	—	~0,15 ~417
15	—	—	~0,19 450±10
16*	466,7	—	
17*	471,2	—	~0,19 465±10
18*	484,6	—	0,29 485±5
19	--	—	0,24 509±5
20	—	—	0,17 535±10
21	609,3	8,21	8,96 609
22*	652,4	0,50	— —
23*	660,9		0,43 666±7
24*	703,2	0,28	0,15 703
25	—	—	0,13 721±7
26	—	—	~0,07 ~740 (excess)
27	768,7	1,05	1,01 769
28*	787,1	0,25	0,23 787
29*	806,3	0,34	0,29 806
30*	821,3	0,15	0,17 837±8
31	—	—	0,07 885±10
32	934,8	0,74	0,62 935
33	—	—	0,09 960±5
34	—	—	0,10 1050±10
35	1120,4	2,95	3,16 1120
36	1155,3	0,45	0,34 1155
37*	1207,1	0,33	0,11 1207
38	1238,3	1,14	1,15 1238
39	1281,3	0,33	0,32 1281
40	1378,2	0,89	0,91 1378
41*	1385,3		
42*	1391,1		
43*	1396,5	0,88	0,77 1403±7
44*	1401,7		
45*	1408,0		
46*	1438,0		
47	1509,3	0,54	0,42 1509
48	—	—	0,16 1541±5
49*	1582,9	0,22	0,21 1583
50*	1605,2	0,07	0,07 1605
51*	1668,4	0,10	0,20 1668
52	1728,3	0,34	0,45 1728
53	1764,4	2,73	3,11 1764
54*	1783,8	0,58	— —
55*	1790,7	0,16	— —
56	1848,5	0,25	0,39 1848
57*	1862,3	0,29	0,15 1862
58**	1900	0,17	0,08 1900±10
59	2016,7	0,06	~0,02 2017 (excess)
60**	2085	0,08	~0,02 2090 (excess)
61	2117,0	0,27	0,26 2117
62	2204,2	1	1 2204
63**	2290	0,07	0,08 2297±10
64	—	—	~0,03 2410 (excess)
65**	2450	0,36	0,30 2446±10

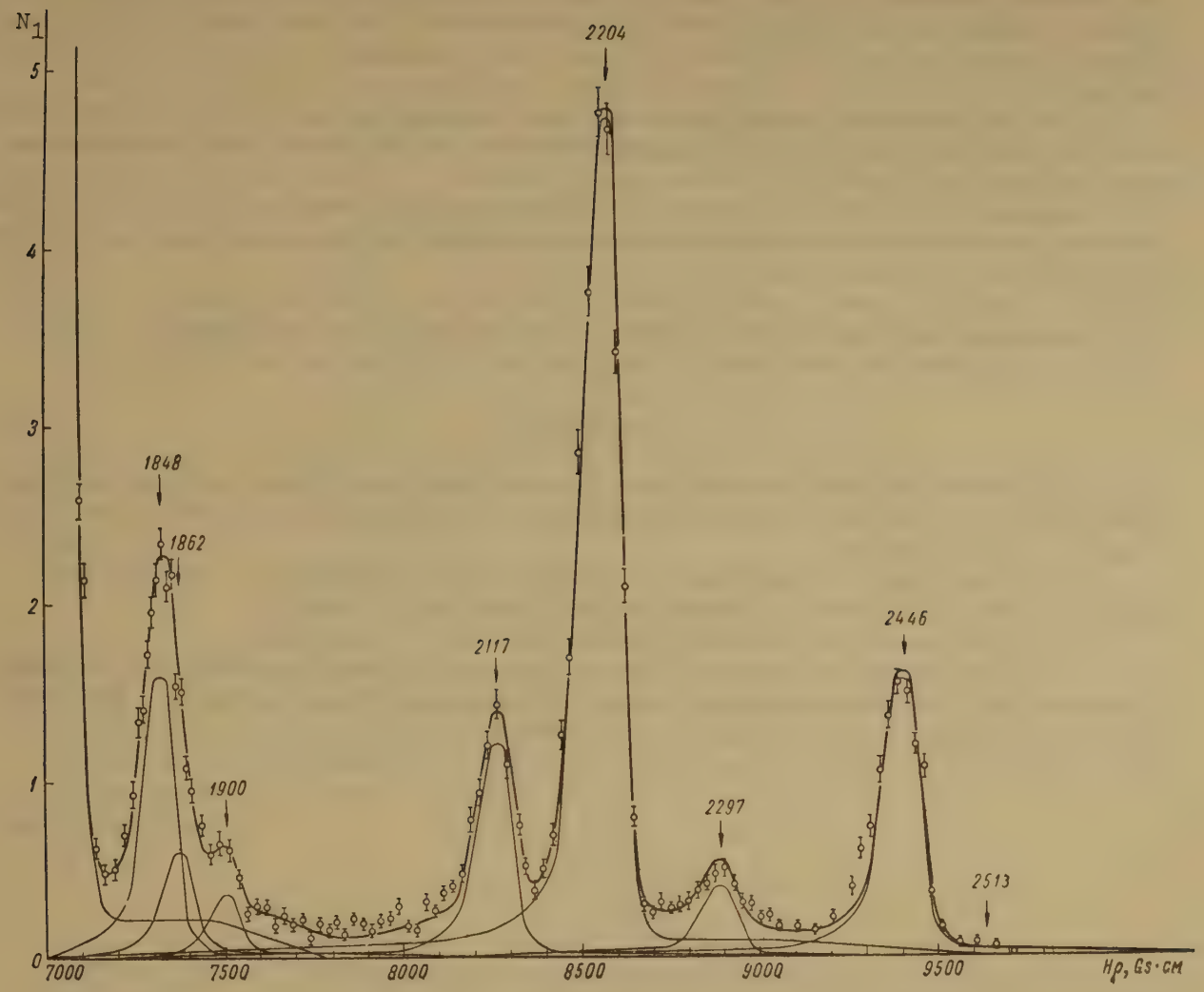

Fig.4. Resolution of the 1780 to 2530 kev section of the Ra γ-spectrum.

Rutherford et al[4] detected a 2513 ± 5 kev excited level in RaC'; hence one might expect the appearance of a γ-line of 2513 kev energy. The 2513 point is indicated by an arrow in Fig.4. If this line does exist, its intensity is less than $4 \cdot 10^{-4}$ photons per disintegration.

To find the relative intensities we determined the areas under each component, reduced to equal Hρ intervals. Then we made appropriate corrections for the efficiency of the counters in detecting electrons of different energies, for self-absorption in the source, for absorption in the walls of the instrument and for the spectral sensitivity of the spectrometer. It was assumed then that the line intensities are proportional to these corrected areas.

The results are listed in the accompanying table. The energy values listed in column 2 are those given by Mladjenovic & Slätis[3]. The lines marked with an asterisk were found among the unidentified conversion lines in Ref.3 and identified by us as K (or in some cases L) electron conversion lines of RaC. Line energies identified by two asterisks are values determined in the measurements of Ref.1.

The relative intensities listed in column 3 are revised values (refinement over the tabular data of Ref.1): the 609.3 kev line is now plotted according to

the standard shape with the observed half-width (earlier the line shape was based on the assumption of a smooth energy dependence of the half-width); the minor revisions in the intensity values for the other lines are connected with improved resolution.

It will be evident from the table that the agreement of the present results with the earlier data is fairly good: intensities of the strong single lines agree within 7-10%.

Graduate students F.A.Predovskii (Leningrad Polytechnic Institute) and N.A. Voinova (Leningrad State University) participated in the measurements; we take this occasion to thank them.

"D.I.Mendeleev" All-Union Scientific Research Institute of Metrology
"V.G.Khlopin" Radium Institute of the Academy of Sciences of the USSR

References

1. B.Dzhelepov & S.Shestopalova, Izv.AN SSSR, Ser.fiz., 21, 990 (1957). (Trans.Bulletin 21, No.7, 992.); B.Dzhelepov & S.Shestopalova, Nuovo Cim., 3, Suppl., 1, 54, (1956).

2. B.Dzhelepov, N.Zhukovskii, V.Nedovesov & G.Shchukin, Izv.AN SSSR, Ser.fiz., 21, 966 (1957). (Trans.Bulletin 21, No.7, 968.)

3. M.Mladjenovic & H.Slätis, Arkiv.för Fys., 8, 65 (1954).

4. E.Rutherford, W.Lewis & B.Bowden, Proc.Roy.Soc., A, 142, 347 (1933); E.Rutherford, C.Wynn-Williams, W.Lewis & B.Bowden, Proc.Roy.Soc. A, 139, 167 (1933); G.Briggs, Revs.Mod.Phys., 26, 1 (1954).

DETERMINATION OF THE NUMBER OF PHOTONS PER DISINTEGRATION OF La^{140}

- E.A.Khol'nova

The procedure for experimental determination of the number of γ-quanta per decay discussed in the present report is based on calorimetric measurement of the amount of heat evolved in the absorption of the β- and γ-radiation emitted by the investigated isotope. Briefly, the procedure consists of the following.[1]

Let us assume that the energies $h\nu_1, h\nu_2 \ldots h\nu_n$ and relative intensities α_1, $\alpha_2 \ldots \alpha_n$ of all the γ-rays of the isotopes under investigation are known from spectroscopic measurement. The relative intensities of the γ-lines are the numbers η_i of γ-rays per disintegration divided by the number of γ-rays per disintegration for the line whose relative intensity is taken as unity, i.e.,

$$\alpha_1 = \frac{\eta_1}{\eta_c}, \quad \alpha_2 = \frac{\eta_2}{\eta_c} \ldots \alpha_c = 1 = \frac{\eta_c}{\eta_c} \ldots \alpha_n = \frac{\eta_n}{\eta_c}. \tag{1}$$

The calorimetrically measured amount of heat Q_γ that is released by the investigated isotope per second in the form of β- and γ-radiation is related to the energy of the γ-rays and the numbers of photons per decay by the following expression

$$Q_\gamma = N_0 \left(\sum_i h\nu_i \eta_i p_i + \overline{E}_\beta \right), \tag{2}$$

where N_0 is the number of decays per sec, $\overline{E}_\beta$ is the mean energy of the β-spectrum and p_i is a coefficient taking into account the fraction of γ-rays absorbed in the γ-calorimeter (in the case of complete absorption p_i equals unity).

Inasmuch as the numbers of photons per decay are usually not known, they can be expressed in terms of the relative intensities using Eq.(1); in this case Eq.(2) becomes

$$Q_\gamma = N_0 \left(\eta_c \sum_i h\nu_i \alpha_i p_i + \overline{E}_\beta \right). \tag{3}$$

In this expression there are two unknown quantities, namely, N_0 the activity of the source and η_c the number of photons per decay for the γ-line whose relative intensity is taken as unity. However, N_0 can be determined by measuring with a β-calorimeter the energy given off by the source in the form of the kinetic energy of β-particles. Thus we obtain a second equation:

$$Q_\beta = N_0 (\overline{E}_\beta + \Delta E_\gamma). \tag{4}$$

Here ΔE_γ is the correction taking into account the absorption of γ-rays in the thin walls of the β-calorimeter.

Solution of these two equations gives us the number of quanta per decay for the line whose relative intensity is taken as unity. The numbers of photons per decay for all the other lines can then be found from (1).

We used the outlined procedure for determining the numbers of photons per decay in the case of La^{140}. In our work we used the energies and relative intensities of the γ-lines obtained by Prokhodtseva & Khol'nov[2] on the Ritron. In calculating the mean β-particle energy we used the La^{140} β-spectrum obtained by Dzhelepov et al[3] on the Leningrad State University Ketron.

Having measured (on the All-Union Scientific Research Institute of Metrology calorimeters[4]) the amount of heat given off by the La^{140} source in the form of β- and γ-radiation and utilizing the above mentioned spectroscopic data, we found that the number of γ-quanta per decay for the most intense 1597 kev γ-line, whose intensity is taken as unity in evaluating the relative intensities[2], equals

Table

Relative intensities and numbers of γ-rays per decay in the radiation from La^{140}

γ-ray energy, kev (Ref. 2)	Relative intensity (Ref. 2)	No. quanta per decay (our data)
323	0,21	0,20
400	0,03	0,028
491	0,42	0,40
748	0,034	0,432
815	0,196	0,186
868	0,053	0,050
923	0,096	0,091
1597	1,00	0,95
2343	0,0078	0,0074
2515	0,03	0,035
2890	0,0008	0,0008

0.95. Using this value and the available relative intensity data, we determined the numbers of photons per decay for all the other γ-lines. The results are listed in the third column of the accompanying table.

We then used these data for calculating the total energy per disintegration. Taking the products of the energy by the number of corresponding γ-rays per decay and summing over all the γ-lines, we found the energy released per disintegration in the form of γ-rays. The computed value was 2200 kev.

We determined the analogous quantity for the β-radiation using the resolution of the La^{140} β-spectrum into components given by Peacock, Quinn & Oser[5]. Knowing the relative intensities of the β-components and their end-point energies, we found that the total energy of the β-particles on the average per disintegration equals 1310 kev. From this the total disintegration energy is found to be 3510 kev, i.e., about 300 kev lower than follows from the available decay schemes.

This gives reason to infer that the relative intensities of the β-components given by Peacock et al and used in our calculations are inaccurate. Presumably, the soft β-components are somewhat less intense than indicated by Peacock et al.

This, however, does not affect the accuracy of determining the number of photons per decay inasmuch as in determining these we did not make use of the resolution of the β-spectrum.

The writer desires to thank L.P.Timofeeva who participated in some of the measurements and in the computations.

"V.I.Mendeleev" All-Union Scientific Research Institute of Metrology

References

1. K.K.Aglintsev & E.A.Khol'nova, Doklady AN SSSR, 98, 357 (1954).

2. V.P.Prikhodtseva & Iu.V.Khol'nov, Izv.AN SSSR, Ser.fiz., 22, 176 (1958). Trans.,Bulletin 22, No.2, 173.)

3. A.A.Bashilov, B.S.Dzhelepov, N.D.Novosil'tseva & L.S.Chervinskaia, Izv. AN SSSR, Ser.fiz., 22, 179 (1958). (Trans.Bulletin, 22, No.2, 176.)

4. K.K.Aglintsev, F.M.Karavaev, A.A.Konstantinov, G.P.Ostromukhova & E.A. Khol'nova, Atomnaia energiia, (Atomic energy) 2, 55 (1956).

5. C.Peacock, J.Quinn & A.Oser, Phys.Rev., 94, 372 (1954).

DETERMINATION OF THE L/K RATIOS FOR Dy^{159} AND Er^{165} AND EVALUATION OF THE $Dy^{159} \rightarrow Tb^{159}$ AND $Er^{165} \rightarrow Ho^{165}$ TRANSITION ENERGIES

- O.I.Grigor'ev, B.S.Kuznetsov, N.S.Shimanskaia & I.A.Iutlandov

Introduction

The disintegration energy ϵ_o of radioactive isotopes undergoing electron capture can be determined in different ways.

1. In the presence of competing β^+-decay, the value of ϵ_o, which in this case is greater than 1 Mev, may be obtained from the data on the end-point energy of the positron spectrum and in the case of transitions to excited levels from the data on the energy of the corresponding γ-rays. Use of this method is predicated on having detailed information on the decay scheme of the isotope.

2. The disintegration energy ϵ_o of an isotope with mass number A and atomic number Z, decaying by K capture, can be determined from the experimentally found value of the threshold of the (p,n) reaction on the isotope with the same mass number and atomic number Z - 1.

3. The transition energy for a given type radioactive transformation can, in some cases, be determined on the basis of the energy relationships in so-called "closed cycles". In such calculations use is made of the energy of the α, β and γ-radiations of the isotopes comprising the cycle and sometimes - for example, in the case of K^{40} - of mass spectroscopic data as well. This method has been successfully used for evaluating the disintegration energy for a number of K capture isotopes, primarily isotopes lying near the end of the periodic table.

4. The end-point energy of the internal bramsstrahlung spectrum accompanying electron capture also give the energy ϵ_o of the transformation. This method can readily be used in the case of "pure" K capture when the decay goes directly to the ground level of the final nucleus and consequently γ-radiation is absent. If, however, the decay scheme is more complicated and there occur transitions to different excited levels of the daughter nucleus, this method is applicable only in rare cases when the energy of the transition to the excited level appreciably exceeds the energy of this level (Cr^{51} - Ref.1 & Sb^{119} - Ref.2).

5. Finally, there is one other method peculiar to electron capture for determining the transformation energy from the ratio of the number of L captures to the number of K captures. It is known that in the decay of radioactive isotopes by orbital electron capture, in addition to capture of K shell electrons there is always a finite probability of capture of electrons from the L shells. The existence of L capture was first proved experimentally by Pontecorvo, Kirkwood & Hanna[3] 1948-9 for the case of A^{37}, although the phenomenon was predicted some years earlier by Marshak[4]. Marshak, who derived a general formula for the lifetimes of nuclei decaying by orbital electron capture, established that the relative probability of L capture increases with increasing Z of the disintegrating nucleus and decreasing transition energy ϵ_o. For allowed transitions the ratio of probabilities of L and K capture is given by the expression

$$\frac{L}{K} = \left(\frac{g_{L_I}^2}{g_K^2}\right)\left(1 + \frac{f_{L_{II}}^2}{g_{L_I}^2}\right)\left(\frac{\varepsilon_0 + E_L}{\varepsilon_0 + E_K}\right)^2, \qquad (1)$$

where the first factor (g_{LI}^2/g_K^2) characterizes the ratio of L_I and K shell electron densities on the nuclear surface.

The magnitude of this ratio and its variation as a function of Z were calculated by Rose & Jackson[5] who give the curve reproduced in Fig.1. Their calculations were carried out by means of relativistic wave functions computed by Reitz for medium and heavy elements ($Z > 20$; curve 1) and Hartree self-consistent field wave functions for light elements ($Z < 30$; curve 2).

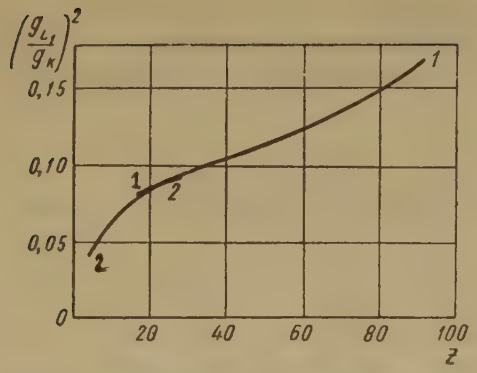

Fig.1. Ratio of L_I and K shell electron densities at the nuclear radius vs Z. Curve 1 computed by means of relativistic wave functions with a Thomas-Fermi field plus exchange; curve 2 computed by means of Hartree self-consistent field wave functions.

Recently, the Rose-Jackson calculations have been refined by Zyrianova, Band & Suslov[6] who took into account finite nuclear size and the presence of orbital electrons. The wave functions used in their calculations were found by the method of numerical integration of the Dirac equation. The results of Zyrianova, Band & Suslov are very close to those of Rose & Jackson for the entire range of variation of Z.

The second factor in Eq.(1) takes into account the probability of capture of electrons from the L_{II} shell; this, even in the region of heavy nuclei, in the case of allowed transitions does not exceed a few percent. Marshak gives the following approximate expression for the ratio of L_{II} and L_I shell electron densities at the nuclear radius:

$$\left(\frac{f_{L_{II}}}{g_{L_I}}\right)^2 = \frac{3}{16}\left(\frac{Z-4{,}15}{137.3}\right)^2. \qquad (2)$$

More precise calculations carried out by Zyrianova, Band & Suslov yield somewhat lower values than given by Eq.(2) for L_{II}/L_I in the region of large Z. Thus for Dy, the fraction of L_{II} captures according to Zyrianova et al amounts to 4.5% instead of 3.7% as given by Eq.(2).

The third, "energy factor" $\left(\frac{\epsilon_0 + E_L}{\epsilon_0 + E_K}\right)^2$ is determined by the transition energy ϵ_0 and E_L and E_K the electron binding energies on the L and K shells, which are known with good accuracy.

In the case of forbidden transitions (except for first forbidden transitions involving a change in parity and either no change or a change of one unit in angular momentum), one cannot directly make use of Eq.(1) for determining the transition energy. The theory of orbital electron capture for forbidden transitions has not been developed to any extent. In most cases it appears impossible to state explicitly, as a separate factor in the probability equation, the unknown value of the matrix element determined by the nuclear wave functions. In addition, inasmuch as forbidden capture may occur from all three L subshells, one must take into account the probability of L_{III} capture, which also presents considerable difficulties. Robinson & Fink[7] in their review article give the results of an unpublished work by Brysk & Rose[8] in which the latter calculated the relative probabilities of electron capture from all the subshells for four cases of forbidden transitions characterized by $\Delta I = \pm 2$, yes. The values of L/K obtained for K^{40}, Ca^{41}, Ni^{59} and Tl^{204} show an appreciable increase in the value of this ratio in the case of forbidden transitions of this type.

The "L/K ratio" procedure has been used by a number of authors for determining disintegration energies. Specifically it has been used for determining the decay energies of K^{40}(Ref.9), Cd^{109} (Ref.10), I^{125} (Ref. 11), Ta^{179} (Ref.12), W^{181} (Ref.13), Os^{185} (Ref.14), Au^{195} (Ref.15) and a number of other isotopes. Unfortunately, only in a few cases has it been possible to carry out a comparison of the disintegration energy evaluated by the L/K ratio method with the value of ϵ_0 determined by some other reliable procedure. The divergence between the respective values of ϵ_0 found for K^{40} (Ref.9), Kr^{79} (Ref.16) and Pd^{103} (Ref.17) may be explained, on the one hand, by inaccuracy in the L/K calculations in the

case of forbidden transitions* and, on the other hand, by errors inherent in the experimental determination of the L/K ratio, errors which are particularly difficult to avoid in the case of complicated decay schemes. The latter reason is probably the more important one. Experimental determination of L/K is in fact connected with serious difficulties due, first, to the low energy of the detected radiation, and, second, to the uncertainty in the assumed values of certain constants (primarily the L fluorescence yield) characterizing the process of rearrangement of the electron shell incident to electron capture.

Obviously, in the simplest case, when the electron capture in a nucleus with atomic number Z goes to the ground level of the nucleus with Z - 1, for determining the number of L and K captures one can measure the intensities I_L and I_K of L and K x-radiation. The value of L/K can then be determined from the equality

$$L/K = \frac{I_L}{I_K} \cdot \frac{\omega_K}{\bar{\omega}_L} - n_{KL}, \qquad (3)$$

where ω_K and $\bar{\omega}_L$ are the fluorescence yields from the K and L shells and n_{KL} is the number of vacancies in the L shell arising incident to filling of the vacancies forming in the K shell.

If, however, the electron capture goes to excited levels of the final nucleus and is accompanied by γ-radiation, in calculating L/K one should take into account the L and K x-radiation accompanying the γ-ray conversion. This is particularly difficult to do in the case of intense and strongly converted γ-radiation. In a number of cases it has proved possible to determine L/K by measuring coincidences[19] and working with the source located inside the radiation detector.

In addition it must be borne in mind that the L/K ratio method can be used for determining the transition energy only in a rather limited region of relatively small values of ϵ_0. Thus it will be evident from Eq.(1) that at high transition energy values the "energy factor" $\left(\frac{\epsilon_0 + E_L}{\epsilon_0 + E_K}\right)$ approaches unity and the value of L/K becomes constant for the given isotope regardless of the disintegration energy. Fig.2 shows the variation of L/K as a function of ϵ_0 for dysprosium (Z = 66) calculated by us by means of Marshak's formula. It will be evident from the curve that only at transitions energies smaller than 200 kev one can make use of the experimentally determined value of L/K for determining the transition energy. At higher energies even a minor error in determining L/K results in a large error in the value of ϵ_0.**

---

*Recently Daudel & Odiot[18] showed that in theoretical evaluation of L/K one must take into account the correlation and the position of the atomic electrons. This effect, which in the case of most K-capture nuclides can be neglected, may play a significant role in the case of light elements (Z < 30). Thus, for example, in the case of Be^7(Z = 4), it results in a three-fold increase of the ratio L/K as compared with that calculated by Marshak's formula; in the case of A^{37} (Z = 18) the increase amounts to about 25%.

**In the case of a complicated decay scheme, when the electron capture may go both to the ground level of the final nucleus and to some of its excited levels, the L/K ratio will obviously be different for transitions to different energy levels and will have a value corresponding to the transition energy given by the difference between the disintegration energy of the isotope and the energy of the given level. Hence if, for example, on the basis of γ-radiation data for the isotope one may expect to have a large disintegration energy ϵ_0, one can attempt to determine ϵ_0 accurately by measuring L/K and the transition energy corresponding to electron capture to the higher lying energy levels where one can expect low transition energies.

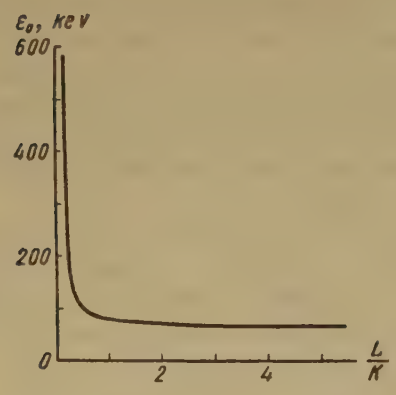

Fig.2. Transition energy ϵ_0 vs L/K for Dy isotopes (Z = 66).

On the contrary, at low energies, i.e., energies close to the K shell binding energy, the L/K ratio naturally strongly depends on the transition energy so that even with a considerable uncertainty in determining L/K the value of the transition energy is obtained with good accuracy.

Thus it may be said that the L/K ratio procedure is promising and convenient for determining the energies of low energy transitions (< 200 kev in isotopes with a relatively simple decay scheme in the absence of strongly converting cascade γ-radiation. The application of this method is at present limited, on the one hand, by the crude state of electron capture theory and, on the other hand, by the inadequacy of our information on the qualitative and quantitative regularities characterizing the process of rearrangement of atomic electron shells.

In the present work we determined the L/K ratio for two neutron-deficient rare earth elements: Dy^{159} and Er^{165}. On the basis of the L/K values obtained, we evaluated the energy of the $Dy^{159} \rightarrow Tb^{159}$ and $Er^{165} \rightarrow Ho^{165}$ transitions.

Experimental Equipment

For measuring the energy and intensity of the L and K x-radiation of the investigated isotopes we used a γ-spectrometer with a proportional counter. The proportional counter technique[20] allows of measuring γ- and x-radition of very low energies (of the order of a few hundreds or even tens of electron volts), i.e., in the range of energies not susceptible of measurement by other techniques.

The resolution of spectrometers of this type is not high. It is appreciably lower than the resolution of modern magnetic and crystal γ-spectrometers. It must be borne in mind, however, that instruments of the latter type require an appreciably stronger activity (than proportional counters) and their employment in the low energy region (< 50 kev) is hampered by practical difficulties.

In the ~50 kev region the resolution of a proportional counter is comparable with that of a scintillation spectrometer and is appreciably higher in the region of still lower energies. Thus, for example, for a ~10 kev line the relative half-width obtained by means of a proportional counter is 12-13%, whereas the half-width for a scintillation counter is greater than 50%.

In recent years proportional counters have been successfully used by a number of Italian and French physicists not only for investigating soft γ-radiation from radioactive isotopes but also for studying K capture and in particular for determining L/K.

Counter and experimental geometry

The proportional counter used in our measurements had a cylindrical aluminum cathode. Its inside diameter was 8.7 cm; the effective length was about 40 cm. At the ends, the counter was covered with circular plexiglass plates with appropriate annular recesses for rubber gaskets. The central electrode, to which the high positive voltage was applied, was a 100 μ diameter tungsten filament which was thoroughly cleaned decontaminated and polished beforehand.

The counter has a side window consisting of a ~2 cm diameter beryllium disk with a superficial density of 148 mg/cm^2. The purity of the beryllium was checked

spectroscopically. The counter was filled with a mixture of argon and methane, usually in the proportion of 9 to 1 at a pressure of about 1 atmosphere. The gaseous mixture was purified beforehand by passing it through calcium heated to 300°.

The present experiments were made with an external source (see Fig.4) which was mounted in a special holder at a fixed distance h from the beryllium window. In most of the measurements described below this distance h was about 4 cm.

Inasmuch as γ- and x-radiation of more than 20-30 kev energy could pass through the 4 millimeter aluminum walls of the counter, a special lead collimator was introduced between the source and the counter. To eliminate the characteristic radiation of lead, the collimator was lined successively with layers of cadmium, copper and aluminum. The counter was surrounded with lead shielding to minimize the background.

Counter efficiency

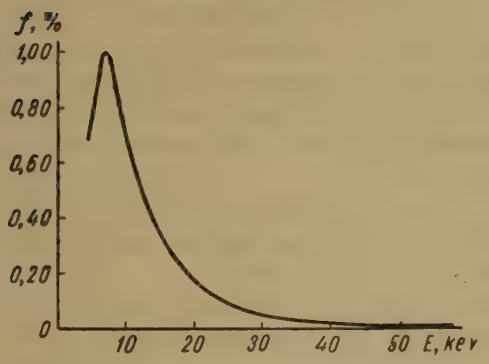

Fig.3. Variation of the counter efficiency as a function of the γ-radiation energy.

The efficiency of the counter for detecting γ- and x-radiations of different energies was calculated on the basis of the known coefficients of absorption in argon and beryllium, (Ref.21) taking into account the specific geometry of the experiment. In view of the size of the sources ($d_s < 5$ mm) and the source to counter distance h used in the experiments, it was feasible to use the formulas given by Bisi and Zappa[22] for calculating the counter efficiency. The calculated curve characterizing the variation of the counter efficiency as a function of the radiation energy is shown in Fig.3. In reducing the experimental data we also took into account absorption from the radiation in air, which for soft radiation could be appreciable (8% for the Dy^{159} L_{α_1} line (6.3 kev) with h = = 4 cm).

Electronic circuit

The pulses from the counter were applied through a high voltage capacitor to the grid of the first tube of the preamplifier which was mounted on one of the end surfaces of the counter. The amplification factor of the preamplifier was 20; the noise level - 35 μv. The main linear non-jamming amplifier had a maximum amplification coefficient of $4 \cdot 10^4$; the pulse rise time was < 0.3 microsec. The pulses were shaped in the amplifier by means of a differentiating RC network with a time constant of 2.2 microsec. The amplifier incorporated a "flattener" which allowed of obtaining pulses with a flat top without altering their amplitude; this made for better analysis of the pulses by the pulse height analyzer. A somewhat modified SV (CB) "Kashtan" type unit was used as the one-channel differential analyzer. Usually the spectrum was recorded semiautomatically by means of an EPPV-51 recorder. Adjustment of the lower threshold of the analyzer discriminator, determining the position of the gate, was realized by means of a potentiometer coupled with the strip-chart feed mechanism of the recorder. The pulses from the analyzer were fed into an integrator; the dc output voltage - proportional to the number of pulses - was applied to the input of the recorder amplifier.

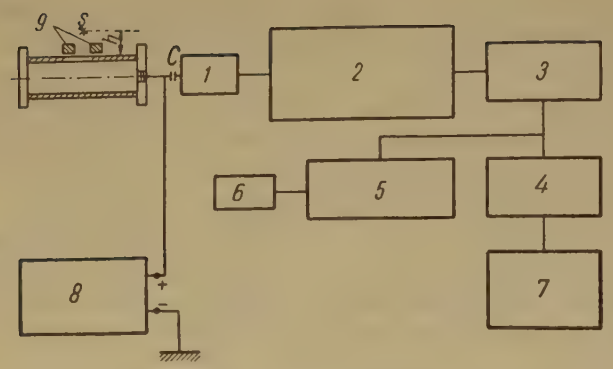

Fig.4. Diagram of experimental set-up: 1) preamplifier (k = 20), 2) linear amplifier (k = $4 \cdot 10^4$), 3) pulse height analyzer, 4) integrator, 5) scaling circuit (1:2048), 6) mechanical register, 7) EPPV-51 recorder, 8) high voltage supply unit, 9) collimator.

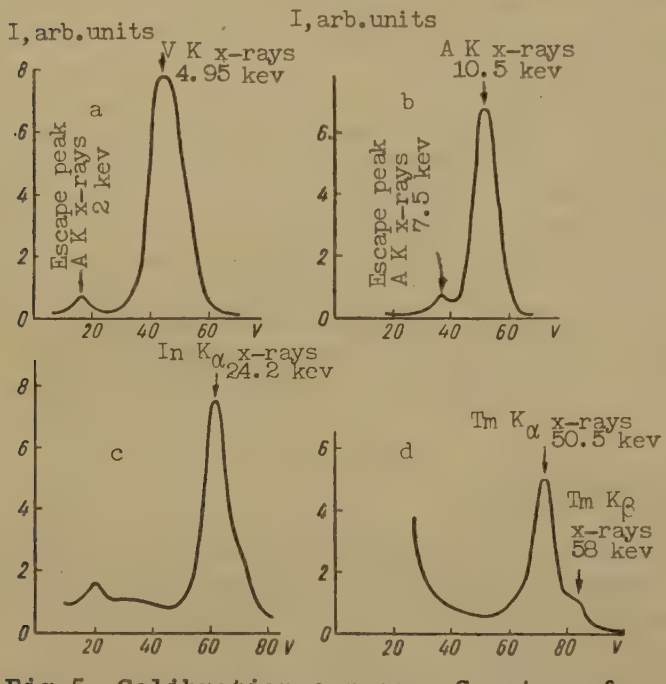

Fig.5. Calibration curves. Spectra of x-rays accompanying the decay of a - Cr^{51} (4.9 kev), b - Se^{75} (10.5 kev), c - Sn^{113} (24.2 kev), d - Yb^{169} (50.7 kev). Horizontal scale - pulse heights; vertical scale - radiation intensity.

A high voltage VS-10 (BC-10) unit was employed to supply the requisite stabilized high potential (usually ~3000 v) for the counter filament. The voltage drift over a period of 8 hours operation was less than 0.02%. A block diagram of the experimental set-up is shown in Fig.4.

Calibration of the instrument

The equipment was calibrated in the range from 2 to 55 kev by means of radioactive sources emitting γ- and x-radiation of known energy: Cr^{51}, Fe^{55}, Zn^{65}, Ge^{71}, Se^{75}, Sn^{113}, Cs^{137}, RaD and others. We checked the linearity of the energy dependence of the pulse heights and determined the resolution for different energy regions and different counter gas pressures and mixtures.

Fig.5 shows the spectra of the x-radiation accompanying the decay of Cr^{51} (4.9 kev), Se^{75} (10.5 kev), Sn^{113} (24.2 kev) and Yb^{169} (50.7 kev). In the case of Cr^{51} and Se^{75} one can clearly see the so-called "escape peaks" due to the characteristic radiation of argon not absorbed in the counter gas. The narrowest line half-width obtained with the counter filled with A + CH_4 at 76 mm Hg pressure was 19% for Fe^{55} (5.9 kev), 15% for Sn^{113} (24.2 kev) and 11% for RaD (46.7 kev). Reduction of the gas pressure resulted in a noticeable improvement of the resolution in the entire region of the detected radiation.

Experimental Results

Dy^{159}

1. The long-lived dysprosium isotope Dy^{159} was first obtained in 1949 by Ketelle[23] by irradiation of a purified dysprosium sample with slow neutrons. Ketelle gives the value of 140 ± 10 days for the period of this isotope; Butement[24] found the half-life to be ~136 days and asserts that Dy^{159} decays solely by electron capture, emitting only Tb L and K x-radiation. Coulomb excitation of Tb^{159} indicated the existence of rotational levels with

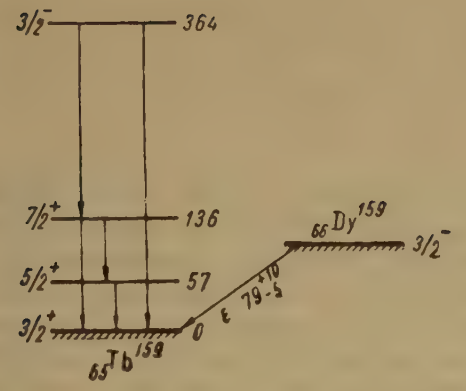

Fig.6. Dy^{159} decay scheme and Tb^{159} level diagram.

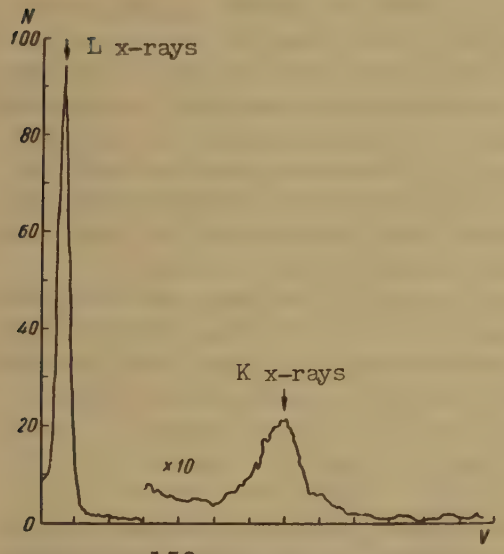

Fig.7. Dy^{159} x-ray spectrum.

energies of 57 and 136 kev.[25] Other energy levels of this isotope are known from studies of the decay of 18-hour Gd^{159} which also transforms to Tb^{159} but by β^--decay.

The level diagram for Tb^{159}, given by Dzhelepov & Peker[26], is reproduced in Fig.6.

2. The Dy^{159} source used in the present experiments was obtained from a tantalum target bombarded with 660 Mev protons in the Joint Institute for Nuclear Research synchrocyclotron. The measurements were performed an appreciable time after separation of the dysprosium fraction when the short-lived activities had virtually died out.

One of the experimental x-ray spectra obtained for Dy^{159} is reproduced in Fig.7. Clearly in evidence are the Tb L and K x-radiation peaks with energies close to the values of $L\alpha_1$ and $K\alpha_1$ for this element (6.3 and 44.5 kev). The small peak (rise in the right side of the K x-ray line) is apparently due to the $K\beta_1$ radiation of terbium (50.4 kev).

From the ratio of the L and K radiation intensities, obtained on the basis of averaging the areas S under all the experimental curves and taking into account the counter efficiency at the respective energies, we obtained a value of 1.0 ± 0.3 for the ratio of the number of L to K captures in Dy^{159} (see table). The ratio was calculated by means of Eq.(3), using the values indicated in the table for the K and L fluorescence yields and the number n_{KL}

The large uncertainty in the deduced value of L/K is due partly to inaccuracy in determining the areas under the experimental curves and evaluating the counter efficiency and primarily to the uncertainty as regards the L fluorescence yield $\bar{\omega}_L$ which was taken equal to 15%. We picked this value of $\bar{\omega}_L$ from a curve drawn through the experimental points for $\bar{\omega}_L$ obtained by different authors on the basis of investigation of electron capture in different elements and recently summarized by Fink[28].*

---

*It is interesting to note that the results of Lay[29], obtained by the photographic technique, for the L shell fluorescence yield with excitation of the atoms by x-rays are systematically higher than the values for the L fluorescence yield found in K capture studies. This fact, if we assume that there is no systematic error in the work of Lay, may indicate that the L shell fluorescence yield depends on the method of excitation of the electron shell and that its value in general is lower in the case of nuclear excitation than in the case of x-ray excitation.[7,28]

Values of the ratio L/K and the quantities used in calculating it

Isotope	S_L/S_K	I_L/I_K	ω_K [27]	$\bar{\omega}_L$ [28]	n_{KL} [7]	L/K	ϵ_0, kev
Dy^{159}	15.3	0.35	0.91	0.18	0.841	1.0±0.3	79^{+10}_{-5}
Er^{165}	22.0	0.40	0.92	0.17	0.834	1.2±0.4	82^{+10}_{-5}

3. The Dy^{159} nucleus, like its daughter Tb^{159}, belongs in the class of deformed nuclei with odd Z. In this case it may be assumed that the ground state spin is determined by the angular momentum of the odd nucleon. According to the work of Mottelson & Nilsson[30] and Peker[31] on the spins of deformed nuclei, the assignments for the ground states of Dy^{159} and Tb^{159} are 3/2+ and 3/2-, respectively (the 3/2- assignment for Tb^{159} has been substantiated experimentally). Consequently, the $Dy^{159} \rightarrow Tb^{159}$ transition must belong in the class of first forbidden transitions.

Using Marshak's formula, we obtained 79^{+10}_{-5} kev for the energy of this transition (this, accordingly, is the value listed in the table and in the Dy^{159} decay scheme reproduced in Fig.6). The lowest (57 kev) level of Tb^{159} is apparently not excited in the decay of Dy^{159}. We searched for this line in the spectrum of Dy^{159} by means of a scintillation spectrometer: neither this nor any other γ-lines were observed. However, inasmuch as such soft radiation must be strongly converted (the theoretical K and L shell conversion coefficients for E1 radiation of this energy are ~1.5 and 0.3, respectively), to determine for certain whether this level is excited, it is desirable to perform L-L coincidence experiments, which we plan to do in the near future (the transition to the 57 kev excited level could obviously occur only by L capture).

An evaluation of log ft, carried out on the basis of the deduced decay energy ϵ_0 = 79 kev and T = 136 days, yielded a value close to 6.2 for the $Dy^{159} \rightarrow Tb^{159}$ transition. This according to the classification of King[32] is consistent with the assumption of first degree forbiddenness for this transition.

Er^{165}

1. This erbium isotope was first discovered by Butement[33] in 1950 in bombarding holmium with fast protons. The 10-hour activity in the erbium fraction was attributed to Er^{165}, forming in the (p,n) reaction on the natural holmium isotope. Er^{165} was also obtained in irradiation of holmium with 10 Mev deuterons, apparently by the (d,2n) reaction.[34] In one of the investigations[34] of this isotope, there is mention of low intensity γ-rays of 220 and 1100 kev energy, presumably detected by absorption. Accordingly, Dzhelepov & Peker[26] in their book give the decay scheme for Er^{165} reproduced in Fig.8. According to this decay scheme, the $Er^{165} \rightarrow Ho^{165}$ transition energy should be greater than 1.1 Mev. The other levels of Ho^{165} indicated in the decay scheme were found in investigating the γ-spectrum of Dy^{165}.

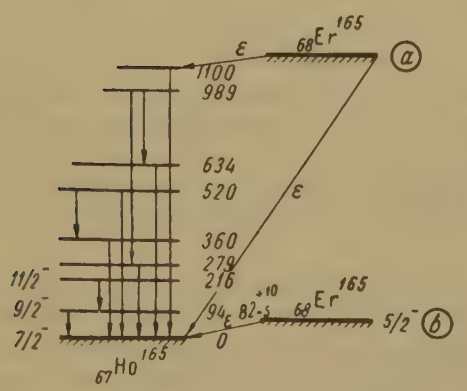

Fig.8. Er^{165} decay scheme: a) location of level according to Ref.26, b) location of level according to our data.

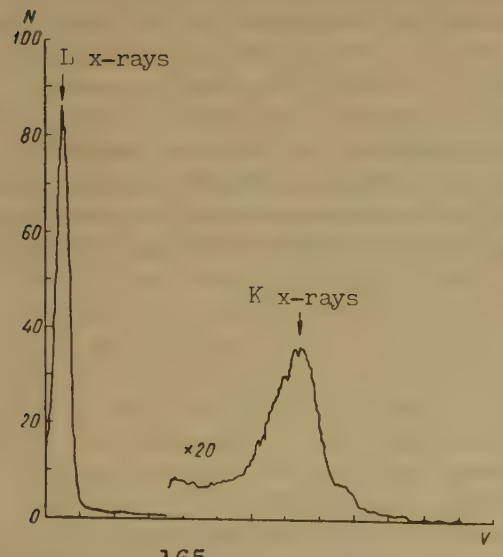

Fig.9. Er^{165} x-ray spectrum.

2. The Er^{165} sources used in our experiments were also obtained by bombardment of tantalum with fast (660 Mev) protons.

The erbium fraction was separated from the thulium fraction 1-2 days after separation of the latter from the bombarded tantalum by the ion exchange procedure. This fraction, as will readily be evident from an examination of all the erbium and thulium isotopes, contained only Er^{165} which is the daughter of 29-hour Tm^{165}. The purity of separation from thulium was checked with reference to the most intense 200 kev γ-line of Tm^{167} and by determining the period which was measured over five half-lives and found to be equal to 10.5 ± 0.5 hours.

We carried out several series of x-ray measurements on different sources obtained from tantalum targets irradiated for different lengths of time. One of the experimental curves obtained by means of the proportional counter is shown in Fig.9. The prominent features are the Ho K and L x-ray peaks (K_{α_1} = 47.5 kev, K_{β_1} = 53.9 kev and L_{α_1} = 6.72 kev).

The intensity ratio I_L/I_K as determined by averaging the results of the different series of measurements proved to be 0.40. Using this value and ω_K = 0.92 (Ref.27), $\bar{\omega}_L$ = 0.17 (Ref.28) and n_{KL} = 0.834 (Ref.7), we obtained L/K = 1.2 ± 0.4.

3. The $Er^{165} \rightarrow Ho^{165}$ decay belongs in the class of allowed transitions inasmuch as the spin of the Er^{165} ground state, according to Mottelson & Nilsson[30] and Peker[31], must be 5/2-, while the assignment for Ho^{165} is 7/2-. Using Marshak's formula, we obtain on the basis of our experimental value for L/K, ϵ_o = $= 82^{+10}_{-5}$ kev for the energy of the $Er^{165} \rightarrow Ho^{165}$ transition. This low transition energy is consistent with the now definitely proved absence of γ-radiation from Er^{165}, including the soft 94 kev and 122 kev γ-radiation corresponding to excitation of first rotational levels with energies of 94 and 216 kev. The absence of 1.1 Mev γ-rays follows not only from our search in this region by means of a scintillation spectrometer, but also from the deduced value of L/K. Thus if the decay scheme for Er^{165} shown in Fig.8 (a) were valid and there occurred K transitions to the 1.1 Mev level, then, regardless of how low the fraction of branching, the transition energy for the principal branch would be greater than the above value and consequently the experimentally determined L/K ratio should be less than 0.14. The divergence between this value and that found by us for L/K lies far beyond the limits of the possible experimental errors.

We calculated log ƒt on the basis of the determined transition energy (ϵ_o = = 82 kev) and the period (T = 10.5 hours) and obtained log ƒt = 3.1, which is consistent with the above inference that this is an allowed transition.

Conclusions

We found that in the case of Dy^{159} and Er^{165} the decay energies are very small, i.e., less than 100 kev. As was emphasized above, in the case of such low transitions energies the "L/K ratio" method yields reasonably accurate results for the transition energy even with a very rough determination of this ratio and, in the absence of γ-radiation, is relatively simple from the experimental standpoint.

The use of most of the other methods listed in the introduction, where Dy^{159} and Er^{165} and other similar isotopes are concerned, is precluded either from the standpoint of principle (methods 1 and 3) or from that of practice (method 4).

It is interesting to note that the empirical formula for atomic masses, given in a recent contribution by Levy[35], yields a value of 70 kev for the decay energy of Dy^{159} and a negative value for the decay energy of Er^{165}. Inasmuch as in 85% of the cases Levy's formula gives good agreement with the experimentally determined disintegration energies in the range to 250 kev, this may be regarded as a partial substantiation of the low energy values obtained by us for the transitions in question.

"V.G.Khlopin" Institute,
Academy of Sciences of the USSR

References

1. A.Bisi, E.Germagnoli & L.Zappa, Nuovo Cim., 11, 1052 (1955).
2. I.Olsen, L.Mann & M.Linder, Phys.Rev., 106, 985 (1957).
3. B.Pontecorvo, D.Kirkwood & G.Hanna, Phys.Rev., 75, 982 (1949).
4. R.Marshak, Phys.Rev., 61, 431 (1942).
5. M.Rose & J.Jackson, Phys.Rev., 76, 1540 (1949).
6. L.Zyrianova, I.Band & Iu.Suslov, Transactions of the Eighth All-Union Conference on Nuclear Spectroscopy, 1958.
7. B.Robinson & R.Fink, Revs.Mod.Phys., 27, 424 (1955).
8. H.Brysk & M.Rose, ORNL.-1830 (1955).
9. J.Heintze, Z.Naturforsch., 92, 469 (1954).
10. G.Bertolini, A.Bisi, E.Lassarini & L.Zappa, Nuovo Com., 11, 539 (1954).
11. G.Friedlander & W.Orr, Phys.Rev., 84, 484 (1951).
12. A.Bisi, L.Zappa & E.Zimmer, Nuovo Com., 4, 307, 539 (1956).
13. A.Bisi, S.Michalowicz & L.Zappa, Nuovo Com., 1, 651 (1955).
14. A.Bisi, E.Germagnoli & L.Zappa, Nuovo Com, 6, 299 (1957).
15. A.Bisi, L.Zappa, Nuovo Com., 12, 539 (1954).
16. P.Padvanyi & M.Langevin, Compt.rend., 238, 77 (1954).
17. O.Kofoed-Hansen, Phys.Rev., 96, 1045 (1954).
18. R.Daudel & S.Odiot, Journ.Phys.Rad., 17, 60 (1956).
19. A.Bisi, E.Germagnoli & L.Zappa, Nucl.Phys., 1, 593 (1956).
20. H.Curran & K.Siegbahn, Beta- and Gamma-ray Spectroscopy, New York,1955.
21. Handbook of Chemistry and Physics, p.2235, -(34th edition), Cleveland, Ohio, 1952.
22. A.Bisi & L.Zappa, Nuovo Com., 12, 211 (1954).
23. B.Ketelle, Phys.Rev., 76, 1256 (1949).
24. F.Butement, Proc.Phys.Soc., A64, 428 (1951).
25. N.Marty, Compt.rend., 241, 385 (1955).
26. B.Dzhelepov & L.Peker, Skhemy raspada radioaktivn. izotopov (Decay schemes of radioactive isotopes), M.-L., 1957.
27. K.Siegbahn, Beta- and Gamma-Ray Spectroscopy, N.Y., 1955.
28. R.Fink, Phys.Rev., 106, 266 (1957).
29. H.Lay, Z.Phys., 91, 533 (1934).
30. B.Mottelson & S.Nilsson, Phys.Rev., 99, 1615 (1955).
31. L.Peker, Izv.AN SSSR, Ser.fiz., 21, 1029 (1957). (Trans.Bulletin 21, No.7, 1030.)
32. R.King, Revs.Mod.Phys., 26, 327 (1954).
33. F.Butement, Proc.Phys.Soc., A63, 775 (1950).
34. D.Kunden, I.Service & M.Pool, Phys.Rev., 87, 203 (1952).
35. H.Levy, Phys.Rev., 106, 1265 (1957).

LIFETIME OF THE FIRST EXCITED STATE OF Mg^{24}

- N.N.Deliagin & V.S.Shpinel'

Introduction

The present investigation was concerned with measurement of the lifetime of the first excited (1.37 Mev) state of Mg^{24} by the method of resonance scattering of γ-rays (nuclear resonance fluorescence). In recent years this method has been successfully used for measuring short lifetimes of excited nuclear states (10^{-10} sec and shorter). The resonance scattering cross section increases with increasing width of the excited level, consequently the range of application of this method is not limited on the side of short lifetimes. The first successful experiments were carried out in 1950 by Moon; subsequently, the method was developed primarily in the work of Metzger. The development and potentialities of the resonance fluorescence method is described in the review of Malmfors[1] and Dzhelepov[2], which includes a complete bibliography.

The lifetime of the 1.37 Mev excited state of Mg^{24} has been measured by Coleman[3] by the method of delayed coincidences. Coleman obtained a value of $3.6 \cdot 10^{-11}$ sec, which is twice the value corresponding to a single-particle transition (Weiskopf formula[4]). In 1956 the present authors[5] and Burgov & Terekhov[6] measured the resonance scattering of γ-rays by Mg^{24}, the γ-ray sources used being either solid compounds containing Na^{24} or their solutions. Although measurements with solid or liquid sources can only give a very rough evaluation of the lifetime, even these measurements showed that the lifetime of the 1.37 Mev state is substantially shorter than 10^{-11} sec. In the work of Helm[7], this lifetime was evaluated from the results of experiments on inelastic scattering of fast electrons and a value of $\sim 1.9 \cdot 10^{-12}$ sec was obtained.

In the present work we used a gaseous Na^{24} source for measuring the resonance fluorescence.

1. Underlying theory

For observation of resonance scattering of γ-rays it is most natural to use as the γ-source the radioactive isotope that decays to the nuclei by which the photons are scattered (for example, for excitation of the 1.37 Mev level of Mg one should use the γ-radiation accompanying the $Na^{24} \rightarrow Mg^{24}$ transition). However, even in this case, the energy of the incident (exciting) γ-rays proves to be insufficient for resonance excitation. In accord with the laws of conservation of energy and momentum, the photon, owing to recoil of the nucleus, loses part of its energy, i.e., an amount of energy equal to $E_0^2/2Mc^2$ (E_0 is the γ-ray energy and M is the mass of the recoiling nucleus). The photon loses an equal part of its energy in absorption (the scattering process); thus the total energy deficit is $\Delta E = E_0^2/Mc^2$. Although this energy loss is relatively small (in the case of Mg^{24} it amounts to 84 ev), it is much greater than the width of the excited level; consequently, the resonance scattering cross section is reduced to a neglibly small value.

The energy of the incident γ-ray can be brought up to the resonance value by utilizing the Doppler effect. If the photon is emitted not from a stationary but from a moving nucleus, the energy of the photon is increased by an amount

$$\delta E = E_0 \frac{v}{c} \cos \vartheta, \qquad (1)$$

where V is the velocity of the nucleus and ϑ is the angle between the direction of motion of the nucleus and the emission of the photon. If δE proves equal to E_0^2/Mc^2 the resonance condition will be restored.

The emitting nuclei can be brought into motion either mechanically or by heating the source to a high temperature. Such methods have been successfully used in the region of medium and heavy nuclei for small excitation energies. In the case of the Mg^{24} 1.37 Mev level, these methods cannot be used inasmuch as the necessary mechanical velocities or temperatures lie outside the range of experimental feasibility.

In the present work we used the method of cascade transitions[8] for increasing the energy of the exciting γ-rays. In this case the nucleus is brought into motion through recoil incident to emission of a particle (β-particle, neutrino or photon) preceding the emission of the exciting γ-ray. If the energy of the preceding radiation is sufficient, the energy of the γ-rays will be increased to the resonance value. The total energy of the incident photon (taking into account the recoil loss) will be

$$E = E_0 - \frac{E_0^2}{Mc^2} + E_0 \frac{v}{c} \cos \vartheta. \qquad (2)$$

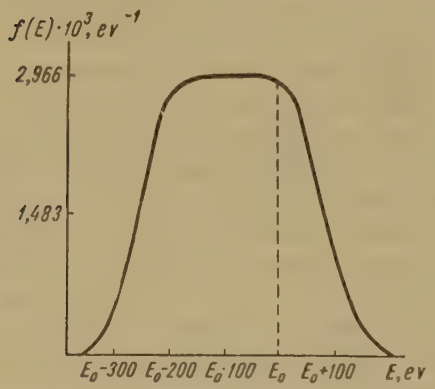

Fig.1. Microspectrum of incident (exciting 1.37 Mev γ-rays calculated on the basis of scalar interaction in β-decay.

It follows from this equation that the incident γ-rays will not be monoenergetic in the sense that their energy will vary as a function of $\cos \vartheta$ and the actual line width (the width of the "microspectrum" of the incident γ-rays) will substantially exceed the natural line width. The necessary condition for part of the γ-rays to have an energy sufficient for resonance excitation is

$$v > E_0 / Mc. \qquad (3)$$

If this condition is fulfilled the resonance scattering cross section is given by the formula[9]:

$$\sigma = \frac{2I_1 + 1}{2I_0 + 1} \cdot \frac{h^2 c^2}{4E_0^2} \Gamma f(E_0), \qquad (4)$$

where I_1 is the spin of the excited and I_0 the spin of the ground state of the nucleus, Γ is the width of the excited level, $f(E_0)$ is the distribution-in-energy density of the incident γ-rays in the microspectrum for the resonance energy E_0. Thus calculation of the cross section reduces in the given case to calculation of the microspectrum of the exciting γ-rays, i.e., the function $f(E)$.

In the $Na^{24} \rightarrow Mg^{24}$ decay scheme the 1.37 Mev γ-ray is preceded by the emission of a 2.75 Mev γ-ray and β-radiation with an end-point energy of 1.39 Mev. Hence condition (3) is fulfilled with an excess. The shape of the 1.37 Mev γ-ray spectrum will depend, in particular, on the spectrum of the recoil nuclei after β-decay, i.e., will be different for different variants of β-decay theory. Actually, however, the values of $f(E_0)$ calculated on the assumption of different types of interaction in β-decay differ from each other by less than 3%. Taking into account γ-γ angular correlation alters the value of $f(E_0)$ calculated for different types of β-decay interaction by 1% on the average. Thermal motion of the nuclei in the given case has virtually no influence on the magnitude of $f(E_0)$ for the thermal velocities are much lower than the velocities of the recoil nuclei following β-decay and emission of the 2.75 Mev γ-rays. Thermal motion can be expected to have a noticeable influence only at the edges of the microspectrum. The microspectrum of the 1.37 Mev γ-rays deduced on the assumption of scalar interaction in β-decay is shown in Fig.1.

Taking into account the uncertainty introduced by the ambiguity in specifying the type of β-decay interaction, the resonance scattering cross section for the given case, calculated by means of Eq.(4), is

$$\sigma = \frac{(1.93 \pm 0.04) \cdot 10^{-38}}{\tau}, \qquad (5)$$

where τ is the lifetime of the 1.37 Mev state of Mg^{24} in seconds.

2. Physical state of the source material

The results obtained above will be valid only when the recoil nuclei have a sufficiently large collision time: specifically, the 1.37 Mev γ-ray must be emitted by the moving recoil nucleus before it loses its velocity as a result of collisions with neighboring atoms. This condition is not fulfilled for a source in the solid or liquid state: in this case most of the 1.37 Mev γ-rays will be emitted by nuclei that have already attained thermal equilibrium with the neighboring atoms in the source. Our knowledge of the collision processes in solids and liquids is insufficient for carrying out a precise calculation of the influence of collisions on the shape of the microspectrum of the exciting γ-rays; at most we can make only a rough evaluation. Hence for purposes of lifetime measurements one must exclude this factor; this can be done by using a gaseous source. In a gaseous source at a pressure of about 1 atmosphere virtually all the 1.37 Mev γ-rays are emitted before the recoil nuclei lose their momentum through collisions.

In some cases in lifetime measurements by the resonance fluorescence procedure an important factor is the nature of the chemical bonds in the compound comprising the source.[8] Gaseous sodium is primarily monatomic. With increasing temperature part of the sodium atoms combine into Na_2 molecules. However, the fraction of Na_2 molecules at a gas temperature of 800-900° is small; moreover the atomic bonding energy is low, while the energy of the recoil atoms is large (170 ev after emission of the 2.75 Mev γ-ray). Hence in the present case we can neglect the influence of chemical bonds on the shape of the γ-ray microspectrum.

3. Description of the experiment

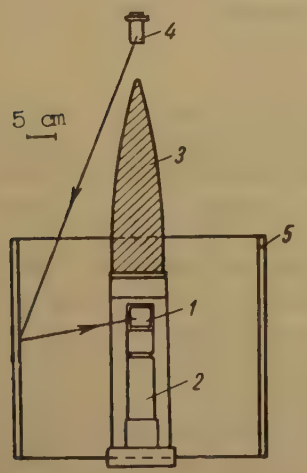

Fig.2. Experimental arrangement: 1) NaI(Tl) crystal, 2) FEU-29 photomultiplier, 3) lead shielding cone, 4) container with source, 5) scatterer.

The experimental arrangement is diagrammed in Fig.2. The scattered γ-rays were recorded by the NaI(Tl) crystal 1, having a thickness and diameter of 4 cm, and a FEU-29 photomultiplier tube. The photomultiplier output pulses were amplified and applied to a differential discriminator. The detector was shielded from direct radiation from the source by the 35 cm high lead cone 3. The tip of the cone also served as the support of the nichrome oven (not shown in the drawing). The temperature was measured by means of a "PP" thermocouple held in contact with the steel container 4, housing the source. The source consisted of 20-30 mg metallic sodium irradiated with slow neutrons in the heavy water reactor of the USSR Academy of Sciences. The activity of the source was 20-30 mC. After irradiation the sodium was placed in the steel container (volume 25 cm^2),

which was then tightly closed, evacuated and mounted in the nichrome oven.

The scatterer was a magnesium ring 5 having a diameter of 44 cm, a height of 40 cm and a wall thickness of 1.2 cm. For comparison we used a similar scatterer of aluminum. Particular attention was paid to stability of operation of the equipment: the scatterers were interchanged every 5 min to exclude the possible influence of slow changes in the operation of the electronic equipment. The 10 volt gate of the differential discriminator was centered on the 1.37 Mev photopeak (the half-width of the photopeak was equal to 4 v). The arrangement precluded detection not only of Compton scattering quanta but also possible chance coincidences of two such quanta. The counting rates with the magnesium and aluminum scatterers were compared at room temperature and at temperatures in the range from 800 to 880°. At room temperature these counting rates were equal within the limits of the experimental error; upon heating of the source the sodium was vaporized and the counting rate with the magnesium scatterer increased due to resonance scattering.

If the activity of the source is N_0 disintegrations per second, the resonance scattering counting rate is given by

$$N_p = N_0 \sigma \nu d \varepsilon_1 S \Omega \varkappa, \tag{6}$$

where ν is the number of Mg^{24} atoms per 1 cm^3, d is the effective thickness of the scatterer, ε_1 is the detecting efficiency for 1.37 Mev γ-rays, S is the area of the detector, Ω is a geometric factor and $\varkappa$ is the fraction of the total mass of the sodium in the gaseous state.

The experimental geometry was computed by integration over the surface of the scatterer. Appropriate corrections were made for the angular distribution of the scattered radiation[10], for absorption of γ-rays in the scatterer and for the geometric dependence of the efficiency.

For determining the resonance fluorescence cross section the counting rate N_p is compared with the counting rate when the source is located at a certain distance r from the detector. This counting rate is

$$N = N_0 (\varepsilon_1 + \varepsilon_2) \frac{S}{4\pi r^2}, \tag{7}$$

where ε_2 is the detecting efficiency for 2.75 Mev γ-rays. From Eqs.(6) & (7) it follows that

$$\sigma = \frac{N_p}{N} \cdot \frac{\varepsilon_1 + \varepsilon_2}{\varepsilon_1} \cdot \frac{1}{\nu d \Omega \, 4\pi r^2 \varkappa}. \tag{8}$$

The ratio $\frac{\varepsilon_1 + \varepsilon_2}{\varepsilon_1}$ is determined from the shape of the Na^{24} γ-radiation spectrum; it equals 1.5 with a possible uncertainty of 5%. The fraction $\varkappa$ is determined from the total mass of the source (weighed) and the mass of the vapor, which was calculated theoretically. The average value of $\varkappa$ for the different series of measurements was 0.2.

4. Results and discussion

The resonance fluorescence measurements were carried out at 5 different temperatures of the source in the range from 800 to 880°. With increasing temperature the amount of sodium vapor in the container (i.e., the fraction $\varkappa$) increases which leads to an increase in the resonance scattering counting rate Knowing the temperature dependence of the sodium vapor pressure, one can readily calculate the temperature dependence of the effect. As will be seen from Fig.3

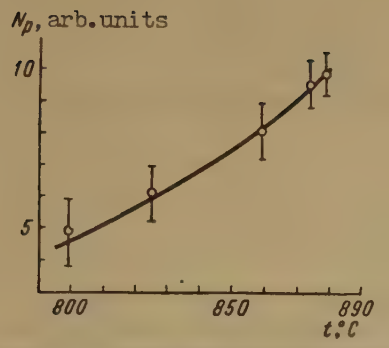

Fig.3. Temperature dependence of the resonance fluorescence effect. Points - experimental; solid line - theoretical curve.

the experimental results are in good agreement with the calculated curve.

At the beginning of measurements the resonance scattering counting rate was on the average 22 pulses per minute at 860°; this amounts to 10-15% of the total counting rate (in addition to the resonance scattering, the background and penetration of direct radiation through the lead shielding make a contribution to the total counting rate).

The experimental cross section for resonance fluorescence, as calculated by means of Eq.(8), was found to be $(1.14 \pm 0.26)\cdot 10^{-26}$ cm^2.

Whence the lifetime of the first excited state of Mg^{24}, computed by means of Eq.(5), is

$$\tau = (1.7 \pm 0.4)\cdot 10^{-12} \text{ sec.} \qquad (9)$$

The indicated uncertainty, in addition to the statistical uncertainty, comprises the error in determining all the quantities entering into Eq.(8), as well as the uncertainty introduced by the ambiguity in choosing the type of β-decay interaction (i.e., in this case the scalar variant of the theory was assumed). The above result is consistent with the lifetime given by Helm[7] on the basis of experiments on inelastic scattering of fast electrons by Mg^{24} nuclei.

The Bohr-Mottelson unified nuclear model[11,12] predicts that for nuclei with $A \approx 24$ the deformed equilibrium shape is energetically more advantageous than the spherically symmetric shape. As is known, the lower excited levels of deformed nuclei are rotational ones. Analysis of the excited state of Mg^{24} showed[13] that the 1.37 Mev state can be regarded as the first excited state of a rotational series with K = 0. If this interpretation is correct, we can calculate the quadrupole moment and the deformation parameter of the Mg^{24} nucleus from the measured lifetime. For an electric quadrupole transition between two rotational states with I = 2 and I = 0 and belonging to the same rotational series (K = 0), the reduced transition probability is[14]

$$B(E2) = \frac{e^2 Q_0^2}{16\pi}, \qquad (10)$$

where Q_0 is the quadrupole moment of the nucleus. A lifetime of $1.7\cdot 10^{-12}$ sec corresponds in this case to an absolute quadrupole moment of 0.7 barns. To calculate the deformation parameter β for the Mg^{24} nucleus, we can make use of the following formula given by Alder et al[15]:

$$Q_0 = \frac{3}{(5\pi)^{1/2}} zR_0^2\beta(1 + 0.16\beta), \quad (R_0 = 1.2\cdot 10^{-13}A^{1/3}). \qquad (11)$$

Numerical computation yields β = 0.59, which exceeds the deformation parameter values for elongated nuclei of the rare earth elements.

Moscow State University

References

1. K.G.Malmfors, in Beta- and Gamma-ray Spectroscopy, edited by K.Siegbahn, N.Y., 1955.
2. B.S.Dzhelepov, Usp.fiz.nauk, 62, 3 (1957).
3. C.Coleman, Phil.Mag., 46, 1135 (1955).
4. J.M.Blatt & V.F.Weisskopf, Theoretical Nuclear Physics, N.Y., 1952. (Cited in Russian trans.)
5. N.N.Deliagin & V.S.Shpinel', Abstracts of reports presented at the Seventh All-Union Conference on Nuclear Spectroscopy, p.42, M.-L., 1957.
6. N.A.Burgov & Iu.V.Terekhov, Atomnaia energiia (Atomic energy), No.6, 514 (1957).
7. R.H.Helm, Phys.Rev., 104, 1466 (1956).
8. F.Metzger, Phys.Rev., 101, 286 (1956); 103, 983 (1956).
9. H.Schopper, Z.Phys., 144, 476 (1956).
10. F.Metzger, Phys.Rev., 97, 1258 (1955).
11. A.Bohr & B.Mottelson, Dan.Mat.-Fys.Medd., 30, 1 (1955).
12. B.L.Birbrair, Zhur.eksp.i teor.fiz., 33, 1235 (1957). (Trans.,Soviet Phys., -JETP.).
13. L.I.Peker, L.V.Gustova & O.V.Chubinskii, Izv.AN SSSR, Ser.fiz, 21, 1013 (1957). (Trans.Bulletin 21, No.7, 1014.)
14. A.Bohr & B.Mottelson, Dan.Mat.-Fys.Medd., 27, 16 (1953).
15. K.Alder, A.Bohr, T.Huus, B.Mottelson & A.Winther, Revs.Mod.Phys., 28, 432 (1956).

CONCERNING DOPPLER BROADENING OF THE LINES ASSOCIATED WITH CONVERSION ELECTRONS EMITTED BY RECOIL NUCLEI

- A.V.Gnedich, L.N.Kriukova, V.V.Murav'eva, V.S.Shpinel' & V.I.Shumshurov

If a conversion electron is emitted by a moving recoil nucleus the change in electron momentum $\Delta p = p - p_0$ due to the Doppler effect is given by

$$\Delta p = p_0 \frac{V}{v_0} \cos\theta,$$

where p_0 is the momentum of an electron emitted by a stationary nucleus, v_0 is the velocity of the electron emitted by the stationary nucleus, V is the velocity of the recoil nucleus and θ is the angle between the velocities of the nucleus and electron.

This effect influences the position and shape of the conversion line; under certain conditions this may be utilized for determining the lifetime of the excited nuclear state.[1,2] Moreover, the distortion of the line shape produced by the effect must be taken into account in determining the relative intensities of conversion lines and the values of conversion coefficients.

The present work was concerned with investigation of the Doppler effect for the conversion lines associated with the transition from the 40 kev level in the Tl^{208} (ThC") nucleus excited in α-decay of Bi^{212} (ThC) to the ground state. The influence of the Doppler effect on the shape of a given conversion line recorded by means of a spectrometer depends on the experimental conditions.

Let us consider the case of an infinitely thin plane source. In the case of isotropic distribution, 50% of the recoil nuclei will move in the direction of the source backing. For the conversion electrons emitted by these nuclei, Δp will depend on the relation between the stopping time T for the nuclei in the backing and the mean lifetime τ of the level. The other 50% of the nuclei will move away from the backing and escape into the vacuum of the spectrometer chamber. The electrons emitted by these nuclei will be detected only if before the emission event the nuclei did not have time to emerge from the region of focusing of the spectrometer. Consequently, the observed Doppler effect must depend on the ratio between τ and the time of flight t of the nuclei in the focusing region. This time t can be evaluated. Assuming the dimensions of the focusing region to be of the order of some tenths of a millimeter, if the velocity of a recoil nucleus is $\sim 10^7$ cm/sec, the time t will be $\sim 10^{-9}$ sec. The stopping time for recoil nuclei in a solid medium is much shorter. For example, for slowing down in aluminum of Tl^{208} recoil nuclei having an initial velocity of $3.3 \cdot 10^7$ cm/sec, the stopping time $T \approx 2 \cdot 10^{-13}$ sec.

If the lifetime of the excited state is much shorter than the slowing down time in the backing ($\tau \ll T$), there must be observed a maximum Doppler line broadening equal to $\frac{2\Delta p}{p_0} = \frac{2V}{v_0}$. In this case the conversion line will be extended equally to both sides. When $\tau \leqslant T$, the nuclei moving into the backing will emit electrons after some slowing down or being stopped completely. In this case the line will become asymmetric; the broadening to the side of high energies will be the same as in the preceding case, while the broadening to the side of low energies will be reduced.

If the lifetime τ lies in the range between T and t, the conversion line will consist of two parts S_1 and S_2 equal in intensity (Fig.1). The part S_1 is due to electrons emitted by nuclei stopped in the backing; this part of the line is somewhat diffused owing to the fact that the electrons are emitted from the depth of the backing. S_2 is due to electrons emerging into the vacuum and

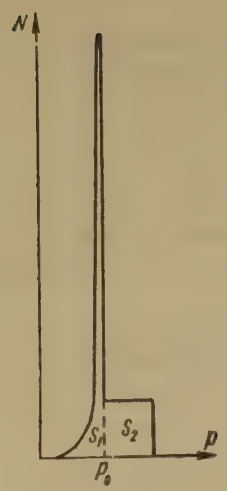

Fig.1.

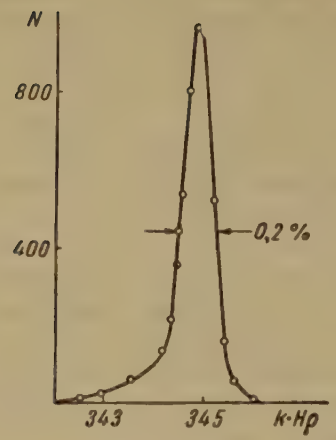

Fig.2

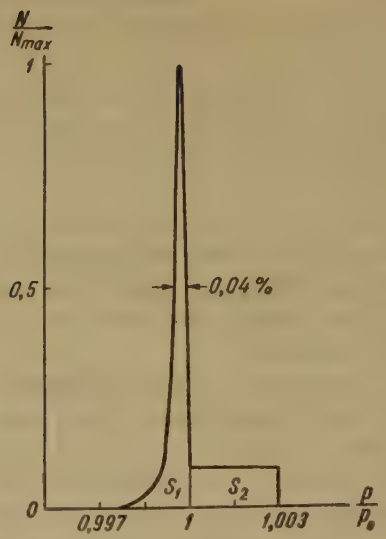

Fig.3

Fig.1. Distribution of electrons in momentum for an infinitely thin plane source when $T < \tau < t$.

Fig.2. F line, E_e = 147 kev.

Fig.3. Momentum distribution of conversion electrons for the B line.

receiving only a positive addition to their velocity.* In the case of isotropic distribution of recoil nuclei and conversion electrons, S_2 has the shape of a rectangle of width V/v_0. When $\tau \gg t$, the recoil nuclei will pass through the focusing region before emitting electrons. In this case there will be observed a decrease in the intensity of the conversion lines, an effect first noted by Flammersfeld[3] in investigating a Th active deposit. If τ is comparable with t, there will be observed both a change in the shape of the line and a reduction of its intensity, from the magnitude of which one can calculate the lifetime of the level.

In practice the thickness of the source has an appreciable influence on the observed effects. Only when the lifetime is much shorter than the stopping time ($\tau \ll T$) are the line shape and intensity independent of the source thickness. In cases when $T < \tau < t$, increase of the source thickness leads to an increase in the number of electrons emitted by completely stopped nuclei. Then the area S_1 increases at the expense of S_2. With $\tau > t$, increase in the thickness of the source leads to increase of the relative number of nuclei emerging into the vacuum. When the thickness of the source greatly exceeds the range of the recoil nuclei, then in all cases, except when $\tau \ll T$, neither Doppler broadening nor a decrease in the intensity of the conversion lines will be observed.

We investigated the conversion line shape on a spiral β-spectrometer. The source was a thorium active deposit on an aluminum strip measuring 15 x 0.4 mm. The activation time was 2 hours. The half-width of the F line (Fig.2) was 0.2%. We determined the effective thickness of the source from the fraction of Tl^{208} nuclei escaping from the source. The fraction of escaping recoil nuclei was evaluated from the change in the intensity of the G and H lines of the Th active deposit with the source open and with the source covered with a thin film.[4] For

---

*This is true in the case when the plane of the source is perpendicular to the axis of the electron beam and the instrument aperture angle is small.

an infinitely thin source the fraction of escaping nuclei should be 0.5. In our case it proved to be 0.34. Whence we obtain a value of 0.6 R (R is the range of the recoil nuclei) for the source thickness.*

The theoretical shape of the lines under study was computed on the assumption that the mean lifetime τ of the 40 kev level lies between T and t. The momentum distribution of the B line electrons (conversion on the M_I shell; electron energy E_e = 36.7 kev) is shown in Fig.3. Here we assume a linear relationship between the range R and the velocity V of the recoil nuclei.**

The width of the S_2 trangle equals 0.003 p_o. In this distribution the area ratio S_1/S_2 is of the order of 2, which is in agreement with the experimentally determined fraction of escaping nuclei. The relative half-width of the S_1 distribution taking into account the total thickness of the source (1.6 R) was evaluated to be 0.04%.

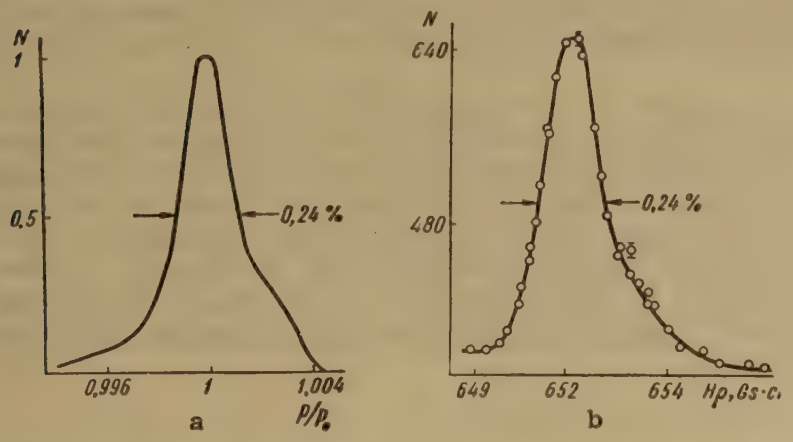

Fig.4. a) Expected shape of the B line allowing for distortion of the electron distribution by the apparatus line; b) B line obtained experimentally. E_e = 36 kev.

The expected shape of the B line, obtained from this distribution taking into account our apparatus line shape, is shown in Fig.4a. From a comparison of Figs.2 and 4a, it will be evident that the Doppler effect leads to broadening of the line to the high energy side. The experimental B line is reproduced in Fig.4b. It will be seen that its shape agrees with the predicted one. We observed an analogous line broadening to the side of high energies for the Aa line (the L_{II} line of the same transition; E_e = 25 kev). We deemed it desirable to make sure that this effect was not due to apparatus distortion of the line shape in the given energy region. To this end we made use of the Ce^{144} conversion spectrum lines which are not distorted by the

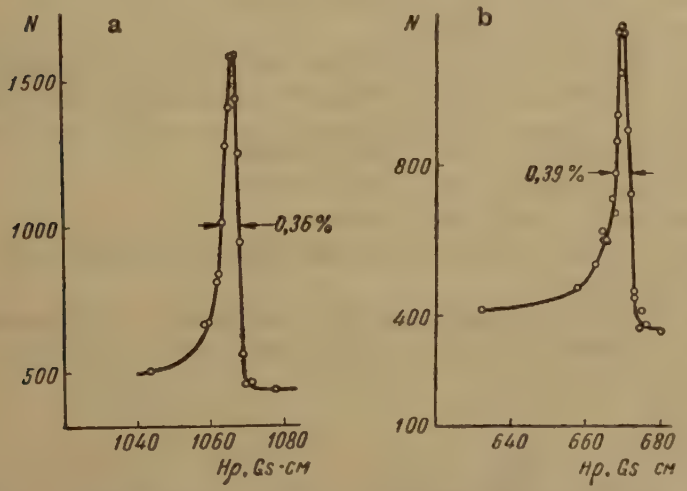

Fig.5. Conversion lines of Ce^{144}: a) E_e = 92 kev (K line of the 134 kev transition), b) E_e = = 39 kev (K line of the 80 kev transition).

---

*The activity of the source is assumed to be uniformly distributed in depth. We did not take into account the effective diffusion into the depth of the backing during activation, an effect recently reported by Siekman & de Waard.[5]

**Assumption of a quadratic relation between the range and velocity ($R = \alpha V^2$) somewhat modifies the shape of S_2, but has very little effect on the final form of the curve shown in Fig.4,a.

Doppler effect. It will be evident from Fig.5 that in going from 92 kev to 39 kev there is no appreciable alteration of the line shape. Consequently, the observed broadening of the B and Aa conversion lines must be due to the Doppler effect. This inference is in agreement with the mean lifetime of the 40 kev transition as determined by Burde & Cohen[2] and Graham & Bell[6].

We could not make use of the most intense conversion line of the 40 kev transition in ThC'' - the A line - inasmuch as it is complex. The increase in the half-width of the A line by 0.2% as compared with the F line with an instrument resolution of 1.2%, observed in the work of Burde & Cohen[7], in our opinion cannot be due exclusively to the Doppler effect. Investigation of this line with high resolution without taking into account the Doppler effect leads to an erroneous evaluation of the relative intensities of the A and A' lines and their half-widths.[8,9]

Thus by investigating the shape of conversion lines due to electrons emitted by moving nuclei one can arrive at an evaluation of the liftime of the corresponding nuclear levels. In analyzing the line shape one must take into account the specific experimental conditions and in particular the thickness of the source. The lifetime can also be evaluated by determining the decrease in intensity of the line due to the escape of recoil nuclei from the source, if the thickness of the source is known. Careful analysis of the shape of conversion lines emitted by moving (recoil) nuclei is essential in evaluating the relative intensities of conversion lines.

Moscow State University

References

1. V.S.Shpinel' & R.I.Moshkina, Zhur.eksp.i teor.fiz., 21, 1127 (1951).
2. J.Burde & G.Cohen, Phys.Rev., 104, 1093 (1956).
3. A.Flammersfeld, Z.Phys., 114, 227 (1939).
4. E.M.Krisiuk, A.D.Vitman, V.D.Vorob'ev, I.V.Vorob'ev, K.I.Il'in, G.D. Latyshev, M.A.Listengarten & A.G.Sergeev, Izv.AN SSSR, Ser.fiz., 20, 883 (1956). (Trans.Bulletin 20, No.8, 803.)
5. J.G.Siekman & H.deWaard, Phys.Rev., 107, 1731 (1957).
6. R.L.Graham & R.E.Bell, Canad.J.Phys., 31, 374 (1957).
7. J.Burde & S.G.Cohen, Phys.Rev., 101, 495 (1956).
8. E.M.Krisiuk, G.D.Latyshev & A.G.Sergeev, Izv.AN SSSR, Ser.fiz., 20, 367 (1956). (Trans.Bulletin 20, No.3, 335.)
9. V.D.Vorob'ev, K.I.Il'in, T.K.Kol'chinskaia, G.D.Latyshev, A.G.Sergeev, Iu.N.Trofimov & V.I.Fadeev, Izv.AN SSSR, Ser.fiz., 21, 954 (1957). (Trans. Bulletin, 21, No.7, 956.)

ELASTIC SCATTERING OF PROTONS BY Si^{28} NUCLEI. SPIN AND PARITY OF THE 4.31 AND 4.73 Mev LEVELS OF P^{29}

- A.K.Val'ter, I.Ia.Malakhov, P.V.Sorokin & A.Ia.Taranov

Introduction

The most convenient procedure for investigating the levels of P^{29} lying above 3 Mev is apparently elastic scattering of protons by Si^{28}. The Si^{28} nucleus has a closed $D_{5/2}$ subshell and spin I = 0, while the proton binding energy is relatively low (2.72 Mev). Presumably the levels of P^{29}, which has one proton outside the closed $D_{5/2}$ subshell, are comparatively widely spaced. All this gives reason to assume that analysis of the experimental p-Si^{28} scattering data should be relatively simple.

Recently, there was published a brief communication by Olness et al[1] concerning measurements of the p-Si^{28} scattering cross section in the energy range from 1.4 to 3.8 Mev. The authors do not give the results of measurements but indicate that they detected resonances at proton energies of 1.65 Mev (width 60 kev), 2.09 Mev (width 25 kev) and a giant resonance at 2.9 Mev.

The purpose of the present work was to measure the p-Si^{28} scattering cross section for the purpose of determining the assignments for the excited states of P^{29} associated with the resonances mentioned by Olness et al.

1. Experimental technique

The apparatus employed for the experiments is diagrammed in Fig.1. The source of protons was the electrostatic generator of the Physical-Technical Institute of the Ukrainian SSR Academy of Sciences. The proton beam was deflected 90° by a magnetic analyzer, passed through the system of collimating annuli A,B and C (diameter 2 mm) and impinged on the silicon target 0 having a thickness of 0.2 mg/cm^2. The energy spread of the protons amounted to 0.05%. The protons scattered in a $4 \cdot 10^{-4}$ sterad solid angle by the target nuclei were detected by a 0.5 mm thick CsI crystal and an FEU-25 photomultiplier. The primary beam current was measured by means of a Faraday cup (F) and a current integrator.

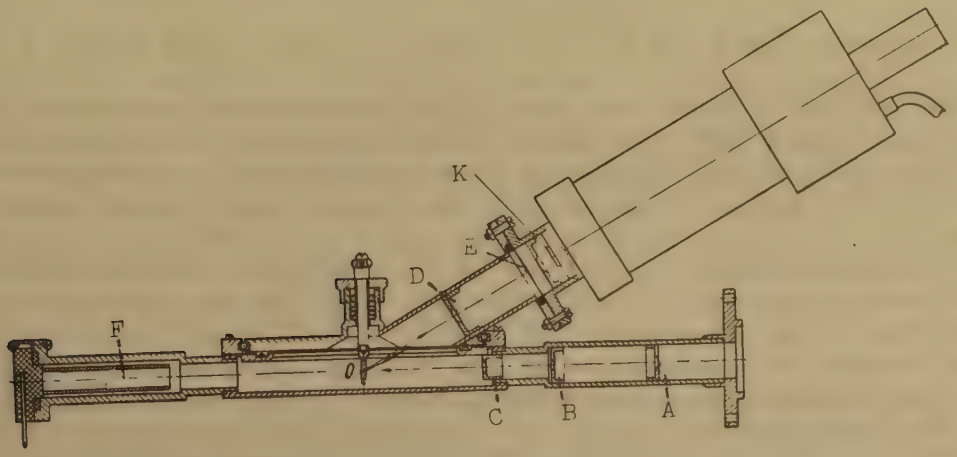

Fig.1. Diagram of apparatus: A,B,C,D & E - defining annuli, F - Faraday cup, K - crystal, 0 - target.

The target was prepared by vacuum evaporation of natural silicon from a carbon crucible onto a polished backing of stainless steel. The silicon film was then pealed off the backing; as a result there was obtained a free-standing silicon target. The thickness of the target was evaluated from the results of an experiment on small angle proton scattering, wherein the principal contribution to the cross section is made by Coulomb scattering.

2. Experimental results

The scattering was measured at angles of 75, 90, 125.5 and 151° in the center of mass system and in the proton energy range from 1.5 to 3.1 Mev. Inasmuch as the target thickness was not determined independently, the scattering cross sections are given in relative units (Figs.2-5).

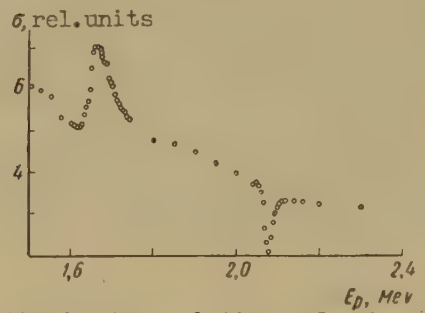

Fig.2. Variation of the relative elastic scattering cross section with the proton energy at $\theta = 75^{\circ}$.

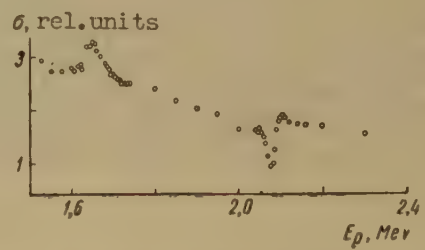

Fig.3. Same as Fig.2 but with $\theta = 90^{\circ}$.

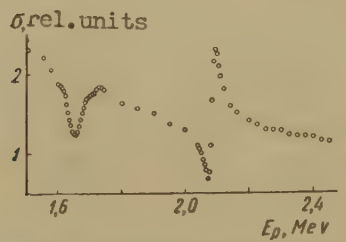

Fig.4. Same as Fig.2 but with $\theta = 125.5^{\circ}$.

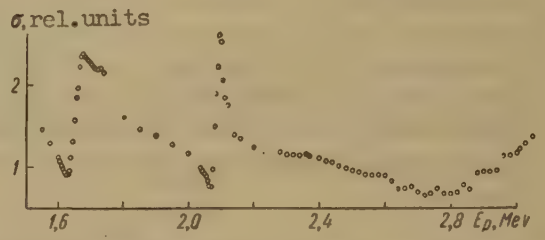

Fig.5. Same as Fig.2 but with $\theta = 151^{\circ}$.

It will be evident from the figures that there are clearly pronounced resonances in the p-Si^{28} scattering cross section at proton energies of 1.65 and 2.08 Mev (half-widths, 50 and 14 kev, respectively). In Fig.5 there is discernible a third resonance extending to the upper bound of the investigated energy range.

A certain anomaly is evident in the variation of the cross section at a proton energy of about 1.75 Mev (Figs.4 & 5). It is connected with resonance scattering of the protons by C^{12} nuclei (Ref.2) which contaminated the target in the process of evaporation of the silicon from the carbon crucible. Our evaluations showed that the carbon content in the target did not exceed 3%.

The experimental results were utilized for determining the spins, parities and reduced widths of the 4.31 and 4.73 Mev levels of P^{29}, i.e., the levels associated with the first two resonances. We did not carry out an analysis of the cross section near 2.9 Mev.

3. Analysis of the results

The cross section for elastic scattering by nuclei with 0 spin is given by the expression[3]

$$\sigma(\theta, E) = \lambda^2 (|A|^2 + |B|^2), \tag{1}$$

where

$$\left.\begin{aligned} A(\theta, E) &= -\frac{1}{2}\eta \operatorname{cosec}^2\frac{\theta}{2} \exp\left(i\eta \ln \operatorname{cosec}^2\frac{\theta}{2}\right) + \\ &+ \sum_{l=0}^{\infty} [(l+1)\exp(i\alpha_l + i\delta_l^+)\sin\delta_l^+ + l\exp(i\alpha_l + i\delta_l^-)\sin\delta_l^-] P_l(\cos\theta) \\ B(\theta, E) &= i\sin\theta \sum_{l=1}^{\infty} P'(\cos\theta)\, e^{i\alpha_l} [\sin\delta_l^- \exp(i\delta_l^-) - \sin\delta_l^+ \exp(i\delta_l^+)]; \end{aligned}\right\} \tag{2}$$

$$\eta = \frac{ze^2}{\hbar v}; \quad \lambda = \frac{\hbar}{mv}; \quad P'(\cos\theta) = \frac{d[P_l(\cos\theta)]}{d[\cos\theta]};$$

$$\alpha_l = 2\sum_{s=1}^{l} \operatorname{arctg}\eta/s \text{ for } l > 0; \ \alpha_0 = 0;$$

the $\delta_l^{\pm}$ are the phase shifts of the l-th partial wave scattered in states with the total momentum $I = l \pm \frac{1}{2}$; Z is the charge of the target nuclei, m is the reduced mass of the system and θ is the angle of scattering in the center of mass system.

According to the theory of Wigner & Eisenbud[4], the phase shifts near the resonances can be represented in the form

$$\delta_l^{\pm} = -\operatorname{arctg}\left(\frac{F_l}{G_l}\right)_{r=a} + \operatorname{arctg}\left[\frac{k\gamma_\lambda^2 / A_l^2}{E_\lambda + \Delta_\lambda - E}\right]_{r=a}, \tag{3}$$

where F_l and G_l are the regular and irregular Coulomb functions, γ_λ^2 is the reduced width of the λ level and E_λ is its characteristic energy;

$$\Delta_\lambda = -\left[\frac{k\gamma_\lambda^2}{\rho}\left(\frac{\rho}{A_l^2}\frac{dA_l}{d\rho} + 1\right)\right]_{\rho = k\alpha};$$

$$A_l^2 = F_l^2 + G_l^2, \quad k = \frac{mv}{\hbar};$$

a is the interaction range which is usually assumed to be the same and equal to $1.45\,[A^{1/3} + 1]\cdot 10^{-13}$ cm for all partial waves.

With the interaction parameter specified, the analytic problem consists of determining the values of l, I and γ_λ^2 so that the cross sections computed by means of Eqs. (1), (2) and (3) will fit the experimental results.

The reduced level width γ_λ^2 is related to the width Γ_λ observed experimentally by the expression

$$\frac{1}{2}\Gamma_\lambda = \left(\frac{k\gamma_\lambda^2}{A_l^2}\right)_{r=a} \tag{4}$$

From Wigner's relation $\gamma_\lambda^2 \leqslant \frac{3\hbar^2}{2ma}$ and Eq. (4), we have the inequality

$$\frac{1}{2}\Gamma_\lambda \leqslant \frac{3\hbar^2 k}{2maA_l^2}. \tag{5}$$

this inequality allows of determining the maximum value of the orbital angular momentum l that can be associated with the resonance width Γ_λ.

On the basis of the experimental widths Γ_λ for the 1.65 and 2.08 Mev resonances and inequality (5), we established that the first resonance is associated with $l < 2$ and the second with $l \leqslant 3$.

It is apparent from Eqs.(1) and (2) that if the resonance is connected with one level, then the 90° scattering cross section has an almost symmetrical maximum only for odd l. On the contrary, the presence of a minimum indicates that the corresponding resonance is associated with an even l.

The results of our measurements at 90° show that the resonance at 1.65 Mev is associated with an odd value of the orbital momentum, which must moreover satisfy the condition $l < 2$. Consequently, the first resonance is associated with $l = 1$ and the corresponding level has odd parity.

An analogous argument leads to the inference that the resonance at 2.08 Mev is associated with an even l, which can be either 0 or 2. The $l = 2$ value must be rejected in view of the shape of the resonance obtained at an angle of 125.5°. For this angle the second Legendre polynomial P_2 (cos θ) is close to zero. If the resonance in question were associated with $l = 2$, then, in accord with Eqs. (1) & (2), the cross section curve would have an almost symmetrical maximum; this, however, is not the case (Fig.4). Hence we must infer that the resonance at 2.08 Mev is associated with $l = 0$ and that the spin and parity of the excited state of P^{29} corresponding to it are 1/2+.

Thus our analysis leads to the conclusion that the assignment for the 4.31 Mev level may be 3/2- or 1/2-; the assignment for the 4.73 Mev level has been determined unambiguously as 1/2+. To choose between the alternatives for the 4.31 Mev level one must carry out a detailed comparison of the theoretical curves with the experimental results.

Using the graphic method described by Laubenstein & Laubenstein[5], we found that the theoretical curves satisfactorily fit the experimental ones if we take $2.23 \cdot 10^{-13}$ Mev cm for the reduced width γ_λ^2 of the first level and $0.13 \cdot 10^{-13}$ Mev cm for that of the second level and assume that the assignment for the first level is 3/2-.

We used these values for calculating the p-Si^{28} scattering cross section in the energy range from 1.6 to 2.2 Mev by means of Eqs.(1), (2) & (3) without introducing any further assumptions regarding the energy dependence of the phases.

Inasmuch as a target having a thickness equivalent to 20 kev was used in the experiments, for comparison of the experimental data with the calculated values the latter were first averaged over the thickness of the target:

$$\bar{\sigma}(E)=\frac{1}{\Delta E}\int_{E}^{E-\Delta E}\sigma(E)dE$$

where $\sigma(E)$ is the calculated cross section for p-Si^{28} scattering and ΔE is the energy loss of the protons in the target.

The results of our calculation are given by the solid lines in Figs.6-9. The points in these figures represent the experimental results, while the dash line in Fig.9 shows the curve calculated on the assumption that the spin and parity of the 4.31 Mev level are 1/2-. It will be seen that this curve shows very poor agreement with experiment; consequently, the 1/2- assignment can be eliminated.

The maximum divergence between the experimental points and the calculated curves (solid lines) does not exceed 25%. This divergence is not excessive in view of the fact that in the experiments we used a silicon target with the natural isotopic composition (92% Si^{28}) which also contained ~3% carbon. Moreover the measurement results, particularly in the regions of the sharp minima and maxima, were undoubtedly influenced by the fact that a target of appreciable thickness was used in the experiments.

The difference between the calculated curve and the experimental points at about 2.2 Mev (Fig.9) is apparently due to the fact that the δ_0 phase behaves

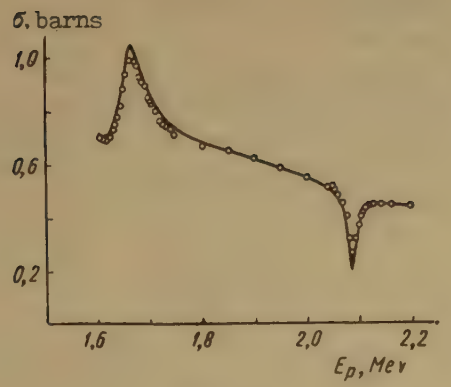

Fig.6

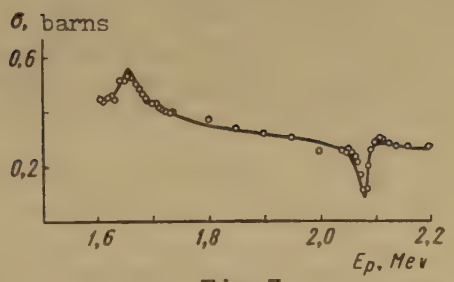

Fig.7

Fig.6. Comparison of experimental and calculated data at $\theta = 75^{\circ}$.
Fig.7. Same as Fig.6, but with $\theta = 90^{\circ}$.

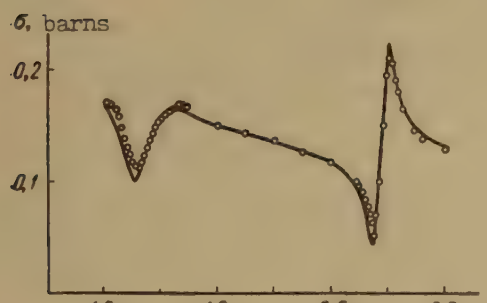

Fig.8

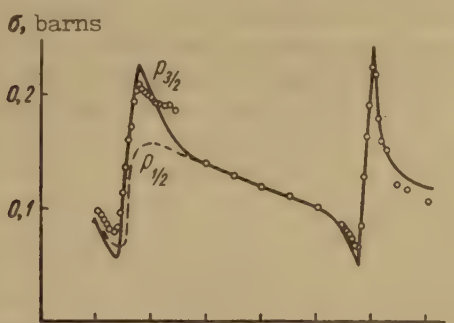

Fig.9

Fig.8. Same as Fig.6 but with $\theta = 125.5^{\circ}$. Fig.9. Same as Fig.6 with $\theta = 151^{\circ}$.

somewhat differently than described by Eq.(3). The cross section at 151° is very sensitive to the δ_0 phase. For complete agreement of the data one need increase δ_0 by only 4°. Such a change in phase has virtually no effect on the calculated results for the other scattering angles.

Conclusions

The experimentally determined half-widths of the resonances at proton energies of 1.65 and 2.08 Mev were found to be 50 and 14 kev, respectively; these values differ substantially from the 60 and 25 kev half-widths reported by Olness et al[1]. Since these authors give virtually no experimental details, it is impossible to suggest a reason for the divergence.

The results of phase analysis are listed in the accompanying table ($a = 5.86 \cdot 10^{-13}$ cm).

The ratios of the cited level widths to the value of $3\hbar^2/2ma$ show that the 4.31 Mev level is apparently a single particle one, while the 4.73 Mev level owes its existence to a more complicated excitation mechanism.

The assignments for the investigated levels listed above are the results of our preliminary measurements of proton polarization in p-Si^{28} elastic scattering.

E_p, Mev	Level energy, kev	Level width, kev, in c.m. system	Spin and parity	Reduced width $\gamma\lambda^2$, Mev cm	Ratio $\gamma^2\lambda/3\hbar^2/2ma$
1.65	4.31	48	$\frac{3}{2}-$	$2.23 \cdot 10^{-13}$	0.2
2.08	4.73	13.5	$\frac{1}{2}+$	$0.13 \cdot 10^{-13}$	0.01

Physical-Technical Institute,
Academy of Sciences of the Ukrainian SSR

References

1. J.W.Olness, W.Heaberli & H.W.Lewis, Bull.Amer.Phys.Soc., 2, 34 (1957).
2. H.L.Jackson & A.J.Galonsky, Phys.Rev., 89, 370 (1953).
3. J.Lepore, Phys.Rev., 79, 137 (1951).
4. E.P.Wigner & L.Eisenbud, Phys.Rev., 72, 29 (1947).
5. R.A.Laubenstein & M.J.W.Laubenstein, Phys.Rev., 84, 18 (1951).

TOROIDAL SECTOR TYPE β-SPECTROMETER

- S.Salai & D.Bereni

In this communication we shall give a brief description of the toroidal β-spectrometer constructed in the Nuclear Research Institute of the Hungarian Academy of Sciences. The first report regarding the design of this spectrometer was published by Horvath[1].

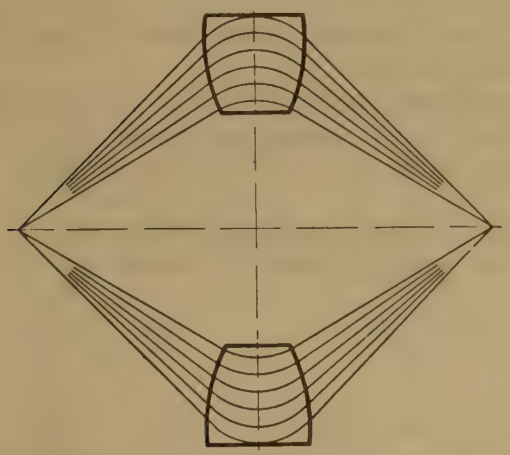

Fig.1. Focusing principle employed in the toroidal sector spectrometer.

The focusing principle of the instrument is illustrated in Fig.1. The core of the toroidal coil is a ring separated into 42 segments by 42 gaps with parallel faces. The figure shows the profile of the iron segments and the electron trajectories in the spectrometer. The magnetic field is perpendicular to the plane of the figure. The magnetic field lines at the points of entry and emergence of the electrons are curved. Through proper design of the segments (field configuration), it proved possible to eliminate spherical aberration.

The magnetic coil surrounds the core segments so that the gaps are free for the passage of electrons. The entire spectrometer is mounted in a vacuum chamber (Fig.2). The source holder is located at one end of the spectrometer on the symmetry axis; at the other end - symmetrical with the source - is an anthracene crystal coupled to a photomultiplier.

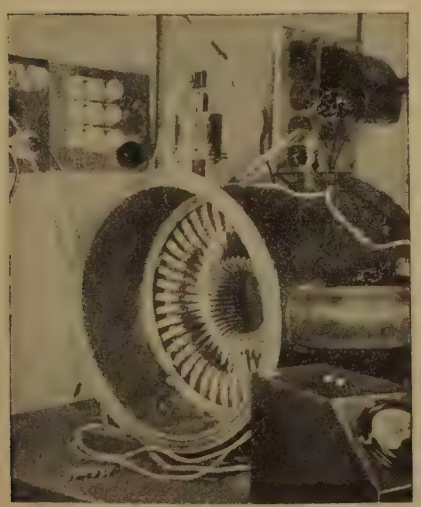

Fig.2.

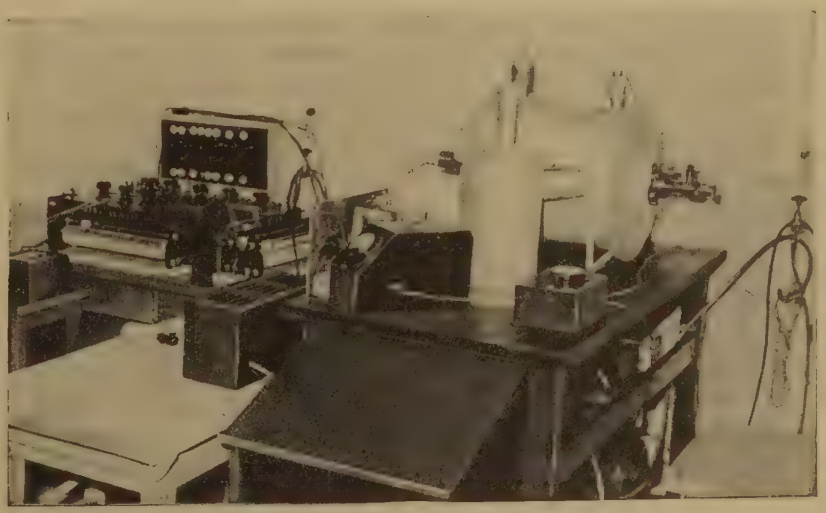

Fig.3

Fig.2. Mounting of the toroidal coil in the vacuum chamber.
Fig.3. General view of the spectrometer.

The focusing properties of the spectrometer were investigated by means of the radiation from Th(B + C) and Cs^{137} and Agfa Texo-R x-ray film. Our preliminary measurements carried out with Cs^{137} showed that the relative line half-width is about 3-4%; the transmission factor 2.5%.

These values are in line with those characteristic of ordinary magnetic lens spectrometers. Our spectrometer, however, has certain new valuable characteristics, namely:

1. As measurements showed, there is no magnetic field at the points of location of the source and detector.

2. The spectrometer requires a relatively low current (less than 3 amp, i.e., one order of magnitude lower than magnetic lenses).

3. The design dispenses with baffles separating electrons from positrons.

The cited characteristics, particularly the first, make this type of β-spectrometer very convenient for the investigation of β-γ, e^--γ. and e^--β-coincidences.

Construction and adjustment of instruments of this type have already started in our Institute. A general view of the spectrometer is shown in Fig.3.

Nuclear Research Institute,
Hungarian Academy of Sciences

References

1. J.I.Horvath, Experientia, 5, 112 (1949).

PRECISION MEASUREMENTS OF THE Co^{60} 1.17 AND 1.33 Mev, Hf^{181} 482 kev AND Au^{199} 158 AND 208 kev γ-LINES

- M.P.Avotina & O.I.Sumbaev

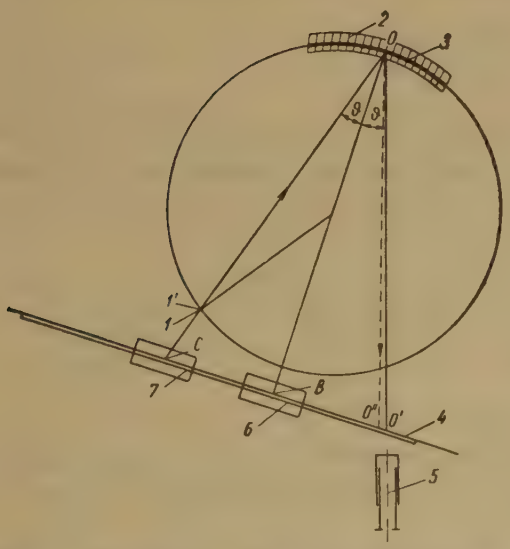

Fig.1. Diagram of sine mechanism with optical indicating device: 1 & 1' - positions of source and cross hairs, 2 - bent crystal, 3 - spherical mirror, 4 - glass scale, 5 - eyepiece micrometer, 6 - crystal carriage, 7 - source carriage.

Table 1

Results of measurements of the Au^{198} 412 kev γ-line energy ($2\bar{l}$ = 51.145 mm)

№	$2l$	$2\bar{l} - 2l$
1	51,146	—0,001
2	51,151	—0,006
3	51,145	0,0
4	51,135	+0,010
5	51,147	—0,002
6	51,146	—0,001
7	51,145	0,0
8	51,139	—0,006
9	51,152	—0,007
10	51,148	+0,002

The principal source of errors involved in wavelength (energy) measurements carried out on the 2-meter curved crystal spectrometer[1,2] of the All-Union Scientific Research Institute of Metrology were elastic and inelastic deformations of the members forming the measurement triangle (COB in Fig.1). Bending of the rod OB, transmitting the motion from the crystal carriage 6 to the crystal 2, led to statistical scatter of the measured values with a mean root square deviation of the order of 0.18 mÅ. Even more important was the possibility of deformation-caused deviations of the spectrometer scale from linearity (changes in the coefficient k in the expression $\lambda = k2l$ relating the γ-radiation wavelength with the distance CB = l between the source and crystal carriages).

In order to exclude the influence of deformable mechanical linkages, the optical indicating system described below was realized.

A diagram of the optical indicating device is shown in Fig.1. The transparent glass scale 4 is rigidly connected with the source carriage 7 and is located in the field of view of the microscope with an eyepiece micrometer 5, designed to read to within 0.01 mm.

A set of cross hairs 1', illuminated by a special lamp, is mounted above the γ-ray source 1; an image of the cross hairs is projected by the spherical mirror 3, rigidly connected with the bent crystal holder 2, onto the scale in the field of view of the microscope 5. The sine mechanism of the instrument is designed[1] so that CB = O'B = l. With ideal operation of this mechanism and absolute rigidity of the arm OB linking the crystal 2 with the crystal carriage 6, the image of the cross hairs must remain stationary relative to the microscope. In practice, however, the cross hair image shifts somewhat but remains in the field of view. The distance CO', obtained by reading the position of the cross hair image on the scale, is a direct measure of the angle of incidence ϑ. Thus any errors connected with deformation or inaccuracies in the functioning of the sine mechanism are almost wholly excluded.

Table 1 shows the results of measurements of the Au^{198} 412 kev line, the energy of which is now known with great accuracy. This was the line used for determining the constant k of the instrument. As will be evident from the table,

the mean root square error of measurement amounted to ±0.005 mm (0.006 mÅ), which indicates good reproducibility of the results.

Taking the value of $\lambda = 30.105 \pm 0.003$ mÅ, obtained by the DuMond group[3] on their crystal spectrometer, we find the constant for our instrument

$$k = \frac{\lambda}{2l} = 0.58862 \pm 0.00007 \text{ mA/mm}.$$

Table 2

Results of measurements of the Co^{60} 1.33 Mev γ-line energy ($2l = 15.803$ mm)

$2l$	$2\bar{l} - 2l$
15,802	+0,001
15,803	0,0
15,804	—0,001
15,804	—0,001
15,802	+0,001

Table 3

Results of measurements of the Co^{60} 1.17 Mev γ-line energy ($2\bar{l} = 17.946$ mm)

$2l$	$2\bar{l} - 2l$
17,942	+0,004
17,950	—0,004
17,945	+0,001
17,944	+0,002
17,949	—0,003

The results of wavelength measurements of the Co^{60} 1.17 & 1.33 Mev and Hf^{181} 482.0 kev lines are listed in Tables 2,3 & 4. The wavelength values obtained for Co^{60} are:

$\lambda_{1.17} = 10.5628 \pm 0.0023$ mA; $E_{1.17} = 1173.3 \pm 0.3$ kev;
$\lambda_{1.33} = 9.3008 \pm 0.0020$ mA; $E_{1.33} = 1333.0 \pm 0.3$ kev;
$\lambda_{0.482} = 25.720 \pm 0.0030$ mA; $E_{0.482} = 482.03 \pm 0.10$ kev.*

These values are in good agreement with the most accurate data reported hitherto in the literature.[4,5]

Table 4

Results of measurements of the Hf^{181} 482 kev γ-line energy ($2\bar{l} = 43.696$ mm)

$2l$	$2\bar{l} - 2l$
43,689	+0,007
43,700	—0,004
43,699	—0,003
43,695	+0,001

Table 5

Results of measurements of the Au^{199} γ-line energies (kev)

Ref.6	Ref.7	Ref.8	Our data
159	158	159	158,27±0,35
209	208	208	208,17±0,12

The 158 and 208 kev lines of Au^{199} lie outside the range (240-1500 kev) in which measurements can be made by means of the above described optical indicating device. In this case the readings were made by measuring the position of the source and crystal carriages with reference to calibrated millimeter scales. Nevertheless possible systematic errors associated with deformations of the measurement triangle could be almost entirely excluded.

The Au^{199} was obtained by irradiation of Au^{197} with thermal neutrons, i.e., by the successive neutron capture reaction: Au^{197} (n,γ) Au^{198} (n,γ) Au^{199}.

In addition to the Au^{199} lines, there was present in the spectrum the intense Au^{198} 412 kev line which was used as the reference. The second and third orders of this line yielded reference points at energies equal to exactly 1/2

---

*All the indicated uncertainties are root mean square values.

and 1/3 of the fundamental value, which made it possible to bring out and exclude possible nonlinearities.

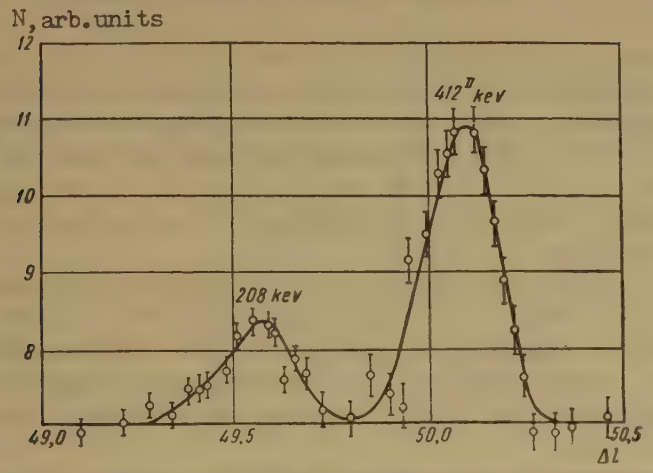

Fig.2. Section of the experimental spectrum comprising the Au^{199} 208 kev and Au^{198} 412 kev lines (in the second order). Horizontal axis laid off in divisions of the spectrometer scale, proportional to the wavelength.

Fig.2 shows the Au^{199} 208 kev and Au^{198} 412 kev lines as observed in the second order ($E_{eff} = E_{412}/2 \approx 206$ kev). The wavelength difference amounts to only

$$\Delta\lambda = 0.647 \pm 0.035 \text{ mÅ},$$

and the error that could be introduced by possible nonlinearity is some 2-3 orders of magnitude less than the indicated uncertainty.

Our data together with those of other investigators for the energy of the γ-lines of Au^{199} are listed in Table 5. The indicated uncertainties are root mean square errors and take into account only chance deviations. On the basis of what has been said above, however, it may be assumed that the systematic errors are not large and do not exceed the indicated uncertainties.

We take this occasion to thank V.S.Stepanov, who supervised the development of the optical indicating system.

"D.I.Mendeleev" All-Union Scientific Research Institute Metrology

References

1. P.I.Lukirskii & O.I.Sumbaev, Izv.AN SSSR, Ser.fiz., 20, 903 (1956). (Trans.Bulletin, 20, No.7, 820.)
2. O.I.Sumbaev, Izmerit. tekhnika (Measurement techniques), No.2 (1957),
3. D.E.Muller, H.C.Hoyt, D.J.Klein & J.W.M.DuMond, Phys.Rev., 88, 775 (1952).
4. G.Lindstrom, A.Hedgran & D.Alburger, Phys.Rev., 89, 1303 (1953).
5. F.Boehm & P.Marmier, Phys.Rev., 103, 343 (1956).
6. P.H.Sherk & R.D.Hill, Phys.Rev., 83, 1097 (1951).
7. K.Siegbahn in Siegbahn Commemorative Volume, p.199. - Upsala, 1951.
8. J.H.Cork, J.M.LeBlanc, F.B.Stumpf & W.H.Nester, Phys.Rev., 86, 415 (1952).

SCATTERING OF LONGITUDINALLY POLARIZED ELECTRONS AND POSITRONS BY POLARIZED ELECTRONS

- A.I.Mukhtarov and Iu.S.Perov

1. Polarization effects in electron-electron and positron-electron scattering have been considered by several authors.[1-3] These papers give the cross sections for scattering of polarized electrons and positrons by polarized electrons without including the polarization of the scattered particle and for scattering of polarized electrons by unpolarized electrons with the polarization after scattering taken into account; in addition, they give the degree of polarization of the scattered electron for the latter case.

In the present communication, we deduce a somewhat more general expression for the cross section as a function not only of the initial spins of the two particles, but also of the final spin. In addition, we find the polarization of the particle after the scattering event. We have considered only longitudinally polarized particles (which is equivalent to considering only the component of the spin along the direction of motion).

The matrix elements were calculated with the spin taken into account by a method described elsewhere.[4]

2. In the first nonvanishing approximation, the cross section for electron-electron scattering is given by

$$d\sigma = \frac{\alpha^2 K^2}{8k^4 \sin^4\theta}(f_1 + s_1 s_2 f_2 + s_1 s' f_3 + s_2 s' f_4)\, d\Omega, \qquad (1)$$

where

$$f_1 = 1 + 2\beta^2 + 6\beta^4 + 3(1 + 2\beta^2 - \beta^4)\cos^2\theta + \beta^4\cos^4\theta,$$
$$f_2 = 1 + 2\beta^2 + 4\beta^4 - (1 + 5\beta^4)\cos^2\theta - \beta^2(2 - \beta^2)\cos^4\theta,$$
$$f_3 = 2(1 + \beta^2)[\beta^2(2 + \cos\theta) + (1 - \beta^2)\cos^2\theta + \cos^3\theta],$$
$$f_4 = 2(1 + \beta^2)[\beta^2(2 - \cos\theta) + (1 - \beta^2)\cos^2\theta - \cos^3\theta].$$

Here $\beta = \frac{v}{c}$, $\hbar k$ is the momentum, $c\hbar K$ is the energy, s_1 and s_2 (equal either to +1 or -1) are the components of the spins along the momenta before scattering (in units of $\hbar/2$), and s' is the component of the spin along the momentum for an electron scattered through an angle θ. All the variables are given in the center-of-mass system.

Eq.(1) can be used to find the degree of longitudinal polarization of the scattered particle. It gives

$$P = \frac{d\sigma(s' = 1) - d\sigma(s' = -1)}{d\sigma(s' = 1) + d\sigma(s' = -1)} = \frac{s_1 f_3 + s_2 f_4}{f_1 + s_1 s_2 f_2}. \qquad (2)$$

The scattering-angle dependence of the polarization of the scattered electron is simplest when the energy of the electrons is small and their spins are parallel before scattering. For this case we have

$$P \approx s_1 \cos\theta.$$

In the even simpler ultrarelativistic case with initially antiparallel spins we have

$$P \approx s_1,$$

which means that the electrons remain longitudinally polarized.

Eqs.(1) and (2) are applicable also in the case in which one or both of the electrons are initially unpolarized. In this case one need only formally set the appropriate spin equal to zero.

3. Consider the scattering of a positron by an electron. We shall treat the cross section as a function of the positron scattering angle and the final positron spin. We will find the polarization after scattering for the positron as well. In order to obtain the analogous expressions for the electron one need only replace all the variables referring to the positron by others referring to the electron, and vice versa (in the center-of-mass system this is equivalent to interchanging the electron and positron spins).

Introducing the quantities

$$F_1 = \frac{1}{(1-\cos\theta)^2}[2+3\beta^4+2\beta^2(2-\beta^2)\cos\theta+\beta^4\cos^2\theta]+$$

$$+\frac{1}{1-\cos\theta}[\beta^2(-3+2\beta^2)-2\beta^4(2-\beta^2)\cos\theta-\beta^6\cos^2\theta]+\beta^4\left(\frac{3}{2}-\beta^2\right)+\frac{1}{2}\beta^8\cos^2\theta,$$

$$F_2 = \frac{1}{(1-\cos\theta)^2}[\beta^2(1+2\beta^2)-2\beta^4\cos\theta-\beta^2\cos^2\theta]+$$

$$+\frac{1}{1-\cos\theta}[\beta^2+2\beta^6\cos\theta+\beta^4(2-\beta^2)\cos^2\theta]-\frac{1}{2}\beta^4-\beta^6\left(1-\frac{1}{2}\beta^2\right)\cos^2\theta,$$

$$F_3 = \frac{1}{(1-\cos\theta)^2}[\beta^2(3+2\beta^2)+2\cos\theta+\beta^2\cos^2\theta]+$$

$$+\frac{1}{1-\cos\theta}[-\beta^4+\beta^2(-3+\beta^4)\cos\theta-\beta^4\cos^2\theta]+\beta^4\cos\theta,$$

$$F_4 = \frac{1}{(1-\cos\theta)^2}[\beta^2(1+2\beta^2)-2\beta^4\cos\theta-\beta^2\cos^2\theta]+$$

$$+\frac{1}{1-\cos\theta}[\beta^4+\beta^2(1+\beta^4)\cos\theta+\beta^4\cos^2\theta]-\beta^4\cos\theta,$$

we find the cross section to be given by

$$d\sigma = \frac{\alpha^2K^2}{16k^4}(F_1+s_1s_2F_2+s_2s'F_3+s_1s'F_4)\,d\Omega. \qquad (3)$$

Here s_1 gives the electron spin component before scattering, while s_2 and s' give the positron spin components before and after scattering, respectively. We note that all the spin variables for the positron (that is, s_2, s' and P) are given in the same way as for the electron.

Eq.(3) gives the following expression for the final longitudinal polarization of the positron:

$$P = \frac{s_2F_3+s_1F_4}{F_1+s_1s_2F_2}. \qquad (4)$$

It will be evident that for the special case of low energies the positron polarization after scattering is independent of the initial electron polarization; in fact, in this case

$$P \approx s_2\cos\theta.$$

We also note that if the particles have high energies and the initial spins are antiparallel, the scattered positrons remain fully polarized:

$$P \approx s_2.$$

Eqs.(3) and (4) remain valid also when the electron, the positron, or both are initially unpolarized; one need only set the respective spin projections equal to zero.

We express our gratitude to A.A.Sokolov for suggesting the subject and helpful advice and to B.K.Kerimov for valuable discussions.

"S.M.Kirov" Azerbaidzhan State University
&
Moscow State University

References

1. A.Bincer, Phys.Rev., 107, 1434 (1957).
2. G.Ford & C.Mullin, Phys.Rev., 108, 477 (1957).
3. A.A.Kresnin & L.N.Rozentsveig, Zhur.eksp.i teor.fiz., 32, 353 (1957). (Trans. Soviet Phys. - JETP).
4. A.Sokolov & D.Ivanenko, Kvantovaia teoriia polia (Quantum field theory), M.-L., 1952.

BREMSSTRAHLUNG FROM A LONGITUDINALLY POLARIZED ELECTRON

- B.K.Kerimov and I.M.Nadzhafov

1. One of the fundamental consequences of parity nonconservation in weak interactions is the emission of longitudinally polarized electrons by unpolarized radioactive nuclei. The longitudinal polarization of electrons emitted in β-decay has recently been observed experimentally in several different ways (double scattering, bremsstrahlung, Møller scattering[1-7]). These experiments give $-v/c$ for the longitudinal polarization of the electrons. The same value is obtained from the two-component theory of the neutrino.[8-10]

McVoy[11] has calculated the circular polarization for the special case in which an incident longitudinally polarized electron emits a photon by bremsstrahlung in its direction of motion.

A theoretical consideration of bremsstrahlung emitted by a completely longitudinally polarized electron in all directions and for all possible energies, taking into account the polarization of the initial and final states, should be of interest.

In the present communication we deduce a formula giving the angular and energy dependence of the degree of circular polarization of bremmstrahlung photons. The formula obtained for the bremsstrahlung cross section is a generalization of the well known Bethe-Heitler formula, accounting for the polarization of the electron spin and of the photon.

The partial circular polarization of bremsstrahlung photons was recently observed experimentally[5] for the electrons emitted by a source consisting of $Y^{90} + Sr^{90}$.

2. When performing quantum mechanical calculations of the probabilities of various processes connected with the transition of a Dirac particle from a state with momentum $\hbar\mathbf{k}$ to one with momentum $\hbar\mathbf{k}$, one usually averages over initial and sums over final spins. In this case the squares of the matrix elements are calculated by Casimir's method. According to this method,

$$\langle\gamma', \gamma\rangle_k \equiv b^+(\mathbf{k})\gamma' b(\mathbf{k}')\, b^+(\mathbf{k}')\gamma b(\mathbf{k}) = \frac{1}{8} Sp\gamma'\left(1 + \varepsilon' \frac{\vec{\alpha}\mathbf{k}' + \rho_3 k_0}{K'}\right)\gamma\left(1 + \varepsilon \frac{\vec{\alpha}\mathbf{k} + \rho_3 k_0}{K}\right), \quad (1)$$

where γ' and γ are Dirac matrices (of which there are 16).

When one uses (1), of course, one cannot find how the cross section depends on the spin orientation.

The 1945 Sokolov[12,13] developed the theory of Dirac particles with oriented spins; this theory can be used to calculate the spin dependence of the cross section for various processes. According to this theory, the squares of the matrix elements for electron transitions from state $(\mathbf{k}, s, \varepsilon)$ to state $(\mathbf{k}', s', \varepsilon')$ are given by (see p.110 of Sokolov and Ivanenko[12])

$$\langle\gamma', \gamma\rangle \equiv b^+(\mathbf{k}, s, \varepsilon)\gamma' b(\mathbf{k}', s', \varepsilon')\, b^+(\mathbf{k}', s', \varepsilon')\gamma b(\mathbf{k}, s, \varepsilon) =$$

$$= \frac{1}{16} Sp\,\gamma'\left(1 + \rho_1\varepsilon' s' \frac{k'}{K'} + \rho_3\varepsilon' \frac{k_0}{K'}\right)\left(1 + s' \frac{\vec{\sigma}\mathbf{k}'}{k'}\right)\gamma \times \left(1 + \rho_1\varepsilon s \frac{k}{K} + \rho_3\varepsilon \frac{k_0}{K}\right)\left(1 + s \frac{\vec{\sigma}\mathbf{k}}{k}\right). \quad (2)$$

Here $s = \pm 1$ and $s' = \pm 1$ give the projection of twice the spin $(\vec{\sigma})$ on the directions of motion of the electron in the initial and final states. When $s = 1$, the spin is along the direction of motion, and when $s = -1$, it is in the opposite direction (complete longitudinal polarization of the electron in the initial state). The quantities $\varepsilon = \pm 1$ and $\varepsilon' = \pm 1$ determine the sign of the energy in the initial and final states.

The variables with primes refer everywhere to the final state, and those without, to the initial state. If we sum in (2) over final and average over initial spins, we obtain Casimir's equation (1).

In the Born approximation, the cross section for bremsstrahlung parallel or anti-parallel to the direction of motion of a relativistic electron is given by (see (37.16) of Ref.12)

$$d\sigma = \frac{Z^2}{\pi^2}\left(\frac{e^2}{c\hbar}\right)^3 \frac{KK'k'\varkappa d\varkappa}{k(\varkappa')^4} S^+S\, d\Omega\, d\Omega', \tag{3}$$

where the square of the matrix element for the $(\mathbf{k}\to\mathbf{k}')$ transition is

$$S^+S = b^+(A + \rho_1\vec{\sigma}\mathbf{B} - i\vec{\sigma}\mathbf{C})\, b'b'^+(A^+ + \rho_1\vec{\sigma}\mathbf{B}^+ + i\vec{\sigma}\mathbf{C}^+)\, b; \tag{4}$$

$$\mathbf{C} = -(R - R')\,[\vec{\varkappa}\mathbf{a}];\quad \mathbf{B} = -\varkappa(R + R')\,\mathbf{a};$$

$$A = -2(\mathbf{k}'R' - \mathbf{k}R)\,\mathbf{a};\quad A^+ = -2(\mathbf{k}'R' - \mathbf{k}R)\,\mathbf{a}^+;$$

$$R = \frac{1}{2}(K\varkappa - \mathbf{k}\vec{\varkappa})^{-1};\quad R' = \frac{1}{2}(K'\varkappa - \mathbf{k}'\vec{\varkappa})^{-1}\ .\text{etc.}$$

Here $\mathbf{p} = \hbar\mathbf{k}$, and $\mathbf{p}' = \hbar\mathbf{k}'$ are the electron momenta before and after scattering, $\hbar\vec{\varkappa}$ is the momentum of the emitted photon, $\hbar\vec{\varkappa'} = \hbar\mathbf{k} - \hbar\mathbf{k}' - \hbar\vec{\varkappa}$ is the momentum transferred to the nucleus, $E = c\hbar K = c\hbar\sqrt{k^2 + k_0^2}$ and $E' = c\hbar K' = c\hbar\sqrt{k'^2 + k_0^2}$ are the total electron energies before and after scattering, $k_0 = \frac{m_0 c}{\hbar}$; Z is the atomic number of the element, $d\Omega = \sin\theta\, d\theta\, d\varphi$ and $d\Omega' = \sin\theta'\, d\theta'\, d\varphi'$ are solid angles for the electron before and after scattering, a and $\mathbf{a}^+$ are the amplitudes of the vector potential of the photon field, $b \equiv b(\mathbf{k}, s, \varepsilon)$ and $b' \equiv b(\mathbf{k}', s', \varepsilon')$ are Dirac spinor amplitudes for the electron, and ρ_1 and $\vec{\sigma}$ are the well known Dirac matrices.

Eqs.(2), (3) and (4) can be used to calculate the cross section for bremsstrahlung by a longitudinally polarized ($s = \pm 1$) electron. We will thus use (2) in calculating the traces that enter into (4).

In order to evaluate the circular polarization of the bremsstrahlung, we must break up a into two components according to

$$\mathbf{a} = \sum_{l=\pm 1} \mathbf{a}_l q_l = \frac{1}{\sqrt{2}} \sum_{l=\pm 1} (\vec{\beta} + il\,[\vec{\varkappa}^0\vec{\beta}])\, q_l, \tag{5}$$

where

$$\vec{\beta} = \frac{[\vec{\varkappa}^0\mathbf{j}]}{\sqrt{1 - (\vec{\varkappa}^0\mathbf{j})^2}}, \tag{6}$$

$$q_{l'}^+ q_l = 0,\quad q_l q_{l'}^+ = \delta_{ll'},\quad l,\ l' = 1,\ -1;$$

Here $\vec{\varkappa}^0 = \frac{\vec{\varkappa}}{\varkappa}$ is the unit vector in the direction of propagation of the radiated photon, and j is any unit vector. When $l = 1$ we have bremsstrahlung with right circular polarization (the photon spin is a "forward" in the direction of motion), and when $l = -1$ the photon is left circularly polarized (spin "backward").

By means of (5) and (6) it is easily shown that

$$\vec{\varkappa}^0 \mathbf{a}_l = \vec{\varkappa}^0 \mathbf{a}_l^+ = 0, \quad \mathbf{a}_l \mathbf{a}_{l'}^+ = \delta_{ll'}$$

$$[\vec{\varkappa}^0 \mathbf{a}_l] = -il\,\mathbf{a}_l, \quad [\mathbf{a}_l \mathbf{a}_{l'}^+] = -il\vec{\varkappa}^0 \delta_{ll'}$$

$$(\mathbf{F}_1 \mathbf{a}_l)(\mathbf{F}_2 \mathbf{a}_1^+) = \frac{1}{2}\{\mathbf{F}_1\mathbf{F}_2 - (\vec{\varkappa}^0\mathbf{F}_1)(\vec{\varkappa}^0\mathbf{F}_2) - il\vec{\varkappa}^0[\mathbf{F}_1\mathbf{F}_2]\}, \tag{7}$$

where $\mathbf{F}_1$ and $\mathbf{F}_2$ are arbitrary vectors. We shall find these relations useful later.

The conservation laws are of the form

$$K - K' - \varkappa = 0, \quad \mathbf{k} - \mathbf{k}' - \vec{\varkappa} - \vec{\varkappa}' = 0. \tag{8}$$

If $\vec{\varkappa}$ is directed along the z axis,

$$\varkappa'^2 = k^2 + k'^2 + \varkappa^2 - 2\vec{\varkappa}\mathbf{k} + 2\vec{\varkappa}\mathbf{k}' - 2\mathbf{k}\mathbf{k}',$$

$$\cos\theta = \frac{\vec{\varkappa}\mathbf{k}}{\varkappa k}, \quad \cos\theta' = \frac{\vec{\varkappa}\mathbf{k}'}{\varkappa k'}, \tag{9}$$

$$\frac{\mathbf{k}\mathbf{k}'}{kk'} = \cos\theta\cos\theta' + \sin\theta\sin\theta'\cos(\varphi' - \varphi).$$

Using (2) and (5), we find the cross section for bremsstrahlung from a longitudinally polarized relativistic electron summed over final spins to be

$$\sum_{s'=\pm 1} d\sigma_{ss'l} = d\sigma_{sl} = \frac{1}{2}\sigma_{B-H}(\theta, \theta')\,d\Omega\,d\Omega' + ls\sigma(\theta, \theta')\,d\Omega\,d\Omega', \tag{10}$$

where

$$\sigma(\theta, \theta') = \frac{Z^2}{\pi^2}\left(\frac{e^2}{c\hbar}\right)^3 \frac{k'\,d\varkappa}{4k^2\varkappa(\varkappa')^4}\left\{\frac{k^2\sin^2\theta}{\Delta^2}(Kk\varkappa\cos\theta + Kk'\varkappa\cos\theta' - K\varkappa^2 + \varkappa k_0^2) + \right.$$

$$+ \frac{k'^2\sin^2\theta'}{(\Delta')^2}(Kk\varkappa\cos\theta + Kk'\varkappa\cos\theta' + K\varkappa^2 - \varkappa k_0^2) -$$

$$- 2\frac{f(\theta,\theta')}{\Delta\Delta'}(Kk\varkappa\cos\theta + Kk'\varkappa\cos\theta') + \frac{k^2\sin^2\theta - k'^2\sin^2\theta'}{\Delta\Delta'}\varkappa(\varkappa K - k_0^2) -$$

$$\left. - \varkappa k_0^2 f(\theta, \theta)\left(\frac{1}{\Delta^2} - \frac{1}{(\Delta')^2}\right) + \frac{(k'^2)\sin^2\theta' - k^2\sin^2\theta}{\Delta^2\Delta'}\varkappa^2 k_0^2\right\}; \tag{11}$$

here

$$\Delta = K - k\cos\theta, \quad \Delta' = K' - k'\cos\theta',$$

$$f(\theta, \theta') = \mathbf{k}\mathbf{k}' - kk'\cos\theta\cos\theta' = kk'\sin\theta\sin\theta'\cos(\varphi' - \varphi). \tag{12}$$

Eqs. (10) and (11) give not only energy and angular distributions, but also the polarization ($l = \pm 1$) of the bremsstrahlung photons emitted in any direction. If we average (10) over initial electron spins, the term proportional to ls vanishes and we obtain the well known Bethe-Heitler cross section $\sigma_{B-H}(\theta,\theta')$.

It is thus seen from (10) that only electrons polarized parallel or antiparallel to their direction of motion can give rise to circularly polarized ($l = \pm 1$) bremsstrahlung.

For the case of radiation forward in the direction of the electron's motion $\left(\theta \to 0,\ \cos\theta = \frac{\vec{\varkappa}\mathbf{k}}{\varkappa k} \to 1\right)$, integration of (10) over the solid angle $d\Omega'$ gives

$$\underset{\theta\to 0}{d\sigma_{sl}} = \frac{Z^2}{2\pi}\left(\frac{e^2}{c\hbar}\right)^3 \frac{k'\,d\varkappa}{k\varkappa}[(1 + sl)\,\Phi_1(\varkappa, K, K') + \Phi_2(\varkappa, K, K')]. \tag{13}$$

The degree of circular polarization of the bremsstrahlung radiation is given by

$$P=\frac{(d\sigma_{sl})_{l=1}-(d\sigma_{sl})_{l=-1}}{(d\sigma_{sl})_{l=1}+(d\sigma_{sl})_{l=-1}}=s\left[1+\frac{(KK'+K'k+k_0^2)I_2-kk'I_1}{\varkappa\left((K+k)I_2+\frac{K-k+\varkappa}{K-k}k'I_1\right)}\right]^{-1}, \tag{14}$$

where

$$\Phi_1(\varkappa, K, K')=\varkappa(K+k)I_2+\frac{\varkappa k'(K-k+\varkappa)}{K-k}I_1,$$

$$\Phi_2(\varkappa, K, K')=(KK'+k_0^2+K'k)I_2-kk'I_1;$$

$$I_2=\frac{k_0^2-KK'}{2k'k^3(K-k)^3}\ln\frac{(k-\varkappa-k')^2(K'+k')}{(k-\varkappa+k')^2(K'-k')}-\frac{1}{k^2(K-k)^2},$$

$$I_1=\frac{1}{2(k')^2(k-\varkappa)^2}\ln\frac{k-\varkappa-k'}{k-\varkappa+k'}-\frac{k_0^2}{4k^2(k')^2(K-k)^2}\ln\frac{(k-\varkappa-k')^2(K'+k')}{(k-\varkappa+k')^2(K'-k')}-$$

$$-[2kk'(k-\varkappa)(K-k)]^{-1}. \tag{15}$$

It is seen from (14) that as $\varkappa\to 0$, the polarization $P\to 0$, and that P increases rapidly with $\varkappa$, reaching its maximum value at $\varepsilon_\Phi=c\hbar\varkappa=E-m_0c^2$. Bearing in mind that $\lim\limits_{k'\to 0}\frac{k'I_1}{I_2}=k_0$, we obtain the maximum polarization as given by (15) to be

$$P_{\max}=\lim_{k'\to 0}P=s\left[1+\frac{(K-k)(K+k_0)}{(2K-k)(K-k_0)}\right]^{-1}. \tag{16}$$

For $s=1$ this gives the value recently obtained by McVoy[11]. It follows from (16) that the bremsstrahlung from longitudinally polarized high-energy ($k\gg k_0$) electrons will be completely circularly polarized ($P_{\max}=s=\pm 1$, meaning that the photon spin is either always along or always opposite to its direction of motion.

Integrating (10) over $d\Omega'$ for the cross section in the general case, we obtain

$$\sigma_{sl}(\theta)\,d\Omega=\frac{1}{2}d\Omega\int\sigma_{B-H}(\theta,\theta')\,d\Omega'+ls\,d\Omega\int\sigma(\theta,\theta')\,d\Omega', \tag{17}$$

where

$$\frac{1}{2}\int\sigma_{B-H}(\theta,\theta')\,d\Omega'=\frac{Z^2}{16\pi}\left(\frac{e^2}{c\hbar}\right)^3\frac{k'}{k}\cdot\frac{d\varkappa}{\varkappa}\left\{\frac{8k_0^2(k_0^2+2K^2)}{k^2\Delta^4}\sin^2\theta-\right.$$

$$-2\frac{5K^2+3k_0^2+2KK'}{k^2\Delta^2}-2\frac{k^2-\varkappa^2}{T^2\Delta^2}+\frac{4K'}{k^2\Delta}+\frac{L}{kk'}\left(\frac{4Kk_0^2(3\varkappa k_0^2-K'k^2)}{k^2\Delta^4}\sin^2\theta+\right.$$

$$+\frac{4K^4+4K^2K'^2-2k_0^2(7K^2+K'^2-3KK'-k_0^2)}{k^2\Delta^2}+\frac{2\varkappa}{k^2\Delta}(KK'+k^2)\Big)+$$

$$\left.+\frac{\varepsilon_0^T}{k'T}\left(4\frac{k_0^2}{\Delta^2}-6\frac{\varkappa}{\Delta}-2\varkappa\frac{k^2-\varkappa^2}{\Delta T^2}\right)-4\frac{\varepsilon_0}{k'\Delta}\right\}. \tag{18}$$

$$\int\sigma(\theta,\theta')\,d\Omega'=\frac{Z^2}{2\pi}\left(\frac{e^2}{c\hbar}\right)^3\frac{k'}{k^2}\frac{d\varkappa}{\varkappa}\left\{-\frac{\varkappa}{k^2\Delta^4}[-Kk(K^2+2k_0^2)\cos\theta+\right.$$

$$\left.+k^2(K^2+k_0^2)]\sin^2\theta-K\frac{k^2-\varkappa^2}{4T^2\Delta^2}-\frac{\varkappa Kk_0^2}{k^2\Delta^3}+\frac{1}{4k^2\Delta^2}[3K^3-2K^2K'+\right.$$

$$+ k_0^2 (K - 2K')] + \frac{L}{kk'} \left[\frac{\varkappa k_0^2 K}{2k^2 \Delta^4} (k (3K\varkappa - k^2) \cos\theta - 2\varkappa k^2) \sin^2\theta - \right.$$

$$- \frac{\varkappa^2 k_0^4}{2k^2\Delta^3} + \frac{\varkappa}{4k^2\Delta^2} (2K^4 + 2K^3K' - k_0^2 (K^2 + 4KK' - k_0^2)) - \left. \frac{\varkappa (K + K')}{4\Delta} \right] +$$

$$+ \frac{\varkappa \varepsilon_0^T}{4k'T} \left(- K \frac{k^2 - \varkappa^2}{\Delta T^2} - \frac{3K}{\Delta} + 2 \frac{k^2}{\Delta^2} \right) \Big\}; \qquad (19)$$

here

$$T = |\mathbf{k} - \vec{\varkappa}|, \quad \Delta = K - k\cos\theta,$$

$$L = \ln \frac{KK' - k_0^2 + kk'}{KK' - k_0^2 - kk'},$$

$$\varepsilon_0 = \ln \frac{K' + k'}{K' - k'}, \quad \varepsilon_0^T = \ln \frac{T + k'}{T - k'}.$$

This means that the degree of circular polarization of the bremsstrahlung photons will be given by

$$P = s \frac{\int \sigma(\theta, \theta')\, d\Omega'}{\frac{1}{2} \int \sigma_{B-H}(\theta, \theta')\, d\Omega'}, \qquad (20)$$

In the ultrarelativistic case for small angles (both θ and θ' of the order of m_0c^2/E) the dependence of the circular polarization on the energy E_e' of the scattered electron and the emitted photon is of the type shown in Fig.1.

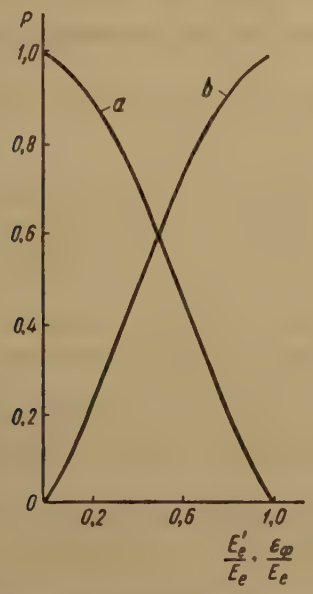

Fig.1. Degree of circular polarization as a function of (a) the scattered electron energy and (b) the radiated photon energy for small angles.

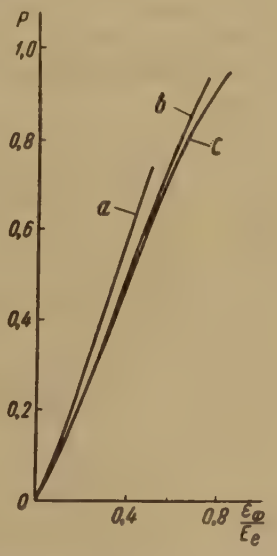

Fig.2. Degree of circular polarization as a function of the energy of the radiated photon: (a) T_k = 0.5 Mev, b) T_k = 1.5 Mev, c) T_k = 3.5 Mev.

The dependence of P on $\frac{\varepsilon_\Phi}{E_e} = \frac{\varkappa}{K}$, as calculated from (15) for the case of s = = +1 is shown in Fig.2 for several electron kinetic energies T_k. P increases rapidly with the bremsstrahlung energy. As the electron energy increases, so does P_{max}, becoming about 100% (complete right circular polarization) at T_k = = 3.5 Mev (or $E = 8m_0c^2$). For s = -1, the bremsstrahlung is completely left circularly polarized (l = -1).

In conclusion, we express our gratitude to A.A.Sokolov for discussions.

Statistical Physics and Mechanics Faculty
Moscow State University.

References

1. H.Fraunenfelder, R.Babone and others, Phys.Rev., 106, 386 (1957).
2. A.I.Alikhanov, G.P.Eliseev, V.A.Lubimov & V.A.Ershler, Zhur.eksp.i teor. fiz., 32, 1344 (1957). (Trans. Soviet Phys.- JETP.); Reports presented at the Eighth All-Union Conference on Nuclear Spectroscopy, 1958.
3. A.I.Alikhanov, G.P.Eliseev, V.A.Lubimov, Reports presented at the Eighth All-Union Conference on Nuclear Spectroscopy, 1958.
4. H.DeWaard & O.I.Poppema, Physica, 23, 597 (1957).
5. M.Goldhaber, L.Grodzins & A.W.Sunyar, Phys.Rev., 106, 826 (1957).
6. H.Fraunfelder, A.O.Hanson, N.Levine, A.Rossi & G.DePasquali, Phys.Rev., 107, 643 (1957).
7. A.DeShalit, S.Kuperman, H.I.Lipkin & T.Rothem, Phys.Rev., 107,1459 (1957).
8. T.D.Lee & C.N.Yang, Phys.Rev., 105, 1671 (1957).
9. L.D.Landau, Zhur.eksp.i teor.fiz., 32, 407 (1957) (Trans. JETP.)
10. A.Salam, Nuovo Cimento, 5, 299 (1957).
11. K.W.McVoy, Phys.Rev., 106, 828 (1957).
12. A.Sokolov & D.Ivanenko, Kvantovaia teoriia polia (Quantum field theory), Part I, M.-L., 1952.
13. A.Sokolow, Jour.Phys.USSR, 9, 363 (1945).

Bulletin of the Academy of Sciences of the USSR - Physical Series
Vol.22, No. 7
Transactions of the Eighth All-Union Conference on Nuclear Spectroscopy
(Continued from Vol.22, No.2)

TABLE OF CONTENTS

	Page Orig.	Trans.
Internal conversion - A review - M.A.Listengarten	759	755
Conversion electrons from Yb^{169} - K.Ia.Gromov, B.S.Dzhelepov & B.K.Preobrazhenskii	775	770
Level diagram of Tl^{208} - A.G.Sergeev, E.M.Krisiuk, G.D.Latyshev, V.D.Vorob'ev & T.I.Kol'chinskaia	785	779
Beta-spectra of the shortlived isotopes Al^{28} and F^{17} - S.S.Vasil'ev & L.Ia.Shavtvalov	788	782
Conversion electron coincidences in $Tb^{155} \rightarrow Gd^{155}$ decay B.S.Dzhelepov, B.K.Preobrazhenskii & V.A.Sergienko	791	785
Coincidences between conversion electrons in the decay of Lu^{173}. Refinement of the $Lu^{173} \rightarrow Yb^{173}$ decay scheme - B.S.Dzhelepov, B.K.Preobrazhenskii & V.A.Sergienko	795	789
Mass numbers of neutron-deficient terbium isotopes - V.I.Baranovskii, A.N.Murin, V.N.Pokrovskii & I.A.Iutlandov	808	802
Mass numbers of 52-day gadolinium and 4.3-day europium isotopes - G.M.Gorodinskii, A.N.Murin & V.N.Pokrovskii	811	805
Mass numbers of neutron-deficient Dy isotopes - A.N.Dobronravova, L.M.Krizhanskii, A.N.Murin & V.N.Pokrovskii	815	809
New neutron-deficient rare earth isotopes. Lutetium isotope with mass number 167 - P.M.Aron, A.V.Kaliamin, A.N.Murin & V.A.Iakovlev	817	811
Lutetium isotope with mass number 173 - G.M.Gorodinskii, A.N.Murin, V.N.Pokrovskii & B.K.Preobrazhensii	818	812
Relative intensities of γ-transitions in Ho^{160} - E.P.Grigor'ev, B.S.Dzhelepov & A.V.Zolotavin	821	815
Investigation of the lower excited levels of Th^{230} by observing α-e_K coincidences - A.P.Komar, G.A.Korolev & G.E.Kocharov	824	818
Investigation of Cs^{134} by the coincidence method - Iu. A. Aleksandrov	827	821
Radiation from As^{74} - E.P.Grigor'ev, B.S.Dzhelepov, A.V.Zolotavin, V.Ia.Mishin, V.P.Prikhodtseva, Iu.V.Khol'nov & G.E.Shchukin	831	825
Gamma-spectrum of Lu^{171} - A.I.Lebedev, A.N.Silant'ev & I.A.Iutlandov	839	833

New data on the relative intensities of the γ-lines of RaC in equilibrium with its decay products - B.S.Dzhelepov, N.N.Zhukovskii, I.F.Uchenatkin & S.A.Shestopalova 841 835

Determination of the number of photons per disintegration of La^{140} - E.A.Khol'nova 848 843

Determination of the L/K ratios for Dy^{159} and Er^{165} and evaluation of the Dy^{159}--Tb^{159} and Er^{165}--Ho^{165} transition energies - O.I.Grigor'ev, B.S.Kuznetsov, N.S.Shimanskaia & I.A.Iutlandov 850 845

Lifetime of the first excited state of Mg^{24} - N.N.Deliagin & V.S.Shpinel' 861 855

Concerning Doppler broadening of the lines associated with conversion electrons emitted by recoil nuclei - A.V.Gnedich, L.N.Kriukova, V.V.Murav'eva, V.S.Shpinel' & V.I.Shumshurov 867 861

Elastic scattering of protons by Si^{28} nuclei. Spin and parity of the 4.31 and 4.73 Mev levels of P^{29} - A.K.Val'ter, I.Ia.Malakhov, P.V.Sorokin & A.Ia.Taranov 871 865

Toroidal sector type β-spectrometer - S.Salai & D.Bereni 877 871

Precision measurements of the Co^{60} 1.17 and 1.33 Mev, Hf^{181} 482 kev and Au^{199} 158 and 208 kev γ-lines - M.P.Avotina & O.I.Sumbaev 879 873

Scattering of longitudinally polarized electrons and positrons by polarized electrons - A.I.Mukhtarov & Iu.S.Perov 883 876

Bremsstrahlung from a longitudinally polarized electron - B.K.Kerimov & I.M.Nadzhafov 886 879

Translated in 1959 by
Columbia Technical Translations
5 Vermont Ave., White Plains, N.Y.

Transactions

of the

Eighth All-Union Conference on Nuclear Spectroscopy

(Continued from Vol.22, Nos.2 and 7)

887e

Gd^{149} CONVERSION ELECTRON SPECTRUM

- N.M.Anton'eva, A.A.Bashilov, B.S.Dzhelepov and B.K.Preobrazhenskii

Introduction

The conversion electron spectrum of the gadolinium fraction separated from a tantalum target irradiated (with protons) in the synchrocyclotron was investigated on the Leningrad State University Ketron[1] magnetic spectrometer at a resolution of 0.5%. The activity was collected on a thin aluminum foil.[2] The counter window was transparent to > 7 kev electrons. Investigation of the spectrum began a few hours after termination of the chemical operations. The general appearance of the conversion spectrum some 90 hours after separation is shown in Fig.1. It was found that the intensity of the conversion lines varied at different rates with time, which indicated the presence of several Gd isotopes or isomers in the source. For the purpose of making mass number assignments the spectrum was measured at successive intervals and the resultant data (areas or simply the heights of the peaks) were used to plot decay curves for each conversion line.

The conversion lines with $T_{1/2}$ = 10 ± 1 days (Fig.2) were attributed to Gd^{149}.

Radioactive Gd^{149} was discovered in 1951 by Hoff, Rasmussen & Thomson[3] who observed the Sm^{147} (α, 2n) Gd^{149} and Eu^{151} (p, 3n) Gd^{149} reactions. Somewhat later it was established[4] that Gd^{149} with a period of 9 ± 1 days converts by electron capture (>99%) to Eu^{149} and by emission of 3 Mev α-particles ($\sim 10^{-3}$%) to Sm^{145}. The conversion electron and γ-ray spectra have not hitherto been studied. Our principal experimental data were presented at the Seventh All-Union Conference on Nuclear Spectroscopy in January, 1957.[5] Below we shall discuss our results together with the data on Gd^{149} published [6-8] in 1957.

1. Experimental results

The transitions we assigned to Gd^{149} are listed in Table 1. The K-149.8 and L-149.8 conversion lines are discernible only in Fig.1. The lines lying in the 220 to 360 and 400 to 550 kev intervals are also shown in Figs.3 & 4 which pertain to a later series of measurements carried out when the short-lived Gd^{147} ($T_{1/2}$ = 35 hours) had already decayed; the long-lived isotopes, Gd^{151} and Gd^{153}, give rise to a number of lines (K-243, K-306, K-350, etc.) in these energy intervals. However, in view of the fact that with short irradiation times these lines are of low intensity they are not apparent in Fig.3.

The values of K/L listed in Table 1 are arithmetic mean values based on ten series of measurements. The value of K/L for the 272 kev transition could not be accurately determined in view of the low intensity of the L-272 line. The large uncertainty in determining K/L for the 298 kev transition is connected with the fact that the L line in question is rather weak and could not be resolved from the strong K-346 line (similar qualifying observations apply to the ratios associated with the 497, 517 and 535 kev transitions.

Murin and his co-workers[6,7] report that by means of a scintillation counter they detected γ-rays from Gd^{149} with the following energies: $E\gamma$ = 150, 300, 347 and 520 kev.

Very recently there appeared a report of Rasmussen and his co-workers[8] on their investigation of the radiation from Gd^{149}. These investigators used a photographic recording β-spectrograph, a double focusing spectrometer (resolution 0.3%) for investigating the strong conversion lines and a scintillation γ-spectrometer. The Gd^{149} was obtained by the Sm + α and Eu + d reactions in which there were also formed other radioactive Gd isotopes. These authors observed the com-

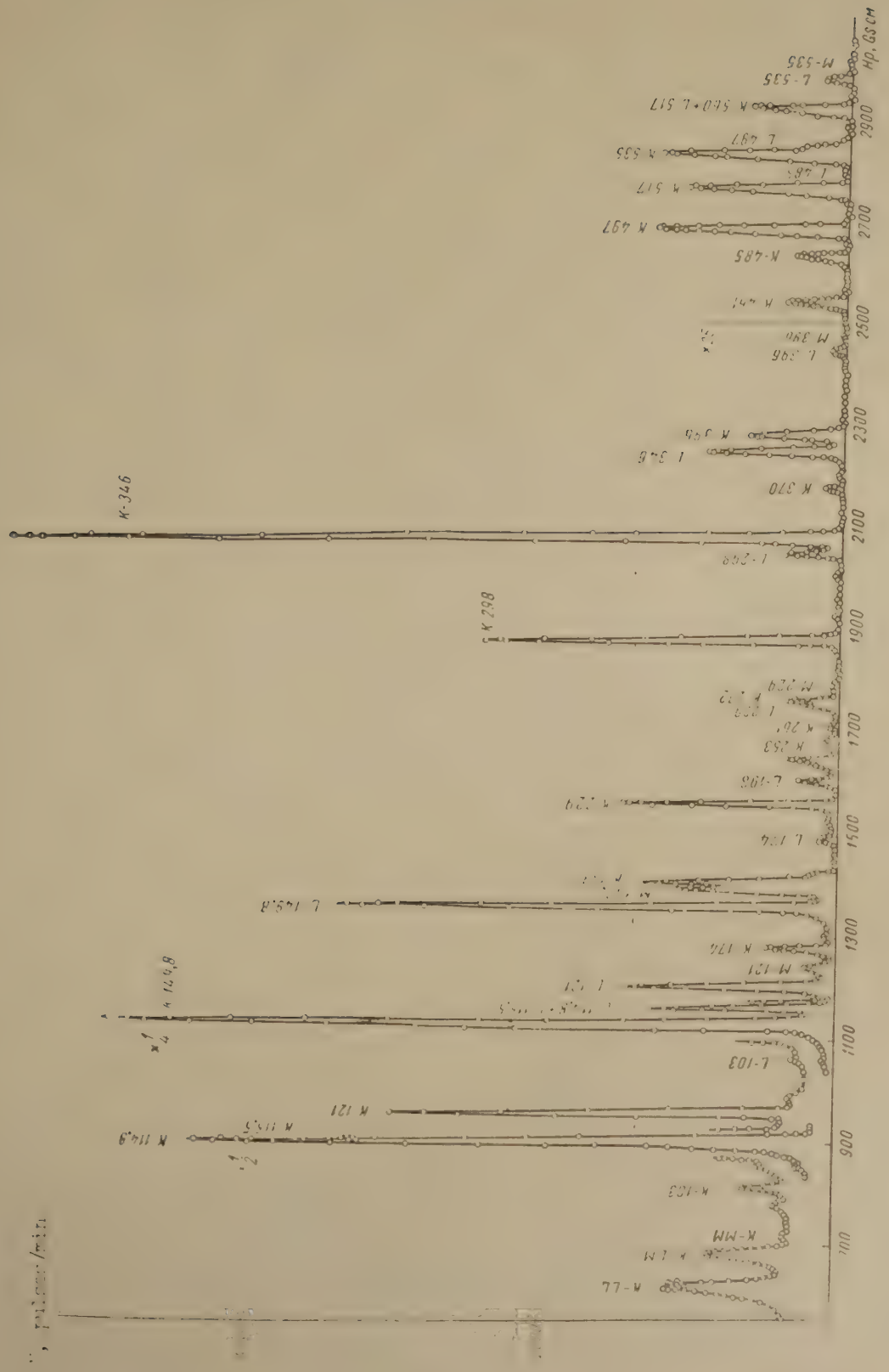

Fig.1. General appearance of the conversion electron spectrum (to 550 kev) of the gadolinium fraction recorded 90 hours after chemical separation.

Table 1

Transition energies and relative conversion line intensities for Gd^{149}

No.	E_γ, kev	Observed conversion lines	K/L	K/K_{346} x 100
1	149,8±0,3 149,9*	K, L, M	6,6±0,3 9,4*	530±20 430*
2	272±1 272,7*	K, L	≈6 —	7,7±0,5 —
3	298±1 298,8*	K, L	6±1 5,5*	45±2 44÷49*
4	346±1 346,7*	K, L, M	5,9±0,3 4,4÷5,0*	100 100*
5	461±1 461*	K	—	0,37±0,03
6	497±1 496*	K, L	3,5±0,5 —	1,0±0,1 —
7	517±1 517*	K, L	7,0±0,5 —	0,8±0,1 —
8	535±1 534*	K, L	6,6±0,6 —	1,0±0,1 —
9	~940	K, L	6,5±1,0	0,23±0,05

* Data of Shirley et al[8].

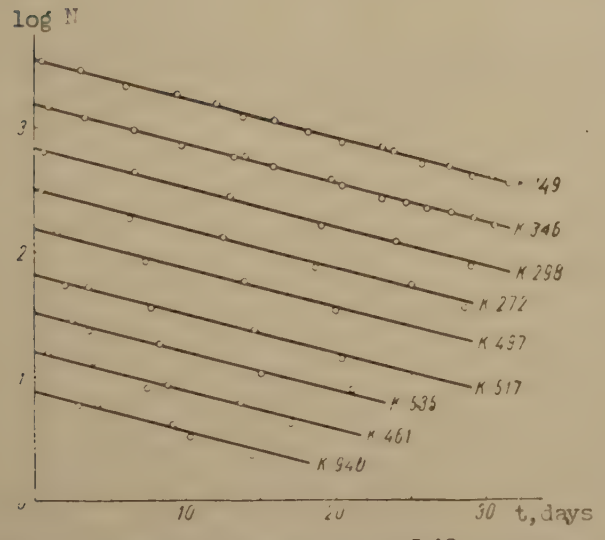

Fig.2. Decay curves for Gd^{149} plotted on the basis of the falling off of intensity of the K conversion lines. For the sake of clarity the decay curves for different lines are shifted vertically.

plex spectrum of the radiation from the resultant mixture of Gd isotopes and their decay products. The data of Rasmussen et al for the strong conversion lines of Gd^{149} are listed in Table 1 together with our results for purposes of comparison. It will be seen that there is excellent agreement (except for the 149.8 kev line). Rasmussen et al attributed a number of additional weak lines corresponding to transitions of energies 107, 120, 126, 134, 244, 253, (650), 750, 790 and 937 kev to Gd^{149}. However, some of their assignments are open to question. Their spectrum actually included the conversion electrons of several gadolinium isotopes and their daughters; evaluation of the periods in the case of the weak low energy lines was carried out from measurements of the spectrogram blackenings, a technique not characterized by particularly high accuracy. Specifically, it must be noted that the conversion lines corresponding to the 126 kev γ-transition were not observed by us in the spectrum of the gadolinium fraction but were clearly apparent in the spectrum of the europium fraction, which we also investigated. The K-132 line, which according to Rasmussen et al is not very weak, should have been but was not observed in our experiments. Further, the 244 kev γ-transition cannot apparently be attributed to Gd^{149}. Our spectrum contains a K conversion line of an unidentified transition of 244 kev energy; however, this transition does not occur in the decay of Gd^{149} inasmuch as while in the case of some sources the K-244 line was comparable in intensity with the K-272 line (of Gd^{149}) in the case of other sources it was much weaker. The K-255 line was also observed by us in the spectrum of one of the sources

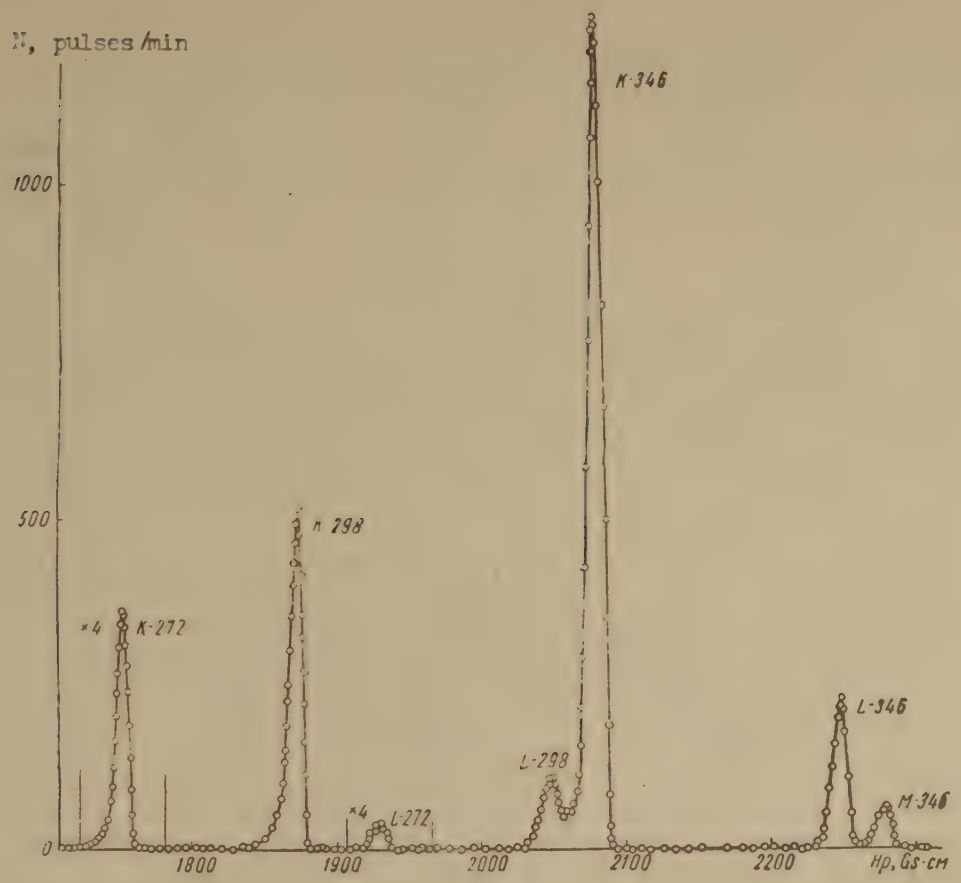

Fig.3. Gd^{149} conversion electron spectrum in the energy range from 200 to 350 kev. The lines associated with the 149.8 kev transition are shown in Fig.1.

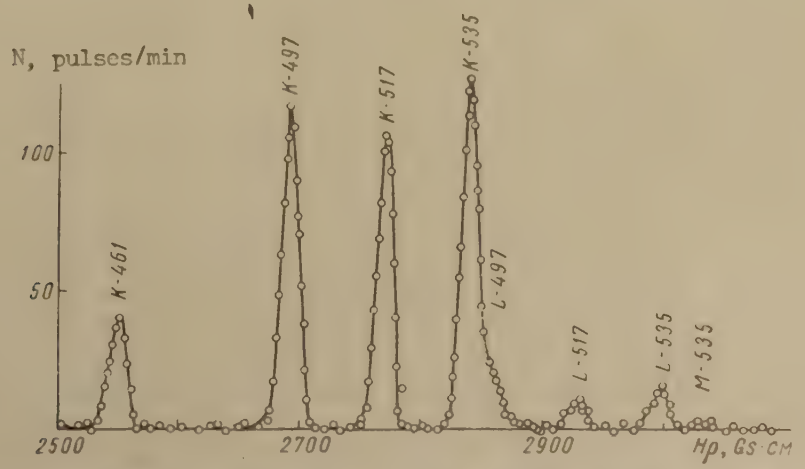

Fig.4. Gd^{149} conversion electron spectrum in the energy range from 400 to 550 kev.

(it had an appreciable intensity relative to the K-272 line), but was not observed in the spectra of the other sources. Moreover, we observed a line of close energy ($E\gamma$ = 255 kev) in the spectrum of the europium fraction. Finally, the conversion

electrons associated with the hard γ-rays ($E_\gamma \approx 650$, 750 and 790) belong, according to our data, to Gd^{147} and the decay products of gadolinium, namely, radioactive isotopes of europium.

At this point it is difficult to say anything definite regarding the other weak lines observed by Rasmussen and his co-workers.

2. Multipole orders

Our data on the conversion electron spectrum of Gd^{149} allow of drawing certain deductions regarding the multipole orders of the nuclear transitions in Eu^{149}. To this end the results of our measurements are compared with the theoretical data in Table 2. The theoretical values of α_K, α_{L_1}, α_{L_2} and α_{L_3} were interpolated from the tables of Sliv & Band. Let us consider the observed transitions in order of increasing energy.

149.8 kev γ-transition. The experimental value of the K/L ratio is in best agreement with the theoretical value for M1.

This inference is substantiated by the supplementary data obtained by V.M. Lobashev and one of the present authors (A.A.Bashilov) in our laboratory by means of a photographic plate spectrograph. In the spectrograms, among the conversion lines of the 149.8 kev transition, there were observed the L_1 line and the L_2 line (weak), while the L_3 line was undiscernible. According to a rough evaluation, the intensities of these lines decrease by a factor of ~10 or more going from L_1 to L_2 to L_3. As will be evident from a comparison with the theoretical data (Table 2) that this proportion is most consistent with the M1 assignment.

Furthermore, in experiments, carried out in our laboratory by Adamchuk et al[9], it was found through comparison of the numbers of conversion and photoelectrons for one and the same source that the K conversion coefficient for the 149.8 kev transition is 0.53 ± 0.07, which is close to the theoretical value of 0.51 for an M1 transition.

Hence it may safely be concluded that the 149.8 kev transition is of the M1 type. We note that Rasmussen et al[8] also inferred that the transition of ~150 kev energy is a magnetic dipole transition.

272 kev γ-transition. This transition is of low intensity and hence it is difficult to draw any definite inferences regarding it.

298 kev γ-transition. One cannot unambiguously identify the type of this transition from the ratio of the K and L shell conversion coefficients in view of the large uncertainty in determining these quantities.

However, according to the data of Adamchuk et al[9] in this case $\alpha_K = 0.066 \pm \pm 0.007$ which indicates that we are dealing with an M1 + E2 transition. Furthermore, if we used the values of the relative intensities of the conversion lines from our measurements ($e_{298}:e_{150} = 0.086$) and take the relative γ-ray intensities from the data of Adamchuk et al[9] ($\gamma_{298}:\gamma_{150} = 0.67$) and bear in mind that the 150 kev transition is M1, we can roughly evaluate the conversion coefficient:

$$\alpha_{298} = \frac{(e_{298}:e_{150})}{(\gamma_{298}:\gamma_{150})}\,\alpha_{150} \approx 0.065.$$

This result also indicates that the 298 kev transition is a mixture of M1 + E2. Probably the M1 contribution amounts to about 70%.

346 kev γ-transition. In this case the experimental value of K/L is in good agreement with an M2 assignment and not at all consistent with E1, E2 and M1; one

Table 2

Data for determination of the multipole orders of γ-transitions in Eu^{149}

E_γ, kev	Ratios & coefficients	Experimental values	Theoretical values					Inferred multipole order
			E1	*M1*	*E2*	*M2*	*E3*	
149,8	$K:L$ $L_1:L_2:L_3$ α_K	$6,6\pm0,4$ $\sim10:1:0,1$ $0,53\pm0,07$	7,0 6,4 : 1 : 1,2 0,080	6,9 12 : 1 : 0,17 0,51	2,3 0,54 : 1 : 0,90 0,37	4,8 8,4 : 1 : 1,0 3,2	0,6 0,10 : 1 : 0,8 1,4	*M1*
272	$K:L$	~6	7,2	7,0	3,9	5,5	1,6	$M1+E2$
298	$K:L$ α_K	6 ± 1 $0,066\pm0,007$	7,2 0,013	7,0 0,075	4,2 0,046	5,6 0,31	1,9 0,13	*M1* 70% + *E2* 30%
346	$K:L$ $L_1:L_2:L_3$ α_K	$5,9\pm0,3$ $L_1 \gg L_2$ & L_3 $0,18\pm0,02$	7,2 11 : 1 : 1,0 0,0089	7,0 16 : 1 : 0,20 0,050	4,6 1,8 : 1 : 0,4 0,030	5,8 9,5 : 1 : 0,41 0,19	2,3 0,59 : 1 : 0,53 0,083	*M2*
497	$K:L$ α_K	$3,5\pm0,5$ $3,1\cdot10^{-2}$	7,3 $4,3\cdot10^{-3}$	7,1 $2,0\cdot10^{-2}$	5,6 $1,1\cdot10^{-2}$	6,2 $6,3\cdot10^{-2}$	3,8 $2,9\cdot10^{-2}$	*E3*
517	$K:L$ α_K	$7,0\pm0,5$ $1\cdot10^{-2}$	7,3 $4,1\cdot10^{-3}$	7,1 $1,8\cdot10^{-2}$	5,7 $1,0\cdot10^{-2}$	6,3 $5,3\cdot10^{-2}$	4,0 $2,5\cdot10^{-2}$	*M1*, *E2*, $M1+E2$
535	$K:L$ α_K	$6,6\pm0,6$ $1,3\cdot10^{-2}$	7,3 $3,9\cdot10^{-3}$	7,1 $1,7\cdot10^{-2}$	5,8 $0,95\cdot10^{-2}$	6,4 $5,0\cdot10^{-2}$	4,1 $2,2\cdot10^{-2}$	*M1*, *E2* $M1+E2$

cannot, however, exclude the possibility of an M1 + E2 mixture.

Measurements carried out in our laboratory by V.M.Lobashev et al on the photographic plate spectrograph showed that the L_1 line appears clearly in the spectrograms, while the L_2 and L_3 lines are indiscernible. This fact is in agreement with the M2 assignment, inconsistent with the E2 possibility, but does not exclude E1 and M1.

Decisive in this respect are the experiments of Adamchuk et al which yielded $\alpha_K = 0.18$, a value corresponding to M2 radiation. Calculation of α_K from the relative intensities of the conversion lines and γ-rays leads to a value of 0.2, if it be assumed that the 149.8 kev transition is M1.

As will be evident from Table 2, the values of K/L, α_K and the ratios of the L subshell coefficients clearly indicate that the 346 kev γ-transition belongs in the M2 class.

461 kev γ-transition. No assignment can be made for this transition inasmuch as the L conversion line is entirely overlapped by the K-497 line and we have no data on the intensity of these γ-rays.

497 kev γ-transition. The K/L ratio could not be determined accurately in this case inasmuch as the L-497 line was poorly resolved from the K-517 line. The relatively low estimated K/L value shows that the transition must have a high multipole order. To evaluate the conversion coefficient it would have been necessary to determine the relative intensity of the given γ-rays and to do this in the presence of the close γ-lines at 461, 517 and 535 kev. Unfortunately, under our circumstances it was not feasible to determine the number of photons for each of these lines separately inasmuch as the activity of the available material was too low for satisfactory measurements on the photoelectric γ-spectrometer, while scintillation spectrometers are incapable of resolving such close lines.

Rasmussen and his co-workers[8], however, give approximate evaluations of the intensity of the hard Gd^{149} γ-lines based on measurements by means of a scintillation counter. Although admittedly the accuracy of these evaluations is not high, using these data and our own data on the relative intensities of the lines, one can evaluate α_K and thus obtain some further indication regarding the multipole order assignment for the 497 kev γ-transition. As may be seen from Table 2 such an evaluation allows of identifying this transition as E3 or M2 or even M1 inasmuch as theoretical values of α_K for the three cases differ little. The M1 and M2 assignments can apparently be rejected in view of the value of K/L. Thus the experimental data do not conflict with the E3 assignment for the 497 kev γ-transition.

517 and 535 kev γ-transitions. These transitions are characterized by a high value of K/L, namely, ~6-7. Although the intensities of the associated K lines were determined with good accuracy, the L lines are very weak so that the K/L ratio was necessarily evaluated very roughly. Nevertheless, from this evaluation we can infer that these transitions are probably E1, M1 or possibly E2 or M2, but can hardly be of a higher multipole order. One can obtain some further indication regarding the multipolarity of these transitions from an evaluation of the conversion coefficients in the same way as was done above in discussing the 497 kev transition. Comparing the deduced and theoretical values of K/L and α_K, we infer that these transitions are probably M1, E2 or a mixture of M1 + E2.

The 940 kev γ-transition has not been investigated in sufficient detail to allow of drawing any unambiguous deduction regarding its multipole order.

On the basis of the above data we can make an approximate evaluation of the total intensities of the nuclear transitions in Eu^{149}:

Bearing this fact in mind and remaining within the framework of the already sketched in portion of the decay scheme, we can suggest two variants for locating the 298 kev transition. Both variants, however, encounter certain difficulties.

Variant 1. It may be hypothesized that the 298 kev transition goes from a 298 kev level to the ground state. According to the single particle model, the characteristics of this 298 kev level can be only $d_{3/2}$ or $s_{1/2}$ inasmuch as the other levels of this shell are already occupied. Inasmuch as the 298 kev transition to the ground state ($d_{\ }$) belongs to the M1 + E2 type, we must discard s and of the indicated configurations choose $d_{3/2}$. Inasmuch as all the intense transitions have already been located in the scheme, we can only infer that the 298 kev level is populated primarily by direct transitions from Gd^{149}. Such transitions are possible with considerable abundance only if of the two possible configurations ($f_{\ }$, $h_{\ }$) of the Gd^{149} ground state the actual one is $f_{7/2}$. However, in this case the probability of excitation of the $h_{9/2}$ level is very low inasmuch as the transition from Gd^{149} is strongly forbidden by the selection rules ($\Delta I = 2$, no). In actual fact, however, the population of the 496 kev ($h_{9/2}$) level is very high.

Thus the assumption that the 298 kev level is an ordinary single particle level consistent with the Mayer model encounters serious difficulties. One could, however, hypothesize that the given level had some other nature and that its spin is 7/2+ (inasmuch as the 298 kev transition is M1 + E2). In this case the ground state of Gd^{149} could be characterized by $h_{9/2}$ and electron capture to this level and the $h_{9/2}$ level would be once forbidden ($\Delta I = 1$, yes). Inasmuch as the disintegration energies to the 496 kev ($h_{9/2}$) and 298 kev (7/2+) levels differ by only about 20% (Ref.11 - see Fig.5), the excitation probabilities for these levels should not differ greatly. This is actually the case.

Variant 2. Alternatively, it may be hypothesized that the 298 kev transition is in cascade with the 346 kev transition. Then the energy of the departure level would be 794 kev. This assumption is apparently not in conflict with the absence of coincidences with the 149.8 kev transition, inasmuch as the 496 kev level must be metastable. According to Weisskopf's formula, the lifetime for the 496→150 kev (M2) transition in Eu^{149} should be $5 \cdot 10^{-8}$ sec, but, as a rule, the actual lifetime in the case of magnetic transitions is appreciably longer. From the standpoint of the intensity balance this arrangement is possible inasmuch as the total intensities of the two transitions are approximately equal. The transitions with energies close to 500 kev have very low intensities and hence can be neglected in the present discussion. Inasmuch as the 298 kev transition is M1 + E2, the possible assignments for the 794 kev level are 9/2-, 11/2- or 13/2-. This level can no longer be interpreted as a single particle level in the framework of the Mayer scheme, inasmuch as there are no longer levels with high spins in the shell under consideration. The 13/2- assignment must be rejected, inasmuch as otherwise the 794 kev level could not be excited. The 11/2- assignment would mean that the selection rules equally allow transitions from Gd^{149} to the 794 kev and to the 496 kev level. From this it would follow that the 346 kev transition should have at least twice the intensity of the 298 kev transition. Actually, however, they are approximately of equal intensity. Finally, the 9/2- assignment makes it necessary to infer the existence of an intense 644 kev E1 type transition to the 150 kev ($g_{\ }$) level. Unfortunately, no such transition is observed. These are the unsatisfactory aspects of the second variant.

The available experimental data do not allow of choosing between the above two variants for situating the 298 kev transition in the decay scheme or of elaborating some other, more consistent variant. More acceptable in our opinion is the variant according to which we postulate the existence of a 298 kev 7/2+ level.

As for the 272 kev transition, it must be borne in mind that in the above mentioned e-e coincidence study[10] there were obtained indications that this transition is in cascade with the 149.8 kev γ-transition. It is not clear, however, whether the 272 kev transition goes directly to the 150 kev level (from a level at 150 + 272 = 422 kev) or is connected with the first excited level through some other unidentified transition.

If we introduce a level at 957 kev, we have two possible alternative arrangements for the 272 and 535 kev transitions. One of these is shown in Fig.5 and infers the existence of a 422 kev ($d_{3/2}$) level. With the other alternative instead of the 422 kev level one must introduce a level at 685 kev. On the basis of evaluation of relative intensities of the transitions in question, it would appear likely that the 272 kev transition goes to the first (150 kev) level.

The introduction of a 957 kev level also provides for locating the 461 kev transition in the decay scheme. The 517 and 940 kev transitions apparently call for the introduction of a new, additional level.

We desire to express our deep gratitude to V.P.Dzhelepov, Director of the Laboratory of Nuclear Problems at the Joint Institute for Nuclear Studies, and the crew of the synchrocyclotron for irradiating the tantalum samples. We wish to thank A.M.Murin, G.M.Gorodinskii, V.N.Pokrovskii & V.A.Sergienko for their interest in the work and for communicating their experimental results prior to publication. We are also indebted to L.A.Sliv and I.M.Band for giving us the values of the theoretical L shell conversion coefficients prior to publication.

Scientific Research Physical Institute
Leningrad State University

References

1. B.S.Dzhelepov & A.A.Bashilov, Izv.AN SSSR, Ser.fiz., 14, 263 (1950).
2. B.K.Preobrazhenskii, O.M.Lilova, A.N.Dobronravova & E.D.Teterin, Zhur. neorgan. khimii (Journ. Inorganic Chem.), 1, 2294 (1956).
3. R.Hoff, J.Rasmussen & S.Thomson, Phys.Rev., 83, 1068 (1951).
4. J.Rasmussen, S.Thomson & A.Chiarso, Phys.Rev., 89, 1068 (1951).
5. N.M.Anton'eva, A.A.Bashilov, B.S.Dzhelepov & B.K.Preobrazhenskii, Abstracts of reports presented at the Seventh All-Union Conference on Nuclear Spectroscopy, M.-L., 1957.
6. G.M.Gorodinskii, A.N.Murin & V.N.Pokrovskii, ibid.
7. G.M.Gorodinskii, A.N.Murin, V.N.Pokrovskii & B.K.Preobrazhenskii, Izv. AN SSSR, Ser.fiz., 21, 1624 (1957). (Trans. Bulletin 21, No.12, 1611.)
8. Y.Shirley, W.Smith & J.Rasmussen, Nucl.Phys., 4, 395 (1957).
9. V.K.Adamchuk, A.A.Bashilov & B.K.Preobrazhenskii, Present issue of the Bulletin, p.
10. B.S.Dzhelepov, B.K.Preobrazhenskii & V.A.Sergienko, Transactions of the Eighth All-Union Conference on Nuclear Spectroscopy, 1958.
11. J.Riddell, Table of Levy's Empirical Atomic Masses, p.654, AECL -CRP, Canada, 1957.

Gd^{147} AND Eu^{147} CONVERSION ELECTRON SPECTRA

- N.M.Anton'eva, A.A.Bashilov, B.S.Dzhelepov & B.K.Preobrazhenskii

Introduction

The present investigation was concerned with the conversion electron spectra of Gd^{147} and its decay product Eu^{147}. The Gd^{147} was obtained by spallation of tantalum. The experimental conditions were the same as in our earlier investigation[1] of Gd^{149}. Our principal experimental results were reported at the Seventh All-Union Conference on Nuclear Spectroscopy in January, 1957.[2]

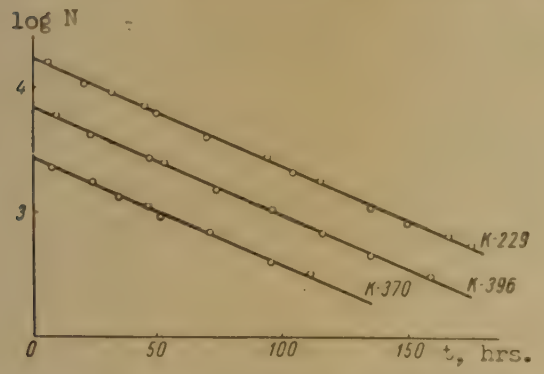

Fig.1. Gd^{147} decay curves characterizing the decrease in the intensity of the K conversion lines associated with γ-transitions with energies of 229, 370 and 396 kev. For the sake of clarity the curves have been shifted vertically.

As the first step, we investigated the integral conversion spectrum of the gadolinium fraction which comprised several isotopes. The decay curves, characterizing the decrease in intensity of the conversion lines with time, indicated that the fraction contained, among other isotopes, a previously unknown Gd isotope with a period of 35 ± 1 hr. The decay curves for the K conversion lines of the principal transitions with energies of 229, 370 and 396 kev are shown in Fig.1. It was established that the conversion electron energy differences were K - L = = 40.5 ± 0.2 kev and K - M = 46.8 ± 0.3 kev. It may be inferred therefore that these transitions occur in the Eu nucleus after electron capture in Gd.

Furthermore, it was noted that there appeared and built up in the gadolinium fraction spectrum conversion lines corresponding to nuclear transitions with energies of ~120 and ~200 kev. The burgeoning and subsequent decay of the K lines associated with these transitions are illustrated in Fig.2. It will be evident that the activity responsible for the build-up of the lines has a period of 35 hours and that after some time their intensity falls off with an appreciably longer period, namely, $T_{1/2}$ = 25 ± 1 days. In this case the conversion line energy differences proved to be K - L = 39.1 ± 0.2 kev and K - M = 45.2 ± 0.3 kev, which indicated unambiguously that the ~120 and ~200 kev transitions occur in Sm. It may be inferred, therefore, that the 35 ± 1 hr Gd isotope transforms into radioactive Eu, which by electron capture with a period $T_{1/2}$ = 25 ±1 days converts to Sm and excites transitions having energies of 120 and 200 kev in the last nucleus.

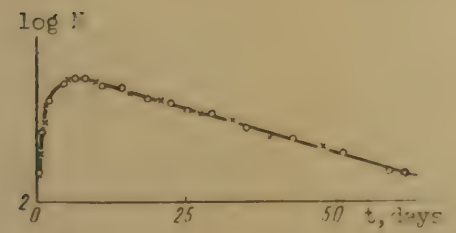

Fig.2. Curve illustrating the growth and decay of Eu^{147} activity in a Gd^{147} source. Observations based on the K-121 (circles) and K-197 (crosses) lines.

We carried out the following control experiment. The gadolinium was purified by separating out the accumulated europium chromatographically. The aforementioned conversion lines associated with the 120 and 200 kev transitions were not evident in the spectrum of the purified Gd, but, as may have been expected, the spectrum of the europium fraction comprised strong conversion lines corresponding to transitions of these energies. The half-life of the Eu isotope as

determined from the decay of these conversion lines again proved to be 25 ± 1 days.

Europium activity with a period of 24 days, accompanied by γ-radiation with energies of 120 and 200 kev , according to Seaborg's Table of Isotopes[3], should be assigned to Eu^{147}. We concluded therefore that the gadolinium isotope decaying with the 35 ± 1 hr period is Gd^{147}.

Concurrently, Murin and his co-workers[4] by successive chromatographic separation of Eu from the gadolinium established that the parent isotope for Eu^{147} is Gd with a period of 1.5 days (36 hours). Murin et al, using a scintillation spectrometer, observed 230, 370 and 390 kev γ-rays from their Gd^{147} source.

Recently, Shirley, Smith & Rasmussen[5] published the results of their investigation on gadolinium isotopes; in this work Gd^{147} was obtained by the Sm + α and Eu + d reactions.

1. Experimental results for Gd^{147}

The complete conversion electron spectrum of the gadolinium fraction in the range up to ~500 kev is shown in Fig.1 of the preceding article.[1] In the present article in Fig.3 we give the section of the Gd^{147} conversion electron spectrum up to ~400 kev with the lines belonging to other Gd isotopes and Eu subtracted. Fig.4 shows the section of the spectrum from ~400 kev to 1.5 Mev; this spectrum includes the lines of other isotopes (hatched in the figure).

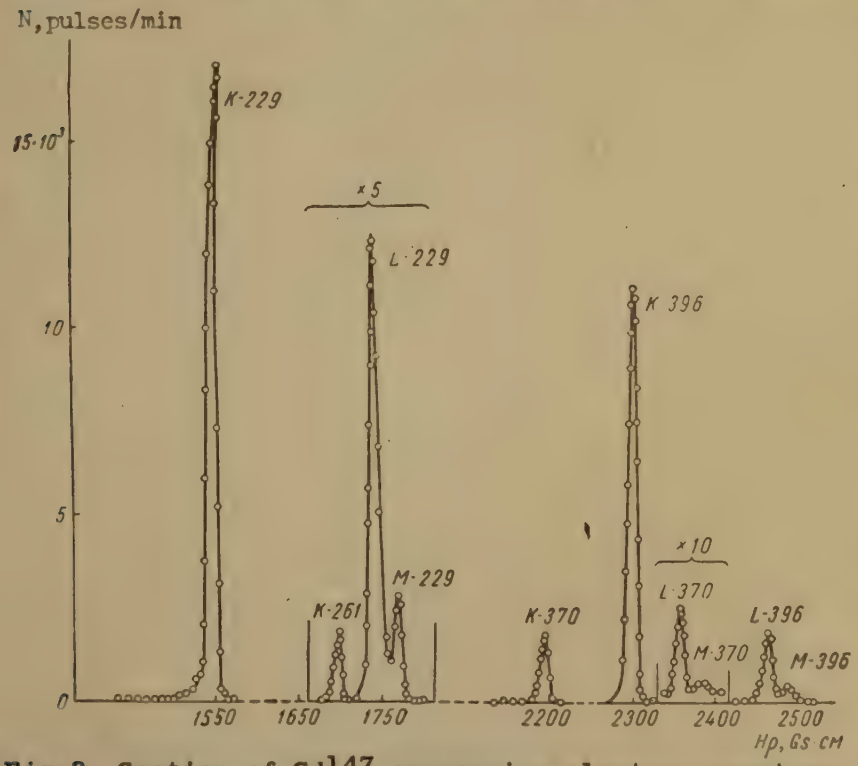

Fig.3. Section of Gd^{147} conversion electron spectrum up to ~400 kev; lines belonging to other Gd isotopes or Eu subtracted.

The detected nuclear transitions excited in the decay of Gd^{147} are listed in Table 1 together with their energies and the relative intensities of the associated conversion lines. Assignment of the weak lines to Gd^{147} (or other isotopes) was made on the basis of the observed period. It proved feasible to determine the K/L ratio for only some of the transitions in view of the fact that the L lines in many cases are weak and poorly resolved. The data pertaining to transitions with energies from ~0.5 to ~1.5 Mev were obtained with only one source and a limited number of successive measurements. Hence the accuracy of the data for this section of the spectrum is lower than for the initial range.

It is interesting to compare our results with the data of Shirley, Smith & Rasmussen[5] who also investigated the conversion electron spectrum of Gd^{147}. All their data pertaining to the conversion lines of the intense 229, 370 and 396 kev γ-transitions are in good agreement with ours. These investigators used an

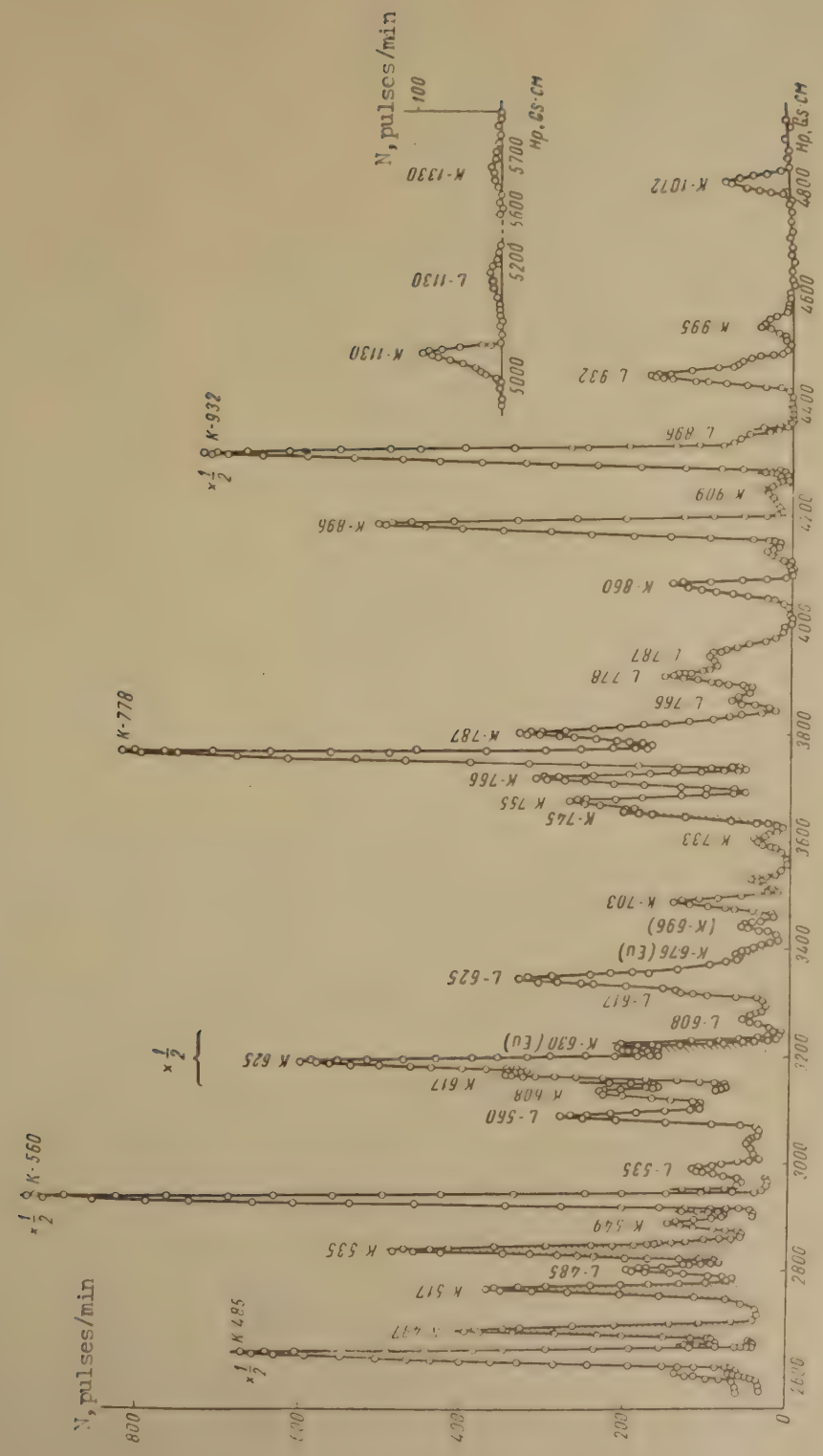

Fig.4. Gd^{147} conversion electron spectrum in the energy range from ~400 kev to 1.5 Mev. The lines belonging to other Gd isotopes or Eu are hatched.

Table 1

Transition energies and relative conversion line intensities for Gd^{147}

No.	E_γ, kev	Lines observed	K/K_{sse} X 100	K/L
1	229±1	K, L, M	220±10	6,9±0,5
2	261±2	K	4,7±0,5	—
3	370±1	K, L, M	15±1	±0,5
4	396±1	K, L, M	100	±0,2
5	485±1	K, L	1,7±0,2	6,8±0,5
6	549±2	K	0,19±0,02	5,8—
7	560±2	K, L	2,4±0,2	7,6±0,5
8	608±3	K, L	0,25±0,02	7,0±1
9	617±3	K, L	0,85±0,10	6—
10	625±3	K, L	1,6±0,2	~4
11	(696)	K	~0,03	—
12	703±3	K	0,17±0,02	—
13	733±3	K	~0,05	—
14	755±3	K, L	~0,4	—
15	766±3	K, L	0,48±0,05	—
16	778±3	K, L	1,2±0,1	—
17	787±3	K, L	~0,5	—
18	860±2	K, L	0,20±0,02	
19	896±2	K	0,65±0,07	
20	909±3	K	~0,05	—
21	932±2	K, L	1,9±0,2	7,1±0,5
22	995±5	K	~0,07	—
23	1072±5	K	~0,16	—
24	1130±5	K, L	~0,13	7±1
25	1330±5	K	~0,013	—

ordinary photographic recording β-spectrograph, a double focusing spectrometer (for investigating strong lines) and a scintillation γ-spectrometer. In addition to the strong conversion lines associated with the above enumerated three transitions, they also detected on their photographic plate weak lines, not observed in our work and corresponding to transitions of energies 136, 142, 217, 226, 241, 310, 348, 374, 391 and 502 kev. According to the visual evaluation of these authors, the conversion lines of all these transitions are "very, very weak" except for the lines associated with the 142 kev transition. The exceedingly low intensity of these lines explains why we did not observe them. The K-226, K-248 and K-391 lines were not separated in our spectra from the other lines. By means of the scintillation spectrometer Shirley, Smith & Rasmussen also observed γ-rays having energies of 517, 570, 635, 770, 900, 1080 and 1298 kev. As will be evident from Table 1, we observed a large number of lines in the corresponding energy region.

2. Multipolarities of the nuclear transitions excited in the decay of Gd^{147}

Table 2

Data for the determination of multipole orders of nuclear transitions in Eu^{147}

E_γ, kev	Ratios & coefficients	Experimental values	Theoretical values E1	M1	E2	M2	E3	Inferred multipole orders
229	K/L	6,9±0,6	7,2	6,9	3,5	5,2	1,2	M1
	α_K	0,16±0,02*	0,027	0,15	0,10	0,74	0,36	
370	K/L	6,8±0,5	7,2	7,0	4,8	5,9	2,6	M1
	α_K	0,051±0,010*	0,0076	0,043	0,025	0,16	0,074	
396	K/L	5,8±0,2	7,2	7,0	4,9	5,9	2,8	M2
	α_K	0,015±0,02*	0,0067	0,035	0,021	0,13	0,062	
485	K/L	7,6±0,5	7,3	7,1	5,5	6,2	3,7	M1 or E1
	α_K	-	0,0043	0,020	0,013	0,065	0,032	

* According to Adamchuk et al[2].

Determination of the multipole orders of nuclear transitions is very important for constructing decay schemes and investigating the structure of nuclear levels. Our results together with certain supplementary data allow of making assignments for the principal transitions in Eu^{147}.

The experimental values of K/L and α_K are compared with the corresponding theoretical values in Table 2. Below we consider the inferences that can be drawn from comparison of these values.

229 kev γ-transition. The experimental value of K/L is in excellent agreement with the theoretical one for M1. This assignment is substantiated by the results obtained in our laboratory by Lobashev and one of the present authors (A.A.Bashilov) who on their β-spectrograph photographic plate obtained an intense L_1 conversion line, an appreciably weaker L_2 line and a very weak L_3 line. However, both these results do not differ greatly from what may be expected on the basis of the theoretical data for E1 and M2 transitions. Decisive as regards the assignment for this transition is the magnitude of α_K obtained in our laboratory by Adamchuk et al[6]. These investigators compared the number of conversion electrons with the number of photoelectrons from the same source. After calibration of the spectrometer with reference to transitions with a known conversion coefficient they found α_K-229 = 0.16, which is in excellent agreement with the theoretical value for M1.

Thus there can be little doubt that the assignment for the 229 kev γ-transition is M1.

370 kev γ-transition. In view of the low intensity of the conversion lines associated with this transition, the experimental K/L ratio has an appreciable uncertainty; it is, however, in good agreement with the theoretical value for M1, although one cannot exclude the possibility of E1. According to the measurements of Adamchuk et al[6], α_K-370 $\approx$ 0.051 which is consistent with the M1 assignment.

396 kev γ-transition. The experimental value of K/L is in good agreement with the theoretical value for M2, but within the limits of the experimental error also allows of identifying this transition as a mixture of M1 + E2. In view of the value α_K-396 = 0.15 obtained by Adamchuk et al, we can safely assert that this transition is of the M2 type.

625 kev γ-transition. In this case the K/L ratio is small (~4) which is typical for transitions having a high multipole order. We suggest that this transition is E3. Unfortunately, in view of the presence of a large number of lines with energies close to 625 kev in the γ-spectrum of this activity, it was impossible to measure the intensities of the individual γ-lines and hence to determine α_K with satisfactory accuracy.

The same observation applies to the other high energy nuclear transitions: the γ-ray intensity measurements of Shirley, Smith & Rasmussen[5] pertain to unresolved groups of γ-lines so that it is not feasible to evaluate the internal conversion coefficients for individual transitions. For this reason no attempt was made to determine the multipole orders of the high energy transitions.

Knowing the multipolarities of nuclear transitions, we can evaluate their total relative inteisites. Such evaluations were carried out for the 229, 370, 396 and 625 kev γ-transitions. In the computations we used the theoretical values of α_K for pure multipoles. We found $I_{229}:I_{370}:I_{396}:I_{625} \approx 2:0.4:1:0.1$.

Among the high energy transitions, some have intensities comparable with that of the 396 kev transition. The most intense, apparently, is the 932 kev transition.

3. Decay scheme for Gd^{147}

Inasmuch as both Gd^{147} and Eu^{147} contain less than 88 neutrons, it may be assumed that these nuclei are spherical. Hence it is logical to consider their

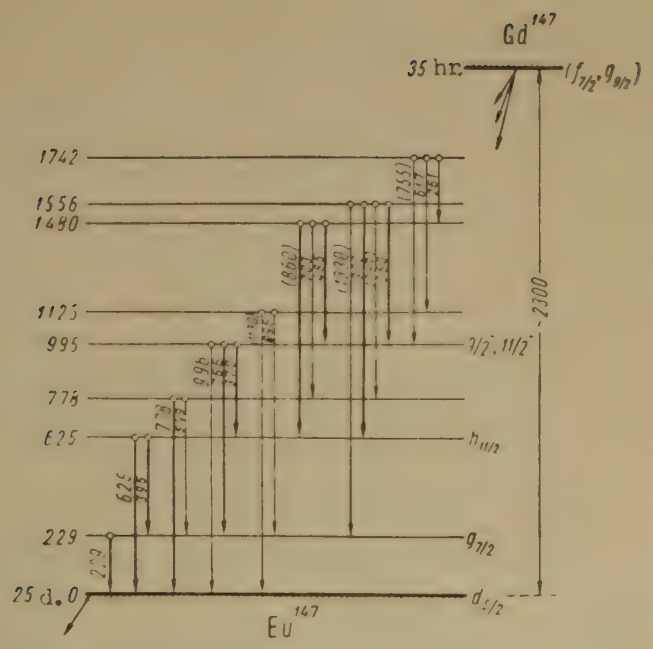

Fig.5. Tentative $Gd^{147} \rightarrow Eu^{147}$ decay scheme.

quantum characteristics from the standpoint of the Mayer model.

According to the single particle model the ground state of Gd^{147} must be $f_{7/2}$ or possibly $h_{9/2}$, while the ground state of Eu^{147} should be either $g_{7/2}$ or $d_{5/2}$. In what follows we shall assume that the configuration of the Eu^{147} ground state is $d_{5/2}$.

As was indicated above the most intense transition is the 229 kev M1 transition. It may safely be assumed that it goes from the first excited level to the ground state (see Fig.5). This assumption is in agreement with the single particle model according to which the first level should be a $g_{7/2}$ level (since we have taken $d_{5/2}$ for the ground state). Thus the energy of the first level is 229 kev.

According to the single particle model, we may expect one of the next excited levels of Eu^{147} to be $h_{11/2}$. The transition from this level to the first level ($g_{7/2}$) must be of the M2 type. As indicated above, the assignment for the 396 kev transition is M2. Hence we infer that it occurs in cascade with the 229 kev transition and that, accordingly, the energy of the second level is 229 + + 396 = 625 kev. This inference is substantiated by the presence of 625 kev γ-rays, corresponding to a cross-over transition from the second 625 ($h_{11/2}$) level to the ground state ($d_{5/2}$). The multipole order of this cross-over transition must be high (E3). As noted above, this apparently is in agreement with the experimental data. Furthermore, our assumption is substantiated by the occurrence of coincidences between the K-229 and K-396 conversion electrons, detected by means of a double magnetic lens spectrometer.[7]

It is impossible to present equally rigorous arguments for the location of the other transitions in the decay scheme. Nevertheless, on the basis of the energy relationships between the transitions and rough evaluations of the relative transition intensities, we propose the decay scheme shown in Fig.5.

For most transitions, energy balances obtain to within 1-3 kev. The transitions for which the balance is less precise are given in parentheses in the figure. The total disintegration energy was computed by means of Levy's empirical formula for atomic masses.[8] The proposed decay scheme does not include a number of observed weak transitions, namely, transitions with energies of 608, 696, 733, 909 and 1072 kev.

4. Experimental results for Eu^{147}

The sections of the conversion electron spectra of the gadolinium fraction containing the Eu^{147} K-121 line are shown in Fig.6; the spectra were recorded six hours and seven days after chemical separation of the Gd. Next to the Eu^{147} K-121 line, for purposes of comparison, we show the slowly varying K-114.8 and K-115.5 lines belonging to Gd^{146} which has a long period (45 days). It will be clear from the figures how the K-121 conversion line has increased in intensity over the ~7-day interval, during which the activity of the 35-hour parent Gd^{147} has virtually died out.

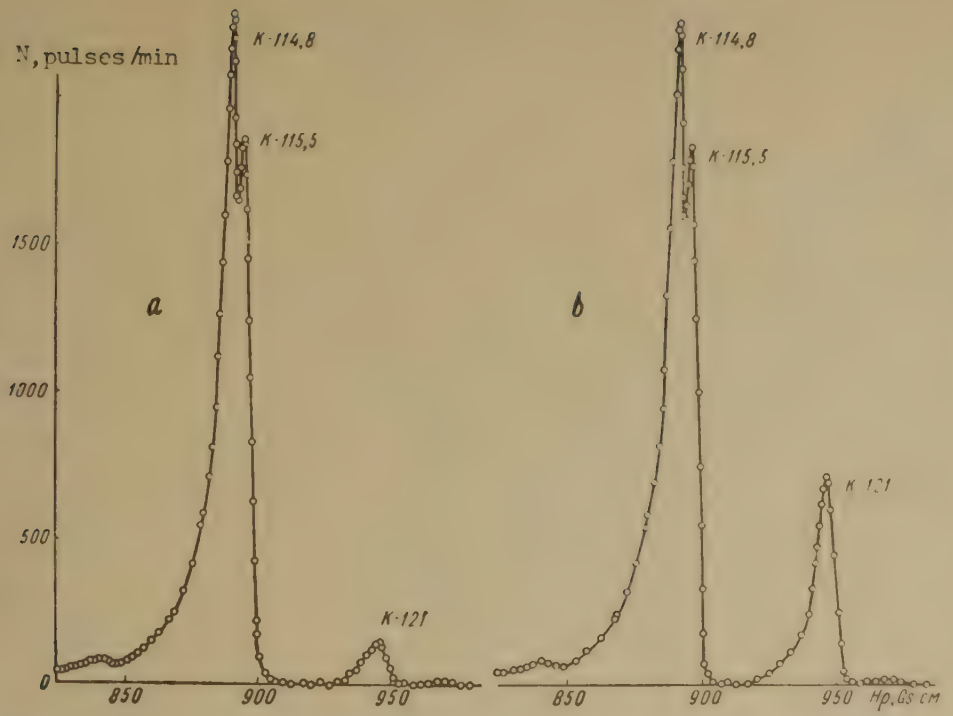

Fig.6. Section of the conversion electron spectrum of the gadolinium fraction illustrating the initial growth of the K-121 line of daughter Eu^{147}. Curve a represents the spectrum 6 hours after chemical separation of the Gd; curve b - 7 days after separation.

Table 3
Transition energies and relative conversion line intensities for Eu^{147}

No.	E_γ, kev	Line observed	K/L	K/K_{197} X 100
1	76,5±0,3	K, L	~6,5	~100
2	121,0±0,3	K, L, M	6,2±0,6	480±30
3	197,6±0,3	K, L, M	3,4±0,3	100
4	600±2	K, L	—	1,9±0,2
5	676±2	K, L	—	1,8±0,2
6	(800±5)	K	—	~0,3

The overall conversion electron spectrum of Eu^{147} is shown in Fig.7. It was obtained in investigating the europium fraction. The spectrum of this fraction contained the conversion lines of several Eu isotopes. The identification of the lines belonging to Eu^{147} was carried out, as in the other cases, from the decay period. Our experimental results are summarized in Table 3. The 800 kev γ-transition was only tentatively assigned to Eu^{147}.

The K and L conversion lines of the 76.5 kev transition are poorly resolved from the K-LL Auger electron group and the K-121 line, respectively. The poor resolution is due to diffusion of the low energy lines because of inadequate uniformity of the active layer. Hence the relative intensities of these lines could be evaluated only very roughly as regards order of magnitude. The ~80 kev transition was first observed by Gorodinskii et al.[4] Later, however, the same authors found by means of a scintillation counter that the intensity of the ~80 kev γ-rays is very low[9] (if they exist at all).

This transition cannot, apparently, be classified as E1, inasmuch as in this case the 76.5 kev γ-ray would have a high relative intensity ($I_{\gamma-76}: I_{\gamma-121} \approx 35\%$) and hence would have been clearly observed. However, if we assume that the assignment for the given transition is E2 or M1, then the intensity ratio $I_{\gamma-76}: I_{\gamma-121}$ would be only 8 or 5%, respectively, and one can readily understand the negative results of the search[9] for the 76.5 kev γ-rays. On the basis of the above, we infer that this transition is either M1 or M1 + E2; this interpretation is substantiated by the other decay scheme data.

Next, let us consider the 197.6 kev γ-transition. Our experimental value of K/L = 3.4 ± 0.3 is consistent with an E2 assignment (Table 4). Gorodinskii et al

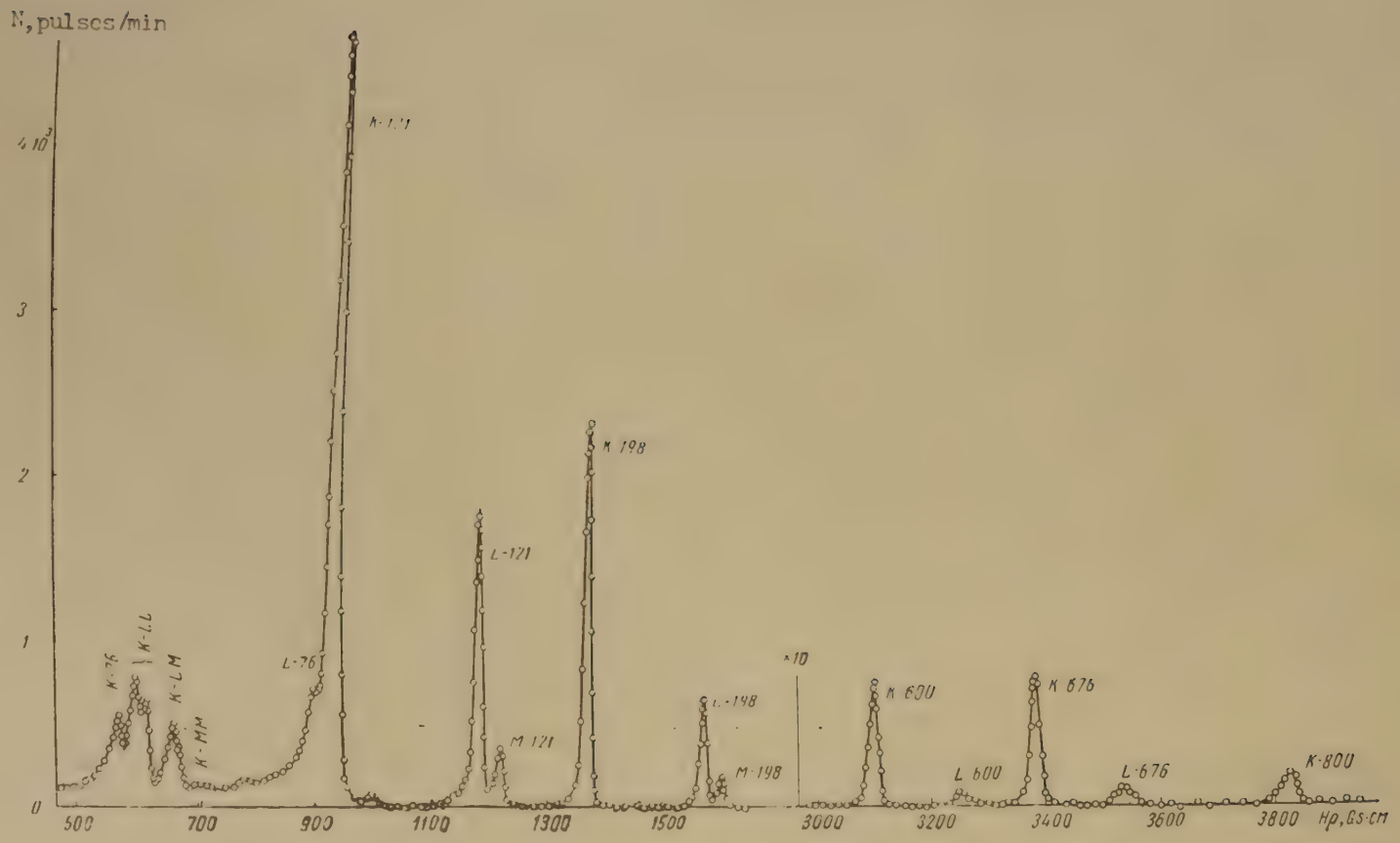

Fig.7. Experimental conversion electron spectrum of Eu^{147}. The curve was obtained in investigating the europium fraction, but the lines belonging to other Eu isotopes have been subtracted. The 800 kev γ-transition has been tentatively attributed to Eu^{147}.

Table 4

Data for the determination of the multipole orders of some transitions in Sm^{147}

E_γ, kev	Ratios & coefficients	Experimental values	Theoretical values					Inferred multipole orders
			E1	M1	E2	M2	E3	
121,0	K/L	6,2±0,6	6,9	6,9	1,8	4,5	0,35	M1
	α_K	1,34*						
		1,2**	0,14	0,83	0,68	6,6	2,8	
197,6	K/L	3,4±0,3	7,1	7,0	3,3	5,2	1,0	E2
	α_K	0,195*	0,03	0,19	0,16	1,0	0,60	

* According to Gorodinskii et al[9].
** Calculated on the basis of the relative γ-ray[9] and K conversion line intensities for the 121 and 197.6 kev transitions.

measured the conversion coefficient for this transition and obtained $\alpha_K = 0.195$, indicating either M1 or E2. Finally, analysis of all the decay scheme data in the aggregate leads us to the conclusion that the most plausible assignment for the 197.6 kev transition is E2.

Accurate determination of the K/L ratio for the 121 kev transition is hampered by the diffusion of the lines and the presence of close lines of somewhat lower energies. The experimentally deduced value of K/L = 6.2 ± 0.6 indicates that this transition is probably M1 + E2. Berlovich et al[10], however, came to the conclusion that the upper bound for the lifetime for this transition ($\tau_\gamma \leqslant 5 \cdot 10^{-10}$ sec) deriving from their measurements is in conflict with the M1 + E2 assignment but is not inconsistent with the transition being pure E1. As may be seen from Table 4, the experimental value of K/L can within the limits of the experimental error be reconciled with the theoretical value for E1, but the data on the internal conversion coefficient conflicts with this interpretation. According to the data of Gorodinskii et al[9], $\alpha_{K\text{-}121} = 1.34$. In addition, the conversion coefficient can be calculated from the relative intensities of the γ-rays and conversion lines. According to the data of Gorodinskii et al, $I_{\gamma\text{-}121} : I_{\gamma\text{-}198} = 1:1.56$, while according to our data $e_{K\text{-}121} : e_{K\text{-}198} = 4.8$. Inasmuch as the 197.6 kev transition may be regarded as pure quadrupole, we can take the theoretical value of 0.16 for its conversion coefficient. Calculation of the K_{121} conversion coefficient on the basis of the indicated quantities gives $\alpha_{K\text{-}121} = 1.2$. Although somewhat high, this value is fairly close to the theoretical value of 0.83 for an M1 transition. Actually, there are no other multipole orders for which the experimental values of K/L and α_K are in better agreement with the theoretical ones (Table 4). The agreement would be better if the ratio of the 121.0 and 197.6 kev γ-ray intensities were closer to unity than follows from the results of Gorodinskii et al. On the basis of the above said, we come to the conclusion that the 121 kev transition must be M1.

For the higher energy transitions - 600 and 676 kev and the possible 800 kev γ-transition - we can only indicate the relative intensities of the K conversion lines. One can say nothing definite regarding the K/L ratios. The possible assignments for these transitions according to the decay scheme are M1, E2 and E3, respectively. Using these multipole orders, the conversion electron data and the theoretical internal conversion coefficients for the corresponding pure multipole orders, we calculated the relative intensities of the nuclear transitions and obtained

$$I_{77} : I_{121} : I_{198} : I_{600} : I_{676} : I_{800} = (0.2) : 1.5 : 1 : 0.20 : 0.48 : (0.02).$$

The most reliable intensity values are those for the 121 and 197.6 kev transitions. The other data, as follows from what has been said above, are only tentative.

It is interesting to compare the principal transition and lower level schemes for Eu^{147} and Eu^{149} with the corresponding schemes for Eu^{151} and Eu^{153} (Ref.15 - Fig.6). In the case of the first three isotopes - Eu^{147}, Eu^{149} and Eu^{151} - the number of neutrons is less than the critical number $N_{cr} = 89$. All these nuclei have a system of low-lying levels satisfactorily described by the Mayer model. Analyzing the respective level diagrams, one is at once struck by their similarity; the principal difference is that the separation between the successive levels decreases as we go from the nucleus with a filled neutron shell towards the region of elongated nuclei. The energy of the first level, equal to 229 kev for Eu^{147}, decreases to 150 kev in Eu^{149} and falls to only 22 kev in Eu^{151}. A similar situation obtains for the $h_{11/2}$ level: in going from Eu^{147} to Eu^{151} its energy decreases from 625 to 497 and then to 197 kev. As is evident from the energies of the corresponding transitions, the energy differences between the levels also decrease.

The system of levels of Eu^{153}, which has a larger than critical number of neutrons is already described by Nilsson's scheme rather than that of Mayer; this nucleus is known to have two rotational states with energies 84 and 194 kev. It is undoubtedly an elongated nucleus.

5. Eu^{147} decay scheme

The decay scheme for $Eu^{147} \rightarrow Sm^{147}$ was discussed and described by Gorodinskii et al[9]. On the basis of our present results it proved feasible to supplement this scheme with the introduction of transitions of 76.5, 600, 676 and 800 kev energy (Fig.8). The disintegration energy was calculated by means of Levy's empirical formula for atomic masses.[8]

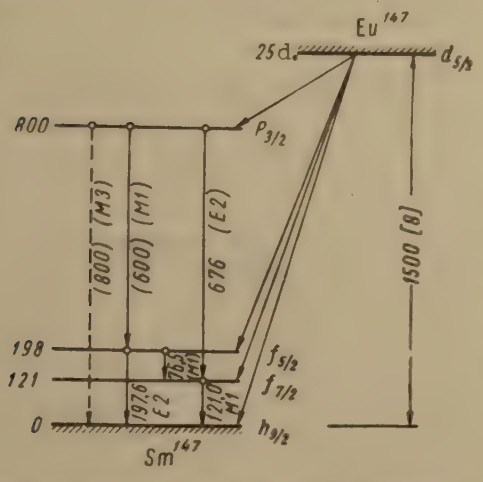

Fig.8. Tentative decay scheme for $Eu^{147} \rightarrow Sm^{147}$. The multipole assignments for the 600 and 676 kev γ-transitions are based only on the decay scheme. The relative abundances of the transitions are given in the text.

As was inferred above in discussing the Gd^{147} decay scheme, the configuration of the ground state of Eu^{147} is $d_{5/2}$. According to Mayer's model the ground state of Sm^{147} must be either $h_{9/2}$ or $f_{7/2}$. While we lack rigorous experimental proof for the choice, we are inclined to give preference to the $h_{9/2}$ assignment on the basis of the proposed decay scheme and the determined multipole orders of the nuclear transitions in Sm^{147}. We note that the $h_{9/2}$ assignment is not in conflict with the Pm^{147}--Sm^{147} β-decay data. According to the Mayer model, the ground state of Pm^{147} must be $d_{5/2}$ or $g_{7/2}$. Consequently, the β^--transition between the ground states must be a first forbidden one ($\Delta I = 1$ or 2, yes). The log ft value of 7.5 is not in conflict with this degree of forbiddenness.

The most intense of the transitions observed in Sm^{147} are those with $E_\gamma = 121.00$ and 197.6 kev. Obviously, these transitions must occur between low-lying levels. In a study[11] of γ-γ coincidences it was established that the 121 and 197.6 kev γ-transitions are not in cascade. Consequently, there must exist levels at 121 and 198 kev.

The existence of the 121 kev level is substantiated by other experiments. Langevin-Joliot[12] reports that in $Pm^{147} \rightarrow Sm^{147}$ β-decay there are emitted weak

γ-rays of 121 kev energy. Inasmuch as the total disintegration energy in this case is 226 kev, the presence of such γ-rays indicates that the first (or one of the first) excited levels in Sm^{147} is located at 121 kev.

The 76.5 kev transition presumably occurs between the 198 and 121 kev levels. If in conformity with the Mayer model, we assume that the first excited level is $f_{7/2}$ and the second $f_{5/2}$, we find that the experimentally determined multipole orders of the 121 kev (M1) and 198 kev (E2) transitions are in excellent agreement with what may be expected on the basis of the proposed level scheme (Fig.8). The assumption that the 76.5 kev transition is of the M1 type is also consistent with the level scheme.

The energies of the two hard γ-lines - 600 and 676 kev - give reason to infer the existence of another level with an energy of 800 kev; the 600 and 676 kev γ-rays correspond to transitions from the 800 kev level to the first and second excited levels (see Fig.8). The 800 kev γ-transition, which we have tentatively attributed to Eu^{147}, may be a cross-over transition from this high-lying level to the ground state. The configuration of the 800 kev leve, according to the Mayer model, is probably $p_{1/2}$. The probable multipole orders of the 600 and 676 kev γ-transitions consistent with the proposed decay scheme are M1 and E2, respectively. The 800 kev transition should be M1. Unfortunately, the available experimental data are not adequate for making reliable multipole order assignments for these transitions. It must be noted, however, that the relative probabilities of these three transitions calculated according to Moszkowski's formula disagree with the relative intensity values calculated from the number of conversion electrons and the inferred multipole orders. The divergence is particularly large in the case of the 800 kev transition: Moszkowski's formula gives a $\sim 10^5$ times lower probability for the transition as compared with the expected.

On the basis of the γ-transition intensities given above (Section 4), we can roughly evaluate the probabilities of electron capture in Eu^{147} to different levels of Sm^{147}. The results of such calculation expressed in the same units as used for the transition intensities (i.e., taking $I_{198} = 1.00$) are the following: intensity of capture to the 800 kev level - 0.70, to the 198 kev level - 1.0 and to the 121 kev level 0.85. In order to determine the probability of capture to the Sm^{147} ground state, one would have to know the total number of Auger electrons. Unfortunately, we did not have sources consisting of pure Eu^{147}; all our sources had appreciable admixtures of other europium isotopes. Gorodinskii et al[9], however, evaluated the relative probability of capture to the ground state of Sm^{147} as 16% and to the excited level as 84%. Using these values, we calculated, on the basis of our data, the relative probabilities of decay of Eu^{147} to the different levels of Sm^{147} and found: 121 kev level - 28%, 198 kev level - 33% and 800 kev level - 23%.

We desire to express our deep gratitude to V.P.Dzhelepov, Director of the Laboratory of Nuclear Problems at the Joint Institute for Nuclear Studies, and the crew of the synchrocyclotron for irradiating the tantalum samples. We wish to thank A.M.Murin, G.M.Gorodinskii, V.N.Pokrovskii and V.A.Sergienko for their interest in the work and for communicating their experimental results prior to publication. We are also indebted to L.A.Sliv and I.M.Band for giving us the values of the theoretical L shell conversion coefficients prior to publication.

Scientific Research Physical Institute,
Leningrad State University

References

1. N.M.Anton'eva, A.A.Bashilov, B.S.Dzhelepov & B.K.Preobrazhenskii, Present issue of the Bulletin, p.889.

2. N.M.Anton'eva, A.A.Bashilov, B.S.Dzhelepov & B.K.Preobrazhenskii, Abstracts of reports presented at the Seventh All-Union Conference on Nuclear Spectroscopy, M.-L., 1957.

3. J.M.Hollander, I.Perlman and G.T.Seaborg, Revs.Mod.Phys., 25, 469 (1953). (Cited in Russian trans., M., 1956.)

4. G.M.Gorodinskii, A.N.Murin & V.N.Pokrovskii, Abstracts of reports presented at the Seventh All-Union Conference on Nuclear Spectroscopy, M.-L., 1957.

5. V.Shirley, W.Smith & J.Rasmussen, Nucl.Phys., 4, 395 (1957).

6. V.K.Adamchuk, A.A.Bashilov & B.K.Preobrazhenskii, Present issue of the Bulletin, p.911.

7. B.S.Dzhelepov, B.K.Preobrazhenskii & V.A.Sergienko, Transactions of the Eighth All-Union Conference on Nuclear Spectroscopy, 1958.

8. J.Riddell, Table of Levy's Empirical Atomic Masses, AECL, CRP, 654, Canada, 1957.

9. G.M.Gorodinskii, A.N.Murin, V.N.Pokrovskii & B.K.Preobrazhenskii, Izv. AN SSSR, Ser.fiz., 21, 1624 (1957). (Trans.Bulletin 21, No.12, 1611.)

10. E.E.Berlovich, K.M.Grotovskii, M.P.Bonits, V.I.Breslav & B.K.Preobrazhenskii, Izv.AN SSSR, Ser.fiz., 21, 1643 (1957). (Trans.Bulletin 21, No.12, 1629.)

11. G.M.Gorodinskii, V.N.Pokrovskii & E.I.Firsov, Uch.zep.(Scientific Notes) Leningrad State Pedagogical Institute, Fiz.-Math.Series, 10, 272 (1957).

12. H.Langevin-Joliot, J.phys.et radium, 17, 497 (1956).

INTERNAL CONVERSION COEFFICIENTS OF SOME NUCLEAR TRANSITIONS IN Eu^{147} AND Eu^{149}

- V.K.Adamchuk, A.A.Bashilov & B.K.Preobrazhenskii

Introduction

The decay of Gd^{147} and Gd^{149} by electron capture leads to the formation of Eu^{147} and Eu^{149} nuclei in different energy states. As investigations[1-3] of the conversion electron spectra have shown, there then occur numerous nuclear transitions in the two europium isotopes. In the case of Eu^{147}, there have been observed over twenty transitions with energies in the range from 230 to ~1000 kev. In the case of Eu^{149}, there are at least eight transitions from 150 to ~500 kev. The $Gd^{147} \rightarrow Eu^{147}$ and $Gd^{149} \rightarrow Eu^{149}$ decay schemes are complicated.[2,3] To construct these schemes one must know the spins and parities of the levels, while to make the assignments one must in turn determine the multipole orders of the nuclear transitions in Eu^{147} and Eu^{149}.

One of the basic methods of determining multipolarities is based on comparison of the experimental and theoretical values of the internal conversion coefficients. For experimental determination of the internal coefficients, however, it is usually necessary to have fairly detailed information on the decay scheme. Hence in the case of complicated decay schemes determination of the conversion coefficients generally proves difficult.

In the present work we used a procedure for determining internal conversion coefficients, which does not require knowledge of the decay scheme. The procedure is based on measurements by means of a magnetic spectrometer of the number of conversion electrons and the number of γ-rays (from observation of photoelectrons) emitted by one and the same source.

Similar experiments have been carried out by Karamian & Prokof'ev[4].

Experimental Procedure

The essentials of the procedure employed in this investigation are the following. Using one and the same radioactive material, we measured by means of a magnetic spectrometer the number n_e of conversion electrons and the number n_γ of photoelectrons. The electron source consisted of the radioactive materials, a copper absorber (0.3 mm), an aluminum absorber (0.1 mm) and a photoelectron radiator, namely, a bismuth foil with a superficial density of 1.6 mg/cm^2. The radioactive source was first mounted at the focus of the spectrometer in the position required for detection of conversion electrons; then it was turned and the photoelectrons were recorded.

The number n_γ of photoelectrons entering the receiving slit of the spectrometer from the radiator may be approximated by the multiple product

$$n_\gamma \approx N_\gamma \omega P D \tau \theta \Omega_\gamma, \qquad (1)$$

where N_γ is the number of γ-rays emitted by the active source, ω is the effective solid angle subtended by the radiator as viewed from the source, $P = P(E_\gamma)$ is a function taking into account the absorption of the γ-rays in the absorber mounted between the source and the radiator, D is the effective thickness of the radiator, τ is the coefficient of photoelectric absorption, $\theta = \theta(E_\gamma)$ is a function taking into account the angular distribution of photoelectrons and depending on the atomic number of the element of which the radiator is made, and Ω_γ is the effective solid angle of the spectrometer for the given radiator geometry.

Thus the number of detected photoelectrons is proportional to the number of γ-rays and the coefficient of photoelectric absorption:

$$n_\gamma = g_\gamma(E_\gamma)\tau N_\gamma. \tag{2}$$

The instrument proportionality factor $g_\gamma(E_\gamma)$ depends on the geometry of the electron source and the instrument and on the energy of the γ-radiation.

It will be evident from Eq.(1) that the function $g_\gamma(E)$ depends on the energy only through the factors $P(E_\gamma)$ and $\theta(E_\gamma)$. With increasing energy of the γ-rays their absorption in the absorber slowly decreases, while $P(E_\gamma)$ increases, tending to a value close to unity. At the same time the angular distribution of the photoelectrons gradually narrows in the direction of motion of the photons and, consequently, the probability of the photoelectrons being within the receiving angle of the spectrometer increases, i.e., the function $\theta(E_\gamma)$ increases. In view of the above considerations, it may be assumed that in a wide energy range the proportionality factor g_γ will be a slowly increasing function of E_γ.

The number of conversion electrons detected by the spectrometer is

$$n_e = \Omega_e N_e. \tag{3}$$

The effective solid angles of the spectrometer for detecting conversion electrons (Ω_e) and photoelectrons (Ω_γ) may differ somewhat because of different instrument geometries and other factors.

Obviously, the internal conversion coefficient $\alpha = N_e/N_\gamma$ is related with the measured quantities n_e and n_γ by

$$\alpha = g\tau\frac{n_e}{n_\gamma}, \tag{4}$$

where g differs from g_γ only by the constant factor

$$g(E_\gamma) = g_\gamma/\Omega_e \approx \omega P D \theta \frac{\Omega_\gamma}{\Omega_e}. \tag{5}$$

While the function $g(E_\gamma)$ can be calculated, we deemed it more expedient to determine a series of values for it by means of calibration experiments using γ-rays with well known conversion coefficients and then to plot an interpolation curve. Our reason for giving preference to empirical determination of $g(E_\gamma)$ is that the theory of the photoeffect is as yet inadequately developed, particularly as regards the angular distribution of photoelectrons and the absolute values of the total absorption coefficient τ. Calibration with reference to known conversion coefficients automatically allows for the angular distribution of photoelectrons and for deviations of the accepted (tabular[5]) values of τ from the true ones. Inasmuch as the possible divergences are not large, they do not have a strong influence on the value of $g(E_\gamma)$. The coefficient τ could be included in the function $g(E_\gamma)$, but in this case the function would have a sharp variation with energy and for a reliable interpolation curve one would have to have a large number of calibration points.

All the calibration measurements were carried out under rigorously identical geometric conditions, i.e., under the same conditions as the main measurements. In all cases we used one and the same photoelectron radiator.

For purposes of calibration, we used the internal conversion coefficients of the 238.6 kev γ-rays of ThB (F-line), 412 γ-rays of Au^{198} and 661.6 kev γ-rays of Cs^{137}. The theoretical and average experimental values of α_K for the listed γ-rays, according to the data in the literature, are summarized in Table 1. In the case of the ThB F-line, the experimental value - $\alpha_K = 0.66 \pm 0.03$ - was obtained by averaging the results of many authors.[6] In addition, recently there have been carried out very careful measurements[7,8] of the ratios of the L_1, L_2

Table 1

Results of calibration experiments

Isotope	Transition energy, kev	Type transition	Experimental value of α_K	Theoretical value of α_K	g, cm
ThB	238.6	$M1$	0.66 ± 0.03	0.69	$1.9 \cdot 10^{-4}$
Au^{198}	411.8	$E2$	0.030 ± 0.001	0.030	$2.1 \cdot 10^{-4}$
Cs^{137}	661.5	$M4$	0.10 ± 0.01	0.11	$2.3 \cdot 10^{-4}$

and L_3 subshell conversion coefficients of the F-line γ-rays. It follows unambiguously from these measurements that the nuclear transition in question is a magnetic dipole one. The possible admixture of E2 does not exceed 1%. In view of this one can justifiably use the theoretical value of α_K for a pure M1 transition for purposes of calibration. The value of $\alpha_K = (0.69)$ listed in the table is taken from the data of Sliv & Band[9].

There have been numerous investigations devoted to determination of the internal conversion coefficient of the 412 kev γ-rays of Au^{198}. It has been established[10-12] that the multipole order of this transition is E2. The most probable experimental value $\alpha_K = 0.030 \pm 0.001$, agrees exactly with the theoretical value given by Sliv & Band[9] for an E2 transition, namely, $\alpha_K = 0.030$.

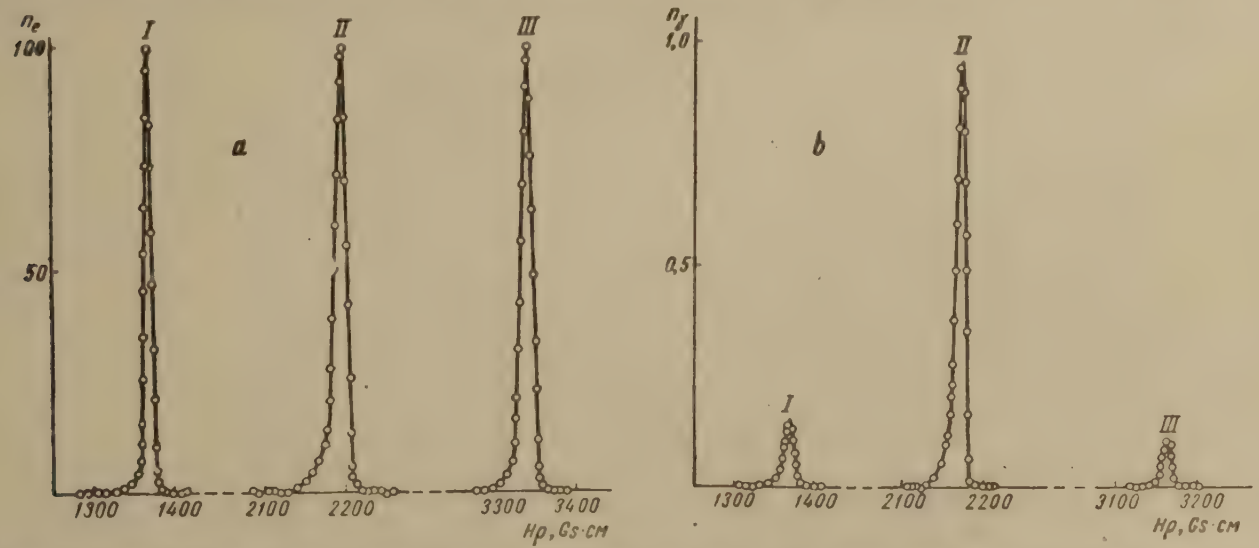

Fig.1. Conversion electron (2) and photoelectron (b) spectra associated with the 238.6 kev γ-rays of ThB(I), 412 kev γ-rays of Au^{198} (II) and 661.5 kev γ-rays of Cs^{137} (III). The background has been subtracted in all cases.

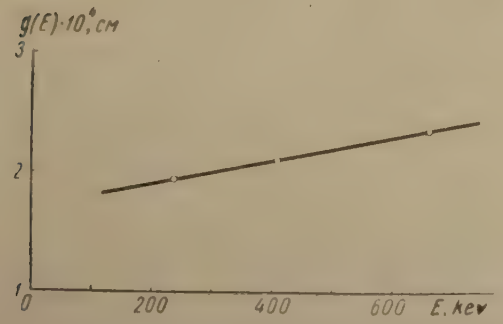

Fig.2. Calibration curve: variation of g as a function of the energy.

The internal conversion coefficient of the 661.6 kev γ-rays of Cs^{137} has also been determined by a number of investigators (Ref.10, 11 & 13). It has been firmly established that the multipole order of this transition is M4. The most probable experimental value of α_K is 0.10 ± 0.01. For our calibration experiments we chose the theoretical value: $\alpha_K = 0.11$.

Typical experimental conversion lines selected for our calibration experiments are shown in Fig.1,a. All the lines were normalized to the same height. The photoelectron lines associated with the same

γ-rays are shown in Fig.1,b. The relative photopeak heights correspond to conversion lines of equal height. The vertical scales in Figs.1, a & b differ by a factor of 100. It should be noted that since a thin absorber was used in these experiments (to increase ω) fast β-particles from Th (B+C+C') and Au^{198} penetrated the filter and gave rise to an appreciable background. In the case of Cs^{137} the background was much weaker. In subsequent experiments we used thicker absorbers and the background due to β-particles was eliminated.

The experimentally determined values of $g(E_\gamma)$ for the selected γ-rays are listed in Table 1. The results of the calibration experiments are plotted in Fig.2. As may have been expected the function $g(E_\gamma)$ varies slowly with the energy, which justifies extrapolation of the curve to cover a rather wide energy range.

The described procedure can also be used for measuring the relative intensities of γ-lines from observation of photoelectrons taking into account their angular distribution. By simple substitution in Eq.(4), we obtain

$$\frac{N_{\gamma_2}}{N_{\gamma_1}} = \frac{g_1\tau_1}{g_2\tau_2}\,\frac{n_{\gamma_2}}{n_{\gamma_1}}. \qquad (6)$$

This relation was used for determining the relative intensities of γ-rays emitted in the decay of Gd^{147} and Gd^{149}.

Measurement Results

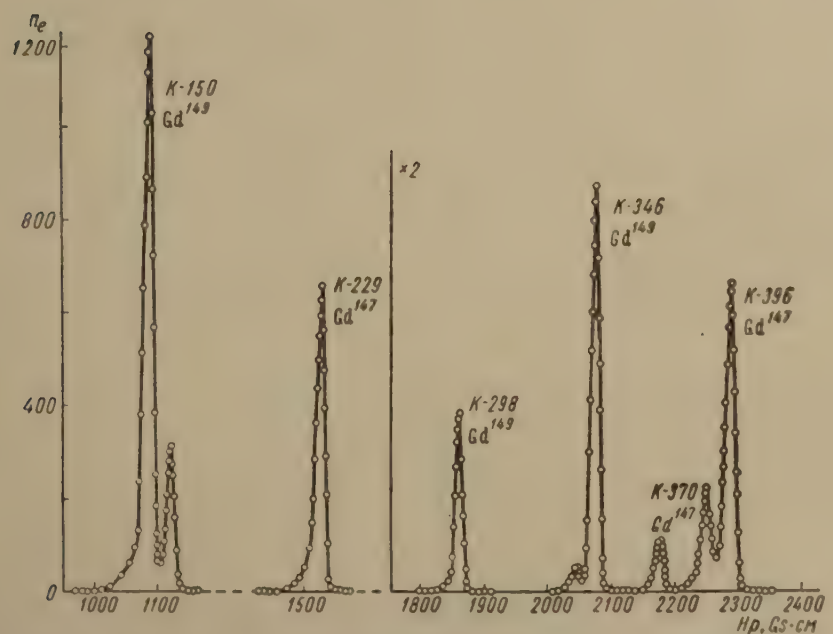

Fig.3. Spectrum of conversion electrons associated with the principal γ-rays of Gd^{147} and Gd^{149}.

Very intense lines associated with nuclear transitions of 229, 370 and 396 kev energy in Eu^{147} appear in the conversion electron spectrum of Gd^{147}. The relative intensities of the other transitions are appreciably lower.

Likewise in the case of electron capture in Gd^{149}, in addition to a number of relatively weak transitions in Eu^{149}, there are excited three very intense transitions having energies of 150, 298 and 346 kev.

In the present investigation we used the described procedure to determine the internal conversion coefficients for the enumerated principal transitions in Eu^{147} and Eu^{149}. All the measurements were carried out under the same standard conditions as the calibartion experiments.

The conversion electron lines corresponding to the principal nuclear transitions in Eu^{147} and Eu^{149} (from radioactive Gd^{147} and Gd^{149}) are shown in Fig.3. The counting rates are given in arbitrary units. The L-114 line of Gd^{146} and the L-298 and L-346 lines of Gd^{149} appear in the spectrum on the side of the K-150

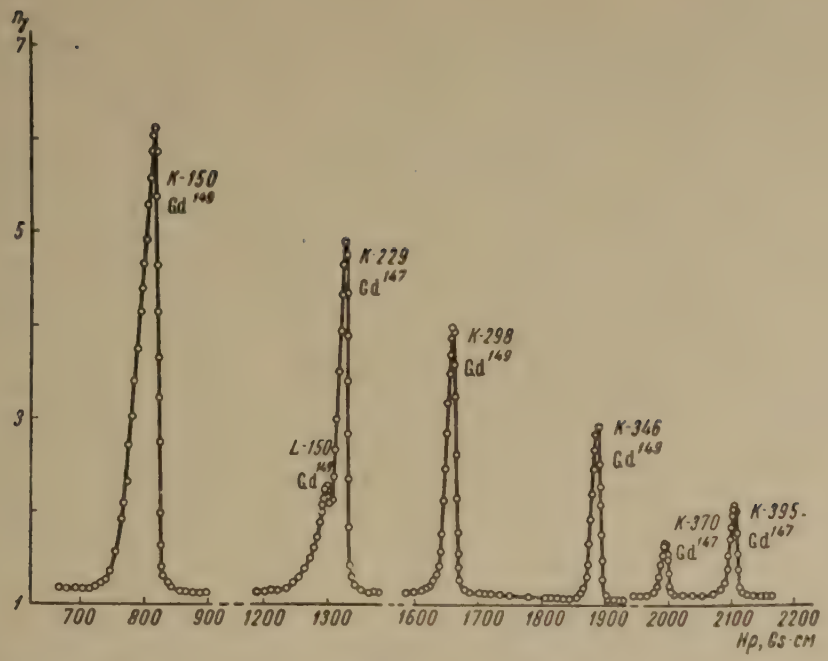

Fig.4. Photoelectron spectra due to the principal γ-rays of Gd^{147} and Gd^{149}.

line and just to the left of the K-346 and K-396 lines, respectively, but this, as will be obvious from the figure, does not interfere with accurate determination of the intensity of the γ-lines under study.

The photoelectron lines associated with the same γ-rays are shown in Fig.4. Here the K-229 and L-150 lines are not fully resolved owing to the rather great superficial density of the radiator (~1.6 mg/cm^2 Bi). Nevertheless, the intensities of the individual lines can be determined with good accuracy inasmuch as the L-150 line (10-day Gd^{149}) can be measured after the Gd^{147} (36-hour) responsible for the K-229 line has completely decayed. The K-150 line has a half-width of 2.5%, inasmuch as the energy of its electrons is low (~60 kev) and they undergo appreciable slowing down in the radiator. The apparent intensity of the K-150 line may be reduced for this reason.

The lines of higher energy have a half-width of 0.57%.

The photoelectron lines are observed against an appreciable background due primarily to Compton electrons from the hard γ-rays of Gd^{147}. The background conditions in the measurements of the short-lived Gd^{147} were somewhat worse than in the case of Gd^{149}. The latter was investigated after the decay of Gd^{147}. The experimentally determined internal conversion coefficients are compared in Table 2 with the theoretical values for transitions of different types. The inferred multipole orders are listed in the last column.

Table 2

Multipole orders of nuclear transitions in Eu^{147} and Eu^{149}

Isotope	Transition energy, kev	Experimental values of α_K	Theoretical values of α_K					Assignment
			E1	M1	E2	M2	E3	
Eu^{149}	150	0,53±0,07	0,080	0,51	0,37	3,2	1,4	M1
Eu^{147}	229	0,16±0,02	0,027	0,15	0,10	0,74	0,36	M1
Eu^{149}	298	0,066±0,007	0,013	0,075	0,046	0,31	0,13	M1
Eu^{149}	346	0,18±0,02	0,0089	0,050	0,030	0,19	0,083	M2
Eu^{147}	370	0,051±0,01	0,0076	0,043	0,025	0,16	0,074	M1
Eu^{147}	396	0,15±0,02	0,0067	0,035	0,021	0,13	0,062	M2

The most interesting inference is that the 396 kev transition in Eu^{147} and the 346 kev transition in Eu^{149} are both M2.

Our inferences regarding the multipole order assignments are substantiated by the data deduced from analysis of the conversion electron spectra of Gd^{147}

and Gd^{149} in Refs.1, 2 & 3. In the cited investigations, the multipole order assignments were based on determination of the conversion coefficient ratios, primarily K/L. This method, however, does not always allow of making a definitive assignment. For example, one of the M2 type transitions referred to above could readily have been interpreted as a mixture of M1 + E2. Thus our method of determining the multipole order from the absolute value of the conversion coefficient proved to be decisive in this case.

As noted above, we also determined the relative intensities of the γ-rays from Gd^{147} and Gd^{149}. The relative intensities obtained in the present investigation are compared with the data of Rasmussen and his co-workers[1] in Table 3.

Table 3

Relative intensities of Gd^{147} and Gd^{149} γ-rays

Isotope	Transition energy, kev	Relative intensity	
		Ref.1	Our data
Gd^{147}	229	2.4	2.1±0.2
	370	0.41	0.48±0.05
	396	1	1
Gd^{149}	150	2.4	1.8±0.4
	298	1.6	1.2±0.1
	346	1	1

It will be seen that the values for Gd^{149} differ appreciably and that the divergence exceeds the limits of the experimental error. This may be partially connected with inaccuracy in taking into account the absorption of photoelectrons in the radiator in the case of the soft 150 kev γ-rays. The photoelectrons from the K shell of bismuth for the indicated line have an energy of 60 kev; admittedly the radiator used in the experiments is too thick for such electrons. On the other hand, the divergence may also be partially connected with the relatively low resolution of the scintillation spectrometer used in the work of Rasmussen and his co-workers for determining the relative γ-ray intensities.

Discussion

Knowing the multipole orders of the principal transitions in Eu^{147} and Eu^{149}, we can construct the skeletal decay schemes for Gd^{147} and Gd^{149}.

The Eu^{147} and Eu^{149} nuclei have an odd number of protons (Z = 63) and an even number of neutrons (84 and 86, respectively). Inasmuch as the number of neutrons is less than the critical number 89, marking the transition from spherical to elongated nuclei, it may be assumed that the Eu nuclei under study are spherical and hence are characterized by the Mayer model. According to the Mayer scheme, the ground states of Eu^{147} and Eu^{149} have the configurations $g_{7/2}$ or $d_{5/2}$. Among the excited levels there must be a $h_{11/2}$ level. Comparing the relative intensities and multipole orders of the principal transitions, we infer that the most intense transitions in Eu^{147} and Eu^{149} of type M1 with energies of 229 and 150 kev and the M2 transitions with energies of 396 and 346 kev, respectively, occur in cascade and are situated in the decay schemes as shown in Fig.5. It must be emphasized that the indicated interpretation of the low-lying levels of Eu^{147} and Eu^{149} hinges upon the multipole order assignments and intensities established in this investigation inasmuch as certain other level characteristics would also be consistent with the Mayer model.

The arrangement of the two principal transitions illustrated in Fig.5 is substantiated by the fact that there are observed E3 type cross-over transitions with energies of 625 kev (Eu^{147}) and 497 kev (Eu^{149}) from the upper $h_{11/2}$ level to the $d_{5/2}$ ground state.[2,3] Further confirmation is furnished by coincidence measurements[1,14] proving the simultaneity of the inferred cascade transitions in the case of both Eu^{147} and Eu^{149}.

Regarding the M1 (or M1 + E2) 370 and 298 kev transitions, it may be assumed that they go from higher-lying levels to the $h_{11/2}$ levels. The characteristics of these higher-lying levels are apparently 9/2 or 11/2. There are, how-

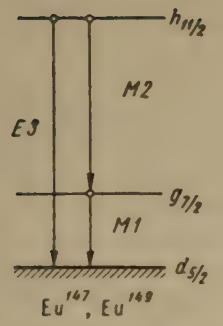

Fig.5. Diagram of principal transitions in Eu^{147} and Eu^{149}.

ever, certain objections to this hypothesis.[2] It must also be noted that the introduction of these hypothetical departure levels cannot be explained within the framework of the Mayer model inasmuch as there are no levels with such high spin values in the shell in question.

It is interesting to compare the schemes for the principal transitions and associated low-lying levels in Eu^{147} and Eu^{149} with corresponding schemes for Eu^{151} and Eu^{153} (Fig. 6).[15] The first three isotopes - Eu^{147}, Eu^{149} & Eu^{151} - have less than the critical number (89) of neutrons. All these nuclei have a system of low-lying levels fully consistent with the Mayer scheme. The similarity of the level systematics will be evident from a glance at Fig.6. The characteristic difference is only that the separation between the levels decreases as we go from the nucleus with a closed neutron shell toward the region of elongated nuclei. The energy of the first level, equal to 229 kev for Eu^{147}, decreases to 150 kev in Eu^{149} and drops to only 22 kev in the case of Eu^{151}. A similar situation obtains for the $h_{11/2}$ level: in going from Eu^{147} to Eu^{151}, its energy decreases from 625 to 497 and then to 197 kev. As will be evident from the energies of the corresponding transitions, the energy differences between the levels also decrease.

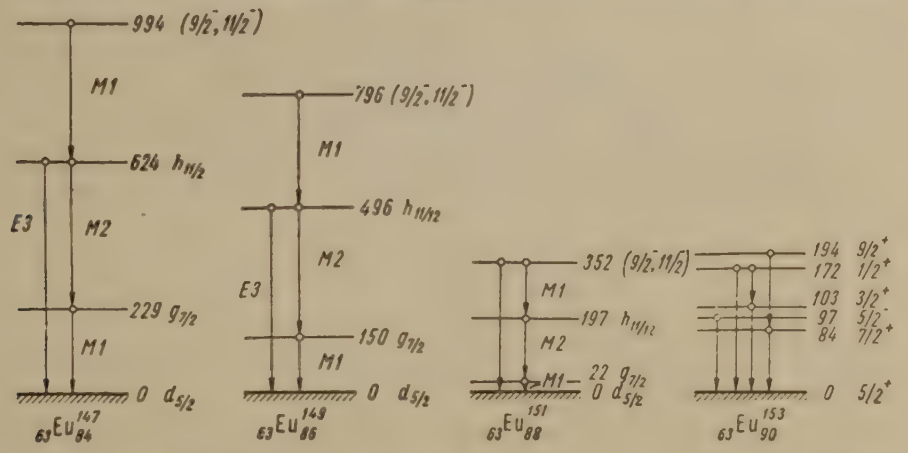

Fig.6. Variation in the arrangement of the low-lying levels in going from spherical nuclei (Eu^{147}, Eu^{149} & Eu^{151}) to elongated ones (Eu^{153}).

In the case of Eu^{153}, which has more than the critical number of neutrons (90), the system of levels is described by Nilsson's scheme rather than that of Mayer; this nucleus is known to have two rotational states with energies of 84 and 194 kev. It is, undoubtedly, an elongated nucleus.

The level diagrams shown in Fig.6 illustrate the character of the variations occurring in going from spherical to elongated nuclei.

We desire to express our gratitude to V.P.Dzhelepov, Director of the Laboratory of Nuclear Problems at the Joint Institute for Nuclear Research and the crew of the synchrocyclotron for irradiation of the tantalum samples.

Scientific Research Physical Institute,
Leningrad State University

References

1. V.Shirley, W.Smith & J.Rasmussen, Nucl.Phys., 4, 395 (1957).
2. N.M.Anton'eva, A.A.Bashilov, B.S.Dzhelepov & B.K.Preobrazhenskii, Present issue of the Bulletin, p.899.
3. N.M.Anton'eva, A.A.Bashilov, B.S.Dzhelepov & B.K.Preobrazhenskii, Present issue of the Bulletin, p.889.
4. P.T.Prokof'ev, Dissertation, All-Union Scientific Research Institute of Metrology.
5. C.DaVisson & R.Evans, Revs.Mod.Phys., 24, 79 (1952).
6. A.Wapstra & G.Nijgh, Nucl.Phys., 1, 245 (1956).
7. V.M.Kel'man, V.A.Romanov & R.Ia.Metskhvarishvili, Doklady AN SSSR, 103, 577 (1955).
8. E.M.Krisiuk, G.D.Latyshev, M.A.Listengarten, L.A.Ostretsov & A.G.Sergeev, Izv.AN SSSR, Ser.fiz., 20, 363 (1956). (Trans.Bulletin, 20, No.3, 332.)
9. L.A.Sliv & I.M.Band, Tablitsy koeffitsientov vnutrennei konversii γ-izlucheniia (Tables of internal conversion coefficients), M.-L., 1956.
10. B.S.Dzhelepov & L.K.Peker, Skhemy raspada radioaktivnykh izotopov (Decay schemes of radioactive isotopes), M.-L., 1957.
11. J.M.Hollander, I.Perlman & G.T.Seaborg, Revs.Mod.Phys., 25, 469 (1953). (Cited in Russian trans., 1956).
12. L.Simons, Phys.Rev., 86, 570 (1952).
13. Yasukozu Yashizama, Nucl.Phys., 5, 122 (1958).
14. B.S.Dzhelepov, B.K.Preobrazhenskii & V.A.Sergienko, Transactions of the Eighth All-Union Conference on Nuclear Spectroscopy, 1958.
15. N.M.Antoneva, A.A.Bashilov, B.S.Dzhelepov & B.K.Presobrazhenskii, Izv. AN SSSR, Ser.fiz., 22, 135 (1958). (Trans.Bulletin, 22, No.2, 134.)

As^{73} CONVERSION ELECTRON SPECTRUM

- E.P.Grigor'ev, B.S.Dzhelepov, A.V.Zolotavin & V.Ia.Mishin

The principal features of the decay scheme of As^{73} are now known: Fig.1 shows the decay scheme proposed by Welker et al[1] and elaborated by Barloutaud and his co-workers[2,3] and Trail & Johnson[4]. We carried out an investigation of the conversion electron spectrum of As^{73} on a β-spectrometer[5] with a resolution of 0.4%. The As^{73} source was obtained by irradiation of natural germanium with 10.8 Mev deuterons and in addition to As^{73} contained residues of As^{74}. The preparation and purification procedure is described in Ref.6.

Inasmuch as the conversion lines of As^{73} rise high above the continuous spectrum of As^{74}, the latter did not interfere with study of the As^{73} spectrum. The high specific activity of our material made it feasible to prepare comparatively thin sources; the electron absorption in the source was very small. Control experiments with a source one eighth the thickness showed that the absorption does not exceed 2-5% for 12 kev electrons. The counter window introduced an appreciable distortion as regards the intensity of the 12 and 50 kev lines. The film forming the counter window passed electrons from 8 kev energy and it was necessary to introduce a very appreciable correction for the 12 kev line.

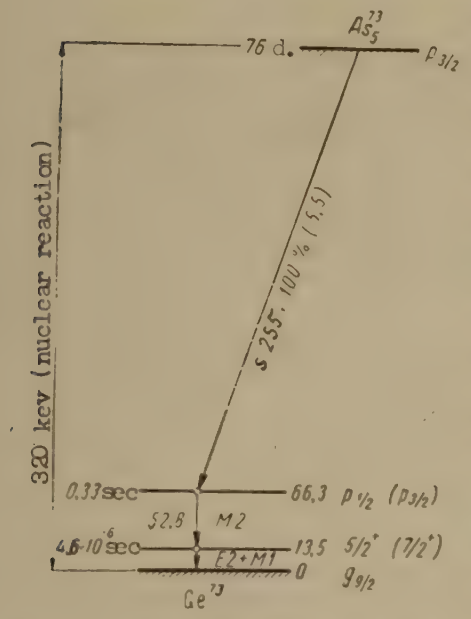

Fig.1. Decay scheme for As^{73}.

We detected conversion lines only from the two transitions indicated in Fig.1. Specifically, we determined the energies and relative intensities of the L and (M + N) lines of the 13.5 kev transition (Fig.2) and the K, L and (M + N) lines of the 52.8 kev transition (Fig.3). Our results are juxtaposed with those of Johansson[7] in Table 1. It will be seen that there is good agreement as regards the transitions energies and only minor divergences as regards the line intensities.

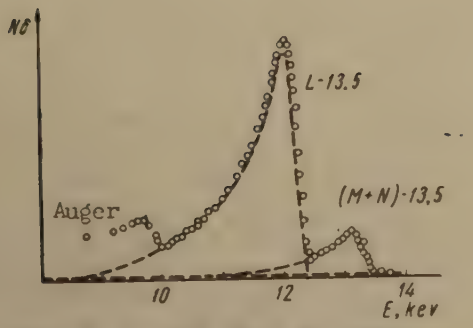

Fig.2. L and (M + N) conversion lines of the 13.5 kev transition.

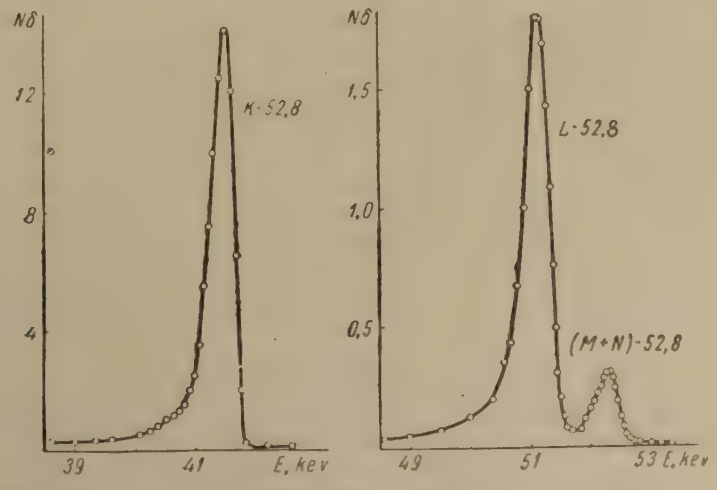

Fig.3. K, L and (M + N) conversion lines of the 52.8 kev transition.

Table 1

Energies and relative intensities of As^{73} conversion lines

Lines	Our results			Johansson's data[7]		
	E_e	$h\nu$	I_e	E_e	$h\nu$	I_e
L_1	12,3	13,5±0,5	7,2±1*	12,1	13,5±0,3	8,3
$M_1 + N_1$	13,4		1,1±0,2	13,3		1,5
K_2	41,8		10,0	42,6		10,0
L_2	51,5	52,8±0,5	1.39±0,05	52,7	53,9±0,5	1,79±0,10
$M_2 + N_2$	52,6		0,22±0,01			
K_3		81	$<10^{-3}$	75	81±8	10^{-2}
K_4		66,3	$<10^{-4}$			

* The uncertainties in determining $L_1/(M_1 + N_1)$ are appreciably smaller: $L_1/(M_1 + N_1) = 6.3 \pm 0.6$.

The K_2, L_2 and $(M_2 + N_2)$ lines (52.8 kev transition) were well resolved in our work, so that we could determine the individual intensities of the L_2 and $(M_2 + N_2)$ lines. The good resolution and low statistical uncertainty (under 1%) attained in our experiments allowed us to indicate the intensities with better accuracy.

Under our conditions, we should have been able to detect the lines associated with the 81 ± 8 kev transition even if it were 10 times weaker than reported by Johansson[7], but we were unable to detect any lines associated with a transition of this energy.

Using a 70 times stronger source, we carefully searched the background in the vicinity of the $(M_2 + N_2)$ line for the purpose of obtaining evidence of a crossover transition (~66 kev) from the second excited level to the ground state. Again, we failed to detect this activity. The upper bound for the intensity of the corresponding K line is indicated in Table 1.

Discussion

Table 2

Conversion coefficients for the 52.8 kev transition (Z = 32).

Multipole order	Theoretical		Experimental			
	α_K	K/L	α_K [2]	α_K [3]		K/L (Our data)
$E1$	0,403	<8				
$E2$	2,8	<2,8				
$E3$	6,9	<0,3				
$M1$	0,40	~8,5				
$M2$	7,1	~6	4	7—8		7,2±0,3
$M3$	105	~2				

1. Our results allow of making more definite the assignment for the 52.8 kev transition. Inasmuch as there are as yet no precise theoretical L shell conversion coefficients for low energies and the values of Z in question, we compared our experimental K_2/L_2 ratio with the values obtained by extrapolation of the coefficients calculated by Sliv & Band. The comparative data are listed in Table 2, which shows that on the basis of K/L and α_K values one can eliminate all assignments except M2.

2. Let us consider now the possible assignments for the second excited level of Ge^{73} in the light of the As^{73} decay scheme. The ground state of this nucleus is probably $p_{3/2}$. This assignment is predicted by Mayer's scheme which is known to be valid for a number of nuclei with odd-A and 31 or 33 protons or neutrons, namely Ga^{73}_{42}, As^{75}_{42}, As^{77}_{44}, Cr^{55}_{31}, Fe^{57}_{31}, Ni^{59}_{31}, Fe^{57}_{33}, and Ni^{61}_{33}.

Evaluation of log ft for the electron capture on the basis of the disintegration energy and lifetime of As^{73} yields log ft = 5.5. This value is typical for allowed transitions; whence it follows that the Ge^{73} could be $p_{1/2}$, $p_{3/2}$ or $f_{5/2}$. On the other hand, the 13.5 kev transition on the basis of the lifetime of the 13.5 kev level in Ge^{73} and the α_K and K/L values must be classified as E2 or E2 + M1. Inasmuch as the ground state of Ge^{73} is 9/2+, this leaves only the 5/2+ and 7/2+ assignments for the 13.5 kev state of Ge^{73}. Since as we have unambiguously identified the 52.8 kev transition as M2, there remain for the 66.3 kev level in Ge^{73} only the assignments 1/2- and 3/2-, the 5/2- possibility being excluded.

Now let us consider the competition of the 66.3 and 52.8 transitions with the alternate 1/2- and 3/2- assignments for the Ge^{73} 66.3 kev level. In Table 3 we give the upper bound for the ratio of the intensities of the K conversion lines associated with the 66.3 and 52.8 kev transitions and, for comparison, the same ratio calculated according to Weisskopf's formula on the assumption that the multipole order of the 66.3 kev transition is E3 or M4.

Table 3

Intensity ratio of the K conversion lines of the 66.3 and 52.8 kev transitions (theoretical values computed on the assumption that the 66.3 kev transition is either E3 or M4)

Experimental	Theoretical	
	$(E3(^9/_2^- \to {}^9/_2^+)$	$M4\ {}^1/_2^- \to {}^9/_2^+)$
$<10^{-5}$	$\sim 10^{-5}$	10^{-13}

An unambiguous deduction from the tabulated values is not feasible. It should be borne in mind, however, that the 52.8 kev transition is retarded by four orders of magnitude: this is evident from a comparison of the lifetimes, i.e., the experimental lifetime and the theoretical one calculated according to Weisskopf. Such a slowing down may be connected with one of the levels being a collective one and the other a single particle one; probably the collective level is the Ge^{73} 13.5 kev level and the 13.5 kev transition is a greatly retarded M1 type transition. If this is the case, the theoretical value in Table 3 should be increased by a factor of 10^4, after which comparison with experiment proves to be more favorable for the 1/2- assignment.

3. Of intrinsic interest is the value of L/(M + N) obtained by us for the 52.8 kev transition, for there are few such values for M2 transitions in the literature.[8] Our value of 6.2 ± 0.5 for this transition differs greatly from L/(M + N) ≈ 3 reported for other multipole orders. The value of L/(M + N) ≈ 6.3 obtained for the 13.5 kev transition is also higher than the average value for E2 transitions (it must be noted, however, that very few L/(M + N) ratios have been determined in the given energy region).

4. The presence of the two isotopes As^{73} and As^{74} in our source material made it possible to compare their relative amounts at the time of measurement and to calculate the ratio of their yields in the nuclear reaction. The ratio of the number of K conversion electrons from the 52.8 kev transition in As^{73} to the number of conversion electrons from the 596 kev transition in As^{74} at the time of measurement equalled 185. Using the decay scheme for As^{74} given in Ref.6 and taking the number of K conversion electrons from the 52.8 kev transition as 8.2 per decay, we find that the reaction yield of As^{73} amounts to 0.8 ± ± 0.3 of the yield of As^{74}.

We desire to thak B.M.Isaev, I.P.Selinov, E.E.Baroni & E.N.Khaprov for assistance in the work.

Scientific Research Physical Institute,
Leningrad State University

References

1. J.Welker, A.Schardt, G.Friedlander & J.Howland, Phys.Rev., 92, 401 (1953); Ibid., 91, 484 (1953).
2. R.Barloutaud & M.Sartory, Compt.Rend., 236, 1872 (1953).
3. R.Barloutaud, R.Ballini & R.Sartory, Ibid., 237, 886 (1953).
4. C.Trail & C.Johnson, Phys.Rev., 91, 474 (1953).
5. A.V.Zolotavin, Izv.AN SSSR, Ser.fiz., 18, 127 (1954).
6. E.P.Grigor'ev, B.S.Dzhelepov, A.V.Zolotavin, V.Ia.Prikhodtseva, Iu.V. Khol'nov & G.E.Shchukin, Izv.AN SSSR, Ser.fiz., 22, 831 (1958). (Trans.Bulletin, 22, No.7, p.825.)
7. S.Johansson, Ark.Fys., 4, 273 (1952).
8. M.A.Listengarten, Izv.AN SSSR, Ser.fiz., 22, 759 (1958). (Trans.Bulletin, 22, No.7, p.755.)

CONVERSION ELECTRON SPECTRUM OF THE CERIUM FRACTION FROM THE SPALLATION PRODUCT OF Ta

- B.S.Dzhelepov, B.K.Preobrazhenskii, I.M.Rogachev & P.A.Tishkin

The cerium fraction, obtained as a result of chromatographic separation of the products of spallation of Ta, was applied to a lightly aluminized collodion film. The diameter of the active spot was 3-4 mm. The electron spectrum of the cerium fraction was measured on two instruments: in the range from 30 kev up on a single magnetic lens β-spectrometer with improved focusing (relative line half-width 1.4%) and in the region of low energies on a magnetic lens β-spectrometer with particle acceleration. This spectrometer had a counter with a window made of thin collodion film which passed electrons having energies > 2-2.5 kev.

The activity of the cerium fraction in all the sources, obtained by irradiation at different times, was relatively low; the counting rate at the most intense conversion line at the beginning of measurement did not exceed 900 pulses/ /min.

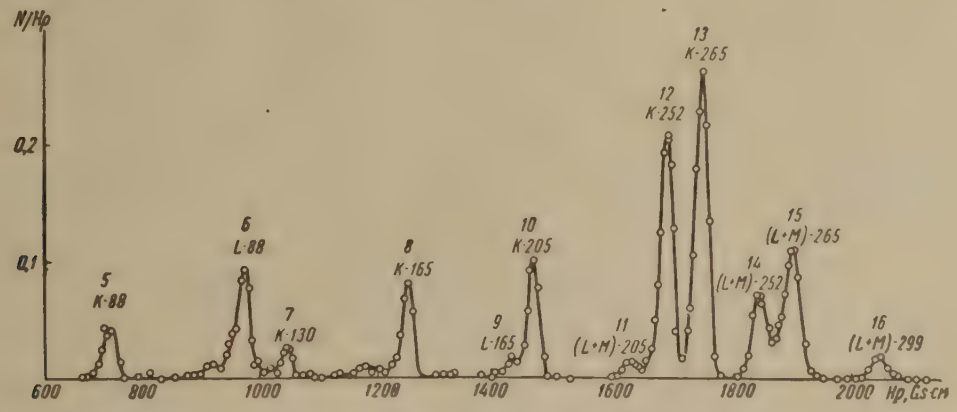

Fig.1. High energy region of the cerium fraction conversion electron spectrum.

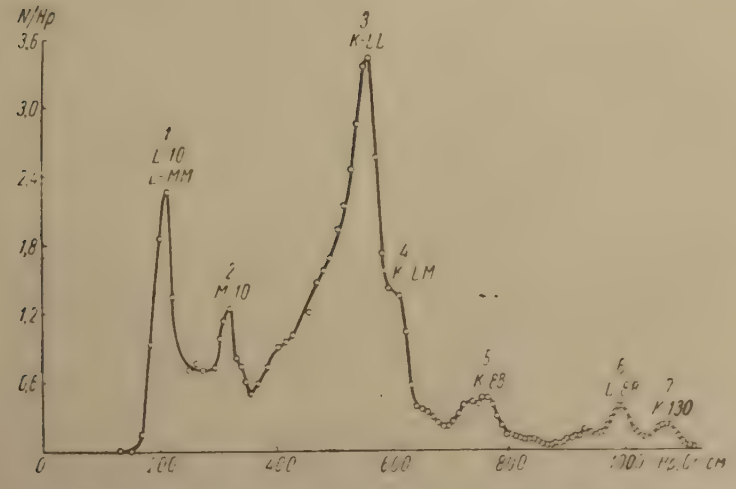

Fig.2. Spectrum of conversion and Auger electrons from the cerium fraction; low energy region.

The experimental conversion spectrum is shown in Figs.1 & 2; the line energies, inferred identifications and relative intensities are listed in Table 1. The 15 detected electron lines fall into three groups according to their decay periods.

1. The intensity of the 126.2 and 159.1 kev electron lines fell off very slowly; these lines are apparently due to the K and (L + M) conversion electrons of the well-known 165 kev transition in Ce^{139} which has a half-life of 140 days.[1] Our experimental intensity ratio, K/(L + M) = = 8.1 ± 0.5, is consistent with the M1 assignment[2,3] for this 165 kev transition.

Table 1

Conversion and Auger electron lines in the spectrum of the cerium fraction

No.	Hρ Gs·cm	E_{e^-}, kev	Identification	Half-life, hrs.	Relative intensity
1	212	4,0±0,3	$L-MM$, L-10	—	—
2	318	9,0±0,3	M-10	—	—
3	560	27,0±0,5	$K-LL$	—	—
4	612	32,0±2,0	$K-LM$	—	—
5	765	49,1±0,5	K-88	19,9	94±10
6	994	80,5±1,0	L-88	17,9±1,0	56±6
7	1064	91,4±1,0	K-130	17,8±5	9,5±2
8	1270	126,1±1,0	K-165 Ce^{139}	Long	24±2
9	1446	159,1±1,0	$(L+M)$-165 Ce^{139}	Long	3,0±0,5
10	1484	166,5±1,0	K-205	16,9±0,3	32±3
11	1658	201,8±3,0	$(L+M)$-205	—	7,3±0,8
12	1710	212,8±1,0	K-252	33,0±0,3	67±5
13	1772	226,1±1,0	K-265	16,7±0,5	100
14	1872	248±3	$(L+M)$-252	36,0±3,0	27±3
15	1926	260±1	$(L+M)$-265	17,7±1,0	44±5
16	2070	293±2	$(L+M)$-299	19,5±3,0	4,4±1

2. The intensity of the 212.8 and 248 kev conversion lines fell off with a period of 33 hours; they can be identified as the K and (L + M) conversion lines of a 252 kev γ-transition. The experimental value of K/(L + M) ratio indicates that this transition is E3 (see Table 2).

Ce^{137} has an isomeric state with an energy of 256 kev and a half-life of 34.5 hours.[7] In view of the closeness of the energy, half-life and multipole order of the transition observed by us with the corresponding characteristics of the isomeric transition in Ce^{137}, we are inclined to attribute the 33-hour activity to Ce^{137}.

We failed to detect conversion electrons from the 445 kev transition observed in Ce^{137} by Brosi & Ketelle[7], which is not surprising in view of the weak activity of our source and the low intensity of this transition: according to the decay scheme proposed by Brosi & Ketelle, the relative intensity of this transition is only 3%.

The electron line with 9 kev energy apparently appears as a result of conversion on the M shell of the 10 kev γ-rays discovered by Brosi & Ketelle.[7] The L conversion electrons of the 10 kev γ-transition should appear in the region of the L-MM Auger electrons.

Our data are not in conflict with the decay scheme proposed by Brosi & Ketelle.

3. The intensity of the other lines listed in the table fell off with a period of 17 hours. The intense 226 and 260 kev electron lines are due to the K and (L + M) conversion electrons of a 265 kev transition. According to Kurbatov et al[8], the isomeric transition in Ba^{135} (28.7 hours) has a close energy, namely, 269 kev, and could occur in the decay of Ce^{135}:

$$Ce^{135} \xrightarrow[22\ hrs]{EC} La^{135} \xrightarrow[19\ hrs]{EC} Ba^{135m} \xrightarrow[28.7\ hrs]{\gamma, e^-} Ba^{135}\ (stable).$$

However, careful observation of the counting rate at the conversion lines showed no indication of any increase of the period above 17 hours; hence the detected 265 kev γ-transition cannot be attributed to the isomeric state of Ba^{135}. According to our evaluation K/(L + M) = 2.27 and the assignment for the 265 kev transition is E3.

Table 2

Multipole order assignments

γ-transition energy, kev	Experimental ratios		Theoretical values of K/L calculated according to Sliv & Band[5] (K-shell) and Rose[6] (L-shell)										Possible assignments
	K/(L + M)	K/L*	α_1	α_2	α_3	α_4	α_5	β_1	β_2	β_3	β_4	β_5	
88	1,62±0,30	2,02	7,42	1,82	0,35	0,060	0,013	7,21	4,63	1,64	0,626	0,231	$E2$, $(E3+M2)$, $(E4+M3)$
165	8,1±0,5	10,1	7,69	3,78	1,51	0,392	0,168	6,98	5,28	3,00	1,67	1,09	$E1$ or $M1$
205	4,38±0,25	5,48	7,68	4,36	2,01	0,591	0,306	7,30	5,63	3,83	2,31	1,51	$E2$, $(E3+M2)$
252	2,48±0,16	3,10	7,95	5,00	2,62	1,09	0,550	7,20	5,95	4,27	3,21	2,05	$E3$, $E4+M3$, $E5+M4$
265	2,27±0,15	2,84	8,00	5,53	2,75	1,10	0,540	7,21	5,97	4,31	3,01	1,95	$E3$, $E4+M3$, $E5+M4$

* Obtained on the assumption that M/L ≈ 0.25, as given in Listengarten's review article[4].

The weak conversion line of 293 kev energy may be interpreted as being due to conversion of a 299 kev γ-transition on the (L + M) shells, for if this line were due to K conversion electrons there should also exist an L line at about 326 kev, yet not indications of a line at this energy were evident.

The K line from the 299 kev transition should be located between the strong L lines associated with the 252 and 265 kev transitions; in some series of measurements we observed a small rise between these lines. In addition, the 293 kev line is asymmetric: its right hand side is flatter, which indicates the possible surposition of M electrons of a lower intensity conversion on the L electrons.

The 49.1 and 80.5 kev electron lines may be identified as the K and (L + M) conversion electron lines of an 88 kev γ-transition. The experimental line intensities listed in Table 1 have been corrected for absorption in the counter window.

Comparison of the experimental K/(L + M) ratio (1.62) with the theoretical value for K/L indicates that the 88 kev transition is probably E2. We identify the 166.5 and 201.8 kev conversion lines as being due to a 205 kev transition.

We also detected a weak line at 91.4 kev and inferred that it is due to the K electrons of a 130 kev transition.

On the basis of the above data it is still impossible to assign the "17-hour" lines to any definite Ce isotope or its daughters or to indicate even a tentative decay scheme.

We wish to express our gratitude to the crew of the Joint Institute for Nuclear Research synchrocyclotron for irradiation of the tantalum target and to I.A. Iutlandov for assistance in preparing the source.

Scientific Research Physical Institute
Leningrad State University

References

1. J.M.Hollander, I.Perlman & G.T.Seaborg, Revs.Mod.Phys., 25, 469 (1953). (Cited in Russian trans., M, 1956.)

2. C.H.Pruett & R.G.Wilkinson, Phys.Rev., 96, 1340 (1956).

3. B.H.Ketelle, H.Thomas & A.R.Brosi, Phys.Rev., 103, 190 (1956).

4. M.A.Listengarten, Izv.AN SSSR, Ser.fiz., 22, 759 (1958). (Trans.Bulletin, 22, No.7, 755.)

5. L.A.Sliv & I.M.Band, Tablitsy KVK γ-izlucheniia, Ch.1. K-obolochka (Tables of internal conversion coefficients. Part 1. K-shell), M.-L, 1956.

6. G.F.Dranitsyna, Koeffitsienty vnutrennei konversii na L_I, L_{II}, L_{III}-podobolochkakh (L_I, L_{II} & L_{III} subshell conversion coefficients), M.-L., 1957.

7. A.R.Brosi & B.H.Ketelle, Phys.Rev., 103, 917 (1956).

8. K.E.Weimer, M.L.Pool & J.D.Kurbatov, Phys.Rev., 63, 59 A (1943). [F.Yu and J.D.Kurbatov, Phys.Rev., 74, 34 (1948).]

CONVERSION ELECTRON SPECTRA OF SOME NEUTRON-DEFICIENT Ho AND Er ISOTOPES

- I.S.Dneprovskii & G.M.Kolesov

The conversion spectra of neutron-deficient isotopes of Ho and Er have been studied by a number of investigators.[1-5] Cork[1] and Dzhelepov and his co-workers (Ref.2,3) investigated 30-hour Ho^{161}. Nihelich, Harmatz & Handley[4] studied the spectra of a number of isotopes but only up to about 300 kev. Handley & Olson[5] recorded the γ-radiation from Er^{161} by means of a scintillation spectrometer.

The present work was devoted to an investigation of the conversion spectra of the erbium isotopes that form in the spallation reaction on tantalum bombarded by high energy (660 Mev) protons. The tantalum target was irradiated for 10 min in the internal beam of the Joint Institute for Nuclear Research synchrocyclotron; following irradiation the group of rare earth elements was separated from the target chemically and then these elements were in turn separated in an ion exchange column by the procedure described in Ref.6.

Drops with maximum activity were taken from the erbium extract and evaporated to drive off the ammonium lactate; then the residue, dissolved in one drop of acetic acid (1:5) was applied to an aluminum strip measuring 20 x 1 x 0.005 mm.

The time from irradiation to extraction of the erbium fraction from the exchange column was 2-2.5 hours; the subsequent source preparation time did not exceed 30 min.

The absence of the characteristic lines of thulium, which was studied in detail under similar experimental conditions by Gromov et al[7], gave reason to assume that the purity of the source was satisfactory.

The measurements were carried out on a $\pi\sqrt{2}$ focusing angle β-spectrometer designed and constructed at the "Fizpribor" Plant. The radius of the central electron trajectory was 22.5 cm. The relative half-width of the Cs^{137} (661.6 kev γ-ray) conversion line with a solid angle of ~0.6% of 4π was 0.4% for a 1 mm wide source. The vacuum in the spectrometer chamber was maintained at $5 \cdot 10^{-5}$ mm Hg.

The magnetic field was measured by means of magnetometer operating on the principle of interaction between a light coil suspended on a horizontal axis and the measured magnetic field. Use of the magnetometer made the measurements independent of the magnetic state of the magnet iron and insured the operative conditions necessary for the investigation of isotopes with a half-life of several hours; the sensitivity of the magnetometer was 0.02% of the magnetic field intensity per scale division. The spectrometer was calibrated with reference to the standard conversion lines of ThB, Au^{198} and Cs^{137}. The high energy electrons were detected by an end-window counter with a mica window having a transmission threshold of ~30 kev. In investigating the soft region of the spectra we used a cylindrical GM counter with a collodion window having a transmission threshold of ~5 kev.

Analyzing the recorded spectra, we can distinguish four groups of lines with periods of ~30, 3.5, 2.5 and 1 hours.

$T_{1/2} \approx 30$ hours

The experimental data on the ~30 hour lines (Table 1) are in satisfactory agreement with the results of Dzhelepov and his co-workers[2,3], in view of which they can be safely attributed to transitions following the decay of Ho^{160}, a daughter of Er^{160}.

It was not our purpose to investigate the spectrum of this isotope since it was thoroughly investigated by the Dzhelepov group[2,3]; it may be noted, however, that despite the brief irradiation of the tantalum, the spectrum was clearly evinced and we could readily identify the lines. Thus we observed the lines

Table 1

Experimental results for the conversion lines of Ho^{160}

Electron energy, kev	Identification	E_γ, kev	Relative intensity
50,6±0,2	L_{I+II}-59	59,5	—
51,2±0,2	L_{III}-59	59,1	—
57,0±0,2	M-59	—	—
78,0±0,2	L_{I+II}-87	86,8	1100±100
78,9±0,2	L_{III}-87	86,7	
85,1±0,2	M-87	87,1	—
85,9±0,3	N-87	—	—
142,9±0,2	K-196	196,7	100
188,4±0,6	L-196	—	—
195,4±0,5	M-196	—	—
591,8±0,8	K-646	645,6	5,1±0,2
635,5±1,0	L-646	—	—
674,3±1,0	K-728	728,1	6,9±0,3
714,7±3,0	L-728	—	—

Table 2

Experimental results for the conversion lines of Er^{161}

Electron energy, kev	Identification	E_γ, kev	Relative intensity
57,8±0,2	$L_I + L_{II}$-67	67,0	250±50
58,8±0,2	L_{III}-67	66,9	
64,8±0,2	M-67	—	90±10
155,2±0,3	K-210	210,8	100
201,7±0,6	L-210	—	130±13
209,1±0,6	M-210	—	50±5
210,0±0,6	N-210	210,4	14±1
770,9±0,8	K-826	826,5	20±3
818,0±1,0	L-826	—	4±0,5
824,5±1,0	M-826	—	~0,5

Table 3

$(L_I - L_{II})/L_{III}$ ratio for the 67.0 kev transition

Experimental	Theoretical					
	$E1$	$E2$	$E3$	$M1$	$M2$	$M3$
1,2±0,5	4,00	1,25	0,85	80,00	4,15	0,70

associated with the most intense transitions of 87, 196, 646 and 728 kev. The 108 kev transition was not specially investigated and in our experiments the lines associated with it were not clearly evinced owing to the masking effect of intense lines from shorter-lived isotopes.

$T_{1/2} \approx 3.5$ hours

An erbium isotope decaying with this period was discovered by Handley & Olson[5] who in their scintillation spectrometer measurements observed γ-rays having energies of 195, 824 and 1120 kev; they also note the possible existence of γ-rays of about 65 kev energy. Mitchel & Templeton[8] determined the mass number of this isotope from the flight time in a mass spectrometer; it equals 161. It may be assumed that the lines falling off with this period in our spectrum may pertain to transitions following the decay of Er^{161} and its daughter Ho^{161}.

Analyzing our data, we can distinguish a group of lines (Fig.1 & Table 2) associated with transitions occurring in a nucleus with Z = 67, as follows from a comparison of the theoretical and experimental data on the differences K - M, K - L and L_{III} - M.

From the data of Table 3 we can establish the presence of the transitions in Ho^{161} with energies of 67.0 ± 0.1, 210 ± 0.2 and 826.5 ± ± 0.5 kev. As a result of resolution of the total L peak of the 67.0 kev transition, we determined the ratio of intensities of the L_I - L_{II} and L_{III} lines. The approximate value is 1.2 (probable uncertainty ±0.5). Comparison of this value with the theoretical ratio (Table 3) indicates that the most probable assignment for this transition is E2, although one cannot fully exclude the possibility of E2 + M3 or M2 + E3.

The 210.6 kev transition is of particular interest. It follows from the data of Table 4 that this transition is E3. The difference between the experimental and theoretical values of K/L (0.75 and 0.95, respectively) may be due to inaccuracy of the theoretical value. Evidence in favor of this assignment is the

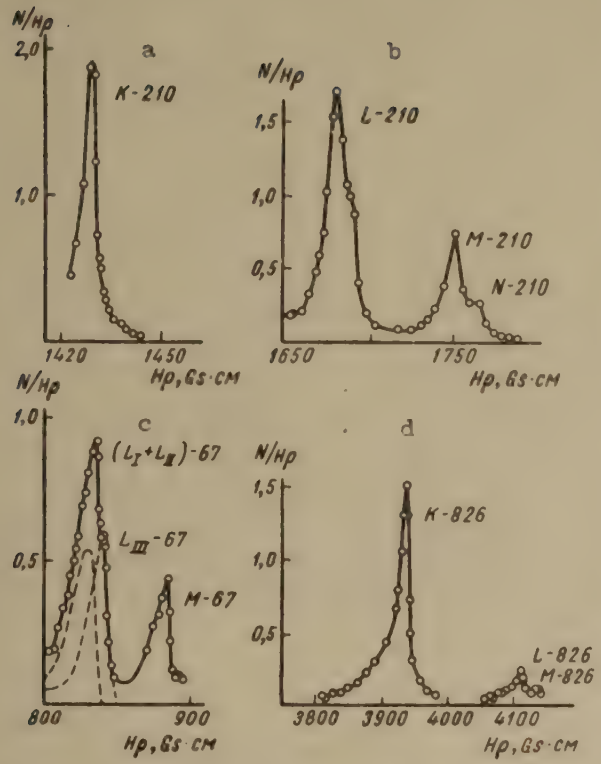

Fig.1. Conversion lines of Er^{161}: a) K line of 210.6 kev transition, b) L and M lines of 210.6 kev transition, c) conversion lines of 67.0 kev transition, d) conversion lines of 826.5 kev transition.

Table 4

K/L and $(L_I - L_{II})/L_{III}$ ratios for the 210.6 kev transition

Ratios	Experimental	Theoretical									
		E1	E2	E3	E4	E5	M1	M2	M3	M4	M5
K/L	0,75	6,7	2,6	0,95	0,27	0,15	6,4	4,5	2,6	1,2	0,3
$(L_I+L_{II})/L_{III}$	1,7	8,0	2,4	2,2	3,0	0,041	110	12	3,3	0,33	0,048

Table 5

Experimental results for the conversion lines of Ho^{161}

Electron energy, kev	Identification	E_γ, kev	Relative intensity
66,6±0,3	L-71	75,4	200±30
68,2±0,2	L-77	77,0	100±20
121,5±0,2	K-175	175,2	100

excellent agreement of our K/L ratio for the 210.6 kev transition with the experimental values of K/L found by Gromov et al[7] and Mihelich et al[4] for the 208 kev transition in Er^{167} for which the assignment is E3. Gromov et al give $K/L \approx 0.71$; Mihelich et al ~0.75. The experimental value of $(L_I + L_{II})/L_{III}$ determined by Mihelich et al[4] for the 208 kev transition in Er^{167} is 1.5 which is also in agreement with our value of 1.7 for the 210.6 kev transition. Thus it may safely be asserted that Ho^{161} has an isomeric E3 transition with an energy of 210.6 kev. As follows from the work of Mottelson & Nilsson[9], the ground state of Ho^{161} must have the same spin as that of Ho^{165} inasmuch as both nuclei have an even number of neutrons and 67 protons. In this case the sequence of levels in deformed nuclei given by Mottelson & Nilsson serves to explain the existence of the Ho^{161} isomer. This isomeric transition is apparently a transition between levels with spins 1/2+ and 7/2-.

On the basis of the data in the literature[1,4], and the results of our measurements, it may be assumed that the lines listed in Table 5 are associated with transitions following the decay of Ho^{161} in equilibrium with Er^{161}. Owing to the overlapping of the lines, we were not able to make an accurate evaluation of their intensities.

We also observed three fairly clear lines at 62.0, 62.9 and 164.2 kev. The first two can be identified as the L and M lines of a 71 kev transition, but it is difficult to decide in what nucleus this transition occurs.

So far we have not been able to identify the 164.2 kev line.

$T_{1/2} \approx 2.5$ hours

We identified the group of lines listed in Table 6 and shown in Fig.2 as lines associated with a 98.6 kev transition. The value deduced from the decay curve in Fig.3 equals 2.4 ± 0.1 hours.

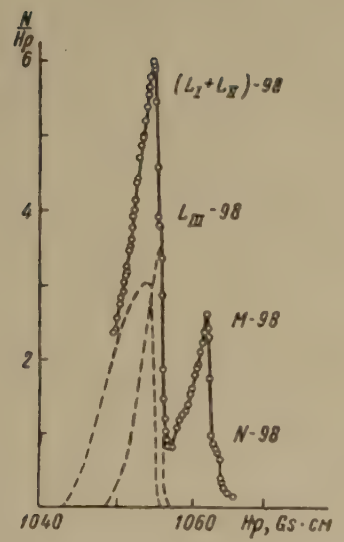

Fig.2. Conversion lines associated with the 98.6 kev transition.

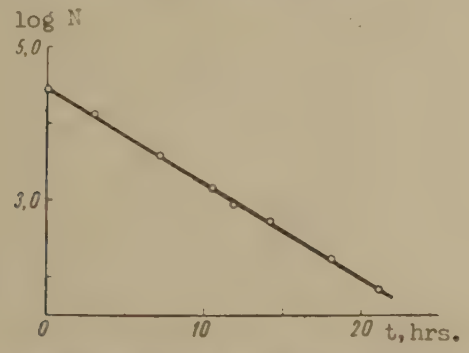

Fig.3. Decay curve for the conversion lines of the 98.6 kev transition.

Table 6

Experimental results for the conversion lines with a period of 2.5 hours

Electron energy, kev	Identification	E_γ, kev	Transition energy, kev
44,9±0,1	*K*-98	98,7	
89,8±0,1	L_{I+II}-98	98,6	
90,8±0,1	*L*-98	98,6	98,6
96,7±0,1	*M*-98	—	
98,2±0,1	*N*-98	98,6	

Table 7

$(L_I + L_{II})/L_{III}$ ratio for the 98.6 kev transition

Experimental	Theoretical					
	E1	*E2*	*E3*	*M1*	*M2*	*M3*
1,87	4,3	1,3	1,7	105	6,1	1,15

From a comparison of the experimental and theoretical differences K - L_{III}, K - M and K - N, it may be inferred that the 98.6 kev transition occurs in a nucleus with Z = 66 (Dy). From a comparison of the experimental and theoretical values of $(L_I + L_{II})/L_{III}$ (Table 7), it would appear probable that this transition is E3, although the E2 + M1 assignment cannot be ruled out.

Ho^{161} is known to have a half-life of 2.5 hours. One cannot, however, attribute the 98.6 kev transition to this isotope inasmuch as under our experimental conditions there should have been in this case a period of 3.5 hours (Er^{161}). We believe it preferable to hypothesize the existence of an Er isotope with a half-life of 2.5 hours.

$T_{1/2} \approx 1$ hour

We observed a number of lines falling off in intensity with a period of about 1 hour. It must be noted, however, that it is difficult to investigate such lines on a spectrometer of the type employed. We were able to establish only the existence of the three lines shown in Fig.4 (data in Table 8) with reasonable reliability.

We associate these lines with a 138 kev transition; a transition of this energy was identified by Mihelich et al[4] as a transition following the decay of Ho^{156}. It may be inferred, therefore, that the above mentioned lines owe their origin to this isotope.

From the value of $(L_I - L_{II})/L_{III}$ for the 138 kev transition, found by resolution of the L peak, it may be inferred that the assignment for this transition is E2 (Table 9). This, too, is assignment given by Mihelich et al.

Table 8

Experimental results for the conversion lines with a period of ~1 hour.

Electron energy, kev	Identification	Relative intensity	E_γ, kev
119,6±0,4	—	~100	
129,5±0,3	L_{I+II}-138	100	138,2
130,3±0,4	L_{III}-138		
135,9±0,4	M-138	~20	

Table 9

$(L_I + L_{II})/L_{III}$ ratio for the 138 kev transition

Experimental	Theoretical					
	E1	E2	E3	M1	M2	M3
1,5	13,5	1,55	1,86	105	7,8	2,0

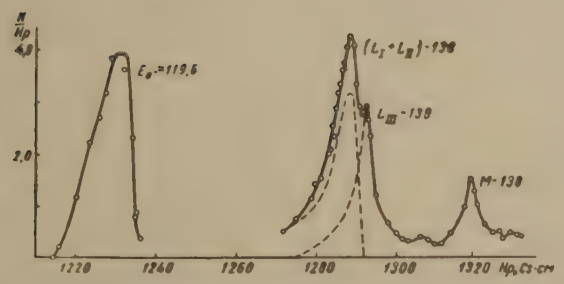

Fig.4. Conversion lines with a period of ~1 hour.

We desire to express our gratitude to K.Ia.Gromov for advice and assistance in the work and A.V.Kaliamin for assuring the chemical separation of the rare earth isotopes.

"V.I.Vernadskii" Institute of Geochemistry and Analytic Chemistry
Academy of Sciences of the USSR

References

1. J.M.Cork, Bull.Amer.Phys. Soc., 2, 297 (1956).
2. B.S.Dzhelepov, B.K.Preobrazhenskii, I.M.Rogachev & P.A. Tishkin, Izv.AN SSSR, Ser.fiz., 21, 962 (1957). (Trans.Bulletin 21, No.7, 964).
3. E.P.Grigor'ev, B.S.Dzhelepov, A.V.Zolotavin, O.E.Kraft, B. Kratsik & L.K.Peker, Report presented at the Eighth All-Union Conference on Nuclear Spectroscopy, 1958.
4. J.W.Mihelich, B.Harmatz & T.H. Handley, Phys.Rev., 108, 989 (1957).
5. T.H.Handley & E.L.Olson, Phys. Rev., 93, 524 (1954).
6. B.K.Preobrazhenskii, O.M.Lilova, A.N.Dobronravova & E.D.Teterin, Zhur. neorgan. khimii (Journ. Inorganic Chem.) 1, 2294 (1956).
7. K.Ia.Gromov, B.S.Dzhelepov & B.K. Preobrazhenskii, Izv.AN SSSR, Ser.fiz., 21, 918 (1957). (Trans.Bulletin 21, No.7, 920.)
8. M.C.Mitchel & D.H.Templeton, Phys.Rev., 93, 1442 (1954).
9. B.Mottelson & S.Nilsson, in Probl.sovrem.fiz (Problems of modern physics), collection of translations and review articles, 1, 186 (1956).

RADIATION FROM Eu^{155}

- M.P.Gazunov & B.F.Gulev

Introduction

Investigation of the β- and γ-spectra of Eu^{155} is both of theoretical and practical interest. This odd-even nucleus lies in the transition region between spherical and deformed nuclei, hence study of its γ-transitions and determination of their multipole orders and relative intensities may be useful from the standpoint of developing and testing nuclear models.

The relatively low energy of the γ-radiation and comparatively long half-life of Eu^{155} make it a useful source of soft γ-rays in materiology and medicine. The period of Eu^{155} is 1.7 years; it converts by β-decay to Gd^{155}. The results of previous investigations[1-7] of Eu^{155} radiation are conflicting.

In our work we used Eu^{155} separated from the fission fragments of uranium. The initial concentrate was prepared six and a half years ago. For preparation of the source, the material was carefully purified to free it of radioactive and stable impurities.

1. Investigation of the β-spectrum of Eu^{155}

The β-spectrum and conversion electron spectrum of Eu^{155} were studied on a combined β-γ spectrometer[8]. The resolution of the instrument with a source and slit width of 0.8 mm and height of 2 cm is 0.7%. The sources were deposited on 2 μ thick aluminum foils. The window of the counter chamber was covered with a collodion film having a thickness of ~40 $\mu g/cm^2$. The instrument was calibrated with reference to the standard lines of Cs^{137}, Co^{60} and Zn^{65}. In the low energy region we tied in our calibration with the well resolved 87 kev γ-line of Eu^{155}.

Table 1

β-radiation from Eu^{155}

$E_{e.p.}$, kev	Relative intensity, %	log ft	Refs.
140±5 185±5 245±5	58 39 3	7.1 7.7 8.8	Our data
150 250	— —	6.8 8.1	Ref.1
152 252	84 16	6.8 8.2	Ref.4
150±10 240±10	77 23	7.9 8.2	Ref.5
150 240	21 79	— —	Ref.6

The spectrum of Eu^{155} was recorded several times over a period of 8 months. Plotting the continuous spectrum in Fermi-Kurie coordinates brought out five partial β-spectra (see figure). We attributed the spectra with end-point energies of 140 ± 5, 185 ± 5 and 245 ± 5 kev and intensities of 58, 39 and 4%, respectively, to Eu^{155}. The spectra with end-point energies of 340 ± 5 and 800 ± 20 kev and intensities of 5 and 7%, respectively, belong to Eu^{154} which was present as an impurity in our source material.

The end-point energies of two of the partial spectra of Eu^{155} are in good agreement with the data of other authors. The component with end-point energy 185 ± 5 kev had not been previously detected. The distribution of intensities of the partial spectra, however, does not agree with the data of other investigators. Our results are compared with those of other authors in Table 1.

It may be inferred from the log ft values and the shape of the β-spectra that the continuous β-spectra of Eu^{155} are once forbidden. The log ft values were calculated according to Moszkowski[9].

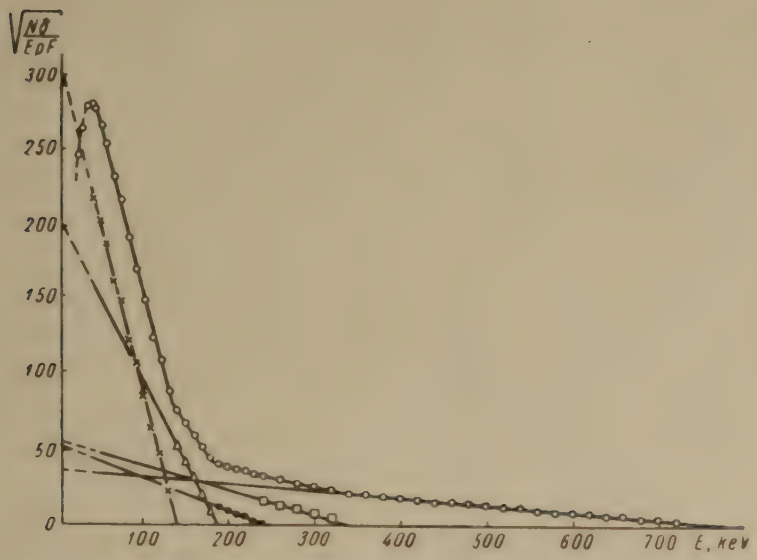

Fermi-Kurie plot of the continuous β-spectrum of Eu^{155}

2. Conversion electron spectrum and γ-spectrum of Eu^{155}

On the basis of repeated investigations of the conversion spectrum of Eu^{155} we were able to establish with good reliability the existence of 63 lines, 8 of which were attributed to Eu^{154} and Eu^{152} impurities and 5 were identified as being due to Auger electrons. Through identification of the conversion lines we inferred the existence of γ-transitions with the following energies (uncertainties here and below ± 0.5): 15, 18, 26, 31.6, 45.6, 61, 87, 100, 102, 106, 118, 125, 132 and 137 kev. We assigned these γ-transitions to Eu^{155}. Lines with energies of 42, 122 and 123 kev were attributed to the γ-radiation of Eu^{154} + Eu^{152}. The above-mentioned five Auger electron lines have energies of 31.5, 32.5, 33.2, 33.7 and 35 kev. The inferred 15, 18, 61, 87, 100, 102, 106, 132 and 137 kev transition energies are in good agreement with the data in the literature; the 26.7, 31.6 and 45.6 kev transition energy values agree with the data of Ward, Jacob & Mihelich[10]. These authors investigated the excited levels of Gd^{155} in positron decay of Tb^{155}.

We succeeded in measuring the areas under the K and L lines associated with some of the γ-transitions. The experimental values of K/L are in good agreement with the corresponding theoretical values given in the tables of Sliv & Band[11] and Dranitsyna[12]. Our results for the γ-radiation from Eu^{155} are summarized in Table 2.

To verify the presence of hard γ-rays of low intensity, which were not evinced in the β-γ spectrometer measurements, the activity was investigated on a scintillation spectrometer with a 50-channel analyzer[13] kindly made available by Iu.A.Surkov. These measurements led to detection of γ-rays having the following energies (the uncertainties here are ± 10): 240, 420, 580, 670, 870, 1000 and 1280 kev.

We attributed all these γ-transitions to the Eu^{154} and Eu^{152} impurities present in the source employed. Judging from the intensity of the Eu^{152} γ-lines (420, 580 and 670 kev), the principal impurity in our source was Eu^{154}. This is substantiated by the β-decay data.

In concluding we must emphasize the difficulty of identifying the β- and γ-radiations from Eu^{155} in view of the virtual impossibility of separating this isotope from radioactive Eu^{154} and Eu^{152} which have complicated β- and γ-spectra. The latest investigations[14,15] of the radiation from Eu^{154} and Eu^{152} are also conflicting and do not give a complete picture of their spectra.

We desire to thank N.E.Brezhnev, V.I.Levin, G.V.Korpusov and N.N.Motorin for making available the radioactive material and supplementary purification thereof and V.A.Ivanov for assistance in the work.

Data on the γ-radiation of Eu^{155} Table 2

No.	E_{e^-}, kev	Identification	E_γ, kev	Relative intensity	K/L ratio		Multipole order
					exper.	theo.	
1	6,6	L_I	15				
2	9,6	L_I	18				
3	10,9	K	61	34	0,7	0,8	$E3$
4	13,2	M_I	15	65			
5	13,5	$M_{II} + M_{III}$	15				
6	16,2	M_I	18				
7	18,4	L_I	26,7				
8	19,3	$L_{II} + L_{III}$	26,7				
9	23,2	L_I	31,6				
10	24,7	L_{II}	31,6				
11	24,9	M_I	26,7				
12	26,4	N_I	26,7				
13	29,5	M_I	31,6				
14	31	N_I	31,6				
15	37	K	87	100	10,4	9	$E1$
16	37,3	L_I	45,6				
17	38,4	$L_{II} + L_{III}$	45,6				
18	43,9	M_I	45,6				
19	44,1	$M_I + M_{II}$	45,6				
20	45,3	N_I	45,6				
21	49,7	K	100	42	7,3		
22	52	K	102,3				
23	52,6	L_I	61	46			
24	53	$L_{II} + L_{III}$	61				
25	55,8	K	106	38	3,3	3,3	$E1$
26	58,2	M_I	61				
27	58,8	M_{II}	61				
28	74,8	K	125	23	3	3,3; 2,5	$E1, M1$
29	78,7	L_I	87	9,6			
30	79,5	$L_I + L_{II}$	87	7,6			
31	68	K	118				
32	80,7	K	132	7,6	4	3,7	$E2$
33	85,7	M_I	87	3,8			
34	86,6	K	137				
35	92	L_I	100	4,6			
36	93,8	$L_{II} + L_{III}$	100	3,8			
37	94,3	L_I	102,3				
38	97,6	L_I	106	11,5			
39	98,8	$L_{II} + L_{III}$	106	8,4			
40	104,1	M_I	106	3			
41	104,5	$M_{II} + M_{III}$	106				
42	105,6	N_I	106				
43	109,2	L_I	118	3			
44	116,6	L_I	125	7,6			
45	123,3	L_I	132	1,9			
46	124,4	$L_{II} + L_{III}$	132				
47	127,6	L_I	137				
48	128,7	$L_{II} + L_{III}$	137				
49	130,1	M_I	132				
50	131,6	N_I	132				

References

1. W.C.Rutledge, J.M.Cork & S.B.Burson, Phys.Rev., 86, 775 (1952).
2. H.W.Wilson & G.M.Lewis, Proc.Phys.Soc., 65A, 656 (1952).
3. M.R.Lee & R.Katz, Phys.Rev., 93, 155 (1954).
4. E.L.Church & M.Goldhaber, Phys.Rev., 95, 626 (1954).
5. V.S.Dubey, C.E.Mandeville & M.A.Rothman, Phys.Rev., 103, 1430 (1956).
6. V.S.Dubey, C.E.Mandeville & M.A.Rothman, Bull.Amer. Phys.Soc., 1, 4, 164 (1956).
7. F.Boehm & E.N.Hatch, Bull.Amer.Phys.Soc., Ser.II, 2, 231 (1957).
8. M.P.Glazunov & V.I.Spitsyn, Izv.AN SSSR, Ser.fiz., 20, 1423 (1956). (Trans.Bulletin 20, No.12a, 1302.)
9. S.Moszkowski, Revs.Mod.Phys., 25, 2, 473 (1953).
10. R.J.Ward, K.P.Jacob & J.W.Mihelich, Bull.Amer.Phys.Soc., Ser.II, 2, 259 (1957).
11. L.A.Sliv & I.M.Band, Tablitsy koeffitsientov vnutrennei konversii γ-izlucheniia (Tables of internal conversion coefficients) Part 1, M.-L, 1956.
12. G.V.Dranitsyna, Koeffitsienty vnutrennei konversii na L_I, L_{II}, L_{III} -podobolochkakh (L_I, L_{II} and L_{III} subshell conversion coefficients), M.-L., 1957.
13. Iu.A.Surkov, Dissertation, GEOKhI AN SSSR, 1958.
14. J.Cork, M.Brice, R.Helmer & D.Sarason, Phys.Rev., 107, 1621 (1957).
15. J.Juliano & F.Stephens, Phys.Rev., 108, 341 (1957).

COINCIDENCES OF CONVERSION ELECTRONS IN $Eu^{147} \rightarrow Sm^{147}$ DECAY

- B.S.Dzhelepov, B.K.Preobrazhenskii & V.A.Sergienko

Coincidences between the conversion electrons forming in the decay of ~25-day Eu^{147} to Sm^{147} were studied by means of a twin magnetic lens β-spectrometer[1]. The Eu^{147} was obtained through bombardment of a tantalum target with 660 Mev protons. The neutron-deficient europium isotopes were separated chromatographically from the rare-earth fraction, which was previously separated chemically from the irradiated tantalum. The active material was collected on a thin lightly aluminized collodion film; the diameter of the source was 5 mm. The coincidence measurements were started several days after the separation, when the shorter-lived activities of Eu had virtually died out.

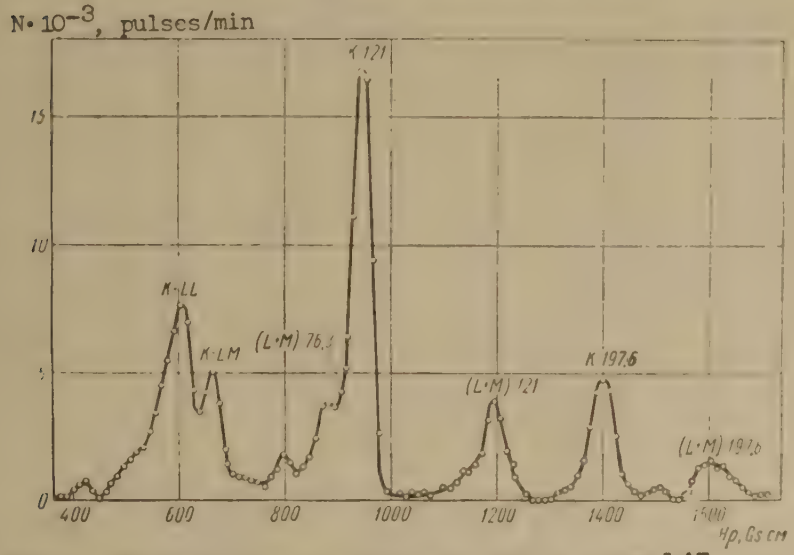

Fig.1. Conversion electron spectrum of Eu^{147} recorded on one half the twin β-spectrometer.

The existence of γ-transitions with energies of 121.0 and 197.6 kev in the decay of Eu^{147} to Sm^{147} has been firmly established (Ref.2-4). An 80 kev transition was initially reported by Gorodinskii et al[3] but was not detected in later experiments[4] by the same investigators. Conversion lines associated with a 76.3 kev transition were observed in the work of Ref.2. Coincidences between the 121.0 and 197.6 kev γ-rays were not observed, but there were detected coincidences between the γ-rays of these transitions and x-rays[4].

The conversion electron spectrum up to 200 kev as recorded by a single (half the twin) spectrometer viewing the activity side of the source is shown in Fig.1. The number of conversion lines, their location in the spectrum and their relative intensities agree with the data of Ref.2. In view of the inadequate resolution of our spectrometers the K and (L + M) lines of the 76.3 kev

Data on electron coincidences in $Eu^{147} \rightarrow Sm^{147}$

Line detected by first spectrometer (thru backing)	Counting rate at peak, $(N_1 - N_{bkgd}) \cdot 10^{-3}$, counts/min	Line detected by second spectrometer	Counting rate at peak, $(N_2 - N_{bkgd}) \cdot 10^{-3}$, counts/min	Coincidences per hour		
				Obs.	Chance	True
	19	K-197,6	6	5	4	1
K-121+ +(L+M)-76,3	21	K-121 + (L + M)-76,3	7,5	74	8	66
		(K — LL) + K-76,3	8,5	189	10	179
		K — LM	4,5	76	8	68
L + M)-121	4,5	(K — LL) + K-76,3	9	22	2	20
		K — LM	6	9	1	8
(L+M)-197,6	1,5	(K — LL) + K-76,3	9	7	1,5	5,5
		K — LM	6	5	1,5	3,5

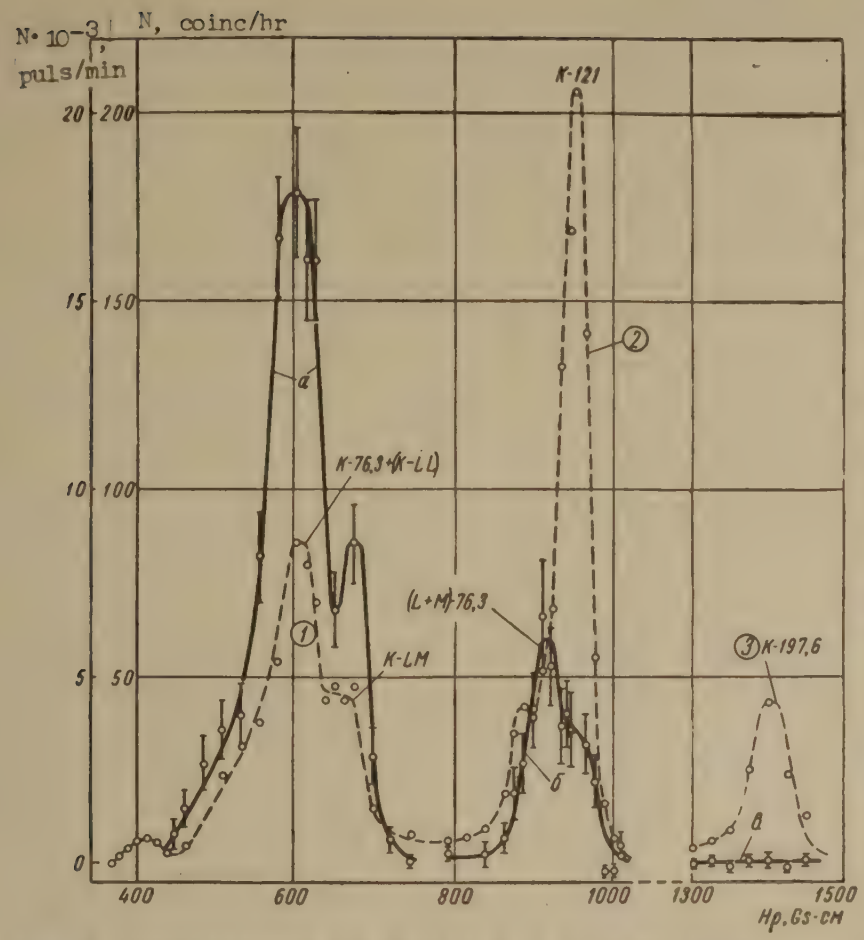

Fig.2. Coincidences of (K-121.0 + (L + M)-76.3) electrons with a) K Auger and K-76.3 electrons, b) (L + M)-76.3 electrons, and c) K-197.6 electrons. Curves 1,2 & 3 - the (K - LL) + K-76.3, K - LM, K-121.0 + (L + M)-76.3 and K-197.6 lines as recorded on a single spectrometer.

transition were not evinced in our measurements; the K line merged with the K - LL Auger electron line and the (L + M) line with the K-121.0 line.

We investigated coincidences between K-121.0 and K-197.6 electrons and (L + M)-121.0 and (L + M)--197.6 electrons with K Auger electrons and also coincidences of K-121.0 electrons "through the backing" for the purpose of detecting the (L + M) line associated with the 76.3 kev transition. In addition, we recorded coincidences between the K-121.0 electrons and the K Auger electrons.

The number of true coincidences varied from 3.5 to 179 per minute with counting rates in the channels from $1.5 \cdot 10^3$ to $21 \cdot 10^3$ pulses/min; the ratio of true to chance coincidences varied from 2 to 18. Experimental results are summarized in the accompanying table and illustrated in Figs.2 & 3.

1. Coincidences between the 76.3 and 121.0 kev transitions

The existence of coincidences between these transitions is clearly evident from the table and the experimental coincidence curve in Fig.2 (curve b). The number of coincidences in both halves of the spectrometer set to detect K-121.0 + + (L + M)-76.3 electrons amounted to 74 per hour; of these, 8 were chance and 66 true. The existence of an appreciable number of (K-121.0) - [(L + M)-76.3] coincidences made it possible to separate the (L - M)-76.3 line and thereby reliably establish the existence of this (76.3 kev) transition in the $Eu^{147} \rightarrow Sm^{147}$ decay scheme.

2. Coincidences between the 197.6 & 121.0 kev and 197.6 & 76.3 kev transitions

There can be no doubt regarding the absence of coincidences between the 197.6 & 121.0 kev and 197.6 & 76.3 kev transitions. This is evident from the table and the experimental curve shown in Fig.2 (curve c). Thus it may be inferred that the 197.6 kev transition is not in cascade with either the 76.3 or the 121.0 kev transition.

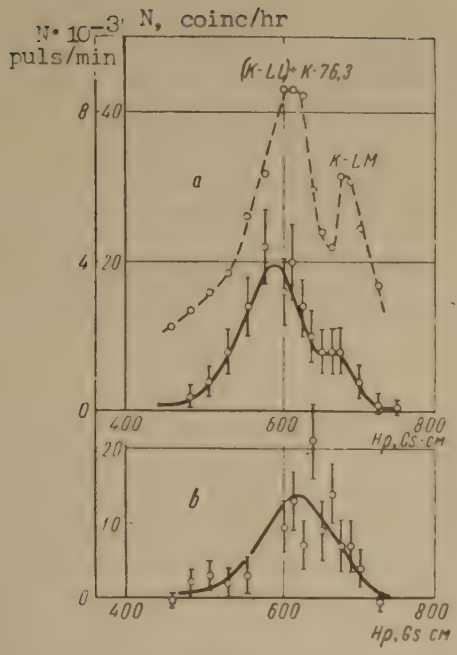

Fig.3. a) Solid curve - [(L + M)-121.0]-[K-76.3 + (K - LL) + (K - LM)] coincidences; b) [(L + M)-197.6]-[(K - LL) + K-76.3 + (K - LM)] coincidences. Upper dash line curve - (K - LL) + K-76.3 and K - LM lines recorded on a single spectrometer.

3. Coincidences between the 121.0 and 197.6 kev transitions and K Auger electrons

Coincidences between (L + M) electrons from the γ-transitions and the K Auger electrons may be taken as evidence of the existence of K capture to excited levels, transitions from which in the product nucleus occur with the emission of the given γ-rays; the coincidence rate is then indicative of the K capture intensity. The experimental [(L + M)-121]-[(K - LL) + K-76.3 + (K - LM)] and [(L + M)-197.6)]-[(K - LL) + (K-76.3) + (K - LM)] coincidence curves are shown in Fig.3.

Inasmuch as the K-76.3 line was not resolved in our experiments from the K - LL line and the (L + M)-121 electrons may give coincidences with the K-76.3 electrons, it is not feasible to determine the number of (K - LL)-[(L + M)-121] coincidences. One can judge of the existence of coincidences of K Auger electrons with (L + M)-121 electrons from the presence of (K - LM)-[(L + M)-121] coincidences; the K - LL and K - LM lines were almost resolved. The number of [(L + M)-121]-(K - LM) coincidences was 8 per hour. We are certain that these coincidences actually do occur; hence K capture goes to the excited level of Sm^{147} from which the 121 kev γ-transition departs.

There should be no (K-76.3)-[(L + M)-197.6] coincidences. Consequently, all the recorded [(L + M)-197.6]-[(K - LL) + K-76.3 + (K - LK)] coincidences must be due to coincidences of (L + M)-197.6 electrons with K Auger electrons. The number of these coincidences were small, namely, 3-3.5 coincidences per hour. We assume that the K capture in the Eu^{147} nucleus goes to the 197.6 kev level.

4. Coincidences between K-121 conversion electrons and K Auger electrons

The experimental [K-121 + (L + M)-76.3]-[(K - LL) + K-76.3 + (K - LM)] coincidence curve is shown in Fig.2 (curve a). Inasmuch as the K-76.3 line was not resolved from the K - LL line and the K-121 electrons must yield coincidences with the K-76.3 electrons and since the contribution from (K-121)-(K-76.3) and [(L + M)-76.3]-(K - LL) coincidences is difficult to evaluate, we can only judge of coincidences between K-121 and K Auger electrons from coincidences of the K-121 electrons with electrons of the (K - LM)-121 line which was almost resolved from the K - LL line. But to do this we must allow for the (K - LM)-[(L + M)-76.3] coincidences. If we assume that the probabilities of coincidence of K Auger electrons formed in K capture with the K and (L + M) electrons from the 76.3 and 121 kev transitions are equal and are determined only by the numbers of these electrons, then of all the [K-121 + (L + M)-76.3]-(K - LM) coincidences, namely, 68 coinc/hr, approximately 66 coinc/hr may be attributed to (K-121)-(K - LM). It should also be borne in mind that these coincidences are due to K Auger electrons forming both as a result of conversion on the K shell and in

K capture to the 121 kev level. Invoking the fact that the K/(L + M) ratio for the 121-kev transition is about 4.5, we obtain 36 coinc/hr for the number of coincidences of K-121 electrons with the K - LM electrons forming in K capture and about 30 coinc/hr for the number of coincidences of K-121 electrons with the K - - LM electrons forming after conversion on the K shell.

Our data are in agreement with the decay scheme for Eu^{147} given in a preceding article[5] (Fig.8 on p.908).

We thank A.A.Bashilov for his interest in the work and valuable discussions. V.Bunakov and Iu.Zvol'skii participated in the measurements.

Scientific Research Physical Institute
Leningrad State University

References

1. V.A.Sergienko, Izv.AN SSSR, Ser.fiz., 22, 198 (1958). (Trans.Bulletin 22, No.2, 195).

2. N.M.Anton'eva, A.A.Bashilov, B.S.Dzhelepov & B.K.Preobrazhenskii, Abstracts of reports presented at the Seventh All-Union Conference on Nuclear Spectroscopy M.-L., 1956.

3. G.M.Gorodinskii, A.N.Murin, V.N.Pokrovskii & B.K.Preobrazhenskii, Doklady AN SSSR, 112, 405 (1957).

4. G.M.Gorodinskii, A.N.Murin, V.N.Pokrovskii & B.K.Preobrazhenskii, Izv. AN SSSR, Ser.fiz., 21, 1624 (1957). (Trans.Bulletin 21, No.12, 1611.)

5. N.M.Anton'eva, A.A.Bashilov, B.S.Dzhelepov & B.K.Preobrazhenskii, Izv. AN SSSR, Present issue of the Bulletin, p.899.

COINCIDENCES OF CONVERSION ELECTRONS IN $Tm^{167} \rightarrow Er^{167}$ DECAY

- B.S.Dzhelepov, B.K.Preobrazhenskii & V.A.Sergienko

We investigated the coincidences between the conversion transitions occurring in the decay of ~9.6-day Tm^{167} to Er^{167} by means of a twin magnetic-lens β-spectrometer[1]. The Tm^{167} was obtained with bombardment of a tantalum target with 660 Mev protons. The neutron-deficient thulium isotopes were separated from the rare earth fraction in an ion exchange column.

The active material was deposited on a thin lightly aluminized collodion film; the diameter of the source was 5 mm. The coincidence measurements were started several days after separation, when the short-lived Tm isotopes had decayed.

The $Tm^{167} \rightarrow Er^{167}$ process is accompanied by γ-transitions of 56.9 and 208.1 kev (average values from the results of Refs.2 and 4). The conversion electron spectrum of Tm^{167} up to about 200 kev recorded on a single (half the twin) spectrometer is shown in Fig.1. It agrees as regards location of the lines and their relative intensities with the spectrum given in Ref.2.

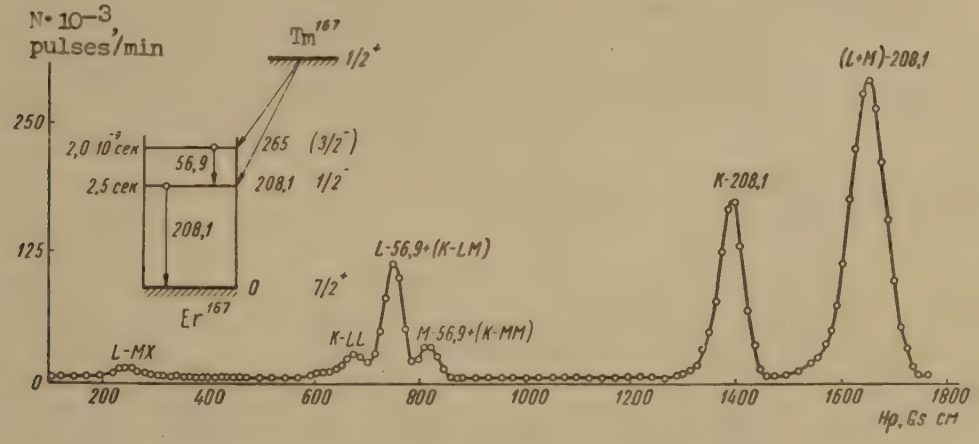

Fig.1. Conversion electron spectrum of Tm^{167}; insert - $Tm^{167} \rightarrow Er^{167}$ decay scheme.

Data on electron coincidences in $Tm^{167} \rightarrow Er^{167}$

Line detected by first spectrometer (thru backing)	Counting rate at peak, $(N_1 - N_{bkgd}) \cdot 10^{-3}$, counts/min	Line detected by second spectrometer	Counting rate at peak, $(N_2 - N_{bkgd}) \cdot 10^{-3}$, counts/min	Coincidences per hour*		
				Obs.	Chance	True
$(L+M)$-208,1	190	$K-LL$	21	104	98	(6)
		L-56,9 + $(K-LM)$	70	590	570	(20)
		M-56,9 + $(K-MM)$	35	288	300	(−12)
L-56,9 + $(K-LM)$	96	$K-LL$	15	208	30	178
		L-56,9 + $(K-LM)$	72	302	112	190
		M-56,9 + $(K-MM)$	25	112	64	44
K-208,1	256	$K-LL$	77	2040	492	1548
		L-56,9 + $(K-LM)$	220	2150	1344	806
		M-56,9 + $(K-MM)$	73	525	90	435

*The values in parentheses are of the same order of magnitude as the experimental uncertainty.

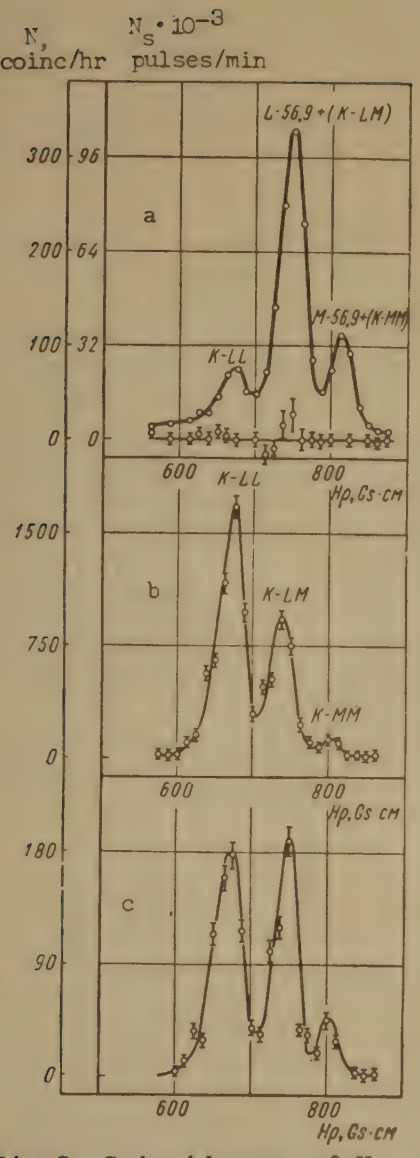

Fig.2. Coincidences of K Auger electrons with conversion electrons: a - (L + M)-208.1, b - K-208.1 and c - L-56.9. The upper curve in a represents the K - LL, L-56.9 + (K - LM) and M-56.9 + (K - MM) lines recorded on a single spectrometer.

We investigated the coincidences between the conversion electrons from the 56.9 and 208.1 kev transitions and also between these electrons and the K Auger electrons. The experimental results are summarized in the accompanying table and illustrated in Fig.2.

1. Coincidences between the 208.1 and 56.9 kev transitions

As was shown in Refs.5 & 6 and substantiated in the investigations of Refs.7 & 8, the lifetime of the 208.1 kev excited state in Er^{167} is 2.5 sec. Hence there should not be coincidences between the conversion electrons of the 208.1 and 56.9 kev transitions or between the (L + M)-208.1 conversion electrons and the K series Auger electrons. The absence of coincidences between the (L + M)-208.1 line and the K Auger and L-56.9 lines is evident from the tabular data and Fig.2 (curve a). Thus our data substantiate the metastable nature of the 208.1 kev level in Er^{167}.

2. Coincidences of K-208.1 electrons with K Auger electrons

There were observed coincidences between the K-208.1 conversion electrons and the K Auger electrons forming after conversion on the K shell. The experimental (K-208.1)-[(K - LL) + (K - LM)] coincidence curve is shown in Fig.2 (curve b). The counting rated for coincidences of K-208.1 electrons with different groups of Auger electrons should be proportional to the probabilities of the Auger effect on different atomic shells. The ratio of the number of (K - LL) electrons to the number of all other K Auger electrons as evaluated from the areas under the K - LL, K - LM and K - MM lines equals 1.6, which agrees within the limits of the experimental error with the corresponding data of Refs.9, 10 & 11 for Z = 57 to 84.

3. Coincidences of L-56.9 electrons with K Auger electrons

That there occur coincidences between the L-56.9 conversion electrons and K Auger electrons will be evident from the table and Fig.2 (curve c).

The number of "self-coincidences" of the [L-56.9 + (K - LM)] line electrons and the number of [L-56.9 + (K - LM)] —(K - LL) coincidences were, respectively, 302 and 208 per hour; of these, according to our evaluation, the respective numbers of chance coincidences were 112 and 30 and of true coincidences 190 and 178. Thus there can be no doubt that there occur coincidences between the L-56.9 electrons and K Auger electrons. The large number of "self-coincidences" of the

[L-56.9 + (K - LM)] line electrons is connected with the fact that in recording the line formed by two groups of electrons of close energy simultaneously in both halves of the spectrometer, the observed number of coincidences is always twice the number of coincidences that would be observed if these two groups of electrons were completely resolved. Taking into account this doubling of the number of "self-coincidences" we find that the ratio of the (L-56.9)-(K - LL) and (L-56.9)--(K - LM) coincidence rates is approximately 1.9. This is consistent with the results of our experiments on coincidences between K-208.1 and K Auger electrons and the data of Refs.9, 10 & 11 on the probability of production of different groups of K Auger electrons. Further, it follows from our experiments that the probability of formation of different groups of K Auger electrons in K capture and conversion are equal and are given approximately by (K - LL): [(K - LM) + + (K - MM)] = 1:0.6.

Inasmuch as K series Auger electrons cannot appear after conversion on the L shell, the observed coincidences indicate that the 56.9 kev transition promptly follows the K capture.[12] These coincidences also substantiate the inference that the 56.9 kev transition occurs in Er^{167} and is not an isomeric transition in Tm^{167}.

The decay scheme for Tm^{167}, proposed in Refs.2 & 3, is shown in Fig.1. The results of our present experiments tend to substantiate this scheme.

We wish to express our gratitude to K.Ia.Gromov for valuable suggestions in discussing the results. Leningrad State University students V.Bunakov and L. Popeko participated in the measurements.

Scientific Research Physical Institute,
Leningrad State University

References

1. V.Sergienko, Izv.AN SSSR, Ser.fiz., 22, 198 (1958). (Trans.Bulletin 22, No.2, 195.)

2. B.Dzhelepov, K.Gromov & B.Preobrazhenskii, Izv.AN SSSR, Ser.fiz., 21, 918 (1957). (Trans.Bulletin 21, No.7, 920.)

3. G.Gorodinskii, A.Murin, V.Pokrovskii & B.Preobrazhenskii, Izv.AN SSSR, Ser.fiz., 21, 1004 (1957). (Trans.Bulletin 21, No.7, 1005.)

4. J.W.Mihelich, B.Harmatz & Handley, Phys.Rev., 108, 989 (1957).

5. E.Campbell, J.Kahn & M.Goodrich, Nucl.Sci., 10, 256 (1956).

6. M.G.Steward, A.M.Bureau & C.L.Hammer, Bul.Amer.Phys.Soc., 1, 206, 4(R2) (1956); Nucl.Sci., 10, 256 (1956).

7. C.L.Hammer & M.G.Steward, Phys.Rev., 106, 1001 (1957).

8. J.W.Mihelich, Phys.Rev., 106, 1232 (1957).

9. K.Gromov, B.Dzhelepov, A.Dmitriev & B.Preobrazhenskii, Izv.AN SSSR, Ser. fiz., 22, 153 (1958). (Trans.Bulletin 22, No.2, 151.)

10. A.Zhernovoi, E.Krisiuk, G.Latyshev, A.Remennyi, A.Sergeev & V.Fadeev, Zhur.eksp.i teor.fiz., 32, 682 (1957). (Trans. Soviet Phys. - JETP.)

11. M.Mladjenovic & H.Slätis, Arkiv.Fys., 9, 41 (1955).

12. E.E.Berlovich, K.M.Grotovskii, M.P.Bonits, V.I.Breslav & B.K.Preobrazhenskii, Izv.AN SSSR, Ser.fiz., 21, 1643 (1957). (Trans.Bulletin 21, No.12, 1629.)

TABLES OF FUNCTIONS NEEDED FOR DETERMINING THE PROBABILITY OF ALLOWED AND FORBIDDEN L CAPTURE

- I.M.Band, L.N.Zyrianova & Iu.P.Suslov

The purpose of the work was to calculate the functions employed in the theory of nuclear transitions by L capture. Analysis of the electron capture branch is necessary in investigating all cases of positron radioactivity. Orbital electron capture is the only decay mode in a considerable number of nuclei. The interest in electron capture has been heightened in recent years in connection with intensive investigations of neutron-deficient isotopes. Tables of the "numerical values of the K electron functions determining the probability of allowed and forbidden K capture" were published in 1956.[1] For L capture, which is also of interest in experimental investigation of decay schemes, there are numerical calculations in the literature only for a few Z; this obviously hampers practical computations.

For calculating the probabilities of transitions by L capture one must know a number of coefficients depend on the L electron wave functions. Below we have tabulated these coefficients, taking into account the effect of screening and finite nuclear size.

1. L electron wave functions

The L_I, L_{II} and L_{III} electron wave functions used in this work were found by the method of numerical integration of the Dirac potential equation taking into account the presence of orbital electrons and finite nuclear size. The atomic potential inside the nuclear volume was taken for a uniform electric charge distribution over a volume of radius $R = 1.20 \cdot A^{1/3} \cdot 10^{-13}$ cm; the field outside the nucleus was assumed to be that of a Thomas-Fermi-Dirac statistical atom. In determining the screening functions, we used the tables of Metropolis & Reitz[2] and Thomas[3], while the exchange interaction was taken into account in the form used by Reitz[4].

The values of the L_I electron wave functions at the nuclear boundary for a number of values of Z, calculated in this manner, are listed in Table 1. In addition to G_{L_I} and F_{L_I}, the large and small components of the radial wave func-

Table 1

Values of the L_I electron wave functions at the nuclear boundary

Z	$U_0 - \sqrt{2R}$	$G_{L_I} R$	$F_{L_I} R$	E_{L_I}
18	0,1500	$3,4457 \cdot 10^{-4}$	$-1,8144 \cdot 10^{-5}$	−0,00064666
25	0,1540	$6,0923 \cdot 10^{-4}$	$-4,4635 \cdot 10^{-5}$	−0,0014979
33	0,16050	$1,1239 \cdot 10^{-3}$	$-1,0899 \cdot 10^{-4}$	−0,0030785
41	0,16777	$1,9093 \cdot 10^{-3}$	$-2,3086 \cdot 10^{-4}$	−0,0053577
49	0,17378	$3,0297 \cdot 10^{-3}$	$-4,3971 \cdot 10^{-4}$	−0,0084177
57	0,17940	$4,6365 \cdot 10^{-3}$	$-7,8676 \cdot 10^{-4}$	−0,012356
61	0,18110	$5,6281 \cdot 10^{-3}$	$-1,0249 \cdot 10^{-3}$	−0,014691
65	0,18352	$6,8544 \cdot 10^{-3}$	$-1,3342 \cdot 10^{-3}$	−0,01 295
73	0,18747	0,010014	$-2,2039 \cdot 10^{-3}$	−0,023382
81	0,19131	0,014550	$-3,5802 \cdot 10^{-3}$	−0,030825
84	0,19280	0,016740	$-4,2847 \cdot 10^{-3}$	−0,034017
88	0,19457	0,020144	$-5,4250 \cdot 10^{-3}$	−0,037722
92	0,19623	0,024257	$-6,8607 \cdot 10^{-3}$	−0,042668
95	0,19746	0,027885	$-8,1727 \cdot 10^{-3}$	−0,047993
98	0,19864	0,031956	$-9,6973 \cdot 10^{-3}$	−0,050841

Table 2

Values of the L_{II} and L_{III} electron wave functions at the nuclear boundary

Z	$G_{L_{II}} R$	$F_{L_{II}} R$	$G_{L_{III}} R$	$F_{L_{III}} R$
18	$1{,}0050 \cdot 10^{-6}$	$1{,}6704 \cdot 10^{-5}$	$1{,}2109 \cdot 10^{-7}$	$-3{,}6388 \cdot 10^{-9}$
25	$3{,}4710 \cdot 10^{-6}$	$4{,}2749 \cdot 10^{-5}$	$3{,}1612 \cdot 10^{-7}$	$-1{,}3203 \cdot 10^{-8}$
33	$1{,}1460 \cdot 10^{-5}$	$1{,}0851 \cdot 10^{-4}$	—	—
41	$3{,}0771 \cdot 10^{-5}$	$2{,}3601 \cdot 10^{-4}$	$1{,}8854 \cdot 10^{-6}$	$-1{,}2945 \cdot 10^{-7}$
49	$7{,}1356 \cdot 10^{-5}$	$4{,}5946 \cdot 10^{-4}$	$3{,}7034 \cdot 10^{-6}$	$-3{,}0439 \cdot 10^{-7}$
57	$1{,}5141 \cdot 10^{-4}$	$8{,}3842 \cdot 10^{-4}$	$6{,}6860 \cdot 10^{-6}$	$-6{,}4050 \cdot 10^{-7}$
61	$2{,}1312 \cdot 10^{-4}$	$1{,}1028 \cdot 10^{-3}$	$8{,}6022 \cdot 10^{-6}$	$-8{,}8283 \cdot 10^{-7}$
65	$2{,}9896 \cdot 10^{-4}$	$1{,}4504 \cdot 10^{-3}$	$1{,}1125 \cdot 10^{-5}$	$-1{,}2180 \cdot 10^{-6}$
73	$5{,}6811 \cdot 10^{-4}$	$2{,}4475 \cdot 10^{-3}$	$1{,}7791 \cdot 10^{-5}$	$-2{,}1931 \cdot 10^{-6}$
81	$1{,}0534 \cdot 10^{-3}$	$4{,}0724 \cdot 10^{-3}$	$2{,}7630 \cdot 10^{-5}$	$-3{,}7899 \cdot 10^{-6}$
84	$1{,}3232 \cdot 10^{-3}$	$4{,}9224 \cdot 10^{-3}$	$3{,}2430 \cdot 10^{-5}$	$-4{,}6184 \cdot 10^{-6}$
88	$1{,}7862 \cdot 10^{-3}$	$6{,}3244 \cdot 10^{-3}$	$3{,}9829 \cdot 10^{-5}$	$-5{,}9515 \cdot 10^{-6}$
92	$2{,}4057 \cdot 10^{-3}$	$8{,}1211 \cdot 10^{-3}$	$4{,}8598 \cdot 10^{-5}$	$-7{,}6048 \cdot 10^{-6}$
95	$3{,}0064 \cdot 10^{-3}$	$9{,}8028 \cdot 10^{-3}$	$5{,}6307 \cdot 10^{-5}$	$-9{,}1103 \cdot 10^{-6}$
98	$3{,}7961 \cdot 10^{-3}$	0,011965	$6{,}5543 \cdot 10^{-5}$	$-1{,}0954 \cdot 10^{-5}$

tions of the $2s$ state, we give E_{L_I}, the theoretical value of the L_I electron binding energy, and the parameter $U_0 = \sqrt{2R}$. Table 2 gives the corresponding values for the L_{II} and L_{III} electrons (for the same U_0).

The data of Table 1 for small Z can be compared with the wave function values calculated by the Hartree-Fock method[5]. At Z = 30, the G_{L_I} evaluated for the statistical atom and by the self consistent field procedure diverge up to 19%. At Z = 18 the difference is 16%. Inasmuch as in the range of small Z one should give preference to the Hartree-Fock method, for Z = 18 we used the following self-consistent field wave functions:

$$G_K^2 = 8{,}61 \cdot 10^{-3} \quad \text{and} \quad G_{L_I}^2 = 6{,}94 \cdot 10^{-4}.$$

II. Allowed L capture

In the usual notation of β-decay theory the probability for allowed L capture is given by

$$W_{L_i} = \frac{g^2}{2\pi^3} M^2 f_{L_i}(E_0, Z), \tag{1}$$

where g is the Fermi β-interaction constant, M^2 is the nuclear matrix element and f_{L_i} is a function depending on the characteristics of the captured electron.

Allowed capture is possible from the L_I and L_{II} subshells and is defined by the functions

$$f_{L_I}(E_0, Z) = \frac{\pi}{2}(E_0 + E_{L_I})^2 G_{L_I}^2, \tag{2}$$

$$f_{L_{II}}(E_0, Z) = \frac{\pi}{2}(E_0 + E_{L_{II}})^2 F_{L_{II}}^2, \tag{3}$$

respectively, where E_0 is the nuclear transition energy (total end-point energy of the positron spectrum) in units of m_0c^2, E_{L_i} is the total energy of the L_i electron in the same units and Z is the atomic number of the decaying nucleus.

The radial wave functions G_{L_I} and $F_{L_{II}}$ should be taken at the point of transformation of the nucleon. As usual, we took the values at the nuclear boundary (radius). In view of the fact that the energies of the L_I and L_{II} electrons are virtually equal, the ratio of their capture probabilities becomes

Table 3

Values of the function f_{L_1}

Z	E_0				
	−0,90	−0,80	−0,70	−0,60	−0,50
18	$1{,}078\cdot10^{-5}$	$4{,}336\cdot10^{-5}$	$9{,}775\cdot10^{-5}$	$1{,}739\cdot10^{-4}$	$2{,}719\cdot10^{-4}$
19	$1{,}366\cdot10^{-5}$	$5{,}502\cdot10^{-5}$	$1{,}241\cdot10^{-4}$	$2{,}208\cdot10^{-4}$	$3{,}453\cdot10^{-4}$
20	$1{,}694\cdot10^{-5}$	$6{,}830\cdot10^{-5}$	$1{,}541\cdot10^{-4}$	$2{,}743\cdot10^{-4}$	$4{,}289\cdot10^{-4}$
21	$2{,}063\cdot10^{-5}$	$8{,}329\cdot10^{-5}$	$1{,}880\cdot10^{-4}$	$3{,}347\cdot10^{-4}$	$5{,}234\cdot10^{-4}$
22	$2{,}478\cdot10^{-5}$	$1{,}002\cdot10^{-4}$	$2{,}261\cdot10^{-4}$	$4{,}027\cdot10^{-4}$	$6{,}298\cdot10^{-4}$
23	$2{,}940\cdot10^{-5}$	$1{,}190\cdot10^{-4}$	$2{,}688\cdot10^{-4}$	$4{,}789\cdot10^{-4}$	$7{,}492\cdot10^{-4}$
24	$3{,}454\cdot10^{-5}$	$1{,}400\cdot10^{-4}$	$3{,}164\cdot10^{-4}$	$5{,}638\cdot10^{-4}$	$8{,}822\cdot10^{-4}$
25	$4{,}024\cdot10^{-5}$	$1{,}634\cdot10^{-4}$	$3{,}695\cdot10^{-4}$	$6{,}585\cdot10^{-4}$	$1{,}030\cdot10^{-3}$
26	$4{,}648\cdot10^{-5}$	$1{,}891\cdot10^{-4}$	$4{,}278\cdot10^{-4}$	$7{,}626\cdot10^{-4}$	$1{,}194\cdot10^{-3}$
27	$5{,}341\cdot10^{-5}$	$2{,}176\cdot10^{-4}$	$4{,}926\cdot10^{-4}$	$8{,}785\cdot10^{-4}$	$1{,}375\cdot10^{-3}$
28	$6{,}107\cdot10^{-5}$	$2{,}493\cdot10^{-4}$	$5{,}646\cdot10^{-4}$	$1{,}007\cdot10^{-3}$	$1{,}577\cdot10^{-3}$
29	$6{,}955\cdot10^{-5}$	$2{,}844\cdot10^{-4}$	$6{,}444\cdot10^{-4}$	$1{,}150\cdot10^{-3}$	$1{,}798\cdot10^{-3}$
30	$7{,}884\cdot10^{-5}$	$3{,}230\cdot10^{-4}$	$7{,}326\cdot10^{-4}$	$1{,}307\cdot10^{-3}$	$2{,}048\cdot10^{-3}$
31	$8{,}908\cdot10^{-5}$	$3{,}657\cdot10^{-4}$	$8{,}299\cdot10^{-4}$	$1{,}482\cdot10^{-3}$	$2{,}321\cdot10^{-3}$
32	$1{,}002\cdot10^{-4}$	$4{,}125\cdot10^{-4}$	$9{,}369\cdot10^{-4}$	$1{,}673\cdot10^{-3}$	$2{,}622\cdot10^{-3}$
33	$1{,}126\cdot10^{-4}$	$4{,}642\cdot10^{-4}$	$1{,}055\cdot10^{-3}$	$1{,}885\cdot10^{-3}$	$2{,}954\cdot10^{-3}$
34	$1{,}261\cdot10^{-4}$	$5{,}215\cdot10^{-4}$	$1{,}186\cdot10^{-3}$	$2{,}120\cdot10^{-3}$	$3{,}324\cdot10^{-3}$
35	$1{,}408\cdot10^{-4}$	$5{,}839\cdot10^{-4}$	$1{,}329\cdot10^{-3}$	$2{,}377\cdot10^{-3}$	$3{,}728\cdot10^{-3}$
36	$1{,}568\cdot10^{-4}$	$6{,}520\cdot10^{-4}$	$1{,}486\cdot10^{-3}$	$2{,}659\cdot10^{-3}$	$4{,}170\cdot10^{-3}$
37	$1{,}742\cdot10^{-4}$	$7{,}263\cdot10^{-4}$	$1{,}657\cdot10^{-3}$	$2{,}966\cdot10^{-3}$	$4{,}653\cdot10^{-3}$
38	$1{,}930\cdot10^{-4}$	$8{,}073\cdot10^{-4}$	$1{,}845\cdot10^{-3}$	$3{,}301\cdot10^{-3}$	$5{,}181\cdot10^{-3}$
39	$2{,}134\cdot10^{-4}$	$8{,}956\cdot10^{-4}$	$2{,}047\cdot10^{-3}$	$3{,}668\cdot10^{-3}$	$5{,}758\cdot10^{-3}$
40	$2{,}353\cdot10^{-4}$	$9{,}912\cdot10^{-4}$	$2{,}268\cdot10^{-3}$	$4{,}067\cdot10^{-3}$	$6{,}386\cdot10^{-3}$
41	$2{,}592\cdot10^{-4}$	$1{,}096\cdot10^{-3}$	$2{,}510\cdot10^{-3}$	$4{,}503\cdot10^{-3}$	$7{,}074\cdot10^{-3}$
42	$2{,}854\cdot10^{-4}$	$1{,}211\cdot10^{-3}$	$2{,}778\cdot10^{-3}$	$4{,}986\cdot10^{-3}$	$7{,}836\cdot10^{-3}$
43	$3{,}138\cdot10^{-4}$	$1{,}336\cdot10^{-3}$	$3{,}068\cdot10^{-3}$	$5{,}511\cdot10^{-3}$	$8{,}663\cdot10^{-3}$
44	$3{,}386\cdot10^{-4}$	$1{,}470\cdot10^{-3}$	$3{,}380\cdot10^{-3}$	$6{,}074\cdot10^{-3}$	$9{,}552\cdot10^{-3}$
45	$3{,}767\cdot10^{-4}$	$1{,}616\cdot10^{-3}$	$3{,}720\cdot10^{-3}$	$6{,}688\cdot10^{-3}$	0,01052
46	$4{,}112\cdot10^{-4}$	$1{,}773\cdot10^{-3}$	$4{,}087\cdot10^{-3}$	$7{,}353\cdot10^{-3}$	0,01157
47	$4{,}488\cdot10^{-4}$	$1{,}942\cdot10^{-3}$	$4{,}484\cdot10^{-3}$	$8{,}079\cdot10^{-3}$	0,01271
48	$4{,}890\cdot10^{-4}$	$2{,}126\cdot10^{-3}$	$4{,}916\cdot10^{-3}$	$8{,}857\cdot10^{-3}$	0,01395
49	$5{,}318\cdot10^{-4}$	$2{,}324\cdot10^{-3}$	$5{,}381\cdot10^{-3}$	$9{,}703\cdot10^{-3}$	0,01529
50	$5{,}775\cdot10^{-4}$	$2{,}536\cdot10^{-3}$	$5{,}882\cdot10^{-3}$	0,01061	0,01673
51	$6{,}269\cdot10^{-4}$	$2{,}767\cdot10^{-3}$	$6{,}427\cdot10^{-3}$	0,01151	0,01831
52	$6{,}794\cdot10^{-4}$	$3{,}016\cdot10^{-3}$	$7{,}017\cdot10^{-3}$	0,01268	0,02002
53	$7{,}357\cdot10^{-4}$	$3{,}285\cdot10^{-3}$	$7{,}657\cdot10^{-3}$	0,01385	0,02187
54	$7{,}961\cdot10^{-4}$	$3{,}576\cdot10^{-3}$	$8{,}351\cdot10^{-3}$	0,01512	0,02389
55	$8{,}606\cdot10^{-4}$	$3{,}890\cdot10^{-3}$	$9{,}102\cdot10^{-3}$	0,01650	0,02607
56	$9{,}296\cdot10^{-4}$	$4{,}229\cdot10^{-3}$	$9{,}915\cdot10^{-3}$	0,01799	0,02845
57	$1{,}003\cdot10^{-3}$	$4{,}594\cdot10^{-3}$	0,01079	0,01959	0,03100
58	$1{,}082\cdot10^{-3}$	$4{,}991\cdot10^{-3}$	0,01175	0,02136	0,03381
59	$1{,}167\cdot10^{-3}$	$5{,}418\cdot10^{-3}$	0,01278	0,02326	0,03684
60	$1{,}256\cdot10^{-3}$	$5{,}872\cdot10^{-3}$	0,01388	0,02529	0,04009
61	$1{,}350\cdot10^{-3}$	$6{,}361\cdot10^{-3}$	0,01507	0,02748	0,04360
62	$1{,}451\cdot10^{-3}$	$6{,}887\cdot10^{-3}$	0,01636	0,02986	0,04739
63	$1{,}557\cdot10^{-3}$	$7{,}452\cdot10^{-3}$	0,01774	0,03242	0,05149
64	$1{,}670\cdot10^{-3}$	$8{,}057\cdot10^{-3}$	0,01923	0,03518	0,05591
65	$1{,}790\cdot10^{-3}$	$8{,}708\cdot10^{-3}$	0,02083	0,03816	0,06069
66	$1{,}917\cdot10^{-3}$	$9{,}414\cdot10^{-3}$	0,02258	0,04142	0,06592
67	$2{,}054\cdot10^{-3}$	0,01018	0,02447	0,04494	0,07158
68	$2{,}196\cdot10^{-3}$	0,01099	0,02649	0,04872	0,07766
69	$2{,}346\cdot10^{-3}$	0,01185	0,02867	0,05278	0,08421
70	$2{,}509\cdot10^{-3}$	0,01279	0,03102	0,05719	0,09131
71	$2{,}676\cdot10^{-3}$	0,01379	0,03357	0,06193	0,09895
72	$2{,}852\cdot10^{-3}$	0,01486	0,03626	0,06704	0,1072
73	$3{,}036\cdot10^{-3}$	0,01601	0,03918	0,07255	0,1161
74	$3{,}233\cdot10^{-3}$	0,01725	0,04236	0,07857	0,1259
75	$3{,}438\cdot10^{-3}$	0,01858	0,04578	0,08505	0,1364
76	$3{,}651\cdot10^{-3}$	0,01999	0,04944	0,09200	0,1477
77	$3{,}875\cdot10^{-3}$	0,02150	0,05338	0,09951	0,1599
78	$4{,}108\cdot10^{-3}$	0,02313	0,05762	0,1076	0,1731
79	$4{,}349\cdot10^{-3}$	0,02485	0,06218	0,1163	0,1873
80	$4{,}601\cdot10^{-3}$	0,02671	0,06709	0,1258	0,2027
81	$4{,}864\cdot10^{-3}$	0,02868	0,07236	0,1359	0,2195
82	$5{,}129\cdot10^{-3}$	0,03080	0,07805	0,1469	0,2373

Table 3 (continued)

	E_0				
/	−0,90	−0,80	−0,70	−0,60	−0,50
83	$5,410 \cdot 10^{-3}$	0,03397	0,08418	0,1587	0,2568
84	$5,696 \cdot 10^{-3}$	0,03548	0,09074	0,1715	0,2777
85	$5,988 \cdot 10^{-3}$	0,03804	0,09778	0,1852	0,3003
86	$6,290 \cdot 10^{-3}$	0,04079	0,1054	0,2001	0,3248
87	$6,601 \cdot 10^{-3}$	0,04374	0,1136	0,2162	0,3515
88	$6,918 \cdot 10^{-3}$	0,04689	0,1224	0,2336	0,3803
89	$7,236 \cdot 10^{-3}$	0,05024	0,1319	0,2523	0,4113
90	$7,565 \cdot 10^{-3}$	0,05384	0,1422	0,2726	0,4452
91	$7,892 \cdot 10^{-3}$	0,05768	0,1533	0,2948	0,4819
92	$8,224 \cdot 10^{-3}$	0,06180	0,1652	0,3186	0,5217
93	$8,550 \cdot 10^{-3}$	0,06616	0,1780	0,3442	0,56 7
94	$8,871 \cdot 10^{-3}$	0,07079	0,1918	0,3719	0,6110
95	$9,176 \cdot 10^{-3}$	0,07566	0,2064	0,4014	0,6607
96	$9,465 \cdot 10^{-3}$	0,08078	0,2220	0,4330	0,7140
97	$9,728 \cdot 10^{-3}$	0,08612	0,2384	0,4666	0,7708
98	$9,964 \cdot 10^{-3}$	0,09170	0,2558	0,5024	0,8314

Table 3 (continued)

	E_0				
	−0,30	−0,20	−0,10	−0,00	
18	$3,917 \cdot 10^{-4}$	$5,334 \cdot 10^{-4}$	$6,967 \cdot 10^{-4}$	$8,820 \cdot 10^{-4}$	$1,089 \cdot 10^{-3}$
19	$4,974 \cdot 10^{-4}$	$6,772 \cdot 10^{-4}$	$8,848 \cdot 10^{-4}$	$1,120 \cdot 10^{-3}$	$1,383 \cdot 10^{-3}$
	$6,179 \cdot 10^{-4}$	$8,413 \cdot 10^{-4}$	$1,099 \cdot 10^{-3}$	$1,391 \cdot 10^{-3}$	$1,718 \cdot 10^{-3}$
1	$7,542 \cdot 10^{-4}$	$1,027 \cdot 10^{-3}$	$1,342 \cdot 10^{-3}$	$1,698 \cdot 10^{-3}$	$2,097 \cdot 10^{-3}$
	$9,076 \cdot 10^{-4}$	$1,236 \cdot 10^{-3}$	$1,615 \cdot 10^{-3}$	$2,044 \cdot 10^{-3}$	$2,525 \cdot 10^{-3}$
	$1,08 \cdot 10^{-3}$	$1,47 \cdot 10^{-3}$	$1,921 \cdot 10^{-3}$	$2,43 \cdot 10^{-3}$	$3,00 \cdot 10^{-3}$
	$1,271 \cdot 10^{-3}$	$1,73 \cdot 10^{-3}$	$2,263 \cdot 10^{-3}$	$2,865 \cdot 10^{-3}$	$3,54 \cdot 10^{-3}$
	$1,48 \cdot 10^{-3}$	$2,0 \cdot 10^{-3}$	$2,644 \cdot 10^{-3}$	$3,34 \cdot 10^{-3}$	$4,14 \cdot 10^{-3}$
	$1,721 \cdot 10^{-3}$	$2,33 \cdot 10^{-3}$	$3,08 \cdot 10^{-3}$	$3,879 \cdot 10^{-3}$	$4,790 \cdot 10^{-3}$
	$1,983 \cdot 10^{-3}$	$2,69 \cdot 10^{-3}$	$3,539 \cdot 10^{-3}$	$4,470 \cdot 10^{-3}$	$5,51 \cdot 10^{-3}$
	$2,28 \cdot 10^{-3}$	$3,08 \cdot 10^{-3}$	$4,049 \cdot 10^{-3}$	$5,127 \cdot 10^{-3}$	$6,31 \cdot 10^{-3}$
	$2,596 \cdot 10^{-3}$	$3,51 \cdot 10^{-3}$	$4,624 \cdot 10^{-3}$	$5,856 \cdot 10^{-3}$	$7,21 \cdot 10^{-3}$
	$2,94 \cdot 10^{-3}$	$3,98 \cdot 10^{-3}$	$5,261 \cdot 10^{-3}$	$6,67 \cdot 10^{-3}$	$8,22 \cdot 10^{-3}$
	$3,348 \cdot 10^{-3}$	$4,54 \cdot 10^{-3}$	$5,964 \cdot 10^{-3}$	$7,57 \cdot 10^{-3}$	$9,33 \cdot 10^{-3}$
	$3,80 \cdot 10^{-3}$	$5,16 \cdot 10^{-3}$	$6,77 \cdot 10^{-3}$	$8,58 \cdot 10^{-3}$	$1,06 \cdot 10^{-2}$
	$4,263 \cdot 10^{-3}$	$5,81 \cdot 10^{-3}$	$7,59 \cdot 10^{-3}$	$9,63 \cdot 10^{-3}$	$1,19 \cdot 10^{-2}$
	$4,78 \cdot 10^{-3}$	$6,52 \cdot 10^{-3}$	$8,51 \cdot 10^{-3}$	$1,08 \cdot 10^{-2}$	$1,33 \cdot 10^{-2}$
	$5,381 \cdot 10^{-3}$	$7,34 \cdot 10^{-3}$	$9,59 \cdot 10^{-3}$	0,01215	0,01495
	$6,020 \cdot 10^{-3}$	$8,209 \cdot 10^{-3}$	0,01074	0,01361	0,01681
	$6,73 \cdot 10^{-3}$	$9,18 \cdot 10^{-3}$	0,01198	0,01518	0,01874
	$7,483 \cdot 10^{-3}$	0,01021	0,01334	0,01691	0,02091
	$8,317 \cdot 10^{-3}$	0,01135	0,01484	0,01881	0,02325
	$9,18 \cdot 10^{-3}$	0,01253	0,01637	0,02078	0,02580
	0,01	0,01384	0,01808	0,02314	0,02860
	0,01133	0,01546	0,02018	0,02565	0,03170
	0,01252	0,01710	0,02238	0,02844	0,03507
	0,01384	0,01886	0,02469	0,03139	0,03870
	0,01522	0,02078	0,02721	0,03450	0,04266
	0,01674	0,02287	0,02994	0,03707	0,04696
	0,018 0	0,02513	0,03290	0,04174	0,05166
	0,0	0,02759	0,03614	0,04585	0,05679
		0,03026	0,03964	0,05028	0,06239
		0,03313	0,04344	0,05508	0,06843
		0,03627	0,04758	0,06031	0,07494
		0,03967	0,05209	0,06599	0,08165
		0,04338	0,05696	0,07217	0,08931
		0,04745	0,06225	0,07889	0,09764
		0,05195	0,06803	0,08619	0,1067
		0,05652	0,07444	0,0945	0,1165
		0,06185	0,08088	0,1027	0,1267

Table 3 (continued)

Z	E_0				
	−0,40	−0,30	−0,20	−0,10	0,00
58	0,04912	0,06728	0,08828	0,1121	0,1388
59	0,05354	0,07335	0,09628	0,1223	0,1515
60	0,05828	0,07987	0,1048	0,1332	0,1650
61	0,06341	0,08692	0,1141	0,1450	0,1797
62	0,06896	0,09455	0,1242	0,1578	0,1955
63	0,07495	0,1028	0,1350	0,1717	0,2127
64	0,08060	0,1117	0,1468	0,1866	0,2313
65	0,08843	0,1214	0,1595	0,2029	0,2514
66	0,09610	0,1320	0,1735	0,2206	0,2735
67	0,1044	0,1434	0,1885	0,2399	0,2974
68	0,1133	0,1557	0,2048	0,2606	0,3231
69	0,1226	0,1690	0,2223	0,2830	0,3509
70	0,1334	0,1834	0,2413	0,3072	0,3810
71	0,1446	0,1989	0,2618	0,3334	0,4136
72	0,1568	0,2158	0,2840	0,3617	0,4488
73	0,1699	0,2339	0,3081	0,3924	0,4870
74	0,1843	0,2538	0,3344	0,4260	0,5288
75	0,1998	0,2752	0,3628	0,4623	0,5740
76	0,2165	0,2984	0,3934	0,5015	0,6227
77	0,2345	0,3234	0,4265	0,5438	0,6755
78	0,2540	0,3504	0,4623	0,5897	0,7326
79	0,2751	0,3797	0,5011	0,6396	0,7944
80	0,2979	0,4114	0,5431	0,6932	0,8615
81	0,3223	0,4457	0,5886	0,7515	0,9342
82	0,3493	0,4829	0,6380	0,8148	1,013
83	0,3782	0,5232	0,6915	0,8834	1,099
84	0,4094	0,5666	0,7493	0,9575	1,191
85	0,4431	0,6136	0,8118	1,038	1,291
86	0,4797	0,6646	0,8797	1,125	1,400
87	0,5195	0,7202	0,9536	1,220	1,519
88	0,5626	0,7804	1,034	1,323	1,648
89	0,6090	0,8454	1,120	1,434	1,787
90	0,6598	0,9165	1,215	1,556	1,939
91	0,7149	0,9937	1,318	1,689	2,105
92	0,7748	1,078	1,430	1,833	2,286
93	0,8394	1,168	1,552	1,989	2,481
94	0,9093	1,268	1,683	2,159	2,693
95	0,9843	1,372	1,824	2,341	2,921
96	1,065	1,486	1,976	2,536	3,168
97	1,151	1,607	2,139	2,746	3,430
98	1,243	1,736	2,313	2,971	3,712

Table 3 (continued)

Z	E_0				
	0,25	0,50	0,75	1,00	1,25
18	$1,702 \cdot 10^{-3}$	$2,451 \cdot 10^{-3}$	$3,336 \cdot 10^{-3}$	$4,358 \cdot 10^{-3}$	$5,516 \cdot 10^{-3}$
19	$2,161 \cdot 10^{-3}$	$3,113 \cdot 10^{-3}$	$4,237 \cdot 10^{-3}$	$5,535 \cdot 10^{-3}$	$7,006 \cdot 10^{-3}$
20	$2,685 \cdot 10^{-3}$	$3,868 \cdot 10^{-3}$	$5,265 \cdot 10^{-3}$	$6,878 \cdot 10^{-3}$	$8,705 \cdot 10^{-3}$
21	$3,278 \cdot 10^{-3}$	$4,722 \cdot 10^{-3}$	$6,428 \cdot 10^{-3}$	$8,397 \cdot 10^{-3}$	0,01063
22	$3,947 \cdot 10^{-3}$	$5,685 \cdot 10^{-3}$	$7,739 \cdot 10^{-3}$	0,01011	0,01280
23	$4,696 \cdot 10^{-3}$	$6,764 \cdot 10^{-3}$	$9,208 \cdot 10^{-3}$	0,01203	0,01523
24	$5,531 \cdot 10^{-3}$	$7,968 \cdot 10^{-3}$	0,01085	0,01417	0,01794
25	$6,463 \cdot 10^{-3}$	$9,310 \cdot 10^{-3}$	0,01268	0,01656	0,02096
26	$7,490 \cdot 10^{-3}$	0,01079	0,01469	0,01919	0,02429
27	$8,633 \cdot 10^{-3}$	0,01244	0,01693	0,02219	0,02800
28	$9,902 \cdot 10^{-3}$	0,01427	0,01943	0,02538	0,03213
29	0,01131	0,01630	0,02219	0,02899	0,03670
30	0,01287	0,01854	0,02525	0,03299	0,04177
31	0,01460	0,02103	0,02864	0,03742	0,04738

Table 3 (continued)

Z	E_0				
	0,25	0,50	0,75	0,00	1,25
32	0,01650	0,02377	0,03238	0,04230	0,05356
33	0,01860	0,02680	0,03650	0,04770	0,06039
34	0,02094	0,03018	0,04110	0,05370	0,06799
35	0,02350	0,03387	0,04613	0,06028	0,07632
36	0,02630	0,03791	0,05164	0,06748	0,08544
37	0,02937	0,04234	0,05767	0,07536	0,09543
38	0,03272	0,04717	0,06426	0,08399	0,1064
39	0,03639	0,05248	0,07148	0,09343	0,1183
40	0,04040	0,05825	0,07936	0,1037	0,1314
41	0,04478	0,06458	0,08798	0,1150	0,1456
42	0,04965	0,07161	0,09757	0,1275	0,1615
43	0,05493	0,07923	0,1080	0,1411	0,1787
44	0,06062	0,08744	0,1192	0,1558	0,1973
45	0,06684	0,09642	0,1314	0,1718	0,2176
46	0,07358	0,1062	0,1447	0,1892	0,2396
47	0,08090	0,1167	0,1591	0,2080	0,2635
48	0,08887	0,1282	0,1748	0,2286	0,2896
49	0,09750	0,1407	0,1918	0,2508	0,3178
50	0,1068	0,1542	0,2102	0,2749	0,3483
51	0,1170	0,1689	0,2303	0,3012	0,3816
52	0,1281	0,1849	0,2521	0,3298	0,4178
53	0,1401	0,2023	0,2759	0,3609	0,4573
54	0,1532	0,2213	0,3018	0,3948	0,5003
55	0,1675	0,2419	0,3299	0,4316	0,5469
56	0,1830	0,2643	0,3605	0,4717	0,5978
57	0,1997	0,2885	0,3936	0,5150	0,6527
58	0,2181	0,3151	0,4300	0,5626	0,7131
59	0,2379	0,3439	0,4693	0,6141	0,7784
60	0,2593	0,3748	0,5115	0,6694	0,8485
61	0,2824	0,4082	0,5572	0,7293	0,9245
62	0,3074	0,4445	0,6067	0,7942	1,007
63	0,3345	0,4838	0,6604	0,8646	1,096
64	0,3638	0,5262	0,7185	0,9407	1,193
65	0,3956	0,5723	0,7815	1,023	1,298
66	0,4305	0,6228	0,8507	1,114	1,413
67	0,4682	0,6775	0,9256	1,212	1,537
68	0,5088	0,7365	1,006	1,318	1,671
69	0,5528	0,8002	1,093	1,432	1,817
70	0,6004	0,8694	1,188	1,556	1,974
71	0,6519	0,9441	1,290	1,690	2,145
72	0,7077	1,025	1,401	1,836	2,330
73	0,7681	1,113	1,522	1,994	2,530
74	0,8343	1,209	1,653	2,167	2,750
75	0,9058	1,313	1,796	2,354	2,987
76	0,9831	1,426	1,950	2,556	3,244
77	1,067	1,547	2,117	2,775	3,523
78	1,158	1,679	2,298	3,013	3,825
79	1,257	1,822	2,494	3,270	4,152
80	1,362	1,977	2,706	3,550	4,507
81	1,478	2,145	2,937	3,853	4,893
82	1,603	2,328	3,188	4,183	5,313
83	1,739	2,527	3,461	4,542	5,769
84	1,887	2,742	3,756	4,929	6,262
85	2,046	2,974	4,075	5,349	6,796
86	2,220	3,227	4,423	5,807	7,379
87	2,409	3,504	4,803	6,307	8,015
88	2,615	3,804	5,216	6,850	8,707
89	2,837	4,129	5,663	7,438	9,456
90	3,080	4,485	6,153	8,083	10,28
91	3,346	4,873	6,687	8,786	11,17
92	3,635	5,296	7,269	9,554	12,15
93	3,949	5,755	7,901	10,39	13,21
94	4,288	6,252	8,586	11,29	14,36
95	4,654	6,788	9,325	12,26	15,60
96	5,048	7,366	10,12	13,31	16,94
97	5,472	7,988	10,98	14,44	18,38
98	5,925	8,654	11,89	15,66	19,93

Table 3 (continued)

Z	E_0				
	1,50	2,00	2,50	3,00	3,50
18	$6{,}810\cdot10^{-3}$	$9{,}808\cdot10^{-3}$	0,01335	0,01744	0,02207
19	$8{,}650\cdot10^{-3}$	0,01246	0,01696	0,02215	0,02803
20	0,01075	0,01548	0,02107	0,02752	0,03483
21	0,01312	0,01890	0,02573	0,03360	0,04253
22	0,01580	0,02275	0,03097	0,04046	0,05121
23	0,01879	0,02708	0,03686	0,04814	0,06094
24	0,02215	0,03190	0,04342	0,05672	0,07179
25	0,02588	0,03728	0,05075	0,06629	0,08390
26	0,03000	0,04321	0,05882	0,07683	0,09725
27	0,03458	0,04981	0,06780	0,08858	0,1121
28	0,03967	0,05714	0,07779	0,1016	0,1286
29	0,04532	0,06528	0,08888	0,1161	0,1470
30	0,05158	0,07430	0,1012	0,1321	0,1672
31	0,05850	0,08427	0,1147	0,1499	0,1897
32	0,06614	0,09528	0,1297	0,1695	0,2145
33	0,07457	0,1074	0,1463	0,1911	0,2419
34	0,08397	0,1210	0,1647	0,2152	0,2724
35	0,09425	0,1358	0,1849	0,2415	0,3058
36	0,1055	0,1520	0,2070	0,2704	0,3424
37	0,1178	0,1698	0,2312	0,3021	0,3824
38	0,1314	0,1892	0,2577	0,3367	0,4262
39	0,1461	0,2105	0,2867	0,3746	0,4742
40	0,1622	0,2338	0,3184	0,4160	0,5266
41	0,1799	0,2592	0,3530	0,4612	0,5839
42	0,1995	0,2875	0,3915	0,5116	0,6477
43	0,2208	0,3182	0,4333	0,5662	0,7169
44	0,2437	0,3512	0,4784	0,6251	0,7919
45	0,2688	0,3874	0,5276	0,6895	0,8733
46	0,2960	0,4266	0,5811	0,7593	0,9618
47	0,3255	0,4692	0,6391	0,8352	1,058
48	0,3577	0,5156	0,7024	0,9180	1,162
49	0,3926	0,5660	0,7710	1,008	1,276
50	0,4303	0,6204	0,8452	1,105	1,399
51	0,4715	0,6798	0,9261	1,210	1,533
52	0,5163	0,7444	1,014	1,326	1,678
53	0,5651	0,8148	1,110	1,451	1,837
54	0,6182	0,8915	1,215	1,588	2,009
55	0,6759	0,9748	1,328	1,736	2,198
56	0,7388	1,065	1,452	1,898	2,404
57	0,8067	1,164	1,586	2,073	2,625
58	0,8814	1,271	1,733	2,265	2,869
59	0,9621	1,388	1,891	2,473	3,132
60	1,049	1,513	2,062	2,696	3,415
61	1,143	1,649	2,248	2,939	3,722
62	1,245	1,796	2,448	3,201	4,055
63	1,355	1,956	2,666	3,486	4,416
64	1,475	2,128	2,901	3,794	4,806
65	1,604	2,316	3,157	4,128	5,230
66	1,747	2,521	3,438	4,496	5,696
67	1,901	2,744	3,741	4,893	6,070
68	2,067	2,984	4,069	5,322	6,586
69	2,247	3,244	4,424	5,787	7,332
70	2,442	3,526	4,809	6,290	7,970
71	2,653	3,831	5,225	6,835	8,661
72	2,882	4,162	5,677	7,426	9,411
73	3,130	4,521	6,167	8,068	10,22
74	3,402	4,915	6,704	8,772	11,12
75	3,696	5,340	7,286	9,532	12,08
76	4,014	5,800	7,914	10,36	13,12
77	4,359	6,300	8,596	11,25	14,06
78	4,733	6,841	9,336	12,22	15,48
79	5,139	7,428	10,14	13,27	16,82
80	5,579	8,066	11,01	14,41	18,27
81	6,057	8,758	11,96	15,65	19,84
82	6,578	9,512	12,99	17,00	21,55
83	7,142	10,33	14,10	18,46	23,41
84	7,754	11,22	15,31	20,05	25,42

Table 3 (continued)

Z	E_e				
	1,50	2,00	2,50	3,00	3,50
85	8,416	12,18	16,63	21,87	27,61
86	9,139	13,22	18,06	23,65	29,99
87	9,928	14,37	19,62	25,70	32,59
88	10,79	15,61	21,32	27,93	35,42
89	11,72	16,96	23,17	30,35	38,49
90	12,73	18,44	25,19	33,00	41,85
91	13,84	20,05	27,40	35,89	45,53
92	15,06	21,81	29,81	39,05	49,54
93	16,37	23,72	32,42	42,48	53,90
94	17,80	25,79	35,26	46,20	58,63
95	19,34	28,03	38,32	51,23	63,73
96	21,01	30,45	41,64	54,57	69,25
97	22,80	33,05	45,20	59,24	75,19
98	24,72	35,84	49,02	64,26	81,57

Table 3 (continued)

Z	E_e				
	4,00	5,00	6,00	8,00	10,00
18	0,02725	0,03924	0,05341	0,08829	0,1319
19	0,03461	0,04984	0,06784	0,1122	0,1675
20	0,04301	0,06193	0,08430	0,1394	0,2082
21	0,05251	0,07562	0,1029	0,1702	0,2542
22	0,06322	0,09105	0,1239	0,2049	0,3061
23	0,07524	0,1084	0,1475	0,2438	0,3642
24	0,08864	0,1276	0,1738	0,2873	0,4291
25	0,1036	0,1492	0,2031	0,3357	0,5016
26	0,1201	0,1729	0,2354	0,3892	0,5814
27	0,1384	0,1994	0,2714	0,4486	0,6702
28	0,1588	0,2287	0,3114	0,5148	0,7690
29	0,1814	0,2613	0,3557	0,5881	0,8786
30	0,2065	0,2974	0,4049	0,6694	1,000
31	0,2342	0,3374	0,4592	0,7593	1,134
32	0,2648	0,3815	0,5193	0,8586	1,283
33	0,2986	0,4301	0,5855	0,9681	1,446
34	0,3363	0,4844	0,6594	1,090	1,629
35	0,3775	0,5438	0,7403	1,224	1,829
36	0,4227	0,6089	0,8289	1,371	2,048
37	0,4722	0,6801	0,9259	1,531	2,287
38	0,5263	0,7581	1,032	1,707	2,550
39	0,5981	0,8846	1,148	1,899	2,837
40	0,6503	0,9367	1,275	2,109	3,151
41	0,7210	1,039	1,414	2,338	3,494
42	0,7998	1,152	1,569	2,594	3,876
43	0,8852	1,275	1,736	2,871	4,290
44	0,9774	1,408	1,9170	3,170	4,737
45	1,078	1,553	2,115	3,497	5,225
46	1,187	1,711	2,329	3,852	5,755
47	1,306	1,882	2,562	4,237	6,332
48	1,435	2,068	2,816	4,657	6,959
49	1,576	2,270	3,091	5,113	7,640
50	1,727	2,489	3,389	5,605	8,377
51	1,893	2,728	3,714	6,143	9,181
52	2,073	2,987	4,068	6,729	10,06
53	2,268	3,270	4,453	7,366	11,01
54	2,483	3,579	4,873	8,061	12,05
55	2,716	3,914	5,330	8,817	13,18
56	2,969	4,279	5,827	9,640	14,41
57	3,243	4,673	6,365	10,53	15,74
58	3,544	5,107	6,956	11,51	17,20
59	3,869	5,576	7,595	12,57	18,78
60	4,213	6,081	8,282	13,70	20,48
61	4,598	6,628	9,028	14,94	22,33
62	5,010	7,221	9,836	16,28	24,33

Table 3 (continued)

Z	E_0				
	4,00	5,00	6,00	8,00	10,00
63	5,455	7,864	10,71	17,72	26,50
64	5,938	8,560	11,66	19,30	28,84
65	6,462	9,315	12,69	21,00	31,39
66	7,037	10,15	13,82	22,87	34,19
67	7,659	11,04	15,04	24,90	37,22
68	8,332	12,01	16,37	27,09	40,50
69	9,059	13,06	17,80	29,46	44,04
70	9,848	14,20	19,35	32,02	47,88
71	10,70	15,43	21,03	34,81	52,04
72	11,63	16,77	22,85	37,83	56,56
73	12,64	18,22	24,83	41,11	61,46
74	13,74	19,82	27,00	44,70	66,84
75	14,93	21,54	29,35	48,59	72,66
76	16,22	23,40	31,89	52,80	78,95
77	17,62	25,42	34,64	57,37	85,78
78	19,14	27,61	37,63	62,32	93,19
79	20,79	29,99	40,88	67,70	101,2
80	22,58	32,58	44,40	73,54	110,0
81	24,52	35,39	48,24	79,89	119,5
82	26,64	38,45	52,41	86,80	129,8
83	28,94	41,77	56,94	94,31	141,1
84	31,43	45,37	61,85	102,4	153,2
85	34,14	49,27	67,17	111,3	166,5
86	37,08	53,53	72,98	120,9	180,9
87	40,30	58,18	79,32	131,4	196,6
88	43,80	63,24	86,23	142,9	213,8
89	47,60	68,73	93,72	155,3	232,4
90	51,76	74,74	101,9	168,9	252,8
91	56,31	81,32	110,9	183,8	275,0
92	61,28	88,50	120,7	200,1	299,4
93	66,67	96,29	131,3	217,7	325,8
94	72,53	104,8	142,9	236,9	354,5
95	78,85	113,9	155,4	257,6	385,6
96	85,68	123,8	168,9	280,0	419,1
97	93,03	134,4	183,4	304,1	455,2
98	100,9	145,8	199,0	330,0	494,0

Table 4

Values of the function $\frac{\pi}{2} G^2{}_{L_I}$

Z	$\frac{\pi}{2} G^2{}_{L_I}$	Z	$\frac{\pi}{2} G^2{}_{L_I}$	Z	$\frac{\pi}{2} G^2{}_{L_I}$	Z	$\frac{\pi}{2} G^2{}_{L_I}$
18	$1{,}090 \cdot 10^{-3}$	39	0,02346	60	0,1697	81	0,9929
19	$1{,}385 \cdot 10^{-3}$	40	0,02606	61	0,1850	82	1,079
20	$1{,}721 \cdot 10^{-3}$	41	0,02890	62	0,2016	83	1,173
21	$2{,}101 \cdot 10^{-3}$	42	0,03206	63	0,2196	84	1,274
22	$2{,}530 \cdot 10^{-3}$	43	0,03548	64	0,2391	85	1,384
23	$3{,}010 \cdot 10^{-3}$	44	0,03919	65	0,2602	86	1,504
24	$3{,}548 \cdot 10^{-3}$	45	0,04324	66	0,2835	87	1,636
25	$4{,}146 \cdot 10^{-3}$	46	0,04763	67	0,3086	88	1,779
26	$4{,}807 \cdot 10^{-3}$	47	0,05240	68	0,3358	89	1,934
27	$5{,}541 \cdot 10^{-3}$	48	0,05759	69	0,3653	90	2,104
28	$6{,}358 \cdot 10^{-3}$	49	0,06323	70	0,3972	91	2,290
29	$7{,}264 \cdot 10^{-3}$	50	0,06934	71	0,4318	92	2,493
30	$8{,}268 \cdot 10^{-3}$	51	0,07600	72	0,4693	93	2,714
31	$9{,}379 \cdot 10^{-3}$	52	0,08325	73	0,5101	94	2,954
32	0,01061	53	0,09115	74	0,5548	95	3,214
33	0,01196	54	0,09976	75	0,6032	96	3,494
34	0,01347	55	0,1091	76	0,6555	97	3,796
35	0,01512	56	0,1193	77	0,7124	98	4,121
36	0,01694	57	0,1304	78	0,7740		
37	0,01892	58	0,1425	79	0,8410		
38	0,02109	59	0,1556	80	0,9138		

$$\frac{W_{L_{II}}}{W_{L_I}} \approx \frac{F^2_{L_{II}}}{G^2_{L_I}}. \qquad (4)$$

Of interest also is the magnitude of the L_I and K electron capture probabilities

$$\frac{W_{L_I}}{W_K} = \frac{(E_0 + E_{L_I})^2}{(E_0 + E_K)^2} \frac{G^2_{L_I}}{G^2_K}. \qquad (5)$$

Here G_K is the value at the nuclear boundary of the large component of the K electron wave function and E_K is the total K electron energy.

Using the data of Tables 1 and 2, we tabulated the values of the functions defined by Eqs.(2)-(5) for all values of Z from 18 to 98. The values of the wave functions for the Z not listed in Tables 1 & 2 were found by interpolation.

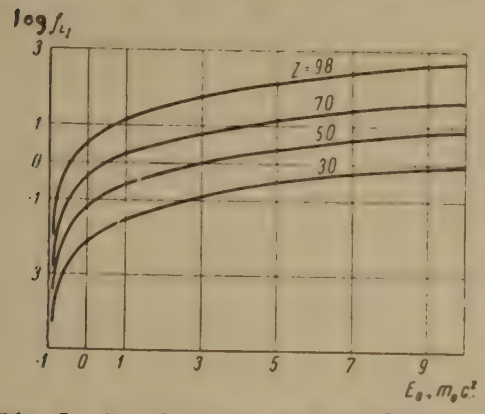

Fig.1. Variation of the function f_{L_I} with the transition energy E_0.

To determine the reduced lifetime $f_{L_I} t_{L_I}$ for L_I capture one must know the function f_{L_I}. Its values as functions of Z and the transition energy E_0 (in the range from -0.90 to 10 m_0c^2) are listed in Table 3. In the calculations we used the experimental values for E_{L_I}. Intermediate values of f_{L_I} can be found by interpolation of the tabular data. The behavior of f_{L_I} as a function of the transition energy is shown in Fig.1.

In regions where f_{L_I} changes rapidly its value can be found by means of Eq.(2). To facilitate such calculations, the values of the function $(\pi/2)\, G^2_{L_I}$ are given in Table 4. For calculating f_{L_I}, the values from Table 4 should be multiplied by $(E_0 + E_{L_I})^2$.

By comparing the present values of f_{L_I} with the results of earlier calcula-

Table 5

Values of the function $\frac{\pi}{2} F^2_{L_{II}}$

Z	$\frac{\pi}{2} F^2_{L_{II}}$	Z	$\frac{\pi}{2} F^2_{L_{II}}$	Z	$\frac{\pi}{2} F^2_{L_{II}}$	Z	$\frac{\pi}{2} F^2_{L_{II}}$
18	$3{,}463 \cdot 10^{-6}$	39	$3{,}220 \cdot 10^{-4}$	60	$6{,}251 \cdot 10^{-3}$	81	0,07778
19	$4{,}562 \cdot 10^{-6}$	40	$3{,}776 \cdot 10^{-4}$	61	$7{,}104 \cdot 10^{-3}$	82	0,08739
20	$5{,}948 \cdot 10^{-6}$	41	$4{,}416 \cdot 10^{-4}$	62	$8{,}079 \cdot 10^{-3}$	83	0,09813
21	$7{,}697 \cdot 10^{-6}$	42	$5{,}151 \cdot 10^{-4}$	63	$9{,}162 \cdot 10^{-3}$	84	0,1102
22	$9{,}928 \cdot 10^{-6}$	43	$6{,}001 \cdot 10^{-4}$	64	0,01037	85	0,1238
23	$1{,}267 \cdot 10^{-5}$	44	$6{,}981 \cdot 10^{-4}$	65	0,01165	86	0,1391
24	$1{,}612 \cdot 10^{-5}$	45	$8{,}110 \cdot 10^{-4}$	66	0,01329	87	0,1562
25	$2{,}042 \cdot 10^{-5}$	46	$9{,}406 \cdot 10^{-4}$	67	0,01504	88	0,1754
26	$2{,}604 \cdot 10^{-5}$	47	$1{,}090 \cdot 10^{-3}$	68	0,01696	89	0,1978
27	$3{,}279 \cdot 10^{-5}$	48	$1{,}260 \cdot 10^{-3}$	69	0,01909	90	0,2222
28	$4{,}087 \cdot 10^{-5}$	49	$1{,}454 \cdot 10^{-3}$	70	0,02148	91	0,2492
29	$5{,}055 \cdot 10^{-5}$	50	$1{,}694 \cdot 10^{-3}$	71	0,02414	92	0,2795
30	$6{,}212 \cdot 10^{-5}$	51	$1{,}956 \cdot 10^{-3}$	72	0,02712	93	0,3136
31	$7{,}585 \cdot 10^{-5}$	52	$2{,}243 \cdot 10^{-3}$	73	0,03047	94	0,3525
32	$9{,}217 \cdot 10^{-5}$	53	$2{,}562 \cdot 10^{-3}$	74	0,03426	95	0,3971
33	$1{,}115 \cdot 10^{-4}$	54	$2{,}914 \cdot 10^{-3}$	75	0,03851	96	0,4488
34	$1{,}358 \cdot 10^{-4}$	55	$3{,}311 \cdot 10^{-3}$	76	0,04327	97	0,5083
35	$1{,}636 \cdot 10^{-4}$	56	$3{,}758 \cdot 10^{-3}$	77	0,04864	98	0,5776
36	$1{,}954 \cdot 10^{-4}$	57	$4{,}264 \cdot 10^{-3}$	78	0,05473		
37	$2{,}319 \cdot 10^{-4}$	58	$4{,}841 \cdot 10^{-3}$	79	0,06108		
38	$2{,}738 \cdot 10^{-4}$	59	$5{,}500 \cdot 10^{-3}$	80	0,06921		

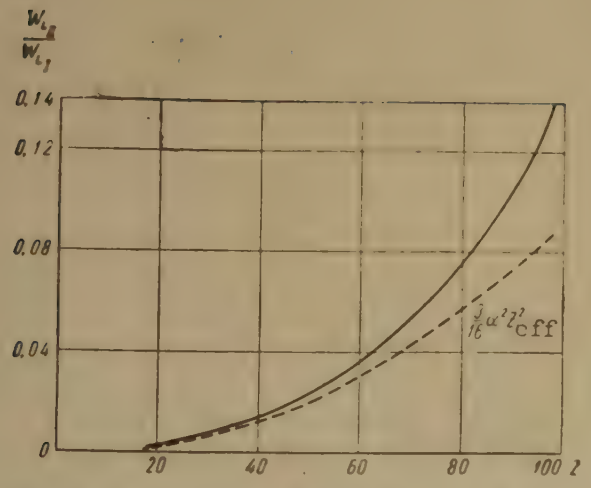

Fig.2. Variation of the L_{II} to L_I electron capture probability ratio.

tions for a pure Coulomb field[6,7] and the data of Reitz[4], in whose work the L electron wave functions for Z = 29, 49, 84 and 92 were found for a statistical atom, we can determine the influence of screening and finite nuclear size on L capture. It is found that for L electrons a significant role is played by the method of taking into account the screening effect of orbital electrons: numerical integration of the Dirac equation with a Thomas-Fermi-Dirac potential leads in the case of high transition energies to corrections which at Z = 50 are 20% and at Z = 90 about 25% greater than the value determined by the approximate method of Slater[8]. In the range of low transition energies when only L capture is energetically possible, the errors of Slater's method attain 60%. The finite nuclear size corrections for L capture prove to be relatively small: 0.3% at Z = 50 and 2.7% at Z = 90.

In view of the fact that the probability of L_{II} electron capture is small compared with L_I capture, we have not included a table for the function $f_{L_{II}}$, but only give values of the coefficient $\frac{\pi}{2} F^2_{L_{II}}$ (Table 5), which after multiplication by $(E_0 + E_{L_{II}})^2$ give the value of the function $f_{L_{II}}(E_0, Z)$. For L_{II} capture, also, the method of taking screening into account is important: as compared with the work of Slater the corrections increase by 30-40%.

It must be borne in mind that the functions f_{L_I} and $f_{L_{II}}$ can be used for determining the ft value only if the partial lifetime of the nucleus with respect to L_I and L_{II} captures is known. If only the total period T is known, the reduced lifetime should be calculated by means of the formula

$$(f_+ + f_K + f_{L_I} + f_{L_{II}})\, T.$$

The values of the ratio $F^2_{L_{II}} / G^2_{L_I}$ corresponding to the ratio of the probabilities of L_{II} and L_I electron capture (neglecting their energy difference), are given in Table 6. In cases when high accuracy in determining L_{II}/L_I is necessary, the values of Table 6 should be multiplied by

$$\left(\frac{E_0 + E_{L_{II}}}{E_0 + E_{L_I}}\right)^2.$$

For purposes of illustration the values of L_{II}/L_I, deduced in the present work, are plotted as a function of Z in Fig.2 (solid line). As may be seen, L_I capture predominates: up to Z = 70, L_{II} electron capture amounts to less than 5% and at Z = 95 comes to 12% of the L_I capture. The dash line in Fig.2 represents the variation of $^3/_{16}\,\alpha^2 Z^2_{eff}$ (Z_{eff} = Z - 4.15), the quantity which has usually been used for calculating the L_{II}/L_I ratio.

Of considerable practical interest is the value of the L_I/K ratio shown in Fig.3 for three elements. The K electron values used in the calculations were taken from Ref.1. In the range of high transition energies L_I/K varies from 0.08 for Z = 18 to 0.18 for Z = 98. At low energies the ratio increases, may become greater than unity and tends to ∞, when only L_I capture is energetically possible.

Values of $B = \frac{F^2_{L_{II}}}{G^2_{L_I}}$ Table 6

Z	B	Z	B	Z	B	Z	B
18	$2{,}350 \cdot 10^{-3}$	39	0,01372	60	0,03683	81	0,07834
19	$2{,}672 \cdot 10^{-3}$	40	0,01449	61	0,03839	82	0,08098
20	$3{,}001 \cdot 10^{-3}$	41	0,01528	62	0,04007	83	0,08368
21	$3{,}304 \cdot 10^{-3}$	42	0,01607	63	0,04172	84	0,08646
22	$3{,}715 \cdot 10^{-3}$	43	0,01691	64	0,04338	85	0,08944
23	$4{,}087 \cdot 10^{-3}$	44	0,01781	65	0,04478	86	0,09239
24	$4{,}492 \cdot 10^{-3}$	45	0,01876	66	0,04689	87	0,09547
25	$4{,}924 \cdot 10^{-3}$	46	0,01975	67	0,04872	88	0,09858
26	$5{,}417 \cdot 10^{-3}$	47	0,02079	68	0,05050	89	0,1023
27	$5{,}917 \cdot 10^{-3}$	48	0,02187	69	0,05227	90	0,1056
28	$6{,}428 \cdot 10^{-3}$	49	0,02299	70	0,05376	91	0,1088
29	$6{,}959 \cdot 10^{-3}$	50	0,02413	71	0,05591	92	0,1121
30	$7{,}513 \cdot 10^{-3}$	51	0,02523	72	0,05780	93	0,1155
31	$8{,}088 \cdot 10^{-3}$	52	0,02644	73	0,05974	94	0,1193
32	$8{,}690 \cdot 10^{-3}$	53	0,02760	74	0,06186	95	0,1236
33	$9{,}322 \cdot 10^{-3}$	54	0,02882	75	0,06405	96	0,1284
34	0,01008	55	0,03034	76	0,06628	97	0,1339
35	0,01082	56	0,03150	77	0,06856	98	0,1402
36	0,01154	57	0,03270	78	0,07091		
37	0,01225	58	0,03397	79	0,07331		
38	0,01298	59	0,03536	80	0,07574		

Values of $D = \frac{G^2_{L_I}}{G^2_K}$ Table 7

Z	D	Z	D	Z	D	Z	D
18	0,0806	39	0,1076	60	0,1279	81	0,1542
19	0,0828	40	0,1085	61	0,1290	82	0,1557
20	0,0848	41	0,1095	62	0,1300	83	0,1570
21	0,0867	42	0,1104	63	0,1311	84	0,1588
22	0,0885	43	0,1114	64	0,1322	85	0,1603
23	0,0902	44	0,1123	65	0,1333	86	0,1619
24	0,0916	45	0,1132	66	0,1345	87	0,1636
25	0,0930	46	0,1142	67	0,1356	88	0,1653
26	0,09423	47	0,1151	68	0,1369	89	0,1670
27	0,09538	48	0,1160	69	0,1380	90	0,1688
28	0,09651	49	0,1170	70	0,1392	91	0,1707
29	0,09762	50	0,1179	71	0,1405	92	0,1726
30	0,09869	51	0,1188	72	0,1418	93	0,1745
31	0,09975	52	0,1198	73	0,1430	94	0,1764
32	0,1008	53	0,1208	74	0,1446	95	0,1782
33	0,1018	54	0,1216	75	0,1460	96	0,1799
34	0,1028	55	0,1227	76	0,1475	97	0,1815
35	0,1038	56	0,1237	77	0,1489	98	0,1829
36	0,1047	57	0,1248	78	0,1502		
37	0,1057	58	0,1258	79	0,1516		
38	0,1066	59	0,1268	80	0,1529		

Lacking space to give the values of L_I/K as a function of the transition energy for all Z, we are listing appropriate values of the ratio $G^2_{L_I}/G^2_K$ in Table 7. For determining L_I/K, the values in Table 7 should be multiplied by $\frac{(E_0 + E_{L_I})^2}{(E_0 + E_K)^2}$ minus the square of the ratio of the energies of the neutrinos emitted in the L_I and K capture, respectively.

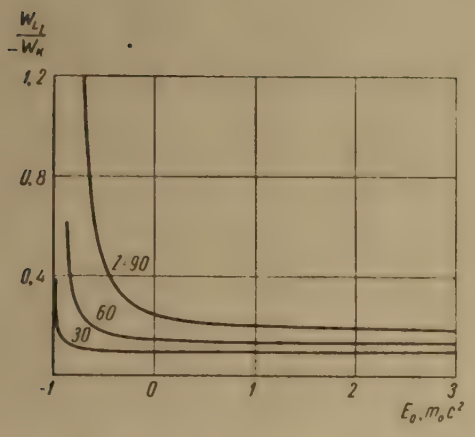

Fig.3. Ratio of L_I to K capture probabilities.

In 1949 quantities similar to the data of Table 7 were published by Rose & Jackson[9] who based their calculations on the Hartree[5] self-consistent field wave functions for the light elements and Reitz's[4] functions for medium and heavy elements. Our results differ from those of Rose & Jackson by the introduction of corrections for infinite nuclear size for the L_I and K electrons. Our L_I/K values lie somewhat higher, but the divergence nowhere exceeds 0.5%.

The variation as a function of Z of the ratio $G^2_{L_I}/G^2_K$ of L_I and K electron densities at the nuclear boundary is shown in Fig.4. The plotted values for Z > 25 are based on the data of Table 1; at Z = 18 the curve is matched

Table 8

Values of the functions L_0, M_0 and N_0 for L_I capture

Z	L_0	M_0	N_0	Z	L_0	M_0	N_0
18	$6{,}940\cdot10^{-4}$	0,02055	$-3{,}777\cdot10^{-3}$	59	0,09904	11,62	−1,073
19	$8{,}816\cdot10^{-4}$	0,02623	$-4{,}80\cdot10^{-3}$	60	0,1080	13,00	−1,185
20	$1{,}096\cdot10^{-3}$	0,03331	$-6{,}040\cdot10^{-3}$	61	0,1178	14,52	−1,308
21	$1{,}338\cdot10^{-3}$	0,04206	$-7{,}501\cdot10^{-3}$	62	0,1284	16,18	−1,441
22	$1{,}611\cdot10^{-3}$	0,05281	$-9{,}222\cdot10^{-3}$	63	0,1398	18,02	−1,587
23	$1{,}916\cdot10^{-3}$	0,06591	−0,01124	64	0,1522	20,03	−1,746
24	$2{,}258\cdot10^{-3}$	0,08174	−0,01359	65	0,1657	22,14	−1,915
25	$2{,}640\cdot10^{-3}$	0,1008	−0,01631	66	0,1805	24,78	−2,115
26	$3{,}060\cdot10^{-3}$	0,1245	−0,01952	67	0,1965	27,54	−2,326
27	$3{,}527\cdot10^{-3}$	0,1522	−0,02317	68	0,2138	30,57	−2,556
28	$4{,}048\cdot10^{-3}$	0,1841	−0,02729	69	0,2325	33,89	−2,807
29	$4{,}624\cdot10^{-3}$	0,2209	−0,03196	70	0,2528	37,55	−3,081
30	$5{,}264\cdot10^{-3}$	0,2634	−0,03723	71	0,2749	41,58	−3,381
31	$5{,}971\cdot10^{-3}$	0,3121	−0,04318	72	0,2988	46,02	−3,708
32	$6{,}752\cdot10^{-3}$	0,3678	−0,04984	73	0,3247	50,93	−4,062
33	$7{,}614\cdot10^{-3}$	0,4316	−0,05733	74	0,3532	56,42	−4,464
34	$8{,}575\cdot10^{-3}$	0,5055	−0,06584	75	0,3840	62,45	−4,897
35	$9{,}628\cdot10^{-3}$	0,5886	−0,07528	76	0,4173	69,08	−5,369
36	0,01078	0,6821	−0,08575	77	0,4535	76,40	−5,886
37	0,01204	0,7872	−0,09737	78	0,4928	84,56	−6,455
38	0,01343	0,9056	−0,1103	79	0,5354	93,51	−7,076
39	0,01494	1,039	−0,1246	80	0,5817	103,4	−7,755
40	0,01659	1,189	−0,1404	81	0,6321	114,3	−8,499
41	0,01840	1,358	−0,1581	82	0,6870	126,2	−9,310
42	0,02041	1,557	−0,1783	83	0,7466	139,3	−10,20
43	0,02259	1,778	−0,2004	84	0,8112	153,8	−11,17
44	0,02495	2,022	−0,2246	85	0,8813	169,9	−12,24
45	0,02753	2,293	−0,2512	86	0,9578	187,7	−13,41
46	0,03032	2,595	−0,2805	87	1,041	207,4	−14,70
47	0,03336	2,931	−0,3127	88	1,132	229,3	−16,11
48	0,03666	3,304	−0,3480	89	1,231	253,3	−17,66
49	0,04026	3,719	−0,3869	90	1,340	280,1	−19,37
50	0,04414	4,169	−0,4290	91	1,458	309,7	−21,25
51	0,04838	4,672	−0,4755	92	1,587	342,6	−23,32
52	0,05300	5,234	−0,5267	93	1,728	378,8	−25,58
53	0,05803	5,864	−0,5833	94	1,881	418,6	−28,06
54	0,06351	6,568	−0,6458	95	2,046	462,3	−30,75
55	0,06947	7,357	−0,7149	96	2,224	510,6	−33,70
56	0,07596	8,240	−0,7911	97	2,416	563,1	−36,87
57	0,08301	9,228	−0,8752	98	2,623	620,6	−40,35
58	0,09071	10,36	−0,9696	$P_0=L_0$; $Q_0=-M_0$; $R_0=N_0$; $L_1=P_1=0$			

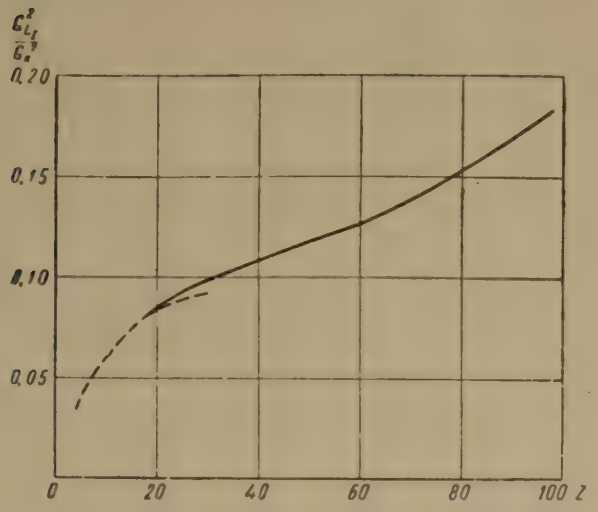

←Fig.4. Ratio of L_I to K electron densities at the nuclear boundary. Solid line - our results; dash line - values calculated using Hartree self-consistent field functions.

Table 9

Values of the functions L_0, M_0 and N_0 for L_{II} capture

Z	L_0	M_0	N_0	Z	L_0	M_0	N_0
18	$2{,}205\cdot10^{-6}$	$6{,}306\cdot10^{-5}$	$-1{,}179\cdot10^{-5}$	59	$3{,}501\cdot10^{-3}$	0,4638	−0,04030
19	$2{,}904\cdot10^{-6}$	$9{,}733\cdot10^{-5}$	$-1{,}681\cdot10^{-5}$	60	$3{,}980\cdot10^{-3}$	0,5401	−0,04636
20	$3{,}786\cdot10^{-6}$	$1{,}397\cdot10^{-4}$	$-2{,}300\cdot10^{-5}$	61	$4{,}522\cdot10^{-3}$	0,6280	−0,05329
21	$4{,}900\cdot10^{-6}$	$1{,}926\cdot10^{-4}$	$-3{,}072\cdot10^{-5}$	62	$5{,}144\cdot10^{-3}$	0,7305	−0,06130
22	$6{,}320\cdot10^{-6}$	$2{,}601\cdot10^{-4}$	$-4{,}055\cdot10^{-5}$	63	$5{,}833\cdot10^{-3}$	0,8459	−0,07024
23	$8{,}063\cdot10^{-6}$	$3{,}473\cdot10^{-4}$	$-5{,}292\cdot10^{-5}$	64	$6{,}603\cdot10^{-3}$	0,9762	−0,08028
24	$1{,}026\cdot10^{-5}$	$4{,}609\cdot10^{-4}$	$-6{,}877\cdot10^{-5}$	65	$7{,}418\cdot10^{-3}$	1,111	−0,09080
25	$1{,}300\cdot10^{-5}$	$6{,}094\cdot10^{-4}$	$-8{,}899\cdot10^{-5}$	66	$8{,}463\cdot10^{-3}$	1,307	−0,1052
26	$1{,}658\cdot10^{-5}$	$8{,}537\cdot10^{-4}$	$-1{,}190\cdot10^{-4}$	67	$9{,}573\cdot10^{-3}$	1,509	−0,1202
27	$2{,}087\cdot10^{-5}$	$1{,}145\cdot10^{-3}$	$-1{,}546\cdot10^{-4}$	68	0,01080	1,735	−0,1369
28	$2{,}602\cdot10^{-5}$	$1{,}493\cdot10^{-3}$	$-1{,}971\cdot10^{-4}$	69	0,01216	1,988	−0,1554
29	$3{,}218\cdot10^{-5}$	$1{,}916\cdot10^{-3}$	$-2{,}483\cdot10^{-4}$	70	0,01368	2,274	−0,1763
30	$3{,}955\cdot10^{-5}$	$2{,}431\cdot10^{-3}$	$-3{,}101\cdot10^{-4}$	71	0,01537	2,597	−0,1998
31	$4{,}829\cdot10^{-5}$	$3{,}058\cdot10^{-3}$	$-3{,}843\cdot10^{-4}$	72	0,01727	2,965	−0,2263
32	$5{,}868\cdot10^{-5}$	$3{,}827\cdot10^{-3}$	$-4{,}739\cdot10^{-4}$	73	0,01940	3,384	−0,2562
33	$7{,}098\cdot10^{-5}$	$4{,}772\cdot10^{-3}$	$-5{,}820\cdot10^{-4}$	74	0,02181	3,875	−0,2907
34	$8{,}647\cdot10^{-5}$	$6{,}149\cdot10^{-3}$	$-7{,}291\cdot10^{-4}$	75	0,02452	4,431	−0,3296
35	$1{,}041\cdot10^{-4}$	$7{,}710\cdot10^{-3}$	$-8{,}961\cdot10^{-4}$	76	0,02755	5,063	−0,3735
36	$1{,}244\cdot10^{-4}$	$9{,}497\cdot10^{-3}$	$-1{,}087\cdot10^{-3}$	77	0,03096	5,785	−0,4232
37	$1{,}476\cdot10^{-4}$	0,01156	$-1{,}306\cdot10^{-3}$	78	0,03484	6,623	−0,4804
38	$1{,}743\cdot10^{-4}$	0,01397	$-1{,}560\cdot10^{-3}$	79	0,03888	7,460	−0,5386
39	$2{,}050\cdot10^{-4}$	0,01680	$-1{,}856\cdot10^{-3}$	80	0,04406	8,661	−0,6178
40	$2{,}404\cdot10^{-4}$	0,02015	$-2{,}201\cdot10^{-3}$	81	0,04952	9,892	−0,6999
41	$2{,}812\cdot10^{-4}$	0,02412	$-2{,}604\cdot10^{-3}$	82	0,05564	11,29	−0,7925
42	$3{,}279\cdot10^{-4}$	0,02913	$-3{,}090\cdot10^{-3}$	83	0,06247	12,87	−0,8966
43	$3{,}820\cdot10^{-4}$	0,03496	$-3{,}655\cdot10^{-3}$	84	0,07014	14,67	−1,014
44	$4{,}444\cdot10^{-4}$	0,04179	$-4{,}309\cdot10^{-3}$	85	0,07883	16,76	−1,149
45	$5{,}163\cdot10^{-4}$	0,04978	$-5{,}069\cdot10^{-3}$	86	0,08854	19,12	−1,301
46	$5{,}988\cdot10^{-4}$	0,05914	$-5{,}951\cdot10^{-3}$	87	0,09942	21,80	−1,472
47	$6{,}936\cdot10^{-4}$	0,07011	$-6{,}974\cdot10^{-3}$	88	0,1116	24,86	−1,666
48	$8{,}020\cdot10^{-4}$	0,08294	$-8{,}156\cdot10^{-3}$	89	0,1259	28,49	−1,894
49	$9{,}256\cdot10^{-4}$	0,09794	$-9{,}521\cdot10^{-3}$	90	0,1415	32,50	−2,144
50	$1{,}078\cdot10^{-3}$	0,1172	−0,01124	91	0,1587	37,00	−2,423
51	$1{,}245\cdot10^{-3}$	0,1385	−0,01313	92	0,1779	42,12	−2,738
52	$1{,}428\cdot10^{-3}$	0,1622	−0,01522	93	0,1996	47,97	−3,095
53	$1{,}630\cdot10^{-3}$	0,1888	−0,01754	94	0,2244	54,74	−3,505
54	$1{,}855\cdot10^{-3}$	0,2193	−0,02017	95	0,2528	62,56	−3,977
55	$2{,}108\cdot10^{-3}$	0,2542	−0,02315	96	0,2857	71,78	−4,528
56	$2{,}392\cdot10^{-3}$	0,2947	−0,02655	97	0,3236	82,51	−5,167
57	$2{,}714\cdot10^{-3}$	0,3418	−0,03046	98	0,3677	95,09	−5,913
58	$3{,}082\cdot10^{-3}$	0,3983	−0,03503	$P_0 = -L_0$; $Q_0 = M_0$; $R_0 = -N_0$; $L_1 = P_1 = 0$			

Table 10

Values of the function L_I for L_{III} capture

Z	L_1	Z	L_1	Z	L_1	Z	L_1
18	$9{,}155\cdot10^{-7}$	39	$6{,}834\cdot10^{-5}$	60	$9{,}194\cdot10^{-4}$	81	$6{,}806\cdot10^{-3}$
19	$1{,}157\cdot10^{-6}$	40	$7{,}872\cdot10^{-5}$	61	$1{,}023\cdot10^{-3}$	82	$7{,}424\cdot10^{-3}$
20	$1{,}480\cdot10^{-6}$	41	$9{,}057\cdot10^{-5}$	62	$1{,}138\cdot10^{-3}$	83	$7{,}806\cdot10^{-3}$
21	$1{,}901\cdot10^{-6}$	42	$1{,}039\cdot10^{-4}$	63	$1{,}263\cdot10^{-3}$	84	$8{,}814\cdot10^{-3}$
22	$2{,}444\cdot10^{-6}$	43	$1{,}193\cdot10^{-4}$	64	$1{,}400\cdot10^{-3}$	85	$9{,}602\cdot10^{-3}$
23	$3{,}131\cdot10^{-6}$	44	$1{,}367\cdot10^{-4}$	65	$1{,}539\cdot10^{-3}$	86	$1{,}045\cdot10^{-2}$
24	$4{,}991\cdot10^{-6}$	45	$1{,}566\cdot10^{-4}$	66	$1{,}710\cdot10^{-3}$	87	$1{,}137\cdot10^{-2}$
25	$5{,}054\cdot10^{-6}$	46	$1{,}789\cdot10^{-4}$	67	$1{,}886\cdot10^{-3}$	88	$1{,}236\cdot10^{-2}$
26	$7{,}074\cdot10^{-6}$	47	$2{,}041\cdot10^{-4}$	68	$2{,}078\cdot10^{-3}$	89	$1{,}342\cdot10^{-2}$
27	$9{,}096\cdot10^{-6}$	48	$2{,}323\cdot10^{-4}$	69	$2{,}286\cdot10^{-3}$	90	$1{,}458\cdot10^{-2}$
28	$1{,}148\cdot10^{-5}$	49	$2{,}638\cdot10^{-4}$	70	$2{,}513\cdot10^{-3}$	91	$1{,}583\cdot10^{-2}$
29	$1{,}413\cdot10^{-5}$	50	$3{,}014\cdot10^{-4}$	71	$2{,}759\cdot10^{-3}$	92	$1{,}719\cdot10^{-2}$
30	$1{,}710\cdot10^{-5}$	51	$3{,}415\cdot10^{-4}$	72	$3{,}027\cdot10^{-3}$	93	$1{,}865\cdot10^{-2}$
31	$2{,}040\cdot10^{-5}$	52	$3{,}847\cdot10^{-4}$	73	$3{,}319\cdot10^{-3}$	94	$2{,}024\cdot10^{-2}$
32	$2{,}412\cdot10^{-5}$	53	$4{,}314\cdot10^{-4}$	74	$3{,}632\cdot10^{-3}$	95	$2{,}194\cdot10^{-2}$
33	$2{,}833\cdot10^{-5}$	54	$4{,}824\cdot10^{-4}$	75	$3{,}974\cdot10^{-3}$	96	$2{,}380\cdot10^{-2}$
34	$3{,}299\cdot10^{-5}$	55	$5{,}380\cdot10^{-4}$	76	$4{,}347\cdot10^{-3}$	97	$2{,}578\cdot10^{-2}$
35	$3{,}831\cdot10^{-5}$	56	$5{,}992\cdot10^{-4}$	77	$4{,}758\cdot10^{-3}$	98	$2{,}835\cdot10^{-2}$
36	$4{,}438\cdot10^{-5}$	57	$6{,}669\cdot10^{-4}$	78	$5{,}210\cdot10^{-3}$	$P_1 = L_1$;	
37	$5{,}132\cdot10^{-5}$	58	$7{,}419\cdot10^{-4}$	79	$5{,}657\cdot10^{-3}$	$L_0=M_0=N_0=P_0=$	
38	$5{,}925\cdot10^{-5}$	59	$8{,}258\cdot10^{-4}$	80	$6{,}232\cdot10^{-3}$	$=Q_0=R_0=0$	

with the self-consistent field functions. In calculating $(L_I + L_{II})/K$ one should use the following formula

$$\frac{W_{L_I} + W_{L_{II}}}{W_K} = \frac{f_{L_I} + f_{L_{II}}}{f_K}. \qquad (6)$$

Numerical values of this ratio can readily be obtained using the data of Table 3 (or 4) and 5 herein and Table 2 (or 3) in Ref.1.

3. Forbidden L capture

The probability of forbidden L capture can be determined by means of the same formulas as are employed for the probability of β-decay if one makes use of the following coefficients expressed in terms of the L electron wave functions:

L_I subshell -

$$L_0 = G^2_{L_I}; \quad M_0 = R^{-2}F^2_{L_I}; \quad N_0 = R^{-1}G_{L_I}F_{L_I}$$
$$P_0 = L_0; \quad Q_0 = -M_0; \quad R_0 = N_0; \quad L_1 = P_1 = 0;$$

L_{II} subshell -

$$L_0 = F^2_{L_{II}}, \quad M_0 = R^{-2}G^2_{L_{II}}; \quad N_0 = -R^{-1}G_{L_{II}}F_{L_{II}};$$
$$P_0 = -L_0; \quad Q_0 = M_0; \quad R_0 = -N_0; \quad L_1 = P_0 = 0;$$

L_{III} subshell -

$$L_1 = R^{-2}G^2_{L_{III}}, \quad P_1 = L_1;$$
$$L_0 = P_0 = M_0 = Q_0 = N_0 = R_1 = 0.$$

We have listed the values of these coefficients, based on the data of Tables 1 & 2, in Tables 8, 9 & 10. Knowledge of these coefficients allows of analyzing forbidden transitions occurring by L capture, which together with analysis of the positron decay and K capture branch data makes it possible to obtain significant information on changes in the state of the nucleus in β-decay.

Leningrad State University

References

1. I.Band, L.Zyrianova & Tsin Chen-Zhui, Izv.AN SSSR, Ser.fiz., 20, 1387 (1956). (Trans.Bulletin 20, No.12a, 1269.)
2. M.Metropolis & J.Reitz, J.Chem.Phys., 19, 55 (1951).
3. L.Thomas, J.Chem.Phys., 22, 1759 (1954).
4. J.Reitz, Phys.Rev., 77, 10 (1950).
5. D.Hartree, Reports on Progress in Physics, XI (1948).
6. R.Marshak, Phys.Rev., 61, 431 (1942).
7. M.Wang, Science Record, 5, 77 (1952).
8. J.Slater, Phys.Rev., 36, 51 (1930).
9. M.Rose & J.Jackson, Phys.Rev., 76, 1540 (1949).

ANGULAR DISTRIBUTION OF GAMMA-RAYS FROM POSITRON ANNIHILATION IN LIQUID HYDROGEN AND HELIUM

- A.S.Basina, K.A.Baskova, B.S.Dzhelepov and M.A.Dolgoborodova

Introduction

The mechanism of positron annihilation in condensed materials cannot be fully understood from a study of hitherto published data. It has been established that the annihilation mechanism differs at least partially in metals and amorphous materials. In metals positron annihilation involves mainly free electrons; the number of positrons falls off exponentially with time and the mean lifetime for all metals is $1.5 \cdot 10^{-10}$ sec.

The decay curves for amorphous materials reveal two components corresponding to different annihilation mechanisms; the respective lifetimes vary somewhat in different materials, but are of the order of $\sim 10^{-9}$ and $\sim 10^{-10}$. An attempt has been made to account for these components through the hypothesis that positronium is formed in amorphous materials. The "long-lived" component is then associated with two-quantum annihilation of orthopositronium by the so-called pickoff process[4], whereby a positron can annihilate with a bound electron which has a suitable spin orientation.

The fast process ($T \approx 10^{-10}$ sec, i.e., close in order of magnitude to T in metals) results from positron annihilation on atoms and ions and is partly due to annihilation of parapositronium.

Measurements by Page and his coworkers[1,2] and by Stewart[3] have shown that positron annihilation in amorphous materials and in metals is marked by different angular correlations of the two annihilation quanta. In metals the angular distributions (angular deviations from 180°) of two-quantum annihilation are represented by parabolic curves with half-width $\sim 1^{\circ}$. In the case of amorphous materials a narrower peak with a relatively broad base is observed. The narrow peak is customarily attributed to the formation of positronium in the para state since the photons diverge at an angle close to 180° when slowed-down parapositronium is annihilated.

The annihilation of free positrons with bound electrons broadens the angular distribution curve.

The velocities of atomic electrons which participate in annihilation account for a greater angular distribution width (the positrons are slowed down before annihilation). The possible two-quantum annihilation of orthopositronium formed in amorphous materials should also broaden the base of the angular distribution curve.

For the purpose of elucidating the positron annihilation mechanism in amorphous materials it would be desirable to perform joint measurements of the lifetime and angular distribution and to determine the probability ratio of three-quantum to two-quantum annihilation. Such experiments would be especially valuable in materials of sufficiently simple structure so that the behavior of positrons in the given material could be calculated at least approximately. Gaseous helium and molecular hydrogen are evidently the best substances for such investigations.

Chang Li[5] made a number of calculations for these gaseous systems. However, inasmuch as low densities create a number of experimental difficulties, actual experiments are performed mainly with liquid hydrogen and helium.

Paul and Graham[6] and Wackerle and Stump[7] have studied the lifetime distribution of positron annihilations in liquid helium. There is agreement as to the existence of three components with the lifetimes of $\sim 2 \cdot 10^{-10}$, $(1.83 \pm 0.15) \cdot 10^{-9}$ and $(9.1 \pm 0.5) \cdot 10^{-8}$ sec.

These investigators associate the lifetimes with three different mechanisms: parapositronium annihilation, interactions between positrons and atomic electrons, and orthopositronium annihilation, respectively. Annihilations through the formation of parapositronium and orthopositronium are estimated to comprise 5 and 16%, respectively, of all annihilations; the remaining 79% of the positrons annihilate with atomic electrons.

Measurements of three-quantum annihilation in gaseous hydrogen and helium by De Benedetti and Siegel[8] also indicate the formation of positronium in these gases.

In the present work we investigated annihilation photon angular distribution in liquid hydrogen and helium.

1. Experimental Arrangement

The experimental set-up and technique used in measuring the angular distribution of photons from positron annihilation in liquid hydrogen and helium were essentially the same as in previous work by some of us.[9] The apparatus is shown schematically in Fig.1. A Dewar vessel placed between two scintillation counters contained liquid hydrogen or helium in which positrons were slowed down and annihilated. A lead collimator with a cylindrical aperture of 2 mm diameter was placed in front of counter 1; a rotating lead disc with annuli (annular slits) of different sizes was placed in front of counter 2. With this geometry it was possible to discriminate annihilation photons in definite angular intervals.

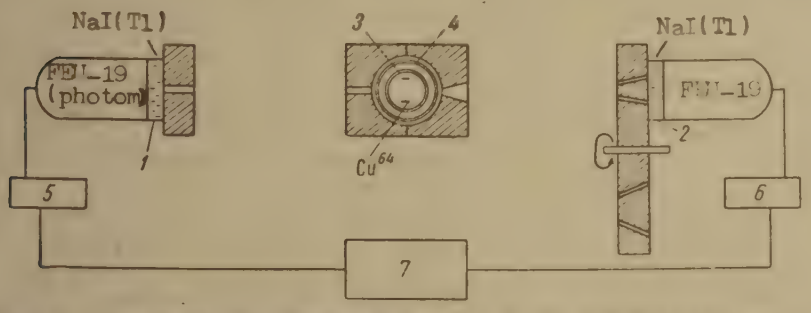

Fig.1. Diagram of experiment: 1 & 2) scintillation counters, 3) Dewar for liquid helium or hydrogen (inside diameter of vessel with helium - 45 mm, with hydrogen - 75 mm), 4) Dewar for liquid nitrogen, 5 & 6) preamplifiers, 7) coincidence circuit.

In the present experiment the positron source was radioactive Cu^{64} in the form of 30-60 μ thick foil. The copper foil was was fastened in a special frame attached to a rod (as shown in Fig.2) by means of which it was lowered into the Dewar. The experimental geometry required a rigorously determined shape of the target in which positrons are slowed down and annihilated. For measurements of positron annihilation in metals the target was a small cylinder of 2 mm diameter. Since our results were to be compared with those from metals, similarity of the experimental conditions had to be approximated by isolating a working volume in the liquid hydrogen or helium in the form of a 2 mm diameter cylinder. To this end the Dewar was enclosed in a lead block with circular openings facing the counters. This lead block also shielded the scintillation counters against direct radiation from the positron source.

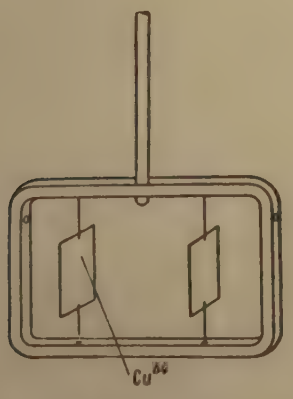

Fig.2. Frame for positron source.

To assure exact definition of the angular intervals it was essential to align precisely the axes of the collimator in front of counter 1, the annulus in front of

counter 2 and the collimator enclosing the Dewar. This adjustment was performed by means of a parallel light beam passing through the collimator openings and impinging on a photoelectric cell behind the last collimator. The units were aligned to obtain a maximum photocurrent reading. In the experiments with liquid hydrogen and helium the correct position of the source-holder frame with respect to the axis defined by the light beam was determined by means of a small mirror attached to the rod holding the frame. A light beam reflected from this mirror to a screen was displaced vertically as the frame moved in a direction perpendicular to the axis of the apparatus. The helium and hydrogen Dewars each had two vertical unsilvered transparent strips 1 cm wide located opposite each other. We could thus determine rotation of the frame about its axis by sending a light beam through openings (in line with the unsilvered strips of the Dewars) drilled in the vertical members of the holder frame.

The scintillation counters used to detect the photons consisted of NaI(Tl) crystals and FEU-19 multiplier tubes. The pulses from the counters were amplified and fed to a coincidence circuit with a resolving time of $\sim 5 \cdot 10^{-8}$ sec.

The angular distribution curve could be plotted from the coincidence counts with different annuli mounted successively in front of counter 2 (making due allowance for solid angles and the transmission of the apparatus in the process of plotting). The γ-rays passing through different annular slits struck different parts of the counter surface. Appropriate corrections were introduced for the variation of counter efficiency from its center to its periphery, as determined by a special experiment. The Dewars were large enough to contain the entire positron range in liquid hydrogen and helium so that positrons were annihilated without reaching the walls of the vessel.

Inasmuch as the Dewar containing the liquid helium was placed in another Dewar containing liquid nitrogen, scattering of annihilation quanta in the liquid nitrogen and from the Dewar walls might have distorted the observed angular distribution. Control experiments showed, however, that this effect was insignificant. The angular distribution of photons was also measured for positrons annihilating in the Cu^{64} source itself, which in this instance was a small cylinder mounted in the target position. The angular distribution was measured with the source in air (Col. I of the Table), in a helium Dewar (Col. II), with the helium Dewar inside the empty liquid nitrogen Dewar (III) and, finally, with liquid nitrogen poured into the outer Dewar (IV). All the values of $f(\theta)$ shown in the table are normalized to the $\theta = 3.5'$ value.

It is evident from the table that all curves agree within the limits of the experimental uncertainty.

Angular distribution $f(\theta)$ of quanta from positron annihilation in copper under different conditions

θ	$f(\theta)$			
	I	II	III	IV
3,5′	161 ±5	161 ±1	161 ±8	161 ±8
21′	120,5 ±1,2	122 ±2	119 ±2	125 ±3
41′	25,9 ±0,5	26,7 ±0,8	26,7 ±0,6	25,1 ±0,8
62′	4,1 ±0,1	5,3 ±0,3	3,7 ±0,3	3,5 ±0,4
1°29′	0,7 ±0,1	0,5 ±0,1	0,6 ±0,1	0,7 ±0,1
2°	0,31±0,02	0,21±0,02	0,22±0,02	0,32±0,03

2. Results

The angular distributions for liquid hydrogen and helium are shown in Fig.3. Each point of the curves represents the number of coincidences per unit solid angle in the angular interval corresponding to a given annulus. For purposes of comparison we also give the distribution curve for positron annihilation in aluminum.

The reduction of experimental results to values per unit solid angle requires special consideration. In measurements with aluminum the working volume from which annihilation quanta might emerge to be detected could be accurately confined to the dimensions required by the geometry. Furthermore, the transmission of the apparatus for different annuli could be calculated accurately.

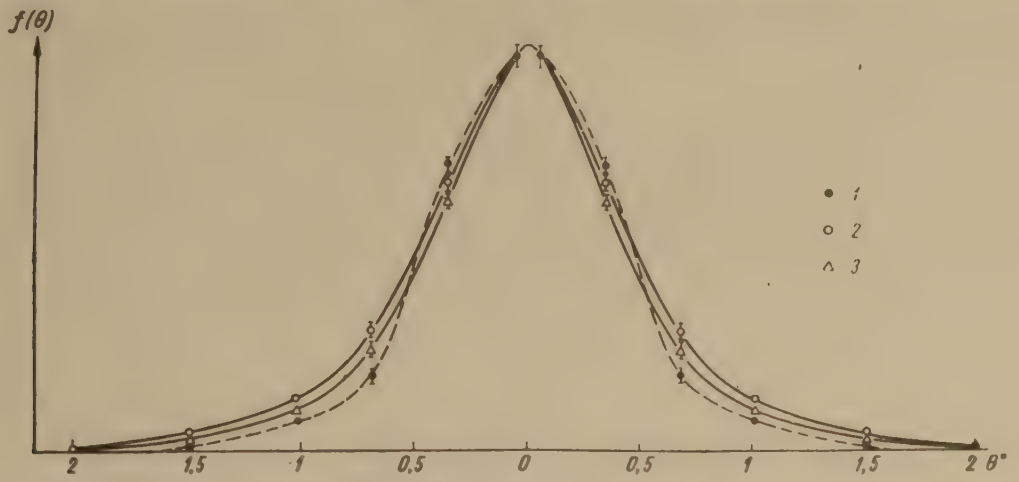

Fig.3. Angular distribution of photons from positron annihilation: 1) in aluminum (dash line), 2) liquid helium, 3) liquid hydrogen.

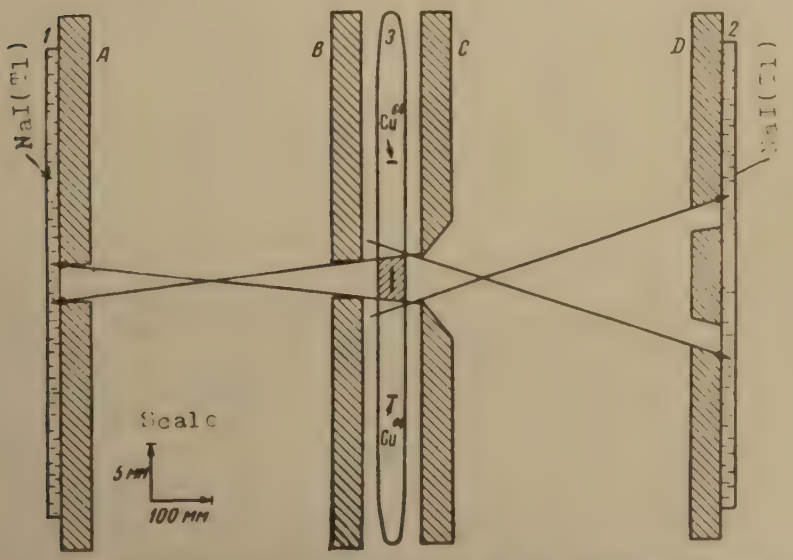

Fig.4. Experimental geometry: 1 & 2) scintillation counters, 3) helium Dewar; A) collimator in front of counter 1; B & C) collimators in front of counter 2.

In measurements with helium and hydrogen the working volume is somewhat greater, as shown by the hatched area in Fig.4. This must be taken into account in determining the effective transmission, which we calculated and verified experimentally. For this purpose the angular distribution for aluminum was measured twice: once with an aluminum cylinder 5 mm long and 2 mm in diameter (the collimator opening diameter) and once with aluminum foil. In the latter instance the volume previously filled with helium or hydrogen was uniformly filled with

crumpled 10μ foil; the crumpled foil had a density equal to that of liquid helium or hydrogen. The geometry of the "annihilation field" was thus, to a first approximation, equal in the experiments with the liquids and with the foil. The experimental curves obtained with the 2 mm diameter aluminum cylinder and with the foil differed, but agreed after introduction of the calculated corrections for the effective transmission, thus confirming the corrections.

It is evident from Fig.3 that the angular distributions for hydrogen and helium differ from the distribution curve for aluminum. Our curve for aluminum agrees with the results obtained by Green & Stewart[10] and by Lang, DeBenedetti and Smoluchowski[11]. The curves for hydrogen and helium have a narrower peak and a considerably broader base. The difference in curve widths lies outside the limits of the experimental error. The statistical error for $\theta > 0.5^{o}$ does not exceed the size of the "points". The distinctive shape of the H and He curves can apparently be accounted for by the formation of positronium in hydrogen and helium with positrons of sufficient energy.

The narrower peak for hydrogen and helium is presumably due to the annihilation of parapositronium formed therein. It should be noted, however, that this peak is considerably broader than that for positron annihilation in amorphous materials, where its width is usually ~20'. This latter narrow peak is associated with the annihilation of fully stopped parapositronium, while the broader peak for hydrogen and helium indicates that the parapositronium is not fully slowed down before annihilation in H and He.

Fig.5. Calculated distribution of photons from positron annihilation in liquid hydrogen.[5] The experimental points were obtained in the present work.

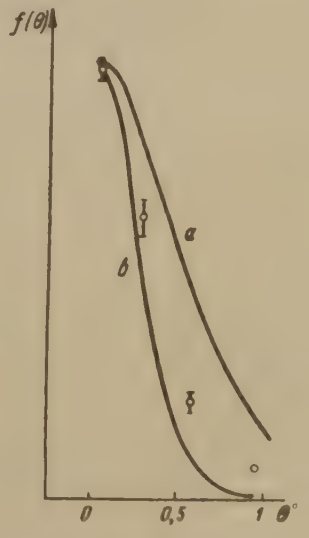

Fig.6. Calculated distribution of photons from positron annihilation in liquid helium.[5] a) theoretical curve neglecting polarization, b) theoretical curve including polarization. The experimental points were obtained in the present work.

For angles $\theta > 0.5^{o}$ the curves for hydrogen and helium are broader than for aluminum. This results from the higher mean velocities of the bound electrons in hydrogen and helium with which the positrons annihilate. The broadening of the curves for hydrogen and helium also seems to result from two-quantum annihilation of the orthopositronium formed with bound electrons possessing suitable spin orientation.

The observed emissions of quanta at large angles ($\theta > 1^{\circ}$) presumably result from the annihilation of not fully slowed-down positrons, since hydrogen and helium contain no electrons with energies corresponding to such large angles. It seems strange to find a considerably smaller number of such events for aluminum.

The angular distribution for helium is broader than for hydrogen as a result of the higher electron velocity in the helium atom.

Our experimental angular distribution of quanta from positron annihilation in liquid hydrogen and helium are compared in Figs.5 and 6 with the curves calculated by Chang Li. In Fig.6, curve a was calculated on the assumption that a positron is acted on by the mean field of the helium atom with which it interacts; in this case the positron lifetime would be $1.5 \cdot 10^{-8}$ sec. Curve b was calculated taking into account the polarization of the atom by the positron; in this case the lifetime is $2.6 \cdot 10^{-9}$ sec, which agrees with the experimental lifetime of free positrons in liquid helium. The experimental angular distribution in Fig.6 occupies an intermediate position between these two curves and is closer to curve b for small angles. The calculated curve for hydrogen in Fig.5 is narrower than that for helium, which is in agreement with experiment. The experimental curve for liquid hydrogen in Fig.5 also differs from the calculated curve.

It should be noted that an analysis of the experimental results indicates the possibility of positronium formation in helium, which was neglected in the calculation.

The angular distribution of the photons can be used to plot the energy spectrum for the center of gravity of the annihilating pairs.

The experimentally observed angular distribution is expressed by

$$N_{\exp}(\theta) = \int_{\beta_{\min}}^{1} N'(\theta, \beta) W(\beta) d\beta,$$

where $\beta_{\min} = \frac{v_{\min}}{c}$ (here $v_{\min}$ is the minimum velocity at which the photons can form the angle of divergence $\pi - \theta$), $N'(\theta, \beta)$ is the number of coincidences per unit solid angle, given by

$$N'(\theta, \beta) = \frac{\mathfrak{N}\{\sqrt{4\beta^2 - \sin^2(\theta - \Delta\theta)} - \sqrt{4\beta^2 - \sin^2(\theta + \Delta\theta)}\}}{\beta \sin\theta \Delta\theta},$$

where $\mathfrak{N}$ is the number of annihilations per second.

It would be complicated mathematically to determine the function $W(\beta)$ (the energy spectrum of the center of gravity of annihilating paris) in the integrand. Such mathematical treatment is not justified in view of the fact that the experimental curve was plotted on the basis of only 6 points. The following approximate analysis is preferable. The entire range of β from 0 to 1 is divided into 6 parts (for the number of experimental values) so that the interval $\beta_1 - \beta_2$ corresponds to photon deviation angles θ from θ_1 to θ_2, the interval $\beta_2 - \beta_3$ corresponds to $\theta_2 - \theta_3$, etc. The integral can then be replaced by the set of equations

$$N(\theta_1) = W_1(\beta) \frac{2N'(\theta_1, \beta)}{\mathfrak{N}} + W_2(\beta) \frac{2N'(\theta_2, \beta)}{\mathfrak{N}} + \cdots + W_6(\beta) \frac{2N'(\theta_6, \beta)}{\mathfrak{N}},$$

. . . . . .

$$N(\theta_5) = W_6(\beta) \frac{2N'(\theta_6, \beta)}{\mathfrak{N}}.$$

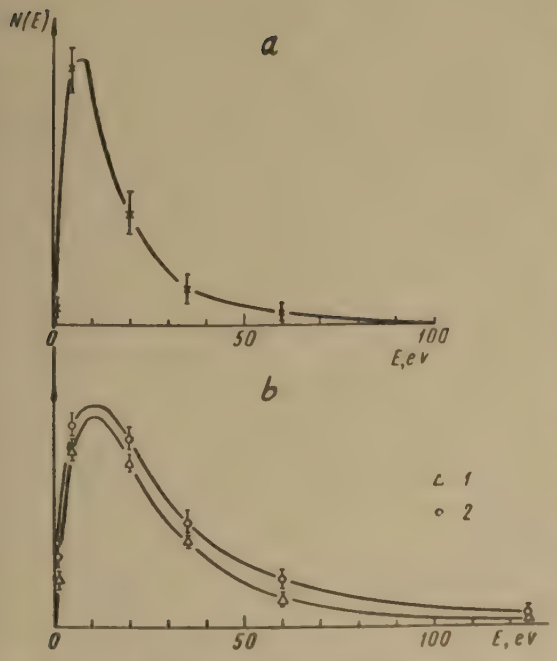

Fig.7. Energy spectrum of center of gravity of annihilating pairs; a) aluminum, b) liquid hydrogen (1) and helium (2).

These equations can be solved successively for $W(\beta)$, working backward from the last equation.

We performed the calculations and obtained the energy spectra for positron annihilation in liquid hydrogen and helium shown in Fig.7 together with the spectrum obtained for aluminum. There is no point in discussing the details of these spectra inasmuch as - as was noted above - each curve is based on only six experimental values.

The authors are deeply grateful to P.L. Kapitsa, director of the "S.I.Vavilov" Institute for Physical Problems, where the experimental work was performed, and to A.I.Shal'nikov for his continued interest.

Scientific Research Physical Institute
Leningrad State University

References

1. L.Page, M.Heinberg, J.Wallace & T.Trout, Phys.Rev., 98, 206 (1955).
2. L.Page & M.Heinberg, Phys.Rev., 102, 1545 (1956).
3. A.Stewart, Phys.Rev., 99, 594 (1955).
4. R.Ferrell, Rev.Mod.Phys., 3, 511 (1956).
5. Chang Li, Vestnik, Leningrad State Univ., Ser.fiz.i khim, No.4, 160 (1958).
6. D.Paul & R.Graham, Phys.Rev., 106, 16 (1957).
7. J.Wackerle & R.Stump, Phys.Rev., 106, 18 (1957).
8. S.DeBenedetti & R.Siegel, Phys.Rev., 94, 955 (1954).
9. K.A.Baskova & B.S.Dzhelepov, Izv.AN SSSR, Ser.fiz., 20, 951 (1956). (Trans.Bulletin, 20, No.8, 860.)
10. R.Green & A.Stewart, Phys.Rev., 98, 486 (1955).
11. G.Lang, S.DeBenedetti & R.Smoluchowski, Phys.Rev., 99, 596 (1955).

COMPENSATION OF THE EARTH'S MAGNETIC FIELD

- E.M.Krisyuk and G.D.Latyshev

Introduction

The design of an iron-free double-focusing β-spectrometer (r_o = 50 cm) required compensation of the earth's magnetic field in the working volume of the spectrometer. To insure linearity of the spectrometer to within about 1 in 10^5, the external magnetic fields had to be weaker than the spectrometer field by a factor of at least 10^5. The weakest spectrometer field with which it is possible to measure conversion lines accurately is ~10 oersted; ~25 kev electrons are focused with a field of this strength. The spectrum of lower-energy electrons will be strongly distorted by electron scattering and absorption in the source, instrument walls and counter window. Therefore external fields must not exceed 10^{-4} oersted inside the instrument. At Leningrad the vertical component of the Earth's field is ~0.5 oersted; the horizontal component is ~0.15 oersted. The vertical component therefore had to be compensated to within $\sim 2\cdot 10^{-4}$ and the horizontal component to within $\sim 6\cdot 10^{-4}$ in the working volume of the spectrometer, which is a cylinder of 60 cm radius and 80 cm height.

The Earth's magnetic field can be represented by a nonvertical vector which varies slowly and continuously in magnitude and direction. At points remote from ferromagnets and other perturbing influences the general field is very uniform. The problem of compensating the Earth's field can be divided into three parts: 1) the choice of location in the laboratory which insures the required initial homogeneity of the field, 2) designing of a system of coils to generate an adequately homogeneous field which will compensate the Earth's field in the working space, and 3) designing of equipment which will automatically adjust the current in the system to compensate variations of the Earth's field.

In the present paper we consider the problem of generating a compensating homogeneous magnetic field. For this purpose a few current-carrying coils arranged symmetrically with respect to a central plane are commonly used. Such systems provide free access to instruments located within them.

1. Magnetic field of two symmetrically placed coils

Within a sphere of radius $r < \rho$, the magnetic field due to the current in a coil can be represented by the series (see Ref.1, for example):

$$H_x = 0.2\ \pi I\omega \frac{\sin^2\psi}{\rho} \sum_{n=0}^{\infty} \left(\frac{r}{\rho}\right)^n P_n(\cos\theta) P'_{n+1}(\cos\psi),$$

$$H_y = 0.2\pi I\omega\ \frac{\sin^2\psi}{\rho} \sin\theta \sum_{n=1}^{\infty} \left(\frac{r}{\rho}\right)^n\ P'_{n+1}(\cos\psi) \left[P_{n+1}(\cos\theta) - \frac{\cos\theta}{n+1} P'_{n+1}(\cos\theta)\right], \qquad (1)$$

where H_x is the field component parallel to the axis of the system in oersteds, H_y is the component perpendicular to the same axis, r and θ are the coordinates of the point at which the field is being determined, ρ and ψ are the coordinates of the coil, ω is the number of turns in the coil, I is the current in amperes, $P_n(x)$ and $P_n'(x)$ are Legendre polynomials and their first derivatives. The coordinate origin is an arbitrary point on the coil axis and the positive direction is assumed to be that of the field.

The expression for the magnetic field of two coils placed symmetrically with respect to the origin contains only even powers of r/ρ. Since I, ω, r, θ and ρ are identical for both coils, while ψ_1 and ψ_2 differ by 180°, in view of the properties of derivatives of the Legendre polynomials, all terms containing odd powers

of r/ρ vanish, while all terms with even powers are doubled. Hence the magnetic field of two symmetrically placed coils will be

$$H_x = 0.4\pi I\omega \frac{\sin^2\psi}{\rho} \sum_{n=0}^{\infty} (r/\rho)^{2n} P_{2n}(\cos\theta) P'_{2n+1}(\cos\psi),$$

$$H_y = 0.4\,\pi I\omega \frac{\sin^2\psi}{\rho} \sin\theta \sum_{n-1}^{\infty} \left(\frac{r}{\rho}\right)^{2n} P'_{2n+1}(\cos\psi) \times \left[P_{2n+1}(\cos\theta) - \frac{\cos\theta}{2n+1} P'_{2n+1}(\cos\theta)\right]. \quad (2)$$

In (2) the term with $n = 0$ is independent of the field (point) coordinates and hence gives a homogeneous field, while the terms with $n > 0$ characterize deviations from homogeneity. Inasmuch as we are interested in the field close to the coordinate origin, i.e., for $r < \rho$, each term in (2) will be smaller than the preceding term. If the geometry of the system is such that the coefficients of terms from $n = 1$ to $n = m - 1$ vanish, the deviation from field homogeneity will be characterized by the term with $n = m$. The index m will be called the order of inhomogeneity of the field; obviously the greater m, the more uniform the magnetic field.

Systems with identical values of m can be distinguished by the value of A_{2m}, which is the coefficient of the term with $n = m$.

A system with two symmetrically placed coils has one free parameter ψ, which can be chosen to cause the term with $n = 1$ to vanish. For this purpose it is sufficient to set $P'_3(\cos\psi) = 0$. Solution of the resultant equation gives

$$\cos^2\psi = \frac{1}{5}. \quad (3)$$

The distance d from the coordinate origin to the plane of the coil will be

$$d = \frac{R}{2}, \quad (4)$$

where R is the coil radius. When (4) is satisfied, we have Helmholtz coils, the magnetic field of which has been thoroughly analyzed and described by Ruark & Peters[2].

From (3) we can readily obtain the magnetic field of Helmholtz coils at any given point x,y in rectangular coordinates:

$$H_x = 0.899176 \frac{I\omega}{R}\left[1 - \frac{0.144}{R^4}(8x^4 - 24x^2y^2 + 3y^4) + \right.$$
$$\left. + \frac{0.078848}{R^6}(16x^6 - 120x^4y^2 + 90x^2y^4 - 5y^6) - \ldots\right],$$
$$H_y = 0{,}517926 \frac{I\omega}{R^5} xy(4x^2 - 3y^2) - 0{,}425390 \frac{I\omega}{R^7} xy(8x^4 - 20x^2y^2 + 5y^4) + \cdots \quad (5)$$

Tables 1 and 2 give relative values of the Helmholtz-coil field components with x and y expressed as fractions of the coil radius R. For convenience all values of H are multiplied by 10^4.

Helmholtz coils can be used to compensate the east-west component of the Earth's field. The extreme variations of the horizontal component are ~0.005 oersted. With a Helmholtz coil radius of 1.75 meters, the east-west component in the working space of the instrument will be reduced by a factor of about 60, giving the required degree of compensation.

It is evident from the tables that the required compensation of the vertical component can be achieved only for $x < 0.1$ R and $y < 0.1$ R. This means that in our case R must be over 6 meters. This coil radius is too large as compared with the dimensions of the spectrometer. Hence for compensation of

Table 1

$$\frac{H_x - H_{x0}}{H_{x0}} \cdot 10^4 = -0.144 \cdot (8x^4 - 24x^2y^2 + 3y^4) \cdot 10^4$$

x	y								
	0	0,05	0,10	0,15	0,20	0,25	0,30	0,35	0,40
0	0	— 0,0270	—0,432	— 2,19	— 6,91	—16,9	—35,0	—64,8	—111
0,05	—0,0720	+ 0,117	+0,360	— 0,315	— 3,53	—11,5	—27,3	—54,3	—96,8
0,10	—1,15	— 0,315	+1,87	+ 4,44	+ 5,76	+ 3,57	— 5,04	—23,6	—56,4
0,15	—5,83	— 3,92	+1,51	+ 9,48	+18,4	+25,9	+29,2	+24,6	+ 7,99
0,20	—18,4	—15,0	— 5,04	+10,5	+30,0	+51,1	+71,0	+86,1	+92,2
0,25	—45,0	—39,6	—23,8	+ 1,41	+34,5	+73,1	+114	+155	+190
0,30	—93,3	—85,6	—62,6	—25,5	+24,2	+84,2	+152	+223	+294
0,35	—173	—162	—131	—79,8	—10,4	+74,9	+173	+281	+394
0,40	—295	—281	—240	—173	—80,6	+33,8	+168	+318	+479

Table 2

$$\frac{H_y}{H_{x0}} \cdot 10^4 = 0.576\ xy\,(4x^2 - 3y^2) \cdot 10^4$$

x	y								
	0	0,05	0,10	0,15	0,20	0,25	0,30	0,35	0,40
0	0	0	0	0	0	0	0	0	0
0,05	0	+ 0,0360	— 0,576	— 2,48	— 6,34	—12,8	—22,5	—36,0	—54,1
0,10	0	+ 0,936	+ 0,576	— 2,38	— 9,22	—21,2	—39,7	—66,0	—101
0,15	0	+ 3,56	+ 5,18	+ 2,92	— 5,18	—21,1	—46,7	—83,9	—135
0,20	0	+ 8,78	+15,0	+16,0	+ 9,22	— 7,92	—38,0	—83,7	—147
0,25	0	+17,5	+31,7	+39,4	+37,4	+22,5	— 8,64	—59,2	—132
0,30	0	+30,5	+57,0	+75,8	+82,9	+74,5	+46,7	— 4,54	—82,9
0,35	0	+48,6	+92,7	+128	+149	+152	+133	+86,4	+8,06
0,40	0	+72,9	+141	+198	+240	+261	+256	+220	+147

both the vertical and horizontal components we must take recourse to some more complicated system, producing a greater field homogeneity.

2. Magnetic field of three coils

Let us consider a system of three coils with the coordinate origin at the center of the central coil and with the outer coils positioned symmetrically in relation to the central coil. The field of these three coils will be

$$H_x = 0.2\pi I \frac{\omega_2}{\rho_2} \sum_{n=0}^{\infty} \left(\frac{r}{\rho_2}\right)^{2n} P_{2n}(\cos\theta) \left[\sin^2\psi \left(\frac{2\omega_1}{\omega_2}\right)\left(\frac{\rho_2}{\rho_1}\right)^{2n+1} P'_{2n+1}(\cos\psi) + P'_{2n+1}(0)\right].$$

$$H_y = 0.2\pi I \frac{\omega_2}{\rho_2} \sin\theta \sum_{n=1}^{\infty} \left(\frac{r}{\rho_2}\right)^{2n} \left[P_{2n+1}(\cos\theta) - \frac{\cos\theta}{2n+1} P'_{2n+1}(\cos\theta)\right] \times$$

$$\times \left[\sin^2\psi \left(\frac{2\omega_1}{\omega_2}\right)\left(\frac{\rho_2}{\rho_1}\right)^{2n+1} P'_{2n+1}(\cos\psi) + P'_{2n+1}(0)\right], \qquad (6)$$

where the indices 1 and 2 pertain to the outer and central coils, respectively.

This system has three free parameters $\cos\psi$, $\frac{2\omega_1}{\omega_2}$ and $\frac{\rho_1}{\rho_2}$; these parameters should be chosen so that the coefficients at $(r/\rho)^2$, $(r/\rho)^4$ and $(r/\rho)^6$ vanish. It can be shown, however, that no values of the three free parameters will cause

all three coefficients to vanish. There are many solutions that will make the $(r/\rho)^2$ and (r/ρ^4) coefficients zero. For the best solution we therefore impose the additional requirement that the coefficient of $(r/\rho)^6$ be minimized.

When the coefficient of $(r/\rho)^6$ is minimized and the coefficients of $(r/\rho)^2$ and $(r/\rho)^4$ vanish, we find that for a given radius of the central coil the magnetic field becomes more homogeneous as the radius of the outer coils is increased and, conversely, for a given outer coil radius the field becomes more homogeneous as the central coil radius is increased. Consequently, with a system of given size, as characterized by the largest coil radius and the distance from the plane of the coil to the center of the system, we obtain the greatest homogeneity when $R_1 = R_2 = R$. The coefficients of $(r/\rho)^2$ and $(r/\rho)^4$ then vanish when

$$u = \cos^2\psi = 0.366157;$$
$$N = \frac{2\omega_1}{\omega_2} = 3.76320; \quad d_1 = 0.760051. \tag{7}$$

When these conditions are satisfied, the magnetic field becomes

$$H_x = 1.82151\,\frac{I\omega_2}{R}\left[1 - 0.0511462\,\frac{1}{R^6}\,(16x^6 - 120x^4y^2 + 90x^2y^4 - 5y^6) + \dots\right],$$
$$H_y = 0.558980\,\frac{I\omega_2}{R^7}\,xy\,(8x^4 - 20x^2y^2 + 5y^4) - \dots \tag{8}$$

It is interesting to compare this solution with that of Maxwell (see Ref.3), wherein $\rho_1 = \rho_2$, N = 49/32 and $u = 3/r$, giving the field

$$H_x = 1.17810\,\frac{I\omega_2}{R_2}\left[1 - 0.127679\,\frac{1}{R_2^6}\,(16x^6 - 120x^4y^2 + 90x^2y^4 - 5y^6) + \dots\right],$$
$$H_y = 0.902507\,\frac{I\omega_2}{R_2^7}\,xy\,(8x^4 - 20x^2y^2 + 5y^4) - \dots \tag{9}$$

The new solution gives a field which is more homogeneous by a factor of 2.5 than that of Maxwell for the same central coil radius.

Scott[4] has suggested that a homogeneous field could be obtained by using two pairs of Helmholtz coils connected in opposition. When the pairs of coils have a common center and axis of symmetry and the number of turns of each pair is proportional to the fifth power of the radius, the $(r/\rho)^4$ term in the expression for the magnetic field vanishes. We thus obtain a system with third order inhomogeneity. The x-th field component is

$$H_x = 0.899176I\left(\frac{\omega_l}{R_l} - \frac{\omega_s}{R_s}\right)\times$$
$$\times\left[1 + 0.078848\,\frac{\left(\frac{\omega_l}{R_l^7} - \frac{\omega_s}{R_s^7}\right)}{\left(\frac{\omega_l}{R_l} - \frac{\omega_s}{R_s}\right)}\,(16x^6 - 120x^4y^2 + 90x^2y^4 - 5y^6) + \dots\right], \tag{10}$$

where the indices l and s denote the outer and inner Helmholtz coils, respectively. Scott used Helmholtz coils differing in size by a factor of 2. In this case

$$H_x = 0.842978\,\frac{I\omega_l}{R_l}\left[1 - 0.252314\,\frac{1}{R_l^6}\,(16x^6 - 120x^4y^2 + 90x^2y^4 - 5y^6) + \dots\right]. \tag{11}$$

$$\frac{H_x - H_{x0}}{H_{x_0}} \cdot 10^4 = -0.0511462\,(16x^6 - 120x^4y^2 + 90x^2y^4 - 5y^6) \cdot 10^4$$

Table 3

x	y								
	0	0,05	0,10	0,15	0,20	0,25	0,30	0,35	0,40
0	0	+ 0,0000400	+ 0,00256	+0,0291	+ 0,164	+ 0,624	+ 1,86	+ 4,70	+10,5
0,05	— 0,000128	+ 0,000152	— 0,00524	—0,0206	— 0,00524	+ 0,199	+ 0,967	+ 3,02	+ 7,59
0,10	— 0,00818	+ 0,00732	+ 0,00972	—0,0740	— 0,336	— 0,798	— 1,32	— 1,46	— 0,336
0,15	— 0,0932	— 0,0220	+ 0,116	+0,111	— 0,344	— 1,57	— 3,82	— 7,13	—11,2
0,20	— 0,524	— 0,290	+ 0,277	+0,783	+ 0,622	— 0,954	— 4,74	—11,4	—21,5
0,25	— 2,00	— 1,42	+ 0,114	+1,97	+ 3,15	+ 2,37	— 1,86	—11,1	—26,8
0,30	— 5,97	— 4,75	— 1,41	+3,15	+ 7,46	+ 9,55	+ 7,08	— 2,53	—22,0
0,35	—15,0	—12,8	— 6,39	+2,85	+12,9	+21,1	+24,0	+17,9	— 1,56
0,40	—33,5	—29,6	—18,5	—1,87	+17,7	+36,5	+50,1	+53,1	+39,8

$$\frac{H_y}{H_{x0}} \cdot 10^4 = 0.306877\,(8x^4 - 20x^2y^2 + 5y^4)xy \cdot 10^4$$

Table 4

x	y								
	0	0,05	0,10	0,15	0,20	0,25	0,30	0,35	0,40
0	0	0	0	0	0	0	0	0	0
0,05	0	— 0,000336	+ 0,000767	+ 0,0335	+ 0,186	+0,631	+ 1,66	+ 3,70	+ 7,39
0,10	0	+ 0,00508	— 0,0215	— 0,0538	+ 0,0491	+0,601	+ 2,15	+ 5,51	+11,9
0,15	0	+ 0,0680	+ 0,00230	— 0,245	— 0,548	—0,523	+ 0,559	+ 3,86	+11,1
0,20	0	+ 0,332	+ 0,325	— 0,246	— 1,37	—2,71	— 3,44	— 2,18	+ 3,14
0,25	0	+ 1,08	+ 1,48	+ 0,651	— 1,65	—5,24	— 9,38	—12,6	—12,5
0,30	0	+ 2,78	+ 4,35	+ 3,71	+ 0,147	—6,48	—15,7	—26,0	—35,1
0,35	0	+ 6,12	+10,3	+10,9	+ 6,46	—3,64	—19,3	—39,5	—61,8
0,40	0	+12,1	+21,3	+24,9	+20,8	+7,47	—15,7	—48,2	—88,0

It is evident from a comparison of (11) and (8) that Scott's system of coils produces a field which is less homogeneous by a factor of 5 than that of our three coils. The homogeneity of Scott's field could be improved by increasing the radius of the inner coils, but this would sharply reduce the efficiency of the system, which we define by

$$S = \frac{H_{x0} R}{I \sum_i \omega_i},$$

representing the field when the total number of ampere-turns and the radius are both equal to unity.

Tables 3 and 4 give the topography of the field calculated for our system of three coils in the same units as for Helmholtz coils. It is evident that a coil radius of 1.75 meters produces the required degree of compensation of the earth's horizontal component within the working space. However, with this coil radius the system of three coils does not provide satisfactory compensation of the vertical component and some method of obtaining a more homogeneous field is needed.

3. Magnetic field of four coils

Let us consider a system of four coils arranged symmetrically with respect to the origin. The indices 1 and 2 will pertain to the coordinates and number of terms of the outer and inner pairs, respectively. Then

$$H_x = 0.4\pi I \omega_2 \sum_{n=0}^{\infty} r^{2n} P_{2n}(\cos\theta) \left[\frac{\omega_1}{\omega_2} \frac{\sin^2\psi_1}{\rho_1^{2n+1}} P'_{2n+1}(\cos\psi_1) + \frac{\sin^2\psi_2}{\rho_2^{2n+1}} P'_{2n+1}(\cos\psi_2) \right],$$

$$H_y = 0.4\pi I \omega_2 \sin\theta \sum_{n=1}^{\infty} r^{2n} \left[P_{2n+1}(\cos\theta) - \frac{\cos\theta}{2n+1} P'_{2n+1}(\cos\theta) \right] \times$$

$$\times \left[\frac{\omega_1}{\omega_2} \frac{\sin^2\psi_1}{\rho_1^{2n+1}} P'_{2n+1}(\cos\psi_1) + \frac{\sin^2\psi_2}{\rho_2^{2n+1}} P'_{2n+1}(\cos\psi_2) \right]. \qquad (12)$$

This system possesses four free parameters: ρ_2/ρ_1, $\cos\psi_1$, $\cos\psi_2$ and ω_1/ω_2; we could thus attempt to have the coefficients of $(r/\rho)^2$, $(r/\rho)^4$, $(r/\rho)^6$ and $(r/\rho)^8$ vanish. However, the solution would certainly be very complicated; in fact it is probable that no solution could be found (as in the case of three coils). We therefore attempted to obtain a special solution of three equations with $R_1 = R_2$, which is convenient from the standpoint of practical design. By successive approximations, we obtained

$$u_1 = 0.469490; \quad u_2 = 0.0558372; \quad N = \frac{\omega_1}{\omega_2} = 2.26044;$$

$$d_1 = 0.940733\,R; \quad d_2 = 0.243186\,R. \qquad (13)$$

The field is then

$$H_x = 2.25047 \frac{I\omega_2}{R} \left[1 - 0.00438737 \frac{1}{R^8} (128 x^8 - 1792 x^6 y^2 + 3360 x^4 y^4 - \right.$$

$$\left. - 1120 x^2 y^6 + 35 y^8) + \ldots \right],$$

$$H_y = 0.0789891 \frac{I\omega_2}{R^9} xy (64 x^6 - 336 x^4 y^2 + 280 x^2 y^4 - 35 y^6) - \ldots \qquad (14)$$

McKeehan[3] obtained a special solution for four coils with $\rho_1 = \rho_2$. In his solution $u_1 = 0.585310$, $u_2 = 0.0813570$ and $N = 0.682111$ and the resultant expressions for the field:

Table 5

$$\frac{H_x - H_{x0}}{H_{x0}} \cdot 10^4 = -\,0.00438737\,[128x^8 - 1792x^6y^2 + 3360x^4y^4 - 1120x^2y^6 + 35y^8]\cdot 10^4$$

x \ y	0	0,05	0,10	0,15	0,20	0,25	0,30	0,35	0,40
0	0	$6,90\cdot10^{-8}$	$-1,54\cdot10^{-5}$	$-3,94\cdot10^{-4}$	$-3,93\cdot10^{-3}$	−0,0234	−0,101	0,346	− 1,01
0,05	$2,19\cdot10^{-7}$	$1,05\cdot10^{-6}$	$+2,74\cdot10^{-5}$	$+5,67\cdot10^{-4}$	$+2,51\cdot10^{-3}$	$3,04\cdot10^{-3}$	−0,0185	−0,134	− 0,527
0,10	$5,62\cdot10^{-5}$	$+5,59\cdot10^{-5}$	$-2,68\cdot10^{-4}$	$-5,46\cdot10^{-4}$	$+7,02\cdot10^{-3}$	+0,0438	+0,145	+0,346	+ 0,641
0,15	$1,44\cdot10^{-3}$	$+3,50\cdot10^{-4}$	$+1,14\cdot10^{-3}$	$-6,87\cdot10^{-3}$	−0,0182	$+9,51\cdot10^{-3}$	+0,180	+0,675	+ 1,75
0,20	−0,0144	$3,24\cdot10^{-3}$	+0,0143	$+1,43\cdot10^{-3}$	−0,0686	−0,165	−0,140	+0,330	+ 1,80
0,25	−0,0857	−0,0413	+0,0517	+0,0893	−0,0466	−0,409	−0,884	−1,08	− 0,183
0,30	−0,368	0,233	+0,0897	+0,367	+0,293	−0,394	−1,76	−3,48	− 4,66
0,35	−1,26	0,917	−0,0546	+0,936	+1,56	+0,573	−1,89	−6,04	−11,1
0,40	−3,68	2,90	−0,830	+1,74	+3,66	+3,60	−0,365	−6,76	−17,6

Table 6

$$\frac{H_y}{H_{y0}} \cdot 10^4 = 0.0350989\ xy\,[64x^6 - 336\ x^4y^2 + 280\ x^2y^4 - 35\ y^6]\cdot 10^4$$

x \ y	0	0,05	0,10	0,15	0,20	0,25	0,30	0,35	0,40
0	0	0	0	0	0	0	0	0	0
0,05	0	$-3,70\cdot10^{-7}$	$+2,63\cdot10^{-5}$	$-2,38\cdot10^{-4}$	$4,22\cdot10^{-3}$	−0,0261	−0,105	−0,332	−0,883
0,10	0	$-5,35\cdot10^{-6}$	$-9,48\cdot10^{-5}$	$+1,72\cdot10^{-3}$	$+6,74\cdot10^{-3}$	$+3,13\cdot10^{-3}$	−0,0610	−0,324	−1,08
0,15	0	$+9,02\cdot10^{-4}$	$-1,98\cdot10^{-3}$	$-2,43\cdot10^{-3}$	+0,0186	−0,0811	+0,173	+0,186	−0,180
0,20	0	$-1,37\cdot10^{-3}$	$-1,37\cdot10^{-3}$	−0,0287	−0,0243	+0,199	+0,440	+1,03	+1,73
0,25	0	+0,0546	−0,0370	−0,0717	−0,195	−0,145	+0,362	+1,63	+3,87
0,30	0	+0,211	+0,231	−0,0351	−0,508	−0,883	−0,622	+0,998	+4,76
0,35	0	+0,647	+0,868	+0,390	−0,771	−2,21	−3,09	−2,13	+2,24
0,40	0	+1,69	+2,54	+1,91	−0,350	−3,83	−7,36	−9,02	−6,21

$$H_x = 1.447140\ \frac{I\omega_2}{R_2}\left[1 - 0.00998465\ \frac{1}{R_2^8}\left(128x^8 - 1792x^6y^2 + 3360x^4y^4 - 1120x^2y^6 + 35y^8\right) + \ldots\right].$$

$$H_y = -0.115593\ \frac{I\omega_2}{R_2^9}\,xy\left(64x^6 - 336x^4y^2 + 280x^2y^4 - 35y^6\right) - \ldots \qquad (15)$$

Our field is seen to be more homogeneous by a factor of about 2.3 than that of McKeehan.

Tables 5 and 6 give the field topography for four coils and show that the vertical component of the Earth's field can be compensated to the required degree in the working volume with a coil radius of 1.75 meters.

The different systems that have been discussed are compared in Table 7, where the first column gives values of m, the order of inhomogeneity of the system; the sixth column gives values of s, the efficiency of the system; and the seventh column gives value of B/D, the ratio of the width to the thickness of the winding that produces the most homogeneous field. Maxwell showed that terms of the order $\frac{B^2r^2}{R^4}$ and $\frac{D^2r^2}{R^6}$ in the expression for the field of a coil, taking the finite dimensions of the winding into account, vanish when the condition

$$\frac{B^2}{D^2} = \frac{12 - 195u + 490u^2 - 315u^3}{15 - 225u + 525u^2 - 315u^3} \qquad (16)$$

is satisfied, leaving terms of the orders $\frac{B^2r^4}{R^6}$: $\frac{D^2r^4}{R^6}$: $\frac{B^4r^2}{R^6}$: $\frac{D^4r^2}{R^6}$. These terms can be neglected when high fields are not required, so that the cross section of the winding may be small.

The table shows that in the case of McKeehan's equations one cannot choose an optimal value of B/D, whereas our solutions are free of this shortcoming.

In conclusion we should consider how the homogeneity of the field is affected by lack of precision in fabricating the coils. Since a rigorous investigation of this question would be laborious we have limited ourselves to an estimate.

Table 7

Comparison of different solutions

m	u	N	d	A_{2m}	S	B/D	Solution
1	2	3	4	5	6	7	8
2	0,2	—	0,5	−0,144	0,449538	0,9280	Helmholtz
3	0 0,428571	1,53125	0 0,654654	−0,127679	0,465421	0,8944 0,8062	Maxwell
3	0 0,366157	3,76320	0 0,760051	−0,0511462	0,382413	0,8944 0,7358	Our solution
4	0,0858579 0,585310	0,682111	0,296364 0,798214	−0,00998465	0,430155	∞ ∞	McKeehan
4	0,0558372 0,469490	2,26044	0,243186 0,940733	−0,00438737	0,345117	0,8020 0,7426	Our solution

Imprecision of the coils could lead to additional field terms of the order $(\alpha/R)(r/\rho)^2$ where α is the deviation from the design dimensions. The allowable tolerances in preparing the coils should be determined accordingly.

Physics Department,
"V.N.Obraztsov" Leningrad Railroad Engineers Institute

References

1. B.M.Ianovskii, Zemnoi magnetizm (Terrestrial magnetism), M.-L., 1953.
2. A.E.Ruark & M.F.Peters, J.Opt.Soc.America, 13, 205 (1926).
3. L.W.McKeehan, Rev.Scient.Instrum., 7, 150 (1936).
4. G.G.Scott, Rev.Scient.Instrum., 28, 270 (1957).

FINITE SIZE CORRECTIONS TO THE LAMB SHIFT

- E.V.Teodorovich

The experimental values of the $^2S_{1/2}-2P_{1/2}$ Lamb shift are 1057.77 ± 0.10 Mc/sec in hydrogen and 1059.00 ± 0.10 Mc/sec in deuterium.[1] These values are accounted for theoretically by the interaction of the electron with fluctuations of the photon and electron-positron vacua. It is also necessary to take into account the mass corrections and relativistic corrections in the two-body problem which were first calculated by Salpeter[2], as well as nuclear recoil[3]. Until recently, a discrepancy of the order of 0.6 Mc/sec between the experimental and theoretical values for the Lamb shift had been unaccounted for.

We now have a new value for the magnetic dipole moment of the electron:

$$\mu_l = \mu_0\left(1 + \frac{\alpha}{2\pi} - 0.328\frac{\alpha^2}{\pi^2}\right) = 1.0011596\mu_0 ;$$

this was determined by Petermann and recently recalculated by Sommerfield[4] this was in good agreement with the latest experimental data of Frankel & Liebes[5]:

$$\mu_l = \mu_0(1{,}001165 \pm 0{,}000011).$$

This has been used to obtain a new value of the fine structure constant, $1/\alpha = 137.039$ (instead of 137.036) and a new value for the higher order electromagnetic corrections to the Lamb shift. We thus have 1057.82 Mc/sec for hydrogen and 1058.47 Mc/sec for deuterium while still neglecting the volume (finite size) of the nucleus.

It was pointed out some time ago by Ivanenko and Kolesnikov[6], as well as in the publications of Schwinger's group, that the Lamb shift should be corrected for the charge distribution in the deuterium nucleus. Recent experiments by Hofstadter and others on scattering of high-energy electrons by protons indicate a rms radius $\bar{r} = 0.77\cdot10^{-13}$ cm for the proton charge distribution[7].

The finite size of the deuterium nucleus was previously taken into account by means of perturbation theory[2,8], which gives $\Delta\varepsilon = \frac{\alpha}{3}\psi(0)^2\,\bar{r}^2$ for the level shift, where $\bar{r}$ is the rms radius of the charge distribution.

Since we now have very exact measurements of the Lamb shift, which is influenced by a number of characteristics of elementary particles (the magnetic moment, charge, structure, etc.), it is important to obtain a more precise correction for finite nuclear and proton size and, in particular, to take into account the distortion of the electron wave function due to "smearing out" of the nuclear or proton charge.

A formula for the finite-size correction has been obtained, using the method of "refined" wave functions[6,9,10]. In this method the solution for the outer region, where a purely Coulomb field obtains, is joined smoothly with the solution for the inner region, in which a non-Coulomb field results from smearing of the charge, to find the level energy correction.

The solution for the outer region is a combination of Whittaker functions converging exponentially at infinity for all values of the principal quantum number n and becoming the usual solution as a combination of hypergeometric functions for integral n.

The change of the level energy is determined by the change in n as compared with the pure Coulomb value:

$$\Delta\varepsilon^{(1)} = \alpha^2 mc^2\frac{\Delta n}{n^3}. \qquad (1)$$

Joining the solutions for the S level gives

$$\Delta n = 2\alpha^4 \left(\frac{R}{r_0}\right)^2 \left(1 + \frac{2}{\alpha}\,\frac{f(R)}{g(R)}\right), \tag{2}$$

where $r_0 = \frac{e^2}{mc^2}$, R is the function-joining radius and f and g are the radial components of the Dirac solution.

In the inner region, we can to a good approximation set $g = a$. We then have

$$f = \alpha a \,\frac{1}{r^2}\int_0^r V(x)\,x^2 dx, \tag{3}$$

where

$$V(x) = \int \frac{\rho(x)}{|\mathbf{r} - \mathbf{x}|}\,d\mathbf{x}, \tag{4}$$

which gives

$$\Delta n = \frac{2}{3}\,\frac{\alpha^4}{r_0^2}\left(\int_0^R \rho(x)\,x^4 dx\right)\left(\int_0^R \rho(x)\,x^2 dx\right)^{-1}, \tag{5}$$

or, taking R sufficiently larger than the region of charge distribution,

$$\Delta n = \frac{2}{3}\,\alpha^4 \left(\frac{\bar{r}}{r_0}\right)^2. \tag{5a}$$

Inserting Δn into the equation for $\Delta\varepsilon^{(1)}$, we obtain a result which agrees with perturbation theory.

It must be emphasized, however, that the method of refined wave functions can be used to obtain an additional shift due to wave function distortion inside the smeared nucleus or proton. For this part of the correction we obtained

$$\Delta\varepsilon^{(2)} = -\Delta\varepsilon_0\alpha^2\left\{\frac{4}{3}\,\frac{\bar{r}^2}{r_0^2} + \frac{2}{r_0}\iint |\mathbf{x} - \mathbf{r}|\,\rho(x)\,\rho(r)\,d\mathbf{x}\,d\mathbf{r} - \int \rho(r)\,dr\left[\frac{1}{r^2}\int_0^r x^2 dx \int \frac{\rho(y)}{|\mathbf{x} - \mathbf{y}|}\,dy\right]_f^2\right|, \tag{6}$$

where the first term takes into account the change of wave function normalization $\frac{\Delta N}{N} = -\frac{\Delta n}{\alpha^2}$, the second term takes into account the change in principal radial component g of the Dirac solution and the third term is due to the effect of the small f component.

It should be noted that our equation for $\Delta\varepsilon^{(2)}$ can be used in hyperfine structure theory and in the experimental determination of the fine structure constant. In Ref.10 a different method was used to obtain the second term in the equation for $\Delta\varepsilon^{(2)}$; $\Delta\varepsilon^{(1)} + \Delta\varepsilon^{(2)}$ was determined by using the value of $\bar{r}$ obtained by Hofstadter et al[7] in scattering experiments. The integral in the second term of $\Delta\varepsilon^{(2)}$ for real charge distributions can be represented very accurately by $4\bar{r}/3$; the third term makes a maximum contribution of 0.006 Mc/sec and may be neglected at the present stage of comparison with experiment.

Thus the finite size correction to the Lamb shift requires only that we know the rms radius of the charge distribution. Hofstadter's results are $\bar{r}_H = 0.77 \cdot 10^{-13}$ cm and $\bar{r}_D = 1.96 \cdot 10^{-13}$ cm. We also calculated the finite size correction for tritium; in this case allowance for the finite size of the proton and a wave function obtained by the variational method yielded $\bar{r}_T = 1.42 \cdot 10^{-13}$ cm.

The best values of the Lamb shift including finite-size corrections are now

$$S_H = 1057.90 \pm 0.13,$$
$$S_D = 1057.10 \pm 0.13,$$
$$S_T = 1058.99 \pm 0.13.$$

It should be noted that the potentialities of experimental techniques for determination of the Lamb shift have still not been exhausted and that increased experimental accuracy may provide information on the size of the charge distribution region and the character of the distribution as well as about the structure of other elementary particles, especially the neutron and electron.

Department of Statistical Physics and Mechanics,
Moscow State University

References

1. S.Triebwasser, E.Dayhoff & W.Lamb, Phys.Rev., 89, 98 (1953).
2. D.Salpeter, Phys.Rev., 89, 92 (1953).
3. T.Fulton & P.Martin, Phys.Rev., 95, 811 (1954).
4. C.Sommerfield, Phys.Rev., 107, 328 (1957).
5. P.Frankel & S.Liebes, Phys.Rev., 104, 1197 (1956).
6. D.Ivanenko & N.Kolesnikov, Doklady AN SSSR, 91, 47 (1953).
7. E.Chambers & R.Hofstadter, Phys.Rev., 103, 1454 (1956).
8. W.Aron & A.Zuchelli, Phys.Rev., 105, 1681 (1957).
9. A.Sokolov & D.Ivanenko, Kvantovaia teoriia polia (Quantum field theory), Part II, Chapt.3, Sec.7., M.-L., 1952.
10. E. V. Teodorovich, Zhur.eksp.i teor.fiz., 33, 823 (1957). (Trans.Soviet Physics, - JETP.)
11. A.Zemach, Phys.Rev., 104, 1771 (1956).

ACCURACY OF MAGNETIC FIELD MEASUREMENTS BY THE NUTATION METHOD

- A. I. Zhernovoi, Iu. S. Egorov and G. D. Latyshev

The principle of magnetic field measurement by the nutation method was described by us in an earlier paper[1]. A continuous stream of water passes successively through a strong magnetizing field, a cavity in the field to be measured, where a high-frequency transverse field is applied (the nutation head), and the usual apparatus for detecting nuclear resonance (Fig.1). The amplitude of the nuclear resonance signal is proportional to the projection, on the external field direction, of the resultant nuclear magnetic moment in a unit volume of the water entering the nuclear magnetic resonance head.

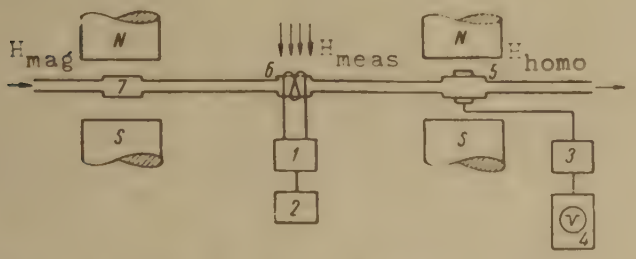

Fig.1. Block diagram of apparatus for measuring inhomogeneous magnetic fields: 1 - high-frequency generator, 2 - frequency meter, 3 - NMR detector, 4 - oscilloscope, 5 - NMR head, 6 - nutation head, 7 - cavity in magnetizing field.

When we neglect relaxation processes, the solution of the Bloch equation in a rotating coordinate system for nuclei leaving the nutation head gives the following expression for this projection:

$$M_z = M_0\left[1 - \frac{H_1^2}{H_1^2 + \Delta H^2}\left(\cos\gamma\sqrt{H_1^2 + \Delta H^2}\,\frac{V_N}{Q} - 1\right)\right], \qquad (1)$$

where H_1 is the half-amplitude of the oscillating field, ΔH is the deviation of the external field from resonance, γ is the proton gyromagnetic ratio, V_N is the volume of the nutation head, Q is the rate of water flow and M_0 is the resultant nuclear magnetic moment in a unit volume of the water entering the nutation head.

At exact resonance in a homogeneous field, the first negative absorption signal appears when

$$\gamma H_1 \frac{V_N}{Q} = \pi. \qquad (2)$$

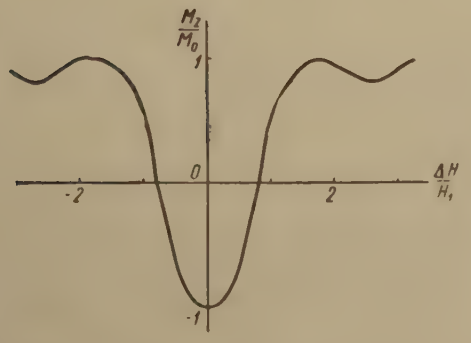

Fig.2. Amplitude of first nutation extremum in a homogeneous field as a function of field departure from resonance.

Subject to this condition, M_z/M_0 from (1) as a function of $\Delta H/H_1$ is shown in Fig. 2. It will be evident from this plot that the absorption signal can possess negative polarity only when the departure from resonance $\Delta H < 0.8\ H_1$. For $0.8\ H_1 < \Delta H < 1.5\ H_1$, the signal is only reduced in amplitude. Thus variation of the absorption signal will be observed only as the field (or frequency) is swept through range $\Delta H = 3\ H_1$; practically no nutation will be observed outside this range.

The center of the nutation region can at worst be determined within 10%. Therefore the error in a homogeneous field is given by

$$\sigma_{homo} = 0.3\,H_1. \qquad (3)$$

From (2) we have

$$H_1 = \frac{Q\pi}{\gamma V_N}, \tag{4}$$

whence

$$\dot{\alpha}_{homo} = 0.3\,\frac{\pi}{\gamma}\,\frac{Q}{V_N} = 3.5\cdot 10^{-5}\,[\text{Oe sec}^{-1}]\,\frac{Q}{V_N}. \tag{5}$$

Now let us consider the case of an inhomogeneous field.

Let the head be a cylinder of diameter d and length l (in the direction of flow). The existence of transverse inhomogeneity with the gradient K_d requires fulfillment of the condition

$$dK_d \leqslant 1.5\,H_1. \tag{6}$$

Otherwise, the nutation is greatly weakened. The error of measurement is now

$$\sigma = 0.1\,(dK_d + 3\,H_1). \tag{7}$$

For longitudinal inhomogeneity with the gradient K_l, the error is given by

$$\sigma = 0.1\,(lK_l + 3\,H_1). \tag{8}$$

When both types of inhomogeneity are present, we have

$$\sigma = 0.1\,(lK_l + dK_d + 3\,H_1). \tag{9}$$

In an inhomogeneous field (2) no longer holds for two reasons: first, the transverse inhomogeneity ΔH reduces the relaxation time T_2^* to $T^* \simeq 1/\gamma\Delta H$; second the condition for exact resonance can no longer be satisfied at all points of the nutation head and, as we see from (1), for a given ΔH the nutation frequency becomes

$$\Omega = \gamma\sqrt{H_1^2 + \Delta H^2}. \tag{10}$$

Evaluations show that when (6) is satisfied, relaxation has no significant effect on the nutation.

When the resonance conditions are satisfied at the center of the head, the "detuning" of the field from resonance is given by

$$\Delta H(x, y) = K_l x + K_d y, \tag{11}$$

where x and y are the longitudinal and transverse coordinates along axes parallel to K_l and K_d, respectively, with the origin at the center of the head. The detuning averaged over the cross section is

$$\overline{\Delta H}(x) = K_l x. \tag{12}$$

Invoking (10) and (12), we obtain the nutation angle of the specific resultant magnetic moment of the nuclei leaving the nutation head:

$$\theta = \frac{\gamma\pi d^2}{4\,Q}\int_{-\frac{l}{2}}^{+\frac{l}{2}}\sqrt{H_1^2 + K_l x}\,dx. \tag{13}$$

After integration we have

$$\theta = \frac{\gamma H_1 l \pi d^2}{4Q} m, \tag{14}$$

where

$$m = \frac{1}{2}\left\{\sqrt{1-\frac{b^2}{4}} + b \ln\left(\frac{\sqrt{1+\frac{b^2}{4}}+\frac{b}{2}}{\sqrt{1+\frac{b^2}{4}}-\frac{b}{2}}\right)\right\}, \tag{15}$$

wherein

$$b = \frac{K_l l}{H_1}.$$

When the condition for the first negative nutation signal is satisfied ($\theta = \pi$), we obtain the following expression for the amplitude of the oscillating field:

$$H_1 = \frac{4Q}{\gamma l d^2 m}. \tag{16}$$

Inserting (16) into (9), we obtain the error of measurement in the inhomogeneous field:

$$\sigma = 0.1\left(K_l l + K_d d + \frac{12Q}{\gamma m l d^2}\right). \tag{17}$$

The optimum conditions together with the requirement (6) give expressions for the dimensions of the head which will produce the minimum error:

$$d_{opt} = \sqrt{\frac{6Q}{\gamma l m K_d}}; \tag{18}$$

$$l_{opt} = \frac{1}{d}\sqrt{\frac{12Q}{\gamma m K_l}}; \tag{19}$$

with $m = 1.07$.

Making use of Eqs. (18) and (19), we can express the dependence of the optimum nutation head parameters and the minimum error on the rate of flow and the magnetic field inhomogeneity. When the longitudinal and transverse gradient are related by $K_d = aK_l$, we have

$$l_{opt} = \sqrt[4]{\frac{45Qa^2}{\gamma K_l}} = 0.2\,[\mathrm{Oe}^{1/4}\,\mathrm{sec}^{1/4}]\sqrt[4]{\frac{Qa^2}{K_l}}, \tag{20}$$

$$d_{opt} = \sqrt{\frac{2.8Q}{\gamma a^2 K_l}} = 0.1\,[\mathrm{Oe}^{1/4}\,\mathrm{sec}^{1/4}]\sqrt[4]{\frac{Q}{a^2 K_l}}, \tag{21}$$

$$H_{1\,opt} = \sqrt{\frac{0.6Qa^2K_l^3}{\gamma}} = 0.07\,[\mathrm{Oe}^{1/4}\,\mathrm{sec}^{1/4}]\sqrt[4]{Qa^2K_l^3}, \tag{22}$$

$$\sigma_{min} = 0.05\,[\mathrm{Oe}^{1/4}\,\mathrm{sec}^{1/4}]\sqrt{Qa^2K_l^3}. \tag{23}$$

The optimum parameters are related simply by

$$K_l l_{opt} = 2K_d d_{opt} = 3H_1;$$

$$\sigma_{min} = 0{,}25\,K_l l_{opt} = 0{,}5\,K_d d_{opt} = 0.75\,H_1.$$

Table 1 gives the optimum parameters for a few values of Q, K_l and a. The choice of Q is dictated by the requirement of obtaining a good signal from the absorption head; K_l is determined by the geometry of the measured field; a depends on the position of the nutation head.

Table 1

Optimum parameters of nutation head

$Q = 100$ cm^3 sec^{-1}, $a = 1$						$Q = 100$ cm^3 cm^{-1}, $a = 0.1$					
K_l, oerst. cm^{-1}	100	10	1	0,1	0,01	Kl, Oe cm^{-1}	100	10	1	0,1	0,01
l, cm	0,20	0,35	0,63	1,1	2,0	l, cm	0,07	0,12	0,20	0,35	0,63
d, cm	0,10	0,17	0,31	0,55	1,0	d, cm	0,4	0,6	1,0	1,7	3,1
σ, Oe	5	0,8	0,16	0,02	0,004	σ, Oe	1,5	0,26	0,05	0,006	0,002
H_1, Oe	8	1,3	0,25	0,03	0,006	H_1, Oe	2,3	0,36	0,07	0,01	0,002

It is obviously advantageous to have the water flowing in the direction of the external field gradient.

Table 2 gives the dependence of the relative error in field measurement on the field strength, assuming an inhomogeneity of 10^{-2} cm^{-1}. The error is defined as σ_{min}/H_{meas}. For nutation head parameters other than the optimum ones, the error must be found from (17).

Table 2

Variation of the relative field measurement error with the field strength

$Q = 100$ cm^3/sec, $a = 0.1$, inhomogeneity 10^{-2} cm^{-1}

H_{meas} Oe	10 000	1000	100	10	1
$\frac{\sigma}{H_{meas}}$	$1.5 \cdot 10^{-4}$	$2.6 \cdot 10^{-4}$	$5 \cdot 10^{-4}$	$6 \cdot 10^{-4}$	10^{-3}

In designing nutation heads, one must observe the condition

$$l < \frac{6\,mQ}{\gamma K_d d^3}.$$

When a head is a parallelepiped with the sides a, b and l, the field gradients parallel to the sides are K_a, K_b and K_l and the water flows along l, the optimum parameters are given by

$$Q_{opt} = \frac{1.5\,H_1}{K_a},\quad b_{opt} = \frac{1.5\,H_1}{K_b},\quad l_{opt} = \frac{3\,H_1}{K_l};$$

$$H_1 = \sqrt[4]{\frac{\pi Q}{\gamma\, 6.7}\,K_a K_b K_l} = 0.07\ [\mathrm{Oe}^{1/4}\,\mathrm{sec}^{1/4}]\ \sqrt[4]{Q K_a K_b K_l};$$

$$\sigma_{min} = 0.75\,H_1.$$

It follows that the nutation method can give good results as regards absolute measurements of fields with steep gradients. The fact that the nutation effect is not dependent on the external field strength makes this method useful for absolute measurements of very weak fields.

In practice the accuracy of measurement can be appreciably higher than indicated by the above formulas, which are based on assumptions that clearly result in overestimation of the errors. This applies especially to weak fields, for which the optimum nutation head parameters can readily be realized. Our preliminary experimental results tend to support the aforesaid.

"V.N.Obraztsov" Leningrad Railroad Engineers Institute

Reference

1. A.I.Zhernovoi, Iu.S.Egorov & G.D.Latishev, PTE (Instruments & experimental techniques), No.5 (1958).

NEW TECHNIQUE FOR MEASURING THE SPIN-LATTICE RELAXATION TIME OF LIQUIDS

- A. I. Zhernovoi and G. D. Latyshev

By using a nuclear magnetic resonance head with a flowing resonating material[1] it is possible to determine the longitudinal relaxation time. If V_1 is the volume placed in the strong polarizing field H_1, H_3 is the weak homogeneous field in which the nuclear resonance head is located, V_3 is the volume traversed by the liquid in field H_3 before entering the head and V_2 is the volume in the stray field H_2 between fields H_1 and H_3, then provided the conditions

$$H_2 \ll H_1 e^{\frac{-V_2}{QT_1}} \quad \text{and} \quad (1 - e^{\frac{-V_3}{QT_1}}) H_3 \ll H_1 e^{\frac{-V_3}{QT_1}}$$

are satisfied, the amplitude of the nuclear magnetic resonance signal is described by

$$A_c \sim H_1 e^{\frac{-V_2}{QT_1}} (1 - e^{\frac{-V_1}{QT_1}}),$$

where Q is the rate of liquid flow. This formula has been checked experimentally.

By studying the dependence of the signal amplitude on the volume V_2 or V_1 with Q constant, we can determine absolute longitudinal relaxation times exceeding 0.05 sec to within a few percent.

The merits of this method are that it can be used with any nuclear magnetic resonance set-up, that it does not involve errors due to the effect of a high-frequency field on nuclear resonance and that it can be used to measure T_1 for nuclei in any magnetic field beginning practically with a zero field.

Results of relaxation time measurements made by means of this technique are consistent with the data obtained by other methods. The procedure can also be used to investigate solvation, the formation of complexes in chemical reactions, catalysis, etc.

"V. N. Obraztsov" Leningrad Railroad Engineers Institute

Reference

1. A. I. Zhernovoi, Iu. S. Egorev & G. D. Latyshev, PTE (Instruments and experimental techniques, No. 5 (1958).

NEW TECHNIQUE FOR MEASURING SPIN-SPIN RELAXATION TIME OF LIQUIDS

- A. I. Zhernovoi and G. D. Latyshev

Measurements of the relaxation times, which characterize complex internal interactions within matter, further our understanding of such interactions. Our technique, unlike all others[1-4], determines the spin-spin relaxation time for nuclei in a very weak magnetic field, which can in principle be nearly zero. The technique can be used in connection with any set-up for recording nuclear resonance, but only for liquid samples with a spin-lattice relaxation time $T_1 > 0.05$ sec.

The sample is first kept in a strong field long enough to attain full polarization of the nuclei and then passes through a connecting tube into a cavity of volume V within a very weak homogeneous field that is shielded from external fields. The inhomogeneity of this field across the liquid stream must not exceed $1/\gamma T_2$, where γ is the gyromagnetic ratio of the nuclei and T_2 is the relaxation time to be measured. This condition can be fulfilled more easily with a low field strength.

In the cavity, the resultant nuclear magnetic moment is rotated by the resonant oscillating field into a direction perpendicular to the external magnetic field; when the sample emerges, the magnetic moment of the nuclei again becomes parallel to the field.

If Q is the rate of liquid flow, the resultant nuclear magnetic moment is reduced by the factor $e^{\frac{-V}{QT_2}}$ during the time the nuclei are in V. This is determined by means of the amplitude of the NMR signal from the nuclear resonance head in the weak homogeneous field that is entered by the liquid from V. If for volumes V_1 and V_2, the NMR amplitudes are A_1 and A_2, respectively, we have

$$T_2 = \frac{V_2 - V_1}{Q \ln \frac{A_1}{A_2}}.$$

When $T_2 < 0.01$ sec, for which a too small volume V is required, we may, by using only one of the oscillating fields, determine T_2 from the dependence of the nutation signal amplitude on the rate of liquid flow[5].

"V. N. Obraztsov" Leningrad Railroad Engineers Institute

References

1. N. Blombergen, E. M. Purcell & R. V. Pound, Phys. Rev., 73, 679 (1948).
2. Gabillard, Rev. Sci. Inst., No. 5 (1952).
3. H. C. Torrey, Phys. Rev., 76, 1059 (1949).
4. E. L. Hahn, Phys. Rev., 80, 580 (1950).
5. A. I. Zhernovoi, Iu. S. Egorev & G. D. Latyshev, PTE (Instruments and experimental techniques, No. 5 (1958).

LEVEL SHIFTS AND THE PROBABILITIES OF CORRESPONDING β- AND γ-TRANSITIONS IN ODD NUCLEI

- V.S.Shpinel'

The independent-particle model provides a qualitative explanation of many properties of low-lying nuclear levels. Quantitative explanations have thus far not been derived, except in the case of strongly deformed nuclei which can be described by the unified nuclear model.

New empirical relations are required for the purpose of making the shell model more exact. The present paper presents a systematics and analysis of experimental data pertaining to excited states of odd-A nuclei adjacent to nuclei with closed shells. Similar discussions can be found in Refs.1-4.

In the light of the independent-particle model, we may expect nuclei with identical numbers of odd particles outside the closed shell to have similar level schemes. Such nuclei with the same number of odd particles may contain either an even number of neutrons or an even number of protons. At present we already know of many such nuclei in which the predicted levels and sequences of levels have been observed. The separations and properties of corresponding levels will vary with the number of pairs in the even nucleon group. It is of interest to determine the character of such variations.

Level Shifts

The experimentally observed level shift which is associated with the addition of a particle to the nucleus can be interpreted with the aid of the following model. Let us first consider two nuclei in which the odd group contains the same number of neutrons, while the even number of protons differs by a single proton pair in the state j_p, with resultant total spin $I_p = 0$. In the general case, this pair of particles will interact with the odd particle group and with the remaining particles. The interaction energy will depend on the states of the given proton pair and of the other particles. Interactions with particles whose states are identical for different nuclear levels can only induce a common shift of the entire spectrum, i.e., an equal shift of all levels. It is evident that only interactions with the odd neutron group, which has different states for different excited levels, can induce relative level shifts.

Let us consider the separation of two levels in a nucleus (Z,N) and the separation of the corresponding levels in a nucleus (Z + 2,N), where Z is an even number of protons. In view of the foregoing, the energy $E_{j_n}(Z+2,N)$ of a state with a given value of j_n in the nucleus (Z + 2,N) can be expressed in terms of the corresponding energy level $E_{j_n}(Z, N)$ in nucleus (Z, N) and the interaction energy as follows:

$$E_j(Z+2,N) = E_j(Z,N) + H_{j_p^2}(Z,N) + V_{jj_p^2}(Z,N), \qquad (1)$$

where $H_{j_p^2}(Z,N)$ is the interaction energy of the proton pair and the core, and $V_{jj_p^2}(Z,N)$ is the interaction energy of an odd neutron in the j_n state with a proton pair in state j_p. The separation of the j and j' levels in the (Z + 2,N) nucleus is given by

$$E_j(Z+2,N) - E_{j'}(Z+2,N) = \Delta_{jj'}(Z+2,N) = \Delta_{jj'}(Z,N) + \Delta V_{jj',j_p^2}(Z,N). \qquad (2)$$

It is thus evident that the relative level shift in our approximation is given by the difference between the interaction energies -

$$\Delta V_{jj',j_p}(Z,N) = V_{j,j_p}(Z,N) - V_{j',j_p}(Z,N) \qquad (3)$$

- in states j and j'. If n proton pairs are added at the j_p level to the (Z,N) nucleus, the general expression for the jj' level separation is

$$\Delta_{jj'}(Z+2n,N) = \Delta_{jj'}(Z,N) + n\Delta V_{jj',j_p}(Z,N) + \sum_{n=1}^{2(n-1)} [\Delta V_{jj',j_p}(Z+2(n-1),N) - \Delta V_{jj',j_p}(Z,N)]. \qquad (4)$$

Eq.(4) contains a sum of terms for the variation of $\Delta V_{jj',j_p}$ with Z because the interaction between an odd particle and a proton pair may depend on the number of protons in the core. If this dependence is neglected, the relative level shift will be given only by the second term in (4), which is proportional to n. In this case the plot of level separation as a function of the even number of particles in the same j_p state would be a straight line; this relation will hereinafter be called the level shift curve. With changing j_p - the level of the last proton pair - the level shift curve will show a bend which is associated with the dependence of $\Delta V_{jj',j_p}$ on j_p.

Similar considerations apply to cases of odd Z and even N, i.e., to isotopes differing by an even number of neutrons.

Figs.1-6 are level shift curves plotted by us on the basis of data in the literature[5]. Fig.1 gives the curve for the proton level separation $g_{9/2} - p_{1/2}$ as a function of the even number of neutrons. The number of protons is indicated for each curve pertaining to a different isotope. The level of the last neutron pair according to the Mayer scheme is shown below the numerals denoting the even

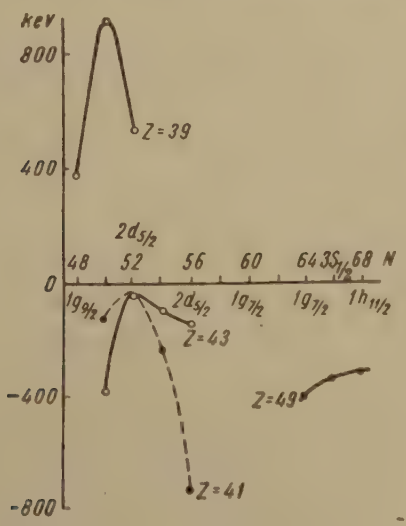

Fig.1

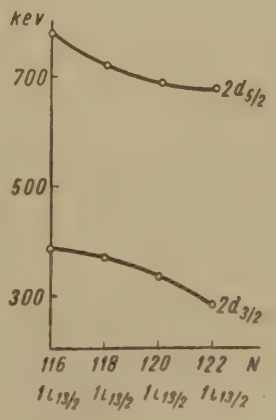

Fig.2

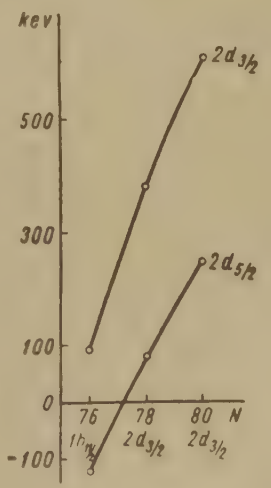

Fig.3

Fig.1. $g_{9/2} - p_{1/2}$ proton level separation in isotopes with odd Z as a function of the even number N of neutrons ("level shift curves"). The number of protons Z is indicated for each curve. The indicated neutron level sequence is based on the Mayer scheme.

Fig.2. Level shift curve for the proton level sequence $3s_{1/2} - 2d_{3/2} - 2d_{5/2}$ in Tl isotopes (Z = 81).

Fig.3. Level shift curve for the proton level sequence $1g_{9/2} - 2d_{3/2} - 2d_{5/2}$ in Cs isotopes (Z = 55).

number of neutrons. A similar figure is given in Ref.2, in which it is assumed that the $g_{9/2} - p_{1/2}$ level pair in Nb^{91} is inverted by comparison with the corresponding levels of the other niobium isotopes and that the ground state of Tc^{97} is $g_{9/2}$. This figure does not include Tc^{93}, which was investigated later. The given assumptions serve the purpose of obtaining a maximum at N = 50 in the curves for niobium (Z = 41) and technetium (Z = 43). When we also consider the point for Tc^{93} and the order of levels obtained in the studies of Refs.6 & 7, the maximum for niobium isotopes is found at N = 52, and for technetium isotopes at N = 52 (as shown in Fig.1), or at N = 54 if the ground level of Tc^{97} is assumed to be $p_{1/2}$. Figs.2 & 3 contain the curves for successive $3s_{1/2} - 2d_{3/2} - 2d_{5/2}$ levels in Tl isotopes and the successive $1g_{7/2} - 2d_{3/2} - 2d_{5/2}$ levels in Cs isotopes, respectively.

In all instances the experimental points lie on curves rather than on straight lines. There is a natural bend at N = 50 for yttrium isotopes (Z = 39), since the last neutron pair in Y^{89} is on the $1g_{9/2}$ level and completes the filling of the 50-neutron shell, while in Y^{91} the last neutron pair, which is on the $2d_{5/2}$ level, begins to fill a new shell. For the same reason , we might expect a maximum at N = 50 for Nb and Tc isotopes, but this is not observed. The different positions of the maxima in these curves are evidently associated with different orders of filling of the $2d_{5/2}$ and $1g_{7/2}$ neutron levels, regarding which orders we still have no direct information. The level shift curve for In isotopes shows the same slight curvature as the curves for Tl and Cs isotopes. In thallium isotopes the last neutron pair is on the $1i_{13/2}$ level and for cesium isotopes on the $2d_{5/2}$ level. The smoothness of the curve for In isotopes indicates that the order of filling of neutron levels here differs from that shown on the basis of the Mayer scheme in Fig.1. In In^{115} and In^{117} the last neutron pair evidently fills the same level, which is most likely $1h_{11/2}$.

The shifts of neutron levels as a function of an even number of protons, which are shown in Figs.4-6, are similar in character. The curves for the $g_{9/2} - p_{1/2}$ neutron level separation in N = 49 isotones (4) shows slight bending at Z = 38 and 40, corresponding to the filling of the $1f_{5/2}$ and $2p_{1/2}$ proton levels.

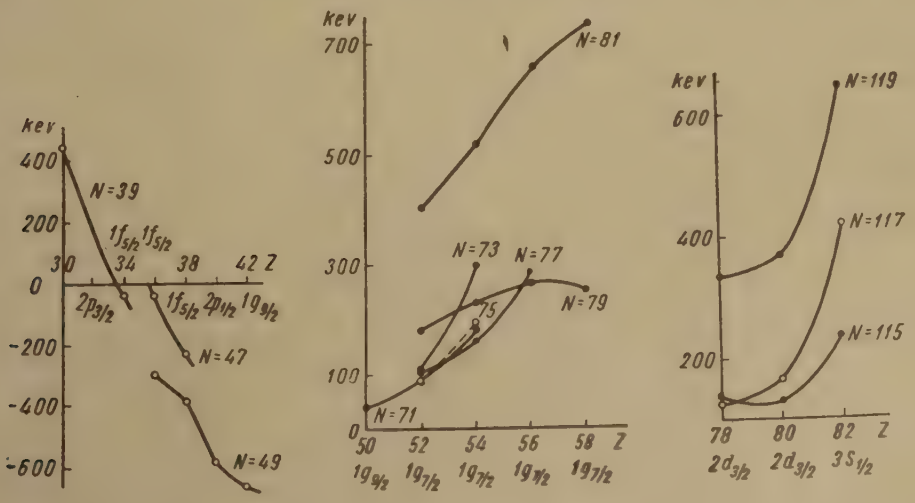

Fig.4. $g_{9/2} - p_{1/2}$ neutron level shifts in isotones with odd N.
Fig.5. $1h_{11/2} - 2d_{5/2}$ neutron level shifts in isotones with odd N.
Fig.6. $1i_{13/2} - 2f_{5/2}$ neutron level shifts in isotones with odd N.

Unfortunately, we have only two points on this curve for N = 39 and 47, so that we do not know the shape of the corresponding curves and only infer that the observed shifts represent a common tendency.

The level shift curves for the $1h_{11/2}$ and $2d_{3/2}$ levels in isotones with N = = 71, 73, 75, 77, 79 and 81 and for the $1i_{13/2} - 2f_{7/2}$ separation in isotones with N = 115, 117 and 119, which are shown in Figs.5 and 6, also exhibit curvature. A sharp rise is observed for the $1i_{13/2} - 2f_{7/2}$ shift as we go from Z = 80 to Z = = 82, when the $2d_{5/2}$ levels have already been filled and the last neutron pair enters the $3s_{1/2}$ level to fill the 82-proton shell.

Figs.1-6 can be summarized as follows. The level shifts are represented by slightly bent curves which vary according to the level that is filled with an even number of particles. This property can be used to elucidate the order of filling of nuclear levels. The given facts indicate, first of all, that the independent-particle model furnishes a very reasonable approximation even for such fine details as level shifts. As has already been mentioned, the deviation of the curves from straight lines can be attributed to the fact that the interaction energy of an odd particle and a proton pair varies with the number of particles in the core. In other words, this interaction energy generally depends on the potential well containing the interacting particles, i.e.,

$$\left.\begin{aligned} V_{j,j_{p^2}}(Z, N) &\neq V_{j,j_{p^2}}(Z+2, N) \\ V_{j,j_{n^2}}(Z, N) &\neq V_{j,j_{n^2}}(Z, N+2) \end{aligned}\right\} \quad (6)$$

and

Gamma-transition probabilities

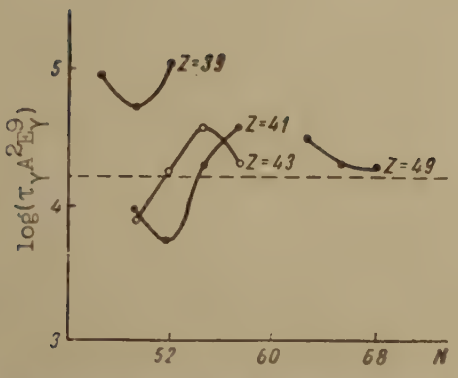

Fig.7. Reduced probabilities of M4 transitions in odd isotopes as a function of even numbers of neutrons. The proton number Z is indicated at each curve. The dashed line represents the theoretical value for a single-particle proton transition.

Single-particle states can no longer be used when a different kind of interaction is involved. The departures from pure one-particle wave functions will affect the γ-transition probabilities and, if, as we can infer from the level shift curves, these departures vary smoothly from nucleus to nucleus, the γ-transition matrix elements for these nuclei will also vary smoothly. The variation of the γ-transition matrix elements for the nuclei represented by the level shift curves can be traced mainly in the case of M4 transitions, for which we have the required experimental lifetimes. The reduced probabilities, log $(\tau_\gamma A^2 E_\gamma^9)$, of M4 transitions for the given nuclei are plotted in Figs.7 & 8 as a function of even numbers of neutrons and protons. Dependence on the nuclear energy and radius is excluded. In these figures the horizontal dashed line represents the theoretical value of the reduced probability, which was calculated by means of the Weisskopf formula.

It is evident from the figures that the expected smooth experimental curves are obtained whenever the corresponding level shift curves are smooth. The bending of the curves for Y, Nb and Tc isotopes can evidently be correlated with the aforementioned maxima in the level shift curves. It must be noted, however, that the experimental points for Nb and Tc isotopes in Figs.1 and 7 are not

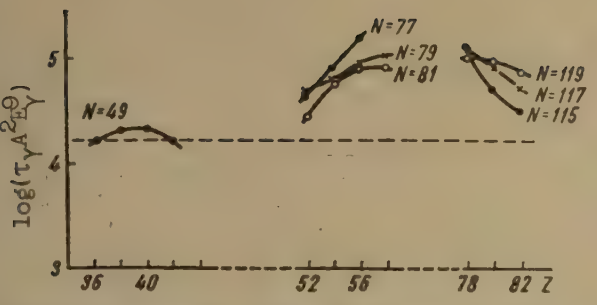

Fig.8. Reduced probabilities of M4 transitions in odd isotones as a function of even Z.

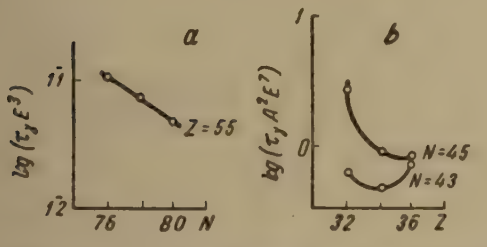

Fig. 9. a - Reduced probabilities of M1 transitions in Cs isotopes as a function of even N; b - reduced probabilities of E3 transitions in isotones with odd N (indicated on the curve) as a function of even Z.

entirely reliable, so that the inflection points are not absolutely certain. We may expect that more exact data will improve the correlation between the level shift curves and the corresponding γ-transition curves.

We have only meager information concerning the lifetimes for other γ-transitions between the levels represented in the level shift curves. Fig. 9 shows the reduced probabilities of M1 transitions in Cs isotopes as a function of the even number of neutrons, and the reduced probabilities of E3 transitions in N = 43 and 45 isotones as a function of the even number of protons. Unfortunately, each of these curves is based on only three points, but the arrangement of the points suggests that there do obtain definite regularities.

While the matrix elements for some multipoles fluctuate considerably for different nuclei, we know that the fluctuation for M4 transitions is relatively minor. The dependence of reduced probabilities for M4 transitions on the number of particles in the nucleus, which we have noted (see also Ref.3), throws light on the nature of these fluctuations.

Beta-transition probabilities

Smooth variations of the wave functions associated with the states of the given nuclei must also affect the probabilities of β-transitions, which depend on the initial-state wave function in the original nucleus and the final wave function in the terminal nucleus. For initial nuclei with the same number of odd-group nucleons, the odd number of particles in the final nuclei will differ by 2, 4,... particles and, conversely, for final nuclei with the same number of odd-group particles, the number in the initial nuclei will not be the same. We cannot find data on enough nuclei to provide a comparison of the matrix elements for "corresponding" β-transitions. The majority of our examples show two (or more seldom three) β-transitions. The curves in Fig.10 for log ft (for corresponding β-transitions) as a function of even N show that in most instances the probabilities of corresponding β-transitions vary smoothly and not very strongly, although each curve has been plotted through only two or three points.

However, the $Zr^{97} \rightarrow Nb^{97}$ β-transition probability differs considerably from the other two corresponding β-transitions, $Zr^{95} \rightarrow Nb^{95}$ and $Zr^{93} \rightarrow Nb^{93}$. This difference can be associated with the way in which the neutron levels with N = = 56 are filled. A similar sharp distinction is observed for the $I^{135} \rightarrow Xe^{135}$ β-transition compared with $I^{131} \rightarrow Xe^{131}$ and $I^{133} \rightarrow Xe^{133}$ β-transitions (7/2+→ →11/2- transitions). We note that in these iodine isotopes the number of neutrons varies from 78 to 82 and that, as shown above, this variation is accompanied by a variation of the level shift curves (Fig.6).

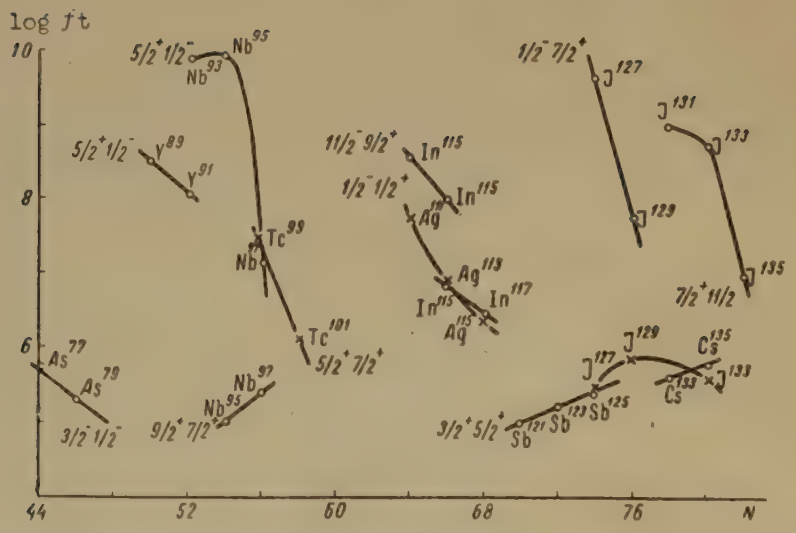

Fig.10. Log ft for β-transitions as a function of even N.

Scientific Research Institute for Nuclear Physics,
at Moscow State University

References

1. V.S.Shpinel', Zhur.eksp.i teor.fiz., 24, 90 (1953).
2. M.Goldhaber & R.D.Hill, Rev.Mod.Phys., 24, 179 (1952).
3. E.P.Mazets & L.I.Rusinov, Doklady AN SSSR, 101, 253 (1955).
4. N.Zeldes, Nucl.Phys., 2, 1 (1956-57).
5. B.S.Dzhelepov & L.K.Peker, Skhemi raspada radioaktivnykh izotopov (Decay schemes for radioactive isotopes). M.-L., 1957.
6. R.W.Hayward, D.D.Hoppes & H.Ernst, Phys.Rev., 98, 231 (1955).
7. C.Levi & L.Papineau, Compt.Rend., 238, 2313 (1954).

COMMERCIAL PHOTOMULTIPLIER WITH IMPROVED TIME RESOLUTION AND LARGER OUTPUT CURRENT

- A.G.Berkovskii, L.G.Leiteizen & V.G.Pol'skii

A report[1] presented at our previous conference gave some preliminary data on a new 13-stage FEU-33 photomultiplier tube designed specifically for investigation of nuclear processes separated by extermely short time intervals. The following results have been obtained in more recent tests of the FEU-33 tube.

1. Static parameters

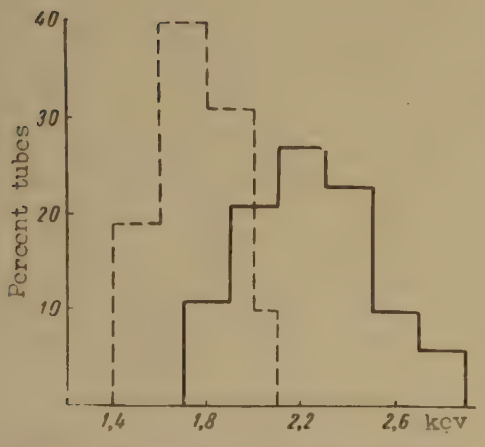

Fig.1. Sensitivity distribution in batch of 124 FEU-33 tubes: applied voltages for sensitivities of 100 amp/lumen (solid line) and 1000 amp/lumen (dashed line).

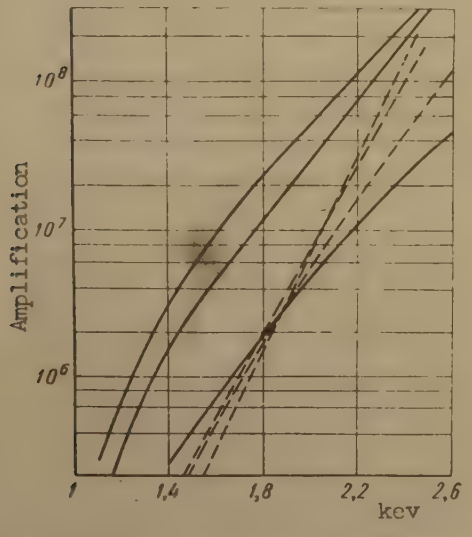

Fig.2. Amplification of FEU-33 (solid curves) and RCA-6810 (dashed curves) as a function of supply voltage.

According to the technical specifications, the integral sensitivity of the FEU-33 cathode, like that of the FEU-29 cathode, must be at least 30 μamp/lumen. The average integral cathode sensitivity of photomultipliers manufactured during the past two months was found to be 40 μamp/lumen. The integral photomultiplier sensitivity is gaged by measuring the voltage required to produce sensitivities of 100 and 1000 amp/lumen, which values correspond approximately to current amplifications of $3 \cdot 10^6$ and $3 \cdot 10^7$. The total voltage was divided equally between the sections of the voltage divider. According to the technical specifications, the voltages corresponding to these amplifications should not exceed 2100 and 2900 v, respectively. Fig.1 shows how 124 FEU-23 samples were distributed with respect to supply voltage for sensitivities of 100 and 1000 amp/lumen. We note that the 100 amp/lumen sensitivity is reached at 1700 v on the average and 1000 amp/lumen at 2200 v on the average.

The solid curves in Fig.2 show the amplification as a function of the supply voltage for three FEU-33 tubes. The dashed lines in the same figure pertain to three RCA-6810 14-stage photomultipliers developed in recent years for the same purposes as the FEU-33. A comparison shows that the FEU-33 provides higher amplification than the RCA-6810 below 2000 v and practically the same amplification at higher voltages. This is accounted for by the fact that below 150-200 v cesium-antimony emitters exhibit higher secondary emission than alloy emitters.

With increasing voltage the secondary emission of the alloy rises more rapidly. The same effect is observed when we compare amplification in FEU-29 (with cesium-antimony emitters) and FEU of the same design with alloy-type emitters.

2. Pulse-height resolution and noise

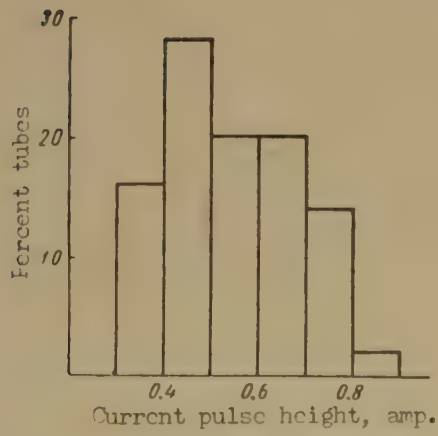

Fig.3. FEU-33 distribution with respect to pulse heights. (Supply voltage - 2800-3200 v.)

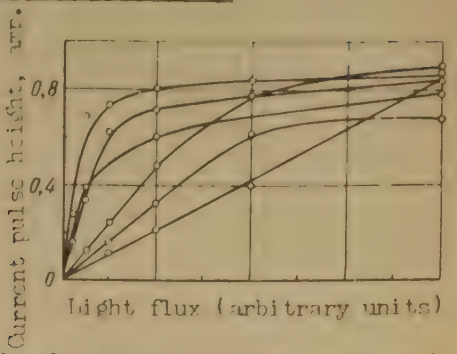

Fig.4. FEU-33 current linearity characteristics.

According to test results the FEU-33 tube is practically as good as other types with respect to pulse-height resolution. In work with a NaI(Tl) crystal and Cs^{137} the relative line half-width for the great majority of tested tubes was in the range from 8.5 to 11%. The noise level was of the order 3-4 kev at a counting rate of 50 pulses per second (Cs^{137} & NaI(Tl) combination).

FEU-33 current pulses were measured with the cathodes exposed to 10^{-9} sec light flashes (sparks) at the rate of a few thousand per second. The luminous flux was sufficient to produce space charge limited pulses. The standard divider with an overall average supply voltage of 3 kv was used in the tests.

Fig.3 shows the current pulse height distribution of 50 FEU-33 tubes. The minimum current was 0.3 amp and the maximum 1 amp. Pulsed currents above 1 amp could be obtained from individual photomultiplier tubes by using a matched special voltage divider.

An investigation of the output current characteristics at an overall voltage of the order 4 kv, of which 1.5 kv was applied between the last emitter and the anode, revealed that the FEU-33 are linear on the average up to 0.5 amp, with values of from 0.4 to 0.8 amp for individual tubes (Fig.4).

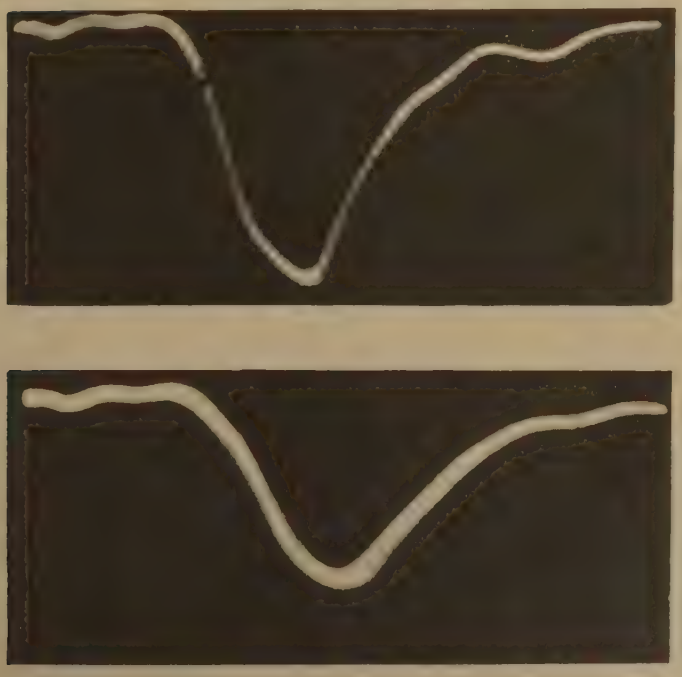

Fig.5. FEU-33 pulse oscillograms.

3. Time characteristics

In a coincidence set-up of two FEU-33 tubes with one crystal and one Co^{60} source, the half-width of coincidence curve fluctu-

ates from 2 to 4 mμ sec (at 50% counting efficiency).

FEU pulse shapes were observed in our laboratory by means of a high-speed oscilloscope. The light source was the same spark discharge as was used for current pulse measurements. Two photographs of anode pulses are shown in Fig. 5. Analysis of the oscillograms showed that the pulse rise times were approximately 2.5-3 mμ sec and the total pulse durations little longer than 10 mμsec. Pulse shape and the appearance of a substantial rise on the trailing edge depend on the voltage division, i.e., the after pulse can be minimized through appropriate modification of the voltage divider.

Reference

1. L.G.Leiteizen, A.G.Berkovskii, I.Ia.Breido, V.M.Glukhovskoi, O.S.Korol'kova & E.I.Tarasova, Izv.AN SSSR, Ser.fiz., 21, 1653 (1957). (Trans.Bulletin 21, No.12, 1639.)

NEW DATA ON COMMERCIAL PHOTOMULTIPLIER TUBES FOR SCINTILLATION SPECTROMETERS

- A.G.Berkovskii, I.Ya.Breido, B.M.Glukhovskoi, O.S.Korol'kova, L.G.Leiteizen and E.I.Tarasova

The principal features of new types of photoelectric multipliers for spectrometers were described[1] at the Seventh All-Union Conference on Nuclear Spectroscopy. The present paper gives new data on previously developed types, which have been put into production, and some information on new tubes developed in 1957.

1. Photomultiplier with 34-mm Diameter Cathode

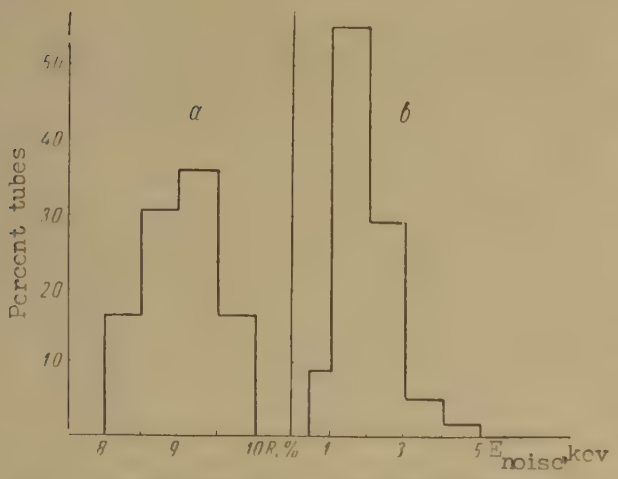

Fig.1. Performance distribution of 500 FEU-29 tubes with a standard voltage division: a - pulse-height resolution with NaI(Tl) and Cs^{137}; b - noise.

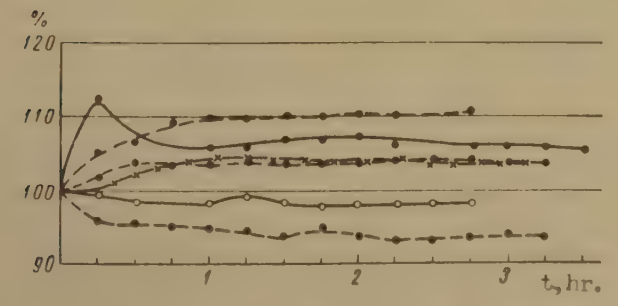

Fig.2. Variation with time of FEU-29 photopeak for several different tubes.

In 1957 a large number of the FEU-29 - the principal spectrometric type - was produced.

Extensive tests were run to determine a standard voltage distribution for the first stages to insure a good pulse-height resolution. The results for 500 photomultipliers manufactured in December 1957 and tested with the standard Cs^{137} - NaI(Tl) combination are shown in Fig.1a. The noise level, measured at 50 pulses per sec with a band width of a 3 Mc/sec, is shown in Fig.1b. Most tubes have a noise level below 3 kev noise and more than half of them below 2 kev.

These data fully refute Khlebnikov's claim[2] that it is inadvisable to combine this multiplier system with an end-window cathode in designing spectrometric photomultipliers.

Fig.2 shows the variation with time of the photopeak from Cs^{137}, measured for a few samples of FEU-29, by means of a single-channel discriminator at $n = 2000$ pulses/sec and pulse height of 4 v. For most of the tubes the measured photopeak variation lies within the usual limits of experimental error after the initial "stabilizing period". The data show that, contrary to Khlebnikov's assertion, at normal loads cesium-antimony emitters are no less stable than alloy emitters. Our earlier measurements[3] of photomultiplier stability at a mean output current of 100 μamp also showed that the emitter material is a minor factor where stability is concerned.

In order to test the possibility of producing spectrometric photomultipliers with higher resolution, we experimented with multiple-alkali cathodes. Small lots of FEU-29 tubes were produced with Sb-Na-K and Sb-Na-Cs cathodes and AMGK(Al-Mg) alloy emitters. The amplification with the Sb-Na-K-Cs cathode was the same as with the usual Sb-Cs cathode and alloy-type emitters. Photomultipliers with

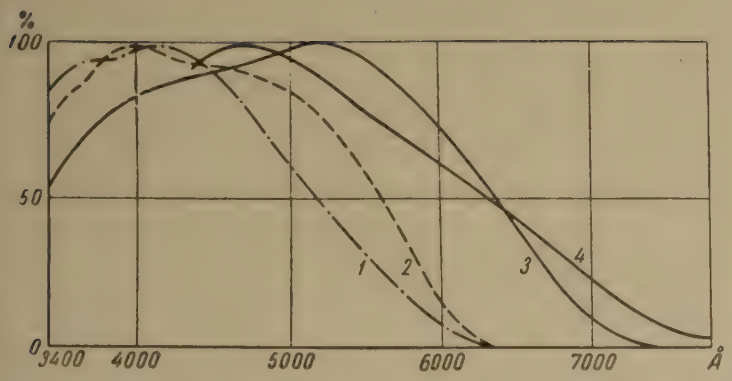

Fig.3. Spectral characteristics of FEU-29 type tubes with different semitransparent photocathodes: 1) Sb-Na-K, 2) Sb-Cs, 3) Bi-Ag-Cs, 4) Sb-Na-K-Cs.

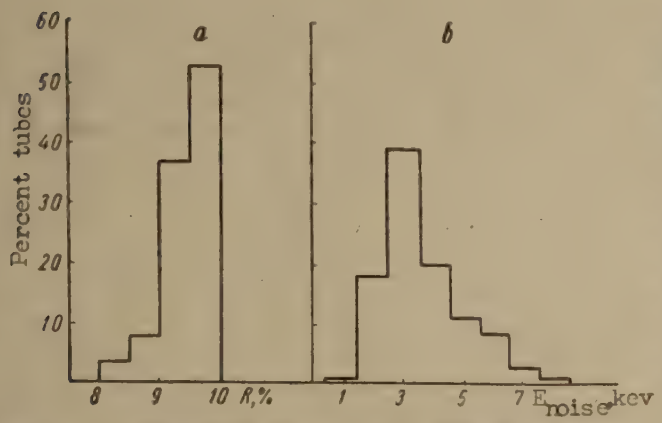

Fig.4. Performance of 250 samples of FEU-24 tubes: a) distribution of pulse heights from Cs^{137} (measured with 30 mm diameter NaI(Tl) crystal at center of cathode); b) noise.

Optimum "standard" stage voltages for FEU-24

Cathode-ring	0.2
Ring-annulus	2.8
Annulus-E_1	1.0
E_1 - E_2	2.5
E_2 - E_3 thru E_{10} - E_{11} (per stage)	1.0
E_{11} - E_{12}	2.0
E_{12} - E_{13}	2.0

cathodes without Cs required voltages about 15-20% higher to produce the same amplification.

The spectral characteristics of these cathodes are shown in Fig.3. The photomultipliers had the following sensitivities: Sb-Na-K - 20-30 μamp/lumen ("blue" - 4-7.5 μamp/lumen), Sb-Na-K-Cs - 80-120 μamp/lumen ("blue" - 8.5-18 μamp/lumen). The best samples exhibited a pulse-height resolution of 8%.

2. Photomultiplier with 75-mm Diameter Cathode

During the past year large-scale production of FEU-24 was begun. The general design data[1] on this tube were given at the Seventh Conference. Fig.4 shows the distribution of relative half-widths (resolution) for 250 samples of FEU-24, from measurements at 3 points of the cathodes, using a 30 mm diameter NaI(Tl) crystal. The measurements were made with the best relative voltages on the first four stages determined individually for each tube. The noise level distribution is shown in Fig.4b.

Tests were run to determine a standard voltage supply. The table gives the optimum "standard" voltage division between stages in relative units. Tests showed that the pulse-height resolution of some of the photomultipliers with the standard potential distribution was reduced by a few percent compared with the optimum with individually selected voltage distributions. The most critical voltage is that on the first section, because of some scatter in the geometry and changes in fabricating conditions. We tested the feasibility of using toroidal dynodes of Al-Mg alloy in tubes of this type. Ten samples prepared with such dynodes showed spectrometric resolution identical with that of the standard FEU-24, but it was found that for these tubes the cathode-ring voltage difference is not critical. Fig.5 compares data on the stability of the toroidal dynode photomultiplier and the

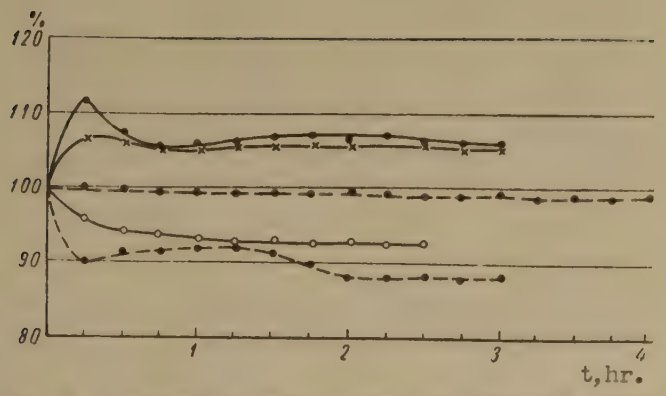

Fig.5. Variation with time of FEU-24 photopeak: solid lines - conventional design; dashed lines - with toroidal dynodes.

conventional FEU-24. The results obtained with the special samples were encouraging and the design studies are being continued.

3. New photomultiplier types

Small tube

A new small spectrometric photomultiplier has the following specifications: cathode diameter - 25 mm, maximum base diameter - 34.5 mm, length - 110 mm. All electrodes are brought out through the base, which facilitates shielding the tube in operation.

This photomultiplier was designed for use with a high-resistance divider; the resistance of the insulation between its electrodes is at least 10^9 ohm. The spectrometric resolution was tested with two qualitatively different NaI(Tl) crystals of 20 mm diameter (R_1) and 14-mm diameter (R_2). Results obtained for a batch of the new tube are given in the table. To allow comparison of the crystal quality, we also give the results of measurements with these crystals on an FEU-29 tube which with a 30-mm diameter crystal gave a resolution R = 8%.

FEU No.	FEU-29	3	6	14	18	30	38	52	50	28	29
R_1	10	10	10	9,5	11,5	10,5	10	10,5	9,5	11,5	12
R_2	7,5	7,5	7,5	7	9	8	7,5	8	7,0	9	9

It will be seen that the resolution of these small photomultipliers is of the same order as that of the FEU-29.

Miniature tube

The main specifications of FEU-31 have been given elsewhere[3]. The spectrometric resolution of ten samples of FEU-31 with a 14-mm diameter crystal was 8.5-11%, obtained with an individual voltage distribution selected for each tube.

Photomultiplier with 300-mm diameter cathode

A tube with large cathode diameter has been developed for work with liquid and plastic scintillators. Its principal features are a cesium-antimony cathode with a sensitivity of at least 20 μamp/lumen. The photomultiplier sensitivity with 2400 v overall voltage is at least 10 amp/lumen. Toroidal dynodes of AMGK (Al-Mg) alloy are used in this tube.

Tube with a Bi-Ag-Cs cathode

Bismuth-silver-cesium type cathodes are advantageous for work with scintillators which emit in the red portion of the spectrum and also at low temperatures. A small photomultiplier incorporating this cathode has been developed at the plant and is being put into production. The specifications have been given

elsewhere[3]. These photomultipliers provide good amplification; their average sensitivity at an overall voltage V = 1000 v is 1 amp/lumen; at 1350 v it is 10 amp/lumen and at 1800 v it is 100 amp/lumen.

The pulse-height resolution of 10 samples tested with a Cs^{137} source and a 20 mm diameter NaI(Tl) crystal varied between 12 and 14%.

References

1. L.G.Leiteizen, A.G.Berkovskii, I.Ia.Breido, V.M.Glukhovskoi, O.S.Korol'-kova & E.I.Tarasova, Izv.AN SSSR, Ser.fiz., 21, 1653 (1957). (Trans.Bulletin 21, No.12, 1639.)

2. N.S.Khlebnikov, Izv.AN SSSR, Ser.fiz., 22, 70 (1958). (Trans.Bulletin 22, No.1, 67.)

3. L.G.Leiteizen, A.G.Berkovskii, B.M.Glukhoskoi, O.S.Korol'kova & E.I. Tarasova, Izv.AN SSSR, Ser.fiz., 22, 513 (1958). (Trans.Bulletin, 22, No.5, 516.)

Λ-NUCLEON FORCES AND THE Λ PARTICLE BINDING ENERGY IN HYPERNUCLEI

- V. I. Filimonov

Let us assume that the interaction of baryons with the π and K meson fields is of the form

$$H = Gi\sum_{i=1}^{3}\int(\bar{N}\tau_i N\pi_i + \bar{\Lambda}\gamma_5\Sigma_i\pi_i + \bar{\Sigma}_i\gamma_5\bar{\Sigma}_i\gamma_5\Lambda\pi_i)\,d\tau +$$

$$+ G\left\{i\int\left[\sum_{i=1}^{3}(\bar{N}\tau_i K^*\gamma_5\Sigma_i) + \bar{N}K^*\gamma_5\Lambda + \bar{\Lambda}K^*\gamma_5\Xi\right]d\tau + \text{Hermitian conjugate}\right\}, \qquad (1)$$

as proposed by d'Espagnat and Prentki[1], and let us use this expression to calculate the Λ-nucleon forces.

Performing the Nelson-Dyson transformation for the case of baryons at rest at points and maintaining only terms linear in the coupling constant in the transformed Hamiltonian, we obtain

$$H = G\frac{i}{2^{3/2}}\sum_{n=1}^{N}\sum_{k}\sum_{i=1}^{3}v(k)(\vec{\sigma}_n\mathbf{k})\,T_i^{(\pi)_n}\hat{a}^n\sqrt{\frac{1}{2\omega\pi}}\,(a_{ik} + a^*_{i,-k})e^{i\mathbf{k}\mathbf{x}_n} +$$

$$+ G\left\{\frac{i}{2^{3/2}}\sum_{n=1}^{N}\sum_{k}\sum_{i=1}^{2}v(k)(\vec{\sigma}_n\mathbf{k})\,T_i^{(K)_n}\hat{a}^n\sqrt{\frac{1}{2\omega^K}}\,(c_{ik} + b^*_{ik})\,e^{i\mathbf{k}\mathbf{x}_n} + \text{Hermitian conjugate}\right\}, \qquad (2)$$

where a_i, c_i, b_i and a_i^*, c_i^*, b_i^* are annihilation and creation operators for π_i, K_i and $\bar{K}_i$ mesons, respectively, $\hat{a}$ is a diagonal matrix whose elements are the inverses of the baryon masses,

$$\omega^\pi = \sqrt{\mu_\pi^2 + k^2} \quad \text{and} \quad \omega^K = \sqrt{\mu_K^2 + k^2}. \qquad (3)$$

In the Hamiltonian of (2) we have introduced the virtual meson momentum cutoff function $v(k)$. Further, N is the number of baryons in our system, and $T_i^{(K)}$ and $T_i^{(\pi)}$ are eight-dimensional matrices which describe the transformation of baryons into each other with emission and absorption of pions and K mesons according to the interaction given in (1).

The Hamiltonian of (2) can be used to calculate those forces between the particle and nucleon which are caused by the exchange of two pions ($V^{2\pi}$), one K meson (V^{1K}), a pion and a K meson ($V^{K\pi}$) and two K mesons (V^{2K}). We calculate the Λ-nucleon forces in the same way as Gartenhaus[2] calculates nucleon-nucleon forces. We then obtain the following expressions for the interaction potentials:

$$V^{2\pi} = -G^4\,\frac{3}{16\,(2\pi)^6 M_\Lambda^2 M_n^2}\int\left\{\frac{(\mathbf{k}_1\mathbf{k}_2)^2}{\omega_1^{(\pi)3}\omega_2^{(\pi)2}} + \frac{\vec{\sigma}_1[\mathbf{k}_1\mathbf{k}_2]\,\vec{\sigma}_2[\mathbf{k}_1\mathbf{k}_2]}{\omega_1^{(\pi)3}(\omega_1^{(\pi)} + \omega_2^{(\pi)})\,\omega_2^{(\pi)}}\right\}\times$$

$$\times v^2(k_1)\,v^2(k_2)\,e^{i(\mathbf{k}_1+\mathbf{k}_2)(\mathbf{x}_1-\mathbf{x}_2)}\,(d\mathbf{k}_1)\,(d\mathbf{k}_2); \qquad (4)$$

$$V^{1K} = -\frac{G^2}{4(2\pi)^3 M_\Lambda M_n}(\lambda_1\lambda_2^* + \lambda_2^*\lambda_1)\int(\vec{\sigma}_1\mathbf{k})(\vec{\sigma}_2\mathbf{k})\,\frac{v^2(k)}{\omega^{(K)2}}\,e^{i\mathbf{k}(\mathbf{x}_1-\mathbf{x}_2)}\,(d\mathbf{k}); \qquad (5)$$

$$V^{K\pi} = -\frac{G^4\cdot 3}{16\,(2\pi)^6 M_\Lambda^2 M_n^2}(\lambda_1\lambda_2^* + \lambda_2\lambda_1^*)\int\left\{(\mathbf{k}_1\mathbf{k}_2)^2\left[\frac{1}{\omega_1^{(K)3}\omega_2^{(\pi)2}} + \frac{1}{\omega_1^{(K)2}\omega_2^{(\pi)3}}\right] +\right.$$

$$\left. + \vec{\sigma}_1[\mathbf{k}_1\mathbf{k}_2]\,\vec{\sigma}_2[\mathbf{k}_1\mathbf{k}_2]\left[\frac{1}{\omega_2^{(\pi)3}(\omega_2^{(\pi)} + \omega_1^{(K)})\,\omega_1^{(K)}} + \frac{1}{\omega_1^{(K)3}(\omega_1^{(K)} + \omega_2^{(\pi)})\,\omega_2^{(\pi)}}\right]\right\}\times$$

$$\times v^2(k_1)\,v^2(k_2)\,e^{i(\mathbf{k}_1+\mathbf{k}_2)(\mathbf{x}_1-\mathbf{x}_2)}\,(d\mathbf{k}_1)\,(d\mathbf{k}_2); \qquad (6)$$

$$V^{2K} = -\frac{G^4}{4(2\pi)^6 M_\Lambda^2 M_n^2}\int\int\left\{\frac{(\mathbf{k}_1\mathbf{k}_2)^2}{\omega_1^{(K)3}\omega_2^{(K)2}} + \frac{\vec{\sigma}_1[\mathbf{k}_1\mathbf{k}_2]\vec{\sigma}_2[\mathbf{k}_1\mathbf{k}_2]}{\omega_1^{(K)3}(\omega_1^{(K)}+\omega_2^{(K)})\omega_2^{(K)}}\right\}$$

$$\times e^{i(\mathbf{k}_1+\mathbf{k}_2)(\mathbf{x}_1-\mathbf{x}_2)} v^2(k_1) v^2(k_2)(d\mathbf{k}_1)(d\mathbf{k}_2) \qquad (7)$$

$$\lambda = \begin{vmatrix} 0 & 1 \\ 0 & 0 \end{vmatrix}; \quad \lambda^* = \begin{vmatrix} 0 & 0 \\ 1 & 0 \end{vmatrix} \qquad (8)$$

The matrices λ and λ^* transform a Λ particle into a nucleon, and vice versa. We treat the Λ particle and nucleon formally as different states of a baryon, describing them by one-row matrices of the type

$$N = \begin{vmatrix} 1 \\ 0 \end{vmatrix}; \quad \Lambda = \begin{vmatrix} 0 \\ 1 \end{vmatrix}. \qquad (9)$$

In order to calculate the binding energy of a Λ particle in a hypernucleus, we shall find the potential energy of interaction between a nucleon of the core nucleus and a Λ particle in the triplet state (energy E_t) and the singlet state (energy E_s). To do this we write down the wave functions of the two particles in the triplet and singlet states, namely,

$$\psi_t = \psi(r_1 r_2)[\Lambda(1)N(2) + \Lambda(2)N(1)]S_s; \qquad (10)$$

$$\psi_s = \psi(r_1 r_2)[\Lambda(1)N(2) - \Lambda(2)N(1)]S_A; \qquad (11)$$

where $\psi(r_1 r_2)$ is a symmetric function of the space coordinates and S_s and S_A are a symmetric and an antisymmetric spin function. The wave functions of (10) and (11) are eigenfunctions of the λ operators of (5) and (6) belonging to the eigenvalues +1 for the singlet state and -1 for the triplet state. Therefore the spin-independent part of the forces described by (6) will give equal but opposite contributions to the potential energies of the singlet and triplet states. This is what causes the potential energy due to the Kπ-forces to be approximately equal to zero in the ${}_\Lambda He^4$ nucleus when its spin is zero.

In performing numerical calculations of the binding energy in light hypernuclei, we chose $\psi(r_1 r_2)$ as the product of the nucleon wave function in the core nucleus and the Λ wave function in the hypernucleus; i.e.,

$$\psi(r_1 r_2) = Ae^{-\frac{\rho_1^2}{4\gamma^2}} A_\Lambda e^{-\frac{\rho_2^2\eta^2}{4\gamma^2}}, \qquad (12)$$

where A and A_Λ are normalizing factors, $\rho_1 = |\mathbf{x}_1|\mu_\pi$, and η is a parameter of variation. The value of γ in (12) was chosen so that the nucleon density in the core nucleus be in agreement with experiments on nuclear Coulomb energies, electron and neutron scattering, etc. Averaging Eqs.(4)-(7) with the aid of (10) and (11), summing over spins, and integrating over the coordinates $\mathbf{x}_1$ and $\mathbf{x}_2$ and over the angles between $\mathbf{k}_1$ and $\mathbf{k}_2$, we obtain the expressions (wherein we write $g^2 = \frac{G^2}{4\pi}$)

$$E^{2\pi} = -g^4 \frac{3m^2}{16\pi^3}\frac{m_\pi c^2}{\gamma_1^6}[F_1^{2\pi}(\gamma_1) + f^{2\pi}F_2^{2\pi}(\gamma_1)]; \qquad (13)$$

$$E^{1K} = g^2 m\nu^3 f^{1K} m_\pi c^2 \frac{1}{\pi}\int_0^{x_m} \frac{x^4 e^{-\gamma_1^2\nu^2x^2}dx}{x^2+1} < f^{1K} g^2 m\nu^3 m_\pi c^2 \frac{1}{\pi}\int_0^{\infty} x^4 e^{-\gamma_1^2\nu^2x^2}dx \approx f^{1K}\frac{0{,}5}{\gamma_1^2\gamma^2}\ \text{Mev} \qquad (14)$$

for the potential energies of the two particles, where

$$\nu = \frac{m_K}{m_\pi} = 3.54, \qquad m = \frac{m_\pi^2}{M_n M_\Lambda} = 0.0186, \quad \gamma_1^2 = \frac{1+\eta^2}{2\eta^2}\gamma^2,$$

m_K is the K meson mass, and f^{1K} is 1/6 for the triplet state and 1/2 for the singlet. In obtaining the last term of (14), we assumed that $g^2 \approx 12$. Further, we obtain

$$E^{K\pi} = -g^4 \frac{3m^2}{8\pi^2}\frac{m_\pi c^2}{\gamma_1^6}\{\pm F_1^{K\pi}(\gamma_1) + f^{K\pi}F_2^{K\pi}(\gamma_1)\}; \qquad (15)$$

where the positive sign is taken for the singlet state and the negative sign for the triplet. Finally,

$$E^{2K} = -g^4 \frac{m^2}{4\pi^2}\frac{m_\pi c^2}{\gamma_1^6}\{F_1^{2K}(\gamma_1) + f^{2K}F_2(\gamma_1)\}, \qquad (16)$$

where $f^{2\pi}$, $f^{K\pi}$ and f^{2K} are constants of the order of unity and take on different values for the singlet and triplet states.

The functions appearing in these expressions are the following:

$$F_1^{2\pi}(\gamma_1) = \int_0^{x_m}\int_0^{x_m} \frac{x_1x_2\varphi(x_1x_2\gamma_1)dx_1dx_2}{(x_1^2+1)^{3/2}(x_2^2+1)}; \qquad (17)$$

$$F_1^{K\pi}(\gamma_1) = \int_0^{x_m}\int_0^{x_m} \frac{1}{2}\left\{\frac{x_1x_2\varphi(x_1x_2\gamma_1)}{(x_1^2+\nu^2)^{3/2}(x_2^2+1)} + \frac{x_1x_2\varphi(x_1x_2\gamma_1)}{(x_2^2+\nu^2)(x_1^2+1)^{3/2}}\right\}dx_1dx_2; \qquad (18)$$

$$F_1^{2K}(\gamma_1) = \int_0^{x_m}\int_0^{x_m} \frac{x_1x_2\varphi(x_1x_2\gamma_1)dx_1dx_2}{(x_1^2+\nu^2)(x_2^2+\nu^2)^{3/2}}; \qquad (19)$$

$$\varphi(x_1x_2\gamma_1) = e^{-\gamma_1^2(x_1-x_2)^2}\left(x_1^2x_2^2\gamma^4 - x_1x_2\gamma_1^2 + \frac{1}{2}\right) - e^{-\gamma_1^2(x_1+x_2)^2}\left(x_1^2x_2^2\gamma^4 + x_1x_2\gamma_1^2 + \frac{1}{2}\right); \qquad (20)$$

where $x = \frac{k}{\mu_\pi}$; $x_m = \frac{k_m}{\mu_\pi}$ and k_m is the cutoff momentum. The F_2 functions are smaller by a factor of about twenty than the F_1 functions and therefore may be ignored. We can also ignore the last term in (20). Then it is seen from (13) and (16) that the potential energy of the 2π and 2K forces is the same in the triplet and singlet states.

Since $\gamma \approx 1$, it is seen from (14) that E^{1K} gives only a small contribution to the potential energy of hypernuclei (of the order of 0.5 Mev, which is about 0.1 of the total potential energy). The potential $E^{K\pi}$ differs significantly for different states. It is negative in the singlet and positive in the triplet state, though its absolute value is about the same for both. We may conclude from this that the singlet is the preferred state for a Λ-nucleon pair, so that in light hypernuclei the lowest energy belongs to states with the greatest number of singlet pairs. In other words, the ground state of a light hypernucleus is that with the lowest spin. In this case the potential energy of the Λ particle in the hypernucleus will be

$$E_p = \frac{3}{2} E_s + \frac{1}{2} E_t \quad \text{for } {}_\Lambda H^3 ;$$
$$E_p = \frac{3}{2} E_s + \frac{3}{2} E_t \quad \text{for } {}_\Lambda H^4, {}_\Lambda He^4 ;$$
$$E_p = E_s + 3E_t \quad \text{for } {}_\Lambda He^5 .$$

The kinetic energy is

$$E_K = \frac{3}{8} \eta^2 \frac{m_\pi}{M'_\Lambda \gamma^2} m_\pi c^2$$

(where M'_Λ is the reduced mass of the particle and the core nucleus).

It is a simple matter to integrate (17)-(19) numerically and find the η-dependence of the energy, thus finding its minimum value, the Λ particle binding energy $B_\Lambda = -E_{min}$. The results of such calculations are presented in the table.

Comparison of theoretical and experimental[3] values of B_Λ

Hyper-nucleus	Spin	γ	η	B_Λ theo., Mev	B_Λ exp., Mev
${}_\Lambda H^3$	1/2	1,0	0,80	0,48	0,25±0,31
${}_\Lambda H^4$, ${}_\Lambda He^4$	0	1,07	0,87	1,53	1,44±0,20 1,70±0,24
${}_\Lambda He^5$	1/2	0,9	0,92	2,30	2,56±0,17

For the purposes of calculation we took $g^2 = 12.3$ and $x_m = 6$. The table indicates satisfactory agreement with experiment, although g^2 must be chosen smaller than the value given by data on nucleon-nucleon forces.

Chair of Statistical Physics and Mechanics,
Physics Faculty, Moscow State University

References

1. B.d'Espagnat & J.Prentki, Nucl. Phys., 1, 38 (1956).
2. S.Gartenhaus, Phys.Rev., 100, 900 (1955).
3. C.Franzinetti & G.Morpurgo, Suppl.Nuovo Cim., 6, 794 (1957).

Bulletin of the Academy of Sciences of the USSR - Physical Series
Vol. 22, No. 8 - August 1958

Transactions of the Eighth All-Union Conference on Nuclear Spectroscopy
(Continued from Vol.22, Nos. 2 and 7)

TABLE OF CONTENTS

	Page Orig.	Trans.
Ge^{149} conversion electron spectrum - N.M.Anton'eva, A.A.Bashilov, B.S.Dzhelepov & B.K.Preobrazhenskii	895	889
Gd^{147} and Eu^{147} conversion electron spectra - N.M.Anton'eva, A.A.Bashilov, B.S.Dzhelepov & B.K.Preobrazhenskii	906	899
Internal conversion coefficients of some nuclear transitions in Eu^{147} and Eu^{149} - V.K.Adamchuk, A.A.Bashilov & B.K. Preobrazhenskii	919	911
As^{73} conversion electron spectrum - E.P.Grigor'ev, B.S.Dzhelepov, A.V.Zolotavin & V.Ia.Mishin	927	919
Conversion electron spectrum of the cerium fraction (from the spallation product of Ta) - B.S.Dzhelepov, B.K.Preobrazhenskii, I.M.Rogachev & P.A.Tishkin	931	923
Conversion electron spectra of some neutron-deficient Ho and Er isotopes - I.S.Dneprovskii & G.M.Kolesov	935	927
Radiation from Eu^{155} - M.P.Glazunov & B.F.Gulev	941	932
Coincidences of conversion electrons in $Eu^{147} \rightarrow Sm^{147}$ decay - B.S.Dzhelepov, B.K.Preobrazhenskii & V.A.Sergienko	945	936
Coincidences of conversion electrons in $Tm^{167} \rightarrow Er^{167}$ decay - B.S.Dzhelepov, B.K.Preobrazhenskii & V.A.Sergienko	949	940
Tables of functions needed for determining the probability of allowed and forbidden L-capture - I.M.Band, L.N.Zyrianova & Iu.P.Suslov	952	943
Angular distribution of gamma-rays from positron annihilation in liquid hydrogen and helium - A.S.Basina, K.A.Baskova, B.S.Dzhelepov & M.A.Dolgoborodova	968	959
Compensation of the Earth's magnetic field - E.M.Krisiuk & G.D.Latyshev	976	966
Finite size corrections to the Lamb shift - E.V.Teodorovich	985	975
Accuracy of magnetic field measurements by the nutation method - A.I.Zhernovoi, Iu.S.Egorov & G.D.Latyshev	988	978
New technique for measuring the spin-lattice relaxation time of liquids - A.I.Zhernovoi & G.D.Latyshev	993	982
New technique for measuring the spin-spin relaxation time of liquids - A.I.Zhernovoi & G.D.Latyshev	994	983
Level shifts and the probabilities of corresponding β- and γ-transitions in odd nuclei - V.S.Shpinel'	995	984
Commercial photomultiplier with improved time resolution and larger output current - A.G.Berkovskii, L.G.Leiteizen & V.G.Pol'skii	1002	990

New data on commercial photomultiplier tubes for scintillation spectrometers - A.G.Berkovskii, I.Ia.Breido, B.M.Glukhovskoi, O.S.Korol'kova, L.G.Leiteizen & E.I.Tarasova 1005 993

Λ-nucleon forces and Λ particle binding energy in hypernuclei - V.A.Filimonov 1009 997

Translated in 1959 by
Columbia Technical Translations
5 Vermont Ave., White Plains, N.Y.

Number 9 Volume 22 1958

BULLETIN

of the

Academy of Sciences of the USSR

- Physical Series -

(Izvestiia Akademii Nauk SSSR)
(Seriia fizicheskaia)

Reproduction rights reserved

by

Columbia Technical Translations
5 Vermont Avenue
White Plains, New York

Single Issues
$20

Annual Subscription
$215

Transactions

of the

Eleventh All-Union Conference on Theoretical Spectroscopy

(Continued from Vol.22, No.6 - to be continued in No.11)

Lithoprinted in U.S.A.
EDWARDS BROTHERS, INC.
Ann Arbor, Michigan

FREE-ELECTRON MODEL CALCULATIONS OF THE ELECTRIC AND MAGNETIC PROPERTIES OF COMPLEX MOLECULES

- M.N.Adamov, M.G.Veselov & T.K.Rebane

In the simplest version of the free-electron (FE) model one assumes that the π-electrons are free to move along the lines forming the structural network of the chemical bonds. This concept has been used by many authors in calculating the polarizability and diamagnetic susceptibility of π-electrons. Several authors[1-3] made further simplifying assumptions, which, naturally, affected the final results. We succeeded in carrying out precise calculations of the above properties within the framework of the FE model (i.e., without any further assumptions).

1. The polarizability α of atoms and molecules is usually calculated by perturbation theory. The calculations amount essentially to finding the correction to the first approximation for the wave function. The solution of this problem leads to the well known infinite-series dispersion formula for α, namely,

$$\alpha_n(\omega) = 2\sum_k{}' \frac{\omega_{kn}|x_{kn}|^2}{\omega_{kn}^2 - \omega^2}. \qquad (1)$$

We have obtained a finite expression for the correction to the first-approximation wave function, and therefore also the polarizability, in the FE model.* For a single electron in a one-dimensional potential box of length L we obtain

$$\alpha_n(\omega) = \frac{4E_n}{L\omega^4}\left[p_n\frac{(-1)^n - \cos p_n L}{\sin p_n L} + q_n\frac{(-1)^n - \cos q_n L}{\sin q_n L}\right] - \frac{1}{\omega^2}, \qquad (2)^{**}$$

where

$$p_n = \sqrt{2(E_n - \omega)}, \quad q_n = \sqrt{2(E_n + \omega)}, \quad E_n = \frac{\pi^2 n^2}{2L^2}, \quad n = 1, 2, \ldots$$

Accordingly, the static polarizability is

$$\alpha_n(0) = \frac{L^4}{12\pi^4 n^2}(15 - \pi^2 n^2) \qquad (3)$$

which is negative for all one-electron excited states.

We used (2) and (3) to calculate the π-electron longitudinal polarizability of $H_{2n+2}C_{2n}$ polyenes, approximating these by a plane broken line. The results are given in Table 1 together with Bolton's[1] less accurate ones.

Table 1

n	$\alpha(\omega_D)$	$\alpha(0)$	$\alpha(0)$, (Bolton[1])
2	66	54	—
3	296	204	300
4	540	513	664
5	12329	1032	1228

We have solved the electron-polarizability problem exactly also for a ring (circle) and for a regular hexagon which are usually taken as models for the benzene molecule. For six electrons in a ring of radius R, we obtain

$$\alpha(\omega) = \frac{12R^4}{9 - 4R^4\omega^2}, \qquad (4)$$

which, setting R = $3a/\pi$ (where a is the length of the C—C bond), gives $\alpha(\omega_D)$ = 56.3 and $\alpha(0)$ = 50.7. For the hexagon we get $\alpha(0)$ = 47. Com-

---

*In the static case one could avoid using perturbation theory, since the exact wave functions in this case can be expressed in terms of known Airey functions.

**Eq.(2) can be obtained directly from (1) with the aid of Watson's formula

$$\sum_k f(k) = -\pi\sum_{z_k} \mathrm{Res}\,[f(z_k)\,\mathrm{ctg}\,\pi z],$$

where z_k are the poles of $f(z)$.

paring this with the experimental value $\alpha = 55$ for the benzene molecule, we see that too small a fraction of the polarizability has been left for the σ-bond. In other words, the calculation gives too high a value for the mobility of the π--electrons.

Adding up the polarizabilities of the $2n$ electrons in the ground state according to (1), we arrive at

$$\alpha = 4 \sum_{i=1}^{n} \sum_{k=n+1}^{\infty} \frac{|x_{ik}|^2}{E - E_i}. \tag{5}$$

Keeping only one term, corresponding to minimum excitation, in this sum, we obtain the approximate expression

$$\alpha = 4 \frac{|x_{n,n+1}|^2}{E_{n+1} - E_n}, \tag{6}$$

a formula which gives almost the same results in the FE model as does the exact one.

2. For the branched one-dimensional free-electron model, we have developed a simple mathematical procedure which can be used to obtain exact expressions for the π-electron wave function and energy spectrum in a magnetic field. On each individual conjugated bond, the π-electron wave function satisfies the equation

$$\left[\frac{\left(p_s + \frac{e}{c} A_s\right)^2}{2m} + V(s)\right] \psi = E\psi, \tag{7}$$

where A_s is the projection of the vector potential onto the bond under consideration. In the case of a homogeneous magnetic field, it can be shown that the general solution of (7) is

$$\psi = \exp\left(-\frac{ie}{ch} A_s s\right) \psi_0, \tag{8}$$

where ψ_0 is a general solution of (7) in the absence of the magnetic field.

Let us now make use of the continuity of the one-dimensional wave function at the nodes of the conjugated bond network, namely,

$$\psi_1 = \psi_2 = \ldots = \psi_N \tag{9}$$

and the subsidiary conditions on the derivatives of the wave functions in the neighborhood of the node. Because the energy operator must be self-adjoint, these conditions can be stated in the form

$$\sum_{l=1}^{N} \left(\psi_l' + \frac{ie}{ch} A_l \psi\right) = K\psi, \quad K = K^*. \tag{10}$$

If the one-dimensional potential on the conjugated bond network vanishes everywhere, the problem reduces to

$$W\psi = 0, \tag{11}$$

i.e., to finding the eigenvectors of the Hermitian matrix whose elements are

$$W_{lm} = -N_l \delta_{lm} \cos \sqrt{\frac{2mE}{h^2}} a + (1 - \delta_{lm}) \eta_{lm} \exp\left(\frac{ie}{ch} H S_{lm}\right). \tag{12}$$

The components of the j-th eigenvector of W are the values of the j-th one-dimensional wave function at the individual C atoms in the conjugated system. In (12), N_l is the number of C atoms neighboring on the C_l atom, a is the mean length

of the conjugated C—C bond, η_{lm} is 1 if C_l and C_m are linked and zero otherwise, S_{lm} is the area of the triangle whose vertices are at C_l, C_m and the origin, and H is the magnetic field strength. The π-electron energy spectrum in the magnetic field and the electron diamagnetic susceptibility are found from the secular equation

$$\det W = 0. \tag{13}$$

We used this method to calculate the diamagnetic susceptibility of the π-electrons for several aromatic molecules. The results are given in Table 2 (column a), together with the results of molecular-orbit calculations with linear combinations of atomic orbits, both neglecting (column b) and including (column c) integrals which account for lack of orthogonality. The values are given in units of the diamagnetic susceptibility of benzene in a perpendicular magnetic field.

Table 2

Molecules	Theory			Experiment
	a	b	c	
Naphthalene	2.011	2.185	2.219	2.06-2.11
Azulene	2.142	2.256	2.269	2.38
Pentalene	-2.840	-2.778	-2.526	-
Heptalene	-9.495	-8.340	-9.926	-
Anthracene	3.077	3.448	3.530	3.08-3.38
Styrene	0.870	0.919	0.923	0.73-1.00
Phenylbutadiene	0.848	0.903	0.902	-
Fulvene	0.133	0.076	0.196	-
Heptafulvene	0.009	0.157	-0.073	-
Diphenyl	1.777	1.868	1.876	1.74-2.00
Stilbene	1.686	1.794	1.801	1.61-1.65
Diphenylbutadiene	1.670	1.760	1.767	1.41-1.89
Difulvene	-1.250	-2.092	-1.565	-

The table shows that our method is sensitive enough to reflect the details of the structure of the system of conjugated bonds (the number of aromatic rings and the length of the chains) and is no less accurate than the molecular-orbit method.

Another representation of the π-electron diamagnetic susceptibility is also useful. For alternate hydrocarbons this representation is

$$\chi = \frac{h^2}{ma^2}\int_0^1 \frac{dz}{z} R\left[i\left(z - \frac{1}{z}\right)\right], \tag{14}$$

where R is a rational fraction of its argument, the numerator and denominator of this fraction being polynomials of the same parity. This formula was used to calculate the limit of the π-electron diamagnetic susceptibility of aromatic molecules of the styrene, diphenyl, and triphenyl methyl type as the length of the chains tends to infinity. The limiting values for molecules of these types are 0.8109, 1.6218 and 2.4327, respectively.

Our method for calculating the diamagnetic susceptibility can be extended to the case of a variable one-dimensional potential V(s), thus making it possible to include periodic fields within the molecule, as well as aperiodic ones (heterocyclin atoms, incomplete equalization of double bonds, etc.).

3. We used the matrix formulation of the problem to study the relation of the FE method to the molecular-orbit method. We showed that the overall correspondence found previously for the electron spectra and π-electron wave functions in these two methods holds also with a magnetic field. From this one can also obtain the following approximate equation relating the electron's effective mass

in the FE model to the geometric characteristics of the conjugated system and the resonance integral β of the molecular-orbit method:

$$m^* = -\frac{ch^2}{N\beta a^2}. \qquad (15)$$

The values of c obtained in various different ways lie between 1.23 and 1.57 and $m^* \approx m$.

From the correspondence of the energy spectra and with the aid of the semi-empirical results of Pariser & Parr and Pople[4], it can be shown that the depth of the potential box at the position of the j-th atom is given in the FE model by

$$V_j = \frac{1}{2}[(2 - q_j) I_j + q_j \varepsilon_j] - N_j \beta. \qquad (16)$$

Here we use the following notation: q_j is the electron charge of the j-th atom, I_j is its ionization potential, ε_j is its electron affinity and N_j is the number of its nearest neighbors. This expression can be used to derive Veselov and Rekasheva's semiempirical rule[5] relating the shape of the bottom of the potential box in the case of conjugated molecules containing heterocyclic atoms with the electron affinities and ionization potentials of the individual atoms.

"A. A. Zhdanov" Leningrad State University

References

1. H.Bolton, Trans. Faraday Soc., 50, 1265 (1954).
2. M.W.Nathans, J.Chem.Phys., 20, 741 (1952).
3. M.V.Vol'kenshtein & L.A.Borovinskii, Doklady AN SSSR, 85, 977 (1952).
4. R.Pariser & R.G.Parr, J.Chem.Phys., 21, 466 (1953); J.A.Pople, Trans. Faraday Soc., 49, 1375 (1953).
5. M.G.Veselov & T.N.Rekasheva, Vestnik, Leningrad State University, No.5, 149 (1954).

CALCULATION OF THE ABSORPTION SPECTRA OF UNSATURATED HYDROCARBON MOLECULES ON THE BASIS OF THE METALLIC MODEL

- L.Z.Borovinskii

This paper is devoted to two problems, namely, calculation of the absorption spectrum of benzene according to the metallic model, taking account of the periodic potential and the interaction between π-electrons, and examination of the joining conditions for the wave functions used in performing calculations for molecules with branched C—C bond chains.

1. As our model of the benzene molecule we shall choose a circle of radius $R = 6a/2\pi$ (where a is the length of the C—C bond; see Fig.1). We write the potential energy of a π-electron on the circle in the form

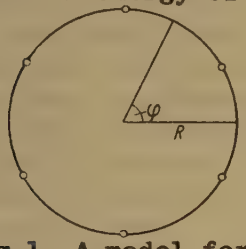

Fig.1. A model for the benzene molecule. The circles indicate the positions of carbon nuclei.

$$V = V_0 \cos 6\varphi.$$

For large distances the electron pair interaction operator may be written

$$U_{ik} = \frac{e_0^2}{|\mathbf{r}_i - \mathbf{r}_k|}.$$

This formula cannot be used for small distances in a one-dimensional model. To remove these divergences one must take account of the finite width of the potential box. We introduce the parameter r_0; physically, we can think of this as the mean distance of the electron from the line passing through the carbon nuclei. We now write the electron pair interaction operator in the form

$$U_{ik} = \frac{e_0^2}{\sqrt{|r_i - r_k|^2 + r_0^2}}. \tag{1}$$

For the above circular model of benzene, this becomes

$$U_{ik} = \frac{e_0^2}{2R\sqrt{\sin^2\dfrac{\varphi_i - \varphi_k}{2} + u^2}}. \tag{1a}$$

where $u = r_0/2R$.

The Hamiltonian of the system consisting of the six π-electrons of benzene is

$$H = -\frac{\hbar^2}{2m}\sum_{i=1}^{6}\frac{d^2}{d\varphi_i^2} + V_0\sum_{i=1}^{6}\cos 6\varphi_i + \frac{e_0^2}{2R}\sum_{6\geqslant i>k}\sum_{k=1}^{6}\frac{1}{\sqrt{\sin^2\dfrac{\varphi_i - \varphi_k}{2} + u^2}}. \tag{2}$$

In order to find the benzene spectrum one must calculate the eigenvalues of this Hamiltonian. We shall assume the wave function of the six π-electrons to be a function of only φ. It must satisfy definite symmetry conditions[1] with respect to interchange of the φ_i. These symmetry conditions are not the same for all values of the resultant spin, so that the energy of the levels depends on the spin. We shall proceed by forming a set of functions satisfying the symmetry conditions and expanding the eigenfunctions of (2) in series of these functions. This may be done in the following way. We consider an orthonormal set of one-electron functions with the required periodicity properties; the most convenient functions of this type are

$$\psi_k = \frac{1}{\sqrt{2\pi R}}e^{i\varphi k}; \quad (k = 0,\ 1,\ -1\ldots).$$

A choice of six ψ_k functions is a configuration. According to the Pauli principle no function may enter a configuration more than twice. Abarenkov has shown[2] that a set of functions satisfying the symmetry requirements can be constructed of six such ψ_k functions. In general to each configuration there correspond several linearly independent functions, their number being determined by the spin of the system and the number of unpaired electrons. Functions belonging to different configurations are automatically orthogonal, and those belonging to the same configuration can be orthogonalized by a suitable linear transformation. The energy levels are found from the secular equation

$$|H_{ik} - \lambda\delta_{ik}| = 0, \tag{3}$$

where H_{ik} are the matrix elements of H between the states whose functions are ψ_i and ψ_k. There will be interactions only between configurations having the same multiplicity and pertaining to the same irreducible representation of the group D_{6h}. Therefore H_{ik} is a quasidiagonal matrix, and Eq.(3) breaks up into equations corresponding to definite symmetries and spin values of the π-electron system. In calculating the matrix elements of (3), the terms involving the kinetic and potential energies of the electrons are obtained by elementary processes. Terms corresponding to the electron interaction are given by integrals of the form

$$I_m = \int_0^{\pi} \frac{\cos 2\beta m}{\sqrt{\sin^2\beta + u^2}}\, d\beta,$$

and for specific values of the empirical parameter u these are obtained by numerical integration. From the practical point of view, we are interested only in the lowest roots of the secular equation for each type of symmetry. The number of configurations of each type of symmetry, making a significant contribution due to electron interaction, is about 13-15. In addition there is a set of configurations which should be taken into account in connection with the periodicity of the potential. Without going into details of the calculation,[3] we give the final results in the accompanying table. The transition energies are given in arbitrary units equal to

$$E_c = \frac{\hbar^2}{2mR^2} = 2.17 \text{ ev}.$$

The values of the empirical parameters are

$$V_0 = 5.5 \text{ arb.units, and } u = 0.18.$$

Level symmetry	Energy, ev		
	Calculated		Measured Refs. in []
$^1A_{1g}$	(0)	(0)	—
$^1B_{2u}$	3,17	2,26	2,17 [5]
$^1B_{1u}$	3,67	2,76	2,75 [4]
$^1E_{1u}$	5,88	4,86	3,12 [4]
$^3B_{1u}$	1,63	1,32	1,75 [6]
$^3B_{2u}$	2,56	2,25	2,51 [4]
$^3E_{1u}$	2,15	2,38	2,22 [7]

In order to illustrate the role of the high-energy configurations, we list in the second column the results of a calculation in which the position of the configurations was taken into account only when two of them have the same energy, and this energy is the minimum for configurations of the given symmetry. The third column gives the energy levels obtained in the calculation which includes the high-energy configurations. When the π-electron interaction is not taken into account, calculations yield the same frequency (energy) value for all six transitions. As may be seen from the fourth column, the results are in satisfactory agreement with experiment for all but the $^1A_{1g} \rightarrow {}^1E_{1u}$ transition. It will also be evident that when the contribution from the high-energy configurations are included, the agreement is improved.

2. In making calculations for molecules with branched C—C bonds, one must establish the joining conditions for the wave functions and their derivatives at the branching point. These conditions are usually written in the form

$$\psi(x_{1p}) = \psi(x_{2p}) = \psi(x_{3p}), \tag{4a}$$

$$\left[\frac{d\psi(x_1)}{dx_1} + \frac{d\psi(x_2)}{dx_2} + \frac{d\psi(x_3)}{dx_3}\right]_p = K\psi(x_p), \tag{4b}$$

where $\psi(x_{1p})$, $\psi(x_{2p})$ and $\psi(x_{3p})$ are the values of the wave functions at the branching point.

Calculations carried out for the energy levels of a number of molecules and free radicals show that (4) leads to some paradoxical conclusions. For instance, the energy of the π-electron system in our model of biphenyl (two linked rings) is found to be greater than that of the π-electron energy in two non-coupled rings. This would mean that linking two benzene rings increases the π-electron energy! This and other paradoxes,[8] led us to undertake a more critical examination of the conditions implied by Eq.(4).

The one-dimensional model rests on the possibility of separating out of the wave function a factor which gives the motion of the π-electrons along the C—C bonds. As our one-dimensional function we may choose the wave function evaluated along the axis of the potential box. This one-dimensional function satisfies the equation

$$-\frac{\hbar^2}{2m}\frac{d^2\psi}{dx^2} = E\psi. \tag{5}$$

It is impossible to separate variables in the neighborhood of the branching point, so that the one-dimensional function does not satisfy (5); hence there is no reason to believe that the solutions of (5), when extrapolated to the branching point, will all be equal. For this reason we believe (4) to be erroneous.

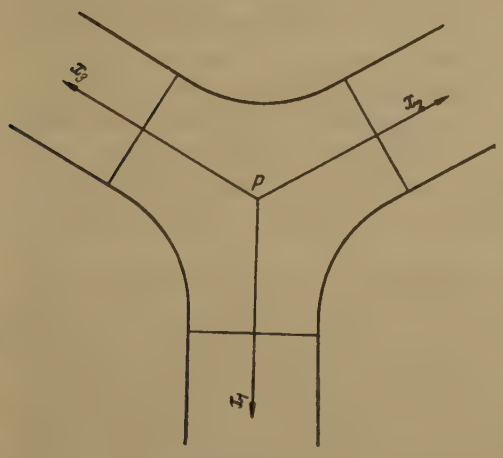

Fig.2

With a view to determining the joining conditions, let us consider a two-dimensional model in the neighborhood of a branching point (Fig.2).

The solutions of the two-dimensional Schroedinger equation at a branching point can be written as the product of two sine functions, one depending on the longitudinal and the other on the transverse coordinates. We shall attempt to find a numerical solution in the vicinity of the branching point by the net method. The requirement that the wave function and its derivative be continuous in the longitudinal coordinate can be used to establish the relations between the values of the wave function and its derivative at the boundaries of the branching region. These relations are of the form

$$\left.\frac{d\psi}{dx_1}\right|_{x_1=b} = \frac{1}{b}\{p\psi|_{x_1=b} + q[\psi|_{x_2=b} + \psi|_{x_3=b}]\}. \tag{6}$$

(Two other such relations are obtained from (6) by cyclic permutation of the indices.)

In (6) b is the width of the potential box, and $p = 1.84$ and $q = 0.91$ are numerical coefficients.

The values of x_1, x_2 and x_3 are calculated along the branches with the origin at the intersection point P. The value of b is obtained empirically.

In our future work we plan to use (6) to calculate the absorption spectra and electron density distributions of polycyclic hydrocarbon molecules.

References

1. V.A.Fok, Zhur.eksp.i teor.fiz., 10, 961 (1940).
2. I.V.Abarenkov, Vestnik, Leningrad State University, No.2, 43 (1956).
3. L.A.Borovinskii, Optika i spektroskopiia, 4, 156 (1958).
4. H.B.Klevens & J.R.Platt, J.Chem.Phys., 17, 470 (1949).
5. V.L.Broude, A.F.Prikhot'ko & V.S.Medvedev, Zhur.eksp. i teor.fiz., 21, 666 (1951).
6. P.Pesteil & L.Pesteil, Compt. rend. Acad.Sci., 240, 1987 (1955).
7. P.Pesteil, L.Pesteil & A.Zmerli, Ibid., 241, 29 (1956).
8. L.A.Borovinskii, Optika i spektroskopiia, 4, 526 (1958).

THEORY OF VIBRATIONAL SPECTRA OF UNSATURATED COMPOUNDS

- L.M.Sverdlov, M.G.Borisov, Iu.V.Klochkovskii, E.P.Krainov, V.S.Kukina & N.V.Tarasova

1. By now there has been accumulated a wealth of experimental data on the vibrational spectra of unsaturated compounds. It may be of interest therefore to carry out a theoretical generalization of the available experimental material in two directions: first, to establish theoretically the characteristic frequencies peculiar to different structural groups, including double bonds, which is of practical importance (in particular, it is desirable to see how the frequencies associated with the $\rangle C{=}C\langle$ group depend on the position of the double bond in the chain, the degree of branching of the chain and on the number and position of double bonds, and to clarify the influence of inclusion of a double bond in the ring), and, second, to examine the question of the intereffect of the different structural elements entering into the composition of unsaturated compounds, which is important from the standpoint of the theory of chemical structure (particularly, the influence of alkyl- and halogen-substitution on the force field of ethylene, cumulation of double bonds, etc.).

Accordingly, we carried out theoretical calculations of the frequencies of the normal vibrations and potential energy constant (by the methods of the theory of small vibrations of polyatomic molecules in the form developed by Vol'kenshtein, El'iashevich & Stepanov[1] and Maiants[2]) for ethylene and the simplest representatives of the olefins, diolefins, cycloolefins, allenes and halogen derivatives of ethylenes. In all we carried out calculations for 39 molecules; ethylene & its deuterium derivatives, propylene and deuteropropylene, butene-1,3-methyl-butene-1, isobutylene, cis-and trans-butene-2, trimethylethylene, tetramethylethylene, 1,4--pentadene, cyclopentene, allene & tetradeuteroallene, 1,1-dimethylallene, monobromoethylene & seven of its deuterium derivatives, cis- & trans-dichloroethylene & their deuterium derivatives and 1,1-difluorethylene and its deuterium derivative In addition, we considered the electrooptics of the vibrations of ethylene and tetradeuteroethylene.

Part of our results have been published earlier[3]; some of the more recent results are given below. The secular equations were solved by the method of successive diagonalization and with the aid of an electronic computer (cyclopentene - symmetry type A_1 and B_1; deuterobromoethylene - symmetry type A_1).*

---

*We take this opportunity to express our gratitude to M.M.Sushchinskii and R.I.Poklovchenko, members of the staff of the Physical Institute of the USSR Academy of Sciences, for solution of these equations on the computer.

2. The following is a summary of our principal results.

A. Replacement of hydrogen atoms in ethylene with alkyl groups has virtually no effect on the force field of the remaining ethylene group (or on that of the alkyl radical). As for the influence of alkyl substitution on the spectrum, here the basic factor is the geometric arrangement of the alkyl groups relative to the double bond:

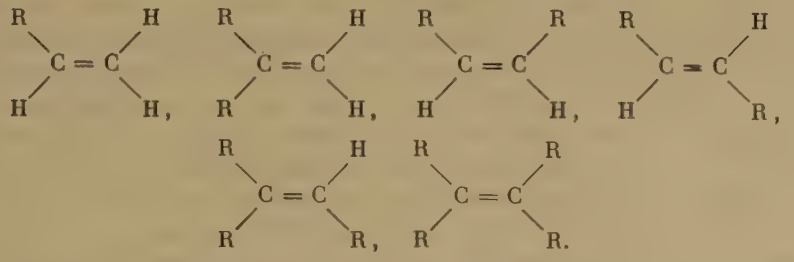

Each of these six classes of olefins is characterized by its own particular set of characteristic frequencies. This deduction is substantiated by the experimental data on the spectra of over 90 olefins. Further substantiation is furnished by the results of calculations carried out for more complex representatives of the above mentioned homologous series, particularly, for butene-1. Utilizing the results of calculation for butene-1 and the data of Stepanov[1] on the calculated spectra of normal paraffins, we were able to interpret and elucidate the salient features in the spectra of all molecules of the $RCH{=}CH_2$ series up to undecene-1.

We considered the influence of branching on the spectrum: if there is branching in the chain at a distance from the double bond, the characteristic features of the vibrations of atoms associated with the double bond are not altered; on the other hand, if the branching occurs at a carbon atom contiguous to a double bond (for example, 3-methylbutene-1), a number of characteristic vibrations are affected.

B. Calculations carried out for compound containing several double bonds showed that in the case of presence in the molecule of two double bonds separated by at least two single bonds (for example, 1,4-pentadene), one can safely use the force constants of butene-1 for calculating the vibrational spectra. It follows therefore that in this case the double bonds have virtually no effect on each other. Most frequencies characteristic for monoalkyl-substituted derivatives of ethylene are also characteristic for diolefins. In particular, we were able to interpret fully the vibrational spectrum of diallyl.

In contrast, in the case of cumulation of double bonds there occurs a certain change in the force field of the ethylene group. Evaluations for 1,1-dimethylallene showed that for calculation of the vibrational spectra of alkyl-derivatives of allene one can use the force constants established for allene and paraffins. We determined the characteristic frequencies of dialkyl-derivatives of allene.

C. On the basis of calculation of the vibration frequencies of cyclopentene we were able for the first time to interpret fully the Raman spectrum of this molecule. From the results of the calculations we conclude, first, that in calculations for cycloolefins one can use the force constants of acyclic olefins as a good zeroth approximation and, second, that the heavy carbon ring of cyclopentene is not plane but somewhat bent (the deformation, however, is relatively small). Calculation of the spectrum of cyclopentene enabled us to establish the characteristic frequencies of alkyl-derivatives of cyclopentene of the following types:

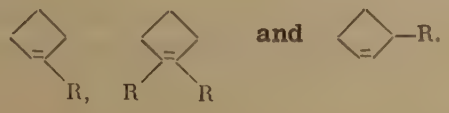

D. We carried out theoretical calculations of the frequencies and force constants of some bromine, chlorine and fluorine derivatives of ethylene for which there were available adequate data on the spectra of the deuterosubstituted molecules so that the force constants could be calculated with a high degree of accuracy. Good agreement of the calculated frequencies with the observed values confirms the reliability of the entire system of deduced constants. Replacement of hydrogen atoms in ethylene with halogen atoms does not lead to any substantial change in the force field of the remaining ethylene group (the strength of the C—H bond is increased by 2-3%) or in the strength of the carbon-halogen bonds. In view of this, it may be concluded that the force constants obtained by calculation can be used as a good zeroth approximation in calculating the vibrational spectra of other Br, Cl and F derivatives of ethylene. The strongest effect is produced by attachment of fluorine atoms to a double bond; this leads to an increase of about 10% in the strength of the double bond.

There is very little difference between the force fields of cis- and trans--dichloroethylene. The difference between their spectra is due primarily to the different symmetry of the molecules.

The strength of C—Br, C—Cl and C—F bonds in the halogen derivatives of unsaturated compounds is somewhat greater than in the corresponding saturated hydrocarbons.

E. Using the procedure of Vol'kenshtein et al[1], we calculated the intensities and polarizations in the Raman and infrared absorption spectra of ethylene and tetradeuteroethylene. We derived general formulas for the derivatives $\partial P_i/\partial Q_j$ of the dipole moment with respect to the normal coordinates, the trace b_i' and anisotropy g_i' of the derivative of the polarizability tensor (valence-optical system in the zeroth approximation). On the basis of recently published experimental data[4] on the absolute integral intensities of the infrared bands of ethylene and C_2D_4, we determined the numberical values of the dipole moment μ_{CH} and the derivative of the dipole moment (μ_{CH}') with respect to the natural coordinate q (change in the length of the C—H bond). The calculations showed the inapplicability of the valence-optical scheme in the zeroth approximation inasmuch as for the vibrations of different types of symmetry B_{1u}, B_{2u} and B_{3u}, there are obtained different values of μ_{CH} and μ_{CH}', which is devoid of physical meaning. In view of this, for the first time, we carried out a calculation of $\partial P_i/\partial Q_j$ in the first approximation of the valence-optical scheme; it was found that in this case there are obtained identical values of μ_{CH} and μ_{CH}' for the vibrations of all types of symmetry, as, in fact, should be the case.

Thus our computations showed that for calculating the intensities in infrared spectra, the valence-optical scheme is applicable only in the first approximation.

Saratov Highway Institute &
All-Union Highway Correspondence Institute

References

1. M.V.Vol'kenshtein, M.A.El'iashevich & B.I.Stepanov, Kolebaniia molekul (Molecular vibrations), Vols.I & II, M.-L., 1949.

2. L.M.Maiants, Trudy (Proceedings), Physical Institute of the USSR Academy of Sciences, 5, 63 (1950).

3. L.M.Sverdlov & N.L.Pakhomova, Zhur.eksp.i teor.fiz., 26,64 (1954); L.M. Sverdlov & O.N.Vinokhodova, Doklady AN SSSR, 100,34 (1955); L.M.Sverdlov, Doklady AN SSSR, 106,80 (1956); Optika i spektroskopiia, 1,752 (1956); Doklady AN SSSR, 112,706 (1957); ibid., 2,540 (1957); Transactions of the Tenth All-Union Conference on Spectroscopy, Vol.1, 278, Pub. L'vov State University, 1957.

4. R.Golike, J.Mills, W.Person & B.Crawford, J.Chem.Phys., 25,1266 (1956).

CONTRIBUTION TO THE QUANTUM MECHANICAL THEORY OF RAMAN LINE INTENSITIES

- I. I. Sobelman

The basic equation for the molecular wave function commonly employed[1,2] in the theory of molecular spectra is the following:

$$\Psi_n^v(\mathbf{r}, Q) = \psi_n(\mathbf{r}, Q)\, U_n^v(Q). \tag{1}$$

Here r indicates the coordinates of the electrons, Q indicates the normal coordinates of the nuclei and n and v are indices identifying the electron and vibrational states, respectively. In this treatment the zeroth approximation involves a nonequilibrium nuclear configuration, so that the electron function $\Psi_n(\mathbf{r},Q)$ contains the nuclear coordinates as parameters.

Actually, it is feasible to simplify the zeroth approximation wave functions to a great extent. When dealing with scattering, it is the electrons alone which determine the interaction with photons, since the interaction of the nuclei with the radiation is negligible. The energy of the radiation field is transferred to the nuclei through the electrons, by means of the nucleus-electron Coulomb interaction. Let us therefore start from the equilibrium configuration of the nuclei, treating the interaction of the electrons with the nuclear displacements as perturbations.*

Let $\Psi_n(\mathbf{r}, \mathbf{R}) = \Psi_n(\mathbf{r})$ correspond to the equilibrium configuration R of the nuclei. Under a small displacement $\delta\mathbf{R}$ of the nuclei, there appears a small increment $W(\mathbf{r}, \delta\mathbf{R})$ in the potential, and this can be interpreted as interaction of the electrons with the nuclear displacements. If this displacement occurs as a result of molecular vibrations, the interaction energy should be taken as

$$w(\mathbf{r}) = \int U_n^v(Q)\, W(\mathbf{r}, \delta\mathbf{R})\, U_n^{v'}(Q)\, dQ. \tag{2}$$

rather than simply $W(\mathbf{r}, \delta\mathbf{R})$.

Let us consider Raman scattering of a molecule. In the process a photon of frequency ω_0 and polarization $\mathbf{e}_\rho$ is absorbed, (perturbation $V \sim e\mathbf{r}\mathbf{e}_\rho = p^\rho$), a photon with the parameters ω and e_σ is emitted (perturbation $V \sim e\mathbf{r}\mathbf{e}_\sigma = p^\sigma$), and the nuclei are excited to a higher vibrational state (perturbation w). Using the general procedures of perturbation theory one easily obtains the matrix element for this process, namely (in the third approximation),

$$M_{n\,0,\,n\,1} \sim \{\beta_{\rho\sigma}\}_{n\,0,\,n\,1} =$$
$$= \sum_{m,\,k}{}' \left\{ \frac{p^\rho_{nm}\, p^\sigma_{nk}\, w_{kn}}{(E_n + \hbar\omega_0 - E_m)(E_n - E_k + \hbar\Omega)} + \begin{array}{l}\text{terms of the same type, differ-}\\ \text{ing in the order of the factors}\\ p^\rho,\ p^\sigma \text{ and } w\end{array} \right\}. \tag{3}$$

The sum in (3) is taken over all intermediate states, including those in the continuous and discrete spectra. In this expression E_i is the energy of the molecule in the i-th state for the equilibrium configuration of the nuclei, i.e., simply the electron energy, and $\hbar\Omega$ is the vibrational quantum.**

---

*We note that what is new here is not that the nuclear motion is treated by perturbation theory (this has often been done in solving other problems; see, for example, Pekar[3], Jahn & Teller[4], and Vol'kenshtein et al.[1,5]), but rather the sequence in which the approximations are obtained for Raman scattering.

**Footnote, next page.

The matrix elements of $p^\rho p^\sigma$ and ω are calculated by means of the $\Psi_n(\mathbf{r})$ function, which is independent of the vibrations. Therefore p^ρ_{nm} is in general independent of the vibrations, while w_{nk} can be written as a product of independent "electron" and "nuclear" factors. In the most general case we can write

$$W(\mathbf{r}, \delta\mathbf{R}) = \sum_i (\partial H / \partial \mathbf{R}_i)\,\delta\mathbf{R}_i = \sum_{i,\alpha} (\partial H / \partial \mathbf{R}_i)\,\mathbf{C}_{i\alpha} Q_\alpha. \qquad (4)$$

Here H is the molecular Hamiltonian, and the indices i and α refer to the molecular nuclei and the normal coordinates, respectively. The $\mathbf{C}_{i\alpha}$ vectors relate the nuclear displacements to the normal coordinates:

$$\delta\mathbf{R}_i = \sum_\alpha \mathbf{C}_{i\alpha} Q_\alpha.$$

With the aid of (4), we can rewrite $\beta_{\rho\sigma}$ in the form

$$\beta_{\rho\sigma} = (Q_\mu)_{01} \sum_i \mathbf{C}_{i\mu} \vec{B}^i_{\rho\sigma} = \sum_i \vec{B}^i_{\rho\sigma} \delta\mathbf{R}^\mu_i. \qquad (5)$$

Each term of the sum in (5) corresponds to the interaction of the molecular electrons with the displacement of one of the nuclei. The vector coefficients $\vec{B}^i_{\rho\sigma}$ are independent of the vibrations and are fully defined by the structure of the electron shells of the molecule (for the equilibrium configuration of the nuclei).

In solving diverse problems[8], it is often convenient to represent the $\beta_{\rho\sigma}$ as in (3) and (5). As an example, we shall show how these equations can be used to calculate the $\beta_{\rho\sigma}$ of molecules containing delocalized π-electrons. As is known, the valence-optics scheme is not applicable to such nuclei. In many cases, however, their properties can be described with sufficient accuracy by the metallic model. Hence, with the aid of this model, one can attempt to calculate the part of the $\beta_{\rho\sigma}$ tensor that is related to the delocalized π-electrons.*

Let us assume that the electron moves in the field of N identical centers of force, so that

$$U(\mathbf{r}) = \sum_{i=1}^{N} U_i(\mathbf{r}),$$

and that these centers are located as shown in the figure. We shall assume further that the electron's motion is restricted by infinitely high potential barriers, described by

$$U(\mathbf{r}) = \infty \quad \text{for } z \leqslant 0 \quad \text{and} \quad z \geqslant L, \quad \text{where } L = \frac{Nd}{2}.$$

---

*The first attempt in this direction has already been taken. In Ref.6 the author calculated the contribution from the delocalized π-electrons to the polarizability of several polyenes by using the simple model of an electron in a one-dimensional potential box. The calculated values for the intensity of the fully symmetric vibrations of polyene chains were found to be in satisfactory agreement with experiment.

**(See preceding page.) Obviously one may consider any nuclear configuration R in the zeroth approximation. The equation

$$\Psi_n(\mathbf{r}, \mathbf{R} + \delta\mathbf{R}) = \Psi_n(\mathbf{r}, \mathbf{R}) + \sum_k{}' \frac{W_{nk}}{E_n - E_k}$$

is independent of the choice of R. The only requirement is that W be small compared to E_n, E_k and $(E_n - E_k)$. In what follows we shall everywhere understand R as the equilibrium configuration of the nuclear ground state.

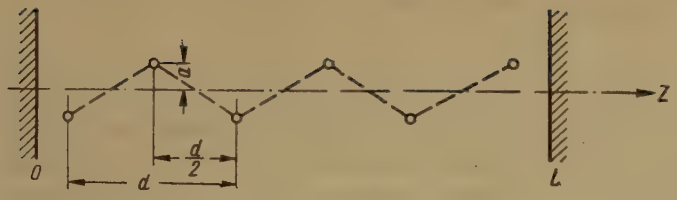

Calculation of electron motion

In the most general case, the electron wave function can be written

$$\Phi_n(\mathbf{r}) \sin \frac{n\pi}{L} z;$$

$$\Phi_n(x, y, z + md) = \Phi_n(x, y, z). \quad (6)$$

We now go on to a calculation of β_{zz} with (6) as the zeroth approximation.*

Let us now assume, as usual, that 2N delocalized electrons occupy the N lowest levels (n = 1,2,...,N). Then the principal role is played by the electrons in the last of the filled levels and n = N. We shall assume that the potential $U_i(\mathbf{r})$ is some function of the form $U(|\mathbf{r} - \mathbf{R}_i|)$. We then may assert that regardless of the specific form of this function, its derivative $(\partial U / \partial \mathbf{R}_i)$ fails to vanish only in a small region $|\mathbf{r} - \mathbf{R}_i| \lesssim d$. This fact and the symmetry properties of $\Phi_n(\mathbf{r})$ can be used to represent $(\partial U/\partial \mathbf{R}_i)_{N,N'}$ as the product of two factors. The first of these factors depends on the position of the i-th nucleus in the chain (on Z_i) and can be calculated explicitly. The second depends entirely on the specific form of $U_i(\mathbf{r})$ and $\Phi_n(\mathbf{r})$. The final expression for β_{zz} is

$$\beta_{zz} = \frac{Z_{N,N+1} Z_{N+1,N+2} (E_N - E_{N+1})}{(E_N - E_{N+2})\left[(E_N - E_{N+1})^2 - \hbar^2\omega_0^2\right]} \times \left\{ C_1 \sum_i (-1)^i \sin \frac{2i-1}{N} \pi \cdot \delta X_i + C_2 \sum_i \sin \frac{2i-1}{N} \pi \cdot \delta Z_i \right\}. \quad (8)$$

The nuclei in the lower row are those with i = 1,3,5. and those in the upper row are those with i = 2,4,6; δX_i and δZ_i are the displacements of the nuclei along the x and z axes.

Let us denote the factor multiplying the braces in (8) by $F(N)$. Then according to (8) β_{zz} is determined by the two unknown parameters $F(N)C_1$ and $F(N)C_2$. These parameters are independent of the vibrations and are fully determined by the equilibrium configuration of the molecule. The parameters C_1 and C_2 are independent of N (i.e., of the length of the chain) and are the same for all chains of the type under study, no matter how many nuclei the chain may contain. The entire N-dependence is "concentrated" in the factor $F(N)$ and can be calculated either in the one-dimensional potential box approximation or from the observed electronic spectrum of the molecule. It may be noted that in a linear chain β_{zz} is of an even simpler form. For such a chain C_1 = 0, and the only parameter that enters into the formula for β_{zz} is $F(N)C_2$. We assumed implicitly above that the vibrations do not alter L. This restriction is easily removed. Any arbitrary displacement of the nuclei in a chain can be written in the form

$$\delta \mathbf{R}_i = \frac{\delta L}{N} i \mathbf{e}_z + \delta \mathbf{R}_i.$$

---

*In the one-electron case it is possible to separate out an independent part of $\beta_{\rho\sigma}$ corresponding to the system of delocalized π-electrons. This is the only part we are considering here. The transverse dimensions of the region in which the electron is localized are of the order of $d/2$, so that the matrix elements of x and y components of the dipole moment are smaller than the z component by a factor of about d/L. This is why β_{zz} is of primary interest.

The first term gives the displacement of the nuclei when the chain is stretched without disturbing its periodicity. Let us consider the zeroth approximation for a chain of length $L = L_0 + \delta L$ with a period

$$d = \frac{L - L_0}{N} 2.$$

We shall denote the polarizability of such a chain by $\alpha(L)$. Additional displacements $\delta R'$, disrupting the periodicity will change the polarizability by an amount $\alpha'(L, \delta R_i')$, which can be calculated in the same way as (8). In the general case the polarization is the sum of α and α'.

Equation (8) can also be used to calculate β_{zz}. For fully symmetrical vibrations, for instance, $\delta R_i' = 0$ and $\beta_{zz} = \frac{\partial \alpha(L)}{\partial L} \cdot \delta L$; $\delta L \sim Q$.

For the calculation of $\partial\alpha / \partial L$ see Iazykova's dissertation.[6] If $\delta L = 0$, we obtain (8) again.

It is relatively simple to generalize (5) to the case in which the molecule is subjected to an external (intermolecular) interaction. There are several interesting evaluations that can be made in this case. In particular, one can establish the relation between the intensity of the forbidden lines in the Raman spectrum of liquids and the intensity I' of the so-called low-frequency Raman spectrum (scattering by intermolecular vibrations). When one knows this ratio and the allowed and forbidden Raman line intensities, one can evaluate the upper bound for I'. This is of definite interest from the standpoint of interpreting the nature of the Rayleigh scattering tail.

We note in conclusion that when the electron functions are sufficiently simple in the zeroth approximation, it becomes possible to calculate $\beta_{\rho\sigma}$ directly from (3). As an example of such a case, we refer to the calculation of the cross section for Raman scattering of x-rays by plasma waves undertaken by the author and Feinberg[7] (also see Ref.8 for more details).

Moscow Physical-Technical Institute

References

1. M.V.Vol'kenshtein, M.A.El'iashevich & B.I.Stepanov, Kolebaniia molekul (Molecular vibrations), M.-L., 1949.

2. G.Plachek, Releevskoe rasseianie i raman-effekt (Rayleigh scattering and the Raman effect), Kharkov, 1935.

3. S.I.Pekar, Zhur.eksp.i teor.fiz., 22, 641 (1952).

4. A.Jahn & E.Teller, Proc.Roy.Soc., 161, 220 (1957).

5. M.V.Vol'kenshtein & M.A.El'iashevich, Izv.AN SSSR,Ser.fiz., 12,5 (1948).

6. S.Iazykova, Dissertation, Phys.Inst., USSR Ac. of Sci., 1955.

7. I.I.Sobel'man & E.L.Feinberg, Zhur,eksp i teor.fiz.,34,494 (1958).(Trans. Soviet Physics - JETP.)

8. I.I.Sobel'man, Sbornik trudov pamiati akademika G.S.Landsberga (Symposium in memory of G.S.Landsberg)., M.,1959.

INTENSITIES AND POLARIZATIONS IN THE RAMAN SPECTRA OF C_6H_6, C_6D_6 AND SYMMETRICAL $C_6H_3D_3$

- M.A.Kovner & B.N.Snegirev

The availability of new experimental data[1] on the Raman spectra of C_6H_6, C_6D_6 and $C_6H_3D_3$ makes it possible to solve the problem of determining the electrooptical parameters (polarizabilities and the derivatives thereof) of the benzene ring for the purpose of clarifying the characteristics of its electron shell and subsequent calculation of the intensities in the spectra of more complex substituted benzenes. We made use of the formulas of the valence-optical theory[2] and the formulas of Ferigle & Weber[3], which dispense with taking into account the equivalence of the angular momentum to zero in explicit form, (generalized by us to the case of bonds not possessing axial symmetry) for calculating the tensors of the polarizability derivatives with respect to the normal coordinates for all vibrations evinced in the Raman spectra of C_6H_6, C_6D_6 and $C_6H_3D_3$. We determined the elements of the L matrices of the normalized vibration coefficients entering into these tensors through solution of the mechanical problem[5,6]. It should be noted that the formulas of Ferigle & Weber[3] comprise elements of the L^{-1} matrix. One can, however, avoid inversion of the L matrix by making use of the relationship $A(L^{-1})' = L$, in which A is a matrix of kinematic coefficients.

Allen & Bernstein[1] give the experimental values of the depolarization coefficients ρ and the ratios

$$S = \frac{(5\alpha_l'^2 + 7g_l'^2)}{(5\alpha'^2 + 7g'^2)_{458}},$$

where α_l', g_l', α' and g' are the traces and anisotropies of the tensors of the polarizability derivatives with respect to the normal coordinates of the l-th normal vibration and the vibration with a frequency of 458 cm^{-1} in the Raman spectrum of CCl_4. For calculating the electrooptical parameters of benzene one must first evaluate

$$(5\alpha'^2 + 7g'^2)_{458}^{-1} = K^2.$$

We did this by means of the formulas of Ref.4 for the tensors pertaining to E_g^- and the values of S for the 849 and 661 cm^{-1} frequencies in the spectra of C_6H_6 and C_6D_6, using the procedure described by Whiffen[7]. Through such calculation there are obtained two values of K^2, namely, $K_I^2 = 0.352$ Å^{-6} and $K_{II}^2 = 0.028$ Å^{-6}.

Inasmuch as a priori choice between these two values is impossible, we carried out all the calculations for both values, i.e., in two variants, hereinafter designated I and II. In addition to the values of K^2, using the above values of S, we determined by means of the formulas of Ref.4 the linear combinations $\alpha_{Q1} + \alpha_{Q2} - 2\alpha_{Q3}$ and $\alpha_{q1} + \alpha_{q2} - 2\alpha_{q3}$* pertaining to the polarizabilities of the C—C and C—H bonds; one can then calculate the values of S for the nonplane E'' vibrations of $C_6H_3D_3$. Finally using the values of K^2 and Eq.(7) of Ref.4 one can calculate S and ρ for the A_{1g} vibrations of C_6H_6 and C_6D_6 and A_1' of $C_6H_3D_3$.

The tensors of the E_g^+ symmetry representations for C_6H_6 and C_6D_6 and E' for $C_6H_3D_3$ contain new electrooptical parameters, namely, the differences $\alpha_{Q1} - \alpha_{Q2}$, $\alpha_{q1} - \alpha_{q2}$ and their derivatives. There are available 15 experimental values of S for their determination. In extracting the square root and solving such a system of excess equations there result many variants of combinations of signs; from

---

*The values of these quantities in Ref.4 and Table 2 (variant I) differ somewhat inasmuch as in the first calculation we used the ordinary masses of H and D and in the second calculation the spectroscopic masses.

among these we chose the variant that appeared most plausible from the physical standpoint.

All the calculations were carried out in the ordinary so-called zeroth approximation of the valence-optical scheme[2]; the results are listed in Tables 1 & 2. In the case of benzene, however, it is expedient to take into account the dependence of the polarizability of the bonds on changes in the length of the other bonds and the values of the valence angles, i.e., to go over to the first approximation in solving the electrooptical problem[2]. In this case there are introduced corrections to the tensors of the polarizability derivatives with respect to the normal coordinates; these corrections can be most readily expressed by means of row matrices of the form

$$(\alpha'_{Qi0}, \alpha'_{Qim}, \alpha'_{Qip}) = H_i; \qquad (\alpha'_{qi0}, \alpha'_{qim}, \alpha'_{qip}) = h_i;$$
$$(\alpha'_{Qi\gamma 0}, \alpha'_{Qi\gamma m}, \alpha'_{Qi\gamma p}) = G_i; \qquad (\alpha'_{qi\gamma 0}, \alpha'_{qi\gamma m}, \alpha'_{qi\gamma p}) = g_i;$$
$$(\alpha'^{(1)}_{Qi\beta 0}, \alpha'^{(2)}_{Qi\beta 0}, \alpha'^{(1)}_{Qi\beta p}, \alpha'^{(2)}_{Qi\beta p}) = B_i; \quad (\alpha'^{(1)}_{qi\beta 0}, \alpha'^{(2)}_{qi\beta 0}, \alpha'^{(1)}_{qi\beta m}, \alpha'^{(2)}_{qi\beta m}) = \beta_i;$$
$$i = 1, 2, 3$$

Table 1

Observed and calculated intensities and depolarizabilities in the Raman spectra of C_6H_6, C_6D_6 and $C_6H_3D_3$

Substance and symmetry type		ν, cm^{-1}	S[1] obs.	$S^{(0)}$ calc. Var. I	$S^{(0)}$ calc. Var. II	$S^{(1)}$ calc. Var. I	$S^{(1)}$ calc. Var. II	S[7] calc.	ρ[1] obs.	$\rho^{(0,1)}$ calc	ρ[7] calc
C_6H_6	E_g^-	849	0,105	0,105	0,105	0,105	0,105	0,105			
C_6D_6		661	0,204	0,204	0,204	0,204	0,204	0,204		0,86	
$C_6H_3D_3$	E''	374	0,013	0,095	0,012	0,075	0,013	0,013			
		710	0,101	0,041	0,133	0,041	0,133	0,131			
		947	—	0,089	0,017	0,089	0,017	0,083			
C_6H_6	A_{1g}	992	4,406	4,47		4,47		4,19	0,11	0,11	0,11
		3062	16,505	16,78		16,78		17,80	0,21	0,21	0,20
C_6D_6		945	4,041	4,56		4,56		4,29	0,12	0,11	0,12
		2292	7,702	6,67		6,67		6,98	0,21	0,23	0,21
$C_6H_3D_3$	A'_1	955	2,785	3,24		2,80		2,92	0,12	0,11	0,12
		1003	0,804	1,20		0,77		1,34	0,11	0,11	0,11
		2283	2,422	3,32		3,03		3,44	0,22	0,23	0,22
		3054	—	8,39		8,70		8,89	—	0,21	0,20
$A'_1 + E'$		3054	7,730	11,06		11,37		10,93	0,36	0,30	0,36
C_6H_6	E_g^+	606	0,181	0,16		0,16		0,20			
		1178	0,584	0,44		0,44		0,58			
		1596	1,084	1,33		1,33		1,15			
		3047	4,608	5,75		5,75		3,66			
C_6D_6		577	0,146	0,15		0,15		0,13			
		867	0,305	0,31		0,31		0,31			
		1560	0,979	0,99		0,99		0,92			
		2264	2,470	2,50		2,50		3,15		0,86	
$C_6H_3D_3$	E'	594	0,180	0,16		0,16		0,16			
		832	0,133	0,08		0,08		0,12			
		1102	0,169	0,18		0,18		0,24			
		1396	0,049	0,12		0,12		0,12			
		1576	0,925	1,28		1,28		1,03			
		2273	0,523	1,70		1,70		1,64			
		3054	—	2,67		2,67		2,04			

Figures in [] are Refs.

Table 2

Calculated electrooptical parameters of the C—C and C—H bonds

Zeroth approximation	First approximation	Calculated values		
		Variant I	Variant II	Ref.7
α'_{Q1}	$\alpha'_{Q1} + H_1 a$	1,32 Å²	4,70 Å²	3,4 Å²
α'_{Q2}	$\alpha'_{Q2} + H_2 a$	0,34 Å²	1,21 Å²	2,5 Å²
α'_{Q3}	$\alpha'_{Q3} + H_3 a$	0,23 Å²	0,80 Å²	0,8 Å²
α'_{q1}	$\alpha'_{q1} + h_1 a$	0,86 Å²	3,04 Å²	2,6 Å²
α'_{q2}	$\alpha'_{q2} + h_2 a$	0,24 Å²	0,83 Å²	1,2 Å²
α'_{q3}	$\alpha'_{q3} + h_3 a$	0,03 Å²	0,11 Å²	0,1 Å²
$\alpha_{Q1} + \alpha_{Q2} - 2\alpha_{Q3}$	$\alpha_{Q1} + \alpha_{Q2} - 2\alpha_{Q3}$	1,75 Å³	1,94 Å³	—
$\alpha_{Q1} - \alpha_{Q2}$	$\alpha_{Q1} - \alpha_{Q2} + \frac{\sqrt{3}}{2}\left[(G_1 - G_2)c + (g_1 - g_2)b + \frac{1}{2}(B_1 - B_2 - \beta_1 + \beta_2)d\right]$	0,22 Å³	0,80 Å³	—
$\alpha_{q1} + \alpha_{q2} - 2\alpha_{q3}$	$\alpha_{q1} + \alpha_{q2} - 2\alpha_{q3}$	0,24 Å³	0,04 Å³	—
$\alpha_{q1} - \alpha_{q2}$	$\alpha_{q1} - \alpha_{q2} + \frac{\sqrt{3}}{2}(B_1 - B_2 - \beta_1 + \beta_2)d$	0,04 Å³	0,14 Å³	—
—	$(G_1 + G_2)f + \frac{1}{2}(\alpha'_{q1\gamma} + \alpha'_{q2\gamma}) + \frac{1}{2}(g_1 + g_2)a$	−0,08 Å³	−0,30 Å³	—
	$G_3 f + \frac{1}{2} g_3 a + \frac{1}{2}\alpha'_{q3\gamma}$	−0,01 Å³	−0,05 Å³	—

and column matrices

$$\begin{pmatrix}2\\2\\1\end{pmatrix} = a; \quad \begin{pmatrix}1\\1\\-1\end{pmatrix} = b; \quad \begin{pmatrix}1\\-2\\1\end{pmatrix} = c; \quad \begin{pmatrix}1\\-1\\-1\\1\end{pmatrix} = d; \quad \begin{pmatrix}1\\1\\1\end{pmatrix} = f.$$

Here α'_{Qi0}, α'_{Qim}, α'_{Qip}, α'_{qi0}, α'_{qim}, α'_{qip} are the derivatives of the polarizabilities of the C—C and C—H bonds in the i directions with respect to the lengths of the C—C and C—H bonds oriented in the ortho-, meta- and para-positions with regard to the given bond; $\alpha'_{Qi\gamma 0,\,m,\,p}$, $\alpha'_{qi\gamma 0,\,m,\,p}$ and $\alpha'_{Qi\beta 0,\,m,\,p}$, $\alpha'_{qi\beta 0,\,m,\,p}$ are the derivatives of the same polarizabilities with respect to the C—C—C and C—C—H angles with the same apex but arranged in a nonequivalent manner with regard to the given gond.

It follows from Tables 1 & 2 that variant II is to be preferred; this becomes evident only when we examine the results of calculation of the values of S for $C_6H_3D_3$. (This calculation was not made in the work of Ref.4.) Variant II was also given preference by Whiffen[7] whose results are listed in the last columns of Tables 1 & 2 for purposes of comparison. The superiority of variant II can be confirmed by an independent calculation. It follows from Ref.2 that

$$K^2 = [20(\alpha'_1 + 2\alpha'_2)^2 N^2]^{-1},$$

where α'_1 is the longitudinal and α'_2 is the transverse polarizability of C—Cl bonds and the normalization factor $N = \nu/\sqrt{k}$; here ν = 458 cm^{-1} and the force constant k for the C—Cl bond equals $6.2 \cdot 10^6$ cm^{-2}.

Substituting α'_1 = 3.07 Å³ and α'_2 = 0.74 Å³ (Ref.2) (the length of the C--Cl bond is expressed in 1.09 Å units and is dimensionless), we find that K^2 = 0.07 $Å^{-6}$. This value is appreciably closer to K^2_{II} than to K^2_I.

In the case of variant II, $\alpha_{q1} + \alpha_{q2} - 2\alpha_{q3} = 0.04$ Å^3 and differs greatly from the corresponding value in paraffins, which indicates that the axial symmetry of the C—H bonds in benzene is disturbed. It will be evident from Table 1 (the $^{(0)}$ and $^{(1)}$ denote the zeroth and first approximations) that the introduction of the first approximation makes it possible to improve substantially the agreement between the calculated and observed values of S in the case of the A_1' vibrations of $C_6H_3D_3$. This improvement is obtained as a result of using the quantities in the last two rows of Table 2.

"N.G.Chernyshevskii" Saratov State University

References

1. G.Allen & H.J.Bernstein, Canad. J. Phys., 33, 1137 (1955).
2. M.V.Vol'kenshtein, M.A.El'iashevich & B.I.Stepanov, Kolebaniia molekul (Molecular vibrations) Vol.II, M.-L., 1949.
3. S.M.Ferigle & A.Weber, Canad. J. Phys., 32, 799 (1954).
4. M.A.Kovner & B.N.Snegirev, Doklady AN SSSR, 112, 835 (1957).
5. M.A.Kovner, Zhur.eksp. i teor.fiz., 26, 598 (1954).
6. M.A.Kovner, Doklady AN SSSR, 97, 65 (1954).
7. D.H.Whiffen, Proc. Phys. Soc. A,69, No.437, 375 (1956).

CORRESPONDENCE OF THE ABSORPTION AND LUMINESCENCE BANDS OF COMPLEX MOLECULES

- B. I. Stepanov

In this contribution we shall show that there obtains the following universal relation between the contour of the fluorescence band and the contour of the long wavelength absorption band of complex molecules, namely,

$$W_\nu^{\text{lum}} = D(T, \text{exc. cond.})\, W_\nu^{\text{ther. em.}} = D \cdot \mathfrak{A}_\nu u_\nu = d \cdot \mathfrak{A}_\nu \nu^3 \frac{1}{e^{h\nu/kT} - 1}, \qquad (1)$$

wherein the proportionality factors D and d depend only on the temperature and excitation conditions and do not depend on the frequency ν.

In Eq. (1) W_ν^{lum} and $W_\nu^{\text{ther. em.}}$ are the luminescence and thermal emissive powers, $\mathfrak{A}_\nu$ is the absorptive capacity and u_ν is the density of the equilibrium emission. Relation (1) is valid if during the time the molecule remains in the excited electronic state there is established statistical equilibrium of the emitting center with the surrounding medium, and consequently, an equilibrium distribution over the vibrational energy levels.*

This assumption is generally considered to hold for solutions.[2] It is invoked to explain the fact that the quantum efficiency and position and contour of the luminescence band are independent of the frequency of the exciting light, the equal persistence of all frequencies of the luminescence band and other experimental facts. The assumption is supposed to be valid not only for solutions of complex molecules but also for other condensed systems. It is also partially valid for vapors of complex molecules inasmuch as during the time the molecules remain in the excited state there occurs extremely rapid redistribution of vibrational energy over individual degrees of freedom and attainment of statistical equilibrium inside each excited molecule (see below).

Before embarking on the proof of the above universal relation, we must recall a fundamental law of thermal emission, namely, Kirchhoff's law. It is applicable to all bodies in the state of equilibrium with the surrounding medium, including complex molecules such as dye molecules. According to Kirchhoff's law

$$W_\nu^{\text{therm. em.}} = \mathfrak{A}_\nu u_\nu. \qquad (2)$$

The absorptive capacity $\mathfrak{A}_\nu$ is proportional to the absorption coefficient k_ν and is known from experiment for many complex molecules. The variation of k_ν with frequency ν is essentially what is usually called the contour of the absorption band. A typical $\mathfrak{A}_\nu$ vs ν curve for dye type molecules is shown in Fig. 1 (curve 1). Curve 2 in the same figure gives the variation of Planck's function in the visible region of the spectrum. For the purpose of our discussion the important point is that as ν decreases the value of u_ν monotonically increases. Curve 3 gives the result of multiplication of the values of $\mathfrak{A}_\nu$ and u_ν, i.e., the thermal emissive power of the given substance. The maximum of the thermal emission band is shifted somewhat to the side of lower frequencies relative to the maximum of the absorption band. According to Eq. (1) the luminescence power is proportional to the thermal emissive power; consequently, knowing the contour of the absorption band from experiment, we can readily calculate the contour of the thermal emission band and compare it with the contour of the luminescence band.

---

*In addition it is assumed that nonexciting absorption can be neglected.[1] Relation (1) is inapplicable to mixtures of two substances absorbing in the same spectral region.

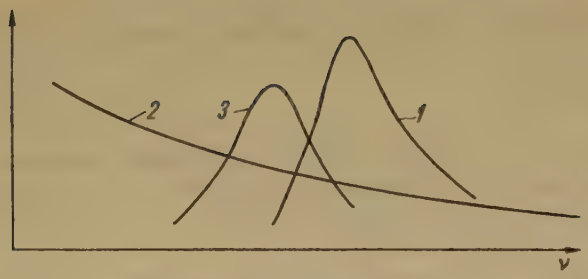

Fig.1. (Scales arbitrary).

Let us consider the level diagram shown in Fig.2. The lower part represents the vibrational levels of the lower electronic state; the upper part the vibrational levels of the upper electronic state. In the general case, the emissive power at frequency ν (in a unit frequency interval) is given by[2]

$$W_\nu = h\nu \int n^*(E^*_{vib})\, A(E^*_{vib}, \nu)\, dE^*_{vib}. \quad (3)$$

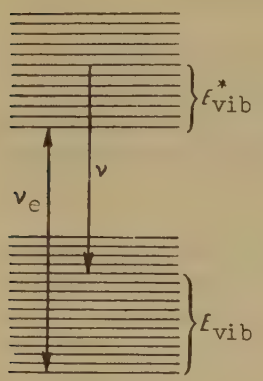

Fig.2.

Here $n^*(E^*_{vib})$ is the number of excited molecules per unit vibrational energy interval, $A(E^*_{vib}, \nu)$ is the probability of a spontaneous transition (Einstein's coefficient) from the vibrational level E^*_{vib} of the upper electronic state to the vibrational level $E_{vib} = E^*_{vib} - h\nu + h\nu_e$ of the lower electronic state. Integration is carried out over all values of the vibrational energy of the excited state.

Let us assume now that complete thermodynamic equilibrium has been attained in the system under study. In this case according to Boltzmann's formula

$$n^*(E^*_{vib}) = C(T)\, n g^*(E^*_{vib}) \exp\left(-\frac{h\nu_e + E^*_{vib}}{kT}\right), \quad (4)$$

where n is the total number of molecules, $g^*(E^*_{vib})$ is the statistical weight of the vibrational levels of the excited electronic state and $h\nu_e + E^*_{vib}$ is the total energy of the vibrational level E^*_{vib}.

Substituting (4) in (3), we obtain the following equation for the thermal emissive power

$$W_\nu^{ther.em.} = h\nu C(T)\, n e^{-h\nu_e/kT} \int g^*(E^*_{vib})\, A(E^*_{vib}, \nu)\, e^{-\frac{E^*_{vib}}{kT}} dE^*_{vib}. \quad (5)$$

Let us now find the luminescence power. According to our initial assumption, prior to the emission event there is established an equilibrium distribution of excited emitting centers over the vibrational energy levels:

$$n^*(E^*_{vib}) = C^*(T)\, n^*\, g^*(E^*_{vib})\, e^{-E^*_{vib}/kT}. \quad (6)$$

Here n^* is the number of excited molecules, which depends on the excitation conditions: the intensity of the incident light, the presence of quenchers, the temperature and properties of the molecule itself. The statistical weight $g^*(E^*_{vib})$ has the same meaning as in Eq.(4); it depends only on the properties of the molecules. The temperature T in the case of solutions is determined by the temperature of the medium; in the case of vapor it may depend, in addition, on the excitation conditions.

Substituting (6) in (3), we obtain for the case of solutions

$$W_\nu^{lum} = h\nu C^*(T)\, n^*(T_{exc.cond.}) \int g^*(E^*_{vib})\, A(E^*_{vib}, \nu)\, e^{-E^*_{vib}/kT} dE^*_{vib}. \quad (7)$$

From (7) and (5) we readily obtain our initial formula: Eq.(1). There may obviously occur deviations from relation (1) in practice. Such deviations, however, should not be taken to mean that the relation itself is invalid but only as indication that the necessary conditions are not fulfilled. If the redistri-

bution of particles over vibrational levels occurs slowly and equilibrium is not established during the time the molecule remains in the excited state, relation (1) loses all meaning. If the deviation from equilibrium is relatively small, comparing the contour of the luminescence band calculated by means of Eq.(1) with the contour of the band measured experimentally, we can draw certain inferences regarding the degree and character of departure from equilibrium and the rate of attainment of equilibrium. Such a case may occur, for example, in studying anti--Stokes fluorescence. Whereas in Stokes excitation the contour of the luminescence band is characterized by Eq.(1), in going over to anti-Stokes excitation the relation no longer holds.[3,4] This indicates that in the case of anti-Stokes excitation, equilibrium distribution of the excited molecules does not have time to become established prior to the emission event.

A distinctive situation occurs in the luminescence of rarefied gases. In this case (with $\nu_{excit} > \nu_e$) equilibrium with the medium is not realized: the excited molecules possess an excess of vibrational energy. At the same time, inside each molecule equilibrium of the individual vibrational degrees of freedom is established.[2] The intrinsic temperature of such molecules is higher than the temperature of the medium and depends directly on the frequency of the exciting light. This is why the contour of the luminescence band of a vapor, although generally close to the contour of the luminescence band of the corresponding solution, differs somewhat from it, the difference increasing with the magnitude of $\nu_{excit} - \nu_e$. If there were no equilibrium in the vapor molecule, the luminescence spectrum would depend much more strongly on ν_{excit} (as, for example, in atoms).

Recently Alentsev[5] called attention to the fact that relation (1) can be applied to vapors. In this case, however, the contour of the luminescence band must be compared with the contour of the thermal emission not at the actual temperature of the experiment but at another, higher temperature equal to the mean intrinsic temperature of the excited molecules.* This suggests an obvious procedure for determining the mean intrinsic temperature of excited vapor molecules.

Verification of relation (1) on the basis of extant experimental material is difficult. Most investigators studying the luminescence of complex molecules measured only W_ν^{lum} and k_ν close to the center of the band and did not make careful measurements at the edges of the band where W_ν^{lum} and k_ν are small. This has been due not so much to experimental difficulties but to the fact that there was no apparent need for such data. The first results of attempts of verification of relation (1) using extant experimental material, carried out in the work of Kazachenko[6], Kazachenko & Stepanov[1] and Alentsev[5], indicate both that the relation is valid in principle and that there are certain deviations from it. Careful investigation of these deviations should help clarify the distinctive features of the luminescence of different types of complex molecules.

Relation (1) has been used[1] for developing a method for determining the frequency of a purely electronic transition from the absorption band alone without measurement of the luminescence spectra or from the luminescence band alone without measurement of the absorption spectrum. Strictly speaking, this method is applicable only to molecules characterized by mirror symmetry of the long wavelength of the absorption band and the luminescence band. In most actual cases

---

*Analyzing a number of earlier experimental data from the standpoint of relation (1) Alentsev came to the conclusion that the mean temperature of excited molecules in a solution is also higher than the nominal temperature of the solution. This may indicate that the exchange of energy with the medium does not have time to go to completion within 10^{-8}-10^{-9} sec and equilibrium is not attained. This hypothesis, which requires further experimental proof, may be important in clarifying the nature of processes occurring after excitation.

precise symmetry does not obtain; as a rule, however, close to the point of intersection of the spectra, a degree of symmetry is realized and the proposed method may lead to useful results.

Institute of Physics and Mathematics
Academy of Sciences of the Belorussion SSR

References

1. B.I.Stepanov, Doklady AN SSSR, 112, 839 (1957); L.P.Kazachenko & B.I.Stepanov, Optika i spektroskopiia, 2, 339 (1957); Doklady AN SSSR, 112, 839 (1957).

2. B.I.Stepanov, Liuminestsentsiia slokhnykh molekul (Luminescence of complex molecules), Pub., Ac. of Sci. of Belorussian SSR; Usp.fiz.nauk,108,3 (1956).

3. L.A.Tumerman, Trudy (Proceedings) Physical Inst., USSR Acad. of Sci., No.4, 77 (1938).

4. B.S.Neporent & N.A.Borisevich, Doklady AN SSSR, 94, 447 (1954).

5. M.N.Alentsev, Optika i spektroskopiia, 4, 690 (1958).

6. L.P.Kazachenko, Usp.zap. (Scientific notes) Belorussian University, No.41, Phys.series, 1957.

DIFFERENT FORMS OF CONCENTRATION QUENCHING AND THE POSSIBILITY OF DISTINGUISHING BETWEEN THEM*

- V.L.Levshin & E.G.Baranova

The present work was a continuation of our earlier investigations[1,2] devoted to clarifying the nature of concentration quenching in dye solutions. As the subject of the present study, we chose solutions of rhodamine 6G and rhodamine 6B in water and ethyl alcohol.

In our opinion there may exist three different types of concentration quenching, namely, quenching due 1) to inactive absorption of the exciting light by nonluminescing associative complexes, 2) to transfer of excitation energy from an excited monomer to a nonluminescing complex and 3) to transfer of energy from an excited monomer to a nonexcited one. In the last case the decrease in luminescence results from the fact that part of the transitions lead to dissipation of the excitation energy.

In this study we noted the formation of nonluminescing aggregates with increasing concentration and determined the degree of association. Further, we developed methods for distinguishing between the above mentioned quenching processes.

Aqueous solutions

In aqueous solutions of rhodamine 6G and 6B there is virtually no association up to a concentration of $4 \cdot 10^{-6}$ mole/liter, for the absorption spectra of both dyes undergo little or no change up to this concentration. Up to this concentration, too, no concentration quenching is observed: the luminance of thin layers of solutions increase in proportion to the concentration.

With further increase in concentration, there occurs a noticeable change in the absorption spectra. The variation of the absorption spectra of rhodamine 3B extra is shown in Fig.1. With increasing concentration, the short wavelength absorption maximum rises, while the long wave absorption maximum flattens out. The absorption curves for both rhodamine 6G and rhodamine 3B solutions pass through a common point of intersection.

For solutions containing dimers the absorption coefficient is given by

$$\alpha = \alpha_m x + \alpha_d (1 - x), \tag{1}$$

where α_m and α_d are the absorption coefficients of solutions of monomers and dimers, respectively, and x is the fraction of monomers in the solution; α_m can readily be determined from the spectra of weak solutions, while α_d is unknown.

For the case of equilibrium of dimers and monomers in the solution

$$\frac{x^2}{1-x} = \frac{D}{C}. \tag{1'}$$

From (1) and (1') we obtain

$$\frac{(\alpha - \alpha_d)^2}{\alpha_m - \alpha} = \frac{D}{C}(\alpha_m - \alpha_d), \tag{2}$$

where D is the equilibrium constant. Obviously, for two different concentrations C_1 and C_2 we can write

---

*Resume of report. Complete text will be published in "Optika i spektroskopiia".

$$\frac{\alpha_1 - \alpha_d}{\alpha_2 - \alpha_d} = \sqrt{\frac{C_2(\alpha_m - \alpha_1)}{C_1(\alpha_m - \alpha_2)}},$$

whence

$$\alpha_d = \frac{\alpha_1 - B\alpha_2}{1 - B}, \qquad (3)$$

where

$$B = \sqrt{\frac{C_2(\alpha_m - \alpha_1)}{C_1(\alpha_m - \alpha_2)}},$$

and α_1 and α_2 are the experimentally determined absorption coefficients for the two solutions having the concentration C_1 and C_2.

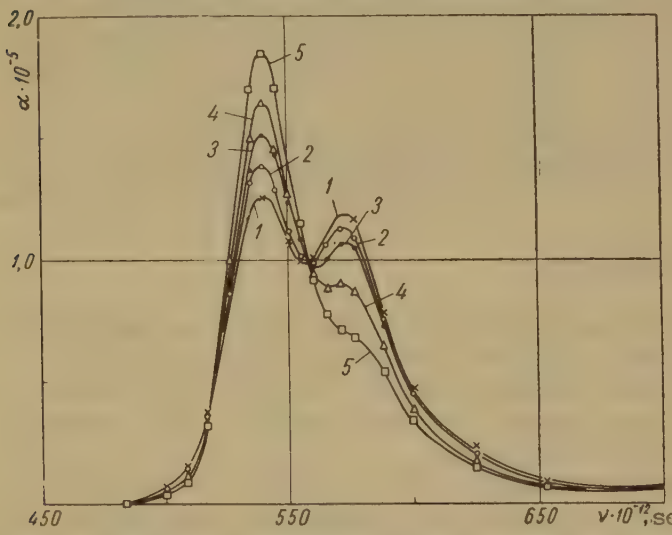

Fig.1. Absorption spectra of aqueous solutions of rhodamine 3B extra at different concentrations: 1) C = $4 \cdot 10^{-3}$, 2) $2 \cdot 10^{-3}$, 3) $1 \cdot 10^{-3}$, 4) $4 \cdot 10^{-4}$, 5) $4 \cdot 10^{-5}$, $2 \cdot 10^{-6}$ & $4 \cdot 10^{-6}$ mole/liter (α = = absorption coefficient).

From (3) we can determine α_d for any given wavelength and then by means of (1) find x. Thus from the absorption spectra we can determine the degree of association in the solution and evaluate the role of inactive absorption.

The effect of migration (energy transfer) quenching can be determined from the decrease in luminescence intensity of a thin layer of solution. The luminescence intensity of a thin layer of solution is given by

$$I = AxC\varkappa_m\varkappa_d, \qquad (4)$$

where A is a constant that depends on the excitation intensity, the thickness of the layer, the absorption coefficient and the luminescence yield at low concentrations but does not depend on the concentration, the association of the dye molecules or transfer of energy; x is the fraction of molecules in the monomer state; $\varkappa_m$ and $\varkappa_d$ are factors taking into account the decrease in intensity due to transfer of excitation energy to monomers and dimers, respectively.

As a result of investigation of the luminescence intensity I of thin layers of rhodamine 6G and 3B solutions, we obtained the data shown in Table 1 (τ/τ_o is the relative change in persistence of luminescence).*

It will be evident from Table 1 that migration of excitation energy from monomers to dimers in solutions of rhodamine 6G becomes noticeable at a concentration at which the mean distance from an excited molecule to a dimer molecule is 100 Å; the corresponding distance in rhodamine 3B solutions is 85 Å.

---

*The measurements on a Tumerman fluorometer were carried out by O.F. Shelaeva, for whom we take this opportunity to thank.

Table 1

Variation in association with increasing concentration of solutions of rhodamines 6G and 3B and development of migration quenching

C, mole/liter	Rhodamine 6G				Rhodamine 6B			
	κ, % (from absorption)	I/CA	$\varkappa_m \varkappa_d$	τ/τ_0	κ, % (from absorption)	I/CA	$\varkappa_m \varkappa_d$	τ/τ_0
$4 \cdot 10^{-6}$	1,00	1,00	1,00	1,00	1,00	1,00	1,00	1,00
$1 \cdot 10^{-4}$	0,72	0,74	1,02	1,00	0,90	0,91	1,01	1,00
$2 \cdot 10^{-4}$	0,61	0,63	1,03	1,00	0,85	0,87	1,02	1,00
$4 \cdot 10^{-4}$	0,50	0,52	1,04	0,80	0,74	0,76	1,02	0,93
$1 \cdot 10^{-3}$	0,35	0,29	0,83	0,70	0,58	0,55	0,95	0,90
$2 \cdot 10^{-3}$	0,26	0,17	0,67	0,60	0,46	0,33	0,72	0,80
$4 \cdot 10^{-3}$	0,20	0,08	0,40	0,41	0,35	0,18	0,51	0,69

Alcohol solutions

The solubility of rhodamines in alcohol is much higher than in water. In alcohol, concentrations of up to $1.6 \cdot 10^{-1}$ mole/liter can be attained.

Concentration quenching becomes evident only at very high concentrations of the order of $1 \cdot 10^{-2}$ mole/liter. The absorption spectra change little up to such concentrations. The quenching is connnected with the formation of associative complexes, inasmuch as upon heating of quenched solutions their luminescence sharply increases. To explain this we must assume that in alcohol solutions the predominant role in quenching is played by energy transfer to dimers. Percentagewise the dimer content in solutions even at high dye concentrations is low. It may be inferred from a comparison of the absorption spectra of water and alcohol solutions that in an alcohol solution of rhodamine 3B with a concentration of $8 \cdot 10^{-2}$ mole/liter the percent of dimers is only ~5%, i.e., $C_d = 4 \cdot 10^{-3}$ mole/liter. Although the percent content of dimers is low, in view of the high concentration of dye at which quenching is observed, the actual absolute concentration of dimers is appreciable and apparently sufficient for the development of inductive concentration quenching.

Table 2

Variation of the luminescence intensity of alcohol solutions of rhodamine 3B as function of the concentration

C, mole/liter	Thin layer	Complete absorption
	$I \sim \varkappa_m \varkappa_d$	$I \sim \varkappa_m \varkappa_d$
$1,4 \cdot 10^{-3}$	1,00	1,00
$1 \cdot 10^{-2}$	0,94	0,94
$2 \cdot 10^{-2}$	0,79	0,65
$4 \cdot 10^{-2}$	0,47	0,37
$8 \cdot 10^{-2}$	0,12	0,12
$1,6 \cdot 10^{-1}$	0,04	0,04

Measurements of the intensity of luminescence of alcohol solutions in thin layers (λ_{excit} = 365 mμ) and with complete absorption (λ_{excit} = 540 mμ) yielded the data listed in Table 2. The luminescence was observed in the orange region of the spectrum (600-650 mμ), where absorption by the solution is weak.

In view of the fact that the dye concentrations in ethyl alcohol were very high, we had reason to expect that here the quenching influence of energy migration from monomer to monomer would be evinced. Actually, however, no quenching was observed up to a concentration of $1 \cdot 10^{-2}$ mole/liter; consequently, this effect is very weak as compared with quenching due to energy transfer to associative complexes (dimers). In water solutions one cannot obtain concentrations better than $3 \cdot 10^{-3}$-10^{-2} mole/liter, hence if the efficiency of quenching due to energy migration from monomer to monomer is equal to the efficiency in alcohol solutions, this effect in water solutions can be neglected; it is highly probable, however, that in water monomer to monomer energy transfer quenching is more effective than in alcohol.

Aggregates in binary solutions

We investigated the possibility of formation of complexes of molecules of two different dyes, namely, rhodamine 6G and rhodamine 3B.

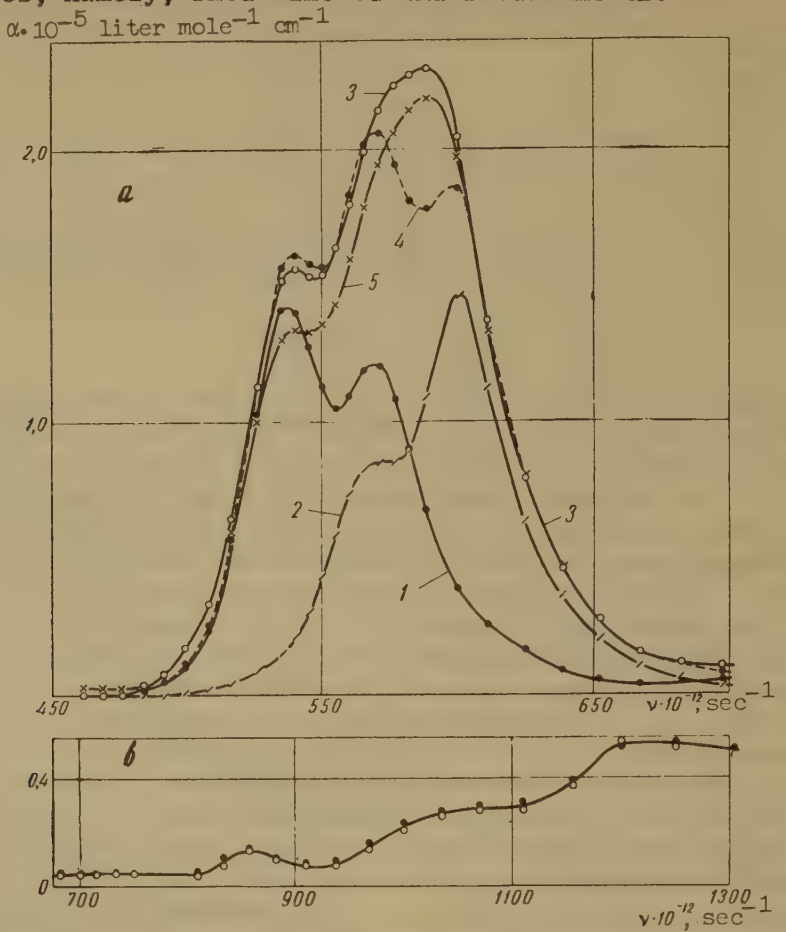

Fig.2. a) Absorption spectra of binary solutions in the principal region of the spectra - appearance of complex aggregates; 1 - C = $= 2 \cdot 10^{-3}$; rhodamine 3B; 2 - C = $2 \cdot 10^{-3}$, rhodamine 6G; 3 - experimental curve for a binary solution of rhodamines 3B and 6G with equal concentrations C = $2 \cdot 10^{-3}$; 4 - curve for the same solution calculated as the sum of curves 1 and 2; 5 - experimental curve for a binary solution of rhodamines 3B and 6G with equal concentrations C = $4 \cdot 10^{-3}$; b) absorption spectrum of binary solutions in ultraviolet region; rhodamines 3B and 6G in equal concentrations: ● - C = $= 1 \cdot 10^{-3}$, o - C = $4 \cdot 10^{-5}$ (all concentrations in mole/liter).

At low concentrations the absorption spectrum of binary solutions proved to be equal to the sum of the spectra of solutions of the individual components. At high concentrations, however, the additivity broke down. Fig.2 shows the spectra of the individual components, the calculated (sum) spectrum for a binary solution (dashed curve) and the observed spectra of binary solutions. It will be seen that the calculated curve differs noticeably from the experimental spectra. The difference is evidence of the formation of complex aggregates. These are less stable than dimers of the individual components and dissociate when the solution is heated to 80°. At this temperature the experimental spectrum of the binary solution becomes identical with the calculated (sum) spectrum.

It must be noted that the change in the absorption spectra incident to association is limited to the first absorption band lying in the visible region of

the spectrum. The ultraviolet part of the spectrum both for ordinary and complex aggregates of rhodamines 3B and 6G agrees with the spectrum of nonassociated molecules and is similar for both dyes.

Thus association affects only the π-electron cloud.

The authors would like to thank L.V.Krotova for assistance in the work.

"P.N.Lebedev" Physical Institute
Academy of Sciences of the USSR

References

1. V.L.Levshin, Z.Phys., 43, 230 (1927); Zhur.fiz.khim., 6,1 (1935); Izv. AN SSSR,Ser.fiz., 20, 397 (1956). (Trans. Bulletin,20, No.4, 362.)

2. V.L.Levshin & E.G.Baranova, Izv.AN SSSR,Ser.fiz., 20, 424 (1956). (Trans. Bulletin, 20, No.4, 387.)

* * * *

ON THE RELATION BETWEEN THE KRAVETS INTEGRAL (AREA OF THE ABSORPTION BAND) AND THE LIFETIME OF THE EXCITED STATE OF MOLECULES

- M.D.Galanin & Z.A.Chizhikova

Introduction

The luminescence of complex molecules is usually associated with electron transitions from the first excited state to the ground state. In absorption these transitions are responsible for the long wavelength absorption band. If, in conformity with the Franck-Condon principle, the electron transition probability is independent of the vibrational-rotational state of the molecule, the transition probability calculated from the first absorption band should be equal to the probability of the inverse transition.

In the case of luminescence with a quantum efficiency of 100% the transition probability from the excited state is obviously equal to the emission probability $1/\tau_o$, where τ_o is the mean lifetime of the excited state. For absorption the transition probability is proportional to the area of the absorption band (the Kravets integral). Thus under the given conditions there is a direct relation between the Kravets integral and $1/\tau_o$. Despite the fact that this relation is a general one and has been repeatedly used in different studies, we have no more or less systematic data on the extent to which it holds in the luminescence of complex molecules. Moreover, the question of the influence of the solvent (in particular the influence of the "effective field") on this relation has not been considered in the literature.

The influence of the effective field on the absorption band integral was taken into account in Kravets' classical work.[1] Later this question was examined by Chako[2]. It was found, however, that the Lorentz corrections to the effective field do not lead to a satisfactory explanation of the observed change in the area of absorption bands in going from vapor spectra to the spectra of solutions (see, for example, the review of Ref.3). The available data on absorption do not allow of determining the reasons for this divergence: it may be due to a difference between the actual effective field and that calculated according to Lorentz or it may be due to changes in the transition probability as a result of some influence of the solvent which cannot be taken into account by means of the effective field.

Below we shall give experimental data illustrating the relation between $1/\tau_0$ and the area of the first absorption band for luminescing substances with a high quantum efficiency.

The influence of the index of refraction of the medium and the effective field on the relation between the probabilities of absorption and emission have been considered in the work of Dexter[4,5]. In a number of treatises on luminescence, however, one can still find formulas that fail to take into account the influence of the effective field on this relation.[6,7] Hence it may be expedient to give a brief derivation of this relation.

1. Derivation of the relation between the probability of emission ($1/\tau_0$) and the area of the absorption band

Let us consider the simplest classical model of an emitter in the form of a dipole oscillator inserted in a spherical cavity in a medium with an index of refraction n. The relationship between τ_0 and the integrated absorption coefficient for a classical oscillator is of course trivial inasmuch as both quantities in this case are fully determined. But this simple classical model serves to show how the relation in question depends on the index of refraction of the medium and the effective field. The damping constant of the oscillator is given by[8]:

$$\frac{1}{\tau_0} = \frac{2}{3}\frac{\omega_0^2 e^2}{mc^3} n. \tag{1}$$

The energy of the electromagnetic wave absorbed by the oscillator per unit time is defined by the following expression (the electric field vector is assumed to be directed along the dipole axis)[7]:

$$\frac{dW_{\text{abs}}}{dt} = \frac{\frac{\gamma\omega^2 e^2}{m} 2E_{\text{eff}}^2}{(\omega_0^2-\omega^2)^2+4\gamma^2\omega^2}, \tag{2}$$

where γ is the damping constant, E_{eff}^2 is the mean square of the electric field strength (frequency ω) of the incident wave in the cavity ("effective field"). Let us characterize dW_{abs}/dt in terms of the absorption coefficient $k(\omega)$. The attenuation of the energy flux S in passing through a layer dx is

$$dS = -k(\omega) S dx = -\frac{dW_{\text{abs}}}{dt}\cdot\frac{N dx}{3}, \tag{3}$$

where $S = (c/4\pi)nE^2$ (here E^2 is the mean square of the external field intensity), N is the number of dipoles per unit volume and the factor 1/3 takes care of averaging over the angle between the direction of the electric field and the axes of the randomly oriented dipoles. From (2) and (3), integrating over the frequencies and comparing with (1), we obtain

$$\frac{1}{\tau_0} = \frac{\omega_0^2}{\pi^2 c^2 N}\left(\frac{E}{E_{\text{eff}}}\right)^2 n^2 \int k(\omega)\, d\omega. \tag{4}$$

A more general derivation of this relation, not connected with any specific model, is based on the relative values of Einstein's coefficients. The ratio of the spectral densities of Einstein's coefficients $A'(\omega)$ and $B'(\omega)$ when the radiating system is located in a medium with an index of refraction n increases by a factor of n^3 (this is because the intensity of equilibrium radiation in the medium increases by a factor of n^2, while the radiation density increases n^3 times). Consequently,

$$\frac{g_2 A'}{g_1 B'} = \frac{\hbar\omega^3}{\pi^2 c^3} n^3, \tag{5}$$

where g_1 and g_2 are the statistical weights of the upper and lower states. The Einstein coefficient A' is related to the emission probability by

$$\frac{1}{\tau_0} = \int A'(\omega)\, d\omega. \tag{6}$$

Coefficient B' determines the absorption probability. The energy absorbed in a layer having an area of 1 cm^2 and a thickness dx in the frequency interval $d\omega$ is

$$dS(\omega) = -NB'(\omega)\, u(\omega)\, \hbar\omega\, dx\, d\omega, \tag{7}$$

where $u(\omega)$ is the energy density at the point where the absorbing system is situated.

Obviously, $u(\omega)$ is proportional to the square of the effective field intensity and, consequently,

$$u(\omega) = \frac{S(\omega)}{c/n}\left(\frac{E_{\text{eff}}}{E}\right)^2. \tag{8}$$

Recalling (3), we obtain the sought relation, fully similar to that deduced from the classical model, but having a more general meaning:

$$\frac{1}{\tau_0} = \frac{g_1}{g_2} \cdot \frac{1}{\pi^2 c^2 N}\left(\frac{E}{E_{\text{eff}}}\right)^2 n^2 \int \omega^2 k(\omega)\, d\omega. \tag{9}$$

For a Lorentz effective field, $\frac{E}{E_{\text{eff}}} = \frac{3}{n^2+2}$, and the factor dependent on n is $\left(\frac{3n}{n^2+2}\right)^2$. For the usual values of this factor is close to unity.

2. Experimental data

Experimental verification of formula (9) requires that certain conditions be fulfilled and is predicated on a number of assumptions. The experimentally measured value of τ will be equal to the "natural" lifetime τ_0 of the excited state only in the absence of quenching. If the quantum efficiency ρ of the luminescence is less than 100%, we can calculate τ_0 from the measured τ by assuming that the quenching is of the second kind. Then $\tau_0 = \tau/\rho$. Obviously, the possibilities of concentration quenching and increase of τ due to reabsorption and secondary emission must be excluded.

We measured τ, the absorption spectra and the quantum luminescence efficiencies for several luminescent solutions. The lifetime of the excited state was measured by means of a phase fluorometer; the absorption spectra were measured on an SF-4 spectrophotometer. The quantum efficiencies were determined by comparison with a standard solution of fluoroscein. The quantum field of fluoroscein was determined anew by the procedure described earlier.[9]

The experimental results are listed in the accompanying table; some of the absorption and luminescence spectra are reproduced in the figure.

In calculating τ_0 from the absorption we used the Lorentz effective field. The precise value of the index of refraction of crystal anthracene is not known but is is close to 2 and hence the factor dependent on n was taken equal to unity. For all the solutions the values of τ_0 determined from the area of the absorption band are in good agreement with the values calculated from measured values of τ and ρ. In the case of acridine and quinine, as will be obvious from the figure, there is some uncertainty as regards the actual area of the first absorption band. There is a considerable divergence for the anthracene crystal. Such a difference between the values for the crystal and the anthracene solutions is not unexpected and may be connected with the intensity of the effective field in the crystal.

Substance	Solvent	ρ (100%)	$\tau \cdot 10^{-9}$ sec meas.	$\tau_0 \cdot 10^{-9}$ sec calculated from τ/ρ	$\tau_0 \cdot 10^{-9}$ sec calculated from absorption
Fluorescein[1]	Glycerol	1.0	4.2	4.2	3.8
1-,1'-,4-,4'-Tetraphenylbutadiene	Polystyrene[2]	1.0	2.1	2.1	1.8
Acridine sulfate	Glycerol	0.8	27	34	28
Quinine sulfate	"	0.9	17	19	17
1,6-Diphenylhexathriene[3]	Benzene	0.7	5.6	8.0	7.9
Anthracene	Toluene	0.27	4.4	16	14.5
	Polystyrene[2]	0.26	5.2	20	23
Anthracene (crystal)[4]	--	1.0	8	8	(23)

Notes: [1]Data on fluorescein taken from Ref.10.
[2]We are indebted to I.M.Rozman for the polystyrene samples.
[3]Data from Ref.11.
[4]Experimental value of τ corrected for reabsorption.

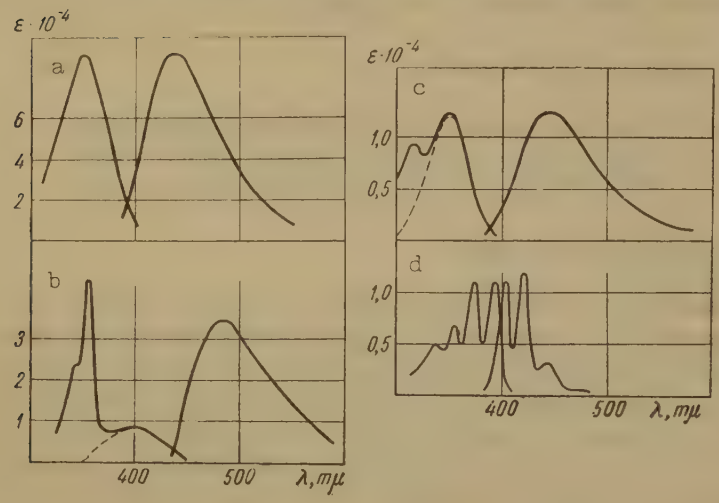

← Absorption and luminescence spectra: a) 1-,1'-,4-,4'-tetraphenylbutadiene in polystyrene, b) acridine sulfate in glycerol, c) quinine sulfate in glycerol, d) anthracene crystal (ε - molar absorption coefficient). The luminescence spectra give the energy distribution in relative units.

"P.N.Lebedev" Physical Institute
Academy of Sciences of the USSR

References

1. T.P.Kravets, Izv.Mosk.inzhenernogo uchilishcha, (Bulletin, Moscow Engineering College) 2, No.6 (1912).
2. N.Q.Chako, J.Chem.Phys., 2, 644 (1934).
3. R.S.Mulliken & C.A.Rieke, Repts.Progr.Phys., 8, 231 (1942).
4. D.L.Dexter, J.Chem.Phys., 21, 836 (1953).
5. D.L.Dexter, Phys.Rev., 101, 48 (1957).
6. E.J.Bowen & F.Wokes, Fluorescence of solutions, London, 1953.
7. B.I.Stepanov, Liuminestsentsiia slozhnukh molekul (Luminescence of complex molecules), Vol.1, Minsk, 1955.
8. M.D.Galanin & I.M.Franck, Zhur.eksp.i teor.fiz., 21, 114 (1951).
9. M.D.Galanin & Z.A.Chizhikova, ibid., 26, 624 (1954).
10. M.D.Galanin, ibid., 28, 485 (1955).
11. A.N.Nikitina, M.D.Galanin, G.S.Ter-Sarkisian & B.M.Mikhailov, Report presented at the Eleventh All-Union Conference on Theoretical Spectroscopy, 1957.

KINETICS OF IMPURITY QUENCHING OF FLUORESCENCE IN SOLUTIONS

- B.Ia.Sveshnikov, V.M.Shirokov, L.A.Kuznetsova & P.I.Kudriashov

Of considerable interest from both the standpoint of theory of fluorescence quenching in solutions and the theory of reactions in solutions is the question of calculating the number of effective collisions between molecules of the reacting substances. Formerly chemists generally held to the opinion that the number of effective collisions is proportional to the total number of collisions between the molecules of the dissolved substances, which in the first approximation does not depend on the viscosity of the solvent.

In 1936 one of us[1] showed that this hypothesis fails to take into account certain singularities in the distribution of collisions between the solvent molecules. Whereas in a gas two molecules taking part in a collision either react or "go their separate ways," in liquids two molecules involved in an encounter may undergo a series of repeat collisions before parting company. Hence the hypothesized viscosity independence of the reaction rate is actually observed only in the limiting case when the probability of reaction is a single collision is low. In contrast, in the other limiting case when the reaction probability $W = 1$, the number of effective collisions equals the number of primary collisions (encounters) and determination of this number reduces to solving the diffusion problem, which gives a virtually linear dependence of the reaction rate on the viscosity. In intermediate cases ($0 < W < 1$), the rate of reaction will increase more slowly than the fluidity.*

The first convincing proof of the possibility of applying the methods of diffusion theory to calculating the number of effective molecular collisions in solutions was actually given by Vavilov[4]. The quenching equation deduced by Vavilov, however, did not give a rigorous quantitative description of the effect. It was predicated on the assumption that the duration and yield of luminescence vary in exactly the same way in the process of quenching and that the ratio of the luminescence yield B_0 of the unquenched solution to the luminescence yield B of the quenched solution is a linear function of the quencher concentration and the fluidity. The experimentally observed regularities proved to be more complicated. In order to reconcile theory with experiment, Vavilov & Frank[5] introduced the hypothesis of additional static quenching. Subsequently, detailed analysis of the kinetics of the diffusion processes developing about an excited molecule enabled one of us[6] in 1935 to deduce a quenching formula explaining the nonlinear dependence of B_0/B on the quencher concentration c without recourse to the static quenching concept. It was shown that the reason for the nonlinear dependence of B_0/B on c may be deviation of the fluorescence decay law for quenched solutions from the exponential. This deviation from the exponential law is due to the fact that the number of encounters of an excited molecule with quencher molecules, as follows from a rigorous solution of the diffusion equation, is a function of time. When this time dependence is taken into account the fluorescence decay law for quenched solutions is described by

$$n = n_0^{-(\alpha t + p\beta\sqrt{t})}. \qquad (1)$$

---

*This distinctive feature of the distribution of collisions between solute molecules and its importance in the kinetics of molecular reactions in solutions were later discussed by Rabinovitch[2] (1937) and Fowler & Slater[3] (1938).

where n is the number of excited molecules at the instant t, n_0 is the number of excited molecules at the instant $t = 0$, p is the probability of quenching during the period of the encounter and

$$\alpha = 4\pi pRDc + \tau_0^{-1} \quad \text{and} \quad \beta = 8\pi^{\frac{1}{2}} D^{\frac{1}{2}} R^2 c. \tag{2}$$

In these formulas R is the interaction range (radius of the sphere of action), D is the diffusion coefficient, c is the number of quencher molecules per unit volume and τ_0 is the lifetime of the excited state of the molecules in unquenched solutions.

From (1) we can readily deduce the following formulas for the yield ratio:

$$\frac{B_0}{B} = \alpha\tau\delta, \tag{3}$$

where

$$\delta = \left[1 - 2\gamma e^{\gamma^2}\left(\sqrt{\frac{\pi}{2}} - \int_0^{\gamma} e^{-z^2} dz\right)\right]^{-1} \quad \text{and} \quad \gamma = 2pR^{\frac{3}{2}} c^{\frac{1}{2}} \left(\frac{4\pi pDRc\tau_0}{4\pi pDRc\tau_0 + 1}\right) \tag{4}$$

and the ratio of fluorescence persistences:

$$\chi \frac{B}{B_0} = \frac{\tau}{\tau_0}, \tag{5}$$

where

$$\chi = \left(1 + \gamma^2 - \frac{\delta - 1}{2}\right)\delta. \tag{6}$$

The calculated values of δ^{-1} and χ^{-1} as functions of γ are plotted in Fig.1. For the given combination (fluorescing substance + quencher + solvent) γ is a function only of the quencher concentration. It should be noted that Eq.(5) contains the quantity τ, the duration of fluorescence, given by

$$\tau = \int t dn' \Big/ \int dn', \tag{7}$$

where n' is the number of molecules de-exciting radiatively.

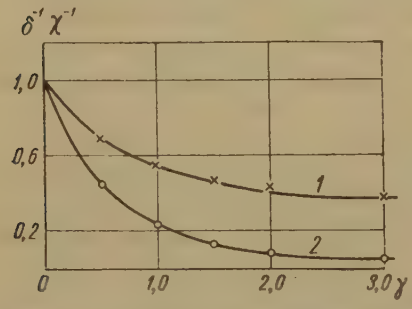

Fig.1. Plot of the functional dependence of χ^{-1} (1) and δ^{-1} (2) on γ.

In the case of a nonexponential decay law τ does not equal τ', the duration or lifetime of the excited state of the molecule, given by

$$\tau' = \int t dn \Big/ \int dn. \tag{8}$$

We must note another important consequence of the nonexponential decay law for quenched solutions. In investigating the polarization of fluorescence of quenched solutions, τ in the Levshin-Perrin formula is usually replaced by $\tau_0(B/B_0)$. When the fluorescence decay law is not exponential this substitution is not permissible. Calculations[7] for this (nonexponential) case lead to the formula

$$\frac{1}{p} - \frac{1}{3} = \left(\frac{1}{p_0} - \frac{1}{3}\right)\left(\frac{kTB}{v\eta B_0}\tau_0\delta + 1\right)\frac{\delta_1}{\delta} \tag{9}$$

where p is the degree of polarization corresponding to the given quencher concentration, p_0 is the limiting polarization, i.e., the polarization for infinitely high viscosity η or as $(B/B_0) \to 0$ and δ_1 is equivalent to the expression obtained by replacing α is (2) by $\alpha + (kT/v\cdot\eta)$ (where v is the molecular volume).

In the case of an exponential decay law $\delta_1 = \delta = 1$ and (9) becomes the usual Levshin-Perrin formula.

Direct proof of the validity of the proposed quenching theory is furnished by the experimentally observed deviation of the decay of fluorescence of quenched solutions from the exponential law, i.e., the observed dependence of the mean persistence of luminescence on the light modulation frequency in the fluorometer.

We measured τ_{fl} for a solution of 3-aminophthalimide in glycerol quenched by a factor of 6 by potassium iodide, with $\omega_1 = 8 \cdot 10^7$ sec^{-1} and $\omega_2 = 16 \cdot 10^7$ sec^{-1}. We found that τ_{fl} does vary with the frequency and that the variation is in qualitative agreement predicted by theory. Glycerol was chosen as the solvent because, as follows from (1), the deviation of the decay law from the exponential should be strongest in a viscous solution.

For qualitative comparison of the experimental results with the theoretical, we calculated τ_{fl}, which for an arbitrary decay law is given by

$$\tau_{fl} = \frac{1}{\omega} \frac{\int_0^\infty n(t) \sin \omega t \, dt}{\int_0^\infty n(t) \cos \omega t \, dt}. \qquad (10)$$

The constants α and $p\beta$ in the expression for the time dependence of n (Eq. (1)) were determined from the experimental values of τ/τ_0 and B/B_0. In these calculations we took τ equal to τ_{fl} measured with $\omega = 8 \cdot 10^7$ sec^{-1}. The actual value of τ is some 3-4% greater than τ_{fl}, which in the given case is unimportant. In view of the impossibility of calculating the integrals in Eq.(10), τ_{fl} was evaluated graphically. The theoretical and experimental values of τ_{fl} are listed in Table 1.

Table 1

Values of τ_{fl}	ω, sec^{-1}		$\Delta\tau_{fl}$, sec
	$8 \cdot 10^7$	$16 \cdot 10^7$	
Experimental	$3.88 \cdot 10^{-9}$	$3.57 \cdot 10^{-9}$	$0.31 \cdot 10^{-9}$
Calculated	$3.74 \cdot 10^{-9}$	$3.44 \cdot 10^{-9}$	$0.30 \cdot 10^{-9}$

It will be seen from the table that the difference between the values of τ_{fl} determined from experiment agrees with the theoretical value. The indicated experimental values of τ_{fl} are averages based on many measurements. We evaluate the uncertainty in the experimental value of $\Delta\tau_{fl}$ as $\pm 0.05 \cdot 10^{-9}$ sec.

A no less convincing proof of the nonsteady character of the Brownian motion during the lifetime of molecules in the excited state is experimental substantiation of Eq.(5). To this end one must compare the changes in yield and the mean duration of fluorescence in the case of fluorescence quenching.

The data obtained by us for the variation of the yield and mean duration of fluorescence as a function of the quencher concentration for an aqueous solution of fluorescein quenched by KI are shown in Fig.2. From the experimental data on B_0/B and τ_0/τ we can readily obtain the experimental curve for χ and by matching it with the corresponding theoretical curve (Fig.1) determine the ratio of γ and c. Having this ratio, one can readily find the expectation value of B for each experimental value of τ. This has been done in Fig.2. The good agreement of the calculated and experimental data is proof that the fluorescence decay law is nonexponential and that a diffusion mechanism is involved in the quenching process.

Finally, for experimental verification of Eq.(9), we investigated the variation in the degree of fluorescence polarization of aqueous solutions in fluorescein quenched with KI. For each KI concentration, we calculated two values of the limiting polarization - one by replacing τ by its fluorometric value, the other by means of Eq.(9); the results are listed in Table 2.

It will be obvious from comparison of the values in the last two columns of the table that calculations by means of Eq.(9) give better results.

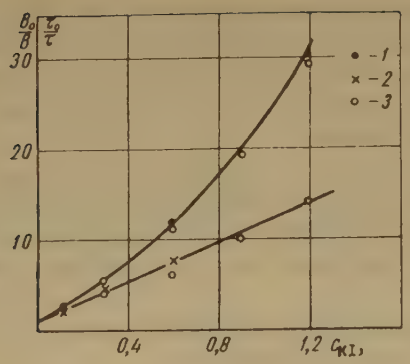

Fig.2. Variation of the yield B and duration τ of the fluorescence of an aqueous solution of fluorescein as a function of the concentration c of the quencher (KI): 1) experimental value of B, 2) experimental values of τ and 3) values of yield and duration obtained by calculation using the values of χ^{-1} and δ^{-1} from Fig.1.

Table 2

Experimental values of the degree of polarization P, the relative yield B/B_0 and the duration τ/τ_0 of fluorescence in KI quenched solutions of fluorescein and the calculated values of the limiting polarization P_0

c_{KI}, mole/liter	$\frac{B}{B_0}$	$\frac{\tau}{\tau_0}$	P, %	δ_1	$\frac{\delta_2}{\delta_1}$	P_0, from (9)	P_0, from τ_{fl}
0,15	0,34	0,336	4,54	1,31	0,8416	39,2	36,3
0,3	0,192	0,21	7,15	1,57	0,763	39,2	38,2
0,6	0,095	0,128	11,43	1,96	0,7370	40,0	40,4
0,9	0,0518	0,085	15,85	2,225	0,7675	41,5	43,3
1,2	0,0351	0,066	19,55	2,485	0,7821	41,5	45,8
1,5	0,0261	0,052	22,83	2,73	0,7828	44,5	46,7
1,8	0,0189	0,041	26,0	2,975	0,7850	42,9	47,1

It should be noted that the experimental proofs of the nonexponential character of the fluorescence decay law for quenched solutions aduced above are not only evidence in favor of the diffusion theory of fluorescence quenching by impurities but are also the first experimental proof of the validity of the Smoluchowski-Leontovich-Kolmogorov formula[8] based on the assumption that the rate of diffusion varies with the time elapsed from the beginning of diffusion (Brownian motion).

References

1. B.Ia.Sveshnikov, Doklady AN SSSR, 3, 61 (1936).
2. E.Rabinovitch, Trans. Faraday Soc., 33, 1225 (1937).
3. R.H.Fowler & N.B.Slater, Trans. Faraday Soc., 34, 81 (1938).
4. S.I.Vavilov, Z.Phys., 53, 665 (1929).
5. S.I.Vavilov & I.M.Frank, Z.Phys., 69, 100 (1931).
6. B.Ia.Sveshnikov, Acta Physiochimica USSR, 3, 257 (1935).
7. B.Ia.Sveshnikov & P.I.Kudriashov, Doklady AN SSSR, 115,984 (1957).
8. M.Smoluchowski, Z.Phys.Chem., 92, 129 (1917); M.A.Leontovich & A.N.Kolmogorov, Phys.Z.Sow., 4, 1 (1933).

EFFECT OF LIGHT GASES ON THE ELECTRONIC ABSORPTION SPECTRA OF AROMATIC COMPOUNDS AND INTERACTION BETWEEN THE MOLECULES

- B.S.Neporent

In this paper we shall review investigations of the influence of light gases on the absorption of light by aromatic compound vapors, an effect discovered by the author[1], and consider how this effect is related to the long range interaction between aromatic compound molecules[2].

In the investigations of Refs.1-3, we discovered and studied the decrease in absorption by aromatic compounds in the vapor state as a result of introduction of light gases. The effect is illustrated in Fig.1, taken from Ref.4. It will be seen that the absorption by the vapor of the investigated substance decreases as helium is added: the higher the intrinsic (partial) vapor pressure of the investigated substance, the more slowly the absorption decreases with addition of helium and the weaker the total effect at the limit.

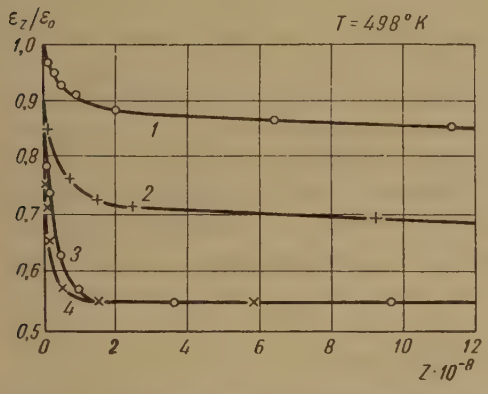

Fig.1. Influence of helium on the absorption coefficient ε of 3-acetylaminophthalimide vapor. Z - number of collisions per second of a vapor molecule with helium atoms. The curves correspond to 3-acetylaminophthalimide vapor pressures of 1) 0.325, 2) 0.086, 3) 0.036 and 4) 0.026 mm Hg.

It was shown in Ref.1 that addition of a heavy gas, for example, pentane, to the system, much as increase of the partial pressure of the investigated substance, leads to diminution of the effect of helium. Increasing the temperature, on the contrary, intensifies the effect, i.e., leads to a decrease of the limiting residual absorption. It is significant that according to evaluations based on our experimental data the aromatic compound molecules may remain for an appreciable time ($>10^{-7}$-10^{-6} sec) in the low-absorption state attained as a result of collision with helium atoms.

On the basis of analysis of the experimental data[1,3,4], we suggested the following explanation for the effect. Light gases produce weakening of the absorption in substances that have conjugated bond chains (except benzene). Collisions with light gas particles produced changes in the structure of the molecules in the normal state N, changes that are accompanied by disturbance of their π-electrons with the result that the absorption is reduced. The forming perturbed states N' have a higher energy than the normal states N and are separated from them by a potential barrier (Fig.2).

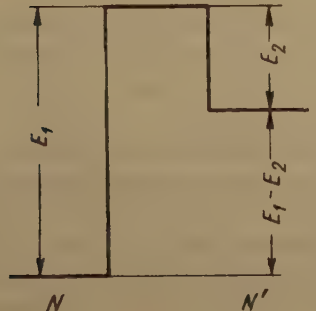

Fig.2. Change in the energy state of molecules as a result of collision with a light gas particle.

The specific effect of light gases is connected with the possibility of an "impact" collision mechanism by virtue of which the aromatic compound molecule can undergo a structural rearrangement representing an N→N' transition in which a barrier of height E_1 is surmounted. Then, if a collision occurs between two complex molecules, the strong Van de Waals field orients the molecules and facilitates close contact between them, thereby prolonging

the encounter during which the inverse transition of the excited molecule from state N' to N may take place with a barrier of height E_2 being surmounted in the process.

Attempts to detect changes in the structure of the investigated molecules incident to their transition from state N to N' from measurements of infrared spectra have so far failed to yield positive results, owing to the narrow spectral interval involved and the obvious experimental difficulties. To clarify the mechanism of the effect we undertook an analysis of its kinetics on the basis of the assumption that there occur the following reactions:

$$N + A \xrightarrow{k_1} N' + A, \quad k_1 = s_1 e^{-\frac{E_1}{RT}} \alpha_A,$$

$$N' + A \xrightarrow{k_2} N + A, \quad k_2 = s_2 e^{-\frac{E_2}{RT}} \alpha_A,$$

$$\left.\begin{aligned} N' + N &\xrightarrow{k_3} N + N, \\ N' + N' &\xrightarrow{k_3} N' + N, \end{aligned}\right\} \quad k_3 = k_4 = s_3 e^{-\frac{E_2}{RT}} \alpha_N,$$

$$N' + M \xrightarrow{k_5} N + M, \quad k_5 = s_5 e^{-\frac{E_2}{RT}} \alpha_M.$$

Here N and N' denote the molecule under study in the normal and perturbed state, respectively, A is a particle of the light extraneous gase, M is a particle of the heavy extraneous gas, the k_i are reaction rate constants, the s_i are probability factors and α_i are conversion coefficients relating the concentrations with the numbers of collisions. For the simple case, when no heavy gas is present (the general case has been treated in Ref.5), we deduced the following expression

$$\frac{\varepsilon_0}{\varepsilon_0 - \varepsilon_c} = \frac{k_1 + k_2}{\gamma k_1}\left(1 + \frac{k_3 C_N}{k_1 + k_2} \cdot \frac{1}{C_A}\right), \qquad (1)$$

where ε_0 is the absorption coefficient in the vapor in the absence of the extraneous light gas, ε_c is the absorption coefficient present at a concentration C_A, C_N is the concentration of the molecules under study and γ is a factor associated with the ratio of the absorption coefficients for molecules in the states N and N' and also (and this is important) comprising a factor η that takes into account the shielding effect of the compound molecules on each other; this shielding reduces the influence of the light gas. An expression similar to (1) was proposed earlier[1] as an empirical formula. It is generally supported by experiment, which makes it possible to calculate the energy $E_1 - E_2$ of the perturbed state and to evaluate the ratios s_2/s_1 and s_3/s_1. In view of what has been said above, the magnitude of s_3 depends on the temperature, inasmuch as the effective collision time must obviously decrease with decreasing temperature.

Calculations for 3-aminophthalimide and 1,4-diphenylbutadiene led to values of $E_1 - E_2$ equal to 3.8 and 5.4 kilocal/mole, values of s_2/s_1 equal to 0.036 and 0.0025 and values of s_1/s_3 varying, respectively, from 0.32 to 1.80 and from 0.24 to 0.18 with variations in temperature from about T = 570° to T = 470°. These values were obtained on the assumption (for the ratios) that $\gamma = 1$ and for $E_1 - E$ only on the assumption that $\gamma(T) = \text{const}$.

It was shown in Ref.5 that this assumption has a certain basis but that it can be made only in the case of experiments at sufficiently low concentrations of the investigated molecules ($C_N < C_0$), inasmuch as experiment, in contradiction to Eq.(1), shows that beginning with a certain critical concentration C_0, the limit towards which the absorption attenuation curves tend begins to increase and that no increase in concentration C_A of the light gas (helium) can lead to the degree

of attenuation that is observed when $C_N < C_o$. It follows that above the concentration C_o all the molecules of the substance under study cannot be regarded as independent: part of them (the greater, the higher C_N) at any given instant are in a state of interaction with each other, mutually shielding themselves against the influence of the light gas. The above mentioned coefficient η takes into account these interactions. For the investigated substances the concentration C_o does not exceed $2 \cdot 10^{15}$ molecules per cm^3, whence it follows that the molecular interaction in question has a very long range.

It must be noted that in an independent investigation carried out by the writer in collaboration with Klochkov[2] on vapors of the same substances, there were established small changes in the absorption spectra beginning at approximately the same critical concentrations C_o that were found in the experiments with helium.

On the basis of all the experimental data it may be inferred that, as suggested in Ref.6, the interactions under consideration are associated with displacement or other changes of the π-electron clouds of the molecules. Investigation of the effect by observation of changes in spectra is extremely difficult and in this connection the results of analysis of the influence of light gases on the absorption of vapors are particularly important, for by introducing the coefficient η we can qualitatively investigate N—N interactions between molecules. One can with a certain degree of plausibility assume that these interactions, just as interactions leading to energy transfer between excited and unexcited molecules, can be described as dipole-dipole interactions and that one can apply to them the theory developed some time ago by Vavilov[7] and more recently by Galanin[8]. It may also be assumed that under certain conditions (since we are dealing with systems that are more nearly alike than normal and excited molecules), the interactions in question will be stronger than those treated by Vavilov and Galanin.

The described investigations may help reveal an as yet unknown mechanism of intermolecular N—N interactions as well as a shielding mechanism protecting the complex molecules against interactions with light gas atoms: $N + A \rightarrow N' + A$. We are continuing our research in the indicated direction. Analysis of the interactions in question should also make it possible to obtain new information on certain important intramolecular processes inasmuch as experiment shows that the shielding N—N interactions differ substantially for molecules belonging to different spectral groups.[6]

References

1. B.S.Neporent, Dissertation, 1945; Doklady AN SSSR, 72,35 (1950).
2. B.S.Neporent & V.P.Klochkov, Doklady AN SSSR, 114,524 (1957).
3. B.S.Neporent & A.A.Solodovnikov, Optika i spektroskopiia, 1,951 (1956).
4. B.S.Neporent & V.P.Klochkov, ibid., 3, 529 (1957).
5. B.S.Neporent, ibid., 4, 703 (1958); Sbornik pamiati akad.G.S.Landsberg (Symposium in memory of G.S.Landsberg), 1959.
6. B.S.Neporent, Zhur.eksp.i teor.fiz., 21,172 (1957). (Trans. Soviet Phys.-JETP.); Zhur.fiz.khimi, 30, 1048 (1956).
7. S.I.Vavilov, Zhur.eksp.i teor.fiz., 13, 13 (1943); Sochineniia, (Collected works) Vol.2, p.153, M.-L., 1952.
8. M.D.Galanin, Zhur,eksp.i teor.fiz., 21, 126 (1951).

SPECTROSCOPIC INVESTIGATION OF THE INTER- AND INTRAMOLECULAR INTERACTION OF NITRO AND AMINO RADICALS IN SOME BENZENE DERIVATIVES

- V.I.Danilova, V.D.Gol'tsev & N.A.Prilezhaeva

The presence of atomic groups of opposite polarity in two different molecules leads, under appropriate conditions, to the formation of complexes held together by electrostatic forces. Spectroscopic studies in such cases may reveal displacement of the usual absorption bands or even the appearance of new bands. When such opposite polarity radicals are present in one and the same molecule, the interaction between them varies, depending on their relative position (ortho-, meta- or para-) and the spectra change accordingly.

We undertook a comparative investigation of the interaction of amino and nitro groups in the case when they enter into the composition of two different molecules (specifically, aniline and nitrobenzene) and in the case when they form part of one and the same molecule (specifically, nitroanilines). Hence our spectroscopic studies consisted of two parts: investigation of the aniline-nitrobenzene system and investigation of nitroanilines.

The intense absorption developing in the visible region of the spectrum when solutions of aniline and nitrobenzene are mixed is considered by some authors to be a result of formation of 1 to 1 complexes. A number of other authors, on the other hand, on the basis of physical-chemical and spectroscopic studies, deny the existence of such complexes. It would appear therefore that the concentration of complexes at ordinary temperatures must be very low, i.e., presumably below the threshold of sensitivity of the procedures employed.

We investigated the aniline-nitrobenzene system by different spectroscopic techniques in the visible and ultraviolet regions. In the ultraviolet region, we studied the absorption spectra of solutions of aniline and nitrobenzene in hexane, mixtures of these solutions and liquid films of aniline, nitrobenzene and mixtures thereof. We found that interaction of aniline with nitrobenzene leads to no noticeable changes in the spectrum in the 2200-3000 Å range. In the visible region, interaction of aniline with nitrobenzene leads to a sharp increase in absorption. We investigated this absorption by the procedure of varying the concentration of one of the components.[1]

Analysis of the experimental data showed that with increasing concentration of the "second" component, in addition to the noted increase in absorption in the visible region, there occurs a shift of the absorption limit of the solutions from the short wavelength to the long wavelength part of the spectrum, which also results in an apparent increase in absorption. By means of a procedure which we cannot describe here, we succeeded in separating these two effect and finding the dependence of the quantity n, characterizing the increase in intensity of absorption, on the concentration of the second component.

In all plots characterizing this dependence there is a clear break in the curve at an aniline to benzene concentration ratio of 1 to 1, indicating the formation of complex compounds of aniline with nitrobenzene in the proportions of 1:1.

The curves for two series of solutions are shown in Fig.1. Curve 1 pertains to measurements in the 4700 to 6300 Å region of the spectrum; curve 2 to the 3600 to 4800 Å region.

We also investigated greatly diluted solutions of aniline and nitrobenzene; the purpose of the dilution was to minimize the influence of the absorption limit shift on the measurements. We measured the optical density of the solutions in the range from 3100 to 4000 Å.

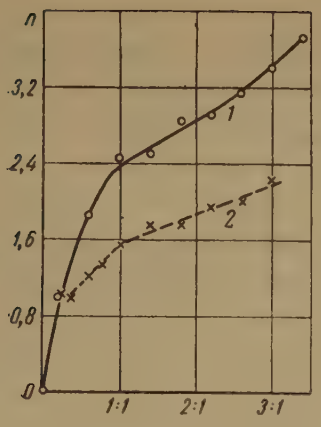

Nitrobenzeze: aniline

Fig.1. Variation of the increase in absorption of aniline with nitrobenzene with the nitrobenzene concentration (aniline concentration constant): 1) 4700 to 6300 Å, 2) 3600 to 4800 Å (appreciable absorption in nitrobenzene). n = increase in intensity of absorption. The calculations were carried out over the entire absorption curves in the indicated wavelength interval.

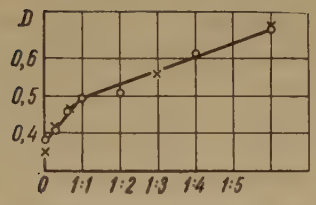

Nitrobenzene: aniline

Fig.2. Variation of the optical density D of solutions of aniline with nitrobenzene in benzene with the aniline concentration (nitrobenzene concentration constant).

The variation of optical density with composition at λ = 3400 Å is shown in Fig.2. Here, too, there is clearly evident a break in the curve at a concentration ratio of 1:1, which substantiates the above inference regarding the formation of complexes with this composition.

To determine the characteristics of the complex compounds formed in the solution, we made use of the procedures described by Hammick & Wardley[2] based on there being a linear dependence between D/b^m and D, where D is the optical density of the solution under study, b is the concentration of one of the components and m is a number indicating how many molecules of one of the components link up with the molecules of the other component in forming a complex. This procedure is applicable in cases when only one type of complex compound forms in the solution. The D-dependences of D/b^m were found to be linear for all wavelengths in the range from 4100 to 4700 Å with m = 1. This indicates that there are formed primarily 1:1 complexes in the solution and that if there do form complexes having a different composition their concentration is negligibly low. From the slope of the straight line plot one can calculate the equilibrium constant K and the absorption coefficient ϵ of the complex. These data for different wavelengths are listed in Table 1.

Table 1

Values of the equilibrium constant K and absorption coefficient ϵ of the complex for different wavelengths

λ, Å	K, liter $mole^{-1}$	ϵ, liter $mole^{-1}$ cm^{-1}
4200	0,04	170
4300	0,02	290
4400	0,02	280
4500	0,01	200
4600	0,02	80

We also measured the temperature dependence of the optical density of solutions of a mixture of aniline with nitrobenzene in the 1:1 ratio; we took appropriate measures to prevent oxidation of the aniline by atmospheric oxygen during heating and took into account the thermal expansion of the liquid.

The temperature was varied from room temperature to 140°; the densities were measured in the range from 4300 to 6400 Å. In all cases, we observed a reversible decrease of the optical density with increasing temperature, which can be explained by thermal dissociation of the complexes.

Fig.3 shows a plot of the temperature dependence of the optical density for λ = 5300 Å (without taking thermal expansion into account). From the observed temperature dependence of the optical density, we evaluated the binding energy of the complexes by means of the formula[3]:

$$U = R\frac{T_1T_2}{T_2-T_1}\ln\frac{K_2}{K_1},$$

where U is the binding energy and K_1 and K_2 are the equilibrium constants corresponding to the temperatures T_1 and T_2. The calculated values of U for different wavelengths are listed in Table 2.

Table 2

Complex binding energy U for different wavelengths

λ, Å	U, Kcal/mole
4400	0.66
4500	0.67
4600	0.67
4700	0.60

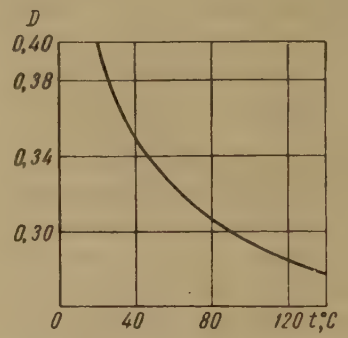

Fig.3. Variation of the optical density D of solutions of aniline and nitrobenzene (1:1) with the temperature (not corrected for thermal expansion.

The absorption spectra of nitroaniline molecules in solution have been investigated by a number of authors.[4] The absorption spectrum of the ortho-isomer in the vapor state has been investigated only qualitatively.[5] In the present work, we carried out a quantitative investigation of the absorption for all three isomers in the vapor state and in solutions in CCl_4, dioxane, H_2O and aqueous solutions of HCl.

In the region from 2000 to 4000 Å ortho- and metanitroaniline both in the vapor form and in solutions have three absorption maxima, while paranitroaniline has only two. The wavelength position of the first, long wavelength maximum varies greatly, depending on the isomer and the solvent. The other maxima undergo relatively little change. The positions of the long wavelength absorption maximum for all three isomers in the vapor state and in solution are listed in Tabl.3.

Table 3

Long wavelength absorption peak of nitroanilines (λ, Å)

Substance	Vapor	Solution					
		in hexane	in CCl_4	in dioxane	in CH_3OH	in H_2O	in HCl water solution
Orthonitroaniline	3600	3800	3760	4010	4040	3970	2690
Metanitroaniline	3250	3500	3450	3690	3750	3630	2620
Paranitroaniline	2875	3200	3360	3525	3740	3750	2610

Conclusions

1. Our experiments show that there form 1:1 complexes in the aniline-nitrobenzene system. The bond strength of these complexes is ~0.6 Kcal/mole.

2. As a result of complex formation, the absorption peak of nitrobenzene is shifted from 3550 to 4300 Å. It can be shown that this shift is due to the fact that the intermolecular binding increases sharply incident to excitation of the nitrobenzene molecules.[6]

3. The intramolecular binding between the NH_2 and NO_2 radicals in nitroaniline molecules increases in going from the para- to the meta- and to the ortho-isomers; at the same time the absorption maximum is shifted increasingly to the side of the longer wavelengths.

4. The shift of the absorption peak of the nitroaniline isomers, like the shift in the aniline-nitrobenzene system, is due to enhanced interaction incident to excitation of the molecules.

5. On the basis of all experimental data, it may be inferred that the nature of the intermolecular and intramolecular interactions between the NH_2 and NO_2 groups is the same.

Siberian Physical-Technical Institute
at Tomsk State University

References

1. A.K.Babko, Fiziko-khimicheskii analiz kompleksnykh soedinenii v rastvorakh (Physical-chemical analysis of complex compounds in solution) Pub. Ukrainian SSR Academy of Sciences, 1955.

2. F.Hammick & A.A.Wardley, J.Chem.Soc., 3817 (1953).

3. S.Naqakura, J.Amer.Chem.Soc., 74, 3070 (1954).

4. L.Dede & A.Rosenberg, Ber.Dtsch.chem.Ges.,67, 147 (1934).

5. I.E.Purvis & N.P.McCleland, J.Chem.Soc., 103, 1088 (1913).

6. V.D.Gol'tsev, Izvestiia (Bulletin), Ministry of Higher Education of the USSR, Physical Series, No.1 (1957).

DEPENDENCE OF THE SPECTRA OF AROMATIC NITRO COMPOUNDS ON THE ANGLE OF ROTATION OF THE NITRO GROUP ABOUT THE C-N BOND

- P.P.Shorygin & Z.F.Il'icheva

The indications of conjugation of π-bonds in molecules of organic compounds depend on the angle of rotation of one of the π-bonds relative to the other and are more strongly evinced when the two bonds are located in the same plane. Thus in nonsubstituted nitrobenzene, which has a plane structure, the dipole moment is appreciably stronger, the nitro group frequency lower and the intensity of the corresponding Raman line much higher than in aliphatic nitro compounds.

The introduction of a substituent in the ortho position into the nitrobenzene molecule disturbs the complanarity of the "benzene ring-nitro group" system and weakens the indications of conjugation. Obviously, the plane in which the nitro group is located may be rotated about the C—N bond relative to the plane of the benzene ring through some angle θ, which in principle may be as great as 90°. At the same time there may occur small changes in some of the valence angles and interatomic distances.

The quantitative correlations between the indications of conjugation and the angle θ have virtually not been studied. Yet such investigation is important for clarifying the nature of the mutual effect of different atomic groups in complex molecules. Different forms of mutual influence should depend in different ways on the angle θ; the manifestation of the inductive effect, however, should depend but little on this angle.

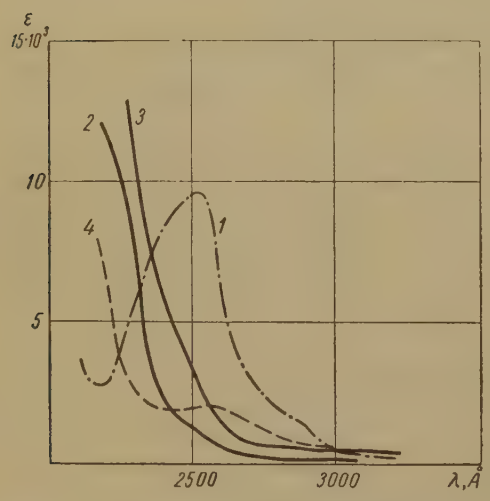

Fig.1. Absorption spectra of compounds of the 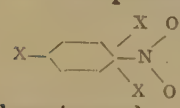 type (solvent-heptane):

1 — X = H, 2 — X = Cl, 3 — X = Br, 4 — X = CH_3

In the present work we investigated the ultraviolet absorption spectra, the Raman spectra and the dipole moments of ortho derivatives of nitrobenzene, including those of the 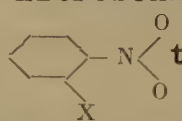 type, with different substituents X. We deliberately chose substituents with minimum ability to influence the nitro group through the benzene ring; one can judge of the extent of this influence indirectly from the data on nitriles (and on type molecules[1]). Indications of conjugation of the C≡N and NO_2 groups with the benzene ring are rather similar; however, the CN group, which has a linear configuration, is little subject to the influence of steric factors.

The following data are listed in the accompanying table for each of the investigated compounds:

1) The different ($\Delta\omega$) between the frequency of the valence symmetric vi-

Compound	ω_{NO_2}, cm^{-1}	$\Delta\omega$, cm^{-1}	NO_2	UV spectra in heptane	ε_{2500}	μ	$\Delta\mu$	θ
$CH_3 \cdot CH_2 \cdot CH_2 \cdot NO_2$		+36	40	—	—	3,2	—0,8	—
	1347	0	700	2850(1,5); 2520(9,6)	9600	4,00	0	0°
		0	1300	2670(11)	—	2,56	+0,15	0°
		+6	600	3080(2,5); 2480(3,5)	3500	4,83	—0,3	30°
		+1	500	2860(1,6); 2500(6)	6000	3,68	—0,2	30°
		+19	170	No maxima	1400	3,53	—0,3	—
		+1	700	2900(1,6); 2450(7)	6600	—	—	35°
		+7	300	2880(1,2); 2450(4);	3800	4,36+	—0,6	60°
		~+7	—	2950(1,3); 2450 (4)	3600	4,20	—0,7	65°
		~+3	—	3050(1,8); 2300(11,3)	4200	3,90	—0,8	70°
		+17	250	No maxima (see Fig.1)	1900	3,66	—0,4	45°
		+18	50		500	~5,0*	~0,5	—
		+14	50		1300	3,22+	—0,7	70°**
		~+9	50		3500	3,17+	—0,7	—
	ω_{CN}	I_{CN}						
	2230	0	330	2720(0,8); 2230(13)	—	4,0	0	
		+2	360	2700(0,8); 2310(15)	—	2,5	+0,1	
		+4	420	2950(1,4); 2450(14)	—	3,75+	—0,15	
		—1	650	2890(3,9); 2300(8,2)	—	—	—	

*The value of μ for dichloronitrobenzene is unreliable (data of different authors differ greatly).

**According to the x-ray diffraction data of Zhdanov & Gol'der[2] $\theta = 64^\circ$ in 3,5-dichloro-4-nitroaniline.

brations of the nitro group of the investigated substance and the corresponding frequency of nitrobenzene (in benzene solutions); for nitriles, we give the corresponding data for the C—N frequencies. In the case of ω_{NO_2} doublets we took the intermediate frequency value (identified by "~").

2) The coefficient of the integral intensity I_{NO_2} of the nitro group line (and, accordingly, I_{CN} for the nitrile group) in the Raman spectra of benzene solutions.* The unit intensity is 0.01 the intensity of the CCl_4 313 cm^{-1} line reduced to 1 mole; accuracy of intensity evaluations ±20%; excitation by the Hg 4358 Å line.

3) The wavelength of the absorption band maxima (in Å);* following these in parentheses are the values of $\varepsilon/1000$, where ε is the molar (decimal) coefficient of absorption at the band peak. In addition, we give the values of ε in the 2500 Å region (ε_{2500}).

4) The dipole moment μ in benzene in Debye units. The values followed by + were obtained by us; the other data are taken from the literature.

5) The difference $\Delta\mu$ between the experimental data and the calculated values of μ for complex molecules computed by the method of vector addition of moments of the corresponding monoderivative of benzene (for the computations we assumed μ = 1.58 for PhCl and μ = = 1.53 for PhBr).

6) The angle Θ calculated on the assumption that the distance between the O atom of the nitro group and the atom of the ortho substituent is close to the sum of the Van der Waals radii of these two atoms. For o-nitrotoluene we assumed that the O···H distances to the two H atoms of the methyl group are identical and equal to 2.5 Å (If we assume CH_3 to be a sphere of radius 2 Å, we obtain Θ = 85 Å; this value is in poorer agreement with the spectroscopic data which favor the assumed configuration with the absence of rotation of the CH_3 about the C—C bond.)

In calculating Θ and $\Delta\mu$ we took into account a probable 1-5° increase of the angles between the C—N and C—X bonds, changes in the O-N-O and C-N-O angles (on the basis of the data on elasticity coefficients) and alterations in the length of the C—N bond in the range from 1.36 to 1.46 Å, bearing in mind the data of Zhdanov & Gol'der[2] for some nitro compounds. In view of the rough evaluation of the corrections allowing for the different factors (including those considered below) that affect the value of Θ, the calculated data listed in the table must be regarded as only approximate.

The molecular model in which the atoms are represented by contiguous rigid spheres gives equal values of Θ for molecules of the

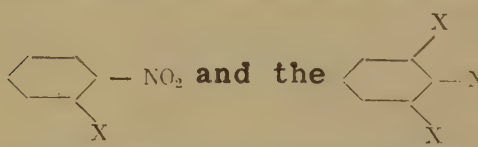

types. Actually, however, the indications of conjugation are weakened to an appreciably greater extent in the latter case.

---

*The measurement technique is described in Ref.1.

Evaluations taking into account the actual variation of the forces of repulsion as a function of the distance between continuous atoms, using the Lenard-Jones potential, and changes in the C-C-X, C-C-N and O-N-O angles indicate that upon the introduction of a second ortho substituent, the angle θ may increase appreciably. One can think of the potential energy U of the molecule as the sum of the plane model energy U_o in the absence of repulsion and the energy expended on overcoming the repulsive forces (U_{rep}), on deformation of the angles (U_{def}) and on rotation of the nitro group through the angle θ relative to the benzene ring (U_θ); thus

$$U = U_{rep} + U_{def} + U_\theta$$

(according to Samoilov & Diatkina $U_\theta = f(\theta)$ is a cosine function[3]).

The tabular data shows that a CH_3 group weakens the indications of conjugation of nitro groups with the benzene ring to a lesser extent than a Cl atom. The inverse situation obtains in the case of ortho derivatives of dimethylanaline. This is connected with geometric factors which determine the possibility of close approach of branched groups.* Moreover, as calculations show, the Coulomb interaction of some excess charges of contiguous atoms of polar NO_2 and X (or CH_3 and X) groups may increase or decrease θ by 1 to 10° (depending on the polarity of the charges). Offhand, one might expect that in the series of ortho derivatives of nitrobenzene with X = F, Cl, Br and I the characteristic NO_2 frequency will increase, while the absorption in the 2500 Å region (the wavelength of the intense absorption band in nonsubstituted benzene) will be attenuated. Actually this is observed only for the first members of the series. In going from chlorine to bromine to iodine derivatives ω_{NO_2} actually decreases and the absorption in the 2500 A region is intensified.

This shows that one cannot indiscriminately utilize the frequency of the nitro group for judging of deviations from complanarity. It is entirely possible that increase of the mass of the substituent X tends to lower ω_{NO_2}; it is also possible that the force field of X may exert a direct influence on ω_{NO_2}. Nevertheless, it is a fact that as a result of introduction of two chlorine atoms, ω_{NO_2} comes closer to the frequency of nitropropane (1383 cm^{-1}) than to the frequency of nonsubstituted nitrobenzene (1347 cm^{-1}). At the same time in similar benzo-nitrile derivatives the frequency increases slightly.

In bromine and iodine derivatives the "benzene ring-halogen" system begins to predominate in the absorption spectra. Iodobenzene has an intense band in the region of 2300 Å, i.e., closer to 2500 Å than the other halogen-benzenes; the absorption spectrum of o-iodonitrobenzene is virtually identical with that of iodobenzene.

---

*The closest approach of methyl groups is attained with the arrangement 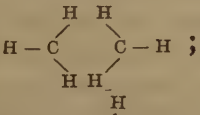 ; the maximum approach of CH_3 and Cl with the arrangement 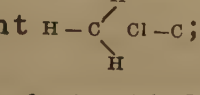 ; in the latter case the formally calculated "radii" are substantially smaller.

The difficulties in interpreting the absorption spectra (partially connected with the direct influence of ortho substituents on the benzene ring and on the absorption spectrum) cannot be reduced by introducing an NH_2 (or similar) group in the para-position in the nitrobenzene molecule. Para-nitroanaline has a closer and more sharply pronounced absorption band, from the changes in which one can more readily determine the effect of ortho substituents; upon the introduction of two Cl atoms this band almost disappears and the spectrum becomes nearly identical with that of nonsubstituted analine (Fig.2). It may be inferred that here interaction with the nitro group is almost entirely suppressed.

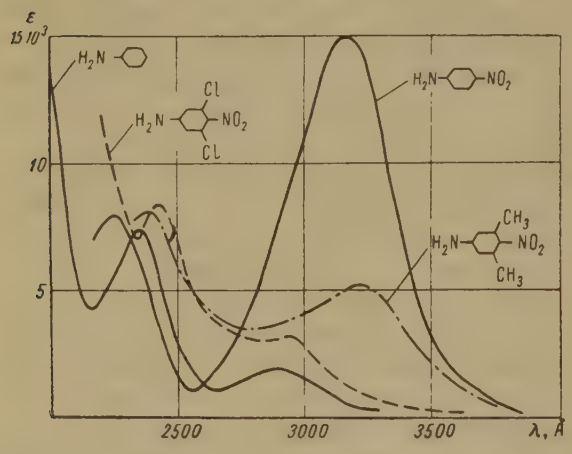

Fig.2. Absorption spectra in heptane. The dash-dot curve is plotted by analogy with the spectra of similar compounds.

Knowing the variation of λ and the energy of the molecule in the ground state as a function of the angle θ, one can determine the θ dependence of the energy of the excited molecule. Inasmuch as λ is virtually independent of θ, it may be assumed that the fraction of double C-N bonds in excited molecules is negligible.

Interpretation of the dipole moments is hindered by the lack of precise information on the C-C-Hal and other angles. According to Zhdanov & Gol'der[2], in 3,5-dichloro-4-nitroanaline (and also in 2,4,6-trichlorobenzonitrile) the C-C-Hal angles equal ~123° and the O-N-O angle equals ~110°; there are no data available for the other compounds in question and we were forced to make rough approximations (thus for tribromonitrobenzene, we took the C-C-Br angle to be 125°). In any case the table shows that the dipole moment anomalies observed in the plane nitrobenzene molecule upon introduction of methyl groups into both ortho positions are appreciably reduced and upon introduction of chlorine or bromine atoms become altogether insignificant.

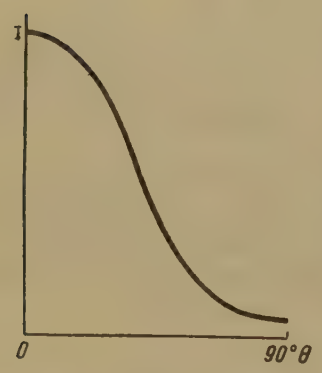

Fig.3. Variation of the intensity I of the nitro group line in the Raman spectra as a function of the angle θ.

With increase in the volume of the substituent X, the intensity of the nitro group line in the Raman spectrum falls off sharply and finally approaches the value characteristic for molecules without conjugated bonds. The probable character of $I = f(\theta)$ is shown in Fig.3. A curve of similar shape is obtained for $\Delta\mu = f(\theta)$.

It must be noted that use of all the molecular parameters considered above for purposes of interpretation is subject to severe limitations. It may, however, be asserted that introduction of two Cl atoms into the ortho positions with $\theta = 60\text{-}70°$ leads to almost complete suppression of the observable indications of conjugation (this applies to a lesser extent to ω_{NO_2}).

Our data show that the inductive effect does not exert any great influence on the properties of nitro compounds. Inasmuch as the nitro group is a highly polar one, it may be inferred that the influence of the inductive effect will be even weaker in the case of other types of compounds.

"L.Ia.Karpov" Physical-Chemical Institute

References

1. P.Shorygin & Z.Egorova, Zhur.fiz.khim., 32, 915 (1958); Doklady AN SSSR, 118, 763 (1958).
2. G.Zhdanov & G.Gol'der, Zhur.fiz.khim., 29, 1248 (1955).
3. S.Samoilov & M.Diatkina, Zhur.fiz.khim., 22, 1294 (1948).

* * * * *

INVESTIGATION OF VIBRATIONAL SPECTRA IN THE REGION OF THE VALENCE VIBRATIONS OF CH

- M.M.Sushchinskii

In the present report we give the results of experimental and theoretical investigations of the Raman and infrared spectra of some hydrocarbons in the region of the CH valence vibrations. Experimental study of this spectral region is fraught with great difficulties inasmuch as it comprises a large number of close and partially overlapping lines. Hence the Raman spectra were investigated using high dispersion instruments. Furthermore, we made extensive use of the technique of measurements in polarized light, which makes it possible to distinguish between lines having different polarizations.

Photographic recording allows of separating out depolarized lines. Using photoelectric recording with modulation of the light beam by means of polaroids, it proved possible to separate out the polarized lines (this new polarization technique will be described in a separate article). The appearance of the Raman spectrum of one of the investigated hydrocarbons is shown in Fig.1. In calculating the frequencies we used the usual procedure[1], appropriately modified for programming on an electronic computer[2].

In investigating spectra of the type in question we are immediately faced with the problem of assigning the observed lines to various groups. Unfortunately, one cannot solve this problem purely theoretically through calculation of the frequencies: owing to the fact that there are many close lines (frequencies) the accuracy of calculation proves to be inadequate for reliable assignments; moreover, the number of lines actually observed usually exceeds the number of lines predicted by theory. In view of this for interpreting the observed spectra one must have recourse to comparison of all the line parameters in the spectra of a series of related compounds. By means of this procedure one can generally make fairly reliable group assignments of the lines observed in the given spectral region.[3,4]

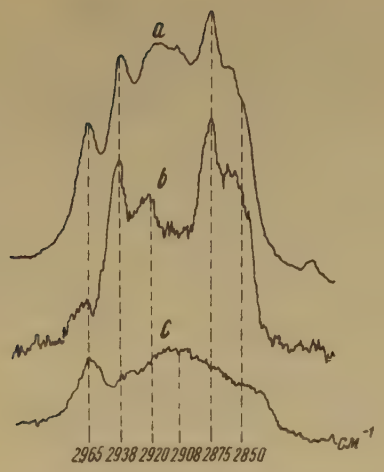

Fig.1. Raman spectrum of n-hexane in the region of valence vibrations of CH: a) natural light, b) polarized component, c) depolarized component.

We turn first to the spectra of regular alkanes. In the spectra of this class of hydrocarbons there are four rather sharp strongly polarized lines having frequencies of about 2850, 2875, 2920 and 2938 cm^{-1}, a somewhat wider depolarized line with a frequency of 2965 cm^{-1} and a very broad line (better termed a band) at 2908 cm^{-1} (Fig.1). Comparison of the spectra of different *n*-paraffins shows[3,4] that the frequencies of these lines are strictly characteristic, that the depolarization factors also change very little and that the normalized (per gram-molecule) intensities behave in different ways with lengthening of the chain. For three of the lines (2850, 2920 & 2908 cm^{-1}) the intensities increase appreciably with increase in the number of CH_2 groups in the molecule, while for the other three lines the increase is appreciably smaller (Fig.2) and may be explained as the result of partial overlapping of the lines.

Of particular interest among the isoparaffins are those which contain only CH_3 groups: tetramethylmethane and hexamethylethane. The spectra of these alkanes comprise a depolarized line at ~2965 cm^{-1}, analogous to the line of the same frequency in the spectra of *n*-paraffins, a strongly polarized 2909 cm^{-1} (the most intense line in the spectrum) and a number of comparatively weak polarized lines in the region from 2870 to 2890 cm^{-1}. No lines in the 2920 to 2940 cm^{-1} region similar to those of *n*-paraffins are observed.

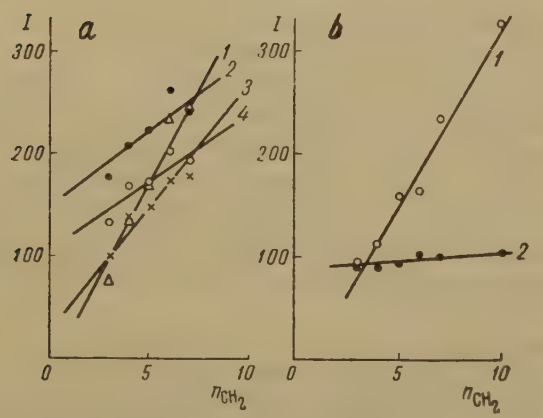

Fig.2. Variation of the line intensities I with the number of CH_2 groups in n-paraffin molecules: a - polarized line: 1) $\nu \approx 2850$ cm^{-1}, 2) 2875 cm^{-1}, 3) 2920 cm^{-1}, 4) 2938 cm^{-1}; b - depolarized lines: 1) 2908 cm^{-1}, 2) 2965 cm^{-1}.

The noted features in the paraffin spectra cannot be explained on the basis of calculations in the approximation used hitherto. The results of calculations carried out by us for several paraffins by means of the rigorous method described in Ref. 2 are listed in Table 1. As may be seen, the calculations always yield one and the same value of 2899 cm^{-1} for the symmetrical line of the CH_3 group. The calculations also give very close values for the nonsymmetrical lines. Thus the calculations can explain the presence of only two lines associated with the CH_3 group in the spectra and moreover indicate a rigorously constant characteristic frequency for these lines. From the standpoint of internal symmetry of the CH_3 group (C_{3v} symmetry) there should also be observed only two lines in the spectra, namely, a symmetrical and a degenerate line. It would seem natural to interpret the 2870 cm^{-1} line in the spectra of *n*-paraffins as the symmetrical one

and the 2965 cm^{-1} line as the degenerate line associated with the CH_3 group. This interpretation, however, encounters certain difficulties.

1. One must find some explanation for the "extra" lines, the presence of which does not follow from our calculations or from the internal symmetry of the CH_3 group.

2. The most intense polarized line in the spectra of tetramethylmethane and hexamethylethane has a frequency of 2909 cm^{-1}. It would seem that this should be identified as the fully symmetrical CH_3 line. However, the observed shift of the symmetrical frequency from 2870 cm^{-1} to 2909 cm^{-1} in going from *n*-paraffins to tetramethylmethane is in conflict with the results of our calculations.

3. The splitting of the fully symmetrical frequency into 2-3 lines is also in conflict with the calculations.

In our opinion, it is reasonable to assume that these difficulties stem from the inadequacies of theory. In all theoretical calculations made until now (including our calculations, the results of which are listed in Table 1), account is taken of the dynamic interaction of only the H atoms comprised in one and the same group, while the dynamic interaction of the CH_2 and CH_3 groups with each other is not allowed for. Yet there undoubtedly is some coupling between the H atoms of one group and those of the other groups (particularly the neighboring groups) and these are precisely the interactions that may serve to explain the varying stability of rotational isomers. These interactions can be taken into account in

Table 1

Calculated frequencies of the valence vibrations of the CH group in paraffins (ν, cm^{-1})

Substance	Symmetry type	Interpretation				
		CH_2 symmetrical	CH_3 symmetrical	CH_2 nonsymmet.	CH_3 nonsymmet.	CH
n-butane	Ag	2927	2899	—	2976	—
	Bg	—	—	2968	2981	—
	Bu	2928	2899	—	2976	—
	Au	—	—	2973	2989	—
n-pentane	A_1	2926 2930	2899	—	2976	—
	B_2	—	—	2970	2985	—
	B_1	2928	2899	—	2976	—
	A_2	—	—	2966 2978	2999	—
tetramethylmethane	A_1	—	2899	—	—	—
	E	—	—	—	2977	—
	F_1	—	—	—	2975	—
	F_2	—	2899	—	2977	—
2,3-dimethylbutane	Ag	—	2899	—	2977 2979	2950
	Bg	—	2899	—	2975 2976	—
	Bu	—	2899	—	2977 2980	2957
	Au	—	2899	—	2975 2976	—

the framework of the usual computation scheme. To this end one need only assign appropriate nonzero values to the dynamic interaction coefficients of the vibrational coordinates q of neighboring H atoms. The interaction scheme is illustrated in Fig.3 and the values of the corresponding interaction coefficients are listed in Table 2.

Table 2

Coefficients of dynamic interaction of the vibrational coordinates

Interacting coordinates	Distance between interacting H atoms, Å	Interaction coefficient	
		Designation	Numerical value
q_1; q_2	1,78	$x_0 = h$	0,05
q_3; q_5	2,49	x_1	0,05
q_3; q_4	3,06	x_2	0,04
q_3; q_7	2,51	x_3	0,05
q_3; q_6	3,08	x_4	0,04
q_1; q_8	4,29	x_5	0,00
q_1; q_7	3,74	x_6	0,00

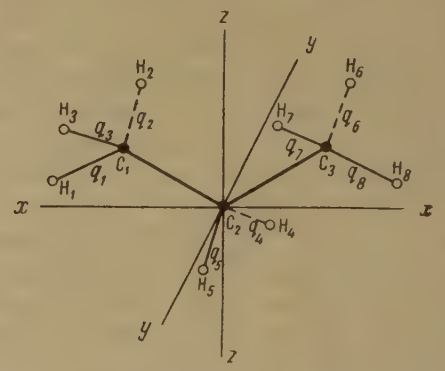

Fig.3. Interaction of hydrogen atoms belonging to neighboring groups.

It is significant that taking into account the interaction of close CH groups leads in a number of cases to correction of the diagonal coefficients of the dynamic interaction matrix. The magnitude of the corrections depends on the symmetry of the molecules and the symmetry type of the vibration in question. Consequently, taking the coefficients into account leads to displacement and splitting of the CH valence vibration frequencies. Thus we obtain an explanation of the experimentally observed behavior of the lines, i.e., the shift and splitting of some of the lines associated with the given group in going from one molecule to another or incident to changes in the position of the group in the same molecule.

In calculating the coefficients x_i, we used the available data for tetramethylmethane; the results are listed in Table.2.

Our calculations show that in the case of n-paraffins the interaction of H atoms belonging to different groups leads to an appreciable change in the frequency of the valence vibrations of only two CH_2 groups, which are located at the center of the molecule with an even number of carbon atoms or adjacent to the central carbon atom with an odd number of carbon atoms in the molecule. These two "central" CH_2 groups should give rise to a distinctive set of frequencies in the spectra of n-paraffins, frequencies differing from those associated with other CH_2 groups. The corrections in the two cases proved to be of the same magnitude.[3]

On the basis of our analysis, we propose the following assignments for the lines observed in the region of CH valence vibrations in the spectra of n-paraffins. The 2875 and 2965 cm^{-1} lines, the intensities of which virtually do not change with increasing length of the chain, should be attributed to vibrations of the CH_3 group; the strongly polarized 2875 cm^{-1} line corresponds to the symmetrical vibrations, while the depolarized 2965 cm^{-1} line corresponds to degenerate vibrations of this group. The 2938 cm^{-1} line, the intensity of which changes very little with increasing number of CH_2 groups in the molecule, may be identified with the symmetrical vi-

brations of the "central" CH_2 groups. Inasmuch as the number of such groups is always the same, namely, two, the intensity of this line does not depend on the length of the chain. According to our calculations, this line should be shifted approximately 20 cm^{-1} relative to the corresponding line of ordinary (noncentral) CH_2 groups, i.e., should be observed at ~2920 cm^{-1}. In this region in the spectra of *n*-paraffins there actually is a strongly polarized line which partially overlaps the broad depolarized line of 2908 cm^{-1} frequency; the intensities of these lines increase with the number of CH_2 groups in the molecule. The depolarized 2908 cm^{-1} line may logically be associated with antisymmetrical vibrations of the CH_2 group. The polarized 2850 cm^{-1} line may be interpreted as an intensified (by virtue of Fermi resonance) overtone of the 1450 cm^{-1} frequency, associated with α-type deformation vibrations of the CH_2 group.

Our analysis of the Raman spectra in the region of the CH valence vibrations shows that in this region additivity obtains in the sense that the observed spectra represent superpositions of lines belonging to individual CH_3, CH_2 and CH groups. The parameters of these lines, however, are not rigorously invariant: they are influenced to a greater or lesser extent by the position of the associated group in the molecule and the general structure of the molecule; a relatively small change in frequency may lead to noticeable shifts and splittings of the lines. The most stable parameters are those of the 2965 cm^{-1} line. The intensity of this line (per CH_3 group) is so characteristic (constant) that it can be used for determining the number of CH groups in paraffins with an unknown structure.

The additivity of the Raman spectra established for the different types of paraffins as regards the CH_3, CH_2 and CH groups also obtains in the infrared spectra. It must be noted, however, that this additivity is sometimes overstressed in infrared spectroscopy. In view of this, some workers fail to note or take into account certain distinctive features in the spectra, associated with deviations from characteristic frequencies.

References

1. M.V.Vol'kenshtein, M.A.El'iashevich & B.I.Stepanov, Kolebaniia molekul (Molecular vibrations), M.-L., 1949.

2. R.I.Podlovchenko & M.M.Sushchinskii, Optika i spektroskopiia, 2, 49 (1957); R.I.Podlovchenko & M.M.Sushchinskii, Fiz.sbornik (Physics reports) L'vov State University, 3, 99 (1957).

3. M.M.Sushchinskii, Dissertation, Physical Institute, USSR Ac. of Sci., 1957.

4. M.M.Sushchinskii, Izv.AN SSSR,Ser.fiz., 11, 348 (1947).

ANHARMONICITY COEFFICIENTS AND RESONANCE INTERACTION OF INTERNAL VIBRATIONS OF THE CH GROUP

- V.D.Bogdanov & M.M.Sushchinskii

Additivity of the vibrational spectra of hydrocarbons as regard the CH_3, CH_2 and CH groups bound in these molecules obtains not only in the region of the fundamentals[1] but also in the overtone regions. We made use of this additivity for determining the anharmonicity coefficients.

We investigated the infrared spectra of a number of regular and some strongly branched paraffins in the regions of the fundamentals of the CH vibrations (~2900 cm^{-1}), the first and second overtones (~5800 and ~8700 cm^{-1}, respectively) and the combination tone (4200 cm^{-1}), as well as the Raman spectra in the region of the first overtone (~5800 cm^{-1}). Comparing the variation in the intensity of the individual lines in the spectra of different hydrocarbons with the number of CH_2 and CH_3 groups in them, one can assign the various lines to the appropriate groups.

Our interpretation of the experimental frequencies and the values of the anharmonicity coefficients x are given in the accompanying table. It will be noted that the values of the coefficients are relatively small.

Interpretation		Frequencies, cm^{-1}	
Group	Type vibration	Experim.	Calculated
CH_3	E_{val}	$\nu_0 = 2958$ $\nu_1 = 5876$ $\nu_2 = 8760$	$\nu = 2998$ $x = 0{,}0067$ $\nu_2 = 8753$
CH_2	B_{1val}	$\nu_0 = 2928$ $\nu_1 = 5784$ $\nu_2 = 8565$	$\nu = 3000$ $x = 0{,}012$ $\nu_2 = 8568$
CH_3	A_{1val}	$\nu_0 = 2872$ $\nu_1 = 5774$ $\nu_2 = 8675$	$\nu = 2842$ $x = -0{,}0052$ $\nu_2 = 8695$
CH_2	A_1 deform	$\nu_1 = 2855$ $\nu_3 = 5690$ $\nu_5 = 8320$	$\nu = 1462$ $x_d = 0{,}006$ $\nu_5 = 8350$

We calculated the resonance interaction of the valence vibrations of the CH_2 group with the deformation vibrations of this group. The method of calculation is in general the same as for CO_2 molecules.[2-4] According to the interpretation given in Ref.1, ν_1 = 2920 cm^{-1} is the frequency of the fully symmetrical valence vibrations of the CH_2 group, ν_2 = 2850 cm^{-1} is the frequency of the first overtone of the internal deformation vibration of this group. Let I_1 and I_2 be the intensities of the Raman lines having the frequencies ν_1 and ν_2 and ρ_1 and ρ_2 be their respective depolarization factors. Our calculations yielded $I_2/I_1 = 0.89$, $\rho_1 = 0.09$ and $\rho_2 = 0.08$. The experimental values for n-dodecane (an n-paraffin in which the number of CH_2 groups appreciably exceeds the number of CH_3 groups) are $I_2/I_1 = 0.96$, $\rho_1 = 0.20$ and $\rho_2 = 0.18$.

In view of the difficulties of measurement under conditions of partial overlapping of the spectral lines and the necessarily approximate nature of the calculations the agreement may be regarded as satisfactory.

References

1. M.M.Sushchinskii, Present issue of the Bulletin, p.
2. E.Fermi, Z.Phys., 71, 250 (1931).
3. M.V.Vol'kenshtein, M.A.El'iashevich & B.I.Stepanov, Kolebania molekul (Molecular vibrations), M.-L., 1949.
4. G.Plachek, Releevskoi rasseianie i raman-effekt (Rayleigh scattering and the Raman effect), M.-L., 1935.

INVESTIGATION OF THE TEMPERATURE DEPENDENCE OF RAMAN SPECTRUM LINE INTENSITIES

- A.I.Sokolevskaia & P.A.Bazhulin

The temperature dependence of the intensity of Raman spectrum lines in liquids has been studied repeatedly.[1-6] Most of the experimantal results, which are in qualitative agreement, indicate that the intensity of Stokes lines decreases with increasing temperature. It must be noted, however, that quantitatively the results obtained by different authors show substantial disagreement.

We undertook a detailed study of this temperature dependence inasmuch as it is of considerable interest from the standpoint of investigation of the inter- and intramolecular interactions in liquids. The present study is a continuation of the work of Ref.7 wherein the experimental technique was briefly described. Hence here we only note that for the temperature experiments we used the tube diagramed in Fig.1. The investigated substance was contained in tube a; nitrogen vapor for low temperatures or hot air for high temperatures was passed through the glass jacket b. The second vacuum jacket c served to prevent frosting of the walls and window of the inner tube during the low temperature measurements. The temperature of the investigated substance was determined by means of a thermocouple. The width of the spectrograph slit varied from the equivalent of 1.5 to 0.5 cm^{-1} at the spectrum depending on the width of the line under study. The line intensities were determined by measuring the contours with a planimeter.

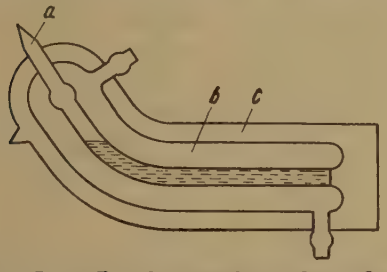

Fig.1. Jacketed tube for investigating Raman spectra at different temperatures.

The true line contours were obtained by reducing the observed contours by the procedure described in Ref.8. In the process we introduced appropriate corrections for temperature induced changes of the density and index of refraction of the substance. Special experiments showed that in our set-up the influence of the index of refraction is evinced only in changes in the brightness of the scattered radiation as it leaves the tube.[9] All the other effects associated with variation of index of refraction (changes in the reflection coefficient at the liquid-glass interface, changes in the configuration of the exciting rays in the tube, changes in the conditions of formation of the image on the spectrograph slit, etc.) were too weak to necessitate any additional corrections.

The temperature was varied over a range of 120°. The intensity of each Raman line was measured at four different temperatures in this range.

Our experiments showed that the intensity of the Stokes lines decreases with increasing temperature but that the changes are not as great as reported by Fishkova[2] and Bobovich et al[3,4]. We also found that the behavior of the line intensities depends on the structure of the molecules involved. By way of illustration, the results for some of the lines of tetramethylethylene and carbon disulfide are shown in Fig.2. These substances represent extreme

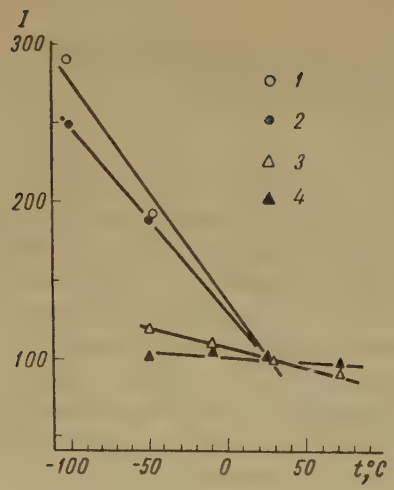

cases: the intensity of the tetraethylmethy lene lines is least subject to the influenc of temperature, while the intensity of car- bon disulfide lines falls off very appreci- ably with increasing temperature.

Fig.2. Temperature dependence of the inten- sity of Raman lines of carbon disulfide (1 - $\Delta\nu$ = 796 cm^{-1} & 2 - $\Delta\nu$ = 656 cm^{-1}) and tetramethylethylene (3 - $\Delta\nu$ = 1670 cm^{-1} & $\Delta\nu$ = 690 cm^{-1}).

Table 1

Temperature dependences of Raman line intensities for a number of liquids (I_{25° = 100)

Substance	$\Delta\nu$, cm^{-1}	ϱ	I_t *		ΔI per 100°
			+10°	−10°	
Toluene	521	0,61	90	110	18
	623	0,73	80	110	27
	786	0,09	88	109	19
	1211	0,13	90	107	15
	1606	0,70	83	111	25
			+40°	−70°	
Cyclopentane	899	0,12	95	130	30
	1031	0,82	95	136	37
	1449	0,72	93	148	50
			+70°	−50°	
Tetramethyl- ethylene	504	0,70	90	116	20
	690	0,15	94	110	13
	1683	0,13	90	117	22
			+100°	−10°	
3-ethylpentene-2	1440—59	0,74	84	112	25
	1670	0,20	90	103	12
			+90°	−10°	
Heptene-1	1642	0,15	77	112	35
			+80°	−50°	
Dipropenyl	1657— —1668	0,35	80	130	38
			+50°	−70°	
Diallyl	1416	*dp*	93	129	30
	1642	0,12	88	138	40

*The present values of I include a correction for the temperature induced change of the index of refraction; this correction was not made in the earlier results of Ref.7.

Further, we found that the temperature variation of the intensity depends not only on the structure of the molecules but also on the type of the bonds participating in the vibration. Results of intensity measurements for a number of substances are listed in Table 1: the intensity changes are referred to the intensity at 25°, taken as 100. The changes in intensity calculated per 100° are given in the last column. The values of the depolarization factor ρ given in the table are taken from Ref.10.

As will be evident from the table, the greatest changes with temperature are, as a rule, exhibited by lines associated with deformation vibrations (for example, the 623 and 1606 cm^{-1} lines of toluene and the 1031 and 1449 cm^{-1} lines of cyclopentane). The intensities of lines associated with valence vibrations of single bonds are less temperature sensitive (the 1211 cm^{-1} line of toluene and the 690 cm^{-1} line of tetramethylethylene). On the other hand, one cannot establish any clear correlation between the intensity behavior and the degree of depolarization of the line. Thus the polarized 992 cm^{-1} line of benzene undergoes an appreciable decrease in intensity when the temperature is raised 50°.[7] The same thing may be said regarding the behavior of Raman lines associated with vibrations of double bonds. We investigated the variation in intensity with temperature of lines associated with vibrations of double bonds in a number of hydrocarbons having a similar structure. If the double bond is located near the end of the chain (heptane-1, diallyl, and for that matter, dipropenyl which contains conjugated double bonds) the associated lines exhibit large changes in intensity. The line intensity falls off somewhat more slowly with increasing temperature in the case of 3-ethylpentane-2 and tetramethylethylene in which the double bonds are screened by neighboring groups.

In the case of the Raman spectrum of carbon disulfide we felt it would be of particular interest to investigate the influence of temperature on the intensity of the 796 cm^{-1} line (the overtone of the 397 cm^{-1} deformation vibrations) and the 648 and 805 cm^{-1} lines associated with vibrations of the CS_2 molecule with an excited lower state. With decrease of the temperature from +25 to -70°, the intensity of the 796 cm^{-1} overtone increases 2.5 times, whereas according to theory it should decrease by only 20%. In the same temperature interval the intensity of the 648 and 805 cm^{-1} lines decreases by only 40%, whereas according to theory there should be observed a fourfold decrease. We were also able to investigate with a fair degree of reliability the temperature behavior of the 656 cm^{-1} anti-Stokes satellite in the spectrum of carbon disulfide. Our measurements showed that the intensity of this anti-Stokes line falls

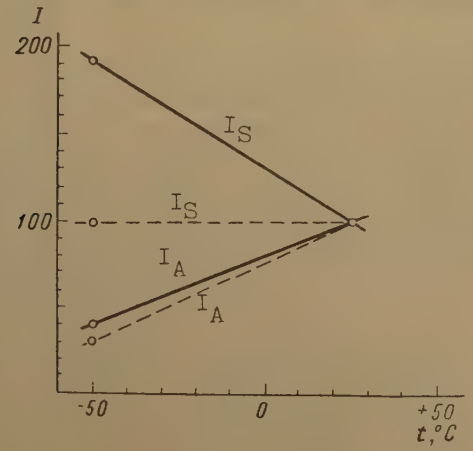

Fig.3. Variation with temperature of the intensity of the Stokes (I_S) and anti-Stokes (I_A) components of the 656 cm^{-1} Raman line of CS_2. Solid lines - experimental data; dashed lines - calculated variation.

off with decreasing temperature, while at the same time the intensity of the Stokes line increases. According to present-day theoretical concepts the intensities of both lines should decrease with increasing temperature.

The experimental and theoretical temperature dependences of the intensities of the anti-Stokes and Stokes 656 cm^{-1} lines of CS_2 in the range from -50 to +25°C are shown in Fig.3. It will be seen that the observed change in the intensity of the anti-Stokes line (60%) is close to the calculated value (70%). The intensity of the Stokes line changes by 90% in the same temperature interval whereas according to theory the intensity should remain constant. It will be obvious that the ratio of the experimental intensities of the Stokes and anti-Stokes 656 cm^{-1} lines of carbon disulfide does not agree with the theoretical value over most of the temperature range from +25 to -50°.

Our experimental results show that the present theory of the temperature dependence of Raman line intensities does not adequately explain the effect. It must be emphasized that the deviation of experiment from theory cannot be attributed to inaccuracy in determining the integral intensity of the temperature broadened lines, i.e., failure to take into account the line wings.[11] Our experiments showed that the temperature dependence of the line half-width and intensity differ. It has been established[7] that the half-width of polarized lines changes little with temperature, while depolarized lines are greatly broadened with increasing temperature. As was noted above, there is no apparent correlation between the intensity

Table 2

Variation of the width δ and intensity I of Raman lines with temperature

Substance	Δν, cm^{-1}	ρ	t°	Line width, δ, cm^{-1}	Change in line width, Δδ, cm^{-1}	$I_t / I_{25°}$
Heptene-1	1642	0,15	−10 +90	4,0 5,5	1,5	1,35
Diallyl	1642	0,12	−70 +55	6,0 6,2	0,2	1,40
Carbon disulfide	656	0,20	−110 +25	0,7 0,8	0,1	2,9
	796	0,20	−110 +25	4,1 4,5	0,4	2,5
Toluene	623	0,73	−10 +100	6,4 15,0	9,0	1,27
	1606	0,70	− 10 +100	6,4 13,4	7,0	1,25

behavior and the degree of depolarization of the Raman lines. Thus the intensity of polarized lines associated with vibrations of a double bond located close to the end of the molecular chain changes appreciably with temperature, whereas the line half-width remains virtually constant (Table 2). Again, the half-width of the polarized 656 and 796 cm^{-1} lines of carbon disulfide are virtually temperature independent, whereas their intensities are strongly dependent on the temperature. On the contrary, the width of the depolarized lines in the spectrum of toluene increases rapidly with temperature, while their integral intensity decreases very slightly. Consequently, the observed effect cannot be explained by temperature induced intensity redistribution in the line wings.[11]

Further, we note that the observed temperature variations of the intensity can hardly be explained by increase of the anharmonicity of the vibrations with temperature[6], inasmuch as under our conditions $kT \ll h\omega$. The hypothesis that increase in anharmonicity is responsible for the temperature variation of intensity is also in conflict with theoretical calculations[12]. The anomalous behavior of the I_S/I_A ratio for the 656 cm^{-1} lines of carbon disulfide indicates that the observed temperature dependence of intensities cannot be wholly explained by intermolecular interactions[12], although at present one cannot assert that the influence of such interactions is negligible. That intermolecular interactions may exert some effect is indicated by the fact that the character of the temperature variation of the intensity does depend on the position of the double bonds in the molecule.

Obviously, the whole question of the temperature dependence of the intensity of Raman lines requires further extensive theoretical and experimental investigation.

"G.S.Landsberg" Optical Laboratory,
"P.N.Lebedev" Physical Institute, Academy of Sciences of the USSR

References

1. G.S.Landsberg & L.I.Mandelshtam, Z.Phys.,60,364 (1930).
2. L.M.Fishkova, Doklady AN SSSR, 75,523 (1950).
3. Ia.S.Bobovich, ibid., 98, 39 (1954).
4. Ia.S.Bobovich & V. M.Pivovarov, ibid.,97, 801 (1954).
5. H.J.Bernstein & G.Allen, JOSA, 45, 237 (1955).
6. A.I.Stekhanov & E.V.Chisler, Zhur.tekh.fiz., 25, 2209 (1955).
7. A.I.Sokolovskaia & P.A.Bazhulin, Transactions of the Tenth All-Union Conference on Spectroscopy, No.1, 225, L'vov, 1957.
8. P.A.Bazhulin, S.G.Rautian, A.I.Sokolovskaia & M.M.Sushchinskii, Zhur.eksp.i teor.fiz., 29, 822 (1955).
9. L.A.Woodward & J.H.B.George, Proc.Phys.Soc., B64, 780 (1951).
10. G.S.Landsberg, P.A.Bazhulin & M.M.Sushchinskii, Osnovnye parametry spektrov kombinatsionnogo rasseianiia uglevodorodov (Principal parameters of Raman spectra of hydrocarbons), M., 1956.
11. F.C.Rosler, Acta.phys.austriaca, 5, 477 (1952).
12. Ia.S.Bobovich & V.M.Pivovarov, Optika i spektroskopiia, 3, 227 (1957).

RAMAN SPECTRA OF SOME UNSATURATED CYCLIC HYDROCARBONS

- V.T.Aleksanian, Kh.E.Sterin, A.A.Mel'nikov & A.F.Plate

In the general class of unsaturated hydrocarbons the Raman spectra of aliphatic mono- and dialkenes have been studied in greatest detail. For monoalkenes Goubeau[1] experimentally established a number of frequencies characterizing six possible types of substitution in ethylene. Subsequently, Goubeau's deductions were substantiated by the theoretical calculations of Sverdlov[2]. It was also found that the intensity and other parameters of lines associated with vibrations of double bonds are characteristic.[3-7] Moreover, Akishin & Tatevskii[5] showed on the example of 21 saturated hydrocarbons, including a number of cyclic ones, that the integral intensity (per mole and per double bond in the absence of conjugation) of lines in the range from 1610 to 1680 cm^{-1} is virtually constant. This fact is particularly significant because, as is known, the intensity of lines is much more sensitive to changes in molecular structure than the frequency. Whereas frequency invariance presumably obtains for cyclic systems as well, one cannot apply Goubeau's frequency indications to some of them, cyclopentene, for example, Hence, bearing in mind the paucity of factual data and the problems involved in analytic determination of unsaturated cyclic hydrocarbons, we had to begin our investigation of the Raman spectra with the initial purpose of determining the characteristic frequencies.

In the present work we investigated the Raman spectra of hydrocarbons with a double bond in the ring: 1-ethylcyclopentene-1, 1-n-propylcyclopentene-1 and 1-n-butylcyclopentene-1 (first series), and with a heptocyclic double bond: ethylidenecyclopentane, n-propylidene cyclopentane and n-butylidenecyclopentane (second series). We also made an attempt to establish a correlation between the characteristic frequency of the C=C bond and the molecular structure of the alkenes.

All the investigated hydrocarbons were obtained by dehydration with oxalic acid of tertiary alcohols synthesized by the Grignard reaction from the appropriate alkylmagnesium bromides and cyclopentanone. In the dehydration of each alcohol there were obtained two unsaturated hydrocarbons, one with a double bond in the five-membered ring and one with a heptacyclic double bond:

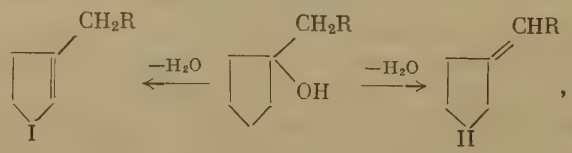

where R = CH_3, C_2H_5 and C_3H_7.

Under our dehydration conditions, the ratio of products I and II was about 7 to 1.

Each binary mixture was distilled in a column with a rating of 80 theoretical plates and then the index of refraction, density and melting point were determined for each of the components. (The solidification curves were obtained in the Chemical Thermodynamics Laboratory of Moscow State University; we take this opportunity to thank A.G.Anikin and G.M.Dugacheva for making the measurements).

The procedure followed in obtaining and measuring the spectra has been described earlier[8,9].

Results and discussion

1-ETHYLCYCLOPENTENE-1. t_{boil} = 106.0° (760 mm Hg); n_D^{20} = 1.4418; d_4^{20} = = 0.7979; found MR_D = 31.88; calculated for C_7H_{12} MR_D = 31.85, t_{melt} = -118.55°; degree of purity 98.6%. According to Ref.10: t_{boil} = 106.3° (760 mm Hg); n_D^{20} = = 1.4410; d_4^{20} = 0.7982; t_{melt} = -118.4°.

Δν (см$^{-1}$) : 215(6,ш),254 (2),275 (1), 300 (4), 354 (8), 401 (15), 432 (2),482 (7,ш),571 (0), 589 (5), 646 (2, ш), 820 (6, ш), 861 (27), 870 (10, ф), 886 (19, ш), 903 (21), 943 (10), 955 (10), 973 (5), 1025 (24), 1050 (5), 1064 (16), 1073 (8), 1130 (7), 1151 (6), 1205 (20), 1233 (11), 1252 (4), 1270(2), 1295(8), 1309(4), 1324(4), 1439 (100, ш), 1464(37, ш), 1618(3), 1651 (120), 2843 (310, ш), 2881 (300), 2897(340, ш), 2983(250, ш), 2961 (210, ш), 3048(60, ш).

1-n-PROPYLCYCLOPENTENE-1. t_{boil} = 131.1° (760 mm Hg); n_D^{20} = 1.4448; d_4^{20} = = 0.8004; found MR_D = 36.63; calculated for C_8H_{14} MR_D = 36.48; t_{melt} = 99.0°; degree of purity 98.9%. According to Ref.11: t_{boil} = 131.5-132.5°, n_D^{20} = 1.4450; d_4^{20} = 0.8015; t_{melt} = -100.3°.

Δν: 238(1), 261(1), 278(1), 295(3), 319 (5, ф), 329(12), 347(11,ш),374(5, ш), 397(2, ш), 432 (2,ш), 448(1), 474(6, ш), 487(5, ш), 536(2, ш), 592(3, ш), 637(2), 679(2), 770(1), 815(3), 855(20), 873(5,ф), 893(42), 911(8, ф), 949(14), 981(4), 996(3, ш), 1029(24, ш), 1075(6), 1093(9), 1133(5), 1151(5), 1204(19), 1217 (14), 1254(4), 1296(16, р), 1332(5), 1347(3), 1440(74, ш), 1466(28, ш, ф), 1495(1), 1523(2), 1652(84, р), 2841(200), 2870(190, ф), 2902(270, ш), 2933(220), 2964(170), 3046(50).

1-n-BUTYLCYCLOPENTENE-1. t_{boil} = 157.1° (760 mm Hg); n_D^{20} = 1.4482; d_4^{20} = = 0.8062; found MR_D = 41.26; calculated for C_9H_{16} MR_D = 41.09; t_{melt} = 88.35°; degree of purity 97.5%. According to Ref.11: t_{boil} = 157.5-158° (760 mm Hg); $n_D^{21,3}$ = 1.4488; $d_4^{17,8}$ = 0.8101; t_{melt} = -95.75°.

Δν: 227(4), 247(4),264(2), 285(9), 305(15), 325(10), 341(9), 370(5), 388(3), 420(10, ш), 433(10, ш), 451 (1), 472(3), 494(4), 512(2), 602(2), 641(2), 670(2), 723(2), 776(3), 820(10), 863(12, ш), 878(10, ш), 898(32, ш), 926(4), 951(13), 969(3), 1000(2), 1023(12), 1042(8), 1055(9), 1079(3), 1099(14), 1131(8), 1150(8), 1177(2), 1200(17), 1234(7), 1258(6), 1295(20, ш), 1334(9), 1359(3), 1440(110, ш), 1465(42), 1500(1), 1523(2), 1569(1), 1621(1), 1650(110, р), 2843(210), 2873(220, ф), 2905(290, ш, дв), 2936(190), 2959(160), 3044(80).

ETHYLIDENECYCLOPENTANE. t_{boil} = 112.4° (760 mm Hg); n_D^{20} = 1.4496; d_4^{20} = = 0.8030; found MR_D= 32.15; calculated for C_7H_{12} MR_D = 31.85; t_{melt} = -129.5°. According to Ref.12: t_{boil} = 112.4° (760 mm Hg); n_D^{20} = 1.4490; d_4^{20} = 0.8030.

Δν: 214(30, ш), 224(3, ш, ф), 259(5), 278(5), 427(30), 456(46), 495(1); 536(2), 569(7), 593(16), 626(1), 717(1), 732(21), 805(16, ш), 840(22), 856(3), 898(90), 944(5), 970(11), 1025(36, ш), 1067(7), 1102(2), 1125(1), 1153(15, ш), 1172(2), 1212(13), 1227(17), 1244(2), 1270(10), 1285(4), 1298(8), 1305(3), 1344(31), 1377(19), 1432(45), 1450(60), 1469(8), 1520(4), 1682(140), 2836(110), 2863 (200, ш), 2886(210, ш, ф.), 2912 (230,ф), 2938(180, ф), 2957(300, ш), 3031(60), 3059(20).

n-PROPYLIDENECYCLOPENTANE. t_{boil} = 135.3° (760 mm Hg); n_D^{20} = 1.4524; d_4^{20} = = 0.8050; found MR_D = 36.96; calculated for C_8H_{14} MR_D = 36.48; t_{melt} = -116.5°. This hydrocarbon was prepared for the first time in this investigation.

---

*Translator's note:

No key to the letters is given in the original. The probable meanings are ш - wide; ф - background, дв - doublet, р - sharp. The figures in () are intensities relative to that of the 802 cm^{-1} cyclohexane line taken as 250.

Δν: 242(5, ш), 249(7, ш), 285(2, ш), 367(15, ш), 432(21), 460(1, ш), 497(1, ш), 520(1), 571(4, ш), 604(5, ш), 670(5), 725(4, ш), 742(3, ш), 799(5), 830(16), 850(22), 898(62, р), 910(10, ф), 949(9), 971(1, ш), 1008(29), 1026(36), 1064(11), 1093(2), 1129(2), 1155(15, р), 1174(2), 1212(7), 1226(15), 1257(5, р), 1272(16, р), 1298(22, р), 1308(15), 1354(12), 1376(8), 1433(39), 1451(48), 1470(15, ш), 1523(8, р), 1574(3), 1650(1), 1679(78, ш), 2837(110), 2869(210), 2890(140, ф), 2908(140, ф), 2933(250), 2962(320), 3042(20).

n-BUTYLIDENECYCLOPENTANE. t_{boil} = 159.4° (760 mm Hg); n_D^{20} = 1.4550; d_4^{20} = = 0.8105; found MR_D = 41.58; calculated for C_9H_{16} MR_D = 41.09; vitrefies. This hydrocarbon was prepared for the first time in this investigation.

Δν: 223(5, ш), 249(4), 266(5), 312(10, ш, ф), 342(8, ш), 406(8, ш), 435(21), 483(3), 507(6), 570(7), 594(4), 608(5), 662(1), 680(0), 727(6), 752(8), 771(1), 811(5, ш), 840(12), 854(5), 871(20), 894(25), 902(72), 912(15), 948(12), 974(3, ш), 1005(10), 1024(32), 1053(6), 1065(9), 1090(17), 1135(2), 1154(16), 1172(1), 1212(8), 1230(20), 1260(7), 1271(7), 1289(3), 1302(15), 1321(12, р), 1342(12, р), 1357(10, р), 1377(5), 1435(54, ш), 1451(62), 1471(15), 1523(4), 1548(1), 1650(2), 1678(110), 2839(90), 2869(160, дв?), 2889(100, ф), 2905(190), 2935(210), 2962(230), 3043(20).

The spectra of the hydrocarbons of the above mentioned first series are already known[13,14]. Important additions to our results are the spectra of cyclopentene and 1-methylcyclopentene-1 (first series) given in Refs. 7 & 14 and of methylenecyclopentane (second series) given in Ref.14. The characteristic frequencies in the spectra of each series are listed in Tables 1 & 2. Some of these will be discussed below.

Table 1

Characteristic frequencies in the spectra of cyclopentene and its 1-alkyl homologues

Ref.7	900(140)	1027(15)	1207(18)	1614(150)	3060(270)
Ref.7	880(50)	1028(22)	1207(17)	1659(160)	3044(120)
	861(27) 886(19) 903(21)	1025(24)	1205(20)	1651(120)	3048(60)
	893(42)	1029(24)	1204(19)	1652(84)	3046(50)
	898(32)	1023(12)	1200(17)	1650(110)	3044(80)

Table 2

Characteristic frequencies in the spectra of methylene- and alkylidenecyclopentanes

Ref.14	417(9)	897(75)	1022(20)	1152(10)	1219(15)	1437(25)	1657(120)	3078(65) 3031(60)
	427(30)	898(90)	1025(36)	1153(15)	1212(13)	1432(45)	1682(140)	3059(20)
	432(21)	898(62)	1026(36)	1155(15)	1212(7)	1433(39)	1679(78)	3042(20)
	435(21)	902(72)	1024(32)	1154(16)	1212(8)	1435(54)	1678(110)	3043(20)

A. Double bond in five-membered ring (Table 1)

The lines in the 860 to 905 cm^{-1} interval are due to pulsating vibrations of the ring[7].* The 1614 cm^{-1} line of cyclopentene - a formal analog of cis-dialkylethylene - (second column in Table 3) and the 1650-1659 cm^{-1} lines of the other hydrocarbons - analogs of trisubstituted ethylene - (third column in Table 3), as well as the lines in the 3044 to 3060 cm^{-1} interval, are undoubtedly characteristic lines of the C=C double bond.**

B. Five-membered ring with a heptacyclic double bond

The 897 to 902 cm^{-1} lines are apparently also associated with pulsation of the five-membered ring. The vibrations of the double bond are represented by the 1657 cm^{-1} line in the spectrum of methylenecyclopentane - a formal analog of unsymmetrical trisubstituted ethylene - (column 1 in Table 3) and the 1678 to 1682 cm^{-1} lines*** in the spectra of the hydrocarbons which are analogs of trisubstituted ethylene (column 4 in Table 3) as well as the 3031 to 3078 cm^{-1} lines. Possibly the 1432-1437 cm^{-1} lines are also due to the presence of the double bond.

Values of the frequency $\nu_{C=C}$ and the structure of cyclic unsaturated hydrocarbons

In the case of monoalkenes the C=C—C valence angles are almost the same with all types of substitution in ethylene. In cyclic systems, however, particularly with 3-, 4- and 5-membered rings, these angles can vary greatly. Hence it is expedient to compare the values of $\nu_{C=C}$ with the spectra of cyclic unsaturated and aliphatic monoalkenes having the same type of double bond substitution. The available data are arranged accordingly in Table 3. Inasmuch as the tabular data has been taken from different sources there may be some divergences, but these can hardly exceed 10 cm^{-1}.

The table shows that in each row, corresponding to 6-, 5- and 4-membered rings, the frequencies increase with the increasing degree of substitution, i.e., that cyclic unsaturated hydrocarbons behave in the same manner as aliphatic monoalkenes (first row). Kohlrausch[15], considering the formal analogs of cis-substituted ethylene (cis-pentene-2, cyclopentene, cyclopentadiene, furan and pyrole) associated the decrease of $\nu_{C=C}$ in this series with narrowing of the C=C—C angle. It would appear more expedient, however, to consider only hydrocarbons with one double bond. Actually in the case of two conjugated double bonds (cyclohexadiene-1,3, cyclopentadiene and indene) the frequency falls off sharply,

---

*There are three bright lines in the spectrum of 1-ethylcyclopentene-1 in this interval: 861(27), 886(19) & 903(21). The line due to pulsation of the ring can be identified on the basis of polarization measurements.

**Levina et al[13] reported weak lines in the vicinity of 1680 cm^{-1} which have been interpreted as a result of splitting of the $\nu_{C=C}$ frequency by Akishin & Tatevskii[5]; in view of the synthesis procedure employed by Levina et al, from the results of our investigation it may be inferred that these lines belong to the corresponding isomers of the second series.

***The weak lines at 1650 cm^{-1} in the spectra of propylidene- and butylidene cyclopentane belong to admixtures (1-2%) of the corresponding isomers from the first series.

Table 3

Values of the frequency of the C=C bond in the spectra of different hydrocarbons (R - radical not containing double bond conjugated with the C=C bond)

$R_2 > C=CH_2$ R_1 1653	$H > C=C < H$ $R_1 \quad R_2$ 1656	$R_1 > C=C < R_2$ $H \quad R_3$ 1670-1680	$R_2 > C=C < R_3$ $R_1 \quad R_4$ 1670-1680
Aliphatic monoalkenes [1]			
	One double bond [17] 1648–1650 Cyclooctene	Two double bonds	
	[17] 1652 Cycloheptene		[17] 1673 1-methyl-cycloheptene-1
[13] 1651 Methylene-cyclohexene	[7] 1654 Cyclohexene	[15] 1676 cyclohexa-diene-1,4	[7,17,21] 1669–1680 1-alkyl-cyclohexene
		[7] 1578 cyclohexa-diene-1,3	[17] 1674–1677
[13] 1653 Methylcyclo-pentane	[7] 1614 Cyclopentene	[15] 1496 Cyclopenta-diene	1650–1660 1-alkyl-cyclopentene
			1678–1682 Alkyl-idene-cyclopentane
[24] 1679 Methyl-cyclobutane	[23] 1566 Cyclobutene		
		[20] 1550 Indene	
	[18] 1568 Bicyclo-(2,2,1)-heptene-2	[18] 1575 Bicyclo-(2,2,1)-heptadiene-2,5	
	[17] 1614 Bicyclo-(2,2,2)-octene-2		

Numbers in [] are References

whereas no such abrupt decrease is observed in the absence of conjugation. It will be seen from Table 3 that the frequency of the double bonds is the same as in monoalkenes as long as the ring is unstrained (cyclooctene, cycloheptene, cyclohexene and their homologues. Diminution of the characteristic frequency of the double bond is observed in cases when the cyclic system is strained (cyclobutene, bicycloheptene and 1-alkyl cyclopentenes). It must be assumed that the decrease of the frequency of double bond in bicyclooctene is also due to strain. Further decrease of the frequency may be expected in the spectra of

cyclopropene and its homologues of the 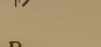 type. It must be noted, however,

that the $\nu_{C=C}$ in the spectra of 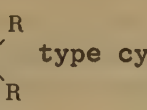 type cyclopentenes (1673-1693 cm^{-1})

are exceptions to the inferred regularity.

Since, as we saw, $\nu_{C=C}$ falls off with diminution of the C=C—C angle, it may logically be assumed that the frequency will increase with increase of this angle. This inference is supported by the spectra of methylene- and isopropylidene-cyclobutanes. Further substantiation could be furnished by the C=C frequencies in the spectra of hydrocarbons of the type 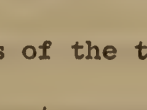 . Inasmuch as the $\nu_{C=C}$ in the spectra of methylene-cyclopentane and alkylidene-cyclopentane are not lower than in the spectra of the corresponding monoalkenes, it may be assumed that the C=C—C angle in these compounds is close to the normal value. This is all the more plausible in view of the fact that the five-membered ring is not plane.[16]

We want to emphasize that all the qualitative regularities inferred above are tentative and must be subjected to the test of further experiments and calculations.

Laboratory of the Commission on Spectroscopy,
Academy of Sciences of the USSR &
Faculty of Petroleum Chemistry,
Moscow State University

References

1. J.Goubeau, Die Ramanspektren von Olefinen. Supplement to Zs.Angew. Chemie, No.156 (1948).

2. L.M.Sverdlov, Fizich.sbornik (Physical review) L'vov State University, 3(8), 1, 278 (1957).

3. P.A.Bazhulin & Kh.E.Sterin, Izv.AN SSSR, Ser.fiz., 11, 456 (1947).

4. E.G.Treshchova, P.A.Akishin & V.M.Tatevskii, Zhur.analit.khimii (Journal of analytic chemistry), 3, 75 (1948).

5. P.A.Akishin & V.M.Tatevskii, Doklady AN SSSR, 76, 527 (1951); Vestnik MGU (Moscow State University), No.2, 103 (1951).

6. V.M.Tatevskii, E.G.Treshchova, V.R.Skvarchenko & R.Ia.Levina, Zhur.fiz. khimii (Journal of Physical Chemistry), 23, 657 (1949).

7. S.V.Markova, P.A.Bazhulin & M.M.Sushchinskii, Optika i spektroskopiia, 1, 41 (1956).

8. V.T.Aleksanian, Kh.E.Sterin, A.L.Liberman, E.A.Mikhailova, M.A.Prianishnikova & B.A.Kazanskii, Izv.AN SSSR, Ser.fiz., 19, 225 (1955). (Trans.Bulletin 19, No.2, 206.)

9. V.T.Aleksanian & Kh.E.Sterin, Optika i spektroskopiia, 2, 562 (1957).

10. F.D.Rossini, a.oth, Selected Values of Physical and Thermodynamic Properties of Hydrocarbons and Related Compounds, 64. -Pittsburgh, 1953.

11. G.Chavanne & P.Becker, Bull.Soc.chim.Belg., 36, 591 (1927).

12. J.R.Van der Bij & E.C.Kosyman, Recueil trav.chim., 71, 837 (1952).

13. R.Ia.Levina, N.N.Mezentsova & P.A.Akishin, Vestnik, Moscow State University, Phys.-Math.,Series, 10, 109 (1949).

14. P.A.Akishin, V.M.Tatevskii, N.G.Rambidi, N.N.Mezentsova & R.Ia.Levina, Zhur.fiz.khimii, 30, 660 (1956).

15. K.Kohlrausch, Ramanspektren, Leipzig (Reprinted 1943 Edwards Bros., Ann Arbor, Mich.). (Cited in Russian trans.)

16. J.E.Kilpatrick, K.S.Pitzer & R.J.Spitzer, J.Amer.Chem.Soc., 69, 2483 (1947).

17. Landolt-Börnstein, Tabellen, B 1, T.2, s.479. - Springer, 1951.

18. V.T.Aleksanian & Kh.E.Sterin, Fizich.sbornik (Physical review), L'vov State University, 3(8), 1, 59 (1957).

19.V.T.Aleksanian, Kh.E.Sterin, M.Iu.Lukina & L.A.Nakhapetian, Fizich.sb. (Physical review), L'vov State University, 3(8), 1, 68 (1957).

20. K.Matsuno & K.Han, Bull.Chem.Soc.Japan., 11, 321 (1936).

21. R.Ia.Levina, N.N.Mezentsova & P.A.Akishin, Vestnik, Moscow State University, No.2, 77 (1951).

22. M.R.Fenske, a.oth., Anal.Chem., 19, 700 (1947).

23. R.C.Lord & D.G.Rea, J.Amer.Chem.Soc., 79, 2401 (1957).

24. Catalog of Selected Raman Spectral Data, Amer.PetrolInst.Research Project 44, - Washington, D.C., 1948.

VIBRATIONAL SPECTRA OF SOME PHOSPHORORGANIC COMPOUNDS

- R.R.Shagidullin

Investigation of the vibrational spectra of phosphororganic compounds, which are becoming of increasing interest, showed that the presence of a number of atomic groupings in their molecules leads to the appearance of characteristic frequencies in the infrared and Raman spectra.[1-5]

The present study was undertaken for the purpose of determining whether some of the groupings can be satisfactorily characterized by spectroscopic data and to gain further information on the structure of some of the new phosphororganic compounds which are now being extensively synthesized and investigated in the Kazan laboratory under the supervision of Academicians A.E. and B.A.Arbuzov. We investigated the Raman and infrared absorption (IR) spectra of 11 substances* (all liquids), which on the basis of the method of preparation and what is known of their structure may be classified in two series (see figure)**. The experimental procedure and equipment have been described earlier.[6,7] Here we shall only give the infrared spectrograms (figure) and list the characteristic frequencies (table).

Discussion of Results

Series A

On the basis of the available chemical data one cannot choose unambiguously between the following two structural formulas for the compounds of series A:

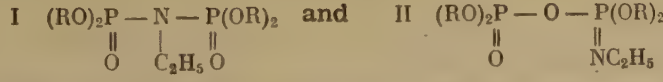

I $(RO)_2P(O)-N(C_2H_5)-P(O)(OR)_2$ and II $(RO)_2P(O)-O-P(NC_2H_5)(OR)_2$.

Inasmuch as the characteristic vibration frequencies of the P=O bond in the interval from 1200 to 1300 cm^{-1} have been reliably established[1], we shall begin our discussion with this region of the spectrum. In the infrared spectrum of compound a, the 1305 cm^{-1} band, according to Harvey & Mayhood[2], pertains to the $PNMe_2$ group***, while the 1232 cm^{-1} band is associated with the P=O bond, where two phosphorus valences are taken up by dimethylamino groups. The 1265 cm^{-1} band should be attributed to P=O in the case of structure I and to P=N in the case of structure II. The corresponding bands in the IR spectra of compounds b (1270 cm^{-1}), c (1270 cm^{-1}) and d (1265/1280 cm^{-1}) should be regarded as the result of surposition of the bands of the two P=O bonds in the case of structure I or of the P=O and P=N bands in the case of structure II. While this inference in the case of structure I is in good agreement with the data in the litera-

---

*The investigated substances were synthesized by P.I.Alimov, N.P.Grechkin and O.N.Fedorov, staff members of the Kazan branch of the USSR Academy of Sciences. I take this opportunity to thank them for making samples of the compounds available for analysis.

**Substance k was 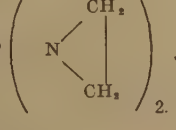 . It was found that the IR spectrum of this substance altered with time.

***Me = CH_3.

Substance					
	Series A				
a	623(60)	1222(14) 1232 s	1257(8) 1265 s	1285(8)	1304(7) 1305 s
b	657 w(26)		1261(21) 1270 s	1286(23)	
c	663 w(26)		1259(24) 1270 s	1280(24)	
d	665 w(21)		1259(14) 1265 s	1279(1) 1280 s	
	Series B				
e		1248(12) 1250 s	1280(42) 1280 s	3005(78)	3076 (38 d)
f		1251(14) 1256 s	1280(46) 1280 s	3002(70)	3071 (30 d)
g		1249(6) 1257 s	1280(29) 1290 s	3003(68)	3075 (30 d)
h	1231(14) 1232 s	1264(11)	1280(74) 1272 s d	3001(150)	3075 (68 d)
i		1265(46) 1272 s		2989 w(130)	3069 (50 d)
j		1255(30) 1264 s		2983 w(120)	3060 (36 d)
k		1257(110 1271 s		2985 w(170)	3061 (88 d)

Notes: The figures in parentheses following the IR frequencies are intensity values in the scale where the intensity of the 802 cm^{-1} line of cyclohexane is taken as 250. The frequencies given under the Raman frequencies are those of the IR absorption peaks. Key: s - strong, d - double, and w - wide.

ture, in the case of structure II it appears unlikely inasmuch as the weights and electronegativities of the O atom and the NC_2H_5 group are different and structure II is unsymmetrical. Unfortunately, one cannot obtain further evidence in favor of either I or II in the 1200-1300 cm^{-1} region from the Raman spectra. At the same time, in the 600 to 670 cm^{-1} region each of the series A compounds has one intense Raman line (table). According to Bellamy[1], the characteristic vibrational frequencies of the P-N bond are evinced in the vicinity of 700 cm^{-1}. It may be assumed therefore that the 600-670 cm^{-1} line in the Raman spectra is associated with symmetrical vibrations of the P—N—P group. A shift to the side of lower frequencies and increase in intensity of this line in the spectrum of compound a is probably due to lengthening of the chain and increase in the number of P—N bonds (P—N—P$\begin{matrix}N\\ \diagup\\ \diagdown\\ N\end{matrix}$). This may also be taken as evidence in favor of structure I. It must be noted that the intense absorption band in the 920 to 975 cm^{-1} region (figure) evinced in the spectra of all four compounds of series A may belong either to P—N—P (structure I, anti-symmetrical vibrations) or to P—O—P (structure II)[3]. In view of this, we cannot positively affirm that the compounds of series A have the imido structure, although the other spectroscopic evidence seems to favor this inference. We plan to investigate the matter further.

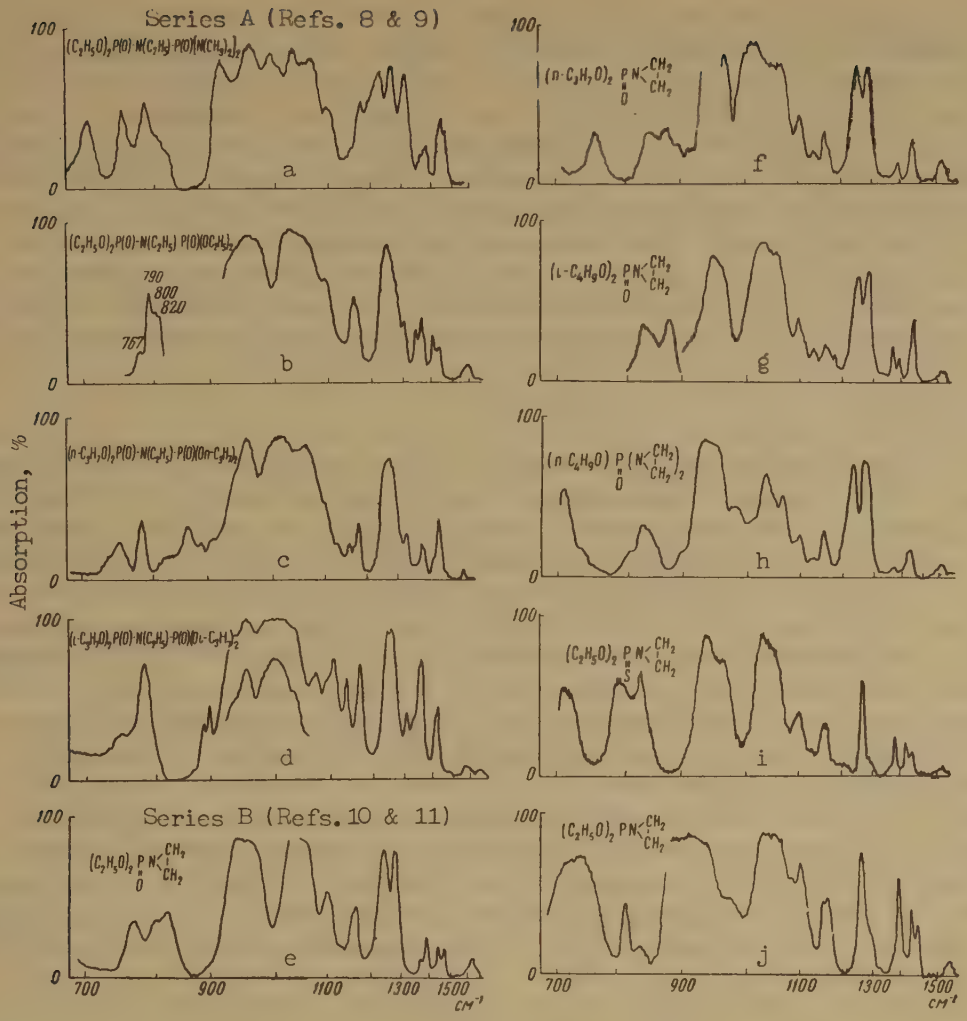

Series B

In the spectra of the compounds of series B we searched for the characteristic frequencies of the ethylenimine ring N<C/C and the double bond P=O. According to Ref.12, the pulsation frequency of ehtylenimine is 1215 cm^{-1}, i.e., is close to the region in which the characteristic vibrations of the P=O bond are evinced. As may be seen from the spectrograms and table, all the compounds of series B have intense IR bands in the 1230 to 1290 cm^{-1} region. But in the spectra of compounds e,f,g and h, which in addition to the ethylenimine ring contain a P=O bond, there are two bands in this interval (1260 cm^{-1} and 1280 cm^{-1}), while in the spectra of compounds i,j and k, whose molecules contain only the ethylenimine ring, there is only one band (1264-1272 cm^{-1}). Inasmuch as according to the data in the literature, no other atomic group in compounds i,j and k absorbs in this region, the said band can safely be attributed to pulsations of the ethylenimine ring.

It is feasible to interpret the Raman lines in the 1230 and 1280 cm^{-1} range. As will be evident from the table, these lines can readily be subdivided into

three groups according to intensities: relatively weak lines (up to 14 in the intensity scale - see note under table), medium (29-46) and strong lines (74-110). On the other hand, the formulas of the series B compounds show that the compounds with strong lines in their spectra have two ethylenimine rings each. Further, it will be noted that the intensities of the strong lines are approximately double those of the medium intensity lines. Hence it may be concluded that the medium and strong lines are associated with vibrations of the ethylenimine ring. The relatively weak lines may be attributed to P=O bonds.

It follows from a comparison of the infrared and Raman spectra that the absorption bands in the IR spectra of compounds e,f,g and h in the 1232 to 1257 cm^{-1} region pertain to the P=O bond and those in the 1272 to 1290 cm^{-1} range to the $N\langle^{C}_{C}$ ring.

Lines having frequencies of about 3000 cm^{-1} and 3070 cm^{-1} appear in the spectra of all the series B compounds. Comparing the spectra of these compounds with the spectrum of ethylenimine[12], one can safely attribute the ~3070 cm^{-1} frequency to antisymmetrical and the 3000 cm^{-1} frequency to symmetrical vibrations of the C—H bonds in the ring. The intensity of these lines is also proportional to the number of ethylenimine rings in the molecules (see table).

It must be noted that the P=O bond and to a lesser extent the P=S bond increase the characteristic frequencies of the ethylenimine ring.

On the other hand, the ethylenimine ring acts to reduce the vibrational frequency of the P=O bond, i.e., has an effect analogous to introduction of a nonelectronegative substituent[4].

As will be evident from the cited data, the frequency of the fully symmetrical vibrations of the ethylenimine ring in the investigated compounds is appreciably higher than the frequency in ethylenimine itself. It is interesting to note that according to chemical data the reactivity of the ring in these compounds is appreciably reduced.[10] It is not impossible that the two effect are related.

Kazan Branch of the USSR Academy of Sciences &
Commission on Spectroscopy of the USSR Academy of Sciences

References

1. L.Bellamy, Infrared spectra of molecules. (Cited in Russian trans.M,1957)
2. R.B.Harvey & J.E.Mayhood, Canad.J.Chem., 33, 1552 (1955).
3. R.A.McIvor, G.A.Grant & C.E.Hubbley, Canad.J.Chem., 34, 1611 (1956).
4. L.W.Daasch & D.C.Smith, Anal.Chem., 23, 853 (1951).
5. M.Baudler, Naturwissenschaften, 6, 124 (1956).
6. V.T.Aleksanian, Kh.E.Sterin, A.L.Liberman, E.A.Mikhailova, M.A.Prianishnikova & B.A.Kazanskii, Izv.AN SSSR, Ser.fiz., 19, 225 (1955). (Trans.Bull.19, No.2, 206.); V.T.Aleksanian & Kh.E.Sterin, Optika i spektroskopiia, 2, 56 (1957).
7. V.I.Malyshev, M.N.Markov & A.A.Shubin, Izv.AN SSSR, Ser.fiz., 17,654(1953
8. B.A.Arbuzov, P.I.Alimov & O.N.Fedorova, Izv.AN SSSR, Otd.khim.nauk (Bulletin, Div.Chem.Sciences), No.8, 932 (1956).
9. B.A.Arbuzov, P.I.Alimov, M.A.Zvereva, I.D.Neklesova & M.A.Kudrina, Izv. AN SSSR, Otd.khim nauk, No.6, 1047 (1954).
10. N.P.Grechkin, Izv.AN SSSR, Otd.khim.nauk, No.5, 538 (1956).
11. N.P.Grechkin, Izv.AN SSSR, Otd.khim.nauk, No.9, 1053 (1957).
12. Landolt-Börnstein, Zahlenwerte und Funktionen, B.I., T.2, p.286, Springer, 1951.

RAMAN SPECTRUM OF VITREOUS GERMANIUM DIOXIDE

- V.V.Obukhov-Denisov, N.N.Sobolev & V.P.Cheremisinov

There have been numerous studies of the vibrational spectra of both crystalline and vitreous silicon dioxide. The results of these investigations indicate that the spectra of these two modifications of silicon dioxide are very similar.

The closest chemical analog of silicon is germanium, the dioxide of which can exist not only in the crystalline but also in the glass-like state. One of the modifications of germanium dioxide (soluble) has the same hexagonal crystal lattice as α-quartz, the principal structural units of which are SiO_4 tetrahedra.

In addition to their intrinsic interest, experimental data on the vibrational spectrum of germanium dioxide may be of value from the standpoint of the theory of the glassy state, particularly in view of the noted analogy of silicon and germanium. Until now, however, the vibrational spectrum of germanium dioxide has received scant attention. The purpose of the present work was, therefore, to investigate the Raman spectrum of germanium dioxide. Unfortunately, we have not yet been able to investigate the Raman spectrum of crystalline germanium dioxide inasmuch as GeO_2 single crystals do not occur in nature and spectroscopic investigation of polycrystals is very difficult.

Below we give the results of our study of the Raman spectrum of glassy germanium dioxide together with a comparison of this spectrum with that of vitreous silicon dioxide[1].

In comparing the two spectra we proceeded on the hypothesis that vitreous germanium dioxide has a structure analogous to that of vitreous silicon dioxide. If this is the case, in comparing the vibrational spectra of the two dioxides it is not unreasonable to regard them as the vibrational spectra of dioxides of the same element but with different atomic weights. This hypothesis is, of course, somewhat far-fetched - silicon and germanium are different elements - but it may be of help in interpreting the vibrational spectra of both GeO_2 and SiO_2.

Table 1

Frequencies and intensities in the Raman and infrared absorption[2] spectra of germanium dioxide (ν, cm^{-1})

Raman spectrum (glassy)	Infrared absorption spectrum	
	glassy	polycrystal
193 (v.w.)		
250 (v.w.)		
312–349; peak – 331 (m)		
373–461; peak – 408 (v.s.)		
520–615; peak 1 – 540 (m)	564 (s)	517 (m)
peak 2 – 600 (m)		551 (m)
		587 (m)
825–894; peak – 866 (w)	888 (v.s.)	872 (v.s.)
935–973; peak – 977 (w)	966 (s)	955 (s)

Intensities: v.w. – very weak, m. – medium, s – strong, v.s. – very strong.

We observed seven bands of different widths and intensities in the Raman spectrum of our specimen of vitreous germanium dioxide. The Raman spectrum obtained with excitation by the 4358 Å line is reproduced in Fig.1 together with the microdensitometer record. The frequency and intensity values are listed in Table 1 together with the frequencies of the infrared absorption peaks of vitreous and polycrystalline GeO_2 according to Sidorov[2]. We note the close similarity of the absorption spectra of the vitreous and polycrystalline modifications and the counterpart of all the infrared absorption bands of vitreous GeO_2 in the Raman spectrum.

In collaboration with Ia.S.Bobovich we carried out a tentative investigation of the polarization of the Raman lines of vitreous germanium dioxide by

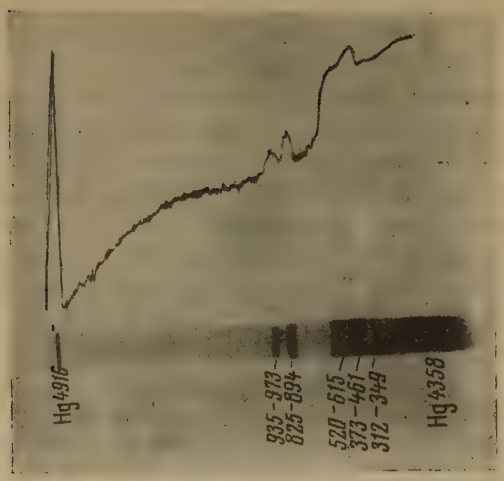

Fig.1

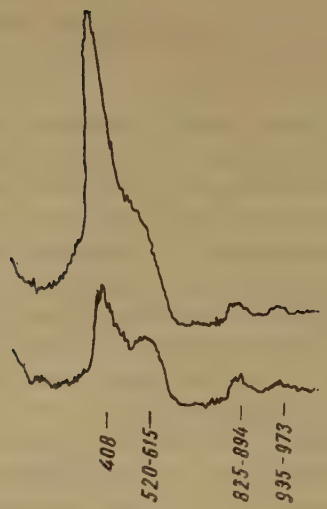

Fig.2

Fig.1. Photograph and microphotogram of the Raman spectrum of vitreous germanium dioxide.

Fig.2. Polarization Raman spectrum of vitreous germanium dioxide. Upper curve - strong component; lower curve - weak component.

means of the diffraction spectrometer with double monochromatization developed by Kiselev[3]. The polarization Raman spectrum is shown in Fig.2. It will be seen that the most intense band peaking at 408 cm^{-1} is strongly polarized, while the other bands (520-615, 825-894 and 935-973 cm^{-1}) are depolarized.

Table 2

Comparison of the Raman spectra of vitreous germanium and silicon dioxide (ν, cm^{-1})

GeO_2 (glassy)	SiO_2 (glassy) (Ref.1)
193 (v.w.)	30-120 (v.s.)
250 (v.w.)	285 (s)
312-349 (m)	370 (s)
373-461 (v.s.)	430 (v.s.)
	495 (s)
520-615	
peak 1 - 540 (m)	635 (w)
peak 2 - 600 (m)	775-846 (m)
825-894 (w)	1022-1098 (w)
935-973 (w)	1140-1246 (w)

For intensity key see Table 1.

In comparing the spectra of GeO_2 and SiO_2, it must be borne in mind that the corresponding bands in the vibrational spectrum of GeO_2 should have lower frequencies than in the SiO_2 spectrum owing to the higher atomic weight of Ge. In comparing the spectra, we also took into account the degree of depolarization and intensity of the Raman lines. The data on the Raman spectra of the two dioxides are juxtaposed in Table 2.

The 825-894, 935-973 and 520-615 cm^{-1} depolarized bands of vitreous germanium dioxide correspond to the 1023-1098, 1140-1246 and 775-846 cm^{-1} depolarized bands in the spectrum of vitreous silicon dioxide. All these bands have their counterparts in the infrared absorption spectrum. The most intense and strongly polarized 373-461 cm^{-1} band of GeO_2 corresponds to the most intense and strongly polarized 430--495 cm^{-1} band of SiO_2. This band of SiO_2 is also present in the infrared spectrum, whereas the corresponding band was not observed in the infrared spectra of GeO_2 (the investigation extended only to 22 μ).

A characteristic feature of the Raman spectrum of germanium dioxide, as of the SiO_2 spectrum, is the presence of a continuous section adjacent to the exciting λ = 4358 Å line; however, the intensity of this continuum is lower in the spectrum of GeO_2.

The above comparison of the Raman spectra of vitreous GeO_2 and SiO_2 may prove useful in the future in interpreting the vibrational spectra of these substances.

"P.N.Lebedev" Physical Institute,
Academy of Sciences of the USSR

References

1. R.S.Krishman, Proc.Ind.Acad.Sci., 37, 1, 377 (1953).
2. T.A.Sidorov, Dissertation, Physical Inst. - USSR Ac.of Sci., 1957.
3. B.A.Kiselev, Optika i spektroskopiia, 1, 597 (1956).

INVESTIGATION OF THE INFLUENCE OF DIFFERENT ELEMENTS ON THE STRUCTURE OF SILICATE GLASSES BY RAMAN SPECTROSCOPY

- Ia.S.Bobovich & T.P.Tulub

1. Determination of the influence of various chemical elements on the structure of glass is important from the standpoint of both theory and practice. Basically, solution of this problem reduces to establishing the atomic-molecular architecture of glass, hence it is expedient to use direct experimental methods. Yet, research in this direction has been based primarily on indirect procedures or on purely speculative inferences regarding the possible role played by different components of the system in the process of vitrification.

Probably the most direct and rational method of attacking the problem is that of vibrational spectra. Hence we undertook an investigation of the influence of different elements on the structure of glass by means of Raman spectroscopy.

2. For our investigation we chose mixed silicates of the $Na_2O \cdot MeO \cdot SiO_2$ type and orthosilicates of the $Na_2O \cdot Me_2O_3 \cdot 2SiO_2$ and $2Na_2O \cdot MeO_2 \cdot 2SiO_2$ types for the cases of di-, tri- and tetravalent elements (Me), respectively. It will be evident that all these contain sodium oxide and the oxides of the other elements in molecular proportions at which no one of the SiO_4 tetrahedra is linked with another common oxygen atom.

This choice of glass compositions was deliberate. It can readily be shown that with this selection any imaginable glass structure can be correlated with its distinctive spectroscopic features. Clearly, if the element Me is present in the orthosilicate glass in the form of cations, there must necessarily be evinced in the spectrum the frequencies associated with vibrations of the SiO_4 tetrahedra, i.e., only one polarized band. If the tetrahedra are so strongly deformed that they have lost all their symmetry elements, this will be evinced by the complete absence of polarized bands. In the case when the Me—O bond is highly covalent, the Me oxide (MeO, Me_2O_3 or MeO_2) may be incorporated in the common network with Na_2O and SiO_2. Then there probably should be observed "continuous" polarized Raman scattering and wide bands, i.e., the spectral features observed for sodium silicate glasses with strongly developed steric coupling of the SiO_4 tetrahedra. This fact was established by us earlier.[1-3] It is not impossible, for example, that the oxides (MeO, Me_2O_3 or MeO_2), particularly if they themselves are glass forming, will not enter at all into the common network. Then there should be observed a surposition of the spectra of the glass-forming oxide and $Na_2O \cdot SiO_2$. The latter has been thoroughly investigated by us[2,3] experimentally and by Stepanov and Prima[4-6] theoretically, and has a highly characteristic appearance. Obviously, there may exist intermediate structures.

Specifically, we investigated the influence of all the more important elements that might be used in practice: Be, Mg, Ca, Sr, Ba, Zn, Cd, Pb, Al, Bi, B, Ti and Zr. Three of these (Be, Al and Zr) were investigated in glasses of somewhat different composition. We were also able to obtain lead glass in the form of the simple orthosilicate $2PbO \cdot SiO_2$. The spectra were investigated by means of a double monochromator developed and constructed in our laboratory.[7] We note that most of the glasses contained the usual and inevitable large defects which preclude investigation by conventional experimental procedures.

3. It was found that as regards their influence on the spectra the enumerated elements may be subdivided into three groups.

The spectra of some members of the largest group are shown in Fig.1. They are characterized by a more or less intense continuous polarized spectrum near the edge of which there appears a low peak (located at approximately the same frequency (~625 cm^{-1}) in all glasses) and a very broad high frequency band peak-

ing at about 980 cm^{-1}. The width of the bands and particularly the presence of the continuum is, in our opinion, a clear indication of partial spatial coupling of the SiO_4 tetrahedra realized through the intermediary of the Me atoms. This inference is substantiated by the appearance of the spectrum of pure lead orthosilicate, which we do not reproduce here. Al, Bi, Pb and B are apparently distinguished by a particularly strong tendency to build into the glass network. Probably a small fraction of the Na_2O and SiO_2 molecules (different in different glasses) forms structures similar to metasilicate chains. Evidence of this is furnished by the presence of bands with a frequency of 625 cm^{-1} and the results of our experiments involving variation of the MeO content (the results of these experiments will be reported elsewhere).

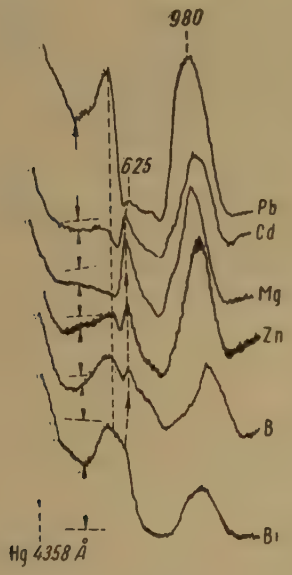

Fig.1

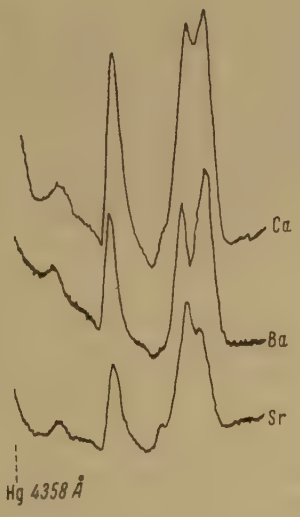

Fig.2

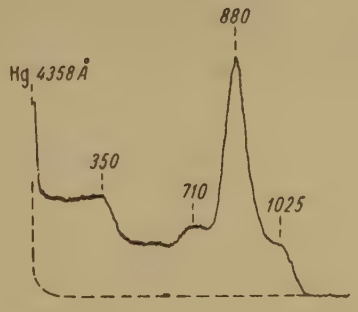

Fig.3

Fig.1. Raman spectra of some glasses having the compositions $Na_2O \cdot MeO \cdot 2SiO_2$ and $Na_2O \cdot Me_2O_3 \cdot 2SiO_2$. The dashed line indicates the level of the background near the exciting line; the arrows identify the continuous spectrum.

Fig.2. Raman spectra of three mixed metasilicates: $Na_2O \cdot MeO \cdot 2SiO_2$, where Me denotes Ca, Ba or Sr.

Fig.3. Raman spectrum of $2Na_2O \cdot TiO_2 \cdot 2SiO_2$ glass. Dashed line - background level.

In the second group, we have three glasses containing CaO, BaO and SrO. Their spectra are shown in Fig.2. They are characterized by somewhat narrow bands, the absence of the continuous polarized spectrum (instead of which there appear two depolarized peaks), good resolution of the structure of the high frequency band and a somewhat different intensity distribution. As regards appearance, these spectra are generally reminiscent of the spectra of sodium metasilicate glasses. The similarity is particularly striking in the case of the glass containing SrO. In view of these facts we infer that structurally all three glasses represent metasilicate chains consisting of Na_2O and SiO_2 molecules.

The $2Na_2O \cdot TiO_2 \cdot 2SiO_2$ glass belongs in the third group. The spectrum of this glass, which is shown in Fig.3, is highly distinctive. In contrast to the foregoing, there are no bands with frequencies of ~625 and ~980 cm^{-1} in the spectrum of this glass; instead there appears a very intense polarized band at ~880 cm^{-1}. Further, there is evident a continuous, also polarized section with a greatly displaced edge (approximately to 800 cm^{-1}). Wide polarized and depolarized bands stand out against this continuous scattering background. A weak de-

polarized satellite adjoins the ~880 cm^{-1} band on the high frequency side.

It would appear that there are evinced in this spectrum the vibrations of free SiO_4 tetrahedra and the complex $TiO_2 \cdot SiO_2$ network. We associate the ~800 cm^{-1} band with the fully symmetrical vibrations of the tetrahedra. This is in agreement with the theoretical data of Stepanov & Prima[4-6]. We associate the continuous scattering with the vibrations of the $TiO_2 \cdot SiO_2$ network. The displacement of its edge is probably due to the appreciably greater rigidity of the Ti—O bond as compared with the Si—O bond. This is apparently connected with the fact that in the Ti atom the outer electrons, that participate in formation of the bond, are 3d electrons.

References

1. Ia.S.Bobovich, O.P.Girin & T.P.Tulub, Doklady AN SSSR, 105, 61 (1955).
2. Ia.S.Bobovich & T.P.Tulub, Zhur.fiz.khim., 30, 1679 (1956).
3. Ia.S.Bobovich & T.P.Tulub, Optika i spektroskopiia 2, 174 (1957).
4. B.I.Stepanov & A.M.Prima, ibid., 4, 734 (1958).
5. B.I.Stepanov & A.M.Prima, ibid., 5, 15 (1958).
6. A.M.Prima, Report presented at the Eleventh Conference on Spectroscopy.
7. B.A.Kiselev, Optika i spektroskopiia, 1, 599 (1956).

SPECTROSCOPY OF NEGATIVE RADIANT ENERGY FLUXES

- B.I.Stepanov & Ia.S.Khvashchevskaia

In most typical problems in spectroscopy we are concerned with nonequilibrium processes occurring due to interaction of light with matter. However, for correct interpretation of the experimental facts, particularly in infrared and high-temperature spectroscopy, it is essential to take into account the background of thermal radiation, namely, the thermal radiation of the investigated substance, the radiation detector and even the material of the absorption cell windows.

Let us consider the substance contained in an absorption cell. We assume that it is in thermodynamic equilibrium with the surrounding medium. The distribution of particles in energy states is characterized by the Boltzmann relation. The thermodynamic equilibrium is maintained by virtue of thermal and radiant exchange with the medium. The radiation fluxes at any point in the cell are described by Planck's formula. If we change the character of the incident radiation, the equilibrium will be disturbed and there will be initiated processes tending to re-establish it. In the case of deviation of the particle distribution from the equilibrium one, there may occur either an increase or a decrease of the mean energy of the system. The first type of disturbance of equilibrium has been thoroughly studied. The second type has received less consideration although actually it is encountered rather frequently and can be detected experimentally.

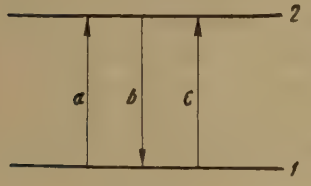

Fig.1

Let us consider a simple system of particles with two energy levels. In the equilibrium condition $n_2^{equi} = n_1^{equi} \cdot e^{-(E-E_1)/kT}$. The commonly encountered disturbance of equilibrium occurs if a radiation source, for example, a body at a higher temperature, is placed near the absorption cell. In this case the radiation flux from the source to the cell will exceed the flux in the opposite direction. Under the influence of the excess flux the system will be excited, that is, part of the quanta will be absorbed and as a result a certain fraction of the particles will be raised from the first level to the second level. This transition between levels 1 and 2 is shown by arrow a in Fig.1. The values of n_2 and n_1 are described by formulas given in Ref.1.

The inverse disturbance of the thermodynamic equilibrium will occur if a cooled body is placed near the cell window. In this case the radiation flux from the cold source in the direction of the cell will be weaker than the reverse flux. As a result of this external influence, part of the particles will undergo transitions from level 2 to level 1. The system will again be brought into an excited state, but of opposite sign, ($n_2 < n_2^{equi}$ and $n_1 > n_1^{equi}$). This negative excitation process is represented by arrow b in Fig.1.

It follows from above that in either case excitation of the system occurs under the influence of a flux $\Delta I = I_{source} - I_{cell}$.

If $\Delta I = 0$, no excitation occurs, i.e., the equilibrium is not disturbed. If $\Delta I > 0$, we have the usual type of excitation. Finally, if the incident flux is negative, we have a unique negative excitation accompanied by decrease of the mean energy of the system. The numbers n_2 and n_1 of particles in the states 2 and 1 are given by the same formulas but with negative values of ΔI. In contrast to positive fluxes, the maximum value of negative fluxes is limited; consequently, the influence of negative fluxes is relatively weak and frequently remains unnoticed.

Under the influence of a negative flux, however, there may occur in a system of particles diverse optical effects equivalent to all the usual effects. A negative flux may be absorbed, scattered or reflected. The negative flux may give rise to negative luminescence or a negative photoeffect.[2-3] If the quantum efficiency of the negative luminescence is 100%, the absorbed negative flux is fully compensated by negative luminescence. Negative luminescence is represented by arrow c in Fig.1.

The purely theoretical considerations[3] outlined above led us to undertake a series of experimental investigations. Our very first attempt showed that negative fluxes can readily be detected and possess many of the usual attributes of positive fluxes. They can be utilized for determining the distribution of levels, absorption coefficients, indices of refraction, lifetimes of excited states, yields and efficiencies, scattering indicatrices, etc. Noticeable negative fluxes are readily obtained in the infrared region. At high temperatures of the cell they can also be detected in the visible region without difficulty.

In investigating the properties of negative fluxes propagated from a cold source to the cell, one must take into account the thermal emission of the radiation detector. This emission is also appreciable and normally remains unnoticed only because it is compensated by the counter fluxes due to the thermal emission of the absorption cell with the investigated substance and other external objects.

If the radiation source, the investigated substance and the radiation detector are all at the same temperature, there will be no nonequilibrium processes and the detector will give a null indication. Any disturbance of the thermodynamic equilibrium will produce a reaction in the detector: it will begin to give an indication (positive or negative), if the source is heated or cooled or if a nonequilibrium source is interposed between it and the thermal radiation source. The detector will also begin to indicate, i.e., give nonzero readings, if the temperature of the cell or even of the detector itself changes. The indications of the radiation detector will be proportional to the difference between the flux incident on it and the flux emitted by it. The former consists of the flux from the source attenuated in the cell and the flux due to thermal emission of the investigated substance. In general the indication of the radiation detector is given by[4]

$$Y = C(1 - R)[E_{sou}e^{-kl} + U_{cell}(1 - e^{-kl}) - U_{rd}]. \quad (1)$$

Here R is the coefficient of reflection from the absorbing layer, U_{cell} and U_{rd} are Planck's functions at $T = T_{cell}$ and $T = T_{rd}$ (rd = radiation detector), k is the coefficient of absorption or scattering, l is the thickness of the absorbing layer, E_{sou} is the emissive capacity of the source and C is a constant dependent on the response of the detector. Usually both the detector and cell are at the same (room) temperature; in this case

$$Y = C(1 - R)(E_{sou} - U_{rd})e^{-kl}. \quad (2)$$

The transmission of the cell is

$$P = \frac{Y}{Y_0} = (1 - R)e^{-kl}; \quad (3)$$

it depends only on the properties of the investigated substance.

It will be evident that the indications of the instrument (radiation detector) may be either positive or negative. The latter case is realized with cold sources ($E_{sou} < U_{rd}$; $T_{sou} < T_{rd} = T_{cell}$). In either case, using (3), we can determine the coefficients of absorption or scattering from the curve

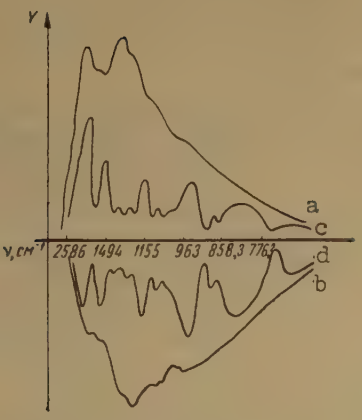

Fig.2. Absorption spectra of nitrobenzene at different source temperatures.

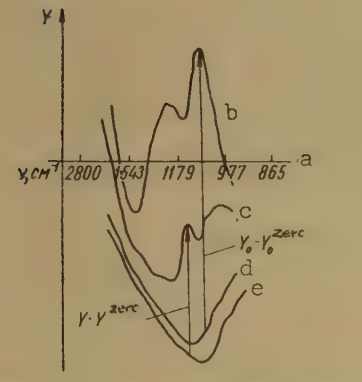

Fig.3. Absorption spectra of cyclohexanone at different source temperatures.

recorded by the instrument. Different negative flux frequencies are attenuated to different degrees; Buger's law holds for negative fluxes as well.

Fig.2 shows the records obtained by means of an IKS-11 spectrometer for the absorption of nitrobenzene. Curve a gives the values of Y_0, i.e., the indications of the instrument with an empty cell and a hot source - in this case the interior of a blackened brass bushing heated to 80°. Curve b gives the value of Y_0 for a cold source - the same brass bushing cooled to -100°. Reduction of the temperature by 120° (below room temperature) leads to approximately the same values of Y_0 (with opposite sign) as heating to 60° above room temperature. The approximate coincidence of the maxima and minima in curves a and b is fortuitous and does not occur at other temperatures. Every cold source (and in particular every cooled metallic surface) has its own specific "negative" emissive capacity. This characteristic can be utilized for analysis and for distinguishing between different objects.

Curves c and d in Fig.2 give the values of Y for an ordinary and a cold source with the cell filled with nitrobenzene. The thickness of the layer was 0.05 mm; the slit width 1.9 mm. Curves c and d are approximately symmetrical with respect to the zero line (horizontal axis); the frequency positions of the bands are essentially the same. The symmetry is approximate and is connected with the symmetry of curves a and b. The values of the absorption coefficient determined from curves a & c and b & d are identical, which is proof that cold sources can be used in solving many spectroscopic problems. Similar data were obtained in a number of other cases.

Frequently, rather complicated regularities are observed in investigating the temperature dependence of absorption spectra. In such cases one must also take into account the thermal emission of the cell windows which are never completely transparent. In some cases the detector may give positive readings for certain wavelengths and negative readings for other wavelengths. Fig.3 shows the records necessary for analysis of the absorption spectrum of cyclohexanone at T = -140°. Curve d characterizes the thermal emission spectrum of the KCl windows of the empty cell at T = -140°, which corresponds to values of Y from (1) at $E_{sou} = U_{rd}$, i.e.,

$$Y = C(1 - R)(U_{cell} - U_{rd})(1 - e^{-kl}).$$

Curve b gives the values of Y obtained with the radiation from a warm source passing through the cold cell windows. In this case the source was the interior of an electric heater coil at T = 240°. It will be seen that in the 2800-1600 cm^{-1} and 1300-970 cm^{-1} spectral intervals the values of Y are positive. This means that the positive flux from the source, weakened in passing through the cell windows (first term in Eq.(1)), exceeds the negative flux from the cell (second and third terms in Eq.(1)). In the 1600-1300 cm^{-1} range and below 970 cm^{-1} the values of Y are negative; consequently, the positive flux is weaker than

the negative flux. Curve e in Fig.3 is the record of the thermal emission of the cell filled with cyclohexanone; curve c is the record of the flux from the source, attenuated in the filled cell, together with the negative flux from the cell. This curve is complex and requires special interpretation.

The cited results indicate that the negative flux concept is a valuable one and that its introduction is justified. It allows of giving a correct interpretation of many experimental facts and extends the range of applicability of most common formulas of theoretical optics.

Recently Veingerov and his co-workers[5] discovered a negative optical--acoustic effect. This phenomenon readily fits into the general scheme of the processes discussed above.

Belorussian State University &
Institute of Physics and Mathematics,
Belorussian SSR Academy of Sciences

References

1. B.I.Stepanov, Liuminestsentsiia slozhnykh molekul (Luminescence of complex molecules). Pub. by Belorussian SSR Ac. of Sci., 1956; Trudy (Transactions) Institute of Phys.& Math., Belorussian SSR Ac.of Sci. No.1 (1956).

2. V.V.Antonov-Romanovskii, B.I.Stepanov, M.V.Fok & A.P.Khapaliuk, Doklady AN SSSR, 105, 50 (1955); B.I.Stepanov, Optika i spektroskopiia, 1, 125 (1956).

3. B.I.Stepanov, Optika i spektroskopiia, 3, 3 (1957).

4. B.I.Stepanov & Ia.S.Khvashchevskaia, Doklady AN SSSR, 116, 558 (1957); Uch.zap.BGU (Scientific Notes, Belorussian State University) 41, 1957.

5. M.L.Veingerov, Ia.I.Gerlovin & N.A.Pankratov, Optika i spektroskopiia, 1, 1023 (1956).

6. M.L.Veingerov, A.A.Sivkov & E.V.Malykh, ibid., 2, 823 (1957).

INFRARED ABSORPTION AND THERMAL RADIATION SPECTRA OF SOME MOLECULAR COMPOUNDS IN DIFFERENT STATES OF AGGREGATION

- O.V.Fialkovskaia

One of the more valuable procedures for studying intermolecular interaction is investigation of the absorption spectra in different states of aggregation.[1] Through comparison of the absorption spectra one can follow how the optical properties of the molecules change under the influence of intermolecular forces as the molecules unite to form a crystal. It is useful to supplement such studies with investigation of the absorption spectra in polarized light when the relative orientation of the electromagnetic wave vector and the molecule in the crystal are known.[2]

We investigated the infrared absorption spectra of naphthalene, anthracene and phenanathrene in different states in the region of the fundamental intramolecular vibrations (700 to 1500 cm^{-1}). In addition to the usually investigated states - the gaseous and crystalline, we studied the absorption spectra of these substances in the dissolved, molten and polycrystalline states at different temperatures. This enabled us to follow the appearance of new absorption bands due to aggregation of the molecules, to elucidate the nature of some of these bands and to detect the effect of thermal radiation of the investigated molecular crystals. The observations were carried out at different temperatures from -231 to +220° in natural and polarized light. All the absorption spectra were obtained under identical experimental conditions, and in some cases with equivalent layer thicknesses (gas, solution, crystal or polycrystal and melt). Measurements were made on a Perkin-Elmer Model 12C infrared spectrometer. The effective slit width was 4.3 cm^{-1} in the 15 μ region, 5.6 cm^{-1} in the 12 μ region, 6.5 cm^{-1} in the 10 μ region, etc. The accuracy of measurement was ±5 cm^{-1} at 2000 cm^{-1}, ±2 cm^{-1} at 1000 cm^{-1} and ±1 cm^{-1} at 600 cm^{-1}.

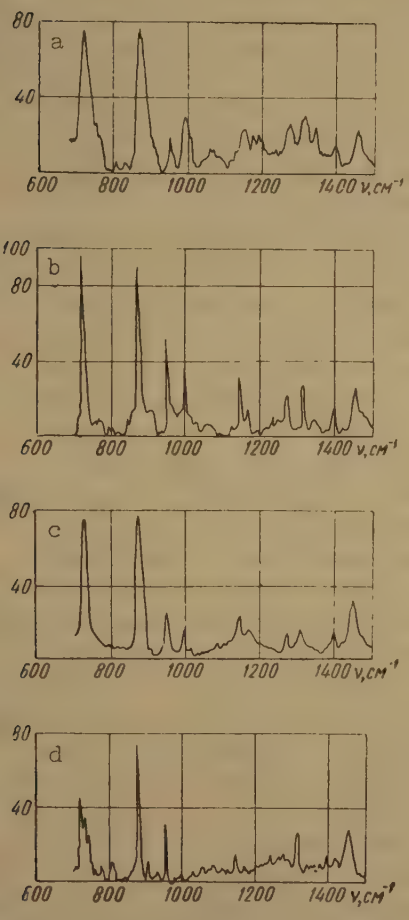

Fig.1. Absorption spectra of anthracene: a) vapor at 40 mm Hg pressure, b) 1% solution in carbon disulfide, c) melt and d) single crystal at 18°.

The scattered light was controlled by means of an LiF shutter located between the specimen and the light source; this arrangement also took care of the parasitic thermal radiation from the heated specimen. Inasmuch as the character of the changes in the spectra in going from one state of aggregation to another is virtually the same for all the investigated molecular crystals, we shall confine our discussion below to one, namely, anthracene. Anthracene crystallizes in the monoclinic system - space group C_{2h}^5 (the symmetry of the free anthracene molecule is D_{2h}). Each unit cell comprises two differently oriented molecules.

The absorption spectra of anthracene in different states of aggregation are shown in Fig.1. Through comparison of these spectra, we can distinguish the principal intramolecular frequencies: 726, 878, 952, 1000, 1148, 1166, 1276, 1315, 1340

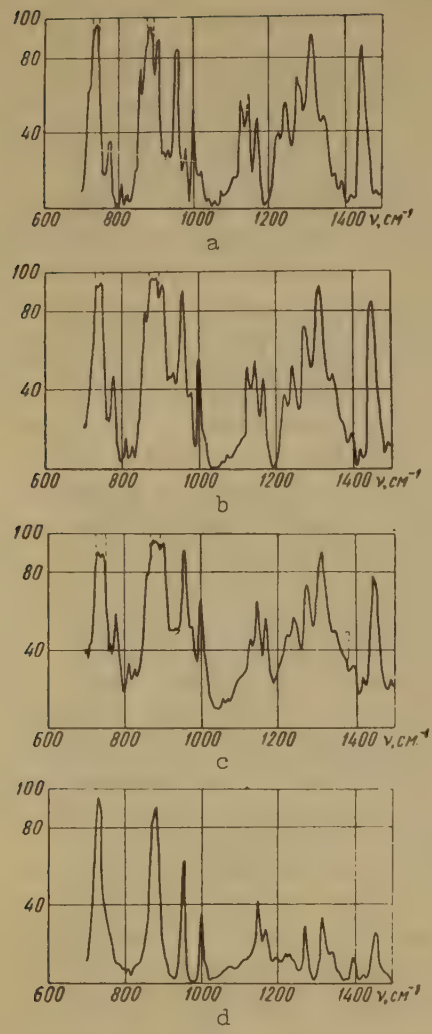

Fig.2. Absorption spectra of anthracene: polycrystal at a) 20°, b) 100°, c) 150° and d) melt.

and 1454 cm^{-1} and so on. The intramolecular vibration frequencies remain virtually the same (within the limits of the experimental error) in all three non-solid states: gas, solution and melt.

In analyzing the absorption spectrum of the single crystal we paid primary attention to the behavior of some of the absorption bands that change their appearance in going from the gaseous to the crystal state and to the appearance of new bands characteristic of the crystal state. The 726 cm^{-1} band decreases in intensity in the crystal and splits into two bands (726 and 740 cm^{-1}). The spli ting of this band in non-polarized light is due to the presence of differently oriented molecules in the unit cells.[3] This is substantiated by the appearance of the spectra obtained with polarized light (see below). In addition there appear in the single crystal spectrum a number of new absorption bands, low in intensity, but quite narrow and sharp; these have no analogs in the spectra of the vapor and melt. These bands appear primarily in the form of satellites at equal distances (20 to 24 cm^{-1}) from the principal intramolecular band. The short wavelength satellites are somewhat more intense than the long wavelength ones.

With a view to clarifying the nature of the satellites, we felt it would be of interest to follow their behavior in going from the crystal to the molten state. These experiments were carried out with polycrystals, which can be had in any thickness and moreover in any size up to the dimensions of the Globar image.

Investigation of the absorption spectrum of a thick (50 μ) polycrystal at different temperature up to the fusion point enabled us to follow the appearance and temperature behavior of the newly discovered "crystalline" bands (Fig.2). In the spectrum of the thick polycrystal there are clearly evident not only the bands associated with the principal intramolecular vibrations, but also the high and low frequency crystalline satellites; as the material goes over into the crystalline state these bands develop and broaden and tend to obscure the weak bands appearing in the liquid and gaseous state spectra (this makes it easier to interpret the crystalline spectrum).

Intramolecular frequencies, cm^{-1}	740		882		956	
Satellite frequencies, cm^{-1}	762	720	904	860	980	934
$\Delta\nu$, cm^{-1}	22	20	22	22	24	22

With increasing temperature, the intensity of the satellite increases, true with simultaneous increase in the intensity of the continuous absorption background. In addition to the satellites accompanying the intramolecular bands, we observed yet another band with a frequency of 1128 cm^{-1}, the temperature behavior of which is the inverse of that of the satellites, i.e., this band becomes weaker

with increasing temperature. Apparently it has an origin different from that of the satellites.

Investigation of the absorption spectrum of an anthracene single crystal in polarized light at -231° further substantiated the "crystalline" origin of the above mentioned new absorption bands. Most of the new absorption bands[4] of crystal anthracene exhibit weak polarization, i.e., only a small change in intensity in going from one polarized component to the other, with the frequency of the bands remaining the same. Aside from these, however, we observed a number of strongly polarized bands; outstanding among these is the 740 cm^{-1} band which corresponds to the 726 cm^{-1} band in the spectrum of the gas. Thus in the a-component there is evident a very intense band at 742 cm^{-1} and a weak band at 728 cm^{-1}, while in the b-component, on the contrary, the 728 cm^{-1} band is intense and the 742 cm^{-1} band is weak, i.e., we have here a case of so called Davydov splitting[3]. The band at 1148 cm^{-1} band exhibits similar behavior.

The satellites surrounding the intramolecular bands are also polarized. We found that the long wavelength satellites are evinced more strongly in the b-component.

By comparing the absorption spectra for different states of aggregation and making use of the results of our temperature and polarization studies, we were not only able to follow the process of appearance of the new crystalline bands but also to determine their nature. From the fact that the satellites systematically appear at approximately the same small (20-24 cm^{-1}) distance from the principal intramolecular bands and from the character of their behavior in polarized light, we conclude that they appear as a result of coupling of lattice vibrations with intramolecular vibrations. As for the strongly polarized bands (726 cm^{-1} in the b—component and 742 cm^{-1} in the a-component), there is reason to assume that they have an exciton origin.

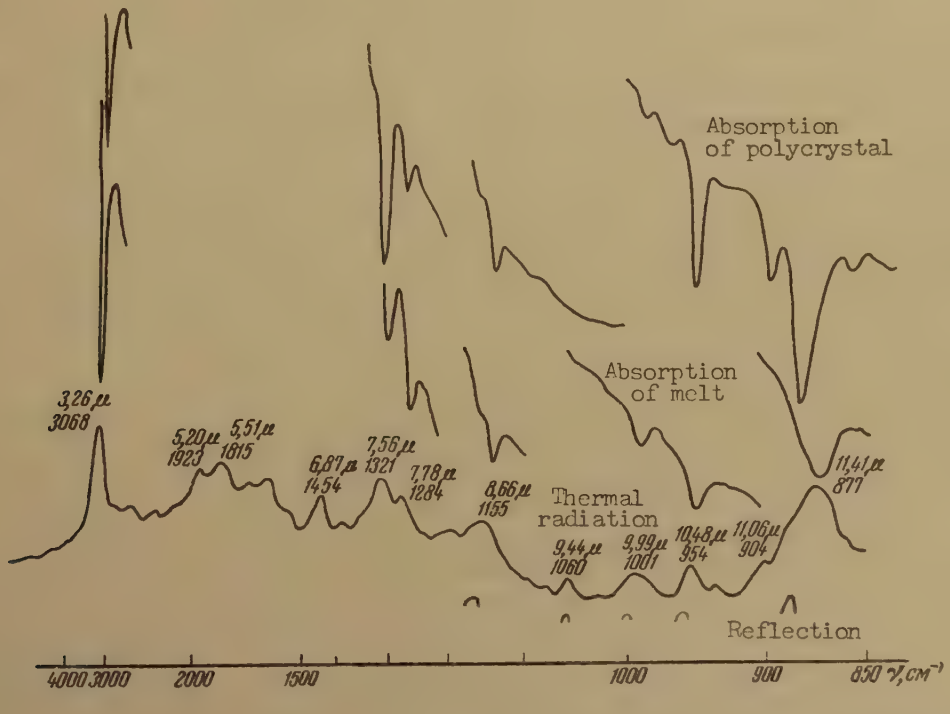

Fig.3. Thermal radiation spectrum of anthracene (below) compared with the absorption spectra of anthracene in different states (above).

In investigating the absorption spectra of anthracene in the molten state, we observed its thermal radiation. The thermal radiation spectrum of anthracene (Fig.3) consists of a number of emission bands, whose maxima in conformity with Kirchhoff's law coincide with the peaks of the absorption band.

Institute of Physics,
Academy of Sciences of the Ukrainian SSR

References

1. A.F.Prikhot'ko, J.Phys., 8, 257; A.F.Prikhot'ko, Izv.AN SSSR, Ser.fiz., 12, 499 (1948); R.S.Halford & O.A.Schaeffer, J.Chem.Phys., 14, 141 (1946)

2. R.D.Mayer & D.F.Hornig, J.Chem.Phys., 17, 1236 (1948); Zwerdling & R.S.Halford, J.Chem.Phys., 23, 2221 (1955); G.S.Pimentel & A.L.McClellan, J. Chem.Phys., 20, 270 (1952); G.S.Pimentel, J.Chem.Phys., 19, 1936 (1951); W.S. Person & G.S.Pimentel, J.Chem.Phys., 20, 230 (1955).

3. A.S.Davydov, Teoriia pogloshcheniia sveta v molekyliarnykh kristallakh (Theory of light absorption in molecular crystals), Kiev, 1951.

4. O.V.Fialkovskaia, Transactions of the Tenth All-Union Conference on Spectroscopy, Vol.1, p.151, Lv'ov, 1957.

INFRARED REFLECTION SPECTRUM OF BORON OXIDE AT HIGH TEMPERATURES

- E.P.Markin & N.N.Sobolev

Earlier a detailed investigation of the vibrational spectrum of boron oxide was carried out in our laboratory.[1-3] Analysis of the Raman and infrared spectra together with special calculations showed that for a satisfactory interpretation of the vibrational spectrum of boron oxide it must be assumed that the fundamental structural unit of this material in the glassy state is the B_4O_6 molecule belonging to the T_d point symmetry group. This was substantiated by the results of investigation of the isotope shift in the infrared spectrum of boron oxide enriched with B^{10} and the observed invariance of the fundamental frequencies in the Raman spectrum of boric acid in going from the glassy to the liquid state.

In the earlier experiments the infrared absorption spectrum of molten boron oxide could not be obtained inasmuch as thin films of the oxide upon melting coagulated into drops. Yet it was felt that data on the infrared spectrum of liquid boron oxide might be helpful in understanding its structure.

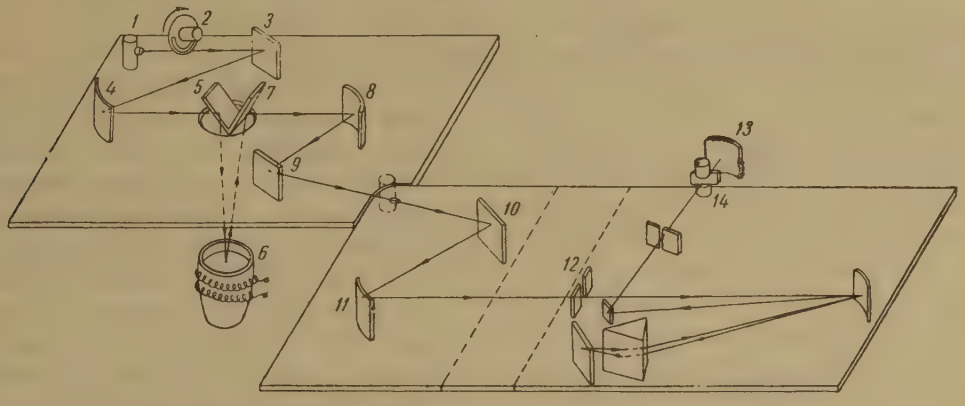

Fig.1. Diagram of the set-up used for investigating infrared reflection spectra of substances at high temperatures.

The present investigation was therefore concerned with the infrared reflection spectrum of boron oxide at high temperatures. For the purpose of such studies we designed and constructed the set-up diagramed in Fig.1. The modulation procedure was adopted to eliminate the continuous spectrum emitted by the investigated substance and the heater at high temperatures.

As shown in the figure, a rotating shutter 2 (9 rps) is mounted in front of the Silit rod 1. The modulated beam is focused by means of the rotatable plane mirror 3, the spherical mirror 4 and the plane nickel mirror 5 onto the surface of the boron oxide sample 6. The reflected beam is focused by means of the system of mirrors 7,8 & 9 onto the vertical plane formerly occupied by the Nernst glower of the IKS-11 monochromator (naturally the glower was removed) and directed by the illuminating system 10 & 11 into the entrance slit of the monochromator 12. The radiation flux from the monochromator is focused by mirror 13 onto the bolometer 14 which is connected to the input of an ac amplifier.[4] Hence only the modulated radiation is detected and measured. The amplified signal after appropriate transformation is recorded on a strip chart by means of an EPP-09 potentiograph.

Results obtained for boron oxide in the temperature range from 20 to 1000° are shown in Fig.2. It will be evident from the curves that the 3241, 1542 and 1184 cm^{-1} bands, observed at room temperatures and belonging to the boric acid

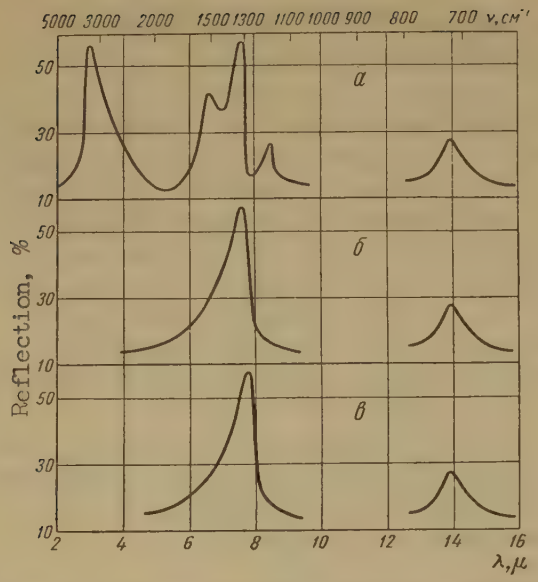

Fig.2. Infrared reflection spectrum of boron oxide at a) 20°, b) 170° and c) 1000°.

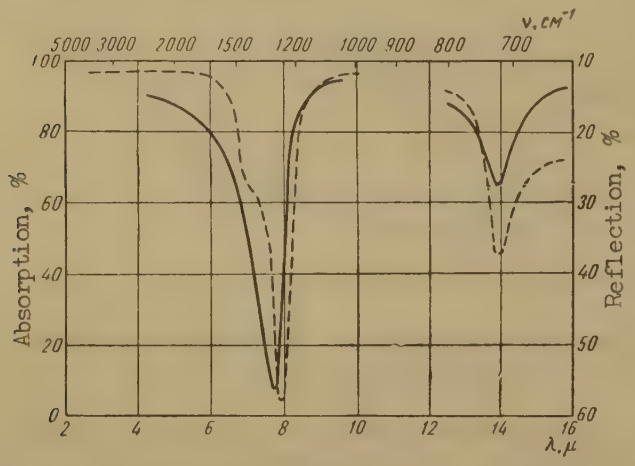

Fig.3. Infrared reflection spectrum of liquid boron oxide at 1000° (solid curve) and infrared absorption spectrum of glassy boron oxide (dashed curve).

forming on the surface of the oxide, disappear at about 170°.

In the range from 170 to 1000°C, there are observed two bands with frequencies of 1316 and 720 cm^{-1}. With increasing temperature, the 1316 cm^{-1} band is shifted to the side of lower frequencies, the displacement attaining 40 cm^{-1} at 1000°. These bands correspond to the 1260 and 718 cm^{-1} infrared absorption bands of glassy boron oxide[2] (Fig.3). Thus the principal infrared bands of boron oxide, evinced in the glassy state, persist in the liquid state as well up to 1000° (viscosity 74 poise)[5]. These results substantiate the earlier inference that the fundamental structural unit continues to be the B_4O_6 molecule even after transformation from the glassy to the liquid state.

In conclusion, we note that the results recently published by Harrand[6] substantiate the above deduction regarding the molecular structure of boron oxide, although Harrand himself suggests a different interpretation of his data. Measurement of the depolarization factor ρ of the fully symmetrical 808 cm^{-1} line of glassy boron oxide showed that $\rho = 0.63$.[1] Yet the fully symmetrical vibration of the B_4O_6 molecule if its point symmetry were T_d should give $\rho = 0$.

The appreciable depolarization of the 808 cm^{-1} line of glassy boron oxide might be explained by the large unremovable anisotropy of the specimen. In going over to the liquid state, one should then expect a decrease in the degree of polarization. This is what was observed in the work of Harrand: the depolarization factor of the 808 cm^{-1} line of liquid boron oxide proved to be 0.2. Thus the work of Harrand, in agreement with our results, substantiates the molecular structure of boron oxide in the liquid as well as in the glassy state and indicates that the B_4O_6 molecule has the point symmetry T_d.

"P.N.Lebedev" Physical Institute,
Academy of Sciences of the USSR

References

1. E.N.Lotkova, V.V.Obukhov-Denisov, N.N.Sobolev & V.P.Cheremisinov, Optika i spektroskopiia, 1, 772 (1956).
2. T.A.Sidorov & N.N.Sobolev, ibid., 3, 560 (1957).
3. T.A.Sidorov & N.N.Sobolev, ibid., 4, 9 (1958).
4. V.I.Malyshev, M.N.Markov & A.A.Shubin, Doklady AN SSSR, 86, 273 (1952); Izv.AN SSSR, Ser.fiz., 17, 654 (1953); M.N.Markov, Zhur.tekh.fiz., 24, 1867 (1954).
5. K.Arndt, Z.Elektrochem., 13, 578 (1907).
6. M.Harrand, Ann.de phys., 2, 309 (1957).

* * * * * * *

INFRARED ABSORPTION SPECTRA OF MOLECULAR COMPOUNDS WITH METAL HALIDES

- A.N.Terenin, V.N.Filimonov & D.S.Bystrov

A characteristic attribute of $AlCl_3$, $AlBr_3$, $SnCl_4$ and certain other metal halides, which act as efficient catalysts for many chemical reactions, is the ability of their molecules to link up with other organic and inorganic molecules at the point of excess electronic density produced by free electron pairs on the N, O and S atoms or by the π-electrons of double bonds. The electron acceptor properties of metal halides are due to the presence of a vacant orbit in the valence electron shell of the metal atom, an orbit which can readily be filled by a free electron pair belonging to the atom of another molecule with the formation of a donor-acceptor bond.

For the purpose of understanding the mechanism of molecular activation by metal halides, it is important to investigate the vibrational spectra of molecular compounds formed by the halides inasmuch as such spectra can yield information on the structure of these compounds and the changes occurring in the combining molecules under the influence of the metal halides.

We investigated the infrared absorption spectra of molecular compounds of NO, acetonitrile, pyridine, acetaldehide, acetone, acetyl chloride, ethyl acetate, diethyl ether, methanol and cyclohexane with $AlBr_3$, $AlCl_3$, $SnCl_4$ and some other metal halides. In most cases the molecular compounds were investigated in the solid state and were prepared by the method of absorption of the vapor of the organic compound (gaseous NO) on the sublimated layer of the halide. The experimental procedure and some of the initial results have been described earlier.[1]

The characteristic 1876 cm^{-1} vibrational frequency of NO is shifted upon formation of molecular compounds of NO with $AlBr_3$ and $SnCl_4$ to 2142 and 2200 cm^{-1}, respectively. Such an appreciable increase in frequency can be explained, in our opinion, by partial transfer of the NO valence electron to the halide molecule, as a result of which the bond between the N and O atoms approaches a triple one: $N{\equiv}O^+$. It is known, for example, that in compounds where NO is present as a positive ion ($NO^+HSO_4^-$, $NO^+ClO_4^-$, etc.) the frequency of its valence vibrations is greatly increased.[2]

We also observed an increase in the frequency of the valence vibration of the interacting group in the molecule upon addition of a metal halide in the case of acetonitrile. The 2267 cm^{-1} frequency of $C{\equiv}N$ is increased in compounds with $AlBr_3$, $AlCl_3$ and $SnCl_4$ by about 65 cm^{-1}; at the same time the 919 cm^{-1} frequency of C—C is increased 20 or 40 cm^{-1}.

Upon the addition of $AlBr_3$ to acetaldehyde molecule, the greatest change is exhibited by the valence vibration frequency of C=O, which is reduced from 1765 cm^{-1} to 1665 cm^{-1}. The other frequencies of the acetaldehyde groups change appreciably less. Considerable decrease of the carbonyl group frequency (85 and 75 cm^{-1}) occurs incident to the formation of molecular compounds of acetone with $AlBr_3$ and $SnCl_4$. Apparently in such cases the metal halides link up with the carbonyl groups of the organic molecules. In the absorption spectrum of the molecular compound of $AlCl_3$ with acetyl chloride, according to data of Susz & Wuhrmann[3] and our results, instead of the 1820 cm^{-1} band, associated with the valence vibrations of C=O, there appear new absorption bands at 2210 and 2315 cm^{-1}. These bands apparently belong to vibrations of the C≡O+ bond forming as a result of linking up of the $AlCl_3$ with the Cl atom of acetyl chloride and transformation of the molecular compound to the ionic form: $H_3C—C{\equiv}O^+AlCl_4^-$.

The formation of molecular compounds of ethyl acetate with $AlBr_3$, $AlCl_3$, $SnCl_4$ and $TiCl_4$ leads to the disappearance of the 1745 and 1250 cm^{-1} absorption bands associated, respectively, with the valence vibrations of the C=O group and the antisymmetrical valence vibrations of the 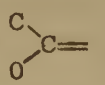 group of ethyl acetate.[4] Instead of these bands, there appear in the absorption spectrum two intense bands at 1605 and 1335 cm^{-1} in the case of molecular compounds with the aluminum halide and at 1630 and 1320 cm^{-1} in the case of the compounds with $SnCl_4$ and $TiCl_4$. The other frequencies of ethyl acetate exhibit little change. Such changes in the vibrational spectrum of $CH_3COOC_2H_5$ cannot be explained by attachment of the halides to the ether oxygen of the ethyl acetate. Actually in this case one could expect only an insignificant change in the C=O frequency and a minor reduction of the frequency of vibration of the 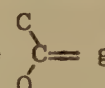 group.

The vanishing of the 1745 cm^{-1} band and the appearance in its stead of a new band shifted 140-115 cm^{-1} to the side of lower frequencies indicate that the metal halide molecule interacts with the carbonyl group of ethyl acetate. The new band is apparently due to vibration of the C=O group disturbed as a result of attachment to it of an electron acceptor agent; the frequency position of the new band approximately coincides with the position of the C=O band of acetone and acetaldehyde in molecular compounds with $AlBr_3$ and $SnCl_4$. This new band might also be attributed to vibrations of a C=C bond forming as a result of transition of the ethyl acetate molecule into the enol form. However, the fact that there is no evidence of the CH valence frequencies characteristic of the $=CH_2$ group in the spectrum indicates that this transition does not occur. The appearance of the new band at 1320-1330 cm^{-1} must apparently be explained by increase of the 1250 cm^{-1} frequency of the 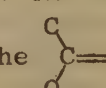 group owing to weakening of the neighboring C=O bond.

Comparison of the infrared spectra of molecular compounds of cyclohexane with $AlBr_3$, $AlCl_3$ and $SnCl_4$ with the absorption spectrum of pure cyclohexane shows that the metal halides have a particularly strong influence on the 1650 cm^{-1} frequency of C=C in cyclohexane, i.e., reduce it to 1525-1535 cm^{-1}. At the same time the 3025 cm^{-1} band associated with the valence vibrations of CH in the =CH groups of cyclohexane disappears. The other frequencies of cyclohexane change much less. Such changes in the cyclohexane spectrum can be explained either by formation of a π-complex with symmetrical attachment of the halides to the double bond or by formation of a molecular compound of the type

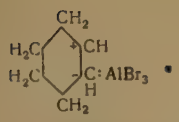

Evidence in favor of the first hypothesis is the magnitude of the decrease of the C=C frequency, which is approximately equal to the decrease of the double bond frequency in complexes of ethylene, propylene and butylene with $PtCl_2$, wherein π-electron interaction is inferred.[5] On the other hand, the great intensity of the 1530 cm^{-1} band as compared with the intensity of the 1650 cm^{-1} band in pure cyclohexane and the disappearance of the 3025 cm^{-1} band support the second hypothesis. In this case the 1530 cm^{-1} frequency must be attributed to vibrations of the semipolar $C^{+}—C^{-}$ bonds.

Studies[6] of the Raman spectra of pyridine in different solvents have shown that some of the frequencies of pyridine increase in a regular manner with enhancement of the proton-donor properties of the solvent. Thus, for example, the 988 cm^{-1} frequency associated with the fully symmetrical vibrations of the pyridine ring increases by 8, 12, 12, 18 and 18 cm^{-1} when pyridine is dissolved in water, ethyl alcohol, chlorophenol, formic and acetic acid, respectively. In $C_5H_5NH^{+}Cl^{-}$ aqueous solutions this frequency is increased by 19 cm^{-1}. In the molecular compounds of pyridine with $AlBr_3$, $AlCl_3$, $SnCl_4$, $TiCl_4$, SnI_4, $FeCl_3$ and $BiCl_3$ investigated by us, the 988 cm^{-1} frequency was increased by 32, 32, 29, 25, 24, 22 and 18 cm^{-1}, respectively.

The sequence of halides arranged in order of increasing shift of the pyridine frequency is (except for $FeCl_3$) identical with the sequence of metal halides arranged in order of increasingly stronger acidic properties as determined by means of electronic absorption spectra[7]. The greater frequency shift observed in the case of the metal halides investigated by us indicates that they possess stronger electron acceptor properties than the molecules of the protonic acids enumerated above. Thus changes in the infrared spectrum show that attachment of metal halides to organic molecules produce in these the same changes as the addition of a proton, i.e., that Al, Sn, Ti and Fe halides, even in the absence of corresponding hydrogen halides, behave like strong acids.

Scientific Research Physical Institute,
"A.A.Zhdanov" Leningrad State University

References

1. V.N.Filimonov & A.N.Terenin, Doklady AN SSSR, 109, 799 (1956); V.N. Filimonov, D.S.Bystrov & A.N.Terenin, Optika i spektroskopiia , 3, 480 (1957).

2. W.R.Angus & A.H.Leckie, Proc.Roy.Soc.A, 149, 327 (1935).

3. B.P.Susz & J.Wuhrmann, Helvetica chim.acta, 40, 971 (1957).

4. S.A.Francis, J.Chem.Phys., 19, 942 (1951).

5. J.Shatt & L.A.Duncanson, J.Chem.Soc., 2939 (1953); H.B.Jonassen & J.E.Field, J.Amer.Chem.Soc., 79, 1275 (1957).

6. R.Mierzecki, Acta phys.polonica, 12, 26 (1953); B.R.Lakshmanan, J.Indian Inst.Sci., 36, 91 (1954); P.Chiorbolis, Ann.Chimica, 47, 443 (1957); G.K.Kastha, Indian J.Phys., 30, 519 (1956).

7. D.L.Hawke & J.Steigman, Anal.Chem., 26, 1989 (1954).

TOWARDS A CLARIFICATION OF THE "HYDROGEN BOND" CONCEPT

- V.M.Chulanovskii

Investigations of the hydrogen bond have been going on for several decades. Nevertheless, no one so far has come up with a fully acceptable definition of the concept. In fact, it is still impossible to give the precise experimental indications or factors that distinguish this type of intermolecular bond* from others. It is interesting to note that this was not done even at the International Symposium on the Hydrogen Bond held in July 1957 in Ljubljana (Yugoslavia) although a special session was devoted to the question.

In its extreme manifestations the hydrogen bond has a very pronounced effect on different properties of matter. Spectroscopically, in such cases it is evinced by a very large shift (to the side of low frequencies) of the principal valence vibration band of the XH group of the molecules joined by the hydrogen bridge and also by the great intensity of the band.

However, neither these effects nor any other can be regarded as distinctive experimental indications characterizing the hydrogen bond exclusively. Thus, the frequency shift may be rather large ($CHCl_3$ in diethyl ether) or negligible (same $CHCl_3$ in dioxane or acetone), although in other respects the hydrogen bond is evinced in approximately the same way. An appreciable increase in intensity characterizes the formation of a saturated intermolecular bond and occurs in cases when the hydrogen atom does not directly participate in the bond.[2]

The purpose of the present paper is to call the attention of investigators working on intermolecular interactions to experimental manifestations of the hydrogen bond that are characteristic only of it and to relate these manifestations with the particular attributes of the hydrogen atom that distinguish it from other atoms.

The first obvious indication of formation of a saturated hydrogen bond should be an appreciable increase in the intensity of absorption at the fundamental of the valence vibrations of the XH groups that participate in the intermolecular bond.[1,2]

Other indications characteristic of the hydrogen bond should be sought in manifestations of those properties of the XH group that are associated with or dependent upon the very small size of the hydrogen nucleus, the proton.

The hydrogen bond is evinced particularly clearly in cases when the hydrogen atom is linked with a halogen or oxygen atom. Let us consider the first case, in which comparison of the hydrogen atom with monovalent alkali metal atoms, which have a much larger core, is particularly simple and straightforward.

A common attribute of hydrogen-halide (HalH) and metal-halogen (HalMe) compounds is that upon being dissolved they break up into ions. The facile electrolytic dissociation is indicative of the ionic character of the molecular bonds in both types of compounds.

On the other hand, we know that the molecules of these two types of compounds cannot be described by the same model. In order not to complicate the discussion, we shall have recourse to the rough characteristic of the electron shell of the ions composing the molecules commonly used in such cases, namely, the magnitude of its radius. The properties of all alkali halide molecules are satisfactorily described by the model pictured in Fig.1,a in which the distance R between the ionic cores is equal to the sum of the ionic radii:

$$R = r_1 + r_2.$$

Comparison of the distance R with the radius r of the negative halogen ion in HalH molecules (Fig.1,b) leads to the inequality $R < r$, that is, in this case

---

*In this article we do not consider intramolecular hydrogen bonds.

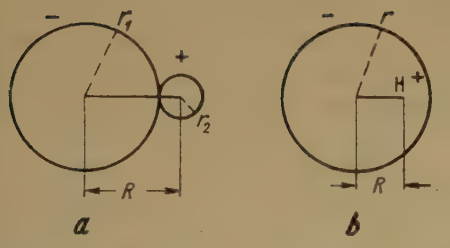

Fig.1. a) Model of HalMe molecule, b) model of HalH molecule.

the proton is located inside the Hal^- electron shell.

The closer the partner element to the beginning of the given row in the periodic table, the deeper the penetration of the proton into its electron shell and hence the weaker the manifestation of the hydrogen bond. In going from elements in the first row to lower lying ones one must bear in mind the deeper penetration of the proton into their atomic shell. In this case, too, the manifestation of the hydrogen bond becomes weaker.

Thus the penetration of the proton into the electron shell of the partner atom is in itself not sufficient to characterize the hydrogen bond. There are a number of other supplementary effects that might be mentioned.

1. In an earlier investigation[3] devoted to the valence band (~1030 cm^{-1}) of the C—O group in methyl alcohol and its solutions, it was shown that upon formation of a hydrogen bridge by the OH group, there appears a new band which is also associated with the valence vibrations of the CO group. It is located about 84 cm^{-1} to the high frequency side of the ~1030 cm^{-1} band. This displaced band disappears when the hydrogen bridge breaks up in the solution or vapor state. To explain this unusual, as regards both magnitude and direction, displacement of the C—O band, it was suggested that upon withdrawal of the proton from the oxygen nucleus as a result of formation of the hydrogen bond, the electron shell is shifted towards the carbon atom, strengthening the C—O bond and increasing the frequency.

The experimental indication of the hydrogen bond in this case is increase of the wave number of the band associated with the neighboring bond and the explanation of this effect should be sought in reduction of the screening of the proton by electrons bound to the oxygen nucleus incident to formation of the hydrogen bridge.

2. Upon formation of a hydrogen bond between carboxylic acid, alcohol and diethylamine molecules, there is observed at the first and higher overtones of the valence vibrations of the XH group an anomalously large decrease in intensity. Thus even in a 50% solution of phenol in CCl_4, the absorption band of the associated molecules at the fundamental appreciably exceeds the intensity of the band characteristic of phenol molecules not linked by a hydrogen bridge. The opposite effect is observed at the overtones.

A similar effect is observed incident to the formation of mixed associations when a hydrogen bond forms, for example, in solutions of chloroform or bromoform in pyridine, quinoline, diethyl ether, acetone, etc.[2,4]

This effect was explained by Mecke[5] as the result of increased ionicity in connection with formation of hydrogen bonds, which in this case is equivalent to reduction of screening of the proton by the electron shell of the partner.

This interpretation of the described effect can yield additional information on the structure of molecules capable of forming a hydrogen bridge. Thus, it follows from the above that in chloroform and bromoform molecules the proton is buried in the 8-electron cloud of the carbon atom. Under the influence of active solvents the proton emerges from this shell (the electron screening diminishes) and there is observed a corresponding anomaly at the first overtone (zero intensity of the band of the associated molecules). Under the influence of other, inactive solvents (CCl_4, hexane and chloroform and bromoform themselves), there are no indications of a saturated bond and hence no intensity anomaly at the first overtone. It may be assumed, therefore, that in this case hydrogen bonds are not formed.

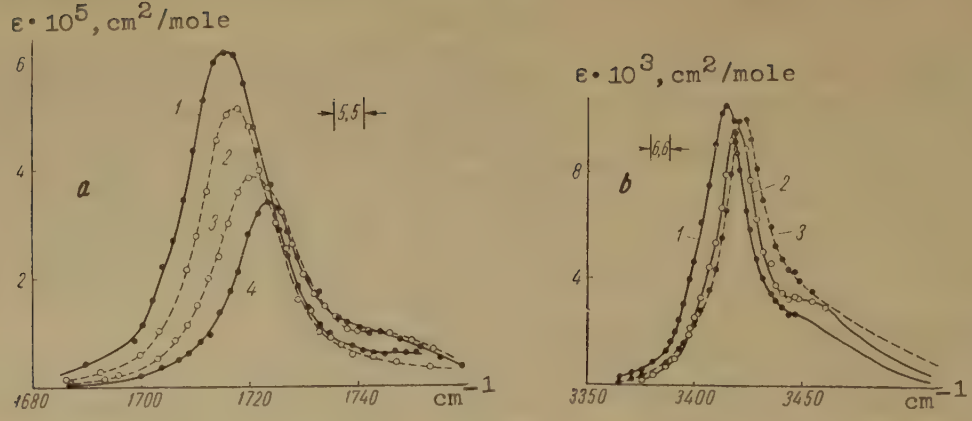

Fig.2. a) Concentration dependence of the absorption coefficient ε of the valence band of the C=O group for solutions of acetone in n-octane with different volume concentrations C_v: 1 - C_v = 100%, 2 - 50%, 3 - 10%, 4 - 1%; b) same for the first overtone: 1 - C_v = 100%, 2 - 30%, 3 - 10%.

Finally, it has been noted that in the known cases of strong associations of the saturated type, yielding an intense vibration band at the fundamental of the valence vibrations, but not containing hydrogen atoms in the intermolecular bond, there is no anomaly at the first overtone.

G.S.Denisov in our laboratory investigated the spectra of acetone which normally associates to the extent of about 35% in the pure liquid form. He observed an appreciable decrease in the intensity of the principal valence band of the C=O group when the acetone was dissolved in normal octane with resultant break-up of the associated molecules (Fig.2,a). At the first overtone of the same vibrations, as may be seen from Fig.2,b, the intensity is virtually independent of the concentration, i.e., there is no anomalous reduction of the absorption due to the presence of associated molecules. A similar effect was observed in our laboratory by E.L.Zhukova for solutions of acrylonitrile in CCl_4.

It is possible that the very great increase in intensity at the fundamental of the valence vibrations of the XH group in associated molecules cannot be explained solely by increase of ionicity, as inferred by Mecke[5]. Regardless of whether other factors are or are not involved, we can obviously consider the described anomalous decrease in intensity in going from the fundamental to the overtone as an experimental indication of the intermolecular hydrogen bond.

3. In his report presented at the Ljubljana symposium, Popl' indicated that the formation of a hydrogen bridge also produces appreciable changes in nuclear magnetic resonance. These changes are interpreted by Popl' as being the result of diminished screening of the proton by the electron shell.

The above facts are still too scanty and fragmentary to allow of giving a satisfactory definition of the hydrogen bond concept. Undoubtedly further investigations will make it possible to supplement and correct some of the above statements. However, juxtaposition of the above data may be useful for systematic work in the direction of interest to us. The common but independently arrived at explanation of the observed effects as being the result of an appreciable decrease of screening of the proton by the electron cloud of the partner appears to be plausible. In particular, it gives us some idea why the outward manifestation of the hydrogen bond becomes weaker in going from elements in the first row of the periodic table to those lying lower, i.e., to elements with an electron shell of larger size.

In this case, just as in the case of going from the upper right hand corner (from fluorine) of the periodic table to its left edge, the degree of participation of the hydrogen bond in the actual intermolecular binding decreases and the hydrogen bond concept becomes increasingly more difficult to define succinctly.

Scientific Research Physical Institute,
"A.A.Zhdanov" Leningrad State University

References

1. V.M.Chulanovskii, M.P.Burgova, G.S.Denisov & E.L.Zhukova, Transactions of the Tenth All-Union Conference on Spectroscopy, Vol., p.42, Lvov, 1957.
2. V.M.Chulanovskii & M.P.Burgova, Optika i spektroskopiia, 2, 330 (1957).
3. V.M.Chulanovskii, Doklady AN SSSR, 101, 649 (1955).
4. M.P.Burgova, Ia.Kuchirek & L.Proskurina, Optika i spectroskopiia 5, 141 (1958).
5. R.Mecke, Z.f.Elektrochem., 54, 88 (1950).
6. M.Van Thiel, E.D.Becker & G.C.Pimentel, J.Chem.Phys., 27, 486 (1957).

INVESTIGATION OF THE HYDROGEN BOND IN GLYCOLS AND CATECHOLS

- V.I.Malyshev & V.N.Murzin

The study was concerned with intermolecular and intramolecular hydrogen bonds in a number of compounds, the molecules of which contain two hydroxyl groups. The investigated compounds were selected so that the conditions of intramolecular interaction of the hydroxyl groups would be different. Specifically, we investigated the infrared spectra of

a) glycols: ethylene glycol, 1,3-butylene glycol and 1,4-butylene glycol, as well as pinacol, and

b) catechols: hydroquinone, resorcinol and pyrocatechol.

The distance between the hydroxyl groups and the relative arrangement of these groups differ in these substances. In addition, for purposes of comparison, we investigated the spectra of ethylene chlorohydrin, quaiacol, *o*- and *m*-nitrophenol and benzoin, the molecules of which differ from those listed above in that in them one of the hydroxyl groups is replaced by a different atom or radical.

The measurements were made in the regions of the fundamental (3200-3600 cm^{-1}) and the first overtone (6200-7100 cm^{-1}) of the vibrations of the H-O group. The enumerated substances were investigated in two forms: in the pure (100%) form in the liquid or solid state and in the form of weak (~0.1%) solutions in carbon tetrachloride. The absorption spectra were recorded at different temperatures in the range from 20 to 250°.

In the regions of the fundamental and first overtone, there are observed in the spectra of the pure substances wide bands associated with vibrations of the H-O group, perturbed due to formation of intermolecular hydrogen bonds. It was found that the shape of these bands in the region of the fundamental differs from the band shape in the region of the first overtone. In the spectra of most of the investigated substances the band in the region of the first overtone has a complex structure with two distinct peaks, the relative intensity of which differs for different compounds. In glycol spectra these peaks are observed at about 6630 cm^{-1} and 6300 cm^{-1}; in the catechol spectra at about 6930 and 6680 cm^{-1}. Furthermore, the relative intensity of these peaks depends on the temperature: with increasing temperature the intensity of the longer wavelength maximum decreases, that of the shorter wavelength increases. At elevated temperatures there also appears at ~7100 cm^{-1} a narrow band due to unperturbed vibrations of the H-O group. A similar picture was observed by us and a number of other investigators in the spectra of alcohols and carboxylic acids. In the case of alcohols these two peaks correspond to the two peaks at ~3500 cm^{-1} and ~3300 cm^{-1} observed in the spectra of weak solutions of alcohol in CCl_4 in the region of the fundamental.

In the region of the fundamental, the band associated with perturbed vibrations of the H-O group in the spectra of most of the investigated substances has only one peak at ~3300 cm^{-1}, corresponding to the longer wavelength maximum of the first overtone band. Only in the spectra of resorcinol, pyrocatechol and quaiacol does this band have two peaks. To explain these results, it may be hypothesized, first, that in these substances there exist two different forms of intermolecular interaction, differing as regards the degree of perturbation of the H-O vibrations and, consequently, as regards bond energy, and, second, that the relative magnitude of the molecular absorption coefficients of these two forms of perturbed vibrations differs in the region of the fundamental from that in the region of the first overtone, which means that the two forms of interaction differ in character. Further, it is assumed that the interaction characterized by the lesser perturbation of the H-O vibrations is primarily

interaction of the hydroxyl group of one molecule with the oxygen atom of another molecule (hydrogen bond proper). The interaction characterized by the stronger perturbation and, consequently, the higher bond energy is due to simultaneous interaction or coupling of two hydroxyl groups, belonging to different molecules, in the case of some particular relative orientation of these groups (hydroxyl bond). The above assumptions allow of explaining all the observed experimental facts pertaining to the intermolecular interactions of molecules containing one or two hydroxyl groups.

In the spectra of dilute solutions of glycols, pinacol and pyrocatechol in CCl_4 there are observed two comparatively narrow bands associated with absorption of the H-O groups of isolated molecules both in the region of the fundamental and in the region of the first overtone. The frequency of one of these bands is virtually the same ($\sim$7100 cm^{-1}) in the spectra of all the investigated substances, while the frequency of the other, shifted band, its width and intensity differ in different substances. The width of the shifted band increases with the magnitude of its displacement. Moreover, the relative intensity of this band in the spectrum of a given substance differs in the region of the fundamental from the intensity in the region of the first overtone (the intensity is greater in the region of the fundamental).

The presence of two H-O vibration bands in the solution spectra indicates the existence in these substances of two molecular configurations with different relative orientations of the hydroxyl groups. In one of these configurations, the hydroxyl groups are isolated from each other, while in the other they interact with each other, perturbing the H-O group vibrations.

It is significant that, contrary to expectation, the degree of perturbation of the H-O vibrations increases with increasing distance between the hydroxyl groups in the molecular chain. Thus the band shift in the spectrum of ethylene glycol is $\sim$40 cm^{-1}, in 1,3-butylene glycol $\sim$80 cm^{-1} and in 1,4-butylene glycol $\sim$170 cm^{-1}. This gives reason to infer that by virtue of the possibility of free rotation about the C—C and C—O bonds, one of the possible configurations of the 1,3- and 1,4-butylene glycol molecules is such that the distance between the hydroxyl groups is small and they interact with each other. Specifically, in the case of 1,4-butylene glycol, the molecule does not have the usual zig-zag chain form but is rather a ring closed by virtue of the interaction of the hydroxyl groups located at its end.

Among the catechols two bands are observed only in the spectrum of solution of pyrocatechol; only one band is distinguishable in the spectra of resorcinol and hydroquinone. This shows that, as might be expected, interaction between the hydroxyl groups is realized only in the orthopositions.

"G.S.Landsberg" Optical Laboratory,
"P.N.Lebedev" Physical Institute,
Academy of Sciences of the USSR

STRUCTURE OF THE OH VIBRATION BAND IN THE SPECTRA OF CRYSTALS CONTAINING HYDROGEN BONDS

- A. I. Stekhanov

At present relatively little is known regarding the appearance of the OH vibration band in the Raman and infrared spectra of crystals. The available experimental data indicate that in most cases in the region of the OH group vibrations in the spectra of crystals there appears a diffuse band having a width of a few hundred cm^{-1}. In the spectra of some crystals containing water of crystallization a few wide low intensity maxima can sometimes be discerned against the background of the OH band.[1-3]

The present work was devoted to a careful investigation of the Raman and infrared absorption spectra of over 20 crystals at room and low temperatures for the purpose of studying the intensity distribution in the OH band, inasmuch as this is important from the standpoint of investigation of the hydrogen bond.

We found that the valence vibrations of the OH group are evinced in the spectra of all the investigated crystals in the form of a very wide band with a complex structure. The structure is revealed particularly clearly at low temperature: in this case instead of the usual wide OH band there are observed individual narrow bands and sharp lines.

Particularly noteworthy are the following characteristic features of the discrete structure of the OH band. First, in the spectra of some crystals, in addition to the intense lines in the band, there is evinced a fairly numerous group of weaker lines. Further, in all the investigated crystals the intense lines either form doublets or are observed in the form of individual lines; the latter usually appear at the short wavelength edge of the OH band.

Thus at room temperature, in the region of the OH vibrations in the Raman spectrum of selenite[4] there appears a band having a width of over 650 cm^{-1}. Near the center of the band there are discernible two intense lines with frequencies $\nu_1 = 3405$ and $\nu_2 = 3495$ cm^{-1}.[3] When the gypsum crystal is cooled to liquid nitrogen temperature, the intensity of the band is greatly diminished and against the weak residual background there appear, in addition to the intense ν_1 and ν_2 lines, six weak but sharp lines arranged symmetrically with respect to ν_1 and ν_2. The spectrum of Rochelle salt contains two doublets (3280-3345 cm^{-1} and 3405-3471 cm^{-1}) and a line at 353 cm^{-1}.

Two doublets and a single line (3263-3322 cm^{-1}, 3396-3453 cm^{-1} and 3559 cm^{-1}) are also evinced in the Raman spectrum of sodium dihydrogen phosphate.

In our opinion, the most probable cause of the doublet structure is the proton tunnel effect[5] which, apparently, may be realized in crystals containing hydrogen bonds. The presence of weak lines in the band region may be explained by coupling of the intramolecular vibrations with translational intermolecular vibrations of the water molecules in the crystal.[4]

References

1. G.P.N.Nayar, Proc.Ind.Acad.Sci., 8, 419 (1938).
2. E.Canals & P.Peyrot, Compt.Rend.Acad.Sci., 207, 224 (1938).
3. G.S.Landsberg & F.S.Baryshanskaia, Izv.AN SSSR, Ser.fiz., 10, 509 (1946).
4. A.I.Stekhanov, Doklady AN SSSR, 92, 281 (1953).
5. A.I.Stekhanov, ibid., 106, 433 (1956).

INFRARED ABSORPTION SPECTRA OF ORGANOLITHIUM COMPOUNDS. THE INTERMOLECULAR LITHIUM BOND

- A.N.Rodionov, D.N.Shigorin, T.V.Talalaeva & K.A.Kocheshkov

Investigation of the vibrational spectra of organolithium compounds of the R—Li and R—O—Li types is important from the standpoint of establishing the structure of these compounds and clarifying the nature of intermolecular coupling, particularly, the hydrogen bond.

Earlier one of us[1-8] investigated a number of systems with a hydrogen (A—H···B) and a metal-element bond (e—Me···e). It was shown that in triatomic A—H···B systems without π-electrons the bands associated with the A—H··· valence vibrations slightly displaced, weakly diffused and have integral intensities only slightly greater than those of the free radical. In this case the hydrogen bond energy E is determined primarily by the acceptor-donor interaction energy E_a (N.D.Sokolov) and to some extent by dipole interaction, i.e., $E = E_a + E_d$.

Furthermore, it was established[1] that in triatomic systems with π-electrons the situation differs radically from that in the preceding case. The A—H··· valence vibration bands are sharply shifted to the side of long wavelengths and strongly diffused. In systems with π-electrons the hydrogen bond energy is given by $E = E_d + E_a + E_\pi$; that is, there appears an additional term, E_π, which takes into account the contribution of the hydrogen atom to the π-electron interaction.

In the studies referred to above, the distinctive characteristics of the hydrogen bond in compounds with π-electrons are explained on the assumption that the p^* orbit of the hydrogen atom is directly involved in the formation of the hydrogen bond; it was inferred that consequently the hydrogen atom interacts simultaneously with the π-electrons of all the nearest neighbors and through these with the π-electrons of the entire molecule. The alteration of the p^* orbit of the hydrogen atom in the molecule is realized by virtue of deformation of its electron cloud in the direction normal to the bond ($\sigma \rightarrow \pi$ deformation). Thus in the formation of hydrogen bonds in molecules such as tropolone, acetylacetone, α-oxyanthraquinone, and the like the magnitude of the energy E_π plays the decisive role. In the case of a metal-element bond, the metal atoms (Li, Mg, Al, etc.) either already have valence electrons in the *p*-state or can acquire such electrons with a minimal expenditure of energy. Hence the participation of the *p* orbit of a metal atom in the formation of a metal-element bond, e—Me···e, should occur with greater facility than in the case of hydrogen.

Investigation of the vibrational spectra of intracomplex compounds[2] has generally substantiated the above argument. Hence it may be asserted that the E_π term in the expression for the metal-element bond energy $E_{Me\cdots e} = E_a + E_d + E_\pi$, which determines the importance of the role played by the *n*-electron of the metal atom in the π-electron interaction, is the most important, decisive term. Obviously, the distinctive attributes of the lithium atom (its small radius, relatively low ionization potential, the relative ease of utilization of the *p* orbit) make it particularly effective in forming e--Li···e bonds, i.e., more active in this sense than hydrogen and other metal atoms. Hence it is of particular interest to investigate e—Li···e bonds in different systems, in systems both with and without π-electrons.

Through investigation of the infrared spectra of compounds of the R—Li and R—O—Li types we discovered and studied the effect of formation of lithium bonds of the types $\overset{-\delta}{C}\overset{+\delta}{Li}\cdots\overset{-\delta}{C}\overset{+\delta}{Li}\cdots$ and $\overset{-\delta}{O}\overset{+\delta}{Li}\cdots\overset{-\delta}{O}\overset{+\delta}{Li}\cdots$. Of particular interest is the investigation of the intermolecular $\overset{+\delta}{Li}\cdots\overset{-\delta}{C}$ bond in view of the fact

that it can form without acceptor-donor interaction.

The compounds used in the present investigation were synthesized and purified by the procedures developed by Kocheshkov and his co-workers.[9,10] The compounds were investigated in the form of vapors, solutions and powders suspended in vaseline oil. The spectra of the investigated compounds are shown in Figs. 1 & 2.

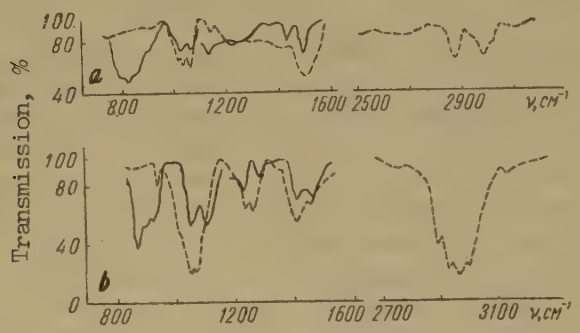

Fig.1

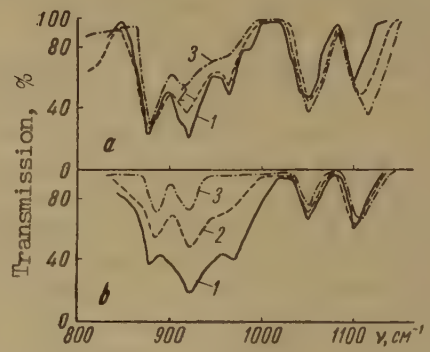

Fig.2

Fig.1. Infrared spectra of a) methyllithium and b) ethyllithium. Solid lines - crystals in vaseline oil; dashed lines - vapors.

Fig.2. Infrared spectra of solutions of ethyllithium in benzene: a - 0.9 N solution of LiC_2H_5 in benzene at different temperatures: 22° (1), 48° (2), 79° (3); b - solutions in benzene with different LiC_2H_5 concentrations: 0.8 N (1), 0.4 N (2) and 0.2 N (3).

The 1052 cm^{-1} and 1092 cm^{-1} bands in the methyllithium vapor spectra obviously correspond to the ν_3 and ν_6 frequencies characteristic of the free C—Li group (Table 1).

Table 1

Compound	ν_3 (a_1)	ν_6 (e)	ν_2 (a_1)	ν_5 (e)	ν_1 (a_1)	ν_4 (e)
CH_3Li	1052	1092	1383	1490	2875	2980

Investigation of the spectrum of $LiCH_3$ powder suspended in vaseline oil brought out a new diffuse and very intense band with a principal peak at ~820 cm^{-1}. We attribute this band to C—Li··· groups participating in the formation of intermolecular lithium bonds. A similar picture was observed in the spectra of ethyl lithium vapor and crystals. In the spectrum of LiC_2H_5 powder there is a broad intense band with a complex structure extending from 882 to 940 cm^{-1}. This band does not appear in the vapor spectrum and hence can be attributed to the valence vibrations of the C—Li··· group participating in the formation of the intermolecular lithium bond. The relative intensity of the 1052 cm^{-1} band in the vapor spectrum is appreciably greater than its intensity in the spectrum of crystalline LiC_2H_5. Hence there is good reason to assign this band to the valence vibrations of free C—Li groups.

The above band assignments are substantiated by the character of the spectra of solutions of ethyl lithium in hexane and benzene. In freshly prepared solutions of ethyl lithium in benzene, the 1050 cm^{-1} band associated with the free C—Li radicals has a low intensity, while the 875 and 926 cm^{-1} bands, which we associate with C—Li··· groups in different associations, are very intense. This

ndicates that in such benzene solutions almost all the molecules are associated, orming two different types of complexes (possibly dimers and hexamers). With ncreasing dilution, the relative intensity of the 926 cm^{-1} band diminishes, that f the 1050 cm^{-1} band increases, while that of the 875 cm^{-1} band remains virtual- y constant. In the spectra of aged LiC_2H_5 solutions and also fresh solutions eated to 70°, the relative intensities of these bands are modified (see Fig.2,a). t may be assumed that the 875 cm^{-1} band pertains to the C—Li··· group in dimers nd the 926 cm^{-1} band to the C—Li··· group in hexamers. Investigation of the pectra of LiC_2H_5 in hexane shows that the fraction of unassociated molecules is reater than the fraction of associated molecules and that the latter decreases harply with dilution.

Dodecyllithium dissolved in hexane exhibits analogous behavior. In dodecyl- ithium solutions the relative intensity of the 927 cm^{-1} band, associated with he C—Li··· groups, decreases with increasing dilution, while the relative in- ensity of the 1052 cm^{-1} band, which we associate with free C—Li radicals, in- reases. Thus the molecules are associated in a different way in crystals chains) as compared with solutions (rings). The degree and character of as- ociation in solutions depend greatly on the nature of the solvent.

Cryoscopic data[12,13] are in agreement with our results. It follows from ur data that the dipole moment of LiC_2H_5 measured in diluted hexane solutions ust approach the dipole moment of the free molecule. Certain data obatined by .N.Vasil'eva (private communication) substantiate this deduction (μ = 1.1 Dp). he question of the nature of the rings forming in solutions will be considered n a later contribution.

We also detected frequencies in the 2756-2805 cm^{-1} region in the spectra of iC_2H_5; we tentatively attribute these to the CH_2 groups, the carbon atom of hich participates in the formation of the intermolecular lithium bond. Calcu- ation of the C—Li bond energy on the basis of the 1050 cm^{-1} frequency using he harmonic oscillator model (and the bond energy vs elastic constant curve) ields a value of about 65 Kcal. Thus comparison of the spectra of vapors, solu- ions and powders suspended in vaseline oil and analysis of the molecular vibra- ions allows of determining the frequencies of the valence vibrations of the —Li groups, both free and involved in lithium bonds (Table 2).

The C—Li frequency assignments given by Brown & Rogers[14] are questionable. n investigating the infrared spectra of compounds of the R—Li and R—O—Li ypes, we detected the formation of intermolecular lithium bonds: —Li···C— nd —Li···O—. The —Li···C— bond is stable ($\Delta\nu/\nu_c$ = 12-19%) despite the fact hat it forms without acceptor-donor interaction. The —Li···O— bond is even ore stable.

As noted, the —Li···C— bond forms without participation of acceptor-donor nteraction. This raises the question of the nature of this bond. It is known hat electrostatic interaction cannot wholly explain the formation and proper- ies of such intermolecular bonds. Apparently, the explanation must be sought n the specific nature of the lithium atom (small radius, low ionization poten- ial, etc.). It may be that in the given case the nature of the lithium bond is etermined primarily by direct interaction (coupling) of the Li atom electron in he *p*-state with the "free portion of the electron density" of the carbon atom nd also partially by dipole interaction.

Table 2

Compound	$\nu_{C-Li(O-Li)}$ free, cm^{-1}	$\nu_{C-Li\cdots(O-Li\cdots)}$ assoc., cm^{-1}	$\frac{\Delta\nu}{\nu_0}$, %
CH_3Li vapor	1052 m	—	—
CH_3Li crystal	1060 m	820 s,b	19
C_2H_5Li vapor	1061 s	—	—
C_2H_5Li crystal	1056 s	882 s,b	16
C_2H_5Li + benzene (0.8 N)	1050 w	918 s,b 875 m	12
C_2H_5Li + benzene (0.1 N)	1050 m	920 m 875 m	12
C_2H_5Li + hexane (1 N)	1052 s	915 m	13
C_2H_5Li + hexane (0.27 N)	1058 m	—	—
C_6H_5Li vapor	1029 m 1045 m	— —	— —
C_6H_5Li crystal	1039 s	838 s,b	19
$C_{12}H_{25}Li$ + hexane (0.53 N)	1052 m	927 s,b	12
$C_{12}H_{25}Li$ + hexane (0.13 N)	1058 s	930 w	13
p-$CH_3C_6H_4Li$ (crystal)	987 m	833 s,b	15
α-$C_{10}H_7Li$ (crystal)	940 m	828 s,b	12
CH_3OLi (crystal)	~1430 s	840 s,b	35

Intensity key: s – strong, w – weak, m – medium, b – broad.

"L.Ia.Karpov" Physical-Chemical Institute

References

1. D.N.Shigorin, Zhur.fiz.khim., 27, 554 (1953).
2. D.N.Shigorin, Izv.AN SSSR, Ser.fiz., 17, 596 (1953).
3. D.N.Shigorin, ibid., 18, 723 (1954). (Trans.Bulletin 18, No.6, 404.)
4. D.N.Shigorin & N.S.Dokunikhin, Doklady AN SSSR, 100, 323 (1955).
5. D.N.Shigorin & N.S.Dokunikhin, ibid., 100, 745 (1955).
6. D.N.Shigorin & N.S.Dokunikhin, Zhur.fiz.khim., 29, 1958 (1955).
7. D.N.Shigorin, M.M.Shemiakin, L.A.Shchukina, N.M.Kolosov & F.A.Mendelevich Doklady, AN SSSR, 108, 672 (1956).
8. D.N.Shigorin, Transactions of the Tenth All-Union Conference on Spectroscopy, No.1, 208,L'vov, 1957.
9. T.V.Talalaeva & K.A.Kocheshkov, Izv.AN SSSR. Otd.khim.nauk (Bulletin USSR Ac.of Sci., Div.Chem.Sciences), 1, 126 (1953).
10. T.V.Talalaeva & K.A.Kocheshkov, Zhur.obshch.khimii., 23, 392 (1953).
11. K.Ziegler & K.Nagel, Z.anorgan und allquem.Chemie, 282, 345 (1955).
12. F.Hein & H.Schramm, Z.phys.Chemie, 151, 234 (1934).
13. K.B.Piotrovskii & M.P.Ranina, Doklady AN SSSR, 115, 4 (1957).
14. T.Brown & M.Rogers, Journ.Amer.Chem.Soc., 79, 8, 1859 (1957).

INVESTIGATION OF INTERMOLECULAR COUPLING IN POLYETHYLENE BY INFRARED ABSORPTION SPECTROSCOPY

- I. I. Novak

The results of x-ray diffraction, dilatometric and spectroscopic studies[1] all indicate that polyethylene is a crystallizing polymer. The amount of crystal phase varies from 40-80% depending on the fabrication procedure. The orthorhombic crystal lattice of polyethylene has the following constants: a = 7.42 Å, b = 4.93 Å and c = 2.534 Å.[2]

The x-ray diffraction data of Bunn & Alcock[2] indicate that with increase of temperature from 18 to 100° the constant a increases from 7.42 to 7.65 A, while b and c remain unchanged.

Electron diffraction studies by Kargin et al[3] showed that elongation of polyethylene by 500% is accompanied by increase of the lattice constant a from 7.47 to 7.56 A.

The alteration of the lattice constants of polyethylene under the influence of heat, deformation and other physical factors leads to a change in the interaction (coupling) between neighboring molecules. This in turn must obviously be evinced in the frequencies of the infrared absorption spectrum of polyethylene associated with the crystal lattice. The present work was concerned with investigation of the influence of temperature, elongation and annealing on the infrared absorption spectra of polyethylene. In addition, we studied the infrared spectra of dicetyl (dotriacontane - $C_{32}H_{66}$), the crystal lattice of which is similar in structure to that of polyethylene.

Experimental Results and Discussion

The infrared absorption spectra of polyethylene and dicetyl were studied by means of IKS-1 and VIKS-MZ spectrometers employing fluorite and rock salt prisms.

The measurement procedure has been described earlier,[4] hence we proceed directly to the experimental results. The spectrum of polyethylene includes two bands at 1464 and 1473 cm^{-1} (at room temperature). The former is associated with deformation vibrations of the CH_2 group.[5] As the temperature is increased from 20 to 120° the intensity of the 1473 cm^{-1} band falls off rapidly and at the melting point (120°) this band disappears completely; at the same time, the intensity of the 1464 cm^{-1} band decreases only slightly. Moreover with increasing temperature the 1473 cm^{-1} frequency is reduced somewhat and at 90° becomes 1471.2 cm^{-1}. With decrease of the temperature from 0 to -175° the peaks of these bands shift to 1462.4 and 1474.8 cm^{-1}, respectively. Thus with change of temperature from -175° to +90°, the splitting of the doublet diminishes from 12.4 to 7 cm^{-1}.

Fivefold elongation of polyethylene under tension produces the following changes in its spectrum: the 1464 & 1473 and 720 & 730 cm^{-1} bands are shifted to 1465.6 & 1470.8 and 720 & 728 cm^{-1}. Thus under the influence of stretching the splittings of the polyethylene doublet in the 7 and 14 μ regions decrease from 9 to 5 cm^{-1} and from 10 to 8 cm^{-1}, respectively. The 720-730 cm^{-1} absorption bands of polyethylene are associated with "rocking" vibrations of the CH_2 group, normal to the chain axis.[6]

Upon rapid cooling of polyethylene from 150 to -196°, the shorter wavelength band remains at 1464 cm^{-1}, while the 1473 cm^{-1} band shifts to 1471 cm^{-1}.

In the 7 μ region of the spectrum of crystalline dicetyl there are two bands with wave numbers 1464 and 1473 cm^{-1}. Only the band at 1464 cm^{-1} is present in the spectrum of liquid dicetyl. On cooling of dicetyl from 20° to -150°, the 1464 and 1473 cm^{-1} frequencies shift to 1462 and 1473 cm^{-1}. Thus

cooling of dicetyl from 20° to -150° increases the splitting of the 7 μ doublet from 9 to 11 cm^{-1}. The doublet structure of the absorption band in the 14 μ region in the spectra of crystalline members of the paraffin series from $C_{18}H_{38}$ to $C_{54}H_{110}$ has been observed by Stein & Sutherland[7]. In the liquid state these substances have only one band at about 720 cm^{-1}. Krimm[8] also showed that the absorption bands of the solid normal paraffin $C_{36}H_{74}$ in the vicinity of 1460 and 720 cm^{-1} have a doublet structure. Moreover the 720 and 730 cm^{-1} bands were found to be polarized along the crystallographic axes *b* and *a*, respectively. The low and high frequency components of the 7 μ doublet are also polarized along the *b* and *a* axes.

In view of all the above experimental facts, it may be inferred that the doublet structure of the polyethylene and high molecular paraffins bands in the 7 and 14 μ regions is associated with the crystal lattice. In other words, the splittings can apparently be explained, in accord with the theory of Davydov[9], by intermolecular resonance coupling of the vibrations of neighboring groups in the crystal lattice.

It follows from Dvaydov's theory that the number of split components is equal to the number of molecules in a unit cell. According to the x-ray diffraction data of Bunn[10] and Müller[10], there are two molecules per unit cell in polyethylene and high molecular paraffins, which is consistent with the observed doublet structure of their absorption bands at 7 and 14 μ. The polarization of the doublet components in the spectrum of the paraffin $C_{36}H_{74}$ along the *b* and *a* crystal axes is also consistent with Davydov's theory.

If we accept the hypothesis that the formation of the doublet structure of the absorption bands of polyethylene and paraffins is associated with resonance coupling of neighboring molecules in the crystal lattice, it would follow that the doublet splitting should increase with enhanced intermolecular coupling.

As was noted above, with increase of temperature from 20 to 90°, the splitting of the 7 μ doublet of polyethylene decreases. This can readily be explained by the fact that with heating the lattice constant *a* of polyethylene increases[2] and, consequently, the coupling between neighboring CH_2 groups is weakened. This leads to diminution of the splitting of the 7 μ doublet. Analogously, the increase in separation of the doublet incident to reduction of the temperature of polyethylene from 20° to -175° is connected with decrease of the lattice constant.

The decrease of the 7 and 14 μ doublet splittings incident to elongation of polyethylene can also be explained by weakening of the interaction between neighboring CH_2 groups owing to increase of the lattice constant *a*. It is interesting to note that the lattice constants of some high molecular paraffins increase by 5-10% in going through the transition point.[11] This, as has been shown by Stein & Sutherland[12], has a noticeable effect on the spectra of these paraffins. In the spectra of the paraffins from $C_{19}H_{40}$ to $C_{54}H_{110}$ there is only one 720 cm^{-1} band at temperatures 0.5° above the transition point, while below this temperature there appear two bands having frequencies of 720 and 730 cm^{-1}.

In view of the results obtained in investigating the infrared absorption spectra of polyethylene, it may be concluded that the doublet structure of the absorption bands at 7 and 14 μ can be explained, according to the theory of Davydov, by resonance coupling of the vibrations of the CH_2 groups of neighboring molecules in the crystal lattice. The magnitude of the doublet splittings can be correlated with the value of the lattice constant *a*.

Leningrad Physical Technical Institute,
Academy of Sciences of the USSR

References

1. S.Krimm, A.Tobolsky, J.Pol.Sci., 7, 57 (1951); E.Hunter & W.G.Oakes, Trans.Faraday Soc., 41, 49 (1945); V.N.Nikitin & E.I.Pokrovskii, Doklady AN SSSR, 95, 109 (1954); R.B.Richards, J.Appl.Chem., 1, 370 (1951).

2. C.W.Bunn & T.C.Alcock, Trans.Faraday Soc., 41, 317 (1945).

3. V.A.Kargin, E.Rylov & V.L.Karpov, Zhur.fiz.khim., 27, 572 (1953).

4. I.I.Novak, Zhur.tekh.fiz., 24, 19 (1954); Optika i spektroskopiia, 2, 62 (1957).

5. J.K.Brown, N.Sheppard & D.M.Simpson, Disc.Faraday Soc., No.9, 261 (1950); H.W.Thompson & P.Torkington, Trans.Faraday Soc., 41, 184 (1945).

6. N.Sheppard & G.Sutherland, Nature, 159, 739 (1947); G.Sutherland & A.V. Jones, Nature, 160, 567 (1947).

7. R.S.Stein & G.Sutherland, J.Chem.Phys., 21, 370 (1953).

8. S.Krimm,J. Chem.Phys., 22, 567 (1954).

9. A.S.Davydov, Teoriia pogloshcheniia sveta v molekuliarnykh kristallakh (Theory of light absorption in molecular crystals), Pub.Inst.of Physics, Ukrainian SSR Ac. of Sci., 1951.

10. C.W.Bunn, Trans.Faraday Soc., 35, 482 (1939); Müller, Proc.Roy.Soc. A, 120, 437 (1938).

11. W.F.Sayer, R.F.Paterson & J.L.Keays, J.Amer.Chem.Soc., 66, 179 (1944); A.Müller, Proc.Roy.Soc. A, 138, 514 (1932).

12. R.S.Stein & G.Sutherland, J.Chem.Phys., 22, 1993 (1954).

INFLUENCE OF TEMPERATURE AND THE STATE OF AGGREGATION ON THE INFRARED ABSORPTION OF CARBON TETRACHLORIDE

- M.P.Lisitsa & V.N.Malinko

Introduction

Of particular importance where determination of the factors affecting the intensity, half-width, shape and structure of vibrational bands is concerned are temperature studies and measurements made at close temperatures with the investigated substance in different states of aggregation. We have carried out such studies for the absorption bands of carbon tetrachloride. The spectrum of this compound has by now been fairly thoroughly studied and most of the frequencies therein reliably identified.[1,2]

We employed the procedure developed earlier and described in Ref.2 for qualitative measurements in the region of intense absorption. To realize the measurements at higher than room temperatures it was necessary to find suitable heat-stable sealing gaskets for the absorption cells, i.e., gaskets of a material not dissolving in or reacting with CCl_4. This proved to be a difficult task. We tested a considerable number of different cements and sealing compounds and found the most suitable for measurements in the range from -25° to $+70^{\circ}$ to be a putty of talc with water glass[4] and a paste made of equal parts of zinc oxide, manganese oxide and chalk stirred in water glass.[5] The temperature gradient along the cell mounted in the center of the cylindrical furnace did not exceed 1°. The temperature was monitored by means of a copper-constantan thermocouple. For measurements in the temperature range from -22.6° to $+22^{\circ}$, the furnace was replaced by a special cryostat designed for work with liquid air and other coolants. In this case, too, the temperature gradient over the investigated layer did not exceed 1°.

The error in determining the absorption coefficient K in most cases did not exceed 7-10%. Only in the region of the fundamental vibrations (ν_3) of CCl_4 could it have been as much as 15% owing to the systematic error involved in determining the effective thickness of the absorbing layer.[3] In all cases, regardless of the temperature and state of aggregation, all measurements of the absorption at a given band were carried out with the same slit width. It was not necessary to take into account the apparatus function of the IKS-6 spectrometer, which was used for all the measurements, inasmuch as in the case of a band half-width not over 3 times the spectral slit width and on condition that this band can be approximated by a Gaussian curve or a triangle, the distorting influence of the apparatus on the integral intensity, as well as on the half-width, does not exceed 1-2% of the measured quantity.[6] These conditions were fulfilled in all our measurements. The reliability of the results given by Willis[6] was substantiated by comparing the fundamental characteristics of the ν_3 absorption band of gaseous CCl_4, obtained with different slit widths.*

1. Influence of temperature

In studying the effect of temperature, we first investigated the very intense double band, one component of which (784 cm^{-1}) corresponds to the fundamental, triply degenerate ν_3 vibrations and the second component (762 cm^{-1}) to the composite $\nu_1 + \nu_4$ vibrations. Owing to Fermi resonance the composite vibration band attains an intensity comparable with that of the fundamental ν_3 vibration band.

---

*All designations in the present report are analogous to those used in Ref.2.

Table 1

Influence of temperature on the fundamental Fermi resonance doublet of CCl_4 in the liquid state

T°, K	$\nu_1 + \nu_4$ (762 см$^{-1}$)			ν_3 (784 см$^{-1}$),		
	$\int K_\nu d\nu \cdot 10^{-4}$, см$^{-2}$	$K \cdot 10^{-2}$, см$^{-1}$	Γ, см$^{-1}$	$\int K_\nu d\nu \cdot 10^{-4}$, см$^{-2}$	$K \cdot 10^{-2}$, см$^{-1}$	Γ, см$^{-1}$
298	34	190	18	50	230	22
323	32	178	18	48	210	23
343	31	170	19	48	200	22

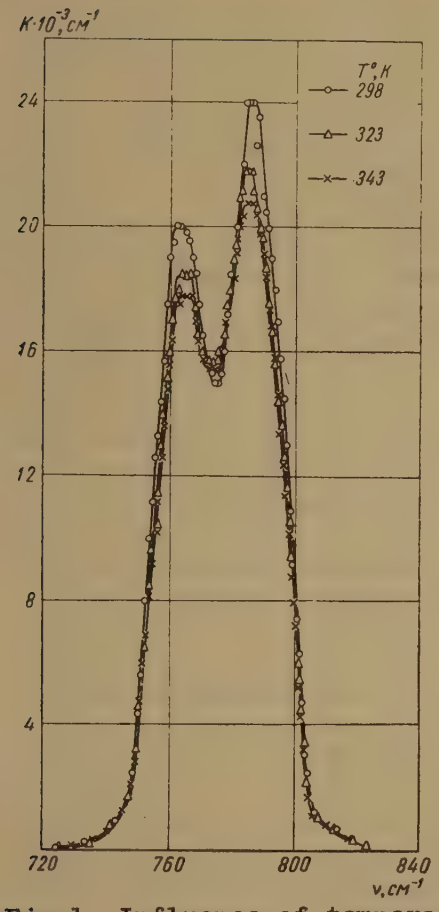

Fig.1. Influence of temperature on the $\nu_1 + \nu_4$ and ν_3 doublet.

Our measurements showed (Table 1 & Fig.1) that when the temperature is increased from 298 to 343°K the integral intensities of both components change little; the intensity of the composite $\nu_1 + \nu_4$ band* decreases to the same degree as the intensity of the fundamental ν_3 band. The experimental data indicate that the half-widths of both components of the doublet remain virtually constant in the indicated temperature interval.

Among the considerable number of other composite bands, for our temperature studies we chose two isolated doublets consisting of components between which Fermi resonance is realized. Resolution of the doublet into components, which was carried out by the conventional graphic procedure, presented no particular difficulties (it was assumed that the shape of both components was symmetrical). The results obtained for one of the doublets are given in Table 2 and Fig.2. It will be seen that in this case there is a much more appreciable decrease of the integral absorption with increasing temperature: increase of T from 251 to 333°K, i.e., by 80°, leads to a decrease of $\int K_\nu d\nu$ by a factor of almost two. Thus these composite bands are appreciably more sensitive to the influence of temperature.

We note that the long wavelength component of each of the two investigated doublets undergoes the same quantitative changes as the short wavelength component, although in both cases the former represents a composite band of higher order than the latter and might be expected to exhibit a stronger temperature dependence. Apparently, the observed effects are connected with Fermi resonance. To substantiate this assertion it would be desirable to carry out temperature studies of the ν_3 and $\nu_1 + \nu_4$ bands for gaseous CCl_4.

Our measurements showed that the half-width of the composite doublet band remains virtually constant in the indicated temperature range.

The integral intensity vs temperature curves for the above mentioned doublets are shown in Fig.3. Unfortunately, owing to the narrow temperature inter-

---

*Here and below composite bands are understood to mean absorption bands corresponding to combination tones.

Table 2

Influence of temperature on the composite absorption bands of liquid CCl_4

T°, K	$\int K_\nu d\nu$, см$^{-2}$	First resolved doublet					Second resolved doublet					
		$\nu_2+\nu_3$(1006 см$^{-1}$)		$\nu_2+(\nu_1+\nu_4)$ (см$^{-1}$)			$\nu_1+\nu_3$ (1249 см$^{-1}$)			$\nu_1+(\nu_1+\nu_4)$ (1216 см$^{-1}$)		
		K, см$^{-1}$	Γ, см$^{-1}$	$\int K_\nu d\nu$, см$^{-2}$	K, см$^{-1}$	Γ *, см$^{-1}$	$\int K_\nu d\nu$, см$^{-2}$	K **, см$^{-1}$,	Γ, см$^{-1}$	$\int K_\nu d\nu$, см$^{-2}$	K, см$^{-2}$	Γ, см$^{-1}$
251	1040	32	26	920	30	23	1080	32	23	1020	26	31
269	950	29	26	840	26	24	970	28	25	900	22	33
293	770	27	26	770	23	24	860	26	24	760	20	32
313	800	26	27	700	22	24	700	22	25	610	17	33
333	600	19	27	550	17	23	640	21	25	500	14	33

* Half-width.
** Absorption at peak.

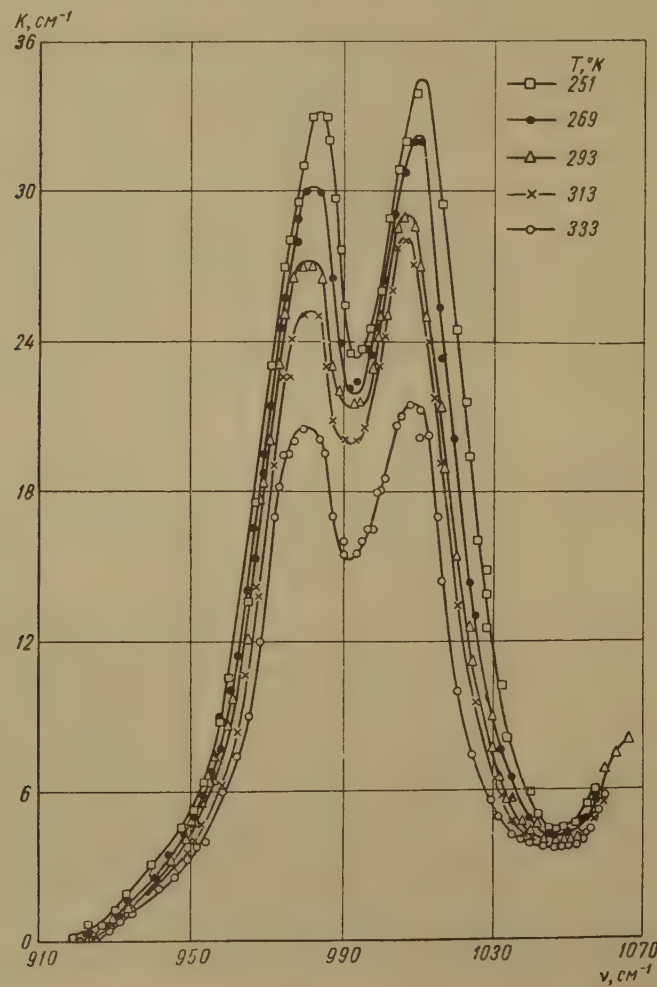

Fig.2. Temperature variation of the composite $\nu_2 + (\nu_1 + \nu_4)$ and $\nu_2 + \nu_3$ bands.

val involved, it is impossible to deduce the empirical law for $\int K_\nu d\nu = f(T)$.

In the 251-333°K interval, however, the variation of the integral absorption with temperature is approximately linear and for both doublets the rate of decrease with increasing temperature is nearly the same. A similar temperature dependence of the intensity of infrared absorption band was obtained by Slowinski

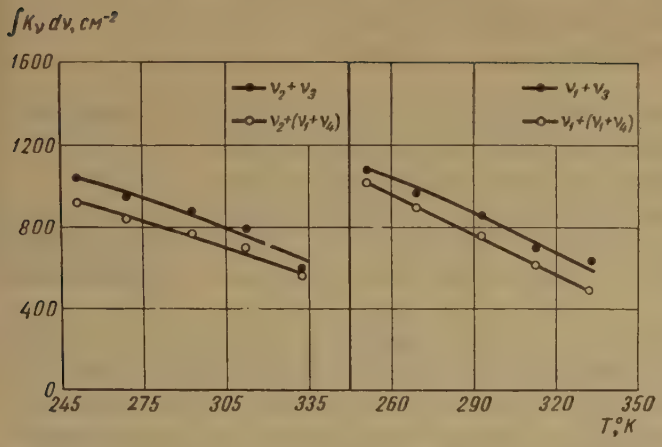

Fig.3. Variation of the integral intensities of the composite bands with temperature.

& Claver[7] for four bands of cyclohexane.

Obviously, on the basis of the above scanty data one cannot attempt to explain the temperature dependence of the infrared absorption band intensities or construct a plausible theory. At present we can only note that in the given case, increase of the temperature leads to decrease of the transition matrix elements, the value of which depends not only on the specific molecule but also on its environment.

2. Influence of the state of aggregation

In an earlier report[2] we described the spectrum of CCl_4 in the 470 to 12,500 cm^{-1} range at room temperature. The measurements were carried out for two states - liquid and gaseous - in the regions of the fundamental vibration frequency ν_3, its first overtone and the combination tone $\nu_1 + \nu_4$. The liquid-gas transition is accompanied by a substantial decrease in intensity, a change in the half-width of the bands and a pronounced weakening of the resonance coupling between the $\nu_1 + \nu_4$ and ν_3 vibrations, evinced by a substantial decrease in the intensity of the former. Subsequently, we undertook a supplementary investigation aimed at clarifying the influence of the state of aggregation of the intensity of the composite absorption bands. The measurements were carried out at room temperature for the frequencies whose temperature dependences have been described above.

Evaluations of the integral intensities showed that incidental to the liquid-gas transition the integral intensity of the long wavelength component of each doublet decreases by a factor of two. In the case of the short wave component and particularly the $\nu_1 + \nu_3$ band, the decrease in intensity is insignificant. It can also be explained by substantial weakening of the resonance coupling between the component vibrations incident to transition from the liquid to the gaseous state. As in the case of the $\nu_1 + \nu_4$ and ν_3 vibrations, weakening of the resonance results in a comparatively greater decrease in intensity of the weaker component. It is significant that in the liquid-gas phase transition the half-width of each component virtually does not change, although the maximum of the long wavelength component acquires an isotopic structure, splitting into 2 or 3 components.

"T.G.Shevchenko" Kiev State University

References

1. K.Schaefer & R.Kern, Z.Phys., 74, 609 (1932).
2. M.P.Lisitsa & V.N.Malinko, Opticka i spektroskopiia, 4, 455 (1958).
3. M.P.Lisitsa & V.N.Malinko, PTE (Instruments and Experimental Techniques), 3, 52 (1957).
4. J.Strong et al, Procedures in Experimental Physics, N.Y., 1944 (Cited in Russian trans., 1948).
5. Spravochnik khimika (Chemist's Handbook) Vol.III, M., 1951.
6. E.J.Slowinski & G.C.Claver, J.Opt.Soc.America, 45, 396 (1955).

CHANGES IN THE INFRARED SPECTRUM OF AMMONIA INCIDENT TO TRANSITION FROM THE GASEOUS TO THE LIQUID STATE

- I.V.Demidenkova & L.D.Shcherba

The present work was devoted to the investigation of the infrared spectrum of liquid ammonia and solutions of ammonia in carbon tetrachloride.

Liquid ammonia, which is an excellent solvent not only for organic compounds but also for many inorganic salts and metals, is finding extensive use in chemistry as a medium for many reactions. In view of this, data on the structure of liquid ammonia - particularly its vibrational spectrum - are of considerable interest.

Investigation of the infrared spectrum of liquid ammonia is also of interest in connection with the more general question of changes occurring in the spectra of materials incident to transitions from the gaseous to the condensed state. Such observations are most conveniently made with simple molecules such as the ammonia molecule.

Hitherto the infrared spectrum of liquid ammonia had not been studied in detail. The infrared spectra of solutions of a number of organic compounds in liquid ammonia were obtained in the 3 μ region in the work of Izrailevich et al[1]. Their data regarding the valence bands of pure ammonia are not particularly accurate in view of the excessive thickness of the absorbing layer. Reding & Hornig[2] obtained the infrared spectrum of crystalline ammonia. The Raman spectrum of liquid ammonia has been investigated by Daure[3] and Bhagavantam[4] and more recently by Marchand[5], Plint, Small & Welsh[6] and Dunumaki & Aida[7].

In our work the spectra were recorded on an IKS-11 spectrometer with LiF and NaCl prisms. The spectrum of liquid ammonia was obtained in the region from 2 to 15 μ at -50°.

The spectrum of ammonia solution in CCl_4 was obtained only in the region of the valence NH vibrations. The absorption cell used for recording the spectra of liquid ammonia was of the conventional low-temperature type in the form of a demountable glass Dewar. The copper plate on which the cell proper was assembled was attached to bottom of the inner flask by means of Wood's alloy. The greatest experimental difficulty was encountered in finding a suitable material for the cell windows inasmuch as alkali halide salts readily dissolve in liquid ammonia. For this reason it was impossible to use AgCl windows which are generally the most convenient for low-temperature measurements. The only suitable window material proved to be KCl (the solubility of KCl in liquid NH_3 is 1.45 g/liter). A 12 μ thick teflon spacer gasket was clamped between the windows; Bakelite varnish was used as the sealant. The ammonia gas was introduced into the cell through a Pyrex tube cemented into the cell window. The given (12 μ) layer thickness proved to be too great for observation of the intense band of liquid NH_3 at 1050 cm^{-1} (ν_2). Hence to obtain approximate data on the frequency position of the band, we used a thin layer of liquid NH_3 condensed directly on a KCl plate.

In all the work we used synthetic NH_3 dehydrated by condensation over metallic sodium.

The infrared absorption spectrum of liquid ammonia in the region of the valence and deformation vibrations is shown in Figs.1 & 2. Table 1 lists the frequencies of the observed bands and their interpretations which agree with the assignments given by Plint et al[6] and Kumanaki & Aida[7] for the Raman spectrum. In earlier Raman spectrum studies[3,4] a different assignment was proposed for the three bands observed in the valence vibration region. Bhagavantam[4] attributed the middle component of the triplet to symmetrical vibration of the NH_3 molecules and the two end components to vibrations of the dimer, presumably present in the liquid.

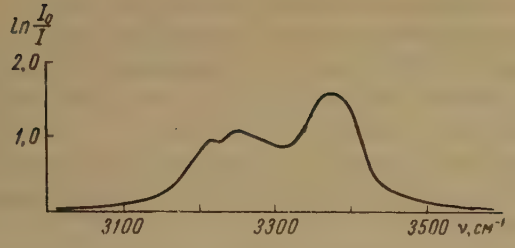

Fig.1. Infrared spectrum of liquid NH_3.

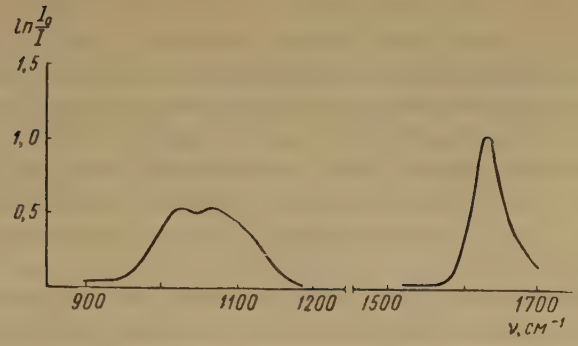

Fig.2. Infrared spectrum of liquid NH_3.

Table 1

Data on the infrared spectrum and Raman spectrum of ammonium (ν, cm^{-1})

Gas (Ref.8)	Infrared spectrum (our data)		Raman spectrum of liquid (Ref.7)	Assignment
	Solution in CCl_4	Liquid		
3444*	3421	3375	3384	ν_3 (E)
3337	3313	3285**	3303	ν_1 (A)
3219	3237	3220	3212	$2\nu_4$
1627	2987,2?	1632	1624	ν_4 (E)
931,6—968,1		1035—1066	1054	ν_2 (A)

* According to Cumming & Welsh[9].
** Value obtained by resolution of the overlapping bands, according to symmetrical contours.

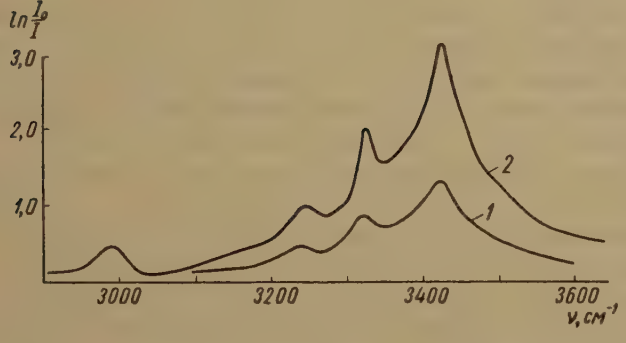

Fig.3. Infrared spectrum of solution of NH_3 in CCl_4. Thickness of absorbing layer: 1 - 1 cm, 2 - 2 cm.

The spectrum of a 0.3 mole/liter ammonia solution in carbon tetrachloride in the region of the valence NH vibrations is given in Fig.3. At so low a concentration there can hardly be any appreciable formation of dimers. Nevertheless, the triplet observed in the liquid is also present in the spectrum of solution.

Thus there is no justification for attributing the 3375 cm^{-1} and 3220 cm^{-1} bands in the spectrum of liquid ammonia to dimer vibrations.

The transition of ammonia from the gaseous to the condensed state is accompanied by a marked change in the relative intensity of the bands corresponding to symmetrical ν_1(A) and antisymmetrical ν_3(E) valence vibrations. In the infrared spectrum of the gas the ν_1 band is more intense than the ν_3 band. In the CCl_4 solution, on the contrary, the ν_3 band becomes somewhat more intense than ν_1. Finally, in going from the liquid to the solid (crystalline) state[2] the intensity of the ν_3 band becomes several times greater than the intensity of the ν_1 band. For liquid NH_3 this will be evident from Fig.1 if one resolves the bands of the triplet. This great change in the relative intensities of the bands is apparently not directly con-

nected with formation of hydrogen bonds inasmuch as an appreciable change is already observed when ammonia is dissolved in carbon tetrachloride.

In the spectrum of gaseous ammonia the 950 cm^{-1} ν_2(A) band is split into two components (inversion splitting), which is connected with there being two equilibrium positions of the nitrogen atom (to either side of the plane of the hydrogen atom). The magnitude of the splitting is 36.5 cm^{-1}. Apparently the inversion splitting persists in liquid NH_3 inasmuch as the ν_2 band (Fig.2) consists of two components with a separation of 30 cm^{-1}.

Fyfe[10] calculated the hydrogen bond energy in liquid NH_3 on the assumption that one NH bond of the molecule interacts with a free electron pair of another molecule and obtained a value of 5.1 Kcal/mole.

On the basis of this assumption regarding the hydrogen bond in ammonia, one should expect an appreciable difference between the spectrum of the liquid and that of the gas, namely, the appearance of a new band associated with perturbed NH vibrations and removal of degeneration due to nonequivalence of the NH bonds. Actually, however, no significant changes in the infrared spectrum incident to the liquid-gas transition are observed except for a considerable increase in the relative intensity of the ν_3 band and a rather noticeable displacement of the bands (see table). This result can be explained if we assume that all three NH bonds of a given molecule interact with the free electron pair of another molecule. In this case all three NH bonds remain equiparate and the hydrogen bonds formed are presumably nonlinear.

State Institute of Applied Chemistry

References

1. E.A.Izrailevich, D.N.Shigorin, I.V.Astaf'ev & A.I.Shatenshtein, Doklady AN SSSR, 111, 617 (1956).
2. F.P.Reding & D.F.Hornig, J.Chem.Phys., 19, 594 (1951).
3. P.Daure, Ann.Phys., 12, 375 (1929).
4. S.Bhagavantam, Ind.J.Phys., 5, 54 (1930).
5. A.Marchand, Compt.rend., Paris, 235, 395 (1951).
6. C.A.Plint, R.M.B.Small & H.L.Welsh, Canad.J.Phys., 32, 653 (1954).
7. Susumu Kunumaki & Koyo Aida, Sci.Repts.Res.Inst.Tohoku Univ.Ser. A6, 186-92 (1954).
8. G.Herzberg, Infrared and Raman Spectra of Polyatomic Molecules. (Cited in Russian trans.)
9. C.Cumming & H.L.Welsh, J.Chem.Phys., 21, 1119 (1953).
10. N.S.Fyfe, J.Chem.Phys., 21, 2 (1953).

INFRARED SPECTRA OF SALT SOLUTIONS

- E.N.Vasenko, A.P.Cherniavskaia & N.V.Chernaia

The vibrational spectra of solutions have been utilized for investigating the effect of ions on liquids having a structure characterized by the presence of intermolecular hydrogen bonds. As the subject of our investigation we chose formamide, the infrared spectrum of which is reasonably well known; in addition formamide is similar to water as regards the character of the intermolecular hydrogen bonds that are responsible for the formation of a spatial net structure encompassing the entire liquid volume.

For purposes of preliminary study we chose the C-N band of formamide in view of the fact that the position of this band changes noticeably incident to formation and rupture of the hydrogen bonds in which both the amino and carbonyl groups of the formamide molecules participate.[1] A further consideration was the fact that this band is relatively intense and remote from the other bands in the spectrum of formamide.

We recorded the absorption spectrum of a saturated solution of potassium nitrate in formamide in the 1200 to 1500 cm^{-1} region on an IKS-11 spectrometer with a rock salt prism.

KNO_3 is a monovalent electrolyte, which exhibits the closest approach to the limiting Debye-Guchel law in determining the activity coefficient of this electrolyte in formamide;[2] hence it was of interest to clarify the influence of its ions on the spectrum of formamide. At an absorbing layer thickness equal to that used in the case of pure formamide, we detected three not fully resolved bands near 1325, 1345 and 1365 cm^{-1}. In this region in the spectrum of pure formamide there is observed a band at 1309 cm^{-1} associated with the valence vibrations of C-N and a band at 1391 cm^{-1} associated with deformation vibrations of C-H. The newly discovered bands can be attributed either to C-N vibrations perturbed by ionic dipole interaction, exceeding in energy the intermolecular hydrogen bond N—H···O=C in liquid formamide, or to vibrations of the NO_3^- anion.

To resolve this question we obtained the spectrum of a saturated solution of potassium bromide in formamide in the same spectral region (1200-1500 cm^{-1}). In this case there were clearly discernible bands near 1330 and 1350 cm^{-1}; consequently, these can be attributed to absorption of formamide in the presence of K^+ and Br^- ions, disturbing its structure in the liquid state.

The absorption spectra of saturated aqueous solutions of the same salt, which we recorded for purposes of comparison, showed an appreciable absorption in the given region not characteristic of pure water (two bands in the case of potassium bromide). We are continuing our research with a view to elucidating the origin of this absorption and determining the concentration dependence of the absorption spectra both in the 1200-1500 cm^{-1} region and in the region of the valence vibrations of the N—H and C=O groups in formamide and the O—H group in water.

L'vov Polytechnical Institute

References

1. E.N.Vasenko, Transactions of the Tenth All-Union Conference on Spectroscopy, Part I, L'vov, 1957.

2. E.N.Vasenko, Zhur.fiz.khim., 23, 959 (1949).

INVESTIGATION OF KETO-TRANS-CIS-ENOL EQUILIBRIUM BY INFRARED ABSORPTION SPECTROSCOPY

- M.E.Movsenian, M.I.Kabachnik, S.T.Ioffe & K.V.Vatsuro

The infrared spectra of keto-enol compounds have been studied by a number of authors, primarily in the regions of the valence vibrations of the C=C, C=O and O—H groups, i.e., in the 3 μ and 6 μ regions. In the latter region, in addition to the lines belonging to the keto form, there have been observed bands belonging to the enol form, usually at somewhat longer wavelengths. In more recent investigations, carried out with improved equipment, Bratoz et al[1] and Le Fevre & Welsh[2] have succeeded in observing in the spectra of β-keto esters individual C=O absorption maxima belonging to the carbonyl and carboxyl groups and also a complex double band in the region of the valence vibrations of the C=C bond. Actually, only one of the latter maxima pertains to the double bond, while the other is associated with the chelated and conjugated carboxyl carbonyl.[3]

Hitherto there have been very few quantitative measurements of keto-enol equilibrium by observation of infrared absorption spectra. Thus, Le Fevre & Welsh[2] compared the intensity of the 1650 cm^{-1} band of acetoacetic ester in different solvents with the amount of enol found chemically. They obtained a smooth curve which, in their opinion, substantiates the accuracy of the chemical determinations. Kuratani[4] comparing the relative intensities of the enol and keto bands of the ethyl acetoacetic ester, found that the amount of enol in solutions of this ester in hexane, diethyl ether, and carbon disulfide is greater than in solutions in pyridine and methyl alcohol. Shigorin[5] evaluated the amount of enol in ethyl ethers of cyclohexanone carboxylic and cyclopentanone carboxylic acids from the intensity of the Raman lines.

In the present work we attempted to determine by means of infrared absorption spectrometry the cis-trans-enol tautomerism in keto-enol compounds and to evaluate the relative amounts of the stereoisomeric forms.

We investigated the infrared absorption spectra of the ethyl esters of acetoacetic, cyclohexanone carboxylic, cyclopentanone carboxylic, α-sec-dibutylacetoacetic and formylphenylacetic acids. By way of solvents we used chloroform, benzene, toluene, diethyl ether, carbon tetrachloride and n-hexane.

In the spectra of compounds with cis-positioned enols (cyclohexanone carboxylic and cyclopentanone carboxylic esters) and of acetacetic ester four bands were observed in the 6 μ region:

1) a band associated with the vibrations of the carboxyl carbonyl group of the keto form,

2) a band associated with the vibrations of the carbonyl group of the keto form,

3) a band of the carboxyl carbonyl, linked by an intermolecular hydrogen bond and conjugated with the ethylene C=C bond, of the enol form, and

4) a band associated with the valence vibrations of the C=C bond of the enol form.

By way of illustration the spectrum of the solution of cyclopentanone carboxylic ester in hexane is shown in Fig.1.

We compared the relative intensities of the absorption bands of the keto and enol forms of all the above enumerated substances with the equilibrium constants (determined chemically) of acetoacetic ester which is usually taken as the standard substance in such work. In determining the optical densities, we took into account the absorption at the band maximum. According to our evaluations, the error in determining the optical density ratios does not exceed 12%.

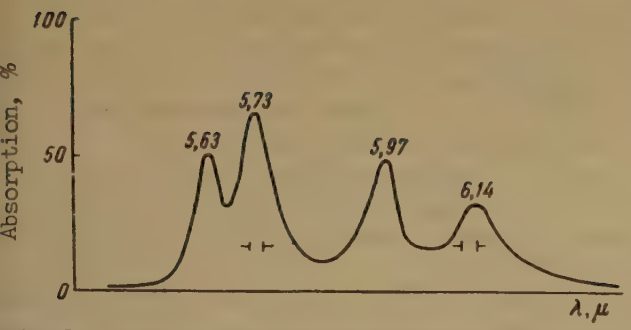

Fig.1. Absorption spectrum of a solution of the ethyl ester of cyclopentanone carboxylic acid in hexane in the 6 μ region.

It can readily be seen that the optical density ratio D'/D'' for the enol band 4 and keto band 2 yields the equilibrium constant K_T with an accuracy to within the factor ϵ_4/ϵ_2:

$$\frac{D'}{D''} = \frac{D_4}{D_2} = \frac{\epsilon_4 \cdot C_4}{\epsilon_2 \cdot C_2} = \frac{\epsilon_4}{\epsilon_2} K_T.$$

Inasmuch as the value of ϵ depends on the solvent, it was clearly necessary to determine whether the ratio ϵ_4/ϵ_2 is a function of the solvent. To this end we plotted the values of the chemically determined equilibrium constants K of acetoacetic ester in different solvents vs the ratio $D'/D'' = D_4/D_2$ in the same solvent. As may be seen in Fig.2 the plot is a straight line; hence it follows that the ratio ϵ_4/ϵ_2 does not depend on the solvent.

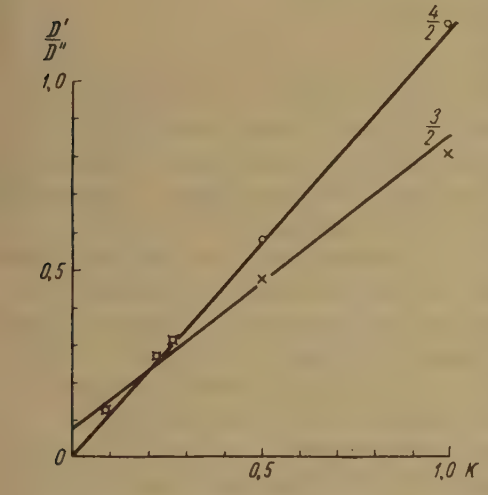

Fig.2.

If it is assumed that in all the investigated solvents all the enol is in the cis form and, moreover, that there is an intermolecular hydrogen bond in all the enol molecules, the D'/D'' (equal in this case to D_3/D_2) vs K plot should be a straight line passing through the origin. As will be seen in Fig.2 (the 3/2 line) this assumption is realized in the case of acetoacetic ester.

Meyer found the following empirical formula for the dependence of the keto-enol equilibrium on the properties of the keto-enol and the solvent:

$$K_T = EL,$$

where K_T is the equilibrium constant, E is the enolizability of the keto and L is the enolizing ability of the solvent.

Subsequently, this formula was derived by Kabachnik[6] utilizing the theory of acids and bases.

Considering the more general case of equilibrium when the enol form may have both the cis and trans configurations, Kabachnik, Ioffe & Vatsuro[7] arrived at the following expression:

$$K_T = EL + E'L'. \qquad (1)$$

Here E and E' are the enolizabilities of the keto forms in the cis- and trans-enol forms, respectively. E and E' are determined only by the keto-enol structure and do not depend on the solvent. L and L' are the enolizing abilities of the solvent; they depend only on the solvent. These quantities (general for all keto-enols) are equal to the tautomeric equilibrium constants of the substances taken as the standards for cis- and trans-enolization. In the absence of trans-enolization, E' = 0 and formula (1) becomes the Meyer formula.

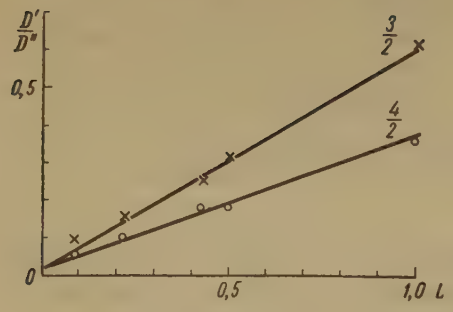

Fig.3.

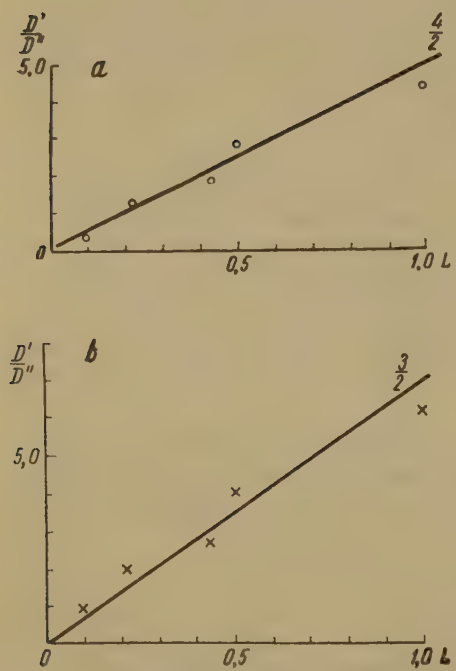

Fig.4.

Experimental chemical investigation[7] of a number of keto-enol compounds showed that substances capable of only cis-enolization (cis-positioned enols) conform to Meyer's formula; the K_T vs L plots for all these substances are straight lines passing through the origin.

In the case of substances which only have the trans-enol form (trans-positioned enols), the equilibrium constant does not depend on the solvent.

It follows from the two series of experiments first, that the choice of acetoacetic ester as the standard for cis-enolization is justified and, second, that L' is a constant. In this case instead of formula (1), we can write[7]:

$$K_T = EL + E_1. \qquad (2)$$

Thus, keto-enols in solutions in which there are present both cis- and trans-enol forms are also characterized by a linear dependence of K_T on L, but in this case the straight-line plots do not pass through the origin but intersect the vertical axis at a point numerically equal to E_1.

It follows from the above that the dependences of the ratio D_4/D_2 on the equilibrium constant of acetoacetic ester should be linear. As may be seen from Figs.3 & 4, the experimental points for cyclopentanone carboxylic ester (Fig.3) and cyclohexanone carboxylic ester (Fig.4) fall on straight lines passing through the origin.

In these figures we have also plotted the values of the ratio D_3/D_2, which are proportional to the ratio of the amounts of the cis-enol and keto forms. As might be expected, the points also fit straight lines passing through the origin.

Of the compounds in which, owing to steric hindrance, primarily trans-enol is present, we investigated α-sec-butylacetylacetic ester. Our choice of this substance was dictated by the fact that it contains a relatively large amount of enol and dissolves in the above listed solvents. In the spectra of this substance, in addition to two bands associated with the carbonyl groups, there is only one band which we assigned to the C=C group. It was found that the ratio of the optical density of this band to that of either of the keto bands remains constant for all the investigated solvents, i.e., the D_3/D_2 vs L plot is a straight line virtually parallel to the horizontal axis (Fig.5). It is interesting to note that the point for chloroform, which in our plot falls below the straight line, also proves to be anomalous in chemical experiments.

Further, we deemed it of interest to investigate a compound in which there simultaneously exist both the cis- and trans-enol forms; as the most suitable substance we chose the ester of formylphenylacetic acid. We investigated solutions of this substance in chloroform, diethyl ether and carbon tetrachloride. In this case, according to the generalized Meyer formula, the straight line given by

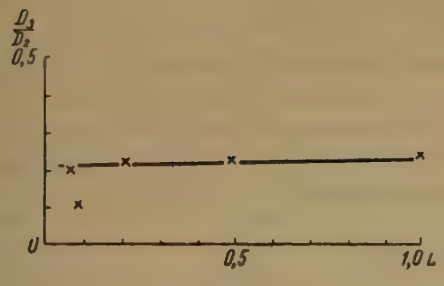

Fig.5.

$$\frac{D_4}{D_2} = f_1(L)$$

should not pass through the origin, while the straight line defined by

$$\frac{D_3}{D_2} = f_2(L)$$

should. Fig.6 shows that this is in fact the case.

The ratio of the ordinates of the points on the D_3/D_2 and D_4/D_2 plots for any given solvent will obviously give

$$\frac{D_3}{D_4} \approx \frac{C_{cis}}{C_{cis} + C_{trans}},$$

where C_{cis} and C_{trans} are the respective concentrations determined by chemical analysis.[7] The ratios $D_3/D_4 : C_{cis}/(C_{cis} + C_{trans})$ proved to be constant, showing that in this case ϵ_3/ϵ_4 does not depend on the solvent.

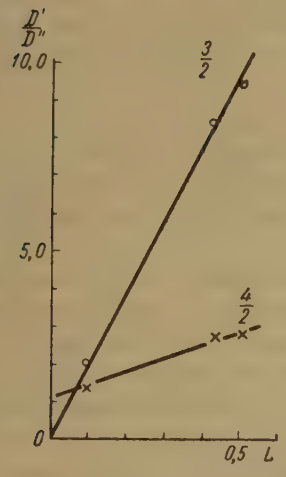

Fig.6.

Conclusions

1. We obtained the infrared spectra of solutions of acetoacetic, α-sec-butylacetoacetic, cyclopentanone carboxylic and cyclohexanone carboxylic esters in chloroform, benzene, diethyl ether, carbon tetrachloride and hexane and solutions of formylphenylacetic ester in chloroform, diethyl ether and carbon tetrachloride.

2. Quantitative determinations of the keto-enol equilibrium by means of the infrared absorption spectra proved to be in good agreement with the results of chemical analyses.

3. The spectroscopic data also substantiate the generalized Meyer formula for the keto-cis-trans-enol tautomerism equilibrium constant.

"P.N.Lebedev" Physical Institute
Commission of Spectroscopy &
IÉOS of the USSR Academy of Sciences

References

1. S.Bratoz, D.Hadzi & G.Rosmi, Trans.Faraday Soc., 52, 464 (1956).
2. R.J.W.Le Fevre & H.Welsh, J.Chem.Soc., 2230 (1949).
3. R.S.Rasmussen, D.D.Tunnicliff, & R.R.Brattain, J.Amer.Chem.Soc., 71, 1068 (1949); N.J.Leonard, H.S.Gutowsky, W.J.Middleton & E.M.Petersen, J.Amer.Chem. Soc., 74, 4070 (1952).
4. K.Kuratani, Rept.Inst.Sci., Tokyo, 5, 25 (1951); Chem.Abstr., 1354 (1952).
5. D.N.Shigorin, Zhur.fiz.khim., 24, 924 (1950).
6. M.I.Kabachnik, Doklady AN SSSR, 83, 407, 859 (1952).
7. M.I.Kabachnik, S.T. Ioffe & K.V.Vatsuro, Izv.AN SSSR, Chem.section, No.6, 755 (1957).

SPECTROSCOPIC INVESTIGATION OF THE STRUCTURE OF SOME COMPLEX COMPOUNDS

- A.A.Babushkin

This report summarizes the results of three investigations devoted to the structure of molecular compounds. Two of these were concerned with the study of complex compounds of boron trifluoride with some nitrogen- and oxygen-containing molecules; the other with investigation of the influence of water of crystallization on the structure of sodium para- and metatungstates.

1. $F_3B \cdot NH_3$ and $F_3B \cdot ND_3$ Complexes*

The infrared absorption and Raman spectra of these compounds were obtained in our laboratory. Calculations of the force field and vibrational spectra were carried out by I.F.Kovalev on the basis of the C_{3v} model for $F_3B \cdot NH_3$ and $F_3B \cdot ND_3$ and the C_s model for $F_3B \cdot NH_2D$ and $F_3B \cdot NHD_2$. The spectra of the last two substances were utilized for checking the calculations.

The interpretation of the fundamental frequencies of $F_3B \cdot NH_3$ and $F_3B \cdot ND_3$ was checked by application of the product rule: the experimental ratios of the squares of the vibration frequencies corresponding to the A_1 and E symmetry types of these compounds exceeded the theoretical values by 0.010 and 0.013, respectively.

In calculating the frequencies on the basis of the deduced force constants, the secular equations (except for the type A symmetry equations for $F_3B \cdot NH_2D$ and $F_3B \cdot NHD_2$) were solved with the aid of the BESM (USSR Academy of Sciences) electronic computer. The calculated vibration frequencies proved to be in good agreement with the experimental values: the mean absolute deviation is 11 cm^{-1}.

Thus it proved feasible on the basis of the assumed C_{3v} model to calculate and interpret the vibrational spectra of the molecular compound $F_3B \cdot NH_3$ and its deuteroderivatives and to evaluate the potential function.

We computed the value of the force constant for the B—N bond, namely, $4.4 \cdot 10^5$ dyne cm^{-1}, which shows that the B—N bond is comparatively strong; the intensity of the Raman spectrum frequency corresponding to the vibrations of the B—N bond indicates that it is a covalent bond.

2. Structure of Molecular Complexes of Boron Trifluoride with Methyl and Ethyl Alcohol and Water**

Boron trifuloride forms two types of molecular compounds with water and alcohols: in one there is one molecule of water or alcohol per F_3B molecule (1:1 compounds); in the other there are two water alcohol molecules per trifluoride molecule (1:2 compounds). Meerwein & Pannwitz[1] hypothesized that in the latter case the second water or alcohol molecule is coupled to the 1:1 complex by means of a hydrogen bond of the type

$$\begin{matrix} H—O\cdots H—O\cdot BF_3 \\ \quad\downarrow X \quad\quad \downarrow X \end{matrix}$$

where X = H or R.

At present a number of authors[2] appear to share the opinion of Paushkin[3] that the 1:2 molecular compounds should be regarded as oxonium type complexes:

---

*Collaborators: A.A.Babushkin, I.F.Kovalev and V.M.Emel'ianova.

**Collaborators: A.A.Babushkin, L.A.Gribov, N.G.Guseva and V.M.Emel'ianova.

$(H_2O)^+(F_3B\cdot OH)^-$ and $(R\cdot OH_2)^+(F_3B\cdot OR)^-$.

It must be admitted, therefore, that the structure of these molecular compounds has not been definitively established.

Experimental Results

A careful search for absorption characteristic specifically of the oxonium ion in the spectrum of $F_3B\cdot 2(ORH)$ proved to be fruitless. In this study, extending over the 2200 to 3800 cm^{-1} range of the spectrum, the thickness of the absorbing layers was varied from 5 to 400 μ. The absorption spectrum was also recorded with the compounds cooled to -20°. In the case of the complexes with alcohols there was detected absorption associated with the valence vibrations of the CH bonds and for each of the investigated compounds absorption at 3565 cm^{-1}. No significant absorption at higher wave numbers was observed.

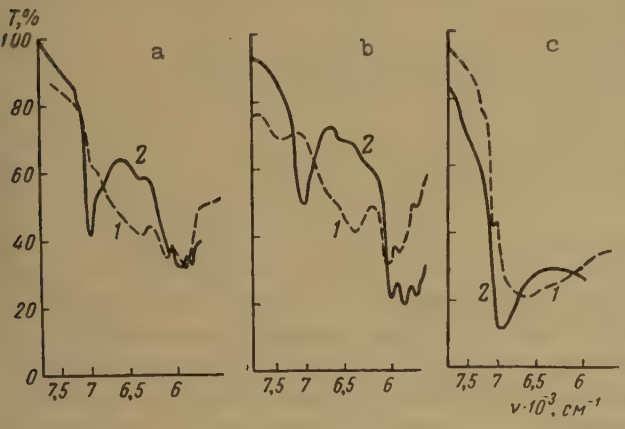

Fig.1. Absorption spectra of the investigated molecular compounds in the 5700 to 7500 cm^{-1} region: a) 1 - $F_3B\cdot CH_3OH$, 2 - $F_3B\cdot 2CH_3OH$; b) 1 - $F_3B\cdot C_2H_5OH$, 2 - $F_3B\cdot 2C_2H_5OH$, c) 1 - $F_3B\cdot H_2O$, 2 - $F_3B\cdot 2H_2O$.

Investigation of the absorption spectra in the region of the first overtone of the OH valence vibrations (Fig. 1) showed that there is a pronounced difference between the spectra of $F_3B\cdot 1(ORH)$ and $F_3B\cdot 2(ORH)$. The spectra of the 1:1 compounds comprise a wide absorption band with a half-width of 450-550 cm^{-1}; the wave numbers of the absorption peaks are 6350, 6335 and 6500 cm^{-1} for the molecular compounds of F_3B with methanol, ethyl alcohol and water, respectively. There are also indications of weak absorption in the 7180-7300 cm^{-1} region; this, however, is clearly evident only in the spectrum of the $F_3B\cdot C_2H_5OH$ complex. The absorption spectra of the 1:2 type compounds are characterized by the presence of a narrow absorption band with a half-width of 90-180 cm^{-1}; the wave number of the peak of these bands is 6985 cm^{-1} in all cases.

Discussion of results

1. The fact that there is no spectroscopic evidence of the oxonium ion indicates that either the oxonium form is not realized in the investigated molecular compounds or that its concentration is negligibly low.

2. Comparison of the wave numbers of the fundamentals and first overtones of the valence vibrations of the OH group in methyl and ethyl alcohol and water in the absence of association (dilute solutions and vapors) with the wave numbers of the absorption peaks of the 1:2 molecular compounds indicates that these compounds are associated by means of hydrogen bonds. The wide absorption bands of 1:1 compounds are also due to association by the intermediary of hydrogen bonds.

3. The difference between the band widths and wave numbers of the absorption peaks in the spectra of the 1:1 and 1:2 complexes must be attributed to differences in the character of formation of the hydrogen bonds. Bearing in mind

the data in the literature on the character of association of alcohols and water, we feel it is logical to connect the wide absorption band of 1:1 compounds with polymer association of the

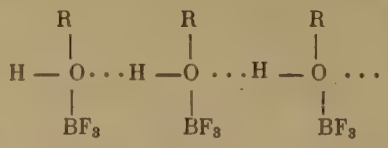

(I)

type.

This form of association infers the presence of end OH groups. In the experimental spectrograms they are evinced in the form of a weak absorption band peaking at 7200 cm^{-1}.

We are inclined to connect the narrow absorption band in the spectra of the 1:2 compounds with association of two complexes in which the four hydrogen bonds form a closed ring:

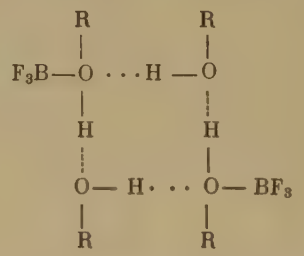

(II)

In this type of formation all the bonds are fully saturated so that there is no possibility of further association. In view of its cyclic character this structure is a stable formation, which, on the one hand, explains the shift and narrowness of the absorption band and, on the other hand, is consistent with the greater chemical stability of the 1:2 compounds as compared with the 1:1 compounds. The fact that there is no absorption characteristic of the end hydroxyl group (not participating in the hydrogen bond) either in the region of the fundamental or of the first overtone of the OH valence vibrations may be taken as further evidence in favor of the II structure.

3. Influence of Water on the Structure of Sodium Para- and Metatungstate*

Spectra of sodium paratungstate hydrates

There were obtained the infrared absorption spectra of sodium paratungstates ($5Na_2O \cdot 12WO_3$) containing $28H_2O$, $19H_2O$, $9H_2O$, $4H_2O$ and $2H_2O$ and of the anhydride. The spectra were investigated in two regions: in the region of the valence and deformation vibrations of the tungstate ion (700 to 1700 cm^{-1}) and in the region most favorable for studying the state of the water in these hydrates (3000 to 3800 cm^{-1}). Investigation of the absorption band of water in the ~3 μ region showed that a pronounced change in the coordination of water occurs in going from the $19H_2O$ to the $9H_2O$ hydrate (Fig.2). This change in the coordination of water produces a change in the structure of the paratungstate ion: the discreet structure of the absorption spectrum in the 700-860 cm^{-1} region, characteristic of the 28-water and 19-water hydrates, is no longer observed in the spectra of the 9-water and lower hydrates. Discreet structure again becomes evident in this region in the spectra of the hydrates with 0.2 H_2O per mole $Na_{10}W_{12}O_{41}$ and the anhydrous tungstate, but it differs in character from that in the spectrum

---

*Collaborators: A.A.Babushkin, G.V.Iukhnevich, Iu.V.Berezkina and V.I. Spitsyn.

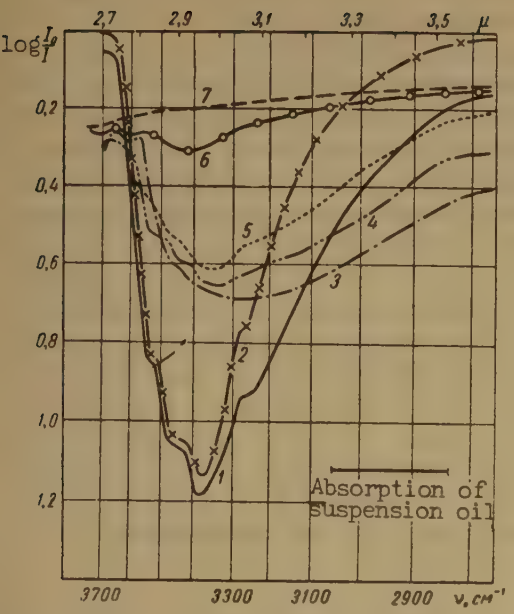

Fig.2. Absorption spectra of different hydrates of sodium paratungstate in the 2800 to 3700 cm^{-1} region: 1 - $28H_2O$, 2 - $19H_2O$, 3 - $9H_2O$, 4 - $4H_2O$, 5 - $2H_2O$, 6 - $0.2H_2O$ per mole $Na_{10}W_{12}O_{41}$, 7 - anhydrous tungstate.

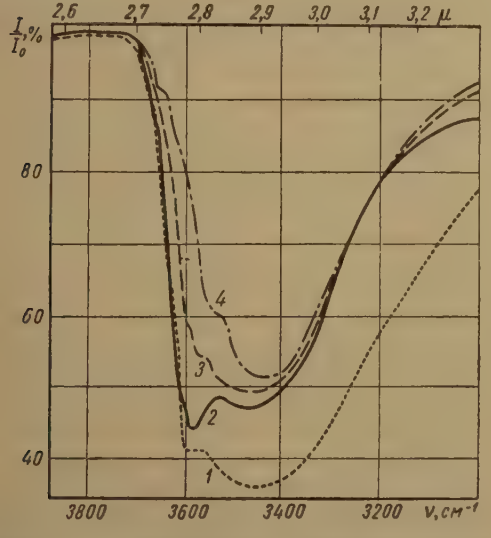

Fig.3. Absorption spectra of $28H_2O$ sodium paratungstate and its solutions in D_2O: 1) solid paratungstate in an oil suspension, 2) immediately after solution in D_2O, 3) after heating at 60° for 2 hours, 4) 10 days after solution. Spectra recorded on an IKS-2 spectrograph.

of the initial 28 H_2O paratungstate.

Comparison of the absorption spectra of the 28-water sodium paratungstate hydrate with the spectra of its solutions in D_2O (95.5% D_2O concentration) (Fig.3), recorded at different times after forming the solution and after heating, show that the isotopic exchange of the hydrogen of the hydrate water for the deuterium of the solvent water proceeds in steps; the individual exchange steps are associated with different regions of spectral manifestation of the water. From these exchange experiments it may be concluded that in the 28 H_2O hydrate there exist three forms of coordination of water, one of them being realized in the form of a hydroxyl directly linked with the tungsten atom (W—OH···). This deduction is based on the fact that there is a narrow band peaking at 3560 cm^{-1} in the water absorption spectrum.

Spectra of sodium metatungstate hydrates

There were obtained the absorption spectra of sodium metatungstate ($Na_2W_4O_{13}$) hydrates containing $10H_2O$, $7H_2O$ and $2H_2O$ and of the anhydrous metatungstate. The absorption band of water in the 3 μ region in the spectra of these hydrates consists of two components: a wide component (maximum at 3400 cm^{-1}) and a narrow component (maximum at 3560 cm^{-1}). (Just as in the case of sodium paratungstate the absorption component peaking at 3560 cm^{-1} could be attributed to the valence vibrations of the hydroxyl group linked directly to the tungsten atom.) The shape of the band as a whole remains the same in all the hydrates; however, the integral intensity of the band decreases, while the relative intensity of the narrow component increases somewhat in going from the higher to the lower hydrates. This invariance of the shape of the water absorption band, in our opinion, indicates that the coordination of the water in the investigated hydrates does not change with gradual dehyrdation of the highest metatungstate hydrate.

The character of the absorption spectra in the region of the valence and deformation vibrations of the metatungstate anion also does not change significantly in going from the highest to the lowest of the investigated hydrates; only the relative intensities of the individual absorption bands are modified to some extent. This invariance of the general

character of the spectrum indicates that the structure of the anion is essentially the same in all the investigated sodium metatungstate hydrates.

On the basis of the results obtained for the different sodium para- and metatungstate hydrates, we can draw the general conclusion that where these substances are concerned there is a direct correlation between the coordination of the water in the hydrate complex and the structure of the anion of the isopoly compound: when the coordination of the water changes incident to dehydration, the structure of the anion is modified, while when the type of coordination remains the same, the initial structure of the complex persists.

Institute of Physical Chemistry
Academy of Sciences of the USSR

References

1. H.Meerwein & W.Pannwitz, J.Prakt.Chem., 141, 123 (1934).
2. N.Greenwood & R.L.Martin, Quart.Reviews, 8, 8 (1954).
3. Ia.M.Paushkin, Zhur.prikladn.khim. (Journal of Applied Chemistry) 21, 1207 (1948).

SPECTROSCOPIC METHODS OF INVESTIGATING CATALYTIC CONVERSIONS ON METAL FILMS

- V.M.Griaznov, V.D.Iagodovskii & V.I.Shimulis

Metal films obtained by vacuum sublimation are distinguished from metallic catalysts prepared in other ways by the high purity and cleanliness of their surface. The catalytic activity of such films, however, is not high and deteriorates rapidly with time, particularly at elevated temperatures. For rapid determination of the extent of catalyzed conversions, we used optical cells onto the walls or windows of which a film of the desired metal could be applied by vacuum evaporation. If one of the substances participating in the catalytic conversion has a far larger absorption coefficient at some frequency than the other compounds present, one can readily follow the course of the reaction by observing the optical density of the reagent vapor in the given frequency interval. By using a recording spectrograph one can obtain a curve of the variation with time of the optical density, i.e., a curve characterizing the kinetics of the reaction.

By observing the ultraviolet absorption spectra we investigated the kinetics of isomerization of allylbenzene to propenylbenzene,

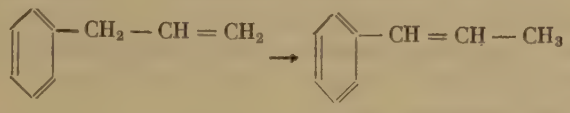

on palladium films. The palladium films were deposited by sublimation at a vacuum of $1 \cdot 10^{-6}$ mm Hg on the walls of a quartz cell 150 mm long with end windows (1 and 1' - Fig.1) 40 mm in diameter.

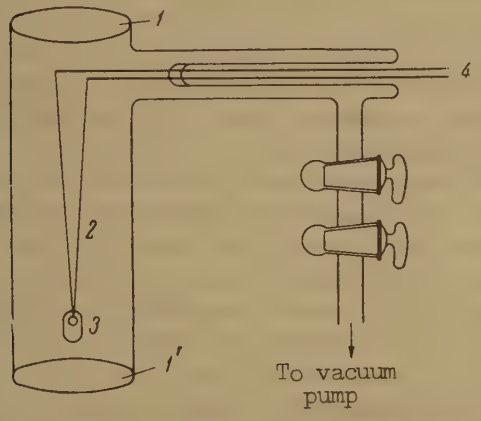

Fig.1. Quartz cell for spectroscopic investigation of catalytic conversions on metallic films.

For sublimation of the metal, the palladium wire 2 was held near the axis of the cell by the weight 3 which simultaneously served to shield the bottom window of the cell. The top window was protected against deposition of palladium by the molybdenum leads 4. After obtaining a specular palladium film of about 1000 Å thickness, the two stopcocks were closed, the cell was detached from the vacuum line and mounted in front of the monochromator slit. In the viewing position, the weight 3 dropped onto the wall of the cell out of the way of the light beam.

We used a ZMR-2 mirror monochromator with a photoelectric attachment for recording the absorption spectra of the allylbenzene and propenylbenzene vapor mixture forming during the catalytic isomerization. There was no provision in the design of the ZMR-2 instrument for protection of the photocell from extraneous light, which greatly hampered the work. The recording was greatly improved by installing a light-proof sleeve with a movable shutter between the exit slit and the photocell. The shutter allowed of beginning and ending the recording at precisely known points.

Investigation of the spectra of mixtures of allylbenzene and propenylbenzene vapor of different composition at a constant total pressure of 0.65 mm Hg showed that the presence of allylbenzene vapor had virtually no effect on the absorption at 2550 Å and that the optical density at this wavelength varied linearly with the propenylbenzene vapor pressure. Thus it was feasible to determine the dependence of the extent of isomerization of allylbenzene on the experimental condi-

tions from the optical density vs time curves. A detailed description of the technique and the results obtained in the experiment have been published earlier[1].

We used an identical cell for investigating the kinetics of conversion of 1,3-cyclohexadiene to benzene and cyclohexene:

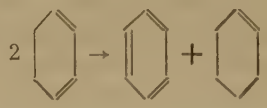

(1)

This reaction goes to completion on a palladium film within a few minutes even at room temperature, but the spectroscopic techniques allows of determining its kinetic sequence.*

The transformation of the cyclohexene forming in the above reaction into benzene and cyclohexane -

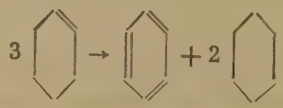

(2)

- proceeds appreciably more slowly. The extent of conversion of the cyclohexadiene was determined from the decrease of absorption at 271 mμ, where the absorption of cyclohexadiene vapor is high, while the vapors of benzene, cyclohexene and cyclohexane do not absorb.

The conversion of cyclohexadiene was also investigated on transparent palladium films of about 100 Å thickness, which were applied directly to the windows of a one-piece quartz cell 16 mm long. The reaction proceeded on these films at a noticeable rate even at room temperature. Experiments were also carried out at 85°. Prior to application of the palladium films to the cell windows, we investigated the pressure dependence of the density of the benzene vapor absorption spectrum. It was found that at the chosen exposure, the most intense absorption bands of benzene are not evident at vapor pressures under 0.3 mm Hg. The vapor pressure of the benzene obtained from cyclohexadiene at an initial vapor pressure of 0.5 mm Hg could not exceed 0.33 mm Hg, as will be evident from Eqs.(1) and (2). Hence it was thought that even after complete conversion of the cyclohexadiene into benzene and cyclohexane the absorption bands of benzene would be very weak. Actually, however, their intensity proved to be almost as high as at a benzene vapor pressure of 0.5 mm, which can be explained only by an apparent increase of the absorption coefficient of benzene adsorbed on the palladium film.

It should be noted that at a pressure of 0.33 mm Hg and a cell length (thickness) of 16 mm there were about $2 \cdot 10^{-7}$ mole benzene vapor in the light beam. The visible illuminated surface of the palladium film on the cell windows was 14 cm^2. Our measurements showed that the total film surface available for absorption of benzene exceeded the visible surface by a factor of about 10. The "sorption area" for a benzene molecule is approximately 40 $Å^2$. Hence in the adsorbed monolayer there could be $6 \cdot 10^{-8}$ mole benzene. Therefore, under our experimental conditions complete "filling" of the monolayer occurred at pressures considerably below 0.1 mm Hg with subsequent formation of polylayers at higher pressures.

Consequently, with a cell length of 16 mm the absorption of ultraviolet radiation by benzene vapor was commensurate with the absorption of the adsorbed benzene layers on the cell windows.

---

*Huo Tiu Ok, Student in the Chemistry Department of Moscow State University, participated in these experiments.

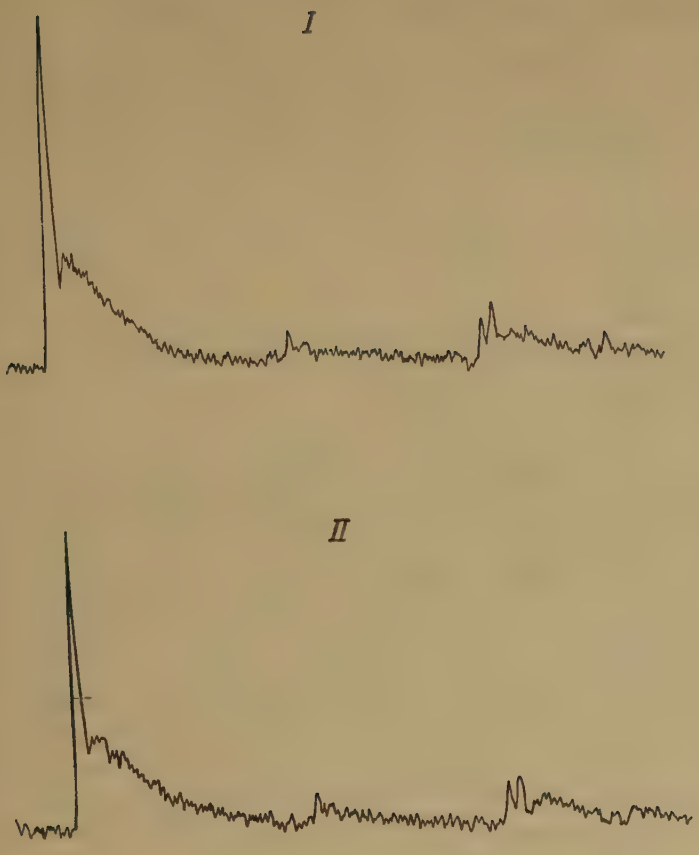

Fig.2. Microphotograms of sections of the absorption spectra of benzene: I - at a pressure of 0.5 mm Hg in a 16 mm cell, II - obtained from cyclohexadiene on films of palladium deposited on the windows of the same 16 mm cell.

We felt it would be of interest to compare the absorption spectrum of benzene obtained under these conditions with the spectrum obtained with a greater vapor layer thickness. For these measurements we used a large DFS-3 diffraction grating spectrograph with a dispersion of 2 Å/mm and a theoretical resolution of 144,000. The spectra were recorded with a slit width of 0.011 mm and an exposure of 2 hours. The continuum source was a superhigh pressure xenon tube. With a layer thickness of 170 mm and a benzene vapor pressure of 0.1 mm Hg, 52 absorption bands were discernible in the spectrum. Most of these were comparable in width with iron arc emission lines.

For determining the frequencies of the benzene absorption bands we plotted dispersion curves with reference to standard iron arc lines; these for <3 Å intervals were straight lines in all cases. The dispersion did not differ by more than 0.05 A/mm in different parts of the spectrum. The positions of the benzene absorption band and iron arc lines were measured by means of an IZA-2 comparator to within 0.002 mm. Each line and band was measured 10 times; the deviations from the arithmetic mean were generally less than 0.003 mm, which corresponds to an accuracy of ±0.4 cm^{-1} in determining frequency. The microscope cross-hair was aligned with the center of the iron lines and the narrow benzene absorption bands; in the case of the wide absorption bands the measurements were made with reference to the short wavelength edge.

The results for a number of bands are listed in column 3 of the accompanying table. Column 1 gives the absorption band assignments according to Sponer, Nordheim, Sklar & Teller[2]. The frequencies determined by Radle & Beck[3] for a 500 mm thick benzene vapor layer are listed in column 2. For the bands with a sharp short-wavelength edge these authors evaluate the accuracy of their determinations as ±1 cm^{-1}. It will be seen that in most cases our frequency values obtained for the 170 mm thick layer agree with the values of Radle & Beck within 0.5 cm^{-1}; for some bands, however, the difference is appreciably greater (column 4).

The deviations from the values of Sponer et al as a rule increase when we go to the spectrum of benzene vapor at 0.5 mm Hg pressure in the 16 mm quartz cell. The frequency values for the 16 mm cell are listed in column 5 of the table.

Frequencies (cm^{-1}) of benzene absorption bands, reduced to vacuum

Assignment (Ref. 2)	500 mm layer, ν_1 (Ref. 3)	170 mm layer, ν_2 (our data)	$\nu_2-\nu_1$	16 mm layer, ν_3 (our data)	$\nu_3-\nu_1$	16 mm layer Pd on window, ν_4 (our data)	$\nu_4-\nu_1$
1	2	3	4	5	6	7	8
B_0^1	37321,1	37321,7	0,6				
B_0^0	37481,9	37481,8	−0,1				
A_1^0	37616,8	37617,6	0,8				
B_1^1	38245,4	38245,4	0,0				
A_0^2	38281,1	38281,3	0,2				
	38285,2	38284,8	−0,4				
	39292,3	39292,9	0,6				
B_1^0	38407,0	38406,5	−0,5				
A_0^1	38448,4	38447,9	−0,5	38447,7	−0,7	39447,7	−0,7
	38452,4	38452,2	−0,2	38452,1	−0,3	38451,5	−0,9
C_0^0	38523,0	38522,9	−0,1	38522,8	−0,2	38522,5	−0,5
A_0^0	38607,5	38605,6	−1,9				
	38612,2	38611,4	−0,8	38610,3	−1,9	38610,1	−2,1
B_2^1	39168,5	39168,1	−0,4				
A_1^2	39204,5	39206,3	1,8				
	39209,3	39207,9	−1,4				
	39215,6	39215,5	−0,1				
C_1^1	39272,1	39271,8	−0,3				
	39281,4	39279,3	−2,1				
	39287,7	39287,8	0,1				
B_2^0	39330,6	39329,9	−0,7				
C_0^2	39371,2	39370,9	−0,3	39370,5	−0,7	39371,4	0,2
	39376,1	39375,6	−0,5				
	40366,4	40365,4	−1,0				

We also obtained the absorption spectrum of benzene forming as a result of catalytic conversion of cyclohexadiene for 15 min at 85° on transparent palladium films applied to the windows of the 16 mm cell. The initial pressure of the cyclohexadiene vapor was 0.5 mm Hg. The band frequencies obtained in this case are listed in column 7.

We noted above that the pressure of benzene in these experiments could not exceed 0.33 mm Hg. The intensities of the absorption bands in this spectrum, however, as may be seen from Fig. 2, scarcely differ from the intensities of the corresponding bands in the spectrum of benzene admitted into the same cell but without Pd films, when the vapor pressure was 0.5 mm Hg.

In addition to the increase in the coefficient of absorption of benzene adsorbed on palladium films, as compared to benzene adsorbed or deposited on the quartz windows, we detected small differences as regards the band frequencies (compare columns 5 and 7). Further investigations of this effect are indicated with a view to determining the reasons for the increase in absorption and the apparent frequency shifts of some of the absorption band.

We take this opportunity to thank V.M.Tatevskii for valuable advice.

Laboratory of Molecular Spectroscopy,
Chemical Faculty of
Moscow State University

References

1. V.I.Shimulis, V.D.Iagodovskii & V.M.Griaznov, Vestnik, Moscow State University, No.4, 257 (1957).
2. H.Sponer, G.Nordheim, A.L.Sklar & E.Teller, J.Chem.Phys., 7, 207 (1939).
3. W.F.Radle & C.A.Beck, J.Chem.Phys., 8, 507 (1940).

* * * * * * *

APPLICATIONS OF THE WEAK-FIELD FREE NUCLEAR INDUCTION TECHNIQUE IN HIGH-RESOLUTION RADIO SPECTROSCOPY

- A.A.Morozov, A.V.Mel'nikov & F.I.Skripov

Some years ago Packard & Varian[1] proposed a new technique for observing free nuclear precession, a technique which made it possible to extend investigations of this effect into the range of very weak magnetic fields (of the order of the Earth's field). What is observed is essentially a decaying chain of oscillations induced in the receiver coil owing to precession of the nuclear magnetization vector, arising after nonadiabatic removal of an auxiliary strong field (the equipment has been described in Ref.2). Until now, the new technique has been used almost exclusively for precision measurements of weak fields. Yet it undoubtedly presents a considerable interest from the viewpoint of radio spectroscopic studies; in particular, in view of the great homogeneity of the Earth's field, the technique allows of realizing a very high absolute resolving power (to fractions of a cycle) with relatively simple equipment.

In the present report we shall give two examples of application of the weak field technique to the problems of radio spectroscopy.

The first problem consists of investigating the fine structure of nuclear resonance signals due to indirect (electron shell) interactions of nonequivalent nuclei in a molecule. It has been noted by Gutowsky et al[3] that the character of the splitting in this case does not depend on the field level, provided the inequality $|\nu_A - \nu_B| \gg a/h$ is fulfilled (a is a coupling constant characterizing the magnitude of the splitting; ν_A and ν_B are the resonance frequencies of the interacting nuclei). Hence in such investigations the absolute resolving power is important and the use of weak fields is justified.

For our investigation we chose tributyl phosphate (TBP): $O = P(-O-CH_2-CH_2-CH_2-CH_3)_3$. In strong fields this molecule would yield a nuclear resonance signal with a very complex structure owing to a) chemical shifts due to nonequivalently located proton groups, b) indirect magnetic interaction between these groups and c) indirect interaction of the protons with the P^{31} nucleus. In the case of a weak (the Earth's) field, the chemical shifts virtually disappear, which in turn should lead to the absence of splitting produced by the indirect magnetic interactions between proton groups (nonfulfillment of the inequality $|\nu_A - \nu_B| \gg a/h$). Such simplification of the spectrum, which makes it possible to separate the mutual influences of nuclei of different types (in this case H^1 and P^{31}), is one of the advantageous features of the weak field technique.

One of the photographs of the free nuclear induction signal obtained from a TBP sample with a volume of 600 cm^3 is reproduced at the top in Fig.1,a. The recording was carried out by means of a loop oscillograph with a film advance rate of 30 mm/sec; so that the individual periods of the signal, which had a frequency of ~2160 cps, are not resolved in the photograph. In order to slow

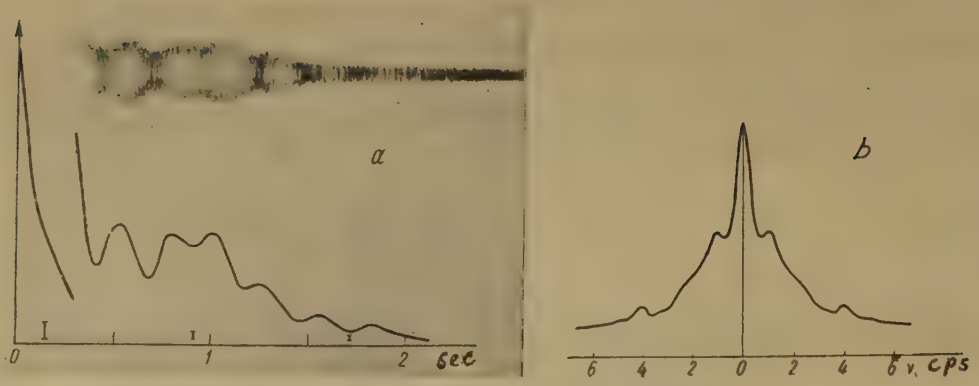

Fig.1. a - Photograph of free proton induction signal from tributyl phosphate (TBP) and its averaged envelope (in the t = 0 to 0.6 sec range the vertical scale is 5 time smaller than for t > 0.6 sec); b - spectral representation of the same signal (Fourier transform).

down the attenuation of the free precession, the sample was heated to 200°. As may be seen in the photograph the signal envelope exhibits a clearly pronounced beat pattern, indicative of the multiplet character of the spectrum.

The initial signal-to-noise ratio exceeds 40. Inasmuch, however, as the beats are evident primarily after the amplitude has decreased by an appreciable factor, further processing of the experimental results was based on careful averaging of the signal envelopes from the 9 best photographs (with preliminary subtraction of the average noise level). The final appearance of the envelope is shown in Fig.1,a (bottom) with evaluations of the probable error at different points. The multiplet structure of the spectrum obtained by numerical conversion (Fourier transforms) is shown in Fig.1,b.* It will be seen that there are clearly resolved components of the signal only ±1 cycles distant from the central peak (it should be noted that the actual resolution of the equipment is even higher, so that essentially the natural line width is observed in this case).

Inasmuch as the spin of the P^{31} nucleus is 1/2, any group of equivalently located protons in the TBP molecule should give a doublet signal. The centers of all the doublets should coincide, while the magnitude of the splitting should be the greater, the stronger the interaction with the P^{31} nucleus. Hence the end components ($\Delta\nu$ = ±4 cps) are obviously due to protons of the three CH_2 groups closest to the P core, etc. The central and most intense line in the spectrum is formed by superposition of the unresolved components from the more remote parts of the molecule. It must be noted, however, that upon more detailed examination of the spectrum there become evident certain anomalies that cannot be explained in the framework of the above simple scheme. Among these anomalies are the presence of the broad peaks at $\Delta\nu$ = ±2.5 cps, the very slow falling off of the spectral curve at large values of $\Delta\nu$, and the very poor agreement between the integral intensities of the observed components and the number of H atoms in

---

*The data at this stage of the work must be regarded as preliminary inasmuch as the method of conversion to the spectrum requires more rigorous justification. In particular, the symmetric character of the spectrum was postulated in carrying out the Fourier transform (in this case symmetry should be expected on the basis of the current concept regarding the mechanism of the effect).

the corresponding groups. The most probable reason for these anomalies, in our opinion, are indirect interactions between protons, which so far have not been taken into account. Although by going over to weak fields the spectrum is undoubtedly simplified, there still remains a certain nonequivalence of the protons, connected with differences in their interaction with the P^{31} nucleus. This nonequivalence is probably sufficient for the spin-spin coupling of the protons to have an appreciable influence on the character of the spectrum. At present we are carrying out a theoretical analysis of this case.*

The second problem we shall touch upon here is of interest from the standpoint of metrology and possibly for the theory of magnetic shielding of nuclei in molecules. As is known, the invariance of the proportionality factor between the field intensity and the nuclear precession frequency $k = \gamma(1 - \sigma)/2\pi$ (where γ is the nuclear gyromagnetic ratio and σ is the coefficient of magnetic shielding of the nucleus by the electron shell) has been thoroughly checked experimentally only in the range of strong fields. In weak fields, the experimentally covered range is still too narrow to permit of drawing a general inference regarding the invariance of k; moreover difficulties connected with precise measurement of the field strength have made it impossible to establish the constancy of k with an uncertainty smaller than 0.01%.[5,6]

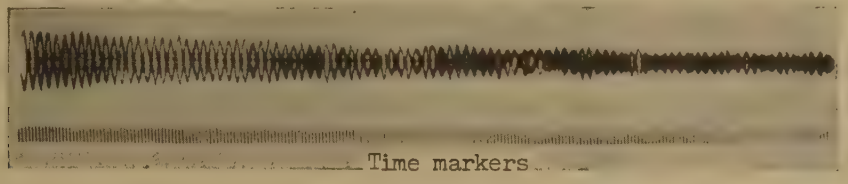

Fig.2. Beats between the precessions of H^1 and F^{19} nuclei; beat frequency ~130 cps.

Hence we undertook measurements of the ratio of the resonance frequencies $\nu(F^{19})/\nu(H^1) = k(F^{19})/k(H^1)$ in the Earth's magnetic field and a comparison of our results with the data available for strong fields. By way of the fluorine containing substances, we used $CH_2Cl\text{-}CFCl_2$ or $CFCl_3$; by way of proton containing substance - distilled water. Both samples were placed in the same receiver coil. The frequency of the beats was measured by comparing with time markers simultaneously recorded on the film (Fig.2). We also tried simultaneous recording of both signals by means of a two-channel system. Upon averaging over a series of measurements, we obtained the following results:

$$CF_2Cl\text{-}CFCl_2 \text{ and } H_2O: \quad k(F^{19})/k(H^1) = 0.940920 \pm 0.000020;$$
$$CFCl_3 \text{ and } H_2O: \quad k(F^{19})/k(H^1) = 0.940987 \pm 0.000030.$$

In strong fields Siegbahn & Lindström[7] obtained a value of 0.940934± ±0.000015 for $k(F^{19})/k(H^1)$ in $CF_2Cl\text{-}CFCl_2$ and water, respectively. Thus the divergence between the data for strong and weak fields in only 0.0015% and well within

---

*After submission of the abstract of this report to the Organizing Committee of the 11th All-Union Conference on Spectroscopy, there appeared the first report[4] in the foreign literature on investigation of the fine structure of nuclear magnetic resonance in the Earth's field. We note that the authors of this contribution with no argumentation assert that in a weak field there should be observed a single averaged beat frequency. Our experimental results for TBP show that this is not necessarily always the case.

the limits of the experimental error. It may safely be assumed that both $k(F^{19})$ and $k(H^1)$ remain constant (at least within the same limits), for otherwise, it would have to be inferred that the changes in $k(F^{19})$ and $k(H^1)$ in going from strong to weak fields are identical, which is scarcely plausible in view of the fact that the substances and their nuclear precession frequencies are different.

There are no data on the $CFCl_3$-water pair in strong fields. However, from our results one can calculate the chemical shift of the F^{19} signal in the Earth's field in going from CF_2Cl-$CFCl_2$ to $CFCl_3$; computations yield $(0.7\pm0.3)\cdot10^{-4}$. Measurements of this quantity in strong fields[8] gave $(0.73\pm0.02)\cdot10^{-4}$, i.e., again we have agreement within the limits of the experimental error. It is interesting to note that for detection of the chemical shift in this case, it was necessary to measure the difference between two resonance frequencies amounting to only 0.14 cycle.

Physical Scientific Research Institute
"A.A.Zhdanov" Leningrad State University

References

1. M.Packard & R.Varian, Phys.Rev., 93, 941 (1954).
2. A.V.Mel'nikov, A.A.Morozov, A.Ia.Rotshtein, F.I.Skripov & S.V.Smirnov, Zhur.tekh.fiz., 28, 901 (1958).
3. H.S.Gutowsky, D.W.McCall & C.P.Slichter, J.Chem.Phys., 21, 279 (1953).
4. D.F.Elliott & R.T.Schumacher, J.Chem.Phys., 26, 1350 (1957).
5. R.M.Brown, Phys.Rev., 78, 530 (1950).
6. W.Wilhelmy, Ann.Physik., 6 Folge, 19, 329 (1957).
7. K.Siegbahn & G.Lindström, Arkiv. Fys., 1, 193 (1949).
8. P.M.Borodin & F.I.Skripov, Transactions of the Tenth All-Union Conference on Spectroscopy, L'vov, 1956.

ROTATIONAL SPECTRUM OF WATER VAPOR IN THE 50 TO 1500 μ REGION*

- N.G. Iaroslavskii & A.E. Stanevich

The rotational spectrum of H_2O has been studied by a number of authors.[1-5] It has been investigated in greatest detail in the 18 to 135 μ region[4,5] and in the middle infrared (4.5-13 μ) region[6] in which the ν_2 (6.26 μ) vibrational absorption band of the H_2O molecule is located. Analysis of the rotational structure of this band made it possible to calculate the rotational energy levels of H_2O for the ground state of the molecule and evaluate the molecular constants.

Recently, a number of investigators[7-10] have obtained the rotational spectrum of H_2O in the longer wavelength section of the infrared range; however, they did not study it in detail, but only recorded it primarily for the purposes of calibration and checking the operation of their long wavelength spectrometers.

Below we give the results of our investigation of the rotational spectrum of H_2O in the 50 to 1500 μ (200 to 7 cm^{-1}) region at different water vapor pressures and under optimum recording conditions.

The absorption spectra of water vapor in room air were recorded on a DIKS-1 vacuum long wavelength grating spectrometer, developed by us and described in Refs.11 & 12. Replacement of the original thermal element with a photoelectron-optical amplifier by the optical acoustical radiometer developed recently by N.A. Pankratov[13] made it feasible to record the absorption spectra of different substances by means of an EPP-09 recorder in the 50 to 1500 μ region with a maximum resolution of 0.2-0.3 cm^{-1}, the average accuracy in determining wave numbers being 0.02 cm^{-1} and intensities <10%.

To encompass the entire spectral region from 50 to 1500 μ, we used 5 interchangeable echelette gratings: 3 gratings with constants of 0.0833, 0.1666 and 0.5 mm (12, 6 and 2 lines per mm, respectively) were prepared in the laboratory of F.M. Gerasimov; the other two gratings with spacing constants of 1.5 and 2.5 mm were ruled on a precision milling machine. The radiation source in the 50 to 100 μ region was a platinum ribbon coated with thorium oxide and heated to 1580° by electric current; the source for the 100 to 1500 μ region was a PRK-4 mercury tube. To exclude the higher order spectra and the scattered short wavelength radiation, we used a) selective modulation with a frequency of 9 cps (compensated KBr interrupter), b) reflecting filters working in the zero order of the echelette gratings with constants 0.3, 0.5 and 0.85 mm for the 140-300, 300-800 and 50--1500 μ spectral ranges, respectively, and c) transmitting filters: a 4 mm thick crystal quartz window over the radiometer and a plate of 1 mm thick polyethylene covered on both sides with a thick layer of turpentine black mounted in front of the radiation detector. In working in the 50-200 μ region we also used crystalline "residual" reflectors. The use of these diverse filtration procedures reduced the amount of scattered radiation in almost the entire spectral range to a few percent; the exceptions were a few grating "glare" intervals in which the background intensity was somewhat higher.

In obtaining the absorption spectra of H_2O vapor in air, the vacuum chambers of the source and spectrometer were connected by means of a sylphon bellows and the entire instrument was evacuated as a whole. The air pressure was reduced to the point where the individual H_2O bands were clearly resolved and their absorption lay in the 30-80% range. With an absorbing layer thickness of 7.5 meters (in the DIKS-1 instrument) and a relative air humidity of 70-80% at 20°, these conditions were attained for the middle wavelength portion of the spectrum at pressures of some tens of millimeters Hg (for the far infrared - at atmospheric pressure).

---

*Detailed report in "Optika i spektroskopiia, 5, 384 (1958).

Wave numbers and wavelengths of absorption bands in the rotational spectrum of H_2O

50—100 μ

Values			Transition $J''_\tau \rightarrow J'_\tau$	Values			Transition $J''_\tau \rightarrow J'_\tau$
Observed		Calculated		Observed		Calculated	
ν, cm^{-1}	λ, μ	ν, cm^{-1}		ν, cm^{-1}	λ, μ	ν, cm^{-1}	
		214,64	$9_{-7}—10_{-7}$			155,61	$8_2 —8_4$
214,35	46,653	213,98	$6_{-2}—7_{-2}$			154,12	$9_1 —9_3$
		212,71	$9_{-6}—10_{-8}$	153,50	65,147	153,47	$5_{-3}—6_{-3}$
		212,66	$10_{-9}—11_{-11}$			152,43	$10_{-7}—10_{-5}$
		212,66	$10_{-10}—11_{-10}$			151,28	$6_{-3}—7_{-5}$
208,40	47,985	208,41	$4_{-1}—5_1$	150,50	66,445	150,49	$2_1 —3_3$
		202,92	$3_2—4_4$			149,89	$10_0 —10_2$
202,80	49,310	202,76	$3_3—4_3$	149,10	67,069	149,10	$2_2 —3_2$
		202,47	$5_{-1}—6_{-1}$	145,00	68,966	144,97	$10_{-8}—10_{-6}$
		200,00	$10_4—10_{-6}$			141,50	$8_{-7}—8_{-5}$
200,10	49,975	200,00	$10_3—10_{-5}$	140,65	71,098	140,64	$4_{-2}—5_{-2}$
		199,23	$9_5—9_7$	139,70	71,582	139,72	$6_{-6}—7_{-6}$
		199,23	$9_4—9_6$	139,00	71,942	139,04	$6_{-5}—7_{-7}$
		198,39	$8_6—8_8$			138,95	$9_0 —10_{-2}$
		198,39	$8_5—8_7$			138,88	$8_{-8}—8_{-6}$
		198,06	$11_{-8}—11_{-10}$			137,83	$10_{-3}—10_{-1}$
		197,77	$11_{-11}—11_{-9}$			135,86	$9_{-6}—9_{-4}$
		197,62	$9_{-2}—10_{-4}$	135,30	73,910	135,30	$10_{-5}—10_{-3}$
197,55	50,620	197,54	$8_{-6}—9_{-6}$			134,45	$9_{-2}—9_0$
195,90	51,046	195,90	$8_{-3}—9_{-5}$	133,45	74,934	133,44	$6_{-1}—7_{-3}$
		194,39	$9_{-9}—10_{-9}$	132,65	75,386	132,68	$2_{-1}—3_1$
194,38	51,467	194,37	$9_{-8}—10_{-10}$			132,41	$8_{-1}—8_1$
		193,52	$8_{-5}—9_{-7}$			131,98	$5_2 —5_4$
188,25	53,121	188,27	$4_0 —5_0$			131,92	$7_0 —7_2$
183,45	54,511	183,43	$5_{-5}—5_1$			131,91	$6_1 —6_3$
181,43	55,118	181,44	$7_{-5}—8_{-5}$			131,76	$5_3 —5_5$
		179,54	$8_4 —8_6$			131,01	$6_2 —6_4$
		179,54	$8_3 —8_5$	128,65	77,730	128,66	$7_1 —7_3$
		179,32	$9_2 —9_4$	127,00	78,740	127,02	$3_{-1}—4_{-1}$
		179,31	$10_1 —10_3$			126,75	$5_{-2}—6_{-4}$
		179,21	$10_{-9}—10_{-7}$	124,90	80,064	124,97	$7_0 —8_{-2}$
		179,18	$9_3 —9_5$	124,35	80,418	124,32	$9_{-4}—9_{-2}$
		178,83	$10_2 —10_4$			124,10	$8_0 —8_{-2}$
		178,63	$10_{-10}—10_{-8}$	123,00	81,301	123,07	$7_{-6}—7_{-4}$
178,60	55,991	178,59	$7_5 —7_7$	121,90	82,032	122,88	$9_{-7}—9_{-5}$
		178,59	$7_4 —7_6$			121,88	$5_{-5}—6_{-5}$
177,55	56,322	177,58	$3_0 —4_2$			120,50	$8_{-5}—8_{-3}$
		176,13	$8_{-8}—9_{-8}$	120,13	83,243	120,12	$5_{-4}—6_{-6}$
176,10	56,786	176,06	$8_{-7}—9_{-9}$	117,93	84,796	117,92	$7_{-7}—7_{-5}$
173,47	57,647	173,47	$7_{-4}—8_{-6}$			116,90	$9_{-1}—9_1$
		173,46	$3_{-2}—4_0$	116,65	85,726	116,64	$8_{-3}—8_{-1}$
170,35	58,703	170,33	$3_1 —4_1$			111,73	$10_{-2}—10_0$
		169,93	$11_{-8}—11_{-6}$	111,11	90,001	111,11	$2_0 —3_0$
166,65	60,006	166,63	$6_{-4}—7_{-4}$			111,11	$7_{-2}—7_0$
		166,44	$7_{-2}—8_{-4}$	107,78	92,782	107,79	$6_{-1}—6_1$
161,85	61,786	161,82	$4_{-4}—4_2$	107,15	93,327	107,15	$7_{-4}—7_{-2}$
		160,29	$9_{-8}—9_{-6}$			106,12	$5_0 —5_2$
160,20	62,422	160,24	$8_{-1}—9_{-3}$	105,67	94,634	105,68	$6_{-5}—6_{-3}$
		158,96	$9_{-9}—9_{-7}$			105,67	$4_1 —4_3$
157,85	63,351	157,86	$7_{-7}—8_{-7}$			105,37	$8_1 —9_{-1}$
		157,66	$7_{-6}—8_{-8}$	104,53	95,666	104,55	$4_{-4}—5_{-4}$
		156,71	$7_{-2}—7_4$			104,31	$4_2 —4_4$
		156,50	$7_3 —7_5$			104,07	$9_1 —10_{-3}$
		156,44	$6_4 —6_6$			101,55	$5_1 —5_3$
156,45	63,918	156,44	$6_3 —6_5$	100,55+	99,453+	100,53	$4_{-3}—5_{-5}$
		156,40	$8_1 —8_3$			100,12	$10_{-6}—10_{-4}$
		156,30	$9_0 —9_2$			100,03	$8_{-6}—8_{-4}$
		155,88	$10_{-1}—10_1$				

Continuation of wave number & wavelength table

100—1500 μ

Values			Transition $J''_\tau \to J'_\tau$	Values			Transition $J''_\tau \to J'_\tau$
Observed		Calculated		Observed		Calculated	
ν, cm^{-1}	λ, μ	ν, cm^{-1}		ν, cm^{-1}	λ, μ	ν, cm^{-1}	
		99,07	$4_{-1}—5_{-3}$	55,42	180,4	55,43	$2_{-1}—2_1$
99,07+	100,9+	99,02	$1_0—2_2$	53,45	187,1	53,44	$4_{-4}—4_{-2}$
		98,67	$5_0—6_{-2}$			53,15	$9_{-5}—8_1$
		96,16	$6_0—6_2$	52,55	190,4	52,56	$7_{-5}—6_1$
96,15+	104,0+	96,16	$6_{-4}—6_{-4}$			51,42	$5_2—6_0$
		96,05	$6_{-3}—6_{-1}$			50,87	$10_7—11_5$
		94,39	$9_2—10_0$			47,47	$10_{-8}—9_{-2}$
92,58+	108,0+	92,54	$1_1—1_2$	47,04+	212,4+	47,05	$5_{-3}—5_{-1}$
89,53	111,7	89,53	$5_{-4}—5_{-2}$			44,79	$8_{-6}—7_0$
		88,87	$7_{-1}—7_1$			44,56	$9_6—10_4$
		88,71	$5_{-3}—4_3$	44,16	226,5	44,13	$5_1—6_{-3}$
88,04	113,6	88,06	$3_{-3}—4_{-3}$			43,62	$9_{-7}—8_{-1}$
		87,88	$5_{-2}—5_0$			43,28	$7_{-1}—8_{-5}$
		85,67	$9_{-1}—10_{-5}$	42,54	235,1	42,56	$6_3—7_1$
85,61	116,8	85,60	$6_1—7_{-1}$	40,98	244,0	40,98	$2_0—2_2$
		84,71	$8_2—9_{-2}$			40,45	$8_5—9_3$
		84,49	$8_0—9_{-4}$	40,23	248,6	40,25	$4_{-2}—4_0$
82,11	121,8	82,11	$4_{-1}—4_1$			39,59	$7_4—8_2$
81,01	123,4	80,98	$9_{-5}—9_{-3}$	38,80	257,7	38,80	$7_5—8_2$
79,77	125,4	79,77	$3_{-2}—4_{-4}$			38,80	$3_{-1}—3_2$
		79,15	$8_{-2}—8_0$			38,63	$5_3—6_{-1}$
79,00	126,6	78,97	$3_0—3_2$			38,45	$2_1—3_{-1}$
78,22	127,8	78,21	$7_{-5}—7_{-3}$			38,27	$8_{-7}—7_{-3}$
77,50	129,0	77,54	$9_{-3}—9_{-1}$			38,24	$10_9—11_7$
		75,79	$10_{-4}—10_{-2}$	37,13	269,3	37,13	$0_0—1_0$
75,55+	132,4+	75,55	$4_{-3}—4_{-1}$			36,95	$10_{-6}—9_0$
		74,91	$7_1—8_{-3}$	36,65	272,8	36,59	$3_{-3}—3_{-1}$
74,12	134,9	74,09	$5_{-5}—5_{-3}$	32,96	303,4	32,93	$1_0—2_{-2}$
73,28	136,5	73,24	$3_1—3_3$	32,09	311,6	32,26	$4_2—5_{-2}$
72,20+	138,5+	72,21	$2_{-2}—3_{-2}$	30,50	327,9	30,48	$3_2—4_0$
		69,64	$8_{-4}—8_{-2}$			28,99	$9_3—10_6$
69,20	144,5	69,20	$3_0—4_{-2}$	27,81	359,6	27,78	$8_{-2}—9_{-6}$
68,10	146,8	68,13	$4_0—4_2$	25,11	398,2	25,11	$2_{-2}—2_0$
		67,70	$10_5—10_3$			21,67	$8_7—9_5$
67,27	148,6	67,25	$6_{-4}—5_2$			20,63	$4_3—5_1$
		65,87	$8_3—9_1$	18,58	538,2	18,58	$1_{-1}—1_1$
		64,96	$9_4—10_2$			16,61	$7_7—8_3$
		64,01	$3_{-2}—3_0$			16,61	$7_6—8_4$
64,00	156,2	64,01	$4_1—5_{-1}$	16,24	615,8	16,24	$7_{-6}—6_{-2}$
		63,21	$4_{-4}—3_2$			15,83	$4_4—5_0$
		62,81	$9_{-8}—8_{-4}$	15,56	642,7	15,60	$5_4—6_2$
62,33+	160,4+	62,29	$5_{-1}—5_1$	15,01	666,2	14,98	$3_3—4_{-1}$
		60,10	$11_8—12_6$	14,76	677,5	14,74	$6_5—7_3$
59,95+	166,8+	59,95	$7_{-3}—7_{-1}$			14,66	$5_5—6_1$
		59,80	$6_{-4}—6_{-2}$	14,52	688,7	14,53	$6_6—7_2$
58,87+	169,9+	58,87	$6_{-2}—6_0$			13,00	$11_{-8}—10_{-4}$
57,28+	174,6+	57,29	$2_{-1}—3_{-3}$	12,63	791,8	12,67	$3_1—4_{-1}$
		57,29	$6_{-6}—5_0$	10,87	920,0	10,86	$4_0—5_{-4}$
		57,13	$5_{-5}—4_1$			10,78	$9_{-3}—10_{-7}$
55,68	179,6	55,69	$1_{-1}—2_{-1}$			6,12	$2_2—3_{-2}$

By way of illustration, the spectrograms obtained for the 145 to 200 μ and 500 to 1450 μ ranges are reproduced in Fig.1. These figures show the resolution attained (0.26 cm^{-1} at 180 μ) and indicate the scanning rates and the signal-to-noise ratios.

In the entire 50 to 1500 μ range there were recorded 150 absorption bands, 94 of which were identified as fundamental frequencies in the rotational spectrum of H_2O and 11 as manifestations of some of the fundamental frequencies in the second order (see table). The measured wave numbers are compared with the wave numbers calculated from the rotational level energies given by Benedict et al[6].

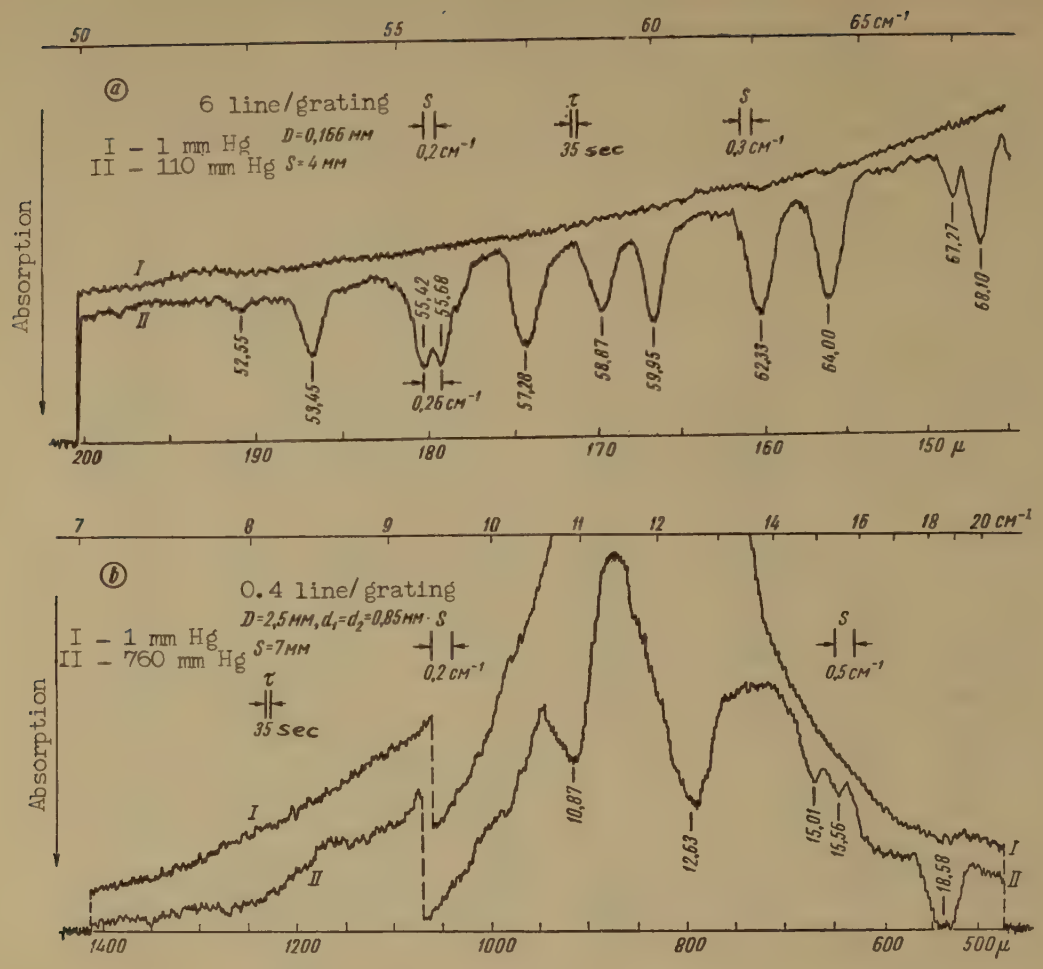

Fig.1. Spectrograms of H_2O vapor in the a) 145-200 μ region and b) 450-1450 μ region.

The plus signs (+) in the table identify wave numbers and wavelengths which were obtained not only in the first but also in the second order. As will be evident from the table, the divergence between the observed and calculated wave numbers is 0.02 cm^{-1} on the average, i.e., does not exceed the measurement error.

Fig.2 gives a diagram of the rotational spectrum of H_2O in the 50 to 1500 μ (200 to 7 cm^{-1}) region. The heights of the heavy vertical bars indicate the relative intensities of the individual bands. The light vertical lines in the upper part of the diagram give the calculated wave numbers; the triangles (▽) indicate the theoretical values of the relative intensities of some of the bands according to Randall et al[3].

It may be of interest to compare our results with the data of other authors. Whereas in the 200 to 75 cm^{-1} (50 to 136 μ) region the spectrum obtained in the present study differs little from the spectrum given by Randall et al[3] and only 3 new bands were detected in this spectral region, in the lower frequency 75 to 7 cm^{-1} (136 to 1500 μ) interval, which was studied earlier only by McCubbin & Sinton[7] and Genzel & Eckhardt[9,10], we found 27 new bands. The transition assignments for them are also given in the table.

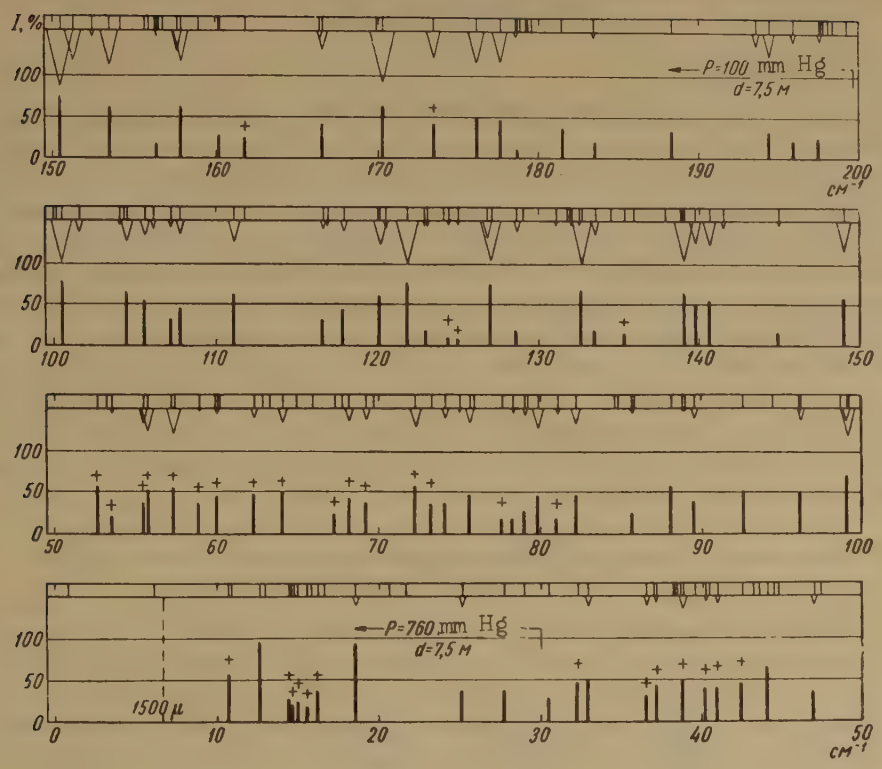

Fig.2. Diagram of rotational spectrum of H_2O in the 50 to 1500 μ region. The bands identified by a + were obtained for the first time in this study.

References

1. R.Mecke, W.Baumann & K.Freudenburg, Zeits.f.Phys., 81, 313, 445, 465 (1933).
2. R.B.Barnes & W.S.Benedict, Phys.Rev., 47, 918 (1935).
3. H.M.Randall, D.M.Dennison, N.Ginsburg & L.R.Weber, Phys.Rev., 52, 160 (1937).
4. N.Fuson, H.M.Randall & D.M.Dennison, Phys.Rev., 56, 982 (1939).
5. D.M.Dennison, Rev.Mod.Phys., 12, 175 (1940).
6. W.S.Benedict, H.H.Classen & J.H.Shaw, J.Res.NBS, 49, 91 (1952).
7. T.K.McCubbin & W.A.Sinton, JOSA, 42, 113 (1952).
8. R.A.Oetjen, W.H.Haynie, W.M.Ward, R.L.Hansler, H.E.Schauwecker & E.E. Bell, JOSA, 42, 559 (1952).
9. L.Genzel & W.Eckhardt, Zeits.f.Phys., 139, 578 (1954).
10. L.Genzel, Zeits.f.Phys., 144, 311 (1956).
11. N.G.Iaroslavskii, B.A.Zheludov & A.E.Stanevich, Optika i spektroskopiia, 1, 507 (1956).
12. N.G.Iaroslavskii, Usp.fiz.nauk, 62, 159 (1957).
13. N.A.Pankratov, Opt.mekh.prom., No.3, 7 (1957).

DETERMINATION OF THE MOLECULAR STRUCTURE OF HDSe FROM ITS ROTATIONAL MICROWAVE SPECTRUM

- V.G.Veselago

In this study the vibrational spectrum of HDSe was investigated by means of a radiofrequency spectroscope with electric molecular modulation. All the measurements were carried out at the temperature of dry ice and a pressure of $\sim 10^{-2}$ mm Hg. The frequencies of the absorption lines were determined by means of a quartz crystal frequency multiplier which was compared with the 200 Kc signal broadcast by station PV-71. In the 8000 to 43,000 Mc range there were detected 10 transitions; these and the corresponding line frequencies are listed in Table 1. The lines corresponding to some transitions in the low abundance isotopes of selenium were not detected. The average accuracy in measuring the line frequencies is evaluated to be 1 in 10^5, while for some strong lines the accuracy is 1 in $5 \cdot 10^6$. The frequencies of the $10_{55} - 10_{56}$ and $11_{65} - 11_{66}$ transitions were measured only by means of a cavity wavemeter and in this case the accuracies were somewhat lower.

Table 1

Transition	Line frequencies, Mc				
	HDSe^{80}	HDSe^{78}	HDSe^{77}	HDSe^{76}	HDSe^{74}
$1_{10} - 1_{11}$	41476,1	41504,5	41534,1	41549,0	41565,4
$2_{20} - 2_{21}$	9127,75	9138,55	9149,65	9155,85	9161,5
$3_{21} - 3_{22}$	43058,4	43106,6	43156,8	43183,1	43209,8
$4_{31} - 4_{32}$	8756,7	8771,05	8786,05	8793,95	8801,85
$5_{32} - 5_{33}$	33023,0	33075,4	33129,7	33157,4	33188,2
$7_{43} - 7_{44}$	22184,4	22230,0	22277,6	22302,3	22327,7
$9_{54} - 9_{55}$	13827,7	13862,65	13899,3	13918,3	13937,8
$10_{55} - 10_{56}$	—	38629	38724	—	—
$11_{65} - 11_{66}$	8215,8	8240,6	8266,6	8280,0	8293,6
$12_{66} - 12_{67}$	—	23249,8	—	—	—

In addition to measuring the line frequencies, we investigated their Stark splittings[1] for the purpose of determining the dipole moment of the HDSe molecul We obtained a value of 0.62 debye for the dipole moment, which is in marked disagreement with the data of Jache et al[2] who obtained a value of 0.24 debye for the dipole moment of the D_2Se molecule. It should be noted, however, that our value of 0.62 debye is in good agreement with theory if one uses the curve for the variation of the ionic character of the bond with the electronegativity of the atoms forming it, given by Townes & Schawlow[3].

As will be seen from Table 1, the observed transitions represent transition with $\Delta J = 0$ (Q branch). Calculations indicate that the given wavelength range includes a series of transitions with $\Delta J = 1$ (R and P branches); but the intensity of these transitions is much lower than that of the Q branch transitions. Tw Q branch transitions, namely, $6_{42} \rightarrow 6_{43}$ and $8_{44} \rightarrow 8_{45}$, lie at frequencies of about 6000 to 60,000 Mc, respectively, and hence were not observed by us inasmuch as these frequencies lie outside the range of our spectroscope.

In the rigid asymmetrical top approximation the frequency of a Q branch transition is given by the relation

$$\nu = \frac{A - C}{2} E'(\varkappa). \qquad (1)$$

Here $E'(\varkappa)$ is a tabulated[4] function of the molecular asymmetry parameter

$\varkappa = \frac{2B-A-C}{A-C}$, and A, B and C are the reciprocals of the moments of inertia of the molecule. Inasmuch as the structure of the HDSe molecule is characterized by only two parameters - the bond length $r_{Se-H} = r_{Se-D} = r$ and the H-Se-D valence angle - for its determination, it is sufficient to know the frequencies of only two transitions. However, if on the basis of the molecular structure determined in this manner one evaluates the frequencies of the other transitions, there is obtained a considerable divergence from the experimental values. This indicates that in carrying out such calculations one must take into account a correction for the presence of centrifugal distortion[5]. The pertinent theory[6] shows that in this case the transition frequency ν_{JK} depends on seven unknown parameters, namely, (A - C)/2, $\varkappa$ and five centrifugal distortion constants: x_1, x_2, x_3, x_4 and x_5, that is,

$$\nu_{JK} = \frac{A-C}{2} E'(\varkappa)\,[1 + KJ(J+1)\,x_1 + (K-1)\,J(J+1)x_2 + K(K^2+2)\,x_3 + \\ + \begin{cases} -x_5, & \text{if } K = 1, \\ x_4 - 2x_5, & \text{if } K \text{ is even}, \\ 4x_4 - x_5, & \text{if } K \text{ is odd}. \end{cases} \qquad (2)$$

Thus in order to determine all the unknowns, one must solve a set of seven nonlinear equations with seven variables. Inasmuch as conventional solution of such a set of equations is extremely difficult, the problem was solved with the aid of the BESM electronic computer. The frequencies of the seven transitions, $1_{10}-1_{11}$, $2_{20}-2_{21}$, $3_{21}-3_{22}$, $4_{31}-4_{32}$, $5_{32}-5_{33}$, $7_{43}-7_{44}$, and $9_{54}-9_{55}$ were used in the computations.

The values obtained are listed in Table 2. The absolute values of (A - C)/2 listed in the table comprise an absolute error of ±3 Mc, the values of $\varkappa$ an uncertainty of ±0.00005. The data of Table 2 were then used for calculating the frequencies of $10_{55}-10_{56}$, $11_{65}-11_{66}$ and $12_{66}-12_{67}$ transitions. The frequencies calculated in this manner are compared in Table 3 with the observed values. The table also lists the frequencies calculated on the basis of the rigid top model; in this case for determining the molecular structure, we used the frequencies of the $1_{10}-1_{11}$ and $2_{20}-2_{21}$ transitions.

Table 2

	$HDSe^{83}$	$HDSe^{80}$	$HDSe^{78}$	$HDSe^{77}$	$HDSe^{76}$
$\frac{A-C}{2}$, Mc	79744	79760	79782	79785	79799
$\varkappa$	−0,47911	−0,47884	−0,47862	−0,47843	−0,47829
$x_1 \cdot 10^4$	−0,410	−0,439	−0,433	−0,506	−0,466
$x_2 \cdot 10^3$	0,162	0,168	0,166	0,177	0,174
$x_3 \cdot 10^3$	−0,510	−0,519	−0,517	−0,525	−0,533
$x_4 \cdot 10^4$	0,597	0,557	0,591	0,531	0,559
$x_5 \cdot 10^4$	−0,132	−0,122	−0,134	−0,135	−0,101

All the data in Table 3 pertain to the $HDSe^{80}$ molecule. As may be seen from the table, taking into account "non-rigidity" of the molecule appreciably improves the agreement of the calculated with the experimental frequency values. The values of (A - C)/2 and $\varkappa$, taken from Table 2, can be used for calculating the structure of the HDSe molecule. The values of (A - C)/2 and $\varkappa$ are related with r and φ by the following expressions:

Table 3

Transition	ν_{exp}, Mc	ν_{calc}, Mc	ν_{rigid}, Mc	$\nu_{calc}-\nu_{exp}$, Mc	$\nu_{rig}-\nu_{exp}$, Mc
$1_{10}-1_{11}$	41504,5				
$2_{20}-2_{21}$	9138,55				
$3_{21}-3_{22}$	43106,6		43104,2		—2,4
$4_{31}-4_{32}$	8771,05		8801,3		30,25
$5_{32}-5_{33}$	33075,4		33138,4		63,0
$7_{43}-7_{44}$	22230,0		22368,2		138,2
$9_{54}-9_{55}$	13862,65		14043,1		180,45
$10_{55}-10_{56}$	38629	38672	38846	43	217
$11_{65}-11_{66}$	8240,6	8237	8424,5	—3,6	183,9
$12_{66}-12_{67}$	23249,8	23274	23483,3	24,2	233,5

$$\left.\begin{aligned} \frac{k^2}{\left(\frac{A-C}{2}\right)^2 [\sqrt{r(1+\varkappa)}+r][\sqrt{r(1+\varkappa)}+1+\varkappa]} &= \frac{M_1M_2M_3}{M_1+M_2+M_3} r^4 \sin^2\varphi, \\ \frac{k}{\left(\frac{A-C}{2}\right)\sqrt{r(1+\varkappa)}} &= \left(\sin^2\frac{\varphi}{2}\cdot\frac{4M_1M_3+M_2(M_1+M_3)}{M_1+M_2+M_3}+\cos^2\frac{\varphi}{2}\cdot\frac{M_2(M_1+M_3)}{M_1+M_2+M_3}\right) r^2, \end{aligned}\right\} \quad (3)$$

where M_1, M_2 and M_3 are the masses of the hydrogen, selenium and deuterium atoms, respectively, and k is a numerical coefficient. If r is expressed in angstroms, M_1, M_2 and M_3 in atomic mass units and (A - C)/2 in megacycles, $k = 5.05531 \cdot 10^5$.

However, an attempt to solve the above equations showed that they are inconsistent; the incompatibility cannot be explained by experimental errors. In order to make the problem tractable it is necessary to assume that the interatomic distances Se—H and Se—D are not equal. This assumption can be justified physically if we bear in mind that in our calculations no account was taken of zero order vibrations. The frequencies measured by us are proportional to (A - C)/2, i.e., to $1/r^2$. Owing to the presence of zero order vibrations, $1/r^2$ varies harmonically with time and (A - C)/2 proves to be proportional to the averaged value of $1/r^2$. In further calculations, however, instead of the averaged value $(\bar{r})^2$, we shall use

$$r_{eff}^2 = \frac{1}{\overline{\frac{1}{r^2}}} \neq (\bar{r})^2.$$

The magnitude of this inequality will undoubtedly be different for the Se—H and Se—D bonds, which vibrate with different frequencies and amplitudes.

Having made this assumption regarding the inequality of the effective length of the Se—H and Se—D bonds, we can readily solve our problem; there are obtained the following values for the structural parameters:

$$r_{Se-D} = 1.446 \pm 0.001 \text{ Å}, \quad r_{Se-H} = 1.452 \pm 0.001 \text{ Å}, \quad \frac{r_{Se-H}}{r_{Se-D}} = 1.004 \pm 0.001 \text{ Å and } \varphi = 90^\circ.$$

It is interesting to compare these data with the results of other measurements of the structure of the H_2Se and D_2Se molecules. Cameron et al[7], on the basis of the vibrational spectra, obtained $r = 1.6$ Å and $\varphi = 90^\circ$ for the H_2Se molecule. In the work of Palik[8], based on the rotational infrared spectrum of H_2Se, r was found to be equal to 1.47 Å and the angle $\varphi = 91^\circ$. Finally, Jache et al[2] give the results of calculation of the structure of D_2Se on the basis of its rotational microwave spectrum. These authors, using different pairs of rotational transitions with low J, obtained values in the range from 1.447 to

1.469 Å for r and from 90.83 to 91.94° for φ. It will be seen that all the authors referred to above obtained values of r greater than ours. This may be explained by the fact that in their calculations the centrifugal distortion was not taken into account and hence their values of r represent bond lengths averaged over all the rotational states of the molecule. It must also be noted that in the investigations of Cameron et al and Palik, which were carried out in the optical range, the lines associated with individual selenium isotopes were not resolved, which obviously leads to additional errors in determining the value of r.

The writer desires to express his sincere gratitude to A.M.Prokhorov for guidance and constant interest in the work and to V.V.Kobelev for assistance in carrying out the computations on the BESM computer.

"P.N.Lebedev" Physical Institute,
Academy of Sciences of the USSR

References

1. V.G.Veselago, Zhur.eksp. i teor.fiz., 32, 620 (1957).
2. A.W.Jache, P.W.Moser & W.Gordy, J.Chem.Phys., 25, 209 (1956).
3. C.H.Townes & A.L.Schawlow, Microwave Spectroscopy, p.236, - N.Y., 1955.
4. C.H.Townes & A.L.Schawlow, ibid., App.IV - N.Y., 1955.
5. V.G.Veselago & A.M.Prokhorov, Zhur.eksp.i teor.fiz., 31, 731 (1956).
6. R.E.Hillger & M.W.P.Straudberg Phys.Rev., 83, 575 (1951).
7. D.M.Cameron, W.C.Sears & H.H.Nielsen, J.Chem.Phys., 7, 994, (1939).
8. E.D.Palik, J.Chem.Phys., 23, 980 (1955).

ROTATIONAL CONSTANTS OF $FH_2C-CH_2Cl^{35}$ MOLECULES

- I.A.Mukhtarov

The present study was devoted to the microwave spectrum of fluorochloroethane. Many molecules of the halogen derivatives of ethane, in particular, H_3C-CH_2F and H_3C-CH_2Cl have been investigated earlier.[1-3]

The fluorochloroethane molecule is of particular interest in view of the fact that it can exist in different isomeric states, owing to rotation of one atomic group (about a single bond) relative to the other. In this case the moments of inertia of the molecule change, whereas in the earlier studied molecules, the moments of inertia do not change incident to rotation of the atomic group about the single bond. Inasmuch as radiospectroscopic measurements give the rotational constants, which are inversely proportional to the principal moments of inertia, having determined the rotational constants, we can find the azimuthal angle, i.e., determine the isomeric state, provided the other molecular parameters (the lengths of the bonds and the angles between them) are known.

Calculations show that change in the azimuthal angle for fluorochloroethane leads to an appreciably greater alteration of the moments of inertia than would follow from merely changes in the interatomic distances and bond angles. Hence having the rotational constants, we can determine the isomeric state of this molecule.

Calculations of the frequencies and intensities of the absorption lines associated with the rotational transitions in fluorochloroethane in the rigid asymmetrical top approximation for different values of the azimuthal angle and for the two natural isotopes of chlorine showed the following:

1. In the 10 and 30 kMc range one can expect to observe lines with an intensity of 10^{-6}-10^{-8} cm^{-1}.

2. The intensities of the lines corresponding to the trans-isomer are low (10^{-9}-10^{-11} cm^{-1}) and hence probably cannot be detected by present-day equipment.

3. The frequencies of the lines associated with individual transitions in molecules with Cl^{35} and Cl^{37} differ by tens and even hundreds of megacycles. In view of the natural abundances of Cl^{35} and Cl^{37}, in an ordinary sample there should be about 25% molecules with Cl^{37}; hence it should be feasible to observe lines pertaining to the $FH_2C-CH_2Cl^{37}$ molecule, although their intensity should be appreciably lower than the intensity of the corresponding $FH_2C-CH_2Cl^{35}$ lines.

For the purpose of our calculations, we took the following structural data[1,3]: interatomic distances: C-C = 1.54 Å, C-H = 1.1 Å, C-F = 1.37 Å, and C-Cl = 1.78 Å; bond angles: for the CH_2F groups - tetrahedral angle ($109^{\circ}28'$), for the CH_2Cl group - the H-C-H angle = $110^{\circ}20'$, the H-C-C angle = $109^{\circ}49'$ and the C-C-Cl angle = $111^{\circ}30'$.

The chlorine nucleus has spin 3/2 and a quadrupole moment. In view of the quadrupole interaction of the chlorine nucleus with the electric field of the molecule there should obtain hyperfine splitting of the absorption lines.

Calculations of the hyperfine structure of individual lines indicated that it should be feasible to resolve the components. Characteristic is the hyperfine structure of the Q branch lines with $\Delta K_{-1} = 1$ and $\Delta K_1 = 1$, where with $J \geqslant 4$, the most intense are four lines, arranged in pairs; the ratios of the distances between pairs to the distance between the lines comprising the pairs does not depend on the molecular parameters but only on the value of J. Hence one can determine the value of J for a given transition from these ratios.

We investigated the absorption lines associated with rotational transitions in fluorochloroethane in the range from 10,000 to 30,000 Mc by means of a radiospectroscope with Stark modulation. The experiments were carried out at different pressures in the absorption cell and at two temperatures: room temperature

and the temperature of dry ice. The frequencies were determined by comparison with the frequency of the harmonics of a crystal oscillator, controlled by a 200 kc frequency standard. The accuracy of measurement was 0.1 Mc.

Over 400 lines of different intensity were detected in the experimental range. At pressures of $2 \cdot 10^{-2}$ to $4 \cdot 10^{-2}$ mm Hg the hyperfine structure of some of the lines was well resolved; this was utilized for identification of the lines.

From the hyperfine splitting ratios, we were able to determine the values of J for two Q branch transitions (J = 4—4 and J = 5—5). Gordi et al[4] give the following expression for the frequencies of the Q branch absorption lines of a rigid asymmetrical rotor:

$$\nu = \frac{A-C}{2}\left[E_{\tau}^{J}(\varkappa) - E_{\tau'}^{J}(\varkappa)\right], \qquad (1)$$

where A and C are rotational constants, $E_{\tau}^{J}(\varkappa)$ is the reduced energy and $\varkappa$ is the asymmetry coefficient. The function $E_{\tau}^{J}(\varkappa)$ is tabulated in Ref.5. Using Eq.(1) and the experimental frequencies of the J = 4—4 and J = 5—5 lines, we determined the values of A - C and $\varkappa$. Then, using these values, we calculated the theoretical frequencies of the Q branch lines; subsequently, the corresponding lines were observed experimentally close to the calculated frequency values (Table 1).

Table 1

Line frequencies

Transitions	Calculated Mc	Observed Mc	Transitions	Calculated Mc	Observed, Mc
$1_{01}—1_{10}$	10729,7	10729,7	$6_{06}—6_{15}$	15504,3	15500,3
$2_{02}—2_{11}$	11155	11155	$3_{13}—4_{04}$	15207	15204,6
$3_{03}—3_{12}$	11815,5	11815,4	$4_{14}—5_{05}$	21983,6	21979,4
$4_{04}—4_{13}$	12737,6	12736,4	$1_{01}—2_{12}$	22236,7	22236,7
$5_{05}—5_{14}$	13954,8	13952,1	$2_{03}—3_{13}$	27788,4	27786,4
			$5_{15}—6_{06}$	28818,2	28812

From analysis of the experimental hyperfine splittings of the $1_{01}—1_{10}$ line, we determined the values of the quadrupole coupling (χ_a, χ_b and χ_c) in the directions of the principal axes.

In addition we observed and identified a number of R and P branch lines, in particular the $1_{01}—2_{12}$ line (ν = 22236.7 Mc), which is located near the familiar absorption line of H_2O (ν = 22235.22Mc).

For a rigid asymmetrical rotor the frequencies of the absorption lines associated with the $1_{01}—1_{10}$ and $1_{01}—2_{12}$ transitions are[4]:

$$\nu_{1_{01}-1_{10}} = A - C, \qquad (2)$$

$$\nu_{1_{01}-2_{12}} = A + 3C. \qquad (3)$$

From the experimental frequency values for these lines, we determined the rotational constants of the $FH_2C\text{-}CH_2Cl^{35}$ molecule (Table 2).

The calculated frequency values in Table 1 were obtained on the basis of the rotational constants determined from the experimental values of the $1_{01}—1_{10}$ and $1_{01}—2_{12}$ line frequencies.

As will be evident from the table, the experimental and calculated frequency values differ, the difference increasing for larger J. Apparently this divergence is due to appreciable centrifugal distortion inasmuch as the non-rigidity of the bonds was not taken into account in evaluating the rotational constants.

Table 2

α	A, Mc	B, Mc	C, Mc	x
		Calculated		
0°	11674	4098	3156	—0,7788
60°	13067	3412	2926	—0,904
70°	13737	3238	2856	—0,9296
80°	14599	3069	2782	—0,9514
120°	20470	2544	2503	—0,9954
180°	30655	2344	2240	—0,9927
		Experimental		
	13606,45	3289,9	2876,75	—0,923

Comparison of the frequency values shows that the general pattern of the arrangement of the experimental lines is in good agreement with the calculated pattern for $\alpha = 70^\circ$ (α is the angle between the projections of the C—F and C—Cl bonds on the plane normal to the C—C bond).

The calculated values of the rotational constants and the asymmetry parameter for different α are listed in Table 2. It will be seen that the experimental data differ little from the calculated values for $\alpha = 70^\circ$.

Thus the experimental results show that there exists a stable isomeric state of the $FH_2C\text{-}CH_2Cl^{35}$ molecule with $\alpha = 70^\circ$. This is the so-called convoluted isomer which can be realized by rotation of an atomic group about the single bond through 110° from the trans-configuration. From symmetry considerations one might expect 120° rotation (i.e., $\alpha = 60^\circ$). This ~10° deviation of the azimuthal angle is apparently connected with the strong repulsion of the fluorine and chlorine atoms.

The following are the parameters of the $FH_2C\text{-}CH_2Cl^{35}$ molecule calculated on the basis of the experimental data listed in Table 2:

$$\chi_a = -23.5 \text{ Mc},$$
$$\chi_b = -8.8 \text{ Mc},$$
$$\chi_c = +32.3 \text{ Mc}.$$

Finally, we note that we also observed and identified a number of Q branch lines associated with transitions in the $FH_2C\text{-}CH_2Cl^{37}$ molecule. This data is now being processed and the results will be published in the near future.

The writer desires to express his gratitude to Dr.A.M.Prokhorov for valuable advice.

"P.N.Lebedev" Physical Institute,
Academy of Sciences of the USSR

References

1. J.Kraitchman & B.P.Dailey, J.Chem.Phys., 23, 184 (1955).
2. A.I.Barchukov, T.M.Murina & A.M.Prokhorov, Zhur.eksp.i teor.fiz., 29, No.6, (1955); Optika i spektroskopiia, 4, 521 (1958).
3. S.Roselin, R.S.Wagner & B.P.Dailey, J.Chem.Phys., 26, 6,1588 (1957).
4. W.Gordy, W.Smith & R.Trambarulo, Microwave Spectroscopy, N.Y., 1953. (Cited in Russian trans.)
5. P.S.Gross, R.M.Hainer & G.W.King, J.Chem.Phys., 12, 222 (1944).

BULLETIN of the Academy of Sciences of the USSR - Physical Series
Vol.22, No.9 - Transactions of the Eleventh All-Union Conference on
Theoretical Spectroscopy

TABLE OF CONTENTS

	Page Orig.	Trans.
Free-electron model calculations of the electric and magnetic properties of complex molecules - M.N.Adamov, M.G.Veselov & T.K.Rebane	1015	1005
Calculation of the absorption spectra of unsaturated hydrocarbon molecules on the basis of the metallic model - L.A.Borovinskii	1019	1009
Theory of vibrational spectra of unsaturated compounds - L.M.Sverdlov, M.G.Borisov, Iu.V.Klochkovskii, E.P.Krainov, V.S.Kukina & N.V.Tarasova	1023	1012
Contribution to the quantum mechanical theory of Raman line intensities - I.I.Sobel'man	1026	1015
Intensities and depolarizations in the Raman spectra of C_6H_6, $C_6D_6$and sym. $C_6H_3D_3$ - M.A.Kovner & B.N.Snegirev	1030	1019
Correspondence of the absorption and luminescence bands of complex molecules - B.I.Stepanov	1034	1023
Different forms of concentration quenching and the possibility of distinguishing between them - V.L.Levshin & E.G.Baranova	1038	1027
On the relation between the Kravets integral (area of the absorption band) and the lifetime of the excited state of molecules - M.D.Galanin & Z.A.Chizhikova	1043	1031
Kinetics of impurity quenching of fluorescence in solutions - B.Ia.Sveshnikov, V.M.Shirokov, L.A.Kuznetsova & P.I. Kudriashov	1047	1035
Effect of light gases on the electron absorption spectra of aromatic compounds and interaction between the molecules of such compounds - B.S.Neporent	1051	1039
Spectroscopic investigation of inter- and intramolecular interaction of nitro and amino radicals in some benzene derivatives - V.I.Danilova, V.D.Gol'tsev & N.A.Prilezhaeva	1054	1042
Dependence of the spectra of aromatic nitro compounds on the angle of rotation of the nitro group about the C-N bond - P.P.Shorygin & Z.F.Il'icheva	1058	1046
Investigation of vibrational spectra in the region of the valence vibrations of CH - M.M.Sushchinskii	1063	1051

Anharmonicity coefficients and resonance interaction of internal vibrations of the CH group - V.D.Bogdanov & M.M.Sushchinskii	1067	1056
Investigation of the temperature dependence of Raman spectrum line intensities - A.I.Sokolovskaia & P.A.Bazhulin	1068	1057
Raman spectra of some unsaturated cyclic hydrocarbons - V.T.Aleksanian, Kh.E.Sterin, A.A.Mel'nikov & A.F.Plate	1073	1062
Vibrational spectra of some phosphorogranic compounds - R.R.Shagidullin	1079	1069
Raman spectrum of vitreous germanium dioxide - V.V.Obukhov-Denisov, N.N.Sobolev & V.P.Cheremisinov	1083	1073
Investigation of the influence of different elements on the structure of silicate glasses by Raman spectroscopy - Ia.S.Bobovich & T.P.Tulub	1086	1076
Spectroscopy of negative radiant energy fluxes - B.I.Stepanov & Ia.S.Khvashchevskaia	1089	1079
Infrared absorption and thermal radiation spectra of some molecular compounds in different states of aggregation - O.V.Fialkovskaia	1093	1083
Infrared reflection spectrum of boron oxide at high temperatures - E.P.Markin & N.N.Sobolev	1097	1087
Infrared absorption spectra of molecular compounds with metal halides - A.N.Terenin, V.N.Filimonov & D.S.Bystrov	1100	1089
Towards a clarification of the "hydrogen bond" concept - V.M.Chulanovskii	1103	1092
Investigation of the hydrogen bond in glycols and catechols - V.I.Malyshev & V.N.Murzin	1107	1096
Structure of the OH vibration band in the spectra of crystals containing hydrogen bonds - A.I.Stekhanov	1109	1098
Infrared absorption spectra of organolithium compounds. The intermolecular lithium bond - A.N.Rodionov, D.N.Shigorin, R.V.Talalaeva & K.A.Kocheshkov	1110	1099
Investigation of intermolecular coupling in polyethylene by infrared absorption spectroscopy - I.I.Novak	1114	1103
Influence of temperature and the state of aggregation on the infrared absorption of carbon tetrachloride - M.P.Lisitsa & V.N.Malinko	1117	1106

Changes in the infrared spectrum of ammonia incident to transition from the gaseous to the liquid state - I.V.Demidenkova & L.D.Shcherba 1122 1110

Infrared spectra of salt solutions - E.N.Vasenko, A.P.Cherniavskaia & N.V.Chernaia 1125 1113

Investigation of keto-trans-cis-enol equilibrium by infrared absorption spectroscopy - M.E.Movsesian, M.I.Kabachnik, S.T.Ioffe & K.V.Vapuro 1126 1114

Spectroscopic investigation of the structure of some complex compounds - A.A.Babushkin 1131 1118

Spectroscopic methods of investigating catalytic conversions on metal films - V.M.Griaznov, V.D.Iagodovskii & V.I.Shimulis 1136 1123

Applications of the weak-field free nuclear induction technique in high-resolution radio spectroscopy - A.A.Morozov, A.V.Mel'nikov & F.I.Skripov 1141 1127

Rotational spectrum of water vapor in the 50 to 1500 μ region - N.G.Iaroslavskii & A.E.Stanevich 1145 1131

Determination of the molecular structure of HDSe from its rotational microwave spectrum - V.G.Veselago 1150 1136

Rotational constants of $FH_2C\text{-}Ch_2Cl^{35}$ - I.A.Mukhtarov 1154 1140

Translated in 1959 by
Columbia Technical Translations
5 Vermont Ave., White Plains, N.Y.

Publisher's Note

Publication of the Transactions of the All-Union Conference on the Physics of Magnetic Materials will be continued in the Vol. 23, No. 3 issue of the Bulletin.

DYNAMIC CONSTANTS OF MAGNETICALLY POLARIZED MAGNETOELASTIC (MAGNETOSTRICTIVE) AND ELECTRICALLY POLARIZED (ELECTROSTRICTIVE) MEDIA

- K.V.Vlasov

We derive equations describing the dynamic behavior of magnetically polarized magnetoelastic and electrically polarized electrostrictive media. These equations take into account nonequilibrium processes occurring in these media, and are obtained by using the methods of what is commonly termed the thermodynamics of irreversible processes (but might better be called simply "thermodynamics" in the full sense of the word, as opposed to "thermostatics").

1. Let us suppose that the state (in general not the equilibrium state) of a magnetoelastic medium is specified by giving the values of the following thermodynamic quantities: the magnetization I_m, the derivatives $\partial u_i/\partial x_j$, where the u_i are the components of the displacement vectors of points in the medium, and in some cases $\partial I_m/\partial x_i$ (this latter, for instance, in the case of ferromagnets). In general, the state of a magnetoelastic medium must be characterized by additional variables, but we shall not consider these as yet.

Let the state of the system be close to some initial state in which $I_m = 0$, $\frac{\partial u_i}{\partial x_j} = 0$ and $\frac{\partial I_m}{\partial x_i} = 0$ and let the medium in the initial state be magnetically polarized, i.e., characterized by a homogeneous magnetization I_0 oriented along the z axis. We consider this system together with a large heat reservoir at a constant temperature T, and write the entropy of the total system in the form

$$TS = \int \left(I_m H_m + \frac{\partial u_i}{\partial x_j} \sigma_{ij} - V \right) d\mathbf{r}, \tag{1}$$

where H_m and σ_{ij} are the variable magnetic field strength and mechanical stresses (both zero in the initial state), and V = -TS', where S' is the entropy density of the system at $H_m = 0$ and $\sigma_{ij} = 0$.

The summation convention is used in (1) and henceforth for repeated indices.

In the neighborhood of the initial state, that is for small I_m, $\frac{\partial u_i}{\partial x_j}$ and $\frac{\partial I_m}{\partial x_i}$, we may write, with Biot,[1]

$$V = -\frac{1}{2}\gamma'_{mn} I_m I_n + \frac{1}{2} a_{mnpq} \frac{\partial I_m}{\partial x_n} \frac{\partial I_p}{\partial x_q} + h'_{m,ij} I_m \frac{\partial u_i}{\partial x_j} + \frac{1}{2} d'_{ijkl} \frac{\partial u_i}{\partial x_j} \frac{\partial u_k}{\partial x_l}. \tag{2}$$

According to (1) and (2), the entropy change corresponding to given values of H_m and σ_{ij} is

$$\delta S = -\frac{1}{T} \int \left[H_m \delta I_m + \sigma_{ij} \delta \left(\frac{\partial u_i}{\partial x_j} \right) - \gamma'_{mn} I_n \delta I_m + a_{mnpq} \frac{\partial^2 I_p}{\partial x_n \partial x_q} \delta I_m - \right.$$

$$\left. - h'_{ij,m} \frac{\partial u_i}{\partial x_j} \delta I_m - h'_{m,ij} I_m \delta \left(\frac{\partial u_i}{\partial x_j} \right) - d'_{ijkl} \frac{\partial u_k}{\partial x_l} \delta \left(\frac{\partial u_i}{\partial x_j} \right) \right] d\mathbf{r} - \int a_{mnpq} \frac{\partial I_p}{\partial x_n} \delta I_m dS_q.$$

We therefore have the following expression for the rise of entropy:

$$-\frac{1}{T} \int \left[\left(H_m + a_{mnpq} \frac{\partial^2 I_p}{\partial x_n \partial x_q} - \gamma'_{mn} I_n - h'_{m,ij} \frac{\partial u_i}{\partial x_j} \right) \dot{I}_m + \left(\sigma_{ij} - d'_{ijkl} \frac{\partial u_k}{\partial x_l} - h'_{ij,m} I_m \right) \frac{\partial \dot{u}_i}{\partial x_j} \right] d\mathbf{r}.$$

If we treat $\dot{I}_m$ and $\frac{\partial u_i}{\partial x_j}$ as thermodynamic fluxes, we obtain the following relations between the fluxes and thermodynamic forces:

$$\left.\begin{aligned}
\dot{I}_l &= \int\Big[K_{lm}(\mathbf{r},\mathbf{r}')\Big(H_m + a_{mnpq}\frac{\partial^2 I_p}{\partial x_n \partial x_q} - \gamma'_{mn} I_n - h'_{m,ij}\frac{\partial u_i}{\partial x_j}\Big) + \\
&\quad + K_{l,ij}(\mathbf{r},\mathbf{r}')\Big(\sigma_{ij} - h'_{ij,m} I_m - d'_{ijkl}\frac{\partial u_k}{\partial x_l}\Big)\Big]\,d\mathbf{r}', \\
\frac{\partial \dot{u}_f}{\partial x_g} &= \int\Big(K_{fg,m}(\mathbf{r},\mathbf{r}')\Big(H_m + a_{mnpq}\frac{\partial^2 I_p}{\partial x_n \partial x_q} - \gamma'_{mn} I_n - h'_{m,ij}\frac{\partial u_i}{\partial x_j}\Big) + \\
&\quad + K_{fgij}(\mathbf{r},\mathbf{r}')\Big(\sigma_{ij} - h'_{ij,m} I_m - d'_{ijkl}\frac{\partial u_k}{\partial x_l}\Big)\Big]\,d\mathbf{r}'.
\end{aligned}\right\} \tag{3}$$

At the same time we have the Onsager relations[2,3]

$$\left.\begin{aligned}
K_{lm}(\mathbf{r},\mathbf{r}';\ I_0) &= K_{ml}(\mathbf{r}',\mathbf{r};\ -I_0); \\
K_{l,ij}(\mathbf{r},\mathbf{r}';\ I_0) &= -K_{ij,l}(\mathbf{r}',\mathbf{r};\ -I_0); \\
K_{fgij}(\mathbf{r},\mathbf{r}';\ I_0) &= K_{ijfg}(\mathbf{r}',\mathbf{r};\ -I_0).
\end{aligned}\right\} \tag{4}$$

Eqs.(3) reduce to

$$\left.\begin{aligned}
\dot{I}_l &= L_{lm}\Big(H_m + a_{mnpq}\frac{\partial^2 I_p}{\partial x_n \partial x_q} - \gamma'_{mn} I_n - h'_{m,ij}\frac{\partial u_i}{\partial x_j}\Big) + \\
&\quad + L_{l,ij}\Big(\sigma_{ij} - h'_{ij,m} I_m - d'_{ijkl}\frac{\partial u_k}{\partial x_l}\Big); \\
\frac{\partial \dot{u}_f}{\partial x_g} &= L_{fg,m}\Big(H_m + a_{mnpq}\frac{\partial^2 I_p}{\partial x_n \partial x_q} - \gamma'_{mn} I_n - h'_{m,ij}\frac{\partial u_i}{\partial x_j}\Big) + \\
&\quad + L_{fgij}\Big(\sigma_{ij} - h'_{ij,m} I_m - d'_{ijkl}\frac{\partial u_k}{\partial x_l}\Big);
\end{aligned}\right\} \tag{5}$$

if

$$\left.\begin{aligned}
K_{lm}(\mathbf{r},\mathbf{r}') = L_{lm}\delta(\mathbf{r},\mathbf{r}'); \quad K_{l,ij}(\mathbf{r},\mathbf{r}') = L_{l,ij}(\mathbf{r},\ \mathbf{r}')\,\delta(\mathbf{r},\mathbf{r}'); \\
K_{fgij}(\mathbf{r},\ \mathbf{r}') = L_{fgij}\delta(\mathbf{r},\mathbf{r}').
\end{aligned}\right\} \tag{6}$$

Using the evenness of the δ-function, we obtain the following expressions for the kinetic coefficients:

$$\left.\begin{aligned}
L_{lm}(I_0) = L_{ml}(-I_0); \quad L_{l,ij}(I_0) = -L_{ij,l}(-I_0); \\
L_{fgij}(I_0) = L_{ijfg}(-I_0).
\end{aligned}\right\} \tag{7}$$

For a quasistatic process, by which we mean a process in which the thermodynamic variables change so slowly that their time-derivatives may be neglected, Eqs.(5) become

$$\left.\begin{aligned}
H_m + a_{mnpq}\frac{\partial^2 I_p}{\partial x_n \partial x_q} &= \gamma'_{mn} I_n + h'_{m,ij}\frac{\partial u_i}{\partial x_j}, \\
\sigma_{kl} &= h'_{kl,n} I_n + d'_{klij}\frac{du_i}{dx_j}.
\end{aligned}\right\} \tag{8}$$

These equations are the equations of state for quasistatic processes and, together with the boundary conditions, they determine the spatial distribution of the magnetization and deformation, as well as the dependence of this distribution on the magnitude and configuration of the magnetic field.

For solving problems involving the dynamic behavior of a magnetoelastic medium, one must solve (5) simultaneously with (7) and the equations of electrodynamics (Maxwell's equations) and elasticity. The elasticity equations involved are

$$\rho \ddot{u}_i = \frac{\partial \sigma_{ji}}{\partial x_j} + f_i, \tag{9}$$

where the f_i are the body forces (for example, the force of gravity) and ρ is the density.

2. Let us now examine the question of the number of independent tensor constants and the number of their independent components entering into (5) and (8).

Eqs.(8) are equations of state. If we neglect those changes in the magnetization which are produced by deformation-determined density changes[4], then, according to (2), there should obtain for these constants the reciprocity conditions:

$$\gamma'_{mn} = \gamma'_{nm}; \qquad h'_{in,\,ij} = h'_{ij,\,m}; \qquad d'_{klij} = d'_{ijkl}, \tag{10}$$

$$a_{mnpq} = a_{pqmn}, \tag{11}$$

which reduce the number of independent tensor constants and the number of independent components of these constants.

For the tensor constants (i.e., the kinetic coefficients) characterizing the dynamic behavior of magnetoelastic media there obtain the Onsager relations (7) rather than the reciprocity relations (10) and (11).

Let us utilize in addition the particular symmetry properties of our magnetoelastic medium. This will also reduce the number of independent constants.

As an example, let us consider a magnetically polarized magnetoelastic medium which in the $I_0 = 0$ state is magnetically and elastically isotropic. Such magnetic symmetry properties are possessed, for instance, by a magnetically polarized paramagnet or ferromagnet whose energy in the external polarizing field is greater than the energy of the crystallographic magnetic anisotropy.

It follows from symmetry considerations that for such a magnetically polarized medium Eqs.(5) and (8) should be invariant under the operation $L_\infty^{\parallel}$, a rotation through any angle about an axis parallel to the polarization magnetization. In addition, (8) should be invariant under $RL_2^{\perp}$, where $L_2^{\perp}$ is a rotation through 180° about any axis perpendicular to the polarization magnetization, and R is the operation of reversing the magnetic field and changing the sign of the time (time reversal).[3] Eqs.(5) need not remain invariant under $RL_2^{\perp}$, since in general they do not describe processes which are time-reversal invariant. It should be noted that magnetically uniaxial crystals possess all the above-mentioned symmetry properties if their mechanical properties are transversely isotropic, so long as the polarization magnetization is directed along the axis of easy magnetization.

From symmetry considerations for an unpolarized medium it follows that (5) and (8) should be invariant under reflection in a plane containing $I_0(C_\infty)$; further, one can establish the parity of the function (whether it be odd or even) which gives the dependence of the tensor constants and kinetic coefficients on the polarization magnetization.

Since Eqs.(5) are invariant under fewer symmetry operations than are (8) and since the constants appearing in (5) are involved in relations (Eqs.(10)) which are somewhat different from those which involve the constants of (8) (Eqs.(7)), it turns out that the number of independent kinetic coefficients and their components will be greater than the number of independent tensor constants and their components (of the same rank and character) appearing in (8), the equations of state.

Using the Onsager relations and the above-mentioned symmetry considerations, we find,[5] that for our particular magnetically polarized, transversely isotropic magnetoelastic medium, the following components of the kinetic coefficients fail to vanish:

$$\left.\begin{aligned}
&L_{22}=L_{11};\quad L_{33};\quad L_{21}=-L_{12};\\
&L_{2,13}=-L_{13,2}=L_{23,1}=-L_{1,23};\quad L_{2,31}=-L_{31,2}=L_{32,1}=-L_{1,32};\\
&L_{3,21}=-L_{21,3}=L_{12,3}=-L_{3,12};\quad L_{3,22}=L_{22,3}=L_{11,3}=L_{3,11};\\
&L_{33,3}=L_{3,33};\quad L_{2,32}=L_{32,2}=L_{31,1}=L_{1,31};\quad L_{2,23}=L_{23,2}=L_{13,1}=L_{1,13};\\
&L_{2222}=L_{1111};\quad L_{3333};\quad L_{2211}=L_{1122};\quad L_{2233}=L_{3322}=L_{3311}=L_{1133};\\
&L_{1313}=L_{2323};\quad L_{3131}=L_{3232};\quad L_{3113}=L_{1331}=L_{3223}=L_{2332};\\
&L_{2121}=L_{1212};\quad L_{2112}=L_{1221};\quad L_{2221}=-L_{2122}=L_{1211}=-L_{1112};\\
&L_{2212}=-L_{1222}=L_{2111}=-L_{1121};\quad L_{3321}=-L_{2133}=L_{1233}=-L_{3312};\\
&L_{1332}=-L_{3213}=L_{3123}=-L_{2331};\quad L_{1323}=-L_{2313};\quad L_{3132}=-L_{3231}.
\end{aligned}\right\}\qquad (12)$$

Further

$$L_{1221}=L_{1111}-L_{1122}-L_{1212}.$$

Kinetic coefficients of the type L_{11}, L_{33}, $L_{1,23}$, $L_{1,32}$, $L_{3,12}$, L_{1111}, L_{3333}, L_{1122}, L_{1133}, L_{2323}, L_{3232}, L_{2332}, L_{1212} and L_{1221} are even functions of I_0, while constants of the form L_{12}, $L_{3,11}$, $L_{3,33}$, $L_{1,31}$, $L_{1,13}$, L_{1112}, L_{1121}, L_{3312}, L_{2331}, L_{2313} and L_{3231} are odd functions.

Using (10) and (11) and symmetry considerations, we find[5] that the constants γ'_{nm}, $h'_{n,kl}$, $h'_{ij,m}$, d'_{ijkl} and a_{mnpq} satisfy entirely similar relations and depend in the same way on I_0 as do the L_{nm}, $L_{n,kl}$, $L_{i,m}$ and L_{ijkl} constants of the same rank, except that constants of the type γ'_{12}, $h'_{1,23}$, $h'_{1,32}$, $h'_{3,12}$, d'_{1112}, d'_{1121}, d'_{3312}, d'_{2331}, d'_{2313}, d'_{3231}, a_{1112}, a_{1121}, a_{3312}, a_{2331}, a_{2313} and a_{3231} vanish.

We note that those terms of (2), (5) and (8) which contain the constant factor a_{mnpq} are determined by the exchange energy. If we ignore the magnetic contribution to the exchange energy[6] and assume that the exchange energy is invariant under rotation of the spin, a_{mnpq} must satisfy the subsidiary condition[7]

$$a_{mnpq}=\delta_{mp}a_{nq}. \qquad (13)$$

As a result, the independent components of this constant reduce to a_{11} and a_{33}.

3. Let us now consider the case of a steady-state process in which the independent variables have a sinusoidal time dependence with an angular frequency ω.

We first solve Eqs.(5) for $H_m+a_{mnpq}\dfrac{\partial^2 I_p}{\partial x_n \partial x_q}$ and σ_{ij}, obtaining a set of equations which is formally the same as (8) except that γ'_{mn}, $h'_{m,ij}$, $h'_{ij,m}$ and d'_{klij} are replaced by the complex constants

$$\left.\begin{aligned}
&\gamma_{mn}=\gamma'_{mn}+i\omega\gamma''_{mn},\qquad h_{m,ij}=h'_{m,ij}+i\omega h''_{m,ij};\\
&h_{ij,m}=h'_{ij,m}+i\omega h''_{ij,m};\quad d_{klij}=d'_{klij}+i\omega d''_{klij}.
\end{aligned}\right\}\qquad (14)$$

The double-primed constants here are determined uniquely by the kinetic coefficients. They and their components are mutually related and depend on I_0 in the same way as do the kinetic coefficients of equal rank, i.e., according to (12).

The complex constants of (14) may be called the dynamical constants of a magnetoelastic medium.

It is easily seen by studying the equations obtained that the stress tensor is not symmetric.

As is usually done in elasticity theory, we introduce the strain and rotation tensors by

$$\varepsilon_g = \frac{1}{2}\left(\frac{\partial u_i}{\partial x_j} + \frac{\partial u_j}{\partial x_i}\right) \quad \text{and} \quad \omega_q = \frac{1}{2}\left(\frac{\partial u_i}{\partial x_j} - \frac{\partial u_j}{\partial x_i}\right), \tag{15}$$

and decompose the stress tensor into its symmetric and antisymmetric parts (the latter gives the moments of the forces per unit volume)

$$\sigma_f = \frac{1}{2}(\sigma_{kl} + \sigma_{lk}) \quad \text{and} \quad T_p = \frac{1}{2}(\sigma_{kl} - \sigma_{lk}). \tag{16}$$

The indices f and g take on the six values 1,2,...,6 (for instance, $\varepsilon_1 = \frac{\partial u_1}{\partial x_1}$, ..., $\varepsilon_6 = \frac{1}{2}\left(\frac{\partial u_1}{\partial x_2} + \frac{\partial u_2}{\partial x_1}\right)$, while p and q take on the three values 4, 5, and 6; for example,

$$\omega_4 = \frac{1}{2}\left(\frac{\partial u_2}{\partial x_3} - \frac{\partial u_3}{\partial x_2}\right), \ldots .$$

We then obtain

$$\left.\begin{aligned} H_m + a_{mnpq}\frac{\partial^2 I_p}{\partial x_n \partial x_q} &= \gamma_{mn} I_n + h_{mg}\varepsilon_g + \overset{*}{h}_{mq}\omega_q, \\ \sigma_f &= \overset{'}{h}_{fn} I_n + c_{fg}\varepsilon_g + \overset{*}{c}_{fq}\omega_q, \\ T_p &= \overset{*'}{h}_{pn} I_n + \overset{*'}{c}_{pg}\varepsilon_g + \overset{**}{c}_{pq}\omega_g, \end{aligned}\right\} \tag{17}$$

where

$$\left.\begin{aligned} &\gamma_{11} = \gamma_{22} = \overset{'}{\gamma}_{11} + i\omega\overset{''}{\gamma}_{11}; \quad \gamma_{33} = \overset{'}{\gamma}_{33} + i\omega\overset{''}{\gamma}_{33}; \\ &h_{33} = \overset{'}{h}_{33} = \overset{'}{h}_{3,33} + i\omega\overset{''}{h}_{3,33}; \quad h_{31} = h_{32} = \overset{'}{h}_{13} = \overset{'}{h}_{23} = \overset{'}{h}_{3,11} + i\omega\overset{''}{h}_{3,11}; \\ &h_{15} = h_{24} = \overset{'}{h}_{51} = \overset{'}{h}_{42} = \frac{1}{2}(\overset{'}{h}_{1,31} + \overset{'}{h}_{1,13}) + \frac{1}{2}i\omega(\overset{''}{h}_{1,31} + \overset{''}{h}_{1,13}); \\ &c_{11} = c_{22} = \overset{'}{d}_{1111} + i\omega\overset{''}{d}_{1111}; \quad c_{12} = c_{21} = \overset{'}{d}_{1122} + i\omega\overset{''}{d}_{1122}; \\ &c_{13} = c_{23} = c_{31} = c_{32} = \overset{'}{d}_{1133} + i\omega\overset{''}{d}_{1133}; \quad c_{33} = \overset{'}{d}_{3333} + i\omega\overset{''}{d}_{3333}; \\ &c_{44} = c_{55} = \frac{1}{4}(\overset{'}{d}_{2323} + \overset{'}{d}_{3232} + 2\overset{'}{d}_{2332}) + \frac{1}{4}i\omega(\overset{''}{d}_{2323} + \overset{''}{d}_{3232} + 2\overset{''}{d}_{2332}); \\ &c_{66} = \frac{1}{2}(c_{11} - c_{12}). \end{aligned}\right\} \tag{18}$$

$$\left.\begin{aligned} &\overset{*}{c}_{44} = -\overset{*}{c}_{55} = \overset{*'}{c}_{44} = -\overset{*'}{c}_{55} = \frac{1}{4}(\overset{'}{d}_{2323} - \overset{'}{d}_{3232}) + \frac{1}{4}i\omega(\overset{''}{d}_{2323} - \overset{''}{d}_{3232}); \\ &\overset{**}{c}_{44} = \overset{**}{c}_{55} = -\frac{1}{4}(\overset{'}{d}_{2323} + \overset{'}{d}_{3232} - 2\overset{'}{d}_{2332}) + \frac{1}{4}i\omega(\overset{''}{d}_{2323} + \overset{''}{d}_{3232} - 2\overset{''}{d}_{2332}); \\ &\overset{**}{c}_{66} = \overset{'}{d}_{1212} + i\omega\overset{''}{d}_{1212} - c_{66}; \end{aligned}\right\} \tag{19}$$

$$\overset{*}{h}_{15} = -\overset{*}{h}_{24} = \overset{*'}{h}_{51} = -\overset{*'}{h}_{42} = \frac{1}{2}(\overset{'}{h}_{1,31} - \overset{'}{h}_{1,13}) + \frac{1}{2}i\omega(\overset{''}{h}_{1,31} - \overset{''}{h}_{1,13}); \tag{20}$$

$$\gamma_{12} = -\gamma_{21} = i\omega\overset{''}{\gamma}_{12}; \tag{21}$$

$$\left.\begin{aligned} h_{14}' = -h_{25}' = -h_{41}' = h_{52}' = -\frac{1}{2} i\omega (h_{1,23}'' + h_{1,32}''); \\ h_{14}^{*} = h_{25}^{*} = h_{41}^{*'} = -h_{52}^{*'} = -\frac{1}{2} i\omega (h_{1,23}'' + h_{1,32}''); \\ h_{36}^{*} = -h_{63}^{*'} = i\omega h_{3,12}''; \end{aligned}\right\} \quad (22)$$

$$\left.\begin{aligned} c_{16} = -c_{26} = -c_{61} = c_{62} = \frac{1}{2} i\omega (d_{1112}'' + d_{1121}''); \\ c_{16}^{*} = c_{26}^{*} = -c_{61}^{*'} = -c_{62}^{*'} = \frac{1}{2} i\omega (d_{1112}'' - d_{1121}''); \quad c_{36}^{*} = -c_{63}^{*'} = i\omega d_{3312}''; \\ c_{45} = -c_{54} = \frac{1}{4} i\omega (d_{3231}'' + d_{2313}'' + 2d_{2331}''); \\ c_{45}^{**} = -c_{54}^{**} = -\frac{1}{4} i\omega (d_{3231}'' + d_{2313}'' - 2d_{2331}''); \\ c_{45}^{*} = c_{54}^{*} = -c_{45}^{*'} = -c_{54}^{*'} = \frac{1}{4} i\omega (d_{3231}'' - d_{2313}''). \end{aligned}\right\} \quad (23)$$

4. Let us analyze the relationships deduced above.

The dynamic constant tensors of (18)-(23) can be divided into two groups:

1) those in (18)-(20), which contain both real and imaginary parts. They fail to vanish both in the dynamic and in the quasistatic states. Their imaginary parts characterize certain relaxation processes and give the amount of energy absorbed;

2) those of (21)-(23), which include only imaginary terms. These fail to vanish only in the dynamic state.

Let us first consider those of the first group.

In elasticity theory it is assumed that the stress tensor is symmetric. This symmetry does not follow from thermodynamic considerations of any kind or from other considerations involving the symmetry of the medium, but is deduced from the premise that the stress is caused by short-range forces.[8] Viswanathan & Raman[9,10] and Laval[11] (on the basis of microscopic theory) have shown, however, that when one takes into account the noncentral nature of intermolecular forces, one concludes that in general the stress tensor should be asymmetric and that the elastic properties of a crystal medium of the lowest symmetry should be described not by 21, but by 45 elasticity coefficients. In our case of a transversely isotropic medium, the above considerations lead to the appearance of the components of the elastic modulus given in (19), i.e., c_{44}^{*}, c_{44}^{**} and c_{66}^{**}. This reason for asymmetry of the stress tensor is valid both in the dynamic and the quasistatic cases.

On the other hand, the asymmetry of the mechanical stress tensor in a magnetically polarized medium may be due to the mechanical torque produced when the resultant magnetization is not parallel to the magnetic field. This explanation was emphasized by Brown.[12] In a transversely isotropic medium this leads to the appearance of the components of the magnetostriction tensor given in (20), namely h_{15}^{*}. Let us consider one of the expressions give by Brown, for example, the one for T_5:

$$T_5 = I_3 H_1 - I_1 H_3,$$

Here I and H are the resultant values of the vectors I_m and H_n, including the polarization magnetic field and the polarization magnetization. It can be shown, using this expression, that for a magnetically uniaxial medium this reason for asymmetry of the stress tensor remains valid in the dynamic and quasistatic cases, while for a magnetically polarized isotropic medium it is valid only in the dy-

namic case. This is because of the phase difference (due to losses) between I_m and H_n. Here one must use Eq.(19) of Ref.13 or Eq.(34) of Ref.4.

Let us now turn to the constants of the second group, i.e., those in (21)-(23). Their physical meaning can be established by considering microscopic kinetic processes in a magnetoelastic medium. We will mention only some of the physical phenomena they may be said to characterize.

Constants describing magnetic properties, i.e., γ_{12} of (21)

Consider, for instance, a homogeneous quasistationary magnetic field with a sinusoidal time dependence. Then in a constrained magnetoelastic medium ($\varepsilon_q = 0$, $\omega_q = 0$) the magnetization in the plane perpendicular to I_0 will be given, according to (17), (18) and (21), by

$$I_1 = \varkappa_{11}^{\varepsilon} H_1 - \varkappa_{12}^{\varepsilon} H_2; \qquad I_2 = \varkappa_{12}^{\varepsilon} H_1 + \varkappa_{11}^{\varepsilon} H_2, \tag{24}$$

where

$$\varkappa_{11}^{\varepsilon} = \frac{1}{\gamma'_{11}} \frac{\omega_1(\omega_1 + i\omega) + \omega_0^2}{(\omega_1 + i\omega)^2 + \omega_0^2}; \quad \varkappa_{12}^{\varepsilon} = i\omega \cdot \frac{1}{\gamma'_{11}} \frac{\omega_0}{(\omega_1 + i\omega)^2 + \omega_0^2}, \tag{25}$$

and

$$\overset{*}{\omega}_1 = \frac{\omega_1^2 + \omega_0^2}{\omega_1}; \qquad \overset{*}{\omega}_0 = \frac{\omega_1^2 + \omega_0^2}{\omega_0}; \qquad \overset{*}{\omega}_1 = \frac{\gamma'_{11}}{\overset{*}{\gamma}_{11}}; \qquad \overset{*}{\omega}_0 = \frac{\gamma'_{11}}{\overset{*}{\gamma}_{12}}. \tag{26}$$

We note that if we set $L_{m,ij} = 0$, we obtain $\omega_1 = I_{11}\gamma'_{11}$ and $\omega_0 = I_{12}\gamma'_{11}$.

Further, writing $I_{12} = g\frac{e}{2mc} I_0$, $\gamma'_{11} = \frac{H_0}{I_0}$ where g is the Landé splitting factor, we obtain the usual formulas for paramagnetic or ferromagnetic resonance (without magnetic anisotropy or shape effects).

Constants describing magnetomechanical properties, i.e., h_{14}, $\overset{*}{h}_{14}$ and $\overset{*}{h}_{36}$ of (22)

As may be seen from (17) and (22), for homogeneous quasistationary variation of the magnetization and deformation, $\overset{*}{h}_{14}$ and $\overset{*}{h}_{36}$ give the anisotropy of the gyromagnetic effects. It is easily seen that h_{14} is related to the same anisotropy.

By way of illustration let us consider a magnetically and elastically isotropic medium in the state $I_0 = 0$. In this state[5] $h_{1,23}(0) = -h_{1,32}(0) = h_{3,12}(0)$.

According to (22), therefore, $\overset{*}{h}_{14}(0) = \overset{*}{h}_{36}(0)$, while $h_{14}(0) = 0$. If $h_{1,23}$, $h_{1,32}$ and $h_{3,12}$ depend on I_0, then $\overset{*}{h}_{14} \neq \overset{*}{h}_{36}$ and h_{14} may not vanish when $I_0 \neq 0$.

Constants describing mechanical properties, i.e., c_{16}, $\overset{*}{c}_{16}$, $\overset{*}{c}_{36}$, c_{45}, $\overset{*}{c}_{45}$ and $\overset{**}{c}_{45}$ of (23)

In a magnetically "constrained" medium ($I_n = 0$) and for quasistationary processes Eqs.(17) and (23) show that these constants should describe, for instance, the following properties: Shear deformation in the xy plane (ε_6) should produce tensile (σ_1) and compressive ($-\sigma_2$) stresses along the x and y axes, and vice versa; that is, for instance, elongation along the x axis (ε_1) should give rise to negative shear in the xy plane ($-\sigma_6$) (described by c_{16}). Rotation about the x axis (ω_4) should give rise to a negative moment about the y axis ($-T_5$), and vice versa, rotation about the y axis (ω_5) should produce a moment about the x axis (T_4) (described by $\overset{**}{c}_{45}$). The constants $\overset{*}{c}_{16}$, $\overset{*}{c}_{36}$, c_{45} and $\overset{*}{c}_{45}$ describe similar effects, likewise easily understood by studying (17) and (23).

In conclusion, we recall that in order to determine the behavior of a magnetoelastic medium in the general case of steady-state (rather than just quasi-

stationary) processes, one must solve Eqs.(5) together with Maxwell's equations and the equations of elasticity, while making use of (12); alternatively, one can solve (17) with Maxwell's and the elasticity equations, using (16) to go over to one type of variables, and taking into account (15) and (18)-(23). These equations describe a wide set of magnetic, mechanical and magnetomechanical phenomena, such as magnetic and magnetomechanical resonance,[14] spin-spin relaxation,[15] the influence of the mechanical state on magnetic resonance, anisotropy of gyromagnetic phenomena, etc.

5. The dynamic behavior of an electrically polarized electrostrictive medium (as opposed to its quasistatic behavior) differs from that of a magnetized magnetostrictive medium.

In order to obtain the equations for this behavior I_n should be replaced by P_n and H_m by E_m in Eqs.(5) and all following equations. Here E_m is the electric field strength and P_n is the electric polarization. Unlike the analogous magnetic case, however, all the equations then obtained for electrostrictive media with transverse symmetry should be invariant under $L_\infty^\perp$ and $IR_2^\perp$, where I is the inversion operator. The Onsager relations for the kinetic coefficients entering these equations will also be somewhat different, namely

$$L'_{lm}(P_0) = L'_{ml}(P_0); \quad L'_{l,ij}(P_0) = L'_{ij,l}(P_0); L'_{fgij}(P_0) = L'_{ijfg}(P_0), \tag{27}$$

which are the same relations as those of (10) and (11).

This all means that the number of independent components of the kinetic coefficients L'_{lm}, $L'_{l,ij}$, $L'_{ij,l}$ and L'_{fgij} will be equal to the number of independent components of the tensor constants γ'_{mn}, $h'_{m,ij}$, $h'_{ij,m}$ and d'_{klij} of equal rank. Here γ'_{mn} is the reciprocal of the dielectric constant and $h'_{m,ij}$ is an electrostrictive constant.

Thus the electric problem is treated by using Eqs.(5) (or (8)) with (12), or Eqs.(17) with (18)-(23), formally replacing H_m by E_m and I_n by P_n. In contrast to the magnetic case, in the electric case the components of the kinetic coefficients which vanish are L'_{12}, $L'_{1,23}$, $L'_{1,32}$, $L'_{3,12}$, L'_{1112}; L'_{1121}, L'_{3312}, L'_{2331}, L'_{2313} and L'_{3231}; therefore so do the components of the tensor constants (appearing in the equations obtained by the above formal substitutions) analogous to those of (21)-(23). All other remarks, such as those concerning the asymmetry of the mechanical stress tensor, remain valid in the case of an electrically polarized electrostrictive medium.

It should be emphasized that in the present work no attempt was made to consider the possibility of exciting internal degrees of freedom in the dynamic state. This possibility has been taken into account, for example, by Finkel'shtein and Fastov[16] in their treatment of the mechanical properties of isotropic media.

Institute of Metal Physics
Academy of Sciences of the USSR

References

1. M.A.Biot, Phys.Rev., 97, 1462 (1955).

2. S.R.deGroot, Thermodynamics of Irreversible Processes, N.Y., 1951. (Cited in Russian trans., M. 1956.)

3. L.D.Landau & E.M.Lifshits, Statisticheskaia fizika (Trans.Statistical Physics), M.-L., 1951.

4. K.B.Vlasov, Izv.AN SSSR, Ser.fiz., 21, 1140 (1957). (Trans.Bulletin 21, No.8, 1125.)

5. K.B.Vlasov, Fiz.met.i metalloved. (Physics of metals & metallography), 5, 385 (1957).

6. S.V.Vonsovskii, K.B.Vlasov & E.A.Turov, Zhur.eks.i teor.fiz., 29, 37 (1955). (Trans.Soviet Physics - JETP.)
7. C.Herring & C.Kittel, Phys.Rev., 81, 869 (1951).
8. L.D.Landau & E.M.Lifshits, Mekhanika sploshnykh sred (Mechanics of continuous media), M., 1953.
9. K.S.Viswanathan, Proc.Ind.Acad.Sci., A41, 98 (1955).
10. C.V.Raman & K.S.Viswanathan, Proc.Ind.Acad.Sci., A42, 51 (1955).
11. J.Laval, C.R., 232, 1947 (1951).
12. W.F.Brown, Revs.Mod.Phys., 25, 131 (1953); Am.J.Phys., 19, 290 and 330 (1951).
13. K.B.Vlasov, Fiz.met.i metalloved., 3, 551 (1956).
14. S.A.Al'tshuler, Doklady AN SSSR, 85, 1235 (1952); Zhur.eksp.i teor.fiz., 28, 38 & 49 (1955). (Latter trans.Soviet Physics - JETP).
15. I.G.Shaposhnikov, Zhur.eksp.i teor.fiz., 18, 533 (1948).
16. B.N.Finkel'shtein & N.S.Fastov, Doklady AN SSSR, 71, 875 (1950).

PHENOMENOLOGICAL THEORY OF FERROMAGNETISM AND ANTIFERROMAGNETISM AT LOW TEMPERATURES (UNIAXIAL CASE)

- E.A.Turov & Iu.P.Irkhin

1. The General Method

From the macroscopic viewpoint a magnet with an ordered magnetic structure (a ferromagnet or antiferromagnet) may be treated as a continuous medium with a certain type of magnetic crystallographic symmetry. Each point in the medium associated with one, two, or more* magnetic moment densities $\mathbf{M}_j(r)$. To describe complete magnetic ordering at absolute zero in the terminology of continuous media, one says that in the lowest energy state the $\mathbf{M}_j(\mathbf{r})$ are constant vectors, i.e., that

$$\mathbf{M}_j(\mathbf{r}) = \mathbf{M}_{0j}.$$

We shall assume in addition that the vector densities remain of constant magnitude, their deviations $\Delta\mathbf{M}_j = \mathbf{M}_j - \mathbf{M}_{0j}$ from equilibrium being due entirely to changes in direction. In other words,

$$\mathbf{M}_j^2(\mathbf{r}) = \mathbf{M}_{0j}^2.$$

We shall restrict our considerations to weak oscillations, that is to $|\Delta\mathbf{M}_j| \ll \mathbf{M}_{0j}$, corresponding to temperatures low compared to the magnetic ordering temperature (the Curie point θ_C and the Néel point θ_N).

Our problem is to find the vibration spectrum of the $\mathbf{M}_j(\mathbf{r})$ for such a medium in an external magnetic field $\mathbf{H}$. As was previously done by one of us and Shavrov[2], we shall proceed from a phenomenological Hamiltonian which, in our case of uniaxial symmetry (e.g., a hexagonal or tetragonal crystal), is of the form

$$\mathcal{H}' = \int \mathcal{H}' d\mathbf{r}, \tag{1}$$

$$\mathcal{H}' = A_{jj'} M_{j\alpha} M_{j'\alpha} + B_{jj'} M_{jz} M_{j'z} + C_{jj'} \nabla M_{j\alpha} \nabla M_{j'\alpha} + D_{jj'} \frac{\partial M_{j\alpha}}{\partial z} \frac{\partial M_{j'\alpha}}{\partial z} - \frac{1}{2} \sum_{j,j'} \mathbf{M}_j \mathbf{H}_{j'}^M - \sum_j \mathbf{M}_j \mathbf{H}, \tag{2}$$

where

$$\mathbf{H}_j^M = \nabla \int \frac{\operatorname{div} \mathbf{M}_j(\mathbf{r}')\, d\mathbf{r}'}{|\mathbf{r} - \mathbf{r}'|}. \tag{3}$$

Here j and j' are numbers designating the magnetic sublattices, $\alpha \equiv x, y, z$, and the summation convention is used for repeated indices. The first four terms in (2) include the exchange energy and the anisotropy energy, the $A_{jj'}$, $B_{jj'}$, $C_{jj'}$ and $D_{jj'}$ being phenomenological constants for the associated interactions. The penultimate term in (2) gives the dipole-dipole interaction,** and the last is the energy of the magnet in the external field.

---

*The number depends on the number of "magnetic sublattices", which in turn is determined by the type of crystal structure and the number of different kinds of magnetic atoms (ions) in a unit cell.

**In taking into account boundary effects (demagnetizing fields) one must add a term of the form $-\nabla \oint \frac{\mathbf{M}_j(\mathbf{r}')\, d\mathbf{r}'}{(\mathbf{r} - \mathbf{r}')}$ to $\mathbf{H}_j^M$ The integration here is over the surface of the magnetic specimen.

The energy spectrum may be calculated in two ways, namely, classically (by setting up and solving the classical equations of motion)[3] or by second quantization.[2] We shall use the latter. To do this we replace the classical c-number vectors $\mathbf{M}_j(\mathbf{r})$ in (1) by operators $\hat{\mathbf{M}}_j(\mathbf{r})$ which satisfy the commutation rules[2]

$$\hat{M}_{j\nu}(\mathbf{r})\,\hat{M}_{j'x}(\mathbf{r}') - \hat{M}_{j'x}(\mathbf{r}')\,\hat{M}_{j\nu}(r) = i\mu_j \hat{M}_{jz}\,\delta_{jj'}\delta(\mathbf{r}-\mathbf{r}') \quad \text{etc.}, \tag{4}$$

where $\mu_j = g_j\beta$; here g_j is the Landé g-factor for the j-th sublattice and β is the Bohr magneton.

If for each j we choose an $X_jY_jZ_j$ coordinate system such that the Z_j axis is the axis of quantization of $\mathbf{M}_j(\mathbf{r})$ (i.e., directed along the classical $\mathbf{M}_{0j}$ vector), the second quantization operators b_r^j and $\overset{+}{b}{}_r^j$ can be introduced by the relations

$$\hat{M}_{jx_j} = (\mu_j M_{0j}/2)^{1/2}(f_j b_r^j + \overset{+}{b}{}_r^j f_j), \quad \hat{M}_{jy_j} = i(\mu_j M_{0j}/2)^{1/2}(f_j b_r^j - \overset{+}{b}{}_r^j f_j),$$

$$\hat{M}_{jz_j} = M_{0j} - \mu_j \overset{+}{b}{}_r^j b_r^j, \quad f_j \equiv \left(1 - \frac{\mu_j \overset{+}{b}{}_r^j b_r^j}{2M_{0j}}\right)^{1/2}. \tag{5}$$

(For simplicity we take the volume V of the sample to be 1.)

We remark that by assumption the expectation values satisfy the relation

$$\overline{\mu_j \overset{+}{b}{}_r^j b_r^j} = \overline{\Delta M}_{jz_j} \ll M_{0j}.$$

Inserting (5) into (4) shows that these new operators satisfy the Bose-Einstein commutation relations

$$b_r^j \overset{+}{b}{}_r^{j'} - \overset{+}{b}{}_r^{j'} b_r^j = \delta_{jj'}\delta(r-r'). \tag{6}$$

In using (5) to go over from the $\mathbf{M}_j(\mathbf{r})$ to the b_r^j and $\overset{+}{b}{}_r^j$ operators in the Hamiltonian, of course, one must express all the $\hat{M}_{jx}$ in a common XYZ coordinate system fixed with respect to the crystal axes. Then the transformation formulas will cause the direction cosines of the $\mathbf{M}_{0j}$ with respect to the fixed system to enter the expression for H. For example, when all the $\mathbf{M}_{0j}$ and the magnetic field $\mathbf{H}$ all lie in the same plane (say, the YZ plane) the transformation formulas are

$$M_{jx} = M_{jx_j}, \quad M_{jy} = \zeta_j M_{jy_j} + \eta_j M_{jz_j}, \quad M_{jz} = \zeta_j M_{jz_j} - \eta_j M_{jy_j}, \tag{7}$$

where $\eta_j = \sin\theta_j$, $\zeta_j = \cos\theta_j$ and θ_j is the angle between $\mathbf{M}_{0j}$ and the Z axis.

After inserting (5) and (7) into (1)-(3) and going over to the Fourier components b_k^j and $\overset{+}{b}{}_k^j$ of the Bose operators, the Hamiltonian of the system can be written in the form of a series

$$\mathcal{H} = \mathcal{H}_0 + \mathcal{H}_1 + \mathcal{H}_2 + \mathcal{H}_3 + \ldots,$$

where $\mathcal{H}_n$ is an n-th order term in the b_k^j and $\overset{+}{b}{}_k^j$.

In order to find the ground state of the system, i.e., the equilibrium values of η_j and ζ_j at T = 0, we minimize $\mathcal{H}_0$ (which is independent of b_k^j and $\overset{+}{b}{}_k^j$) with respect to η_j and ζ_j. For these equilibrium values $\mathcal{H}_1$ vanishes identically* while the expression for $\mathcal{H}_2$ becomes such that when it is diagonalized it is the sum of the elementary spin-wave energies. In other words, it gives the first approximation to the desired intrinsic vibration spectrum. The higher order

---

*In fact the ground state may be found simply from the condition that $\mathcal{H}_0$ vanishes.

terms in the expansion describe collision processes between spin waves (that is, between ferromagnons or antiferromagnons), so that if they are included, one is able to study various kinetic phenomena in magnets.

In what follows we shall apply this method to the specific examples of a ferromagnet and an antiferromagnet.

2. Ferromagnet

Consider a uniaxial ferromagnetic single crystal, which is essentially a single magnetic domain. Let the direction of easy magnetization coincide with the symmetry axis (Z axis).

Bearing in mind that j has only one value (there is only one sublattice) and proceeding as indicated in Section 1, we obtain

$$\mathcal{H}_0 = \text{const} - \frac{1}{2} H_A M_0 \zeta^2 - M_0 \eta_l H_y - M_0 \zeta H_z, \tag{8}$$

$$E \equiv \mathcal{H}_2 = \Delta\mathcal{H}_0 + \sum_k \varepsilon_k n_k. \tag{9}$$

Here $H_A = -2B_{11}M_0$ is the effective magnetic anisotropy field, $M_0 = M_{01}$ is the magnetization at absolute zero, $\Delta H_0 = -\frac{1}{2}\sum_k (\alpha_k - \sqrt{\alpha_k^2 - |\beta_k|^2})$ is the zero-point energy of the spin waves, which contributes to the ground state energy,

$$\varepsilon_k = \sqrt{\alpha_k^2 - |\beta_k|^2} \tag{10}$$

is the energy of the spin wave with wave vector k and n_k is the number of spin waves in this state; further

$$\alpha_k = \left(\zeta^2 - \frac{1}{2}\eta^2\right)\mu H_A + J_k + \eta_l \mu H_y + \zeta \mu H_z + 2\pi\mu M_0 \frac{k'_+ k'_-}{k^2},$$

$$\beta_k = \frac{1}{2}\eta^2 \mu H_A + 2\pi\mu M_0 \left(\frac{k'_-}{k}\right)^2, \quad J_k = 2\mu M_0 (C_{11}k^2 + D_{11}k_z^2),$$

$$k'_\pm = k_{x_l} \pm i k_{y_l} = k_x \pm i\zeta k_y \mp i\eta_l k_z.$$

Let us now consider in detail the two cases $\mathbf{H} \parallel OZ$ and $\mathbf{H} \perp OZ$.

I. Field parallel to the Z-axis

In this case $H_y = 0$, $H_z = H$ and the condition that $\mathcal{H}_0$ be a minimum leads to a $\zeta = 1$ and $\eta = 0$, which means that the magnetization is along the field. We then get

$$\varepsilon_k = \left\{\left[J_k + \mu(H + H_A)\right]\left[J_k + \mu(H + H_A) + 4\pi\mu M_0 \frac{k_x^2 + k_y^2}{k^2}\right]\right\}^{1/2}, \tag{11}$$

which virtually coincides with the well-known results of Holstein & Primakoff[4] and Herring & Kittel.[5]

II. Field perpendicular to the Z-axis

In this case $H_y = H$, $H_z = 0$, and the condition that $\mathcal{H}_0$ be a minimum leads to the following two possibilities:

a) if $H \ll H_A$, then $\eta_l = \frac{H}{H_A}$, $M_{0y} = M_0 \frac{H}{H_A}$,

$$\varepsilon_k = \left\{(J_k + \mu H_A)\left[J_k + \mu H_A\left(1 - \frac{H^2}{H_A^2}\right) + 4\pi\mu M_0 \frac{k'_+ k'_-}{k^2}\right] - 2\pi\mu^2 \frac{M_0 H^2}{H_A} \frac{3k_x^2 - (\zeta k_y - \eta_l k_z)^2}{k^2}\right\}^{1/2}; \tag{12}$$

b) if $H \geqslant H_A$, then $\eta = 1$, $M_{0y} = M_0$,

$$\varepsilon_k = \left\{(J_k + \mu H)\left[J_k + \mu(H - H_A) + 4\pi\mu M_0 \frac{k_x^2 + k_y^2}{k^2}\right] - 2\pi\mu^2 M_0 H_A \frac{3k_x^2 - k_z^2}{k^2}\right\}^{1/2}. \quad (13)$$

To illustrate the application of the energy spectrum so obtained, let us consider the field and temperature dependence of the magnetization of a ferromagnet for case II*. We restrict our considerations to temperatures which satisfy

$$\varkappa T \gg \mu H, \quad \mu H_A, \quad 2\pi\mu M_0 \quad (14)$$

(and, of course, $T \ll \theta_C$).

Iakovlev[6] solved a similar problem for a uniaxial ferrite.

Straightforward calculation using the formula

$$M_y(T, H) = -\frac{\partial}{\partial H}(\mathcal{H}_0 + \Delta\mathcal{H}_0) - \sum_k \frac{\partial \varepsilon_k}{\partial H}\bar{n}_k$$

leads to

$$M_y(T, H) \approx M_0 \frac{H}{H_A}\left(1 + \frac{\mu}{M_0}\sum \bar{n}_k\right) \quad \text{for} \quad H \leqslant H_A, \quad (15)$$

$$M_y(T, H) \approx M_0\left(1 - \frac{\mu}{M_0}\sum \bar{n}_k\right) \quad \text{for} \quad H \geqslant H_A, \quad (16)$$

where $\bar{n}_k$ is the average number of spin waves with energy ε_k (the boson distribution function).

It is easily shown that (15) leads to M_y values greater than M_0 when H is sufficiently close to H_A, which contradicts our initial assumption. Furthermore, at $H = H_A$ there is a discontinuity in the magnetization, and this too lacks physical meaning.** These difficulties are due to the fact that one does not usually include in the calculations the temperature dependence of the equilibrium position of the magnetization vector,*** which is related to the temperature dependence of the anisotropy constant. When the temperature dependence of η is properly included, one must minimize not $\mathcal{H}_0$ for $T > 0$, but the total thermodynamic potential of the system, namely,

$$\Omega = \mathcal{H}_0 + \Delta\mathcal{H}_0 + \varkappa T \sum_k \ln(1 - e^{-\varepsilon_k/\varkappa T}),$$

where ε_k is given by the general expression (10) with an undetermined value of η.

From the condition that Ω be a minimum, we find in case II (using (14)) that

a) $\eta = H/H_A^T$ for $H \leqslant H_A^T$, b) $\eta = 1$ for $H > H_A^T$,

where

$$H_A^T = H_A \frac{M_0 - 3\mu\sum \bar{n}_k}{M_0 - \mu\sum \bar{n}_k}. \quad (17)$$

Thus the transition from state (a) to state (b) takes place at a magnetic field value which is temperature dependent (decreases with increasing tempera-

---

*For case I the H and T dependences of M have no properties different from those discovered by Holstein and Primakoff.[4]

**Similar deductions follow from Iakovlev's work.[6]

***That is, the temperature dependence of the equilibrium direction of the axis of quantization for M which in the present case is characterized by η.

ture).* In this process Eqs.(15) and (16) for the temperature dependence of M_y remain entirely valid; one need only bear in mind that the transition from one of these formulas to the other takes place not at H = H_A, but at H = H_A^T (this observation also holds for the corresponding equations of Ref.6).

Assuming that $J_k \approx /k^2$ and bearing in mind that $\sum \bar{n}_k \approx 0.06\,(\varkappa T / I)^{3/2}$, we finally arrive at

a) $M_y(T,\ H) \approx (M_0 H / H_A)\,[1 + 0.06\,(\mu / M_0)\,(\varkappa T / I)^{3/2}]$ **for** $H \ll H_A^T$

and

b) $M_y(T,\ H) \approx M_0\,[1 - 0.06\,(\mu / M_0)\,(\varkappa T / I)^{3/2}]$ **for** $H \gg H_A^T$,

where

$$H_A^T \approx H_A\,[1 - 0.12\,(\mu / M_0)\,(\varkappa T / I)^{3/2}]. \tag{18}$$

We note that now $M_y^a(T,\ H_A^T) = M_y^b(T,\ H_A^T)$.

3. Antiferromagnets

Let us apply the general method of Section 1 to a uniaxial antiferromagnet whose symmetry axis (Z-axis) lies in the direction of intrinsic antiferromagnetism. We restrict our considerations to an antiferromagnet with two magnetic sublattices, and we assume that for j = 1 and 2, we have $M_{01} = M_{02} = M_0$ and $\mu_1 = \mu_2 = \mu$. Then

$$\mathcal{H}_0 = \text{const} + 2A_1\,(\eta_{j1}\eta_{j2} + \zeta_{j1}\zeta_{j2})\,M_0^2 + 2B_1\zeta_{j1}\zeta_{j2}M_0^2 + B\,(\zeta_{j1}^2 + \zeta_{j2}^2)\,M_0^2 - \\ - (\eta_{j1} + \eta_{j2})\,M_0 H_y - (\zeta_{j1} + \zeta_{j2})\,M_0 H_z, \tag{19}$$

where $A_1 = A_{12} = A_{21}$ is the sublattice exchange coupling constant and $B = B_{11} = B_{22}$ and $B_1 = B_{12} = B_{21}$ are anisotropic interaction coupling constants (within and between sublattices).

In the general case of an arbitrary field direction the operator $\mathcal{H}_2$ and the two types of spin-wave energies obtained from its diagonalized form are characterized by very complicated expressions which we shall not give here. We shall restrict our discussion to the ground state and the spin-wave spectrum when H is parallel or perpendicular to the Z-axis.

A detailed solution of the problem of minimizing $\mathcal{H}_0$ gives the following results for the ground state (i.e., for the values of $\eta_j = \sin\vartheta_j$ and $\zeta_j = \cos\vartheta_j$, which characterize the equilibrium position of the quantization axis of M_j at T = 0). First the conditions for the occurrence of antiferromagnetism with the intrinsic direction along the Z axis are that $A_1 > 0$ and $B_1 - B > 0$. Further, the field dependence of the magnetization differs significantly depending on whether $H \parallel OZ$ or $H \perp OZ$.

I. $H \parallel OZ$

In this case we treat two possibilities, namely, $B > 0$ and $B < 0$.

For convenience we introduce the notation

---

*Equation (17) actually gives the temperature dependence of the anisotropy constant (see also (18)). It is interesting to note that if this expression is considered as formally valid in the entire temperature interval from 0 to θ_C, it will in principle explain the experimentally observed change in the sign of the anisotropy constant of uniaxial ferromagnets.

$$H_{\parallel} = 2M_0\sqrt{(B_1 - B)(2A_1 + B_1 - B)}, \qquad H_{\perp} = H_{\parallel}\frac{2A_1 + B_1 + B}{2A_1 + B_1 - B}$$

and

$$H_e = 2M_0(2A_1 + B_1 + B),$$

fields whose meaning will become clear later. We obtain the following expressions for the H dependence of the equilibrium position of the axes of quantization of M_{0j}, of $M_z = M_{1z} + M_{2z}$ and of the susceptibility $\chi = \partial M_z/\partial H$ at T = 0.

1. $B > 0$ or $H_{\perp} > H_{\parallel}$

a) $0 \leqslant H \leqslant H_{\parallel}$; $\zeta_1 = -\zeta_2 = 1$, $M_z = 0$, $\chi = 0$.

In this state the antiferromagnetism Δ is directed along the Z axis, which is along H. In other words, it is in the direction of intrinsic antiferromagnetism.* We shall denote such a state by $(z, \parallel)$. The first index characterizes the axis along which H is directed, and the second gives the spatial relation between H and Δ.

b) $H_{\parallel} \leqslant H \leqslant H_{\perp}$; $\sin^2\psi = \dfrac{H - H_{\parallel}}{H_{\perp} - H_{\parallel}}$, $\sin^2\varphi = \dfrac{H_{\perp}^2}{H_e^2}\sin^2\psi$.

Here ψ is the angle between Δ and the Z axis, and φ is the angle between the axis of quantization M_{0j} and Δ. In this state, which we denote by (z, ψ), we have

$$M_z = 2M_0\frac{(H - H_{\parallel})H_{\perp}}{(H_{\perp} - H_{\parallel})H_e} \text{ and } \chi = \frac{2M_0H_{\perp}}{(H_{\perp} - H_{\parallel})H_e} = \frac{1}{2B}.$$

c) $H_{\perp} \leqslant H \leqslant H_e$; $\zeta_1 = \zeta_2 = \zeta = H/H_e$, $\eta_1 = -\eta_2 = \sqrt{1 - \zeta^2}$.

This state may be denoted by $(z, \perp)$, since Δ ⊥ H ; we then have

$$M_z = 2M_0\frac{H}{H_e} \quad \text{and} \quad \chi = \frac{2M_0}{H_e} = \frac{1}{2A_1 + B_1 + B}.$$

d) $H \geqslant H_e$; $\zeta_1 = \zeta_2 = 1$, $\eta_1 = \eta_2 = 0$, $M_z = 2M_0$.

This is the state of saturation along the Z axis.

2. $B < 0$ or $H_{\perp} < H_{\parallel}$

This case has been treated in detail by Néel,[7] who showed that in the interval $H_{\perp} \leqslant H \leqslant H_{\parallel}$ there may exist metastable states, so that there will be hysteresis in the magnetization.**

If the system passes only through states of thermodynamic equilibrium, we obtain the following results:

a) if $0 \leqslant H \leqslant H_0 = \sqrt{H_{\parallel}H_{\perp}}$, we have a state of the $(z, \parallel)$ type,

b) if $H_0 \leqslant H \leqslant H_e$ we have a state of the $(z, \perp)$ type,

c) if $H \geqslant H_e$ we have a state of saturation along the Z axis.

In this case, therefore, there is a discontinuous change in the direction of the antiferromagnetism and a discontinuity in the magnetization M_z at the threshold value H_0 of the field.

When one takes into account the existence of metastable states, however, one finds that the discontinuous transition to the $(z, \perp)$ state takes place at $H_{\parallel} > H_0$, while when the field is decreasing the return to the original $(z, \parallel)$

---

*The direction of the antiferromagnetism Δ is the direction of $M_{01} - M_{02}$.

** In his work Néel did not mention the first possibility (B > 0) in which no hysteresis can occur.

state takes place at $H_\perp < H_0$. In other words, hysteresis obtains.*

II. H$\perp OZ$

In this case the system behaves the same way regardless of the sign of We have

a) $0 \leqslant H \leqslant H'_e = 2M_0(2A_1 + B_1 - B)$; $\eta_1 = \eta_2 = \eta = H/H'_e$, $\zeta_1 = -\zeta_2 = \sqrt{1-\eta^2}$.

In such a state $\Delta \perp$ H and since H $\parallel OY$, we may denote this state by $(y, \perp)$. Then at T = 0

$$M_y = M_{1y} + M_{2y} = 2M_0 H/H'_e \quad \text{and} \quad \chi = 2M_0/H'_e = 1/(2A_1 + B_1 - B).$$

b) $H \geqslant H'_e$; $\eta_1 = \eta_2 = 1$, $\zeta_1 = \zeta_2 = 0$, $M_y = 2M_0$.

This is the state of saturation along the Y axis.

We present below the results of energy calculations for the spin waves in some of the cases enumerated above.

The $(z, \parallel)$ State

$$\varepsilon_k^{(1,2)} = \{p_1(p_2 + 2\lambda) \pm 2\sqrt{p_1(p_2 + 2\lambda)(\mu H)^2 + p_1^2\lambda^2}\}^{1/2}, \tag{20}$$

where

$$p_1 = K_1 - K + J_k - J_{1k}, \quad p_2 = K_2 - K + J_k + J_{1k},$$
$$K_1 = 2\mu M_0 B_1,$$
$$K = 2\mu M_0 B,$$
$$J_k = 2\mu M_0(A_1 + Ck^2 + Dk_z^2), \qquad C = C_{11} = C_{22},$$
$$J_{1k} = 2\mu M_0(A_1 + C_1 k^2 + D_1 k_z^2), \qquad C_1 = C_{12} = C_{21},$$
$$D = D_{11} = D_{22}, \qquad D_1 = D_{12} = D_{21}, \qquad \lambda = 2\pi\mu M_0 \frac{k_x^2 + k_y^2}{k^2}.$$

The λ in (20) comes from the dipole interaction. As can be seen, this interaction causes the spin-wave spectrum to be split into two branches even at H = 0. Its contribution to the energy is, however, relatively insignificant. This will be readily evident if we simply set H = 0. We obtain

$$\varepsilon_k^{(1)} = \{(K_1 - K + J_k - J_{1k})(K_1 - K + J_k + J_{1k} + 4\lambda)\}^{1/2},$$
$$\varepsilon_k^{(2)} = \{(K_1 - K + J_k - J_{1k})(K_1 - K + J_k + J_{1k})\}^{1/2}.$$

Thus the dipole interaction term ($\sim \mu M_0$) is added to the exchange interaction term ($\sim \mu M_0 A_1$) and hence hardly affects the energy of the spin waves.

If we neglect the dipole interaction, (20) is replaced by

$$\varepsilon_k^{(1,2)} = \{(K_1 - K + J_k - J_{1k})(K_1 - K + J_k + J_{1k})\}^{1/2} \pm \mu H. \tag{21}$$

In particular, if we set $k = 0$, we obtain the widths of the energy gaps, i.e., the minimum energies needed to excite spin waves. These energies determine the two antiferromagnetic resonance frequencies:

---

*It should be noted that the transition region $|H_\parallel - H_\perp|$ is relatively very narrow, for $|H_\parallel - H_\perp|/H_\perp \sim B/A_1$.

Hence the fact that hysteresis has not been observed experimentally may be explained, for instance, either by the fact that B $\geqslant$ 0 for the substances that have been examined or by the extreme narrowness of the hysteresis loop.

$$\varepsilon_0^{(1,2)} = \hbar\omega_{1,2} = \mu(H_\parallel \pm H). \tag{22}$$

The $(z, \perp)$ State

In general with the dipole interaction taken into account, the resultant expressions for $\varepsilon_k^{1,2}$ in this state are extremely cumbersome. We therefore give the result obtained when the dipole interaction terms are dropped, which is valid in almost all cases of practical interest, namely, for $H \ll H_e$ or $\varkappa T \gg 2\pi\mu M_0$. We then have

$$\varepsilon_k^{(1)} = \left\{(J_k - J_{1k})\left[J_k + \left(1 - 2\frac{H^2}{H_e^2}\right)J_{1k} + \left(1 - \frac{H^2}{H_e^2}\right)(K_1 + K)\right]\right\}^{1/2},$$
$$\varepsilon_k^{(2)} = \left\{(J_k + J_{1k})\left[J_k - \left(1 - 2\frac{H^2}{H_e^2}\right)J_{1k} - \left(1 - \frac{H^2}{H_e^2}\right)(K_1 - K)\right]\right\}^{1/2}. \tag{23}$$

It is interesting that in these states one of the branches has no energy gap. Specifically, for $k = 0$, we have

$$\varepsilon_0^{(1)} = \hbar\omega_1 = 0, \quad \varepsilon_0^{(2)} = \hbar\omega_2 = \left\{2J_0(K_1 - K)\left(\frac{H^2}{H_1^2} - 1\right)\right\}^{1/2}, \tag{24}$$

where $J_0 = 2\mu M_0 A_1$.

The $(y, \perp)$ State

As in the previous case, we present the result which does not include the dipole interaction and which is valid under similar circumstances. This is

$$\varepsilon_k^{(1)} = \left\{(K_1 - K + J_k - J_{1k})\left[J_k + \left(1 - 2\frac{H^2}{H_e'^2}\right)J_{1k} + \left(1 - \frac{H^2}{H_e'^2}\right)\right]\right\}^{1/2},$$
$$\varepsilon_k^{(2)} = \left\{(K_1 - K + J_k + J_{1k})\left[J_k - \left(1 - 2\frac{H^2}{H_e'^2}\right)J_{1k} + K_1 - K + \frac{H^2}{H_e'^2}(K_1 + K)\right]\right\}^{1/2}. \tag{25}$$

For $k = 0$, we obtain

$$\varepsilon_0^{(1)} = \hbar\omega_1 = \mu H_\parallel \sqrt{1 - \frac{H^2}{H_e'^2}}, \quad \varepsilon_0^{(2)} = \hbar\omega_2 = \mu\sqrt{H_\parallel^2 + H^2\frac{H_\perp}{H_\parallel}}. \tag{26}$$

Comparison of (22), (24) and (26) shows that the widths of the energy gaps (and therefore also the antiferromagnetic resonance frequencies) and even the form of their field dependence are very different for different types of states and for different field directions.*

The available experimental data on antiferromagnetic resonance[8] agrees well with the theory. Unfortunately, however, this data pertains only to fields $H < H_\parallel$. It would thus be of considerable interest to extend the investigations to fields $H > H_\parallel$ (usually $H_\parallel \sim 10^4$ oersted) in order to verify Eq. (24).

Because the transition region between the $(z, \parallel)$ and $(z, \perp)$ states is so narrow** one may assume, for the purposes of most problems, that these states join at $H = H_0 \approx 2M_0\sqrt{2A_1(B_1 - B)}$, which is equivalent to assuming $H_\perp = H_\parallel = H_0$.

---

*We have not presented the energy spectrum in the intermediate (z, ψ) state for B > 0 because it is so very complicated even when the dipole interaction is omitted. We remark only that in the narrow field interval $H_\parallel \leqslant H \leqslant H_\perp$ Eqs. (21) and (22) gradually change over to (23) and (24).

**See footnote on page 1164.

Then for fields $H \ll H_e$ the spin-wave energy spectrum may be written in the simpler approximate form

a) in the $(z, \parallel)$ state, i.e., for $\mathbf{H} \parallel OZ$ and $H \leqslant H_0$:

$$\varepsilon_k^{(1,2)} = \sqrt{(\mu H_0)^2 + l^2 k^2} \pm \mu H; \tag{27}$$

b) in the $(z, \perp)$ state, i.e., for $\mathbf{H} \parallel OZ$ and $H \geqslant H_0$:

$$\varepsilon_k^{(1)} = lk, \quad \varepsilon_k^{(2)} = \sqrt{\mu^2 (H^2 - H_0^2) + l^2 k^2}; \tag{28}$$

c) in the $(y, \perp)$ state, i.e., for $\mathbf{H} \perp OZ$:

$$\varepsilon_k^{(1)} = \sqrt{(\mu H_0)^2 + l^2 k^2}, \quad \varepsilon_k^{(2)} = \sqrt{\mu^2 (H^2 + H_0^2) + l^2 k^2}. \tag{29}$$

In Eqs.(27)-(29) we have neglected the anisotropy constants K_1 and K compared with the first exchange coupling constant J_0 and have introduced the second exchange coupling constant according to the relation $2J_0(J_k - J_{1k}) \approx l^2 k^2$.

Eqs.(27)-(29) were used by one of us to calculate the temperature dependence of magnetic susceptibility $\Delta\chi = \chi_T - \chi_0$, as well as the spin specific heat C_s (the specific heat at constant H) in all three states.* These results have been reported elsewhere.[10] Supplementing this report, we note that C_s can be found from the experimental data for $\Delta\chi$ by using the general relation between these two quantities. For $H < H_0$ and $\varkappa T \gg \mu H_0$, for instance, we have

$$\frac{C_s}{T\Delta\chi} = \frac{4\pi^2}{5}\left(\frac{\varkappa}{\mu}\right)^2 \approx 3.8 \cdot 10^8.$$

In conclusion, the authors express their deep gratitude to K.B.Vlasov and S.V.Vonsovskii for advice and discussions.

Institute of Metal Physics
Academy of Sciences of the USSR

References

1. L.D.Landau & E.M.Lifshits, Elektrodinamika sploshnykh sred (Electrodynamics of continuous media), 1957.

2. E.A.Turov & V.G.Shavrov, Trudy (proceedings) Inst.Metal Phys., Ural Branch, USSR Ac.of Sci., No.20, 101 (1958).

3. I.R.MacDonald, Proc.Phys.Soc., 64, 968 (1951).

4. T.Holstein & H.Primakoff, Phys.Rev., 58, 1098 (1940).

5. C.Herring & C.Kittel, Phys.Rev., 81, 869 (1951).

6. E.N.Iakovlev, Doklady AN SSSR, 115, 699 (1957).

7. L.Néel, Ann.Phys., 5, 232 (1936); Izv.AN SSSR, Ser.fiz., 21, 890 (1957). (Trans.Bulletin, 21, No.6, 889.)

8. E.S.Dayhoff, Phys.Rev., 107, 84 (1957).

9. M.I.Kaganov & V.M.Tsukernik, Report presented at the Conference on the Physics of Low Temperatures, M.1957.

10. E.A.Turov, Zhur.eksp.i teor.fiz., 34, 1009 (1958). (Trans.Soviet Physics - JETP.)

---

*Kaganov and Tsukernik[9] have performed similar calculations for the $(z, \parallel)$ and $(y, \perp)$ states, using a phenomenological method.

MAGNETIC STRUCTURE AND TECHNICAL MAGNETIZATION PROCESSES IN HIGH-COERCIVITY FERROMAGNETS

- Ia.S.Shur

Introduction

The magnetic properties of ferromagnets that are involved in technical magnetization can be correlated with their magnetic structure: the size and shape of the domains and the orientation of magnetization therein. This explains the growing interest evinced in the magnetic structure of different types of ferromagnets. It should be noted, however, that hitherto this structure as well as the process of technical magnetization, has been studied only to a limited extent and at that primarily in magnetically soft (low-coercivity) materials. Hence an urgent problem in the field of high-coercivity alloys is clarification of their magnetic structure and determination of the nature of the technical magnetization processes associated with it.

Research has been carried on for a number of years in the Institute of Metal Physics on the structure of high-coercivity ferromagnets. The present report is devoted to a description of the principal results of these studies.

Experimental procedures and results

1. It is a familiar fact that where magnetically soft materials are concerned our broad concepts regarding magnetic structure have been derived from investigation of the magnetic properties of single crystals and magnetically anisotropic polycrystals. Hence with the final aim of establishing the magnetic structure of high-coercivity of ferromagnets, we deliberately chose for study magnetically anisotropic samples of the high-coercivity alloys, Alnico and Vicalloy. The magnetic anisotropy in Alnico was realized by thermomagnetic treatment (heat treatment in a magnetic field); that in Vicalloy by cold deformation followed by annealing. The development of magnetic texture in these alloys as a result of the indicated treatments was evinced by changes in a number of their physical properties.

On the basis of comparison of different characteristics (magnetization curves and hysteresis loops[1], magnetostriction curves[2] and magnetostriction hysteresis loops[3], and variation of the resistivity in a magnetic field[4]), obtained for textured (grain-oriented) samples along and across the texture axis and for magnetically isotropic samples, it was inferred that in high-coercivity alloys technical magnetization processes are realized primarily through rotation. This occurs by virtue of the distinctive magnetic structure of these alloys, i.e., the single-domain type structure, wherein each grain or particle is a single domain. It follows from general energetic considerations that such a structure is only possible when the alloy is comprised of very small ferromagnetic particles; in the case of large particles a multiple domain structure must obtain. Thus, from the assumption of a single domain structure in high-coercivity alloys it follows that in this type of alloy there must exist a heterogeneous structure, wherein the individual minute ferromagnetic formations are isolated from each other by nonferromagnetic or weakly magnetic layers.

In order to obtain high values of the coercive force H_c, however, in addition to a single domain structure, a necessary condition is that there be an appreciable magnetic anisotropy in the domains; this may be induced by diverse factors.[5] In elucidating the nature of magnetic anisotropy in high-coercivity alloys much valuable information can be obtained by investigating the temperature dependence of the magnetization curves and hysteresis loops. Thus it was

found that in the case of Alnico and Vicalloy both H_c and the saturation magnetization are only weakly temperature dependent in a wide temperature range.[6] This is possible only if the magnetic anisotropy is caused by anisotropy of the shape of the ferromagnetic particles. From this and other data[1-4] it was concluded that ferromagnetic particles have a lamellar structure. It was also hypothesized[1] that in the process of thermomagnetic treatment of Alnico the applied magnetic field acts so that the laminae forming during the cooling of the alloy are oriented with their long axis parallel to the field. By virtue of this orientation of the particles, a magnetically uniaxial structure is realized in the specimen.

The proposed magnetic structure model was subsequently substantiated experimentally. Electron microscopic studies of Alnico showed that this alloy in the high-coercivity state is characterized by a heterogeneous structure with the strongly magnetic phase segregating in the form of laminae. As a result of thermomagnetic treatment there develops anisotropy in the arrangement of the laminae: the long axis of the particles is oriented parallel to the direction of the field applied during the magnetic heat treatment[7].

2. The proposed magnetic structure model is apparently applicable to all high-coercivity alloys, although in general the magnetic anisotropy may be caused by factors other than geometric anisotropy. Experiments showed that the coercive force in Vicalloy may be greatly increased by unilateral elongation[8]. Thus when a Vicalloy wire is stretched by a tensile load of 300 kg/mm^2 the value of H_c increases from 270 to 880 oersted. The experimentally observed increase in H_c is in good agreement with the theoretically calculated increase, if it is assumed that there develops in the single domain particles an additional magnetic anisotropy due to the stress anisotropy.

It follows from the above results that artificial increase of the magnetic anisotropy in alloys with a single domain structure may be an effective procedure for increasing the magnetic energy of alloys intended for permanent magnets. An appropriate treatment was therefore proposed for plastically deformable high-coercivity alloys.[9] The proposed treatment consists of subjecting the specimen to unilateral stretching during the tempering leading to the high-coercivity state. This treatment proved to be very effective in the case of Vicalloy: the coercive force increased from 440 to 550 oersted; the maximum magnetic energy increased by 50%.[9]

3. Inasmuch as the high-coercivity state is observed only in ferromagnetic formations of small size, it may naturally be inferred that with reduction of the ferromagnet dimensions, i.e., in going from large particles with a multiple domain structure to fine particles characterized by the single-domain structure, the magnetic structure must change in a regular, consistent manner. In view of this there is obvious interest in investigating the dependence of the magnetic structure on the size of the ferromagnetic formations. As a result of work with ferromagnetic powders of different degrees of dispersion, it was established that reduction of grain size is accompanied by growth of the coercive force, the growth becoming increasingly more rapid as the particle size is reduced.[10] There is good reason to assume, therefore, that the change in coercive force is connected with changes in the magnetic structure of the ferromagnetic material.

On the basis of the available data on the magnetic structure of different ferromagnets one can establish a regular sequence in the variation of this structure with decreasing grain size. Comparatively large particles are always characterized by a multiple domain structure consisting of principal and subsidiary (closure) domains[11]. With structures of this type translation processes (wall displacements) play a predominant role in technical magnetization. As long as this type of structure persists, the value of H_c remains virtually constant. With further decrease in grain size, however, the subsidiary domains begin to

vanish; only a few of them, located at the edges of the crystal, remain. This rearrangement of the structure increases the total energy of the crystal and hampers wall displacements, which leads to an increase of H_c. Further decrease in grain size leads to the multiple domain structure becoming energetically disadvantageous. At this degree of fineness, within each powder particle there exists only one principal magnetic domain with a few minute subsidiary domains persisting at the edges. This magnetic structure should be regarded as a transitional one, intermediate between the multiple domain structure of large particles and the true single domain structure of very fine grains. The development of this structure should produce further increase of H_c inasmuch as under these conditions, the growth of magnetization reversal nuclei (some of the subsidiary edge domains may play the part of such nuclei) is hampered. Finally, in the case of very small powder grains the existence of the subsidiary domains becomes energetically disadvantageous and then we have a true single domain structure with which reversal of magnetization can be realized only through rotation processes (rotation of the domain magnetization vectors); this structure gives the highest values of H_c.

4. Highly important at the present stage of study of coercivity is investigation of transition magnetic structures.

It was shown on the basis of measurements of the variation of H_c of Mn-Bi alloy powder as a function of the particle size at different temperatures that the changes in magnetic structure connected with decrease in the size of the individual ferromagnets (particles) depend on their physical properties.[12] In particular, the greater the total magnetic anisotropy, the larger the critical grain size at which the transition and single domain structures develop.

The transition structure is evinced in many properties of ferromagnets. Thus in the case of fine powders of Mn-Bi alloy, the existence of the transition structure is brought out by comparing the shape of the magnetization curve with the curve characterizing the variation of the residual magnetization and coercive force as functions of the magnetizing field.[3] It was established that the magnetization curve attains saturation at appreciably lower fields than those necessary for attaining the maximum values of residual magnetization and coercive force. These results can be explained if we bear in mind that these parameters are affected in different ways by the subsidiary domains persisting at the particle edges in the transition structure.

5. Valuable information on the magnetic structure of high coercivity ferromagnets and technical magnetization processes therein has been obtained by means of powder patterns (Bitter figures) on Mn-Bi alloy specimens.[14] It proved possible to observe the single domain structure in minute particles and the process of reversal of magnetization in such particles, a process which occurs only by rotation of the domain magnetization vectors. We were also able to detect and isolate particles with the transition magnetic structure. It was found that these, after magnetization in a strong field and subsequent reversal of magnetization, behave as single domain particles. In this case the strong magnetic field completely destroys the reverse magnetization nuclei. The same particles after demagnetization and remagnetization in a weak field behave as multiple domain particles.

Conclusions

It follows from the cited data that the magnetic properties of ferromagnets vary in a consistent, regular fashion with changes in their magnetic structure. As the ferromagnetic particle size decreases, the magnetic structure is simplified, i.e., the multiple domain structure is replaced by a transition structure

and then by a single domain structure, and technical magnetization processes are increasingly hampered. The high coercivity state can develop in ferromagnetic particles only when their structure is of the transition or single domain type. The specific particle sizes at which these magnetic structures arise depend on the physical properties of the ferromagnet and to an appreciable extent on its magnetic anisotropy.

The above concepts allow only of making qualitative judgments regarding the magnetic structure of high coercivity alloys; many important details of this structure are still unclear. Hence we attach particular importance to further comprehensive investigation of the magnetic structure of high-coercivity ferromagnets.

A more detailed review of the subject will be found in Ref.15.

Institute of Metal Physics
Academy of Sciences of the USSR

References

1. L.A.Shubina & Ia.S.Shur, Zhur.tekh.fiz., 19, 88 (1949).
2. D.A.Shturkin & Ia.S.Shur, ibid., 19, 235 (1949).
3. D.A.Shturkin & Ia.S.Shur, ibid., 20, 1393 (1950).
4. V.I.Drozhzhina, M.G.Luzhinskaia & Ia.S.Shur, ibid., 19, 95 (1949).
5. S.V.Vonsovskii & Ia.S.Shur, Ferromagnetizm (Ferromagnetism), M-L.,1948.
6. Ia.S.Shur & N.A.Baranova, Trudy (Proceedings), Institute of Metal Physics, Ural Branch, Ac.of Sci., 15, 19 (1954).
7. H.Fahlenbrach, Naturwissenschaft, 42, 64 (1955).
8. Ia.S.Shur, M.G.Luzhinskaia & L.A.Shubina, Fiz.met.i metallovedenie, 4, 54 (1957). (Trans.Phys. of Metals & Metallography.)
9. Ia.S.Shur, M.G.Luzhinskaia & L.A.Shubina, ibid., 4, 60 (1957).
10. Ia.S.Shur, T.D.Zotov & I.A.Chebotarev, Doklady AN SSSR, 81, 387 (1951); E.V.Shtol'ts & Ia.S.Shur, ibid., 95, 781 (1954).
11. Ia.S.Shur & V.R.Abel's, ibid., 104, 209 (1955); Fiz.met.i metallovedenie, 1, 11 (1955).
12. Ia.S.Shur, E.V.Shtol'ts & G.S.Kandaurova, Fiz.met.i metallovedenie, 6, 420 (1958).
13. Ia.S.Shur, E.V.Shtol'ts & G.S.Kandaurova, ibid., 2, 569 (1956); Izv.AN SSSR, Ser.fiz., 21, 1215 (1957). (Trans.Bulletin, 21, No.7, 1205.)
14. Ia.S.Shur, E.V.Shtol'ts & G.S.Kandaurova & L.V.Bulatova, Fiz.met.i metallovedenie, 5, 234 (1957). (Trans.P.M.M.)
15. Ia.S.Shur, Trudy (Proceedings) Institute of Metal Physics, Ural Branch, Ac.of Sci., 20, 111 (1958).

DOMAIN STRUCTURE DYNAMICS IN TRANSFORMER IRON CRYSTALS UNDER THE INFLUENCE OF STRESSES

- L.V.Kirenskii, M.K.Savchenko & A.M.Rodichev

We used the Akulov-Bitter[1] figure technique to investigate the influence of elongation under tensile stress on the domain structure of crystals of cold rolled transformer iron (3.4% Si). It was found that the domain structure changes substantially as a result of stretching and that the character of the changes depends on the direction of the applied load. Changes in the domain structure were also observed by recording Barkhausen jumps.

Equipment and Procedure

For observation we chose crystals with a surface parallel to the (110) planes. The samples were cut in the form of 0.5 x 4 x 60 mm plates. Prior to observation of the powder patterns the specimens were annealed in vacuum at 1000° for 3-4 hours and then polished electrolytically. The specimens were stretched in a special device in which one end of the specimen was held in a stationary vise, the other in a slider coupled to a tension gage and actuated by a motor. The powder patterns were observed and photographed by means of an MIM-5 microscope. The Barkhausen jumps were recorded by means of a search coil, circling the specimen, and PS-64 scalers with a resolving power of 6400 pulses per sec.

Experimental Results

The powder patterns on the (110) surface of the crystals consist of parallel lines extending in the direction of the easy magnetization axis closest to the surface. This pattern indicates that the domain structure consists of plane-parallel laminar domains oriented (and magnetized) in the direction of the powder pattern lines. The most important changes occurring in the powder patterns, and hence in the domains themselves, are the following.

1. Stretching in the [001] direction

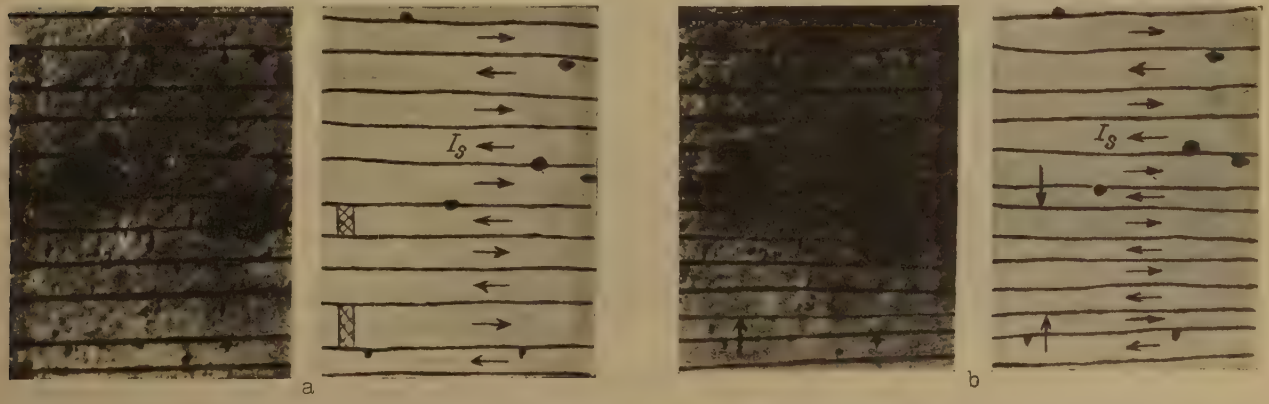

Fig.1. Splitting of domains by newly forming walls (indicated by arrows). Direction of stretching horizontal. Magnification 50 X. The diagrams at the right show the distribution of magnetization I_s in the domains. Stresses: a - 10, b - 15 kg/mm^2.

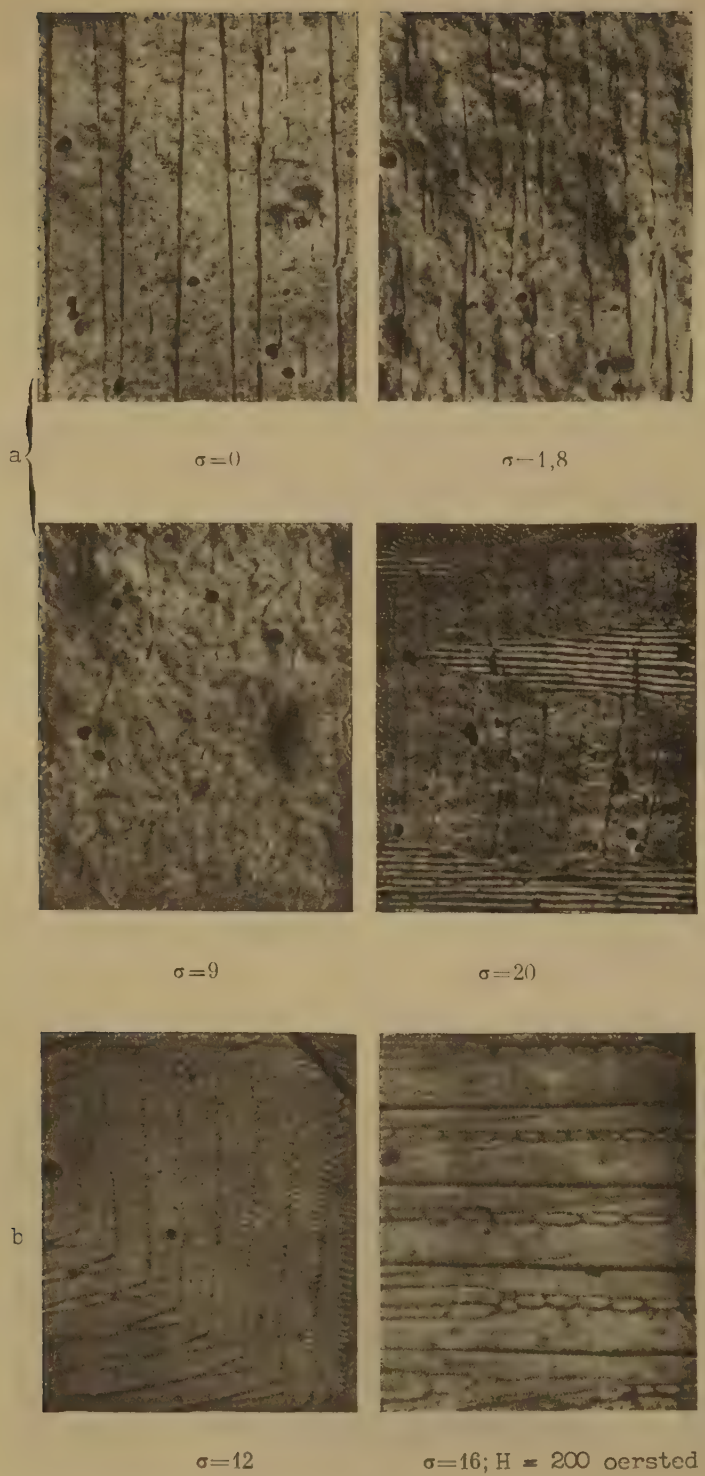

Fig.2. Powder patterns of specimens elongated in the [110] direction (horizontal in the figure): a - rearrangement of structure, magnification 60 X; b & c - drops and chains at boundaries between type 1 domains, magnification 150 X. Stresses σ in kg/mm^2.

The plane-parallel laminar domains in any given specimen are never equal in width owing to residual stresses persisting in the specimens despite the prolonged annealing. Application of the external load equalizes the general stress in the specimen; in consequence, the domain structure is also equalized.

In the course of elongation we frequently observed fissioning of the domains by newly forming walls (Fig.1). The appearance of new boundaries inside the domains indicates reversal of magnetization in parts of the crystal, specifically in the volumes between the newly forming walls. This subdivision of the domains by new walls is a consequence of the more general effect of narrowing of the domains as a result of increase of the effective magnetic crystallographic anisotropy incident to elongation. Such reduction in the domain width is obviously possible only by splitting of some of the domains by newly forming walls. It must be noted that the reversal of magnetization is realized not by wall movements but by sudden flipping of whole domains.

2. Stretching in the [110] direction

Stresses applied in the [110] direction lead to complete rearrangement of the initial domain structure (Fig.2). At a sufficiently high tensile stress there appeared two new types of figures: horizontal and vertical bands which we shall designate type 1 and type 2 figures, respectively; the vertical bands in turn exhibit a fine mosaic structure. Both types of figures tend to form a complex closed system. With increasing

stress, the area occupied by type 2 figures increases at the expense of the type 1 figure area. This indicates that the magnetization in the case of both types of figures is directed perpendicular to the direction of the bands. Measurements of the type 1 bands indicate that the width of these bands is inversely proportional to the logarithm of the stress. In view of this, from the type 1 figures one can determine the stress in the metal, not merely qualitatively but quantitatively.

The described changes in the appearance of the powder patterns are connected with rearrangement of the domain structure owing to redistribution of the easy magnetization axes in the crystal under the influence of stress. The initial magnetization axis - [001] - makes an angle of 90° with the direction of stretching; hence under stress it is replaced either by the [100] or [010] axis, which, although they do not lie in the plane of the crystal, are oriented at 45° to the direction of elongation.

Fine grain specimens. So far we have been speaking of comparatively large crystals, each comprising an entire specimen. For purposes of comparison we also carried out observations on fine crystal specimens consisting of grains having linear dimensions of 1-1.5 mm. Similar observations were carried out some years ago by Dijxtra & Martius[2]; however, they failed to notice certain interesting details. On small crystals, type 2 patterns appear first at the grain boundaries, where the stresses are higher compared with the rest of the grain. In most cases the appearance and development of type 2 patterns is furthered by "drops" forming at the boundaries of type 1 domains (Fig.2,b). The volume of these drops increases with increasing stress; at a certain stress the drops swell to such an extent that they become unstable, break up and retreat, drawing along the type 2 mosaic pattern. Thus the area occupied by type 2 domains in the crystal increases. Regarding the magnetization of the drops, it may be inferred that they are magnetized along their long sides, i.e., in the same way as the type 2 figures; along any given wall the magnetization of all the drops is directed in the same way. This is substantiated by the observed increase in the size of the drops with longitudinal stretching and the absence of sharp boundaries between them and type 2 figures.

Aside from drops, at the boundaries between type 1 domains there may also appear a "chain" pattern. Such chains appear when the crystal is magnetized by a field directed along these boundaries. With one direction of the field, the chains form along one half of all the walls (alternate boundaries); when the field is reversed, the chains form on the other alternate walls. Like that of the drops, the magnetization of the chains is aligned with the field. The appearance of these patterns is shown in Fig.2,b. The appearance of drops and chains is apparently connected with emergence to the surface of internal ferromagnetic domains, while type 1 domains are initially a superficial phenomenon.

In the case of small crystals, just as in the case of large ones, the width of type 1 domains decreases with increasing stress. However, in this case we were unable to establish any simple relationship between the domain widths and the magnitude of the stress. This may be explained by the fact that by virtue of the closeness of the grain boundaries to other portions of the grain, the different parts of the grain have different stresses, i.e., by the fact that small grains are characterized by steeper stress gradients. In addition, as a result of rearrangement of the domain structure under the influence of stress, there form on the crystal boundaries stray magnetic fields which also leave their imprint on the domain structure (powder pattern).

3. Stretching in the [111] direction

Our observations show that when a crystal is stretched in a direction of difficult magnetization, the domain structure changes much as in the case of stretching along an axis of easy magnetization. It must be noted, however, that at high stresses, just as in the case of elongation in an intermediate direction, there is observed rotation of the entire structure through 90°. More detailed investigations of variations in structure during stretching in [111] direction are hampered by the fact that in this case the powder patterns remain indistinct right up to the elastic limit of the material.

4. Powder figures on the (100) surface

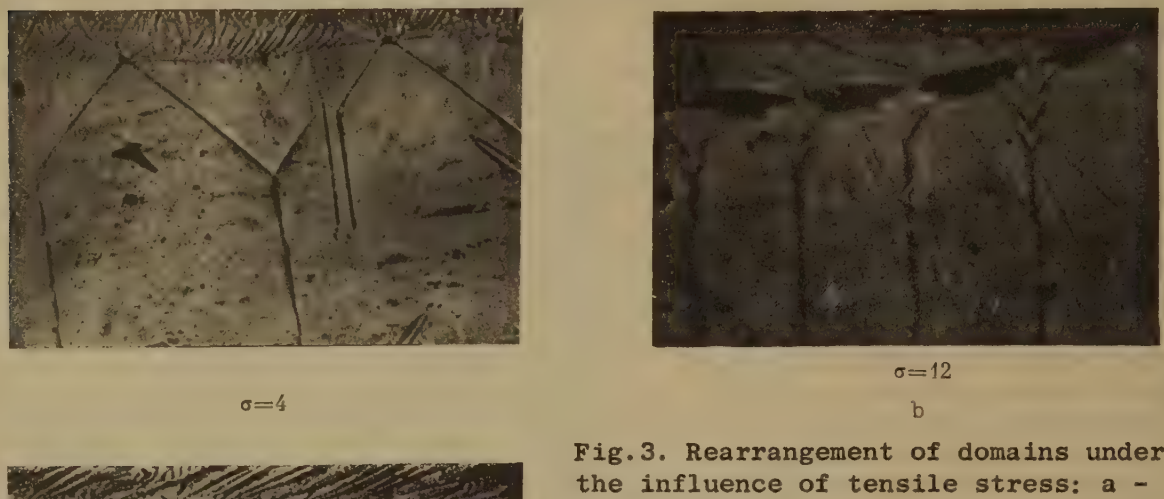

Fig.3. Rearrangement of domains under the influence of tensile stress: a - fragmentation of closure and principal domains (stretching in the horizontal direction); b - formation of poles (stretching in vertical direction). Magnification 150 X; stresses σ in kg/mm^2.

We studied the variation in closure type domains under the influence of elongation on crystals whose surface coincided with a (100) plane. The investigations were carried out on specimens composed of grains with linear dimensions of 1-1.5 mm. When the directions of elongation and of magnetization in the prismatic closure domains are parallel, the domains increased in size with increasing stress. However, this growth is limited; at a certain point the closure domains begin to fragment, i.e., break up into smaller domains, and the rearrangement of the main plane-parallel laminar structure is correlated with the size of these new, smaller prismatic domains (Fig.3). Reversal of magnetization is realized not by wall displacement, but, as noted above, by sudden magnetization flips of appreciable sections of the crystal.

If the direction of magnetization in the prismatic domains forms an angle of about 90° with the direction of elongation, in the process of stretching the domains contract and as a result stray magnetic fields form at the edges of the crystals. In Fig.3,b such stray fields are evinced by the accumulation of magnetic powder in the interstices between the closure domains.

The reproduced powder pattern photographs show that stray fields do not form only if the plane-parallel laminar domain structure includes closure domains. In most cases there are no closure domains at the crystal boundaries in fine grain specimens (the same is true in the case of no stress in the material). Ferromagnetic domains of individual crystals tend to arrange themselves so that the magnetic flux from one crystal passes into the next and so on. It may be said that the domain structure tends to extend through the grain boundaries. This is possible if the neighboring grains have an identical (or close) crystallographic orientation. The weak stray fields arising due to minor misalignments are reduced by the formation of wedge-shaped or similar triangular domains at the crystal boundaries. Closure domains form on the (100) surface only when the orientations of neighboring grains differ appreciably.

5. Concurrent observation of powder patterns and recording of Barkhausen jumps

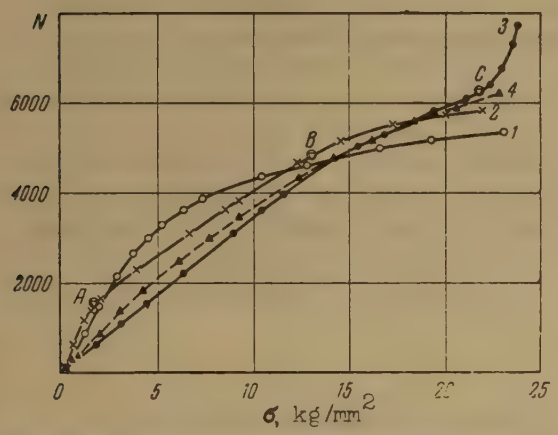

Fig.4. Variation in the number N of Barkhausen jumps with the applied stress in the [001] (curve 1), [110] (curve 2) and [111] directions (curve 3) of a single crystal. Curve 4 is for a polycrystalline specimen.

Although the Bitter figure technique has great potentialities as regards study of the domain structure, it also suffers from a number of serious shortcomings. Among these is the appreciable lag of the pattern changes, the fact that only a limited area on the surface of the material can be observed and the restricted temperature range in which the procedure is applicable. Hence in further investigations of the domain structure of materials it may be useful to supplement the Bitter figure technique with some other procedure. In the present work, in addition to observing powder patterns, we recorded the Barkhausen jumps incident to elongation of single crystals along different crystallographic axes. The results are shown in Fig.4 in the form of curves giving the variation in the number of jumps per mm^3 with the load for different specimens.

a) Elongation in the [001] direction. The initial sharp rise of the curve is connected with elimination of surface domains and intense displacements of the walls between the principal domains in the process of their equalization in width. Further, the curve flattens out; there are only minor domain wall movements corresponding to this stress interval.

b) Elongation in the [110] direction. The initial section of the curve is connected with break-up of the initial structure under the influence of stress. This process terminates only at point A; here the curve exhibits a break (inflection) and thereafter is rectilinear to point B. The interval AB, characterized by the powder patterns of Fig.2, corresponds to the interval when there is no clearly pronounced domain structure in the crystal (transition interval from complete liquidation of the initial structure to the appearance of type 1 and 2 domains). Thereafter the recorded jumps occur in type 1 and 2 domains.

c) Elongation in the [111] direction. The curve in this case is almost a straight line up to stresses of the order of 22 kg/mm^2 (point C). The domain structure in this interval undergoes no changes except some parallel wall displacements and eliminations of the surface domains. The sharp rise of the curve

after point C is connected with rearrangement of the entire structure.

Fig.4 also shows the curve (4) for a polycrystalline specimen (nontextured hot rolled transformer iron with a grain size of 1-1.5 mm). As may be expected this curve does not show any sharp bend inasmuch as all the crystallographic directions are equally probable and the number of jumps is equal to their sum in all directions.

The reproduced Barkhausen jump curves show that such curves faithfully reflect all the changes occurring in the domain structure. Hence this technique can be particularly valuable for investigations at low and high temperatures, that is, in temperature ranges where the powder pattern technique in its present form cannot be employed.

References

1. N.S.Akulov & M.Dekhtiar, Ann.Phys., 15, 750 (1932); F.Bitter, Phys.Rev., 38, 1903 (1931); 41, 507 (1932).

2. L.J.Dijkstra & U.M.Martius, Rev.Mod.Phys., 23, 146 (1953).

CHANGES IN THE MAGNETIC STRUCTURE OF SILICON IRON CRYSTALS UNDER THE INFLUENCE OF ELASTIC STRESS

- V.A.Zaikova & Ia.S.Shur

The magnetic properties of ferromagnets involved and evinced in technical magnetization may change appreciably under the influence of elastic stresses. This is apparently due to the fact that unilateral strains may alter the character of the total anisotropy in the crystal and, in consequence, its entire magnetic structure. Detailed investigation of the changes exhibited by the magnetic structure under the influence of elastic stresses can help us understand the nature of the process of technical magnetization in ferromagnets. In addition, such studies can yield much valuable information on the relation between the magnetic structure and the crystal structure of ferromagnets. It must be noted, however, that hitherto there have been comparatively few studies of this type.[1,2,3]

The purpose of the present work was to establish the general regularities characterizing the variation in the magnetic structure in ferromagnetic crystals under the influence of elastic stress.

The studies were carried out by the powder pattern procedure on coarse grain samples of silicon iron containing about 3.5% Si. The samples were prepared in the form of strips measuring 40 x 4-5 x 0.1-0.2 mm. Specimens with different orientations of the surface relative to the crystallographic planes were studied; the observed area was sufficiently far removed from the clamped ends of the specimens. The dimensions of the individual crystallites varied from 1.0 to 0.2 mm. The straining equipment and the observation and photographing procedures have been described elsewhere.[4]

Results

Of the many observed changes in the powder patterns on the surface of crystallites with different orientations under the influence of elastic elongation, we shall describe below two characteristic cases: 1) when the surface of the specimen is close to a (001) crystallographic plane and 2) when the surface is close to a (011) plane.

Fig.1 shows a series of photographs of the powder patterns observed on a (001) surface of a crystallite, i.e., on the surface of the specimen, the plane of which includes the two directions of easy magnetization: [100] and [010].*

The orientations of the magnetization vectors I_s are indicated by arrows in the photographs. In the initial (unstressed) state there can be seen on the surface of the crystal two principal domains separated by a 180° wall parallel to the [100] axis and the I_s in the principal domains (Fig.1,a). At the ends of this wall there appear triangular closure domains with magnetization vectors parallel to the [010] axis. A number of subdomains can be discerned inside the principal domains.

When a weak stress is applied in the [010] direction, i.e., parallel to the I_s of the closure domains and at right angles to the I_s of the principal domains, at first there is observed growth of the closure domains and some displacement of the wall between the principal domains. Increase of the load leads to an appreciable increase of the area occupied by the domains the I_s of which are parallel to the direction of elongation. At the same time there appear new 180° walls aligned with the strain direction (Fig.1,b).

---

*We denote the tetragonal crystal axis closest to the surface of the specimen as [100], the axis deviating furthest from the surface as [001] and the intermediate axis as [010].

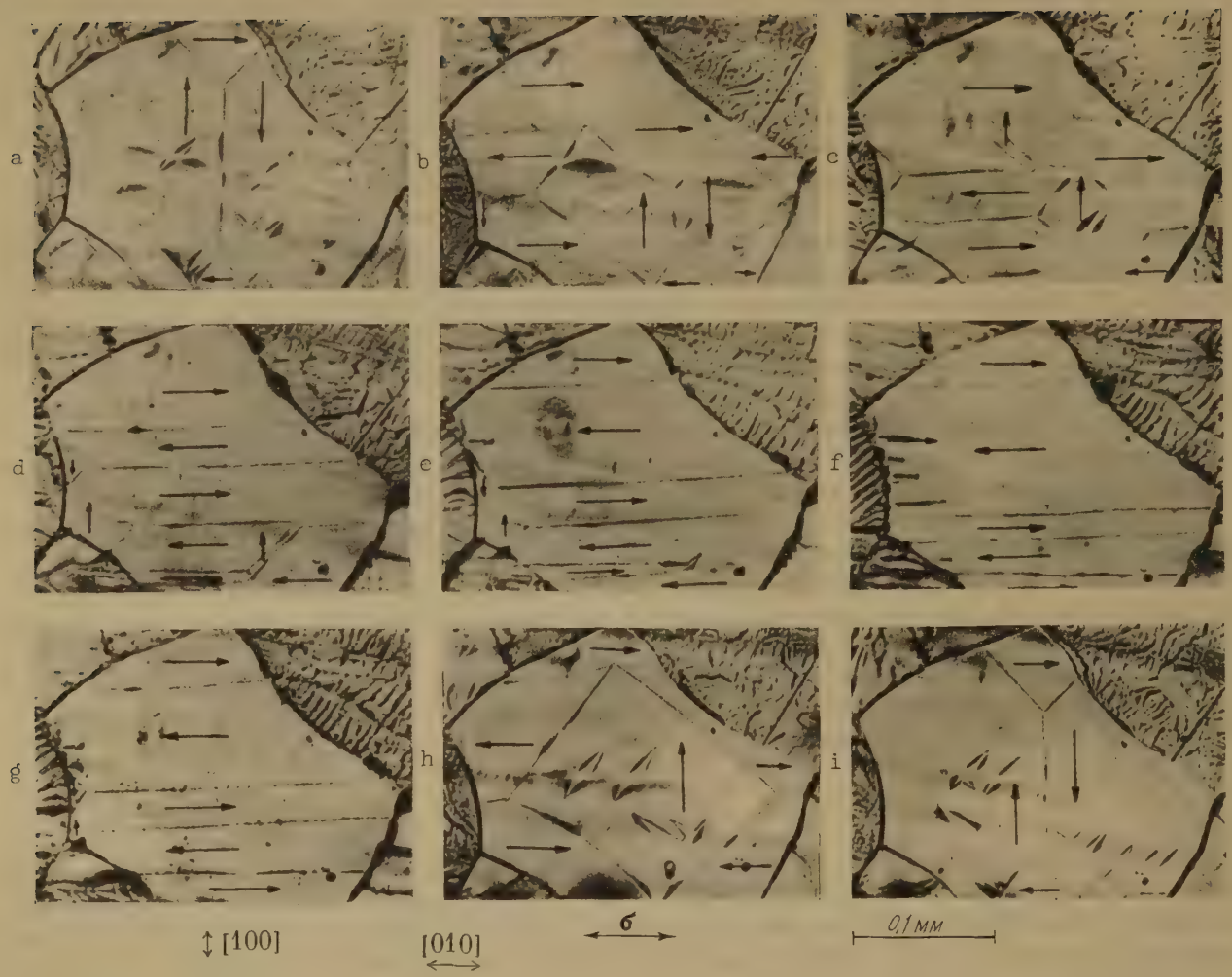

Fig.1. Variation in the powder patterns on the (001) surface of a silicon iron specimen under the influence of elastic elongation. Stress σ in kg/mm^2: a - 0, b - 1.6, c - 3.2, d - 9.5, e - 16, f - 19.0, g - 9.5 and h - 0; i - 0 (after demagnetization).

Further increase of the stress leads to further decrease in the volume of the domains disadvantageously magnetized with respect to the direction of elongation (Fig.1,c) and growth of the new principal domains. For carrying over the magnetic flux of these principal domains there appear (at the left edge of the crystal in the photograph) triangular closure domains, the resultant magnetization in which is perpendicular to the elongation. At a sufficiently high stress (9.5 kg/mm^2), the domains in the center of the crystallite with I_s perpendicular to the line of elongation virtually vanish (Fig.1,d). Further decrease of the load leads first to displacement of some of the walls separating the new principal domains and to reduction of the volume occupied by the closure domains (Fig.1,e) and then to fragmentation of the principal domains and complete disappearance of the closure domains (Fig.1,f). It is important to note that at high tensile stresses there appear at the ends of the principal domains subsidiary dagger-shaped domains (Fig.1,f). These domains reduce the energy of the free poles located at the ends of the principal domains. At lower stresses this role is played by the closure domains, the existence of which at high tensile loads

becomes energetically disadvantageous, inasmuch as the I_s of these domains are perpendicular to the direction of elongation.

Even minor stretching of the specimen alters the shape of the subdomains and the orientation of the magnetization vectors therein. Higher loads result in complete disappearance of the subdomains. With reduction of the load there are observed irreversible changes in the magnetic structure. This will be evident, for example, from comparison of the powder patterns of Fig.1,d and g recorded at the same value of the stress (σ = 9.5 kg/mm^2) but with increasing and decreasing loads, respectively. The walls between the principal domains formed during elongation do not return to their initial positions. Moreover, the number of walls in Fig.1,g is greater than in Fig.1,d. Further reduction of the stress is accompanied by decrease in the number of walls parallel to the direction of stretching. Complete removal of the load leads to the appearance at the center of the grain of a region with I_s perpendicular to the original stress direction (Fig.1,h); the magnetic structure does not, however, completely return to its initial appearance. The initial magnetic structure is restored only after demagnetization of the specimen (Fig.1,i). This indicates that the observed irreversibility of the magnetic structure is purely magnetic in character and is not

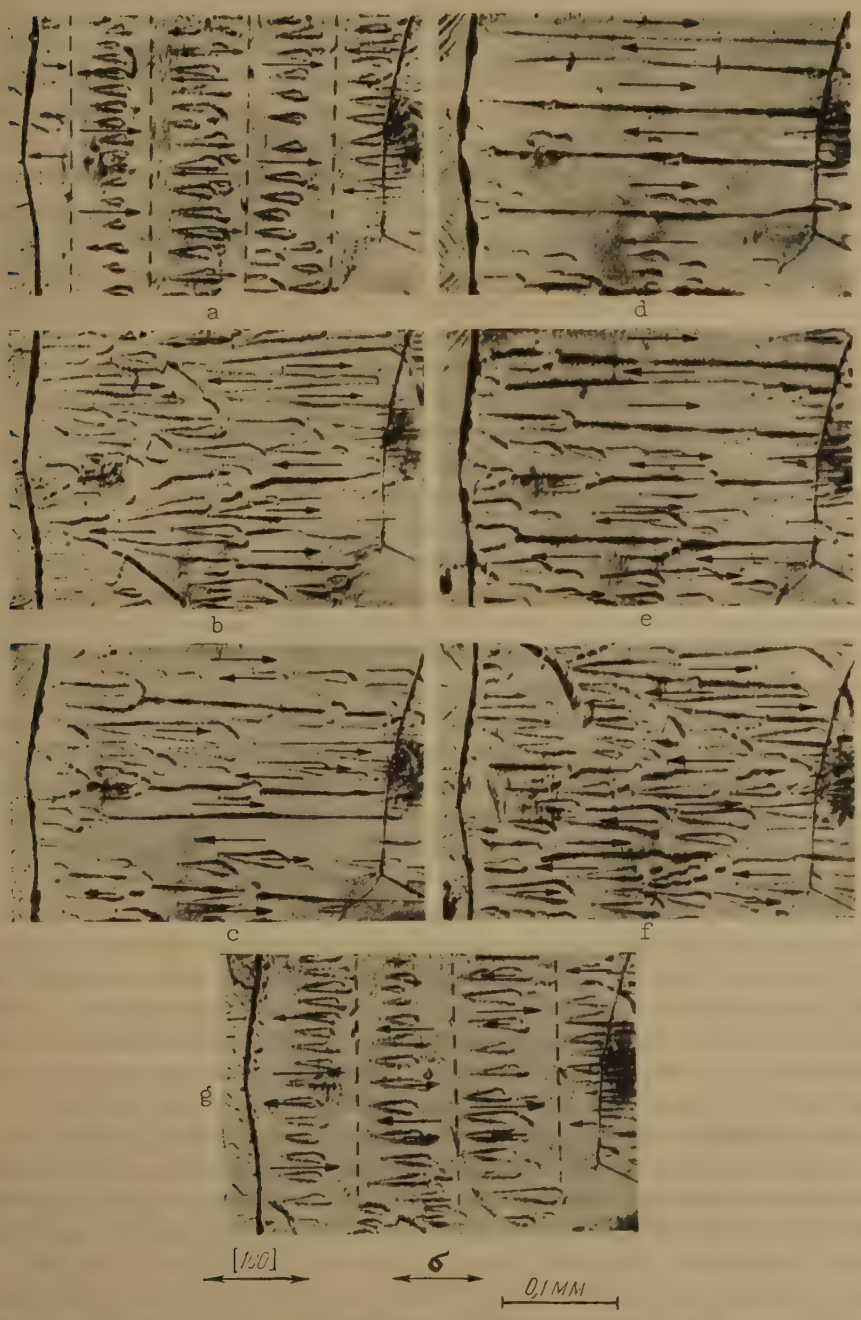

Fig.2. Variation of the powder patterns on a surface close to a (011) plane under the influence of elastic strain. Stress σ in kg/mm^2: a - 0, b - 2.0, c - 4.7, d - 12.5, e - 4.7 and f - 0; g - 0 (after demagnetization).

connected with irreversible changes in the crystal lattice of the ferromagnet under the influence of deformation.

A series of photographs of the powder patterns on the surface close to a (011) plane is reproduced in Fig.2. The [100] direction forms a small angle with the surface of this specimen; the other two directions, namely [010] and [001] are at large angles to the specimen surface. In the initial state the pattern comprises several rows of drop-shaped subsidiary domains (Fig.2,a). It was inferred earlier[5] that in this case the entire surface of the specimen is covered with closure domains with the subsidiary drop-shaped domains inside them. The walls between the closure domains are located between the rows of drops, but owing to the weakness of the stray fields, these walls are not brought out by the powder technique (in Fig.2,a the location of these walls is indicated by the dashed lines). The magnetization vectors of the closure domains are parallel to the [100] axis and perpendicular to the walls separating these domains. The principal domains in this case are magnetized along either the [010] or the [001] axis and do not emerge to the surface of the specimen. In Ref.5 this structure was called type B.

When the crystallite is stretched parallel to the magnetization vector of the closure domains, there is observed a strong growth of the drop-shaped domains (Fig.2,b); the entire surface of the crystallite becomes covered with subsidiary drop domains and expanded dagger domains (the latter prior to stretching of the specimen were located at the right boundary of the crystal). Further increase of the load leads to the appearance of new walls parallel to the direction of elongation. These walls divide new principal domains in which the I_s are parallel to these walls. Thus there develops the structure called type A in Ref.5. At the same time there is an appreciable decrease in the number and area of the subsidiary domains (Fig.2,c). With further increase of the stress, the number of principal domains increases, while the drop domains nearly disappear (Fig.2,d).

Then,with decreasing load, there is observed a gradual increase in the volume and number of drop domains. At the same time the number of walls parallel to the direction of elongation decreases (Fig.2,e & f). In this case, as in the case of the (001) surface described above, the changes in the powder patterns observed incident to application and removal of the load are irreversible. This will be evident from a comparison of Fig.2,c & e photographed at the same value of σ (4.7 kg/mm^2). In Fig.2,e (decreasing load), the area occupied by subsidiary domains is smaller and the number of walls parallel to the direction of elongation larger than in Fig.2,c (increasing load). The principal irreversible feature in this case is that the type A structure, appearing as a result of elongation, persists even after complete removal of the load (Fig.2,f). In this photograph one can see 180° walls and chaotically distributed subsidiary drop-shaped domains. The initial magnetic structure is restored only after demagnetization of the specimen (Fig.2,g). The drop domains are again arranged in rows perpendicular to the direction of elongation. It will be evident from a comparison of Fig.2,a & g that in this case, too, the irreversible changes are of purely magnetic character and not connected with any irreversible alterations in the crystal lattice of the ferromagnet.

Analysis of the experimental results

It will be evident from the cited data that highly complex rearrangements occur in the magnetic structure of silicon iron crystals under the influence of stresses. Let us try to establish the general regularities characterizing the variations in magnetic structure incident to unilateral elastic elongation of ferromagnetic crystals.

In a crystal with type A structure with triangular closure domains, upon elongation of the crystal at right angles to the I_s of the principal domains and parallel to the I_s of the closure domains, there occurs a rearrangement of the structure as a result of which the orientation of the I_s of the principal domains becomes parallel to the direction of elongation. This rearrangement is caused by the fact that the direction parallel to the line of elongation becomes the direction of easy magnetization (Fig.1). The rearrangement is connected with a positive value of magnetostriction in silicon iron. At the same time closure domains grow when the crystal is elongated parallel to the I_s in these domains (Fig.1,a & b) and contract or even disappear when the crystal is stretched in the perpendicular direction (Fig.1,c & f). In the first case, the increase of the closure domains is explained by the fact that elongation makes the [010] direction, lying in the plane of the specimen, energetically more advantageous; this is the direction parallel to the elongation and the orientation of the I_s of the closure domains. Consequently, as the load is increased, the entire structure of the crystal alters. There appears a structure consisting of plane-parallel principal domains with magnetization vectors I_s parallel to this [010] direction and the direction of elongation and new triangular closure domains in which the I_s are perpendicular to the strain direction.

In the second case, the contraction and final disappearance of the closure domains is explained by the fact that with elongation of the specimen the existence of domains in which the I_s are perpendicular to the direction of elongation becomes energetically disadvantageous.[2,4]

In the case of stretching of a crystal with type B structure (Fig.2,a) parallel to the projection of the [100] axis on the plane of the specimen, there is at first observed an appreciable increase in the area occupied by the drop-shaped subsidiary domains (Fig.2,b). This, apparently, is connected with rearrangement of the entire magnetic structure of the crystal, and hence, as a result of elongation, the [100] axis becomes the direction of easy magnetization (instead of the [010] or[001] axis in the initial state). As the stress is increased, the type B structure gives way to the type A structure in which the I_s of the principal domains become parallel to the [100] direction and the line of elongation (Fig.2,b). Further increase of the load is accompanied by decrease of the subsidiary domains (Fig.2,d); this is explained by the fact that with increasing load, the angle between the I_s and the surface of the crystal decreases. This leads to decrease of the free magnetic poles on the surface of the crystal and, consequently, to diminution and disappearance of the subsidiary domains.

Under the influence of elastic deformation parallel to the I_s of the principal domains, there is observed displacement of the walls between them (Fig.1,d & e) and splitting of the principal domains (Figs.1,e & f and 2,c & d). The wall movements can be explained by the fact that incident to elongation of the specimen there appear new regions in the crystal wherein the wall energy has a minimum value. Consequently, the walls shift to these minimum energy locations. Fragmentation of the principal domains is connected with increase of the stray field at the crystal boundaries, in the direction parallel to the line of elongation and the orientation of the I_s in the principal domains. A substantial role is also played in all this by the crystallographic orientation of the neighboring grains.

In some caseselongation leads to a change in the type of magnetic structure (Fig.2,a-c). This rearrangement of the magnetic structure occurs because under the influence of elongation the tetragonal axis closest to the direction of elongation becomes the axis of easy magnetization.

As noted above, incident to application and removal of a tensile load there are observed irreversible changes in the magnetic structure of ferromagnetic

crystals. These changes consist of irreversible displacements of the walls between the principal domains (Fig.1,d-g) and irreversible alterations of the closure and subsidiary domains. Hence, as a rule, the appearance of the powder patterns after removal of the load differs from their initial appearance (Figs. 1,a & h and 2,a & f). This irreversibility in the variation of the magnetic structure is due to the existence of several relatively stable magnetic-structure states in the crystal.

Conclusions

Noticeable changes occur in the magnetic structure of silicon iron crystals under the influence of elastic elongation. These alterations consist of wall displacements, changes in the size of the subsidiary and closure domains and modifications of the type of magnetic structure; they depend on the magnitude of applied stress, the type of initial magnetic structure and the orientation of the stress relative to the crystallographic axes. Some of the changes in magnetic structure occurring incident to elongation of the crystal are irreversible.

The experimental results can be interpreted qualitatively if it be assumed that under the influence of stresses the magnetization vectors of the domains are rotated parallel to the direction of elongation, that regions with minimum energy are redistributed in the crystal and that the tetragonal axis closest to the direction of elongation becomes the direction of easiest magnetization.

It may be hypothesized that the character of the changes in magnetic structure under the influence of stresses below the elastic limit will be similar in other low-coercivity magnetic materials. This applies particularly to triaxial ferromagnets.

Institute of Metal Physics,
Academy of Sciences of the USSR

References

1. H.Williams, R.Bozorth & W.Shockley, Phys.Rev., 75, 155 (1949).
2. L.Dykstra & U.Martius, Revs.Mod.Phys., 25, 146 (1953).
3. L.V.Kirenskii, V.D.Dylgerov & M.K.Savchenko, Izv.AN SSSR, Ser.fiz., 21, 1168 (1957). (Trans.Bulletin 21, No.8, 1157.)
4. Ia.S.Shur & V.A.Zaikova, Fiz.met.i metallovedenie, 6, 545 (1958). (Trans. Physics of metals and metallography.)
5. Ia.S.Shur & V.R.Abel's, ibid., 1, 11 (1955).

MAGNETIC STRUCTURE OF A FERROMAGNET IN THE REMANENCE STATE AND CHANGES THEREIN INCIDENT TO DEMAGNETIZATION BY AN ALTERNATING FIELD

- I.E.Startseva & Ia.S.Shur

Introduction

In earlier contributions[1,2] we drew certain inferences regarding some characteristics of the magnetic structure of ferromagnets in the remanence state and on the influence of these characteristics on the stability of the residual magnetization. These inferences were based on investigations of the influence of the crystal structure of a ferromagnet on the magnitude of the residual magnetization and its stability as regards various demagnetizing factors.

It is known that experimentally determined values of the remanence I_r are, as a rule, considerably lower than the theoretical values calculated on the assumption that the remanent induction is a result of rotation of the spontaneous magnetization vector I_s from the direction parallel to the field in which the sample was magnetized to saturation to the direction of easy magnetization closest to the orientation of this field. It was suggested in Refs.1 & 2 that the difference between the experimental and theoretical values of I_r is due primarily to the fact that in addition to the principal magnetic domains in which the magnetization vectors I_s are oriented in the directions of easy magnetization closest to the direction of the magnetizing field, in the remanence state there also exist subsidiary (closure) and reverse magnetic domains in which the orientation of I_s differs from that of the vector in the principal domains. It was also hypothesized on the basis of our experimental results that the subsidiary and reverse magnetization domains play a determining part in the process of removal of residual magnetization by different demagnetizing influences.

The purpose of the present research was to check these inferences and hypotheses by direct observation of the magnetic structure of a ferromagnet both in the remanence state and during removal of the residual magnetization by means of an alternating magnetic field.

1. Samples and procedure

The study was carried out on polycrystalline specimens of silicon iron (4% Si). The linear dimensions of the individual crystallites were 0.5 to 2 mm. To minimize self-demagnetization, commonly observed in open-circuit specimens, the specimens were prepared in the form of rings with an outside diameter of 40 mm, an inside diameter of 28 mm and a thickness of 0.1-0.2 mm.

The magnetic structure was observed by the powder pattern technique. In polishing the observed surfaces and preparing the magnetic suspension, we followed the procedure described in Refs.3 & 4.

The samples were magnetized in a steady circular magnetic field. For demagnetization we employed a circular alternating (50 cps) field.

The value of I_r was evaluated qualitatively from the appearance of the magnetic structure. Since the thickness of our samples was less than 0.2 mm the walls between the principal domains extended through the entire thickness of the crystal. The degree of stability of the remanence state was evaluated qualitatively from the strength of the alternating field producing a noticeable rearrangement of the magnetic structure resulting in a decrease of I_r.

2. Results of powder pattern observations

To elucidate the characteristics of the magnetic structure of residually magnetized ferromagnets, we carried out observations on a large number of crystallites with surfaces parallel to different crystallographic planes. It was found that the appearance of the magnetic structure in the remanence state depends on the crystallographic orientation of the crystallite surface, on the orientation of the field magnetizing the specimen with respect to the crystallographic axis, and on the crystallographic orientation of the neighboring crystallites.

If the surface of the crystallite lies in one of the crystal planes containing at least one direction of easy magnetization and the magnetization is realized by a field parallel to this direction, usually no subsidiary and reverse magnetization domains are observed on the surface of the crystallite in the remanence state. Sometimes there are seen a few subsidiary domains near the edges of the crystallite and subdomains clustered about defects. In such crystallites, the residual magnetization is close to the saturation magnetization. Generally, in the demagnetized state, such a crystallite fragments into a number of antiparallel domains so that the integral magnetization equals zero. The number of such domains and their dimensions depend on the geometry of the crystallite.

If the direction of easy magnetization deviates from the surface of the crystallite even by a small angle, diverse subsidiary (closure) domains (drops), firtrees, trunks, daggers, combs, etc.) appear on the surface. Similar domains have been observed[5,6] in the surface of demagnetized crystals. The appearance and character of the subsidiary domains depend on the orientation of the sample surface relative to the crystallographic axes and the orientation of the field in which the crystal was magnetized.

In cases when the surface of the specimen lies in a crystal plane containing two directions of easy magnetization, the magnetic structure in the remanence state differs appreciably from the structure in the demagnetized state. Thus, for example, we observe cases when in the demagnetized state the crystal is broken up into a series of antiparallel principal domains separated by 180° walls, while in the remanence state (after magnetization by a field oriented at 45° to both directions of easy magnetization and parallel to the surface of the crystal) the crystal consists of plane-parallel domains with the magnetization vectors in neighboring domains oriented at 90° to each other.[7]

With increase of the angle between the direction of easy magnetization and the surface of the crystal, the number and volume of the subsidiary domains increase and there appear reverse magnetization domains in which the I_s are oriented antiparallel to the I_s in the principal domains.

Thus our earlier inference that the experimental values of I_s are always lower than the theoretical because of the formation of subsidiary and reverse magnetization domains is substantiated by the evidence of the powder patterns.

In investigating the variation in the magnetic structure of our ferromagnetic specimens under the influence of an alternating magnetic field, it was established that the stability of the magnetic structure in individual crystallites depends to an appreciable extent on the crystallographic orientation of the crystal surface and on the orientation of the demagnetizing field.

If the surface of a crystallite fully coincides with a crystallographic plane containing a direction of easy magnetization (i.e., if in the remanence state there are no subsidiary and reverse domains in the crystallite), its magnetic structure is more stable; that is, a stronger (higher amplitude) magnetic

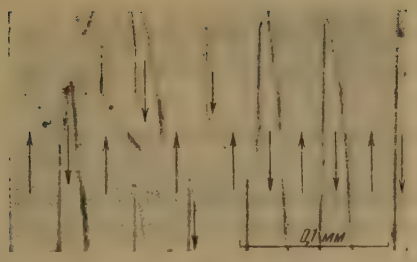

Fig.1. Remanance state after magnetization by a field directed upward (↑H); surface of the crystal close to a (110) plane; ↑[001].

Fig.2. Same after exposure of the specimen to an alternating field with a peak amplitude of 0.3 oersted.

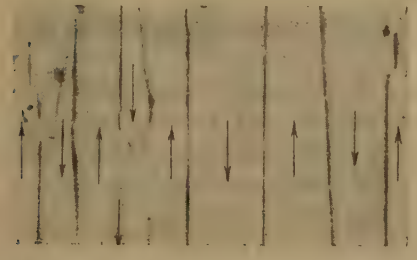

Fig.3. Same after exposure of the specimen to an alternating field with a peak amplitude of 0.7 oersted.

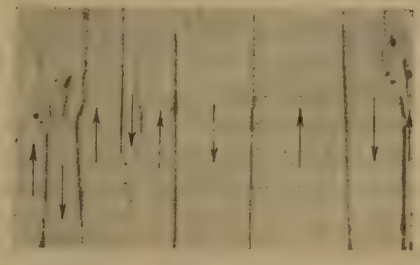

Fig.4. Same after exposure of the specimen to an alternating field with a peak amplitude of 0.9 oersted.

field is necessary to demagnetize such a crystallite. It should be noted that often the appearance of reverse magnetization domains in such crystallites appears to be triggered or induced by the appearance of reverse domains in neighboring crystallites.

As a rule, subdomains do not transform into reverse magnetization domains, i.e., do not act as nuclei of magnetization reversal.

When there is some deviation of the crystallite surface from the crystal plane containing a direction of easy magnetization and there are subsidiary domains present on the surface of the sample in the remanence state, the process of removal of residual magnetization is facilitated. In this case under the influence of the alternating field, one can observe how some of the subsidiary domains grow and transform into reverse magnetization domains, which subsequently fragment.

Demagnetization of a crystallite is most easily realized when there already exist reverse magnetization domains in the remanence state. In this case domain wall displacements are observed even in a weak alternating field. This effect can readily be understood if we bear in mind that movement of the walls of the reverse domains generally does not involve an appreciable change in the area of the walls, whereas transformation of subsidiary domains into reverse magnetization domains is always connected with an appreciable increase of the area of the interdomain walls.

The photographs reproduced in Figs. 1-4 will serve to illustrate how the powder patterns on the surface of a crystallite change under the influence of an alternating field, i.e., incident to removal of the residual magnetization. The surface of this crystallite nearly coincided with a (110) plane. The initial magnetizing field was parallel to the direction of easy magnetization, oriented at a small angle to the surface of the specimen. In the remanence state the entire crystal consisted of one principal magnetic domain magnetized in the direction of easy magnetization. In addition, there can be discerned on the surface of the crystal a number of subsidiary domains in the form of "drops" and "wedges" (Fig.1), in which the magnetization vectors are oriented antiparallel to the magnetization of the principal domain. Under the influence of a weak alternating field, one of the subsidiary domains transforms into a reverse magnetization domain (Fig.2). With further increase of

the field amplitude, this reverse magnetization domain expands and within it there forms a new principal domain in which the magnetization vector is parallel to the vector in the initial principal domain (Fig.3). Further increase of the field amplitude causes displacement of the walls between these new magnetic domains (Fig.4).

Thus in the demagnetized state this crystallite contains an array of domains with antiparallel magnetizations.

It must be noted that upon repeat magnetization of the specimen with a constant field of the same intensity as the initial magnetizing field, the magnetic structure in the remanence state is not fully reconstructed. Nor is the magnetic structure fully reproduced when the crystallite is again demagnetized by an alternating field of the same amplitude.

In polycrystalline specimens, the crystallographic orientation of neighboring grains has an appreciable effect on the domain structure of individual crystallites in the remanence state and on the variation of this structure under the influence of an alternating field. This influence becomes stronger with decreasing grain size.

More detailed data on the appearance of the magnetic structure in the remanence state and the changes in the structure incident to demagnetization by an alternating field will be found in Refs.7 & 8.

Conclusions

The results of our observations of powder patterns on the surface of individual crystallites of polycrystalline silicon iron specimens may be summarized as follows.

1. In the remanence state, in addition to the principal magnetization domains in which the magnetization vector is oriented in the direction of easy magnetization closest to the orientation of the field in which the specimen was magnetized, there are present in the crystallites reverse magnetization domains and subsidiary (closure) domains of different types, including subdomains. These domains are responsible for the experimental values of the residual magnetization being lower than the theoretically calculated values.

2. The appearance of the magnetic structure in the remanence state depends on the crystallographic orientation of the crystal surface and on the orientation of the original magnetizing field with respect to the crystallographic axes.

3. Subsidiary and reverse magnetization domains, when present in the crystal in the remanence state, act to reduce the stability of its magnetic structure as regards demagnetizing factors (specifically, an alternating field).

4. Subdomains generally do not transform into nuclei of magnetization reversal (reverse domains).

5. The changes observed in the magnetic structure of a crystallite in the remanence state in the process of demagnetization by an alternating field are the following: some surface subsidiary domains grow and transform into reverse magnetization domains; these expand with increase in the amplitude in the alternating field. Sometimes in sufficiently strong alternating fields these reverse magnetization domains break up into smaller reverse domains.

6. In polycrystalline specimens the crystallographic orientation of neighboring grains has a noticeable influence on the magnetic structure of individual crystallites in the remanence state and on the changes occurring in the structure in the process of demagnetization.

Institute of Metal Physics
Academy of Sciences of the USSR

References

1. Ia.S.Shur & I.E.Startseva, Fiz.met.i metallovedenie, 2, 568 (1956).
2. Ia.S.Shur & I.E.Startseva, Izv.AN SSSR, Ser.fiz., 21, 1240 (1957). (Trans.Bulletin 21, No.9, 1229.)
3. H.J.Williams, R.M.Bozorth & W.Shockley, Phys.Rev., 75, 155 (1949).
4. W.C.Elmor, Phys.Rev., 54, 1092 (1938).
5. Ia.S.Shur & V.R.Abel's, Fiz.met.i metallovedenie, 1, 5 (1955).
6. Ia.S.Shur & V.R.Abel's, ibid., 1, 11 (1955).
7. I.E.Startseva & Ia.S.Shur, Trudy (Proceedings), Inst.of Metal Physics, Ural Branch Ac.of Sci., 20, 125 (1958).
8. Ia.S.Shur & I.E.Startseva, Fiz.met.i metallovedenie, 6, 614 (1958). (Trans.Physics of Metals & Metallography.)

TEMPERATURE STABILIZATION OF THE MAGNETIC PROPERTIES OF ALLOYS

- I.M.Puzei

In engineering applications of ferromagnetic materials one frequently has to allow for a strong temperature dependence of their magnetic properties. In the case of low-coercivity materials increase of the temperature as a rule leads to increase of the permeability. If the operating temperature range is far from the Curie point, this temperature dependence of the permeability (and of the coercive force) is due primarily to the temperature dependence of the magnetic anisotropy and magnetostriction constants. The anisotropy energy has a particularly strong influence inasmuch as it may vary over a wide range with temperature; the magnetostriction generally varies much less.

In the work of Ref.1 we discovered the effect of the inverse temperature dependence of the anisotropy energy in the binary alloy Ni_3Fe and this alloy with 4% Cu as well as in Mo-Permalloy type alloys; in the first two alloys this inverse temperature dependence is observed in the state obtained after quenching in oil from 600°; in the latter alloys - in states with a certain degree of ordering.

Neutron diffraction studies of Mo-Permalloys showed[2] that in these alloys long-range order is absent even after 25 days annealing at temperatures of 300-500°, yet at the same time the magnetic anisotropy changes from virtually zero to 10^4 erg/cm^3. Thus the transformations in the alloy responsible for the large change in magnetic anisotropy are short-range order transformations.

Hence it may be concluded that the forces giving rise to magnetic anisotropy are local, short-range forces.

This can also be understood from the standpoint of quantum mechanical theory. According to Vonsovskii[3] the mean exchange energy of an alloy is characterized by

$$A = \frac{A_{aa}N_{aa} + A_{bb}N_{bb} + A_{ab}N_{ab} + A_{ba}N_{ba}}{N_{aa} + N_{bb} + N_{ab} + N_{ba}},$$

where A_{aa} and A_{bb} are the exchange energies of the pure components a and b, A_{ab} and A_{ba} are the exchange energies of the component pairs, and N's are the numbers of nearest neighbor atomic pairs.

If spin-spin and spin-orbit interaction are taken into account, the exchange interaction can be regarded as anisotropic and the exchange integral is replaced by the exchange interaction tensor.[4] However, the expression for the average exchange energy of the alloy given by Vonsovskii remains valid. Bearing in mind that the total exchange interaction is determined primarily by the exchange interaction of nearest neighbors, it may be inferred that transformations of the short-range order type will have a strong influence on the anisotropy energy; this is in fact borne out by experiment.

It will be apparent from the above formula for the average exchange energy that if the alloy components have anisotropy constants of opposite sign, at some concentrations one can expect the anisotropy of the alloy to be zero. This is observed, for example, in Ni-Fe alloy with 27% Fe (Ref.5), Fe-Co alloy with 56% Fe (Ref.6) and others. If the pure components have anisotropy constants of opposite sign and the temperature dependences of the constants are of the conventional type, then for the alloy one can expect an inverse temperature dependence of the magnetic anisotropy constant in some temperature interval. This effect must be particularly clearly evinced at small values of the anisotropy energy, i.e., in the region close to the magnetically isotropic state, when even small variations of the anisotropy energy can change the temperature dependence.

In the general class of magnetic alloys, alloys with a magnetically isotropic state are not rare. The anisotropy constants of some alloys in the Ni-

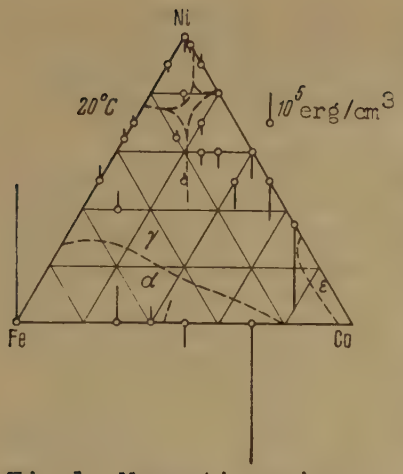

Fig.1. Magnetic anisotropy constants of some Fe-Co-Ni alloys.

-Fe-Co system[6] are shown in Fig.1. We see that in this ternary system there are many concentrations corresponding to a magnetically isotropic state of the alloy. If, further, we take into account the influence of ordering, the number of such concentrations will be even greater. This can be seen in case of the Ni-Fe system[5] in which magnetically isotropic alloys can be obtained not just at one concentration but in the entire range from 28 to 42% Fe. An analogous situation probably obtains for Fe-Co alloys, as well as for Perminvar type alloys wherein ordering processes are known to occur.

In the work of Ref.1 we demonstrated the possibility of temperature stabilization of the magnetic properties of Mo-Permalloy. In the present work we established that utilizing the unique temperature dependence of the anisotropy energy this temperature stabilization procedure can be extended to magnetically soft alloys.

The procedure employed in measuring the magnetic anisotropy was the same as that used in our earlier investigation and has been described in Ref.1.

Investigations of the temperature dependence of the magnetic anisotropy constants of alloys close to their isotropic state showed that as a rule an inverse temperature dependence of the anisotropy energy is observed in some temperature intervals.

In Ref.1 we gave the curve of the temperature dependence of the anisotropy constant of an Ni-Fe alloy in which an inverse temperature dependence obtains in the temperature range from +60 to -196°. Inasmuch as with increase in the degree of order in the alloy, the magnetically isotropic alloy concentration is shifted to the side of iron, the inverse temperature dependence apparently is shifted into the same range of concentrations.

From Fig.1 we see that among the Fe-Co alloys, the alloy with 44% Co is characterized by magnetic isotropy.

The temperature dependence of the anisotropy constant of the 57.3% Fe + 42.7% Co alloy is shown in Fig.2. In the -200 to 0° region there is a weak growth of the constant, i.e., the temperature variation is normal. In the region above 0° the variation is anomalous. At high temperatures ordering occurs and leads to irreversible changes in the anisotropy constant.

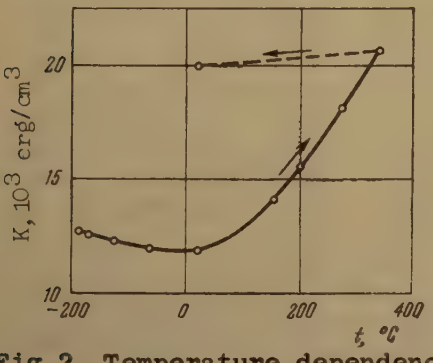

Fig.2. Temperature dependence of the magnetic anisotropy constant K of 57.3% Fe + + 42.7% Co alloy after quenching in oil from 800°.

As in the case of Ni-Fe alloys, with ordering one should expect displacement of the concentration corresponding to the magnetically isotropic alloy and the inverse temperature dependence of the anisotropy to the side of higher Co contents.

According to the data of Ref.6 Ni-Co alloys are magnetically isotropic at Co concentrations of 5 and 18%.

Figs.3,4 & 5 show the temperature dependences of the magnetic anisotropy constants of Ni-Co alloys with 5.3, 19 and 25% Co. It will be seen that the 5.3% Co alloy is characterized by an inverse temperature dependence in the -20 to +50° range

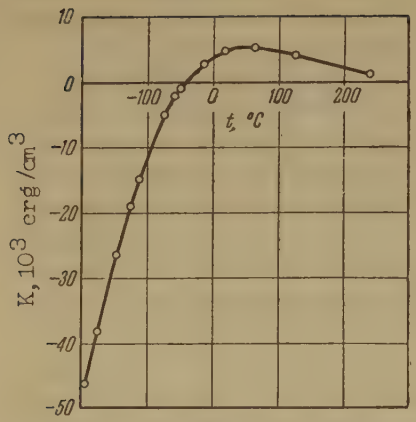

Fig.3. Temperature dependence of K of 5.3% Co + 94.7% Ni alloy.

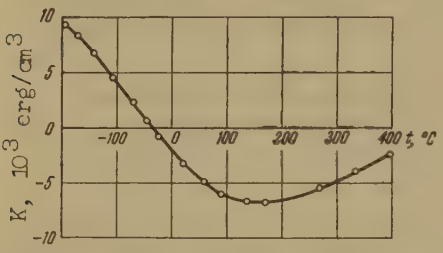

Fig.4. Temperature dependence of K of 19% Co + 81% Ni alloy.

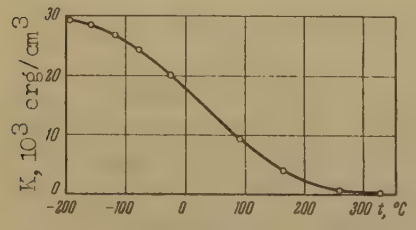

Fig.6. Temperature dependence of the anisotropy constant of 10.2% Co + + 89.8% Ni alloy.

Fig.7. Variation of the anisotropy constant of Mo-Permalloy as a function of the isothermal annealing temperature T. K measured at +20° (1 & 1') and -195.8° (2 & 2').

(Fig.3). In the 19% Co alloy the inverse temperature dependence is observed from -40 to +150° (Fig.4), while in the alloy with 25% Co the temperature variation of the anisotropy is anomalous from +20° down (Fig.5).

Prolonged low temperature (500 to 400°) annealing for 5 days of the Ni-Co alloys did not lead to any substantial changes of the anisotropy constant. Apparently, this heat treatment results in little or no ordering in Ni-Co alloys.

It is interesting to note that according to Fig.1 the alloys with concentrations of Co from 5 to 18% have a positive anisotropy constant at room temperature, although the anisotropy of nickel and cobalt (in the face-centered cubic modifications) is negative. Fig.6 shows the temperature dependence of the anisotropy constant of Ni-Co alloy with 10.2% Co. No anomalies are observed in this case: the temperature variation is the same as in pure metals, for example, iron. Probably here the anisotropy is largely determined by the correlation terms $A_{ab}N_{ab}$ and $A_{ba}N_{ba}$.

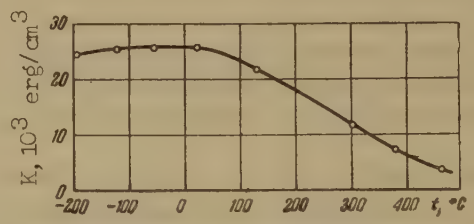

Fig.5. Temperature dependence of K of 25% Co + 75% Ni alloy.

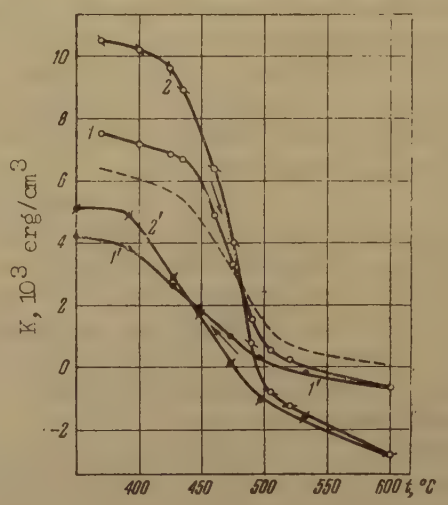

Fig.7 shows the variation of the anisotropy constant of Mo-Permalloy (78.3% Ni + 17.9% Fe + + 3.8% Mo) at +20° and -196° as a function of the isothermal annealing temperature. The arrows at the curves indicate the direction of temperature change in successive anneals. (Curves 1 & 2 are for the Mo-Permalloy sample annealed at successively higher temperatures.) In addition the sample characterized by curves 1' and 2' was annealed for shorter periods (at successively lower temperatures) - see Ref.1: Fig.7 and text.

One can distinguish three different sections of the temperature dependence curves. Let us consider the lower curves 1' and 2'. In the case of isothermal

anneals at temperatures under 435° or above 490°, the temperature variation of the anisotropy constant is normal in the range from +20 to -196°. In the range of annealing temperatures from 435 to 475°, we observe the inverse variation of the anisotropy constant. In the case of annealing in the interval from 475 to 520°, the anisotropy constant changes sign. Details of the temperature dependence of the anisotropy constant after isothermal heat treatments corresponding to the upper curves in Fig.7 are given in Ref.1 (see Figs.9 & 10 in Ref.1).

The strong dependence of the anisotropy constant of Mo-Permalloy with the degree of short-range order is explained by variation of the numbers $N_{aa} \ldots N_{ba}$. With increase in the degree of order N_{ab} and N_{ba} increase, whereas with disordering N_{aa} and N_{bb} increase, while N_{ab} and N_{ba} decrease, i.e., in the disordered state the individual properties of the components make a stronger contribution.

Our discovery and investigation of the inverse temperature dependence of the magnetic anisotropy energy led to development of a procedure for temperature stabilization of the magnetic properties of alloys.

A. Mo-Permalloy. With a view to checking and supplementing the results of Tiablikov[4], we investigated the magnetic properties of standard Mo-Permalloy and two other alloys of similar composition. In all we experimented on seven samples, the compositions of which are listed in Table 1.

Table 1

Composition of investigated samples of Mo-Permalloy type alloys

Sample No.	Composition, %					
	Ni	Mo	Si	Mn	C	Fe
1	79,0	3,8	0,15—0,3	0,3—0,6	0,03	Remainder
2						
3						
4						
5	80,71	3,58	0,23	0,64	0,03	
6	80,35	4,19	0,19	0,64	0,03	
7						

Samples of identical composition in the form of ribbon toroids or disks (thickness 0.35 mm) were subjected successively to the following heat treatments in vacuum: 1) heating for 3 hours at 1100°, cooling at 200° per hour to 600° followed by cooling in the container in air and 2) heating for 3 hours at 600°, 24 hours at 530°, 36 hours at 490°, 36 hours at 470°, followed by cooling in a stream of air.

The first treatment is the standard one. The second corresponds to the lower curves (1' & 2') in Fig.7. After these heat treatments we measured the magnetic properties at -196°, +20° and +100°.

We characterize the temperature stability of the magnetic properties by the value of the permeability in a constant field close to the maximum permeability field. This method of characterization is more representative of actual working conditions than comparison of maximum permeabilities.

The results obtained in our tests are summarized in Table 2.

We obtain quantitatively similar results if we characterize the stability in terms of the initial and maximum permeabilities.

It will be evident from Table 2 that after the standard heat treatment recommended in the GOST (State All-Union Standards) for Mo-Permalloy, the magnetic properties of the material change greatly with temperature particularly in the range of low temperatures. Thus, in the case of sample No.1 at -196° the permeability fell off to 1/10 its value at room temperature. Comparable decreases

Table 2

Magnetic permeability in Gauss/Oersted in a constant field of the Mo-Permalloy type alloys at different temperatures

Sample No.	Thickness, mm	Treatment 1 Field, oersted	Treatment 1 −196°	Treatment 1 +20°	Treatment 1 +100°	Treatment 2 Field, oersted	Treatment 2 −196°	Treatment 2 +20°	Treatment 2 +100°
1	0,2	0,032	10 750	116 000	134 000	0,035	93 000	105 000	114 000
2	0,2	0,032	10 000	110 000	130 000	0,035	100 000	114 000	120 000
3	0,35	0,018	48 000	203 000	238 000	0,027	135 000	149 000	167 000
4	0,35	0,018	51 000	205 000	240 000	0,027	119 000	128 000	147 000
5	0,2	0,016	15 000	206 000	232 000	0,023	168 000	185 000	195 000
6	0,1	0,016	43 000	151 000	103 000	0,023	133 000	152 000	163 000
7	0,1	0,016	13 000	155 000	203 000	0,023	143 000	147 000	166 000

were observed in the case of samples Nos.5,6 and 7. In thicker samples the permeability decreased by a factor of five.

An entirely different situation prevails after the stabilizing heat treatment. Here the average decrease in permeability is only 9.2% in going from +20 to -196°. Further, the increase in permeability with increase of temperature from +20 to +100° amounts to 20% after the standard heat treatment and to only 7.5% after the stabilizing treatment.

It will be apparent that the stabilizing heat treatment evolved on the basis of our investigation of anisotropy constants radically improves the temperature stability of Permalloy particularly in the "difficult" range of low temperature.

B. Ni-Co alloys. As noted in connection with Fig.4, the Ni-Co alloy with 19% Co exhibits an inverse temperature dependence of the anisotropy constant in the range from -40 to +150°.

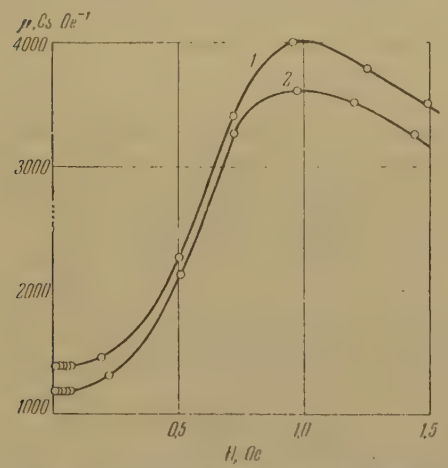

Fig.8. Variation of the magnetic permeability μ of 82% Ni + 18% Co alloy with the field H at +20° (1) and +100° (2).

Fig.8 shows the variation of the permeability of Ni-Co alloy with 18% Co with the magnetic field at +20 and +100°. It will be seen that at +100° the permeability in all fields is lower than at room temperature. This is consistent with the temperature dependence of the magnetic anisotropy of this alloy. Fig.4 shows that increase of temperature from +20 to +100° leads to an increase in the absolute magnitude of the anisotropy constant from $3.2 \cdot 10^3$ to $5.7 \cdot 10^3$ erg/cm^3. This the inverse temperature variation of the anisotropy constant can even result in a reduction of the permeability with increasing temperature.

It is interesting to note that the magnetostriction of the 19% Co alloy is $-2.4 \cdot 10^{-5}$. Consequently, stabilization of the magnetic properties is theoretically feasible not only in materials with a low magnetostriction such as Mo-Permalloy. This is not unexpected particularly if we recall that since the residual stresses in the annealed material are of the order of 3 kg/mm^2 and the saturation magnetostriction $\lambda_1 \approx 10^{-5}$, the magnetoelastic energy equals $3 \cdot 10^3$ erg/cm^3, i.e., is of the same order of magnitude as the anisotropy energy. Consequently, even in the case of large values of magnetostriction, it should be possible to compensate its adverse influence.

Obviously, if we alter slightly the composition of the above mentioned Ni-Co alloy, we can expect to obtain good stability of its permeability in the region of elevated temperatures.

It is evident from Fig.4, the inverse temperature dependence of the magnetic anisotropy constant obtains up to $+150^{o}$. Hence it should be feasible to stabilize the magnetic properties up to this temperature. However, permeability measurements at this temperature have not been made.

Thus we have shown, here and in Ref.1, that alloys in a state close to a magnetically isotropic one, i.e., having small values of the anisotropy energy, may exhibit a unique (inverse) temperature dependence of the magnetic anisotropy constant, which makes it possible to stabilize their magnetic properties as regards temperature variation through appropriate heat treatment.

There are numerous such alloys particularly in the Ni-Fe-Co system and their number can be further increased if one makes use of their potentiality for ordering. Hence the proposed method of stabilizing the magnetic properties of alloys is presumably applicable to a large number of diverse alloys.

References

1. I.M.Puzei, Izv.AN SSSR, Ser.fiz., 21, 1094 (& 1088) (1957). (Trans. Bulletin 21, No.8, 1083 (& 1077).)

2. B.G.Liashchenko, D.F.Litvin, I.M.Puzei & Iu.G.Abov, Kristallografiia 2, 64 (1957). (Trans.Soviet Physics - Crystallography.)

3. S.V.Vonsovskii, Doklady AN SSSR, 26,564 (1940).

4. S.V.Tiablokov, Zhur.eksp.i teor.fiz., 20, 661 (1950).

5. I.M.Puzei, Izv.AN SSSR, Ser.fiz., 16, 549 (1952).

6. R.M.Bozorth, Ferromagnetism, N.Y., 1951. (Cited in Russ.trans.)

MAGNETIC ANISOTROPY AND HYSTERESIS LOSS IN ROTATING MAGNETIC FIELDS IN A MAGNETITE SINGLE CRYSTAL AT LOW TEMPERATURES

- N.N.Narovskaia

Magnetite, which has a cubic lattice at room temperature, undergoes a transition at -160°: the symmetry changes from cubic to orthorhombic. This transition is connected with ordering of the initial random distribution of the Fe^{2+} and Fe^{3+} ions. Li[1] was the first to observe that the character of magnetic anisotropy of magnetite at temperatures below the transition point depends on whether a field is applied during the cooling. Briukhatov[2] showed that an axis of easy magnetization is formed in the (001) plane of a magnetite single crystal when the crystal is cooled in a strong magnetic field, while when it is cooled in a zero field the character of the magnetic anisotropy remains the same as at room temperature.

To explain the influence of a magnetic field on the transition of magnetite Williams, Bozorth & Goertz[3] proposed the following model to characterize the mosaic (or "hybrid") structure of a magnetite single crystal at temperatures below the transition point: if the crystal is cooled in an external magnetic field parallel to one of the cube edges, it becomes an orthorhombic crystal with the axis directed along the field; this axis becomes the axis of easy magnetization; if the crystal is cooled in a field parallel to the [110] direction, it fragments into domains, the *c* axes of which are distributed with equal probability in the [100] and [010] directions. A mosaic structure is formed. If the crystal is cooled in the absence of a magnetic field, the *c* axes of the mosaic domains are distributed with equal probability in the [100], [010] and [001] directions (all the indicated directions pertain to the cubic lattice).

The properties of a crystal as a whole are obtained by summing the properties of the individual portions. Calculations of the torque acting on a crystal in a magnetic field and torque measurements carried out by Williams, Bozorth & Goertz substantiate this hypothesis. We shall make use of it in explaining the results of our experiments.

Briukhatov[4] investigated the hysteresis loss in rotating magnetic fields in a magnetite single crystal cooled to -195° both in the absence of a magnetic field and in a strong field. His measurements for the case of zero field cooling showed a distinctive field dependence of the hysteresis loss. Whereas in ordinary ferromagnets the loss in rotating fields after going through a maximum falls off to zero, in the case in question the loss curve after the maximum has a minimum and with further increase in the field strength again rises. No tendency to saturation or evidence of a second maximum was observed in fields up to 10,000 oersted.

Briukhatov's measurements were carried out only at -195°. The purpose of the present work was to investigate the hysteresis loss in rotating magnetic fields for different fields and temperatures. The measurements were carried out on a single crystal of natural magnetite cut in the form of a sphere and mounted in the holder of the torquemeter so that the plane of rotation of the electromagnet coincided with a (001) plane of the specimen. The torque curves were recorded by measuring the torque acting on the crystal at different successive angles of the magnetic field. The hysteresis losses were then calculated from these torque curves. The crystal was first cooled under appropriate conditions to -195°. Then the measurements were made at successively higher temperatures as the crystal was slowly warmed to -160°.

The experimental results for the case of cooling in zero field are shown in Fig.1. It will be seen that the loss increases with increasing temperature from -195°, attains a maximum in the -170 to -166° interval and then falls off

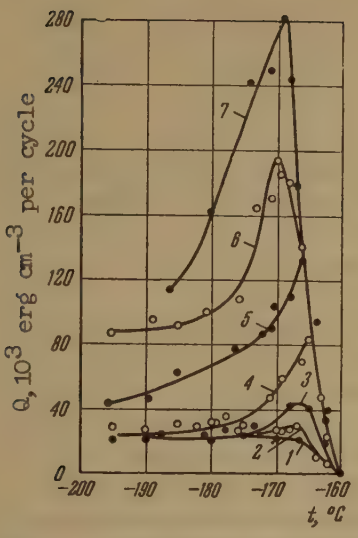

Fig.1. Temperature dependence of the hysteresis loss Q in rotating fields in magnetite cooled through the transition point with no external magnetic field. Measurement field H: 1) 1000, 2) 2000, 3) 3000, 4) 4000, 5) 5000, 6) 6000, 7) 7000 oersted.

sharply to zero at -160° for all the measurement fields used. The magnitude of the loss also depends on the field and at all temperatures increases with the field intensity.

One can propose the following mechanism for explaining the origin and characteristics of the hysteresis loss in magnetite in rotating fields. The underlying concept follows from the axis switching effect discovered by Bickford[5]: the orthorhombic c axis switches under the influence of a magnetic field from one <100> type direction to another direction of the same type. Such switching can occur only under the influence of a strong field (about 15,000 oersted) and at temperatures from -160 to -180°. Calhoun[8] suggested that such axis transfers are connected with redistribution of electrons between the Fe^{2+} and Fe^{3+} ions forming the ordered structure.

As noted above, the low temperature phase of magnetite is characterized by an ordered distribution of the Fe^{2+} and Fe^{3+} ions. The redistribution of electrons could not occur only in a small portion of the crystal, inasmuch as this would lead to disordering if the ions in the neighboring regions retained their original distribution. For a nonmosaic crystal with a single uniquely oriented c axis, switching of the c axis to another direction can occur only in the crystal as a whole or at least in a large portion of the crystal. For this to occur a sufficiently strong field is essential. On the other hand, if the crystal consists of individual domains or regions with differently oriented c axes, upon application of a field, redistribution of electrons can occur in portions of the crystal adjacent to the domain boundaries both owing to the action of the field and to the orienting influence of one domain on another; as a result the interdomain wall will be displaced: one domain will increase in size at the expense of the other. This will obviously be reflected in the torque curves.

Let us next consider the case of cooling of magnetite in an external field parallel to the [110] direction. According to the hypothesis outlined above, the crystal will break up into two groups of domains, equal in volume. According to Williams, Bozorth & Goertz[3], the torques can be calculated with the aid of the following general expression for the magnetic anisotropy energy:

$$E = K_a \sin^2\theta_a + K'_a \sin^4\theta_a + K_b \sin^2\theta_b + K'_b \sin^4\theta_b + K_c \sin^2\theta_c + K'_c \sin^4\theta_c, \qquad (1)$$

where θ_a, θ_b and θ_c are the angles between the saturation magnetization vector J and the respective orthorhombic axes and K_a, K'_a, K_b, K'_b, K_c and K'_c are the anisotropy constants.

From Eq.(1) we obtain the following expression for the torque in the (001) plane for the region in which the c axis is parallel to [100]:

$$L = -\frac{1}{4}(2K_a + 2K_b - 4K_c + 3K'_a + 3K'_b - 4K'_c)\sin 2\theta - \frac{1}{8}(K'_a + K'_b + 4K'_c)\sin 4\theta. \qquad (2)$$

The expression for the torque in the same plane for the region in which the c axis is parallel to [010] is derived from (2) by substituting ($\theta + \pi/2$) for θ and is

$$L = \frac{1}{4}(2K_a + 2K_b - 4K_c + 3K'_a + 3K'_b - 4K'_c)\sin 2\theta - \frac{1}{8}(K'_a + K'_b + 4K'_c)\sin 4\theta. \quad (3)$$

From (2) and (3) we readily obtain the following expression for the torque acting on a crystal with an equal volume of domains of the above two types:

$$L = -\frac{1}{8}(K'_a + K'_b + 4K'_c)\sin 4\theta. \quad (4)$$

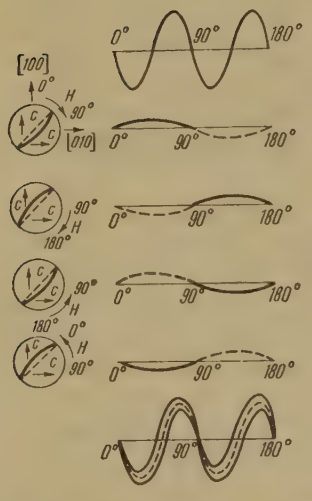

Fig.2. Diagram illustrating origin of hysteresis in a crystal cooled in an external field parallel to [100].

In the proposed model, after displacement of the walls between the domains, these domains will obviously no longer occupy equal volumes and as a result a component with sin 2θ will again appear in the torque curve. However, the direction of the wall displacement and, consequently, the phase of the component with sin 2θ must depend on the direction in which the measurement magnetic field is rotated. The diagram of Fig.2 illustrates how hysteresis arises in the case of two groups of mosaic structure domains.

In our work, for obtaining two volumetrically equal regions (as shown schematically in Fig.2), the magnetite single crystal was cooled from +20 to -195° in a magnetic field aligned accurately with the diagonal of a (001) face. One of the experimental torque curves obtained in the -160 to -195° interval is shown in Fig.3. It will be seen that this curve is generally similar to the resultant curve given in Fig.2. To insure an appreciable displacement of the walls between the mosaic structure regions, we used a rotating field of 9000 oersted. Our measurements showed that the hysteresis loss at -195° in this case is zero; an appreciable loss begins to appear only at -190°, then increases rapidly, attaining a maximum at about -170°. Finally it falls to zero at -160°. The variation of the hysteresis loss in the indicated temperature range is shown in Fig.4.

Obviously, with increasing temperature the field causes an increasingly large displacement of the walls between the mosaic domains and the hysteresis loss increases; this explains the maximum at -170°. The proposed model can also help ex-

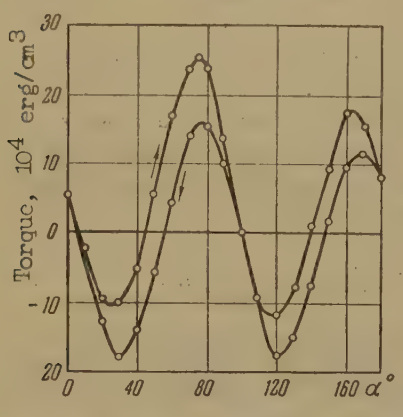

Fig.3. Torque curve for the (001) plane recorded at -175° in a 9000 oersted rotating field for a crystal cooled to -195° in a field parallel to the [110] direction. Angle θ measured from an edge of the cube.

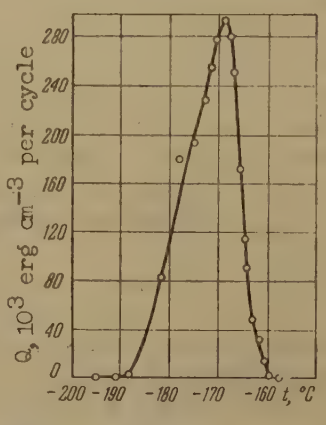

Fig.4. Temperature variation of the hysteresis loss Q for a magnetite specimen cooled in a magnetic field parallel to the [110] axis. Both cooling and measurement carried out in a 9000 oersted field.

plain why the hysteresis loss always falls off in the -170 to -160° interval, going to zero at -160°. The reverse orthorhombic→cubic transition begins at temperatures just above -170°. In the case of magnetite we are probably dealing not with a transition *point* but with a transition *region* extending over about 10°. Thus, viewing our torque curves we can follow how with increase in temperature the volume of the crystal going over into the cubic modification increases. This is evinced by the decrease of the torque and alteration of the period of the torque curves until at -160° the torque curves acquire the appearance characteristic of the cubic modification.

To explain the origin of the hysteresis loss in rotating fields in a magnetite crystal cooled through the transition point in the absence of a magnetic field we must bear in mind the equally probable [100], [010] and [001] orientations of the *c* axes in this case. In such a crystal there can obviously be also displacements of the walls between the mosaic domains. In this case there is also observed an increase of the hysteresis loss with increasing temperature with a maximum at about -170°. The field dependence of this maximum can be explained from the standpoint of the wall displacement mechanism inasmuch as a stronger field is capable of producing a greater wall displacement.

The presence of hysteresis at -195° in the case of a crystal cooled in the absence of a magnetic field is explained by the peculiar processes occurring in the regions of the crystal wherein the *c* axis is oriented perpendicular to the plane of rotation of the measurement field.

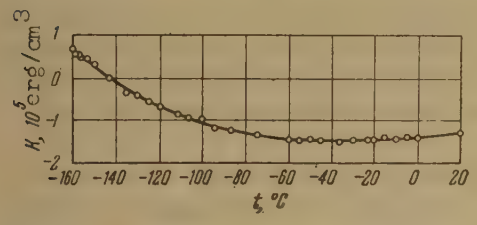

Fig.5. Temperature dependence of the anisotropy constant of the cubic phase of magnetite.

In addition to investigating the hysteresis effect in the low temperature modification of magnetite, we studied the temperature dependence and the anisotropy constant of the cubic phase in the range from +20 to -160° by the torque measurement procedure. The results are shown in Fig.5. The measurements indicate that the anisotropy constant changes sign, going through zero at -143°. This is in agreement with the results Bickford[5] obtained in investigating ferromagnetic resonance absorption.

I wish to thank N.L.Briukhatov for suggesting the subject and guidance in the work.

Faculty of Physics,
Moscow Institute of Railway Transport Engineers

References

1. C.H.Li, Phys.Rev., 40, 1002 (1932).
2. N.L.Briukhatov, Abstracts of reports presented at the Sverdlovsk 1951 conference on magnetism.
3. H.J.Williams, R.M.Bozorth & M.Goertz, Phys.Rev.M., 91, 1107 (1953).
4. N.L.Briukhatov, Izv.AN SSSR, Ser.fiz., 21, 1268 (1957). (Trans.Bulletin 21, No.9, 1257.)
5. L.R.Bickford, Phys.Rev., 78, 449 (1950).
6. B.A.Calhoun, Phys.Rev., 94, 1577 (1954).

NATURE OF THE EFFECT OF THERMOMAGNETIC TREATMENT IN MAGNETICALLY SOFT FERROMAGNETS

- A.A.Glazer & Ia.S.Shur

Introduction

It is a matter of common knowledge that in some ferromagnetic materials cooling in the presence of an external magnetic field (thermomagnetic treatment - hereinafter TMT) leads to uniaxial magnetic anisotropy.[1] The physical nature of this effect is still unclear.

The available experimental data would appear to indicate that TMT is effective primarily when applied to alloys that are ordering solid solutions; accordingly, attempts have been made to relate the TMT mechanism with ordering processes. It was hypothesized that the magnetic field exerts an orienting influence on these processes, thus bringing about the uniaxial magnetic structure.[2,3] Néel[4] suggested that, aside from the direct connection between the TMT effect and ordering processes, there must exist an "oriented superstructure" due to dipole-dipole atomic interaction within each domain in ferromagnetic solid solutions below the Curie point. The axis of this "superstructure" in the domain is aligned with the magnetization vector I_s. At high temperatures, in the presence of a magnetic field, the magnetization vector and, consequently, the superstructure axes align themselves in the direction of the field. In the process of cooling this structure is "frozen", resulting in the observed "magnetic uniaxiality".

It must be noted, however, that at present we have no convincing experimental data indicating that there is a direct relation or connection between the TMT effect and ordering processes.

The present work was done to determine whether such a connection exists. To this end we a) determined the temperature range in which TMT can be effective, b) investigated the influence of TMT on the temperature dependence of saturation magnetization and c) studied the kinetics of TMT of ordered and disordered alloys as well as the kinetics of ordering in alloys previously subjected to TMT.

1. Samples and measurement procedure

The measurements were carried out on the following ordering ferromagnetic alloys: Permalloy with 78 and 66% Ni and Perminvar having the composition 34% Ni, 34% Fe, 29% Co and 3% Mo. The samples were in the form of strips 60 x 4 x 0.2 mm.

To evaluate the effectiveness of TMT, we measured the saturation magnetostriction λ_s and the coercive force H_c, which serve as indications of magnetic structure. The ordering was realized by prolonged (up to 100 hours) annealing at a temperature somewhat below the critical ordering temperature T_c. We judged of the degree of ordering from its influence on the saturation magnetostriction λ_s, the coercive force H_c and the saturation magnetization I_s. The coercive force and the temperature dependence of I_s were measured on a vertical astatic magnetometer. The saturation magnetostriction was determined by means of an apparatus operating on the optical lever principle.

2. Temperature range in which thermomagnetic treatment is effective

The first stage of our work was devoted to determining the temperature range in which TMT is effective. We deemed it expedient to determine whether this temperature interval overlaps with that in which ordering occurs or whether TMT

can also be effective above the critical ordering temperature T_c. Obviously, if long-range order plays an important role in the mechanism of TMT, the treatment must be effective only at temperature below T_c.

Sometime ago Bozorth & Dillinger[5] determined the interval in which TMT is effective in the case of 66 Permalloy. According to their data, TMT is most effective in the 500 to 400° range, i.e., at temperatures at which ordering occurs. In these experiments, however, the samples were cooled in a magnetic field only down to 400-500°, further cooling being carried out in zero field. Hence the upper bound of the effective temperature range could have been an underestimate owing to the fact that in this case the magnetic structure formed at the high temperature could conceivably break down during the latter part of the cooling in the absence of a field. In order to avoid this source of error, we employed the following procedure. The samples, which had been annealed beforehand for 3 hours at 1100° were reheated to 700°, i.e., above the Curie point, then cooled at the rate of 200° per hour. Individual samples were quenched from temperatures in the range from 700 to 400°. Then the H_c and λ_s of the different samples were measured; this gave us the variation of H_c and λ_s with the quenching temperature T. Further, the same samples were reannealed for 3 hours at 1100°, which restored their initial properties. Next the samples were again cooled from 700° at the rate of 200° per hour to the same quenching temperatures, but in this case in a 50 oersted external field. Again the values of H_c and λ_s were measured. The results obtained were subtracted from the previous values (zero field cooling). The differences ΔH_c and $\Delta\lambda_s$ obviously characterize the change in magnetic properties due only to the presence of the magnetic field during the cooling from 700° to T. The values of ΔH_c and $\Delta\lambda_s$ obtained in this manner are listed in the accompanying table.

Changes in the coercive force and saturation magnetostriction as a result of TMT

T, °C	Perminvar		66 Permalloy		78 Permalloy	
	ΔH_c, Oe	$\Delta\lambda_s \cdot 10^6$	ΔH_c, Oe	$\Delta\lambda_s \cdot 10^6$	ΔH_c, Oe	$\Delta\lambda_s \cdot 10^6$
600	0,11	4,5	—	—	—	—
570	0,25	8,0	0,03	2,3	0,00	0,3
540	0,40	9,5	0,14	4,2	0,01	0,1
510	0,50	9,5	0,13	8,8	0,07	0,5
480	0,50	9,5	0,14	11,7	0,08	0,7
450	0,49	9,5	0,16	11,9	0,08	1,0
20	0,48	10,0	0,28	9,7	0,09	1,5

T - temperature to which the samples were cooled from 700° without and with an external field and from which they were quenched.

It will be seen from the table that in the case of 78 Permalloy decrease of H_c and λ_s due to the presence of a magnetic field during cooling is already evident at 540°. The major change in H_c occurs in the 540 to 500° interval, i.e., above the critical ordering temperature for this alloy (T_c = 490°). The saturation magnetostriction continues to decrease even at lower temperatures. This indicates that the formation of uniaxial anisotropy incident to TMT occurs at lower temperatures as well. It follows from these results that TMT is effective not only below but also above T_c. This deduction is substantiated by the data obtained for 66 Permalloy in which appreciable changes in H_c and λ_s also occur above T_c (480°). In Perminvar the major changes in H_c and λ_s, i.e., the formation of magnetic structure, occur at temperatures in the 600-525° interval. In

the case of Perminvar, cooling below T_c (525°) does not lead to any further modification of its properties.

Our experimental results indicate that TMT can be carried out above the critical ordering temperature and that, consequently, ordering per se cannot play any significant role in the TMT mechanism.

3. Influence of thermomagnetic treatment on the temperature dependence of the saturation magnetization

It has been reported[6] that in alloys of the Permalloy type ordering affects the saturation magnetization and the Curie point. In view of this we felt it would be of interest to compare the temperature dependence of the saturation magnetization I_s of a sample subjected to TMT with the temperature dependences of I_s of ordered and disordered samples, for if ordering processes play a significant role in TMT, the I_s vs T curve for a specimen subjected to TMT should be close to the curve for an ordered specimen.

The results of our measurements of the temperature dependence of I_s for samples of 78 and 66 Permalloy and Perminvar are shown in Figs.1 & 2. Fig.1 shows the temperature variation of the saturation magnetization I_s during heating of the samples from room temperature to 700° (above the Curie point) and the subse-

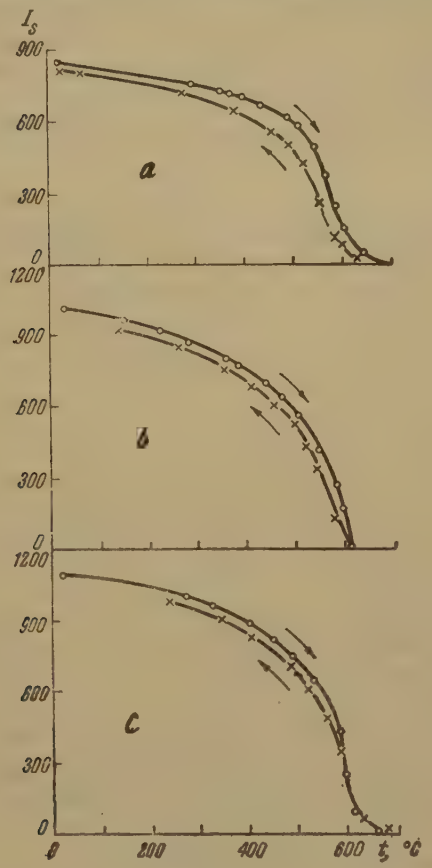

Fig.1

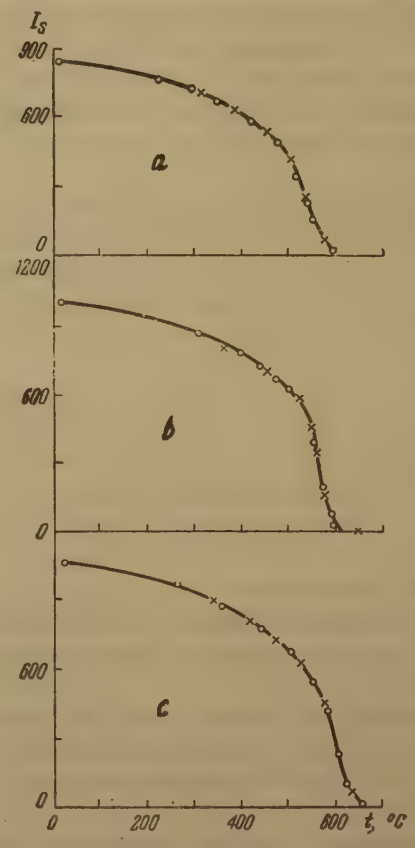

Fig.2

Fig.1. Temperature variation of the saturation magnetization I_s: a) 78 Permalloy, b) 66 Permalloy and c) Perminvar; o - heating, x - cooling. All samples initially in the ordered state.

Fig.2. Same as Fig.1 but for samples subjected to TMT beforehand.

quent cooling to room temperature. In the initial state these samples had the ordered structure obtained by holding for 100 hours at 480°. Heating for 30 min. at 700° (i.e., above T_c) leads to complete disordering. Hence the lower curve in each case - the cooling curve - pertains to the specimen in the disordered state, since no ordering could occur during the brief cooling interval. It will be seen from Fig.1 that the heating curves (ordered state) consistently lie above the cooling curves (disordered state) and that the separation between them is greater at higher temperatures. It follows therefore that the alloys under study have higher value of I_s and Curie point in the ordered state than in the disordered state. This result is in agreement with the data of Wakelin & Yates.[6]

Fig.2 shows the temperature dependences of I_s for similar samples but subjected to preliminary TMT and hence possessing magnetic structure. Obviously, in each case the heating curve pertains to the specimen in the state resulting from TMT. This state persists to the Curie temperature. After holding for about 30 min at 700°, the magnetic texture is "resorbed" and, consequently, the cooling curve pertains to the disordered specimen devoid of magnetic texture. It will be evident from Fig.2 that the heating and cooling curves virtually coincide. This shows that after TMT the alloys under study have the same I_s (and Curie point) as the material in the disordered state. This means that even if some change in the crystal structure does occur during TMT, only a minor fraction of the atoms are involved. Furthermore, these results disprove Kaya's hypothesis according to which 50% of the volume of 78 Permalloy specimens is in the ordered state with an enhanced saturation magnetization after TMT.

4. Thermomagnetic treatment of ordered alloys

In order to determine the influence of superstructure on the course of processes involved in TMT, we subjected samples of 78 Permalloy, 66 Permalloy and Perminvar in the ordered state to TMT. In each case, in order to conserve the ordered structure, the treatment was carried out at temperatures below the critical ordering temperature T_c. For purposes of comparison, identical samples in the disordered state were subjected to the same TMT.

The experimental procedure was the following. Samples of the investigated alloys, brought to the disordered or ordered state by appropriate heat treatment beforehand, were heated at 450° (below T_c) in an external 50 oersted field. At successive intervals samples were quenched and H_c and λ_s were measured at room temperature. After measurement the samples were again heated in the magnetic field to 450° and the TMT continued. Thus we obtained the variation of H_c and λ_s as a function of the annealing time τ at 450° in a magnetic field.

Fig.3 shows the dependences obtained for Perminvar. It will be seen that the values of H_c and λ_s decrease with increasing annealing time for both the ordered and disordered samples. In every case after a certain annealing time both H_c and λ_s approach a constant value. Thus H_c of the quenched (disordered) alloy (curve 2) levels off after only 30 min, while H_c of the ordered alloy (curve 1) continues to decrease even after 3 hours annealing. It was established in further experiments that H_c of the ordered sample attains a constant value only after seven hours heating in a magnetic field; after this period curves 1 & 2 coincide. An analogous effect is observed for λ_s, which in the disordered alloy (curve 4) decreases more rapidly than in the ordered one (curve 3). It may be noted that in the case of both ordered and disordered samples longer annealing times are required to bring λ_s (as compared with H_c) to a constant value.

The corresponding data for 78 and 66 Permalloy samples also indicate that the processes induced by TMT go to completion within a shorter annealing period

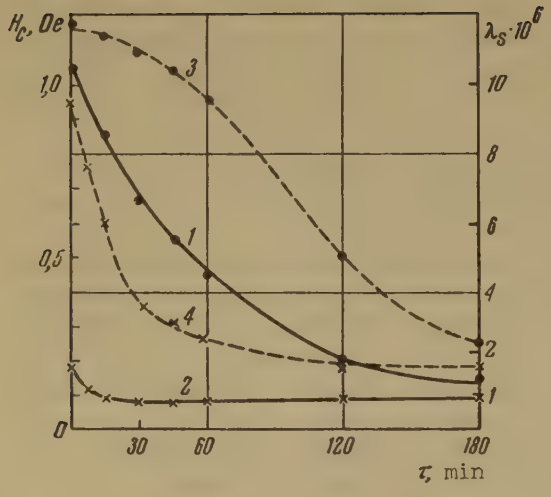

Fig.3. Variation of the coercive force H_c (solid line) and the saturation magnetostriction λ_s (dashed line) of ordered (1 & 3) and disordered (2 & 4) samples of Perminvar with the annealing time τ at 450° in a 50 oersted magnetic field.

in disordered alloys. It follows therefore that the ordered arrangement of atoms inhibits the TMT process. Apparently during TMT there occurs redistribution of the atoms in the crystal lattice, i.e., a new crystal structure forms. This redistribution is hindered in the ordered alloy inasmuch as in it most of the atoms are in energy minima. It is possible that only a small fraction of the atoms, namely, the atoms in excess of the stoichiometric composition, participate in the formation of the crystal structure responsible for the uniaxial anisotropy. This inference is supported by the following experimental fact. In ordered 78 Permalloy, in which almost all the atoms are located at regular sites (inasmuch as the composition of this alloy is close to Ni_3Fe), processes caused by TMT proceed very slowly and even after 15 hours annealing at 450° in a magnetic field the properties of a 78 Permalloy sample were inferior to those of a quenched sample subjected to similar TMT. In ordered 66 Permalloy (somewhat further removed from Ni_3Fe) and in Perminvar (composition far from stoichiometry) the processes induced by TMT occur much more rapidly and go to completion.

5. Ordering of alloys previously subjected to TMT

As was noted above, TMT is apparently accompanied by a redistribution of atoms in the alloy leading to a new and different crystal structure. This structure might reasonably be expected to affect the process of ordering of the alloy. To check this inference, we carried out ordering (annealing at 450°) of quenched samples of all the above enumerated alloys and also of samples subjected to TMT. For all the samples we determined the variation of H_c and λ_s as a function of the annealing time at 450°. One can judge of the degree of ordering from the variation of H_c inasmuch as the value of H_c increases with ordering. Increase of λ_s serves as an indication of breakdown of the magnetic structure inasmuch as in Perminvar the values of λ_s are close in the ordered and disordered states. The results obtained for the Perminvar samples are shown in Fig.4. Curves 1 & 3 pertain to quenched samples; curves 2 & 4 to samples previously subjected to TMT (magnetically uniaxial structure).

It will be evident from the figure that with increasing annealing time, H_c of quenched samples increases to an appreciably greater extent than H_c of samples subjected to previous TMT. The saturation magnetostriction of quenched Perminvar samples has a high value and increases very little with annealing time at 450°. In contrast λ_s in the sample previously subjected to TMT increases appreciably and the growth of λ_s continues over the entire 100 hour interval. It follows from curve 1 that in ordinary disordered samples, ordering develops rapidly and results in a rapid increase of H_c, whereas in samples subjected to TMT ordering occurs slowly and hence H_c increases at a low rate. The gradual increase of λ_s

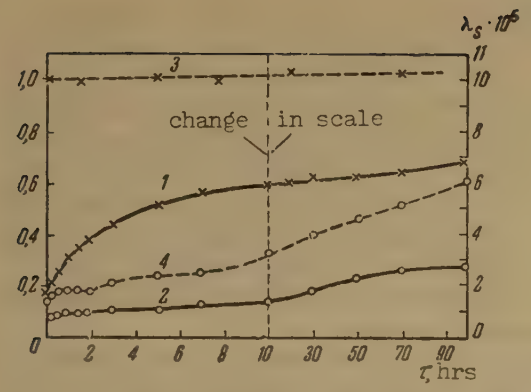

Fig.4. Variation of the coercive force H_c (solid line) and saturation magnetostriction λ_s (dashed lines) of disordered (1 & 3) and thermomagnetically treated (2 & 4) samples of Perminvar with the annealing time τ at 450°.

in samples previously subjected to TMT (curve 4) indicates slow disintegration of the crystal structure responsible for the magnetic uniaxiality.

Thus we established that ordering in samples subjected to TMT occurred more slowly than in ordinary disordered samples. This indicates that TMT gives rise to a distinctive crystal structure, transition from which to the ordered state is more difficult than from the normal disordered state.

Conclusions

The following conclusions may be drawn on the basis of our experimental results.

1. Long-range order does not play any significant part in the mechanism of thermomagnetic treatment (TMT). This follows from the fact that TMT is effective not only below but also above the critical ordering temperature and from the fact that after TMT the saturation magnetization remains virtually the same as in the disordered state.

2. The state obtained as a result of TMT is not the ordinary disordered state characterized by a random arrangement of the atoms, for the kinetics of ordering in samples in the disordered state and those previously subjected to TMT are different.

3. The state forming as a result of TMT differs from both the ordinary ordered and the normal disordered state and is probably a distinctive structural state, in the formation of which only a comparatively small number of atoms is involved. Inasmuch as this state breaks down incident to ordering, a process in which electrostatic forces are involved, it may be inferred that the given structure is created under the influence of magnetic forces. A structure of this form was theoretically predicted by Néel.[4]

Institute of Metal Physics,
Academy of Sciences of the USSR

References

1. S.V.Vonsovskii & Ia.S.Shur, Ferromagnetizm (Ferromagnetism), M., 1948.
2. S.Kaya, Revs.Mod.Phys., 25, 49 (1953).
3. S.Chikazumi, J.Phys.Soc. (Japan), 5, 333 (1950).
4. L.Néel, J.Phys.et radium, 15, 225 (1954).
5. R.Bozorth & J.Dillinger, Physics, 6, 285 (1935).
6. R.F.Wakelin & E.Yates, Proc.Phys.Soc.B 66, 221 (1953).

INVESTIGATION OF THE KINETICS OF MAGNETIC DOMAIN-ORIENTATION IN 65% PERMALLOY

- Sh.I.Zusman

The shape of the hysteresis loop and other magnetic properties of iron--nickel alloys of the Permalloy type are greatly dependent on the previous heat treatment of the material. It is known[1], for example, that after prolonged low-temperature annealing, the hysteresis loops of these alloys acquire a characteristic "necked in" shape.* Rapid cooling from a temperature above the Curie point (600-700°) leads to the appearance of ordinary "undistorted" hysteresis loops. Finally, as a result of low-temperature heat treatment in a magnetic field (thermomagnetic treatment), the hysteresis loops become rectangular.

These attributes are not peculiar to Permalloy but are common to a number of other similar alloys. Analysis of the data in the literature shows that alloys exhibiting deformed, "necked in" hysteresis loops are at the same time alloys particularly sensitive to thermomagnetic treatment. This gives reason to assume that the processes giving rise to the rectangular loops and the processes responsible for the deformed hysteresis loops are related. Yet until recently, the factors responsible for the appearance of the rectangular and deformed loops have been interpreted from different standpoints.

It has been established experimentally that the effect of thermomagnetic treatment is connected with the appearance of a certain stable magnetic structure, namely, preferred orientation of the domains in the direction of the external field applied during the heat treatment.[2] On the other hand, the appearance of the deformed hysteresis loops has usually been regarded as a result of interaction between two alloy phases with distinctly different magnetic properties.[3] The phase heterogeneity of the alloy, in turn, was associated with ordering processes.[4] In the framework of the theory developed in recent years by Néel[5] and independently by Taniguchi & Yamamoto[6], the development of the magnetic structure responsible for the rectangular loops is explained by ordered oriented distribution of the atoms in the alloy lattice. Recently, Yamamoto, Taniguchi & Aoyagi[7] succeeded in explaining some of the features of deformed hysteresis loops in the framework of the directed ordering theory.

In the present work we investigated the variation in the magnetic properties of 65 Permalloy in the process of low-temperature heat treatment. The research was undertaken for the purpose of establishing the possible connection between the processes responsible for the appearance of rectangular and deformed, "necked in" hysteresis loops. Most of the measurements were made by the oscillographic technique.

1. Experimental Procedure and Samples

The measurement apparatus has been described earlier[8] and does not differ in principle from similar set-ups used by other investigators.[9,10] An indication of the accuracy of the set-up is furnished by the oscillogram of the dynamic hysteresis loop of a nickel-zinc ferrite sample reproduced in Fig.1 upon which we have marked the experimental points on the initial magnetization curve and hysteresis loop obtained by the conventional ballistic procedure.

The measurements were carried out on toroidal ribbon cores: ribbon thickness - 0.05 mm, ribbon width - 10 mm; inside diameter of toroid - 20 mm, outside diameter of toroid - 22-23 mm. Prior to forming the toroids, the ribbon was coated

---

*This unusual "necked in" hysteresis loop is one of the manifestations of the "Perminvar" properties of these alloys.

Fig.1. Dynamic hysteresis loop of Ni-Zn ferrite; crosses - points obtained by the conventional ballistic procedure.

with an insulating layer of magnesium oxide.

The samples were subjected to two different preliminary heat treatments: a) slow cooling treatment: heating in vacuum to 1100°, holding at this temperature for 3 hours, followed by cooling at the rate of 100° per hour to 200°; b) quenching treatment: the samples, after being subjected to the above slow cooling treatment, were sealed under vacuum in quartz tubes; the tubes containing the samples were then held for 30 min at 650° and quenched in water.

After heat treatment the samples were placed in individual porcelain forms upon which the magnetizing and measuring windings of wire with heat resistant insulation were wound.

Measurements were carried out in a quartz vacuum furnace; the thermocouple and instrument leads were brought into the furnace through appropriate picein plugs. The hot junction of the thermocouple was in direct contact with the sample. The instrument leads were connected either to the oscillograph (usually) or to a conventional ballistic set-up. All the measurements were carried out at the maximum - 1 oersted - strength of the magnetizing field. Prior to each series of measurements, the sample was demagnetized in a diminishing alternating field.

2. Measurement Results

Heating above the Curie point. Fig.2 shows a series of oscillograms obtained during heating one of the samples to a temperature above the Curie point. This sample had been subjected to the slow cooling treatment.

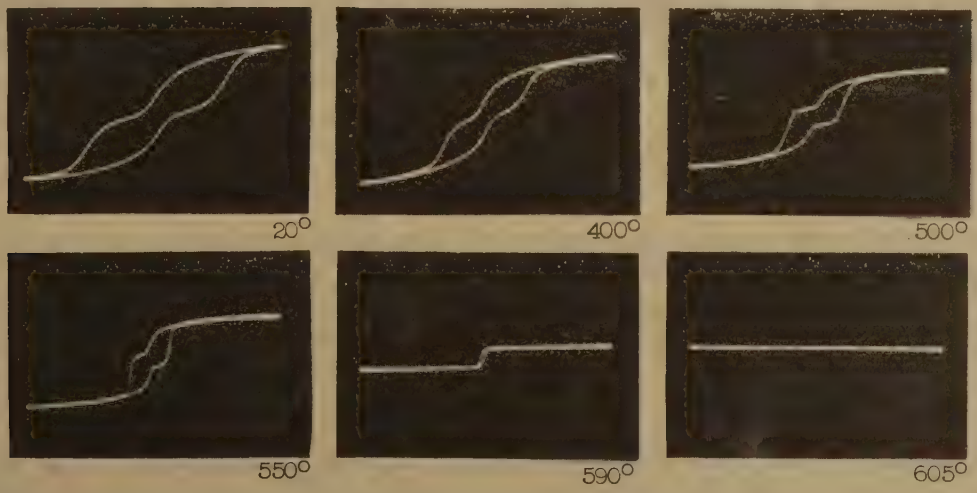

Fig.2. Dynamic hysteresis loops obtained for a sample of 65 Permalloy at different temperatures in the process of heating. Sample subjected to slow cooling treatment beforehand.

In the process of heating the sample was held at each of the indicated temperatures for 30 min and then connected to the oscillograph. During the period of measurement the sample was exposed to the influence of the magnetic field for 10-15 sec.

As may be seen in Fig.2, in the initial state, after high temperature annealing, the hysteresis loop has the "necked in" shape. With increasing temperature there is a monotonic decrease of the coercive force and maximum inductance. The initial hysteresis loop undergoes little change in shape up to about 500°. In this temperature region, a characteristic "step" appears on the back of the hysteresis loop: the coercive force increases appreciably. With approach to the Curie point, the loop gradually narrows and flattens and in the immediate vicinity of the Curie point assumes the normal shape. The "step" on the back of the loop was observed up to about 580°, i.e., at temperatures appreciably above the ordering range (the Kurnakov point for this alloy lies below 500°).

The Curie point of this alloy is situated between 600 and 605°.

3. Realization of Rectangular Hysteresis Loop in Slowly Cooled Samples

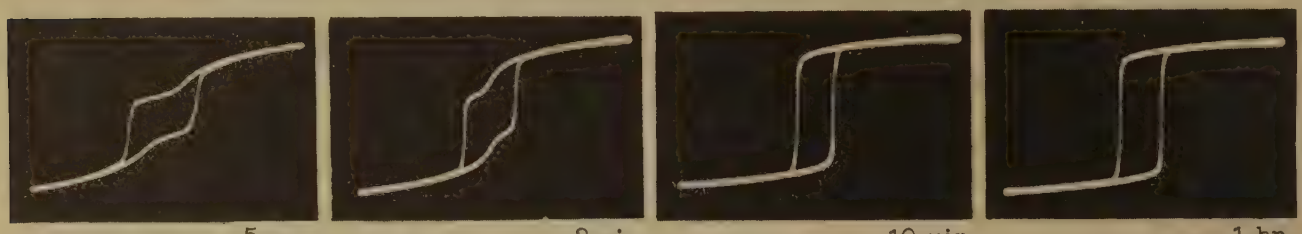

Fig.3. Genesis and development of rectangular hysteresis loop in a sample of slowly cooled 65 Permalloy at 515°.

The oscillograms reproduced in Fig.3 illustrate the genesis of a rectangular loop in a slowly cooled sample of 65 Permalloy at 515°. The sample was held at this temperature for 30 min before being connected to the measurement set-up. The current through the magnetizing winding was such that the peak value of the alternating field was 1 oersted. As may be seen from the successive oscillograms, the initial "stepped" hysteresis loop gradually changes shape under the influence of the magnetic field and becomes rectangular.* The principal alteration of the loop occurs during the first 10 min. Further exposure to the magnetic field leads only to some improvement of the rectangularity. With increasing heat treatment temperature, the establishment of the rectangular hysteresis loop proceeds more intensely, as will be evident from the oscillograms reproduced in Fig.4; at 550° the rectangular loop is formed within 1.5-2 min after application of the magnetic field.**

---

*A certain asymmetry of the deformed hysteresis loops is evident. We observed similar asymmetry in the case of the loops of other alloys; in some cases it was appreciably more pronounced and persisted to room temperatures. A careful check by the ballistic technique at room temperature showed that this asymmetry of the loops is not due to distortions introduced by the oscillographic procedure.

**A noticeable increase in the dynamic coercive force with time in the magnetic field, evinced in the oscillograms of Figs.3,4 & 6, is a purely dynamic effect. This was substantiated by ballistic measurements. This increase is, apparently, due to growth of the eddy-current loss occurring in consequence of enhanced rectangularity of the hysteresis loops.

Fig.4. Genesis and development of rectangular hysteresis loop in a sample of slowly cooled 65 Permalloy at 550°.

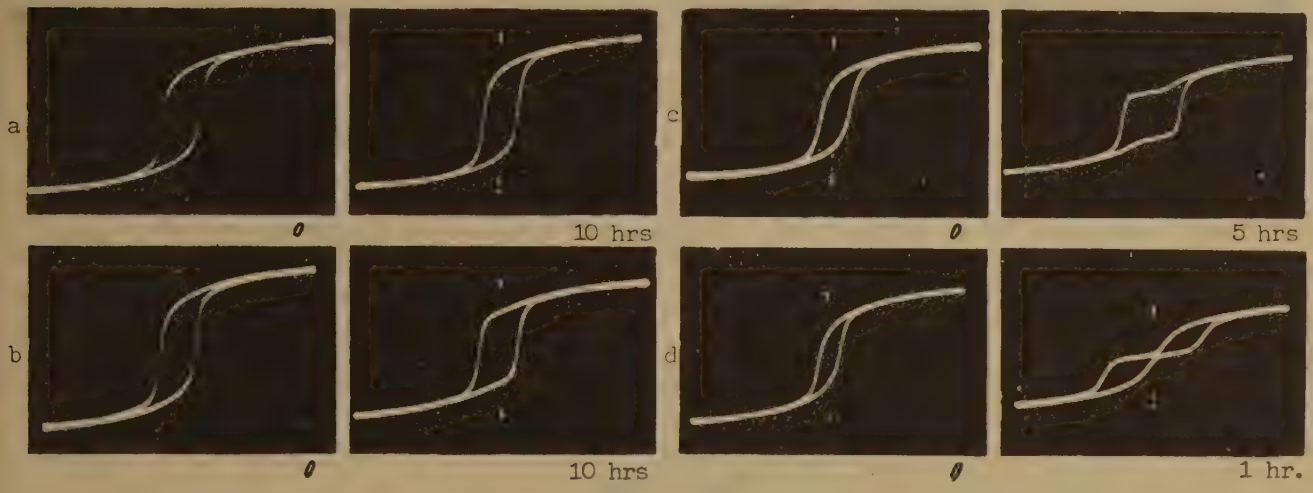

Fig.5. Variation of the hysteresis loops in quenched samples of 65 Permalloy in the course of heating in zero field at different temperatures: a - 380°, b - 400°, c - 440°, d - 500°.

4. Realization of Deformed and Rectangular Hysteresis Loops in Quenched Samples

In this series of experiments two identical quenched samples were placed in a preheated furnace which was then rapidly brought to the desired temperature. The measurements were made at 380, 400, 440 and 500°. When the desired temperature was attained, a direct current producing a 1 oersted field was sent through the windings surrounding one of the samples; the other sample was in zero field. The field measurements were made at appropriate intervals. The formation of the "necked in" loops was studied by the oscillographic procedure; in the case of the rectangular loops, in addition to the oscillographic technique, we used the ballistic procedure for determining the remanence. In other respects the measurement procedure was essentially as described above; in both cases the measurement time did not exceed 10 sec. The results are shown in Figs.5,6 & 7. It will be evident from the figures that the processes responsible for formation of rectangular and deformed hysteresis loops occur in approximately the same temperature region.

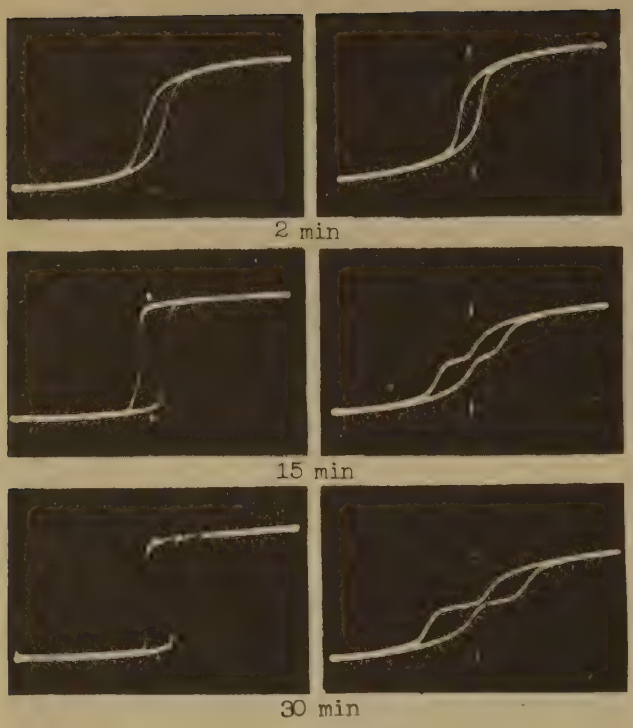

Fig.6. Genesis of rectangular and deformed hysteresis loops in quenched 65 Permalloy samples in the course of heating at 500°: 1 - 2 min, 2 - 15 min, 3 - 30 min. Left - 1 oersted field; right - zero field.

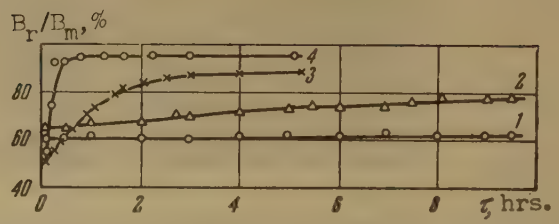

Fig.7. Variation of the rectangularity of the hysteresis loop (B_r/B_m) with the heating time τ in a magnetic field at different temperatures for quenched 65 Permalloy samples: 1 - 380°, 2 - 400°, 3 - 440°, 4 - 500°.

The lower bound of this temperature region lies between 380 and 400°. At this lower bound the processes occurring in the alloy proceed very slowly; at 400° a noticeable change in the shape in the hysteresis loop is observed only after heating for 5 to 10 hours. At 440° a heating period of 2-3 hours is required to obtain well defined rectangular or deformed loops. With increasing temperature the tempo of the processes increases.

As will be evident from the series of oscillograms reproduced in Fig.6 the processes leading to formation of rectangular and deformed hysteresis loops proceed at approximately the same rate: both go to completion within 15-30 min.

Discussion

1. As noted above, usually the appearance of deformed, "necked in" hysteresis loops is attributed to heterogeneity of the alloy which, in turn, is associated with phase differences in ordering. This hypothesis is negated by the fact that the deformed hysteresis loops persist up through temperatures appreciably higher than the ordering temperature.

2. The results obtained in the present work, taken in conjunction with previously known facts, make it possible to establish an analogy between the processes leading to the formation of rectangular hysteresis loops in samples previously subjected to thermomagnetic treatment and the processes responsible for the formation of "necked in" hysteresis loops: a) as previously noted, alloys which exhibit deformed hysteresis loops are at the same time the most sensitive to thermomagnetic treatment; b) deformed hysteresis loops form in the same temperature range as rectangular loops, i.e., in the range in which thermomagnetic treatment is effective (in the case of 65 Permalloy the lower bound of this temperature range lies between 380 and 400°); c) the kinetics of formation of rectangular and deformed hysteresis loops would appear to be subject to the same regularities. With increasing temperature the formation of both rectangular and deformed loops proceeds at a faster rate. The time to formation of well defined

rectangular and deformed hysteresis loops is the same and equals 2-3 hours at 440° and 15-30 min at 500° (in 65 Permalloy).

3. In view of our results, it may be inferred that the formation of both deformed and rectangular hysteresis loops is attributable to the same factor, namely, the formation of magnetic texture. Obviously, the type of texture in the two cases must be entirely different: the rectangular hysteresis loops, as is known, are due to preferred orientation of the domain magnetization in the direction of the field applied during the thermomagnetic treatment, whereas the deformed hysteresis loops are presumably associated with a much more complicated distribution of the domain magnetizations.

It is possible that the common factor responsible for the appearance of both deformed and rectangular hysteresis loops is oriented or directional ordering of the atoms in the alloy lattice.[5,6]

4. Our results regarding the kinetics of formation of rectangular hysteresis loops in 65 Permalloy may prove helpful in determining the optimum thermomagnetic treatment conditions for this alloy.

I desire to express my sincere gratitude to O.N.Al'tgauzen for his constant interest in the work and valuable suggestions in the course of discussions.

References

1. R.M.Bozorth, Ferromagnetism, N.Y., 1951. (Cited in Russ.trans. M.1956.)
2. Ia.S.Shur, Izv.AN SSSR, Ser.fiz., 11, 570 (1947).
3. A.Auwers & H.Kühlewein, Ann.Phys., 17, 2 (1933).
4. S.Kaya & M.Nakayama, Z.Phys., 112, 420 (1939).
5. L.Néel, J.phys.et radium, 15, 225 (1954).
6. S.Taniguchi & M.Yamamoto, Sci.Rep.of the Res.Inst.Tohoku Univ., Ser. A., 6, 4, 330 (1954).
7. M.Yamamoto, S.Taniguchi & K.Aoyagi, Phys.Rev., 102, 1295 (1956).
8. Sh.I.Zusman, in Sbornik trudov TsIIChM "Pretsizionnye splavy" (Symposium on "Precision Alloys"), M., 1959.
9. Sovremennyi katodnyi ostsillograf (The modern cathode-ray oscillograph): Collected articles, Part II, M., 1951.
10. G.S.Veksler & P.S.Tomashevskii, Zhur.tekh.fiz., 24, 1594 (1954).

SYNTHESIS AND MAGNETIC PROPERTIES OF FERRITES WITH A RECTANGULAR HYSTERESIS LOOP

- L. I. Rabkin, S. A. Soskin & B. Sh. Epshtein

Introduction

Ferrites with a rectangular hysteresis loop constitute one of the most promising groups of nonmetallic ferromagnets for applications in computer engineering, automatic telephony and allied fields. Such ferrites must have a high residual induction B_r/B_m, a low dynamic coercive force in pulse fields, a short magnetization reversal time, and time and temperature stable characteristics.

A high value of B_r/B_m, after appropriate treatment, is characteristic of many ferrites: manganese monoferrite, cobalt-manganese and cobalt-manganesium biferrites and a number of polyferrites. A high value of relative remanence in conjunction with a low dynamic coercive force can be obtained in ferrites synthesized of the oxides of iron, manganese and magnesium.[1]

Aside from the chemical composition, the magnetic properties of ferrites are influenced by the presence as well as the shape, size and distribution of pores and other inclusions. These factors are in turn dependent on the conditions of preparation of the initial mixture and of synthesis.

1. Physical-chemical influence of the medium on highly dispersed materials

The process of preparation of ferrites comprises two principal stages: the first stage is the preparation of a homogeneous mixture with the requisite proportion of the different oxides; the second is sintering. The requisite homogeneity of the mixture and high activity of the oxides are realized by chemical, thermal or mechanical procedures.

In the commonly employed precipitation procedure, a mixture of the appropriate water soluble salts in the proper proportions is precipitated with suitable reagents: ammonium carbonate or oxalate, ammonia or alkalis. The precipitate is then washed with water to the requisite degree of purity.

In the precipitation techniques employed in practice the components are all subjected to the action water, the influence of which on such finely dispersed substances has scarcely been investigated; that is, it has been tacitly assumed that the aqueous medium is inert as regards the finely divided powders in the same way as for the bulk material. In the finely dispersed state, i.e., in the case of quasicolloidal particles, the large specific surface cannot but affect the chemical and physical properties of the substance. Under these conditions a medium that is inert under ordinary circumstances may become active. In particular the solubility of the material is altered[2], which in the case of a mixture of several oxides makes it difficult to obtain exactly the specified composition in employing the precipitation technique.

Specifically, in the system of interest to us, namely, Fe_2O_3-MgO-MnO, different quantities of the various oxides are dissolved and carried off with the solution; moreover, some of the oxides may evince binding properties. Thus, for example, magnesium oxide and calcium hydroxide, which is sometimes introduced into the ferrite mixture, form chains of the OH-Mg-O-$(MgO)_n$-Mg-OH type in water.

Intertwined, strongly hydrated chains of this type form structures characteristic of binding substances (cements). Particles of the other oxides are enveloped by such chains, forming stable aggregates. This is evinced in the form of structural viscosity and hampers and counteracts defloccation. Strong hydration of the individual oxides hinders removal of the water and has deleterious effects on the properties of the resultant ferrite.[3]

It is known that in many cases wet grinding makes it possible to obtain finer particles than dry grinding[4] and results in better mixing. In view of these advantages of wet grinding, it would appear expedient to realize it in a liquid medium free of the shortcomings of water. Such a medium may be a nonpolar liquid that does not dissolve the ferrite raw materials or cause solvation of the oxide particle. Suitable nonpolar liquids are benzene, toluene, gasoline, kerosene and the like.

In the course of preparation, ferrite materials are subjected to the influence not only of a liquid but also of a gaseous medium, specifically the sintering medium. Many investigators[5,6] have called attention to the influence of the sintering medium on the properties of the resultant ferrite. As far as we know, there has been no investigation of the influence of the sintering medium on the properties of magnesium-manganese ferrites.

Hence to elucidate the influence of the sintering medium, we undertook a series of experiments involving sintering in different media: air, argon, nitrogen and carbon dioxide. In synthesizing the ferrites we used both quenching from a high temperature and slow cooling. Quenching has a favorable influence on the properties of magnesium-manganese ferrites. There is reason to assume that this is due either to prevention of oxidation of the manganese or to "freezing" of the ferrite structure in a metastable state. A further purpose of the present research was to determine the influence of these factors.

2. Experimental Work

A. Preparation of specimens

The specimens were prepared in the following manner. Mixtures of iron, magnesium and calcium oxide and manganese carbonate were ground in a ball mill for 20 hours either in water or a nonpolar liquid. Then after removal of the liquid, the mixture was briquetted and roasted at 950°. The sintered pellets were ground in a ball mill and the powder compressed to form toroidal cores. By way of binder we used polyvinyl alcohol. The cores were sintered at 1350° in air followed by rapid cooling in a stream of inert gas.

B. Measurements procedure

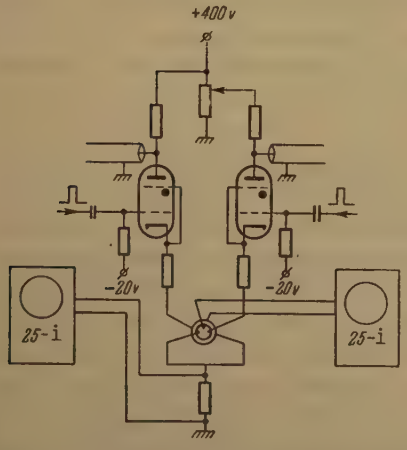

Fig.1. Circuit for measuring the magnetization reversal time τ of toroidal cores.

The magnetic parameters were determined from the dynamic magnetization reversal loops recorded by means of an electron-beam ferrometer in a sinusoidal field of a frequency of 30 kc. This frequency was chosen because it characterizes the properties of ferromagnets under the pulse operation conditions obtaining in many modern automatic circuits.

The magnetization reversal time was measured with pulses of 4 microsec duration and a rise time of 0.02 microsec. The measurement circuit employing a thyratron generator is diagrammed in Fig.1. Pulses of opposite polarity are applied in sequence to the two primary windings on the core. The amplitude of the pulses of one polarity is maintained constant, while the amplitude of the other pulses can be varied from 1 amp to a maximum value (I_{pulse}).

The output signal, characterizing the voltage in the secondary winding, is observed on the screen of the synchroscope. (The synchroscope amplifier is bypassed in this case.) The magnetic polarity reversal time τ is determined as the duration of the output signal corresponding to the jump of the field strength from zero to the maximum value. For each field intensity a reading was also made at the 0.1 level of the peak value of the output signal.

C. Influence of the dispersing medium

In order to investigate the influence of the dispersing medium on the magnetic properties of magnesium-manganese ferrites, we compared samples having the same composition but prepared by precipitation, by grinding of the oxides in water and by grinding of the oxides in a nonpolar liquid (specifically, gasoline). In the last two cases the manganese was used in the form of its carbonate. The average parameters obtained for specimens of the three types are listed in Table 1.

Table 1

Magnetic properties of magnesium-manganese ferrites prepared by different procedures

Method of preparation	Composition, mole %					Magnetic parameters at f = 30 kc; H_m = 2 oerst.		
	Fe_2O_3	MnO	MgO	ZnO	CaO	B_m, Gs	B_r/B_m	H_c, Oe
Precipitation	39	41	5,3	12,3	2,4	2600	0,86	0,85
Grinding in water						2200	0,86	1,6
Grinding in gasoline						2800	0,87	0,77

It will be evident from the table that these ferrites are characterized by almost the same rectangularity of the loop but differ as regards value of the induction and coercive force at H_m = 2 oersted.

The advantages of preparing ferrites from the oxides by grinding in gasoline over the precipitation procedure become clearer if we compare the magnetic parameters of a large number of samples prepared by each of these procedures. It will be evident from the curves of Fig.2 that the best properties and the minimum scatter of magnetic parameters are exhibited by ferrites prepared by the method of grinding in a nonpolar liquid.

D. Influence of the sintering atmosphere and cooling rate

The influence of oxidation of the manganese and persistence of the metastable state structure on the magnetic properties of magnesium-manganese ferrites was investigated using samples subjected, after sintering, to rapid or slow cooling in air, in inert media (argon and nitrogen) and carbon dioxide. It was established that in the case of sintering Mg-Mn ferrites in an inert medium the cooling rate is relatively unimportant. This indicates that the redistribution of ions connected with the rate of cooling does not have an appreciable influence on the magnetic properties of the ferrites. Slow cooling in air, however, seriously impairs the magnetic properties (Table 2).

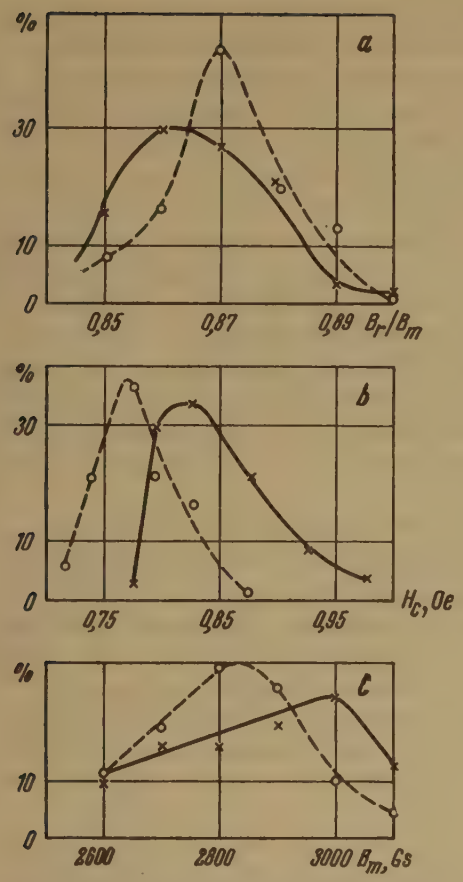

Fig.2. Curves characterizing the statistical distribution of the magnetization reversal loop parameters of ferrite cores for which the initial oxide mixture was prepared by precipitation (solid curves) and by combined grinding of the oxides in a nonpolar liquid (dashed curves): a - relative remanence $[\Delta(B_r/B_m) = 0.01]$, b - coercive force ($\Delta H_c = 0.02$ oersted), c - induction B_m at $H_m = 2$ oersted ($\Delta B = 100$ gauss). Data based on measurements of 500 cores from 10 different batches.

Table 2

Magnetic properties of Mg-Mn ferrites sintered and cooled by different procedures (ferrite composition same as in Table 1)

Conditions of synthesis and cooling	Magnetization reversal loop parameters; f = 30 Kc; H_m = 2 oersted		
	B_m, Gs	B_r/B_m	H_c, Oe
Heating in CO_2 Slow cooling	2800	0,89	0,87
Heating in air Rapid cooling in stream of CO_2	2760	0,87	0,88
Heating in air Rapid cooling	2650	0,85	0,87
Heating in air Slow cooling (in furnace)	400	0,5	0,5

It follows that to obtain ferrites with good magnetic properties it is important to protect the manganese from oxidation. This can be done by sintering in an inert medium or in air followed by rapid cooling.

E. Influence of chemical composition on the magnetic properties of ferrites with a rectangular hysteresis loop

For computer applications, particularly logic circuits, one must have magnetic cores with a rectangular hysteresis loop and possessing a low dynamic coercive force. Hence it has become necessary to find additives that reduce the coercive force without lowering the maximum and relative residual induction. It is known that in order to obtain ferrites with a low coercive force it is essential to strive for a maximum density of the material, which requires a high sintering temperature.[7] Introduction of small amounts of SiO_2 (Ref.5) or CaO (Ref.8) tends to reduce the effective sintering temperature and increase the density of the ferrite. The coercive force can also be diminished by adding a certain amount of zinc oxide, which lowers the Curie point.

In order to determine the ferrite composition with optimum loop parameters we synthesized a series of samples with different proportions of components.

Fig.3 shows the variation of B_m, B_r/B_m and H_c at $H_m = 4$ oersted with the ratio of ZnO to MgO in ferrites containing 40%* Fe_2O_3, 40% MnO and 2.5% CaO.[9]

---

*All % here and below are mole percent.

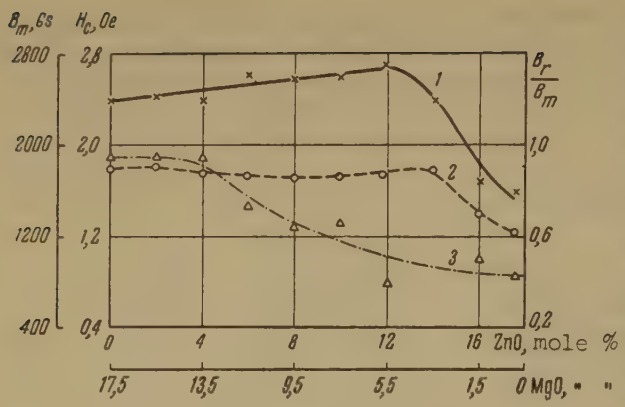

Fig.3. Variation of B_m (1), B_r/B_m (2), and H_c (3) with the ratio of ZnO to MgO in ferrites containing 40% Fe_2O_3, 40% MnO and 2.5% CaO. f = 30 kc and H_m = 4 oersted.

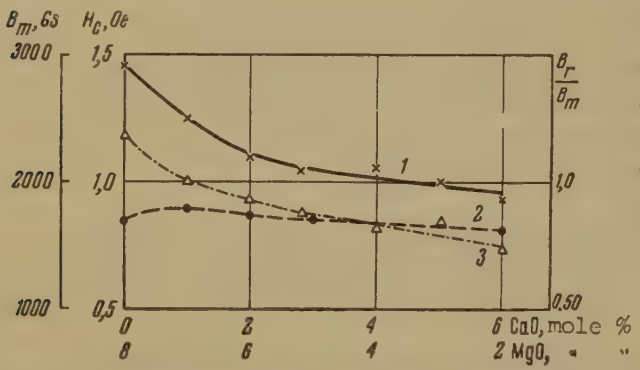

Fig.4. Same as Fig.3 but as a function of the ratio of CaO to MgO with 12% ZnO: 1 - B_m, 2 - B_r/B_m, 3 - H_c.

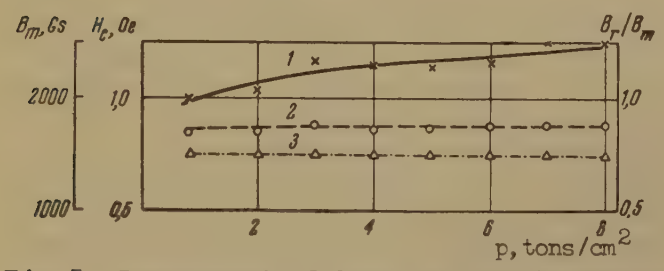

Fig.5. Same as Fig.3 but for PP-24 ferrite cores as a function of the compacting pressure: 1 - B_m, 2 - B_r/B_m and 3 - H_c.

It will be seen that with increase of zinc up to 14%, the coercive force decreases while the maximum induction increases. The optimum magnetic parameters are obtained with 12% ZnO. Further increase of the ZnO content depresses B_m, B_r/B_m and the Curie point.

The variation of the same parameters as a function of the CaO to MgO ratio for ferrites containing 40% Fe_2O_3, 40% MnO and 12% ZnO is shown in Fig.4. It will be seen that the introduction of a small amount of CaO (instead of MgO) reduces the coercive force. At the same time both B_m and B_r/B_m are also reduced to some extent.

Fig.5 shows the variation of B_m, B_r/B_m and H_c at H_m = 2 oersted as a function of the compacting pressure of ferrite cores containing 40% Fe_2O_3, 40% MnO, 12% ZnO, 5.5% MgO and 2.5% CaO. It will be seen that the maximum induction increases with increasing compacting pressure, but that the pressure has little effect on the remanence and coercive force.

F. Principal parameters of ferrites with a rectangular hysteresis loop

On the basis of the experimental results outlined above there were developed a number of types of ferrites with rectangular hysteresis loops; the principal parameters of these ferrites are listed in Table 3. In working out the batching proportions we also took into account the composition of the ferrites developed under the supervision of Kosarev[9].

The magnetic properties of the ferrites under dynamic conditions were investigated by determining the amplitude, frequency and temperature characteristics.

As the field amplitude characteristics for PP-2 ferrite (Fig.6) show, the relative remanence exhibits a maximum at a certain field strength; the coercive force increases with increasing field amplitude more rapidly than the maximum induction. In view of this it is expedient to utilize ferrites with a rectangular hysteresis loop in the range of relatively low field values wherein the relative remanence has a maximum value. The frequency charac-

Table 3

Magnetic properties of some ferrites with a rectangular hysteresis loop

Type	Magnetic parameters						Max. working temperature, °C
	quasistatic conditions H_m = 10 oersted			dynamic conditions f = 30 kc; H_m = 2 oerst.			
	B_m, Gs	B_r/B_m	H_c, Oe	B_m, Gs	B_r/B_m	H_c, Oe	
PP-1 (ПП-1)	2600	0,90	0,68	2500	0,89	1,5	+80
PP-2 (ПП-2)	2400	0,87	0,55	2300	0,86	0,9	+60
PP-24 (ПП-24)	2900	0,89	0,38	2800	0,87	0,75	+60
PP-4 (ПП-4)	2700	0,92	0,80	2590	0,92	1,65	+100
PP-5 (ПП-5)	2600	0,91	0,9	2400	0,90	2,0	+100

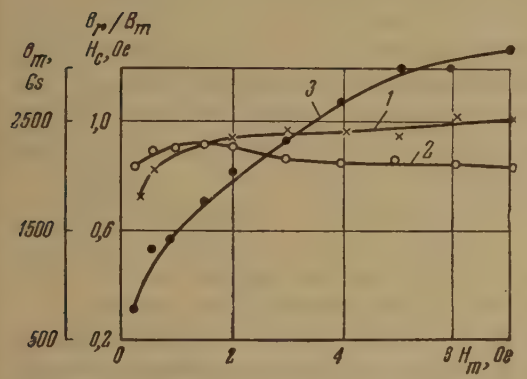

Fig.6. Variation of the magnetic parameters of PP-2 ferrite cores as a function of the field amplitude: 1 - B_m, 2 - B_r/B_m, 3 - H_c.

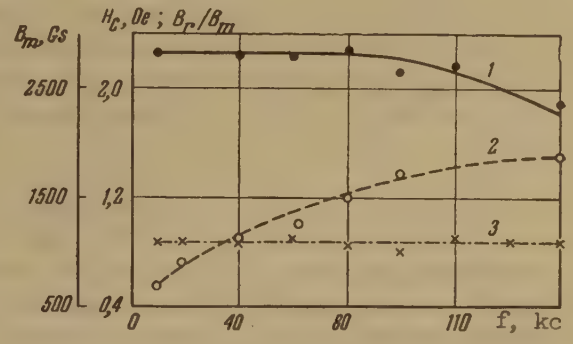

Fig.7. Variation of the magnetic parameters of PP-24 ferrite cores as a function of the frequency at H_m = 2 oersted: 1 - B_m, 2 - B_r/B_m, 3 - H_c.

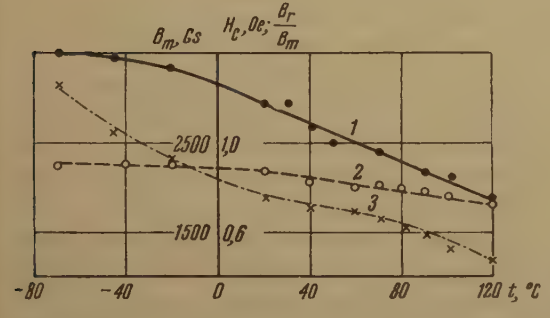

Fig.8. Variation of the magnetic parameters of PP-24 ferrite cores as a function of the temperature at f = 30 kc and H_m = 2 oersted: 1 - B_m, 2 - B_r/B_m, 3 - H_c.

characteristics of PP-24 ferrite (Fig.7) show that B_m and B_r/B_m are characterized by a relatively weak frequency dependence in the range from 10 to 100 kc.

The temperature characteristics of PP-24 ferrite in the range from -70 to +120° are shown in Fig.8. It will be seen that all three parameters decrease with increasing temperature.

Fig.9 shows the variation of τ (the magnetic polarity reversal time) and $1/\tau$ as a function of the field intensity for PP-1, PP-5 and PP-24 ferrites measured at a pulse repetition frequency of 100 per sec (4 μsec square pulses). It will be seen that $1/\tau$ increases linearly with the

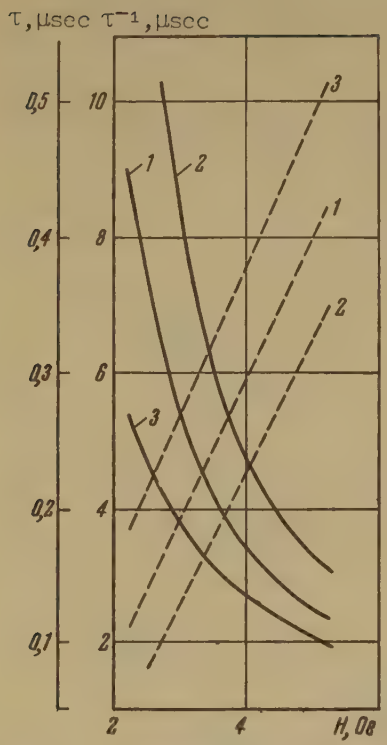

Fig.9. Variation of the magnetization reversal time τ (solid curves) and τ^{-1} (dashed curves) as a function of the field strength for PP-1 (1), PP-5 (2) and PP-24 (3) ferrite cores.

magnetic field strength. Type PP-1 and PP-5 ferrites, which have a higher dynamic coercive force than PP-24 ferrites, are characterized by longer magnetization reversal times.

Scientific Research Telephone Communication Institute

References

1. E.Albers-Schoenberg, J.Appl.Physiks, 25, 152 (1954).
2. G.Hüllet, Z.Phys.Chem., 37, 325 (1901).
3. D.L.Fresh, Proc.IRE, 44, 1303 (1956).
4. M.L.Morgulis, Vibratsionnoe izmel'chenie materiala (Vibrational pulverization of materials), M. 1957.
5. J.L.Snoek, New Developments in Ferromagnetic Materials (Cited in Russian trans., M.1949.)
6. G.Economos, J.Amer.Cer.Soc., 38, 241 (1955).
7. H.P.Wijn, E.W.Gorter, C.I.Esweldt & P.Geldermans, Philips Techn.Rev., 16, 49, 1954.
8. G.Rado, R.Wright & W.Emerson, Phys.Rev., 80, 273 (1950).
9. V.P.Sal'nikova, Tekhnologiia izgotovleniia ferritovykh serdechnikov s priamougol'noi petlei gisterezisa marok VT-1, VT-2 i VT-4 (Technology of preparation of type VT-1, VT-2 and VT-4 ferrite cores with rectangular hysteresis loops), M.1957.

KINETICS OF THERMOMECHANICAL TREATMENT OF FERROMAGNETS

- F.N.Dunaev

Introduction

One of the procedures for producing a stable magnetic texture in ferromagnets consists of subjecting it to an external stress at high temperature and is called "thermomechanical treatment"[1].

Although the effect of thermomechanical treatment has been considered by a number of authors[1-12], it has not yet been adequately studied. For example, there have been no investigations devoted to the rate of the internal processes occurring during thermomechanical treatment. Yet investigations of the kinetics of thermomechanical treatment are of considerable theoretical and practical interest: on the one hand, they can yield certain information on the nature of the processes in the material and, on the other hand, they can be useful in specifying the optimum conditions of treatment.

The present work was concerned with the kinetics of thermomechanical treatment of samples of 65 Permalloy (65% Ni, remainder Fe) and transformer steel (3.7% Si). The 65 Permalloy specimens were in the form of wires 1 mm in diameter and 150 mm in length; the transformer steel samples were strips measuring 150 x x 2 x 0.35 mm. Prior to the experiments the specimens were annealed at 1200° in a current of hydrogen and then at 1000° in a high vacuum.

1. Measurements

The tests were carried out in a special set-up designed to measure the magnetization and magnetostriction at high temperatures under vacuum and at the same time to permit application and removal of an external load evenly but at a fairly rapid rate. The magnetostriction was measured by the mechano-optical procedure; the magnetization - by means of an astatic magnetometer; the temperature - by means of a platinum-rhodium·platinum thermocouple.

The saturation magnetostriction and magnetization in the field range corresponding to maximum susceptibility are highly sensitive to changes in magnetic structure. Hence we utilized these parameters for investigating the texture kinetics in the process of thermomechanical treatment.

The measurement procedure was the following. The specimen was heated without load up to a certain temperature T, then a load producing a tensile stress σ_A^* was applied and the saturation magnetostriction λ_s (in a 700 oersted field) was measured at certain intervals. Prior to each measurement the load was removed and the specimen demagnetized, i.e., the measurements of λ_s were made at zero load. As a result we obtained isothermal λ_s vs τ curves characterizing the variation of saturation magnetostriction with time under the influence of stress, i.e., curves characterizing the formation or establishment of magnetic structure.

After the texturing process had gone to completion, i.e., when continued application of the stress did not produce any further change in λ_s, the load was removed and we observed the process of breakdown or elimination of the magnetic structure at the same temperature T. Upon termination of the elimination of texture process, the load was again applied and we observed the process of re-

---

*In the case of 65 Permalloy σ_A = 1.5 kg/mm^2; in the case of transformer steel σ_A = 2 kg/mm^2. The optimum loads were determined experimentally; they were chosen so as to produce the maximum thermomechanical treatment effect and not cause any appreciable plastic deformation at the test temperatures.[10]

establishment of magnetic structure, i.e., made the same measurements as in obtaining the initial λ_s vs τ curve. Such a cycle of measurements was carried out at different temperatures: in the case of 65 Permalloy at T = 400, 460, 500 and 540° and in the case of transformer steel at T = 420, 470, 520, 570, 620 and 660°C.

A different lot of 65 Permalloy specimens was used to investigate the thermomechanical treatment by measuring the magnetization at a constant magnetic field H corresponding to maximum susceptibility. In principle the procedure was the same as outlined above for λ_s. The field was applied only at the instants of measurement after removal of the load and demagnetization of the specimen. In this case we obtained I_H vs τ curves characterizing the processes of establishment, elimination and reestablishment of magnetic texture at different temperatures T = 400, 420, 440, 460, 480 and 500°.

In order to see how the magnetic texture induced by thermomechanical treatment changes in the process of cooling we recorded saturation magnetostriction vs temperature curves for the following temperature cycle: heating without load to T, cooling without load after prolonged heating at T under stress σ_A, cooling under stress σ_A after prolonged heating under load at T. The holding time at T in both cases was sufficient for the texturing process to go to completion.

We emphasize that in all cases the measurements were made *after* removal of the load and demagnetization of the specimen. Consequently, the observed variations of the magnetization and magnetostriction reflect stable, i.e., more or less permanent, changes occurring inside the specimen.

The sensitivity of our equipment as regards measurements of magnetization was 0.13 gauss mm^{-1}, as regards magnetostriction $2 \cdot 10^{-7}$ mm^{-1}. The uncertainty in the magnetization measurements did not exceed 5%, in the magnetostriction measurements 7% and in the temperature measurements 3°.

2. Experimental results

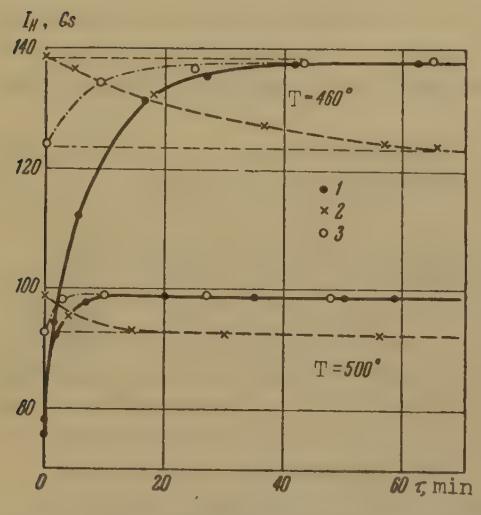

Fig.1. Variation with time τ of the intensity of magnetization of 65 Permalloy during establishment (1), removal (2) and reestablishment (3) of magnetic structure with σ_A = 1.5 kg/mm².

To illustrate the observed regularities, in Fig.1 we give the variation of the magnetization of 65 Permalloy with time in the processes of the initial establishment, removal and reestablishment of magnetic structure at T = 460 and 500°. It will be evident from the curves that changes in the magnetic structure occur more rapidly at higher temperatures: whereas at T = 400° more than two hours are necessary for the processes to go to completion, only 15-20 minutes are required for their consummation at T = 500°.

In the process of removal of texture, i.e., during prolonged holding at T with no load, the magnetic texture breaks down only partially; this is evinced by the fact that at the end of the process I_H does not return to its initial value, i.e., the one that obtained before application of the load.

In the process of reestablishment of the texture, however, I_H returns to the same value as upon completion of the initial texturing process, that is, the magnetic texture is reestablished to the full extent of its breakdown

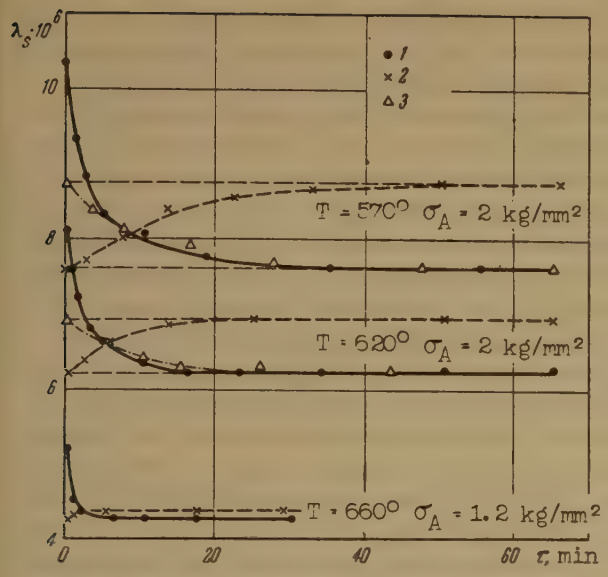

Fig.2. Variation with time τ of the saturation magnetostriction λ_s of transformer steel (3.7% Si) during establishment (1), removal (2) and reestablishment (3) of magnetic structure.

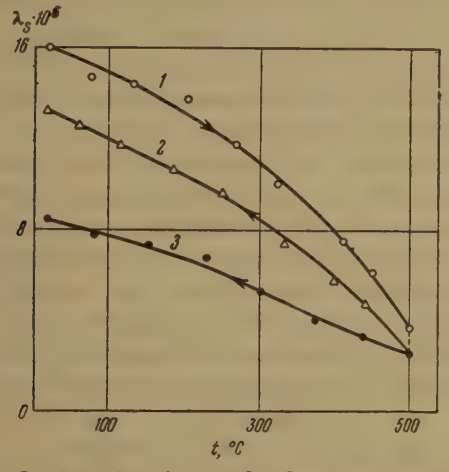

Fig.3. Variation of the saturation magnetostriction λ_s of 65 Permalloy as a function of the measurement temperature t. Heating temperature T = 500°; stresses: 1 - σ_A = 0, 2 - 1.5 kg/mm² during heating, cooling with σ = 0, 3 - σ_A = 1.5 kg/mm².

during heating with no load. Thus the thermomechanical treatment effect apparently comprises an irreversible and a reversible part.

The magnetostriction vs time curve for transformer steel at T = 570, 620 and 660° are shown in Fig.2. It will be evident that the same regularities are observed for transformer steel as for 65 Permalloy. With increasing T, the reversible part of the effect in both materials diminishes. Thus if we characterize the reversible fraction of the effect in terms of the ratio of the change in saturation magnetostriction or magnetization in the process of breakdown of texture to the change in these quantities in the initial process of establishment of structure we find that in the case of transformer steel $\Delta\lambda_{s(rev)}/\Delta\lambda_{s(init)}$ = 0.42, 0.37 and 0.16 for T = =570, 620 and 660°; for Permalloy the ratios are 0.50, 0.42 and 0.35 at 400, 460 and 500°, respectively. The rate of breakdown of texture is somewhat slower than the initial establishment process.

Further, comparing the rates of respective processes at the same temperature in 65 Permalloy and in transformer steel, we see that the rates are lower in transformer steel. For example, at T = 500°, completion of the initial texturing process in transformer steel requires at least 60 minutes, whereas only about 20 minutes are required in the case of Permalloy. A twenty minute texturing time for transformer steel is obtained only when T is increased to 620°.

We note, however, that the completion times for the same material determined from the λ_s and the I_H curves are virtually equal. For example, the time for consummation of the texture formation process for 65 Permalloy at T = 460° yielded by both curves is ~40 min.

The temperature dependences of the magnetostriction λ_s of 65 Permalloy are shown in Fig.3. It will be seen that λ_s decreases with increasing temperature. Curve 1 was obtained in heating with no load, curve 2 in cooling with no load after holding at T = 500° with σ_A = 1.5 kg/mm² and curve 3 in cooling with the load σ_A = 1.5 kg/mm². It will be seen that texture is formed not only during heating under stress but also in the process of cooling under stress. This is evinced by the fact that curve 3 lies considerably below curve 2.

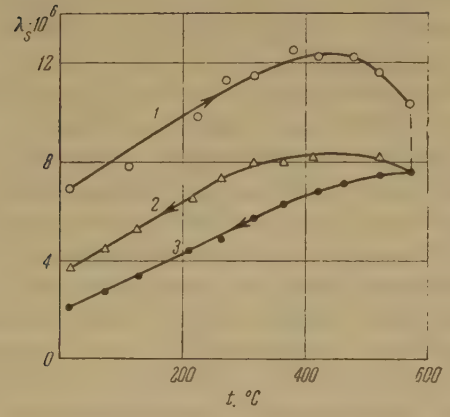

Fig.4. Variation of the saturation magnetostriction λ_s of transformer steel with the temperature. T = 570°, 1 - $\sigma = 0$, 2 $\sigma_A = 2$ kg/mm^2, cooling with $\sigma = 0$, 3 - $\sigma_A = 2$ kg/mm^2.

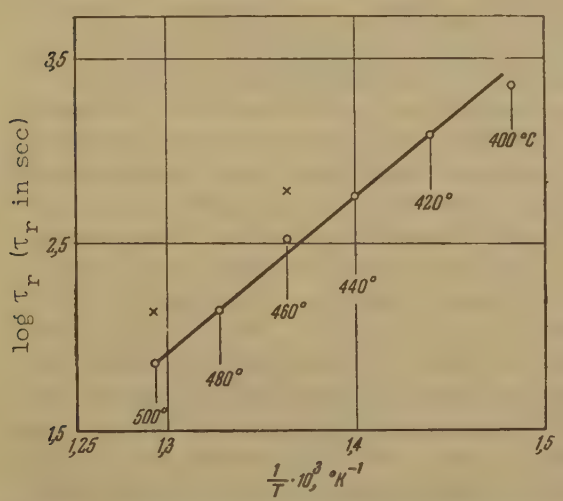

Fig.5. Variation of the relaxation time τ_r of the formation of the magnetic structure as a function of the temperature in 65 Permalloy: o - τ_r calculated from the I_H curves; X - values computed from the λ_s curves.

From analysis of similar λ_s vs temperature curves obtained for different T it was found that the growth of magnetic structure in the process of cooling is intensified for higher values of T, but that the growth only goes on down to about 400-380°, i.e., that the formation of structure stops at approximately this temperature. The degree of texturing can be characterized at least roughly by the ratio of the difference between the values of λ_s on curves 1 & 3 to the corresponding value of λ_s on curve 1. This ratio increases only down to the indicated temperature. For example, from the curve shown in Fig.3, we obtain 0.31, 0.49, 0.53 and 0.53 for $\Delta\lambda_s/\lambda_s$ at 500, 450, 400 and 350° respectively.

The temperature dependences of λ_s of transformer steel for T = 570° are given in Fig.4. In contrast to the case of 65 Permalloy, here λ_s increases with temperature up to a certain point. However, analysis of these curves and similar curves obtained at other values of T leads to the same regularities as regards the variation of magnetic texture as in the case of 65 Permalloy.

Fig.5 shows the dependence of the relaxation time of the texturing process in 65 Permalloy as a function of the reciprocal of the absolute temperature of thermomechanical treatment. It will be seen that the variation of log τ_r with 1/T is nearly linear. Consequently this dependence can be approximated by the relation

$$\tau_r = Ae^{\frac{W}{kT}},$$

i.e., the relation characteristic of diffusion processes. Here k is Boltzmann's constant and A and W are constants which, according to our calculations, have the following values:

$$A = 1.2 \cdot 10^{-9} \text{ sec and}$$
$$W = 2.48 \cdot 10^{-12} \text{ erg} = 1.55 \text{ ev}$$

With a view to comparing the effect of thermomechanical and thermomagnetic treatments, we investigated the kinetics of thermomagnetic treatment at T = 460°, carrying the specimens through a number of cooling cycles in zero field and in a 400 oersted field. All the measurements were made in the same way as in investigating the kinetics of thermomechanical treatment, i.e., the magnetostriction

and magnetization were measured only after removal of the field and demagnetization of the specimen.

The results obtained were similar to those evinced in thermomechanical treatment and described above.

In particular, we observe the process of partial breakdown of the texture in heating in zero field and the process of reestablishment of texture. The time to completion of the initial formation of texture process differs little from the time for consummation of the texturing process during thermomechanical treatment. This result is substantiated by comparison with the data of Bozorth & Dillinger[13] and the results of Zusman[14].

Moreover, in general thermomechanical treatment appears to be most effective for the same materials that are susceptible to thermomagnetic treatment.

All this would indicate that the processes induced in ferromagnetic materials by the two types of treatment are similar or at least have certain traits in common.

It will be seen from Fig.5 that the relaxation times determined from the magnetostriction curves are somewhat longer than the relaxation times computed on the basis of the magnetic intensity curves, even though the times to completion of the texturing process yielded by the two curves are equal. It must be inferred, therefore, that the changes occurring in the specimen during thermomechanical treatment first affect I_H more strongly than λ_s and that these initial changes are primarily irreversible in the sense defined above. Actually, the fraction of the reversible part of the effect as determined from the I_H vs τ curves is smaller than the fraction computed on the basis of the λ_s vs τ curve. For example, for 65 Permalloy with $T = 460^\circ$ we have $\Delta I_{H(rev)}/\Delta I_H = 0.24$, while $\Delta\lambda_{s(rev)}/\Delta\lambda_s = 0.42$. Careful scrutiny of Fig.5 shows that variation of $\log \tau_r$ as a function of $1/T$ is only roughly approximated by a straight line. A better approximation is given by a curve bulging upward.

Arkharov[15] notes that owing to the unquestioned assumption that the kinetics of a given process must be characterized by the simple exponential law investigators frequently tend to disregard deviations of the experimental points from a straight line even when the deviations indicate a different regularity. Such systematic deviation is observed in the case of thermomechanical treatment. The $\log \tau_r$ vs $1/T$ curves calculated both from the I_H and the λ_s vs time curves for 65 Permalloy show an unmistakable upward convexity. The curves for transformer steel also exhibit a noticeable camber. Consequently, with increasing temperature the rate of texture formation is somewhat greater than would follow from the diffusion law.

Apparently other processes in addition to diffusion are involved in thermomechanical treatment. Possibly under the influence of the external load there are set up large local stresses producing plastic deformations in microregions. This may explain the fact that the activation energy determined by us for 65 Permalloy is less than that found by Bozorth & Dillinger[13] for the same material in the process of thermomagnetic treatment. Logically, additional stresses and strains induced in the material by the external load during thermomechanical treatment should reduce the activation energy.

The principal cause of the thermomechanical treatment effect may be oriented superstructure of the type hypothesized by Néel[12]. It is not impossible that a significant role in this effect is also played by diffusional redistribution of internal stresses, resulting in increase of the volumes of regions subjected to internal tensile stresses in the direction of the applied load.

One of the possible causes of partial breakdown of the magnetic texture during heating with no load, i.e., the factor responsible for the reversible

part of the thermomechanical treatment effect, may be the elastic aftereffect known as spring-back.

Faculty of Experimental Physics,
"A.M.Gorki" Ural State University

References

1. S.V.Vonsovskii & Ia.S.Shur, Ferromagnetizm (Ferromagnetism) 1948.
2. Nishina, Sci.Reports, Tohoku Univ., 25, 225 (1939).
3. Ia.S.Shur & A.S.Khokhlov, Zhur.eksp.i teor.fiz., 10, 1113 (1940).
4. Ia.S.Shur & A.S.Khokhlov, Doklady AN SSSR, 53, 39 (1946).
5. Ia.S.Shur, Izv.AN SSSR, Ser.fiz., 11, 570 (1947).
6. S.V.Vonsovskii, Zhur.eksp.i teor.fiz., 17, 1094 (1947).
7. M.V.Dekhtiar, Doklady AN SSSR, 69, 527 (1949).
8. B.A.Vaisman, Dissertation, Kharkhov Machine Building Institute, 1949.
9. Ia.S.Shur & F.N.Dunaev, Doklady AN SSSR, 7, 293 (1950).
10. Ia.S.Shur & F.N.Dunaev, Izv.AN SSSR, Ser.fiz., 16, 640 (1952).
11. Ia.S.Shur & F.N.Dunaev, Trudy (Proceedings), Inst.of Metal Physics, Ural Branch of the USSR Acad.of Sciences, 15, 29 (1954).
12. L.J.Néel, Phys.et radium, 15, 225 (1954).
13. R.M.Bozorth & J.F.Dillinger, Physics, 6, 285 (1935).
14. Sh.I.Zusman, Tezisy dokladov na soveshchanii po fizike magnitnykh materialov (Abstracts of reports presented to the Conference on the Physics of Magnetic Materials), p.14, M.-L., 1957.
15. V.I.Arkharov, Zhur.tekh.fiz., 24, 375 (1954).

GRAIN-ORIENTATION IN THE PROCESS OF ANNEALING COLD-ROLLED TRANSFORMER STEEL*

- L.V.Mironov

A distinctive characteristic of cold-rolled transformer steel being produced at present by our (USSR) plants is its crystallographic structure which is characterized by alignment of the (100) planes in the plane of rolling and of the [100] cube edges in the direction of rolling.[1] Inasmuch as the [100] direction in the α-Fe lattice is a direction of easy magnetization, high magnetic properties can be realized in the rolling direction if a pronounced texture (grain orientation) is obtained in the material. For example, in the case of texture characterized by 90-95% oriented grains, the magnetic induction (B_{25}) with a field strength of 25 ampere-turns per centimeter amounts to 19,300-19,500 gauss, while the specific loss ($P_{10/50}$) at 10,000 gauss and 50 cps is 0.85-0.90 watt/kg. In contrast, samples from the same melt but with less pronounced structure, i.e., having about 25% oriented grains, have B_{25} = 15,500 gauss and $P_{10/50}$ = = 1.40 watt/kg.

In developing rapid procedures for the final annealing of cold-rolled transformer steel, it was found that when the rate of heating is increased about 100-150 degree/hour the grain orientation processes are hindered or suppressed. In case of rapid heating, even after annealing at high temperatures, poor texture was obtained, while samples from the same strips annealed under the same conditions but with a slow heating rate had a texture characterized by 95% oriented grains.

In view of this it appeared desirable to investigate the kinetics of texture formation. The research was carried out on cold-rolled commercial strips 0.35 and 0.50 mm thick from different smelts that had gone through the entire technological process except for the final high-temperature anneal. The samples were deliberately taken from smelts yielding final sheets with different characteristics. The results of chemical analyses of the smelts from which the samples were taken are given in the accompanying table.

Composition of sample batches (values in %)

Smelt No.	C	Si	Mn	P	S	Ni
2	0,04	3,05	0,03	0,010	0,005	0,09
4	0,02	3,09	0,10	0,008	0,004	0,11
6	0,04	3,10	0,07	0,011	0,006	0,11
8	0,04	2,96	0,02	0,009	0,007	0,11

The samples were in the form of 30 mm diameter disks cut from the cold-rolled strips. The samples were heated in the laboratory electric vacuum furnace, or in some cases by the contact procedure. The rate of heating was varied from 1 degree/ /min to 1000 degree/sec.

After annealing, we determined the texture by measuring the normal component of the magnetization (I_n) as a function of the angle φ between the direction of the applied magnetic field and the direction of rolling (Aksenov-Grigorov method[2]). The magnetization measurements were made by means of a ballistic galvanometer at a field intensity of 300 oersted. In addition, using the same samples, we determined the grain size by the conventional metallographic procedure.

Fig.1 shows the variation of I_n with the angle φ for samples from smelt No.8 subjected to different heat treatments. In general such curves are analyzed (harmonic analysis) to obtain the amplitudes of the even harmonics and from these, using Akulov's equation for the magnetic anisotropy[3], one can determine the rela-

---

*G.N.Shubina participated in part of the research.

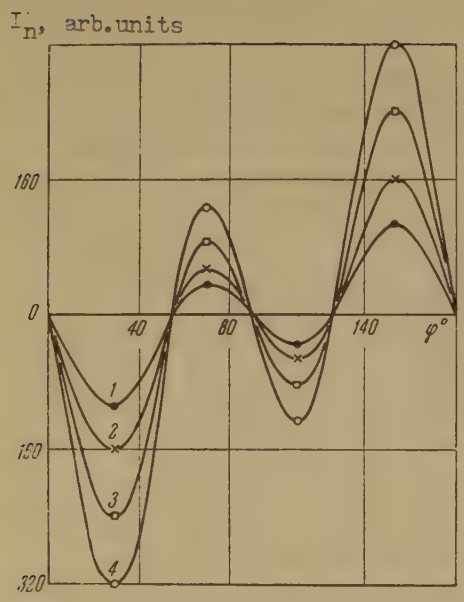

Fig.1. Curves characterizing the anisotropy of samples from smelt No.8. I_n - normal component of the magnetization; φ - angle of field relative to the direction of rolling. Heat treatments: 1) 6 hrs at 850°, 2) 6 hrs at 925°, 3) 4 hrs at 1000°, 4) 2 hrs at 1100°.

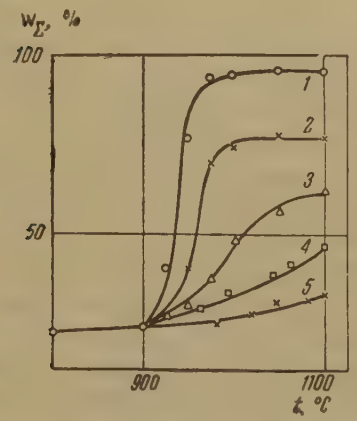

Fig.2. Influence of the rate of heating on the degree of perfection of texture as characterized by W_Σ; samples from smelt No.8: 1) 1.0 degree/min, 2) 35 degree/min, 3) 400 degree/min, 4) 100 degree/sec, 5) 1000 degree/sec.

tive volume of crystallites oriented in conformity with a given type of texture. However, in our particular case, when there are no changes in the type of texture and only the degree of perfection of the texture varies, one can have recourse to a simplified procedure and characterize the degree of perfection by the mean amplitude of the I_n vs φ curves.[4] In our work we subjected three samples to the same heat treatment in each case and as the quantity characterizing the degree of perfection of texture took the arithmetic mean value of I_n for these three samples; hereinafter we shall denote this arithmetic mean value by W_Σ. In a few cases, when there were obtained very large grains, we treated an additional 6-8 samples to enhance the statistical accuracy. The scatter of experimental points did not exceed 10%.

Fig.2 shows the influence of the heating rate on the degree of perfection of texture of samples from smelt No.8 in heating to 800-1100° (zero holding time). It will be evident from the curves that with increase of the rate of heating to 1100° the degree of perfection progressively decreases from 95% in the case of heating at the rate of 1 degree/min to 30% in the case of heating at 1000 degree/sec. It is interesting to note that with slow heating the greatest increment in the degree of perfection occurs in the 900 to 1000° interval. Measurements of grain size showed that in heating to 1100-1200° at a rapid rate (100 to 1000 degree/sec) there occurs complete recrystallization with appreciable development of grain size - sometimes the grain dimensions become commensurate with the thickness of the plate; holding at the high temperature in this case has little effect on the grain size. Consequently, rapid heating does not suppress grain development in general but only preferential growth of oriented grains.

Isothermal experiments yielded an even clearer picture of the processes involved in texture formation. In these experiments the samples were heated at a rate of about 2000 degree/min to different temperatures and held at heat for 5 min to 6 hours. It was found that when cold-rolled transformer steel is annealed at temperatures above 850-900° there occurs secondary recrystallization which has a decisive effect on grain orientation.

After the recrystallization treatment, the samples are characterized by a recrystallization texture, the degree of perfection of which is

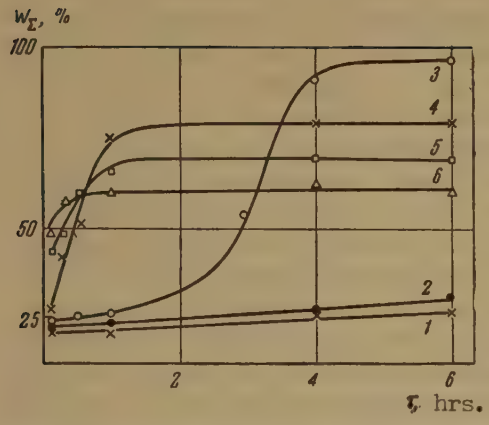

Fig.3. Influence of holding time at different temperatures on the degree of perfection of texture (total texture as characterized by W) for samples from smelt No.8: 1) 850°, 2) 900°, 3) 925°, 4) 975°, 5) 1050°, 6) 1100°.

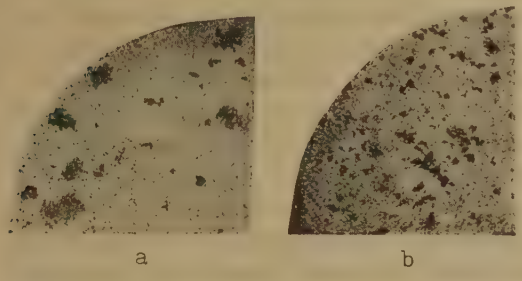

Fig.4. Microstructure of samples from smelt No.8 annealed for a) 15 min at 925° and b) 5 min at 1000°.

about 20% and does not depend on the heating rate. When either the heating time or the temperature are increased, there occurs agglomerative recrystallization accompanied by increase in the degree of perfection. The extent of this improvement depends on the mechanism of grain growth. In the case of ordinary continuous grain growth (usually occurring at temperatures up to 900°), the increase in degree of perfection is insignificant. If, however, there occurs secondary recrystallization, an appreciable increase in perfection may be realized. Decisive in this case are the process parameters, namely, the number N of "growth centers" and the linear growth rate G. The kinetic curves characterizing the process of texture formation in samples from smelt No.8 are shown in Fig.3.

The greatest increase in degree of perfection occurs at temperatures marking the beginning of secondary recrystallization, when there appears a small number of precisely oriented "growth centers". Secondary recrystallization in this case develops primarily through enlargement of the growth centers (not through the genesis of new centers) and terminates when the growing grains "meet". At 925°, owing to the relatively low linear growth rate, the process requires an appreciable time (4 to 5 hours) to go to completion.

Increase of the maximum annealing temperature is accompanied by increase in the number of growth centers which are characterized by increasingly random orientation. The process of secondary recrystallization is accelerated, but the effective grain size is reduced and accordingly the degree of perfection of texture decreases. Apparently, the most accurately oriented grains are the most stable ones and their growth is most advantageous as regards reduction of internal energy; hence they serve as "growth centers" in the range of low temperatures. By the same token, less precisely oriented grains have less tendency to grow and hence can become "growth centers" only at higher temperatures. This is why increase of the annealing temperature is accompanied by increase in the number of "growth centers" and at the same time a decrease as regards the accuracy of their "total" orientation. Photographs of samples annealed at 925° and 1000° and etched to bring out the microstructure are reproduced in Fig.4. These photographs show how greatly the number of "growth centers" (dark specks in the photographs) increases with increase in temperature.

In view of the specific kinetics of secondary recrystallization, the variation of the degree of perfection of texture of transformer steel as a function of the annealing temperature is characterized by curves with maxima. Typical curves for samples from smelt No.8 are shown in Fig.5. It will be seen that the most perfect texture is obtained at temperatures corresponding to the beginning

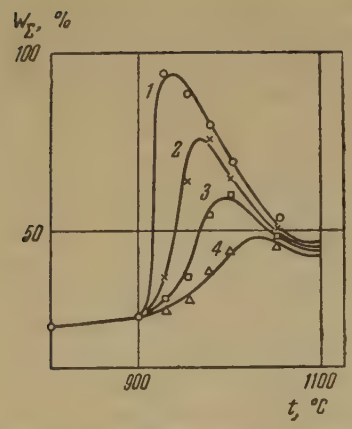

Fig.5. Influence of the annealing temperature on the degree of perfection of texture (as characterized by W_Σ) in samples from smelt No.8. Holding times at heat: 1) 4 hrs, 2) 1 hr, 3) 30 min, 4) 5 min.

of secondary recrystallization, provided the sample is held at heat for a sufficiently long time for the recrystallization process to be consumated. Annealing at a higher or lower temperature results in decrease of the degree of perfection. It will be seen that as the holding time is shortened the maxima in the W_Σ curves shift to the side of higher temperatures.

On the basis of the above described experimental results, one can explain the influence of the rate of heating on the recrystallization texture obtained in annealing cold-rolled transformer steel. In the case of slow heating, the process of secondary recrystallization goes to completion under conditions favorable for texture formation, i.e., when there appear precisely oriented "growth centers". Increase of the heating rate shifts the secondary recrystallization into the region of higher temperatures and this is accompanied by a great increase in a number of "growth centers", many of which are more or less randomly oriented; as a result the texture is impaired.

Tests on samples taken from other smelts showed that different batches of transformer steel are characterized by individual distinctive attributes which are evinced in variation of the temperature of beginning of secondary recrystallization and of the number of "growth centers". In contrast, the linear growth rate appears to be independent of the individual properties of different smelts, i.e., is virtually the same for all smelts.

In some cases the individual attributes of a given smelt are evinced only by an increase or decrease of the temperature of beginning of secondary recrystallization. In such cases the minimum number of "growth centers" and the maximum degree of perfection of texture are observed at different temperatures, which is obviously reflected in the kinetics of the texture formation process. If the secondary recrystallization begins at higher temperatures, the process, owing to a higher linear growth rate, is consumated more rapidly than in samples from smelts with a lower temperature of secondary recrystallization. Figs.6 and 7 show the variation of the parameters N and G and the degree of perfection of texture as a function of the annealing temperature for samples characterized by different temperatures of the beginning of secondary recrystallization. Depending on the temperature of beginning of secondary recrystallization, the time necessary for obtaining the greatest degree of perfection may vary from 4-5 hours (at 900-920°) to 15-20 min (at 1000-1020°). Tests on a large number of samples from different commercial smelts showed that in most cases secondary recrystallization is observed at temperatures between 920 and 970°, which corresponds to holding times of 3-4 hours.

Some individual smelts do not have a clearly defined temperature of beginning of secondary recrystallization: in samples from these smelts a large number of "growth centers" appears at all temperatures from 820-850° up. The degree of perfection that can be attained by annealing specimens from such smelts is relatively low and sheets fabricated from such smelts as a rule have inferior magnetic properties.

As a result of a special series of experiments designed to study the influence of different factors on secondary recrystallization, it was established that preliminary low-temperature annealing (below 850°) even with holding times of up

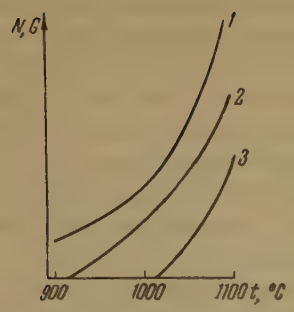

Fig.6

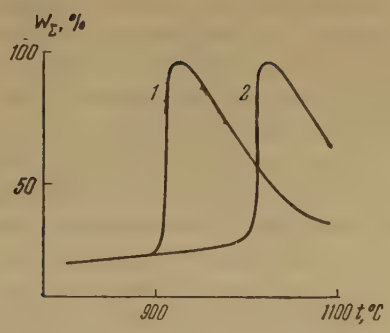

Fig.7

Fig.6. Influence of annealing temperature on the secondary recrystallization parameters: 1) linear growth rate G in samples from smelts Nos.2 & 8, 2) number N of growth centers in a sample from smelt No.8, 3) same for sample from smelt No.2.

Fig.7. Influence of annealing temperature on texture formation (as characterized by W_Σ): 1) smelt No.8, holding time at heat 4 hours; 2) smelt No.2, holding time 20 min.

to 18-20 hours, has little or no effect on the secondary recrystallization parameters and hence on texture formation. On the other hand, preliminary annealing at elevated temperatures (above 1000-1050°), even in the case of rapid electric heating, when no strong grain growth occurs, precludes the possibility of secondary recrystallization at lower temperatures and sharply reduces the "total" texture obtained in the subsequent final annealing. These facts should be borne in mind in specifying conditions for preliminary decarbonizing heat treatment in the fabrication of transformer steel sheets.

Subjecting cold-rolled samples to low temperature annealing (below 850°) followed by rolling with critical reduction leads to complete suppression of secondary recrystallization and a sharp reduction of the degree of texture perfection obtained in subsequent annealing. It is interesting to note that the critical deformation for samples of cold-rolled transformer steel subjected previously to low temperature annealing does not exceed 5%, whereas it is known that the critical reduction for hot-rolled steel is 10-12%. This lower value of the critical reduction for cold-rolled steel can be explained if we assume that the low temperature anneal does not relieve all the stresses in the material. The results of recent etch figure studies[5] of cold-rolled and annealed transformer steels are consistent with this explanation.

All the above observations apply to the processes occurring in commercial strips obtained by two-pass cold rolling with intermediate tempering. Preliminary investigations show, however, that secondary recrystallization effects with the same characteristics occur in steel strips fabricated by single rolling with over 75% reduction. The difference as compared with strips fabricated by two-stage rolling is that secondary recrystallization with the formation of precisely oriented "growth centers" begins, as a rule, at lower temperatures and requires a more prolonged heating time (8-12 hours) to go to completion. This apparently is the reason for the widely held opinion that one cannot obtain recrystallization structure with a high degree of perfection in singly rolled strips.

Conclusions

1. During annealing of cold-rolled transformer steel fabricated by two-stage rolling with intermediate tempering or single rolling with over 75% reduction there occurs secondary recrystallization under conditions favoring preferential growth of oriented grains.

2. The most favorable temperature for obtaining texture with a high degree of perfection is the temperature of beginning of secondary recrystallization when there appear the most precisely oriented "growth centers". In view of the fact that at this temperature the number of "growth centers" is small and the linear growth rate is low, the process requires an appreciable time - up to 6 hours - to go to completion. Increasing the annealing temperature leads to an increase in the number of "growth centers" but with more random orientations; the process is accelerated but leads to the formation of small poorly oriented grains.

3. In the case of slow increase of temperature, the secondary recrystallization is consumated at optimum temperatures; rapid heating shifts the recrystallization into the region of higher temperatures, which is accompanied by reduction of the grain size and decrease in the degree of perfection of texture. Hence under industrial conditions if the heating rate cannot be made slow enough to insure the material remaining in the 900 to 1000° range for a sufficiently long time, it would be expedient to employ two-stage heating, i.e., to hold the material for an appropriate time at just above 900° before bringing it up to the final annealing temperature.

4. The development of secondary recrystallization is also influenced by such factors as the individual characteristics of the smelt, preliminary high-temperature heating and rolling with critical reduction. Low-temperature annealing does not have any appreciable effect on secondary recrystallization.

6. The existence and kinetics of secondary recrystallization must be taken into account in developing and specifying the fabricating operations for different types of cold-rolled transformer steel.

Ural Scientific Research Institute for Ferrous Metals

References

1. A.L.Gol'dman & V.V.Druzhinin, Sbornik, posviashchennyi 70-letiiu Akademika Ioffe (Symposium dedicated to the 70th Anniversary of Academician Ioffe), M.1950.

2. K.V.Grigorov, Izv.AN SSSR, Ser.fiz., 11, 6, 679 (1947).

3. N.S.Akulov, Ferromagnetizm (Ferromagnetism), M., 1939.

4. L.V.Mironov & G.N.Shubin, O kinetike teksturoobrazovaniia transformatornoi stali.Biul.informatsii Ural'sk. NII chernykh metallov (On the kinetics of texture formation in transformer steel. Information Bulletin, Ural Scientific Research Institute for Ferrous Metals), No.2, 1957.

5. C.G.Dunn & E.F.Koch, Acta metallurgica, 5, 10, 548 (1957).

MAGNETIC ANALYSIS OF THE DEFORMATION STRUCTURE DUE TO COLD ROLLING AND RECRYSTALLIZATION IN PURE ELECTROLYTIC NICKEL

- N.L.Briukhatov, N.A.Grinchar & I.Ia.Ekamasov

Introduction

Among the different types of texture or grain-orientation obtained in rolled metals by recrystallization, of particular interest is the so-called "cube texture" which can be realized in some metals and alloys possessing a face-centered cubic lattice.[1]

This texture is characterized by orientation of one set of cube-faces in the plane of rolling and alignment of the crystallographic axis parallel to the cube edge in the direction of rolling; accordingly it is usually denoted by (100), [001]. The cube texture makes it possible to utilize the pronounced anisotropy of some physical properties of single crystals. In particular, as one of us showed earlier[2], it is feasible to utilize the maximum value of the magnetostriction ($-54 \cdot 10^{-6}$) of nickel single crystals by producing the cube structure in polycrystalline material through agglomerative recrystallization.

Despite the fact that the process of recrystallization of nickel, leading to realization of the cube structure, has been investigated by a number of authors, we still have only scant information on the conditions governing the development of cold-rolling deformation texture and recrystallization texture in nickel.

The purpose of the present work was to develop a method of magnetic analysis of deformation and recrystallization textures in pure electrolytic nickel and to elucidate the influence of the degree of purity of the metal and of the conditions of cold rolling and heat treatment on the development and character of the texture and the residual internal stresses.

1. Magnetic Analysis of Texture of Rolled Nickel

For investigating the texture in nickel we used the method of measuring the mechanical torques by means of a magnetic dynamometer (torquemeter).[5] Resolution of the resultant magnetograms (torque curves) into harmonics by the method of harmonic analysis leads, as a rule, to the following general expression for the torque:

$$M = A_4 \sin 4\alpha + A_2 \sin 2\alpha, \qquad (1)$$

where α is the angle between the direction of rolling and the applied magnetic field and A_4 and A_2 are amplitude coefficients depending on the anisotropy constant.

The calculations are generally carried out for an averaged "effective" texture equivalent to the real texture with a certain scatter of the crystallographic axes. We based our analyses and calculations on the x-ray diffraction data which indicate the presence of a primary texture characterized by alignment of the (011) planes with the rolling plane and orientation of the [112] axis in the direction of rolling[1] with possible deviations of up to 8° from this direction[6] and a less pronounced secondary texture in which the (112) planes are in the plane of rolling and the [111] axis is aligned with the direction of rolling.[1] Expressions for the torques can be deduced from the formula for the magnetic anisotropy energy.[5,7] Using ω_j to denote the angle between the cube edge and the direction of rolling for the crystallites of the first groups, W_j to denote the relative volume of such crystallites and W_2 to denote the volumetric proportion

of crystallites of the second group with the (112), [111] orientation, we can write the following expressions for the torques due to the crystalites of the first and second groups:

$$M_1 = \frac{3}{8} K (\Sigma W_j \cos 4\omega_j) \sin 4\alpha + \frac{1}{4} K (\Sigma W_j \cos 2\omega_j) \sin 2\alpha, \tag{2}$$

$$M_2 = -\frac{1}{24} K W_2 (7 \sin 4\alpha + 2 \sin 2\alpha), \tag{3}$$

where K is the anisotropy constant for nickel.

The total torque M is the sum of the component torques M_1, M_2 and the torque M_3 due to oriented internal stresses:

$$M = M_1 + M_2 + M_3, \tag{4}$$

where

$$M_3 = X_2 \sin 2\alpha. \tag{5}$$

Approximating the actual structure with the [112] axes "scattered" about the rolling direction by an "effective" texture with precise orientation of [112] in this direction, i.e., replacing the spread of angles ω_j by a single angle ω_1 for which $\cos\omega_1 = \sqrt{6/3}$ and replacing the W_j by a single W_1, we can write the expression for the total torque in the following form:

$$M = \frac{K}{24} W_1 (2 \sin 2\alpha - 7 \sin 4\alpha) - \frac{K}{24} W_2 (2 \sin 2\alpha + 7 \sin 4\alpha) + X_2 \sin 2\alpha, \tag{6}$$

or

$$M = \left[\frac{K}{12} (W_1 - W_2) + X_2\right] \sin 2\alpha - \frac{7}{24} K (W_1 + W_2) \sin 4\alpha. \tag{7}$$

Obviously, the two equations (1) and (7) alone are not sufficient for determining the three unknowns W_1, W_2 and X_2. However, taking advantage of the strong temperature dependence of the harmonics associated with the crystallographic anisotropy and of the harmonics due to internal stresses[8], we can obtain a third equation. To this end we need only record a magnetogram (torque curve) at a low temperature (for example, at liquid nitrogen temperature). We then have the following three equations for solving our problem:

$$\left.\begin{aligned} \frac{K}{12} (W_1 - W_2) + X_2 &= A_2, \\ -\frac{7 \cdot K}{24} (W_1 + W_2) &= A_4, \\ \frac{K'}{12} (W_1 - W_2) + 1{,}5 X_2 &= A'_2. \end{aligned}\right\} \tag{8}$$

Here A_2 and A_4 are the amplitudes of the harmonics in the torque curve obtained at room temperature and A'_2 is the amplitude at liquid nitrogen temperature. The values of K can be taken from the experimentally determined temperature dependence of the anisotropy constant of nickel[9]; K' is the value of the anisotropy constant at liquid nitrogen temperature.

In the case of the given degree of cooling (i.e., to liquid nitrogen temperature), the change in the amplitude of the second harmonic due to stresses is connected with the corresponding temperature change of the magnetostriction.[10] It may be assumed with reasonable accuracy that the magnetostriction in this case decreases by a factor of 1.5.

2. Experimental Results

The tests were carried out on samples of high purity, grade N0000 electrolytic nickel, analyzing only 0.03% total impurities, including 0.012% cobalt. We employed two rolling procedures: gradual rolling involving 200 passes in which the samples were reduced 90% and rapid rolling in which the samples were reduced 94--95% in 15-20 passes. The recrystallization annealing carried out under vacuum involved either 4 hours heating at 1000° or 2 hours at 1100° followed, in both cases, by slow cooling with the furnace.

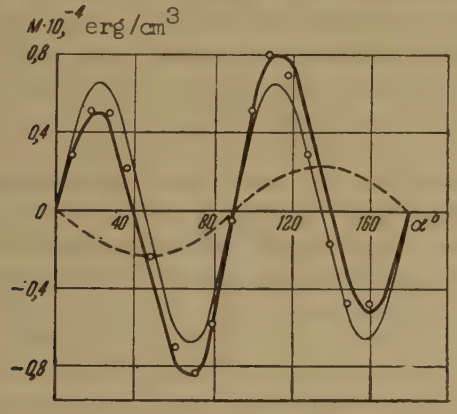

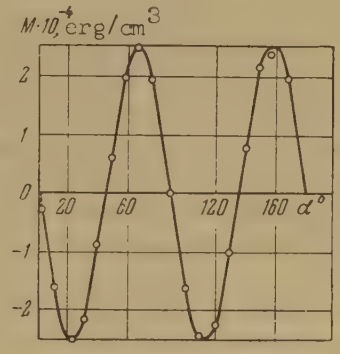

Fig.1. Magnetogram obtained at room temperature for sample No.17 of high purity nickel prior to heat treatment. Gradual 90% reduction by cold rolling. Torque - $M = 0.65 \cdot 10^4 \sin 4\alpha - 0.22 \cdot 10^4 \sin 2\alpha$.

Fig.2. Magnetogram obtained at room temperature for sample No.17 after annealing for 2 hours at 1100°. Torque - $M = -2.49 \cdot 10^4 \sin 4\alpha$.

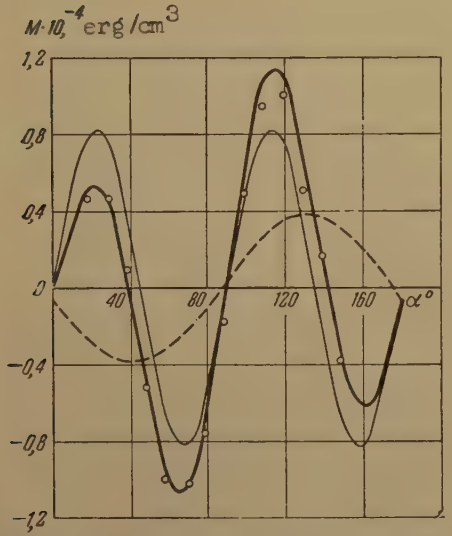

Fig.3. Magnetogram obtained at room temperature for sample No. 10 of high purity nickel after rapid 95.3% reduction. $M = 0.83 \cdot 10^4 \sin 4\alpha - 0.38 \cdot 10^4 \sin 2(\alpha + 4^\circ)$.

A. Realization of cube texture

In samples subjected to gradual 90% reduction there is realized as a result of 2 hours annealing at 1100° a perfect cube texture, i.e., 100% of the crystallites assume the indicated orientation. The torque curve obtained at room temperature for sample No.17 immediately after gradual 90% reduction is shown in Fig.1. Fig.2 shows the torque curve after annealing for the same sample; this curve is virtually identical with that obtained for a nickel single crystal in the cube-face plane[9].

In the case of samples subjected to rapid 90 to 95% reduction, one cannot obtain a perfect cube texture by the same 2 hours at 1100° heat treatment. In this case there is observed a certain quantitative change in the cold rolling texture and only partial development of cube texture. Moreover, in the case of these rapidly deformed samples, 4 hour heating at 1000° failed to yield a perfect cube texture. Fig.3 shows the torque curve obtained at room temperature for sample No.10 immediately after cold rolling with

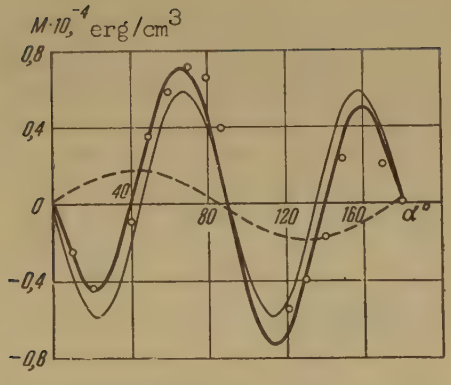

Fig.4. Magnetogram obtained at room temperature for sample No. 10 after 4 hours heating at 1000°. $M = -0.59 \cdot 10^4 \sin 4\alpha + 0.19 \cdot 10^4 \sin 2(\alpha + 6^\circ)$.

rapid 95.3% reduction; Fig.4 shows the torque curve obtained for the same sample after annealing.

B. Analysis of texture and stresses

The results of analysis of the texture and stresses in the high purity electrolytic samples are listed in Table 1.

The torque curves obtained for samples Nos. 17 and 10 after rolling (gradual and rapid reduction, respectively) are given in Figs.5 & 6, respectively. These are the curves needed for writing the third equation in set (8). In all cases the measurements show that the second harmonic X_2, associated with the internal stresses, has a negative amplitude, the magnitude of which increases with increasing degree and rate of reduction.

Table 1

Results of quantitative calculation of the texture and harmonics associated with internal stresses for samples of N0000 nickel after cold rolling (before annealing)

Sample No.	Reduction rate	Percentage reduction	W_1, %	W_2, %	Amplitude of second harmonic, X_2, erg/cm³
17	Gradual	90	22	21	—0,21·10⁴
10	Rapid	95,3	7	55	—0,6·10⁴
24	Rapid	94,8	3,5	54	—0,66·10⁴
25	Rapid	94,1	5	54	—0,7·10⁴
26	Rapid	94,6	3	58	—0,7·10⁴

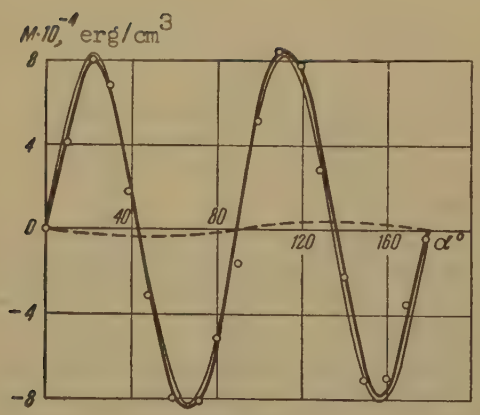

Fig.5

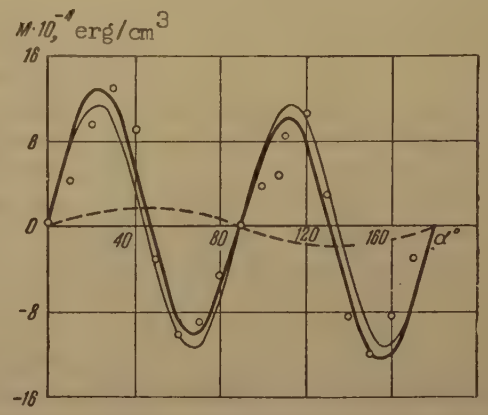

Fig.6

Fig.5. Magnetogram for sample No.17 of high purity nickel before heat treatment. $M = 8.15 \cdot 10^4 \sin 4\alpha - 0.35 \cdot 10^4 \sin 2\alpha$.

Fig.6. Magnetogram for sample No.10 of high purity nickel before heat treatment. $M = 11.54 \cdot 10^4 \sin 4\alpha + 1.73 \cdot 10^4 \sin 2\alpha$.

C. Reflief of internal stresses and formation of recrystallization texture

Table 2

Variation of internal stresses during annealing

Sample No.	Annealing temp., °C	Heating time	Amplitude of second harmonic, X_2, erg/cm³
24	+200	2	$-0.39 \cdot 10^4$
25	+300	2	$-0.03 \cdot 10^4$
26	+400	2	0

In order to bring out the variation of the internal stresses during annealing samples Nos.24, 25 & 26 were heated in vacuum for 2 hours at 200°, 300° and 400°, respectively. Then from the magnetograms obtained for these samples we calculated the total percentages of oriented crystallites and the amplitudes of the second harmonics X_2 due to internal stresses.

The analyses show that the total number of crystallites oriented by cold rolling changes little with the indicated heat treatments but that the magnitude of X_2 decreases rapidly with increasing annealing temperature, going to zero as a result of heating at 400°, which indicates complete removal of the internal stresses. The variation of the amplitude of the second harmonic is shown in Table 2. Analysis of the torque curve obtained for sample No.26 also shows that simultaneously with the relief of the internal stresses there begins to appear a third group of oriented crystallites forming a cube texture.

This third group, forming as a result of annealing and occupying a volume W_0, gives rise to its own harmonic

$$M_4 = \frac{K}{2} W_0 \sin 4\alpha. \tag{9}$$

Hence in this case the second equation in the set (8) must be rewritten:

$$-\frac{7K}{24}(W_1 + W_2) + \frac{1}{2} KW_0 = A_4. \tag{10}$$

Assuming that the total number of oriented crystallites of the first and second groups also changes little, as is evident from determinations of the texture for samples Nos.24 and 25 after annealing, we obtain a value of about 20% for W_0.

Thus, unlike the internal stresses, the initial cold rolling texture cannot be wholly destroyed by annealing: gradually decreasing, the cold rolling texture is replaced by the recrystallization structure with accompanying development of the third group of crystallites forming the cube texture. In the process, the integral torque curve, which is always essentially the sum of several torque curves corresponding to the altering crystallite groups, changes shape. Hence in general one cannot infer the disappearance of texture from the fact that the amplitude of the integral curve harmonics goes to zero.

D. Influence of the degree of purity of the nickel on the formation of texture and relief of internal stresses

For purposes of comparison we also carried out tests with samples of technical grade N2 nickel containing 2.5% total impurities, including 1% cobalt. The results obtained are shown in Table 3.

As will be evident from the table, crystallites of the primary group predominate quantitatively and the internal stresses have a high value.

The results for the same samples after annealing are listed in Table 4.

Table 3

Results of quantitative calculation of the texture and harmonics associated with internal stresses for samples of technical grade N2 nickel after cold rolling (before annealing)

Sample No.	Reduction rate	Percentage reduction	W_1, %	W_2, %	Amplitude of second harmonic, X_2, erg/cm^3
6	Rapid	76	23	11.4	$-0.44 \cdot 10^4$
2		92.4	35	27	$-0.86 \cdot 10^4$

Table 4

Results of quantitative calculation of the texture and harmonics associated with internal stresses for N2 nickel after annealing for 4 hours at 1000°

Sample No.	Reduction rate	Percentage reduction	W_1, %	W_2, %	Amplitude of second harmonic, X_2, erg/cm^3
6	Rapid	76	22	12	$-0.07 \cdot 10^4$
2		92.4	32	13	$-0.06 \cdot 10^4$

As will be evident from Table 4, even 4 hours annealing at 1000° produces little change (decrease) of the cold rolling texture and does not fully relieve the internal stresses, whereas in the case of high purity N0000 nickel the comparatively high stresses produced by cold rolling (Table 1) are completely relieved by annealing at only 400° (Table 2).

Conclusions

1. In analyzing the texture produced by cold rolling in nickel it is necessary to take into account not only the primary group of oriented crystallites, corresponding to the (110), [112] texture but also a group forming a texture characterized by (112), [111]. The relative abundances of the oriented crystallites in each of the groups and the degree of development of the internal stresses serve to explain the change in sign of the second harmonics in the torque curves observed in the case of cooling nickel specimens to liquid nitrogen temperature and as a result of annealing.

2. Separating the effects of the crystallographic structure and internal oriented stresses by the method of recording torque curves at liquid nitrogen temperature, one can determine the relative number of oriented crystallites in both textures and the amplitudes of the second harmonics characterizing the internal stresses.

3. The results of our measurements show that in high purity (N0000) nickel there is produced as a result of cold rolling with rapid 94-95% reduction (15--20 passes) the (112), [111] texture, in which the crystallites of the second group predominate, together with strong internal stresses. In the case of gradual 90% reduction (200 passes) there is formed in the same high purity nickel a texture characterized by the uniform distribution of the crystallites between the two groups and virtually negligible internal stresses.

4. The formation of cube structure incident to annealing, i.e., in the process of agglomerative recrystallization, is accompanied by a change in sign of the fourth harmonic appearing in the magnetograms recorded after annealing. Analysis of the torque curves recorded after heat treatment shows that after 2 hours

heating at 1000° there is formed in high purity nickel previously subjected to gradual 90% reduction a perfect cube texture encompassing 100% of the crystallites. Such complete "monocrystallization" of the nickel is realized only in the case of gradual reduction (90% reduction in 200 passes) and only in nickel containing less than 0.03% impurities.

5. In technical grade N2 nickel in which the total impurity content is 2.5% there is formed under the influence of cold rolling with rapid reduction the (110), [112] type structure with predominance of the first group of crystallites and appreciable internal stresses. High temperature annealing produces little change of the cold rolling texture and does not lead to formation of a pronounced cube structure.

6. In the case of high purity nickel, the internal stresses produced by cold rolling are completely relieved by annealing at 400°. In contrast, in technical grade nickel annealing at 1000° reduces the internal stresses but does not relieve them entirely.

Faculty of Physics
Moscow Institute of Railroad Transport Engineers

References

1. C.S.Barrett, Structure of Metals: Crystallographic Methods, Principles and Data, N.Y., 1943. (Cited in Russian trans.)

2. N.L.Briukhatov, Otchety i materialy NIIF MGU (Reports and proceedings of the Scientific Research Institute of Physics, Moscow State Univ.) 1948-49.

3. H.G.Müller, Metallkunde, 31, 161 (1939).

4. H.Bittel, Ann.d.Physik, 31, 219 (1938); Ibid.,32, 608 (1938).

5. N.S.Akulov & N.L.Briukhatov, Zhur.eksp.i teor.fiz., 3, 59 (1933); N.L. Briukhatov, Zavodsk. laboratoriia, No.10, 42 (1933); N.Akulov & N.Brüchatov, Ann. d.Physik, 15, 741 (1932).

6. S.T.Konobeevskii, Zhur.prikl.fiziki, 2, 107 (1925).

7. R.Bozorth, Phys.Rev., 50, 1076 (1936).

8. N.L.Briukhatov, Izv.AN SSSR, Ser.fiz., 11, 519 (1947).

9. N.L.Briukhatov & L.V.Kirenskii, Zhur.eksp.i teor.fiz., 8, 198 (1938); N.Brüchatov & L.Kirensky, Tech.Phys.USSR, 5, 1 (1938); N.L.Brüchatov & L.V. Kirensky, Phys.Z.Sowjetunion, 12, 602 (1937).

10. G.P.D'iakov, Izv.AN SSSR, Ser.fiz., 11, 667 (1947).

MAGNETOSTRICTION OF NICKEL-IRON-MOLYBDENUM ALLOYS

- I.M.Puzei & B.V.Molotilov

Introduction

In the presence of elastic stresses magnetostrictive changes in a material involve an expenditure of energy, i.e., work is done in overcoming the stresses. Consequently, in the presence of elastic stresses the magnetization process will be determined not only by the anisotropy energy but also by the behavior of the magnetoelastic energy.

Whereas in the case of polycrystals, we can speak of zero magnetostriction in general, in the case of single crystals we can speak of zero magnetostriction only in a given crystallographic direction.

From the two-constant formula for the magnetostriction of a single crystal

$$\lambda = \frac{3}{2}\lambda_{100}\left(\alpha_1^2\beta_1^2 + \alpha_2^2\beta_2^2 + \alpha_3^2\beta_3^2 - \frac{1}{3}\right) + 3\lambda_{111}\left(\alpha_1\alpha_2\beta_1\beta_2 + \alpha_1\alpha_3\beta_1\beta_3 + \alpha_2\alpha_3\beta_2\beta_3\right),$$

it follows that the magnetostriction will be zero in the [100] direction when $\lambda_{100} = 0$ and in the [111] direction with $\lambda_{111} = 0$. Zero magnetostriction in intermediate directions is possible if λ_{100} and λ_{111} have opposite signs.

Let us find the direction of zero magnetostriction in a single crystal. We set $\lambda = 0$ and $\alpha_i = \beta_i$. Then from the above magnetostriction formula we obtain the following equation in polar coordinates:

$$\frac{1}{2}(\sin 2\varphi - 1)\sin^4\theta + \sin^2\theta = \frac{\lambda_{100}}{3(\lambda_{100} - \lambda_{111})}.$$

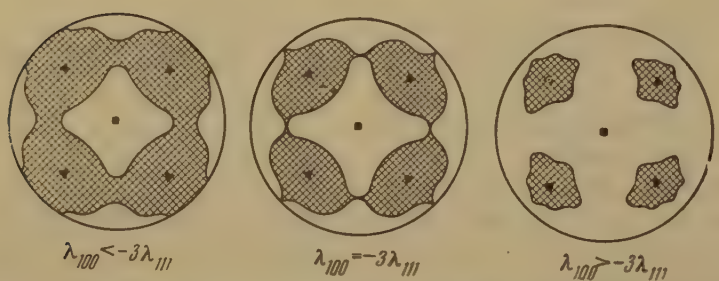

Fig.1. Regions on a single crystal sphere with positive and negative magnetostriction and lines of zero magnetostriction. Squares - points of emergence of [100] axes; triangles - points of emergence of [111] axes, shaded areas correspond to $\lambda < 0$, light areas to $\lambda > 0$.

Solution of this equation shows that the $\lambda = f(\varphi)$ lines form a multiply connected region of positive and negative magnetostriction on the surface of the single crystal sphere. The shape and connectivity of this region depend on the relation between λ_{100} and λ_{111}. With $\lambda_{100} < -3\lambda_{111}$, the connectivity equals 6; with $\lambda_{100} > -3\lambda_{111}$, it equals 8. There is an abrupt transition from one connectivity to the other at the $\lambda_{100} = -3\lambda_{111}$ point. Fig.1 shows the connective region on the surface of a single crystal sphere, the tetragonal axis of which is perpendicular to the plane of the drawing.

The longitudinal magnetostriction is zero along the contours of the regions. Incident to its magnetization in a direction of zero magnetostriction, the sphere does not undergo deformation, i.e., if the magnetostriction in all directions were zero, the magnetoelastic energy would also be zero. Actually, however, there are many directions of magnetization for which the sphere does undergo deformation. Let us determine the directions of magnetization associated with the minimal magnetoelastic energy.

The potential energy of a cubic single crystal is given by

$$W = \frac{1}{2} c_{11}(\tau_{11}^2 + \tau_{22}^2 + \tau_{33}^2) + c_{12}(\tau_{22}\tau_{33} + \tau_{11}\tau_{33} + \tau_{11}\tau_{22}) + \frac{1}{2} c_{44}(\tau_{23}^2 + \tau_{13}^2 + \tau_{12}^2),$$

where c_{11}, c_{12} and c_{44} are elasticity coefficients and the τ_{ij} are components of the deformation tensor. The deformation of a single crystal magnetized in α_i direction is described by the Akulov[1] anisotropy tensor:

$$\begin{vmatrix} (a_0 + a_1 s_1^2) & a_2 s_1 s_2 & a_2 s_1 s_3 \\ a_2 s_2 s_1 & (a_0 + a_1 s_2^2) & a_2 s_2 s_3 \\ a_2 s_3 s_1 & a_2 s_3 s_2 & (a_0 + a_1 s_3^2) \end{vmatrix}.$$

If we express the constants a_0, a_1 and a_2 in terms of the magnetostriction parameters λ_{100} and λ_{111}, and substitute the components of the magnetostrictive deformation tensor into the formula for the potential energy, we obtain the following expression:

$$W = \left(\frac{81}{8}\lambda_{100}^2 c_{11} + 18\lambda_{100}^2 c_{12}\right) + \frac{9}{4}\left(-\lambda_{100}^2 c_{11} + \lambda_{100}^2 c_{12} + \frac{1}{4}\lambda_{111}^2 c_{44}\right)(s_2^2 s_3^2 + s_1^2 s_3^2 + s_1^2 s_2^2).$$

Let us assume that the anisotropy energy is zero and find the potential energy for different values of λ_{100} and λ_{111}.

1. Let $\lambda_{100} = 0$ and $\lambda_{111} \neq 0$. The energy W will be minimal (W = 0) when the spontaneous magnetization vectors are aligned with the cube edges ($\alpha_i = 0$, $\alpha_j \neq 0$ and $\alpha_k \neq 0$). This means that in this case there is no change in the shape and size of the sphere. Hence the directions of easy magnetization will be the directions of the cube edges. The permeability maximum will correspond to $\lambda_{100} = 0$. According to Bozorth[2], in Ni-Fe alloys with 45% Ni, in which $\lambda_{100} = 0$, there is observed a maximum of the initial (and maximum) permeability.

2. Let $\lambda_{111} = 0$ and $\lambda_{100} \neq 0$. In this case the energy W will be minimal with $s_1^2 = s_2^2 = s_3^2 = 1/3$, inasmuch as C_{11} and $C_{12} > 0$ and $C_{11} > C_{12}$. Hence in this case the directions of easy magnetization will be those of the cube diagonals. The permeability peak observed for Ni-Fe alloy with 78% Ni can be explained by the fact that at this concentration λ_{111} is very small;[3] moreover the anisotropy constant is also small and negative.

According to the data of Bozorth[3] for Ni-Fe alloys $\lambda_{100} < 0$ in the Ni concentration range from 100 to 83%, $\lambda_{100} > 0$ in the 83 to 45% Ni range, $\lambda_{111} < 0$ in the 100 to 81% Ni range and $\lambda_{111} > 0$ in the range of Ni concentrations below 81%. Upon the addition of a third component (for example, Mo) to the binary alloy, the concentrations corresponding to zero values of λ_{100} and λ_{111} are shifted into the concentration triangle, forming boundary lines along which $\lambda_{100} = \lambda_{111} = 0$.

In the middle, between these boundary lines, λ_{100} and λ_{111} will have opposite signs. Hence the line of zero magnetostriction of a polycrystal must be located between these two boundary lines. This will obtain for the condition $\lambda_s = \frac{2\lambda_{100} + 3\lambda_{111}}{5} = 0$, i.e., when $\lambda_{100} = -\frac{3}{2}\lambda_{111}$.

It was shown in Ref.5 that if one takes into account the capacity of Ni-Fe-Cr alloys for ordering, the conditions necessary for the anisotropy and magnetostriction constants to be zero are fulfilled not at a single concentration but at a series of concentrations located along a line segment in the diagram. An analogous situation obtains in another important system of alloys, namely, Ni-Fe-Mo. It should be noted, however, that in alloys of the Cr Permalloy type the process of ordering occurs with formation of long-range order, whereas in Mo Permalloys long-range order has not been detected. Apparently, the changes in many of the properties of Mo Permalloys induced by heat treatment are associated with short-range order processes.

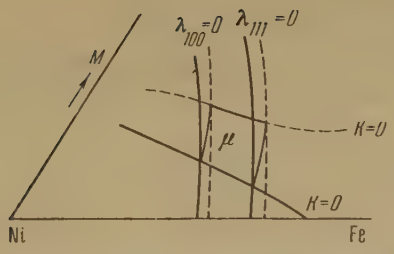

Fig.2. Region of high permeability alloys in the Ni-Fe-Mo system (μ-region). Solid lines - disordered state; dashed lines - ordered state.

How does the region of concentrations of alloys with zero constants vary if one takes into account two magnetostriction constants for single crystals.

With K = 0 and $\lambda_{100} = 0$, the directions of easy magnetization will be the cube edges, while with $\lambda_{111} = 0$, they will be the cube diagonals.

Hence in this case the region of concentrations with small or zero constants in a ternary system will no longer be a line segment but a quandrangle bounded on two sides by the lines $K_{disorder} = 0$ and $K_{order} = 0$ and on the other two sides by the lines $\lambda_{100} = 0$ and $\lambda_{111} = 0$. This region is shown schematically in Fig.2 (μ-region).

The above arguments are based on the magnetostriction formula with two constants. Taking into account a larger number of constants should not alter the deductions significantly in view of the smallness of the additional constants.[3]

The purpose of the present work was to investigate the magnetostriction of Ni-Fe-Mo alloys as a function of ordering and temperature.

1. Measurement Procedure

The magnetostriction measurements were made by means of a strain-gage bridge. As usual the bridge network comprised two active and two inactive resistances (50, 150 or 200 ohm). All four gages were mounted on a common base and the entire assembly was inserted into the Dewar which insured all the gages being at the same temperature. The active gages were cemented to opposite sides of the specimen.

Inasmuch as the alloys under study were characterized by minimal values of magnetostriction (10^{-6}-10^{-7}) a conventional indicator could not provide the requisite degree of accuracy. Hence the bridge output was connected to a special amplifying circuit consisting of a primary galvanometer, a differential photocell, a secondary galvanometer and a light flux stabilizing unit. In view of its high sensitivity this amplifying-indicating arrangement required careful shielding against electromagnetic interference and mechanical vibration, the use of long period galvanometers, temperature control, a stabilized current supply, etc. The operating current in the bridge was 2-3 milliamp. The strain gage resistors were made of

a) beryllium bronze for measurements from -200 to +20°,

b) 80NKhIuD (80НХЮД) nichrome for measurements from +20 to +500°,

c) constantan for measurements from -30 to +100°.

The strain sensitivity coefficient of beryllium bronze (after cold drawing to 30 μ) proved to be 3.9; that of nichrome after high temperature annealing in vacuum 0.40; that of constantan 2.05. Special tests showed that the strain gage coefficients varied very little with temperature.

The use of beryllium bronze proved to be necessary owing to the appearance of ferromagnetism in constantan and nichrome at low temperatures with resultant galvanomagnetic and magnetostrictive effects in the gages themselves.

Initially great difficulty was encountered in bonding the high temperature-range strain gages to the specimens. None of the readily available varnishes and cements are suitable for use at temperatures up to 500°. After numerous experiments we found a cement that proved satisfactory up to +500°. By way of binder we used silicone electric insulating varnish; by way of filler a finely

powdered mixture of MgO, Al_2O_3 and TiO_2 or TiO_2 alone. Actually, the adhesive made with titanium oxide was found to be stable up to 600°, provided only a thin coating was used.

The high temperature gage grid was cemented onto a layer of cement previously applied to the specimen. Lengths of copper lead were welded to the ends of the strain gage.

For the low temperature experiments we constructed a special cryostat by means of which it was possible to obtain all intermediate temperatures in the range from -196° to +100°. In this cryostat design the specimen with a suitable heater is enclosed in an evacuated glass tube; the entire assembly is lowered into the Dewar in which a constant level of liquid nitrogen is maintained. By sending a small current through the heater coil one can obtain any desired intermediate temperature and maintain it reasonably constant over the measurement interval. For the high temperature measurements the specimen and sample were mounted in an evacuated quartz tube.

The low temperatures were measured by a copper-constantan thermocouple; the high temperatures by a chromel-alumel thermocouple. The thermocouple emf was read on a KL-48 voltmeter. The accuracy of temperature measurement was ±0.5. The accuracy of the magnetostriction measurements was evaluated to be ~3% at low temperatures and 5% at high temperatures. The relative accuracy was 1-2%.

The magnetostriction measurements were carried out in an IPS-1 electromagnet in fields of up to 17,000 oersted.[5] The linear magnetostriction was determined by extrapolation from the paraprocess (change of intrinsic magnetization) region to zero field.

The polycrystalline forged Ni-Fe-Mo alloy specimens in the form of disks 18 mm in diameter and 1 mm thick were subjected to the following heat treatments: 1) heating to 1100°, holding for 3 hours, cooling with the furnace to 600°, quenching in oil, or 2) heating to 1100°, holding for 3 hours, cooling with the furnace, heating to 500°, holding for 12 hours followed by step cooling: 12 hours at 490--480°, 48 hours each at 470, 430, 420, 410, 400, 375, 350, 325 and 300° (total time 540 hours).

In addition to the polycrystalline specimens, we investigated four single crystals, grown from a melt under vacuum and subjected to the same heat treatments. These were in the form of disks 11 mm in diameter and 3 mm thick. The disk surfaces were in the (110) planes. The measurements on the single crystals were carried out in two stages. The strain gages were cemented on in the [100] and [111] directions. Then preliminary measurements were made to determine the precise positions of the [100] and [111] axes. After this the main measurements were made.

2. Measurement Results and Discussion

The experimental data obtained for the polycrystalline specimens are shown in Fig.3. The solid lines indicate alloy concentrations with zero magnetostriction after quenching and after extended annealing (the second heat treatment). These lines were obtained by linear extrapolation of the experimental results to zero field. It will be seen that ordering leads to displacement of the zero line to the side of nickel by not more than 1%.

More extensive data on the magnetostrictive properties of the Fe-Ni-Mo alloys is yielded by the single crystal measurements. Below we give the magnetostriction constants of four single crystal specimens of alloys having compositions close to those characterized by zero magnetostriction.

Table 1

Composition and magnetostriction of Ni-Fe-Mo single crystal specimens

Specimen No.	Composition; % by wt.			$\lambda_{100} \cdot 10^6$		$\lambda_{111} \cdot 10^6$	
	Ni	Mo	Fe	Quenched	Annealed	Quenched	Annealed
1	81,0	3,50	Remainder	+1,67	+1,12	—1,18	—0,89
2	80,36	4,26		+2,77	+2,11	+0,125	+0,22
3	84,0	2,69		—1,94	—2,12	—2,00	—2,34
4	82,0	5,0		+0,85	+0,63	—0,81	—0,45

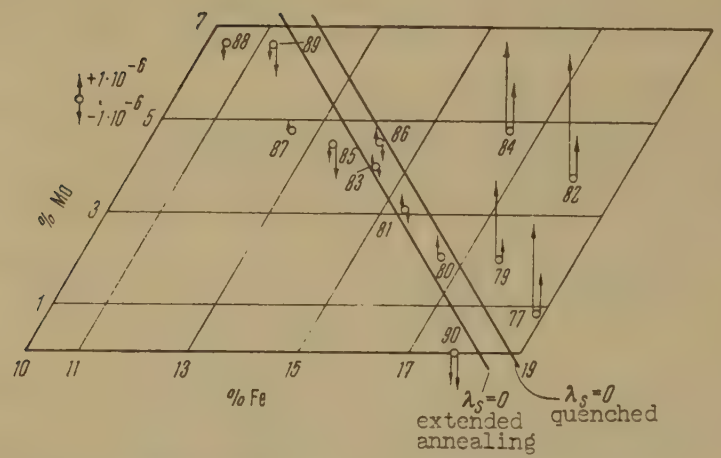

Fig.3. Magnetostriction of Fe-Ni-Mo alloys (polycrystalline specimens) after different heat treatments. The right hand arrows characterize the value λ_s after quenching; the left hand arrows its value after extended annealing (the scale for the arrows is indicated in the upper left hand corner).

The positions of the zero lines ($\lambda_{100} = 0$ and $\lambda_{111} = 0$) after quenching and annealing are shown in Fig.4. As in the case of polycrystals these lines were obtained by extrapolation of the experimental data (Table 1). Additional points at the edge of the Ni-Fe triangle were taken from the experimental results of Bozorth[3].

As may be seen, in the case of single crystals as well, there is noticeable displacement of the zero lines as a result of ordering (prolonged annealing).

The possibility of modifying the magnetostriction constants and of changing the sign of these constants through alteration of the short-range order parameter (this is particularly important in the case of Ni-Fe-Mo alloys inasmuch as in them, as neutron diffraction studies[6] have shown,

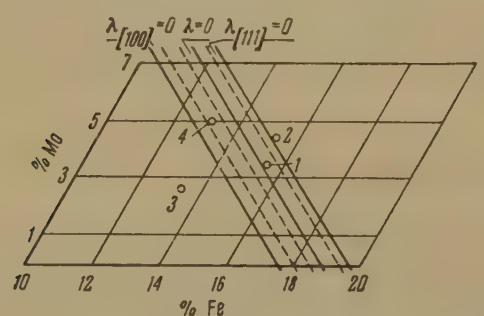

Fig.4

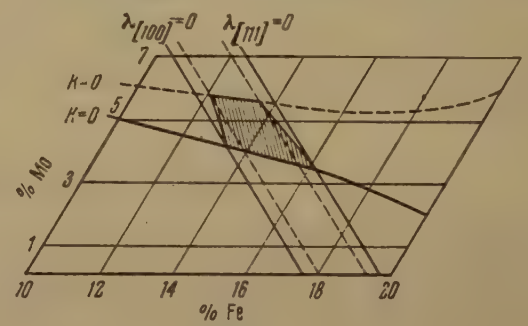

Fig.5

Fig.4. Zero magnetostriction lines for single crystal specimens of Ni-Fe-Mo alloys: dashed lines - after annealing; solid lines - after quenching. The figures at the points correspond to the specimen numbers in Table 1.

Fig.5. Location of the μ-region (hatched area) for alloys of the Fe-Ni-Mo system. Dashed lines - after annealing; solid lines - after quenching.

long-range order is absent) follows from the work of Vonsovskii[4]. In this work it was shown that owing to interaction of atoms of different kinds there may appear in an alloy constants with signs differing from those of the alloy component constants.

We have also plotted in Fig.4 the zero lines for polycrystalline specimens. As might be expected these lines lie between the zero lines for single crystals.

By plotting the zero lines ($\lambda_{100} = 0$ and $\lambda_{111} = 0$) on the Ni-Fe-Mo system concentration triangle, we can define the position of the μ-region (see Fig.2). The μ-region identified in this manner is shown in Fig.5.

All the alloys with compositions in this region have physical constants that favor a high permeability. In practice this region may be somewhat larger; specifically, it may be extended to the side of higher molybdenum concentrations inasmuch as increase of the molybdenum content tends to lower the constants of other alloy components. Moreover, more prolonged and perfect annealing will probably raise the upper boundary of the region to some extent.

It is interesting to note that commercial Mo Permalloys lie outside the indicated μ-region. For the purpose of comparison of the magnetic properties of Mo Permalloy and alloys in the μ-region, we prepared toroidal specimens using exactly the same procedure. The specimens were given heat treatments insuring minimal values of the constants in the μ-region.

Table 2

Temperature dependence of the saturation magnetostriction of polycrystalline specimens of alloys 82 and 86

Alloy 82				Alloy 86			
Quenched		Annealed		Quenched		Annealed	
$t°$,C	λ/λ_{20}	$t°$, C	λ/λ_{20}	$t°$, C	λ/λ_{20}	$t°$, C	λ/λ_{20}
—194	1,26	—194	1,16	—196	1,14	—194	2,22
—145	1,11	—75	1,11	+20	1,0	—125	1,39
+ 20	1,0	—41	1,11	+70	0,91	—81	1,30
+115	0,72	+20	1,0	+184	0,64	+20	1,0
+177	0,57	+86	0,91	+227	0,49	+167	0,73
+276	0,40	+158	0,61	+305	0,27	+253	0,54
+287	0,28	+202	0,54	+427	0,0	+280	0,50
		+244	0,45				
		+340	0,36				
		+380	0,28				

Table 3

Temperature dependence of the magnetostriction parameters of Fe-Ni-Mo alloy single crystals quenched from 600°

Sample No.	Temperature °C	$\frac{\lambda^t_{100}}{\lambda^{20}_{(111)}} = \frac{\lambda^t_{100}}{\lambda^{20}_{(111)}}$	Sample No.	Temperature °C	$\frac{\lambda^t_{100}}{\lambda^{20}_{(111)}} = \frac{\lambda^t_{100}}{\lambda^{20}_{(111)}}$
1	—180	1,07	3	—180	1,1
	—150	1,05		—116	1,02
	—113	1,05		—59	1,02
	+20	1,0		+20	1,0
2	—180	1,33	4	—180	1,05
	—146	1,25		—152	1,05
	—95	1,08		—79	1,0
	—59	1,08		+20	1,0
	+20	1,0			

Measurements of the magnetic properties of the two specimens showed that in the μ-region alloys they are higher than in Mo permalloy by a factor of ~1.5.

Despite the fact that the magnetostriction of the investigated alloys is low (of the order of 10^{-6}), we succeeded in investigating its temperature dependence. Table 2 gives the pertinent data for two polycrystalline alloys: Mo Permalloy (alloy 82: 37% Mo, 18.1% Fe, rest Ni) and an alloy located in the μ-region (alloy 86: 4.5% Mo, 14.25% Fe, rest Ni).

The temperature dependence of the magnetostriction parameters of single crystals is similar to that of polycrystalline specimens (Table 3).

In both single crystal and polycrystalline specimens the magnetostriction decreases monotonically with increasing temperature. We did not observe a change in sign of the magnetostriction constants even though the investigated alloys lie in the region of zero magnetostriction concentrations.

On the basis of Vonsovskii's work[4] one can expect a change in sign of the magnetostriction constants with variation in temperature in cases when the signs of the constants of the alloy components and of the alloys are opposite and when the temperature variations of the constants are different.

Apparently, the temperature dependence of the magnetostriction of the investigated alloys in the region of elevated temperatures obeys Akulov's law[1],

$$\lambda_{sT} = \lambda_{s0}\left(1 - \frac{T}{\theta}\right),$$

where θ is the Curie temperature.

Some deviation from linearity in our data is to be explained by ordering occurring at elevated temperatures during the period of measurement.

References

1. N.S.Akulov, Ferromagnetizm (Ferromagnetism), M., 1939.
2. R.M.Bozorth, Ferromagnetism, N.Y., 1951. (Cited in Russian trans.)
3. R.M.Bozorth, Revs.Mod.Phys., 25, 42 (1953).
4. S.V.Vonsovskii, Zhur.eksp.i teor.fiz., 10, 762 (1940).
5. I.M.Puzei, Izv.AN SSSR, Ser.fiz., 14, 549 (1952).
6. B.G.Liashchenko, D.F.Litvin, I.M.Puzei & Iu.G.Abov, Kristallografiia, 2, 64 (1957).

VOLUME MAGNETOSTRICTION IN IRON-NICKEL-MOLYBDENUM ALLOYS

- I.M.Puzei, B.V.Molotilov & A.I.Rad'kov

The volume magnetostriction of Fe-Ni-Mo alloys was investigated by means of the strain gage-bridge apparatus described in the preceding article.[1] All the measurements were made on samples in the form of disks cut from forged bar stock. The disk specimens were magnetized in fields of up to 18,000 oersted. Particular attention was paid to insuring isothermal conditions since, as is known, adiabatic magnetization distorts the results of magnetostriction measurements owing to magnetocaloric effects.

In order to check the sensitivity of our equipment we investigated the magnetostriction of iron in the paraprocess range (range of high fields, where the change in intrinsic magnetization is due to rotation of the spin magnetic moments). It was found that in fields exceeding 3000 oersted the value of $\partial\omega/\partial H$ (ω is the volume magnetostriction, equal to 3 times the linear and H is the magnetizing field) equals $+4\cdot10^{-10}$ oersted^{-1}. Kornetzki[2] obtained a somewhat higher value, namely, $+6\cdot10^{-10}$. Careful investigation of the paraprocess magnetostriction of nickel showed that in contrast to iron the derivative for nickel is negative, i.e.,

$$\frac{\partial\omega}{\partial H} = -2.5\cdot10^{-10} \text{ oersted}^{-1}.$$

The data in the literature on the magnetostriction of nickel are divergent and often conflicting. Thus, according to data reported in Vonsovskii's text[3] $\partial\omega/\partial H$ $+1.0\cdot10^{-10}$, while according to Azumi & Goldman[4] $\partial\omega/\partial H = -0.55\cdot10^{-10}$, i.e., there is a difference not only in absolute value but also in sign.

High-field magnetostriction of permalloy type alloys was investigated on samples having the compositions listed in the accompanying table, i.e., compositions characterized by values of the technical saturation magnetostriction close to zero.

Compositions of investigated Fe-Ni-Mo alloys

Alloy designation	Composition; % by wt.		
	Mo	Fe	Ni
77	0,81	18,90	Balance
79	1,96	17,60	
80	2,00	16,55	
81	3,05	15,45	
82	3,70	18,10	
83	3,95	14,45	
84	4,78	16,45	
85	4,80	13,40	
86	4,80	14,25	
87	4,80	12,50	
88	6,64	10,35	
89	6,60	11,25	
90	0,0	17,80	

The alloy samples were subjected to the following two heat treatments:

1) Heating to 1100°, holding for 3 hours, cooling to 600°, quenching in water;

2) Heating to 1100°, holding for 3 hours, step cooling in the range from 500 to 300° over a total period of 540 hours.

The field dependence of the magnetostriction in alloys subjected to the prolonged annealing is shown in Fig.1; that in quenched alloys in Fig.2. The value of $\partial\omega/\partial H$ in these alloys was found to be of the order of $3\cdot10^{-10}$ or lower.

Alloys whose compositions lie close to the zero magnetostriction line on the nickel side[1] (see diagrams in preceding article) have a higher absolute value of $\partial\omega/\partial H$ in the quenched state than in the state after prolonged annealing. On the contrary, alloys lying close to the zero magnetostriction line on the iron side are characterized by a high absolute value of $\partial\omega/\partial H$ after annealing.

Furthermore, as may be seen from Fig.1, alloys lying close to the zero magnetostriction line on the nickel side, like nickel itself, have a negative value of $\partial\omega/\partial H$.

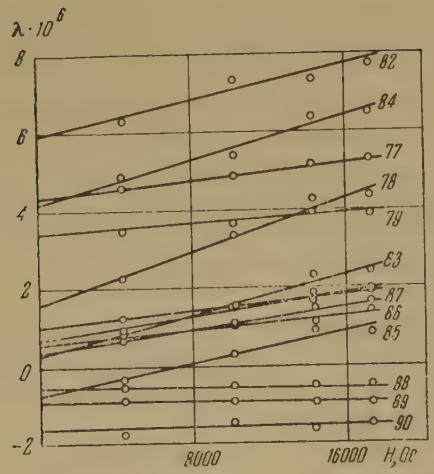

Fig. 1

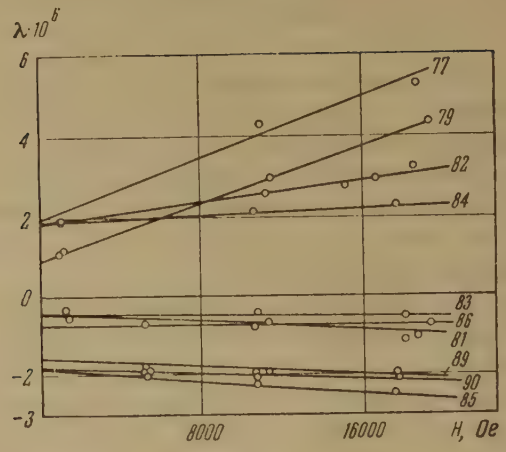

Fig. 2

Fig.1. Field dependence of the magnetostriction λ of a number of Fe-Ni-Mo alloys. Heat treatment - extended annealing.

Fig.2. Field dependence of the Fe-Ni-Mo alloys after quenching. The figures at the curves correspond to the alloy designations in the accompanying table.

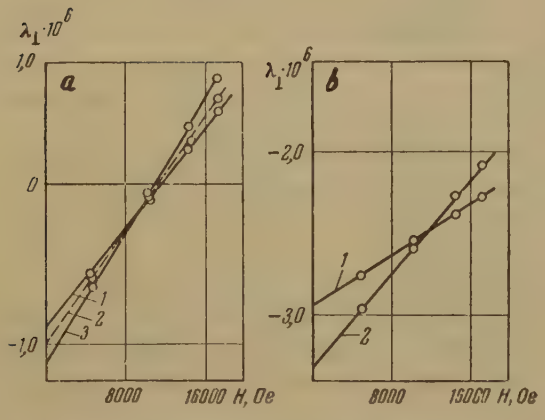

Fig.3. Influence of temperature on the field dependence of the magnetostriction in alloy 82: a - after quenching: 1) +20°, 2) -145° and 3) -180°; b - after extended annealing: 1) +20° and 2) -180°.

The temperature dependences of the magnetostriction of quenched and annealed samples of alloy 82 (3.7% Mo and 18.1% Ni) are shown in Fig.3. The value of $\partial\omega/\partial H$ decreases with increasing temperature in both cases, but the temperature dependence is sharper in the annealed alloy.

Knowing the sign of the volume magnetostriction, one can on the basis of the general thermodynamic relationship

$$\frac{\partial\omega}{\partial H} = -\frac{T}{\varkappa}\cdot\frac{\partial I_s}{\partial T}\cdot\frac{1}{\bar{A}}\cdot\frac{\partial\bar{A}}{\partial\omega}$$

(where $\varkappa$ is the compressibility, I_s is the magnetic saturation and $\bar{A}$ is the mean value of the exchange integral) determine the sign of $\partial\bar{A}/\partial\omega$ and, consequently, the position of the given alloy on the Bethe-Slater interaction curve.

The isothermal volume magnetostriction in nickel is negative. Consequently, $\partial\bar{A}/\partial\omega$ is also negative. Thus the point for nickel must be located on the descending part of the Bethe curve. Decrease of the interatomic spacing in this case must increase the Curie point inasmuch as the mean value of the exchange integral in this case increases. This deduction is substantiated by the results of measurements of the shift of the ferromagnetic Curie points with pressure[5].

In iron the volume magnetostriction is positive. Consequently, the point for iron must lie on the ascending part of the Bethe curve.

It is interesting to note that in the case of some of the alloys the volume magnetostriction changes sign as a result of ordering (for example alloy 86) or falls to zero (alloys 88, 89 & 90). Apparently, all these alloys lie in the region of the maximum of the Bethe curve. The alloys that exhibit a change in sign of the volume magnetostriction as a result of different heat treatments lie in the vicinity of the zero linear magnetostriction lines[1]. Mo Permalloy as regards composition lies at a distance from these lines and its volume magnetostriction does not changes sign and, in fact, changes very little in value in going from the quenched to the annealed state.

Institute of Precision Alloys
Central Scientific Research Institute of Ferrous Metals

References

1. I.M.Puzei & B.V.Molotilov, Present issue of the Bulletin, p.1236.
2. M.Kornetzki, Z.Phys., 87, 560 (1933).
3. S.V.Vonsovskii & Ia.S.Shur, Ferromagnetiz (Ferromagnetism), M., 1948.
4. K.Azumi & J.E.Goldman, Phys.Rev., 93, 630 (1954).
5. L.Patrick, Phys.Rev., 93, 384 (1954).

MAGNETOSTRICTIVE PROPERTIES OF BINARY ALLOYS

- G.P.D'iakov

The theory of magnetostriction is one of the most important in the sciences of ferromagnetism. This is due to the fact that magnetostriction is a significant factor in calculating the hysteresis loss, in determining the coercive force and in investigating the influence of elastic stresses on different physical properties of metals and alloys. Recently, application of the magnetostrictive effect for the generation and detection of ultrasound has enhanced the interest in this phenomenon. Yet, although magnetostriction is such an exceptionally important characteristic of ferromagnetic materials, it has until now been relatively little studied, particularly in single crystals.

At first determinations of magnetostriction constants were carried out only on single crystals. However, in view of the great difficulty (or sometimes impossibility) of obtaining alloy single crystals, it soon became necessary to develop a method for determining the magnetostriction constants λ_{100} and λ_{111} from measurements on polycrystalline samples.

This problem was solved by the writer in 1949 in connection with derivation of the law of approach to saturation of magnetostriction and other even effects.[1] According to this law,

$$\lambda = \frac{2}{5}\lambda_{100} + \frac{3}{5}\lambda_{111} - \frac{8}{35}(\lambda_{111} - \lambda_{100})\frac{k_1}{I_s H} - \left(\frac{32}{7\cdot 11\cdot 13}\lambda_{100} + \frac{984}{5\cdot 7\cdot 11\cdot 13}\lambda_{111}\right)\frac{k_1^2}{I_s^2 H^2}, \qquad (1)$$

where k_1 is the first anisotropy energy constant, I_s is the magnetization at saturation and H is the applied magnetic field.

At saturation, when the magnetizing field H may be regarded as infinitely high, we obtain from Eq.(1) the expression for the saturation magnetostriction deduced earlier by Akulov[2]:

$$\lambda_s = \frac{2}{5}\lambda_{100} + \frac{3}{5}\lambda_{111}. \qquad (2)$$

Factoring out λ_s in Eq.(1), we obtain

$$\lambda = \lambda_s\left(1 - \frac{A}{H} - \frac{B}{H^2}\right), \qquad (3)$$

where

$$A = \frac{8}{35}(\lambda_{111} - \lambda_{100})\frac{k_1}{I_s\lambda_s}, \qquad (4)$$

$$B = \left(\frac{32}{7\cdot 11\cdot 13}\lambda_{100} + \frac{984}{5\cdot 7\cdot 11\cdot 13}\lambda_{111}\right)\frac{k_1^2}{I_s^2\lambda_s}. \qquad (5)$$

The regularities for magnetostriction deduced by the writer in Ref.1 pertained to the case when there is no paraprocess. In the region of high fields, however, in addition to the process of rotation there may also occur the paraprocess. Akulov[2] took into account the influence of the paraprocess on even effects. He showed that at temperatures not very close to the Curie point, the magnitude of an even effect, associated with the paraprocess, is linearly dependent on the magnetic field. The investigations of Belov[3] and others substantiated these deductions. Hence to make the law of approach to saturation more general it should be supplemented by the introduction of a term taking into account the influence of the paraprocess. Thus, instead of Eq.(3), for the general case we should write

$$\lambda = \lambda_s\left(1 - \frac{A}{H} - \frac{B}{H^2}\right) + \varkappa_{\lambda p} H, \qquad (6)$$

where $\varkappa_{\lambda p}$ is the magnetostrictive susceptibility associated with the paraprocess. Relationships (3), (4) and (5) make it possible to determine experimentally the values of λ_{100} and λ_{111}, as well as the magnetic anisotropy constant, by measuring the magnetostrictive susceptibility on polycrystalline specimens, i.e., allow us to dispense with the need for preparing single crystals. By means of this procedure, we[4] first succeeded in determining the values of the anisotropy constant for iron-nickel alloy and later the magnetostriction constants λ_{100} and λ_{111} of nickel[5].

The coefficients A and B in Eq.(3) may depend substantially on elastic stresses in the ferromagnetic material. The writer deduced expressions for these coefficients for the two limiting cases, namely, when the stresses are diffused (wholly random orientation) and when the stresses are aligned with the direction of the magnetic field.[6] In some cases, however, expressions (4) and (5) prove to be inadequate. The exacting requirements now set for many magnetic materials, on the one hand, and the increasing refinement of experimental techniques, on the other, make it necessary to introduce a further term proportional to H^{-3} into Eq.(1) and to take into account the second anisotropy constant k_2. In previous communications, the writer deduced relationships taking into account the second anisotropy constant[7], a term proportional to H^{-3} and diffusely scattered elastic stresses.[8] The results of these investigations made it possible to derive a more precise expression for the law of approach to saturation of magnetostriction and other even effects.

In recent years there have been a number of investigations by foreign scientists devoted to magnetostriction in high fields. In 1954, five years after publication of the writer's first studies, Lee[9] carried out a theoretical analysis of the behavior of magnetostriction in the region of approach to saturation and arrived at the regularities[10] established earlier by the present writer. Soon thereafter, Néel[11] took into account the influence of magnetic interaction on the behavior of magnetostriction in strong magnetic fields. This influence as inferred by Néel, however, appears to be exaggerated, as was pointed out by the writer in Ref.5.

In the present report we give the results of a recent investigation of magnetostriction in binary Fe-Ni alloys. These alloys have attracted the attention of investigators not only because of their practical utility but also owing to the unique variation of magnetostriction in them[12]. The complex behavior of the magnetostriction in polycrystalline specimens is to some extent due to the distinctive magnetostrictive characteristics of Fe-Ni single crystals in different crystallographic directions. Unfortunately, until now there has been no complete investigation of the magnetostriction in Fe-Ni single crystals. The magnetostriction in the [100], [110] and [111] directions in single crystals in the range of Ni concentrations from 30 to 100% was investigated by Lichtenberger[13], who showed that the magnetostriction of single crystals in different crystallographic directions differed not only as regards magnitude but also as regards sign. Moreover, there are two alloys with Ni concentrations of 50 and 86% in which the values of the magnetostriction along the three principal crystallographic directions are equal. The anisotropy constant in these alloys has been thoroughly studied. The results of Puzei's basic studies[14] give us a good idea of the magnitude of the anisotropy constants and their variation depending on the composition of the alloy and the heat treatment to which it is subjected.

Thus the distinctive magnetostrictive properties of Fe-Ni alloys and the now available dependable data on their anisotropy constants lend interest to these alloys and make them particularly valuable for checking the regularities deduced by us theoretically.

For the purpose of our investigation, we took five specimens with nickel concentrations ranging from 40 to 100%. In preparing the specimens we used Armco iron supplied by the "Serp i molot" (Sickle and Hammer) Plant and high purity electrolytic nickel. The specimens of the alloys containing 39.92, 79.3 and 89% Ni were prepared in the form of 7:70 ellipsoids; this axis ratio corresponds to a demagnetizing factor N = 0.256. The 59.78% Ni specimen was in the form of a rod 2.5 mm in diameter and 260 mm long. Finally, the specimen of pure electrolytic nickel was in the form of a strip 150 x 10 x 0.1 mm.

The heat treatments given the alloy specimens were similar to those used by Puzei for single crystals. Our use of the same heat treatments was dictated by the fact that the anisotropy constant depends substantially on the heat treatment. Hence for each alloy we took the anisotropy constant corresponding to the given type of heat treatment.

In the case of the pure nickel specimen it was necessary to select the annealing temperature so as to fully remove the cold-rolling texture. This temperature in principle may vary from 300 to 600° depending on the degree of reduction realized in rolling. We analyzed the texture (to check for absence of cold-rolling texture) by recording torque curves on a magnetic torquemeter.

The magnetostriction measurements were made by the strain gage-bridge procedure. The indicator in the bridge diagonal was a photoelectrooptical amplifier. Use of this amplifier greatly enhanced the sensitivity of the set-up and thus made it possible to measure the magnetostrictive susceptibility with great accuracy.

Knowing the magnetostrictive susceptibility $d\lambda/dH$ of the polycrystalline material one can readily determine the constants λ_{100} and λ_{111}. Differentiating (3) with respect to the field, we obtain

$$\frac{d\lambda}{dH} = \frac{A\lambda_s}{H^2} + \frac{2B\lambda_s}{H^3}. \tag{7}$$

Multiplying both sides of (7) by H^2 and substituting the values of A and B from (4) and (5), we obtain

$$\frac{d\lambda}{dH} \cdot H^2 = \frac{8k_1}{35I_s}(\lambda_{111} - \lambda_{100}) + \frac{2k_1^2}{I_s^2}\left(\frac{32}{1001}\lambda_{100} + \frac{984}{5005}\lambda_{111}\right)\frac{1}{H} \tag{8}$$

or

$$\frac{d\lambda}{dH} \cdot H^2 = a + bH^{-1}, \tag{9}$$

where

$$a = \frac{8k_1}{35I_s}(\lambda_{111} - \lambda_{100}), \tag{10}$$

$$b = \frac{k_1^2}{I_s^2}\left(\frac{64}{1001}\lambda_{100} + \frac{1968}{5005}\lambda_{111}\right). \tag{11}$$

It will be evident from Eq.(9) that the magnetostrictive susceptibility multiplied by H^2 should vary linearly with 1/H. The experimental results, which are plotted in Fig.1, show that the magnetostrictive susceptibility in the region of approach to saturation actually is a linear function of 1/H. The ordinate at the point of intersection of the straightline plot with the vertical axis gives us a, the first term in Eq.(9), while the slope of the straight line gives us b.

The respective numerical values are $a = -50 \cdot 10^{-5}$ and $b = -1.4 \cdot 10^{-1}$.

Assuming $k_1 = 5 \cdot 10^4$ erg/cm^3 and $I_s = 500$ gauss and taking the above values for a and b, we readily obtain by substituting in Eqs.(10) and (11) $\lambda_{100} = -49 \cdot 10^{-6}$ and $\lambda_{111} = -27 \cdot 10^{-6}$.

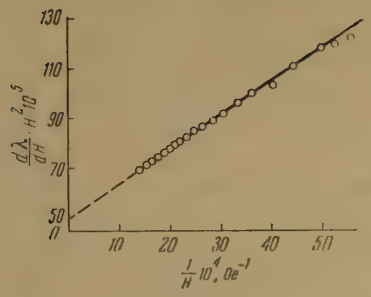

Fig.1

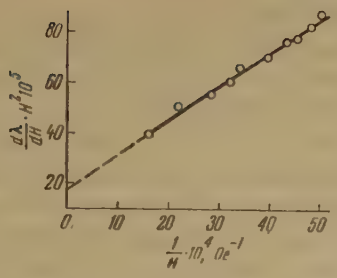

Fig.2

Fig.1. Experimental variation of $(d\lambda/dH)H^2$ with 1/H for nickel.

Fig.2. Variation of $(d\lambda/dH)H^2$ as a function of 1/H for nickel plotted on the basis of Lee's data[15].

Unfortunately, there have been few measurements of magnetostriction in the region of approach to saturation. The only thorough investigation is that of Lee[15] who used nickel strips annealed at 820° for 4 hours followed by cooling at the rate of 100° per hour. The fact that Lee gives no tabular data hampers comparison of his experimental results with our theory. We were therefore forced to pick values off his curves in order to plot the variation of $(d\lambda/dH)H^2$ shown in Fig.2. Then using the vertical axis intercept and the slope of the straight line as in the preceding case, we computed the values of λ_{100} and λ_{111}. They proved to be $-41\cdot10^{-6}$ and $-33\cdot10^{-6}$, respectively.

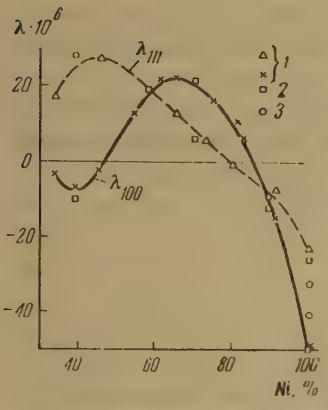

Fig.3. Variation of the magnetostriction constants λ_{100} and λ_{111} with the Ni content in Fe-Ni alloys calculated from the data of different investigators: 1 - Lichtenberger, 2 - Lee and 3 - the author.

The minor differences between our values for the constants and those derived from Lee's measurements may be attributed to differences between our respective specimens as regards purity and heat treatment inasmuch as both these factors exert a considerable influence on the magnetostrictive susceptibility.

The magnetostriction constant of the enumerated alloys were determined in the same manner as for pure nickel. The results are given in Fig.3 together with the data of Lichtenberger[13] for purposes of comparison.

It will be seen that our results for λ_{100} and λ_{111} deriving from measurements on polycrystalline specimens are in good agreement with the results of Lichtenberger. The greatest divergence occurs for the alloy with 39.92% Ni. Here apparently one should take into account more fully the contribution of the paraprocess to the magnetostrictive susceptibility. It is evidently desirable to carry out further measurements on this alloy both in stronger fields and at low temperatures.

Faculty of Physics,
Moscow State University

References

1. G.P.D'iakov, Doklady AN SSSR, 68, 33 (1949).
2. N.S.Akulov, Ferromagnetizm (Ferromagnetism), p.31, M., 1939.
3. K.P.Belov, Doctoral thesis, Moscow State University, 1952.
4. G.P.D'iakov & R.A.Reznikova, Doklady AN SSSR, 97, 663 (1954).
5. G.P.D'iakov, Izv.AN SSSR, Ser.fiz., 21, 1133 (1957). (Trans. Bulletin 21, No.8, 1118.)
6. G.P.D'iakov, Doklady AN SSSR, 82, 867 (1952).

7. G.P.D'iakov, Fiz.metallov i metallovedeniia, 5, 101 (1957). (Trans. Physics of Metals and Metallography.)
8. G.P.D'iakov, Vestnik, Moscow State University, 3, 75 (1957).
9. E.W.Lee, Proc.Phys.Soc., A, 67, 381 (1954).
10. E.W.Lee, Phys.Soc., 18, 209 (1955).
11. L.Néel, Phys.et radium, 15, 376 (1954).
12. S.V.Vonsovskii & Ia.S.Shur, Ferromagnetizm, p.662, M., 1948.
13. F.Lichtenberger, Ann.Phys., 15, 45 (1932).
14. I.M.Puzei, Izv.AN SSSR, Ser.fiz., 16, 540 (1952).
15. E.W.Lee, Proc.Phys.Soc., B,65, 162 (1952).

* * * * *

DEPENDENCE OF THE SENSITIVITY OF MAGNETOSTRICTIVE ULTRASONIC DETECTORS ON THEIR MAGNETIC CHARACTERISTICS

- Ia.S.Shur, M.G.Luzhinskaia, K.B.Vlasov, O.I.Shiraeva & V.A.Zaikova

1. According to theoretical calculations[1-3] the sensitivity of a magnetostrictive detector is related with the magnetic characteristics of the material by

$$e \sim \mu_{\sim} \frac{\partial \lambda}{\partial B}, \tag{1}$$

$$e_{max} \sim \mu_{\sim}(B_{opt}) \frac{\lambda_s}{I_s}, \tag{2}$$

$$e_{max} \sim \mu_0 \frac{\lambda_s}{I_s}, \tag{3}$$

where e is the sensitivity, $\mu_{\sim}$ is the apparent permeability, λ is the magnetostriction, B is the induction, λ_s is the saturation magnetostriction, I_s is the saturation magnetization, μ_0 is the initial permeability and e_{max} is the maximum sensitivity of the detector obtaining at a certain optimal value of the polarization induction B_{opt}.

Eq.(1) characterizes the variation of the detector sensitivity with the intensity of the constant magnetizing field (or the corresponding induction); Eqs. (2) and (3) are valid for the maximum values of the sensitivity of a sound detector made of the given material, obtained at the given optimum polarization B_{opt}.

Up to the present there have been few attempts to verify these formulas experimentally. The purpose of the present work was to check the validity of these theoretical relationships and to evaluate the possibility of utilizing them for the selection of materials for magnetostrictive sound receivers on the basis of the known magnetic properties of different materials.

2. For the purposes of our investigation we chose materials with markedly different magnetic properties, namely, nickel, Permindur, 66 Permalloy, iron-chromium alloys containing from 10 to 30% chromium and iron-aluminum alloys containing from 9 to 15% aluminum. The alloys were rolled into ribbons 0.1 mm thick and subjected to different heat treatments. Ring-shaped specimens were used for obtaining the magnetization curves and hysteresis loops. Specimens in the shape of disks were used to obtain to magnetostriction and magnetization curves. These data were used to deduce the λ vs B curves, from which, in turn, we obtained the $\partial\lambda/\partial B$ vs B curves by graphic differentiation.

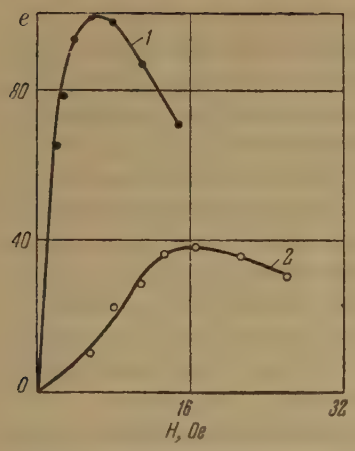

Fig.1. Variation of the sensitivity e of a magnetostrictive detector with the constant field H for two specimens of Permindur: 1) specimen tempered at 800°, H_c = = 1.6 oersted, 2) tempered at 690°, H_c = 16 oersted.

The receiving sensitivity was determined using specimens in the form of tubes 30 mm in diameter and 140 mm in length. The acoustic pressure in the test basin was provided by a magnetostrictive radiator supplied from a noise generator. The electromotive force induced in a coil surrounding the tube was taken as the measure of the detector sensitivity. The sensitivity measurements were comparative, i.e., the emf induced in the coil surrounding a given specimen was referred to the emf obtained under the same conditions for a "standard" specimen. These same tubular specimens were used to measure the internal impedance (the coil inductance was subtracted) which was then used to calculate the ac permeability $\mu_\sim$ of the material.

The sensitivity and internal impedance measurements were carried out at frequencies from 6 to 30 kc. At each frequency we determined the variation of these quantities with the intensity of the polarizing field. The value of $\mu_\sim$ corresponding to a given frequency and polarization was measured at the same alternating induction that obtained in the specimen in measuring the sensitivity at the given acoustic frequency and with the given polarization.

3. The measurements showed that the investigated alloy specimens after different heat treatments are characterized by markedly different magnetic properties (I_s varied from 495 to 1830 gauss, μ_0 in the range from 200 to 2100 gauss/oersted and λ_s in the range from 7 to $84 \cdot 10^{-6}$) and different sensitivity values (the range of variation was 1 to 10).

By way of illustration in Fig.1, we reproduce the sensitivity vs magnetizing field curves for two Permindur specimens subjected to different heat treatments. These specimens were characterized by close values of I_s and λ_s, but differed markedly as regards μ_0. As will be evident from the figure, one can obtain higher values of the sensitivity for the specimen tempered at 800° as compared with that tempered at 700°. Moreover, the peak sensitivity values are obtained in weaker fields in the case of magnetically softer specimen. Among the investigated materials the following are characterized by the highest sensitivity values: Permindur annealed at 800-900°C, quenched Fe-Al alloy with 15% Al and 66 Permalloy.

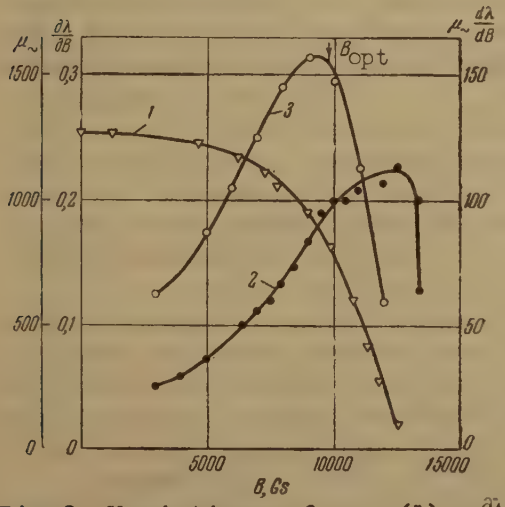

Fig.2. Variations of $\mu_\sim$ (1), $\frac{\partial\lambda}{\partial B}$ (2) and $\mu_\sim \frac{\partial\lambda}{\partial B}$ (3) with the induction B for 66 Permalloy.

Fig.2 shows the B-dependences of $\mu_\sim$ measured at 15 kc, $\partial\lambda/\partial B$ and the product $\mu_\sim(\partial\lambda/\partial B)$ for 66 Permalloy. According to Eq.(1), this product should be proportional to the sensitivity of the detector; it will be seen from the figure that the maximum in the curve is obtained at an induction of 9300 gauss. The sensitivity measurements showed that the maximum sensitivity value for a 66 Permalloy

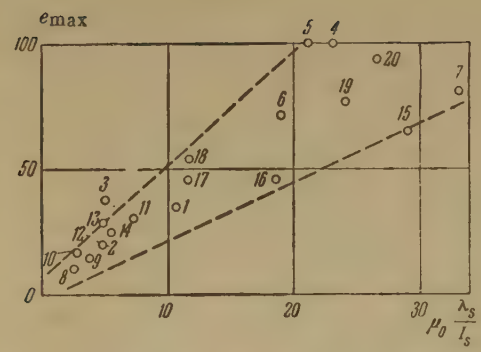

Fig.3. Variation of the maximum sensitivity e_{max} with $\mu_0(\lambda_s/I_s)$ for 1) Ni annealed at 1050°, 2-6) Permindur annealed at 600, 690, 800, 900 and 1000°, respectively, 7) 66 Permalloy annealed at 1050°, 8-13) Fe-Cr alloy with 14, 18, 20, 24, 27 & 30% Cr annealed at 1100°C, 14) Fe-Al-Cr alloy with 9% Al and 5% Cr, 15) Fe-Al alloy with 12% Al, 16) Fe-Al-Mn alloy with 15% Al and 3% Mn, 17) Fe-Al alloy with 15% Al (alloys 14 through 17 annealed at 1000°); 18-20) same alloys as 15--17 but quenched from 700°.

detector is obtained at an induction of 9800 gauss (see arrow in Fig.2). Thus, in agreement with the theoretical formula (1), the value of the induction corresponding to maximum sensitivity is virtually identical with the induction at which the $\mu_\sim(\partial\lambda/\partial B)$ curve peaks. Similar results were obtained for the other alloys. Thus from the magnetic characteristics one can determine the polarization fields necessary for optimum polarization of an ultrasonic detector of the given material.

In Fig.3 we have plotted the sensitivity e_{max} at optimum magnetization against $\mu_0(\lambda_s/I_s)$ (see Eq.(3)) for all the investigated alloy specimens. Although there is an appreciable scatter of the points, one can discern a consistent relation between these two quantities. A similar scatter within limits is obtained in plotting e_{max} against $\mu_\sim$ B_{opt} (λ_s/I_s) for different materials.

Measurements of the specific sensitivity $\gamma_{max} = e_{max}/\sqrt{Z}$ showed that the γ_{max} ratio for different materials may differ appreciably from the e_{max} ratio. Thus the γ_{max} ratio for nickel and Permindur is close to unity, whereas the e_{max} ratio is 0.4. This is explained by the fact that the e_{max} ratio depends on ratio of the permeabilities of the materials, while the γ_{max} ratio depends on the ratio of the square roots of their permeabilities.

It should be noted, however, that in design of ultrasonic detectors, γ is calculated on the basis of Z for the receiver, which includes not only the Z of the material (as in our case) but also the Z of the receiver winding.

4. Thus the experimental data show that the variation of the sensitivity of an ultrasonic detector with the magnetic state of the material is correctly described by Eq.(1).

Eqs.(2) and (3), characterizing the maximum sensitivities of detectors of different alloys, while generally valid, are not precise relationships. Possibly one of the reasons for the disagreement are errors in experimental determination of the different parameters involved. It follows from our results, however, that by means of Eq.(3) one can arrive at an approximate relative evaluation of the sensitivity of different materials if the values of μ_0, λ_s and I_s are known.

The results of the present investigation are described in greater detail in Ref.3.

Institute of Metal Physics,
Academy of Sciences of the USSR

References

1. R.M.Bozorth & S.R.Williams, Revs.Mod.Phys., 17, 72 (1945).
2. C.M.Van der Burgt, Philips.Res.Rep., 8, 91 (1953).
3. Ia.S.Shur, M.G.Luzhinskaia, K.B.Vlasov, O.I.Shiriaeva & V.A.Zaikova, Trudy (Proceedings) Institute of Metal Physics, Ural Branch, USSR Acad.ofSci., No.20, 131 (1958).

MOLYBDENUM INDUCED MODIFICATIONS OF THE STRUCTURAL TRANSFORMATIONS IN PERMALLOY

- Iu.S.Avraamov, B.G.Livshits & V.B.Osvenskii

It has been definitely established that in binary Fe-Ni alloys close in composition to classical Permalloy (78.5% Ni) there forms in a certain critical temperature interval superstructure of the Ni_3Fe type with resultant modification of the physical properties of the alloy.

In Permalloys to which molybdenum has been added, appropriate heat treatment leads to an unusual (for an ordering alloy) change in properties. There are a number of different views in the literature regarding the nature of this transformation in Permalloys doped with over 1% molybdenum.

Some investigators[1-3] have concluded that the process occurring in Fe-Ni-Mo alloys is also essentially ordering and that the Mo acts only to retard this process. Other authors[4,5] infer that tempering of quenched Fe-Ni-Mo alloys at 400-500° leads to the formation of a distinctive state different from the ordered one, a state characterized by higher resistivity. Inasmuch as the alloys in question are in the single phase region of the alloy diagram, there is no separation of a new phase. Lifshits & Ravdel'[5] suggested that in Mo Permalloy in the critical temperature interval there occur processes identical with those discovered by Thomas[6] in nichrome. Hence these authors, following Thomas, have called this distinctive state in Fe-Ni-Mo alloy the "K-state". They conclude that there form in the alloy atomic segregations (zones) with the participation of molybdenum and possibly iron atoms. The increase in resistivity is presumably due to the fact that the conduction electrons undergo additional scattering in these zones, the dimensions of which are of the same order of magnitude as the free path length of the conduction electrons.

In the present work we have attempted to elucidate the nature of the structural transformations in Fe-Ni-Mo alloys, as well as to define the critical temperature interval for these alloys, on the basis of measurements of the resistivity, hardness and the temperature dependences of the internal friction and saturation magnetization.

Experimental results and discussion

We investigated four alloys, the chemical compositions of which are listed in the accompanying table.

Alloy No.	Composition, %			
	Ni	Fe	Mo	C
1	75,05	24,15	—	0,0094
2	76,80	22,50	1,04	0,0094
3	74,50	20,95	3,08	0,0093
4	76,00	18,80	5,15	0,0092

In order to determine the temperature interval in which the transformations occur in these alloys, we measured the electric resistivity in the process of heating and cooling.*

When alloy 1 is heated after quenching there is observed a decrease of its resistivity in the temperature interval from 250 to 450°; this is connected with

---

*The experimental procedure and the results obtained for the temperature dependences of the resistivity, hardness and saturation magnetization are fully described in Ref.7.

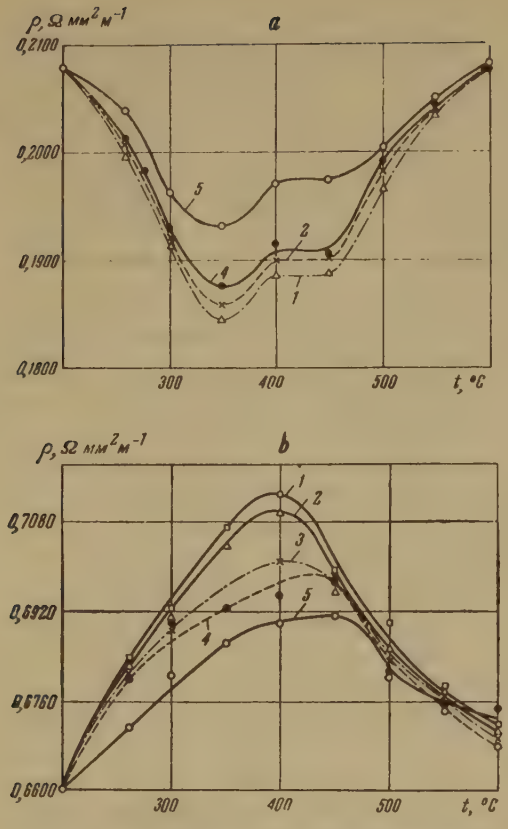

Fig.1. Variation of the resistivity ρ with the tempering temperature t after quenching for different tempering times: a - alloy 1 (Ni_3Fe), b - alloy 4 (5% Mo). Tempering times: 1) 10 hours, 2) 3 hours, 3) 1.5 hours, 4) 30 min, 5) 10 min.

the formation of superstructure. In alloy 4 under the same conditions, the resistivity increases in this temperature interval, which is evidence of formation of the K-state in this alloy. This substantiates the results of Lifshits & Ravdel'.[5]

Fig.1 shows the variation of the resistivity of quenched alloys 1 and 4 as a function of the tempering temperature. It will be seen that the critical temperature intervals for the formation of superstructure and of the K-state coincide and that both processes take a certain time, which indicates that they are diffusive. The presence of an intermediate step in the 400-500° interval in the curve for alloy 1 (Fig.1,a) may be interpreted as being due to the existence of two ordering stages in this alloy.

Our hardness measurements proved that the hardness of the alloys increases as a result of both ordering and formation of the K-state. The change in hardness of alloy 2 (1% Mo) incident to heating in the critical temperature interval indicates that in it there occur both ordering and formation of the K-state. Inasmuch as both these processes effectively increase the hardness, when they are superimposed, the hardness of the alloy is appreciably enhanced. On the other hand, the effect of ordering and formation of the K-state on the resistivity are opposite; hence they tend to compensate each other in the alloy with 1% Mo so that the resistivity changes little incident to tempering. Thus it will be seen that the transition from ordering to the K-state with increasing molybdenum content occurs gradually in the investigated alloys.

We also determined the influence of heat treatment of alloy 4 on the temperature dependence of the saturation magnetization and on the Curie point. After tempering at 400°, a bend appears in the magnetization vs temperature curve; in addition, the Curie point is raised somewhat (Fig.2). This is in agreement with the results of Dekhtiar.[8] The inflection in the curve is not in conflict with the inference that there are present in the molybdenum-containing alloy zones (segregations) having their own Curie point, different from that of the main solid solution. Analysis of the results obtained in an earlier study by two of the present authors[7] showed that in case of tempering at the temperature of K-state formation there form in the Fe-Ni-Mo alloy Heine-Preston type zones containing Mo atoms.

In investigating the transformations in Fe-Ni-Mo alloys, we also used measurements of the internal friction. This approach is based on the fact that the diameter of the Mo atoms entering into the substitutional solid solution is appreciably different from the diameter of the Ni and Fe atoms. According to the data in the literature[9], in such solid solutions there may appear an internal friction peak associated with ordering in a stress field.

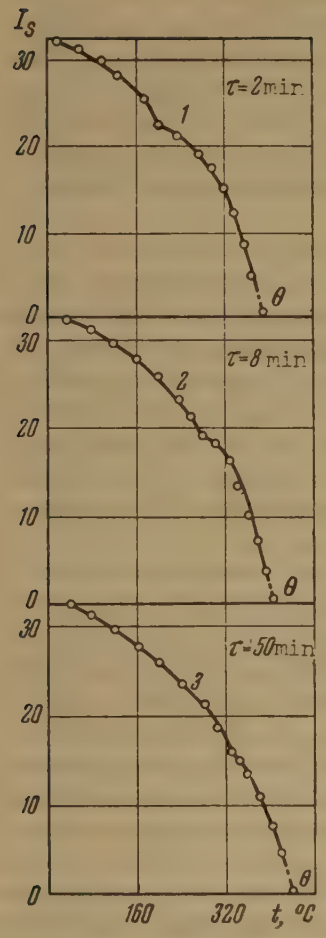

Fig.2. Influence of tempering time τ at 400° on the temperature dependence of the saturation magnetization I_S and on the Curie point θ of alloy 4 (5% Mo).

The determinations of the temperature dependence of the internal friction during heating were carried out by the method of Ke Ting-Sui on the vacuum relaxation tester in the Department of Physics in the Moscow Steel Institute[10] (method of damping of free torsional oscillations). The measurements were carried out on wire specimens 0.8 mm in diameter and 30 mm in length. The specimens were heated to a maximum temperature of 750°; the heating rate was 50° per hour. The measurement temperatures were maintained constant to within ±0.2° by means of a thermostat. The potentiometric temperature measurements were accurate to within ±0.5°. A vacuum of 10^{-4}-10^{-5} mm Hg was maintained during the time of measurement, which protected the specimens from oxidation and reduced external friction losses to a minimum. Concurrently with the internal friction measurements, we measured the temperature dependence of the modulus of elasticity in shear. The free oscillation frequency was measured directly and then the square of the frequency was plotted against the temperature. The measurements were carried out at a frequency of 0.8 cps (at room temperature). The "initial" state was arbitrarily taken to be that obtained in quenching from 1050° in water.

The full curve characterizing the temperature dependence of the internal friction in a quenched specimen of alloy 1 is shown in Fig.3. It will be seen that the internal friction remains virtually constant up to 380°. The high temperature part of the curve, where the internal friction begins to increase with increasing temperature, begins at 380°. At 700° the damping was so strong that it was difficult to measure. There is a pronounced bump in the high temperature part of the internal friction curve in the 595-665° interval. This bump is a result of surposition of a peak on the background represented by the dashed line. The character of this peak E does not change with changes in molybdenum content. On the basis of the data in the literature we inferred that this peak might be associated with viscous behavior of the grain boundaries. To check this inference it was obviously necessary to determine the influence of grain size on this peak. To this end a specimen was treated to induce grain growth, namely, heated for 40 hours at 1000° after preliminary critical reduction. The resultant grain size

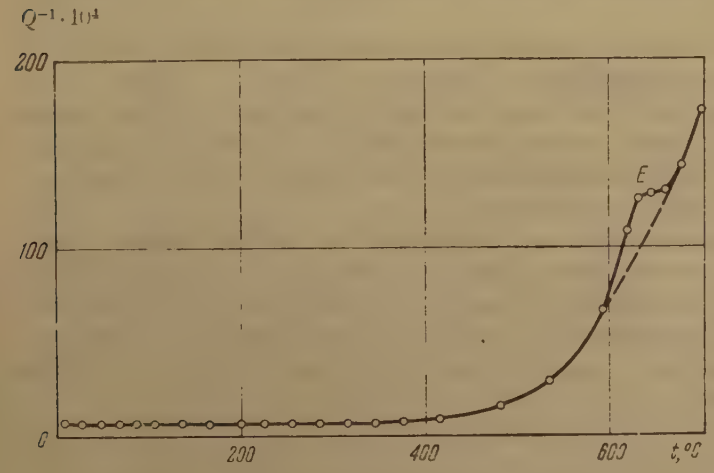

←Fig.3. Temperature dependence of the internal friction obtained for a quenched specimen of alloy 1 (Ni_3Fe).

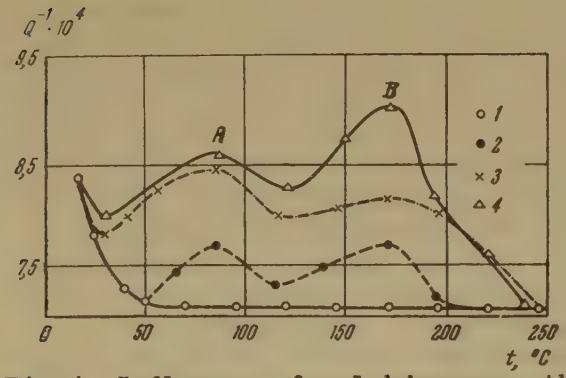

Fig.4. Influence of molybdenum on the temperature dependence of internal friction in quenched Fe-Ni-(Mo) alloys. Mo content: 1) 0, 2) 1%, 3) 3%, 4) 5%. All measurements performed at a frequency of 0.8 cps.

was several times larger than in the initial state. Measurements of the internal friction showed that with increasing grain size the peak E was shifted to the side of higher temperatures. This is in agreement with the data of Ke Ting-Sui[11] and proves that this peak is associated with grain boundary viscosity.

Similar curves with a bump were obtained as a result of measurements on alloys containing molybdenum. The influence of molybdenum on the internal friction is evinced only in the low temperature part of the curve. Hence in Fig.4, which illustrates the influence of Mo on the temperature dependence of internal friction, the high temperature portion of the curve has been omitted.

It will be seen that the curves for all the investigated alloys start with a falling section which extends from 15 to 30-50°. The reason for this decrease is not known.

In alloy 2 (1% Mo) the internal friction in the 50 to 200° interval is higher than in alloy 1 (no Mo). The curve exhibits two peaks: one in the region of 85° (peak A); the other at 170° (peak B). Within the 100 to 150° interval there is apparently superposition of the wings of both peaks; hence the internal friction does not fall to the level characteristic of the alloy with no molybdenum. The height of these peaks above the background is 8%, which is appreciably more than the experimental error.

In the case of alloy 3 (3% Mo) we again have two peaks at approximately the same temperatures. Here the height of the peaks has increased to 19%. The dip between the peaks is less pronounced. The peaks are still higher for alloy 4 (5% Mo); peak B is particularly prominent and rises 27% above the background.

In view of the relatively low height of the peaks, we were not able to determine their precise configuration. However, in all cases a maximum of the internal friction was observed at 170° (peak B), and a second maximum (peak A) at 85° was observed for almost all the specimens. In addition, it is clearly evident that the height of the peaks increases with increasing molybdenum content. This, in conjunction with the fact that there are no peaks evident in the curve for alloy 1, proves that these peaks are associated with the presence of molybdenum atoms in the solid solution.

The existence of two internal friction peaks indicates that there occur in the alloy two different processes with different relaxation times. Where our immediate problem is concerned, however, the precise configuration of the peaks is unimportant; what is important is that there is a rise of internal friction associated with Mo atoms. Hence to avoid controversy and simplify the discussion we shall hereinafter speak of a double peak.

To show that the double peak is not due to intrusion of carbon atoms, we subjected a specimen to a carbonizing treatment which increased the carbon content to 0.3%. For this specimen we obtained a clear internal friction peak at 260°, obviously associated with the presence of C atoms in the solid solution. It may therefore be safely concluded that peaks A and B are not due to the presence of carbon in the solid solution.

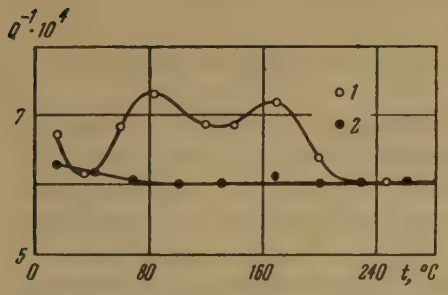

Fig.5. Influence of tempering at 400° on the temperature dependence of the internal friction in alloy 3 (3% Mo). Measurements made at a frequency of 0.8 cps. 1) quenched specimen, 2) specimen tempered at 400° for 12 hours.

The double peak could also be due to some deformation effect. To check this possibility we carried out measurements on deformed specimens (95% deformation in cross section). In the case of all alloys there appeared a new peak at 220°. Consequently, the double peak is not due to deformation.

Further we investigated the influence of heat treatment on the height of the double peak. To this end quenched alloys were tempered at 350 and 400° for 6 and 12 hours. These temperatures and tempering times were chosen on the basis of the kinetic resistivity curves for the given alloys.

Fig.5 shows the temperature dependences of internal friction obtained for two specimens of alloy 3: one for a quenched specimen, the other for a specimen tempered for 12 hours at 400°. It will be seen that the characteristic double peak disappears after tempering. Thus tempering of quenched Fe-Ni-Mo alloys at the temperature of K-state formation eliminates the internal friction peak associated with the presence of molybdenum in the solid solution.

The above experimental results may be interpreted as follows. In the quenched solid solutions the Mo atoms are in a free state. Hence ordering, i.e., reorientation of the Mo atomic pairs (according to the Zener model), readily occurs under the influence of an external stress. When the alloy is subjected to heat treatment inducing the K-state, there form in it Heine-Preston type zones containing Mo atoms. The alloy then behaves as though there occurred intraphase segregation within it. As a result the Mo atoms are no longer in the free state and hence cannot participate in ordering under stress; consequently, the internal stress peak first diminishes and then with continued tempering vanishes entirely.

Thus the results of our internal friction measurement show that incident to formation of the K-state the Mo atoms are taken out of the solid solution. Presumably, as a result of tempering, there form in the solid solution zones containing higher concentrations of Mo atoms and differing in composition from the main solid solution.

Investigations of the temperature dependence of the modulus of elasticity of Fe-Ni-Mo alloys showed the modulus increases upon formation of the K-state.

Metallography Laboratory
"I.V.Stalin" Moscow Steel Institute

References

1. J.Nix, L.Beyer & B.Danning, Phys.Rev., 58, 1031 (1940).
2. E.Jösso, Rev.Metallurgie, 10, 87 (1950).
3. I.M.Puzei, Otchet (Report) TsNIIChM, No.476.
4. Assmus & Pfeifer, Z.Metallkunde, 42, 295 (1951).
5. B.G.Livshits & M.P.Ravdel', Doklady AN SSSR, 93, 6 (1953), also see B.G. Livshits, Bulletin, USSR Ac.of Sci., Phys.Ser., 21, No.9, 1216 (1957).
6. H.Thomas, Z.Phys., 129, 219 (1951).
7. Iu.S.Avraamov & V.B.Osvenskii, Nauchnye doklady vysshei shkoly (College scientific reports), Vo.1, p.2, 1953.
8. M.V.Dekhtiar, Fiz.metallov i metallovedenie, 3, 3 (1953).
9. A.S.Novik, in "Uspekhi fiziki metallov" (Advances in the physics of metals), Vol.I, p.7 (1956).
10. V.S.Nostnikov, Doklady AN SSSR, 91, 79 (1953).
11. Ke Ting-Sui, in "Uprugost' i neuprugost' metallov" (Elasticity and non-elasticity of metals), p.223, M., 1954.

ANISOTROPY OF THE COERCIVE FORCE IN MAGNETICALLY ANISOTROPIC FINE-POWDER SPECIMENS

- E.V.Shtol'ts, Ia.S.Shur & G.S.Kandaurova

One of the most important characteristics of ferromagnets is their magnetic structure. Experimental investigations of this structure, which is of great interest from the standpoint of the theory of ferromagnetism, may be carried out either by direct observation or by studying the several attributes of ferromagnets that depend on the magnetic structure. In the case of finely powdered materials the former procedure is difficult or impossible and hence the latter must generally be used.

One can obtain the clearest idea of the magnetic structure of particles if the investigated specimens are single crystals or pseudo-single crystals, i.e., uniaxial in the sense that they consist of a large number of crystallites with their easy magnetization axes oriented in the same direction. In particular, for such specimens one may expect a definite correlation between the anisotropy of the coercive force and the magnetic structure. The primary purpose of the present work was to verify this correlation experimentally.

Specifically, we carried out measurements of the coercive force on magnetically uniaxial specimens of powders of the following materials: cobalt, Mn-Bi alloy, magnetite and γ-iron oxide. The Mn-Bi alloy was prepared by heating at 300° and 550°; inasmuch as the values of the coercive force for the alloys obtained at these temperatures were ~1000 and 100 oersted, respectively, we shall hereinafter refer to them as the "high-coercivity" and "low-coercivity" Mn-Bi alloys. The MnγBi alloy and cobalt powders were prepared by mechanical grinding; after pulverization the cobalt powder was annealed at 600°.[1] The particle size of these powders varied from about a millimeter to several microns (the particles were uniaxial). The magnetic uniaxiality of cobalt and Mn-Bi alloy particles is due to crystallographic anisotropy. The magnetite and γ-iron oxide powders were prepared chemically in the Sound Recording Institute. These powder particles were needle shaped, hence magnetically uniaxial. The length of the long axis of the magnetite and γ-iron oxide particles from different batches varied from about one micron to a fraction of a micron. The investigated specimens were prepared in the form of disks with artificially produced magnetic texture. To obtain the texture the powder was thoroughly mixed with a suitable binder and the mixture allowed to set in a magnetic field between the poles of an electromagnet.

Fig.1 shows the angular dependence of the coercive force for powder specimens of the different materials. The horizontal scale is laid off in values of φ, the angle between the direction of the magnetic field applied in preparing the specimen (the texture axis) and the direction of the magnetic field during measurement. The vertical scale is laid off in values of the ratio of the coercive force H_c at the given φ to the coercive force along the texture axis, i.e., $H_c^{\varphi}/H_c^{\varphi=0}$.

It will be seen that in the case of the cobalt specimen composed of 4μ particles (curve 1), the coercive force increases with increasing angle, attains a maximum value at $\varphi \approx 70^{\circ}$ and then decreases somewhat. The value of H_c in the direction perpendicular to the texture axis ($\varphi = 90^{\circ}$) is larger than the value in the direction of the texture axis ($\varphi = 0^{\circ}$). The φ-dependence of H_c of the magnetite specimen composed of 0.5 μ particles is similar (curve 2); in this case, however, the anisotropy of H_c is less pronounced and the maximum in the H_c vs φ curve lies at a lower value of φ. In the γ-iron oxide powder specimen, formed of particles measuring from 0.1 to 1.0 μ, H_c at first increases up to $\varphi \approx 50^{\circ}$ and then decreases (curve 3). It will be noted that in this case H_c in the directional normal to the texture axis is smaller than H_c along the texture axis.

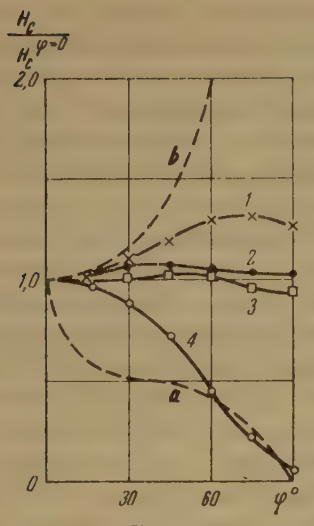

Fig. 1

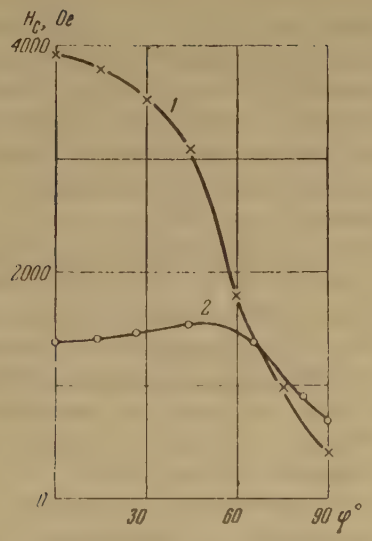

Fig. 2

Fig.1. Angular dependence of the coercive force determined for magnetically anisotropic specimens of different powdered materials: 1 - cobalt (particle size - 4 μ), 2 - magnetite (0.5 μ), 3 - γ-iron oxide (0.1-1.0 μ), 4 - high-coercivity Mn-Bi alloy (9 μ). Dashed lines - theoretical curves: a) for a single domain and b) for a multiple domain structure.

Fig.2. Angular dependence of the coercive force in specimens of low-coercivity Mn-Bi alloy; particle size: 1 - 30 μ and 2 - 90 μ.

The specimen composed of 9 μ particles of high-coercivity Mn-Bi alloy exhibits an entirely different variation of H_c with φ: in this case H_c consistently decreases with increasing φ and the value of H_c in the $\varphi = 90^\circ$ direction is much smaller than its value along the texture axis.

Thus it will be seen that the angular dependence of H_c may differ appreciably in textured specimens prepared of magnetically uniaxial powders.

For purposes of comparison, we also show in Fig.1 the theoretical curve for $H_c = f(\varphi)$ calculated for a single domain (a) and a multiple domain (b) magnetic structure. Curve a was plotted for the case of a uniaxial spherical particle with a large anisotropy constant on the basis of calculations of the hysteresis loop at different φ.[2] It will be seen that in this case H_c has a maximum value along the texture axis; the curve at first falls off sharply, then levels off in the 30 to 60° interval and then again swings downward. At $\varphi = 90^\circ$, $H_c = 0$. Calculations yield a similar φ-dependence of H_c for a geometrically anisotropic single domain particle of a material with weak crystallographic anisotropy.[3]

The experimental curve closest to theoretical curve a is curve 4 obtained for the 9 μ particle high-coercivity Mn-Bi alloy. In the range of small φ, however, there is an appreciable difference between these curves. Consequently, the process of technical magnetization in directions close to the texture axis differs from the process of irreversible rotation of the magnetization vectors. Possibly the difference is due to the fact that the given alloy particles still do not have a true single domain structure. On the basis of investigations of other magnetic properties of powder specimens, it has hypothesized[4] that such particles may have a distinctive domain structure consisting of one principal domain and several closure domains. In such particles, a decisive role in the process of technical magnetization is played by nucleation, growth and subsequent decrease or shrinking of the closure domains. The existence of this distinctive

structure has been substantiated by powder pattern studies.[5]

In the case of a multiple domain structure the coercive force is theoretically inversely proportional to cos φ.[6] Consequently, the coercive force increases with φ, becoming infinitely great as $\varphi \rightarrow 90^{\circ}$ (curve b). In this case, however, the process of technical magnetization may occur through reversible rotations of the magnetization vectors so that H_c drops to 0. Hence in practice one may expect a complicated φ-dependence with H_c passing through a maximum at some value of φ between 0 and 90°.

It will be noted that a dependence of this kind is observed for the cobalt, magnetite and γ-iron oxide specimens (curves 1, 2 & 3). Apparently, the magnetic structure of these powders is largely a multiple domain one. However, the coercive force of these powders is appreciably higher than of the corresponding bulk material. Thus H_c of cobalt powders with the indicated grain size is 96 oersted, while that of the initial material is only 20 oersted. The coercive force of 0.5 μ particle magnetite powder is 314 oersted, while H_c of bulk synthetic magnetite is about 10 oersted[7]. It would appear therefore that the magnetic structure of such particles already differs appreciably from the domain structure of the bulk material. Apparently, in this case the role played by closure domains in the process of technical magnetization is greatly enhanced even though each particle still presumably comprises several principal domains. Admittedly this inference is tentative and requires further verification by direct observation of the domain structure.

In the case of the above described materials we did not observe any change in the character of the coercive force anisotropy with variation in particle size. The reasons for this are the following: a) the magnetite and γ-iron oxide were investigated in only a narrow range of particle sizes; b) the high-coercivity Mn-Bi alloy had a high coercive force in its initial state and in its individual particles there already obtained the single domain (or nearly) structure (hence with increasing fineness only the number of particles with single domain structure, rather than the relative proportion of such particles, increased); c) the particle size of the investigated cobalt powders was far from the theoretical critical size for transition from multiple to single domain structure; hence any variation in particle size within the given range could scarcely affect the character of the H_c anisotropy.

We were able to observe variation of the H_c anisotropy with decreasing particle size in investigating specimens of the low-coercivity Mn-Bi alloy. The φ-dependences obtained in this case are shown in Fig.2. In the case of the specimen composed of 30 μ particles (curve 1), H_c decreases with increasing φ over the entire range of angles. In the case of 90 μ particles (curve 2) there is a slight increase of H_c in the range from 0 to 45°; then at larger values of φ the coercive force decreases, dropping to its lowest value at $\varphi = 90^{\circ}$.

Consequently, in the case of the low-coercivity Mn-Bi alloy reduction of the particle size leads to a change in the magnetic structure that is clearly evinced in the appearance of the H_c vs φ curve.

It will be evident from the described results that data on the anisotropy of the coercive force in magnetically anisotropic ferromagnets, in addition to certain other characteristics, can yield valuable information on the type of magnetic structure.

Institute of Metal Physics,
Academy of Sciences of the USSR &
Physical-Mathematical Faculty,
Ural State University

References

1. G.S.Kandaurova, Fiz.met.i metallovedenie, 4, 548 (1957). (Trans.Physics of Metals and Metallography.)

2. G.S.Kandaurova, Ia.S.Shur & E.V.Shtol'ts, ibid., 6, 229 (1958).

3. I.S.Jacobs & C.P.Bean, Phys.Rev., 100, 1060 (1955).

4. Ia.S.Shur, E.V.Shtol'ts & G.S.Kandaurova, Izv.AN SSSR, Ser.fiz., 21, 1215 (1957), (Trans.Bulletin, 21, No.9, 1205.); E.V.Shtol'ts, Ia.S.Shur & G.S. Kandaurova, Fiz.met.i metallovedeni, 5, 412 (1957). (Trans.Physics of Metals & Metallography.)

5. Ia.S.Shur, E.V.Shtol'ts, G.S.Kandaurova & L.V.Bulatova, Fiz.met.i metallovedenie, 5, 234 (1957). (Trans.Phys.of Metals & Metallography.)

6. S.V.Vonsovskii & Ia.S.Shur, Ferromagnetizm (Ferromagnetism) p.524, M.1948.

7. V.H.Gottschalk, Physics, 6, 127 (1935).

CONCERNING THE TEMPERATURE DEPENDENCE OF THE MAGNETIC PROPERTIES OF HIGH-COERCIVITY ALLOYS

- N.A.Baranova & Ia.S.Shur

Introduction

Our understanding of the physical nature of the high coercive force in magnetically hard ferromagnets is still inadequate. We have no clear information on the magnetic structure of this class of ferromagnets or on the processes of technical magnetization therein. Significant data on the subject can be obtained by investigating the temperature dependences of some of the magnetic properties of high-coercivity ferromagnets, particularly in the case of magnetically anisotropic samples. Consequently, in the present work we studied the temperature dependence of the principal magnetic characteristics of magnetically anisotropy high-coercivity alloys.

1. Specimens and Procedure

The study was carried out on specimens of Alnico (51% Fe, 24% Co, 14% Ni, 8% Al & 3% Cu) and Vicalloy (35% Fe, 52% Co & 13% V). The Alnico specimens were in the form of rods 2.8-3.0 mm in diameter and 48-50 mm in length. The Vicalloy samples were in the form of wires 1.0 mm in diameter and 65 mm in length.

The Alnico specimens were subjected to appropriate thermomagnetic treatment to produce different types (transverse or longitudinal) magnetic texture.[1] The Vicalloy specimens were subjected to cold drawing, followed by tempering and as a result had longitudinal magnetic texture.[1] The measurements were carried out in the temperature range from -195 to +600°. The crystal structure of the alloys was stable in this temperature range inasmuch as the samples had been subjected to prolonged annealing. Hence the changes induced in the magnetic properties of the specimens in the process of measurement were reversible. The principal magnetic characteristics of the alloy specimens were measured by the magnetometric procedure.

2. Results and Analysis

Fig.1 shows the temperature variation of the coercive force H_c obtained for Alnico specimens heat treated in a longitudinal and in a transverse magnetic field and for Vicalloy specimens. It will be seen that in Vicalloy H_c decreases slightly but steadily with increasing temperature.

In Alnico specimens, H_c both along and normal to the magnetic texture axis at first increases with temperature, passes through a maximum at about 200° and then begins to decrease.

The variation of the saturation magnetization $4\pi I_s'$ with temperature in the investigated alloys is shown in Fig.2. It will be seen that in the case of Vicalloy the saturation magnetization decreases monotonically with increasing temperature; in the curves for Alnico, however, there is a break at about 200°.*

In the high coercivity state Vicalloy consists of two phases: a ferromagnetic α-phase and a paramagnetic γ-phase. Owing to the fact that only one phase is ferromagnetic, the temperature dependence of the saturation magnetization of Vicalloy exhibits no singularities.

---

*In earlier contributions[1,2] we failed to note the break in the saturation magnetization vs temperature curves for Alnico; this was due to the fact that our experimental points in the 200° region were too widely spaced.

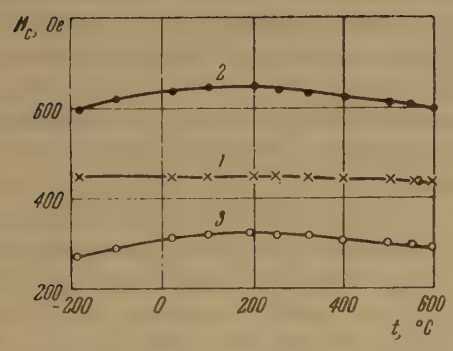

Fig.1

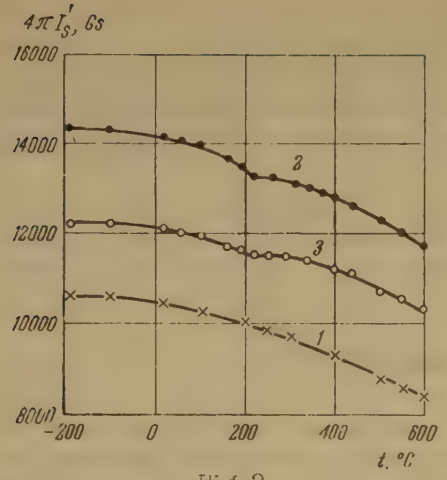

Fig.2

Fig.1. Temperature dependence of the coercive force H_c for specimens of Vicalloy (1) and Alnico subjected to thermomagnetic treatment in a longitudinal (2) and a transverse (3) magnetic field.

Fig.2. Temperature dependence of the saturation magnetization $4\pi I_s'$ (measured in a 1400 oersted field) for Vicalloy and Alnico specimens. Curve designations same as in Fig.1.

Alnico, on the other hand, in the high coercivity state is known to consist of two phases, both ferromagnetic but differing as regards their saturation magnetization I_s' and Curie point. With increasing temperature I_s' of each phase decreases. Experimentally we observed the integral or summation curve. Since the saturation magnetization of the phase with the lower Curie point decreases more rapidly with increasing temperature and at a certain temperature becomes negligibly small, we obtain the noted break in the I_s' vs t curve at this temperature. The higher temperature section of the curve is due to decrease of I_s' of the higher Curie point phase. Thus the break in the temperature dependence curve for I_s' of Alnico is connected with the presence of two ferromagnetic phases having different Curie points.*

Comparison of the temperature dependences of I_s and H_c of Alnico samples showed that beginning with the temperature corresponding to the maximum value of H_c the curves exhibit a parallel variation. This indicates that here H_c apparently depends on I_s'. Such a dependence is possible if the ferromagnet has a single domain magnetic structure and the cause of the anisotropy is geometric or "shape" anisotropy of the ferromagnetic formations. These results substantiate the inference made in Ref.4 that the factor responsible for the high coercive force in the investigated alloys is the single domain character of the ferromagnetic formations which have shape anisotropy, i.e., are laminae.

In connection with this, it is of interest to compare the magnetization curves and hysteresis loops obtained at different temperatures for Alnico specimens subjected to thermomagnetic treatment in a longitudinal field (Figs.3 & 4).

It will be evident from Fig.3 that the general character of the magnetization curves remains the same in the entire experimental temperature range.

---

*After completion of the present study there appeared a report by Clege & McCail[3] on their investigation of Alcomax-3; the saturation magnetization vs temperature curves for this alloy also exhibits a break. The authors associate this singularity with the presence of several ferromagnetic phases with different Curie points in the alloy.

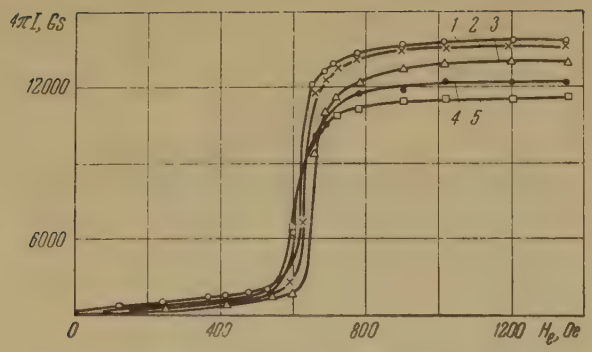

Fig.3. Magnetization curves for a longitudinally textured specimen of Alnico measured at different temperatures: 1) -195°, 2) +20°, 3) +250°, 4) +500° and 5) +600°.

Specifically, in the region of weak fields, the magnetization remains low; in a field numerically equal to the coercive force, the magnetization rises sharply, almost immediately reaching the saturation value. This shows that there has been realized in the ferromagnetic specimens a magnetic texture consisting of single domain formations.[4] From the similarity of the I vs magnetizing field curves it follows that this magnetic structure persists in a wide temperature range. It also follows that the anisotropy in this case is shape anisotropy inasmuch as anisotropy due to any other factors could remain invariant over a temperature range of 800°. It will be seen from the curves of Fig.4 that the ratio I_r/I_s' in the investigated temperature interval changes little; the value of I_r amounts to about 90-95% of I_s'. This indicates that the magnetic texture remains unchanged in the given temperature range.

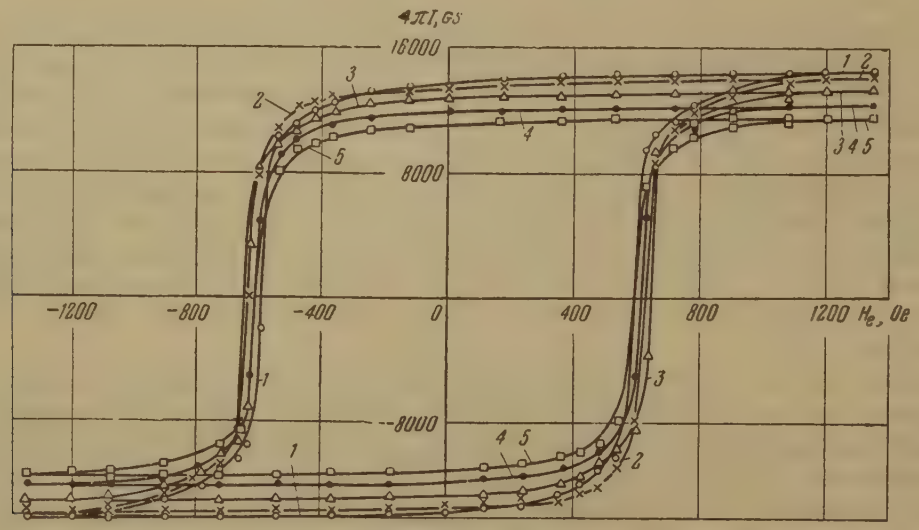

Fig.4. Hysteresis loops obtained for a longitudinally textured specimen of Alnico at different temperatures. Curve designations same as Fig.3.

Thus we infer that in Alnico the phase that determines the magnitude of the coercive force consists of single domain formations characterized by shape anisotropy. These single domain formations are isolated from each other by layers of the other phase with lower magnetic saturation. Owing to decrease with increasing temperature of the saturation magnetization of the weakly magnetic phase, the interaction between the single domain formations of the first phase is weakened (shielding effect). This can obviously lead to increase of the coercive force. Such increase of the coercive force will continue up to the temperature at which the magnetization of the weakly magnetic phase becomes negligibly small, namely, to the temperature of the break in the I_s' vs t curve.

Thus there are two factors influencing the coercive force in Alnico: one, associated with weakening of the interaction between the single domain formations, leads to increase of the coercive force with temperature; the other, due to dependence of H_c on I_s', results in decrease of H_c with increasing temperature. Hence in the case of Alnico we observe a maximum in the H_c vs t curve at the temperature of the break in the I_s' vs t curve.

In Vicalloy, which has only one ferromagnetic phase, the coercive force decreases monotonically with increasing temperature, which is connected with decrease of the saturation magnetization of the alloy with rising temperature.

Institute of Metal Physics,
Academy of Sciences of the USSR

References

1. Ia.S.Shur, N.A.Baranova, Trudy (Proceedings) Institute of Metal Physics, Ural Branch, USSR Ac.of Sci., No.15, 19 (1954).
2. Ia.S.Shur & N.A.Baranova, Doklady AN SSSR, 74, 225 (1950).
3. A.G.Clege & M.McCail, Proc.Phys.Soc., B70, 817 (1957).
4. L.A.Shubina & Ia.S.Shur, Zhur.tekh.fiz., 19, 88 (1949).

ON THE PHYSICS OF MAGNETODIELECTRICS

- L. I. Rabkin

1. Magnetic properties of ferroparticles

Low-coercivity magnetodielectric components are commonly fabricated of powders consisting of "ferroparticles" having linear dimensions in the range from 10^{-4} to 10^{-1} cm. Such particles are not homogeneous as regards magnetic properties. Usually the permeability has a high value in the central region of the particle and falls off towards the peripheries; this is apparently due to the cracks, unevennesses and a large number of closure domains which, being distributed over and near the surface of the particles, hamper displacement of the boundary layer between the ferromagnetic domains.

Hence the average magnetic properties of particles of the same ferromagnetic material but of different size differ, owing to the fact that the smaller the particle, the greater the relative amount of surface layer with a high coercive force and low permeability.

In the study of the properties of magnetodielectrics it is important to define the "permeability" of the ferroparticles. In view of the inhomogeneity of their magnetic properties one must introduce and define some average value of the permeability. Hereinafter we take the average permeability to mean the permeability of a magnetodielectric consisting of particles of the investigated powder with a fill coefficient of the ferromagnetic phase equal to unity and with the same average distribution in the size of the particles as obtains in the electronic components for which the powder is intended. In some cases the permeability of the powder particles determined in this manner can be established experimentally with good approximation. One of the procedures employed by us to this end consists of compacting the powder without a binder at high pressure to the point where the density of the pellet approaches the density of the individual particles. For most metallic low-coercivity powders there exists a critical compacting pressure yielding a saturation value of the permeability, i.e., increasing the compacting pressure yields no further increase of the permeability. Depending on the hardness of the initial powder, this pressure varies between $1.2 \cdot 10^3$ and $3 \cdot 10^4$ atmospheres. Particles of carbonyl iron, incidentally, can be compacted directly in the chamber in which they are formed.

The permeability obtained from measurements on compacted powder pellets has a lower value than the permeability obtained from measurements on sheets or wires of the same material and having a thickness equal to the average dimensions of the particles because in sheets regions or formations with low permeability are oriented only parallel to the magnetic field, whereas in pellets such low permeability sections are distributed at random.

With decreasing size (particle diameter and sheet thickness) the divergence between the respective permeabilities increases.

We determined the initial permeability $\hat{\mu}$ as a function of the particle size for a number of ferromagnetic powders subjected to different heat treatments. The dependences obtained for 80 Permalloy and alsifer (iron-silicon-aluminum alloy) are shown in Figs.1 & 2, respectively.

However, the ferromagnetic powders used for commercial production of magnetodielectric components are not uniform as regards particle size. The permeability of such nonuniform powders can be determined from the permeabilities of the individual fractions, taking into account the fill factors p_n, by means of

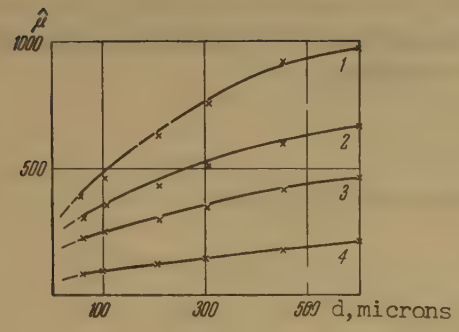

Fig.1

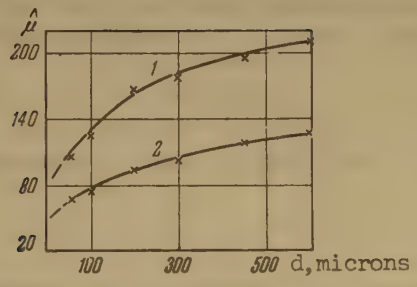

Fig.2

Fig.1. Variation of the average permeability $\hat{\mu}$ of 80 Permalloy powder with the particle size d. Material annealed at 1) 650°, 2) 550°, 3) 520°; 4) not annealed.

Fig.2. Same as Fig.1 but for alsifer: 1) annealed at 750°, 2) not annealed.

Lichtenecker's equation[1]:

$$\log \hat{\mu} = \log \hat{\mu}_1^{p_1} + \log \hat{\mu}_2^{p_2} + \ldots + \log \hat{\mu}_n^{p_n}, \qquad (1)$$

where

$$p_1 + p_2 + \ldots + p_n = 1.$$

2. Variation of the permeability of magnetodielectrics with the fill factor

The variation of the average permeability $\bar{\mu}$ of a magnetodielectric with the fill factor p cannot be characterized by a single function inasmuch as it depends on the distribution of the ferromagnetic and nonferromagnetic phases in the magnetodielectric specimens. As a rule, the permeability of the magnetodielectric decreases with decrease in the number of direct contacts between the ferroparticles and with increasing homogeneity of the distribution of the inert "insulating" material between the particles.

In order to determine the influence of nonuniform distribution of the interparticle insulating material on the magnetic properties of magnetodielectrics, we carried out the following experiments. Using ferromagnetic bodies of sufficiently large size to permit of direct measurement of their permeability, we prepared magnetic circuits with different proportions of the ferromagnetic and nonferromagnetic phases. The results of some of our measurements of $\bar{\mu}$ as a function of p are shown in Fig.3. Curve 1 was obtained for magnetic circuits consisting of several toroidal plates of a ferromagnetic material with distributed 2 mm in diameter circular or polyhedral openings. Curve 2 shows the variation of $\bar{\mu}$ with the fill coefficient p for a magnetic circuit consisting of an isotropic mixture of 2 mm diameter iron and quartz sand particles. Lastly, curve 3 characterizes magnetodielectric specimens consisting of iron particles of the same size (2 mm) uniformly distributed in a dielectric binder. All the specimens were prepared of low carbon steel with an initial permeability $\hat{\mu}_H$ = 253 gauss/oersted* and were subjected to the same heat treatment. It will be seen from the curves of Fig.3 that the magnetodielectrics with a uniformly distributed insulating phase are characterized by the lowest permeability values.

---

*Translator's note: The meaning of the subscript H is not made clear in the text. Presumably, it stands for "initial", i.e., μ_H = initial permeability of the parent material.

In the same figure we give the theoretical curves for the variation of $\bar{\mu}$ as a function of p calculated using $\hat{\mu}$ = 253 gauss/oersted by means of different formulas: curve c is based on the Ollendorf[2] equation:

$$\mu = \frac{3\mu\hat{\mu} + 2(\hat{\mu} - 1)(1 - p)}{3 + (\hat{\mu} - 1)(1 - p)}, \tag{2}$$

curve b is based on the Lichtenecker[1] and Leff-Given[3] formula:

$$\mu = \hat{\mu}(p) \tag{3}$$

and curve a is based on the Kondorskii[4] formula:

$$\bar{\mu} = a + \sqrt{a^2 + \frac{1}{2}\hat{\mu}}, \tag{4}$$

where

$$a = \frac{1}{4}[2 - 3p + (3p - 1)\hat{\mu}].$$

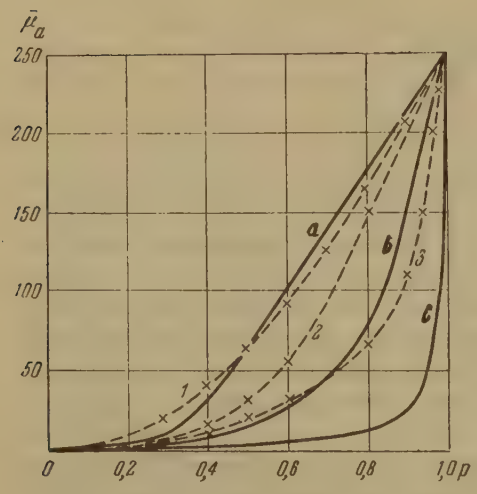

Fig. 3. Variation of the permeability $\bar{\mu}$ with the fill factor p of the ferromagnetic phase. Dashed curves - experimental; solid curves - calculated.

Experimental curve 3, which pertains to magnetodielectrics with a uniform distribution of the dielectric phase, lies below the theoretical curve a and above the theoretical curve c. Curve 3 intersects curve b given by the Lichtenecker & Legg-Given formula. In the region of large fill factors curve a, based on Kondorskii's equation, runs close to experimental curve 1 for a conglomerate in which the ferromagnetic phase is the matrix and the dielectric phase is discontinuous (i.e., holes in annular iron plates).

As we showed earlier[5], formula (3) is in good agreement with the experimental results for magnetodielectrics prepared of alsifer powder provided the permeability of the powders is taken equal to the permeability of a magnetodielectric specimen with p = 1. The fact that Eq. (3) gives better agreement with experiment for actual isotropic magnetodielectrics consisting of fine ferromagnetic particles than do models consisting of relatively large "bodies" is apparently a consequence of the considerable inhomogeneity of magnetic properties of the fine ferroparticles used for the fabrication of commercial magnetodielectrics.

The Lichtenecker formula (3) was also checked by us on magnetodielectrics prepared of nitrided carbonyl iron powder and also of Permalloy powder consisting of lamellar (flaky) particles.

In the first case the permeability $\hat{\mu}$ of the ferromagnetic phase was determined from measurements on annular cores prepared from dense deposits of carbonyl iron formed in the pentacarbonyl decomposition chamber. The permeability varied from 23 to 32 gauss/oersted, depending on the precipitation conditions.

The calculated permeability values are compared with the values obtained by measurements on compact specimens in Table 1. It will be seen that the calculated and experimental values are in satisfactory agreement.

The magnetodielectric specimens prepared of lamellar Permalloy powder had a diameter of about 1 mm and a thickness from 15 to 20 μ. The permeability of the powder was determined by measurements on toroidal specimens compressed with-

Table 1

Calculated and experimental values of the permeability $\bar{\mu}_H$ for magnetodielectrics of carbonyl iron and "flaky" Permalloy

Material	p	$\hat{\mu}_H$ gs/oerst.	μ, gs/oersted	
			calculated	experimental
Nitrided carbonyl iron	0,65	34	9,5	10,4
	0,65	23	7,7	8,4
	0,30	23	2,56	2,8
Flaky Permalloy	0,95	1150	808	730
	0,90	1150	568	550
	0,85	1150	317	288
	0,75	1150	195	170
	0,60	1150	69	61

out a binder at a pressure of 18,000 atmospheres. Further increase of the compacting pressure does not alter the permeability. The cores were annealed at 880° after compacting.

The permeability measurements on these cores, which are also given in Fig.1, show that calculations for anisotropic magnetodielectrics by means of the Lichtenecker formula yield values differing by less than 15% from the experimental data.

3. Permeability of multiple component magnetodielectrics

The permeability of multiple component magnetodielectrics consisting of n powders differing as regards type of particles, permeability and fill coefficients can be calculated by means of the generalized Lichtenecker formula[6]:

$$\log \bar{\mu} = \sum_{k=1}^{n} p_k \log \hat{\mu}_k. \qquad (5)$$

For a two component magnetodielectric this formula reduces to

$$\log \bar{\mu} = p_1 \log \hat{\mu}_1 + p_2 \log \hat{\mu}_2, \qquad (6)$$

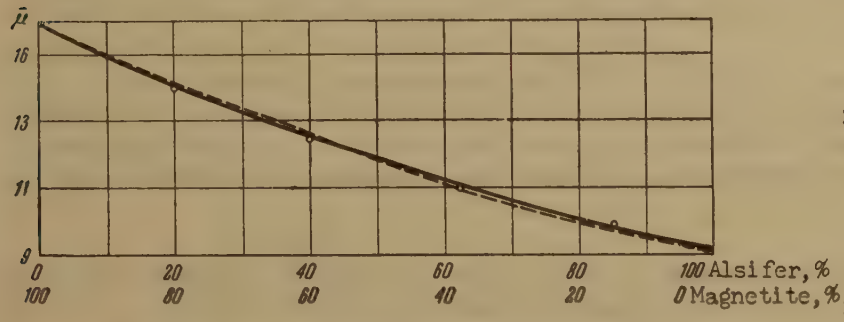

Fig.4. Variation of the permeability of a two component magnetodielectric with the ratio of the ferromagnetic components. Solid curve - experimental; dashed curve - calculated.

We checked Eq.(6) with reference to a number of different compositions. In all cases the agreement with experiment was satisfactory. Fig.4 shows the curves characterizing the variation of $\bar{\mu}$ with the composition of a two component magnetodielectric with a ferromagnetic fill factor $p = 0.7$. The solid curve is based on measurements of specimens consisting of a mixture of RCh-6 alsifer powder with $\hat{\mu}_H = 53$ gauss/oersted and magnetite powder with $\hat{\mu}_H = 23$ gauss/oersted. The dashed curve was calculated by means of Eq.(6). It will be seen that the two curves virtually coincide.

4. Magnetodielectric loss factors

By analogy with the above described assumption regarding the permeability of the "parent" ferromagnetic powder, we assumed that the hysteresis loss factor δ_h, the high-frequency loss factor δ_{rf}, and the initial loss factor δ_i of

Table 2

Loss factors of two cores of 80 Permalloy annealed at 550° for 0.5 hour

Core type	$\hat{\mu}_H$, gs/oersted	$\hat{\delta}_h/\hat{\mu}_H^2$	$\hat{\delta}_i/\hat{\mu}_H$
Core of 0.008 cm thick sheets	960	$420 \cdot 10^{-9}$	$0.95 \cdot 10^{-5}$
Core of 0.070–0.008 cm diameter particles compacted without insulating binder	280	$610 \cdot 10^{-9}$	$1.35 \cdot 10^{-5}$

the "parent" ferromagnetic substance are equal to the corresponding loss factors of magnetodielectric specimens formed of the given powder with a fill factor equal to unity. Measurements of the specific loss factors, $\hat{\delta}_h/\hat{\mu}_H^2$, $\hat{\delta}_i/\hat{\mu}_H$, etc., under these conditions (i.e., using compacted specimens) yield higher values than those obtained for the same ferromagnetic materials in the form of sheets or wires. The comparative initial loss and hysteresis loss factors for laminated and compacted powder cores of 80 Permalloy are listed in Table 2.

The higher loss coefficients for a powder core, as compared with a core assembled of ferromagnetic sheets, are due to inhomogeneity of the field in the powder particles. Whereas in a laminated core every magnetic line of force passes through a homogeneous medium, in a powder core, even one compacted without an insulating binder, each line of force in going from inhomogeneous particle to another must necessarily pass through sections with different properties.

Some years ago the writer[5] proposed a method for calculating the average loss factors of magnetodielectrics from the factors for the initial,"parent" ferromagnetic substance. The deduced equations were

$$\bar{\delta}_h = \hat{\delta}_h (\bar{\mu}_H : \hat{\mu}_H)^2 \frac{1}{p}; \tag{7}$$

$$\bar{\delta}_{rf} = \hat{\delta}_{rf} (\bar{\mu}_H : \hat{\mu}_H)^2 \frac{1}{p}; \tag{8}$$

$$\bar{\delta}_i = \hat{\delta}_i (\bar{\mu}_H : \hat{\mu}_H)^2 \frac{1}{p}. \tag{9}$$

These equations give satisfactory agreement with experiment in the range of fill factors $p > 0.8$.

Table 3

Variation of the hysteresis loss factor δ_h of toroidal cores of alsifer with the fill coefficient p ($\hat{\mu}$ = 111 gauss/oersted; $\hat{\delta}_2 = 12.8 \cdot 10^{-3}$)

Fill factor p	μ, Gs Oe^{-1}	$\delta_h \cdot 10^3$	
		Experimental	Calculated by Eq. (2)
0.5	66	4.28	4.15
0.88	10.8	0.98	0.51

By way of illustration, we list in Table 3 the comparative values of the hysteresis loss factor calculated by means of Eq.(7) and found experimentally for ferrocores of alsifer powder, subjected in the process of core preparation to a pressure of 22,000 atmospheres and annealing in air at 780°.

It will be seen that for the magnetodielectric with $p = 0.5$ the calculated value of δ_h is in satisfactory agreement with the experimental value. In the case of the magnetodielectric with $p = 0.88$, however, there is an appreciable divergence: the experimental loss coefficient is almost twice the calculated one. This divergence is due to increasing inhomogeneity of the magnetic flux

in the particles with reduction of the fill factor p; this inhomogeneity effect is not taken into account in Eqs.(7), (8) and (9).

Our experiments show that the inhomogeneity of the field depends on the particle shape and the fill factor p. Consequently, corrections taking into account the increase of the loss factors owing to inhomogeneity of the field should be introduced into the above equations. The equations become somewhat more complicated:

$$\bar{\delta}_h = \hat{\delta}_h(\bar{\mu}_н : \hat{\mu}_н)^2 \frac{1}{p^{2(1+\Xi)}}; \tag{10}$$

$$\bar{\delta}_{rf} = \hat{\delta}_{rf}(\bar{\mu}_н : \hat{\mu}_н) \frac{1}{p^{(1+\Xi)}}; \tag{11}$$

$$\bar{\delta}_i = \hat{\delta}_i(\bar{\mu}_н : \hat{\mu}_н) \frac{1}{p^{(1+\Xi)}}. \tag{12}$$

The correction term Ξ in the above equations depends on the shape and the mechanical properties of the powder particles. Thus, for example, for powders consisting of spherical particles (carbonyl iron and powders obtained by electroerosion) Ξ is close to zero. For annealed powders of electrolytic iron and Permalloy Ξ lies in the range from 0.2 to 0.3, while for ferrite and alsifer powders the range of values is 0.4 to 0.5.

References

1. K.Lichtenecker, Phys.Z., 25, 172 (1924).
2. F.Ollendorf, Arch.Elecktr., 25, 436 (1931).
3. V.E.Legg & F.J.Given, Bell System Tech.J., 19, 385 (1940).
4. E.I.Kondorskii, Izv.AN SSSR, Ser.fiz., 16, 398 (1952).
5. L.I.Rabkin & N.N.Shol'ts, Magnetodielektriki i ferrokatushki (Magnetodielectrics and ferrocoils), M.-L., 1948.
6. L.I.Rabkin, Magnetodielektriki i ferrokatushki dlia vysokochastotnoi telofonnoi apparatury (Magnetodielectrics and ferrocoils for high frequency telephone equipment), in Symposium "Magnetodielektriki v tekhnike vysokochastotnoi sviazi" (Magnetodielectrics in high frequency communication engineering), M.-L., 1948.

MAGNETIC PROPERTIES OF FERRITES WITH A COMPENSATION POINT

- K.P.Belov, K.M.Bol'shova, T.A.Elkina & M.A.Zaitseva

Some ferrites exhibit an anomalous temperature dependence of the spontaneous magnetization. Of greatest interest in this respect are ferrites that have a "compensation point". In these ferrites the magnetization goes to zero not only at the Curie point but also at the compensation point where the ferrite transforms into an ordinary antiferromagnet.

The possible existence of σ_s vs T curves with a compensation point was predicted by Néel[1] in his treatment of the theoretical model based on application of the Weiss molecular field to ferrites. Ferrites with a compensation point were first detected experimentally by Gorter and his co-workers[2].

Simple physical considerations show that σ_s vs T curves with a compensation point may be expected for ferrites in which the difference between the sublattice magnetizations (at 0°K) is small, i.e., for ferrites which as regards their magnetic properties are close to ordinary antiferromagnets. Different temperature dependences of the magnetizations of the sublattices in such ferrites may lead to the appearance of σ_s vs T curves with a compensation point; in such cases the resultant magnetization up to the compensation point temperature will have the direction of the magnetization of one of the sublattices, while above the compensation temperature, the net magnetization will be aligned with the magnetization of the other sublattice. At the compensation temperature, the magnetizations of the two sublattices become even and since they are oriented antiparallel, the resultant magnetization is zero.

There is little information in the literature on the magnetic behavior of ferrites of this type. In addition to Gorter, Pauthenet[3] reported observing curves with a compensation point for rare earth ferrites.

In the present work we carried out measurements of the magnetic characteristics of mixed ferrites-lithium chromites in the annealed and quenched states and after different heat treatments following quenching. For the purposes of the investigation we prepared a series of ferromagnetic lithium spinels containing chromium; the general formula for these substances is

$$Li_2O\cdot(5 - 2a)Fe_2O_3\cdot 2aCr_2O_3 \text{ (wherein } a = 1.25,\ 1.5,\ 1.6 \text{ and } 1.7).$$

1. Preparation of Specimens and Measurement Procedure

The specimens were prepared by mixing pure (reagent grade) finely ground iron oxide, chromium oxide and lithium carbonate. The several components were weighed off in the requisite amounts and thoroughly pulverized in an agate mortar for several hours. The mixture was compressed into pellets which were sintered for 9 hours at about 1050° in air. The sintered product was again thoroughly ground in an agate mortar. The resultant powder was mixed with a binder and compressed to form the parallelepiped specimens (edge dimensions: 60 mm, 6 mm and 4 mm). These specimens were roasted at 1150° for 3 hours and cooled slowly with the furnace.

The following magnetic characteristics were measured:

1) The temperature dependence of the spontaneous magnetization $\sigma_s = f(T)$; the value of σ_s was determined from the magnetic isotherms by extrapolation to zero field; close to the Curie point, where extrapolation is impossible, σ_s was determined by means of the thermodynamic formula

$$\sigma_s = \sqrt{-\frac{\alpha}{\beta}}$$

(this follows from the thermodynamic equation for the magnetization of a ferromagnet near the Curie point, i.e., the curve $\alpha\sigma - \beta\sigma^3 = H$ at $H = 0$). The thermodynamic procedure also allows of more accurate determination of the Curie point; the Curie point was determined as the temperature at which $\alpha \rightarrow 0$.[6]

2) The atomic magnetic moments, which were determined from the magnetic saturation at the boiling point of liquid helium (these measurements were carried out by A.V.Ped'ko).

3) The temperature dependence of the residual magnetization (as given by the saturation loop) in the temperature range from -30° to a temperature 10-20° above the compensation point (these measurements were made on an astatic magnetometer).

4) The temperature dependence of the paramagnetic susceptibility (determined by the ponderomotive procedure).

The measurement procedures have been described in detail in Refs.4,5 & 6.

2. Results

A. Specimens in the initial (annealed) state

All the investigated compositions exhibited an anomalous temperature dependence of the spontaneous magnetization. A compensation point was evident in the σ_s vs T curves for all the specimens; the curves for the specimens in the initial (annealed) state are shown in Figs.1 through 4. In contradistinction to the results of Gorter, however, we found that in our specimens there obtained "incomplete compensation", i.e., there was evident a certain nonzero spontaneous magnetization at the compensation temperature. This will be evident from Fig.5 in which we show for purposes of comparison the magnetization curves for the $Li_2O \cdot 2.5Fe_2O_3 \cdot 2.5Cr_2O_3$ specimen at the compensation temperature (+44°), at slightly lower and higher temperatures and in the vicinity of the Curie point (+217°C). The compensation temperature curve (curve 1), although it does flatten out, is still distinctly "ferromagnetic" and exhibits approach to saturation. The value of σ_s at this temperature is certainly not less than 0.2 gauss $cm^3\ g^{-1}$. An analogous behavior was observed for all the other alloys.*

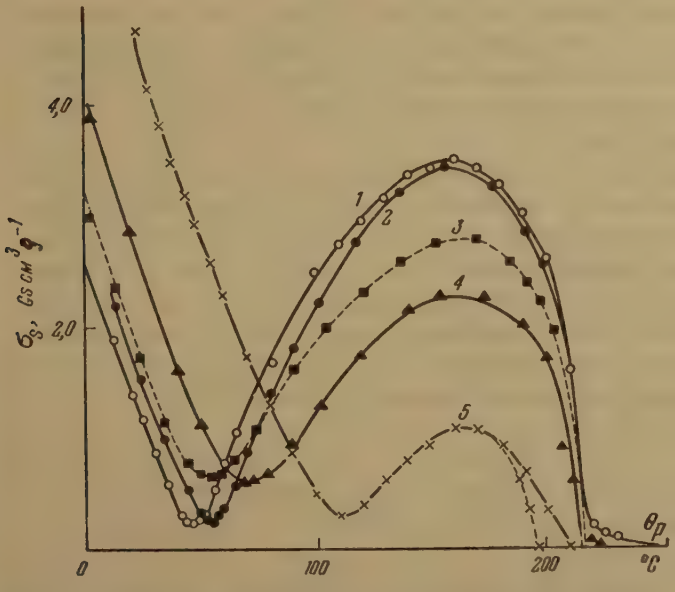

Fig.1 Temperature dependence of the spontaneous magnetization of $Li_2O \cdot 2.5Fe_2O_3 \cdot 2.5Cr_2O_3$ after different heat treatments: 1) initial state, 2) quenching from 1000° in air, 3) heating at 500° for 5 hours, 4) heating at 500° for 24 hours, 5) heating at 800° for 8 hours. Dashed curve in the region of the Curie temperature - variation of σ_s calculated by means of the formula $\sigma_s = \sqrt{-(\alpha/\beta)}$. θ_p - paramagnetic Curie point.

---

*In the case of $Li_2O \cdot 2Fe_2O_3 \cdot 3Cr_2O_3$ the compensation point fell below 0°C and the magnetization curve at this temperature could not be recorded on the ballistic set-up. The compensation point was determined by means of the magnetometer utilizing the fact that the residual magnetization goes to zero at this temperature.

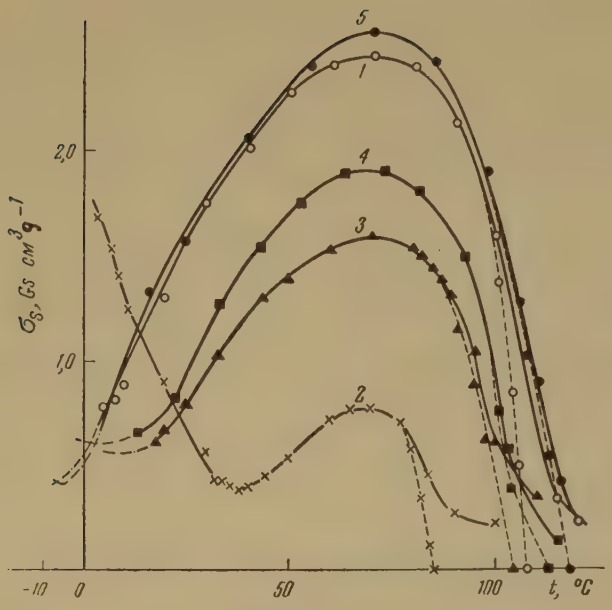

Fig.2

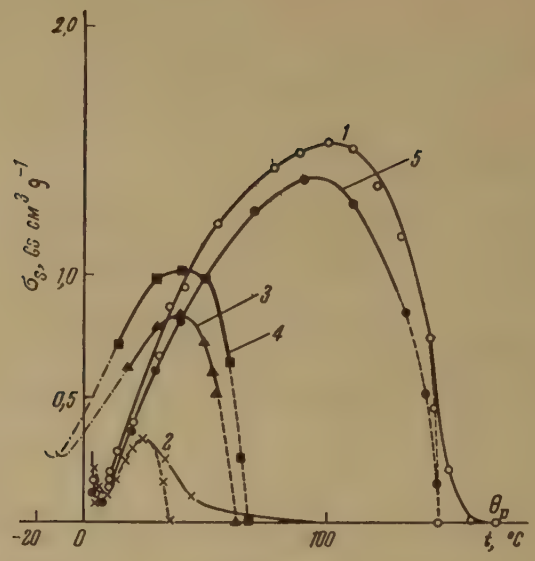

Fig.3

Fig.2. Temperature dependence of the spontaneous magnetization of $Li_2O \cdot 2Fe_2O_3 \cdot 3Cr_2O_3$ after different heat treatments: 1) initial state, 2) quenching from 1000° in air, 3) heating at 500° for 5 hours, 4) heating at 500° for 24 hours, 5) heating at 1000° for 5 hours. Dashed curve in the Curie temperature region - variation of σ_s calculated by means of the formula $\sigma_s = \sqrt{-(\alpha/\beta)}$. The compensation temperature was obtained by means of magnetometric measurements of the temperature dependence of the residual magnetization (dash-dot curves in the vicinity of 0°C).

Fig.3. Temperature dependence of the spontaneous magnetization of $Li_2O \cdot 1.8Fe_2O_3 \cdot 3.2Cr_2O_3$ after different heat treatments: 1) initial state, 2) quenching from 1000° in air, 3) heating at 500° for 5 hours, 4) heating at 500° for 24 hours, 5) heating at 1000° for 5 hours. θ_p - paramagnetic Curie point. The compensation temperature for 3 and 4 was obtained only from measurements of the temperature dependence of the residual magnetization (dash-dot sections of the curves in the vicinity of 0°C). The dashed curve in the Curie temperature region - variation of σ_s calculated by means of the formula $\sigma_s = \sqrt{-(\alpha/\beta)}$.

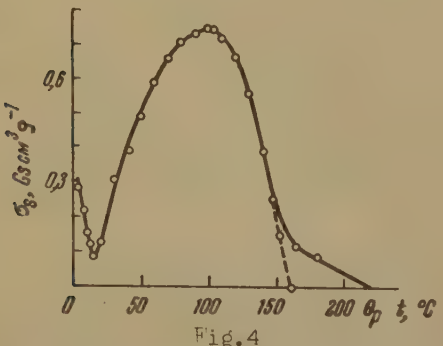

Fig.4

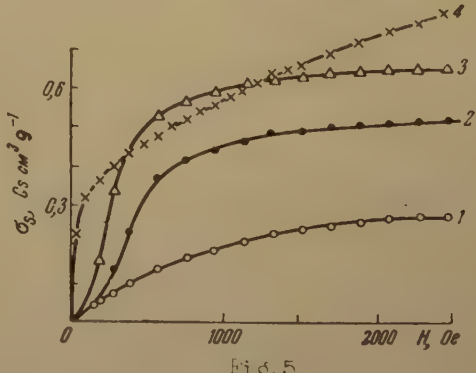

Fig.5

Fig.4. Temperature dependence of the spontaneous magnetization of $Li_2O \cdot 1.6Fe_2O_3 \cdot 3.4Cr_2O_3$ ferrite (initial state). Dashed line in the Curie temperature region - variation of σ_s calculated by means of the formula $\sigma_s = \sqrt{-(\alpha/\beta)}$.

Fig.5. Magnetization curves for $Li_2O \cdot 2.5Fe_2O_3 \cdot 2.5Cr_2O_3$ at different temperatures: 1) +44°, 2) +36.5°, 3) +55° and 4) +217°C.

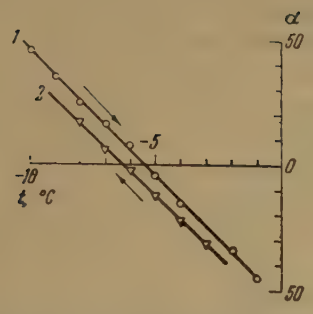

Fig.6. Temperature dependence of the remanence of an $Li_2O \cdot 2Fe_2O_3 \cdot 3Cr_2O_3$ specimen in the initial state in the region of the compensation point T_c. α - magnetometer deflection proportional to the remanence. Curve 1 - heating; curve 2 - cooling.

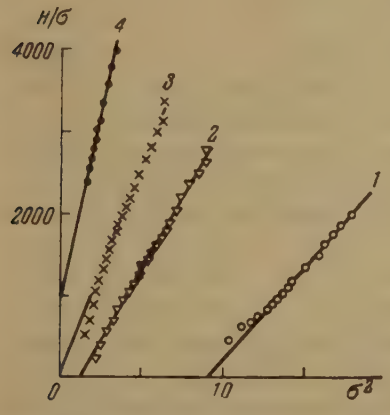

Fig.7. Verification of the thermodynamic formula for the magnetization curve ($\alpha + \beta\sigma^2 = H/\sigma$) at temperatures close to the Curie point for $Li_2O \cdot 2.5Fe_2O_3 \cdot 2.5Cr_2O_3$: 1) +213.5° ($\sigma_s = 0.95$), 2) 216° ($\sigma_s = 0.37$), 3) 217° and 4) 218°.

In order to prove that at the minimum in the σ_s vs T curve there actually does obtain compensation of the magnetic moments of the sublattices, we determined the temperature dependence of the remanence (saturation loop value) for specimens of all compositions. In all cases, i.e., for all compositions and all heat treatments, the remanence curve went through zero at the temperature at which the corresponding σ_s vs T curve had a minimum (within the limits of measurement accuracy, evaluated to be ±0.5°) (Fig.6).

Having the temperature dependences of σ_s up to the Curie point for all the specimens, we were able to check the applicability of the thermodynamic equation[7] for the magnetization in the region of the Curie point,

$$\alpha\sigma + \beta\sigma^3 = H, \qquad (1)$$

to ferrites of this type.

It was found that this equation is valid for all four investigated compositions both in the initial state and after all the types of heat treatment essayed. In each case the plot of H/σ vs σ^2 at the Curie temperature for fields in the range from 100 to 2500 oersted was a straight line passing through the origin (Fig.7).

The Curie and compensation point temperatures found for all our specimens proved to be fairly close to the corresponding values given by Gorter - see Table 1.

It may be noted that the accuracy in determining the compensation temperature was higher in our experiments (as compared with Gorter's), inasmuch as we obtained more experimental points in the given temperature interval (our measurements were made at 1-2° intervals). The fact that Gorter had comparatively few points in the compensation temperature region also probably explains why he failed to detect "incomplete compensation". The method of determining the Curie point is not described in Gorter's report. Presumably, the Curie temperature was determined from the σ vs T curves by extending the tangent to the steep part of the curves to its intersection with the temperature axis. In our experiments the Curie temperature was determined from the coefficient α becoming equal to 0. It was demonstrated earlier by one of us in collaboration with Goriaga[6] that one cannot determine the Curie point from the σ vs T curve since, owing to the paraprocess, the Curie point determined in this manner will depend on the field in which the σ vs T curve was recorded.

We determined the atomic magnetic moments from the values of the absolute magnetic saturation σ_o as given by the magnetization curves recorded at the boiling point of helium.* Our results together with the data of Gorter are listed in Table 2.

---

*See footnote bottom of next page.

Table 1

Compensation and Curie points of different ferrites

Ferrite composition	Compensation point, °C		Curie point, °C	
	Gorter[2]	Our data	Gorter[2]	Our data
$Li_2O \cdot 2.5Fe_2O_3 \cdot 2.5Cr_2O_3$	+38	+45	+214	+217
$Li_2O \cdot 2Fe_2O_3 \cdot 3Cr_2O_3$	−16	− 6	+119	+108
$Li_2O \cdot 1.8Fe_2O_3 \cdot 3.2Cr_2O_3$	+11	+ 7	+167	+147
$Li_2O \cdot 1.6Fe_2O_3 \cdot 3.4Cr_2O_3$	+20	+15	+155	+160

Table 2

Atomic magnetic moments (μ_o in Bohr magnetons per atom)

Composition	μ_o according to Gorter	μ_o, our data for specimens in initial state	μ_o, our data for quenched specimens	μ_o, theoretical after Néel (initial state)
1	2	3	4	5
$Li_2O \cdot 2.5Fe_2O_3 \cdot 2.5\ Cr_2O_3$	0.61	0.68	0.74	0.9
$Li_2O \cdot 1.8Fe_2O_3 \cdot 3.2\ Cr_2O_3$	0.42	0.39	0.57	2.9
$Li_2O \cdot 1.6Fe_2O_3 \cdot 3.4\ Cr_2O_3$	0.22	0.24	0.31	3.7

The values of μ_o listed in column 5 of Table 2 were calculated according to the Néel theory. Knowing the distribution of Li ions in these ferrites[2] and assuming (as inferred by Gorter) that the Cr ions occupy only octahedral sites, one can obtain for each of the investigated ferrites the complete cation distribution between the sublattices A and B. Further, utilizing Néel's formula for the case of antiparallel magnetic moments of the cations in sublattices A and B, i.e., setting

$$M = M_B - M_A, \qquad (2)$$

we obtain the data listed in column 5 of Table 2. Here M_B and M_A are the sums of the magnetic moments of the cations occupying sites in the sublattices B and A, respectively, and M is the resultant magnetic moment of the ferrite. The pure spin values are taken for the magnetic moments of the iron and chromium cations, i.e., $3\mu_B$ for the Cr ion and $5\mu_B$ for the Fe ion. As will be evident from Table 2, the values of μ_o for our ferrites cannot be calculated by means of the Néel theory. Even for the first of our ferrites, the theoretical value greatly exceeds the experimental one and the divergence increases rapidly with increasing Cr content.

B. Specimens in the quenched state and after different heat treatments

We felt it would be of interest to see how heat treatment can affect the properties of the ferrites under study. To this end all the specimens were subjected to quenching from 1000° in air (the holding time at 1000° was 40 min) and then, after measurement of their properties in the quenched state, they were subjected to step anneals under the following conditions: 1) 5 hours at 500°, 2)

---

*(See preceding page) In the case of $Li_2O \cdot 2Fe_2O_3 \cdot 3Cr_2O_3$ saturation was not attained at liquid helium temperature even in a 4500 oersted field; consequently σ_o for this ferrite was not determined.

24 hours at 500° and 3) 8 hours at 800° for some of the compositions or 5 hours at 1000° for the others.

All these heat treatments radically changed the temperature dependence of σ_s. In all cases quenching led to suppression of the reverse magnetization* and reduction of the interval between the compensation point T_c and the Curie point θ (see Figs.1,2 & 3 and Table 3).

It is noteworthy that in the specimen with the lowest Cr content (a = 1.25) the diminution of the $\theta - T_c$ interval occurs due to displacement of the compensation point (the Curie point shifts very little). In the specimen with a high chromium content (a = 1.6) the decrease of the $\theta - T_c$ interval occurs exclusively due to displacement of the Curie point, while the compensation temperature remains virtually the same as in the initial state. In the specimen with the intermediate Cr content (a = 1.5) the $\theta - T_c$ interval is reduced owing to shifting of both the compensation point and the Curie point. Thus the displacement of the compensation point incident to quenching decreases, while the displacement of the Curie point increases with increasing chromium content.

Table 3

Displacement of the compensation and Curie points as a result of quenching

a	T_c in quenched state, °C	θ in quenched state, °C	$\theta - T_c$ in initial state	$\theta - T_c$ in quenched state
1.25	+110	+199	172	86
1.5	+ 37	+ 85	114	47
1.6	+ 9	+ 35	140	26
1.7	None	~— 50	145	—

It is interesting to note that in the case of the composition with the highest Cr content, namely, in $Li_2O \cdot 1.6Fe_2O_3 \cdot 3.4Cr_2O_3$, quenching led to complete suppression of the reverse magnetization. This specimen had no compensation point after quenching, as was evinced by measurements of the remanence carried out on a magnetometer in the temperature range from liquid nitrogen to room temperature. The magnetometric measurements showed that this ferrite becomes ferromagnetic only at low temperatures (beginning approximately from -50°). The remanence does not change polarity in the interval from -50° to liquid nitrogen temperature.

In all the investigated specimens that had a compensation point the compensation was incomplete not only in the initial state but after the different heat treatments (Figs.1,2 & 3). Measurements of the absolute magnetic saturation at liquid helium temperature were carried on quenched specimens having the compositions: $Li_2O \cdot 215Fe_2O_3 \cdot 2.5Cr_2O_3$, $Li_2O \cdot 1.8Fe_2O_3 \cdot 3.2Cr_2O_3$ and $Li_2O \cdot 1.6Fe_2O_3 \cdot 3.4Cr_2O_3$.

Quenching resulted in increase of the magnetic moment. A particularly great increase (~1.5) was observed for $Li_2O \cdot 1.8Fe_2O_3 \cdot 3.2Cr_2O_3$ (see Table 2). As noted above, initially all the specimens were held at 1000° for 40 min. In order to check whether this holding time is sufficient for attainment of equilibrium distribution of the cations at this temperature, we held a number of specimens at 1000° for 10 hours. The longer heating time did not result in any significant modification of the σ_s vs T curves for the quenched specimens.

As noted above, after quenching the specimens were subjected to step anneals. The σ_s vs T curves for the annealed-after-quenching specimens increasingly ap-

---

*Reverse magnetization is here understood to mean the magnetization obtaining in the ferrite above the compensation temperature and directed antiparallel to the resultant magnetization below this temperature.

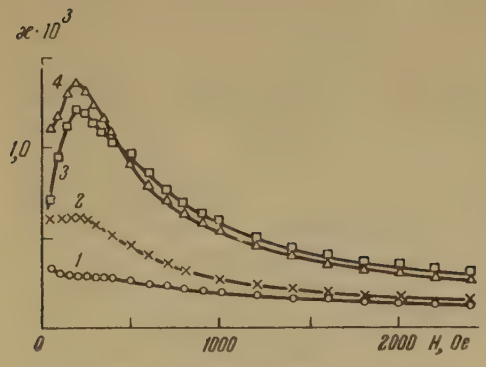

Fig.8. Field dependence of the susceptibility at the compensation temperature for $Li_2O \cdot 2.5Fe_2O_3 \cdot 2.5Cr_2O_3$ ferrite after different heat treatments: 1) initial state, 2) quenching from 1000° in air, 3) annealing for 5 hours at 500°, 4) annealing for 24 hours at 500°.

proached the corresponding curve for the given substance in the initial state as the annealing temperature and time increased (Figs.1,2 & 3). In the case of $Li_2O \cdot 1.6Fe_2O_3 \cdot 3.4Cr_2O_3$ a compensation point appeared in the curves only after annealing at 1000°; the curve in this case was virtually identical with the curve for the initial state.

Incomplete compensation, i.e., the persistence of a certain spontaneous magnetization at the compensation temperature, obtained also in the annealed states. This is evident in Fig.8 which shows the field dependences of the susceptibility at the compensation temperature for $Li_2O \cdot 2.5Fe_2O_3 \cdot 2.5Cr_2O_3$ specimens subjected to different heat treatments. The curves evince a pronounced ferromagnetic character.

Thus heat treatment (quenching and annealing) exerts a strong influence on the appearance of the σ_s vs T curves and the compensation and Curie point temperatures. Apparently all heat treatments substantially modify the cation distribution between the sublattices; quenching apparently results in breakdown of the ordered distribution of cations in the tetrahedral sublattice, the existence of which in lithium chromium ferrites was inferred by Gorter.[2]

3. Discussion

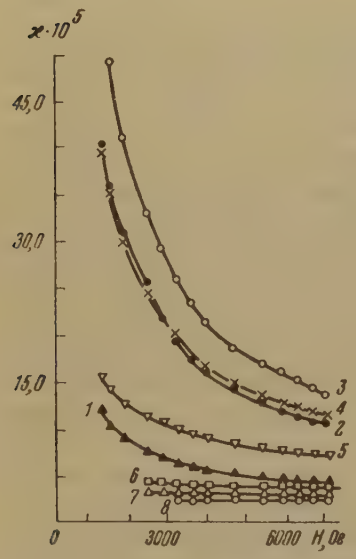

Fig.9. Field dependence of the paramagnetic susceptibility of $Li_2O \cdot 1.6Fe_2O_3 \cdot 3.4Cr_2O_3$ ferrite in the initial state at different temperatures: 1) +21.3°, 2) 55.5°, 3) 101.6°, 4) 130°, 5) 150°, 6) 169.2°, 7) 183° and 8) 219.5°C.

The results of our measurements show that in a certain range of compositions ferromagnetic Li-Fe-Cr spinels actually do have an anomalous temperature dependence of the spontaneous magnetization σ_s with a compensation point, which was earlier predicted by Néel. In conflict with theory, however, we found that the compensation is never complete. Initially it was hypothesized that the incomplete compensation might be due to the presence of some extraneous ferromagnetic impurity, for example, magnetite, which could conceivably form in the process of synthesis. To check this hypothesis we measured the magnetization on a ballistic setup in a certain temperature range beyond the Curie point and also carried out measurements of the paramagnetic susceptibility by the ponderomotive procedure up through temperatures well above the Curie point of magnetite (+587°). The results of these measurements showed that there was no magnetite present in our specimens. This is clearly evident from Fig.9 which shows the field dependence of the susceptibility of one of the investigated compositions at different temperatures. Above +219° the susceptibility becomes independent of the field; this indicates that the specimen is in the paramagnetic state.

The incomplete compensation effect can be explained by heterogeneity, i.e., inhomogeneity of the investigated specimens, associated with fluctuations of the chemical composition over the volume. Inasmuch as the compensation temperature depends on the composition, in the case of heterogeneous composition, the compensation points will be different in different regions of the specimen.

Let us assume, therefore, that there are regions in the material with different - if only slightly - compensation points. Then at the average temperature in the compensation temperature range there will obtain "spurious compensation". At this temperature, we can distinguish two groups of regions, characterized by spontaneous magnetization vectors aligned in opposite directions. At the "spurious compensation" temperature the residual magnetization of the material goes to zero inasmuch as after removal of the external magnetic field, the residual magnetization of one group of regions will be equal in magnitude and opposite in direction to the residual magnetization of the other group (Fig.10). Upon the application of an external field, however, the compensation will be disturbed inasmuch as the regions of the first and second groups, owing to the presence in them of a certain resultant magnetization at the "spurious compensation" temperature, will tend to align themselves with the field and, consequently, the material as a whole will possess a certain spontaneous magnetization. The value of this spontaneous magnetization at the compensation temperature will be the higher, the stronger the composition dependence of the compensation temperature. In the Li-Fe-Cr system this dependence is relatively weak and, consequently, the magnitude of σ_s at the compensation temperature is relatively low.

Another, more serious divergence between theory and experiment is that the absolute saturation calculated according to Néel from the cation distribution differs substantially from the experimental data (column 3 & 5 in Table 2).

The modification of the Néel theory proposed by Yafets & Kittel[8] is capable of explaining the observed divergence. The important point is that inasmuch as in these ferrites the measured value of the magnetic moment is smaller than that calculated by the Néel theory and M_B is greater than M_A, in this case one cannot neglect the negative exchange interaction in the B sublattice (B-B interaction) as compared with the interactions between the A and B sublattices (A-B interaction). The existence of the B-B interaction leads to subdivision of the B sublattice into two sublattices with magnetic moments at an angle to each other (triangular case). This leads to reduction of the total magnetic moment of sublattice B and, consequently, to decrease of the magnetic moment of the ferrite as a whole. True, in the presence of angles between the magnetic moments in the sublattices, the shape of the σ_s vs T curve cannot be anomalous, while in our case it is obviously anomalous. However, it has been shown in the work of Yafet & Kittel[8] and Gorter[2] and later by Lotgering[9] that there cannot be a direct transition from the triangular state to the paramagnetic state. The angles existing in the B sublattice at low temperatures "break down" incident to heating; only after this and realization of antiparallel orientation of the magnetic moments of the sublattices, can the material become paramagnetic upon further heating. The appearance of anomalous σ_s vs T curves does become possible, however, if we assume that the angles break down at some temperature below the compensation temperature.

Knowing the resultant moment from experiment, we can calculate the angle between the magnetic moments in sublattice B, obtaining at low temperatures, by making use of the expression for the resultant moment at $0^{\circ}K$ deduced by Yafet & Kittel. According to Yafet & Kittel, in the case of the triangular configuration in sublattice B, the resultant moment of the ferrite is

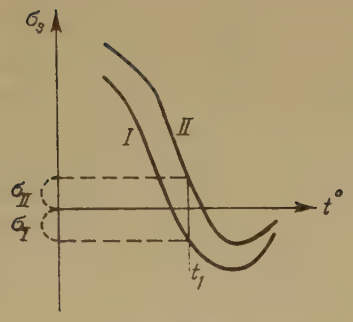

Fig.10

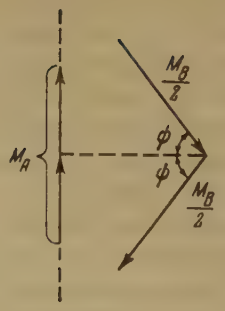

Fig.11

Fig.10. Diagram illustrating "incomplete compensation": I - temperature dependence of the spontaneous magnetization of group I regions in the temperature interval including the compensation point; II - temperature dependence of the spontaneous magnetization of group II regions in the same temperature interval; t_1 - "spurious compensation" temperature at which $\sigma_I = -\sigma_{II}$.

Fig.11. Arrangement of ionic magnetic moments in sublattices A and B in the presence of negative B-B interaction comparable to A-B interaction.

$$M = M_B \sin \varphi - M_A. \qquad (3)$$

Here M_A and M_B are the sums of the ionic magnetic moments in sublattices A and B, respectively, and $(180 - 2\varphi)$ is the angle between the directions of the magnetic moments in sublattice B (Fig.11).

For example, according to the data given by Gorter, distribution of ions in $Li_2O \cdot 2.5Fe_2O_3 \cdot 2.5Cr_2O_3$ ferrite is characterized by

$$Fe_{0.91}Li_{0.009}[Li_{0.41} \cdot Fe_{0.34} \cdot Cr_{1.25}]O_4.$$

Using the spin values of the magnetic moments for the Fe^{3+} and Cr^{3+} ions ($5\mu_B$ and $3\mu_B$, respectively), we obtain for this ferrite $M_A = 4.55$ and $M_B = 5.45$. The measured magnetic moment in the initial state is $M = 0.68$. Thus making use of Eq.(3), we can calculate the angle between the magnetic moments in sublattice B. Such calculations yield reasonable values for the angles for all the ferrites for which we have values of σ_o in the initial state.

Our measurements show that the absolute value of the magnetic saturation in the Li-Fe-Cr system increases as a result of quenching. There are data in the literature on the influence of quenching on σ_o in different simple and mixed ferrites[10,11] and there have been proposed theories[12-14] for explaining the experimental results. According to theories, σ_o depends on the distribution of cations among the A and B sites, while the cation distribution in turn depends on the temperature. Quenching "freezes" the cation distribution obtaining at the quenching temperature, which obviously leads to a change of σ_o as compared with the initial state. Smart[13] gives a method for determining the cation distribution in mixed ferrites with three metallic ions from the experimental 0°K values of the magnetic moment and g factor. In his treatment Smart assumes that the antiparallel arrangement of the magnetic moments in sublattices A and B is retained in all cases. In our case the situation is somewhat more complicated inasmuch as in our ferrites incident to quenching there may occur not only redistribution of the cations but also a change of the angles between the magnetic moments in the sublattices. The possible and unpredictable influence of these two factors precludes comparing our experimental results for the saturation after quenching with the present theories.

The degree of influence of these two factors can probably be determined on the basis of x-ray and particularly neutron diffraction studies.

We take this opportunity to express our gratitude to K.G.Khomiakov and T.I. Bulgakova for facilitating the preparation of the specimens in their laboratory and for valuable advice and suggestions.

Faculty of Physics
Moscow State University

References

1. L.Néel, Ann.phys., 3, 137 (1948).
2. E.W.Gorter, Philips Res.Repts.,9, 295 (1954).
3. R.Pauthenet, Compt. rend., 242, 1859 (1956).
4. K.P.Belov, K.M.Bol'shova & T.A.Elkina, Izv.AN SSSR, Ser.fiz., 21, 1047 (1957). (Trans.Bulletin 21, No.8, 1051.)
5. K.M.Bol'shova & T.A.Elkina, Vestnik, Moscow State Univ., 2, 95 (1957).
6. K.P.Belov & A.N.Goriaga, Fiz.met.i metallovedenie, 2, 1 (1956).
7. V.L.Ginzburg, Zhur.eksp.i teor.fiz., 17, 833 (1947).
8. Y.Yafet & C.Kittel, Phys.Rev., 87, 290 (1952).
9. F.K.Lotgering, Philips Res.Repts., 11, 190-249 (1956).
10. R.Pauthenet & L.Bochirol, J.Phys. et radium, 12, 249 (1951).
11. N.Sakamoto, T.Asahi & S.Miyahara, J.Phys.Soc., Japan, 8,677 (1953).
12. L.Néel, Ct.rend., 230, 190 (1950).
13. J.Smart, Phys.Rev., 94, 847 (1954).
14. H.B.Callen, S.E.Harrison & C.J.Kriessman, Phys.Rev., 103, 851 (1956).

Bulletin of the Academy of Sciences of the USSR - Physical Series
Vol. 22, No. 10 - October 1958
Transactions of the All-Union Conference on the Physics of Magnetic Materials

TABLE OF CONTENTS

	Page Orig.	Trans.
Dynamic constants of magnetically polarized magnetoelastic (magnetostrictive) and electrically polarized (electrostrictive) media - K.B.Vlasov	1159	1149
Phenomenological theory of ferromagnetism and antiferromagnetism at low temperatures (uniaxial case) - E.A.Turov & Iu.P.Irkhin	1168	1158
Magnetic structure and technical magnetization processes in high-coercivity ferromagnets - Ia.S.Shur	1177	1167
Domain structure dynamics in transformer iron crystals under the influence of stresses - L.V.Kirenskii, M.K.Savchenko & A.M. Rodichev	1181	1171
Changes in the magnetic structure of silicon iron crystals under the influence of elastic stress - V.A.Zaikova & Ia.S.Shur	1185	1177
Magnetic structure of a ferromagnet in the remanence state and changes therein incident to demagnetization by an alternating field - I.E.Startseva & Ia.S.Shur	1189	1183
Temperature stabilization of the magnetic properties of alloys - I.M.Puzei	1194	1188
Magnetic anisotropy and hysteresis loss in rotating magnetic fields in a magnetite single crystal at low temperatures - N.N.Narovskaia	1200	1194
Nature of the effect of thermomagnetic treatment in magnetically soft ferromagnets - A.A.Glazer & Ia.S.Shur	1205	1198
Investigation of the kinetics of magnetic domain-orientation in 65% Permalloy - Sh.I.Zusman	1212	1204
Synthesis and magnetic properties of ferrites with a rectangular hysteresis loop - L.I.Rabkin, S.A.Soskin & B.Sh.Epshtein	1217	1210
Kinetics of thermomechanical treatment of ferromagnets - F.N.Dunaev	1225	1217
Grain-orientation in the process of annealing cold-rolled transformer steel - L.V.Mironov	1231	1223
Magnetic analysis of the deformation structure due to cold rolling and recrystallization in pure electrolytic nickel - N.L. Briukhatov, N.A.Grinchar & I.Ia.Ekamasov	1237	1229

Magnetostriction of nickel-iron-molybdenum alloys - I.M.Puzei & B.V.Molotilov 1244 1236

Volume magnetostriction in iron-nickel-molybdenum alloys - I.M.Puzei, B.V.Molotilov & A.I.Rad'kov 1251 1243

Magnetostrictive properties of binary alloys - G.P.D'iakov 1254 1246

Dependence of the sensitivity of magnetostrictive ultrasonic detectors on their magnetic characteristics - Ia.S.Shur, M.G.Luzhinskaia, K.B.Vlasov, O.I.Shiraeva & V.A.Zaikova 1259 1250

Molybdenum induced modifications of the structural transformations in Permalloy - Iu.S.Avraamov, B.G.Livshits & V.B.Osvenskii 1263 1253

Anisotropy of the coercive force in magnetically anisotropic fine-powder specimens - E.V.Shtol'ts, Ia.S.Shur & G.S.Kandaurova 1269 1258

Concerning the temperature dependence of the magnetic properties of high-coercivity alloys - N.A.Baranova & Ia.S.Shur 1272 1262

On the physics of magnetodielectrics - L.I.Rabkin 1276 1266

Magnetic properties of ferrites with a compensation point - K.P.Belov, K.N.Bol'shova, T.A.Elkina & M.A.Zaitseva 1282 1272

The transactions of the conference will be continued in the Vol. 23, No. 3 issue.

Translated in 1959 by
Columbia Technical Translations
5 Vermont Ave., White Plains, N.Y.

Number 11 Volume 22 1958

BULLETIN

of the

Academy of Sciences of the USSR

- Physical Series -

(Izvestiia Akademii Nauk SSSR)
(Seriia fizicheskaia)

Reproduction rights reserved

by

Columbia Technical Translations
5 Vermont Avenue
White Plains, New York

Single Issues
$20

Annual Subscription
$215

Title page →

Transactions

of the

Eleventh All-Union Conference on Theoretical Spectroscopy

(Continued from Vol.22, No.6 and No.9.)

MEASUREMENT AND CALCULATION OF THE POLARIZATION OF THE EMISSION OF HELIUM ATOMS EXCITED BY ELECTRON IMPACT

- L.A.Vainshtein & G.G.Dolgov

Experimental and theoretical investigation of the polarization of impact induced emission is important from the standpoint of the theory of electron-atom collisions. The polarization of emission as a function of the velocity of the incident electrons in the case of excitation of Hg atoms was investigated by Skinner & Appleyard[1], who showed that the variation of the polarization with the electron velocity is not monotonic, but goes through a maximum some 3-4 ev above the excitation threshold. This result disagrees both quantitatively and qualitatively with the theory based on the first Born approximation[2]. There have been no experimental or theoretical investigations of this important problem since the publication of Skinner & Appleyard's work.

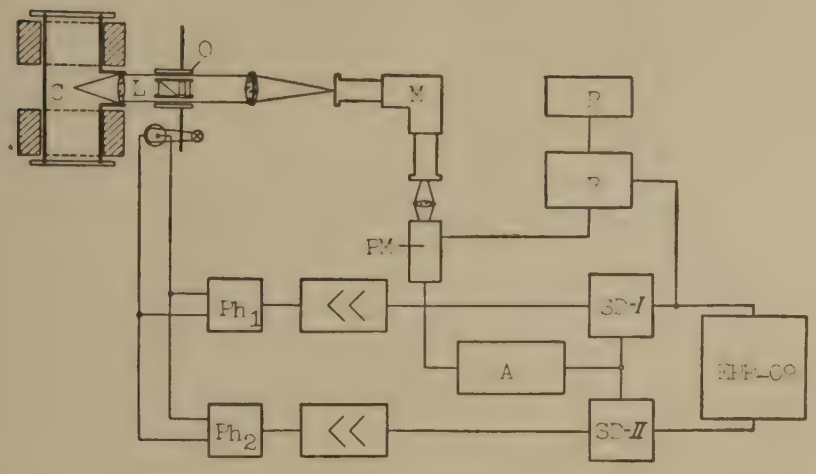

Fig.1. Diagram of apparatus: C - chamber in which gas is excited, L - lens, O - shutter, M - monochromator, B - battery, R - regulated photomultiplier voltage supply, A - narrow band amplifier, Ph_1 & Ph_2 phase-shifting network, PM - photomultiplier.

We undertook an experimental and theoretical investigation of the polarization in the excitation of helium atoms. A block diagram of the experimental apparatus is shown in Fig.1. The investigated gas, contained in chamber C at a pressure of $2\cdot10^{-4}$ mm Hg, was excited by an electron beam with a current density of up to $5\mu a/mm^2$. The electron energy spread was 0.5-0.7 ev on the average. The exciting electron beam was in a uniform magnetic field, directed along the beam. Thus the focusing of the beam did not change with variation of the voltage on the control electrode of the electron gun. Control experiments showed that the polarization of the emission was not affected by the intensity of the magnetic field in the range from 0 to 1000 gauss. All the measurements were carried out at a field strength of 100 gauss.

The parallel light beam from the lens L passed through the sector shutter in the center of which was a polaroid. The desired spectral line was selected by the monochromator M. The modulated light beam fell on the photomultiplier, the signal from which was amplified by the narrow band amplifier A. It can be shown that the signal at the amplifier output is described by

$$A = (I_{\parallel} + I_{\perp})\cos 2\omega t + (I_{\parallel} - I_{\perp})\sin 2\omega t, \qquad (1)$$

where $I_{\parallel}$ and $I_{\perp}$ are the intensities of the beam components polarized parallel and perpendicular to the electron beam, respectively, and ω is the frequency of the shutter.

The amplified signal is applied to the two synchronous detectors SD-I and SD-II, the voltages on which are shifted 90° relative to each other. As a result,

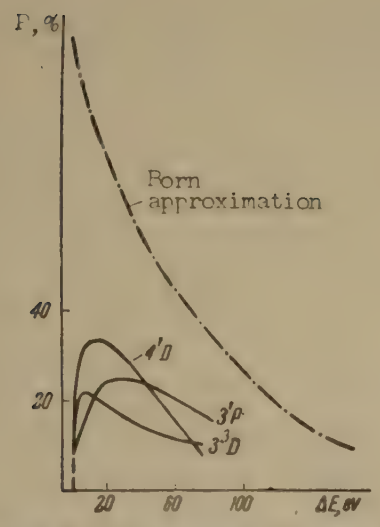

Fig.2. Variation of the polarization with the electron energy.

the voltage at the output of the first detector is proportional to $I_{\parallel} - I_{\perp}$; that on the output of the second to $I_{\parallel} + I_{\perp}$. The signal from the second detector was applied to an EPP-09 rheochord (slide wire rheostat); that from the first detector to the slider of the rheochord. Thus, varying the voltage on the control electrode of the electron gun, we obtain the variation of the degree of polarization as a function of the incident electron velocity:

$$P(v) = \frac{I_{\parallel} - I_{\perp}}{I_{\parallel} + I_{\perp}}. \qquad (2)$$

Fig.2 shows the variation of the polarization as a function of the incident electron velocity for three He lines. It will be evident that the energy dependence of the polarization is nonmonotonic. In the case of excitation of the 3^1P state (polarization of the emission with λ = 5016 Å), the maximum degree of polarization is attained at an energy ~20 ev above the threshold; in the case of the 3^3D and 4^1D states (λ = 4471 and 4921 Å) at energies of ~5 ev and ~15 ev above the excitation threshold, respectively.

In the theoretical discussion of the results we shall consider only excitation of $1^1S - n^1P$ atomic transitions. The polarization curve obtained for this case in the first Born approximation is also shown in Fig.2.

The relation $P(v_{thresh}) = 1$ is readily obtained from consideration of the partial waves of the exciting electrons. At low electron energies the principal contribution is made by the partial waves with the minimum value of l allowed by the conservation law. Hence where excitation of the $^1S - {}^1P$ transition is concerned, one should consider the $s - p$ and $p - s$ transitions of the incident electron. The cross sections σ_{s-p} and σ_{p-s} for these two processes are found independently.

In the $p - s$ transition there are excited atomic sublevels with $m_z = 0$ (z is the direction of the incident electron beam); in the $s - p$ transition there are excited sublevels with m_z = -1, 0 and +1 with equal probability. Hence we obtain the following formula for the polarization of the emission in the direction perpendicular to the incident beam:

$$P(v) = \frac{\sigma_{p-s}}{\sigma_{p-s} + \frac{2}{3}\sigma_{s-p}}. \qquad (3)$$

It can readily be shown that in the first Born approximation

$$\sigma \sim k_0^{2l_0} \cdot k_1^{2l_1}, \qquad (4)$$

where the subscripts 0 and 1 denote the initial and final states. It follows from the above that near the threshold $\sigma_{s-p} \gg \sigma_{p-s}$ and $P(v_{thresh}) = 1$. Taking exchange terms into account does not affect this result.

Taking into account the distortion of the incident and scattered waves by the mean field of the atom does not substantially change the relation between $s - p$ and $p - s$ scattering near the threshold.[3] This is due to the short effective range of the exponentially decreasing atomic field.

To obtain a more precise description of the variation of polarization near the threshold one must apparently take into account long-range terms in the Schrödinger equations for the incident and scattered waves. An illustrative example here is furnished by the term characterizing the interaction between the elastically and inelastically scattered waves. When this term is included in the elastic scattering equation (strong coupling treatment), the radial equations become

$$\left.\begin{aligned} &\frac{d^2f_1}{dr^2} + (k_0^2 + v_{00})\, f_1 = v_{01} f_2; \\ &\frac{d^2f_2}{dr^2} + \left(k_1^2 + v'_{nn} - \frac{2}{r^2}\right) f_2 = v_{01} f_1; \end{aligned}\right\} \quad (s-p)$$

$$\left.\begin{aligned} &\frac{d^2f_3}{dr^2} + \left(k_0^2 + v_{00} - \frac{2}{r^2}\right) f_3 = v'_{01} f_4; \\ &\frac{d^2f_4}{dr^2} + (k_1^2 + v_{nn})\, f_4 = v'_{01} f_3; \end{aligned}\right\} \quad (p-s) \qquad (5)$$

The potential v'_{nn} differs from v_{nn} by the presence of a dipole interaction term (also long-range); v_{01} and v'_{01} differ only by a constant factor.

The set of equations (5) was solved on a "Strela" electronic computer. The computer program was set up to allow of solution of the collision problem for an extensive class of atoms and transitions. The program provides for simultaneous solution of four equations such as (5), determination of the phases from the asymptotic solution trend and evaluation of two cross sections (for example, σ_{s-p} and σ_{p-s}).

So far only preliminary results have been obtained. Specifically it was determined that for the 1^1S-3^1P transition in the He atom with $k_1 = 0.2$, $\sigma_{s-p} > \sigma_{p-s}$.

"P.N.Lebedev" Physical Institute,
Academy of Sciences of the USSR

References

1. H.W.Skinner & E.T.S.Appleyard, Proc.Roy.Soc., 117A, 224 (1928).
2. H.A.Bethe, Quantum Mechanics of One- and Two-Electron Atoms (Cited in Russian trans.).
3. G.G.Dolgov, Optika i spektroskopiia, 4, 268 (1958).

MEASUREMENT AND CALCULATION OF THE POLARIZATION OF THE EMISSION OF HELIUM ATOMS EXCITED BY ELECTRON IMPACT

- L.A.Vainshtein & G.G.Dolgov

Experimental and theoretical investigation of the polarization of impact induced emission is important from the standpoint of the theory of electron-atom collisions. The polarization of emission as a function of the velocity of the incident electrons in the case of excitation of Hg atoms was investigated by Skinner & Appleyard[1], who showed that the variation of the polarization with the electron velocity is not monotonic, but goes through a maximum some 3-4 ev above the excitation threshold. This result disagrees both quantitatively and qualitatively with the theory based on the first Born approximation[2]. There have been no experimental or theoretical investigations of this important problem since the publication of Skinner & Appleyard's work.

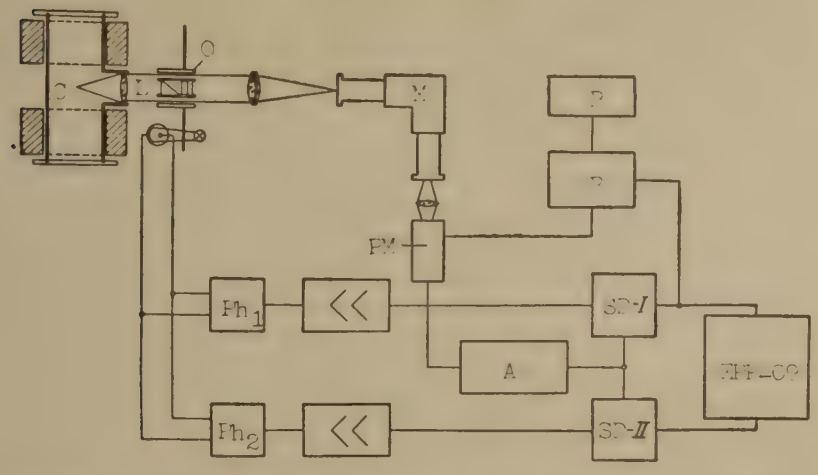

Fig.1. Diagram of apparatus: C - chamber in which gas is excited, L - lens, O - shutter, M - monochromator, B - battery, R - regulated photomultiplier voltage supply, A - narrow band amplifier, Ph_1 & Ph_2 phase-shifting network, PM - photomultiplier.

We undertook an experimental and theoretical investigation of the polarization in the excitation of helium atoms. A block diagram of the experimental apparatus is shown in Fig.1. The investigated gas, contained in chamber C at a pressure of $2 \cdot 10^{-4}$ mm Hg, was excited by an electron beam with a current density of up to $5 \mu a/mm^2$. The electron energy spread was 0.5-0.7 ev on the average. The exciting electron beam was in a uniform magnetic field, directed along the beam. Thus the focusing of the beam did not change with variation of the voltage on the control electrode of the electron gun. Control experiments showed that the polarization of the emission was not affected by the intensity of the magnetic field in the range from 0 to 1000 gauss. All the measurements were carried out at a field strength of 100 gauss.

The parallel light beam from the lens L passed through the sector shutter in the center of which was a polaroid. The desired spectral line was selected by the monochromator M. The modulated light beam fell on the photomultiplier, the signal from which was amplified by the narrow band amplifier A. It can be shown that the signal at the amplifier output is described by

$$A = (I_{\parallel} + I_{\perp}) \cos 2\omega t + (I_{\parallel} - I_{\perp}) \sin 2\omega t, \qquad (1)$$

where $I_{\parallel}$ and $I_{\perp}$ are the intensities of the beam components polarized parallel and perpendicular to the electron beam, respectively, and ω is the frequency of the shutter.

The amplified signal is applied to the two synchronous detectors SD-I and SD-II, the voltages on which are shifted 90° relative to each other. As a result,

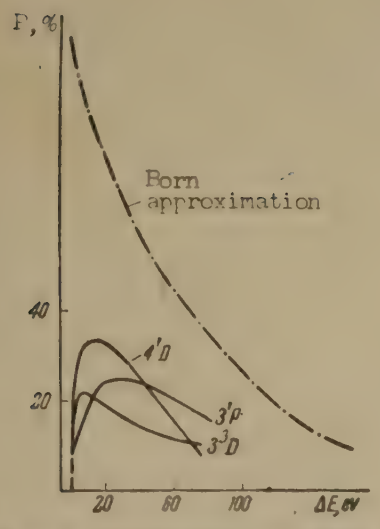

Fig.2. Variation of the polarization with the electron energy.

the voltage at the output of the first detector is proportional to $I_{\parallel} - I_{\perp}$; that on the output of the second to $I_{\parallel} + I_{\perp}$. The signal from the second detector was applied to an EPP-09 rheochord (slide wire rheostat); that from the first detector to the slider of the rheochord. Thus, varying the voltage on the control electrode of the electron gun, we obtain the variation of the degree of polarization as a function of the incident electron velocity:

$$P(v) = \frac{I_{\parallel} - I_{\perp}}{I_{\parallel} + I_{\perp}}. \qquad (2)$$

Fig.2 shows the variation of the polarization as a function of the incident electron velocity for three He lines. It will be evident that the energy dependence of the polarization is nonmonotonic. In the case of excitation of the 3^1P state (polarization of the emission with λ = 5016 Å), the maximum degree of polarization is attained at an energy ~20 ev above the threshold; in the case of the 3^3D and 4^1D states (λ = 4471 and 4921 Å) at energies of ~5 ev and ~15 ev above the excitation threshold, respectively.

In the theoretical discussion of the results we shall consider only excitation of $1^1S - n^1P$ atomic transitions. The polarization curve obtained for this case in the first Born approximation is also shown in Fig.2.

The relation $P(v_{thresh}) = 1$ is readily obtained from consideration of the partial waves of the exciting electrons. At low electron energies the principal contribution is made by the partial waves with the minimum value of l allowed by the conservation law. Hence where excitation of the $^1S - {}^1P$ transition is concerned, one should consider the $s - p$ and $p - s$ transitions of the incident electron. The cross sections σ_{s-p} and σ_{p-s} for these two processes are found independently.

In the $p - s$ transition there are excited atomic sublevels with $m_z = 0$ (z is the direction of the incident electron beam); in the $s - p$ transition there are excited sublevels with $m_z = -1$, 0 and +1 with equal probability. Hence we obtain the following formula for the polarization of the emission in the direction perpendicular to the incident beam:

$$P(v) = \frac{\sigma_{p-s}}{\sigma_{p-s} + \frac{2}{3}\sigma_{s-p}}. \qquad (3)$$

It can readily be shown that in the first Born approximation

$$\sigma \sim k_0^{2l_0} \cdot k_1^{2l_1}, \qquad (4)$$

where the subscripts 0 and 1 denote the initial and final states. It follows from the above that near the threshold $\sigma_{s-p} \gg \sigma_{p-s}$ and $P(v_{thresh}) = 1$. Taking exchange terms into account does not affect this result.

Taking into account the distortion of the incident and scattered waves by the mean field of the atom does not substantially change the relation between $s - p$ and $p - s$ scattering near the threshold.[3] This is due to the short effective range of the exponentially decreasing atomic field.

To obtain a more precise description of the variation of polarization near the threshold one must apparently take into account long-range terms in the Schrödinger equations for the incident and scattered waves. An illustrative example here is furnished by the term characterizing the interaction between the elastically and inelastically scattered waves. When this term is included in the elastic scattering equation (strong coupling treatment), the radial equations become

$$\left.\begin{aligned} &\frac{d^2f_1}{dr^2} + (k_0^2 + v_{00})\, f_1 = v_{01}\, f_2; \\ &\frac{d^2f_2}{dr^2} + \left(k_1^2 + v'_{nn} - \frac{2}{r^2}\right) f_2 = v_{01}\, f_1; \end{aligned}\right\} \quad (s-p)$$

$$\left.\begin{aligned} &\frac{d^2f_3}{} + \left(k_0^2 + v_{00} - \frac{2}{r^2}\right) f_3 = v'_{01}\, f_4; \\ &\frac{d^2f_4}{dr^2} + (k_1^2 + v_{nn})\, f_4 = v'_{01}\, f_3; \end{aligned}\right\} \quad (p-s) \qquad (5)$$

The potential v'_{nn} differs from v_{nn} by the presence of a dipole interaction term (also long-range); v_{01} and v'_{01} differ only by a constant factor.

The set of equations (5) was solved on a "Strela" electronic computer. The computer program was set up to allow of solution of the collision problem for an extensive class of atoms and transitions. The program provides for simultaneous solution of four equations such as (5), determination of the phases from the asymptotic solution trend and evaluation of two cross sections (for example, σ_{s-p} and σ_{p-s}).

So far only preliminary results have been obtained. Specifically it was determined that for the 1^1S-3^1P transition in the He atom with $k_1 = 0.2$, $\sigma_{s-p} > \sigma_{p-s}$.

"P.N.Lebedev" Physical Institute,
Academy of Sciences of the USSR

References

1. H.W.Skinner & E.T.S.Appleyard, Proc.Roy.Soc., 117A, 224 (1928).
2. H.A.Bethe, Quantum Mechanics of One- and Two-Electron Atoms (Cited in Russian trans.).
3. G.G.Dolgov, Optika i spektroskopiia, 4, 268 (1958).

EMISSION OF THE NEGATIVE HYDROGEN ION

- W.Lochte-Holtgreven

The processes of attachment of electrons to neutral hydrogen atoms and radiation by the negative hydrogen ions occur on an enormous scale on the surface of the Sun. The conditions on the Sun are such that, on the one hand, there is a thick atmosphere of H atoms inasmuch as the temperature of the Sun's surface is sufficiently high for complete dissociation of the H_2 molecules and, on the other hand, there are many free electrons as a result of ionization of both hydrogen atoms and metal atoms, particularly alkali metals. Such free electrons from time to time combine with the H atoms and form H^- ions. The energy released in the process reaches us in the form of radiation. Inasmuch as the relative velocity of the H atoms and electrons varies over a very wide range, there is emitted a continuous spectrum, which we all know as daylight. This hypothesis to explain the origin of daylight was proposed by Wildt[1]. The results of calculations made by Chandrasekhar regarding the intensity and wavelength distribution of the radiation from negative hydrogen ions are in such good agreement with solar observations that at present no astrophysicist doubts that sunlight must be attributed to H^- radiation.

The fundamental process is described by

$$H_{atom} + \epsilon = H^- + h\nu .$$

H^- is a stable ion with the helium configuration. Its stability has been established by mass spectroscopic studies. Actually, however, the H^- ion was first detected by Nernst in electrolysis of molten LiH which, contrary to expectations at the time, dissociated into Li^+ and H^-. The ionization energy of an H^- ion, i.e., the energy released as a result of attachment of an electron to the H atom, is only 0.75 v. Whereas for the other elements the continuous spectrum extends from the series limit to the side of shortwave lengths, in the given case the energy of the free-free electron transitions in the field of the H atom is of the same order as the ionization "work". Hence the H^- continuum associated with both free-bound and with free-free electron transitions extends from the infrared through the entire visible region into the far ultraviolet. The precise distribution of intensities can only be determined by calculations, which, in contrast to the case for other atoms, can be carried out precisely for hydrogen.

While the intensity distribution in the solar spectrum corresponds to the calculations of Chandrasekhar, physicists are faced with the problem of why Geissler tubes filled with hydrogen do not emit "sunlight". It would obviously be of scientific interest to reproduce sunlight artificially in a hydrogen filled discharge tube. Clearly, production of such radiation on a large scale would be of practical value. It turns out, however, that the formation of H^- ions is not readily susceptible of observation inasmuch as the processes occurring at different temperatures differ radically.

If the temperature is too low, there are no H atoms present (only H_2 molecules) and, naturally, the H^- continuum cannot appear.

If the temperature exceeds 3000°, an ample number of molecules dissociates, i.e., H atoms are present, but an adequate supply of free electrons is still lacking.

At still higher temperatures, part of the H atoms are ionized. Now there are both electrons and atoms in a sufficient number for formation of H^- ions and, accordingly, the H^- continuum can appear.

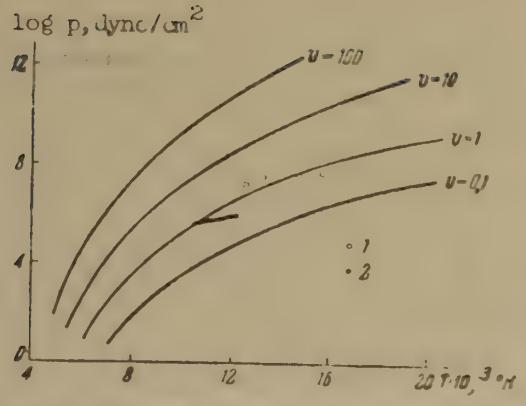

Fig.1. Theoretical ratio $v = I_{H^-}/I_H$ for a pure hydrogen atmosphere as a function of the temperature and pressure (after Vitense), 1 - values obtained in an arc discharge, 2 - values obtained for a spark.

If the temperature is still somewhat higher, there form many H^+ ions which "intercept" the free electrons. Consequently, ordinary recombination

$$H^+ + \epsilon = H + h\nu$$

obtains.

The situation is illustrated in Fig.1. Each curve corresponds to a constant value of the ratio $v = I_{H^-}/I_H$, the ratio of the intensity of H^- radiation to recombination radiation. It will be seen that in order to obtain a high intensity H^- continuum one must have a temperature somewhat under 8000°K and the highest possible pressure.

The curves of Fig.1 were calculated for a pure hydrogen atmosphere. What are the conditions on the Sun? The surface temperature there is of the order of 5000-6000°; the pressure about 10^4-10^5 dyne/cm^2. Hence the intensity ratio $v \approx 100$. It must be recalled, however, that in the solar atmosphere there are more free electrons than in a pure hydrogen atmosphere owing to the presence of readily ionized elements. Thus virtually the entire continuous spectrum of the Sun is due to H^- radiation. Would there be any advantage under laboratory conditions to add easily ionized elements to the hydrogen in the discharge tube in order to increase the free electron density and thereby the H^- radiation intensity? Analysis shows, however, that the problem cannot be solved so easily. The addition of a sufficient amount of impurities to increase noticeably the number of free electrons is accompanied by an increase in the intensity of the continuous radiation of the ionized atoms of these impurity elements and this radiation masks the H^- continuum. Hence there is no practical advantage to introducing easily ionized elements into the discharge tube. In this respect our laboratory equipment is at a disadvantage: owing to the huge size of the Sun, the influence of even a minute amount of alkali elements becomes noticeable. We shall return to this point below.

Thus in order to obtain intense H^- ion formation in the laboratory one must, according to Fig.1, produce a thermal plasma with the highest possible pressure and a temperature not exceeding 8000°. The use of an arc or spark discharge would seem indicated. At this point, however, we encounter a serious difficulty, namely, the good heat conductivity of gaseous hydrogen. Hence to maintain the arc one must supply a large amount of energy, i.e., there must necessarily be a high temperature at the arc axis. At atmospheric pressure, the temperature attains 11,000°K or higher, i.e., is too high for intense H^- emission. In attempting to obtain the continuous spectrum of H^-, we tried several approaches.

1) We observed an arc discharge at a temperature of 11-12,000°K in H_2 at atmospheric pressure[2]; as can be seen from Fig.1, in this case $v = I_{H^-}/I_H$ is only of the order of unity.

2) We observed a spark discharge through a capillary[3] filled with H_2; the discharge spectrum was observed by means of a rotating mirror. Inasmuch as after the discharge the temperature falls off rapidly, it proved feasible to work in the 12,500-16,000° interval with P = 30 atmos. Here again v is of the order of unity.

3) We observed arc discharges at pressures from 150 to 500 atoms, true, not in pure hydrogen but in an atmosphere of water vapor[4]; in this case the temperature was about 12,000°; hence $v \approx 15$.

What is the measurement technique for the H^- continuum? First the temperature and electron density are determined from the contours of the Balmer lines and then the I_{H^-}/I_H from Fig.1. If the absolute intensity of the observed continuous spectrum corresponds to the sum of the H^- and H continuums as calculated according to Chandrasekhar and, respectively, according to Lorentz, this substantiates the interpretation. If in addition the measured absolute intensity varies with the wavelength and temperature as predicted for the sum of the H^- and H spectra, we must assume that the interpretation of the measured spectrum is correct.

Inasmuch as the intensity of the Balmer lines at a given temperature can be calculated theoretically with high accuracy, one can with good precision determine the absolute intensity of the continuous spectrum from the relative measurements by experimental comparison of the lines and background.

We would now like to describe in some detail the new results obtained by the shock wave technique. As you know, the tube in which the shock wave is set up consists of a high pressure chamber, a diaphragm and a low pressure chamber. Upon rupture of the diaphragm, the shock wave is propagated in the low pressure chamber. The temperature of the shock wave depends on the gases used and the initial pressure ratio. The highest temperatures are attained for a high pressure ratio and in addition when a light diatomic gas drives a heavy monatomic one. The emission occurs in the low pressure, driven gas. Hence to observe the hydrogen continuum one must fill the low pressure chamber with hydrogen.

Since the driving gas must be as light as possible, again hydrogen would seem an obvious choice. In this case, however, too low a temperature is obtained: a weak emission is observed only in the reflected shock wave at the end of the tube. Hence for the low pressure gas one must use a mixture containing some heavy gas, preferrably one of the noble gases. We chose a mixture of krypton with hydrogen.[5] In this case one can expect a sufficiently high temperature, which can be regulated by varying the krypton concentration or the pressure ratio. The ionization potentials of hydrogen and krypton are almost equal. Hence the contribution of positive krypton ions to the intensity of the continuum will be of the same order of magnitude as the contribution of the positive H ions. Moreover, the degree of ionization of krypton is 12 times greater than the degree of ionization of hydrogen inasmuch as the ratios of the sums of the ion and neutral atom states that enter into the Saha equation for determining the electron concentration are 6 for krypton and 1/2 for hydrogen. Because of this krypton acts as an additional electron donor, i.e., gives the effect we originally tried to obtain by adding easily ionized elements. The temperature in the reflected shock wave* lay within the range from 8000 to 10,500°K; the pressure in the 8 to 29 atmos range. Hence we have a value of about 50 for the I_{H^-}/I_H ratio.

Fig.2 shows the calculated temperature dependence of this ratio. It will be seen that actually a nearly pure H^- continuum is observed.

Of great interest also is the variation of the H^- continuum with wavelength. This is plotted in Fig.3. It will be seen that the intensity falls off consistently as we go to shorter wavelengths, as required by theory. At about 4100 Å

---

*The observations were carried out for the reflected shock wave. According to the data of oscillographic measurements with an expanded sweep, the emission and, hence, the temperature were constant over an appreciable interval. The decrease of emission and temperature owing to attenuation of the shock wave distorts the results by not more than 10%.

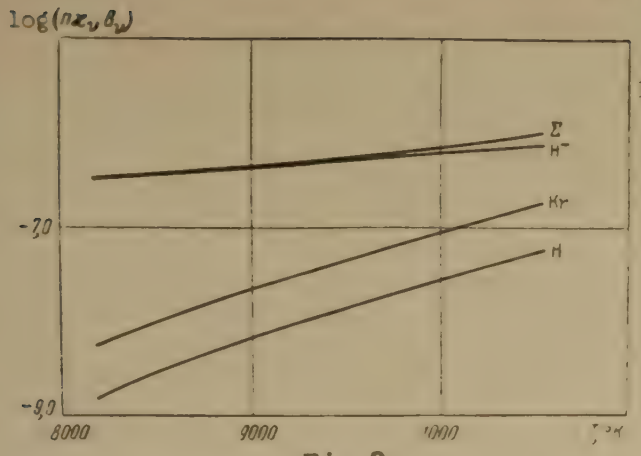

Fig.2

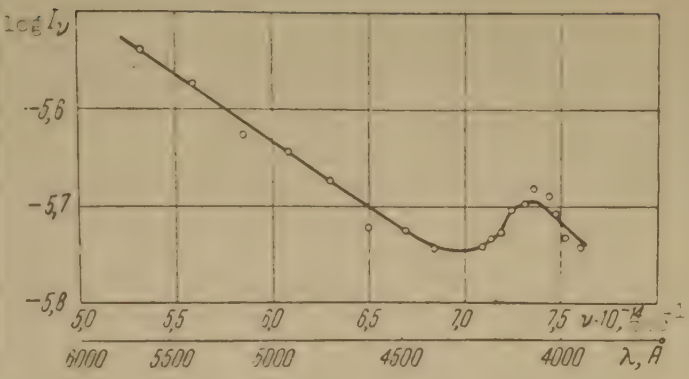

Fig.3

Fig.2. Calculated intensities of the continuous spectra of Kr, H and H^- as functions of the temperature (for λ = 4565 Å).

Fig.3. Measured variation of the H^- continuum with the wavelength.

there is a rise in intensity, which appears puzzling at first glance. It can be shown, however, that the jump in intensity at the Balmer series limit is due to broadening of the Balmer lines shifted to the side of longer wavelengths. Evaluation of the electron density on the basis of this displacement carried out by means of the Inglis-Teller[6] equation, led to a value which differs little from that obtained on the basis of the shock wave data. We also calculated the magnitude of the intensity jump. In Fig.4 we have plotted the calculated jump and its sum with the continuous spectra of krypton and H^- (logarithmic scale!). The integral curve is in close quantitative agreement with the measurement results.

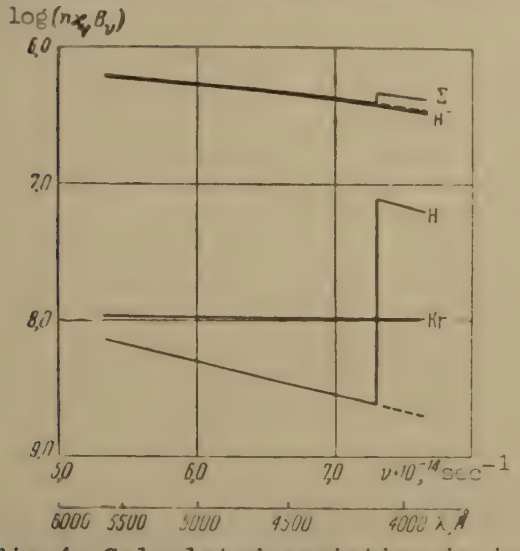

Fig.4. Calculated variation in intensity of the continuous spectra of Kr and H^- and of the H spectrum with the displaced series limit corresponding to an electron density $n_e = 1.5 \cdot 10^{17}$ cm^{-3}.

Thus we find that the H^- continuum can be detected in diverse light sources. In an arc or spark discharge there are superimposed upon it other continuous spectra of approximately the same intensity. In a shock wave there is observed an almost pure H^- spectrum, i.e., with an intensity 50 times greater than the continuous spectrum due to other factors. While we are still far from being able to make practical use of H^- radiation, we can safely assert that we have experimentally proved the mechanism of solar radiation.

To make sure that we have actually been dealing with the continuous spectrum of H^-, the experimental results were constantly compared with theory. Finally, we note that, as Fig.4 shows, the intensity of the H^- spectrum increases in going from shorter to longer wavelengths. At present we plan to follow the H^- spectrum into the infrared.

Institute of Experimental Physics,
Kiel University, Kiel, Germany

References

1. R.Wildt, Astrophys.J., 89, 295 (1939); Ibid., 90, 611 (1939).
2. W.Lochte-Holtgreven & W.Nissen, Z.Phys., 133, 124 (1952).
3. R.Fuchs, Z.Phys., 130, 69 (1951).
4. T.Peters, Z.Phys., 135, 573 (1953).
5. O.Weber, ZS.f.Phys. (to be published).
6. R.R.Inglis & E.Teller, Astrophys.J., 90, 439 (1939).

SPECTROSCOPIC INVESTIGATION OF THE ROTATIONAL MOBILITY OF MOLECULES IN QUASILIQUID CAMPHENE AND TRICYCLENE CRYSTALS

- Ang Men Tok, M.F.Vuks & D.S.Nedzvetskii

So-called quasiliquid crystals have a number of distinctive attributes. The investigations of Gross & Raskin[1] have shown that the Raman spectra of such crystals exhibit many similarities with the spectra for the liquid phase. Thus, for example, in the spectra of crystalline camphene and hexachloro ethane, they observed almost the same wings near the lines as in the spectra of the molten substances.

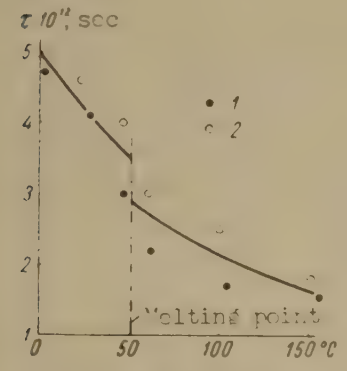

Temperature dependence of the orientational relaxation time τ of the camphene molecule: 1 - points obtained by the spectrographic method; 2 - points obtained by the resonance filter method.

The methods developed in our laboratory for investigating line broadening - the resonance filter procedure and the spectrographic method[2,3] - made it feasible to carry out a more careful comparison. We investigated two quasiliquid crystals, namely, camphene and tricyclene; the first substance melts at 51°; the second at 64°. The measurements were carried out in the range from 0 to 150°. Both substances, and particularly tricyclene, are characterized by very weak anisotropic scattering. This naturally hampered the investigation.

The accompanying figure shows the results obtained for camphene. The relaxation times were calculated by means of the Leontovich formula

$$I = \frac{1}{1+\tau^2\Delta\omega^2}, \qquad (1)$$

where I is the intensity at the distance $\Delta\omega$ from the center of the line and τ is the relaxation time. Measurements were made both by the spectrographic and the resonance filter methods. Allowing for the additional error due to the weak scattering, the results of both methods are in good agreement. This shows that Eq.(1) correctly describes the intensity distribution over the line contour. The curve shows that in the case of camphene there is only a slight decrease of the relaxation time in going from the solid crystalline to the liquid state. This means that the width of the scattering line remains virtually constant.

The same thing applies to the intensity of anisotropic scattering which, as may be seen from Table 1, increases very slightly. A more substantial change is observed in the isotropic component: its intensity almost doubles (second line in Table 1).

Table 1

Scattering intensity in camphene

Polarized component	Crystal at 22°	Liquid at 54°
Weak ($I_\parallel$)*	0.17	0.20
Strong ($I_\perp$)	0.8	1.5

*$I_\parallel$ for benzene taken equal to 1.

Similar results were obtained for tricyclene, except that in the case of this substance no abrupt change in the line width was detected at the melting point. It should be noted, however, that we could not come closer than 20° to the melting point owing to the development of opalescence which increases rapidly as the melting point is approached.

The relaxation times τ for camphene and tricyclene at three different temperatures are listed in Table 2. We note that the relaxation times in both substances are virtually equal, which, of course, is connected with the similarity of the structure and size of these two isomeric molecules.

Table 2

Relaxation times τ in 10^{-12} sec

Substance	Temperature		
	20°	Melting point	150°
Camphene	4.3	3.5; 2.9	1.6
Tricyclene	3.5	2.7	1.6

Our relaxation times are in good agreement with the values of $\tau_{dip}/3$ obtained by Gol'tsman & Raskin[4] for a number of quasi-liquid crystals with a similar chemical structure - camphor, bornyl chloride and α-chlorocamphor - by the method of anomalous dispersion of electromagnetic waves.

If we plot our data in 1/T vs log τ coordinates, we find that all the points for tricyclene fall on one straight line and those for camphene on two close straight lines - one for the crystal, the other for the liquid. This means that the temperature dependence of the relaxation time is adequately described by the familiar Frenkel formula: $\tau = \tau_0 e^{\frac{U}{kT}}$, where U is the height of the potential barrier for molecular reorientation. On the basis of our data we obtained the following values for U:

Camphene, crystalline	1.5 Kcal/mole
Camphine, liquid	1.3 " "
Tricyclene	1.3 " "

What conclusions can be drawn from our results?

The small change in the intensity of the anisotropic scattering in going through the melting point indicates that the orientational disorder in the crystal virtually does not differ from the disorder in the liquid. The fact that the line width is the same in the spectra of both the crystal and the liquid shows that the rotational mobility of the molecules in the quasiliquid crystal is virtually equal to the mobility in the liquid. These data substantiate Frenkel's inference[5] regarding orientational melting in quasiliquid crystals.

The absence of orientational order and the possibility of rapid molecular reorientation in wuch crystals are consequences of the low anisotropy and small elongation of the molecules. This is evinced by the low value of the molecular reorientation energy (1.3-1.5 Kcal/mole) which amounts to only twice the mean energy for one degree of freedom of vibrational motion.

References

1. E.F.Gross & A.I.Raskin, Zhur.eksp.i teor.fiz., 12, 409 (1942).

2. A.K.Atakhodzhaev, M.F.Vuks & V.L.Litvinov, Transactions of the Seventh All-Union Conference on Spectroscopy, Vol.1, p.118, L'vov Univ., 1957.

3. M.F.Vuks & A.K.Atakhodzhaev, Optika i spektroskopiia, 5, 52 (1958).

4. F.M.Gol'tsman & A.I.Raskin, Doklady AN SSSR, 89, 817 (1953).

5. Ia.I.Frenkel, Kineticheskaia teoriia zhidkostei, M.1945. (Translated as Kinetic theory of liquids, Oxford, 1946; N.Y., 1954.)

PHOSPHORESCENCE SPECTRA OF SOME AROMATIC ACIDS AT LIQUID AIR TEMPERATURE

- B.A.Piatnitskii

I. Benzene and its derivatives, including the aromatic acids, phosphoresce at low temperatures. Earlier[1,2], we studied the phosphorescence decay law and the lifetime of the metastable state in molecules of aromatic compounds at low temperatures. In the present work, we investigated the phosphorescence spectra of alcohol solutions of benzoic $[C_6H_5COOH]$, phthalic $[C_6H_4(COOH)_2]$, and gallic $[C_6H_2COOH(OH)_3]$ acids at the temperature of liquid air.

The phosphorescence spectra of phthalic and gallic acids were not investigated in previous studies[3-7] devoted to the phosphorescence of aromatic compounds at low temperatures[3-7]. Only Kowalski[3] gives some data on the phosphorescence spectrum of benzoic acid. The phosphorescence spectra of aromatic compounds at the temperature of liquid air consist of bands of different intensities and have a vibrational structure[6]. The phosphorescence bands are associated with transitions from an excited metastable level to the various vibrational levels of the ground state.

As was shown by Terenin[8], the metastable state of organic molecules is a triplet state, which is characteristic of the benzene ring in all aromatic compounds.

Phosphorescence involves violation of one of the fundamental spectroscopic selection rules - the rule forbidding intercombination - and frequently simultaneous infraction of another rule - that imposed by symmetry considerations[6]. Hence investigation of phosphorescence makes it possible to establish the limits of applicability of these basic assumptions of spectroscopy and to obtain some information on the triplet state of organic molecules. A study of the latter is meaningful since the triplet (biradical) state of organic molecules is supposedly the first stage in several important chemical reactions, especially oxidation.[9]

II. The phosphorescence was excited with a PRK-2 mercury tube. The spectra were photographed using an IS[illegible]-51 (1:2.3) three-prism glass spectrograph with an 0.04 mm slit. The alcohol solutions of the aromatic acids were placed in metallic cells of special design[2]. The luminescence was concentrated on the spectrograph slit by means of a mirror. The photographic shutter was located in front of the spectrograph slit. The spectrograms were scanned on an MF-2 photoelectric microphotometer.

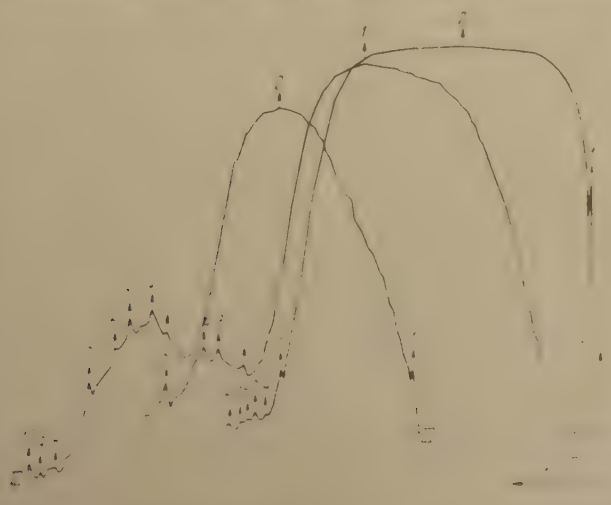

Fig.1. Microphotograms of the visible region of the phosphorescence spectra of: I) benzoic acid, II) phthalic acid, and III) gallic acid.

The microphotograms of the phosphorescence spectra of the alcohol solutions of benzoic, phthalic, and gallic acids are shown in Fig.1. The wavelengths were determined by interpolation between the lines of mercury, using Hartmann's formula.

III. Since the bands in phosphorescence spectra are usually explained as the result of transitions of the molecules from an excited (metastable) electronic level to the various vibrational levels of the ground state, the frequency differences between the band peaks in the phosphorescence spectra should be equal to the vibrational frequencies in the unexcited state or to combinations thereof.

Analyzing, in each of the spectra, the frequency difference between the peaks of the successive bands, we came to the conclusion that there were present in our spectra the specific vibrational frequencies ν^{I}, ν^{II}, ν^{III} and ν^{IV}. Using these we can calculate the frequencies of the band maxima in the phosphorescence spectra by means of the following equation:

$$\nu = \nu_0 - n_1\nu^{I} - n_2\nu^{II} - n_3\nu^{III} - n_4\nu^{IV}, \qquad (1)$$

where ν_0 is the frequency of the highest frequency peak and n_1, n_2, n_3 and n_4 are constants for each maximum. This equation also gives the series formula for each of the spectra. The values of ν_0 and the vibrational frequencies in each spectrum are listed in Table 1.

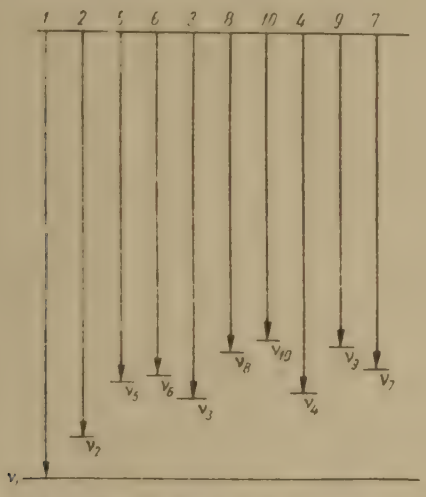

Fig.2. Diagram characterizing the bands in the phosphorescence spectrum of gallic acid.

Table 1

Acid	ν_0, cm^{-1}	vibrational frequencies, cm^{-1}			
		ν^{I}	ν^{II}	ν^{III}	ν^{IV}
Benzoic	24685	313	608	1187	826
Phthalic	21739	313	608	1182	992
Gallic	23283	313	608	1187	—

The vibrational frequencies of Table 1 were also observed in the spectra of other aromatic compounds[6,10]. The frequencies of the band peaks determined from the microphotograms and those calculated from the series formulas are given in Table 2. The formative diagram for the phosphorescence spectrum of gallic acid is given in Fig.2; here, the band peak lines are arranged in a series according to Table 2. An analysis of the phosphorescence spectra leads to the following conclusions.

1. The phosphorescence spectra of aromatic acids consist of a series of bands having maxima of different intensities. The phosphorescence spectrum of benzoic acid in the visible region extends from 4047 to 5431 Å and contains eight bands. The phosphorescence spectrum of phthalic acid is located in the 4034 to 5837 Å region and consists of five bands. The phosphorescence spectrum of gallic acid is located in the 4276 to 6293 Å region and contains 10 bands.

2. Phosphorescence spectra of aromatic acids at the temperature of liquid air have a vibrational structure.

3. All the acid spectra comprise two common vibrational frequencies ν^{I} = = 313 cm^{-1} and ν^{II} = 608 cm^{-1}, associated with vibrations in the C-H and C-C bonds of the benzene ring[6-9].

4. The frequencies of the band peaks satisfy Eq.(1) for all of the phosphorescence spectra.

5. Identical series of the form $\nu = \nu_0 - n_1\nu^{I}$ and $\nu = \nu_0 - n_2\nu^{II}$ appear in the phosphorescence spectra of benzoic and gallic acids.

Table 2

Peak No.	λ, Å	ν, cm^{-1} exper.	ν, cm^{-1} calc.	Series No.	Series formula	n
			I. Benzoic acid			
4	5133	19482	19472	I	$\nu=\nu_0-2\nu^{IV}-3\nu^{III}-n_1\nu^{I}$	$n_1=0$
7	5305	18850	18846			$n_1=2$
8	5388	18560	18533			$n_1=3$
1	4051	24685	24685	II	$\nu=\nu_0-n_2\nu^{II}$	$n_2=0$
3	5045	19822	19821			$n_2=8$
5	5203	19220	19213			$n_2=9$
2	4339	23047	23033	III	$\nu=\nu^0-2\nu^{IV}-n_3\nu^{III}$	$n_3=0$
4	5133	19482	19472			$n_3=3$
1	4051	24685	24685	IV	$\nu=\nu_0-n_1\nu^{I}$	$n_1=0$
6	5254	19033	19051			$n_1=18$
			II. Phthalic acid			
1	4600	21739	21739			
4	5433	18406	18383	I	$\nu=\nu_0-2\nu^{III}-\nu^{IV}-n_1\nu^{I}$	$n_1=0$
5	5735	17437	17444			$n_1=3$
2	5161	19376	19375	II	$\nu=\nu_0-2\nu^{III}-n_2\nu^{II}$	$n_2=0$
3	5328	18769	18767			$n_2=1$
			III. Gallic acid			
1	4295	23283	23283	I	$\nu=\nu_0-n_1\nu^{I}$	$n_1=0$
2	4739	21101	21092			$n_1=7$
5	5473	18271	18275			$n_1=16$
6	5569	17956	17962			$n_1=17$
1	4295	23283	23283	II	$\nu=\nu_0-n_2\nu^{II}$	$n_2=0$
3	5252	19040	19027			$r_2=7$
8	6021	16608	16595			$n_2=11$
10	6257	15982	15987			$n_2=12$
4	5337	18737	18714	III	$\nu=\nu_0-\nu^{I}-7\nu^{II}-n_3\nu^{III}$	$n_3=0$
9	6152	16355	16340			$n_3=2$
3	5252	19040	19027	V	$\nu=\nu_0-7\nu^{II}-n_1\nu^{I}$	$n_1=0$
7	5753	17482	17462			$n_1=5$

References

1. B.A.Piatnitskii, Izv.AN SSSR, Ser.fiz., 15, 597 (1951).
2. B.A.Piatnitskii, Doklady AN SSSR, 57, 771 (1947).
3. J.Kowalski, Z.Phys., 12, 956 (1911).
4. A.Krönenberger, Z.Phys., 63, 494 (1930).
5. I.V.Obreimov and A.F.Prikhot'ko, in Symposium "In Memory of S.I.Vavilov", p.197. M., 1952.
6. P.P.Dikun and B.Ia.Sveshnikov, Zhur.eksp.i teor.fiz., 19, 11, 1000 (1949).
7. E.V.Shpol'skii and A.A.Il'ina, Izv.AN SSSR, Ser.fiz., 15, 585 (1951); Zhur. eksp.i teor.fiz., 21, 2, 142 (1951).
8. A.N.Terenin, Acta Phys.Chim.URSS, 18, 210 (1943); Zhur.fiz.khim., 18, 1-2 (1944).
9. A.N.Terenin, Fotokhimiya krasitelei (Photochemistry of dyes), M., 1947.
10. M.V.Vol'kenshtein, M.A.El'iashevich and B.I.Stepanov, Kolebaniya molekul (Molecular Vibrations), Vol.II, M., 1949.

DETERMINATION OF THE ROTATIONAL CONSTANTS OF CH_3GeCl_3 FROM ITS MICROWAVE ABSORPTION SPECTRUM (Summary)

- N.A. Irisova

The report comprises data from a preliminary investigation[1] of the microwave absorption spectrum of CH_3GeCl_3 as well as new results on determination of the rotational constants A and C.

For the purpose of determining A and C, we recorded the absorption spectra of the compounds $CH_3GeCl_2^{35}Cl^{37}$ and $CH_3GeCl^{35}Cl_2^{37}$, which are asymmetrical-top rotators, at the natural concentrations of Cl^{35} and Cl^{37} for the J = 2→3, 4→5, 5→6 and 7→8 transitions. The experimental conditions for these new measurements were the same as described in Ref.1.

Owing to the low intensity of the $CH_3GeCl^{35}Cl_2^{37}$ lines, the uncertainty in determining their frequencies was ±15 Mc.

Transition J→J + 1	Average frequencies of $CH_3GeCl_2^{35}Cl^{37}$ absorption lines, Mc	Average frequencies of $CH_3GeCl^{35}Cl_2^{37}$ absorption lines Mc
2→3	9455	9315
4→5	15755	15530
5→6	18910	18665
7→8	25220	

We determined the frequencies and intensities of all (2J + 1) the asymmetrical-top components for each observed J transition and plotted the usual curves. The curve envelopes showed that the average frequencies of the observed lines correspond within the limits of the experimental error to the frequencies of the following transition components:

$2_{12}-\!\!>3_{22}$, $4_{14}-\!\!>5_{24}$, $5_{14}-\!\!>6_{26}$, $7_{26}-\!\!>8_{36}$.

Then by the method of successive approximations we determined the values of A, B and C at which the calculated frequency values agreed with the experimental values for the corresponding transitions.

For $C^{12}H_3Ge^{74}Cl_2^{35}Cl^{37}$ we finally obtained A = 1585 ± 2 Mc, B = 1567 ± 2 Mc and C = 1192 ± 25 Mc.

The large uncertainty for C is explained by the fact that the structure of the given molecule is close to a symmetrical-top rotator.

The writer desires to express her deep gratitude to A.M. Prokhorov for valuable discussions.

"P.N. Lebedev" Physical Institute,
Academy of Sciences of the USSR

Reference

1. N.A. Irisova, Optika i spektroskopiia, 4, 543 (1958).

METHOD OF QUASINORMAL COORDINATES IN CRYSTAL OPTICS

- V.S.Mashkevich

Introduction

There are two methods for treating electromagnetic waves in crystals. In the first, the wave field is considered to be external with respect to the particles constituting the crystal and thus the wave causes forced vibrations of the crystal lattice. This method may be called the external field method or the method of forced vibrations.

The other approach is more consistent and may be called the internal field method or the method of natural vibrations. It is based on the extinction theorem[1], according to which an incident electromagnetic wave does not penetrate into the crystal, but merely excites natural vibrations in it. One then deals not with forced vibrations, but with free vibrations of the system consisting of the internal field and the oscillating dipoles.

Accordingly, there exist two different ways of treating the absorption of infrared light by lattice vibrations. From the standpoint of the forced-vibration method, the light wave is absorbed as it transfers its energy to the lattice vibrations.[2] From the natural-vibration point of view, the absorption is due to anharmonic scattering of the energy of the vibrations which "carry the light". The fundamental process in the first method is first-order absorption. But in the usual treatment by the natural-vibration method one-phonon absorption is impossible since in the harmonic approximation the normal vibrations of the crystal lattice are independent. Thus the fundamental process in this method is second-order absorption.

In my opinion the reason for this disagreement is the following. The absence of one-phonon absorption in the natural vibration method results from assigning the propagation of an electromagnetic wave with a given wave vector $\mathbf{k}$ to a single normal vibration (with the same $\mathbf{k}$). I have shown,[3] however, that in a homopolar crystal a wave described by a single normal vibration with a definite frequency does not behave like a light wave. A wave that behaves like a light wave can be represented only by a superposition of two normal vibrations with the same $\mathbf{k}$, but with different frequencies. A wave represented in this way and having the character of a light wave can, however, undergo one-phonon absorption. I have given the name "quasinormal coordinates" to the superposition of normal coordinates designed to describe the propagation of light and its one-phonon absorption, since in a homopolar crystal the coupling between the vibrations of these coordinates is very small.

The present paper is a general description of the method of quasinormal coordinates and gives an application of this method to ionic crystals of the NaCl type.

Quasinormal Coordinates

There are at present two approximations used in the theory of crystal lattice vibrations. These are the point-particle (atom or ion) approximation[4] and the dipole approximation.[3,5] In the point-particle approximation, the state of a particle in the crystal is described by its displacement u (where l is the number of the unit cell, and s is the number of the particle in it). In the more accurate dipole approximation one must use, in addition to the displacement, the dipole moments due to deformation of the electron shells. One may write p, u and p' as superpositions of normal vibrations in the form

$$\mathbf{u}_s^l = \sum_{\alpha, \mathbf{k}} q^\alpha(\mathbf{k})\, \mathbf{u}_s^\alpha(\mathbf{k})\, e^{i\mathbf{k}\mathbf{r}_s^l},$$

$$\mathbf{p}_s^l = \sum_{\alpha, \mathbf{k}} q^\alpha(\mathbf{k})\, \mathbf{p}_s^\alpha(\mathbf{k})\, e^{i\mathbf{k}\mathbf{r}_s^l}, \tag{1}$$

where α is the number of the branch of the normal-vibration spectrum, the $\mathbf{u}_s^\alpha(\mathbf{k})$ and $\mathbf{p}_s^\alpha(\mathbf{k})$ are the normal-vibration amplitudes and the $q^\alpha(\mathbf{k})$ are normal coordinates.

According to the equations of motion, the $q^\alpha(\mathbf{k})$ are harmonic functions of the time. Hence with appropriate normalization of the displacement and dipole-moment amplitudes, the crystal energy in the harmonic approximation becomes

$$H = \sum_{\alpha, \mathbf{k}} [\dot{q}^\alpha(\mathbf{k})\, \dot{q}^\alpha(\mathbf{k}) + \omega_\alpha^2(\mathbf{k})\, q^\alpha(\mathbf{k})\, q^\alpha(\mathbf{k})], \tag{2}$$

where $\omega_\alpha(\mathbf{k})$ is the frequency of the corresponding normal vibration.

We introduce new generalized coordinates $Q^\alpha(\mathbf{k})$ by

$$q^\alpha(\mathbf{k}) = \sum_\beta c_{\alpha\beta}(\mathbf{k})\, Q^\beta(\mathbf{k}); \tag{3}$$

and then (1) becomes

$$\mathbf{u}_s^l = \sum_{\alpha, \mathbf{k}} Q^\alpha(\mathbf{k})\, \mathbf{U}_s^\alpha(\mathbf{k})\, e^{i\mathbf{k}\mathbf{r}_s^l},$$

$$\mathbf{p}_s^l = \sum_{\alpha, \mathbf{k}} Q^\alpha(\mathbf{k})\, \mathbf{P}_s^\alpha(\mathbf{k})\, e^{i\mathbf{k}\mathbf{r}_s^l}, \tag{4}$$

where

$$\mathbf{U}_s^\alpha(\mathbf{k}) = \sum_\beta c_{\beta\alpha}(\mathbf{k})\, \mathbf{u}_s^\beta(\mathbf{k}), \quad \mathbf{P}_s^\alpha(\mathbf{k}) = \sum_\beta c_{\beta\alpha}(\mathbf{k})\, \mathbf{p}_s^\beta(\mathbf{k}) \tag{5}$$

are new displacement and dipole-moment amplitudes. We normalize the $c_{\alpha\beta}$ by

$$\sum_\beta |\, c_{\beta\alpha}(\mathbf{k})|^2 = 1, \tag{6}$$

indicating equivalence of normalization of the new and old amplitudes; then in the Q coordinates H becomes

$$H = H^0 + H', \tag{7}$$

$$H^0 = \sum_{\alpha, \mathbf{k}} [\dot{Q}^\alpha(\mathbf{k})\, \dot{Q}^\alpha(\mathbf{k}) + \Omega_\alpha^2(\mathbf{k})\, \dot{Q}^\alpha(\mathbf{k})\, Q^\alpha(\mathbf{k})], \tag{8}$$

$$H' = \sum_{\mathbf{k}} \sum_{\alpha, \gamma} \Big[\sum_\beta \dot{c}_{\beta\gamma}(\mathbf{k})\, c_{\beta\alpha}(\mathbf{k})\, \dot{Q}^\gamma(\mathbf{k})\, \dot{Q}^\alpha(\mathbf{k}) + \sum_\beta{}' \omega_\beta^2(\mathbf{k})\, \dot{c}_{\beta\gamma}(\mathbf{k})\, c_{\beta\alpha}(\mathbf{k})\, \dot{Q}^\gamma(\mathbf{k})\, Q^\alpha(\mathbf{k}) \Big] + \text{c. c.}, \tag{9}$$

where c.c. denotes the complex conjugate quantity, and

$$\Omega_\alpha^2(\mathbf{k}) = \sum_\beta \omega_\beta^2(\mathbf{k})\, |\, c_{\beta\alpha}(\mathbf{k})|^2 \tag{10}$$

are the squares of the coordinates corresponding to the Q coordinates.

The essence of the quasinormal coordinate method is to choose the $c_{\alpha\beta}$ so as to obtain Q^α which will describe both light waves and vibrations which are known not to have the characteristics of light waves. Then H', which gives the coupling of different Q vibrations in the harmonic approximation, will describe one-phonon light absorption, and will thus give qualitative agreement with the forced-vibration method.

The specific choice of the $c_{\alpha\beta}$ is dictated, of course, by the particular type of crystal, but it must satisfy some general requirements that may be established by examining the internal electric field

$$\vec{\varepsilon}_s^{\,l} = \sum_{\alpha,\,\mathbf{k}} q^{\alpha}(\mathbf{k})\, \vec{\varepsilon}_s^{\,\alpha}(\mathbf{k})\, e^{i\mathbf{k}\mathbf{r}_s^l}, \tag{11}$$

where $\vec{\varepsilon}_s^{\,l}$ is the field strength at $\mathbf{r}_s^l$ due to all the dipoles in the crystal except that at the given point, and $\vec{\varepsilon}_s^{\,\alpha}(\mathbf{k})$ is the amplitude corresponding to the $\alpha\mathbf{k}$ normal vibration, and is given by

$$\vec{\varepsilon}_s^{\,\alpha} = \frac{1}{\Delta}\left\{\frac{4\pi}{3}\mathbf{p}^{\alpha} - 4\pi\frac{n_{\alpha}^2(\mathbf{p}^{\alpha}, \mathbf{s})\,\mathbf{s} - \mathbf{p}^{\alpha}}{n_{\alpha}^2 - 1}\right\} + \mathbf{f}_s(\mathbf{u}_1^{\alpha}, \ldots, \mathbf{p}_1^{\alpha}, \ldots, \mathbf{k}). \tag{12}$$

Here Δ is the volume of a unit cell,

$$\mathbf{p}^{\alpha} = \sum_s (\mathbf{p}_s^{\alpha} + e_s \mathbf{u}_s^{\alpha}), \tag{13}$$

is the charge of the s-th particle of the cell, $n_{\alpha}(\mathbf{k})$ is the index of refraction for the $\alpha\mathbf{k}$ vibration, $\mathbf{f}_s$ is a linear function of the displacements and dipole moments which approaches zero together with $\mathbf{k}$ and $\mathbf{s}$ is the unit vector in the $\mathbf{k}$ direction.

Transforming to Q coordinates in (11), we obtain

$$\mathbf{E}_s^l = \sum_{\alpha\mathbf{k}} Q^{\alpha}(\mathbf{k})\, \vec{\mathcal{E}}_s^{\,\alpha}(\mathbf{k})\, e^{i\mathbf{k}\mathbf{r}_s^l}, \tag{14}$$

where the new amplitude is

$$\vec{\mathcal{E}}_s^{\,\alpha} = \sum_{\beta} c_{\beta\alpha}\, \vec{\varepsilon}_s^{\,\beta}. \tag{15}$$

It is natural to require that for light waves $\vec{\mathcal{E}}_s^{\,\alpha}$ have a structure analogous to (12), and that it vanish for other vibrations. This requirement gives

$$\sum_{\beta} c_{\beta\alpha}\frac{n_{\beta}^2(\mathbf{p}^{\beta}, \mathbf{s})\,\mathbf{s} - \mathbf{p}^{\beta}}{n_{\beta}^2 - 1} = \frac{N_{\alpha}^2(\mathbf{P}^{\alpha}, \mathbf{s})\,\mathbf{s} - \mathbf{P}^{\alpha}}{N_{\alpha}^2 - 1} \tag{16}$$

where α signifies the light-wave branch, and

$$\sum_{\beta} c_{\beta\alpha}\, \vec{\varepsilon}_s^{\,\beta} = 0 \tag{17}$$

where α now signifies the nonlight-wave branch.

The $\mathbf{P}^{\alpha}$ are defined in analogy with (13); $N_{\alpha}(\mathbf{k})$ is the index of refraction corresponding to $Q^{\alpha}(\mathbf{k})$, and it follows from (10) that

$$\frac{1}{N_{\alpha}^2} = \sum_{\beta}\frac{|c_{\beta\alpha}|^2}{n_{\beta}^2}. \tag{18}$$

NaCl Type Ionic Crystals

The inclusion of the polarizability of the particles gives only quantitative corrections for ionic crystals, corrections which do not affect the qualitative aspects of the spectrum.[3,5] Since we are not attempting here to obtain quantitative results, we shall therefore make the point-ion approximation. The vibration spectrum consists of eight branches, three of which are acoustical and the rest optical (one longitudinal and four transverse). Of these, we shall consider the transverse optical vibrations since these are the ones that actively participate in the light propagation. For an ionic crystal H' is nonzero even in the

zeroth approximation in k: we shall restrict our treatment to this approximation. Then the frequencies pertaining to the two different polarizations are equal; this is therefore true of all other results. We shall therefore supress the polarization index.

The two indices in the $c_{\alpha\beta}$ take on the values 1 and 2, corresponding to the two q and two Q coordinates. Let Q^1 correspond to light vibrations; then the $c_{\alpha\beta}$ can be found from the general equations (16) and (17). Making use of the transverse polarization and inserting (12) into (17), we obtain

$$c_{12}\left(\frac{1}{3}+\frac{1}{n_1^2-1}\right)+c_{22}D\left(\frac{1}{3}+\frac{1}{n_2^2-1}\right)=0, \tag{19}$$

where D is a quantity which appears as a result of the normalization of amplitudes. Together with (6), (19) is sufficient for the determination of c_{12} and c_{22}. From (16), we obtain

$$\frac{c_{11}}{n_1^2-1}+\frac{c_{21}D}{n_2^2-1}=\frac{c_{11}+c_{21}D}{N_1^2-1}. \tag{20}$$

Inserting (18) and using (6) we find that

$$c_{11}\,c_{21}\left[\frac{c_{11}D}{n_1^2(n_2^2-1)}-\frac{c_{21}}{n_2^2(n_1^2-1)}\right]=0. \tag{21}$$

The vanishing solutions are discarded, for they lead to the initial original normal vibrations; therefore

$$\frac{c_{11}D}{n_1^2(n_2^2-1)}-\frac{c_{21}}{n_2^2(n_1^2-1)}=0. \tag{22}$$

Together with (6), Eq.(22) determines c_{11} and c_{21}. Thus the introduction of quasinormal coordinates has served its purpose.

Kiev Polytechnic Institute

References

1. C.W.Oseen, Ann.Phys., 42, 1 (1915); P.P.Edwald, Ann.Phys., 49, 1 (1916); W.Bothe, Ann.Phys. 64, 693 (1921).

2. R.E.Peierls, Quantum Theory of Solids, Oxford 1955.(Cited in Russian trans.)

3. V.S.Mashkevich, Thesis. Kiev 1956.

4. M.Born & M.Geppert-Meyer, Theory of Solids. (Cited in Russian trans., M.1938).

5. K.B.Tolpygo, Dissertation, Kiev, 1947; Zhur.eksp.i teor.fiz., 20, 497 (1950).

SPECTROSCOPIC INVESTIGATION OF CRYSTALS

- A.F.Prikhot'ko

Optical and spectral studies occupy an important place in the physics of non-metallic solids; such studies facilitate direct investigation of the energy structure of crystals, observation of processes occurring in them under different conditions and elucidation of the mechanism of a number of effects, particularly luminescence and photoconduction. Systematic investigation of crystal spectra began with the work of I.V.Obreimov who suggested that the continuous absorption of solids is due to disordered interaction of particles caused by thermal vibrations. Upon cooling an organic crystal - azobenzene - to liquid helium temperature, instead of the usual continuous absorption observed at room temperature, Obreimov[1] obtained a discrete line spectrum with clearly discernible electronic-vibrational characteristics.

The intrinsic absorption of anisotropic crystals is pleochroic. Many if not all the bands in their spectra are sharply polarized. Comparison of the absorption spectra of crystals with the spectra of the corresponding vapors makes it possible to assign some of the bands of this type to excitation waves or quasi-particles - excitons - propagating in the lattice and possessing translational symmetry.[2,3] The exciton mechanism is important in theoretical interpretation of absorption and, particularly, luminescence.

In absorbing light a crystal acquires energy, the amount of which depends on its electronic and vibrational states. These states in the case of molecular crystals may be divided into intra- and intermolecular states. In the case of weak interaction of the electronic and vibrational excitations, the absorption bands at low temperatures are, as a rule, narrow and form clear series, through analysis of which one can establish the electronic and vibrational terms. By way of example, one can cite the familiar example of simple aromatic compounds - benzene and its numerous homologues, naphthalene and phenanthrene - in the regions of weak absorption.

Strong interaction of the excitations, which usually occurs in the case of high oscillator strengths, leads to an appreciable broadening of the bands, such as is observed, for example, in the spectra of anthracene, naphthacene, stilbene and tolan crystals. Typical series regularities obtain in the absorption, but are often difficult to distinguish and analyze.[4]

It is significant that the spectra of the same strongly absorbing compounds, if their molecules are separated by an extraneous crystalline medium, become line spectra with distinct series and serve as a source of valuable information on intramolecular vibrations.[5,6]

In all cases the bands of a crystal spectrum are connected by a continuous background, which is generally the stronger, the greater the excitation interaction and the higher the transition energy. The fact that the background weakens with decreasing temperature allows us to associate it with phonons (lattice vibrations).

An excited crystal spontaneously returning to the ground state releases the energy acquired by it in excitation; this energy is transformed into heat, luminescence or a photocurrent or may be expended on a photochemical transformation. Depending on the structure and character of the crystal, one or another of these processes may dominate: in semiconductor crystals photoconductivity predominates; in phosphors - luminescence. The luminescence mechanism in crystals is unique. Regardless of the state of electronic excitation of the crystal, the luminescence is radiated only incident to a transition from the lowest excitation state to the ground state. The process occurs as though the crystal changed all the energy it absorbed by radiationless transitions into a multitude of phonon waves

and the exchange was barred only by the potential barrier between the ground and first excited states. In an ideal crystal at absolute zero the lines associated with the transitions between these states should have a common frequency in the absorption and luminescence spectra. Actually, however, the effect is more complicated.

Careful comparison of the intrinsic absorption and luminescence of a crystal shows that there is a frequency gap between the beginning of the two series of lines, a gap that persists even if reabsorption of the luminescence is taken into account. It is filled with weak bands and absorption lines, differently polarized and not directly related with the series absorption. Usually such bands are single although sometimes they have some repetitions in the spectrum. They are always weak; located in the immediate proximity of the beginning of intrinsic absorption, which in the case of thick crystals frequently seems to be continuous, they form what is frequently called the "structure of the absorption edge". This structure frequently proves to be variable, i.e., the shape, polarization, intensity and frequencies of the bands vary not only from crystal to crystal but sometimes from one section of a crystal to another. Part of these bands, the longer wavelength ones, penetrates into the luminescence region coinciding in frequency with the initial lines of its series, which are characterized by the same variability as the absorption. This effect in cadmium sulfide crystals was explained by Broude, Eremenko & Rashba[7] as being connected with the absorption and emission of energy by a lattice with defects disturbing the translational symmetry of the ideal crystal. The energy levels of such an imperfect lattice are located close to the levels of an ideal crystal. Their relative fewness is evinced by the weakness of the absorption corresponding to transitions to these levels. The variability of the absorption and the ensuing luminescence is due to variations in the distribution of defects in different crystals and different sections of the same crystal. The "resonance" of such absorption lines with the initial lines of the luminescence series means that the de-excitation - emission - occurs from levels due to lattice defects. Such defects can arise as a result of lodging of particles at interstitial sites, the formation of vacancies, introduction of impurities, structural discontinuities, etc.

Similar effects obtain in molecular crystals: phenanthrene, stilbene, anthracene, etc. Anthracene, in view of its good scintillation properties, is being intensively investigated. Data on its spectrum, while generally in agreement for the region of intrinsic absorption, are conflicting for the weak long wave absorption bands and luminescence. The variability of the luminescence of anthracene crystals was remarked on years ago by Obreimov et al[8]. Detailed investigations of the polarized luminescence and absorption of the crystal at liquid hydrogen temperature showed that the initial lines of the luminescence series coincide in frequency with a number of lines preceding the strong series absorption. Their variability is connected with the variability of the luminescence.[9] Heat treatment of stilbene crystals (heating for different times at different temperatures) results in appreciable changes in the absorption preceding the intrinsic absorption region and to changes in the luminescence associated with this absorption.

Impurities in the form of "natural contaminants" are frequently encountered in organic crystals. These are often difficult to eliminate. The closer the "dimensions" of the impurity molecules to those of the host molecules, the more readily these enter into the lattice, where they act as defects. It is known, for example, that an admixture of naphthacene is difficult to remove from anthracene crystals, just as stilbene is only eliminated with difficulty from tolan and dibenzyl crystals. In the case of the latter the readily deformable stilbene molecule tends to assume the shape of the host crystal molecules. Such distorted

molecules play the part of lattice defects; these result in variability of the absorption and luminescence; the emission occurs from the levels of the imperfect lattice.[5] In addition to the effects obtaining in ideal crystals, in such imperfect crystals there occurs transfer of the energy absorbed by the crystal to the impurity molecules. At sufficiently high impurity concentrations, the entire emission occurs from levels due to the contaminant. With increasing purity of the substance the luminescence series associated with the impurity disappear and the intrinsic radiation of the host material increases in intensity, attaining its full strength only when perfect purity is attained. This intrinsic radiation, however, proves to be connected with defects of the host lattice, as has been demonstrated for the cases of anthracene and phenanthrene[9]. Thus the intrinsic defects of the host lattice and defects introduced from outside (impurities) play similar roles, i.e., act as spatially separated centers distorting the ideal lattice and disturbing its translational symmetry. They may give rise to imperfect-lattice levels and new potential barriers that bar the radiationless transitions and facilitate emission of the absorbed energy. The general similarity of the effects observed in crystals of different classes and types, in ionic and molecular crystals, stems from the fact that they have a common cause, namely, disturbances of the translational symmetry of the ideal crystal.

The spectra of crystals are extremely sensitive to such disturbances and hence can serve for investigating them. Crystal spectra are also sensitive to many other external influences. Heating and cooling have a strong effect on the position, shape, width and intensity of the spectral bands; deformations of the lattice, compression or stretching, lead to displacement and broadening of the bands, changes in intensity and polarization. The change in absorption of naphthalene crystals subjected to two-dimensional elongation is particularly noticeable. As a result of such nonuniform deformation the numerous narrow absorption lines constituting its familiar spectrum at 20°K transform into wide displaced diffuse bands, making the spectrum reminiscent of that observed at room temperature. Compression of organic crystals and cadmium sulfide crystals cooled to low temperatures produces diverse alterations of the spectrum, including disappearance of individual bands and the appearance of new ones, and radical changes in luminescence.[10]

Diverse structural changes - phase transitions, photochemical transformations, changes in molecular structure as a result of deuteration or other substitution - are also evinced in crystal spectra.[11] All these factors greatly expand the field of application of spectroscopy of crystals, extending it beyond mere spectral analysis, and make it a useful tool for the solution of many problems in the physics of crystals.

In connection with the development of the theory of absorption and dispersion of light in media in which excitons can exist[12], we undertook a detailed investigation of these effects in crystals. Some preliminary results have already been obtained. We are making use of spectroscopic procedures developed for work at low temperatures for the solution of theoretical problems; it is hoped that this will extend the potentialities and further the development of spectroscopy of crystals.

Physical Institute
Academy of Sciences of the Ukrainian SSR

References

1. I.V.Obreimov & W.I.deHaas, Leiden Comm., 191, 3 (1929); Ibid., 204c, 25 (1930).

2. A.F.Prikhot'ko, Zhur.eksp.i teor.fiz., 19, 383 (1949).

3. A.S.Davydov, Teoriia pogloshcheniia sveta v molekuliarnykh kristallakh (Theory of light absorption in molecular crystals), Kiev, 1951.

4. A.F.Prikhot'ko, Optika i spektroskopiia, 3, 434 (1957).

5. A.F.Prikhot'ko & M.T.Shpak, Transactions of the Tenth Conference on Spectroscopy, Vol.I, p.21, L'vov, 1957; Optika i spektroskopiia, 4, 17, 30 (1958).

6. E.V.Shpol'skii, Doklady AN SSSR, 111, 1227 (1956).

7. V.L.Broude, V.V.Eremenko & E.I.Rashba, Ukr.fiz.zhur. (Ukrainian Physics Journal), 2, 96 (1957); Doklady AN SSSR, 114, 520 (1957).

8. I.V.Obreimov, A.F.Prikhot'ko & K.G.Shabaldas, Zhur.eksp.i teor.fiz., 6, 1062 (1936).

9. A.F.Prikhot'ko & I.Ia.Fugol', Optika i spektroskopiia, 4, 335 (1958).

10. V.L.Broude, V.V.Eremenko, O.S.Pakhomova, V.S.Medvedev & A.F.Prikhot'ko, Ukr.fiz.zhur., 3, 232 (1958).

11. V.L.Broude & A.F.Prikhot'ko, Kristallografiia (Crystallography), 1, 1022 (1957). (Trans.Soviet Physics - Crystallography.)

12. S.I.Pekar, Zhur.eksp.i teor.fiz., 33, 1022 (1957). (Trans.Soviet Phys. - JETP.)

RELATION BETWEEN THE ABSORPTION AND DISPERSION IN CRYSTALS AS EVINCED IN THE CASE OF 1,2-BENZANTHRACENE

- M.S.Brodin & M.S.Soskin

Introduction

While dispersion of light in non-condensed media has been studied rather thoroughly (Rozhdestvenskii, Zellmeyer, Lorentz[2] and others), this can hardly be said of dispersion in crystals. The real beginnings of experimental investigation of dispersion in molecular crystals are the studies of I.V.Obreimov, A.F. Prikhot'ko and their associates. The most general theory of dispersion with a phenomenological basis, which gives an integral relationship between dispersion and absorption, is the Kramers[1] theory which depends on Maxwellian electrodynamics. Davydov[2] proposed a theory of dispersion in the region of exciton absorption in molecular crystals. At present, Pekar[3] is developing a theory of dispersion in media in which excitons appear.

The purpose of the present work was to study simultaneously the absorption and dispersion spectra of some molecular crystals and to compare the experimental results with formulae of the Kramers type. Most molecular crystals have complex absorption and dispersion spectra. It is most convenient, however, to work with a substance whose absorption bands are as far separated and intense as possible. Accordingly, we chose 1,2-benzanthracene. Its advantage as compared to many crystals was also the fact that two principal indicatrix axes of the refraction indices lie in the plane of the platelets obtained by sublimation.

Experimental part

The benzanthracene crystal belongs to the monoclinic system (space group C_2^2 (P_{2_1})), i.e., it has only one symmetry element: a screw axis of the second order. The molecules preserve a plane structure in the crystal, although the C-C bond length is somewhat distorted.

The single crystal 1,2-benzanthracene platelets were grown from the pure material by sublimation (the melting point of benzanthracene is 160°). These were very perfect films, uniform in thickness and with a specular surface. As was done previously[4], they were placed in optical contact with a plane-parallel quartz plate. In this case there was some danger that stresses might develop in the crystal owing to different values of the coefficients of thermal expansion of the support and crystal; these stresses could lead to modification of the spectrum[5]. However, a comparison of the absorption spectra of benzanthracene crystals of different thickness (0.25 to 0.6 μ), photographed under identical conditions, did not show significant differences. Repeated investigation on a Fedorov stage showed that the plane of the crystalline platelets obtained by sublimation coincided with the N_m, N_p plane of the index of refraction ellipsoid (N_m is the middle axis of the ellipsoid and N_g is its minor axis). According to x-ray diffraction data[6], this plane is also the crystallographic ab, in which N_m coincides with the monoclinic b axis and N_p with a.

Since we did not find any data in the literature on the indices of refraction of 1,2-benzanthracene crystals and these were needed for determining the thickness of the crystals, we determined the indices for λ = 5461 Å. The smallest index of refraction n_g was determined by the immersion technique and was found to be 1.635 ± 0.001. The value of n_p for the same wavelength was determined from interferometric measurements in polarized light on crystals of known thickness and proved to be 1.98 ± 0.005. Thus, birefringence in the plane of the platelet is significant, i.e., 0.345.

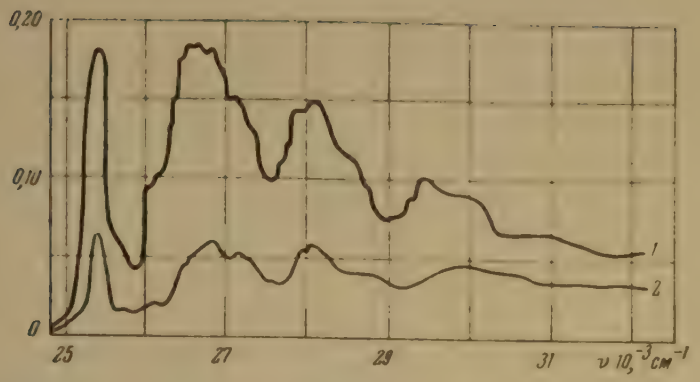

Fig.1. Absorption curves for a 1,2-benzanthracene crystal at T = 20°K: 1) $\| b$, 2) $\| a$.

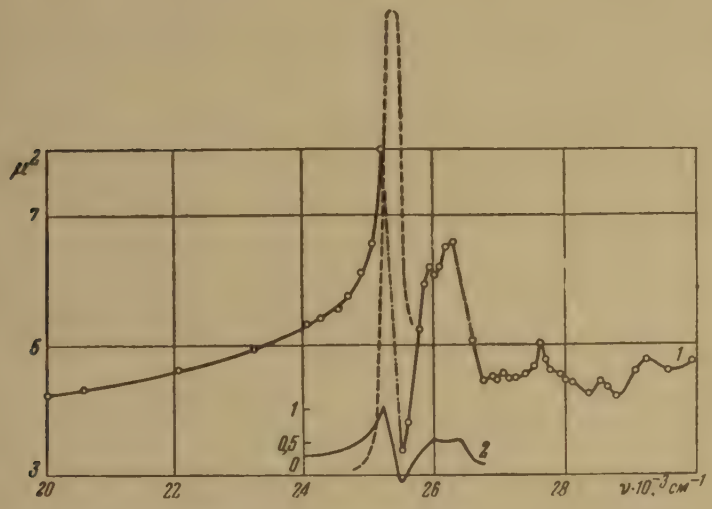

Fig.2. Dispersion curves for a 1,2-benzanthracene crystal at T = 20°K, $\| b$: 1) experimental, 2) calculated by means of Eq.(5). Dashed curve - absorption band.

The absorption curve was determined, as in the earlier studies[4], by the photoelectric null procedure using a FEU-18 photomultiplier coupled to a spectrograph having medium dispersion. The absorption coefficients were calculated, allowing for reflection of light at both surfaces of the crystal, by the formula:

$$\varkappa(\nu) = \frac{\lg \frac{I_0}{I}}{4\pi d \cdot 0.434\,\nu}, \qquad (1)$$

where $\log (I_0/I)$ is the optical density of the crystal corrected for reflection and d is the thickness of the crystal. The amount of reflection was determined from experimental dispersion curves using the familiar Fresnel formula.

The dispersion curves were determined by the interference method, using a Zhamen interferometer. The interferometer, together with the crystal, was placed in a special cryostat[7], cooled by liquid hydrogen. The indices of refraction were calculated by the formula:

$$\mu(\nu) - 1 = \frac{\Delta Y(\nu)}{H(\nu)} \cdot \frac{1}{d\nu}, \qquad (2)$$

where $\Delta Y(\nu)$ is the shift of the zero interference band caused by the crystal at the given point of the spectrum, and $H(\nu)$ is the width of the interference band. The error in determining μ amounted to 2-4%.

Fig.1 shows the absorption curves obtained for the benzanthracene crystal for oscillations of the light vector along the N_m and N_p axes. The oscillator strengths for the first transition of the 1,2-benzanthracene crystal in the two spectrum components, as calculated on the basis of the integral absorption were found to be $f_{N_m} = 0.09$ and $f_{N_p} = 0.03$, respectively.

The dispersion curves obtained for a crystal having a thickness $d = 0.37$ μ are shown in Fig.2.

Comparison with theory and discussion

For comparing the dispersion and absorption curves, we used the general integral relationships which were deduced by Kramers phenomenologically and which can be obtained on the basis of microtheory[8]:

$$\alpha_{ij}(\omega) = \frac{2}{\pi}\int_0^\infty \frac{\sigma_{ij}(\omega)}{(\omega')^2 - \omega^2}\, d\omega', \tag{3}$$

where the α_{ij} and σ_{ij} are the polarizability and electrical conductivity tensors. If the electrical vector of the light wave is aligned with the monoclinic axis of the crystal, the coefficient of absorption $\varkappa$ and index of refraction μ are related by the usual formulas with α_{11} and σ_{11} (index 1 refers to the monoclinic axis). It then follows directly from Eq.(3) that:

$$\mu^2 - \varkappa^2 - 1 = \frac{4}{\pi}\int_0^\infty \frac{\omega'\mu(\omega')\varkappa(\omega')}{(\omega')^2 - \omega^2}\, d\omega'. \tag{4}$$

For any other orientation of the electrical vector, the values of $\varkappa$ and μ are determined by several of the components of the tensors α_{ij} and σ_{ij} and the dispersion curve for any given spectrum component cannot be constructed solely from measurements of the absorption of this component. In order to avoid numerical integration in Eq.(4), the $\varkappa\mu$ curve can be represented as the sum of the Gaussian curves $A_i e^{-\frac{(\nu-\nu_{mi})^2}{(\delta_i)^2}}$. Then, as was shown by Rashba[8], μ^2 is given by the simple equation:

$$\mu^2 = 1 + \varkappa^2 - \sum \frac{4A_i}{V\pi} W\left(\frac{\nu - \nu_{mi}}{\delta_i}\right), \tag{5}$$

where

$$W(x) = e^{-x^2}\int_0^x e^{y^2}\, dy.$$

Since the $W(x)$ function is available in tabular form, calculations present no particular difficulty.

It should be noted that Eq.(4) was compared with the experimental results at room temperature for the b component of naphthacene[8] and the N_p component of tolan. In both cases the agreement between theory and experiment was satisfactory.

The experimental data for comparing the dispersion and absorption curves according to the theory presented are shown in Figs.1 and 2. The sections of the dispersion curve showing anomalous variation for the given thicknesses were not worked over. However, we determined the values of the index of refraction for the wavelengths corresponding to the bands; consequently, the values obtained are close to the extremum ones (but still do not exceed the upper bound). The experimental $\varkappa\mu$ curve for the b component in the range from 25000 to 30000 cm^{-1} was approximated by fifteen Gaussian curves. The results of calculations by means of Eq.(5) in the region of the first two characteristic bands are shown in Fig.2 (curve 2). The calculated values represent the fraction of μ^2 attributable to the 25,000 to 30,000 cm^{-1} spectrum region. More remote (ultraviolet) transitions practically do not alter the relative peak amplitudes of the curve, but only displace the entire curve upward. Comparing the amplitudes of the rises in the experimental and calculated curves, we note a clear divergence which substantially exceeds the limit of possible errors of measurement and calculation (the calculated upswings are at least three times smaller than the experimental values). This lack of agreement was observed for all of the 1,2-benzanthracene crystals studied.

For the same components of the benzanthracene spectrum, the said divergences decrease at room temperature but nevertheless remain substantial. It should be noted that similar effects were previously observed at low temperatures in crystals of other substances[4] (tolan at 80°K and stilbene at 20°K).

Thus, it has been found for several different molecular crystals that the swings (amplitudes) of the dispersion curves calculated according to Kramers type formulas are significantly smaller than those observed experimentally, and that this discrepancy increases at lower temperatures.

Institute of Physics
Academy of Science of the Ukrainian SSR

References

1. Propagation of Short Radio Waves, Edited by D.E.Kerr, Sec.8, 1, N.Y.,1951.
2. A.S.Davydov, Zhur.eksp.i teor.fiz., 19, 930 (1949).
3. S.I.Pekar, Zhur.eksp.i teor.fiz., 33, 1022 (1957).
4. M.S.Brodin, Dissertation, Kiev, 1956; M.S.Brodin and A.F.Prikhot'ko, Optika i spektroskopiia, 2, 448 (1957).
5. V.L.Broude, O.S.Pakhomova and A.F.Prikhot'ko, Optika i spektroskopiia, 2, 323 (1957).
6. I.Iball, Z.Kristallographie, A, 99, 230 (1938).
7. M.S.Brodin, V.S.Medvedev and A.F.Prikhot'ko, PTE (Instruments and Experimental Techniques), No.3, 96 (1956).
8. E.I.Rashba, Dissertation, Kiev, 1955.

QUANTUM MECHANICAL DESCRIPTION OF F-CENTERS IN ALKALI HALIDE CRYSTALS

- I.V. Abarenkov

The present paper is an attempt to provide a consistent quantum mechanical description of F-centers in alkali halide crystals (that is, to deduce the wave function of the system consisting of the F-center and the crystal) without the use of any empirical data other than the fundamental constants. In these calculations we shall use the usual model of an F-center, namely, an electron localized at a vacant anion site. We shall call the trapped electron "optical", and refer to the rest of the electrons and nuclei in the crystal as the "core" of the system.

The energy of the entire crystal may be written as

$$W = W_0 + W_1. \qquad (1)$$

where W_0 is the energy of the core, and W_1 is the energy of the optical electron in the field of the core (this latter term also includes all the electron-core interaction energy). We must find the wave function of the system which will minimize W_1. Let us attempt to find it in the approximation of full separability of the variables.[1] We shall proceed with the minimization in several successive steps. First assuming the ions to be fixed at the sites of an ideal lattice and the optical electron to be absent, we find from the minimization condition for W_0 the one-electron functions Ψ_i for the core electrons. Then from condition for minimum energy W with these core electron functions and still with the ions fixed on the ideal lattice sites, we deduce the one-electron function for the optical electron. Having solved this equation and minimizing the system energy with these one-electron functions for the whole system, we determine the equilibrium positions of the ions. If it is further necessary, we again solve the equation for the optical electron function now using the equilibrium positions of the ions, and again minimize W with respect to the ion displacements.

Löwdin[2] has shown that orthogonal combinations of free-ion one-electron functions give a good approximation to the core one-electron functions obtained by minimizing W_0. We shall use Löwdin's results.

The one-electron function $\Psi(r)$ of the optical electron is given by

$$\left[-\frac{1}{2}\Delta - \sum_i \frac{Z_i}{|r-R_i|} + \int \frac{\rho(r',r')}{|r-r'|}dr' - \sum_i \lambda_i \int \frac{\Psi_i(r')\Psi(r')}{|r-r'|}dr'\right]\Psi(r) = \varepsilon\Psi(r) + \sum_i \lambda_i \Psi_i(r) \qquad (2)$$

Here the $\Psi_i(r)$ are the core one-electron functions, Z_i and R_i are the charge and radius vector of the i-th ion, and $\rho(r',r')$ is the "mixed" density of the core electrons.

The Lagrange multipliers λ_i, which arise from the orthogonality of the optical and core electron functions, can not be set equal to zero, for Ψ and Ψ_i will not automatically be orthogonal. Now the problem can be solved approximately only by expanding the one-electron functions in a complete set of functions depending on the angle variables. The angle dependent parts of the one-electron functions are calculated from different centers, and the radial parts are eigenfunctions of different operators. Therefore neither one nor the other will be orthogonal. Thus the orthogonality must be accounted for explicitly in the minimization.

In order to find the equilibrium positions of the ions one must minimize W with respect to the nuclear displacements. Since the one-electron functions of the entire system are already known, one might reasonably use a method similar to Löwdin's. The use of all kinds of empirical formulas for repulsive forces is not, however, reconcilable with a consistent theoretical calculation of the system.

The equation for Ψ can be solved by a method of successive approximations. But this requires an initial approximation good enough to give reasonable initial values for the exchange term and the Lagrange multipliers. Such an initial approximation could be obtained by the Rayleigh-Ritz method with analytic functions, but this process is very difficult and is strongly dependent on the choice of the type of function. It is better to obtain the initial approximation by solving a somewhat simpler problem corresponding to a rougher physical model. To simplify Eq.(2) we must drop the exchange term and - what is more important - the sum on the right, for in order to find these quantities one must already have an approximation to the desired function.

The electrostatic potential can be calculated, but it should not be naively inserted into the equation if the eigenvalues of this equation are to be identified in any sense with the energy of the system. For we are attempting to minimize the energy by varying only a single one-electron function. It is known that the function so obtained will not be orthogonal to the core electron functions, which means that the optical electron state will be a mixture including some core electron states. This makes it possible for the optical electron to be in a state whose energy is much lower than that allowed by the Pauli principle.

Therefore we shall concentrate on that part of the potential which corresponds to the ions at the lattice sites being replaced by point charges[3] of magnitude ±1. We treat the rest of the potential, which we will not include in the first approximation, as a correction for the fact that the ions surrounding the F-center are not point charges. Our simplified equation is

$$\left[-\frac{1}{2}\Delta - \sum_{i=1}^{n} \frac{e_i}{|\mathbf{r}-\mathbf{R}_i|}\right]\Psi(\mathbf{r}) = \lambda\Psi(\mathbf{r}). \tag{3}$$

where e_i is the magnitude of the i-th charge.

We shall assume for the sake of simplicity that the charges are at the sites of an ideal lattice. This assumption will not significantly alter the energy or the optical one-electron function, for according to all available data the displacement of the ions from their equilibrium positions in the ideal lattice is quite small. We may consider λ as the energy of the system reckoned from some suitably chosen value. Physically, Eq.(3) corresponds to an electron within an ideal point lattice in which one negative charge is missing.

The eigenfunctions and eigenvalues of (3) can be found only approximately, by expanding the potential and the desired function in a series angle-dependent functions forming a complete set. The most convenient and natural functions for this purpose are the cubic harmonics $K_n(\nu, \varphi)$ We may write

$$\sum_i \frac{e_i}{|\mathbf{r}-\mathbf{R}_i|} = \sum_{n=0}^{\infty} V_n(r)\, K_n^{(\alpha)}(\vartheta, \varphi); \tag{4}$$

$$\Psi(\mathbf{r}) = \sum_{n=0}^{\infty} \frac{1}{r} f_n(r)\, K_n(\vartheta, \varphi). \tag{5}$$

The $f_n(r)$ are given by an infinite set of differential equations, exact solution of which is not possible. An approximate solution is most easily obtained if (3) is replaced by the corresponding variational problem with the trial function a finite sum of the terms in the infinite series of (5). Using just one term we obtain

$$f_0'' + F_0 f_0 + \lambda f_0 = 0. \tag{6}$$

Taking the sum of two terms as a second approximation, we obtain

$$\begin{cases} f_0'' + F_0 f_0 + \lambda f_0 = \Phi_0 f_1, \\ f_1'' + F_1 f_1 + \lambda f_1 = \Phi_0 f_0. \end{cases} \tag{7}$$

This process may be continued ad infinitum. In the above equations F_0, F_1 and Φ_0 can be written in terms of $V_0(r)$ and integrals of products of three cubic harmonics.

Eq. (6) was solved for the $1s$ and $2p$ states of the optical electron in LiCl and NaCl crystals. The solutions were obtained in two ways:

I. Eq. (6) was integrated numerically and the eigenfunctions and eigenvalues were found by a method of successive approximation.

II. The boundary value problem for (6) was replaced by the equivalent variational problem, and this was solved by the Rayleigh-Ritz method using $f = \sqrt{4\alpha^3}\, re^{-\alpha r}$ for the $1s$ state, and $f = \sqrt{\frac{4}{3}}\beta^5 r^2 e^{-\beta r}$ for the $2p$ state of the optical electron.

The results are presented in the table (columns I and II, resp.). In addition we solved the even more simplified equation with the potential

$$V(r) = \begin{cases} \frac{M}{a} & r \leqslant a \\ 0 & r > a, \end{cases}$$

where a is the lattice constant, and M is the Madelung constant. This is the way the crystal field was characterized in the work of Petrashen' et al.[3] The results for the energy of the optical electron of NaCl in such a potential well are listed in column III of the table.

Energy*	LiCl			NaCl			
	I	II	Exp.	I	II	III	Exp.
E_{1s}	−0,255	−0,228		−0,239	−0,214	0,217	
E_{2p}	−0,154	−0,139		−0,151	−0,142	−0,123	
ΔE	−0,101	0,089	0,118	0,088	0,072	0,094	0,098

*Energy values are given in atomic units.

By integrating (7) for NaCl it was found that the energy of the $1s$ state is -0.294, that of the $2p$ state is -0.201, and the difference between them is 0.093 atomic units. Further it was found that $\int_0^\infty f_1^2 dr$ is 20% of $\int_0^\infty f_0 dr$ in the ground state, and 30% in the excited state.

We are now attempting to obtain a solution of the exact equation (2) for LiCl and NaCl crystals.

The author is deeply grateful to M. I. Petrashen', under whose supervision the work was done, for constant attention and help.

Scientific Research Physics Institute,
"A. A. Zhdanov" Leningrad State University

References

1. V.A.Fok, Iubileinyi sbornik Akademii nauk, posveshchennyi tridtsatiletiiu Velikoi oktiabr'skoi revoliutsii (Jubilee symposium of the Academy of Sciences dedicated to the Thirtieth Anniversary of the Great October Revolution), p.255. M. 1947.

2. P.O.Löwdin, Thesis, Uppsala, 1948.

3. M.I.Petrashen', A.V.Ivanova & G.Vol'f, Vestnik, Leningrad State University, No.10, 29 (1956).

* * * * *

PROPERTIES AND STRUCTURE OF THE INITIAL AGGREGATIONS OF F-CENTERS IN THE PROCESS OF THEIR COLLOIDAL COAGULATION

- A.A.Shatalov

1. Investigation of the thermal equilibrium of F-centers with their coagulation products

In earlier contributions[1,2] we showed that in heating alkali halide crystals containing medium or low F-center concentrations there occurs a photochemical transformation leading to complete disappearance of the F-band and the appearance of a similar, new absorption band displaced to the long wavelength side. In the case of KCl, the peak of this band lies at 740 mμ.

A similar transformation also occurs in the dark as a result of appropriate heat treatment, provided the initial concentration of F-centers is sufficiently high. In the absorption spectrum of colored potassium chloride with a concentration of over $2 \cdot 10^{17}$ F-centers per cm^3 there appears in the process of cooling from high temperatures a new peak very similar to that of the above mentioned band of photochemical origin. This new peak of thermal origin lies at a slightly longer wavelength (750-780 mμ), is slightly broader and varies greatly in height, depending on the initial F-center concentration. Further, in contrast to the photochemical case, in the thermal case the F-band in KCl does not fully disappear but merely fades and is always observed together with the new band.

In Fig.1 we show, by way of illustration, the absorption curves obtained for one and the same colored KCl crystal annealed for 5 hours at 330° in the warm equilibrium (curve a) and frozen (curve b) states.

We investigated the thermal equilibrium of F-centers with their coagulation products on a large number of KCl specimens. Fig.2 shows the series of absorption curves obtained at room temperature for crystals with different initial F--center concentrations after 5 hours heating at 350°. Fig.3 shows the absorption curves obtained for a colored specimen at different intervals from 15 minutes to 5 hours after the beginning of heating in the process of realization of thermal equilibrium at 400°. Fig.4, like Fig.2, gives the results of measurements of absorption in crystals with different initial F-center concentrations, but frozen (quenched) after 5 hours heating at 400°.

It will be seen that isothermal heating leads to alteration of both bands and that this alteration is temperature dependent. At temperatures of [illegible]-350° (supplementary observations) there occurs a noticeable change in the height of

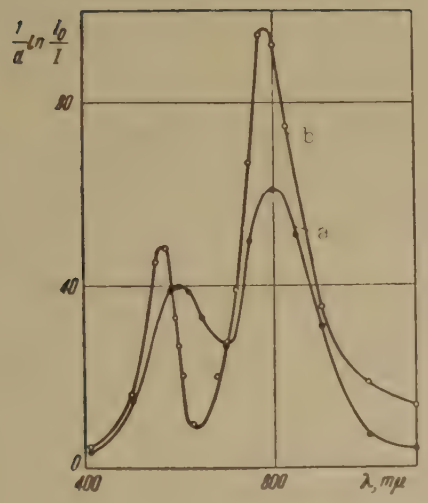

Fig.1. Absorption curves for KCl crystal heated for 5 hours at 350°: a) curve recorded at 350°; b) at 18°.

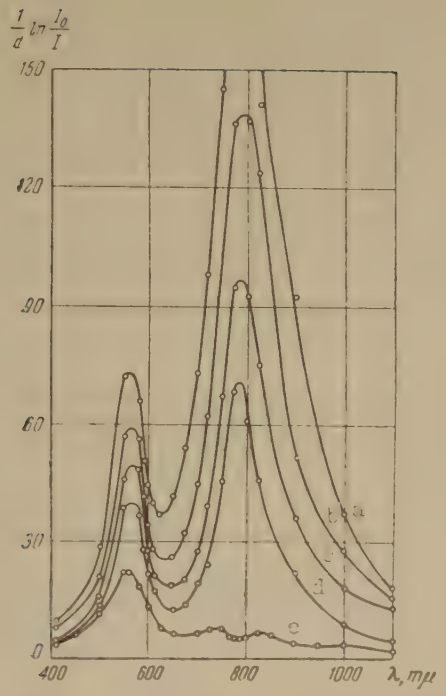

Fig.2. Absorption curves for KCl crystals annealed for 5 hours at 350°. Curves recorded at room temperature. Crystals colored at a) 740°, b) 720°, c) 700°, d) 650° and e) 580°.

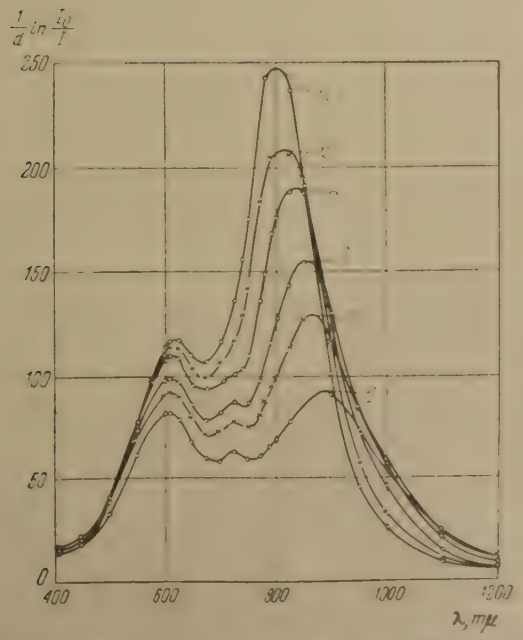

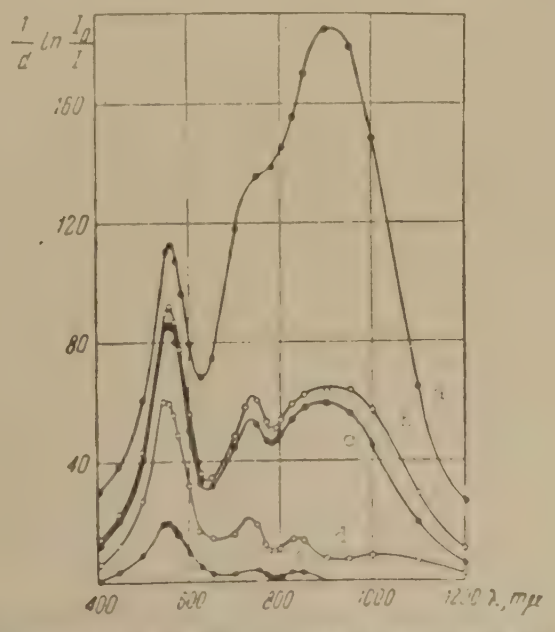

Fig.3. Absorption curves for KCl crystal annealed at 400°. Curves recorded at the following times after the beginning of heating: a) 15 min, b) 30 min, c) 1 hr, d) 2 hrs, e) 3 hrs, f) 5 hrs.

Fig.4. Absorption curves for KCl crystals quenched after heating for 5 hours at 400°. Curves recorded at room temperature. Curve designations same as in Fig.2.

the peaks, a small shift of the right-hand band to the long wavelength side and only minor broadening of this band. The absorption spectrum for equilibrium at 350° is shown in Fig.2. Much more noticeable changes occur at 400-500°. Particularly noticeable at this temperature is the lowering and broadening of the right-hand peak (Fig.3), which at the same time is displaced to the long wave-length side (to 900 mμ). Moreover, in the process of heating the bands "spread" and a new incipient peak appears in the absorption spectrum at approximately the wavelength of the "photochemical transformation" band (Figs.3 & 4).

In view of the properties of the shorter wavelength peaks appearing as a result of thermal coagulation of F-centers (specifically, their wavelength, half-width, temperature dependence and variation in the process of heating), we are inclined to attribute their absorption to a mixture of F_2-centers with larger aggregations of F-centers, but still incorporated in the alkali halide (host) crystal lattice.

The development sequence, shape and wavelength of the longer wavelength peaks (Figs.3 & 4), evinced at higher temperatures, give reason to infer that they are associated with potassium colloids constituting a separate metallic lattice.

The pronounced variation of the equilibrium heights of the absorption peaks with the initial concentration of both F-centers and their coagulation products (Fig.2, 350°) indicates that the equilibrium is established after solution of both the former and the latter centers approximately in equal proportions, i.e., the observed thermal equilibrium is homogeneous. Complex equilibrium of three types of centers, which is clearly evinced only at higher temperatures, must be regarded as thermal equilibrium between colloids and F-center aggregations, on the one hand, and F-center aggregations and "pure" F-centers, on the other hand. The first equilibrium is heterogeneous; the second is homogeneous in this case as well.

The slope (tangent) of the logarithmic straight-line plot of the temperature dependence of the equilibrium concentration of F-centers in the case of thermal transformations may be interpreted as the dissociation energy of the smallest F-center aggregations. The numerical value obtained by us for this energy (0.29 ev) is very close to the thermal dissociation energy for F_2-centers (0.31 ev) determined by a different procedure by Kalabukhov et al[3,4].

Some time ago Scott, Smith and Thompson[5,6], using different coloring and measurement procedures, also obtained "thermal" absorption bands in alkali halide crystals with an appreciable initial F-center concentration. For KCl these bands lie in the region of 750-775 mμ, i.e., at the same wavelength as those observed by us. These authors, however, give a different interpretation of these bands. Not having investigated the influence of exposure to light on F-centers in heated crystals, Scott and his co-workers failed to detect photochemical transformations. Reasoning on the basis of their experimental data, which indicate that the "equilibrium" density of F-centers does not depend on their initial concentration and increases with temperature, these authors conclude that the forming centers constitute a new phase and that the equilibrium attained is heterogeneous. From this they infer that the aggregates obtained by thermal coagulation of F-centers are colloidal. They take the slope of the plot of the logarithm of the "equilibrium" concentration vs 1/T to be indicative of the heat of evaporation of the F-centers from the colloidal particles.

It must be noted, however, that in carrying out their studies Scott and his co-workers used excessively short heating times (3 to 15 min) during which true equilibrium could not have been attained (see Figs.3 & 4). Furthermore, Scott et al made their measurements only at room temperature, i.e., under conditions of

"forced" equilibrium. It must also be noted that "freezing" greatly distorts the ratio of initial concentrations. Using such short heat treatment times, these authors could not observe the formation of large colloids in KCl and other crystals.

The evaporation energy values (0.35-0.5 ev) found by these authors for a number of alkali halide crystals are approximately one third the known values for this quantity for atoms of pure alkali metals.

In view of this and our experimental results, we cannot agree with the hypothesis of Scott et al regarding the colloidal nature of the smallest products of thermal coagulation of F-centers.

2. Structure of the smallest products of photochemical and thermal coagulation of F-centers

Earlier[1,2,7] we published a number of proofs that the new color centers obtained as a result of photochemical treatment of F-centers in heated alkali halide crystals are initial aggregations, i.e., aggregations with which the process of colloid formation begins.

Let us list briefly the results of new investigations substantiating this conclusion and proving that the formations which we originally termed x-centers have the structure of F_2-centers.

1. By solution of simple kinetic equations, set up on the assumption that the photochemical transformation discovered by us is described by $2F \rightarrow F_2$, we obtained time dependences of the F- and x-center concentrations in qualitative agreement with the experimental curves for KCl.[8] The combining of F-centers and decomposition of x-centers are monomolecular reactions.

2. Explanations of the low quantum efficiency and its temperature dependence are consistent with the F_2 model for x-centers.[9]

3. Plots of the ratios, similar to the Mollwo ratio, for the x-bands of KCl, NaCl, KBr, KI and LiF yield as constant a value of the product $\nu_{max}d^2$ as similar plots for the F-bands.[8] This proves that the structure of the F--centers is monotypic in different alkali halide crystals and that the x-centers are formations associated with the properties of the solvent crystal lattice.

4. In photochemical transformation of the "red" centers in sodium chloride to F-centers[8] the influence of monochromatic radiation corresponding to any section of the x-band, leads to its proportional, although not equally rapid, weakening without the formation of local dips, as observed in the irradiation of colloids. Consequently, all x-centers are similar to each other and the x-band, like the F-band, does not constitute the surposition of many different bands.

5. The temperature dependence observed by us is peculiar to the absorption peaks of the smallest products of optical[2] and thermal coagulation of F-centers; such a dependence would not be exhibited by colloidal bands.

6. Investigations of photochemical transformation of the "red" centers of sodium chloride carried out by us by means of polarized light indicate that the x-centers are anisotropic and are oriented along the second order symmetry axes.

7. In addition to F_2-centers, however, other anisotropic combinations of centers and ionic vacancies, for example, F_2^+-centers can be characterized by this orientation in the host crystal lattice. Measurements carried out at our request by A.M.Prokhorov and S.Kaitmarov ("P.N.Lebedev" Physical Institute of the USSR Academy of Sciences) showed that the paramagnetic absorption of KCl crystals colored with F-centers fully disappears after photochemical transformation of the F-centers into x-centers. This proves that the number of electrons at x-centers is even; it will be recalled that an even number of electrons is most easily

CONDITIONS GOVERNING THE EXISTENCE AND SPECTROSCOPIC MANIFESTATION OF EXCITONS IN SEMICONDUCTORS

- I.Z.Fisher

There can no longer be any doubt regarding the existence of excitons and the significant role played by them in physical processes in dielectric crystals. Also clearly evident is the impossibility of exciton excitations in conducting media (metals). Between insulators and metals, however, we have the wide field of semiconductors and there naturally arises the question of the possibility of existence of electrons in semiconductors and the degree of their stability as a function of the conductivity of the material. This question is of great interest since excitons make a significant contribution to optical, photoelectric and other processes associated with exchange or transfer of energy not only in dielectric crystals but in many semiconductors as well.

We base our treatment on the hydrogen-like model of a nonpolarizing exciton, taking into account the crystal lattice field by the effective mass method. The exciton energy levels in an insulator reckoned from the dissociation threshold are given by

$$E_N = -\frac{m^* e^4}{2D^2\hbar^2} \cdot \frac{1}{N^2} \quad (N = 1, 2, 3, \ldots), \tag{1}$$

where m^* is the effective reduced mass of an electron or hole and D is the specific inductive capacitance in the optical frequency region.

The stable existence of the exciton is limited by the thermal vibrations of the crystal lattice capable of producing its thermal dissociation. At a given temperature T only levels with $|E_N| \geq kT$ will be stable. If we introduce the "atomic" temperature units

$$\theta = \frac{2D^2\hbar^2}{m^* e^4} kT = 6.41 \cdot 10^{-6} \left(\frac{m}{m^*}\right) D^2 T, \tag{2}$$

then from the condition $(1/N^2) \geq \theta$, we obtain for the number of exciton states stable as regards thermal dissociation

$$N' = \left[\frac{1}{\sqrt{\theta}}\right], \tag{3}$$

where the brackets indicate an "integral part". With increasing θ the number of exciton levels N' decreases and at $\theta > 1$ the existence of an exciton even in the ground state becomes impossible.

In a semiconductor not only the vibrations of the crystal lattice but also the background of free charges, that provide the conduction electrons, inhibit the existence and stability of exciton levels. Below we shall analyze this situation and deduce a generalization of the basic relationship (3). The presence of the background of conduction electrons or free holes (or both) distorts the interaction of charge pairs thus giving rise to screening of the Coulomb potential. In the Debye-Huckel statistical treatment

$$U(r) = -\frac{e^2}{Dr} e^{-kr}, \tag{4}$$

the screening constant k is determined by

$$k = \frac{\Phi}{\quad} \tag{5}$$

where Φ is the Gibbs potential of the free charges. (For simplicity we hereinafter assume that all the screening charges are of the same polarity, i.e., only

electrons or only holes.) Eqs.(4) and (5) are valid in the framework of the Debye-Huckel approximation for any degree of Fermi degeneration of the electrons (holes) and at T = 0 become identical with the results of the Thomas-Fermi[2] treatment. There are better methods of taking screening into account in the case of metals[3], but their generalization for the case of semiconductors and, particularly, determination of the screening radius for $T \neq 0$ are fraught with great difficulties.[4] Hence below we shall make use of the approximations of Eqs.(4) and (5).

In preceding papers[5,6] we solve the Schrödinger equation for the bound states of an exciton in a semiconductor with an arbitrary degree of screening according to (4)-(5), using Fermi statistics for the free charges. We found the energy levels ε_{Nl} as a function of $\varkappa$ in terms of the "atomic" units of length, energy and the screening constant,

$$r = \frac{D\hbar^2}{m^* e^2}\rho, \quad E = \frac{m^* e^4}{2D^2\hbar^2}\varepsilon, \quad K = \frac{2m^* e^2}{D\hbar^2}\varkappa. \tag{6}$$

For the case of weak screening we obtained

$$\varepsilon_{Nl}(\varkappa) = -\frac{1}{N^2} + 4\varkappa - 2\varkappa^2(3N^2 - l(l+1)) + 4\varkappa^3 N^2(5N^2 + 1 - 3l(l+1)) + \ldots, \tag{7}$$

where N and l are the principal and azimuthal quantum numbers. The quantity $\varkappa$ itself depends on the temperature T and free charge density n:

$$\varkappa = 3.83\cdot 10^{-10}\left(\frac{m}{m^*}\right)\left(\frac{Dn}{T}\right)^{1/2}(1 - 0.7071x + 0.8292x^2 + \ldots), \tag{8}$$

where m is the true electron mass and

$$x = 5.50\cdot 10^{-17}\left(\frac{m}{m_1^*}\right)^{3/2} nT^{-3/2}. \tag{9}$$

Here m_1^* is the effective mass of the screening charges.

In the case of strong screening, the expressions for $\varepsilon_{Nl}(x)$ and $\varkappa(n', T)$ are more complicated; they were evaluated numerically in Refs.5 & 6 and presented in graphic form. In Fig.1 we reproduce the variation of ε_{Nl} with $\varkappa$ for the $1s$, $2s$, $2p$ and $3d$ states. It will be seen that with increase of $\varkappa$ the absolute values of ε_{Nl} decrease rapidly and then vanish, the more rapidly the larger N and l. The limit values of $\varkappa$ at which the ε_{Nl} vanish for the $1s$, $2s$, $2p$ and $3d$ states are 0.5951, 0.1250, 0.1017 and 0.241, respectively.

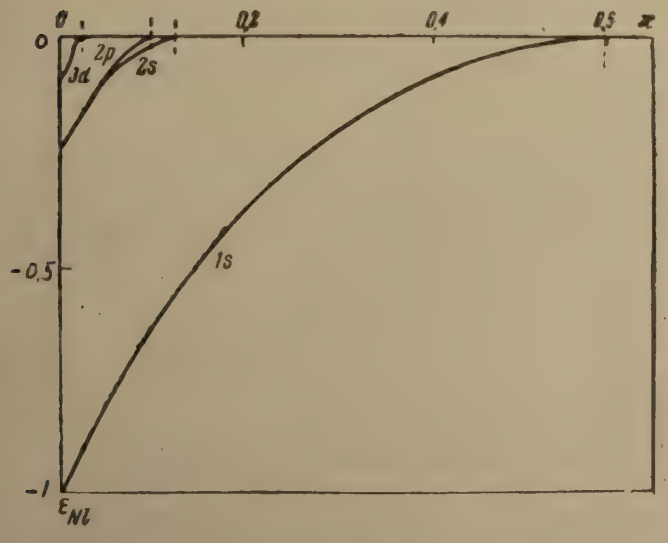

Fig.1. Variation of ε_{Nl} with $\varkappa$ for the $1s, 2s, 2p$ and $3d$ states (strong screening case).

In Ref.6 we also investigated the specific widening of the exciton energy levels associated with fluctuations of the screening field. The existence of such fluctuations inevitably follows from the statistical mechanism of screening. At an appreciable density of the screening charges, the fluctuation of the field and widening of the levels are so great that the exciton proves to be unstable before the limiting equilibrium values of $\varkappa$ shown in Fig.1 are attained.

Denoting the quadratic widening of level ε_{Nl} by $(\overline{\Delta\varepsilon_{Nl}})^2$, we find that the condition for stability of the exciton, taking into account its possible thermal dissociation, is now (see (2)):

$$|\varepsilon_{Nl}(\varkappa)| \geq \theta + \sqrt{\overline{(\Delta\varepsilon_{Nl})^2}}. \qquad (10)$$

If the values of n and T are not too low, the number of levels satisfying this condition is relatively small. By way of illustration in Fig.2 we show the energy levels of an exciton at T = 100°K and T = 300°K for different values of n. For purposes of concreteness we took the specific values of the dielectric constant and effective mass for cuprous oxide, namely, D = 6.25 and $m/m^* = 3.5$. Only the s-levels are shown in the diagram. It will be seen that the levels vanish rapidly with increasing n.

The number of stable levels at given values of n and T can be determined approximately if in (10) we neglect widening and take for N its limit value at which $\varepsilon_{Nl} = \theta$. If $\varepsilon_{Nl}(\varkappa)$ is evaluated by means of the first two terms in (7), we obtain for the number of levels in the exciton energy spectrum

$$N' = \left[\frac{1}{\sqrt{\theta + 4\varkappa}}\right], \qquad (11)$$

instead of Eq.(3) which is valid only for an insulator.

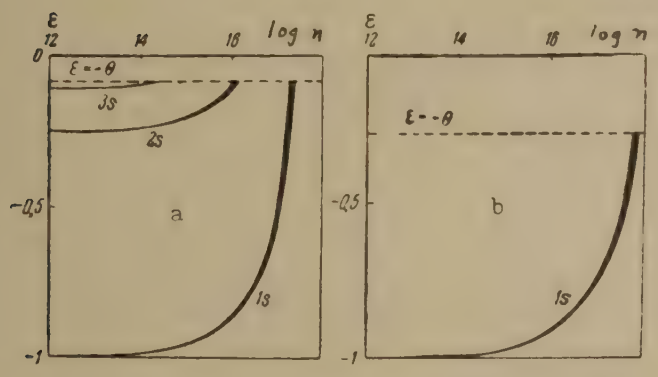

Fig.2. Energy levels of an exciton at T = 100°K (a) and 300°K (b) for different values of n.

It will be evident from the above analysis that stable existence of excitons is inhibited equally by high temperature and good conductivity of the crystal. Excitons in the ground state can exist in a relatively wide range of temperatures and free charge densities. Hence processes involving inactive absorption of light and energy exchange and transfer, wherein only the existence of excitons per se is important, can under ordinary conditions be observed in almost all semiconductors except those with a high conductivity.

To obtain a more or less complete exciton absorption spectrum one must have low values of T and n, i.e., a crystal with good insulating properties. In the absence of light, in good semiconductors decrease of the temperature automatically reduces n, which enhances the possibility of the existence of excited exciton states.

Belorussian State University

References

1. L.D.Landau & E.M.Lifshits, Statisticheskaia fizika (Statistical physics), M.-L., 1951.
2. N.F.Mott, Proc.Cambr.Phil.Soc., 32, 281 (1936).
3. D.Bohm & D.Pines, Phys.Rev., 92, 609 (1953).
4. V.L.Bonch-Bruevich, Zhur.eksp.i teor.fiz., 32, 1092 (1957).
5. I.Z.Fisher & V.I.Krylovich, Zhur.tekh.fiz., 27, 1289 (1957).
6. I.Z.Fisher, Ibid., 27, 632 (1957).

INVESTIGATION OF THE ROLE OF TRAPPED AND FREE EXCITONS IN THE LUMINESCENCE OF MOLECULAR CRYSTALS BY POLARIZATION METHODS

- N.D. Zhevandrov

In the simplest model of the crystal lattice of molecular crystals, interaction between molecules is not taken into account and the crystal is regarded as an "oriented gas". Unfortunately, this simple concept is inconsistent with diverse experimental data.

In particular, this simple model cannot explain the fact that the polarization of luminescence is independent of the polarization of the exciting light, an effect observed for all molecular crystals.[1] Inasmuch as there are several different forms of orientation in the lattices of molecular crystals, this effect can be explained only by transfer of the excitation energy from excited molecules to neighboring molecules, i.e., by redistribution of this energy among molecules with different orientations.

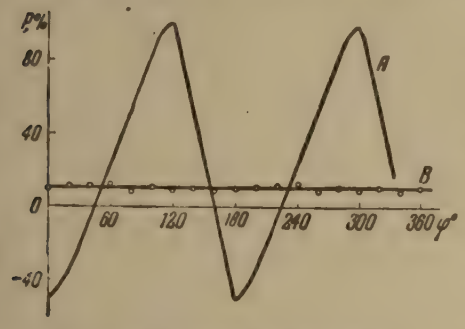

Fig.1. Variation of the fluorescence polarization P of an anthracene crystal with the orientation of the electric vector φ of the incident light: A - calculated, B - experimental.

Curve B in Fig.1 illustrates the experimentally observed behavior of the polarization of fluorescence of an anthracene crystal; curve A gives the calculated dependence on the electric vector of the exciting light that would obtain in the absence of energy transfer.

It will be evident that in actual fact the luminescence polarization is determined only by the orientation of the molecules in the lattice and does not depend on the anisotropy of the excitation. This proves the existence of energy transfer and invalidates the hypothesis that the molecules in a crystal absorb and emit light independently of each other.

An obvious question is: what is the nature of this transfer?

The theory, originated by Frenkel[2] and subsequently developed by Davydov[3], indicates the existence in crystals of two types of excitons: trapped and free excitons. These differ in particular as regards their polarization properties. The polarization of transitions corresponding to trapped excitons is determined by the symmetry of the molecules and their orientation in the lattice, while transitions associated with free excitons are polarized along the crystallographic axes, in other words their polarization is determined by the symmetry of the crystal lattice as a whole.

It is important to note that, as Craig[4] has shown, the ratio of intensity components due to transitions associated with free excitons and polarized along the different crystal axes differs substantially from the ratio of the components of the radiation of the molecules along these axes. In other words, we have the possibility of distinguishing between free and trapped excitons on the basis of polarization.

The experiments of Obreimov & Prikhot'ko[5] and other investigators proved that both types of excitons participate in the process of light absorption by crystals.

An interesting question is how these two types of excitons behave in the process of luminescence. Apparently, the answer to this question can be found by investigating the luminescence spectrum of crystals at a sufficiently low temperature, when the usual bands split into narrow bands and lines, and determining the polarization of the individual lines. Some information, however, can

be obtained from measurements of polarization at room temperature.

We investigated the spatial distribution of the polarization of luminescence of crystals for different orientations of the crystals (i.e., obtained so-called polarization diagrams). Initially these studies were carried out on crystal plates of anthracene.[6]

From the experimental standpoint it is convenient to vary the angle between the direction of observation and the normal to the crystal in the horizontal plane. The spatial distribution of the polarization can be fully characterized by obtaining "polarization diagrams" for two orientations of the crystal, corresponding to the positive and negative polarization maxima (we shall hereinafter refer to these as the "positive" and "negative" polarization diagrams).

In practice it proved necessary to calculate and introduce rather substantial corrections for birefringence, which distorts the true polarization of the luminescence. Our results show that the corrected experimental diagrams and diagrams calculated on the basis of x-ray diffraction data are qualitatively similar, but differ quantitatively.

Evaluations of the corrections showed that they are relatively small for directions forming a small angle with the normal to the crystal surface. Hence it was expedient to design the experiments so that this condition would obtain, thus doing away with the necessity of introducing corrections. One obvious procedure was to use spherical crystals and excite the luminescence at their center. Since the preparation of spherical crystals of anthracene proved to be difficult, the subsequent investigations were carried out with stilbene and tolan.[7] The spheres were cut into hemispheres along determined crystallographic planes; the cut surface was covered with a diaphragm with a central aperture, limiting the excitation of luminescence to a small region at the center of the sphere.

Fig.2 shows the positive and negative polarization diagrams for stilbene obtained for the following hemispherical specimens: I cut in the *ab* plane, *c'* axis aligned with the apparatus axis; II cut in the *bc'* plane, *a* aligned with the apparatus axis; III cut in the *ac'* plane, *b* aligned with the apparatus axis.

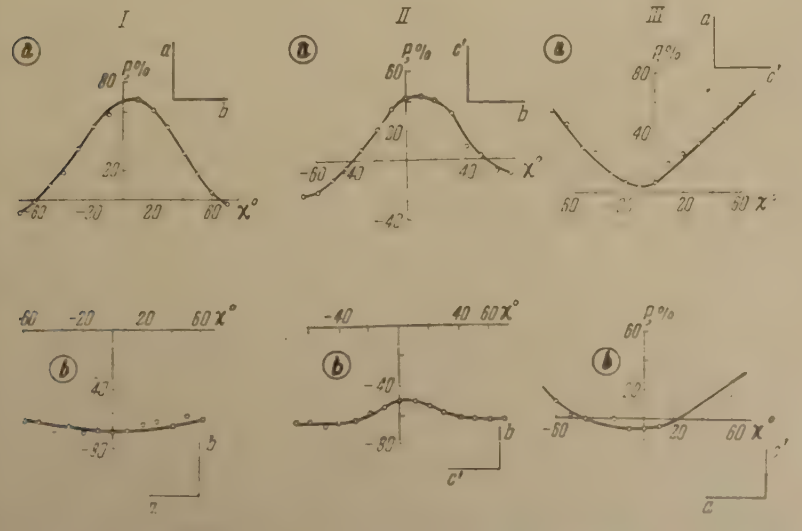

Fig.2. Experimental polarization diagrams obtained for hemispherical stilbene crystals (a - positive and b - negative): I - cut in *ab* plane, II - cut in *bc'* plane and III - cut in *ac'* plane.

The polarization diagrams calculated on the basis of the x-ray diffraction data for the same cases are shown in Fig.3. It will be seen that the calculated and experimental diagrams are in good qualitative agreement without any correction of the experimental data for birefringence. Just as in the case of anthracene, however, the diagrams differ quantitatively: the experimental values of the degree of polarization are always smaller than the calculated ones.

One cannot explain this diminution of polarization by the influence of thermal rotational

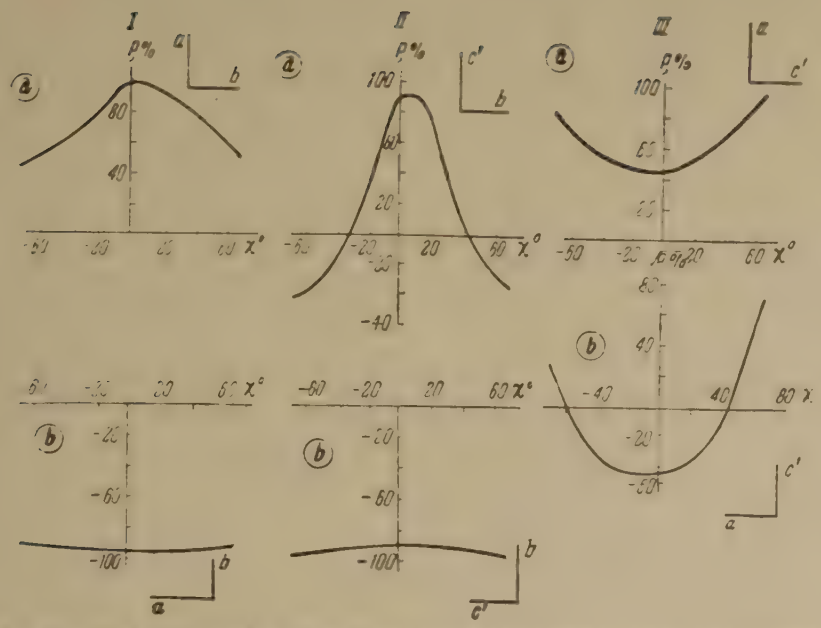

Fig.3. Calculated polarization diagrams for stilbene. Designations same as in Fig.2.

vibrations of the molecules inasmuch as in molecular crystals, as we showed elsewhere[7], the influence of temperature on the polarization of luminescence is very minor.

One can attempt to account for these results on the basis of the presence in the crystal of trapped and free excitons. In calculating the polarization diagrams from the x-ray data, we assumed that the polarization of the luminescence is fully determined by the symmetry of the molecules and their orientation in the lattice, i.e., that the luminescence is due solely to trapped excitons. If in addition to the trapped, free excitons participate in the luminescence, the polarization of the total emission will be different inasmuch as the transitions associated with free excitons are polarized along the crystallographic axes. If the polarization is along the horizontal axis, the degree of total polarization is decreased; if it is along the vertical - increased. From this point of view the polarization diagrams can be regarded as a method for investigating the role of trapped and free electrons in the process of luminescence. By means of these diagrams one can determine the axes along which the emission of the free excitons is polarized and evaluate its relative intensity.

By way of illustration let us analyze the polarization diagrams for stilbene from this standpoint. The axis orientations corresponding to the different diagrams are indicated in Fig.2. Diagrams I (ab cut) indicate that there is radiation polarized along the b axis (inasmuch as both experimental diagrams, the positive and the negative, lie closer to the horizontal axis than the calculated diagrams; consequently, the "additional" radiation is polarized horizontally in the former case and vertically in the latter). Analogously, diagrams III show that the radiation of the free excitons has a component polarized along the c' axis. Using the familiar formula for summation of the degrees of polarization

$$P = \frac{\sum_i I_i P_i}{\sum_i I_i},$$

one can calculate the relative intensity of the radiations of the trapped and free excitons from the ratio of the degrees of polarization of the total luminescence and the emission of the trapped and free excitons. Such calculations indicate that the emission due to trapped excitons accounts for 60-70% of the total luminescence, while each of the two components of the free exciton radiation, polarized along the b and c' axes, amounts to 15-20%, the intensity of the b polarized component being somewhat greater than that of the c' component.

Our inference that the luminescence is due primarily to trapped excitons is in good agreement with the results of Sidman[8] who came to the same conclusion through analysis of the gap between the fluorescence spectrum and the absorption of anthracene crystals.

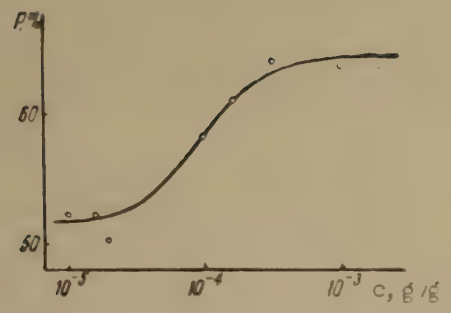

Fig.4. Variation of the degree of polarization of the fluorescence of anthracene with the concentration of naphthacene.

Our results pertaining to the polarization of the free exciton radiation are in agreement with the theory of Davydov[3]. Using the methods of group theory, Davydov treated the case of a monoclinic crystal with space group symmetry C_{2h}^5 containing two molecules per unit cell. Stilbene belongs in this crystal class. Davydov showed that in such a crystal the molecular energy term splits into two terms, one polarized so that the oscillations of the electric vector are parallell to the b axis; the other so that the oscillations are in the plane perpendicular to the b axis.

One more experimental proof can be cited in support of the above interpretation. If we assume with Agranovich[9] that in activated anthracene--naphthacene crystals the transfer of excitation energy from the host substance to the impurity is realized by free excitons, we must expect the relative intensity of the trapped exciton radiation in the host substance to increase with the addition of the impurity. Consequently, the degree of polarization of the host substance luminescence must increase with increasing impurity concentration.

Experiments substantiates this. Fig.4 shows the variation of the polarization of the fluorescence of anthracene as a function of the naphthacene impurity concentration. It will be seen that the polarization increases substantially up to a concentration of $\sim 5 \cdot 10^{-4}$ g/g, at which point the increase slows down and saturation is attained. This is to be expected inasmuch as the fluorescence efficiency of naphthacene attains a saturation value at approximately this concentration.[10]

"P.N.Lebedev" Physical Institute
Academy of Sciences of the USSR

References

1. N.D.Zhevandrov, Doklady AN SSSR, 83, 677 (1952); 100, 455 (1955).
2. Ia.(J.) Frenkel, Phys.Rev., 37, 17 (1931); Phys.Z.Sow., 9, 158 (1936).
3. A.S.Davydov, Teoriia pogloshcheniia sveta v molekuliarnykh kristallakh (Theory of light absorption in molecular crystals), Kiev, 1951; Sbornik pamiati S.I.Vavilova (Symposium in memory of S.I.Vavilov), M., 1952.
4. D.P.Craig, J.Chem.Soc., 2302 (1955).
5. I.V.Obreimov & A.F.Prikhot'ko, Sbornik pamiati S.I.Vavilova, M., 1952.
6. N.D.Zhevandrov, Izv.AN SSSR, Ser.fiz., 20, 553 (1956). (Trans.Bulletin, 20, No.5, 505.)
7. V.N.Varfolomeeva & N.D.Zhevandrov, Doklady AN SSSR, 115, 1115 (1957); Optika i spektroskopiia, 5, 571 (1958).
8. J.W.Sidman, Phys.Rev., 102, 96 (1956).
9. V.M.Agranovich, Optika i spektroskopiia, 4, 586 (1958).
10. E.J.Bowen, E.Mickiewicz & F.W.Smith, Proc.Phys.Soc., 62A, 26 (1949).

IMPURITY SCATTERING OF LIGHT IN CRYSTALS AT LOW TEMPERATURES

- Iu.E.Perlin

Impurity centers in crystals may serve not only as absorption and luminescence centers, but also as scattering centers. Below we shall consider light scattering by impurity centers in an ionic crystal in which the strong-coupling criterion for the interaction between the optical electrons and the lattice vibrations is satisfied. We assume that the frequency Ω_0 of the incident radiation lies within the impurity absorption band. We now use a generalization of Weisskopf's method[1] for dealing with atomic resonance fluorescence and limit our consideration to the ground and first excited states of all the possible discrete electronic levels of the impurity center. This gives the following equation for the probability amplitude of scattering:

$$c[n_\varkappa^0,\ n_\varkappa'] = \frac{V_{s_1 s_2}(\Omega)\, V_{s_2 s_1}(\Omega_0)}{\hbar^2\left[(\Omega-\Omega_0+l\omega)+\frac{i\Gamma}{2}\right]} S[n_\varkappa^0,\ n_\varkappa']; \tag{1}$$

here

$$S[n_\varkappa^0,\ n_\varkappa'] = \sum_{n_\varkappa} \frac{\prod_\varkappa s_{n_\varkappa^0 n_\varkappa}\, s_{n_\varkappa n_\varkappa'}}{(\Omega-\nu+l_2\omega)+\frac{i\gamma}{2}}, \tag{2}$$

where the indices s_1 and s_2 refer to the ground and excited levels, respectively, $n_\varkappa^0$, $n_\varkappa$ and $n_\varkappa'$ are the quantum numbers of the phonon field oscillators in the initial, intermediate and final states of the system, Ω is the frequency of the scattered light, $1/\Gamma$ and $1/\gamma$ are the optical lifetimes of the impurity center in the s_1 and s_2 states, respectively, ω is the limit frequency of the longitudinal polarization vibrations of the lattice, ν is the frequency of the "pure electron" transition, given by

$$h\nu = W \tag{3}$$

(where W is the thermal excitation energy of the center), and

$$l = \sum_\varkappa (n_\varkappa' - n_\varkappa^0); \quad l_2 = \sum_\varkappa (n_\varkappa' - n_\varkappa). \tag{4}$$

The matrix element of the phototransition is the product of an electronic factor $V_{s_1 s_2}$ and a factor of the form

$$s_{n_\varkappa n_\varkappa'} = \int \Phi_{n_\varkappa}(q_\varkappa - q_{\varkappa s_2})\, \Phi_{n_\varkappa'}(q_\varkappa - q_{\varkappa s_1})\, dq_\varkappa, \tag{5}$$

where $\Phi_{n_\varkappa}$ is the wave function of the oscillator, and $q_{\varkappa s}$ is the equilibrium value (in the given electronic state) of the normal coordinate $q_\varkappa$.

A detailed derivation of (1) will be found elsewhere.[2] An analogous expression for solutions was obtained somewhat earlier by Ovander.[3]

The summation in (2) can be carried out using the Fourier transform

$$\left[(l_2-r)\omega+\frac{i\gamma}{2}\right]^{-1} = \frac{1}{i\omega}\int_0^\infty dt \exp[-\delta t + i(l_2-r)t], \tag{6}$$

where

$$\delta = \gamma/2\omega \quad 1. \tag{7}$$

and the familiar expression for the oscillator density matrix

$$\rho(q, \bar{q} \mid \xi) \equiv \sum_{n=0}^{\infty} e^{-(\bar{n}+\frac{1}{2})\xi} \Phi_n(q)\, \Phi_n(\bar{q}) =$$

$$= (2\pi \operatorname{sh}\xi)^{-\frac{1}{2}} \exp\left\{-\frac{1}{4}\left[(q+\bar{q})^2 \operatorname{th}\frac{\xi}{2} + (q-\bar{q})^2 \operatorname{cth}\frac{\xi}{2}\right]\right\}. \qquad (8)$$

Expression (8) was first used by Kubo[4] in summing the probability for multiple-phonon transitions.

Eq. (2) becomes

$$S[n_\varkappa^0,\ n'_\varkappa] = \frac{1}{i\omega}\int_0^\infty dt \exp\left\{-\delta t + i\left[\sum_\varkappa\left(n'_\varkappa + \frac{1}{2}\right) - r\right]t\right\} \times \prod_\varkappa (2\pi i \sin t)^{-\frac{1}{2}} \int\int_{-\infty}^{\infty} dq_\varkappa\, d\bar{q}_\varkappa\, \Phi_{n_\varkappa^0}(q_\varkappa)\, \Phi_{n_\varkappa^0}(\bar{q}_\varkappa) \times$$

$$\times \exp\left\{-\frac{i}{4}\left[(q_\varkappa + \bar{q}_\varkappa + \Delta_\varkappa)^2 \operatorname{tg}\frac{t}{2} - (q_\varkappa - \bar{q}_\varkappa)^2 \operatorname{ctg}\frac{t}{2}\right]\right\}, \qquad (9)$$

where

$$\Delta_\varkappa = 2(q_{\varkappa s_1} - q_{\varkappa s_2}), \qquad (10)$$

$$r = (\nu - \Omega)/\omega. \qquad (11)$$

The probability of light scattering is calculated from (1), using the formula

$$w(\Omega) = \sum_{\ldots n_\varkappa^0 \ldots} \sum_{\ldots n'_\varkappa \ldots} p[n_\varkappa^0]\, |c[n_\varkappa^0, n'_\varkappa]|^2, \qquad (12)$$

which already contains the statistical average over the initial states and the sum over the final states of the lattice oscillators. The Boltzmann factor $p[n_\varkappa^0]$ is given by

$$p[n_\varkappa^0] = \left(2\operatorname{sh}\frac{\beta}{2}\right)^N \exp\left[-\beta\sum_\varkappa\left(n_\varkappa^0 + \frac{1}{2}\right)\right]. \qquad (13)$$

where $\beta = \frac{\hbar\omega}{kT}$. Now writing

$$p = (\Omega_0 - \Omega)/\omega \qquad (14)$$

again using the Fourier transform and (8), we are able, after some manipulation, to perform the summation in (12), bringing it to the form

$$w(\Omega) = \frac{4\pi\, V_{s_1 s_2}(\Omega)\, V_{s_1 s_2}(\Omega_0)\, e^{-\frac{a}{2}}}{\hbar^4 \omega^2 T} \int_0^\infty\int_{-\infty}^{\infty} dt\, dt' \cdot$$

$$\exp\left\{-\beta(t+t') + i\left(\frac{p}{2} - r\right)(t-t') - \frac{a}{2\operatorname{sh}\frac{\beta}{2}}\left[\cos\left(t + \frac{i\beta}{2}\right) + \right.\right.$$

$$\left.\left. + \cos\left(t' - \frac{i\beta}{2}\right)\right]\right\} \times I_T\left(\frac{2a\sin\frac{t}{2}\sin\frac{t'}{2}}{\operatorname{sh}\frac{\beta}{2}}\right) \sum_n^\infty \delta(p-n), \qquad (15)$$

where

$$a = \sum_\varkappa (q_{\varkappa s_1} - q_{\varkappa s_2})^2. \qquad (16)$$

According to Pekar[5], the Stokes shift of the luminescence band relative to the impurity absorption band is ω; hence a can easily be obtained from available experimental data.

The integration in (15) can be carried out fully for the limiting case of low temperatures, when

$$\quad 1 \text{ and } \quad 1. \tag{17}$$

for then the Bessel function $I_{\ }$ of an imaginary argument can be represented by its leading term in a power series, and (15) becomes (for $p \quad 0$)

$$w(\Omega) = \frac{\pi |V_{s_1 s_2}(\Omega) V_{s_2 s_1}(\Omega_0)|^2 (2a)^p e^{\ }}{\hbar^4 \omega^3 \Gamma (\pi^2 \delta^2 + \sin^2 \pi f) \Gamma (p + 1)} \quad I_{pf}{}^2 \sum_{n=-\infty}^{\infty} \delta (p - n), \tag{18}$$

where

$$f = (\Omega_0 - \nu) \quad \omega, \tag{19}$$

$$I_{pf} = \frac{2}{(2i)^{p+1}} \oint_C (1 - \zeta)^p e^{\frac{a}{2}\left(\zeta - \frac{1}{\zeta}\right)} \frac{d\zeta}{\zeta^{f+1}}, \tag{20}$$

where the path of integration C goes clockwise about the point $\zeta = 0$.

Using the integral representation of the confluent hypergeometric function $F(\alpha, \gamma, z)$ (see Landau and Lifshits[6]), we obtain

$$|I_{pf}| = \frac{2\pi \Gamma (p+1)}{2^p |\Gamma (f+1) \Gamma (p-f+1)|} \left| F\left(-f, p-f+1, \frac{a}{2}\right) \right|. \tag{21}$$

Eq. (18) can now be written in the form

$$w(\Omega) = w(r, f) \sum_{n=-\infty}^{\infty} \delta (r + f - n), \tag{22}$$

where

$$w(r, f) = \frac{4\pi^3 |V_{s_1 s_2}(\Omega) V_{s_2 s_1}(\Omega_0)|^2}{\hbar^4 \omega^3 \Gamma (\pi^2 \delta^2 + \sin^2 \pi f)} \times \frac{\left(\frac{a}{2}\right)^p e^{-a} \Gamma (p+1)}{|\Gamma (f+1) \Gamma (p-f+1)|^2} \left| F\left(-f, p-f+1, \frac{a}{2}\right) \right|^2. \tag{23}$$

The spectroscopic intensity distribution of the scattered light depends, as usual, on the incident radiation, and may be written

$$I(\Omega) = N_0 \hbar \Omega \rho (\Omega) \int I_0 (f)\, w(\Omega)\, df, \tag{24}$$

where $I_0(f)\, df$ is the intensity of the incident radiation and N_0 is the number of scattering centers.

Inserting (22) into (24), we obtain

$$I(\Omega) = N_0 \hbar \Omega \rho (\Omega) \sum_{n=-\infty}^{\infty} w(r, n-r)\, I_0 (n-2). \tag{25}$$

Assuming further that the incident radiation has a sharp peak at $f = f_m$, we arrive at

$$I(\Omega) \sim \frac{\left(\frac{a}{2}\right)^{r+f_m} \Gamma (r + f_m + 1)}{(\pi^2 \delta^2 + \sin^2 \pi f_m) |\Gamma (f_m + 1) \Gamma (r+1)|^2} \left| F\left(-f_m, r+1, \frac{a}{2}\right) \right|^2. \tag{26}$$

Further simplification of (26) is hampered by the fact that in actual cases (large a and large r) the usual asymptotic approximation of the confluent hypergeometric functions is not valid. It is interesting to note, however, that if $f_m = 0$ the spectroscopic distribution of the scattered light is given by

$\left(\frac{a}{2}\right)^r \Big/ \Gamma (r+1)$ an expression which gives a "bell-shaped" curve with maximum

at $r = a/2$, i.e.,

$$\Omega_m = \nu - \frac{a\omega}{2}. \qquad (27)$$

The position of the maximum of this curve, its shape, and its half-width agree exactly with the corresponding parameters of the impurity luminescence curve.[5] In the general case (i.e., for $f_m \neq 0$), the intensity distribution given by (26) is more complicated and can only be evaluated by numerical computations.

I wish to express my gratitude to S.I.Pekar for valuable discussions.

Kishinev State University
Moldavian Branch, USSR Academy of Sciences

References

1. V.Weisskopf, Ann.Phys., 9, 23 (1931).
2. Iu.E.Perlin, Uch.zep. (Scientific notes) Kishinev Univ., 36, 6 (1958).
3. L.N.Ovander, Optika i spektroskopiia, 3, 221 (1957).
4. R.Kubo, Phys.Rev., 86, 929 (1952).
5. S.I.Pekar, Zhur.eksp.i teor.fiz., 22, 641 (1952).
6. L.D.Landau & E.M.Lifshitz, Kvantovaiia mekhanika (Quantum Mechanics), M. 1948.

PARAMAGNETIC RESONANCE OF IMPURITY CENTERS IN IONIC CRYSTALS

- M.F.Deigen

Introduction

Although electron spin and nuclear spin resonance methods for investigating impurity centers in semiconductors are relatively new, they have already yielded a number of fundamental results. For instance, the fine deviation in g-values was discovered[1], it became possible to estimate the magnitude of the ψ function of a trapped F-center electron at different points in the crystal[2], to make certain inferences regarding the nature of the F-centers[3], etc.

Theoretical work in this field has dealt with only two problems. These are the explanation of the width of the electron spin absorption line of F-centers in alkali halide crystals[2] and calculation of the wavelength of the electron spin resonance line in Group V impurity atoms in silicon[5]. Kip et al[2] state that even a rough orbital model of an F-center leads to a reasonable value for the broadening, while the generally accepted continuum model is not capable of explaining this effect and leads to a difference of four orders of magnitude between theory and experiment. I have shown elsewhere[5] that this result is not valid (see also Section 2 of the present paper).

Below I give some results of the theory of paramagnetic resonance of local electron centers in crystals as developed by me and my coworkers.

1. Spin Hamiltonian of the Hyperfine Interaction of a Trapped Electron[6,7]

The operator giving the hyperfine interaction of an electron with the magnetic moments of the nuclei in the crystal lattice may be written

$$\hat{H}_1 = -\sum_k \frac{\mu_k}{I_k} \mathbf{I}_k \mathbf{H}_{sk}, \tag{1}$$

where μ_k is the magnetic moment of the nucleus at the k-th site, $\mathbf{I}_k$ is the spin of this nucleus, $\mathbf{H}_{sk}$ is the magnetic field produced by the spin of the electron at the k-th site and is given by

$$\mathbf{H}_{sk} = \int \left[\operatorname{grad} \frac{1}{\rho_k}, \mathbf{j} \right] d\tau, \tag{2}$$

ρ_k is the distance from the k-th site to the electron, and $\mathbf{j}$ is the current density produced by the spin $\mathbf{S}$ of the electron:

$$\mathbf{j} = \operatorname{rot} \frac{\mu}{S} |\psi|^2 \mathbf{S}. \tag{3}$$

Inserting (2) and (3) into (1) and performing some manipulations, we arrive at the general form for the spin Hamiltonian giving the hyperfine interaction of the electron in the crystal lattice, namely

$$\hat{H}_s = 4\pi \sum_k \frac{\mu\mu_k}{SI_k} |\psi(\rho_k = 0)|^2 (\mathbf{I}_k \mathbf{S}) + \sum_k \frac{\mu\mu_k}{SI_k} \int (\mathbf{I}_k \operatorname{grad} |\psi|^2) \frac{S\rho_k}{\rho^3_k} d\tau. \tag{4}$$

Eq.(4) can be brought into more convenient form by using the strong-coupling approximation to construct the wave function ψ of the trapped electron.

For local centers with a spherically symmetric potential (such defect-centers are F-centers, impurity atoms in ionic and homopolar crystals, considered from the standpoint of the continuum model, and others), we have

$$\psi = \sum_k \psi_k (r,\ \rho_k). \qquad (5)$$

In the continuum model of local centers with smoothed out functions, we have

$$\sum_k \psi_k (r,\ \rho_k) = \varphi (r),$$

and when using detailed functions we have

$$\psi_k = \varphi (r)\, u_k (\rho_k),$$

where $u_k(\rho_k)$ is the wave function of the "extra" electron in the vicinity of the k-th site; finally, in the orbital model we have $\psi_k = u_k$, but now the sum in (5) must be extended to include the impurity nucleus.

After inserting (5) into (4) and performing several operations, we obtain

$$\hat{H}_s = \sum_k \frac{\mu\mu_k}{SI_k} [A_k (\mathbf{I}_k \mathbf{S}) + B_k (\mathbf{I}_k \mathbf{R}_k)(\mathbf{S}\mathbf{R}_k)] + \sum \frac{\mu\mu_k}{SI_k} \sum_{p,\ q} A_{pqk} (\mathbf{I}_k \vec{\tau}_{pk})(\mathbf{S}\vec{\tau}_{qk}). \qquad (6)$$

Here τ_{1k}, τ_{2k}, τ_{3k} are unit vectors along the Cartesian x_{1k}, x_{2k}, x_{3k} axes, whose origin lies at the k-th site (the x_{3k} axis lies along the vector $\mathbf{R}_k$ which gives the position of the k-th site relative to the defect); p and q take on the values 1, 2, and 3.

In the spin Hamiltonian (6) the spin and coordinate parts are separated. Therefore its form depends only on the symmetry of the problem. Different choices of functions in different approximations change only the values of the coefficients.

2. Theory of Electron Spin Resonance in F-Centers[5-7,9]

In considering the interaction of an F-center electron with the magnetic moments of the nuclei in the lattice, it is often sufficient to extend the sum in (6) only to the two coordination spheres closest to the vacancy. This is justified by the fact that in alkali halides, for instance, the radius of the F-center electron state is barely larger than the lattice constant.[10,2] For this reason the coefficients in the spin Hamiltonian decrease rapidly with distance from the vacancy.

If we now make use of the symmetry of the problem, the spin Hamiltonian giving the hyperfine interaction of an F-center electron with the first coordination sphere in an alkali halide crystal (with the metal nuclei) becomes

$$\hat{H}_s^{(1)} = A \sum_{k=1}^{6} \mathbf{I}_k \mathbf{S} + B \sum_{k=1}^{6} (\mathbf{I}_k \mathbf{R}_k)(\mathbf{S}\mathbf{R}_k). \qquad (7)$$

A characteristic property of (7) is the presence of the second, anisotropic term.

The continuum model with detailed wave functions leads, after cumbersome but not fundamentally difficult calculations, to analytic expressions for the coefficients in the spin Hamiltonian; it is then possible to carry out calculations for specific crystals.

The eigenvalues of (7) are given by

$$W = S_z \sum_{k=1}^{6} A_k I_k. \qquad (8)$$

Here S_z and I_k are the eigenvalues of $\hat{S}_z$ and $\hat{I}_k$ respectively. The static external field is aligned with the z axis of the system, and

$$\Delta_k = \sqrt{A^2 + BR_{kz}^2(2A + BR^2)}. \tag{9}$$

By using (8) one can find the frequencies of the transitions caused by the incident wave and the half-width of the absorption band. In addition, one can find the shape of this band by calculating the statistical weights of the individual states. Calculations of the half-widths for KCl and NaCl crystals give order of magnitude agreement with experiment.

Because the weight factor Δ_k depends on the mass number of the nucleus, the band shape differs somewhat from the Gaussian, although, as numerical calculations for alkali halide crystals show, the deviation is not large.

Thus Kip et al[2] notwithstanding, the correct application of the continuum model does give reasonable results both for the width and for the shape of the absorption curve.

We note also that in analogy with (7) the operator giving the hyperfine interaction of the F-center electron with the nearest halide nucleus is given by

$$\hat{H}_s^{(2)} = A'(\mathbf{I}_k\mathbf{S}) + B'(\mathbf{I}_k\mathbf{R}_k)(\mathbf{S}\mathbf{R}_k) + C I_{x_{sk}} S_{x_{1k}}. \tag{10}$$

3. Variation of the F-Center Hyperfine Structure with the Orientation of the Crystal in an External Magnetic Field[6]

Feher[11] studied microwave induced transitions (with $\Delta S = 0$ and $\Delta I = \pm 1$) in phosphorus-doped silicon. Similar transitions were observed experimentally in the nuclei of metal and halide ions surrounding F-centers in KCl.[12] For these transitions, we can write

$$h\nu = g_I \beta_I H + E_{S_H, I_H} - E_{S_H, I_H - 1}, \tag{11}$$

where g_I is the nuclear g-factor, β_I = the magneton, and E_{S_H, I_H} is the energy of the hyper-fine interaction.

Assuming that the field H is perpendicular to the [001] direction and makes an angle θ with the [100] direction, we can apply (10) to chlorine ions, for example, to obtain theoretical expressions for the frequencies of nuclear spin transitions as functions of θ. These functional dependences are shown in the form of curves in Fig.1a.

Fig.1 shows also the good agreement obtained with experiment (points). Thus for $\theta = 0$, the frequencies ν'_{001}, ν''_{001} and ν_{010} coincide; as θ is varied from 0 to 45° ν''_{001} increases, while the other two frequencies decrease. At $\theta = 0$, ν_{100} is lower than ν_{010} but becomes equal to it at $\theta = 45°$.

By comparing the experimental and theoretical curves, we can find the constants in the spin Hamiltonians of (7) and (10); then by simple numerical calculations we can obtain the squares of the electron wave functions at the potassium and chlorine sites. It was found that in KCl, for instance, $\psi_F^2(\mathrm{K}) = 0.70 \cdot 10^{24} \mathrm{cm}^{-3}$ and $\psi_F^2(\mathrm{Cl}) = 0.11 \cdot 10^{24}\ \mathrm{cm}^{-3}$. Thus the ratio of these values is 6.4, which indicates that the F-center electron is localized in the immediate proximity of the vacancy.

The constants in the spin Hamiltonian can be calculated from expressions deduced in Refs.5,6,7 & 9. The calculations show that both the continuum and the orbital models of F-centers lead to order-of-magnitude agreement between the theoretical and experimental values of the coefficients.

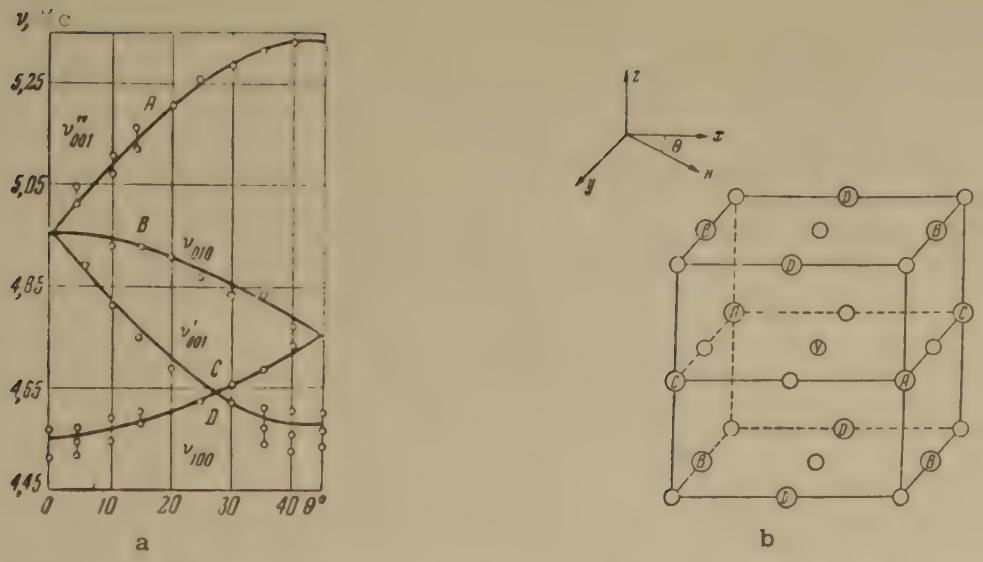

a b

Fig.1. a) Variation of the hyperfine structure of an F-center as a function of the crystal orientation in an external magnetic field. The curves correspond to the different groups of chlorine atoms identified in Fig.1b. The circle points are experimental values. b) Unit crystal cell. V - vacancy.

Finally, we note that the frequencies of nuclear spin transitions are about 1.2 times lower for Cl^{35} than they are for Cl^{37}, which corresponds to the value of the μ ratio for Cl^{35} and Cl^{37}.[5-7,9]

4. Electron Spin Resonance in Surstoichiometric Metal in NaCl type Crystals[13]

Electron spin resonance has been studied in the excess metal in NaCl type crystals (for instance, Na in NaCl). Methods similar to those of Sections 1 and 2 were used to deduce the spin Hamiltonian of the hyperfine interaction of the metal valence electron with its surroundings:

$$H_s = A_0\mathbf{I}_0\mathbf{S} + \sum_k B_{0k}(\mathbf{I}_0\mathbf{R}_k)(\mathbf{S}\mathbf{R}_k) + \sum_k A_k(\mathbf{I}_k\mathbf{S}) + \sum_k B_{1k}(\mathbf{I}_k\mathbf{R}_k)(\mathbf{S}\mathbf{R}_k). \qquad (12)$$

The first two terms give the energy of interaction of the electron with its own nucleus; the second two, with the surrounding nuclei.

Having the eigenvalues of (12), the frequencies of the transitions induced by the incident electromagnetic wave and the intensities of the corresponding electron spin transitions, we can determine the shape of the absorption curve.

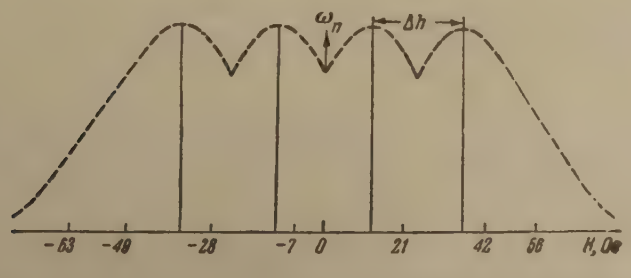

Fig.2. Absorption curve of interstitial Na atoms in NaCl.

This curve for the case of Na in NaCl is shown in Fig.2. The absorption band was the following properties. The contour is symmetric about the Zeeman frequency; it comprises four lines of equal intensity, associated with the interaction of the electron spin with the spin of the impurity nucleus. For this reason the absorption curve is not Gaussian (as was shown in Section 2, such a curve would be characteristic

for electron spin resonance in the case of a DeBoer model F-center. This mechanism can therefore be used to differentiate between the DeBoer model and that of Hilch and Pohl.

Numerical calculations for NaCl show that it should be feasible to resolve the most intense lines experimentally.

Finally, in this case there should be a characteristic dependence of the hyperfine structure on the crystal orientation in an external static magnetic field. This follows from the anisotropic terms in (12).

5. Hyperfine Interaction and Electron Spin Resonance in Polarons and Excitons[14]

Let us consider electron spin resonance in systems whose energy operator has translational symmetry.

It can readily be shown that in such systems (which include polarons and excitons) the energy correction due to the hyperfine interaction vanishes in the first approximation. This is because of the nonlocal nature of the wave functions, in view of the fact that the electrons interact to the same extent with the magnetic moments of all the nuclei in the crystal. Thus the hyperfine interaction is proportional to the average nuclear magnetic moment per unit volume, which is obviously zero.

It follows that, in contrast to the case of local centers, hyperfine interaction where excitons and polarons are concerned will not lead to broadening of the spin resonance absorption line. This can be used to differentiate experimentally between polarons and local electron centers.

The author has shown theoretically[15-17] that in ammonia solutions the atoms of an alkali metal dissociate and the freed electrons form polarons. These polarons are responsible for the electrical conductivity and optical properties of ammonia solutions of metals.

Experimental studies of electron spin resonance in color centers in metal-ammonia solutions[18] have shown that the width of the spin resonance absorption region is of the order of 0.1 gauss, i.e., about 10^{-4} the width in F-centers.

This obviously indicates that these color centers are not local electron centers, but polarons. This was first pointed out by Pekar.[19]

Evaluations of equilibrium exciton concentrations lead to values of 10^{15} to 10^{16} cm^{-3}. With such concentrations it should be possible to observe spin resonance absorption experimentally.

It must be noted that the total spin of the electrons in a dielectric in its ground state is zero. In the case of optical transitions, the total spin remains zero. When, however, an rf quantum is absorbed by an exciton, the total electron spin becomes ± 1, so that the reverse transition from the exciton to the ground state is essentially forbidden. It follows then that an exciton produced by absorption of an rf quantum will normally have a much longer lifetime than an ordinary exciton.

Physical Institute
Academy of Sciences of the Ukrainian SSR

References

1. C.A.Hutchison & G.A.Noble, Phys.Rev., 87, 1125 (1952).
2. A.F.Kip, C.Kittel, R.A.Levy & A.M.Portis, Phys.Rev., 91, 1066 (1953).
3. C.J.Delbecq, B.Smuller & P.H.Juster, Phys.Rev., 104, 599 (1956).
4. W.Kohn & I.M.Luttinger, Phys.Rev., 97, 883 (1955).
5. M.F.Deigen, Zhur.eksp.i teor.fiz., 33, 773 (1957). (Trans.Soviet Physics - JETP.)

6. M.F.Deigen & V.Ia.Zevin, Ibid., 34, 86 (1958).
7. V.Ia.Zevin, Optika i spektroskopiia, 3, 660 (1957).
8. S.I.Pekar, Issledovanie po elektronnoi teorii kristalov (Studies in the electronic theory of crystals), M.-L., 1951.
9. M.F.Deigen & L.A.Shul'man, Optika i spektro., 3, 21 (1957).
10. M.F.Deigen & S.I.Pekar, Zhur.eksp.i teor.fiz., 18, 481 (1948).
11. G.Feher, Phys.Rev., 103, 834 (1956).
12. G.Feher, Phys.Rev., 105, 1122 (1957).
13. M.F.Deigen & M.D.Glinchuk, Zhur.eksp.i teor.fiz., 28, 1981 (1956).
14. M.F.Deigen & S.I.Pekar, Zhur.eksp.i teor.fiz., 34, 684 (1958). (Trans. Soviet Phys. - JETP.)
15. M.F.Deigen, Zhur.eksp.i teor.fiz., 26, 293 (1954).
16. M.F.Deigen, Ibid., 26, 300 (1954).
17. M.F.Deigen & Ia.A.Tsvirko, Ukr.fiz.zhur. (Ukrainian Phys.Journal), 1, 245 (1956).
18. C.A.Hutchison & R.C.Pastor, Phys.Rev., 81, 282 (1951).
19. G.E.Pikus & Iu.A.Firsov, Zhur.tekh.fiz., 25, 2381 (1955).

ABSORPTION AND LUMINESCENCE SPECTRA OF ALKALI-HALIDE CRYSTALS CONTAINING IMPURITY IONS WITH ISOELECTRONIC SHELLS

- M.L.Kats

Introduction

A very real, and at the same time hardly studied, problem in the physics of crystal phosphors is the problem of luminescence centers and the mechanism of selective absorption of light by activating impurities. One of the assumptions made at present regarding the nature of absorption and luminescence centers in activated crystals is that these are ions or atoms of the activating impurity whose electron shells are deformed and whose energy levels are shifted or even split (as compared with the levels of the free impurity)owing to interaction of the activating impurity with the ions of the host lattice. In other words, it is assumed that impurity absorption and luminescence bands are associated with electron transitions between the energy levels of the activating impurity itself.

It follows that, provided the electron shell is not excessively distorted, the absorption and emission spectra and other properties of crystals containing impurity ions of different heavy metals should exhibit considerable similarity if these ions have isoelectronic shells. Such similarity, if observed, would serve as a confirmation of the above hypothesis concerning the mechanism of impurity absorption and the nature of luminescence centers in crystal phosphors. Consequently, a detailed investigation of the absorption and luminescence spectra of alkali-halide crystals activated by ions of heavy metals having isoelectronic shells was undertaken in our laboratory.

Crystals activated by In^+ and Sn^{2+} ions

The single crystals studied were grown from melts of KBr + InBr and KBr + + $SnBr_2$ with comparatively low concentrations of the activating impurities; these presumably were incorporated into the lattice as In^+ and Sn^{2+} ions, which have isoelectronic shells with identical electron configurations.

Absorption and emission spectra of alkali-halide crystals activated by tin were studied in the work of Refs.1-4. An interpretation of the mentioned spectra, based on a study of the changes in the spectra which developed under the influence of hard radiation and additive coloring, was given by the author in Refs.2-4.

The absorption spectra were investigated by means of an SF-4 quartz photoelectric spectrophotometer; the luminescence spectra were studied by the photographic procedure on an ISP-51 spectrograph in the visible region and an ISP-66 instrument in the ultraviolet region. The spectrograms were scanned on an MF-2 microphotometer. The monochromator of an SF-4 spectrophotometer was used for studying the excitation spectra; the usual photocell assembly was replaced by an FEU-19 photomultiplier; special light filters were inserted between the latter and the crystal phosphor in order to shield the photomultiplier photocathode from the direct exciting light.

It will be evident from curve a in the accompanying figure that the absorption spectrum of KBr:In single crystals consists of a very intense short wavelength band with a maximum at 2435 Å and a considerably less intense longer wavelength group of bands peaking 274, 293 and 303 mμ.[5] In the same figure, we present for comparison curve b which characterizes the absorption of the KBr-Sn crystal phosphor. It can be seen that the two spectra are virtually identical, except for the presence of structure in the short wavelength band of KBr:Sn (curve b). The longer wavelength group of bands in the KBr:Sn spectrum is appreciably less intense than the short wavelength band and, as in the case of KBr:In, has three maxima: at 278, 304 and 318 mμ.

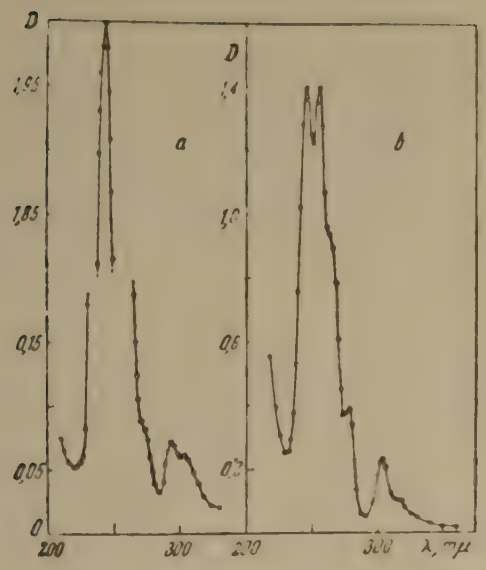

Intensity distribution curves for the absorption of single crystals: a) KBr: In and b) KBr: Sn. D - optical density values from spectrograms.

Such great similarity of the absorption spectra cannot be fortuitous and is, without doubt, due to the fact that the excitation processes take place in the activator ions per se. Thus, to interpret the absorption spectrum of the KBr: In crystal, one can start, as in the case of KBr: Sn (Refs. 2-4), from the level diagram for an isolated In^+ ion, keeping in mind the displacement of these levels under the influence of the lattice field of the host substance. According to the said level diagram, we can attribute the short wavelength band to $5s^2\,{}^1S_0 \rightarrow 5s5p\,{}^1P_1$ transitions. The "fine" structure of this band in the case of KBr: Sn may be due to splitting the $5s5p\,{}^1P_1$ level, owing to an intracrystalline Stark effect.

It is easy to understand the absence of a similar structure in the spectrum of KBr: In if we recall that the In^+ ion deforms the intracrystalline field much less than the doubly-charged Sn^{2+} ion.

The longer wavelength group of bands in the case of KBr: In, as in the case of KBr: Sn, is due to the triplet structure of the $5s5p\,{}^3P$ term and the possibility of intercombinational transitions between the $5s^2\,{}^1S_0$ ground state and the triplet components $5s5p\,{}^3P_2$, $5s5p\,{}^3P_1$ and $5s5p\,{}^3P_0$. We note that the selection rule for ${}^1S_0 \rightarrow {}^3P_2$ and ${}^1S_0 \rightarrow {}^3P_0$ transitions does not hold strictly even for gases[6], and that the forbiddenness may be mitigated or removed in a crystal lattice under the influence of the intracrystalline field.

After irradiation of the phosphor with x-rays, the absorption at the intense short wavelength band decreases; at the same time, the absorption at 274, 293 and 303 mμ increases owing to the formation of V-centers in the crystal. This inference is substantiated by the appearance in x-irradiated KBr: In of an additional absorption band at about 270 mμ; this value agrees within the limits of the experimental error with the peak wavelength of the V-band (267 mμ) in pure KBr crystals.[7]

It follows from analysis of the experimental results that a reduction in the concentration of the ionic activator centers occurs after irradiation of the phosphor with x-rays. Similar effects in other alkali-halide phosphors[8] are usually caused by the trapping of electrons by the ionic activator centers and by the formation of atomic centers, which have characteristic absorption bands. In the case of KBr: In, a new additional absorption band peaking at 325 mμ also develops; however, it appears only after the F-band is bleached, a process which involves trapping of electrons by the ionic centers. The absorption at the V-band also decreases at the same time in consequence of recombination of the V-centers with electrons freed in the optical dissociation of the F-centers.

As in the case of KBr: Sn, the fluorescence spectrum of KBr: In consists only of one band with a maximum at 425 mμ; the shape and wavelength of the band are independent of the frequency of the exciting light.

Again, for KBr: In, as for KBr: Sn, the spectral distribution curve for the effective excitation fully reproduces the curve for the spectral distribution of the absorption.

The experimental data show that emission from KBr:In and KBr:Sn phosphors occurs as a result of electron transitions only from a single discrete excitation level to the ground state. From the fact that the fluorescence spectra are independent of the excitation frequency, it follows that the departure level for these transitions must be the lowest lying excited level. Electron transitions to this level from higher levels are evidently nonradiative.

Crystals activated by Tl^+ and Pb^{2+} ions

Tl^+ and Pb^{2+} ions also have isoelectronic shells and alkali-halide phosphors activated by them (especially thallium) have been the subjects of numerous experimental and theoretical investigations. A comparison of the data in the literature shows that the absorption and luminescence spectra, as well as other properties, of alkali-halide phosphors activated by Tl^+ and Pb^{2+} ions also exhibit marked similarities.

Although no one noted it explicitly, it should have been obvious even from the early measurements of Hilsch[9] that the absorption spectra of alkali-halide crystals doped with thallium or lead are entirely identical as regards the number and shape of the bands. In both cases, regardless of the host cation or anion, the spectrum consists of two main bands: an intense short wavelength band and a less intense longer wavelength one in the 2000-3000 Å region. The location and shape of these bands are completely identical in different alkali-halide crystals having a common anion; upon replacement of the anion - going from Cl^- to Br^- to I^- - the shape does not change but the bands are progressively shifted to longer wavelengths.

However, comparison of the absorption spectra of activated and pure alkali-halide crystals shows that the said shift is not associated with direct participation of the halogen ions in absorption processes. It is caused by enhanced interaction of the activator ions with neighboring halogen ions, whose radii and polarizabilities increase in going from Cl^- to Br^- to I^-.

The luminescence spectra of alkali-halide crystals activated by thallium and lead are also identical in structure. In contrast to the luminescence spectra of alkali-halide crystals doped with indium and tin, which comprise only a single band in the visible region, the spectra of alkali-halide crystals activated with thallium and lead contain two bands, one in the visible, the other in the ultraviolet region. Thus, the luminescence bands of NaCl:Pb peak at 4530 and 3180 Å, while those of KCl:Tl are centered at 4750 and 2980 Å.

Recent studies[10] of the absorption and excitation spectra of NaCl:Pb phosphors showed that the longer wavelength absorption band is complex and actually consists of at least two bands: one in the 2600 to 2950 Å region with a maximum at 2730 Å, and the second in the 2750 to 3100 Å region with a maximum at 2900 Å. An additional excitation band at 2600 Å was observed for NaCl:Pb phosphors grown from solutions. Thus, the longer wavelength absorption band in the NaCl:Pb spectrum has a structure which may be associated with the triplet structure of the $6s6p^3P$ term and by intercombinational transitions between the $6s^2\,{}^1S_0$ ground state and the triplet components $6s6p^3P_2$, $6s6p^3P_1$ and $6s6p^3P_0$.

So far triplet structure of the longer wavelength absorption band has not been observed in the case of Tl-activated single crystals.

However, in some cases, the triplet structure of the term associated with the longer wavelength absorption band is evinced very clearly in the luminescence spectrum. Thus, for example, the ultraviolet band in phosphorescence of a NaBr:Tl crystal splits at low temperature into three bands[11] peaking at 3.36, 3.46 and 3.56 μ. According to the calculations of Williams[12], the longer wavelength absorption band and the ultraviolet luminescence band in Tl-activated alkali-halide phosphors are associated with $^1S_0 - {}^3P$ transitions.

In addition to the bands mentioned above, another band has been observed in the luminescence spectra of KCl:Tl and NaCl:Pb (at 3775 Å and 3850 Å, respectively). These bands are highly sensitive to the activator concentration, and, according to Schulman & Ginther[10] and Williams et al[12], are caused by activator ion pairs, the luminescence spectrum of which changes with time owing to interaction between them.

Conclusions

Alkali-halide crystals activated with ions having isoelectronic shells show very marked similarities as regards their absorption, excitation and luminescence spectra, and other properties. Such congruences indicate that the processes of absorption and emission in such crystals are associated with electron transitions between activator ion levels that are shifted, under the influence of the intra-crystalline field, relative to their "normal" positions in the free impurity atoms.

"N.G.Chernyshevskii" Saratov State University

References

1. M.Huniger & J.Rudolf, Z.Phys., 117, 81 (1941).
2. A.S.Andrianov & M.L.Kats, Doklady AN SSSR, 96, 253 (1954).
3. A.S.Andrianov & M.L.Kats, Transactions of the Fifth Conference on Luminescence, p.67, Tartu, 1956. (Translated abstract - Bulletin 21, No.4, 547).
4. M.L.Kats, Optika i spektroskopiia, 3, 602 (1957).
5. M.L.Kats & V.K.Nikol'skii, Optika i spektro., 4, 354 (1958).
6. G.Herzberg, Atomic Spectra and Atomic Structure. (Cited in Russian trans.)
7. H.Pick, Fundamental Mechanisms of Photographic Sensitivity, p.9. - London, 1951; H.Pick & R.Pohl, Z.Naturforsch, a, 6, 360 (1951).
8. M.L.Kats, Doklady AN SSSR, 85, 539 & 757 (1952); Zhur.eksp.i teor.fiz., 23, 720 (1952); M.L.Kats & B.Z.Semenov, Doklady AN SSSR, 106, 415 (1956).
9. R.Hilsch, Z.Phys., 44, 860 (1927).
10. I.H.Schulman & R.Ginther, JOSA, 40, 854 (1950).
11. W.Meyeren, Z.Phys., 61, 341 (1930).
12. F.E.Williams, Chem.Phys., 19, 457 (1951); P.D.Johnson & F.E.Williams, J.Chem.Phys., 20, 124 (1952).

SPECTROSCOPY OF LUMINESCENCE CENTERS IN ALKALI HALIDE CRYSTAL PHOSPHORS ACTIVATED BY MERCURY-LIKE IONS

- Ch.B.Lushchik & N.E.Lushchik

The spectral characteristics of free "mercury-like ions" (Ga^+, Ge^{2+}, In^+, Sn^{2+}, Tl^+ and Pb^{2+}) have been thoroughly studied. The luminescent characteristics of alkali halide phosphors activated by thallium, lead and tin have also been investigated (for a review of the work in this field see Refs. 1-3). In the past year KCl and KBr phosphors activated by indium, gallium and germanium were synthesized by one of the present authors[4-6] (see also Ref.7). This made possible a detailed comparison of the characteristics of free mercury-like ions and of luminescence centers in the corresponding crystal phosphors[3,8]. We obtained the absorption, excitation and emission spectra of KCl and KBr single crystals activated by Ga^+, Ge^{2+}, In^+, Sn^{2+}, Tl^+ and Pb^{2+} ions (Figs. 1 & 2). For several of these phosphors, Shvarts[9] determined the activation energy of temperature quenching of luminescence. The trapping centers in these phosphors and their recombination luminescence were studied in the work of Refs. 4 & 10-13.

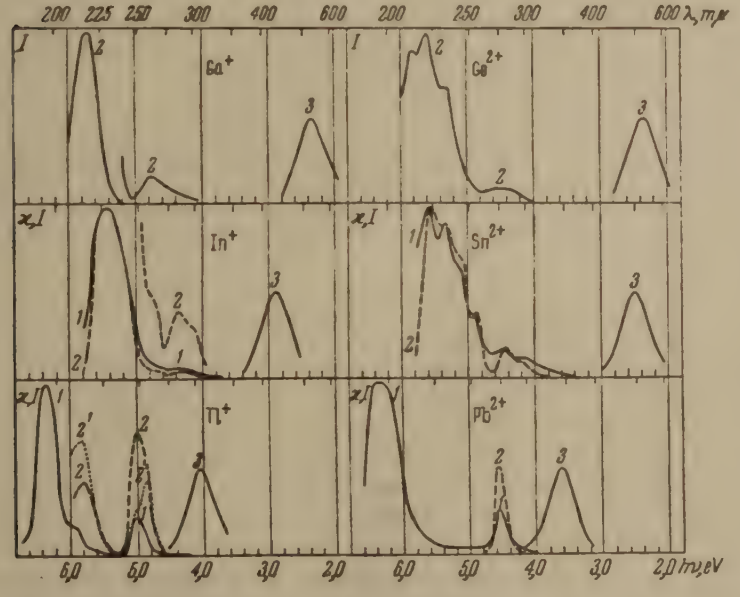

Fig.1. Absorption (1), excitation (2) and emission (3) spectra of KCl single crystals activated by mercury-like ions; (2') - excitation spectrum of the band peaking at 475 mμ.

The absorption (excitation) spectra of all of the phosphors are similar as regards electronic structure; all the spectra comprise one wide intense band (split in some cases) and a group of three weaker, longer wavelength bands. Comparison of several energy and probability relationships for the homologous series of the free activator ions and the homologous series of the phosphors showed[3] that these bands can be attributed to $^1S_0 \longleftrightarrow$ $\longleftrightarrow {}^1P_1$ and $^1S_0 \rightarrow {}^3P_{0,1,2}$ transitions (analogous assignments for individual bands of a number of phosphors were made in Refs.1,10,14, 15 & 17).

A quantitative comparison of the characteristics of the free ions and luminescence centers indicates, however that the intracrystalline field changes the properties of the mercury-like ions to a greater extent than it does those of rare earth ions (see Ref.18).

A convenient parameter for characterizing the change in the separation between the levels of an impurity ion when it is introduced into the host lattice is the ratio of the transition energy E_f in the free ion to the transition energy E_C in the impurity center in the crystal (we take $E_C = E_m^x$, the energy corresponding to the peak

of the absorption band). From the standpoint of principle, it is worth noting that the "compression coefficient" $\rho = E_f / E_c$ is greater than unity for all of the investigated metallic impurities in alkali halide crystals, i.e., the lattice field reduces the spacing between the energy levels of all cationic impurity centers. For anionic impurity centers, one may expect the inverse relationship: $\rho < 1$, and this does actually obtain for H^- centers in KCl:KH ($\rho \approx 0.13$). The difference in the value of ρ for cationic and anionic impurities is probably associated with the fact that negative ions (unlike positive ones) are "compressed" in the lattice field.[19,20]

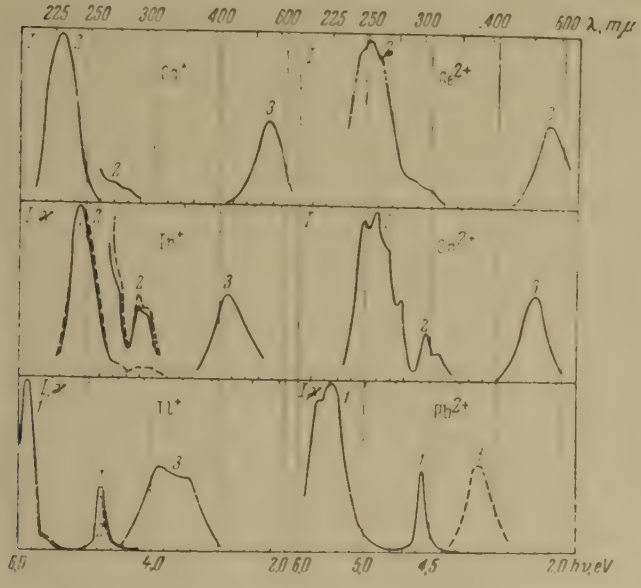

Fig.2. Absorption (1), excitation (2) and emission (3) spectra of KBr single crystals activated by mercury-like ions.

Upon introduction of the ion into the lattice field, the relative locations of the energy levels of a given configuration ($^3P_0$, $^3P_1$, $^3P_2$ and $^1P_1$) are altered in a manner indicating weakening of the Russel-Saunders (L-S) coupling by the crystal field[3].

It was found that $\rho \approx 1 + aE_f$.[3] This approximate relationship allows of making several important, although necessarily rough evaluations. Thus, using the transition energies in the free ions and this relationship, we were able to predict correctly the location of the main absorption (excitation) bands of the heretofore unprepared phosphors KCl:Ga and KCl:Ge[3,6] and the location of the absorption bands, which have not been investigated up to the present, corresponding to the $n^1S_0 \rightarrow (n+1)^1P_1$ transitions in a series of phosphors activated by mercury-like ions[3].

The intracrystalline field causes splitting of the level of mercury-like ions into three sublevels. This effect is particularly clearly evinced in phosphors activated by Sn^{2+} and Ge^{2+} and corresponds to a complete splitting into (2J + 1) components, which, according to Bethe[21,18], is possible in a field having rhombic or lower symmetry. This should be related to local changes in the symmetry of the field caused by microdefects in the crystal lattice (for example, vacant sites, dislocations) or to non-fully symmetrical vibrations of the surrounding host ions.

The crystal field of the lattice only insignificantly weakens the forbiddenness with respect to ΔS (by less than a factor of 10), but it very strongly affects the ΔJ selection rules. In crystals activated by Ga^+, In^+, and Tl^+, the probability of the forced dipole $^1S_0 \rightarrow {}^3P_0$ and $^1S_0 \rightarrow {}^3P_2$ transitions is increased by at least a million-fold.[3,5]

The electronic-vibrational structure of the spectra was studied most completely and systematically by Pekar and his co-workers[22-25] with two principal simplifying assumptions: that the vibrations are purely harmonic and that the change in the vibration frequency of

the ion after excitation of the center is negligibly small.* For impurity centers of relatively large radius, the "frequency change effect" is apparently small ($\omega_1 = \omega_2$); consequently, the Pekar theory agrees satisfactorily with experiment in a number of cases (for example, for F_2 centers[28]).

However, as was shown by micro-calculations[15,29], the effective radii of the luminescence centers in alkali halide phosphors activated by Tl^+ and Ag^+ ions are small. In this case the "effect of frequency change incident to phototransitions" ($\omega_1 \neq \omega_2$) may be significant. This is indicated by several experimental facts[3,8]. Here we note only the most important of these, namely, the large difference between the half-widths of the absorption and emission bands, δ^x and δ^l, corresponding to the very same electronic-vibrational $^1S_0 \rightarrow {}^3P$ transition in the luminescence centers of all of the crystal phosphors studied in the present work (also see Refs. 26 & 27).

Simple calculations in the framework of the "method of potential curves"[15,16,30], using the semi-classical Franck-Condon principle, showed that at temperatures which exceed the "characteristic temperature of the luminescence center", $l = (\omega_1 - \omega_2)^2 = (\delta^l / \delta^x)^2$ (Ref. 3). For the phosphors we investigated, the value of l varies in the range from 1.5 to 2.5, i.e., the "frequency change effect" after a phototransition is significant, which is evidence of interaction of the center with local lattice vibrations. In the same approximation, we generalized the Pekar-Krivoglaz relations[22,23] between the absorption energy E_m^x and the radiated energy E_m^l, the half-widths δ^x and δ^l, the energy E_c of a pure electronic transition and the activation energy Q for temperature quenching:

$$E_m^x - E_c^l = \frac{1}{8kT\ln 2} \cdot \frac{l(l+1)}{2} (\delta^x)^2 = \frac{1}{8kT\ln 2} \cdot \frac{l+1}{2l^2} (\delta^l)^2; \quad (1)$$

$$Q = \frac{E_m^x - E_m^l}{l+1} \left[\frac{\left(\frac{E_m^x l^2 - E_m^l}{E_m^x - E_m^l} \right)^{1/2} - l}{l-1} \right]^2; \quad (2)$$

$$\frac{E_c - E_m^l}{E_m^x - E_c} = l. \quad (3)$$

The more rigorous Pekar-Krivoglaz relationships can be obtained from these expressions for $l = 1$. In the case when $l = 1$, the calculated activation energy (2) for temperature quenching differs from the experimental value[9] by an appreciable factor. The difference between the theoretical and experimental values of $l' - l$ is also considerable. Using $l = l(\omega) \neq 1$ significantly improves the agreement between the theoretical and experimental values of Q and $E_m^x - E_m^l$, but does not completely eliminate the discrepancy.[8] The nature of the deviation between the theoretical and the experimental values and, also, the rather significant shift of the absorption and emission band peaks with temperature indicate that it is necessary to take into account anharmonicity of the lattice vibrations.

---

*An attempt was made in Refs. 26 & 27 to calculate the "frequency factor".

Because of the large Stokes loss (1-2 ev) in the luminescence centers of phosphors activated by mercury-like ions, the elementary emission and absorption bands have the Gaussian shape, as predicted by the Pekar theory[22] and as follows from the Klick model[16] A detailed study of band contours reveals a small asymmetry in the spectra because of changes of the vibrational frequencies during photoexcitation. Mirror symmetry of the absorption and emission bands is not realized and the asymmetry of the absorption bands at temperatures above the characteristic temperature is anomalous,[8] as should be the case for $\omega_1 > \omega_2$.

Calculations of the potential curve parameters for the luminescence centers, using the experimental data obtained at various temperatures, showed[31,8] that l, Q and E_0 depend on the temperature. This, as was predicted by Lax[30], indicates that the single-coordinate approximation is inadequate for describing such complex systems as luminescence centers in crystal phosphors. The inadequacy of the Klick-Williams model, which takes into account only fully symmetrical vibrations of the surrounding ions, is also evident from a number of other experimental factors[3,8].

However, the Klick-Williams model can be regarded as a fairly good first approximation for describing the luminescence centers in phosphors activated by mercury-like ions. Using this model it is feasible to study semiquantitatively a number of important spectral regularities·(for example, the relation between the optical and thermal attributes) characteristic of luminescence centers and to make approximate evaluations that may be of value to experimenters.

The existence of a new physical phenomenon, namely, "optical quenching" in impurity centers, was recently predicted using this model, and, on the basis of this effect, analysis was made of the criteria for the occurrence of luminescence and for deviations from Vavilov's law.[32,3,33,8]

Institute of Physics and Astronomy,
Academy of Sciences of the Estonian SSR

References

1. K.V.Shalimova, Dissertation, Physical Institute of the Academy of Sciences of the USSR, M., 1953.
2. F.D.Klement, Trudy (Proceedings, Inst. Physics & Astronomy, Acad. of Sci., Estonian SSR), No.1, 3 (1955).
3. N.E.Lushchik & Ch.B.Lushchik, ibid., No.6, 5 (1957).
4. N.E.Lushchik, ibid., No.6, 149 (1957); Izv.AN SSSR,Ser.fiz., 21, 754 (1958). (Trans. Bulletin, 21, No.5, 748.)
5. N.E.Lushchik, Trudy (Proceedings, Inst. Physics & Astronomy, Estonian SSR Ac. of Sci.), No.7, 119 (1958).
6. N.E.Lushchik, ibid., No.7, 134 (1958).
7. Iu.N.Zhvanko, Z.L.Morgenshtern & L.M.Shamovskii, Optika i spektroskopiia, 2, 821 (1957).
8. Ch.B.Lushchik, N.E.Lushchik & K.K.Shvarts, Trudy (Proceedings, Inst. Physics & Astronomy, Estonian SSR Ac. of Sci.), No.8, 3 (1958).
9. K.K.Shvarts, ibid., No.7, 153 (1958).
10. Ch.B.Lushchik, ibid., No.3 (1955).
11. Ch.B.Lushchik & V.I.Volin, ibid., No.7, 311 (1958).

12. Ch.B.Lushchik, N.E.Lushchik, G.G.Liidkia & L.A.Teiss, ibid., No.6, 63 (1957).
13. Ch.B.Lushchik & G.G.Liid'ia, ibid., No.7, 193 (1958).
14. F.Seitz, J. Chem. Phys., 1, 150 (1938).
15. F.Williams, J.Chem.Phys., 19, 457 (1951); ibid.,57, 780 (1953).
16. C.Klick, Phys.Rev., 85, 154 (1952); C.Klick & J.Schulman, JOSA, 42, 910 (1952).
17. P.Yuster & C.Delbecq, J.Chem.Phys., 21, 892 (1953).
18. M.A.El'iashevich, Spektry redkikh zemel' (Spectra of the Rare Earths), M., 1953.
19. M.I.Petrashen', A.V.Ivanova & G.Vol'f, Vestnik, Leningrad State University, No.10, 29 (1956).
20. N.N.Kristofel', Trudy (Proceedings, Inst., Physics & Astronomy, Estonian SSR Ac. of Sci.), No.7, 85 (1958).
21. H.Bethe, Ann.Phys., 3, 133 (1929).
22. S.I.Pekar, Zhur.eksp.i teor.fiz., 22, 641 (1952); Usp.fiz.nauk, 50, 197 (1953); Izv.AN SSSR,Ser.fiz., 18, 712 (1954).
23. M.A.Krivoglaz, Zhur.eksp.i teor.fiz., 25, 191 (1953).
24. M.A.Krivoglaz & S.I.Pekar, Trudy (Proceedings, Physics Institute, Ukrainian SSR Ac. of Sci.) No.4, 37 (1953).
25. M.A.Krivoglaz, Optika i spektroskopiia, 1, 54 (1956).
26. R.Kubo, Phys.Rev., 86, 929 (1952); R.Kubo & V.Toyozawa, Progr.Theor. Phys., 13, 160 (1955).
27. A.F.Lubchenko, Optika i spektroskopiia, 2, 195 (1957).
28. G.A.Tishchenko & P.P.Feofilov, Izv.AN SSSR,Ser.fiz., 20, 482 (1956). (Trans. Bulletin, 20, No.4, 440.)
29. N.D.Potekhina, Optika i spektroskopiia, 2, 388 (1957).
30. M.Lax, J. Chem. Phys., 20, 1752 (1952).
31. D.Patterson & C.Klick, Phys.Rev., 105, 401 (1957).
32. C.Klick, D.Dexter & G.Russell, Phys.Rev., 100, 603 (1955).
33. K.K.Rebane, Trudy (Proceedings, Inst. Phys.& Astr., Estonian SSR Ac. of Science), No. 7, 62 (1957).

FLUORESCENCE OF PURE CADMIUM SULFIDE AT LOW TEMPERATURES

- E.Grillot and M.Bancie-Grillot

It is known from the work of Ewles[1], Randall[2] and Kröger[3], dating back nearly a quarter of a century, that very pure cadmium sulfide cooled to the temperature of liquid air emits a bright green luminescence in the 5000-5400 Å region. It is noteworthy that this luminescence band comprises several equally spaced peaks which become increasingly prominent as the temperature is reduced. The origin and nature of this fluorescence in the neighborhood of the principal absorption edge, which are of considerable importance from the standpoint of theory, cannot be explained by the presence of impurities and hence merit special consideration.

There are two contradictory points of view regarding the origin of this fluorescence. According to one, the green fluorescence at the absorption edge is associated with the recombination of electrons and holes, occurring at unidentifiable points in the crystalline lattice. This led to coining of the term "lattice emission". The green fluorescence of pure cadmium sulfide at low temperatures is an indication of the fact that direct optical transitions from the conduction band to the valence band are not absolutely forbidden. Apparently, this forbiddenness is of the first degree and, in the absence of impurity luminescence centers, the conduction to valence band transition probability is not strictly zero. The presence of the several equally-spaced peaks in this case is explained by lattice vibrations.

Three years ago, Kröger and Meyer[4] noted that the green fluorescence of very pure cadmium sulfide at low temperatures is an attribute of an ideal, undisturbed lattice. However, theoretical analyses, assuming the participation of photons, excitons or phonons in the optical transitions, showed that the photon contribution must be significantly smaller than that of the other two quasiparticles.

Certain other facts, observed by Klick[5], give reason to infer that the green luminescence may be attributed not to electron transitions from band to band, but to exciton transitions. Klick, however, did not share this opinion[5]. In a paper published in 1953, he insisted that it was impossible to decide definitively between a nonlocalizable and a localizable lattice mechanism. He regarded another hypothesis as more probable and supported this by a number of arguments, particularly by reference to the infrared absorption band observed at room temperature by Plyler at about 34 μ. Since there were no clear data for settling this important question, we decided in 1955 that it was necessary to study the entire problem more deeply from other positions.

If, as assumed in the first hypothesis, the green fluorescence of very pure cadmium sulfide at low temperatures is caused by a nonlocalizable mechanism, it should depend only on the properties of the crystal lattice. In all of the cases in question, we have a lattice of the hexagonal type, the parameters of which can change under the influence of a number of physical factors (temperature, pressure); however, the lattice properties should not depend on the procedure employed in preparing the crystal. That is, regardless of how the crystal is prepared, a green fluorescence should be observed at very low temperatures. On the contrary, if the emission is due to a mechanism localized in the lattice, i.e., associated

with some defects that act as luminescence centers at low temperatures, the green fluorescence should vary depending on the procedure used for preparing the crystals, since the concentration and even the nature of the lattice defects are influenced by the crystal growth technique.

This approach proved fruitful. It enabled us to show that the green fluorescence of cadmium sulfide at low temperatures must be attributed to discrete luminescence centers distributed through the crystal lattice. Moreover, in one special case of preparation, in which the green fluorescence of the crystal was insignificant, we were able to observe an intense blue emission consisting of lines forming a quasi-hydrogen-like series.

Until now the luminescent emission at the absorption edge of the cadmium sulfide has been studied using polycrystalline specimens or very recently single crystals synthesized from the gaseous phase. In the present work, we experimented with six types of high purity cadmium sulfide specimens prepared by different procedures.

None of the specimens exhibited fluorescence in the visible and infrared regions of the spectrum at ordinary temperatures. The inclusion of traces of silver, however, caused a bright red fluorescence, regardless of whether we were dealing with a polycrystalline powder[6] or single crystals[7]. Traces of copper gave rise to infrared luminescence[8]. Consequently, the absence of luminescence in our samples may be taken as an indication of their high purity, at least as regards impurity centers causing luminescence or quenching thereof.

Sample No.1 consisted of powdery polycrystalline cadmium sulfide, prepared from cadmium disulfide. This substance was obtained by the prolonged evaporation of a highly concentrated solution of Cd^{2+} and $S_2O_3^{2-}$. When heated above 500°, the disulfide transforms into well-crystallized cadmium sulfide, free of excess sulfur. This purification, which avoids the formation of a sulfur lattice, has the advantage that almost all traces of oxygen, which has a very strong effect on luminescence[9], are removed.

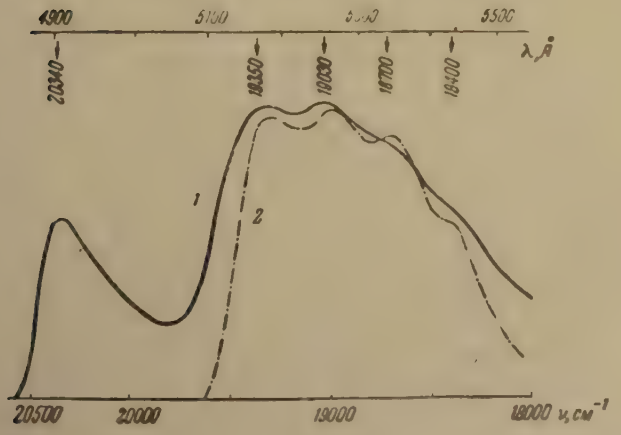

Fig.1. Fluorescence of pure CdS at 20°K: 1 - fine crystalline powder heated at 1000°C with 2% NaCl (Sample No.2), 2 - fine crystalline powder heated at 1000°C without "flux" (Sample No.1).

The resultant substance after being roasted at 1000°C in a nitrogen atmoshpere, began to luminesce only when cooled to below 90°K. Here, the bright green fluorescence in question could be observed. The position of the band in the spectrum and its structure depended on temperature. In Fig.1 we show (dash-dot line) the spectral distribution of the fluorescence of this substance at 20°K. In

agreement with the data of other authors, we found that it extends from 5100 to 5600 Å and has four well defined maxima spaced 300 ± ± 10 cm^{-1} apart. No blue luminescence was observed from this specimen (between the absorption edge and the green band), nor was there any emission above 5600 Å.

Sample No.2 was the same crystalline powder prepared from the same starting materials. In this case, however, 2% pure NaCl was added to it before heating at 1000° in nitrogen. The fluorescence at low temperature was more complex: a blue band appeared in addition to the green band. At 20°K the green band was very bright (Fig.1, solid curve), and had the very same structure as in the spectrum of Sample No.1, although somewhat less sharply pronounced. The individual structure peaks coincided with the peaks in the fluorescence of Sample No.1. The blue band was less bright (than the green), showed no structure and had only one peak, located at about 4900 Å (20,340 cm^{-1}). Since the only difference in preparation was the addition of NaCl, it is natural to assume that the additional blue band is due to the influence of the "flux". At present we do not know whether the effect is a surface one or involves an internal change in the lattice.

We also investigated cadmium sulfide prepared by synthesis in the gaseous phase by reaction of hydrogen sulfide on cadmium vapor at a temperature above 850°. The procedure, which we proposed in 1952, differed somewhat from that described by Frerichs[11]. Our equipment was simpler and did not require entrapping the cadmium vapor by an inert gas[7]. Specifically, our procedure was the following: a stream of hydrogen sulfide was passed through a quartz tube inside which was a second smaller tube which was sealed at one end and partly plugged at the other end by a quartz test tube. The small tube contained pure cadmium in a small boat. At 850° the cadmium vapor filled the small tube and met the hydrogen sulfide which gradually penetrated into it. As with the Frerichs procedure, prismatic single crystal needles together with transparent striated platelets (Sample No.3) were obtained at the open end of the tube. In addition a dull polycrystalline film was formed on the interior of the small tube. It could be supposed that this polycrystalline coating would have different properties from the needles or the platelets, since it was the simultaneous result of synthesis in the gas phase and sublimation. We shall refer to the polycrystalline film as Sample No.4.

For Sample No.3 we obtained a fluorescence spectrum which agreed with the spectrum of Sample No.1. The emission spectrum at 20° is shown in Fig.2 by the solid curve. The peaks coincide with the luminescence peaks of the microcrystalline powder (dot-dash line); in this case, however, the band structure is more developed and one can distinguish five peaks instead of three.

The green fluorescence of Sample No.4 at 20°K was very bright (Fig.2, dashed curve). Like No.4, Sample No.2 did not yield a blue band. Although the emissions of samples Nos.1 and 3 are similar in general, there are differences of detail. The emission of Sample No.4 extends somewhat farther into the long wavelength region and comprises six peaks which differ in relative brightness.

Sample No.5 was a large single crystal prepared by sublimation at low temperatures, using a technique which we described earlier.[12]

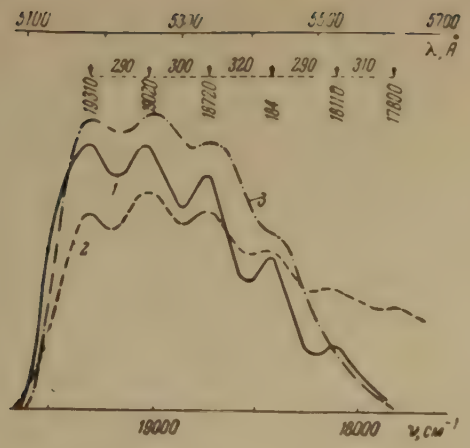

Fig.2. Fluorescence of pure CdS at 20°K: 1 - single crystal (Sample No.3), 2 - film obtained by synthesis in the gas sphase (Sample No.4), 3 - microcrystalline powder calcined at 1000°C without "flux" (Sample No.1).

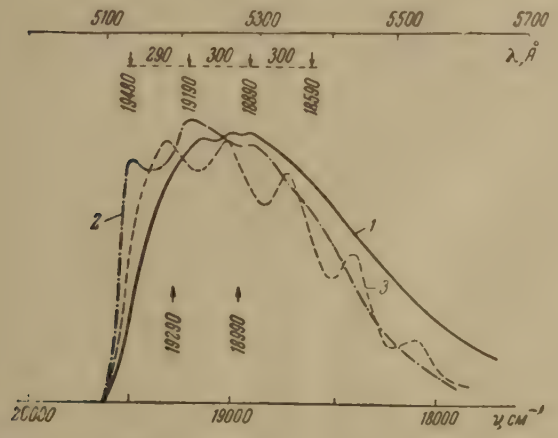

Fig.3. Fluorescence of pure CdS at 20°K: 1 - single crystal obtained by sublimation at 1150°C (Sample No.5), freshly prepared sample, 10 min exposure; 2 - the same crystal after 6 months aging, 3 hrs exposure; 3 - single crystal synthesized from the vapor phase, 12 min exposure.

A large diameter quartz tube (or one of aluminum oxide or titanium oxide) was heated to 1000°. A small diameter tube with a flat bottom, containing microcrystalline powdered cadmium sulfide, was inserted into the large tube. The small tube was partly plugged with a quartz test tube. A slow flow of gas (hydrogen, hydrogen sulfide, or nitrogen, purified of oxygen), passing through the larger tube, cooled the end of the small tube and maintained the temperature of its flat bottom several degrees below the temperature of the powdered cadmium sulfide. Dense crystal plates formed on the flat bottom; these were single crystals, the size of which was found to increase with the initial temperature of sublimation. Thus we were able to obtain crystals with a surface of 1 cm^2 and about 5 mm thick. The crystals had the greenockite structure (hexagonal system).

In studying the green fluorescence of these crystals at low temperature on a relatively freshly prepared sample, we observed the following: the luminescence brightness was approximately the same as for crystals synthesized from the vapor phase; the spectral distribution at 20°K (Fig.3, solid line) showed, however, a less clearly pronounced structure than for the other samples. Several peaks agree with the peaks of other samples; moreover, there are new peaks which are spaced 300 cm^{-1} apart and are located between the peaks common to other samples. The very same crystal tested 6 months later gave weaker fluorescence: the luminescence yield was lower by a factor of about 20. The spectral distribution curve underwent a more profound change: there remained only the series of peaks (more prominent now) that lay between the peaks of the previous samples (Fig.3, dot-dash curve). The separation between these maxima was about 300 cm^{-1} as before. The new peaks of this second series stood out particularly well on the short wavelength side of the fluorescence band.

This new series of peaks located between the first series of peaks is also sometimes evinced in the emission of crystals pre-

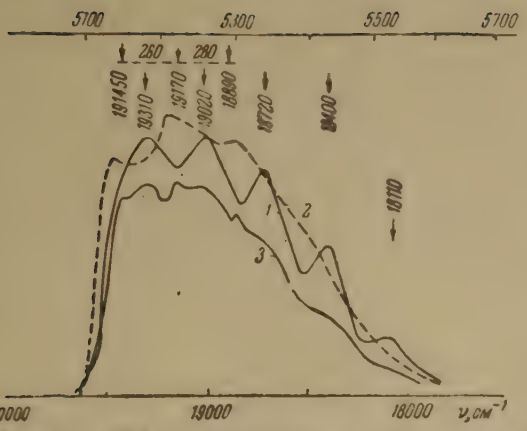

Fig.4. Fluorescence of pure CdS at 20°K: 1 - single crystal obtained by synthesis from gaseous phase, 12 min exposure; 2 - single crystal obtained by sublimation at 1150°C after 6 months aging, 3 hrs exposure; 3 - complex spectrum of crystal obtained by synthesis from the gaseous phase, showing peaks belonging to the first and second series.

pared by synthesis from the gaseous phase. This was also noted by Furlong[13]. In Fig.4 we show the complex spectral distribution curve for the fluorescence of such a sample. For comparison, we also give the curves comprising the first and second series peaks. It can be seen that the peaks of both series are represented in the complex curve.

As we see, study of the low temperature green fluorescence of the first five samples of pure cadmium sulfide prepared by different procedures yields an answer to the question whether the mechanism of the green fluorescence is or is not localized in the lattice. Depending on the preparation procedure and the age of the crystals, very significant differences are evinced in the green fluorescence. The fluorescence spectra differ as regards

1) the nature of the band structure: the separation, number and relative intensity of the peaks,

2) the yield, and

3) the location of the structure peaks which tend to form two series. Each series may be observed separately in different spectra or both exist together in the spectra of some crystals.

These variations can only be explained by assuming that the emission of green fluorescence is localized at discrete luminescence centers formed by individual lattice defects.

As has already been noted by several authors, the 300 cm^{-1} spacing between the peaks (of both series) can be associated with lattice vibrations.

The existence of two series of peaks (Fig.5), in each of which the spacing is about 300 cm^{-1}, leads us to infer the existence of two kinds of luminescence centers, and, consequently, to the hypothesis that there are two kinds of lattice defects connected with lattice vibrations. The energy levels of these defects rise above the top of the valence band only at temperatures below 100°K.

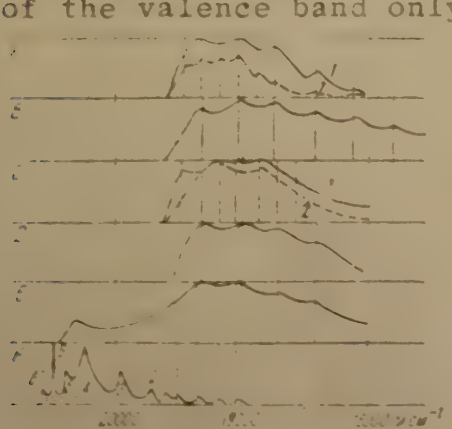

Fig.5. Comparison of the 20°K fluorescence spectra of pure CdS crystals obtained under different conditions: A - Sample No.3 (1 and 2 are for two different crystals prepared at the same time); B - Sample No.4; C - Sample No.5 (1 - immediately after preparation, 2 - after 6 months aging); D - Sample No.1; E - Sample No.2; F - Sample No.6.

It can be assumed that these two types of lattice defects are cadmium and sulfur vacancies. The formation of two kinds of vacancies should lead to the appearance of two series of luminescence peaks in the spectra of these crystals. The predominance of one type of defect over the other, which might depend on the manner of preparation, would lead to predominance of one or the other series of peaks. If this is so, then equilibrium dissociation of cadmium sulfide vapor,

$$CdS \rightleftharpoons Cd + S,$$

should lead to the formation of approximately equal numbers of each kind of vacancy in the crystal during sublimation of the vapor at 1250°C. However, in the process of aging, even at ordinary temperatures, these vacancies can be slowly filled through diffusion. This explains the gradual reduction in the luminescence yield, its low residual value, and the fact that the spectrum of aged crystals comprises only one series of peaks, the one corresponding to the type of vacancy initially present in greater numbers.

These considerations led us to the conclusion that dissociation of the CdS vapor should be the less, the lower the temperature. Consequently, if crystal growth during sublimation were to take place at the lowest temperature possible, the concentrations of the two kinds of vacancies should be very low.

Accordingly, we prepared single crystals of CdS under steep temperature gradient conditions. CdS vapor from powder placed in a tube with a small aperture, which was heated to 1250°C, was carried off slowly by a stream of pure nitrogen into a cooler portion of the furnace, where crystal growth occurred at 700°C. Small prismatic single crystals 1-2 mm long were obtained in this manner (Smpl.No.6).

Like the other samples, Sample No.6 did not exhibit noticeable fluorescence at room temperature. In contrast to the first five samples, however, it did not emit green fluorescence when cooled to 77°K; it began to fluoresce only when cooled to a very low temperature - 20°K. Moreover, the luminescence in this case[14] differed greatly from that observed for the first five samples. The green luminescence band was in evidence but was very weak. On the other hand, an intense blue luminescence consisting of lines, seven of which were very sharp, was observed.

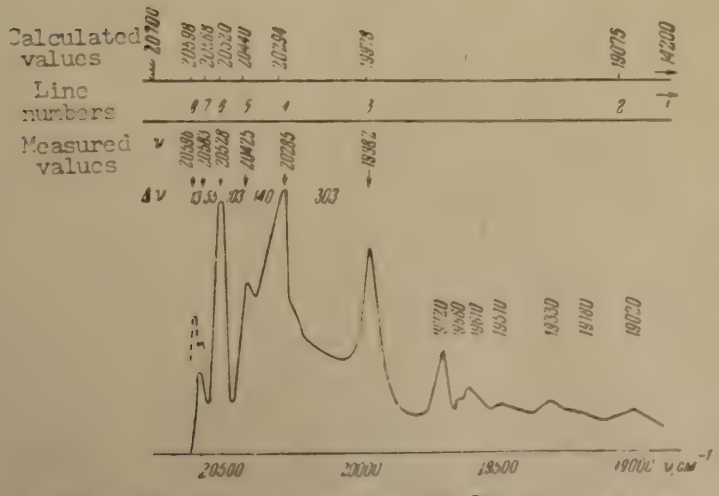

Fig.6. Fluorescence at 20°K of a pure CdS single crystal obtained by sublimation with a steep temperature gradient.

It can be seen from the microphotogram (Fig.6) that this luminescence differs from that of the preceding samples. Instead of equally spaced bands, there obtains a spectrum with sharp peaks, i.e. a spectrum reminiscent of atomic line spectra. In the long wavelength region we have the green luminescence with four equally spaced peaks belonging to the two above mentioned series. However, this green luminescence is appreciably less

intense than the blue line emission.

Leaving aside for the present the line at 19,720 cm^{-1} and two neighboring weakly evident lines which, as we will show below, are associated with it, we can establish that the six remaining lines form a series converging at the absorption limit, located close to 20,700 cm^{-1}.

Although the spectrograph used did not have high resolving power, all of these lines were so sharp that their frequencies could be determined to within 1 cm^{-1}. The frequencies of these six lines satisfy the quasi-hydrogen-like regularity

$$\Delta\nu_n = A - \frac{B}{n^2},$$

where A = 20,700 cm^{-1} (the absorption edge in CdS at 20°K), B = 6500 cm^{-1}, and n takes on values from 3 to 8. Because of some uncertainty in determining the constants A and B, values calculated by means of this formula differ somewhat from the measured values (see Fig.6).

The hypothesis of an exciton mechanism, which was discarded in considering the green luminescence, can be used for explaining the blue line luminescence. This hypothesis should, however, be considered with caution in view of our limited experimental and theoretical information concerning excitons.

In our opinion, it is reasonable to turn to this hypothesis only if the observed spectrum consists of fine lines most of which form a quasi-hydrogen-like series to a first approximation. The coincidence of some of the fluorescence lines with absorption lines may yield further confirmation of this hypothesis.

In the case of pure cadmium sulfide, we saw that the equally-spaced green fluorescence bands cannot be attributed to excitons, as had been believed earlier. Moreover, one must not take as an incontrovertible proof of the exciton mechanism the existence in the fluorescence spectrum of several broad bands, the spacing between which increases in going to longer wavelengths.

For powdered CdS heated with NaCl flux, we observed a blue band together with a more intense and complex green band; if the sample contains traces of silver, then a red band (maximum at 6500 A at 20°K) is observed in addition to these two bands; traces of copper give rise to a band extending into the infrared region (maximum at about 7200 Å at 20°K). Thus, the existence of lines in the absorption spectrum or in the fluorescence spectrum is in itself not a sufficient proof of an exciton mechanism. Such lines may be due to other factors. Krüger, Klick and others observed blue lines and an intense green emission simultaneously in the emission of CdS at low temperatures. Furlong & Ravilious[15] showed that some of the blue lines are undoubtedly caused by surface phenomena associated with adsorption of gases.

The distinctive fluorescence of our Sample No.6, prepared by sublimation with a steep temperature gradient, furnishes stronger arguments in favor of the exciton hypothesis. We recall that this fluorescence is only observed in crystals in whose spectra the usual green fluorescence is either weak or lacking. In addition, we are dealing here with a set of lines, six of which, to a close approximation, form a quasi-hydrogen-like series. Finally, we note the fact that the three lines with the shortest wavelengths, corresponding to levels 8, 7 and 6, agree within satisfactory accuracy

with the most intense absorption lines observed at 4°K in the spectrum of cadmium sulfide by Gross & Iakobson[16], while the fourth (n = 5) differs only slightly from the last absorption line detected by these authors.

Of course, the absorption spectrum observed by Gross & Iakobson is more complex. It also contains other lines, mainly five lines clustered near 4867 Å. Actually, this complexity may be due to the very low experimental temperature: as we shall see, at 4°K the fluorescence spectrum also becomes more complex. Gross further observed that the relative intensity of the different absorption lines varied from sample to sample; some of them, especially those grouped near 4867 Å, disappeared entirely from the spectrum of some samples. It is even more remarkable that despite such variation, the 4853, 4858 and 4870 Å lines, which are all associated with high lying levels that are evinced in the fluorescence, always appear in all of the absorption spectra.

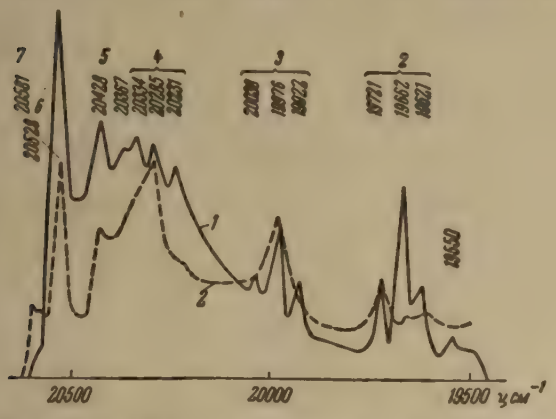

Fig.7. Fluorescence of a pure CdS single crystal obtained by sublimation with a steep temperature gradient: 1) at 4°K, 2) at 20°K.

As mentioned above, we observed a more complicated fluorescence spectrum when we cooled Sample No. 6 to the temperature of liquid helium[17]. All of the sharp lines evinced at 20°K, were observed at 4°K at exactly the same wavelengths. However, their relative intensity changed: the lines corresponding to levels 8 and 7 fell off in intensity. Moreover, new fine structure lines appeared (Fig.7). Lines corresponding to n = 3 and n = 4, now formed triplets, while the n = 5 line formed a doublet. All the separations between the fine structure components were about 50 cm^{-1}.

The three lines with frequencies of 19,720, 19,660 and 19,610 cm^{-1} observed at 20°K, appeared even more clearly at 4°K in the form of a triplet with a component spacing of 50 cm^{-1}; the central line of the triplet was the most intense. It seems to us that these three lines could be explained by the very same mechanism and could belong to the very same system as the others. They might represent the n = 2 level deviating from the hydrogen-like regularity. Such behavior of low lying levels is not precluded from the theoretical standpoint.

We note in conclusion that the exciton, the existence of which has so far been proved experimentally only in absorption of light, can also be evinced in fluorescence.

However, very different conditions are required for these two manifestations of the exciton. The "birth" of the exciton as a result of light absorption at some point in the crystal lattice depends somewhat on lattice defects. If the absorption edge is not masked by the effect of impurities, we need only have a sufficiently thin crystal for the exciton absorption spectrum to be evident.

In contrast, annihilation of an exciton during emission of fluorescence is a rarer effect. The fluorescence is observed only in CdS crystals in which the concentration of lattice defects is exceptionally low.

References

1. J.Ewles, Proc.Roy.Soc.A., 167, 34 (1938).
2. F.T.Randall, Trans. Faraday Soc., 33, 1 (1939).
3. F.A.Kröger, Physica, 7, 1 (1940).
4. F.A.Kröger & H.T.G.Meyer, ibid., 20, 1149 (1954).
5. C.C.Klick, JOSA, 41, 816 (1951); Phys.Rev., 89, 274 (1953).
6. E.Grillot, Compt. rend., 230, 1159 (1950); J.chim.phys., 48, 115 (1951).
7. E.Grillot, Compt. rend., 230, 1280 (1950).
8. E.Grillot & P.Guintini, Compt. rend., 236, 802 (1953); 239, 418 (1954); E.Grillot, J.phys. et radium, 17, 624 (1956).
9. E.Grillot, Compt. rend., 230, 543 (1950); Bull.Soc.chim., France, 19, 39 (1951).
10. R.Lorenz, Berichte, 24, 1501 (1891).
11. R.Frerichs, Naturwiss., 33, 281 (1946); Phys.Rev., 72, 594 (1947).
12. E.Grillot, Compt. rend., 242, 779 (1956); J.Phys.et radium, 17, 795 (1956).
13. R.L.Furlong, Phys.Rev., 95, 1086 (1954).
14. E.Grillot, M.Bancie-Grillot, P.Pesteil & A.Zmerli, Compt. rend., 242, 1794 (1956).
15. R.L.Furlong & C.F.Ravilious, Phys.Rev., 98, 954 (1955).
16. E.F.Gross & M.A.Iakobson, Doklady AN SSSR, 102, 485 (1955).
17. E.Grillot, Phys. et radium, 17, 822 (1956).

Transactions of the Sixth Conference on Luminescence (Molecular luminescence and luminescence analysis) (Leningrad, 17-23 February 1958)

On the following pages we begin publication of the Transactions of the Sixth Conference on Luminescence (Molecular Luminescence and Luminescence Analysis). The reports on Molecular Luminescence will be continued in the Vol.23, No.1 issue of the Bulletin.

The reports on Luminescence Analysis will be published by the Academy of Sciences of the Belorussian SSR.

OPENING ADDRESS

- A.N.Terenin

Today we open the Sixth Conference on Luminescence. The importance of such periodic conferences, intended for exchange of information regarding research work being carried out in our country, cannot be overrated.

The first and second conferences on luminescence were held in Moscow in 1944 and 1948 under the Chairmanship of S.I.Vavilov. The third conference held in 1951 in Moscow was dedicated to his memory. At these conferences we heard reports on a large number of topics, extending from the luminescence of vapors, solutions and crystals to synthesis of luminophors and luminescence analysis in its broadest sense.

In view of the constantly expanding scope of research in the field of luminescence, the Commission on Luminescence of the USSR Academy of Sciences decided to introduce a thematic division and to hold alternate conferences on molecular luminescence and on crystal phosphors.

Thus the Fourth Conference in Minsk in 1955 was devoted solely to molecular luminescence, while the Fifth Conference held in 1956 in Tartu was concerned with crystal phosphors and allied topics in the physics of semiconductors.

The present, Sixth Conference on Luminescence, the first conference on this topic to meet in Leningrad, has limited its program to questions of molecular luminescence and luminescence analysis which has seen great development in recent years, particularly in the fields of biology and medicine.

Despite the fact that the Eleventh Conference on Spectroscopy, held in December 1957, included a number of reports on luminescence, the number of reports scheduled for presentation at the present conference - 117 - has broken all records.

This record number of reports bears evidence of the scope of theoretical research in luminescence and the extent of its application in the USSR.

Before we proceed with our work, I want to recall the name of one who made great contributions to the development of theoretical and practical luminescence in our country, the name of Sergei Ivanovich Vavilov, outstanding scientist and public figure, father of the Soviet school of luminescence. I request all present to rise in his memory.

* * *

By authority of the Organizing Committee I hereby declare the Sixth Conference on Luminescence, organized by the Physical Institute of the USSR Academy of Sciences, the "S.I.Vavilov" State Optical Institute and the Academy of Sciences of the Belorussian SSR, open.

CORRELATION BETWEEN THE LUMINESCENCE AND ABSORPTION SPECTRA OF COMPLEX MOLECULES

- B. I. Stepanov

It was shown in Ref.1 that the contour Π_ν^{lum} of the fluorescence band of a complex molecule is related to the contour $\mathfrak{A}_\nu$ of the long wavelength absorption band by the simple expression:

$$W_\nu^{lum} = D\Pi_\nu^{therm\,rad} = d\mathfrak{A}_\nu \nu^3 \frac{1}{e^{h\nu/kT} - 1} \approx d\mathfrak{A}_\nu \nu^3 e^{-h\nu/kT}. \qquad (1)$$

The proportionality factors D and d depend only on temperature and excitation conditions. Relationship (1) is valid for solutions of all complex molecules (and a number of other condensed systems), provided certain conditions are satisfied, and has a universal character. The principal necessary condition is that there be established an equilibrium energy distribution over the vibrational levels of the excited molecule well prior to the emission event. Moreover, it is assumed that one need not consider transitions between the vibrational levels of the electronic grouns state. These assumptions have been widely accepted with respect to solutions and have been frequently used for explaining experimental facts.

The implications of Eq.(1) are very simple, and it is expedient to repeat them. In previous derivations, we assumed for clarity that the entire energy of a molecule could be divided into two parts: vibrational and electronic. However, the final results are not restricted by this particular assumption and are fully applicable even in the case of strong coupling between the motion of the electrons and the vibrations of the nuclei. In the present derivation, we make no assumption regarding separation of the variable motions of the nuclei and electrons.

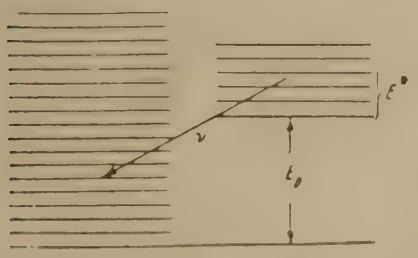

Fig.1. Diagram of energy levels.

In Fig.1, the sublevels of the ground state are shown on the left side; the sublevels of the excited state are shown on the right side. The existence of the excited state is proved by the fact of luminescence. In the case of infinitely strong interaction between the electrons and nuclei, there is no excited state and, therefore, no luminescence. Emission of light occurs as a result of transitions from various sublevels of the excited state to different sublevels of the ground state.

The power of any emission (equilibrium or nonequilibrium) is described in the most general form by [2]

$$W_\nu = h\nu \int n^*(E^*) A(E^*, \nu)\, dE^*. \qquad (2)$$

Here $n^*(E^*)$ is the number of excited molecules present per unit interval of sublevels, $A(E^*, \nu)$ is the probability of a spontaneous transition from sublevel E* of the excited state into a lower state with emission at frequency ν. There is very little forced emission in the visible region of the spectrum and, consequently, it will not be taken into account. The integration is carried out from the lower boundary E_0 of the excited state over all of its sublevels.*

If complete thermodynamic equilibrium obtains in the system,

---

*It should be borne in mind that, with strong coupling between the motions of the electrons and the nuclei, the lower bound E_0 of the excited state can be very low and in general tends to zero at the limit. The properties of the excited levels and the probability $A(E^*, \nu)$ in the case of strong coupling have been treated in Ref.3.

$$n^*(E^*) = C(T)\, n g^*(E^*)\, e^{-\frac{E_0 - E^*}{kT}}. \tag{3}$$

Here n is the total number of molecules and $g^*(E^*)$ is the statistical weight of the excited state sublevels. Inserting (3) in (2), we obtain the thermal radiation power:

$$W_\nu^{\text{therm rad}} = h\nu C(T) n e^{-E_0/kT} \int g^*(E^*) A(E^*, \nu) e^{-E^*/kT} dE^*. \tag{4}$$

According to our initial assumption, the distribution of the molecules over the excited state sublevels during luminescence is described by

$$n^*(E^*) = C^*(T)\, n^* g^*(E^*) e^{-E^*/kT}. \tag{5}$$

Here n^* is the number of excited molecules; it depends on the intensity of the incident light, the temperature and the properties of the molecules. Substituting (5) in Eq.(2), we obtain the luminescence power:

$$W_\nu^{\text{lum}} = h\nu C^*(T)\, n^*(T_{\text{excit.}}) \int g^*(E^*) A(E^*, \nu) e^{-E^*/kT} dE^*. \tag{6}$$

Comparing Eqs.(6) and (4), and invoking Kirchhoff's law

$$W_\nu^{\text{therm rad}} = \mathfrak{A}_\nu u_\nu, \tag{7}$$

we obtain Eq.(1).

The first verification of Eq.(1) was attempted by Kazachenko[4]. It did not achieve a decisive result. Significant results were obtained by Alentsev[5], who wrote Eq.(1) in the form:

$$\ln \frac{\mathfrak{A}_\nu}{W_\nu^{\text{lum}}} + 3 \ln \nu = \frac{h\nu}{kT} + \text{const}. \tag{8}$$

and utilized certain experimental data obtained in 1931 and 1935. Plotting the left-hand part of (8) as a function of the frequency, he obtained satisfactory straight lines, which indicates agreement of the theory with experiment. However, the values of T* determined from the slopes of plots are greater than the actual temperature of the medium. In view of this, Alentsev concluded that the redistribution of energy between the fluorescing molecules and the molecules of the solvent occurs relatively slowly and that while the molecules are in the excited state they transfer only a fraction of the excitation energy to the solvent. Consequently, the excited molecules have a higher average temperature.

Similar curves were plotted at our request by L.G.Pikulik and L.A.Kravtsov. Pikulik used experimental data he obtained for other purposes. In the calculations, no account was taken of reabsorption or of the intrinsic luminescence of the solvent in the same spectral region. Analysis shows that these factors partly compensate each other. Kravtsov made new measurements, fully allowing for reabsorption.[6] Pikulik's results are shown in Fig.2 and in the accompanying table.

Kravtsov's data are given in Fig.3*. They have particular value since chlorophyll and pheophytin are characterized by the strong overlapping of their absorption and luminescence bands; this makes it possible to effect measurements at large values of W_ν^{lum} and $\mathfrak{A}_\nu$ thus assuring high accuracy in determining the $\mathfrak{A}_\nu / W_\nu^{\text{lum}}$ ratio.

---

*More detailed information is contained in L.A.Kravtsov's report to this Conference.

Substance	Solvent	T, °K	Curve No. in Fig.2.
4-Amino-N-methyl-phthalimide	Glycerol	610	1
	Acetoacetic ester	300	6
	Ethyl benzoate	350	9
3-Monomethylamino-phthalimide	Benzyl alcohol	300	2
	Ethyl benzoate	345	5
	Acetoacetic ester	300	4
3-Aminophthalimide	Benzyl alcohol	370	7
	Ethyl benzoate	290	10
	Acetoacetic ester	270	8
4-Aminophthalimide	Glycerol	550	3

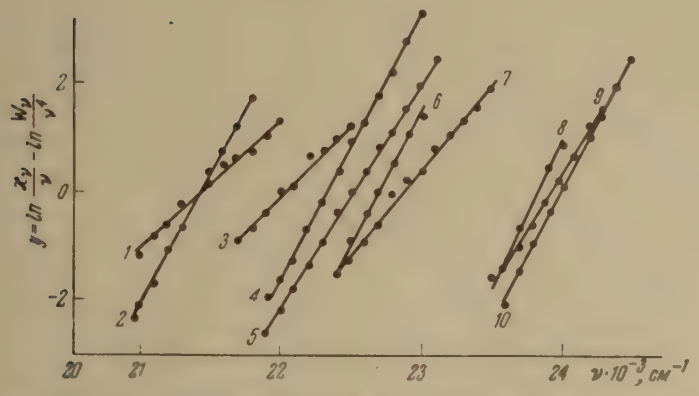

Fig.2. Verification of Eq.(8) on the basis of Pikulik's data (for key to curve numbers see table).

It follows from Figs.2 and 3 that the left side of Eq.(8) is satisfactorily represented by straight lines; this substantiates the validity of Eq.(1). The absorption and emission bands of chlorophyll and pheophytin are comparatively narrow and hence the contribution of the $3 \ln \nu$ term in Eq.(8) is relatively minor and can be neglected. On the contrary, the bands of phthalimides are very broad and Eqs.(8) and (1) no longer hold if the $3 \ln \nu$ term in Eq.(8) or the factor in front of ν^3 in Eq.(1) is disregarded.

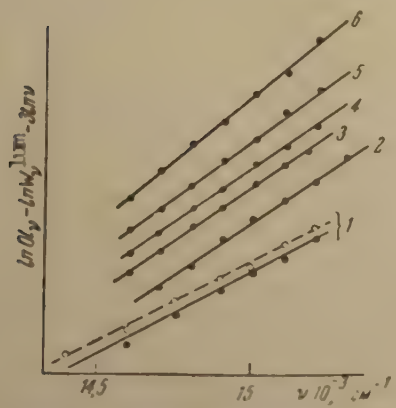

Fig.3. Verification of Eq.(8) on the basis of Kravtsov's data. Pheophytin *a*: 1) in isobutanol (T* = 620°K), 2) in methanol (520°K), 3) in ethanol (500°K), 4) in isoamyl alcohol (500°K). Chlorophyll: 5) chlorophyll *b* in ethanol (450°K), 6) chlorophyll *a* in ethanol (420°K).

As can be seen from the curves and from the table, the value of the temperature T* calculated from the slope of the straight lines (8) corresponds in some cases to the experimental temperature (the uncertainty in calculating T* is <20°). In these cases, the initial assumption as to equilibrium distribution is rigorously fulfilled. In most cases, however, T* > T. The value of T* depends both on the type of the molecule and on the type of solvent. It sometimes attains 620°. According to preliminary data, the value of (T* - T) also depends on the temperature of the experiment.

Thus, Alentsev's inference regarding the absence of complete equilibrium between the degrees of freedom of the excited molecules and the molecules of the solvent has been substantiated by new experimental data. In many cases, the "intrinsic" temperature of the excited molecules is higher than the temperature of the solvent. The concept of the "intrinsic" temperature of excited molecules, which is realized as a consequence of the interaction of varying degrees of freedom within the luminescent molecules, among the luminescent molecules, and also between them and the solvent, and the formation

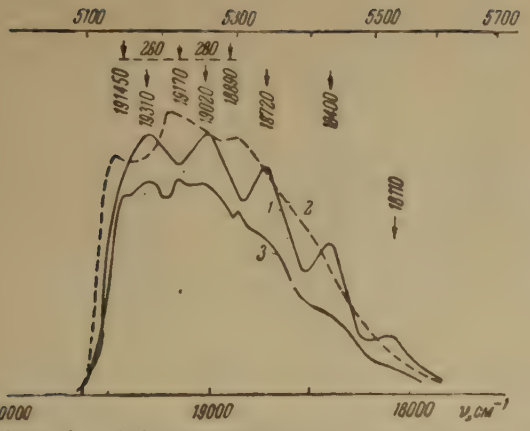

Fig.4. Fluorescence of pure CdS at 20°K: 1 - single crystal obtained by synthesis from gaseous phase, 12 min exposure; 2 - single crystal obtained by sublimation at 1150°C after 6 months aging, 3 hrs exposure; 3 - complex spectrum of crystal obtained by synthesis from the gaseous phase, showing peaks belonging to the first and second series.

pared by synthesis from the gaseous phase. This was also noted by Furlong[13]. In Fig.4 we show the complex spectral distribution curve for the fluorescence of such a sample. For comparison, we also give the curves comprising the first and second series peaks. It can be seen that the peaks of both series are represented in the complex curve.

As we see, study of the low temperature green fluorescence of the first five samples of pure cadmium sulfide prepared by different procedures yields an answer to the question whether the mechanism of the green fluorescence is or is not localized in the lattice. Depending on the preparation procedure and the age of the crystals, very significant differences are evinced in the green fluorescence. The fluorescence spectra differ as regards

1) the nature of the band structure: the separation, number and relative intensity of the peaks,

2) the yield, and

3) the location of the structure peaks which tend to form two series. Each series may be observed separately in different spectra or both exist together in the spectra of some crystals.

These variations can only be explained by assuming that the emission of green fluorescence is localized at discrete luminescence centers formed by individual lattice defects.

As has already been noted by several authors, the 300 cm^{-1} spacing between the peaks (of both series) can be associated with lattice vibrations.

The existence of two series of peaks (Fig.5), in each of which the spacing is about 300 cm^{-1}, leads us to infer the existence of two kinds of luminescence centers, and, consequently, to the hypothesis that there are two kinds of lattice defects connected with lattice vibrations. The energy levels of these defects rise above the top of the valence band only at temperatures below 100°K.

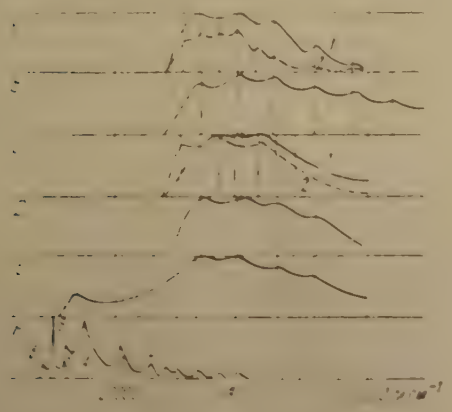

Fig.5. Comparison of the 20°K fluorescence spectra of pure CdS crystals obtained under different conditions: A - Sample No.3 (1 and 2 are for two different crystals prepared at the same time); B - Sample No.4; C - Sample No.5 (1 - immediately after preparation, 2 - after 6 months aging); D - Sample No.1; E - Sample No.2; F - Sample No.6.

(during the interval $t \ll \tau$) of an equilibrium distribution over the sublevels of the excited state, undoubtedly has physical meaning. Otherwise, Eqs.(1) and (8) would not be valid and the left-hand part of Eq.(8) would not be represented by straight-line plots.

For the $T^* \geqslant T$ case, Alentsev[5] proposed a more general equation in place of Eq.(1), namely,

$$W_\nu^{\text{lum}}(T) = d\mathfrak{A}_\nu(T^*)\, e^{-h\nu/kT}. \tag{9}$$

Eq.(9) is easy to derive. If the "intrinsic" temperature of the excited molecules T* is higher than T, we must substitute T* for T in Eq.(6). The expressions under the integral in Eqs.(6) and (4) are equal if $W_\nu^{\text{ther.rad.}}$ is calculated at $T = T^*$. The absorption capacity $\mathfrak{A}_\nu$ must be measured at this same temperature. Then Eq.(9), instead of (8), gives us

$$\ln \frac{\mathfrak{A}_\nu(T^*)}{W_\nu^{\text{lum}}(T)} + 3 \ln \nu = \frac{h\nu}{kT^*} + \text{const}. \tag{10}$$

To verify Eq.(9), we must insert the value of $\mathfrak{A}_\nu$ at the temperature T* into Eq.(10). We tried to carry out the calculation for pheophytin, measuring W_ν^{lum} at room temperature and $\mathfrak{A}_\nu$ at the temperature deduced from the slope of the straight line plot given by the part of Eq.(8) on the left. The straight line obtained from Eq.(10) lay somewhat higher, but it had the same slope (dashed line in Fig.3).

The inequality $T^* \neq T$ observed experimentally in some cases by no means negates the fundamental relation (1). It will be recalled that this relation was formulated only for those systems for which certain specified conditions obtain, particularly the condition of equilibrium between the excited molecules and the surrounding medium. Violation of Eq.(1) in any specific experimental case only means that these necessary conditions are not being satisfied. Thus, Eq.(1) may serve as a criterion to indicate whether an equilibrium distribution over the levels of the excited molecules has been attained. The value of $(T^* - T)$ is a measure of the degree of interaction with the solvent and the rate of transfer of the excess energy.

The question of whether Eq.(9) or (1) is applicable to the vapor of a fluorescing substance calls for special consideration. Neporent[7] showed experimentally that in some cases the same increase in the energy of excited molecules by optical or thermal means led to the same effect (decreased yield or reduction of τ). This is correct despite the undoubted difference in the energy level distribution function for the excited molecules. As a result, Neporent was able to set up an original optical procedure for determining the specific heat of complex molecules. Relation (9) should be applicable precisely to such cases. The average "intrinsic" temperature of the excited molecules in a vapor is defined by

$$h\nu_{\text{exc}} - h\nu_0 = C_\nu(T^* - T). \tag{11}$$

Relation (9) may be used together with Eq.(11) for the experimental determination of C_ν.

The inequality $T^* \neq T$, observed experimentally for some solutions, should be accompanied by certain consequences or effects susceptible of experimental detection. It is natural to assume that the value of T* may depend on the frequency of the exciting light, especially if $(T^* - T)$ is sufficiently large. This, in its turn, can be accompanied by excitation frequency-dependence of both the quantum efficiency of the luminescence and the shape of the band. Such dependences have not been observed as yet, and special experiments may be necessary to detect

them. It is doubtful whether one should search for these dependences at large values of $(\nu_{exc} - \nu_{\epsilon})$ (ϵ = electronic), since energy transfer to the medium will take place more intensively at large excesses of vibrational energy. The dependences would most likely be observed at values of ν_{exc} close to ν_{ϵ}.

Dependence of the luminescence spectra of solutions on the frequency of the exciting radiation was detected[8] in the anti-Stokes region with $\nu_{exc} < \nu_{\epsilon}$. In explaining this effect, Neporent & Borisovich hypothesize that the deficiency in the vibrational energy of the excited molecules is not made up by energy transfer from the solvent. This leads to shifting the bands. One may assume that in this case, too, an equilibrium distribution over the vibrational levels is attained, but with $T^* < T$. Preliminary calculations support the assumption that Eq.(9) is also applicable in this case.

Institute of Physics and Mathematics
Academy of Sciences of the Belorussian SSR

References

1. B.I.Stepanov, Doklady AN SSSR, 112, 839 (1957); Izv.AN SSSR, Ser.fiz., 22, 1089 (1958) (Trans.Bulletin, 22, No.9, 1079); B.I.Stepanov and L.P.Kazachenko, Optika i spektro., 2, 339 (1957).

2. B.I.Stepanov, Luminestsentsiia slozhnykh molekul (Luminescence of complex molecules), Belorussian SSR, 1956.

3. B.I.Stepanov, Zhur.eksp.i teor.fiz., 15, 435 (1945).

4. L.P.Kazachenko, Uch.zap. (Scientific Notes), Belorussian State University, No.41, ser.fiz., 151 (1958).

5. M.N.Alentsev, Optika i spektro., 4, 690 (1958).

6. L.A.Kravtsov and N.P.Ivanov, Inzh.fiz.zhur., (Engineering Phys.Journ,) 1 (1958).

7. B.S.Neporent, Zhur.fiz.khim., 21, 1111 (1947); Usp.fiz.nauk, 43, 380 (1951).

8. B.S.Neporent and N.A.Borisovich, Optika i spektro., 1, 143 (1956).

CORRELATION BETWEEN LUMINESCENCE AND ABSORPTION SPECTRA OF POLYATOMIC MOLECULES

- B.S.Neporent

I

The shape of the spectral bands of complex organic molecules and the correlation between the other attributes of their absorption and fluorescence spectra have been the subjects of many investigations, some of which have been reviewed briefly in Ref.1. It is sufficient here to note that the problem has been treated on the basis of the one- or two-dimensional models of the potential curves for the potential energy by comparing the probabilities of direct and reverse "elementary" transitions between various vibrational levels of molecules in the normal or excited electronic states[2-6], and also by summing these elementary transitions (Refs.7-9). Stepanov[9] showed that the fluorescence spectrum is proportional to the thermal radiation spectrum of the system, multiplied by a factor depending on the temperature and conditions of excitation. The relationships were obtained assuming an equilibrium distribution of normal and excited molecules with respect to vibrational energy, and assuming the absence of absorption not accompanied by electronic excitation of molecules.

In my opinion the problem of the general relationship between molecular absorption and luminescence spectra should be solved by a procedure which was logically the reverse of that employed by Stepanov[9], namely, that one should start by defining the relationships between the absorption and emission spectra of a system in the state of thermal equilibrium.

Proceeding by analogy with the usual treatment of systems with narrow levels, we can readily deduce the relationships between the absorption and emissive capacities of the molecules under consideration; these relationships can then be used for investigating non-equilibrium processes, for example, luminescence, provided the conditions formulated by Stepanov[9] and by the writer[10] are satisfied. This is the approach essayed in Ref.10.

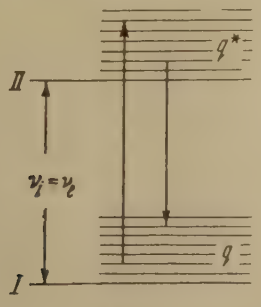

Fig.1

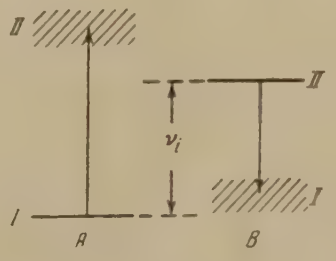

Fig.2

To start, let us consider a simple system having two electronic states, a ground state I and an excited state II (Fig.1). To characterize the densities, we introduce mean values of the Einstein coefficients $\bar{A}_\nu$ and $\bar{B}_\nu$ and use n and n^* to denote the equilibrium concentrations of the molecules in states I and II, respectively. We can then write the equilibrium condition in the form

$$n^*\bar{A}_\nu = n\bar{B}_\nu U_\nu, \qquad (1)$$

where U_ν is the spectral density of the equilibrium radiation, which we express by the Wein formula, bearing in mind that $h\nu \gg kT$. It will be noted that we neglect forced emission.

The ratio n/n^* for equilibrium concentrations is uniquely determined by the separation $h\nu_i$ between the levels of the electronic states I and II and by the multiplicities of these states, which, for the sake of simplicity, we shall provisionally consider to be equal, allowing for the possibility of introducing appropriate corrections later. Obviously,

$$\frac{n}{n^*} = e^{h\nu / kT},$$

and the relation of interest to us can be written in the form

$$\frac{\bar{A}_\nu}{\frac{8\pi h}{c^3}\nu^3 \bar{B}_\nu} = e^{\frac{h}{kT}(\nu_i - \nu)}. \qquad (2)$$

We can readily convert from the mean probabilities B_ν and A_ν to experimentally determined quantities by means of the relations

$$\frac{h}{c}\nu\bar{B}_\nu = \varepsilon_\nu \text{ and } \bar{A}_\nu = \frac{\gamma_\nu}{\tau'},$$

where ε_ν is the molecular absorption coefficient, γ_ν is the spectral density of the quantum yield, and τ' is the experimentally measured lifetime of the excited state.

We note that although the values of γ_ν and τ' are determined experimentally in many current studies, there is no need to do so since the absorption spectra can be measured in relative units I_ν of the quantum luminescence intensity, normalizing the area under the spectral curve so that it equals the area under the $\nu^2\varepsilon_\nu$ curve. The necessity for this choice of "scale" has been proved in Ref. 10 and established experimentally for diverse molecular spectra in the paper by the writer and Bakhshiev[11]. As a result, Eq.(2) can be written as:

$$\frac{I_\nu}{\nu^2\varepsilon_\nu} = e^{-\frac{h}{kT}(\nu_i - \nu)}. \qquad (3)$$

If the spectra are normalized with respect to area, Eq.(3) contains no numerical coefficients. The generally employed procedure of normalizing absorption and fluorescence spectra with respect to the maxima of the spectral curves is erroneous, as is also the general practice of expressing them in units of ε_ν and I_ν (or ε_ν and $E_\nu \sim \nu I_\nu$). This last has been noted by Blokhintsev[7], Förster[8] and Stepanov[9], who proposed using the quantities I_ν/ν^3 and ε_ν/ν, which are proportional to $\bar{B}_\nu$, for characterizing the spectra. It should be noted that there is no basis for giving preference to the «B_ν» (I_ν/ν^3, ε_ν/ν) system over the «A_ν» (I_ν, $\nu^2\varepsilon$) system. Finally, from the standpoint of practical utility, we should also consider the «ε_ν» (I_ν/ν^2, ε_ν) system.

We emphasize that with correct normalization with respect to area, the spectral curves in any system of units should intersect at a point corresponding to the frequency $\nu = \nu_i$. Here the frequency ν_i equals the electronic transition frequency ν_e only in the idealized case pictured in Fig.1. In the general case of the scheme proposed in Refs.1 & 12 and diagramed in Fig.2, the frequency ν_i is associated with the separation between the IA and IIB levels, if the corresponding electronic states of the molecules under study are stable under the given experimental conditions. We shall return to a discussion of the level diagrams of Figs.1 and 2 below.

Attention should be directed to the fact that Stepanov & Kazachenko[9,13] do not consider the necessity of normalizing the spectral curves, and do not give a procedure for such normalization. Consequently, the attempt made in Ref.13 to check the relationships between the spectra based on available experimental data is faulty in that section which pertains to spectra devoid of mirror symmetry.

Turning to the problem of the symmetry of absorption and luminescence spectra, we note that the shapes of the spectra and the relation between them should differ somewhat even in the «A_ν» and «B_ν» unit "physical" systems and, consequently, our concepts as to the correlation between the shape and symmetry of absorption and luminescence spectra become somewhat arbitrary.

Let us consider symmetry relations in the «B_ν» representation. For simplicity, we introduce the quantity $B^*_\nu = \frac{c^3}{8\pi h}\cdot\frac{A_\nu}{\nu^3}$. The symmetry condition (Fig.3) can evidently be written

$$\overline{B}^*_{\nu_i \pm \Delta\nu} = \overline{B}_{\nu_i \mp \Delta\nu}. \tag{4}$$

Substituting the values of $\overline{B}^*_\nu$ and $\overline{B}_\nu$ into this equation, and bearing in mind that if $q < \nu_i - \nu$, then $\overline{B}(q, \nu) = 0$, and if $q^* < \nu - \nu_i$, then $B^*(q^*, \nu) = 0$, it is easy to obtain the symmetry condition formulated some time ago by Levshin[2] (see Ref.10):

$$\begin{gathered} B^*(q^*, \nu \pm \Delta\nu) = B(q, \nu \mp \Delta\nu); \\ \rho^*(q^*) = \rho(q)_{(q=q^*)}, \end{gathered} \tag{5}$$

according to which, for each value of $\Delta\nu$ (Fig.3) the probability of direct and reverse transitions having mirror symmetry should be equal, and the distribution functions $\rho^*(q^*)$ and $\rho(q)$ of the molecules with respect to vibrational levels should also be identically equal. We note that these conditions are fulfilled either with complete identity for both electronic states of the sets of normal vibrations or with such strong coupling of these vibrations that their specific properties disappear and we are dealing essentially with complex molecules possessing modulation spectra, rather than with simple polyatomic molecules. On this basis, we showed[5] that spectra with mirror symmetry represent a limiting case (regularity).

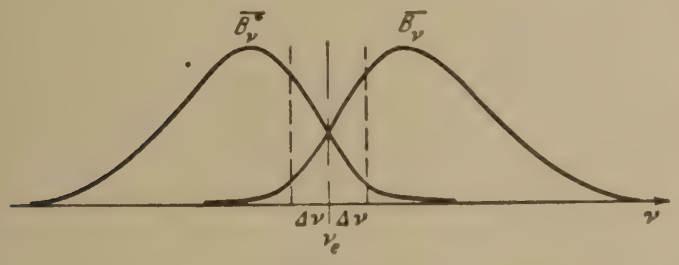

Fig.3

II

We showed[14] that mirror-symmetrical modulation spectra are characteristic of molecules which occupy a median position in a series of related compounds (specifically, phthalimide derivatives), having progressively more complex structures, and that further advance within this series, which is associated with a corresponding enhancement of the intramolecular interactions, leads to the formation of spectra of a new type which have different width relationships, and which we called "attenuation spectra". A review of further investigations of molecules having spectra of this type is given in Refs.12 and 1, together with a discussion of how they are formed.

The proposal that spectra of complex molecules should be divided into two categories is contradicted in the work of Kazachenko & Stepanov[13], who, having converted the spectra of several of the compounds in the series of 12 phthalimide derivatives we investigated[14] to the «$B_\nu I_{\nu_i}(\nu)$, $\varepsilon_{\nu_i}(\nu)$» system, showed that, naturally, all of the spectra here varied in shape somewhat, and that mirror symmetry was more completely realized for the 9th member rather than for the 5-7th members of the series. Moreover, in the opinion of these authors, the

change in the shape of the spectra violates the width relationship established in Ref.5 for attenuation spectra. Kazachenko & Stepanov propose explaining all the spectral relationships by using an appropriate selection of the potential energy curves based on the generalized vibrational coordinate model originally introduced by the writer.[5]

Some points made by Kazachenko & Stepanov[13] appear ill founded to us: first, treatment of the spectra using potential curves in the form presented in Ref. 13 seems to be more of a procedure for describing rather than for interpreting the effect; second, proper comment as to the disturbance of mirror symmetry in the spectra of certain substances (for 3-aminophthalimide this agrees with the results of the study by the writer and Klochkov[15] on the absorption spectra of this substance) does not invalidate the conclusion presented in our papers, since the median position of the compounds with mirror-symmetrical spectra in the series under consideration is preserved in all systems of units. Finally, the width relationship $\Delta\nu = k\nu^2_{max}$ for attenuation spectra, is retained to some extent in all systems of units; this is confirmed by the results of conversions for 3,6--tetramethyldiaminophthalimide, as given in the Table.*

Half-widths of the spectra of two phthalimide derivatives in different representations

	$\Delta\nu$, см$^{-1}$						$k=\Delta\nu/\nu^2_{max}$, mμ					
	I/ν^3	ε/ν	I/ν^3	ε	I	$\nu^2\varepsilon$	I/ν^3	ε/ν	I/ν^3	ε	I	$\nu^2\varepsilon$
3-aminophthalimide												
Vapor	4500	3900	4200	3900	4000	4200						
Solvents:												
Ether	4500	3600	4300	3900	4000	3900						
Xylene	4400	3600	4200	3600	4000	3800						
Dioxane	4100	3600	3900	3700	3600	3900						
Water	4400	3800	4400	3900	3900	4100						
3,6-tetramethyldiaminophthalimide												
Vapor	3300	5000	3000	4700	3200	5000	92	89	87	88	88	91
Solvents:												
Ether	3600	4600	3200	4400	4400	4300	104	87	97	88	87	90
Xylene	3400	3900	3100	3900	2700	4200	105	86	99	86	84	91
Dioxane	3400	4100	3200	4200	2900	4400	102	90	102	91	92	93
Water	2900	5100	2700	5200	2700	5100	100	93	93	95	92	89

It can be readily seen that the values of the constant k for each group of spectra remain approximately the same for the vapor and for solutions in different solvents, but that the values of this constant are not equal for the absorption and fluorescence spectra in the A_ν and B_ν representations. In this connection, it should be noted that an explanation of this equality by means of the concepts developed in Ref.12 would involve introducing additional hypotheses.

The data and discussion presented confirm the fact that the differences noted[1,2,14] in the spectra persist in all the representations (systems of units) and, consequently, they, together with other differences between molecules characterized by other spectroscopic relationships, should serve as the basis for further investigations. As noted earlier[1], the ideas presented in Refs.12 and 1 as to the origin of each type of spectrum cannot be regarded as the final solution of the problem. Nevertheless, these ideas do allow of drawing certain

---

*More detailed data for all of the substances will be published in the near future.

deductions regarding the correlations between the spectra and the nature of intermolecular interaction. Among these results, we regard as important the conclusion that one must take into account the interdependence between the electronic states and nuclear structures in the case of complex molecules and, consequently, the "relaxation" of the molecular core and of the electron cloud after an electron transition; all this leads to a system of electronic states characterized by the four-level diagram of Fig.2. In this scheme, degeneration of this arrangement into one with two levels (Fig.1) represents a special case for complex molecules in the same way as exact mirror-symmetry of the spectra.

Actual complex molecules have a system of electronic states of the Fig.2 type, differing to a greater or lesser degree from the idealized Fig.1 system generally utilized at the present time. So far we do not know the limiting form of coupling between the levels of Fig.2; up to the present, the experimentally detected limiting case is that of the above mentioned spectra described by the relation $\Delta\nu = k\nu^2_{max}$. An analysis of the width relationships in absorption and fluorescence spectra should serve for determining the characteristics of the level system; further studies should show to what extent the widths of typical attenuation spectra are determined by the rate of relaxation of a molecular system after an electron transition. In some cases, the Fig.2 arrangement of levels may also be applicable to molecules having modulation spectra.

References

1. B.S.Neporent, Trudy (Proceedings) State Opt.Inst., 150, 3 (1957).
2. V.L.Levshin, Zhur.fiz.khimi, 2, 641 (1931); 6, 1, 991 (1935); 9, 1 (1937).
3. Jablonsky, Z.Physik, 73, 460 (1931); Acta Physica Polonica, 5, 271 (1936).
4. A.N.Terenin, Zhur.fiz.khimi, 18, 1 (1944).
5. B.S.Neporent, Zhur.eksp.i teor.fiz., 21, 172 (1951).
6. B.I.Stepanov, Izv.AN SSSR, Ser.fiz., 20, 458 (1956). (Trans.Bulletin 20, No.4, 416.)
7. D.I.Blokhintsev, Zhur.eksp.i teor.fiz., 9, 459 (1939).
8. T.Förster, Fluoreszenz organischer Verbindungen. Göttingen, 1951.
9. B.I.Stepanov, Doklady AN SSSR, 112, 839 (1957).
10. B.S.Neporent, Ibid., 20, 30 (1958).
11. B.S.Neporent & N.G.Bakhshiev, Optika i spektroskopiia, 5, 634 (1958).
12. B.S.Neporent, Izv.AN SSSR, Ser.fiz.,20, 455 (1956), (Trans.Bulletin, 20, No.4, 413.); Zhur.fiz.khimi, 30, 1048 (1956).
13. L.P.Kazachenko & B.I.Stepanov, Optika i spektroskopiia, 2, 339 (1957).
14. B.S.Neporent, V.V.Zelinskii & V.P.Klochkov, Doklady AN SSSR, 92, 927 (1953).
15. B.S.Neporent & V.P.Klochkov, Ibid., 114, 524 (1957).

RELATION BETWEEN THE LUMINESCENCE AND ABSORPTION SPECTRA OF AN AQUEOUS SOLUTION OF FLUORESCEIN

- M.N.Alentsev and L.A.Pakhomycheva

Stepanov[1] obtained the following theoretical relation between the luminescence and absorption spectra of complex molecules:

$$\frac{W_\nu^{lum}}{\varkappa_\nu} = d(T)\,\nu^3 e^{-h\nu/kT}. \qquad (1)$$

This formula was deduced on the assumption that between the absorption event and the emission there is established an equilibrium distribution of the molecules over the range of vibrational energy values of the excited electronic state, appropriate to the temperature of the medium.

In a previous contribution[2] one of the present authors attempted to verify Eq.(1) on the basis of certain absorption and luminescence data in the literature. This was done by computing and plotting the values of $F_\nu = 3 \ln \nu - \ln (W_\nu/\varkappa_\nu)$ as a function of the frequency ν. If the relation (1) is valid, the plot should be a straight line, the slope of which should give the temperature T.

The plots obtained actually were straight lines; however, in most cases the temperature T_1 calculated from the slopes was found to be higher than the experimental temperature T, not only in the case of vapors but also for luminescent solutions, where intimate contact with the medium should promote the rapid loss of the excess vibrational energy by the excited molecules.

However, it should be noted that the overlapping of the luminescence and absorption spectra, within the range in which they can be compared, is not large, and in general authors, whose data we utilized, did not specifically aim at obtaining high accuracy at the limits of the spectra.

Consequently, we felt it would be of interest to perform special measurements over as wide an interval of frequencies as possible, in order to see how extensive the noted difference between T and T_1 actually is.

For our work we used solutions of fluorescein in water, containing 1% NaOH by weight. The basic measurements were performed with a fluorescein concentration c of $5 \cdot 10^{-6}$ g/cm^3, at which the correction for reabsorption of the luminescence is small. Additional measurements were performed at a concentration of 10^{-4} g/cm^3 in order to evaluate the effect of reabsorption on the experimental results.

The Hg 436 mμ line was used for excitation. The cell thickness used in studying the luminescence spectra was 0.5 cm. The absorption spectra were recorded with cells of varying thickness - up to 10 cm.

The results are presented in Fig.1. As may be seen, at the $5 \cdot 10^{-6}$ g/cm^3 concentration, the ν dependence of F_ν remains linear over 1 to 10^5 range in the magnitude of F_ν (curve 1). The temperature T_1 determined from the slope of the straight line is 305°K, which agrees well with the experimental value of T = 297°K.

In the case of the 10^{-4} g/cm^3 concentration data, the temperature T_1 calculated from the slope of the line obtained without correcting for reabsorption (line 2) was 278°K, while a value of 322°K was deduced from the slope of line 3, which was obtained after correction for reabsorption, on the assumption that the secondary absorption is wholly inactive.[3] This indicates that the reabsorbed radiation is not entirely lost, i.e., that some of it stimulates further emission.

Thus, one can safely assert that in the given case an equilibrium energy distribution of the molecules over the excited electronic levels is established prior to the emission of luminescence.

We also felt it would be of interest to determine whether the molecular vibrational energy distributions over the upper and lower (ground) electronic states were similar. In case they are similar, as was first noted by Blokhintsev[4], mirror

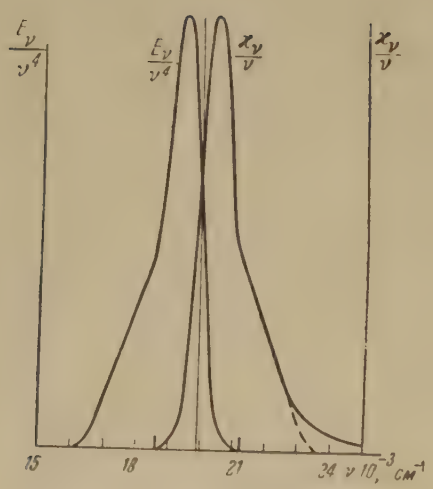

Fig.1. Variation of $F_\nu' = 3\ln\nu - \ln\frac{W_\nu}{\varkappa_\nu}$ with ν: 1) $c = 5\cdot10^{-6}$ g/cm^3, $T_1 = 305^\circ$K; 2) $c = 10^{-4}$ g/cm^3, without correction for reabsorption, $T_1 = 278^\circ$K; 3) $c = 10^{-4}$ g/cm^3, corrected for reabsorption; $T_1 = 322^\circ$K.

Fig.2. Absorption and luminescence spectra of aqueous fluorescein solutions: $c = 5\cdot10^{-6}$ g/cm^3; $\nu_{el} = 19.9\cdot10^3$ cm^{-1}.

symmetry should be observed between the functions W_ν/ν^4 and $\varkappa_\nu/\nu$ expressed in the ν scale. The pertinent data are given in Fig.2, from which it follows that close symmetry does obtain.

We plan to carry out similar experiments on other substances in order to establish whether Eq.(1) is universally applicable.

"P.N.Lebedev" Physical Institute,
Academy of Sciences of the USSR

References

1. B.I.Stepanov, Doklady AN SSSR, 112, 839 (1957).
2. M.N.Alentsev, Optika i spektroskopiia, 4, 690 (1958).
3. V.L.Levshin, Fotoliuminestsentsiia tverdykh i zhidkikh veshchestv (Photoluminescence of solids and liquids), p.51, M.-L., 1951.
4. D.I.Blokhintsev, Zhur.eksp.i teor.fiz., 9, 452 (1939).

Discussion following the reports of B.I.Stepanov, B.S.Neporent and M.N.Alentsev & L.A.Pakhomycheva

M.N.Alentsev: I would like to suggest another derivation for the relationship obtained by Stepanov.

We first consider a luminescent substance, for example, an elementary volume under conditions of thermodynamic equilibrium with black body radiation for the temperature T. In this case, two conditions which are compulsory for any body including luminescent materials, must be fulfilled: first, the emission from the given volume, which in this case will be thermal radiation, must obey Kirchoff's law,

$$W_{\nu}^{\text{forced}} = \mathfrak{A}_{\nu} u_{\nu,T};$$

and, second, the distribution of the molecules with respect to their energy E must be described by the Boltzmann statistical formula:

$$dn(E) = D\varphi(E)\, e^{-E/kT} dE.$$

We now turn to luminescence, i.e., to the case when the number of molecules in the excited electronic state exceeds the equilibrium number. We assume that by the instant of emisson of luminescence there is established a relative energy distribution of the molecules over the levels of the excited electronic state, describable by the same Boltzmann formula (naturally, with a different normalizing factor D').

Since with no forced emission and no interaction of the excited molecules with one another, the energy ratios at the individual frequencies of the luminescence spectrum are determined only by the energy distribution of the molecules over the levels of the excited state and by the corresponding transition probabilities (which depend only on the properties of the molecules themselves and not their numbers), the luminescence spectrum under these conditions should be similar to the thermal radiation spectrum, i.e.,

$$W_{\nu}^{\text{lum}} = \frac{D'}{D} \mathfrak{A}_{\nu} u_{\nu,T}.$$

It seems to me, that it is easier to see from this derivation that fulfilment of the Stepanov relationship only indicates establishment in the excited state of an equilibrium distribution of the molecules with respect to the values of vibrational energy determined by the test temperature, and, on the contrary, if this relationship does not hold, this simply means that either the equilibrium distribution has not been attained by the instant of emission or that the distribution differs from that for T.

B.S.Neporent: It is significant that the very careful measurements of Alentsev & Pakhomycheva led to calculated temperatures in close agreement with average experimental values. It would be hard to agree with the assumption that excited molecules in solutions do not have time to reach thermal equilibrium with the medium before emission. This assumption is in conflict with the experimental data on the rate of transfer of vibrational energy, and, moreover, cannot explain the divergences observed in certain investigations.

ON THE MEANING OF PHOTOLUMINESCENCE AND SCATTERING

- B. I. Stepanov & P. A. Apanasevich

The incidence of radiation on matter results in secondary emission which, depending on its properties, is classified as scattering or photoluminescence. At present the distinction between luminescence and scattering is usually made on the basis of the persistence criterion proposed by S. I. Vavilov. According to this criterion, luminescence possesses a noticeably afterglow and can be quenched, whereas scattering is unquenchable and has no afterglow.

Application of the persistence criterion made it possible to elucidate the nature of the Vavilov-Čerenkov effect and of the so-called universal blue emission. This criterion is also widely used for distinguishing between luminescence and the Raman effect. It must be noted, however, that the persistence criterion is purely empirical and as yet has not been validated theoretically. In a number of cases serious difficulties are encountered in attempting to apply this criterion. An obvious example is furnished by attempts to classify resonance radiation of atoms and simple molecules. Some authors call this emission "resonance fluorescence", while others refer to it as "resonance scattering". Use of the term "resonance radiation" itself is designed to emphasize the specific character of this type of secondary emission. Resonance radiation of rarified vapors is readily quenched by extraneous gases and in this respect is reminiscent of fluorescence. At the same time with increase in the pressure of the luminous vapor the resonance radiation gradually transforms into mirror reflection which is a special case of scattering.

Clearly, there is need for detailed theoretical investigation of the process of transformation of light by matter, i.e., of the process of weakening or complete disappearance of the incident radiation accompanied by the appearance of new secondary emission. The properties of this secondary irradiation must be intimately associated with the character of the transformation process; that is, the difference between scattering and photoluminescence must be defined in a manner consistent with the difference between the mechanisms of interaction of light with matter involved.

Actually scattering and photoluminescence are different, often complementary aspects or parts of the same process of transformation of light by matter. In present day theories, however, luminescence, scattering and the Raman effect are considered separately, often on the basis of different models or approximations. In classical electrodynamics scattering and resonance radiation are regarded as emission of light due to forced oscillations of an electric dipole. Both cease when the stimulating radiation is cut off. After this there begin free, gradually damped vibrations of the dipole, accompanied by afterglow which is classified as luminescence. Luminescence under steady state conditions is not described at all in the classical theory. Quantum mechanics treats only forced processes and does not consistently describe spontaneous emission. From the standpoint of quantum electrodynamics, luminescence is usually treated on the basis of the first approximation of the theory of interaction of an electromagnetic field with matter as a spontaneously decaying one-photon emission process. At the same time, scattering (as well as resonance radiation) is treated as a two-photon process on the basis of the second approximation of this theory.

Fluorescence in the steady state is also a typical two-photon process, a process involving the disappearance of one photon and the appearance of another photon, and from this standpoint is undoubtedly akin to scattering.

Let us turn first to the results of classical theory. For some obscure reason, until now no one has noted that the deductions of classical theory are in direct conflict with the classification based on the persistence criterion.

Yet the results of quantum electrodynamics as regards scattering are analogous to the results of classical electrodynamics and, consequently, it must be inferred that the latter correctly picture reality. In classical theory, we consider the oscillations of a dipole, described by the familiar equation:

$$\ddot{r} + 2\gamma\dot{r} + \omega_0^2 r = \frac{e}{m} E_0 e^{-i\omega t}, \tag{1}$$

where

$$\gamma = \gamma_{em}^{cl} + \gamma_{tr},$$

here

$$\gamma_{em}^{cl} = \frac{e^2\omega^2}{3mc^3}. \tag{2}$$

Under steady state conditions a dipole, set in forced oscillation with the frequency of the incident radiation, emits secondary radiation with an intensity

$$I_{em}(\omega) = \frac{8\pi}{3}\frac{e^4}{m^2c^4}\frac{\omega^4 I_0(\omega)}{(\omega^2-\omega_0^2)^2 + 4\gamma^2\omega^2}. \tag{3}$$

This is forced radiation and is treated by all authors as scattering. The absorption is given by

$$I_{abs}(\omega) = \frac{8\pi^2\omega^2}{mc}\frac{(\gamma_{em}^{cl} + \gamma_{tr})\, I_0(\omega)}{(\omega^2-\omega_0^2)^2 + 4\gamma^2\omega^2}. \tag{4}$$

The relative yield or efficiency, i.e., the ratio of the emitted to the absorbed energy, is

$$\Gamma = \frac{I_{em}(\omega)}{I_{abs}(\omega)} = \frac{\gamma_{em}^{cl}}{\gamma_{em}^{cl} + \gamma_{tr}}. \tag{5}$$

The ratio equals unity (100% efficiency) only in the absence of processes involving transfer of energy to the surrounding medium, i.e., energy loss. Increase of γ_{tr}, for example, by the introduction of an extraneous gas or increase in the number of collisions leads to decrease of the efficiency and, consequently, to quenching of the scattering.

Such quenching of scattering undoubtedly exists but in practice is usually masked by the persisting high level of emission. Fig.1 shows the variation of the emission intensity with the frequency ω for two values of γ_{tr}. If the frequency of the irradiating light differs greatly from the natural frequency ω_0 of the dipole, the intensity of the scattered light is independent of γ_{tr}. Decrease of the emission yield with increase of γ_{tr} is connected not with decrease of the emission intensity, but with increase of the absorption owing to broadening of the absorption line. In the $\omega \approx \omega_0$ region, i.e., for resonance radiation, increase of γ_{tr} is accompanied by decrease of both the emission intensity and its yield.

It must be noted that, according to classical theory, the steady state emission spectrum (scattering spectrum) depends substantially on the spectral composition of the irradiating light. If the irradiating line is very narrow, the contours of the emission line and the irradiation line coincide. Obviously, different scattering lines will have different intensities (Fig.2). If the irradiation is realized with a continuum, there appears in the secondary emission spectrum a line (or band), the contour of which is determined exclusively by the properties of the dipole and is described by the dispersion formula (3) with $I_0(\omega)$ = = const. (Fig.2); however, in this case, too, there is realized the same type of transformation of light. Separating the irradiating light into narrow spectral bands, one finds that each of them is transformed with retention of its specific frequency and contour (but with changes in intensity).

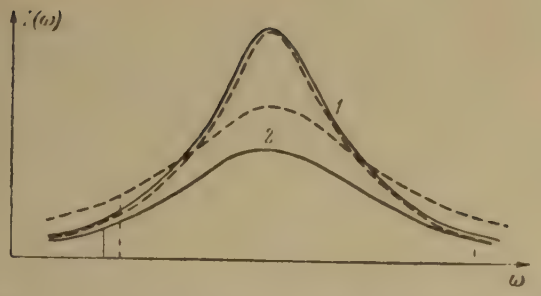

Fig.1. Variation of the intensity of emission (solid lines) and absorption (dashed lines) of light of frequency with 1) $\gamma_{tr} = 0$, 2) $\gamma_{tr} = 0.5\ \gamma_{em}$.

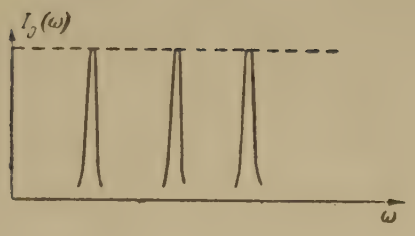

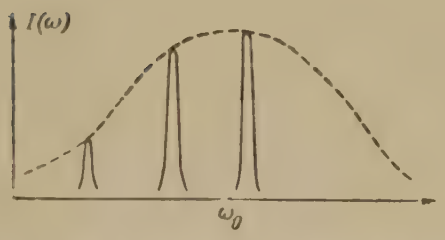

Fig.2. Relation between the contours and absorption of the lines of the secondary and the primary light.

According to classical theory, after cessation of irradiation there always exists an afterglow whose intensity I_{aft} varies with the frequency ω and time t. The integral intensities are given by

$$\left.\begin{aligned}\int_0^\infty I_{aft}(\omega,\ t)\,d\omega &\sim e^{-2\gamma(t-t_0)};\\ \int_{\tau_0}^\infty I_{aft}(\omega,t)\,dt &\sim \frac{1}{(\omega-\omega_0)^2+\gamma^2}.\end{aligned}\right\} \qquad (6)$$

The duration of this afterglow is of the usual order of magnitude characteristic of fluorescence (with $\gamma_{tr} = 0$, $\tau \approx 10^{-8}$ sec). The persistence does not depend on the excitation conditions. In the general case, however, the afterglow spectrum differs radically from the spectrum of the irradiating light: it consists of the intrinsic line of the dipole with the contour given by (6). In case of irradiation far from resonance, at the instant of cessation there occurs a sharp change in the emission spectrum which is evinced by the absence of afterglow. The spectral composition of the secondary emission under steady state conditions coincides with the spectral composition of the afterglow only in the case of resonance irradiation by a continuous spectrum. In this case the properties of the secondary emission are fully reminiscent of the properties of fluorescence, although actually the effect differs in no way from secondary emission in the absence of resonance, naturally treated as scattering.

Thus, if we assume that the classical theory of forced emission of a dipole correctly pictures the principal characteristics of scattering and resonance radiation, the persistence criterion (quenching) cannot be utilized for classification of the secondary emission; as we noted, forced emission a) is quenched and b) may be accompanied by more or less prolonged afterglow.

The same deduction follows from quantum electrodynamics. In addition to Rayleigh scattering and resonance radiation, quantum electrodynamics makes it possible to consider jointly all the other variants of secondary emission (photoluminescence and Raman scattering) and hence allows of consecutive solution of the problem of classification.

In quantum electrodynamics the behavior of a system consisting of matter and an electromagnetic field is described by the wave function Ψ satisfying the Schrödinger equation:

$$(H_0 + H_f + U)\Psi = ih\frac{\partial}{\partial t}\Psi, \tag{7}$$

where H_0 and H_f are the Hamiltonians of the substance and the field and U is the interaction operator.

Expanding Ψ in terms of the eigenfunctions of the substance and the field, one can write Eq.(7) in the form:[1]

$$ih\frac{\partial c_{i(n_\varkappa)}}{\partial t} = -\sum_{j,\varkappa'}\frac{(P_{\varkappa'})_{ij}\sqrt{n_{\varkappa'}+1}}{\sqrt{V\omega_{\varkappa'}}}e^{i(\omega_{ij}-\omega_{\varkappa'})t}c'_{j(n_\varkappa+\delta_{\varkappa\varkappa'})} -$$

$$-\sum_{j,\varkappa'}\frac{(P^{+}_{\varkappa'})_{ij}\sqrt{n_{\varkappa'}}}{\sqrt{V\omega_{\varkappa'}}}e^{i(\omega_{ij}+\omega_{\varkappa'})t}c_{j(n_\varkappa-\delta_{\varkappa\varkappa'})} + \sum_j M_{ij}e^{i\omega_{ij}t}c_{j(n_\varkappa)}; \tag{8}$$

here the $c_{i(n_\varkappa)}$ are the wave function expansion coefficients, the $(P_{\varkappa'})_{ij}$ and M_{ij} are the matrix elements of the optical and nonoptical transitions, respectively, and the $n_\varkappa$ are the numbers of photons.

Eqs.(8) describe the interaction of the electromagnetic field with the substance (matter). Solving these under different assumptions corresponding to different experimental conditions, one can comprehensively investigate the transformation of light. Extant solutions are not suitable for this purpose inasmuch as they treat the different variants of secondary emission separately and do not take into account the specific nature of the experimental problem involved. For example, Weisskopf's solution, which can be found in a number of monographs and has been widely used in different investigations, is a decaying one, i.e., does not correspond to the steady state conditions usually realized in experiments. In order to determine the principal characteristics of transformation of light one must find a solution of Eqs.(8) for the steady irradiation state when $n_\varkappa = n^0_\varkappa$ and $|c_{i(n_\varkappa)}|^2 = a_i$ are constant, and then for after cessation of irradiation when $n_\varkappa = 0$ and $c_{i(0)} = c_i^S t$.

As will be evident from Eqs.(8), at least two transitions of the system are involved in each transformation event: a transition to an intermediate state, accompanied by the disappearance of the incident photon ω' and a transition from this or some other intermediate state to the final state leading to the appearance of a new photon ω''.

These transitions may follow each other promptly or may be separated from one another by intermediate (optical or nonoptical) transitions leading to redistribution of the light transforming system over the excited levels. In complex molecules such processes may be redistribution of the vibrational energy over individual degrees of freedom. According to the number of such intermediate transitions, the complex process of transformation may be subdivided into partial processes[1], the attributes of which are readily determined on the basis of Eqs.(8).

The transformation of light occurring without participation of intermediate transitions is described by the expression

$$I_{i\to j}(\omega'\to\omega'') = \frac{\omega''^2 I_0(\omega')}{4\pi^2\hbar^2c^4\omega'^2}\left|\sum_k\left[\frac{(P^{+}_{\varkappa''})_{jk}(P_{\varkappa'})_{ki}}{-i\gamma_k+\omega_{ki}-\omega'} + \frac{(P_{\varkappa'})_{jk}(P^{+}_{\varkappa''})_{ki}}{\omega_{ki}+\omega''}\right]\right|^2 \sum_i a_i\delta(\omega_{ij}-\omega'+\omega''). \tag{9}$$

where $I_{i\to j}(\omega'\to\omega'')$ is the intensity of the secondary emission resulting from the transition $i\to j$ under the influence of the incident radiation $I_0(\omega')$. The quantity $2\gamma_k$ represents the probability of the light transforming system leaving state k. It consists of the probability $2\gamma^{(\omega'')}_k$ of transitions with emission of light, the

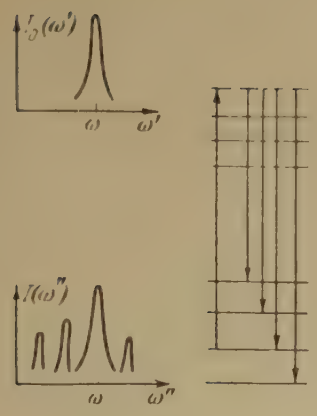

Fig.3

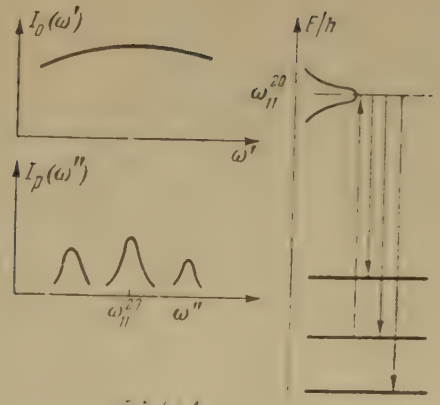

Fig.4

Fig.3. Transformation of light in the case of irradiation by a narrow line.
Fig.4. Transformation of light in the case of resonance irradiation with a wide line.

probability $2\gamma_k^{rl}$ of radiationless transitions and the probability $2\gamma_k^{red}$ of redistribution.

With $i = j$, Eq.(9) describes the transformation of light without change of frequency ($\omega' = \omega''$). This secondary emission has the attributes discussed above in connection with the classical dipole (Figs.1 & 2). Expression (9) differs from (3) only as regards the model assumed for the matter interacting with the field. In the case of an harmonic oscillator, these formulas become identical, ($\gamma_k^{red} = 0$; $\gamma_k^{rl} = \gamma_{tr}$). Hence the radiation described by Eq.(9), with $i = j$, just as the emission of a classical dipole, should be regarded as scattering of light. With $i \neq j$, the secondary emission described by (9) possesses Raman frequencies:

$$\omega'' = \omega' - \omega_{ij}.$$

It also consists of lines, the positions and contours of which depend on the spectral composition of the radiating light (Figs.3 & 4). Essentially this is the Raman effect.

The quantum efficiency of this process of transformation of light is given by

$$B_0 \sim \frac{\gamma_{em}}{\gamma_{em} + \gamma_{rl} + \gamma_{red}}, \tag{10}$$

where γ_{em}, γ_{rl} and γ_{red} are the respective probabilities averaged over all k.

The transformation of light occurring with the participation of only one intermediate transition is described by

$$I_j(\omega'') = \frac{|(P_{x''})_{jk}|^2 |Q_k(\omega')|^2}{\gamma_k^2 + (\omega_{kj} - \omega'')^2}. \tag{11}$$

Its quantum efficiency is

$$B_1 \sim \frac{\gamma_{red}}{\gamma_{em} + \gamma_{rl} + \gamma_{red}} \cdot \frac{\gamma_{em}}{\gamma_{em} + \gamma_{rl} + \gamma_{red}}. \tag{12}$$

It is evident from (11) that this part of the emission is a conjunction of the natural lines of the substance, the positions and contours of which do not depend on the irradiation conditions. Only the value of Q_k which is closely associated with the level population k, depends on the frequency and intensity of the exciting radiation.

In contrast to the radiation characterized by (9), for which far from resonance decrease of B_0 does not involve any change in the emission intensity, change in the quantum efficiency of the emission described by (11) is always accompanied by a corresponding change in the integral intensity.

The radiations arising as a result of the transformation of light with the participation of two, three or more intermediate energy redistributions consist of natural lines of the substance with the same wavelength and contours.

The intensity of lines corresponding to processes with different numbers of intermediate transitions may be different (depending on the values of Q_k). Such lines are superimposed on each other and cannot be resolved experimentally; they must therefore be considered jointly as a single line.

The quantum efficiency of the transformation with participation of all the intermediate transitions is given approximately by

$$B_l \sim \frac{\gamma_{red}}{\gamma_{em} + \gamma_{rl} + \gamma_{red}} \cdot \frac{\gamma_{el}}{\gamma_{em} + \gamma_{rl}}. \qquad (13)$$

In complicated systems the redistributions occur very rapidly ($\gamma_{red} \gg \gamma_{em} + \gamma_{rl}$) the major portion of the light is emitted after a large number of redistributions and hence the contours of the emission bands do not depend on the irradiation conditions. In such systems, as will be evident from (10), transformation without redistribution, i.e., scattering, is virtually completely quenched by rapidly occurring redistributions. In other words, virtually all the emission occurs with participation of redistributions and its quantum efficiency is described by the familiar formula that is obtained from (13) with $\gamma_{red} \gg \gamma_{el} + \gamma_{rl}$.

Utilizing Eq.(8), one can determine the attributes of the radiation emitted after cessation of irradiation.[1] Calculations show that all steady state emission terminates in an afterglow, the line contours and wavelengths of which do not depend on the excitation conditions. The entire afterglow consists of natural lines. Hence the part of the afterglow corresponding to transformation of light without intermediate processes, as regards its spectral composition, is, in general, not identical with the emission during the steady state irradiation. At the same time, the steady state spectrum of the radiation involving participation of redistributions fully matches the spectrum of the corresponding afterglow.

In the present discussion we have not touched on the problem of coherence of the secondary emission inasmuch as coherence cannot be used as a criterion for classifying the emission. Both theory and experiment show that Rayleigh scattering (including resonance radiation) is coherent. In contrast, photoluminescence and Raman scattering are incoherent.

Thus from the standpoint of quantum electrodynamics all secondary emission can be divided into two parts differing as regards their mechanism and possessing substantially different attributes.

One part is comprised of the emission produced with the participation of intermediate transitions. This part of the emission is characterized by the following properties: a) the contours and wavelengths of the lines of which it consists do not depend on the properties of the incident light; b) decrease (or sometimes increase) of the quantum efficiency is always accompanied by a corresponding change in the intensity of emission; c) the steady irradiation spectrum is identical with the afterglow spectrum. All the forms of emission that are commonly regarded as photoluminescence possess such properties. This is why, in accord with generally accepted concepts, this part of the secondary emission should be treated as photoluminescence. It should be noted, however, that the enumerated properties can be clearly observed only for line spectra. In other cases, when the lines overlap, the contours and wavelengths of the resultant bands will depend both on the properties of the irradiated substance and the

attributes of the irradiating light. In complicated systems where the predominant part of the emission is emitted with participation of a large number of redistributions, the emission band contours and wavelengths are usually determined only by the properties of the substance.

The second part is comprised of emission originating without participation of intermediate transitions. In classical theory it is regarded as radiation associated with forced oscillations of a dipole. This part of the emission has the following characteristics: a) the contours and frequencies of the lines depend on the spectral composition of the irradiating light; b) decrease of the quantum efficiency is not always accompanied by decrease of the emission intensity; c) the steady state spectrum in general does not coincide with the spectrum of the corresponding afterglow. Only in one particular case, namely, in the case of irradiation with a broad resonance line does this emission exhibit properties superficially similar to those of emission with participation of redistribution.

With no exceptions radiation produced without participation of intermediate processes should be treated as Rayleigh and Raman scattering. From this viewpoint, resonance radiation and part of the so-called fluorescence of rarefied atomic or simple molecular gases should be regarded as resonance scattering.

It follows from Eqs.(10) and (13) that the ratio of the quantum efficiency of luminescence B_l to the quantum efficiency of scattering $B_s = B_o$, as regards order of magnitude, is given by

$$\frac{B_l}{B_s} \sim \frac{\gamma_{red}}{\gamma_{em} + \gamma_{rl}}. \qquad (14)$$

It will be evident from this relation that with increasing probability of radiationless transitions B_l falls off more rapidly than B_s. If in addition we bear in mind that in the nonresonance case with decrease of B_s the scattering intensity remains unchanged, it will be evident that by using different quenchers one can fully suppress photoluminescence as compared with scattering. This explains the practical significance of utilizing the quenching criterion for distinguishing between scattering and photoluminescence. Thus the quantum electrodynamic solution of the problem of transformation of light furnishes a theoretical justification of the quenching criterion and allows us to establish the range of its applicability.

With reference to the mechanism of secondary emission, S.I.Vavilov also noted that photoluminescence differs from scattering in that it involves intermediate processes. Vavilov did not, however, give a detailed discussion of this problem.

Institute of Physics and Mathematics,
Academy of Sciences of the Belorussian SSR

References

1. P.A.Apanasevich, Trudy (Proceedings), Institute of Physics and Mathematics, Belorussian SSR Acad.of Sciences, No.2, 55; No.3, 140 (1959).

INTERNAL FIELD AND SPECTRA OF COMPLEX MOLECULES IN SOLUTIONS

- N.G.Bakhshiev

It was shown in earlier contributions[1,2] for a number of complex aromatic molecules having continuous electronic absorption and luminescence spectra, that changes in the integral probabilities of absorption (absorption integrals) and emission (lifetime of the excited state) in going from the vapor state to solutions can be quantitatively explained if we regard the solvent as an external dielectric medium which does not directly affect the transition probabilities but only alters the effective internal field of the light wave acting upon it. Hence there is reason to assume that, at least for substances in the given class, the influence of the solvent on the spectrum wavelengths can be explained from the same viewpoint. This assumption is fully justified inasmuch as a number of investigators[3-9] have observed characteristic dependences of the absorption and luminescence wavelengths on the physical properties of the solvent. Recently, there appeared a number of theoretical investigations[10-12] in which attempts were made to relate the position of the electronic spectra of molecules with the physical parameters of the medium, namely, with the dielectric constant ϵ and the index of refraction n. The validity of the expression deduced in these investigations for the magnitude of the displacement of the absorption and emission bands has so far not been substantiated experimentally. The reason for this, we believe, is the following. In theoretical analysis of the influence of the solvent on the position of the electronic levels of molecules only the electronic states were considered, so that the expressions deduced, as has been noted by Bayliss[10] and McRae (Ref.12), pertain only to the frequency shift corresponding to the 0—0 transition and having the physical meaning of a quantity characterizing the electronic excitation energy. In most experimental studies, on the other hand, owing to the difficulty or impossibility of direct determination of the 0—0 frequency, what was investigated essentially was the influence of the solvent on the displacement of the absorption and luminescence spectra peaks, although it is known that in the case of broad electronic-vibrational bands the positions of the maxima do not have the clear physical meaning as, for example, in the case of narrow atomic or molecular spectra. Furthermore, the positions of the peaks in the electronic spectra of polyatomic organic molecules also depend on different factors (the separation between electronic levels, the aggregate transition probabilities between vibrational sublevels of the lower and upper electronic states, the degree to which the Franck-Condon principle is adhered to, etc.), the role of which may change substantially in going from one solvent to another, thereby complicating the effect and masking the investigated regularity.

In view of the above, we undertook an investigation of the variation of the 0—0 frequency (we shall hereinafter refer to it as the purely electronic transition frequency ν_e) of a number of substances as a function of the physical properties of the solvent. In our work we made use of the deductions arrived at in the latest theoretical treatments. Analyzing the results of Bayliss[10], Ooshika[11] and McRae[12] and applying the expressions deduced by them to the frequency shift $\Delta\nu_e$, we can write the following somewhat simplified expression relating the red frequency shift of the electronic transition in a solution relative to the vapor (we have in mind the most common case of increase of the constant dipole moment of the dissolved molecule upon excitation) with the dielectric constant ϵ and the index of refraction n of the solvent:

$$\Delta\nu_c = \nu_{c.vap} - \nu_{e.solv} = \frac{1}{r^3}\left[c_1\frac{2\epsilon-2}{2\epsilon+1} + (c_2 + fc_3)\frac{2n^2-2}{2n^2+1}\right], \qquad (1)$$

where r is the effective Onsager radius[13], which is virtually equal to the radius of the molecule, f is the oscillator strength of the given electronic-vibrational transition and c_1, c_2 and c_3 are constants (c_1 is associated with the change in the constant dipole moment incident to excitation, while c_2 and c_3 are connected with the presence of induced dipole moments in the molecule).

For the purposes of the present investigation we chose five aromatic compounds from among the previously thoroughly studied phthalimide derivatives, namely, 4-aminophthalimide, 3-aminophthalimide, 3-monomethylaminophthalimide, 3-dimethylaminophthalimide and 3-acetylaminophthalimide. All these have continuous absorption and luminescences spectra characterized by mirror symmetry, which allows of accurate determination of ν_e. In the case of these molecules, which according to the classification of Neporent[4] belong to the group of molecules possessing modulation spectra, the frequency ν_e coincides with the point of intersection of the absorption and luminescence spectra. In view of the high degree of symmetry of the spectra, ν_e was determined as the arithmetic average of the frequencies of the absorption (ν_{ma}) and luminescence (ν_{mf}) maxima, i.e.,

$$\nu_e = \frac{\nu_{ma} + \nu_{mf}}{2}.$$

By way of solvents we used n-hexane, n-heptane, carbon tetrachloride, benzene, xylene, dioxane, diethyl ether, methyl phenyl ether, chloroform, acetone, isoamilether, ethyl ether, methyl ether, glycerol, butyl alcohol and water.

The data on the frequencies of the absorption and luminescence spectra in the vapor state were taken from Klochkov[15].*

Before turning to the experimental results, let us adapt Eq.(1) to our case. The results obtained in the work of Ref.1 showed that the oscillator strengths of the investigated substances are constant (within 10%) in all the diverse solvents used. Hence we can set $c_2 f / c_3 = c_4$ and rewrite (1) in the following form

$$\Delta\nu_c = \frac{c_1}{r^3}\left[\frac{2\varepsilon - 2}{2\varepsilon + 1} + p\,\frac{2n^2 - 2}{2n^2 + 1}\right], \qquad (2)$$

where

$$p = \frac{c_4}{c_1}.$$

The variation of ν_e is a function of the term in brackets in Eq.(2) for all the investigated substances is shown in Figs.1,2 & 3 (the values of c_1/r^3 and p are listed in the accompanying table). The points at the origin are for the respective vapors. As will be seen, the experimental points fit the plots of Eq.(2) fairly well.

An interesting fact is the constant value of p for all 3-amino derivatives of phthalimide. This indicates that the relative contribution to the shift connected with changes in the constant and induced dipole moment is the same for all three amino derivatives. The fact that the value of p for 4-aminophthalimide is different indicates that the relative (and apparently absolute) change in the value of the constant dipole moment incident to excitation is greater in 4-aminophthalimide as compared with the 3-amino derivatives. In addition the similarity of the properties of the 3-amino derivatives gives reason to infer that for all these substances c_1 = const. In this case the great difference in the magnitude of the shifts should be due only to differences in the size of the molecules (the Onsager radii).

---

*We note that the frequencies of the absorption and emission spectra of the investigated substances in the vapor state are virtually temperature independent, so that in making comparisons with the spectra in solutions at 20° one can with little error use the vapor data obtained at temperatures of 200-300°.

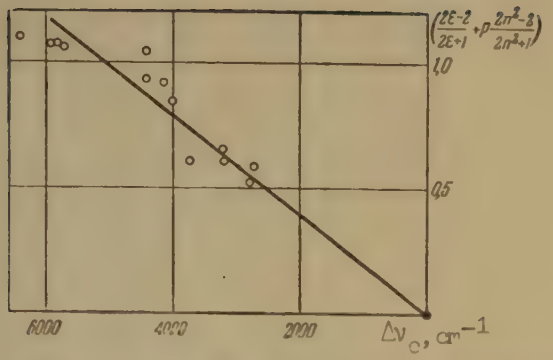

Fig.1. Plot of the functional dependence given by Eq.(2) and experimental points for 4-aminophthalimide.

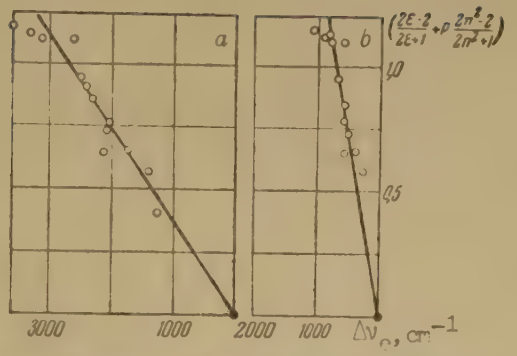

Fig.2. Same as Fig.1 but for a) 3-aminophthalimide and b) 3-acetylaminophthalimide.

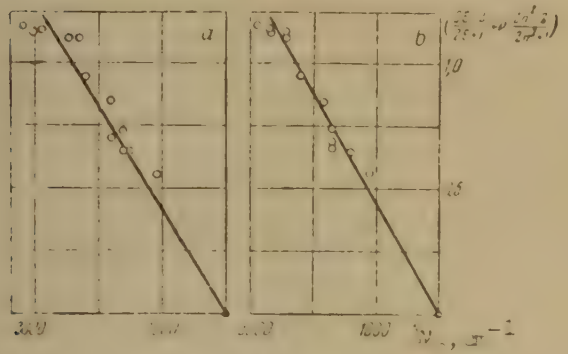

Fig.3. Same as Fig.1 but for a) 3-monoethylaminophthalimide and b) 3-dimethylaminophthalimide.

In column 5 of the accompanying table we list the data taken from Borisevich[16] on the radii (r) of the investigated molecules as determined from the structural models. In column 6 we list the radii (r') of the same molecules calculated from the magnitude of the shift assuming c_1 = = const. (the size of the 3-aminophthalimide molecule was taken as unity).

It will be seen that the relative sizes of the molecules as calculated from the magnitude of the shift are in good agreement with the results deduced from structural models.

Substance	c_1, cm^{-1}	c_2, cm^{-1}	c_2/c_1	r, Å	r', Å
3-aminophthalimide	2800	1400	0,50	3,8	3,8
3-monomethylaminophthalimide	2250	1150	0,51	3,9	4,1
3-dimethylaminophthalimide	2250	1150	0,51	3,9	4,1
3-acetylaminophthalimide	770	390	0,51	5,0	5,3
4-aminophthalimide	5150	1900	0,37	—	

The cited results show that the experimental data on the frequency shift of the electronic transition in a number of complex aromatic compounds in solutions are in good agreement with the deductions of the theory relating the magnitude of the shift with the physical parameters of solvents.

It must be noted, however, that the frequencies of the absorption and luminescence peaks of the investigated substances are generally in poorer agreement with the regularity defined by formula (2).

"S.I.Vavilov" State Optical Institute

References

1. B.S.Neporent & N.G.Bakhshiev, Optika i spektroskopiia, 5, 634 (1958).
2. N.G.Bakhshiev, Ibid., 5, 646 (1958).
3. P.Margulies, Acta phys.polon., 18, 292 (1950).

4. H.Ungnade, J.Amer.Chem.Soc., 75, 432 (1953).
5. L.Forster, J.Amer.Chem.Soc., 77, 1417 (1955).
6. L.Brooker, G.Keyes & D.Heseltine, J.Amer.Chem.Soc., 73, 5350 (1951).
7. E.Lippert & F.Moll, Z.Electrochem., 88, 718 (1954).
8. V.P.Klochkov, Optika i spektroskopiia, 1, 546 (1956).
9. N.Bayliss, J.Chem.Phys., 18, 292 (1950).
10. N.Bayliss & E.McRae, J.Phys.Chem., 58, 1002 (1954).
11. I.Ooshika, J.Phys.Soc.Japan, 9, 594 (1954).
12. E.McRae, J.Amer.Chem.Soc., 58, 1986 (1936).
13. L.Onsager, J.Amer.Chem.Soc., 58, 1986 (1936).
14. B.S.Neporent, Zhur.eksp.i teor.fiz., 21, 172 (1951); Izv.AN SSSR, Ser. fiz., 15, 533 (1951).
15. V.P.Klochkov, Zhur.fiz.khim., 29, 1432 (1955).
16. N.A.Borisevich, Dissertation, State Optical Institute, 1954.

DISCUSSION

V.V.Zelinskii: The report presented by N.G.Bakhshiev is very interesting. Since the changes in the positions (frequencies) of the fluorescence spectra in going from one solvent to another in the case of phthalimide derivatives depends greatly on the structure of the phthalimides and does not depend on the frequency of the fluorescence spectra of the given substance in different solvents, it must be assumed that the effect of the solvent is to produce certain changes in the structure of the molecule. As noted, the fluorescence and absorption spectra change in different ways under the influence of different solvents; in some cases the shifts in different solvents are in opposite directions. This gives reason to infer that the influence of the solvent on the structure of a molecule leads not only to change in the frequency of the electronic transition but also alters the equilibrium state.

Use of the electronic transition frequency as a criterion of the changes occurring in the spectra may serve to unify the information that can be obtained from the absorption and fluorescence spectra regarding the changes in the molecule of the dissolved substance. The observed dependence of the electronic transition frequency on the dielectric constant may be apparent and may be due simply to the fact that the magnitude of the dielectric constant is determined by the same elementary dipoles and by the same polarizabilities of the individual bonds that determine the effect of the solvent on the absorption and fluorescence spectra, but which can, however, be so combined that their net influence on the spectra remains unchanged, while the macrocharacteristic of the solvent, namely, the dielectric constant, changes. In our report we gave data indicating that the electronic transition frequency does not necessarily change with the dielectric constant. Consequently, the magnitude of the dielectric constant per se does not necessarily determine the frequency of the electronic transition.

N.G.Bakhshiev: The fact that the influence of the solvent may not be limited to a shift of the frequency ν_e is obvious and is substantiated by our data. Yet the first stage in the investigation of the influence of solvents on spectra must consist of investigations of the changes in the positions of the electronic levels due to intermolecular interactions of the dielectric type which, as the results of numerous investigations show, are the most common type of interaction in solutions associated with frequency shifts of the dissolved molecules.

TEMPERATURE DEPENDENCES OF THE ELECTRONIC SPECTRA OF SOME PHTHALIMIDES

- L.G.Pikulik & M.A.Solomakho

Stepanov[1] in his monograph gives a review of many experimental studies of the influence of temperature on the electronic spectra of complex molecules. From the results of these early studies it appeared that the frequency of the spectral bands of complex molecules is only weakly dependent on the temperature. It has been established in more recent studies, however, that an appreciable shift occurs in the luminescence spectra of phthalimides in solutions with changes in temperature from +20 to +250° (Refs.2 & 3) and from +20 to -196° (Ref.4). In the latter interval the shift may be comparable with the band half-width. Thus the early assumption regarding the weak temperature dependence of the spectra of solutions of complex molecules is open to question, and there is obvious need for extensive investigation of the temperature dependences of the electronic spectra of solutions of complex molecules in a wide range of temperatures.

Displacement of the emission spectra to the short wavelength side with increasing temperature of the medium[2] may be due to different causes. The fluorescence spectra of solutions of complex molecules are almost always located at longer wavelengths than the fluorescence spectra of the corresponding vapor. The shift of the emission spectra to the shorter wavelength side with increasing temperature may be connected with weakening of the influence of the solvent. In this case, the absorption bands should also exhibit a displacement[5] which, like the displacement of the fluorescence spectra, should be in the shorter wavelength direction, i.e., towards the spectra in the vapor state.

The theory of spectral band contours of complex molecules developed by Stepanov[1,6] for isolated molecules predicts displacement of the emission peak to the short wavelength side with increasing temperature. In this theory, however, the shift is determined by the properties of the molecule itself rather than by the external influence of the medium. According to this theory, the absorption band should be shifted with increasing temperature towards the fluorescence band, i.e., to the side of longer wavelengths from its initial position.

With a view to clarifying the causes of the temperature shift of the spectral bands of solutions, we investigated the absorption and emission spectra of a number of phthalimides (3-aminophthalimide, 3-monomethylaminophthalimide, 4-aminophthalimide, 4-amino-N-methylphthalimide) in high boiling-point solvents (glycerol, benzyl alcohol, isobutyl alcohol, cyclohexanol, ethyl acetoacetate, ethyl benzoate, dibutylphthalate, and vaseline oil). The fluorescence spectra were investigated on a photoelectric set-up assembled about a glass optics UM-2 monochromator; the absorption spectra were studied on an SF-4 spectrophotometer.

As will be evident from Fig.1, in the case of 3-aminophthalimide in cyclohexanol there is observed an appreciable displacement of the absorption and emission bands as the temperature of the medium is increased from +30 to +150°. The simultaneous displacement of the absorption and fluorescence to the shorter wavelength side gives reason to infer that this effect is due to weakening of the influence of the solvent on the molecule. A similar displacement of the spectral bands was observed for all the investigated substances in the other enumerated solvents except vaseline oil.

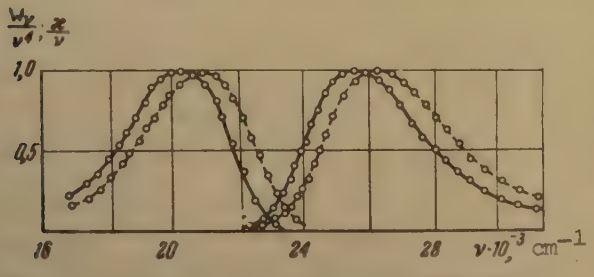

Fig.1. Fluorescence and absorption spectra of 3-aminophthalimide in cyclohexanol at +30° (solid line) and +150° (dashed line).

The magnitude of the effect of the temperature of the medium on the position of

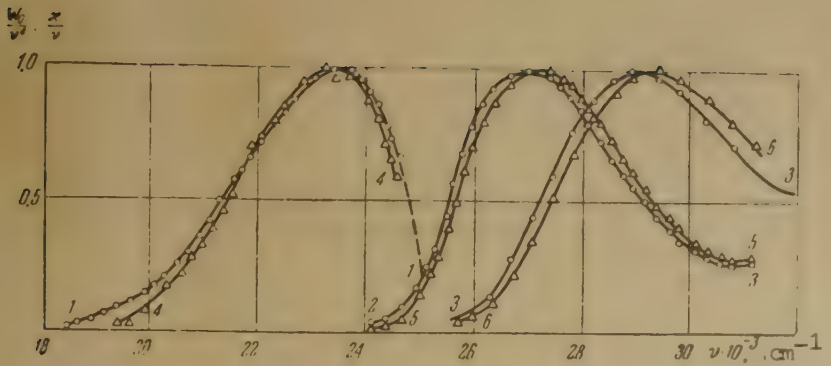

Fig.2. Fluorescence and absorption spectra of 3--aminophthalimide (1,2,4, & 5) and absorption spectra of 4-amino-N-methylphthalimide (3 & 6) in vaseline oil at +20° (1,2 & 3), +155° (4 & 5) and +180° (6).

the bands varies with their initial wavelengths in the given solvent. For example, in the case of 3-aminophthalimide in cyclohexanol at +30° (Fig.1) the fluorescence peak is located at 20,300 cm^{-1}; the absorption peak at 25,600 cm^{-1}. The band shifts with increase of temperature to +150° are 800 and 700 cm^{-1}, respectively. For the same compounds in vaseline oil (Fig.2), where the peaks at 30° are located at shorter wavelengths (ν_{fluo} = 23,400 cm^{-1} and ν_{abs} = 27,000 cm^{-1}), the band shifts incident to heating to +155° are negligible.

In Fig.2 we also give the absorption spectra of 4-amino-N-methylphthalimide in vaseline oil at different temperatures; it will be seen that in this case, too, the band shifts are insignificant.

In order to obtain the greatest displacement of the spectra the solutions were heated almost to the boiling point;* hence the spectra in the different solvents were obtained at different maximum temperatures. For purposes of comparing the spectrum shifts in different solvents, we divided the average value of the absorption and emission band shifts $\nu_{av} = (\Delta\nu_{flu} + \Delta\nu_{abs})/2$ (in some cases only $\Delta\nu_{flu}$) by the corresponding temperature interval. The shift coefficients $\Delta\nu_{av}/\Delta T$ obtained in this manner are plotted in Fig.3. The solvents are laid off in the horizontal frequency scale according to the frequencies of the fluorescence peak

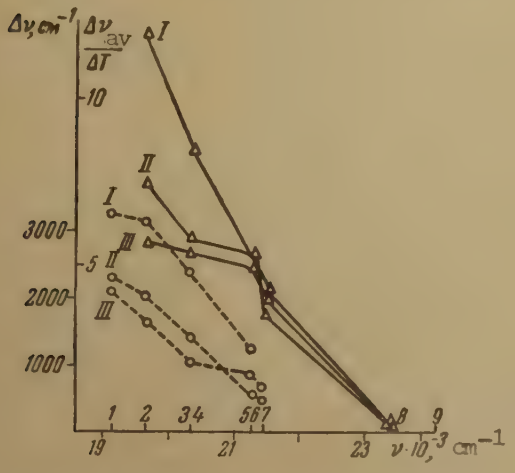

Fig.3. Variation of the temperature induced shift in the spectra of phthalimide derivatives ($\Delta\nu_{av}/\Delta T$ and $\Delta\nu$) with the position of the fluorescence spectrum in the given solvent at +20° relative to its position in the vapor spectrum. Substances: I) 4-amino-N-methylphthalimide and 4-aminophthalimide, II) 3-aminophthalimide and III) 3-monomethyl aminophthalimide. Solvents: 1) glycerol, 2) benzyl alcohol, 3) isobutyl alcohol, 4) cyclohexanol, 5) ethyl acetoacetate, 6) ethyl benzoate, 7) dimethylphthalate, 8) vaseline oil, 9) vapor. Solid lines - shift due to heating; dashed lines - shift due to cooling.

of 3-aminophthalimide in them. Thus, this solvent scale characterizes the decrease of the solvent-induced shift of the fluorescence spectrum of 3-aminophthalimide with respect to the fluorescence spectrum of the vapor. Actually, this sequence of the degree of influence of the solvent on the fluorescence spectrum at +20°

---

*We checked for the absence of decomposition by comparing the spectrum after cooling with the initial room temperature spectrum of the solution.

obtains for the other phthalimide derivatives as well. As will be evident from Fig.3, the variation of $\Delta\nu_{av}/\Delta T$ with the relative position of the spectra in the given solvent at +20° (solid lines) is characterized by decrease of the spectral band displacements as the fluorescence spectrum in the given solvent at +20° approaches the fluorescence spectrum of the vapor. An exception is the value of $\Delta\nu_{av}/\Delta T$ for glycerol, in which the coefficient is always smaller than in ethyl acetoacetate.

Thus increase of the temperature of the medium (solvent) can lead to an appreciable shift in the spectra of phthalimides if prior to heating (i.e., at room temperature) the spectrum of the phthalimide in the given solvent is appreciably displaced relative to the spectrum of the vapor; in other words, the degree of temperature displacement of the bands of a given substance depends on their position (relative to the vapor spectrum) at room temperature. The observed temperature effect is apparently due primarily to variation in the influence of the solvent on the phthalimide molecule.

It must be noted that the indicated regularities obtain only in a limited temperature range, i.e., in heating from room temperature to near the boiling point of the solvent.

The displacement of the spectral bands of phthalimides in the temperature range from +20° to -196° is entirely different. We were able to investigate the absorption spectra of the phthalimide derivatives only in solutions of ethyl alcohol, since the other solvents become opaque at low temperatures owing to cracking and fissuring of the frozen mass. The fluorescence and absorption spectra of 3-monomethylaminophthalimide in ethyl alcohol are shown in Fig.4. It will be seen that when the temperature is reduced from +20° to -196° the peak of the absorption band is shifted to the side of lower frequencies. At the same time the emission band is displaced to the side of higher frequencies.* Thus the absorption and emission band peaks move towards each other.** Similar shifts were observed for all the investigated phthalimide derivatives in ethyl alcohol; presumably the mutual approach of the absorption and emission bands would obtain in all the other solvents since in all cases the emission spectra shifted to the shorter wavelength side with reduction of temperature.

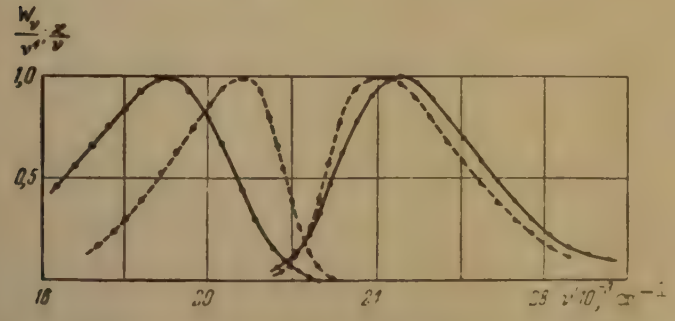

Fig.4. Fluorescence and absorption spectra of 3-monomethylaminophthalimide in ethyl alcohol at +20° (solid lines) and -196° (dashed lines).

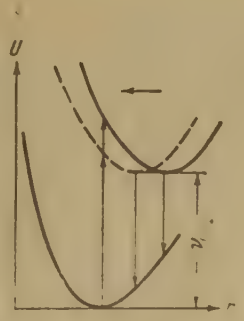

Fig.5.

---

*In this case also there is a correlation between the shift of the emission band and its position at 20°. This dependence for our solvents is shone in Fig. 3 by the dashed lines.

**A similar effect was observed for some acridines.[7]

We note in passing that in going from ~+200° to -196° the width of both the fluorescence and absorption bands decreases noticeably.

The observed regularities of the phthalimide spectrum displacements in the +20° to -196° temperature range can be characterized by means of the one-dimensional potential curve model. This model was used earlier[8] to explain the influence of the solvent on molecular spectra. Fig.5 shows the potential curves for the ground and excited states, shifted relative to each other due to the difference between the generalized equilibrium radii of the lower and upper electronic states (r_0 and r_0^*). The vertical transition from the minimum of the lower curve corresponds to the maximum of the absorption band and, analogously, the vertical transition from the minimum of the upper curve corresponds to the maximum of the emission band. The distance between the minima determines the frequency of the electronic transition.

The displacement of the absorption and emission bands towards each other with decreasing temperature corresponds to displacement of the upper potential curve relative to the lower curve horizontally to the left, i.e., to diminution of the difference between the equilibrium radii of the upper and lower electronic states. Obviously, the absorption maximum is shifted to the side of lower frequencies; the emission maximum, to the side of higher frequencies. In this case, if the shifts are equal, the electronic transition frequency should remain unchanged. As may be seen from Fig.4, however, the point of intersection of the absorption and emission bands (which gives the probable position of ν_e) is shifted noticeably in going from +20° to -196°. Since the spectra of Fig.4 are only for alcohol solutions further investigation of the absorption spectra at low temperatures in different solvents is indicated.

We desire to thank V.V.Zelinskii, A.N.Sevchenko and B.I.Stepanov for valuable suggestions.

Institute of Physics and Mathematics,
Academy of Sciences of the Belorussian SSR

References

1. B.I.Stepanov, Liuminestsentsiia slozhnykh molekul (Luminescence of complex molecules) Minsk, 1956.

2. L.G.Pikulik, Optika i spektroskopiia, 2, 676 (1957).

3. B.S.Neporent, N.A.Borisevich, V.P.Klochkov & O.A.Motovilov, Izv.AN SSSR, Ser.fiz., 18, 674 (1954). (Trans.Bulletin 18, No.6, 358.)

4. V.V.Zelinskii & V.P.Kolobkov, Program of the Sixth Conference on Luminescence (Molecular Luminescence and Luminescence Analysis).

5. V.P.Klochkov, Zhur.fiz.khim., 29, 1432 (1955).

6. L.P.Kazachenko & B.I.Stepanov, Optika i spektroskopiia, 2, 339 (1957).

7. V.L.Levshin & T.M.Tarasova, Izv.AN SSSR, Ser.fiz., 15, 573 (1951).

8. V.V.Zelinskii, V.P.Kolobkov & L.G.Pikulik, Optika i spektroskopiia, 2, 402 (1957).

LUMINESCENCE OF POWDERED MATERIALS

- Iu.I.Chekalinskaia

1. In connection with diverse research problems it is sometimes necessary to investigate the spectra and other optical attributes of powdered luminescent substances. The powdery, dispersed state of luminophors greatly complicates investigation of their optical properties inasmuch as in such cases there occurs multiple scattering of the exciting radiation and of the luminescence inside the powder. The optical properties of luminophor powders depend not only on the quantities characterizing the substance in the bulk (the coefficient of absorption, the quantum efficiency, the persistence of emission, etc.), but also on the size of the particles, the properties of the binding medium, the degree of packing and other factors. Hence in interpreting the experimental data one must take into account multiple scattering of light in the powder. Many authors neglect the effect of scattering as an insignificant factor but do not justify this either experimentally or theoretically. It is possible that in some cases scattering is combined with other effects, but even in such cases to clarify their mechanism, it is important to separate the effects associated with scattering.

The present report is devoted to the problem of allowing for the effect of scattering on the optical properties of powdered luminescent substances. For the purposes of determining the dependence of the intensity of luminescence on the parameters of the light-scattering layer one can make use of the model of a light-scattering layer[1,2] proposed by Antonov-Romanovskii, Girin & Stepanov and Bodo. According to this model, the light-scattering layer is regarded as a system of elementary laminae whose thickness corresponds to the mean dimensions of the particles and whose absorption coefficient is equal to the absorption coefficient of the bulk material.

Using this model and taking into account the invariance of the properties of the light-scattering layer as regards the addition of an elementary lamina,[1] one can deduce the following expressions for the intensity of luminescence of a plane powder layer:

$$I_N^{(1)} = I_0 \frac{\gamma\varphi(\nu')(b-1)(1-R_\infty)(b'+R'_\infty)}{2(b^{2N}-R_\infty^2)(b'^{2N}-R'^2_\infty)} \begin{vmatrix} \frac{b^N-b'^N}{b-b'}, & R_\infty b'^N + R'_\infty b^N \\ \frac{(bb')^N-1}{bb'-1}, & (bb')^N + R_\infty R'_\infty \end{vmatrix}, \qquad (1)$$

$$I_N^{(2)} = I_0 \frac{\gamma\varphi(\nu')(b-1)(1-R_\infty)(b'+R'_\infty)}{2(b^{2N}-R_\infty^2)(b'^{2N}-R'^2_\infty)} \begin{vmatrix} \frac{(bb')^N-1}{bb'-1}, & R_\infty b'^N + R'_\infty b^N \\ \frac{b^N-b'^N}{b-b'}, & (bb')^N + R_\infty R'_\infty \end{vmatrix}. \qquad (2)$$

Here I_0 is the flux of radiation incident on the "front" of layer, $I_N^{(1)}$ and $I_N^{(2)}$ are the luminescence fluxes emerging from the layer in the direction of the incident light (from the back) and in the opposite direction (from the front) respectively, N is the number of laminae, γ is the quantum yield, $\varphi(\nu')$ is a function characterizing the energy distribution over the luminescence spectrum, R_∞ and R'_∞ are the coefficients of reflection of the exciting radiation and of the luminescence from an infinitely thick layer and b and b' are parameters of the light scattering layer (here and below the primes denote quantities pertaining to the luminescence). According to Stokes[3], R_∞ and b are given by

$$R_\infty = \frac{1}{2R_1}(1 - T_1^2 + R_1^2 - \Delta), \text{ and } b = \frac{1}{2T_1}(1 + T_1^2 - R_1^2 + \Delta). \quad (3)$$

Here

$$\Delta = \sqrt{(1 + R_1 + T_1)(1 - R_1 + T_1)(1 + R_1 - T_1)(1 - R_1 - T_1)},$$

where

$$R_1 = r_0 + \frac{(1-r_0)^2 r_0 e^{-2kl}}{1 - r_0^2 e^{-2kl}} \text{ and } T_1 = \frac{(1-r_0)^2 e^{-kl}}{1 - r_0^2 e^{-2kl}}$$

are the coefficients of reflection and transmission of one lamina, l is the thickness of a lamina (equal to the mean dimensions of the particles), k is the coefficient of absorption of the dispersed material, r_0 is the coefficient of reflection at the binding medium-dispersed substance interface, i.e., at the particle boundaries.

Eqs.(1) and (2)* give the dependence of the luminescence flux on the parameters of the light-scattering layer: the absorption coefficients for the exciting radiation (k) and the luminescence (k'), the particle size, and the indices of refraction of the dispersed substance and the binding medium. Knowing these constants and the true luminescence spectrum, we can predict the luminescence spectrum of the powdered luminophor and the way it will change when the parameters are varied. We can also solve the inverse problem, namely, find the true spectrum and the luminescence yield of the material from the measured spectrum and the technical yield of the powder.

If the luminescence is not absorbed, Eqs.(1) and (2) become

$$I_N^{(1)} = I_0 \frac{\gamma\varphi(\nu')(1 - R_\infty)}{2[1 + (N-1)r'](1 - R_\infty^2 b^{-2-N})} \left\{(1 - b^{-N})(1 - R_\infty b^{-N}) + \right.$$
$$\left. + 2r'\left[\frac{(1 - b^{-N})(b^{-1} + R_\infty b^{-N}) - Nb^{-N}(1 - b^{-1})(1 + R_\infty)}{(1 - b^{-1})}\right]\right\}, \quad (4)$$

$$I_N^{(2)} = I_0 \frac{\gamma\varphi(\nu')(1 - R_\infty)(1 - b^{-N})}{1 + R_\infty b^{-N}} - I_N^{(1)}, \quad (5)$$

where $r' = \frac{2r_0}{1 + r_0}$. In working with Eqs.(1), (2), (4) & (5) one must employ numerical calculations. Eqs.(1) and (2) differ mainly as regards the positions of the elements in the first column, which greatly facilitates tabulation.

Below we shall consider the dependence of the luminescence flux on only some of the parameters of light-scattering layers.[1]

2. The variation of the luminescence fluxes as a function of the number of elementary laminae for two values of the coefficient of reflection at the particle boundaries is shown in Fig.1. It will be seen that the luminescence flux emerging from the front (i.e., towards the source of incident light) with increasing number N of laminae always increases, tending to a limiting value, while the flux emerging from the back of the layer first increases, goes through a maximum and then falls off. For media with a small value of the reflection coefficient ($r_0 = 0.01$) the number of elementary lamina at which the maximum flux is attained is larger than for media with a large value of r_0. The luminescence maximum is shifted to the side of smaller values of N with increase of $k'l$. If the radiation is wholly absorbed in the front elementary lamina, there is obviously no maximum.

---

*These expressions can be used for evaluating the luminescence flux of a stack of plates.

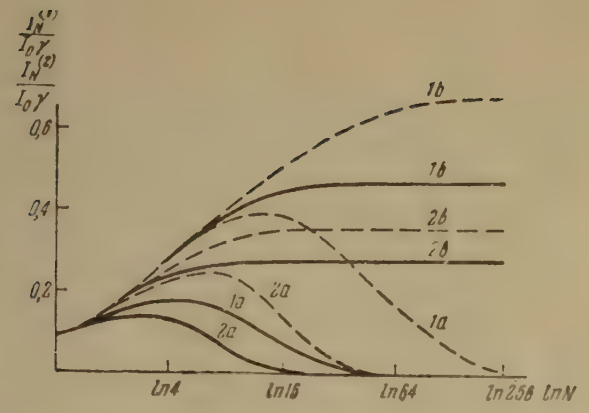

Fig.1. Variation of the luminescence fluxes as a function of the number of elementary lamina with $kl = 0.2$; $r_0 = r_0' = 0.2$ (solid lines) and $r_0 = r_0' = 0.01$ (dash lines): a - $I_N^{(1)}$, b - $I_N^{(2)}$; 1 - $k'l = 0.005$; 2 - $k'l = 0.1$.

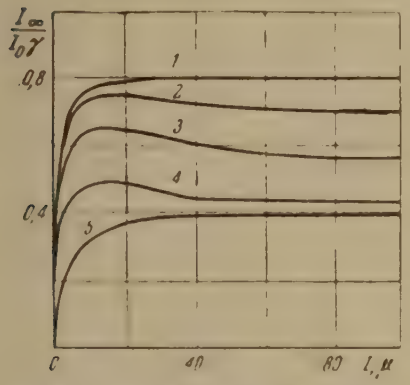

Fig.2. Variation of the luminescence flux for an infinitely thick layer as a function of the particle size with $r_0 = r_0' = 0.2$; 1 - $k' = 0$, 2 - $k' = 0.001k$, 3 - $k' = 0.01k$, 4 - $k' = 0.1k$, 5 - $k' = k$; $k = 1000$ cm^{-1}.

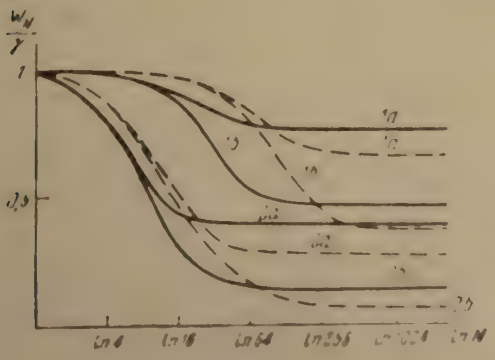

Fig.3. Variation of the technical yield as a function of the number of elementary laminae with $r_0 = 0.2$ (solid lines) and $r_0 = 0.01$ (dash lines): a - $kl = 0.1$, b - $kl = 0.005$; 1 - $k'l = 0.005$, 2 - $k'l = 0.1$.

It also follows from Fig.1 that the luminescence flux emerging from the layer towards the source of radiation (from the front) is always greater than the flux emerging from the back.

3. Fig.2 shows the variation of the luminescence flux from an infinitely thick layer as a function of the particle size for $k = 1000$ cm^{-1} and different values of k'. In the presence of reabsorption ($k' \neq 0$) and $k > k'$, with increasing particle size the flux at first increases, goes through a maximum and then slowly decreases. Consequently, fragmentation of the phosphor (reduction of particle size) in some cases may lead not to diminution of the brightness, as usually observed experimentally[4,12], but to increase of the brightness due to enhanced scattering. In the absence of reabsorption, increase of the particle size is always accompanied by increase of the brightness of an infinitely thick layer.

Although scattering undoubtedly plays a certain role in the variation of brightness with reduction of particle size, the changes observed in a number of cases cannot be explained entirely by scattering. Thus for example the strong decrease in brightness incident to fragmentation of the phosphor NaCl:TlCl cannot be due exclusively to scattering; other factors must be invoked to explain the observed[4] attenuation.

The dependences described above are in agreement with the experimental and theoretical data of Ivanov.[6]

Having elucidated the influence of different parameters on the effective luminescence yield of powdered materials, we can determine the conditions for their most efficient utilization.[6]

4. The technical yield (efficiency) of a layer of finite thickness is given by

$$W_N = \frac{I_N^{(1)} + I_N^{(2)}}{I_0(1 - R_N - T_N)},$$

where R_N and T_N are the coefficients of reflection and transmission of the layer for the exciting radiation. The variation of W_N as a function of the number of elementary laminae is shown in Fig.3; from this figure it follows that

1) with increasing layer thickness the technical yield decreases, tending to a limit, i.e., to the value of the technical yield of an infinitely thick layer;

2) the technical yield of weakly scattering layers ($r_0 = 0.01$) of finite thickness is greater than the technical yield of strongly scattering ($r_0 = 0.2$) layers (for infinitely thick layers the opposite obtains);

3) for weakly scattering media, the technical yield of layers of finite thickness is strongly dependent on $k'l$ and with a small number of laminae is almost independent of kl; in strongly scattering media the kl dependence is stronger, particularly in the range of large $k'l$.

These results show that scattering may have an appreciable influence on the optical properties of powdered phosphors and that, consequently, it must be taken into account in practical applications. Through appropriate variation or selection of the binding medium and the particle size, one can attain the most efficient utilization of a given phosphor.

5. Luminescent layers are generally applied to a backing or base which affects the character of the luminescence. The coefficients of reflection of the base for the exciting radiation and the luminescence are generally not equal. Taking into account multiple reflection of the exciting radiation and the luminescence from the backing, we obtain

$$I_N = I_N^{(2)} + I_N^{(1)} \frac{T_N R}{1 - R_N R} + \frac{[I_N^{(2)} T_N R + I_N^{(1)}(1 - R_N R)] T'_N R'}{(1 - R_N R)(1 - R'_N R')}, \qquad (6)$$

where R and R' are the coefficients of reflection from the backing of the exciting radiation and the luminescence, respectively.

As a rule backings with equally good reflection in a wide spectral range are not available. Analysis of Eq.(6) shows that in most cases (and in the absence of reabsorption always), it is more advantageous to use a backing with high reflection for the luminescence.

In conclusion, I wish to express my gratitude to B.I.Stepanov for guidance in the work and valuable advice.

Institute of Physics and Mathematics,
Academy of Sciences of the Belorussian SSR

References

1. B.I.Stepanov & Iu.I.Chekalinskaia, Trudy (Proceedings), Inst. of Physics & Math., Belorussian Acad.of Sci., No.2, 19 (1957); Iu.I.Chekalinskaia, Trudy (Proceedings), Inst. of Physics & Math., Belorussian Acad.of Sci., No.2, 38 (1957).

2. Z.Bodo & I.Hangos, Acta Phys.Acad.scient.Hung., 5, 295 (1955).

3. G.Stokes, Math. and Phys. Papers., 4, 145 (1904).

4. F.D.Klement & R.K.Gindina, Trudy (Proceedings), Institute of Physics and Astronomy, Estonian SSR Acad. of Sci., No.4, 3 (1956).

5. V.L.Levshin & I.V.Veits, Zhur.eksp.i teor.fiz., 20, 411 (1950).

6. A.P.Ivanov, Optika i spektroskopiia (Optics and Spectroscopy), 4, 225 & 236 (1958).

RESONANCE LUMINESCENCE OF MATTER IN FINITE VOLUMES

- A.M. Samson

Secondary absorption and emission processes occurring in the bulk of the investigated substance generally affect the intensity, efficiency, line shape, rate of decay and other spectroscopic characteristics of the emerging radiation. This influence of secondary processes obviously hampers interpretation of the experimental data.

Under laboratory conditions, the influence of secondary processes can be minimized by investigating the substance in small volumes or at low concentrations. This, however, involves diminution of the total luminescence, which is not always acceptable. In some cases (propagation of radiation through the atmosphere, emission of stars[1,2], etc.), this method of eliminating the influence of secondary processes is impossible.

There have been many studies devoted to investigation of the propagation of radiation in finite volumes. Astrophysicists[1,2] have achieved notable successes in this field, but on the whole, many aspects of this effect have not been adequately studied.

In the present work we derived a general integro-differential equation for volumes of any shape, which makes it possible to allow for the influence of forced emission, the thermal background and nonoptical excitation. Solution of the general equation for particular cases allows of evaluating the influence of secondary absorption and emission processes on the spectroscopic characteristics of resonance luminescence.

If the number of excited and unexcited particles (emissive power and absorption) at each point is known, one can determine all the spectroscopic characteristics of the radiation. The nonlinear integro-differential equation for the number of excited particles at every point can be derived from the usual relation for systems of particles with two energy levels[3]:

$$\frac{dn_2}{dt} = -n_2[A + 2B(u_1 + u_2 + u_3) + d_{21} + d_{12}] + n[B(u_1 + u_2 + u_3) + d_{12}]. \qquad (1)$$

Here n_2 is the density of the excited particles, n is the total particle density, t is the time, A and B are the Einstein probability coefficients and d_{21} and d_{12} are the nonoptical transition probabilities. Finally, u_1, u_2 and u_3 denote the radiation densities associated with the thermal background, the external source and the luminescence of the investigated substance in a given finite volume, respectively; they all depend on the coordinates (see Ref.4).

If the nonoptical and thermal excitations are small compared with the excitation from the external source and one can neglect forced emission, the particular solution of the general equation is

$$y(\rho_0, \vartheta) = \gamma \int_{-\infty}^{\vartheta} e^{-(\vartheta - \vartheta')} w(\vartheta')\, d\vartheta' \sum_{i=0}^{\infty} \frac{\gamma^i (\vartheta - \vartheta')^i}{i!} \Phi_i(\rho_0). \qquad (2)$$

Here

$$y = \frac{n_2}{n}; \quad \gamma = \frac{A}{A + d_{21}}; \quad \vartheta = (A + d_{21})\, t; \qquad (3)$$

ρ represents the product of the radius vector of the point in the volume (specimen) by the absorption coefficient $\varkappa_0$, γ is the quantum efficiency of the elementary volume and $w(\vartheta)$ is proportional to the emissive power of the light source. The Φ_i are defined by

$$\Phi_0(\rho_0) = \Phi(\rho_0); \quad \Phi_i(\rho_0) = \frac{1}{4\pi} \int_{V'} \Phi_{i-1}(\rho) \frac{e^{-|\rho - \rho_0|}}{|\rho - \rho_0|^2}\, dV'. \qquad (4)$$

4. H.Ungnade, J.Amer.Chem.Soc., 75, 432 (1953).
5. L.Forster, J.Amer.Chem.Soc., 77, 1417 (1955).
6. L.Brooker, G.Keyes & D.Heseltine, J.Amer.Chem.Soc., 73, 5350 (1951).
7. E.Lippert & F.Moll, Z.Electrochem., 88, 718 (1954).
8. V.P.Klochkov, Optika i spektroskopiia, 1, 546 (1956).
9. N.Bayliss, J.Chem.Phys., 18, 292 (1950).
10. N.Bayliss & E.McRae, J.Phys.Chem., 58, 1002 (1954).
11. I.Ooshika, J.Phys.Soc.Japan, 9, 594 (1954).
12. E.McRae, J.Amer.Chem.Soc., 58, 1986 (1936).
13. L.Onsager, J.Amer.Chem.Soc., 58, 1986 (1936).
14. B.S.Neporent, Zhur.eksp.i teor.fiz., 21, 172 (1951); Izv.AN SSSR, Ser. fiz., 15, 533 (1951).
15. V.P.Klochkov, Zhur.fiz.khim., 29, 1432 (1955).
16. N.A.Borisevich, Dissertation, State Optical Institute, 1954.

DISCUSSION

V.V.Zelinskii: The report presented by N.G.Bakhshiev is very interesting. Since the changes in the positions (frequencies) of the fluorescence spectra in going from one solvent to another in the case of phthalimide derivatives depends greatly on the structure of the phthalimides and does not depend on the frequency of the fluorescence spectra of the given substance in different solvents, it must be assumed that the effect of the solvent is to produce certain changes in the structure of the molecule. As noted, the fluorescence and absorption spectra change in different ways under the influence of different solvents; in some cases the shifts in different solvents are in opposite directions. This gives reason to infer that the influence of the solvent on the structure of a molecule leads not only to change in the frequency of the electronic transition but also alters the equilibrium state.

Use of the electronic transition frequency as a criterion of the changes occurring in the spectra may serve to unify the information that can be obtained from the absorption and fluorescence spectra regarding the changes in the molecule of the dissolved substance. The observed dependence of the electronic transition frequency on the dielectric constant may be apparent and may be due simply to the fact that the magnitude of the dielectric constant is determined by the same elementary dipoles and by the same polarizabilities of the individual bonds that determine the effect of the solvent on the absorption and fluorescence spectra, but which can, however, be so combined that their net influence on the spectra remains unchanged, while the macrocharacteristic of the solvent, namely, the dielectric constant, changes. In our report we gave data indicating that the electronic transition frequency does not necessarily change with the dielectric constant. Consequently, the magnitude of the dielectric constant per se does not necessarily determine the frequency of the electronic transition.

N.G.Bakhshiev: The fact that the influence of the solvent may not be limited to a shift of the frequency ν_e is obvious and is substantiated by our data. Yet the first stage in the investigation of the influence of solvents on spectra must consist of investigations of the changes in the positions of the electronic levels due to intermolecular interactions of the dielectric type which, as the results of numerous investigations show, are the most common type of interaction in solutions associated with frequency shifts of the dissolved molecules.

TEMPERATURE DEPENDENCES OF THE ELECTRONIC SPECTRA OF SOME PHTHALIMIDES

- L.G.Pikulik & M.A.Solomakho

Stepanov[1] in his monograph gives a review of many experimental studies of the influence of temperature on the electronic spectra of complex molecules. From the results of these early studies it appeared that the frequency of the spectral bands of complex molecules is only weakly dependent on the temperature. It has been established in more recent studies, however, that an appreciable shift occurs in the luminescence spectra of phthalimides in solutions with changes in temperature from +20 to +250° (Refs.2 & 3) and from +20 to -196° (Ref.4). In the latter interval the shift may be comparable with the band half-width. Thus the early assumption regarding the weak temperature dependence of the spectra of solutions of complex molecules is open to question, and there is obvious need for extensive investigation of the temperature dependences of the electronic spectra of solutions of complex molecules in a wide range of temperatures.

Displacement of the emission spectra to the short wavelength side with increasing temperature of the medium[2] may be due to different causes. The fluorescence spectra of solutions of complex molecules are almost always located at longer wavelengths than the fluorescence spectra of the corresponding vapor. The shift of the emission spectra to the shorter wavelength side with increasing temperature may be connected with weakening of the influence of the solvent. In this case, the absorption bands should also exhibit a displacement[5] which, like the displacement of the fluorescence spectra, should be in the shorter wavelength direction, i.e., towards the spectra in the vapor state.

The theory of spectral band contours of complex molecules developed by Stepanov[1,6] for isolated molecules predicts displacement of the emission peak to the short wavelength side with increasing temperature. In this theory, however, the shift is determined by the properties of the molecule itself rather than by the external influence of the medium. According to this theory, the absorption band should be shifted with increasing temperature towards the fluorescence band, i.e., to the side of longer wavelengths from its initial position.

With a view to clarifying the causes of the temperature shift of the spectral bands of solutions, we investigated the absorption and emission spectra of a number of phthalimides (3-aminophthalimide, 3-monomethylaminophthalimide, 4-aminophthalimide, 4-amino-N-methylphthalimide) in high boiling-point solvents (glycerol, benzyl alcohol, isobutyl alcohol, cyclohexanol, ethyl acetoacetate, ethyl benzoate, dibutylphthalate, and vaseline oil). The fluorescence spectra were investigated on a photoelectric set-up assembled about a glass optics UM-2 monochromator; the absorption spectra were studied on an SF-4 spectrophotometer.

As will be evident from Fig.1, in the case of 3-aminophthalimide in cyclohexanol there is observed an appreciable displacement of the absorption and emission bands as the temperature of the medium is increased from +30 to +150°. The simultaneous displacement of the absorption and fluorescence to the shorter wavelength side gives reason to infer that this effect is due to weakening of the influence of the solvent on the molecule. A similar displacement of the spectral bands was observed for all the investigated substances in the other enumerated solvents except vaseline oil.

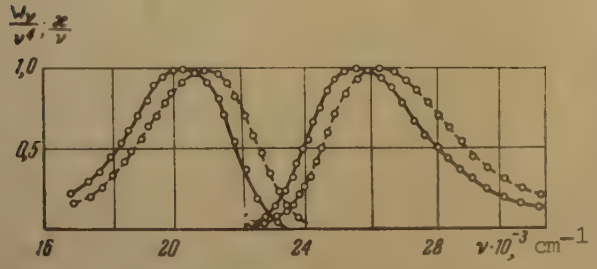

Fig.1. Fluorescence and absorption spectra of 3-aminophthalimide in cyclohexanol at +30° (solid line) and +150° (dashed line).

The magnitude of the effect of the temperature of the medium on the position of

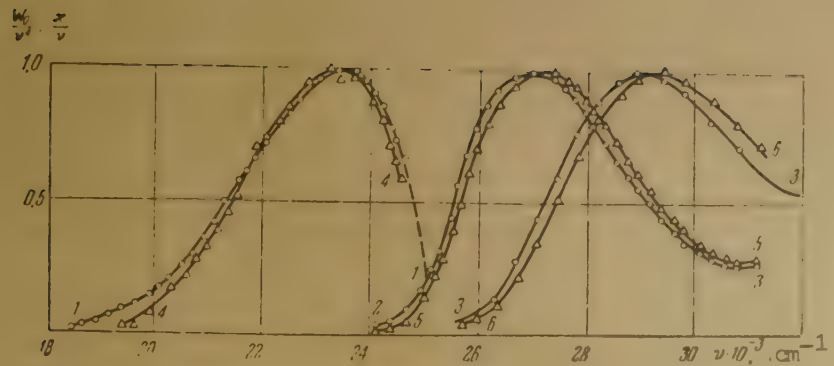

Fig.2. Fluorescence and absorption spectra of 3--aminophthalimide (1,2,4, & 5) and absorption spectra of 4-amino-N-methylphthalimide (3 & 6) in vaseline oil at +20° (1,2 & 3), +155° (4 & 5) and +180° (6).

the bands varies with their initial wavelengths in the given solvent. For example, in the case of 3-aminophthalimide in cyclohexanol at +30° (Fig.1) the fluorescence peak is located at 20,300 cm^{-1}; the absorption peak at 25,600 cm^{-1}. The band shifts with increase of temperature to +150° are 800 and 700 cm^{-1}, respectively. For the same compounds in vaseline oil (Fig.2), where the peaks at 30° are located at shorter wavelengths (ν_{fluo} = 23,400 cm^{-1} and ν_{abs} = 27,000 cm^{-1}), the band shifts incident to heating to +155° are negligible.

In Fig.2 we also give the absorption spectra of 4-amino-N-methylphthalimide in vaseline oil at different temperatures; it will be seen that in this case, too, the band shifts are insignificant.

In order to obtain the greatest displacement of the spectra the solutions were heated almost to the boiling point;* hence the spectra in the different solvents were obtained at different maximum temperatures. For purposes of comparing the spectrum shifts in different solvents, we divided the average value of the absorption and emission band shifts $\nu_{av} = (\Delta\nu_{flu} + \Delta\nu_{abs})/2$ (in some cases only $\Delta\nu_{flu}$) by the corresponding temperature interval. The shift coefficients $\Delta\nu_{av}/\Delta T$ obtained in this manner are plotted in Fig.3. The solvents are laid off in the horizontal frequency scale according to the frequencies of the fluorescence peak

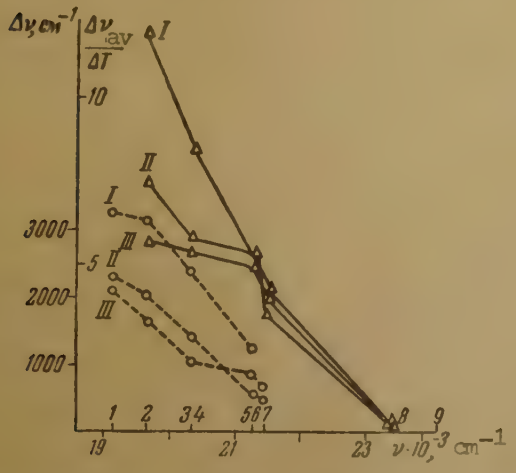

Fig.3. Variation of the temperature induced shift in the spectra of phthalimide derivatives ($\Delta\nu_{av}/\Delta T$ and $\Delta\nu$) with the position of the fluorescence spectrum in the given solvent at +20° relative to its position in the vapor spectrum. Substances: I) 4-amino-N-methylphthalimide and 4-aminophthalimide, II) 3-aminophthalimide and III) 3-monomethyl aminophthalimide. Solvents: 1) glycerol, 2) benzyl alcohol, 3) isobutyl alcohol, 4) cyclohexanol, 5) ethyl acetoacetate, 6) ethyl benzoate, 7) dimethylphthalate, 8) vaseline oil, 9) vapor. Solid lines - shift due to heating; dashed lines - shift due to cooling.

of 3-aminophthalimide in them. Thus, this solvent scale characterizes the decrease of the solvent-induced shift of the fluorescence spectrum of 3-aminophthalimide with respect to the fluorescence spectrum of the vapor. Actually, this sequence of the degree of influence of the solvent on the fluorescence spectrum at +20°

---

*We checked for the absence of decomposition by comparing the spectrum after cooling with the initial room temperature spectrum of the solution.

obtains for the other phthalimide derivatives as well. As will be evident from Fig.3, the variation of $\Delta\nu_{av}/\Delta T$ with the relative position of the spectra in the given solvent at +20° (solid lines) is characterized by decrease of the spectral band displacements as the fluorescence spectrum in the given solvent at +20° approaches the fluorescence spectrum of the vapor. An exception is the value of $\Delta\nu_{av}/\Delta T$ for glycerol, in which the coefficient is always smaller than in ethyl acetoacetate.

Thus increase of the temperature of the medium (solvent) can lead to an appreciable shift in the spectra of phthalimides if prior to heating (i.e., at room temperature) the spectrum of the phthalimide in the given solvent is appreciably displaced relative to the spectrum of the vapor; in other words, the degree of temperature displacement of the bands of a given substance depends on their position (relative to the vapor spectrum) at room temperature. The observed temperature effect is apparently due primarily to variation in the influence of the solvent on the phthalimide molecule.

It must be noted that the indicated regularities obtain only in a limited temperature range, i.e., in heating from room temperature to near the boiling point of the solvent.

The displacement of the spectral bands of phthalimides in the temperature range from +20° to -196° is entirely different. We were able to investigate the absorption spectra of the phthalimide derivatives only in solutions of ethyl alcohol, since the other solvents become opaque at low temperatures owing to cracking and fissuring of the frozen mass. The fluorescence and absorption spectra of 3-monomethylaminophthalimide in ethyl alcohol are shown in Fig.4. It will be seen that when the temperature is reduced from +20° to -196° the peak of the absorption band is shifted to the side of lower frequencies. At the same time the emission band is displaced to the side of higher frequencies.* Thus the absorption and emission band peaks move towards each other.** Similar shifts were observed for all the investigated phthalimide derivatives in ethyl alcohol; presumably the mutual approach of the absorption and emission bands would obtain in all the other solvents since in all cases the emission spectra shifted to the shorter wavelength side with reduction of temperature.

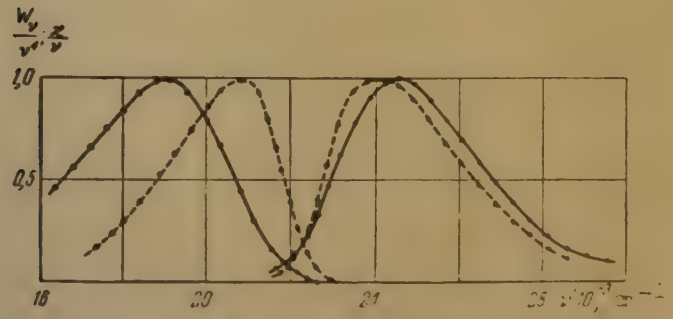

Fig.4. Fluorescence and absorption spectra of 3-monomethylaminophthalimide in ethyl alcohol at +20° (solid lines) and -196° (dashed lines).

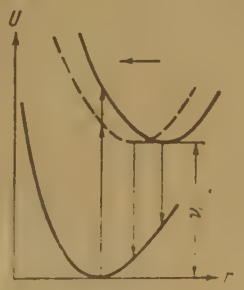

Fig.5.

---

*In this case also there is a correlation between the shift of the emission band and its position at 20°. This dependence for our solvents is shone in Fig. 3 by the dashed lines.

**A similar effect was observed for some acridines.[7]

We note in passing that in going from ~+200° to -196° the width of both the fluorescence and absorption bands decreases noticeably.

The observed regularities of the phthalimide spectrum displacements in the +20° to -196° temperature range can be characterized by means of the one-dimensional potential curve model. This model was used earlier[8] to explain the influence of the solvent on molecular spectra. Fig.5 shows the potential curves for the ground and excited states, shifted relative to each other due to the difference between the generalized equilibrium radii of the lower and upper electronic states (r_0 and r_0^*). The vertical transition from the minimum of the lower curve corresponds to the maximum of the absorption band and, analogously, the vertical transition from the minimum of the upper curve corresponds to the maximum of the emission band. The distance between the minima determines the frequency of the electronic transition.

The displacement of the absorption and emission bands towards each other with decreasing temperature corresponds to displacement of the upper potential curve relative to the lower curve horizontally to the left, i.e., to diminution of the difference between the equilibrium radii of the upper and lower electronic states. Obviously, the absorption maximum is shifted to the side of lower frequencies; the emission maximum, to the side of higher frequencies. In this case, if the shifts are equal, the electronic transition frequency should remain unchanged. As may be seen from Fig.4, however, the point of intersection of the absorption and emission bands (which gives the probable position of ν_e) is shifted noticeably in going from +20° to -196°. Since the spectra of Fig.4 are only for alcohol solutions further investigation of the absorption spectra at low temperatures in different solvents is indicated.

We desire to thank V.V.Zelinskii, A.N.Sevchenko and B.I.Stepanov for valuable suggestions.

Institute of Physics and Mathematics,
Academy of Sciences of the Belorussian SSR

References

1. B.I.Stepanov, Liuminestsentsiia slozhnykh molekul (Luminescence of complex molecules) Minsk, 1956.

2. L.G.Pikulik, Optika i spektroskopiia, 2, 676 (1957).

3. B.S.Neporent, N.A.Borisevich, V.P.Klochkov & O.A.Motovilov, Izv.AN SSSR, Ser.fiz., 18, 674 (1954). (Trans.Bulletin 18, No.6, 358.)

4. V.V.Zelinskii & V.P.Kolobkov, Program of the Sixth Conference on Luminescence (Molecular Luminescence and Luminescence Analysis).

5. V.P.Klochkov, Zhur.fiz.khim., 29, 1432 (1955).

6. L.P.Kazachenko & B.I.Stepanov, Optika i spektroskopiia, 2, 339 (1957).

7. V.L.Levshin & T.M.Tarasova, Izv.AN SSSR, Ser.fiz., 15, 573 (1951).

8. V.V.Zelinskii, V.P.Kolobkov & L.G.Pikulik, Optika i spektroskopiia, 2, 402 (1957).

LUMINESCENCE OF POWDERED MATERIALS

- Iu.I.Chekalinskaia

1. In connection with diverse research problems it is sometimes necessary to investigate the spectra and other optical attributes of powdered luminescent substances. The powdery, dispersed state of luminophors greatly complicates investigation of their optical properties inasmuch as in such cases there occurs multiple scattering of the exciting radiation and of the luminescence inside the powder. The optical properties of luminophor powders depend not only on the quantities characterizing the substance in the bulk (the coefficient of absorption, the quantum efficiency, the persistence of emission, etc.), but also on the size of the particles, the properties of the binding medium, the degree of packing and other factors. Hence in interpreting the experimental data one must take into account multiple scattering of light in the powder. Many authors neglect the effect of scattering as an insignificant factor but do not justify this either experimentally or theoretically. It is possible that in some cases scattering is combined with other effects, but even in such cases to clarify their mechanism, it is important to separate the effects associated with scattering.

The present report is devoted to the problem of allowing for the effect of scattering on the optical properties of powdered luminescent substances. For the purposes of determining the dependence of the intensity of luminescence on the parameters of the light-scattering layer one can make use of the model of a light-scattering layer[1,2] proposed by Antonov-Romanovskii, Girin & Stepanov and Bodo. According to this model, the light-scattering layer is regarded as a system of elementary laminae whose thickness corresponds to the mean dimensions of the particles and whose absorption coefficient is equal to the absorption coefficient of the bulk material.

Using this model and taking into account the invariance of the properties of the light-scattering layer as regards the addition of an elementary lamina,[1] one can deduce the following expressions for the intensity of luminescence of a plane powder layer:

$$I_N^{(1)} = I_0 \frac{\gamma\varphi(\nu')(b-1)(1-R_\infty)(b'+R'_\infty)}{2(b^{2N}-R_\infty^2)(b'^{2N}-R'^2_\infty)} \begin{vmatrix} \frac{b^N-b'^N}{b-b'}, & R_\infty b'^N + R'_\infty b^N \\ \frac{(bb')^N-1}{bb'-1}, & (bb')^N + R_\infty R'_\infty \end{vmatrix}, \qquad (1)$$

$$I_N^{(2)} = I_0 \frac{\gamma\varphi(\nu')(b-1)(1-R_\infty)(b'+R'_\infty)}{2(b^{2N}-R_\infty^2)(b'^{2N}-R'^2_\infty)} \begin{vmatrix} \frac{(bb')^N-1}{bb'-1}, & R_\infty b'^N + R'_\infty b^N \\ \frac{b^N-b'^N}{b-b'}, & (bb')^N + R_\infty R'_\infty \end{vmatrix}. \qquad (2)$$

Here I_0 is the flux of radiation incident on the "front" of layer, $I_N^{(1)}$ and $I_N^{(2)}$ are the luminescence fluxes emerging from the layer in the direction of the incident light (from the back) and in the opposite direction (from the front) respectively, N is the number of laminae, γ is the quantum yield, $\varphi(\nu')$ is a function characterizing the energy distribution over the luminescence spectrum, R_∞ and R'_∞ are the coefficients of reflection of the exciting radiation and of the luminescence from an infinitely thick layer and b and b' are parameters of the light scattering layer (here and below the primes denote quantities pertaining to the luminescence). According to Stokes[3], R_∞ and b are given by

$$R_\infty = \frac{1}{2R_1}(1 - T_1^2 + R_1^2 - \Delta), \text{ and } b = \frac{1}{2T_1}(1 + T_1^2 - R_1^2 + \Delta). \quad (3)$$

Here

$$\Delta = \sqrt{(1 + R_1 + T_1)(1 - R_1 + T_1)(1 + R_1 - T_1)(1 - R_1 - T_1)},$$

where

$$R_1 = r_0 + \frac{(1-r_0)^2 r_0 e^{-2kl}}{1 - r_0^2 e^{-2kl}} \text{ and } T_1 = \frac{(1-r_0)^2 e^{-kl}}{1 - r_0^2 e^{-2kl}}$$

are the coefficients of reflection and transmission of one lamina, l is the thickness of a lamina (equal to the mean dimensions of the particles), k is the coefficient of absorption of the dispersed material, r_0 is the coefficient of reflection at the binding medium-dispersed substance interface, i.e., at the particle boundaries.

Eqs.(1) and (2)* give the dependence of the luminescence flux on the parameters of the light-scattering layer: the absorption coefficients for the exciting radiation (k) and the luminescence (k'), the particle size, and the indices of refraction of the dispersed substance and the binding medium. Knowing these constants and the true luminescence spectrum, we can predict the luminescence spectrum of the powdered luminophor and the way it will change when the parameters are varied. We can also solve the inverse problem, namely, find the true spectrum and the luminescence yield of the material from the measured spectrum and the technical yield of the powder.

If the luminescence is not absorbed, Eqs.(1) and (2) become

$$I_N^{(1)} = I_0 \frac{\gamma\varphi(\nu')(1 - R_\infty)}{2[1 + (N-1)r'](1 - R_\infty^2 b^{-2N})} \left\{(1 - b^{-N})(1 - R_\infty b^{-N}) + \right.$$

$$\left. + 2r'\left[\frac{(1 - b^{-N})(b^{-1} + R_\infty b^{-N}) - Nb^{-N}(1 - b^{-1})(1 + R_\infty)}{(1 - b^{-1})}\right]\right\}, \quad (4)$$

$$I_N^{(2)} = I_0 \frac{\gamma\varphi(\nu')(1 - R_\infty)(1 - b^{-N})}{1 + R_\infty b^{-N}} - I_N^{(1)}, \quad (5)$$

where $r' = \frac{2r_0'}{1 + r_0}$. In working with Eqs.(1), (2), (4) & (5) one must employ numerical calculations. Eqs.(1) and (2) differ mainly as regards the positions of the elements in the first column, which greatly facilitates tabulation.

Below we shall consider the dependence of the luminescence flux on only some of the parameters of light-scattering layers.[1]

2. The variation of the luminescence fluxes as a function of the number of elementary laminae for two values of the coefficient of reflection at the particle boundaries is shown in Fig.1. It will be seen that the luminescence flux emerging from the front (i.e., towards the source of incident light) with increasing number N of laminae always increases, tending to a limiting value, while the flux emerging from the back of the layer first increases, goes through a maximum and then falls off. For media with a small value of the reflection coefficient ($r_0 = 0.01$) the number of elementary lamina at which the maximum flux is attained is larger than for media with a large value of r_0. The luminescence maximum is shifted to the side of smaller values of N with increase of $k'l$. If the radiation is wholly absorbed in the front elementary lamina, there is obviously no maximum.

---

*These expressions can be used for evaluating the luminescence flux of a stack of plates.

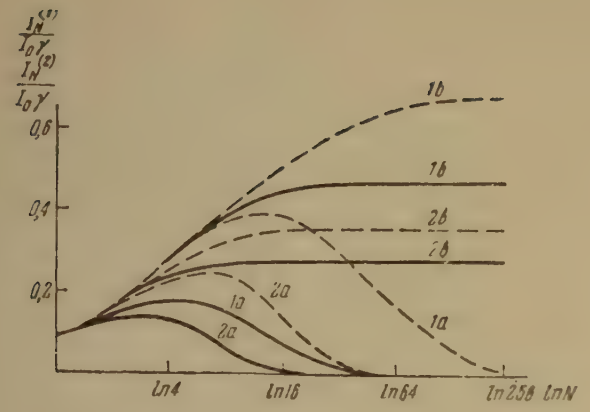

Fig.1. Variation of the luminescence fluxes as a function of the number of elementary lamina with $kl = 0.2$; $r_0 = r_0' = 0.2$ (solid lines) and $r_0 = r_0' = 0.01$ (dash lines): a - $I_N^{(1)}$, b - $I_N^{(2)}$; 1 - $k'l = 0.005$; 2 - $k'l = 0.1$.

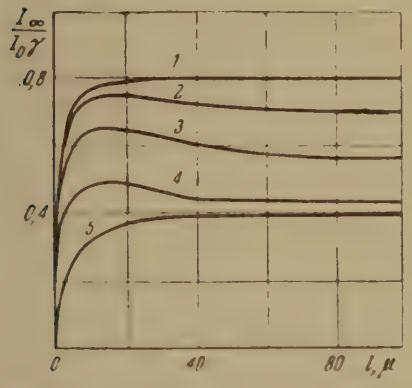

Fig.2. Variation of the luminescence flux for an infinitely thick layer as a function of the particle size with $r_0 = r_0' = 0.2$; 1 - $k' = 0$, 2 - $k' = 0.001k$, 3 - $k' = 0.01k$, 4 - $k' = 0.1k$, 5 - $k' = k$; $k = 1000$ cm^{-1}.

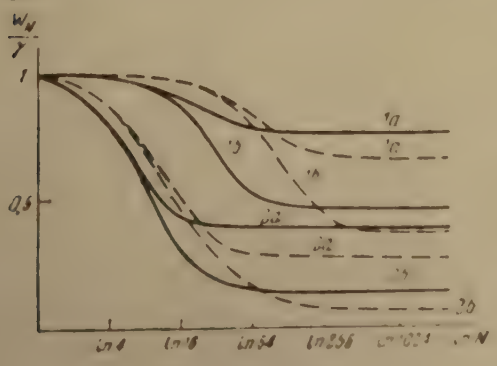

Fig.3. Variation of the technical yield as a function of the number of elementary laminae with $r_0 = 0.2$ (solid lines) and $r_0 = 0.01$ (dash lines): a - $kl = 0.1$, b - $kl = 0.005$; 1 - $k'l = 0.005$, 2 - $k'l = 0.1$.

It also follows from Fig.1 that the luminescence flux emerging from the layer towards the source of radiation (from the front) is always greater than the flux emerging from the back.

3. Fig.2 shows the variation of the luminescence flux from an infinitely thick layer as a function of the particle size for $k = 1000$ cm^{-1} and different values of k'. In the presence of reabsorption ($k' \neq 0$) and $k > k'$, with increasing particle size the flux at first increases, goes through a maximum and then slowly decreases. Consequently, fragmentation of the phosphor (reduction of particle size) in some cases may lead not to diminution of the brightness, as usually observed experimentally[4,12], but to increase of the brightness due to enhanced scattering. In the absence of reabsorption, increase of the particle size is always accompanied by increase of the brightness of an infinitely thick layer.

Although scattering undoubtedly plays a certain role in the variation of brightness with reduction of particle size, the changes observed in a number of cases cannot be explained entirely by scattering. Thus for example the strong decrease in brightness incident to fragmentation of the phosphor NaCl:TlCl cannot be due exclusively to scattering; other factors must be invoked to explain the observed[4] attenuation.

The dependences described above are in agreement with the experimental and theoretical data of Ivanov.[6]

Having elucidated the influence of different parameters on the effective luminescence yield of powdered materials, we can determine the conditions for their most efficient utilization.[6]

4. The technical yield (efficiency) of a layer of finite thickness is given by

$$W_N = \frac{I_N^{(1)} + I_N^{(2)}}{I_0(1 - R_N - T_N)},$$

where R_N and T_N are the coefficients of reflection and transmission of the layer for the exciting radiation. The variation of W_N as a function of the number of elementary laminae is shown in Fig.3; from this figure it follows that

1) with increasing layer thickness the technical yield decreases, tending to a limit, i.e., to the value of the technical yield of an infinitely thick layer;

2) the technical yield of weakly scattering layers ($r_0 = 0.01$) of finite thickness is greater than the technical yield of strongly scattering ($r_0 = 0.2$) layers (for infinitely thick layers the opposite obtains);

3) for weakly scattering media, the technical yield of layers of finite thickness is strongly dependent on $k'l$ and with a small number of laminae is almost independent of kl; in strongly scattering media the kl dependence is stronger, particularly in the range of large $k'l$.

These results show that scattering may have an appreciable influence on the optical properties of powdered phosphors and that, consequently, it must be taken into account in practical applications. Through appropriate variation or selection of the binding medium and the particle size, one can attain the most efficient utilization of a given phosphor.

5. Luminescent layers are generally applied to a backing or base which affects the character of the luminescence. The coefficients of reflection of the base for the exciting radiation and the luminescence are generally not equal. Taking into account multiple reflection of the exciting radiation and the luminescence from the backing, we obtain

$$I_N = I_N^{(2)} + I_N^{(1)} \frac{T_N R}{1 - R_N R} + \frac{[I_N^{(2)} T_N R + I_N^{(1)}(1 - R_N R)] T_N' R'}{(1 - R_N R)(1 - R_N' R')}. \qquad (6)$$

where R and R' are the coefficients of reflection from the backing of the exciting radiation and the luminescence, respectively.

As a rule backings with equally good reflection in a wide spectral range are not available. Analysis of Eq.(6) shows that in most cases (and in the absence of reabsorption always), it is more advantageous to use a backing with high reflection for the luminescence.

In conclusion, I wish to express my gratitude to B.I.Stepanov for guidance in the work and valuable advice.

Institute of Physics and Mathematics,
Academy of Sciences of the Belorussian SSR

References

1. B.I.Stepanov & Iu.I.Chekalinskaia, Trudy (Proceedings), Inst. of Physics & Math., Belorussian Acad.of Sci., No.2, 19 (1957); Iu.I.Chekalinskaia, Trudy (Proceedings), Inst. of Physics & Math., Belorussian Acad.of Sci., No.2, 38 (1957).

2. Z.Bodo & I.Hangos, Acta Phys.Acad.scient.Hung., 5, 295 (1955).

3. G.Stokes, Math. and Phys. Papers., 4, 145 (1904).

4. F.D.Klement & R.K.Gindina, Trudy (Proceedings), Institute of Physics and Astronomy, Estonian SSR Acad. of Sci., No.4, 3 (1956).

5. V.L.Levshin & I.V.Veits, Zhur.eksp.i teor.fiz., 20, 411 (1950).

6. A.P.Ivanov, Optika i spektroskopiia (Optics and Spectroscopy), 4, 225 & 236 (1958).

RESONANCE LUMINESCENCE OF MATTER IN FINITE VOLUMES

- A.M. Samson

Secondary absorption and emission processes occurring in the bulk of the investigated substance generally affect the intensity, efficiency, line shape, rate of decay and other spectroscopic characteristics of the emerging radiation. This influence of secondary processes obviously hampers interpretation of the experimental data.

Under laboratory conditions, the influence of secondary processes can be minimized by investigating the substance in small volumes or at low concentrations. This, however, involves diminution of the total luminescence, which is not always acceptable. In some cases (propagation of radiation through the atmosphere, emission of stars[1,2], etc.), this method of eliminating the influence of secondary processes is impossible.

There have been many studies devoted to investigation of the propagation of radiation in finite volumes. Astrophysicists[1,2] have achieved notable successes in this field, but on the whole, many aspects of this effect have not been adequately studied.

In the present work we derived a general integro-differential equation for volumes of any shape, which makes it possible to allow for the influence of forced emission, the thermal background and nonoptical excitation. Solution of the general equation for particular cases allows of evaluating the influence of secondary absorption and emission processes on the spectroscopic characteristics of resonance luminescence.

If the number of excited and unexcited particles (emissive power and absorption) at each point is known, one can determine all the spectroscopic characteristics of the radiation. The nonlinear integro-differential equation for the number of excited particles at every point can be derived from the usual relation for systems of particles with two energy levels[3]:

$$\frac{dn_2}{dt} = -n_2 [A + 2B(u_1 + u_2 + u_3) + d_{21} + d_{12}] + n[B(u_1 + u_2 + u_3) + d_{12}]. \qquad (1)$$

Here n_2 is the density of the excited particles, n is the total particle density, t is the time, A and B are the Einstein probability coefficients and d_{21} and d_{12} are the nonoptical transition probabilities. Finally, u_1, u_2 and u_3 denote the radiation densities associated with the thermal background, the external source and the luminescence of the investigated substance in a given finite volume, respectively; they all depend on the coordinates (see Ref.4).

If the nonoptical and thermal excitations are small compared with the excitation from the external source and one can neglect forced emission, the particular solution of the general equation is

$$y(\rho_0, \vartheta) = \gamma \int_{-\infty}^{\vartheta} e^{-(\vartheta - \vartheta')} w(\vartheta')\, d\vartheta' \sum_{i=0}^{\infty} \frac{\gamma^i (\vartheta - \vartheta')^i}{i!} \Phi_i(\rho_0). \qquad (2)$$

Here

$$y = \frac{n_2}{n}; \quad \gamma = \frac{A}{A + d_{21}}; \quad \vartheta = (A + d_{21})\, t; \qquad (3)$$

ρ represents the product of the radius vector of the point in the volume (specimen) by the absorption coefficient $\varkappa_0$, γ is the quantum efficiency of the elementary volume and $w(\vartheta)$ is proportional to the emissive power of the light source. The Φ_i are defined by

$$\Phi_0(\rho_0) = \Phi(\rho_0); \quad \Phi_i(\rho_0) = \frac{1}{4\pi} \int_V \Phi_{i-1}(\rho) \frac{e^{-|\rho - \rho_0|}}{|\rho - \rho_0|^2}\, dV'. \qquad (4)$$

$\Phi(\zeta)$ equals the ratio of the radiation density from the external source attenuated by the absorption in the volume to the density of the nonattenuated radiation.

Eq.(2) gives the number of excited particles at point ρ_0 at the instant θ. Different particular cases (growth, decay or steady state) are characterized by the appropriate form of $w(\theta)$. Specifically, for steady state conditions ($w(\theta) = w_0$) it follows from (2) that

$$y(\rho_0) = \gamma w_0 [\Phi_0 + \gamma\Phi_1 + \gamma^2\Phi_2 + \gamma^3\Phi_3 + \ldots] = \gamma w_0 \sum_{i=0}^{\infty} \gamma^i \Phi_i. \qquad (5)$$

Each term in the series (5) has definite physical meaning, namely, the first term Φ_0 is proportional to the density of the radiation arriving from outside at the given point ρ_0; the second term $\gamma\Phi_1$ to the density of primary luminescence, i.e., the radiation due to emission of the particles excited by the external radiation; the third term $\gamma^2\Phi_2$ to the density of secondary luminescence, i.e., the radiation due to excitation of the particles by the primary luminescence, and so on.

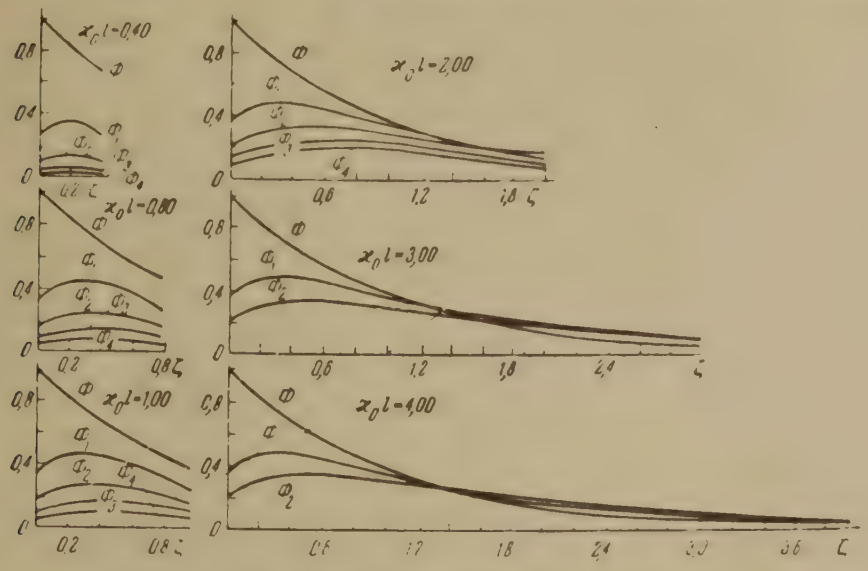

Fig.1. Variation of radiation densities with the optical depth.

The curves of Fig.1 show the variation of different orders of Φ with the optical depth for a plane-parallel layer irradiated by a light beam normal to it.[4] The curves have been plotted on the basis of numerical integration for several optical layer thicknesses: $\varkappa_0 l$ = 0.40, 0.80, 1.00, 2.00, 3.00 and 4.00 (l is the geometric thickness of the layer). It will be seen that all the curves (naturally except that for Φ_0) have a maximum within the front half of the layer. With increasing optical thickness, the height and position of the maximum tends to the limiting value corresponding to $\varkappa_0 l = \infty$. It will also be evident that for small optical thicknesses ($\varkappa_0 l$ = 0.40, 0.80 and 1.00) the primary luminescence density at each point is lower than the density of the radiation from the external source, the density of the secondary luminescence is lower than the density of the primary luminescence, the density of the tertiary luminescence is lower than that of the secondary, etc. For large optical thicknesses and at sufficiently high values of γ, the density of the preceding order of radiation may be lower than the density of the succeeding order.

If the variation of the Φ_i as a function of the optical depth is known, one can, by means of (5), find the total luminescence density $\left(\sum_{i=1}^{\infty} \gamma^i \Phi_i\right)$ and the number of excited particles $\left(\sum_{i=0}^{\infty} \gamma^i \Phi_i\right)$ for any value of the quantum efficiency γ. The cal-

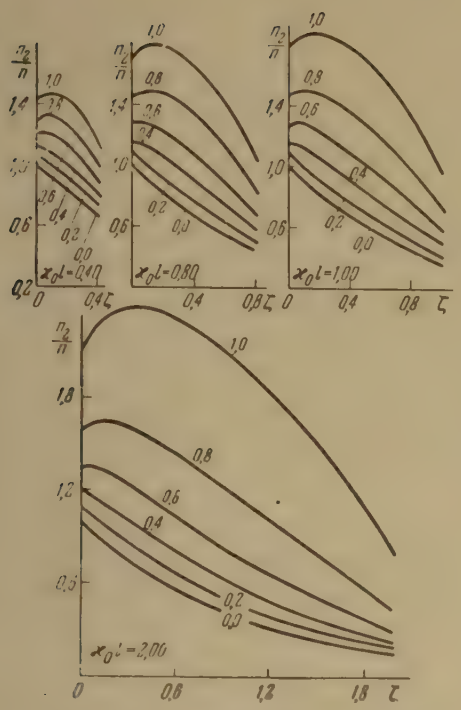

Fig.2. Distribution of excited particles over the depth. Figures at the curves are values of γ.

culated distributions (in relative units) of excited particles over the depth for different and γ are shown in Fig.2. It will be seen that for large γ the curves have a maximum close to the front surface and that the height of this maximum increases with increasing layer thickness. Even with $\gamma = 0.2$ the distribution of excited particles differs appreciably from the distribution in the absence of secondary processes (the last is characterized by the 0.0 curve). The excess of excited particles over the number corresponding solely to direct excitation by the external source even for $x_0 l = 0.40$ and $\gamma = 0.2$ is only 10%. However, with increasing layer thickness this difference increases rapidly. For appreciable layer thicknesses (large $x_0 l$) the density of the external radiation (and, consequently, the number of particles excited by this radiation) at points near the back wall amounts to only a small fraction of the total density even at medium values of γ.

According to Eq.(2) the distribution of excited particles and, consequently, the intensity of the emitted radiation varies in a complex manner with time. Analysis of Eq.(2) shows, for example, that the decay law depends not only on the amount of matter in the finite volume and the quantum efficiency but also on the conditions of excitation and observation. In the case of a plane-parallel layer the persistence of luminescence will differ for observation "from the front" and "from the back". The apparent duration of luminescence will also depend on the angle of incidence of the exciting radiation and on the angle of observation.

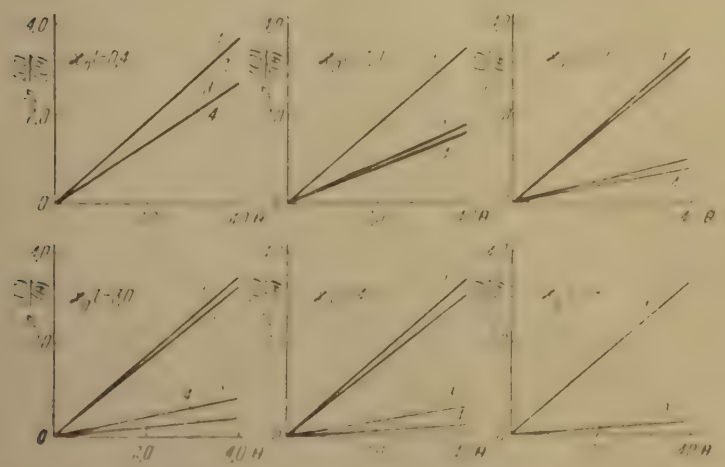

Fig.3. Luminescence decay curves: 1) $\gamma = 0.20$, observation "from the front", 2) $\gamma = 0.20$, observation "from the back", 3) $\gamma = 1.00$, observation "from the front", 4) $\gamma = 1.00$, observation "from the back".

Fig.3 shows a number of decay curves calculated on the basis of Eq.(2), using the approximate formulas derived earlier[5] for the case of irradiation and observation normal to the layer surface. It will be seen that in all cases the decay is appreciably slower than given by the usual exponential law (the slope of the curves is smaller than unity). The thicker the layer, the slower the luminescence decay. The persistence of luminescence also increases with increasing quantum efficiency.

At small layer thicknesses ($x_0 l = 0.40$) the decay is the same for observation "from the front" and "from the back" (at least for relatively short periods after cessation of excitation). In the case of large thicknesses there is a larger difference, which increases with increasing thickness. The duration of luminescence

for observation "from the back" is always greater than for observation "from in front". The increase in the duration of luminescence of finite volumes as compared with the duration of infinitesimal, elementary volumes may be appreciable (as much as several orders of magnitude for large volumes). Thus, for example, the duration of luminescence with observation "from the back" for $\varkappa_0 l = 4.00$ and $\gamma = 1.00$ increases by a factor of 20 as compared with the duration of an infinitely small volume.

One cannot judge of the actual deviation from exponential decay from Fig.3. Analysis of Eq.(2) shows that in general decay is not strictly exponential and that the deviation from the exponential law is greater for longer times.

In conclusion I wish to express my deep gratitude to B.I.Stepanov for suggesting the subject and for his interest in the work.

Institute of Physics and Mathematics,
Academy of Sciences of the Belorussian SSR

References

1. V.V.Sobolev, Perenos luchistoi energii v atmosferakh zvezd i planet. (Transfer of radiant energy in the atmospheres of stars and planets), M, 1956.

2. S.Chandrasekhar, Radiative Transfer, Oxford, 1950. (Cited in Russian trans.)

3. B.I.Stepanov, Liumenstsentsiia slozhnykh molekul (Luminescence of complex molecules), Minsk, 1956.

4. A.M.Samson, Optika i spektroskopiia, 5, 500 (1958).

5. A.M.Samson, Inzhenerno-fizicheskii zhur. (Engineering-Physics Journal), 1, 65 (1958).

DEPENDENCE OF THE POLARIZATION OF PHOSPHORESCENCE OF ORGANIC MATERIALS ON THE VISCOSITY OF THE SOLUTION

- B.Ia.Sveshnikov and P.I.Kudriashov

Many years ago Vavilov & Levshin[1] in an early investigation concerned with the properties of polarized luminescence established that with rare exceptions the degree of polarization of the emission of a solution depends on its viscosity and is virtually independent of the nature of the solvent per se. Thereby Vavilov & Levshin showed that the depolarization of fluorescence in solutions is due to Brownian rotational motion. A quantitative interpretation of the effect was first given by Levshin.[2] More rigorous calculations were subsequently carried out by Perrin.[3] According to his formula, the reciprocal of the polarization of the fluorescence is a linear function of the fluidity and depends on three molecular constants, namely, the lifetime of the excited state of the molecule, the molecular volume and the so-called limit polarization of the fluorescence. This last quantity is equivalent to the polarization of fluorescence for an infinitely great viscosity. For most fluorescent substances in which the lifetime of the excited state is $2\text{-}5\cdot10^{-9}$ sec and the molecular volume $0.5\text{-}5\cdot10^{-21}$ cm^3, the limit polarization is virtually attained at a viscosity of 1-2 poise.

The viscosity dependence of the polarization predicted by Perrin's formula was checked by Sevchenko[4] on a number of fluorescent solutions. It is particularly important to note the satisfactory agreement of the experimental and theoretical values of the polarization in the viscosity range from hundredths through some tenths of a poise, where, with the above-mentioned values of the excited state lifetime and molecular volume, the viscosity dependence of the degree of polarization is very appreciable. Vavilov[5] considered this to be one of the more weighty proofs of the equality of the molecular and molar viscosities of liquid solutions. Inasmuch as the matter of concordance of these viscosities has often been questioned, we felt it would be of interest to repeat the polarization experiments for liquid solutions with greater precision and to extend these studies to solutions with viscosities in the range of hundreds and thousands of poise. Obviously, for this it was necessary to use fluorescent substances with excited lifetimes of the order of 10^{-6} sec.

We felt it would be of even greater interest to elucidate the influence of viscosity on the polarization of the phosphorescence of organic compounds which, as is known, in some cases have emission times of the order of a second and for the most part are solid solutions, the viscosity of which exceeds billions of poise.

For our investigation we chose sugar candy activated by acridine orange. It is known from the work of Levshin[2], Vavilov, Pringsheim & Carelli[6] and a number of other investigators that the phosphorescence and fluorescence (long and short persistence emissions) of these phosphors are identical not only as regards their spectrum but also as regards polarization.

We investigated the polarization of the persistent luminescence of our sugar samples by means of three different set-ups. The common components of all were a mercury tube, a heat filter, a light filter transmitting the Hg 436 mμ line, a collimator lens providing a parallel light beam, a thermostat for the specimen, a photomultiplier-amplifier combination and two 20 x 20 mm Glan prisms one of which - the analyzer - could be rapidly switched from one set position to another. The auxiliary components of the first set-up were a high-speed Becquerel phosphoroscope and an electronic oscillograph. In the second set-up the phosphoroscope was replaced by a special shutter by means of which the phosphor could be illuminated for a precise interval (0.015 or 0.5 sec*), while a loop oscillograph was used as

---

*The window of the photomultiplier was opened 0.02 sec after illumination of the phosphor.

the measuring instrument proper. The third set-up differed from the second in that the excitation time in it was not rigorously controlled but was always greater than 2 sec.

The principal experiments were carried out on the second and third set-ups; specifically, we obtained the phosphorescence decay curves for the two positions of the analyzer. Comparison of the phosphorescence intensities corresponding to the two analyzer positions allowed us to determine the initial values of the polarization and its variation in the process of decay. The first set-up was used to check the initial phosphorescence polarization values obtained on the third set-up and for comparing the polarization of the phosphorescence with the polarization of the integral luminescence.

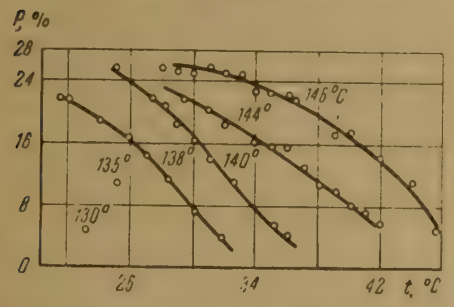

Fig.1. Variation of the degree of polarization of the phosphorescence of sugar specimens activated with acridine orange during heating (the temperatures at the curves are the temperatures of the syrup at the time of pouring the specimen).

The very first experiments showed that with prolonged excitation the initial values of polarization of phosphorescence fall off as the specimen is heated.*

The temperature region in which sharpest decrease of polarization occurs is shifted somewhat, depending on the temperature of the sugar syrup at the time of pouring (Fig.1). If the pouring temperature is reduced to 135-130°, which is 10--15° lower than the temperature recommended by most authors for preparing sugar phosphors, there is obtained an elastic candy exhibiting a low degree of initial polarization of the phosphorescence (Fig.1). In contrast, the degree of polarization of fluorescence of all the other specimens proved to be nearly the same (27%) within 2-3%** and virtually did not change upon heating of the specimen from 20 to 40°.

We believe these results are convincing proof that the degree of polarization of the persistent luminescence depends on the viscosity or structure of the medium. With a view to elucidating the mechanism of the effect, we attempted to determine the variation in degree of polarization in the process of the decay of phosphorescence.

In Fig.2 we give the decay curves obtained for the two positions of the analyzer and with prolonged excitation (> 2 sec). It will be seen from the figure that when the initial degree of polarization of the phosphorescence equals the degree of polarization of the fluorescence (27%), there is no decrease in polarization in the process of decay (Fig.2,a), but the polarization does decrease appreciably when there is a noticeable falling off of the polarization of the luminescence by the instant of opening of the photomultiplier window (Fig.2,b & c).

If we bear in mind that the investigated persistent luminescence of acridine orange in sugar in the 20-40° temperature range occurs essentially from the fluorescence levels and that the polarization of the fluorescence in the given temperature range does not change, it is difficult to explain the experimental results without assuming that the molecules undergo rotation while in the metastable state. We do not know how this rotation occurs, but tentatively assume that it represents

---

*It should be noted that in our experiments we avoided intense illumination of the specimen. It is known that in case of prolonged illumination with intense polarized light and a high phosphorescence yield the polarization of phosphorescence falls off sharply (light saturation effect). In our experiments this effect was absent.

**This depended on the quality of the surface and degree of homogeneity of the specimen.

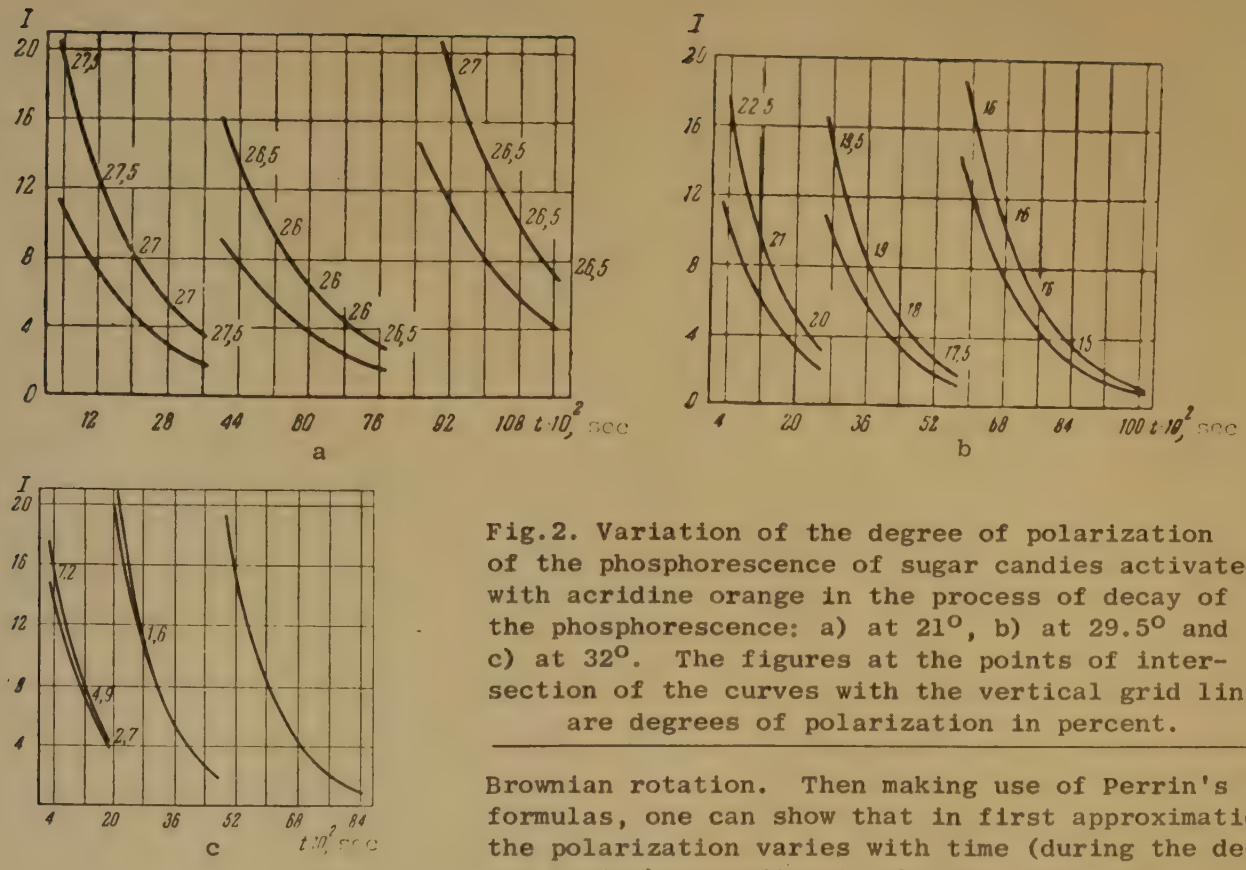

Fig.2. Variation of the degree of polarization of the phosphorescence of sugar candies activated with acridine orange in the process of decay of the phosphorescence: a) at 21°, b) at 29.5° and c) at 32°. The figures at the points of intersection of the curves with the vertical grid lines are degrees of polarization in percent.

Brownian rotation. Then making use of Perrin's formulas, one can show that in first approximation the polarization varies with time (during the decay period) according to the following law:

$$\frac{P_{t_1}}{P_{t_2}} = e^{-\varphi(t_1-t_2)}, \qquad (1)$$

where P_{t_1} and P_{t_2} are the degrees of polarization at the instants t_1 and t_2 and φ is a constant.

Having determined φ from the experimental data, we can introduce the appropriate correction for the decrease of polarization during the period of operation of the shutter. In our case this correction does not exceed 20-25% even for the most highly heated phosphor.

Having the value of φ, we can readily check the validity of the Brownian rotational motion hypothesis. We can excite the phosphor so rapidly that $e^{-\varphi t}$ will differ little from unity during the excitation interval. Then introducing the appropriate correction for the operation of the shutter, we should for any temperature obtain at the moment of cessation of excitation an initial value of polarization equal to the above mentioned value of 27%.

Yet our measurements for a specimen heated to 32.5° (excitation time 0.015 sec) after all corrections yielded a value of 13-14% for the initial polarization of the phosphorescence instead of the expected 27%. Thus the phosphorescence polarization of the sugar phosphor at 32.5° falls off by a factor of 2 in an interval from 10^{-8} to 10^{-2} sec, whereas each further factor of two change in the polarization requires almost 10^{-1} sec. It follows therefore that the hypothesis that the depolarization of phosphorescence is due to Brownian rotational motion must be rejected at least as far as the initial stages of phosphorescence are concerned.

In conclusion, it may be of interest to compare the values of the macroscopic viscosity of the sugar candy with the values of the molecular viscosity deduced on

the assumption that the depolarization of phosphorescence observed after 10^{-2} sec is due to Brownian rotational motion. In this case

$$\varphi = \frac{kT}{v\eta},$$

where v is the molecular volume and η is the molecular viscosity. The value of v for sugar-candy is not known. However, if we take it to be $1 \cdot 10^{-21}$ cm^3, from the curves of Fig.2 we obtain $1.5 \cdot 10^{-6}$ poise for 32.5° and 10^7 poise for 29.5°. The macroscopic values of the viscosity at 32.5° and 29.5° are much higher, namely, 10^{11} and 10^{12} poise, respectively.*

"S.I.Vavilov" State Optical Institute

References

1. S.I.Vavilov & W.L.Levshin, Z.Phys., 35, 920 (1926); Ibid., 44, 539 (1927).
2. W.L.Lewschin, Z.Phys., 32, 307 (1925).
3. F.Perrin, Ann.phys, 12, 169 (1929).
4. A.N.Sevchenko, Trudy (Proceedings) State Optical Institute, 14, 65 (1941).
5. S.I.Vavilov, Izv.AN SSSR, OMEN, Ser.fiz., 3, 345 (1937).
6. P.Pringsheim, S.I.Vavilov, Z.Phys.37, 705 (1926); A.Carelli & P.Pringsheim, Z.Phys., 17, 287 (1923).

---

*For determining the viscosity of the sugar specimens we used the apparatus of V.T.Slavianskii (we take this occasion to thank him), in which the viscosity of solids is determined by comparing the rate of penetration of a loaded round rod into the investigated specimen with the rate of penetration of the same rod into a reference glass sample at a certain temperature. A calibration viscosity vs temperature curve for the glass was obtained beforehand on the basis of experiments involving stretching of glass filaments under load.

VARIATION OF THE DEGREE OF POLARIZATION WITH THE FLUORESCENCE WAVELENGTH

- G.P.Gurinovich & A.N.Sevchenko

Over three decades ago Levshin[1] was among the first to observe variations in the degree of polarization of luminescence with the wavelength of the exciting light. Levshin varied the exciting wavelength within the range of the long wavelength absorption band and noted a decrease in the degree of polarization with increase of the incident light frequency. Since then a similar decrease in the degree of polarization has been observed for almost all investigated luminescent dyes.[2]

This phenomenon can be explained by the influence of vibrations of the molecule in the excited electronic state.[3] Indeed, the asymmetry properties of the electronic state are fundamental to the theory of the polarization of luminescence of complex molecules; together with multipolarity these symmetry properties are basic classification criteria in molecular spectroscopy. In the case of diatomic molecules, the valence vibrations which occur along the molecular axis do not alter the symmetry state and hence cannot influence the luminescence polarization. The situation is different in the case of complex molecules wherein deformation vibrations can substantially distort the molecular configuration. In this case, even with the classical oscillator model, one cannot assume a single oscillator direction but must consider a group of directions inasmuch as the coupling of the oscillators with the molecular skeleton so to say loses its rigidity.

From the standpoint of quantum mechanics one can say that the characteristics of polarization of fluorescence depend on the transition matrix element components in certain specific directions which, in turn, are determined by the symmtery properties of the combining states. Clearly, these components may have different values if the transitions go to different vibrational sublevels of the upper electronic state, associated with the molecular deformations. Thus one can to some extent explain the fact that the limiting value of the degree of polarization of isotropic solutions does not attain the theoretical values (1/2 or -1/3) and the observed decrease in degree of polarization with increase of the exciting photon energy within the limits of the long wavelength absorption band.

An analogous argument leads to the deduction that the limiting value of the degree of polarization can also be reduced due to nonequal values of the matrix element components associated with transitions from the excited electronic state to different vibrational sublevels of the ground state. Accordingly, the degree of polarization of luminescence should obviously decrease in going towards the long wavelength edge of the luminescence band. Moreover, if the mirror symmetry rule[4] holds for the given substance, then as Stepanov[5] has shown

$$\psi_{vib}(E_{vib}) = \psi^*_{vib}(E^*_{vib}) \text{ with } E_{vib} = E^*_{vib},$$

i.e., the wave functions characterizing the vibrational sublevels of the lower and upper electronic states are equal for the same reserve of vibrational energy. This situation imposes certain requirements which must obviously be evinced in an equal influence of the vibrations of the molecule in both states (ground and excited) on the relative orientation of the transition dipole moment. In this case the polarization of fluorescence must also possess mirror symmetry relative to the frequency of the purely electronic transition. This is yet another consequence of the law of mirror symmetry. If there is no mirror symmetry, the polarization will simply decrease to both sides of the frequency of the pure electronic transition.

The influence of the molecular vibrations on the limiting degree of polarization can be quantitatively taken into account by means of Jablonski's theory[6]

according to which the maximum polarization P_0 is connected with $\varepsilon = \sin^2\gamma$ (γ is the angle through which the oscillator axis turns during the vibrations) by the relation

$$P_0 = \frac{9\varepsilon^2 - 12\varepsilon + 4}{3\varepsilon^2 - 4\varepsilon + 8}.$$

To check the above reasoning we carried out an experimental investigation of the variation in the degree of polarization with the wavelength of the exciting and emitted radiation. The experimental arrangement is diagramed in Fig.1. The light from the SVDSh-250 mercury tube S, after passing through the quartz monochromator M_1 and the polarizer N_1, excited the luminescence of the investigated solution in cell K. The luminescence, after passing through the analyzer N_2 and the glass monochromator M_2, was detected by the photomultiplier PM connected through the dc amplifier A to the galvanometer G. In order to minimize possible errors, in investigating the variation of the degree of polarization with the luminescence wavelength, the analyzer N_2, rather than the polarizer N_1, was rotated 90°; on the other hand, in determining the variation in polarization with the wavelength of the exciting light, the analyzer N_2 was rotated. An appropriate correction (constant for each experiment) was made for the partial polarization of the light by the monochromators.

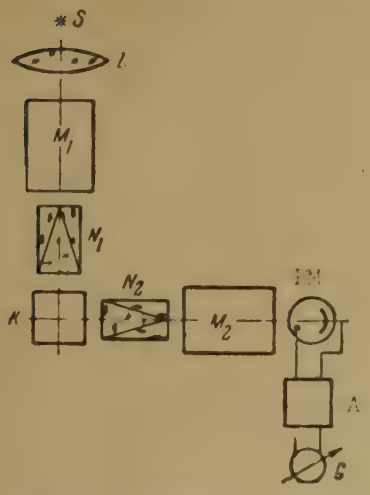

Fig.1. Diagram of experimental set-up.

The results obtained for 3-monomethylaminophthalimide, in which mirror symmetry obtains to a fairly high degree, are shown in Fig.2. The emission and luminescence spectra were obtained by L.G.Pikulik. It will be seen that the degree of polarization falls off noticeably to either side of the frequency of the electronic transition. It will be noted that the polarization curves are also characterized by a high degree of mirror symmetry. The left-hand arrow in Fig.2 indicates the luminescence frequency for which the polarization measurements at different frequencies of the exciting light were made, while the right-hand arrow indicates the frequency of the exciting light at which the variation in the degree of polarization over the luminescence spectrum was measured.

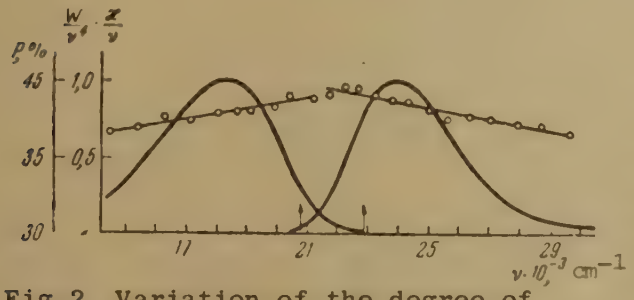

Fig.2. Variation of the degree of polarization with the excitation and luminescence wavelength for 3-monomethylaminophthalimide in glycerol.

Similar measurements were carried out for fluorescein and rhodamine B, extra. The results for these substances are listed in Tables 1 and 2.

It will be evident that the tabular data substantiates the argument set forth above. It may be noted that similar measurements were performed many years ago by Vavilov[7] who came to the conclusion that the polarization does not depend on the fluorescence wavelength within the limits of the experimental error. This disagreement with our results may be explained by the fact that the König-Martens spectrophotometer used by Vavilov did not afford the necessary accuracy; moreover Vavilov investigated only a very narrow spectrum interval.

As is known, the theoretical value of the maximum degree of polarization for isotropic solutions is 1/2. In view of the above, we felt it would be of interest to determine the actual limiting degree of polarization under different conditions

Table 1
Wavelength dependence of P for fluorescein in glycerol

on λ_{lum} (λ_{exc}=500 mμ)		от λ_{exc} (λ_{lum}=545 mμ)	
λ_{lum}, mμ	P, %	λ_{exc}, mμ	P, %
693	35,0	380	34,5
667,4	35,4	400	35,6
652	38,6	420	36,2
618	38,8	440	37,0
589	39,7	460	38,0
564	40,1	480	39,4
543	40,7	500	40,1
535	40,5	520	40,5

Table 2
Wavelength dependence of P for rhodamine B (extra) in glycerol

on λ_{lum} (λ_{exc}=546 mμ)		от λ_{exc} (λ_{lum}=580 mμ)	
λ_{lum}, mμ	P, %	λ_{exc}, mμ	P, %
660	34,6	470	36,0
650	36,2	480	36,8
640	39,0	490	37,3
630	39,4	500	37,9
610	39,7	510	38,1
600	41,2	520	38,9
590	41,0	530	39,1
580	41,2	540	41,1
570	41,4	550	41,9
560	42,1	560	43,0
		570	43,1

Table 3

η, poise	P, % (λ_{exc}=435 mμ, λ_{lum}=465 mμ)	P, % (λ_{exc}=365 mμ, λ_{lum}=716 mμ)
0,024	2,0	1,8
0,092	6,1	5,8
0,142	9,0	8,4
0,240	13,6	12,6
4,84	21,0	18,0
7,27	43,0	35,7
P, %	46,0	38,0*

*The maximum degree of polarization under the usual conditions (depolarization averaged over the entire fluorescence spectrum) reported by A.N. Sarzhevskii is 40%.

experimentally. The results obtained for 3--monomethylaminophthalimide are listed in Table 3. The viscosity in these experiments was varied by changing the water content of the water--glycerol solvent.

It will be seen that the maximum degree of polarization in the first case (λ_{exc} = 435 mμ, λ_{lum} = 465 mμ) increased appreciably with increase of η, but did not attain 50%, which indicates the presence of depolarizing factors. Apparently, if one could excite the luminescence at the frequency of the pure electronic transition and measure the degree of polarization of the fluorescence at the same frequency, one might obtain a higher value for the degree of polarization. In practice, however, such measurements are hindered by obvious experimental difficulties.

We also felt it would be of interest to investigate the variation of the degree of polarization with the luminescence wavelength for porphin type dyes (these compounds are related to the natural pigment, chlorophyll), inasmuch as these substances have complex luminescent spectra, consisting of two, three or more bands. In fact, investigations of this kind may help understand the structure of these dyes.

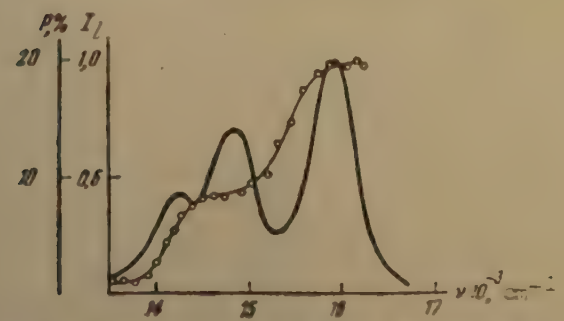

Fig.3. Variation of the degree of polarization with the luminescence wavelength for protoporphyrin IX.

Our experiments showed that the luminescence wavelength dependence of the degree of polarization differs from that characteristic of other dyes. As may be seen from Fig.3, which shows the results obtained for a solution of protoporphyrin IX in a cyclohexanol-glycerin mixture, each band is characterized by a different degree of polarization. The luminescence was excited by light from an SVDSh-250 mercury tube filtered through black glass. The greatest degree of polarization is observed in the short wavelength fluorescence band; the degree of polarization falls off by half in the second

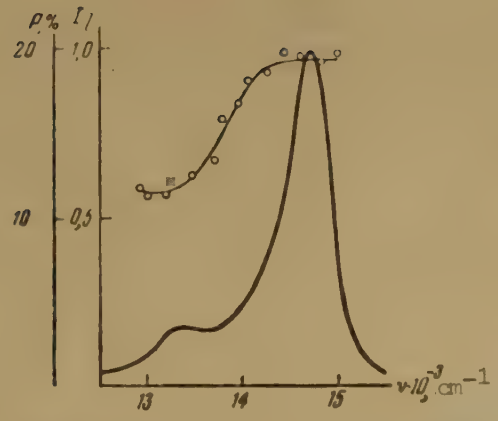

Fig.4. Variation of the degree of polarization with the luminescence wavelength for magnesium phthalocyanin.

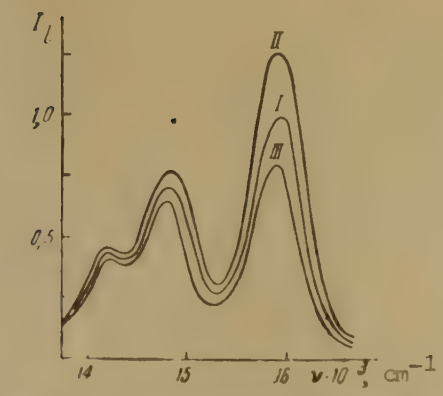

Fig.5. Luminescence spectra of protoporphyrin IX obtained under different conditions.

band and virtually to zero in the third.

The analogous results for magnesium phthalocyanin are shown in Fig.4 (λ_{exc} = 670 mμ). So strong a wavelength dependence cannot be explained by the influence of molecular vibrations and indicates that a number of electronic transitions contribute to the luminescence of compounds in this class. It must be noted that the polarization spectra given in the literature for compounds of this type were obtained for the integral luminescence spectrum and hence are of little value as characteristics of the spatial distribution of the absorption and emission oscillators. From this standpoint one must record polarization spectra for each fluorescence band separately. However, for chlorophyll, phthalocyanin, chlorophyllide and a number of similar compounds this is not important inasmuch as the intensity of the second band is much lower than that of the first and its influence on the polarization is therefore negligible. This does not apply of course to protoporphyrin and most dyes of this type.

Another interesting fact connected with the observed strong luminescence wavelength dependence of the degree of polarization is the dependence of the luminescence spectra of viscous solutions of porphin dyes recorded through a polarizer on the state of polarization and wavelength of the exciting light.

By way of illustration, three luminescence spectra of a solution of protoporphyrin IX in a mixture of cyclohexanol and glycerol are shown in Fig.5. Spectrum I was recorded with excitation by natural light and without an analyzer, i.e., under the "usual" experimental conditions. Owing to the low luminescence intensity, the spectrum was excited by nonmonochromatic light (light from a SVDSh-250 mercury tube filtered through black glass). This spectrum agrees within the limits of the experimental error with the spectrum with excitation from one side and observation from the other. Spectrum II was obtained with excitation by polarized light with vertical oscillations of the electric vector and the luminescence passing through an analyzer set to transmit the vertical oscillations, i.e., polarization in the same plane as the exciting light. Finally, spectrum III was recorded with excitation by horizontally polarized light with the same vertical position of the analyzer.

As will be evident from the figure, the three spectra virtually coincide at the long wavelength luminescence band, differ somewhat at the middle band and differ very appreciably at the short wavelength band. The ratio of intensities of the second and third spectra at the short wavelength band is about 1.5; at the middle band, 1.2 and at the long wavelength band 1.1. It is interesting to note that with excitation of the luminescence through a filter transmitting the Hg 404.6 mμ line the three spectra recorded under the same conditions are virtually identical.

The results of all the above measurements are in satisfactory agreement with determinations of degree of polarization over the fluorescence spectrum.

Analogous results were obtained for a solution of magnesium phthalocyanin in the same solvent. However, in view of the fact that the second band in the spectrum of this compound is very weak compared with the first one, the accuracy of measurement within this band was necessarily relatively low. Some difference between the luminescence band contours should obviously be observed under the given experimental conditions for all typical dyes in viscous solvents. These differences, however, are not great.

We desire to acknowledge our indebtedness to T.N.Godnev for making available the various dyes and reagents.

Institute of Physics and Mathematics
Academy of Sciences of the Belorussian SSR

References

1. V.L.Levshin, Zhurn.rus.fiz.-khim.obshch., Chast' fizicheskaia (Journal of the Russian Physical-Chemical Society, Physics Section), 56, 235 (1924).

2. P.P.Feofilov, Usp.fiz.nauk, 34, 417 (1948).

3. P.P.Feofilov, Dissertation, State Optical Institute, 1955.

4. V.L.Levshin, Zhur.fiz.khim., 2, 641 (1931); 6, 1 (1935); 6, 991 (1935); 9,1, (1937).

5. B.I.Stepanov, Liuminestsentsiia slozhnykh molekul (Luminescence of complex molecules), Minsk, 1955.

6. A.Jablonski, Acta phys.polonica, 10, 33 (1950).

7. S.I.Vavilov, Zhur.prikl.fiz., (Journal of applied physics), 2, 273 (1925); Collected Works, Vol.1, pp.157 & 182 (1954).

8. R.Stupp & H.Kuhn, Helv.Chim.Acta, 35, 2469 (1952).

9. I.C.Goedheer, Nature, 176, 928 (1955).

10. G.P.Gurinovich, I.N.Ermolenko, A.N.Sevchenko & K.N.Solov'ev, Optika i spektroskopiia, 3, p.237 (1957).

POLARIZATION OF THE LUMINESCENCE OF PHTHALIMIDES

- A.M. Sarzhevskii & A.N. Sevchenko

The luminescence of phthalimides in viscous solutions is polarized. With excitation by polarized light in the region of the long wavelength absorption band, the polarization of luminescence for all the investigated phthalimides exceeds 30%. The degree of polarization was determined visually by means of a Sawyer polariscope and by a photoelectric technique based on the use of an SF-4 spectrophotometer especially adopted for polarization measurements.[1]

All the polarization measurements were carried out in glycerol solutions and mixtures of glycerol with water and alcohol (methyl, ethyl and isobutyl). The concentration in all the experiments was $5 \cdot 10^{-6}$ g/cm^3.

There have been many investigations devoted to the influence of the temperature and nature of the solvent on the polarization of luminescence, but most of them are concerned with diverse different substances. We, on the other hand, concentrated on one type of substance, namely, phthalimide derivatives.

The relation between the luminescence polarization, the temperature and the viscosity is given by the familiar Levshin-Perrin formula:

$$\frac{1}{P} = \frac{1}{P_0} + \left(\frac{1}{P_0} - \frac{1}{3}\right)\frac{kT}{V\eta}\tau. \qquad (1)$$

This formula predicts a linear dependence of 1/P on T/η.

We investigated the degree of polarization of the luminescence of a number of phthalimides as a function of the temperature in the range from 20 to 100°. The variation of 1/P with T/η proved to be linear for all the investigated compounds (Fig.1). The degree of polarization of the luminescence falls off rapidly with increase in temperature. For example, for 3-monomethylaminophthalimide (curve 2) the degree of polarization falls off from 37 to 4.5% as the temperature is increased from 20 to 90°; for 3-aminophthalimide (curve 4) the decrease is even

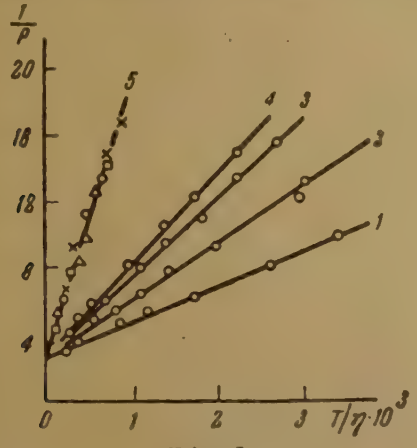

Fig.1

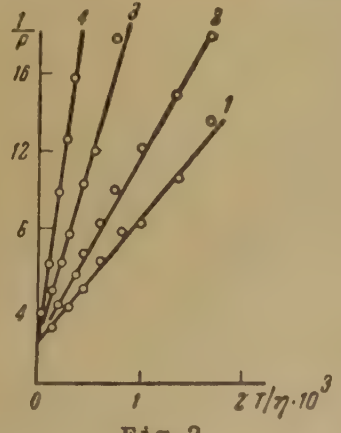

Fig.2

Fig.1. Temperature dependence of the polarization of luminescence of phthalimides: 1) 3-dimethylamino-6-aminophthalimide, 2) 3-monomethylaminophthalimide, 3) 4--formylamino-N-methylphthalimide and 4) 3-aminophthalimide.

Fig.2. Variation of the polarization of luminescence with the viscosity for 3-dimethylamino-6-aminophthalimide: 1) water glycerol solution, 2) methyl alcohol-glycerol solution, 3) ethyl alcohol-glycerol solution, 4) isobutyl alcohol-glycerol solution, and 5) for 4-formylamino-N-methylphthalimide.

more rapid: the polarization falls to 6% at 55°. Similar dependences were observed for all the investigated phthalimide derivatives.

In addition to the temperature dependences, we also investigated the influence of the nature of the solvent. The data for two phthalimide derivatives, namely, 3-dimethylamino-6-aminophthalimide and 4-formylamino-N-methylphthalimide, which represent typical extreme cases, are shown in Fig.2. In the case of 3-dimethylamino-6-aminophthalimide, in going from a water-glycerol solution to a mixture of isobutyl alcohol with glycerol the dependence of 1/P on T/η is noticeably altered. Whereas for the water-glycerol solution P = 14.3% at T/η = 2000, for the isobutyl-glycerol solution of the same viscosity P = 6.8%, i.e., the polarization of the solution in isobutyl alcohol with glycerol falls off twice as fast as in the water-glycerol solution. No such appreciable difference is observed in the case of 4-formylamino-N-methylphthalimide: the straight line plots for the water--glycerol and alcohol-glycerol mixtures virtually coincide. The dependence characteristic of 3-dimethylamino-6-aminophthalimide is also observed for 3-amino-N--methylphthalimide, 4-aminophthalimide, 3- monomethylaminophthalimide, 3,6-diamino--N-methylphthalimide, 3-acetylamino-N-methylphthalimide and 3,6-diacetylamino-N--methylphthalimide. On the other hand, the behavior of 3-aminophthalimide, 3--amino-N-phthalimide and 3-oxy-N-methylphthalimide is similar to that of 4-formylamino-N-methylphthalimide.

Thus the experimental data indicate that the Levshin-Perrin formula is valid for this case of substances and that there is a consistent correspondence between the molar and molecular viscosities. Years ago this formula was used for determining the lifetime of the excited state. The molecular volume entering into the formula was determined by a diffusion procedure. At present the lifetime τ can be measured with good accuracy by means of fluorometers. Hence this formula can now be utilized for determining the molecular volume including the surrounding solvate shell. Accordingly, we determined the molecular volumes of the different phthalimide derivatives in different solvents and mixtures thereof. The excited state lifetimes were measured on a Bonch-Bruevich phase fluorometer. The determined values together with the values of P_o are listed in Table 1.

As will be evident from the data given in Table 2, the molecular volumes of the phthalimides increase appreciably in solution as compared with the volume in the solid state. For example, the 3-dimethylamino-6-aminophthalimide molecule, which has a gram molecular volume of 70 cm^3 in the solid state, when dissolved in ethylene glycol attains a volume of 750 cm^3, in glycerol - 269 cm^3 and in isobutyl alcohol - 572 cm^3. The greatest volume is observed in the water-glycerol mixture, namely, 993 cm^3 or 15 times greater than in the solid state. Similar solvation effects are characteristic of the other phthalimide derivative molecules.

In order to check our results we also investigated fluorescein, rhodamine B and chlorophyll, the gram molecular weights of which were measured by Marinesco[2] by the diffusion procedure. Marinesco reports the following values: fluorescein in glycerol - 480 cm^3, rhodamine B in glycerol - 520 cm^3 and chlorophyll in castor oil - 2600 $Å^3$. Our measurements for the same substances in the same solvents yielded close values: fluorescein - 490 cm^3, rhodamine B - 580 cm^3 and chlorophyll - 2500 $Å^3$.

However, the results of measurements of the molecular volumes by the same procedure carried out by Gribkov & Zhevandrov[3] and Zhevandrov & Nikolaev[4] do not agree among themselves or with our results. Thus, for example, for 3-aminophthalimide in glycerol in the first case G & Z obtained $\tau = 6.3 \cdot 10^{-8}$ sec, P_o = 34% and V = 61 cm^3, while in the second case Z & N obtained $\tau = 11.5 \cdot 10^{-9}$ sec, P_o = 40% and V = 190 $Å^3$ (114 cm^3). It must be noted that in the later report[5] nothing is said concerning this descrepancy.

Table 1

Lifetime of the excited state ($\tau \cdot 10^{-9}$ sec) in different solvents and values of the maximum degree of polarization P_o

Substance	Solvents									P_o, %
	ethylene glycol	cyclo-hexanol	glycerol	iso-butyl alcohol	iso-amyl alcohol	water-glycerol	methyl-glycerol	ethyl-glycerol	iso-butyl-glycerol	
3-dimethylamino-6-aminophthalimide	9,7	10,6	9,4	7,4	10,1	10,6	10,4	9,7	9,2	39,2
3,6-diacetylamino-N-methylphthalimide	12,2	10,4	11,6	11,7	11,0	11,8	12,2	11,8	11,6	39,4
3,6-diamino-N-methylphthalimid	14,0	13,0	10,3	12,2	12,3	12,2	12,2	11,5	11,3	36,6
3-hydroxy-N-methylphthalimide	11,7	9,0	7,5	8,3	6,2	13,0	11,3	12,4	9,6	35,8
3-aminophthalimide	13,5	15,0	13,6	14,2	15,0	13,0	14,3	14,8	14,6	32,2
3-monomethylphthalimide	6,6	9,5	4,0	7,7	9,5	3,2	4,1	4,4	4,8	40,0
3-amino-N-methylphthalimid	14,2	15,7	14,0	15,5	14,8	13,8	15,6	15,6	15,5	35,8
3-acetylamino-N-methylphthalimide	3,9	4,6	4,0	3,3	4,6	4,5	4,0	4,0	3,8	39,4
4-aminophthalimide	8,2	12,6	4,6	10,3	12,7	3,6	4,9	5,1	5,9	39,0
4-formylamino-N-methylphthalimide	18,7	15,7	18,7	16,5	17,0	18,3	17,9	18,2	18,5	32,2
4-amino-N-methylphthalimid	8,9	12,3	4,3	9,8	12,1	2,6	4,5	4,7	5,6	40,0

Table 2

Molecular volumes of phthalimide derivatives in different solvents and mixtures thereof

Substance	Solvents									In solid state
	ethyl ne glycol	cyclo-hexanol	glycerol	iso-butyl alcohol	iso-amyl alcohol	water-glycerol	methyl-glycerol	ethyl-glycerol	iso-butyl-glycerol	
3-dimethylamino-6-aminophthalimide	756	161	269	414	572	993	653	438	346	70
3,6-diacetylamino-N-methylphthalimide	182	86	157	334	281	253	145	139	91	76
3,6-diamino-N-methylphthalimide	343	159	83	340	307	191	124	95	79	66
3-hydroxy-N-methylphthalimid	183	96	93	210	221	142	138	117	111	59
3-aminophthalimide	281	235	78	261	146	125	122	120	151	60
3-monomethylphthalimide	110	120	78	189	143	131	110	86	117	64
3-amino-N-methylphthalimide	204	216	83	—	236	138	142	133	136	64
3-acetylamino-N-methylphthalimide	126	123	170	—	146	143	90	83	81	69
4-aminophthalimide	331	316	109	977	511	290	201	198	247	60
4-formylamino-N-methylphthalimide	354	221	259	—	—	266	260	259	249	69
4-amino-N-methylphthalimide	281	330	121	920	356	211	206	132	163	64

According to our measurements, the data for 3-aminophthalimide are $\tau = 13.6 \cdot 10^{-9}$ sec, $P_0 = 32.2\%$ and $V = 78$ cm^3. We note that our data on the lifetimes for such thoroughly studied substances as fluorescein and rhodamine B agree with the results of measurements by different authors[5,6] using different procedures. Moreover, the results of our polarization measurements for 3-aminophthalimide and other substances are not in conflict with the data of Feofilov.[7]

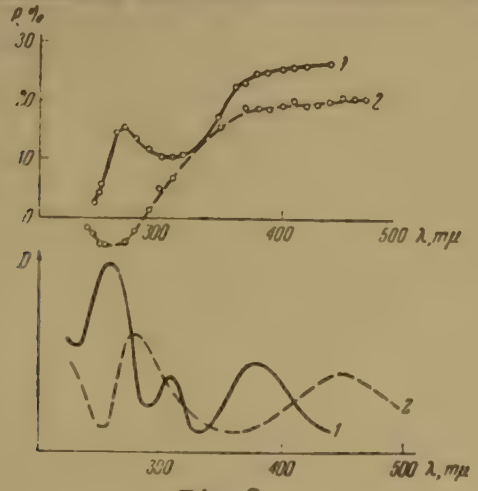

Fig.3

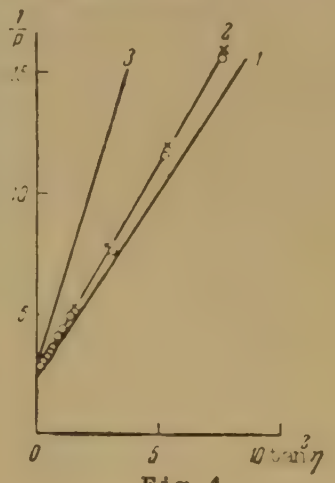

Fig.4

Fig.3. Polarization and absorption spectra of 4-amino-N-methylphthalimide (1) and 3-dimethylamino-6-aminophthalimide (2) in glycerol.

Fig.4. Nature of the elementary emitter of 4-amino-N-methylphthalimide.

In the light of our data the deduction of Zhevandrov & Nikolaev[4] regarding the nonequivalence of the micro- and macroviscosities of phthalimides in glycerol solutions appears questionable. If one assumes, as would follow from the data of Z & N, that the microviscosity is lower than the macroviscosity, it becomes difficult to understand the high value for the limiting polarization obtained by these authors.

In addition to the above described measurements, we investigated the polarization spectra of eleven phthalimide derivatives (the polarization spectra of 3-aminophthalimide, 3-monoethylaminophthalimide and 4-aminophthalimide had been studied earlier by Feofilov[7]). By way of illustration, the spectra of two of these are reproduced in Fig.3. It will be seen that the values of polarization corresponding to each absorption band are different. Consequently, the absorption and polarization spectra can serve as reliable indicators of the chemical structure of these substances. A regular decrease in polarization is observed in the region of the long wavelength absorption band.

Finally, we used Vavilov's method to determine the nature of the elementary oscillators. According to Feofilov[8] when the emitting and absorbing oscillators are dipoles and have the same direction for $P_{max} < 0.5$, the following relationship obtains

$$P(\eta) = P_0 \frac{\cos^2 \eta}{1 - P_0 \sin^2 \eta}, \qquad (2)$$

where η is the angle between the exciting vector and the vertical. If we rewrite this expression in the form

$$\frac{1}{P} = \frac{1}{P_0} + \left(\frac{1}{P_0} - 1\right) \tan^2 \eta, \qquad (3)$$

then in 1/P vs $\tan^2 \eta$ coordinates we obtain a straight line. In the case of dipole absorption and quadrupole emission ($d \rightarrow q$) we will also have a straight line, but with a slope differing from that in the $d \rightarrow d$ case[9]. In Fig.4 we show three straight line plots for 4-amino-N-methylphthalimide: 1 - the theoretical plot for the $d \rightarrow d$ case, 2 - the experimental plot, and 3 - the theoretical plot for $d \rightarrow q$. It will be seen that the first and second plots are very close, while the third has an appreciably steeper slope. This indicates that for 4-amino-N-methylphthalimide we have the $d \rightarrow d$ case. The data obtained for the other phthalimide derivatives also indicate that the absorption and emission oscillators are dipoles.

We desire to express our sincere gratitude to V.V.Zelinskii for providing the phthalimide samples and to A.M.Bonch-Bruevich, V.I.Shirokov and G.A.Tishchenko for making it possible to perform the fluorometric measurements.

Institute of Physics and Mathematics
Academy of Sciences of the Belorussian SSR

References

1. G.P.Gurinovich, A.M.Sarzhevskii & A.N.Sevchenko, Izv.AN Belorussian SSR, Ser.fiz., takh., 2 (1956).
2. N.S.Marinesco, J.Chim.phys., 572 (1927).
3. V.I.Gribkov & N.D.Zhevandrov, Doklady AN SSSR, 98, 565 (1954).
4. N.D.Zhevandrov & V.P.Nikolaev, Ibid., 113, 1025 (1957).
5. A.N.Sevchenko, Trudy (Proceedings), State Opt.Inst., 15, 65 (1941).
6. V.L.Levshin, Fotoliuminestsentsiia zhidkikh i tverdykh veshchestv (Photoluminescence of liquids and solids), 1951.
7. P.P.Feofilov, Dissertation, Ioshkar-Ola, 1943.
8. P.P.Feofilov, Doklady AN SSSR, 44, 159 (1944).
9. G.P.Gurinovich & A.N.Sevchenko, Trudy (Proceedings), Inst. of Physics & Mathematics, Belorussian SSR, Ac.of Sci., No.2, 3 (1957).

CHARACTERISTICS OF THE LUMINESCENCE OF DIFURYLPOLYENES

- P.F.Nepochatykh

Difur(fur)ylpolyenes are organic compounds the molecules of which consist of two furan five-membered rings linked by chains comprising alternating single and double conjugated bonds: —CH=CH.

We investigated the following compounds containing a CO or COCO group in the chain:

A) 1,6-difuryl-hexadiene-1,5-dion-3,4:

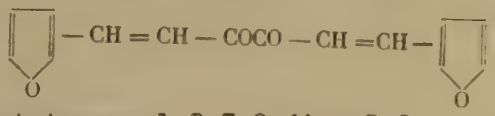

B) difuryl-1,10-decatetraene-1,3,7,9-dion-5,6:

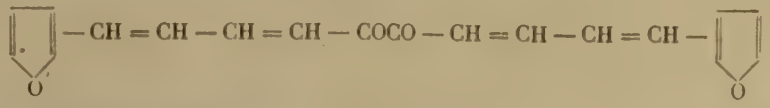

C) difuryl-1,9-decatetraene-1,3,7,9-dion-5:

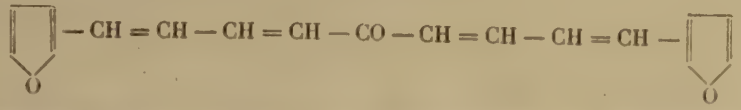

All these compounds are crystalline substances not soluble in water but dissolving in ethyl and methyl alcohols, glycol, hexane and acetone.

The configuration of the atoms in the five-membered furan ring is planar[1]; the angles between the bonds are C-O-C = 107°, O-C-C = 109° and C-C-C = 107° in the equilibrium state; the interatomic distances are: 1.35 Å for C=C, 1.46 Å for C—C and 1.41 Å for C—O.

The long chains consisting of C—C and C=C bonds are characterized by a plane structure. The angles between the single and double bonds are 120°; the separations between the polyene chain atoms are 1.54 Å in the case of the single bonds and 1.34 Å in the case of the double bonds.

Comparing the difurylpolyene molecules with the molecules of such thoroughly studied polycyclic compounds as naphthalene, anthracene and other dyes we note that 1) both groups are characterized by a plane configuration of the atoms and bonds and 2) the polyene molecules have a comparatively elongated structure, in view of which they may be regarded as fine fibers, whereas the polycyclic compound molecules may be thought of as sheets or ribbons.

In undertaking the present research our purpose was to elucidate how these differences in the atomic and bond configurations affect the polarization characteristics of the luminescence; in addition, we deemed it desirable to determine to what extent the Levshin-Perrin formula

$$\frac{1}{P} = \frac{1}{P_0} + \left(\frac{1}{P_0} + \frac{1}{3}\right)\frac{kT}{r\eta}\tau, \qquad (1)$$

which correctly describes the properties of many dyes and polycyclic compounds, is applicable to polyenes.

In Eq.(1) P_0 is the limit polarization, P is the degree of polarization under the experimental conditions, η is the macroscopic viscosity, r is the molecular volume and τ is the lifetime of the excited state. The formula was deduced on the basis of the theory of Brownian motion and the laws of hydrodynamics, it being assumed in the derivation that the molecules are spherical.

However, as was noted above, actually difurylpolyene molecules are more like fibers burdened with complex atomic groups (the furan rings). Hence one might reasonably expect an appreciable difference between the values of τ calculated by means of Eq.(1) and the values determined experimentally on a fluorometer. The results of our experiments and calculations are given below.

We investigated the polyenes in alcohol and glycerol solutions. Measurements of the degree of polarization of the luminescence were made by means of a Sawyer polariscope with a compensating stack; for control purposes we also made a number of measurements by means of a Cornu polarimeter. The viscosity of the solutions were determined in a Hepler viscometer (falling ball method) to within 0.1%. The temperatures in the luminescence cell and the viscometer were maintained constant by means of a thermostat to within ±1°. The measurements were made at 10° intervals in the range from 293 to 393°K.

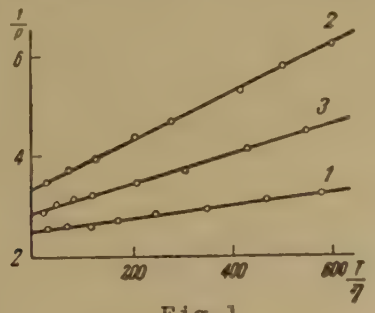

Fig.1

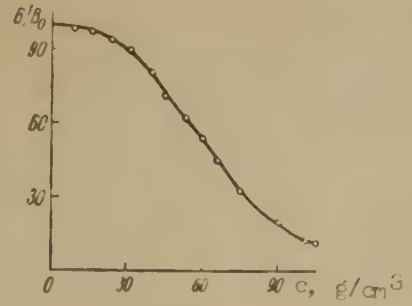

Fig.2

Fig.1. Polarization of luminescence: 1) 1,6-difuryl-hexadiene-1,5-dion-3,4, 2) difuryl-1,10-decatetraene-1,3,7,9-dion-5,6 and 3) difuryl-1,9-decatetraene-1,3,7,9--dion-5.

Fig.2. Quenching of luminescence by aniline in an alcohol solution of difuryl-1,9-decatetraene-1,3,7,9-dion-5.

Substance	P_0, %	$\tau \cdot 10^9$, sec	$\tau_1 \cdot 10^9$, sec	v, Å³	v_1, Å³	$c \cdot 10^6$	$\tau_2 \cdot 10^9$,
1,6-difuryl-hexadiene-1,5-dion-3,4	41,5	2,5	2,2	350	158	2,1	4,1
difuryl-1,10-decatetraene-1,3,7,9-dion-5,6	29,4	1,6	2,1	215	276	2,0	3,3
difuryl-1,9-decatetraene-1,3,7,9-dion-5	35,1	1,6	1,9	185	223	5,0	3,3

Notes: P_0 is the limit polarization in glycerol solutions. Excited state lifetimes: τ - measured on the fluorometer at 293° in glycerol solution, τ_1 determined from the polarization measurements by means of Eq.(1), τ_2 - measured on the fluorometer in an alcohol solution at 77°K. v - molecular volume determined by means of Eq.(1), v_1 - volume determined from the density in the solid state. c - concentration in g $cm^{-3} \cdot 10^{-6}$.

The experimental results are plotted in Fig.1 and listed in the accompanying table. It will be evident from Fig.1 that the linear relation between 1/P and T/η predicted by Eq.(1) obtains for all the investigated compounds.

The excited state lifetimes were determined on the phase fluorometer of the Physical Institute of the USSR Academy of Sciences. The molecular volumes of the fluorescent particles, needed for determining τ by means of Eq.(1) were determined from the molecular weight and the density in the solid state.[2]

Conclusions

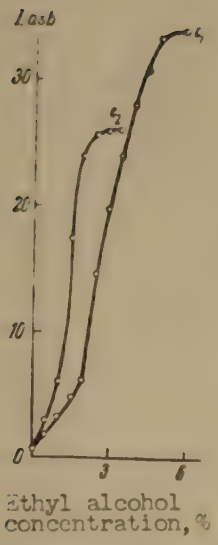

Fig.3. Effect of addition of a polar liquid on the fluorescence of a hexane solution of compound C: $c_1 = 1.87 \cdot 10^{-4}$ g/cm^3; $c_2 = 3.80 \cdot 10^{-4}$ g/cm^3.

1. Increase in the length of the chain comprised by the single and double conjugated bonds leads to a decrease of the limit polarization: for example, introduction of a chain of four links, —CH=CH—CH=CH- reduces the limit polarization by 12.1%.

2. The CO group has a very appreciable influence on the degree of polarization. Introduction of this group into the polyene chain brings down the degree of polarization by 5.7%. This will be evident from a comparison of the limit polarization values for compounds B and C.

3. The excited state lifetimes as determined on the fluorometer and from the polarization measurements do not agree, which can be explained by a deviation of the actual molecular shape from the spherical. The difference between the respective values does not exceed 20%.

4. The fluorescence of solutions of the investigated compounds is quenched by aniline (Fig.2); other quenching agents such as KaI, NaI and NaBr have no noticeable effect. In a nonpolar solvent - hexane - the fluorescence yield is very low. If a polar solvent (ethyl alcohol) is gradually added to the hexane, the luminescence intensity gradually increases to a certain peak value. The variation of the luminescence intensity with the polar solvent concentration is shown in Fig.3. Heating of the solution results in quenching of the luminescence.

We believe the increase in intensity is due to the influence of the polar molecules on the interaction between the solute and solvent molecules.

We desire to thank V.L.Levshin for his interest in the work, M.D.Galanin for assistance in the fluorometric measurements and B.A.Arbuzova for supplying the investigated compounds.

Kazan State Pedagogical and Teachers Institute

References

1. M.V.Vol'kenshtein, B.I.Stepanov & B.I.El'iashevich, Kolebaniia molekul (Molecular vibrations) Vol.1, pp.29 & 41, M., 1949.

2. S.I.Vavilov, Sobr.soch.(Collected Works), Vol.II, pp.11 & 14, M., 1952.

3. V.L.Levshin, Izv.AN SSSR, Ser.fiz., 20, 419 (1956). (Trans.Bulletin 20, No.4, 382.)

Bulletin of the Academy of Sciences of the USSR - Physical Series
Vol. 22, No. 11 - November 1958

TABLE OF CONTENTS

Transactions of the Eleventh All-Union Conference on Theoretical Spectroscopy
(Continued from Vol.22, Nos.6 & 9)

	Page Orig.	Trans.
Measurement and calculation of the polarization of the emission of helium atoms excited by electron impact - L.A.Vainshtein & G.G.Dolgov	1294	1287
Emission of the negative hydrogen ion - W.Lochte-Holtgreven	1297	1290
Spectroscopic investigation of the rotational mobility of molecules in quasiliquid camphene and tricyclene crystals - Ang Meng Tok, M.F.Vuks & D.S.Nedzvetskii	1302	1294
Phosphorescence spectra of some aromatic acids at liquid air temperature - B.A.Piatnitskii	1304	1296
Determination of the rotational constants of CH_3GeCl_3 from its microwave absorption spectrum (summary) - N.A.Irisova	1307	1299
Method of quasinormal coordinates in crystal optics - V.S.Mashkevich	1308	1300
Spectroscopic investigation of crystals - A.F.Prikhot'ko	1312	1304
Relation between the absorption and dispersion in crystals as evinced in the case of 1,2-benzanthrene - M.S.Brodin & M.S.Soskin	1316	1308
Quantum mechanical description of F-centers in alkali halide crystals - I.V.Abarenkov	1320	1312
Properties and structure of the initial aggregations of F-centers in the process of their colloidal coagulation - A.A.Shatalov	1324	1315
Conditions governing the existence and spectroscopic manifestation of excitons in semiconductors - I.Z.Fisher	1329	1320
Investigation of the role of trapped and free excitons in the luminescence of molecular crystals by polarization methods - N.D.Zhevandrov	1332	1323
Impurity scattering of light in crystals at low temperatures - Iu.E.Perlin	1337	1327
Paramagnetic resonance of impurity centers in ionic crystals - M.F.Deigen	1341	1331
Absorption and luminescence spectra of alkali halide crystals containing impurity ions with isoelectronic shells - M.L.Kats	1347	1337

DISCUSSION FOLLOWING THE REPORTS OF SARZHEVSKII & SEVCHENKO AND NEPOCHATYKH

N.D.Zhevandrov: The two-fold difference between our experimental molecular volumes, mentioned by Sevchenko, can readily be explained: there was an interval of three years between the two studies (Refs.3 & 4 of the S & S report) and the data pertain to different batches of glycerol. Even distilled glycerol always contains a certain amount of water and the sensitivity of the method to the solvent has been demonstrated repeatedly (it follows from the work of S & S).

As for interpretation of the results from the viewpoint of solvate shells or differences between the macroscopic and molecular viscosities, we feel that this is an argument about definitions inasmuch as the physical nature of the effect consists in the interaction of the fields of the dissolved molecules with the molecules of the solvent.

M.D.Galanin: Use of the Perrin formula for determining molecular volumes is based on two assumptions: first, that the microviscosity, which plays a role in rotation of molecules, is exactly equal to the macroviscosity measured on a viscometer, and, second, that the molecule can be represented by a solid sphere model with radius r, the molecular volume being equal to $4\pi r^3/3$. Obviously, both assumptions are approximate and cannot be rigorously justified. Hence I believe use of this procedure for determining molecular volumes and, in particular, for deciding the question of the existence of "solvate shells" is erroneous. One can expect agreement between the calculated value of the molecular volume and the true volume of the molecule solely as regards order of magnitude and the results should be interpreted only as an indication that the micro- and macro-viscosities are not too dissimilar.

A.N.Sevchenko: A certain difference between the micro and macroviscosities is possible in principle. However, the extensive experimental data on polarization obtained at different times by different investigators unquestionably indicate that there is a linear relation between the molecular and the molar viscosity. This is why Vavilov proposed this method for determining the volume of solvate shells. On the basis of our experimental data for different molecules, it may be asserted that in a solvent the shape of the molecules is nearly spherical. A direct proof of the accuracy of this method is the fact that the values of solvate shell volumes determined by independent methods (Perrin, Marinesco and others) agree. Hence, I feel that M.D.Galanin's reasoning is not convincing.

Spectroscopy of luminescence centers in alkali halide crystal phosphors activated by mercury-like ions - Ch.B.Lushchik & N.E.Lushchik 1351 1341

Fluorescence of pure cadmium sulfide at low temperatures - E.Grillot & M.Bancie-Grillot 1356 1346

Transactions of the Sixth Conference on Luminescence (Molecular luminescence)
(to be continued in Vol. 23, No.1)

Opening address - A.N.Terenin 1366 1356

Correlation between the luminescence and absorption spectra of complex molecules - B.I.Stepanov 1367 1357

Correlation between the luminescence and absorption spectra of polyatomic molecules - B.S.Neporent 1372 1362

Relation between the luminescence and absorption spectra of an aqueous solution of fluorescein - M.N.Alentsev & L.A.Pakhomycheva 1377 1367

On the meaning of photoluminescence and scattering - B.I.Stepanov & P.A.Apanasevich 1380 1370

Internal field and spectra of complex molecules in solutions - N.G.Bakhshiev 1387 1377

Temperature dependences of the electronic spectra of some phthalimides - L.G.Pikulik & M.A.Solomakho 1391 1381

Luminescence of powdered materials - Iu.I.Chekalinskaia 1395 1385

Resonance luminescence of matter in finite volumes - A.M.Samson 1399 1389

Dependence of the polarization of phosphorescence of organic materials on the viscosity of the solution - B.Ia.Sveshnikov & P.I.Kudriashov 1403 1393

Variation of the degree of polarization with the fluorescence wavelength - G.P.Gurinovich & A.N.Sevchenko 1407 1397

Polarization of the luminescence of phthalimides - A.M.Sarzhevskii & A.N.Sevchenko 1412 1402

Characteristics of the luminescence of difurylpolyenes - P.F.Nepochatykh 1417 1407

Translated in 1959 by
Columbia Technical Translations
5 Vermont Ave., White Plains, N.Y.

Number 12 Volume 22 1958

BULLETIN

of the

Academy of Sciences of the USSR

- Physical Series -

(Izvestiia Akademii Nauk SSSR)
(Seriia fizicheskaia)

Reproduction rights reserved

by

Columbia Technical Translations
5 Vermont Avenue
White Plains, New York

Single Issues
$20

Annual Subscription
$215

TRANSACTIONS

of the

SECOND ALL-UNION CONFERENCE ON FERROELECTRICITY

Rostov on the Don - 12-20 November 1957

CONTRIBUTION TO THE QUANTUM MECHANICAL THEORY OF FERROELECTRICITY

- R.E.Pasynkov

The aim of the present paper is to examine some of the aspects of the quantum mechanicam theory of ferroelectricity.

At present there are two outstanding treatments of ferroelectricity in which the formalism of quantum mechanics is employed: the theory of Barrett[1] and the "electronic theory" of Jaynes-Wigner.[2] The two treatments are based on essentially different mechanisms.

Barrett's theory may be described as a quantum mechanical treatment of Slater's model[3] of anharmonic oscillators. The rise of spontaneous polarization is assumed to be due to displacement of the central Ti or Sr ions, which execute anharmonic vibrations inside the stationary oxygen octahedra.

The physical mechanism fundamental to the electronic theory of Jaynes-Wigner is in a sense opposite to that assumed by Barrett. In Jaynes' work the quantum mechanical effects are taken into account only in considering the states of the electronic structure of the entire complex of ferroactive ions. The source of spontaneous polarization is perturbation of this structure. In Jaynes' treatment electronic displacements are relegated to a minor role, essentially similar to that attributed to deformations of the electron shells in the work of Barrett[1] and Slater[3]. There are a number of objections to the basic premises of the electronic theory.[4] The most serious difficulty, in our opinion, is the impossibility of explaining the frequency relaxation effect, resulting in a great decrease of the dielectric constant. At the same time the possibility - demonstrated by Jaynes - that spontaneous polarization can arise as a result solely of spontaneous deformations of the electron shells is an important result which cannot be ignored in constructing a microscopic theory.

Hence it would appear expedient to consider both sources of ferroelectricity, electronic and ionic, jointly. By way of the first step in this direction we propose the following model.

The ferroelectrically active ionic complex (in the case of the perovskite structure, the oxygen octahedron and the central ion) may be regarded as an independent molecule. The interaction of such molecules with each other is taken into account by introducing an effective field

$$\mathbf{F}_{ef j} = \nu_j \mathbf{E} + \sum_j \beta_{kj} (\mathbf{P}_i + \mathbf{P}_e), \qquad (1)$$

where $\mathbf{P}_i$ is the component of the polarization due to displacement of the ions, $\mathbf{P}_e$ is the electronic polarization, $\mathbf{E}$ is the applied field and ν_j and β_{kj} are constants. The individual ions comprising the molecule can perform anharmonic oscillations.

Let us consider the Hamiltonian operator for such a system of microparticles:

$$\hat{H} = \frac{1}{2}\sum_j' -\frac{h^2}{4\pi^2 m_j}\nabla_j^2 + \sum_{jk}' a_{jk}x_j x_k - \sum_j' q_j E_j x_j + \sum_{jkl}' c_{jkl}x_j x_k x_l + \sum_{jklm}' b_{jklm}x_j x_k x_l x_m, \qquad (2)$$

where the x_j are the displacements and the m_j the masses of the particles. The indices j, k, l and m depend both on the number of the particle and the number of the coordinate characterizing the displacement of the given microparticle from the equilibrium position.

If in (2) we discard terms of powers higher than $x_i x_k$, as well as mixed "electronic-ionic" terms, and introduce normal coordinates, $\hat{H}$ will be a quadratic function of the normal coordinates. In this case we will have additivity of the particle energies and then the partition function

$$Z = \frac{1}{N!}(Z_e \cdot Z_i)^N,$$

here

$$Z_e = \sum_{jkl} \exp\left\{-\frac{W_{ejkl}}{kT}\right\},$$

$$Z_i = \sum_{jkl} \exp\left\{-\frac{W_{ijkl}}{kT}\right\},$$

where W_{ejkl} and W_{ijkl} are the corresponding matrix elements.

In this approximation ferroelectricity can arise only owing to electronic effects, inasmuch as here, as in the work of Jaynes[2], we obtain an equation of state linear with respection to ionic polarization. In order to take into account the ionic source of spontaneous polarization one must include in the expression for $\hat{H}$ terms of higher powers pertaining to the ionic displacements (but no mixed electronic-ionic terms). This problem can be solved in the framework of perturbation theory, i.e., by a procedure analogous to that employed by Barrett[1], and represents a significant step forward inasmuch as in this case the equation of state is nonlinear with respect to both the electronic and the ionic components of the total polarization; in other words, we have taken into account both sources of ferroelectricity without making any assumptions rougher than those made in the work of Barrett and Jaynes. Just as in these works, the electronic-ionic interaction is taken into account only through the effective field. If we wish to take into account the correlation between the electronic and ionic states directly we must use the general form of the Hamiltonian (see Ref.2), which involves determining the interaction coefficients c_{jkl} and b_{jkln}. This problem is a complicated one inasmuch as it requires theoretical solution of the problem of the coupling between the structural elements of the ferroelectric unit cell.

Institute of Semiconductors
Academy of Sciences of the USSR

References

1. J.H.Barrett, Phys.Rev., 86, 118 (1952).
2. E.T.Jaynes, Ferroelectricity, Princeton, 1953.
3. J.S.Slater, Phys.Rev., 78, 748 (1950).
4. R.E.Pasynkov, Izv.AN SSSR, Ser.fiz., 21, 340 (1957). (Trans.Bulletin, 21, No.3, 346.)

ON THE ELECTRIC FIELD DEPENDENCE OF THE DIELECTRIC CONSTANTS OF FERROELECTRICS

- I.V.Liagin & Ia.I.Geivashovich

The physical properties of many ferroelectric materials, including barium titanate, are highly sensitive to external influences. In some cases the nonlinear effects involved are so appreciable that they cannot be neglected. The nonlinear effects in ferroelectrics connected with the external field dependence of the dielectric constant were first discussed almost a decade ago by Ginzburg.[1] Subsequently, this nonlinearity has been considered from both the theoretical and experimental standpoints by Rzhanov[2], Verbitskaia[3] and Vul[4] and others.

The theory of ferroelectrics[1,5,6,7] in which domain structure is not taken into account leads to correct order of magnitude values for the dielectric constant and generally satisfactorily explains the experimentally observed temperature dependence of the constant. However, attempts[7,8] to interpret the hysteresis loops from the standpoint of the single domain thermodynamic theory proved to be less successful: theoretical calculations yielded an excessively high value for the coercive force. Apparently, the domain structure plays a significant role in hysteresis effects. Owing to the displacement of domain walls and the formation of new domains, a crystal may transform from the state in which the polarization vector P is antiparallel to the field to the state in which the vector is parallel to the field before the former state becomes thermodynamically unstable for the crystal as a whole. Nevertheless, the heightened interest in domain structure (particularly, in barium titanate), although it helped clarify some of the regularities involved, led, we feel, to an overevaluation of the importance of domains in ferroelectric effects on the part of certain investigators. We believe that domain structure, particularly in the range of low fields, plays a subsidiary role and that here one can apply with good approximation the single domain thermodynamic theory.

In the present paper we shall consider the dependence of the dielectric susceptibility tensor components on the external electric field in the low field region from the standpoint of the thermodynamic theory of a single domain single crystal.

Usually in calculating the dielectric susceptibility tensor

$$\varkappa_{ni} = \frac{\partial P_n}{\partial E_i} \tag{1}$$

the variation of the polarization vector with the electric field is assumed to be linear, i.e., all higher order terms are disregarded.[1,5,6,9] Obviously, in this case the tensor components are constant. Actually, in order to obtain the true field dependence of the susceptibility, one must take into account the nonlinear field dependence of the polarization.

Limiting our consideration to quadratic terms, we can write*

$$P_n(E_x, E_y, E_z) = P_{0n} + \varkappa^0_{ni}E_i + g_{nik}E_iE_k. \tag{2}$$

Then, from (1) and (2) we have

$$\varkappa_{ni}(E_x, E_y, E_z) = \varkappa^0_{ni} + (g_{nik} + g_{nki})E_k. \tag{3}$$

The twice repeating indices imply summation; the indices i and k independently take on the values of x, y, z and $n = x, y, z$.

---

*This type of field dependence of the dielectric constant of dielectrics is used for explaining the Kerr effect in the optical region.[10]

Relationship (3) can be interpreted as follows: in the assumed approximation the components of the dielectric susceptibility tensor are represented in the form of the sum of two terms. The first term is the initial susceptibility; the second term may be called the induced susceptibility.* It is a linear function of the field. It can readily be shown that the g_{nik} components form a tensor of the third rank symmetrical with respect to all three indices. It is calculated in the usual manner by minimizing the thermodynamic potential; the potential minimum for a barium titanate type single crystal is of the form[5]

$$\Phi = \Phi_0 + \alpha P^2 + \frac{1}{2}\beta_1 P^4 + \beta_2 (P_x^2 P_y^2 + P_y^2 P_z^2 + P_z^2 P_x^2) + \frac{1}{3}\gamma_1 P^6 +$$
$$+ \gamma_2 [P_x^4 (P_y^2 + P_z^2) + P_y^4 (P_z^2 + P_x^2) + P_z^4 (P_x^2 + P_y^2)] + \gamma_3 P_x^2 P_y^2 P_z^2 - \mathrm{PE}. \qquad (4)$$

We omit the calculations and give only the final results: in the paraelectric phase the induced effect is zero;** in the ferroelectric phases (tetragonal, orthorhombic and rhombohedral) the effect obtains and is evinced by the appearance of induced additions to the components of the initial susceptibility and by new non-diagonal components, which do not appear in the calculations in the linear approximation. The appearance of these components is connected with distortion of the crystal symmetry under the influence of the field.

Let us consider the tetragonal phase in more detail. Assuming that the z axis is aligned with the spontaneous polarization vector, we obtain the following dielectric susceptibility tensor

$$\begin{aligned} \varkappa_{xx} &= \varkappa_{xx}^0 + 2g_{xxz}E_z, \\ \varkappa_{xz} &= \varkappa_{zx} = 2g_{xzx}E_x, \\ \varkappa_{yy} &= \varkappa_{yy}^0 + 2g_{yyz}E_z, \\ \varkappa_{yz} &= \varkappa_{zy} = 2g_{yzy}E_y, \\ \varkappa_{zz} &= \varkappa_{zz}^0 + 2g_{zzz}E_z, \\ \varkappa_{xy} &= \varkappa_{yx} = 0, \end{aligned} \qquad (5)$$

where

$$g_{xxz} = g_{yyz} = g_{zxx} = g_{xzx} = g_{yzy} = g_{zyy} = -\frac{\beta_1 + \beta_2 + 2(\gamma_1 + \gamma_2)P_0^2}{8(\beta_2 + \gamma_2 P_0^2)^2 \cdot (\beta_1 + 2\gamma_1 P_0^2) P_0^5} \qquad (6)$$

and

$$g_{zzz} = -\frac{3\beta_1 + 10\gamma_1 P_0^2}{32(\beta_1 + 2\gamma_1 P_0^2)^3 P_0^5}. \qquad (7)$$

In the region of stability of the tetragonal phase $\beta_1 + 2\gamma_1 P_0^2 > 0$ (see, for example, Kholodenko[12]) and $\gamma_1 > 0$; consequently, $g_{zzz} < 0$. It follows that in a field with the z component directed along the spontaneous polarization vector, the $\varkappa_{zz}$ component will decrease under the influence of the field, which is the experimentally observed case[3,4,13,14,15].*** The available experimental data are insufficient for reliably establishing the sign of the other components of g_{nik}. According to numerical evaluations the induced addition to the $\varkappa_{zz}$ component for barium

---

*This term is not intended to imply any molecular polarization mechanism; it is introduced by analogy with the induced piezoelectric effect.[11]

**More accurately speaking, the effect is absent in the assumed approximation. In the next approximation there is obtained a quadratic field dependence of the susceptibility.

***Most of the available experimental data pertain to the ceramic or to single domain single crystals. In the latter case, movement of the domain walls gives rise to an effect which is superposed on the effect in question and in some cases may mask it.

titanate at room temperature and in a dc field of 3 kv/cm amounts to about 1% of the initial susceptibility. It can be shown, however, that near the phase transition point the induced susceptibility varies more rapidly with temperature than the initial susceptibility. Thus, for example, according to Kholodenko[11], in the transition to the cubic phase (at the temperature T_{21}, $\varkappa^0_{zz} \sim 1/(T_{21}-T)^{1/2}$ and $g_{zzz} \sim 1/(T_{21}-T)^{1/2}$; $\varkappa^0_{xx} = \varkappa^0_{yy}$ at the transition point remain finite, while the additions to them are of the order of $1/(T_{21}-T)^{1/2}$. A similar temperature dependence is characteristic of the induced nondiagonal components. In the transition to the orthorhombic phase (at $T = T_{23}$), g_{zzz} has no singularities, while g_{xxz} behaves as $1/(T-T_{23})$ near the transition point.

We desire to thank L.P.Kholodenko for constant interest in the work.

"K.Marx" Smolensk State Pedagogical Institute

References

1. V.L.Ginzburg, Usp.fiz.nauk, 38, 490 (1949).
2. A.V.Rzhanov, Zhur.eksp.i teor.fiz., 19, 335-345 (1949).
3. T.N.Verbitskaia, Izv.AN SSSR, Ser.fiz., 20, 185 (1956). (Trans.Bulletin, 20, No.2, 169.)
4. V.M.Vul, Izv.AN SSSR, Ser.fiz., 21, 379 (1957). (Trans.Bulletin, 21, No. 3, 383.)
5. M.Ia.Shirobokov & L.P.Kholodenko, Zhur.eksp.i teor.fiz., 21, 1239 (1951).
6. G.A.Smolenskii & R.E.Pasynkov, Ibid., 24, 69 (1953).
7. G.A.Smolenskii & V.Kh.Kozlovskii, Ibid., 23, 63,645 (1953).
8. L.P.Kholodenko, Kristallografiia, 1, 4, 393 (1956).
9. A.E.Devonshire, Phil.Mag., 40, 1040 (1949).
10. L.D.Landau & E.M.Lifshits, Elektrodinamika sploshnykh sred (Electrodynamics of continuous media), p.416, M., 1957.
11. L.P.Kholodenko, Zhur.eksp.i teor.fiz., 31, 244 (1956). (Trans.Soviet Phys.-JETP.)
12. L.P.Kholodenko, Ibid., 31, 1034 (1956). (Trans.Soviet Physics - JETP.)
13. N.S.Novosil'tsev & A.L.Khodakov, Zhur.tekh.fiz., 26, 2, 310 (1956).
14. A.L.Khodakov, Zhur.tekh.fiz., 26, 51 (1956). (Trans.Soviet Phys. - Tech. Phys.).
15. V.A.Bokov, Izv.AN SSSR, Ser.fiz., 21, 382 (1957). (Trans.Bulletin 21, No.3, 386.)

PHASE TRAJECTORY OF AN OSCILLATING CIRCUIT WITH A FERROELECTRIC

- N.S.Novosil'tsev

In designing and employing circuits incorporating capacitors containing ferroelectric materials one must take into account the distinctive features of the processes occurring in such materials. Andronov & Khaikin[1] in their book consider a nonlinear circuit with a ferroelectric, but limit their analysis to a conservative approximation. As far back as 1916 Andreev[2] called attention to the fact that in most cases the parameters of dielectrics are measured under dynamic conditions. In connection with this he analyzed the problem of an oscillating circuit taking into account the resonance properties of the dielectric in the capacitor as a system with two degrees of freedom (however, he assumed the system to be a linear one).

In employing ferroelectrics we encounter what are essentially nonlinear oscillatory systems, in general with several degrees of freedom and a specific form of hysteresis loss.

Hysteresis and Ambiguity

To elucidate the limits of applicability of thermodynamic potentials in treating rapid oscillatory processes, let us see what restrictions must be imposed on using the familiar expression for the free energy F from the thermodynamic theory of ferroelectricity as the potential function.

The derivative with respect to polarization

$$\left(\frac{dF}{dP}\right)_T = E \qquad (1)$$

gives the electric equation of state. It must be recalled, however, that for ferroelectrics the curve below the Curie point has two inflection points (bends), where loss of stability occurs.

Rigorously speaking, thermodynamic curves represent a chain or series of equilibrium states, but in our case the initial polarization - the field E - changes with time at a finite rate; consequently, differentiating (1) with respect to time, we write

$$\frac{dP}{dt} = \frac{\frac{dE}{dt}}{\frac{d^2F}{dP^2}}, \qquad (2)$$

At the instant of loss of stability

$$\frac{d^2F}{dP^2} = \frac{dE}{dP} = 0; \qquad (3)$$

consequently, the polarization changes suddenly, skipping the serpentine part corresponding to unstable states in the curve of the thermodynamic equation of state (1).[3] Thus the actual variation of the generalized coordinate (P) with the generalized force (-E) is represented not by the theoretical thermodynamic curve (1), but by a hysteresis loop.

Hysteresis Loss

To determine how the hysteresis loss should be taken into account, let us consider the form of the differential equation for an oscillating circuit with a ferroelectric in the capacitor.

We denote the circuit inductance by L, the thickness of the dielectric by /,

the area of the capacitor plates by S and the charge on the capacitor by q. The specific potential energy U_1 of the field in the ferroelectric is equal to the free energy in the thermodynamic sense:

$$U_1 = \alpha P^2 + \frac{\beta}{2} P^4, \tag{4}$$

where

$$P = \frac{q}{S}.$$

The Lagrangian in the present approximation will be

$$\frac{d}{dt}\left(\frac{\partial T}{\partial \dot{q}}\right) + lS \frac{\partial U_1}{\partial P} \frac{dP}{dq} = 0. \tag{5}$$

Taking the polarization P rather than the charge q as the generalized coordinate, we transform Eq.(5) to the form

$$SL\ddot{P} + l(2\alpha P + 2\beta P^3) = 0. \tag{6}$$

Here

$$l(2\alpha P + 2\beta P^3) = l\frac{\partial F}{\partial P} = lE = V$$

(the difference in potentials on the capacitor plates). Eq.(6) describes the anharmonic oscillatory process and can be investigated by the methods of nonlinear oscillation theory[4-6]. This, however, is of no interest to us inasmuch as actually this equation describes the processes in the circuit with the ferroelectric only above the Curie point where there is no hysteresis.[3]

In the presence of hysteresis the generalized forces are no longer single-valued functions of the coordinates and then we must use some other expression rather than the thermodynamic equation (4). Hysteresis, ambiguity and loss of stability are all interconnected and follow from each other. In order to take hysteresis into account, instead of (5) we must write a new equation:

$$L\ddot{P} + \Phi(P) = 0, \tag{7}$$

where $\Phi(P)$ is a two-valued function. Its curve is given by the hysteresis loop appearing on the oscillograph screen. Eq.(7) also does not have the usual dissipative term with P, nevertheless it describes a process with losses because dissipative forces in systems with hysteresis are expressed not in terms of velocity (i.e., the rate of the process), but through the coordinates. Thus, for example, the area of the hysteresis loop does not depend on the rate at which the loop is traced (velocity of the tracing beam) in a rather wide range of values. Davidenkov (Ref.7) calls attention to analogous relationships in his work on the dissipation of energy in vibrating mechanical systems. As far as we know, however, no one has so far used this approach for taking into account hysteresis losses in considering processes in electric oscillating systems. The question of forced vibrations in mechanical systems with hysteresis has been treated by Bat'[9] and Lur'e & Chekmarev[10] who reduced the essentially nonlinear problem to solution in parts by linear means. In 1952-53 a number of Japanese physicists[6] studied the allied problem of losses in ferromagnets with irreversible magnetization of the domains. By way of mathematical formalism they used Duffing's equation. However, as was pointed out above, for analysis of a system with hysteresis one cannot use a single equation, even a nonlinear one.

Construction of the Phase Trajectory from the Hysteresis Loop

Disregarding the usual dissipative forces that are velocity-dependent, let us rewrite (7) in the form

$$\ddot{x} = f(x) = 0. \tag{7a}$$

The function $f(x)$ is understood to include everything connected with ambiguity and nonlinearity of the dissipative and quasielastic forces in hysteresis. We note that, although in the case of hysteresis the dissipative components of $f(x)$ are described as regards magnitude in terms of the coordinates, as regards direction they are as usual opposed to the velocity; the quasielastic components as regards both sign (direction) and magnitude are determined only by the coordinates. Consequently, in the odd quadrants of the phase plane both components of $f(x)$ are oriented in the same direction, while in even quadrants they are opposed to each other. The electron beam in the oscillograph simultaneously traces both the elastic and the viscous reaction of the ferroelectric.

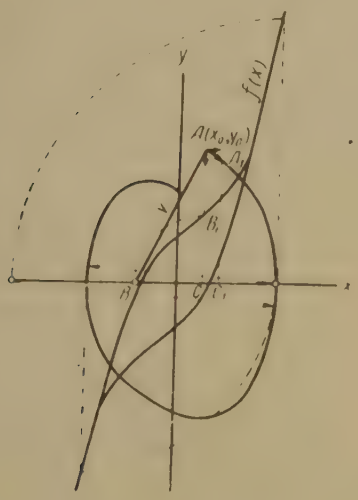

One can always introduce the dimensionless time $\tau = \omega$, where ω is described as usual by a linear term associated with the rigidity and the inertia of the system, and transform our equation to the new variable τ:

$$\frac{d^2x}{d\tau^2} = f_1(x). \tag{8}$$

Eqs. (7) and (8) are particular cases of the Duffing equation:

$$\ddot{x} + \varphi(\dot{x}) + \psi(x) = 0. \tag{9}$$

When $\varphi \neq 0$ and ψ is linear, the integral curves are constructed by the method due to Lienard[11,12]. In our case, when $\varphi = 0$ and ψ is nonlinear, one can use the following procedure for constructing the phase trajectory (see accompanying figure). The process coordinate x is laid off along the horizontal axis of the phase plane. In our case this will be a quantity proportional to the charge on the capacitor plates or, if preferred, to the polarization P. The rate of the process is laid off along the vertical axis. After conversion to the dimensionless time, the velocity and acceleration have the dimensionality of the coordinate. Hence one can plot the dependence given by Eq. (8) in the same coordinate axes.

It will be obvious from what has been said above that this dependence is given by the hysteresis loop to an appropriate scale. The unusual position of the loop is due to the fact that the role of the generalized force in the electric equation of state is played by the field intensity taken with opposite sign (-E).

To plot the phase trajectory, we take the initial conditions x_0, $y_0 = \frac{dx_0}{d\tau}$ (point A in the figure). From A we drop a perpendicular to the x axis. B_1C is obviously equal to the acceleration in the initial instant, while AC equals the velocity. Rotating the segment B_1C counterclockwise 90°, i.e., to the x axis, from the end of B we draw the radius vector BA to point A. As regards magnitude, the vector equals the phase velocity corresponding to point A (x_0, y_0).

The angular velocity of BA is

$$\Omega = \lim_{\Delta\tau \to 0} \frac{A\breve{A}_1}{\Delta\tau BA} = 1$$

(clockwise rotation). From point A_1 we again drop a perpendicular to the x axis, find a new value of the radius vector and so on. It is expedient always to rotate the radius vector through the same angle about the instantaneous center. This is very useful in choosing of coordinates for plotting other curves with respect to the ordinary time axis on the basis of the phase trajectory obtained by the above procedure. As will be evident from the illustrated construction, the phase trajectory is a diminishing spiral characteristic of a decaying process.

Thus, although in Eqs.(7) and (8) $\varphi = 0$, i.e., although these equations contain no ordinary velocity-dependent dissipative terms, they describe decaying oscillations.

Scientific Research Physical-Mathematical Institute at
Rostov-on-the-Don State University

References

1. A.A.Andronov & S.E.Khaikin, Teoriia kolebanii, Part 1, M.1937. (Trans. Theory of Oscillations, Princeton, 1949.)

2. N.N.Andreev, Zhur.Russk.fiz.khim.obshch. (Jour.of the Russian Physical & Chemical Society), 11, 62 (1916).

3. N.S.Novosil'tsev, Dielektricheskii gisterezis, poverkhnost' svobodnoi energii i uravnenie sostoianiia segnetoelektrika (Dielectric hysteresis, free energy surface and equation of state of ferroelectrics), Pub.AKIAN, June, 1955.

4. B.V.Bulgakov, Kolebaniia (Vibrations), Chapt.6, p.355, M., 1954.

5. J.J.Stoker, Nonlinear Vibrations in Mechanical and Electrical Systems, N.Y., 1950. (Cited in Russian trans.)

6. Ken-iti Munakata, J.Phys.Japan., 7, No.4, 515 (1952).

7. N.N.Davidenkov, Zhur.tekh.fiz., 8, 6 (1938).

8. Ia.G.Panovko, ibid., 23, 3, 486 (1953).

9. M.I.Bat', Prikl. matem. i mekhan., 4, 3, 13 (1940).

10. A.I.Lur'e & A.I.Chekmarev, Prikl.matem.i mekhan., Nov.Ser.(Applied Math. and Mech., New Series), 1, 3, 307 (1938).

11. A.Lienard, Rev.gen.electr., 23, 901 (1928).

12. N.N.Bogoliubov & Iu.A.Metropol'skii, Asimptoticheskie metody v teorii nelineinykh kolebanii (Asymptotic methods in the theory of nonlinear vibrations) p.168, M., 1955.

CONTRIBUTING TO THE THEORY OF DOMAIN WALLS IN FERROELECTRICS

- V.A.Zhirnov

It is known from optical studies[1,6,7] that the thickness of the transition layers - walls - between the 180° domains in barium titanate is of the order of the lattice constant (~$4\cdot10^{-8}$ cm), while the thickness of the walls between the 90° domains is ~$5\cdot10^{-5}$ cm. In view of the dipole character of the interaction between the electric moments, the surface energy density associated with the domain walls should decrease with increasing wall thickness. Hence one can expect the surface energy of the 90° domain walls to be appreciably lower than that of the 180° domain walls. This assumption is also supported by the experimentally observed preferential nucleation of 90° domains and the relatively greater ease with which the 90° walls are displaced under the influence of external mechanical stresses.

The present work is devoted to a quantitative evaluation of the thickness and energy of the walls between the 180 and 90° domains in barium titanate and 180° domains in Rochelle salt.

In contrast to the case of ferromagnets, where, owing to exchange interaction the absolute magnitude of the magnetization remains constant so that all changes occur through rotation of the magnetization vector, in the case of ferroelectrics one must take into account the possibility that the magnitude of the spontaneous polarization in the transition layer can vary.

Then, as has been shown by Ginzburg[2] for a ferroelectric crystal in electrical equilibrium, the condition $\operatorname{div} \mathbf{P} = 0$ must obtain. Further, we solve the variational problem of finding the minimum thermodynamic potential[2], to which is added the energy associated with nonuniform distribution of the spontaneous polarization in the transition layer (wall):

$$\frac{\varkappa}{2}\left[(\nabla P_x)^2 + (\nabla P_y)^2 + (\nabla P_z)^2\right],$$

for barium titanate $\varkappa$ is assumed to lie in the range from $3\cdot10^{-15}$ to $3\cdot10^{-16}$ cm^2 and the polarization vector P and displacement vector D are taken as the independent variables.

For a 180° domain wall in $BaTiO_3$, located in a (100) plane when P in the domains is parallel or antiparallel to the z axis, the solution of the variational problem is of the form[4]:

$$P_x = P_y = 0; \quad P_z = P_0 \operatorname{th} \frac{x}{\delta},$$

where $\delta = \frac{1}{P_0}\left(\frac{\varkappa}{\beta_1 - q_{12}^2/c_{11}}\right)^{1/2}$ characterizes the effective dimensions of the transition region.

Taking $\beta_1 - q_{12}^2/c_{11} \approx 1.5\cdot10^8$ cm^4/coulomb^2 (Devonshire[5]), we obtain $\delta \approx 2\cdot10^{-7}$ to $5\cdot10^{-8}$ cm, which amounts to a few lattice constants and, consequently, agrees with the experimental results.[1]

We obtain the following expression for the excess surface energy associated with the presence of the 180° domain wall:

$$\sigma = \int_{-\infty}^{\infty} (\Phi - \Phi_0)\, dx = \frac{8}{3} P_0^2 \left[\varkappa\left(\beta_1 - \frac{q_{12}^2}{c_{11}}\right)\right]^{\frac{1}{2}} \approx 10 \ \text{erg/cm}^2 .$$

This estimate is in agreement with the value given by Merz[6].

For the 90° domain walls in $BaTiO_3$, located in a (101) plane, when P in the domains is directed along the z and x axes, the solution of the variational problem is

$$P_x = \frac{P_0}{2}\left(1 + \operatorname{th} \frac{x+z}{\delta_1}\right); \quad P_y = 0; \quad P_z = \frac{P_0}{2}\left(1 - \operatorname{th} \frac{x+z}{\delta_1}\right),$$

where $\delta_1 = \frac{2}{P_0}\left(\frac{\varkappa}{C}\right)^{1/3}$ and $C = \beta_1 + \beta_2 - \frac{(q_{11} - q_{12} - 2q_{44})^2}{c_{11} - c_{12} + 2c_{44}}$.

Evaluations lead to a value of C = 10^7 cm^4/coulomb^2, whence we obtain $\delta_1 \approx 10^6$ to $5 \cdot 10^{-7}$ cm, which is about one order of magnitude higher than for the 180° case. The divergence from the experimental value of $\sim 10^{-5}$ cm may be due to the fact that in her work Little[1] observed 90° domains having dimensions comparable to the wall thickness; in this case one cannot, as was done in the calculations, assume that the crystal is unstressed through the thickness of the domains.

We obtained the following expression for the surface energy of the 90° domain walls in barium titanate:

$$\sigma_1 = \frac{2}{3} P_0^3 (\varkappa C)^{1/3}.$$

Numerical evaluation in this case yields $\sigma_1 \approx$ 2-4 erg/cm^2.

Comparison with the 180° domains shows that variation of the vector P is energetically favored in the 90° domain walls inasmuch as in this case the minimum magnitude of the polarization is $P_0/\sqrt{2}$ instead of 0. This accounts for the ease with which the 90° domain walls appear and move.

Finally, let us consider the 180° walls of a Rochelle salt single crystal in the actually observed case when the polarization vectors in neighboring domains are directed parallel and antiparallel to the x axis. In the expression for the thermodynamic potential one must take into account the energy of the nonuniform polarization, the anisotropy, the elastic energy (allowing for rhombic symmetry), the linear piezoelectric effect and the quadratic electrostrictive effect. Here the solution of the variational problem is of the form

$$P_x = P_y = 0; \quad P_z = P_0 \operatorname{th} \frac{x}{\delta_2};$$

where $\delta_2 = \frac{1}{P_0}\left(\frac{\varkappa}{D}\right)^{1/3}$ and $D = \beta_3 - \frac{q_{13}^2}{c_{11}}$.

In this case the expression for the surface energy associated with the domain walls is $\sigma_2 = \frac{4}{3}[2\varkappa D]^{1/3} P_0^3$.

We have from the work of Mitsui & Furuichi[7] that at T = 0°C, $P_0 = 2.5 \cdot 10^{-7}$ coulomb/cm^2, $\beta_3 \approx 3.3 \cdot 10^{11}$ cm^4/coulomb^2 and $q_{13} \approx 90$, while at T = 20°C, $P_0 \approx 1.4 \cdot 10^{-7}$ coulomb/cm^2, $\beta_3 \approx 4 \cdot 10^{11}$ cm^4/coulomb^2 and $q_{13} \approx 150$.

Taking $\varkappa \approx d^2 \approx 10^{-4}$ cm^2 and $c_{11} = 4 \cdot 10^{-8}$ coulomb^2/cm^4, we obtain $\delta_2 \approx 1.2 \cdot 10^{-7}$ and $\sigma_2 \approx 6 \cdot 10^{-2}$ erg/cm^2 for 0°C and $\delta_2 \approx 2 \cdot 10^{-6}$ cm and $\sigma_2 \approx 1 \cdot 10^{-2}$ erg/cm^2 for 20°.

These estimates are in good agreement with the results of Mitsui & Furuichi[7], even though it must be noted that in their work electrostriction is not taken consistently into account and the deformations do not satisfy St.Venant's continuity conditions.

The cited evaluations of the domain wall surface energy in ferroelectrics make it feasible to investigate different domain configurations corresponding to the minimum thermodynamic potential.

I desire to express my sincere gratitude to V.L.Ginzburg and E.M.Lifshits for valuable advice and helpful discussions.

"P.N.Lebedev" Physical Institute
Academy of Sciences of the USSR

References

1. E.A.Little, Phys.Rev., 98, 978 (1955).
2. V.L.Ginzburg, Zhur.eksp.i teor.fiz., 15, 739 (1945).
3. G.A.Smolenskii & R.E.Pasynkov, Ibid., 24, 69 (1953).
4. V.A.Zhirnov, Ibid., 35, 1175 (1958). (Trans.Soviet Physics, - JETP, 35, (8), 822.)
5. A.F.Devonshire, Phil.Mag., 40, 1040 (1949).
6. W.J.Merz, Phys.Rev., 95, 690 (1954).
7. T.Mitsui & J.Furuichi, Phys.Rev., 90, 193 (1953).

APERIODIC OPERATION OF CAPACITORS CONTAINING A FERROELECTRIC

- N.F.Shmoilov

The practical utilization of capacitors containing ferroelectrics calls for theoretical analysis of the processes occurring in circuits with nonlinear components. In particular, it is of interest to investigate aperiodic charging and discharging of a nonlinear capacitor in different circuits.

In the case of a circuit with one nonlinear component and a fixed resistance, the conditions of equilibrium is described by

$$IR + U - U_0 = 0, \tag{1}$$

where U is the voltage on the linear component, I is the current in the circuit and U_0 is the voltage of the source. With any realistic approximation of $U = \varphi(q)$ and its inverse, we obtain differential equations for the charge and potential, which can be integrated by separation of variables (assuming a constant source voltage). Formally, the problem can be fully solved, but separation of the variables leads to implicit dependences, which hampers their investigation.

The most suitable proved to be the following approximation, used by Bessonov[1] in analyzing circuits with a nonlinear inductance

$$U = \eta(e^{\delta q} - 1). \tag{2}$$

Using (1), (2) and the appropriate formulas in Ref.2, we obtain the following expression for the variation with time of the charge on the capacitor during charging:*

$$q_3 = \frac{1}{\delta} \ln \frac{U_0 + \eta}{U_0 \exp\left[-(U_0 + \eta)\frac{\delta}{R_3} t\right] + \eta}. \tag{3}$$

From (2) and (3) we obtain the following expressions for the variation of the potential and current during charging:

$$U_3 = \frac{\eta U_0 \left\{1 - \exp\left[-(U_0 + \eta)\frac{\delta}{R_3} t\right]\right\}}{U_0 \exp\left[-(U_0 + \eta)\frac{\delta}{R_3} t\right] + \eta}; \tag{4}$$

$$I_3 = \frac{U_0}{R_3} \cdot \frac{(U_0 + \eta)\exp\left[-(U_0 + \eta)\frac{\delta}{R_3} t\right]}{U_0 \exp\left[-(U_0 + \eta)\frac{\delta}{R_3} t\right] + \eta}. \tag{5}$$

Analogously for the discharge circuit, we find

$$q_p = \frac{1}{\delta} \ln \frac{1}{1 + (e^{-\delta q_0} - 1)\exp\left[-\frac{\eta\delta}{R_p} t\right]}; \tag{6}$$

$$U_p = \frac{\eta U_0}{(U_0 + \eta)\exp\left(\frac{\eta\delta}{R_p} t\right) - U_0}; \tag{7}$$

$$I_p = \frac{\eta I_0}{(\eta + I_0 R_p)\exp\left(\frac{\eta\delta}{R_p} t\right) - I_0 R_p}. \tag{8}$$

Ferroelectrics are characterized by residual induction; to take this into account, we introduce an additional parameter into (1), namely,

---

*Here and below the subscript 3 stands for charging; the subscript p denotes discharging.

$$U = \xi(e^{\sigma\eta} - \varkappa). \tag{9}$$

This does not affect the integrability of the differential equations. Hence, performing the same operations, we obtain

$$q_3 = \frac{1}{\sigma} \ln \frac{\xi\varkappa + U_0}{[\xi(\varkappa - 1) + U_0] \exp\left[-(\xi\varkappa + U_0)\frac{\sigma}{R_3} t\right] + \xi(\xi\varkappa + U_0)}; \tag{10}$$

$$U_3 = \frac{U_0 - \varkappa[\xi(\varkappa - 1) + U_0] \exp\left[-(\xi\varkappa + U_0)\frac{\sigma}{R_3} t\right]}{\left(\varkappa - 1 + \frac{U_0}{\xi}\right) \exp\left[-(\xi\varkappa + U_0)\frac{\sigma}{R_3} t\right] + 1}; \tag{11}$$

$$I_3 = \frac{\xi\varkappa + U_0}{R_3\left\{1 + \frac{\xi}{\xi(\varkappa - 1) + U_0} \exp\left[(\xi\varkappa + U_0)\frac{\sigma}{R_3} t\right]\right\}}. \tag{12}$$

With $\varkappa = 1$, (9) transforms to (1) and, accordingly, (10), (11) and (12) become (3), (4) and (5), respectively. The discharge functions taking residual induction into account are

$$q_p = \frac{1}{\sigma} \ln \frac{\varkappa}{1 + (\varkappa e^{-\sigma q_0} - 1) \exp\left[\frac{-\xi\sigma\varkappa}{R_p} t\right]}; \tag{13}$$

$$U_p = \frac{\xi\varkappa U_0}{(U_0 + \xi\varkappa) \exp\left(\frac{\xi\varkappa\sigma}{R_p} t\right) - U_0}; \tag{14}$$

$$I_p = \frac{\varkappa\xi I_0}{(\varkappa\xi + I_0 R_p) \exp\left(\frac{\xi\varkappa\sigma}{R_p} t\right) - I_0 R_p}. \tag{15}$$

If the source voltage is reversed, i.e., if instead of U_0 we have $-U_0$, the variation of the charge will be given by

$$q = \frac{1}{\delta} \ln \frac{\eta_1^2 - U_0^2}{\eta_1(\eta_1 + U_0) - 2\eta_1 U_0 \exp\left[-(\eta_1 - U_0)\frac{\delta}{R} t\right]}. \tag{16}$$

If $q(0) = q_0$, then $q(\infty) = q(-U_0)$ and not $-q_0$. These two values differ owing to the nonsymmetry of (2).

Using (16) and (2), we obtain

$$U = \frac{\eta_1^2 - U_0^2}{\eta_1 + U_0 - 2U_0 \exp\left[-(\eta_1 - U_0)\frac{\delta}{R} t\right]} - \eta_1; \tag{17}$$

$$I = \frac{2U_0}{R} \frac{\eta_1 - U_0}{(\eta_1 + U_0) \exp\left[(\eta_1 - U_0)\frac{\delta}{R} t\right] - 2U_0}. \tag{18}$$

Let us consider the effect of a steady periodic sequence of identical polarity, square pulses on a nonlinear capacitor. In this case we determine the arbitrary constants in both integrals by matching them for the instants t_1 of the pulse and t_2 of the interpulse interval:

$$q_1 = \frac{1}{\delta} \ln \frac{(U_0 + \eta_1)\left\{1 - \exp\left[-(U_0 t_1 + \eta_1 T)\frac{\delta}{R}\right]\right\}}{U_0\left(1 - e^{-\frac{\delta}{R} t_2}\right) \exp\left[-(U_0 + \eta_1)\frac{\delta}{R} t\right] + \eta_1\left\{1 - \exp\left[-(U_0 t_1 + \eta_1 T)\frac{\delta}{R}\right]\right\}}; \tag{19}$$

$$q_2 = \frac{1}{\delta} \ln \times \frac{(U_0 + \eta_1)\left\{1 - \exp\left[-(U_0 t_1 + \eta_1 T)\frac{\delta}{R}\right]\right\}}{(U_0 + \eta_1)\left\{1 - \exp\left[-(U_0 t_1 + \eta_1 T)\frac{\delta}{R}\right]\right\} - U_0\left\{1 - \exp\left[-(U_0 + \eta_1)\frac{\delta}{R} t_1\right]\right\}\exp\left(-\frac{\eta_1 \delta}{R} t\right)}. \quad (20)$$

Eq.(19) applies during the pulse; (20) during the quiescent interval. According to Ref.3, Eq.(2) can be approximated in the form

$$q = \frac{1}{\delta}\left[\frac{U}{\eta_1} - \frac{1}{2}\left(\frac{U}{\eta_1}\right)^2 + \ldots\right]. \quad (21)$$

With $U/\eta \ll 1$ the series can be limited to the linear term; then all the dependences deduced above become the corresponding expressions for a linear capacitor. By means of the derived relationships one can investigate the influence of any parameter on the processes occurring in circuits with a nonlinear capacitance.

I desire to express my sincere gratitude and obligation to A.L.Khodakov for guidance and valuable discussions.

Rostov-on-the-Don State University &
Novocherkassk Polytechnic Institute

References

1. L.A.Bessonov, Perekhodnye protsessy v nelineinykh elektricheskikh tsepiakh so staliu (Transient processes in nonlinear electric circuits with steel), p.10, M.-L., 1951.

2. E.Kamke, Spravochnikh po obyknovennym differentsial'nykh uravneniiam (Reference on ordinary differential equations), p.53, M., 1950.

3. I.M.Ryzhik & I.S.Gradshtein, Tablitsy integralov, summ, riadov i proizvedenii (Tables of integrals, sums, series and products), p.57, M.-L., 1951.

DEPENDENCE OF THE FERROELECTRIC PROPERTIES OF PEROVSKITE TYPE CRYSTALS ON THE CHARACTER OF THE CHEMICAL BONDS

- I.N.Beliaev

1. There is general agreement that the B-O bonds in ABO_3 perovskite type crystals are partially covalent.[1-6] Nevertheless, many authors consider the perovskite type lattice to be primarily ionic and attribute the occurrence of spontaneous polarization exclusively to ionic interaction.

There can be little doubt, however, that partially covalent bonds, in addition to ionic ones, must play a significant if not decisive role in the appearance of spontaneous polarization inasmuch as spontaneous polarization (the formation of noncompensated dipoles) is a consequence of the formation of nonequivalent uncompensated chemical bonds. The formation of nonequivalent bonds is possible only in mixed ionic-covalent lattices owing to saturation and "directionality" (specific orientation) of the covalent bonds and is scarcely probable in purely ionic lattices, in view of the unsaturated and nondirectional character of ionic bonds.

2. It follows from comparison of the electric negativities of titanium and oxygen atoms (after Pauling) that even in TiO_2 the Ti-O bonds are not purely ionic: the titanium ion is not quadruply charged; the oxygen ion is not doubly charged.*

Consequently, the TiO_2 (rutile, anatase) lattice is not ionic but intermediate between ionic and molecular. For the same reason, the Ti-O bonds in rutile are not equivalent: according to Werner[7] four bonds are located in one plane and have a length of 1.944 Å, while the ionic separation for the other two is 1.988 Å.**

Unfortunately, at present it is impossible to calculate the exact degree of covalence of the Ti-O bonds in TiO_2. An approximate evaluation according to Nekrasov[9,10] and Pauling[11] yields a value of 50%. This means that in TiO_2 the titanium ion retains about two valence electrons; apparently, these are d electrons. Inasmuch as all the valence electrons of Ti participate in formation of the Ti-O bonds it may be inferred that two electrons are completely surrendered to the oxygen atoms with the resultant formation of a doubly charged positive Ti ion and two singly charged negative ions, while the two remaining titanium ion electrons form covalent bonds with the remaining unpaired electron of each oxygen ion.

In $BaTiO_3$ there are two types of bonds with oxygen, namely, Ba-O and Ti-O. The character of these bonds is presumably similar to that in the corresponding oxides. The difference between the bonds in the oxides and in $BaTiO_3$ stems exclusively from the polarization characteristics of the barium and titanium ions. Each of these ions tends to deform the bond of the other ion with oxygen, increasing its ionic character and decreasing the ionic character of its own bond with oxygen. The Ba ion, having a larger radius (1.43 Å), a higher polarizability ($2.008 \cdot 10^{-23}$ cm^3 - Ref.12) and a comparatively weak force field ($Ze/r^2 = 0.97$), does not exert a strong polarizing effect on the Ti-O bond; on the contrary, the Ti ion, when doubly charged, has a smaller radius (0.76 Å) and a comparatively strong force field ($Ze/r^2 = 3.45$) and therefore exerts an appreciably stronger polarizing the ionic character of its own Ti-O bond. As a result the Ti ion in $BaTiO_3$ has a smaller effective charge than in TiO_2, while the O ion has a somewhat larger charge.***

---

*This means that the titanium ion does not give up all four of its valence electrons to the oxygen in forming the ionic bonds; part of the valence electrons "retained" by the titanium ion participates in formation of covalent bonds.

**According to Ref.8, in rutile the Ti-O ionic distances are 1.937 Å for four of the bonds and 1.964 Å for the other two.

***(See footnote bottom of next page).

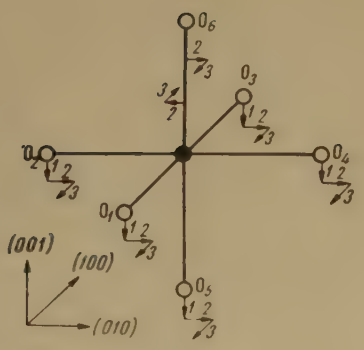

Fig.1

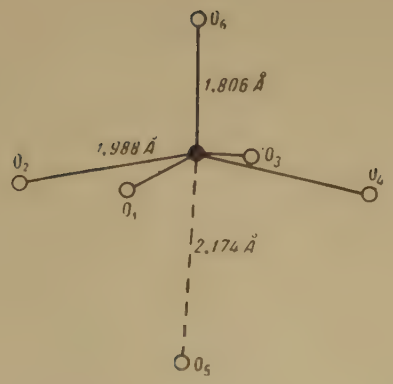

Fig. 2

Fig.1. Arrangement of titanium and oxygen ions in cubic $BaTiO_3$. (The arrows indicate directions of ionic displacements.)
Fig.2. Arrangement of titanium and oxygen ions in tetragonal $BaTiO_3$.

Thus in $BaTiO_3$ the titanium ion is not more than doubly charged and has not less than two electrons participating in the formation of covalent bonds. Accordingly, the oxygen ion, given the double positive charge on the barium ions, is somewhat less than singly charged. In $PbTiO_3$, owing to the appreciably greater polarizability of Pb as compared with Ba ions, the Ti-O bonds are more covalent than in $BaTiO_3$.[14,15]

3. At temperatures above 120°C the Ti ions in cubic $BaTiO_3$ are located at the centers of the oxygen octahedra (Fig.1). All Ti-O distances are equal, all the O-Ti-O valence angles are identical and equal to 90° and all the Ti-O-Ti valence angles are also identical and equal to 180°. Directionality of the covalent bonds is not evinced. All the covalent Ti-O bonds are uniformly distributed between the six O ions surrounding the Ti ion. Below 120° one of the covalent Ti-O bonds begins to evince specific orientation; as a result the Ti ion is displaced towards one of the six O ions and this O ion is displaced in the opposite direction. The covalent parts of the Ti-O bonds are redistributed so that the Ti-O bonds as a whole become nonequivalent and are not mutually compensated: the crystal transforms from cubic to tetragonal symmetry (Fig.2). As a result of the rearrangement, in tetragonal $BaTiO_3$ there is a noticeable separation of TiO_5 groups in the form of rectangular pyramids[2] which form continuous layers on the planes of the 1-4 oxygen ions and are linked by the 5 and 6 oxygen and barium ions (Fig.3).

The directionality of the second covalent Ti-O bond becomes manifest at ~5°C; that of the third at -70°C. As a result, the titanium and oxygen ions undergo new displacements and there occurs further redistribution of the covalent part of the Ti-O bonds and valence angles. From tetragonal the crystal becomes orthorhombic (Fig.4) and then rhombohedral (Fig.5). The new redistribution of the bonds leads to appreciable separation in the orthorhombic crystals of TiO_4 groups having the form of tetrahedra, connected (by the 1 and 2 oxygen ions) into chains extending parallel to the direction of the 1 and 2 oxygens. In the rhombohedral phase the bond rearrangements lead to isolation of TiO_3 groups in the form of trihedral pyramids (Fig.5), similar to the CO_3 groups in calcite.

***Our inference regarding the significantly covalent character of the Ti-O bonds in $BaTiO_3$ is substantiated by the theoretical calculations by Känzig[13] and the experimental data of Blokhin[14,15]. (See previous page.)

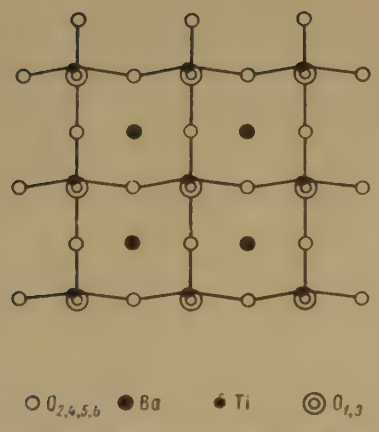

Fig.3. Projection of the lattice of tetragonal $BaTiO_3$ on the O_2-O_6-O_4-O_5 plane.

It follows, therefore, that spontaneous polarization and phase transitions in $BaTiO_3$ are connected with the tendency of the titanium and oxygen ions to acquire directionality of the covalent bonds peculiar to them. There does not, apparently, occur any noticeable enhancement of the covalence of the bonds at the Curie point but only a redistribution of the covalent bonds between the oxygen ions. The presence of covalent bonds, in addition to ionic, as a necessary condition for the occurrence of spontaneous polarization does not conflict with the conditions for spontaneous polarization formulated earlier by Vul[16,17], Skanavi[18], Smolenskii[1], Matthias[19] and others. Nonequivalent, uncompensated bonds in an ABO_3 type lattice, in the presence of covalent bonds, are possible only in structures with an infinite three-dimensional lattice (perovskite, ilmenite and pyrochlore), wherein the framework of oxygen

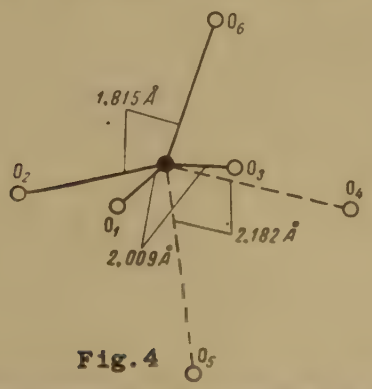

Fig.4

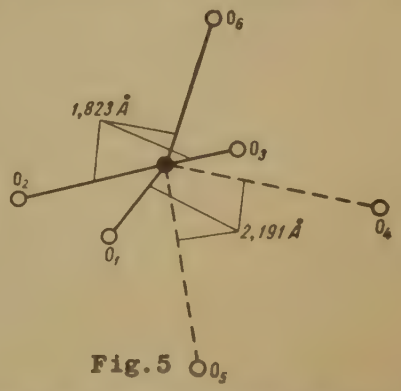

Fig.5

Fig.4. Arrangement of titanium and oxygen ions in orthorhombic $BaTiO_3$.
Fig.5. Arrangement of titanium and oxygen ions in rhombohedral (trigonal) $BaTiO_3$.

octahedra, linked by rigid ionic-covalent ...O-Ti-O... bonds, hinders compensation of the nonequivalent bonds.

At present it is impossible to evaluate quantitatively the degree of covalence of the B-O bonds necessary for the rise of spontaneous polarization. Apparently, the degree of covalence of the B-O bonds must be such that the states with specifically directed covalent bonds and with nondirected bonds would be energetically close; then thermal motion of the ions may be sufficient to disturb the directionality of the bonds. However, taking the degree of covalence of the Ti-O bond in $BaTiO_3$ as a sort of "standard", we can qualitatively evaluate the influence of strengthening or weakening of the covalence of the B-O bond on the ferroelectric properties of crystals of the ABO_3 type. It will be obvious from what has been said above that the higher the degree of covalence of the B-O bond, the more difficult it is to overcome the specific directionality of the covalent bonds and the higher, consequently, must be the transition temperature from the ferroelectric to the nonferroelectric state and hence the wider the ferroelectric temperature interval. In principle, there may even exist ferroelectrics in which the transition to the nonferroelectric state lies above their melting point. Obviously, the contrary also holds true: the lower the degree of covalence, the lower will be the temperature of the ferroelectric-nonferroelectric transition and the narrower the ferroelectric temperature interval. At the limit, these

properties will disappear inasmuch as the covalence of the B-O bond will be so minor that its directionality will not be evinced.

4. In the light of what has been said above, one can readily explain the absence of ferroelectricity in calcium and magnesium titanate and the zirconates of alkali earth metals, the increase in the number of ferro- and antiferroelectrics among the niobates and tantalates, as compared with titanates and zirconates, and, finally, the absence of ferroelectrics among molybdates, tungstates and chromates. All this depends exclusively on the relation of the polarization characteristics of the A and B ions.*

In the series of alkali-earth metals, the highest degree of polarization is exhibited by barium; hence in the series of titanates of the alkali metals the highest degree of covalence of the Ti-O bonds obtains in $BaTiO_3$, and, consequently, $BaTiO_3$ has the widest ferroelectric temperature interval. Replacement of the barium ion by the even more readily polarized lead ion leads to enhancement of the covalence of the Ti-O bond (in $PbTiO_3$ as compared to $BaTiO_3$) and, consequently, the temperature range for the existence of ferroelectric properties is extended accordingly (to 500°). The absence of ferroelectrics among the zirconates and hafnates of the alkali-earth metals is connected with the appreciable weakening of the covalence of the Zr-O (or Hf-O) bonds as compared with the Ti-O bonds in barium titanate. This also explains why the Curie points of lead zirconate and hafnate (235 and 215°, respectively[21]) are lower than the Curie point of lead titanate. The greater number of ferroelectrics among the niobates and tantalates is connected with the increase in the degree of covalence of the B-O bonds as compared with the Ti-O bonds in titanates.[2] In view of this it would seem that the number of ferro- and antiferroelectrics among the molybdates and tungstates should be even greater, since going from the compounds of Group V to Group VI is accompanied by further enhancement of the degree of covalence of the B-O bonds[22]. Actually, however, there is not a single ferroelectric among the molybdates and tungstates. This is due to the fact that in these compounds the degree of covalence of the Mo-O and W-O bonds is so high that the MeO_4 (Me = Mo, W or Cr) tetrahedra, forming owing to the directionality of the covalent bonds, are incorporated into the lattice as single entities. For the same reason there are no ferroelectrics among the vanadates and chromates.

Thus the increased degree of covalence of the B-O bond as compared with that of the Ti-O bond in $BaTiO_3$ at first leads to widening of the temperature range of existence of ferroelectricity; this widening continues as long as the coordination lattice of oxygen octahedra is retained. Further increase in the degree of covalence of the B-O bond, however, leads to disturbance of the oxygen octahedra framework, separation of BO_4 groups and the disappearance of ferroelectric properties.

5. We conclude therefore that a necessary conditions for the occurrence of spontaneous polarization in ABO_3 type crystals is the presence of mixed ionic-covalent B-O bonds. Only in the presence of covalent B-O bonds (in addition to ionic ones) can there form nonequivalent bonds not compensating each other and, consequently, uncompensated dipole moments. However, the presence of covalent bonds although a necessary condition is not the sole one for ferroelectricity: in addition, the crystal lattice must consist of an infinite three-dimensional framework of oxygen octahedra linked by rigid ionic-covalent bonds that hinder the mutual compensation of the nonequivalent bonds, and the B ion must be formed from an

---

*Inasmuch as WO_3 is reported to be a ferroelectric[20], apparently the presence of an A ion is not an essential condition for the occurrence of spontaneous polarization; but WO_3 is the only ferroelectric among BO_x compounds. Hence it may be assumed that the occurrence of spontaneous polarization does depend to an appreciable extent on the nature of the A ion.

atom having not less than four valence electrons of which not less than one and not more than three form covalent bonds. If these conditions are not fulfilled the covalent bonding will either be so weak that its directionality will not be evinced, or it will be so strong that the directionality will predominate in the formation of the crystal lattice. The A ion, depending on the nature of the B ion, must have polarization characteristics that will appropriately strengthen or weaken the covalent character of the B-O bond.

Conclusions

A. We have shown for the case of $BaTiO_3$ that nonequivalent, noncompensated chemical bonds (spontaneous polarization) can occur only in lattices with an infinite oxygen octahedra framework, owing to the tendency of the titanium and oxygen ions to form specifically directed covalent bonds.

B. Increase in the degree of covalence of the B-O bond in ABO_3 type compounds (as compared with the covalence of the Ti-O bond in $BaTiO_3$) through replacement of the Ti ions by other ions leads to widening of the temperature interval in which the substance exhibits ferroelectric properties, and, vice versa, weakening of the covalence results in narrowing of the ferroelectric interval.

C. The role of the A ion in ABO_3 type compounds reduces to regulation of the degree of covalence of the B-O bonds.

D. The analyzed dependence of the ferroelectric properties on the character of the chemical bonds may serve as a criterion in the search for new ferro- and antiferroelectric materials.

Rostov-on-the-Don State University

References

1. G.A.Smolenskii, Zhur.tekh.fiz., 20, 137 (1950); Doklady AN SSSR, 70, 405 (1950).
2. H.D.Megaw, Acta crystallogr., 5, 739 (1952).
3. H.D.Megaw, Acta crystallogr., 7, 187 (1954).
4. P.Vousden, Acta crystallogr., 4, 545 (1951).
5. Iu.N.Venevtsev & G.S.Zhdanov, Izv.AN SSSR, Ser.fiz., 21, 275 (1957). (Trans.Bulletin 21, No.2, 277.)
6. W.P.Meson & B.T.Matthias, Phys.Rev., 74, 1622 (1948).
7. B.Werner, Naturwissenschaften, 42, 10, 295 (1955).
8. T.DonCromer & K.Herrington, J.Amer.Chem.Soc., 77, 8, 4708 (1955).
9. B.V.Nekrasov, Zhur.obshch.Khim., 16, 983 (1946).
10. B.V.Nekrasov, Ibid., 16, 1797 (1946).
11. A.F.Wells, Structural Inorganic Chemistry (Cited in Russian trans.).
12. A.A.Grinberg, Vvedenie v khimiiu kompleksnykh soedinenii (Introductions to the chemistry of complex compounds), p.258, M., 1951.
13. W.Känzig, Helv.phys.acta, 24, 189 (1954).
14. M.A.Blokhin, Doklady AN SSSR, 95, 965 (1954).
15. M.A.Blokhin, Ibid., 95, 1165 (1954).
16. B.M.Vul, Obshch.sobr.(Gen.Coll.)USSR Ac.of Sci., 15-16 Jan., p.111, Pub. USSR Ac.of Sci., 1946.
17. B.M.Vul, Elektrichestvo, No.3, 12 (1946).
18. G.I.Skanavi, Fizika dielektrikov (Physics of dielectrics), p.177, M.1949.
19. B.T.Matthias, Helv.phys.acta, 23, 167 (1950).
20. G.Shirane & R.Pepinsky, Phys.Rev., 91, 812 (1953).
21. B.T.Matthias, Phys.Rev., 76, 430 (1949).
22. M.A.Pchelkina & A.V.Lapitskii, Zhur.obshch.khim., 24, 1101 (1954). (Trans. J.General Chemistry.)

ON THE SEARCH FOR NEW FERROELECTRIC MATERIALS

- I.S.Zheludev & A.S.Sonin

A number of new ferroelectrics have been discovered in recent years. Substances that have been found to exhibit ferroelectric behavior include lead metaniobate and metatantalate, strontium pyrotantalate, guanidine aluminum sulfate hexahydrate (GASH), some alums, ammonium sulfate[1], tri-glycine sulfate[2], tri-glycine fluoberyllate[3], thiourea[4], ammonium monochloracetate[5], colemanite[6], glycine silver nitrate[7], and dicalcium strontium propionate[8].

The Curie temperatures of only a few of the enumerated substances lie above room temperature (an important factor where practical applications are concerned): these are lead metaniobate (T_C = 570°), lead metatantalate (T_C = 260°), GASH (T_C = 100°), tri-glycine sulfate (T_C = 49°) and tri-glycine fluoberyllate (T_C = 70°). Hence both from the standpoint of electronic engineering and that of science, there is urgent need to search for new substances possessing ferroelectric properties.

Efficient search for new ferroelectrics can obviously be carried out only on the basis of certain criteria indicating that spontaneous polarization can develop in the material. Such criteria may be established through analysis of the characteristic properties of known ferroelectrics. An important indication for classifying a substance as a possible ferroelectric is the presence in it of domain structure. Another important indication of ferroelectric properties stems from the fact that substances possessing these properties exhibit phase transitions of the first or second order.* There are other indications that may serve as specific criteria for "oxy-octahedral type" ferroelectrics (ferroelectrics containing oxygen octahedra) and ferroelectrics with hydrogen bonds.

For "oxy-octahedral" ferroelectrics such an indication is the crystallochemical Smolenskii[9]-Matthias[10] criterion. From this criterion it follows that "oxy-octahedral" ferroelectrics should be sought among substances crystallizing in structures in which the comparitively small cations, situated in the oxygen octahedra, have the electronic configuration of a noble gas after removal of the s- and d-electrons; ions of this type form from atoms with an unfilled next to the last shell. Using this crystallochemical criterion in his work, Smolenskii discovered a number of new ferroelectrics of the "oxy-octahedral type" (see, for example, Ref.1).

The situation is considerably more complicated when it comes to ferroelectrics containing hydrogen. Here it is more difficult to formulate the essential criteria due to the complexity and diversity of the chemical composition and structure of compounds in this category and owing to the fact that the nature of the mechanism responsible for the onset of spontaneous polarization is still obscure[11]. Obviously, one can simply say that hydrogen-containing

---

*At present there is only one ferroelectric - GASH - in which a phase transition has not been observed. Presumably, the phase transition in this compound should occur above its decomposition temperature (90-100°C).

ferroelectrics are characterized by the presence of O—H···O, N—H···F and particularly N—H···O bonds[2], the location of which in the structure favors the rise of spontaneous polarization.

Ferroelectrics with hydrogen bonds contain acentric configurations of the following type:

a) tetrahedral: $(NH_4)^+$, $(SO_4)^{2-}$, $(SeO_4)^{2-}$, $(PO_4)^{3-}$, $(BeF_4)^{2-}$,
b) bent chain: (CH_2NH_2COOH), $(C_4H_4O_6)^{2-}$, $(CH_2ClCO_2)^-$, or
c) plane trigonal: $(NO_3)^-$, $[C(NH_2)_3]^+$.

Apparently, atomic configurations of the first two types are determining for such ferroelectrics. Hereinafter we shall refer to the above indications for hydrogen-containing ferroelectrics as the crystallochemical criterion for ferroelectrics with hydrogen bonds.

It would obviously be of interest to find a criterion or test common for all ferroelectrics, indicating the potential appearance of spontaneous polarization. Recently one of us in collaboration with Shuvalov[12,13] examined the change in point symmetry of crystals, associated with the rise of spontaneous polarization or a change in the direction of polarization. Analysis shows that the morphological symmetry of each (final) domain differs from the symmetry which the crystal (or domain) had prior to the phase transition. This is due to the fact that the structural changes incident to a ferroelectric phase transition in a crystal are accompanied by a change of its point symmetry. Careful examination of the nature of the changes occurring in ferroelectrics incident to phase transitions leads to the conclusion that the changes in the symmetry of the crystal (or domain) are governed by certain regularities, which allow of predicting, for example, the change in the point symmetry of a crystal belonging to a given class, when and if the crystal undergoes a ferroelectric phase transition.

The principal effect characterizing phase transitions in ferroelectrics is the appearance (or disappearance) of spontaneous polarization or change in the direction of spontaneous polarization in the crystal. Spontaneous polarization is described by the polar vector P_s having the symmetry $\infty \cdot m$. The change in symmetry incident to a ferroelectric phase transition may be found from the Curie symmetry principle. Application of this principle shows that the new symmetry of the crystal in the case of onset in it of spontaneous polarization can be defined as the highest common subgroup of the symmetry group of the crystallographic class to which the crystal in question belongs in the nonferroelectric phase and of the symmetry group of the polar vector P_s with the given arrangement of the symmetry elements of both groups. As was noted in Ref.13, the changes in symmetry of all known ferroelectrics incident to phase transitions is characterized by the regularity described above. The changes in symmetry of some known ferroelectric incident to phase transitions are listed in Table 1. This table supplements the data given in Ref.13. For the substances for which the point groups after the phase transition have not been determined, we give the most probable (in our opinion) point symmetry groups in parentheses.

In view of what has been said above, it may be inferred that for all dielectrics an indication of ferroelectric phase transitions is a change in point symmetry such that the transformed material in the case of appearance of domains will belong to a symmetry group that is a subgroup of the $\infty \cdot m$ symmetry group, i.e.,

Table 1

Changes in point symmetry incident to phase transition in known ferroelectrics

Compound	Formula	Point symmetry of crystal or domain prior to phase transition	T_{trans}, °C	Point symmetry of domain after phase transition
Barium titanate	$BaTiO_3$	$\bar{6}/4$	120	$4 \cdot m$
			5	$2 \cdot m$
			−70	$3 \cdot m$
Rochelle salt	$KNaC_4H_4O_6 \cdot 4H_2O$	2 : 2	24	2
		2	−18	2 : 2
Potassium orthophosphate	KH_2PO_4	$\bar{4} \cdot m$	−153	$2 \cdot m$
Potassium orthoarsenate	KH_2AsO_4	$\bar{4} \cdot m$	−182	$2 \cdot m$
Ammonium monochloroacetate	$NH_4O_2ClCH_2$	$2 : m$	−150	2
Tri-glycine sulfate	$(CH_2NH_2COOH)_3 \cdot H_2SO_4$	$2 : m$	49	2
Tri-glycine fluoberyllate	$(CH_2NH_2COOH)_3 \cdot H_2BeF_4$	$2 : m$	70	2
Ammonium sulfate	$(NH_4)_2SO_4$	$m \cdot 2 : m$	−50	(2)
Ammonium cadmium sulfate	$(NH_4)_2Cd_2(SO_4)_3$	3/2	−190	(3)
Alums	$M^I[M^{III}(SO_4)_2] \cdot 12H_2O$	$\bar{6}/2$	∼−220	(2)
Colemanite	$Ca_2B_6O_{11} \cdot 5H_2O$	$2 : m$	−6	(2)
Glycine silver nitrate	$(CH_2NH_2COOH) \cdot AgNO_3$	$2 : m$	−55	(2)
Thiourea	CH_4N_2S	$m \cdot 2 : m$	−105	$(2 \cdot m)$

will belong to one of the pyroelectric classes. We shall call this indication the crystallographic criterion for spontaneous polarization.

Accordingly, we checked through the literature to find substances in which the change in symmetry incident to phase transitions satisfies this spontaneous polarization criterion (Table 2). It would be expedient to test these substances for ferroelectric behavior.

It should be emphasized that the above described crystallographic criteria for hydrogen-containing ferroelectrics and for the rise of spontaneous polarization are necessary but not per se sufficient indications. Although they should facilitate the search for new ferroelectrics, they should not be interpreted as unambiguous theoretical indications of ferroelectric behavior. Hence it is necessary to pursue further experimental investigations of the dielectric properties listed in Table 2 and to continue the search for the necessary and sufficient conditions for the existence of spontaneous polarization in crystals.

Table 2

Changes in point symmetry incident to phase transitions

Compound	Formula	Point sym. of cryst. or domain prior to phase trans.	T_{trans}, °C	Point symmetry of domain after phase transition
Rubidium nitrate	$RbNO_3$	$\bar{6}/4$	164	$3 \cdot m$
Cesium nitrate	$CsNO_3$	$\bar{6}/4$	154	$3 \cdot m$
Sodium nitrate	$NaNO_2$	$m \cdot 2 : m$	158	$2 \cdot m$
Silver cyanide	$AgCN$	$\bar{6}/4$	190	$3 \cdot m$
Copper sulfide	Cu_2S	$m \cdot 6 : m$	103	$2 \cdot m$
Baracite	$Mg_3B_7O_{13}Cl$	$3/\bar{4}$	265	$2 \cdot m$

We desire to express our gratitude to L.A.Rusakov, I.S.Rez and V.V.Gladkii for assistance in the work.

Institute of Crystallography of the
Academy of Sciences of the USSR;
TsNILP of the Committee on Radioelectronics
under the Soviet of Ministers of the USSR

References

1. G.A.Smolenskii, Usp.fiz.nauk, 62, 41 (1957).
2. B.T.Matthias, C.E.Miller & J.P.Remeika, Phys.Rev., 104, 849 (1956).
3. S.Hoshino, B.T.Matthias, F.Jona & R.Pepinsky, Phys.Rev., 107, 1255 (1957).
4. A.L.Solomon, Phys.Rev., 104, 1191 (1956).
5. R.Pepinsky, Y.Okaya & B.T.Matthias, Acta Crystallogr., 10, 600 (1957).
6. A.C.Chynoweth, Acta Crystallogr., 10, 511 (1957).
7. R.Pepinsky, Y.Okaya, D.E.Eastmann & B.T.Matthias, Phys.Rev., 107, 1538 (1957).
8. B.T.Matthias & J.P.Remeika, Phys.Rev., 107, 1727 (1957).
9. G.A.Smolenskii & N.V.Kozhevnikova, Doklady AN SSSR, 76, 519 (1951).
10. B.T.Matthias, Phys.Rev., 75, 1771 (1949).
11. H.D.Megaw, Acta Crystallogr., 7, 187 (1954).
12. I.S.Zheludev & L.A.Shuvalov, Izv., AN SSSR, Ser.fiz., 21, 264 (1957). (Trans. Bulletin, 21, No.2, 266.)
13. I.S.Zheludev & L.A.Shuvalov, Kristallografiia, 1, 681 (1956).

PREPARATION AND THE DIELECTRIC PROPERTIES OF SOME BARIUM TITANATE-STANATE SOLID-SOLUTION SINGLE CRYSTALS

- A.L.Khodakov & M.L.Sholokhovich

Among ferroelectric solid solutions the $BaTiO_3$-$BaSnO_3$ system is of particular interest. It was established in a number of investigations[1-4], devoted to the properties of polycrystalline barium titanate-stanate solid solutions, that this system is characterized by a strong variation of the dielectric constant ϵ with the applied electric field. For the composition Ba(90% Ti, 10% Sn)SnO_3 the value of ϵ exceeds 20,000 in relatively weak fields (< 2 kv/cm).

By doping barium titanate with appropriate additives Verbitskaia obtained ferroelectrics - Varikonds[5,6] - with highly pronounced nonlinear characteristics. The nonlinearity coefficient for Varikonds is $\epsilon_m/\epsilon_o > 9$ (ϵ_m is the maximum value of the dielectric constant and ϵ_o is the weak field value), the maximum value of the coefficient being attained in a field of 0.5 kv/cm. $BaTiO_3$-$BaSnO_3$ solid solutions also exhibit strong dependence of the reversible dielectric constant on the biasing dc field.

In view of these properties, such ferroelectrics are already finding special applications in electronic engineering; hence we felt that the preparation of $BaTiO_3$-$BaSnO_3$ single crystals would be not only of scientific interest but also of potential practical value.

Earlier[7-9] we obtained single crystals of (Ba-Sr)TiO_3 and (Ba-Pb)TiO_3 solid solutions; our first attempts to grow $BaTiO_3$-$BaSnO_3$ single crystals showed, however, that this is considerably more difficult.

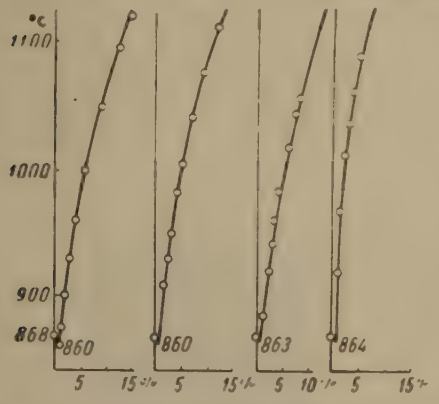

Fig. 1. Crystallization curves

By way of solvent for obtaining single crystals of isomorphous mixtures of $BaTiO_3$ and $BaSnO_3$, we used a solution of potassium fluoride. This choice was based on our investigation of crystallization in the K_2F_2-$BaTiO_3$-$BaSnO_3$ system, which indicated that in this system there is formed a continuous series of $BaTiO_3$-$BaSnO_3$ solid solutions.

A number of crystallization curves for the system are shown in Fig.1. The presence of isomorphous mixtures of $BaTiO_3$ and $BaSnO_3$ in solidified melts with K_2F_2 is substantiated by the results of x-ray diffraction studies carried out by E.G.Fesenko.

We carried out the two series of experiments: in the first series, the initial materials were various mixtures of $BaTiO_3$ and SnO_2, previously subjected to heating at 1200°; in the second series, the initial materials were previously prepared polycrystalline $BaTiO_3$-$BaSnO_3$ solid solutions of different relative concentrations.

The crystals were grown in a covered platinum crucible in a Silit resistance furnace. In all cases 0.01% by weight of Fe_2O_3 were added to the initial mixture. The grown crystals were washed with hot water slightly acidified with HNO_3. In the present report we shall describe only two batches of crystals, the properties of which were investigated in greatest detail. Other batches of crystals have been prepared and their properties are now being studied.

The principal data on the two batches are given in Table 1. It will be evi- from the spectroscopic data for the crystals of Batch 2 that the substitution reaction in $BaTiO_3$ and the formation of the solid solutions do not proceed readily. This was also noted earlier in investigating the melting-point diagram of the K_2F_2-$BaTiO_3$-SnO_2 system. It was established that complete solution does not occur in mixtures of $BaTiO_3$ and SnO_2 containing over 10% SnO_2*. Spectroscopic

*The percentages throughout are molecular.

Table 1

Data on the crystals of batches 1 and 2

Initial melt	Heat treatment	Spectroscopic data	Appearance of crystals
	Batch 1		
82% K_2F_2 + 18%(95% $BaTiO_3$ + 5% SnO_2)	Heating to 1350° Holding at heat for 8 hours Cooling to 860° at 20°/hour	95% BaTiO + 5% $BaSnO_3$	Light yellow transparent crystals, mostly small. Shape imperfect. Some in the form of trihedral plates and cubes 2-2.5 mm on edge (Fig.2).
	Batch 2		
82% K_2F_2 + 18%(90% $BaTiO_3$ + 10% SnO_2)	Heating to 1350° Holding at heat for 12 hours Cooling at 50°/hour	Composition of crystals obtained in different parts of the crucible varied: a) 95% $BaTiO_3$ + 5% $BaSnO_3$ b) 90% $BaTiO_3$ + 10% $BaSnO_3$ c) 89% $BaTiO_3$ + 11% $BaSnO_3$	Light yellow transparent crystals in the form of cubes 1.5 mm on edge.

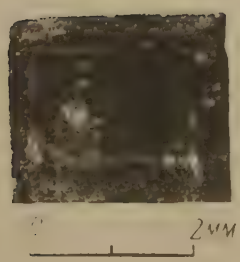

Fig.2. Typical crystal of Batch 1.

analysis showed that the insoluble part of the mixture is tin dioxide. Apparently, 10-11% is the maximum amount of SnO_2 that can replace TiO_2 in $BaTiO_3$ with subsequent formation of a $BaTiO_3$-$BaSnO_3$ solid solution.

We are continuing our investigation of the SnO_2 substitution reaction, but even the available data indicates that in order to obtain single crystals of $BaTiO_3$-$BaSnO_3$ containing more than 10-11% $BaSnO_3$ one must add $BaCO_3$ in stoichiometric proportions with respect to SnO_2 to the $BaTiO_3$ + SnO_2 mixture.

The dielectric properties of the crystals were measured with a Q-meter at $f = 10^6$ cps, with an IEN-2 bridge at 10^3 cps and with an unbalanced bridge at 50 cps. The reversible dielectric constant was measured in an ac field of 25 v/cm and a frequency of 10^6 cps. The conventional oscillographic procedure was employed.

The solid solution crystals were subjected to heat treatment which consisted of heating at 1200° for 2 hours. The crystals became somewhat darker as a result of heat treatment. (Hereinafter we shall designate untreated crystals by A and heat treated crystals by B.) The desirability of such heating, which improves the ferroelectric properties, was established earlier for a number of single crystals of other solid solutions of ferroelectric materials.[7-10]

Before heat treatment crystals of Batch 1 have two dielectric constant peaks: one at +18°, the other at -7° (Fig.3). After heat treatment, the first maximum appears at 82° which agrees with the Curie point of the initial $BaTiO_3$-$BaSnO_3$

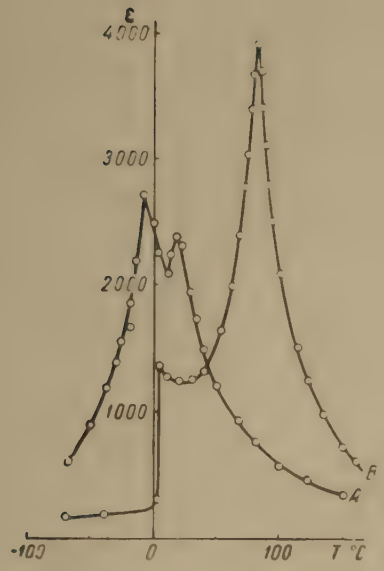

Fig.3. Temperature dependence of the dielectric constant ε of crystals of Batch 1. A - crystal not subjected to heat treatment and B - after heat treatment. $f = 10^6$ cps; E = = 25 v/cm.

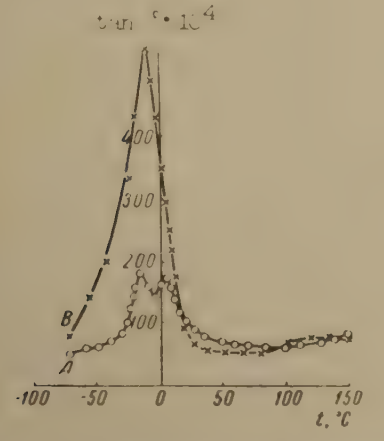

Fig.4. Temperature dependence of tan δ for crystals of Batch 1. $f = 10^6$ cps; E = 25 v/cm.

Table 2

Temperatures (°C) of the maxima of ε in crystals and the ceramic

	1st maximum	2nd maximum	3rd maximum
Crystals A	18	-7	
Crystals B	82	6	
Polycrystalline ceramic	83	37	2

ceramic and with the data in the literature; the second peak appears at 2°. It may be assumed that the observed anomalies are due to mechanical stresses developing in the process of crystallization, owing to unfavorable temperature conditions. This leads to reduction of the tetragonality of the crystal lattice and, therefore, to displacement of the phase transition point. With heat treatment the mechanical stresses are reduced, the tetragonality of the lattice is increased and the crystal becomes "normal". It must be noted, however, that heating does not always fully "remove" the lattice distortions. In this case the temperature of the upper phase transition corresponds to that characteristic of the given composition. In the case of many crystals, despite heat treatment, there persists a small but noticeable growth of ε at the Curie point; these crystals also exhibit a weaker (compared with the initial ceramic) field dependence of the dielectric constant. Heating at higher temperatures (1300--1400°) did not yield better results. Crystals of Batch 1 not subjected to heat treatment exhibit the usual hysteresis loops at temperatures not exceeding the ϵ_{max} temperature by more than 50°. This is apparently connected with the fact that in these crystals with a distorted lattice, in the vicinity of the phase transition temperature, the tetragonality of the lattice increases under the influence of an electric field of a few kv/cm and, consequently, the phase transition temperature is shifted to the side of higher temperatures. Apparently, the electric field partially "compensates" the mechanical stresses and in this sense has an effect analogous to heat treatment.

The temperature of the lower transition point in crystals of Batch 1 appears to be somewhat abnormal. The temperatures of the dielectric constant maxima of our crystals and of $BaTiO_3$-$BaSnO_3$ are listed in Table 2. Whereas the temperatures of the upper phase transition in the ceramic and in crystals subjected to heat treatment are virtually identical, the temperatures of the lower maxima differ by more than 30°.

Possibly the unusual position (temperature) of the ε maxima for this composition is connected with incomplete relief of the mechanical stresses during heat treatment, so that the temperature range of the tetragonal region is somewhat extended.

The dielectric loss, as will be evident from Fig.4, is not high; actually it is lower than in polycrystalline specimens of the same composition.

The crystals of Batch 2 containing 5% $BaSnO_3$ exhibit dielectric properties very similar to those of the crystals of Batch 1. They also showed a significant improvement of their ferroelectric properties after heat treatments at 1200°. The dielectric parameters of Batch 2 crystals containing 10-11% $BaSnO_3$ have not yet been measured. Measurements on these crystals are rendered difficult by their small size.

In conclusion I desire to thank N.S.Novosil'tsev for his interest in the work.

Scientific Research Physical-Mathematical Institute at
Rostov-on-the-Don University

References

1. G.A.Smolenskii & K.I.Rozgachev, Doklady AN SSSR, 79, 53 (1951).
2. G.A.Smolenskii & V.A.Iusupov, Zhur.tekh.fiz., 24, 1375 (1954).
3. S.Nomura, J.Phys.Soc.Japan, 10, 112 (1955).
4. N.S.Novosil'tsev & A.L.Khodakov, Zhur.tekh.fiz., 26, 310 (1956). (Trans. Soviet Physics - Tech.Phys.)
5. T.N.Verbitskaia, Doklady AN SSSR, 100, 29 (1955).
6. T.N.Verbitskaia, Izvestiia, Tomsk Polytechnic Inst., 91, 355 (1956).
7. A.L.Khodakov, M.L.Sholokhovich, E.G.Fesenko & O.P.Kramarov, Doklady AN SSSR, 108, 825 (1956). (Trans.Soviet Phys. - Doklady.)
8. M.L.Sholokhovich, E.G.Fesenko, O.P.Kramarov & A.L.Khodakov, Doklady AN SSSR, 111, 1025 (1956). (Trans.Soviet Phys. - Doklady.)
9. A.L.Khodakov, M.L.Sholokhovich, E.G.Fesenko & O.P.Kramarov, Rost kristallov (Growth of Crystals), p. 294, M., 1957.
10. N.S.Novosil'tsev & A.L.Khodakov, Doklady AN SSSR, 85, 1263 (1952).

INVESTIGATION OF THE $PbO-BaO-B_2O_3-TiO_2$ SYSTEM

- M.L.Sholokhovich & V.I.Varicheva

The choice of medium (solvent) for growing lead-containing ferroelectric single crystals from the melt is complicated by the fact that many substances in the fused state tend to lower the stability of the melt.[1] The choice of solvents becomes even more difficult when it comes to obtaining single crystals of ferroelectric isomorphous mixtures with lead compounds. In this case we have the additional difficulty that many solvents reduce the strength and stability of the solid solutions and lead to their dissociation into components.

An earlier search[2] for solvents suitable for obtaining $PbTiO_3$ single crystals indicated the suitability of melts of $PbO-B_2O_3-TiO_2$ for this purpose. From this melt there form light, transparent, well-defined crystals at relatively moderate temperatures (900-950°).

The purpose of the present work was to investigate the interaction of lead and barium borates with lead and barium titanates with a view to determining the influence of the borates on the stability of barium and lead titanate solid solutions and evaluating the possibility of obtaining single crystals of this mixed titanate from the given melt.

The $PbO-TiO_2-B_2O_3-BaO$ system in the molten state is a complex four-component system and may be represented graphically by a tetrahedron. In this report we give data on the surface of crystallization of the $[50\%\ PbO + 50\%\ B_2O_3]-PbTiO_3-Ba(BO_2)_2-BaTiO_3$ profile of this tetrahedron. The investigation was carried out in platinum crucibles by the visual-polythermal procedure. As initial materials we used chemically pure B_2O_3 and $BaCO_3$; reagent grade pure PbO and reagent grade pure TiO_2 further purified by boiling in 10% HCl.

Specifically, we investigated the side surfaces and 24 internal sections of the tetrahedral diagram. The location of the sections is indicated in Fig.1; the experimental data for the different sections and sides are shown in Figs.2,3 & 4. The side $[50\%\ PbO + 50\%\ B_2O_3]-PbTiO_3$* (Fig.3, curve II) presents a cross section of the $PbO-TiO_2-B_2O_3$ system[2] which is a side face of the tetrahedron. The fusibility diagram of this surface consists of a short branch of a glass-like phase (exact composition not established) and a branch characterizing well crystallizing lead titanate. On the $[50\%\ PbO + 50\%\ B_2O_3]\rightarrow Ba(BO_2)_2$ side (curve I), owing to vitrification, we succeeded in investigating only the branch of crystallization of $Ba(BO_2)_2$. On the $Ba(BO_2)_2-BaTiO_3$ face (curve III), in addition to the component lines, there is also a branch corresponding to crystallization of a phase, the composition of which we have not yet established and which we therefore provisionally designate as phase A. Owing to the high melting point and the instability of $PbTiO_3$, we did not investigate the fusibility of the $BaTiO_3-PbTiO_3$ system; however, a number of investigators[3-6] have demonstrated the formation of a continuous series of isomorphous mixtures in the solid phases of this system.

The crystallization surface of the $[50\%\ PbO + 50\%\ B_2O_3]-BaTiO_3-Ba(BO_2)_2-PbTiO_3$ section plotted on the basis of our data is shown in Fig.1. We see that the largest field of the system belongs to the continuous series of isomorphous $(Ba-Pb)TiO_3$ mixtures. The region of TiO_2 forming as a result of decomposition of $PbTiO_3$ at high temperatures is indicated by a dashed line. The relative sizes of the areas pertaining to different phases of the system are listed in Table 1.

Despite the large field of the isomorphous $(Ba-Pb)TiO_3$ mixtures, crystallization of mixed crystals can occur only at relatively high concentrations of $BaTiO_3$ and $PbTiO_3$ and high temperatures. At lower temperatures lead titanate crystallizes

---

*All percentages are molecular.

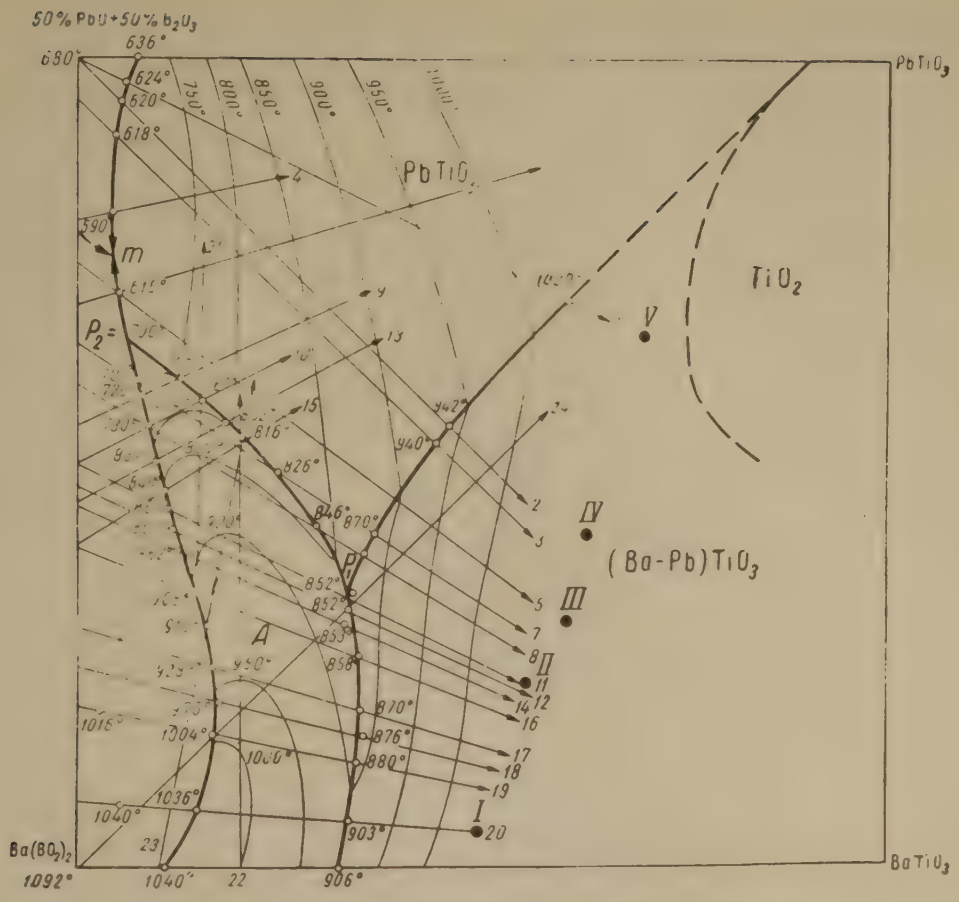

Fig.1. Location of sections.

Table 1

Field No.	Crystallizing phase	Area in % relative to the total area of the crystallization surface in the section
1	Fields of glass-like phases of PbO and B_2O_3 in the field of $Ba(BO_2)_2$*	9.8331
2	A	9.8359
3	(Ba-Pb)TiO_3 and TiO_2**	49.8872
4	$PbTiO_3$	30.4438

*Fields not delimited owing to vitrification.

**Boundary of crystallization fields not established.

from melts located in the upper part of the system and phase A from melts in the lower part of the system. At 852°, at point P_1 we have the simultaneous existence of two phases: (Ba-Pb)-TiO_3 and phase A. At 700° phase A decomposes at point P_2, while at temperatures between 615 and 690° at point m - the lowest point in the surface - there occurs crystallization of $PbTiO_3$ and a phase consisting of a mixture of PbO and B_2O_3 in undetermined proportions.

Thus the existence of a large field of crystallization of isomorphous (Ba-Pb)TiO_3 mixtures in the investigated surface (section) makes it possible to utilize these melts for obtaining $BaTiO_3$-$PbTiO_3$ single crystals with different

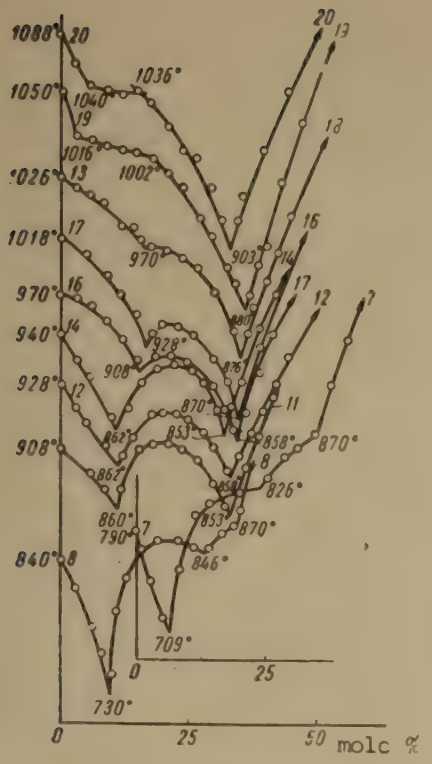

Fig.2

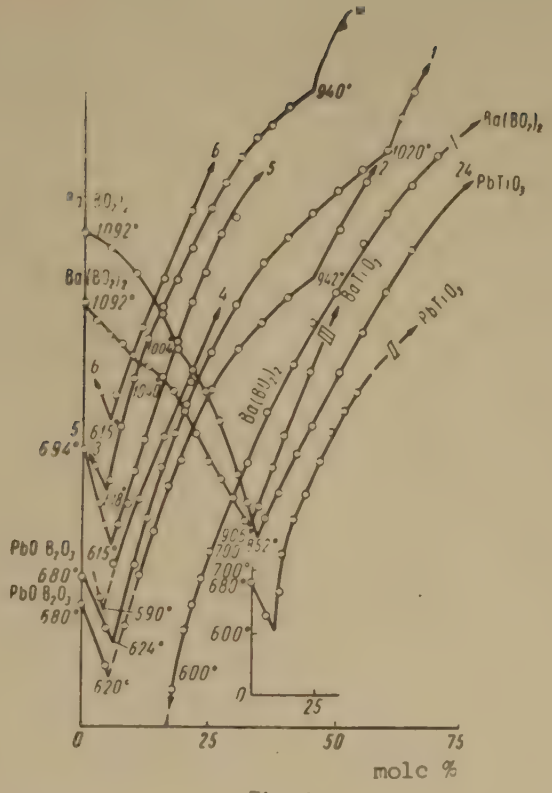

Fig.3

Fig.2. Fusibility of sections 7,8,11,12,16 & 20 through the [50% PbO + 50% B_2O_3] - $-PbTiO_3-Ba(BO_2)_2-BaTiO_3$ surface.

Fig.3. Fusiblity of sections 1 through 6 and the size of the investigated surface.

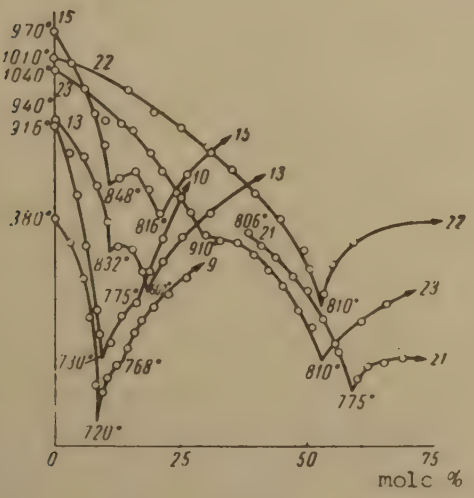

Fig.4

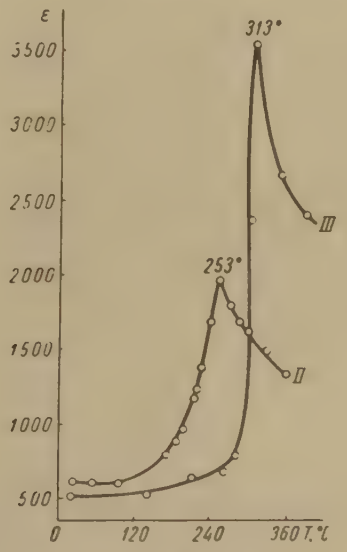

Fig.5

Fig.4. Fusibility of sections 9,19,13,15,21,22 & 23.

Fig.5. Temperature dependence of the dielectric constants of crystals of batches II and III (see Table 2).

Table 2

Batch No.	Composition of initial melt	Expected composition of crystals	Actual composition of crystals	Curie point
I	$8\%[50\%PbO + 50\%B_2O_3] + 92\%Ba(BO_2)_2 \rightarrow 50\%BaTiO_3$	$(Ba_{0,92}-Pb_{0,08})TiO_3$	$(Ba_{0,92}-Pb_{0,08})TiO_3$	152
II	$50\%[50\%PbO + 50\%B_2O_3] + 50\%Ba(BO_2)_2 \rightarrow 55\%BaTiO_3$	$(Ba_{0,59}-Pb_{0,41})TiO_3$	$(Ba_{0,64}-Pb_{0,36})TiO_3$	253
III	$75\%[50\%PbO + 50\%B_2O_3] + 25\%Ba(BO_2)_2 \rightarrow 60\%BaTiO_3$	$(Ba_{0,50}-Pb_{0,50})TiO_3$	$(Ba_{0,50}-Pb_{0,50})TiO_3$	313
IV	$[50\%PbO - 50\%B_2O_3] \rightarrow 63\%BaTiO_3$	$(Ba_{0,41}-Pb_{0,59})TiO_3$	$(Ba_{0,44}-Pb_{0,56})TiO_3$	322
V	$30\%[50\%PbO - 50\%B_2O_3] \rightarrow 70\%[50\%BaTiO_3 + 50\%PbTiO_3]$	$(Ba_{0,10}-Pb_{0,90})TiO_3$	$(Ba_{0,25}-Pb_{0,75})TiO_3$	401

component concentrations. However, it must be borne in mind that in addition to mixed titanate crystals, $PbTiO_3$ crystals form in the solidified melt. Hence one should grow the $(Ba-Pb)TiO_3$ crystals at the highest feasible temperature and then at about 950° pour off the remaining liquid phase.

We grew crystals in a platinum crucible in a Silit furnace by cooling the appropriate melts from about 1350 to 950°, at which point the furnace was turned off. The component concentrations and temperature conditions were chosen on the basis of the data shown in Figs.1 through 4. The resultant crystals were treated with molten potassium fluoride; the fine crystals falling out in the process of rapid cooling were melted and thus eliminated. The large crystals were then picked out, washed with concentrated nitric acid and then with water. The variation of the dielectric constant with temperature for two batches of crystals prepared in this manner is shown in Fig.5.

The compositions of these two batches and three others are listed in Table 2. The composition of crystals of batches II and IV is shifted somewhat to the side of lower $PbTiO_3$ concentrations. A particularly noticeable shift in composition obtains for crystals of batch V, which may be explained by the fact that this melt was held at high temperature for a longer period.

The formation of $(Ba-Pb)TiO_3$ solid solution crystals was substantiated in all cases by x-ray diffraction studies (performed by E.G.Fesenko). It must be noted that the crystals obtained were not perfect as regards shape. The crystals of batches IV and V were light yellow and transparent; the crystals of batches I, II & III were dark. Only the finer crystals in all batches were characterized by a true single domain structure. Crystals of all batches were investigated after heating for 2 hours at 1200°. The measurements were carried out on a Q-meter at a frequency of 10^6 cps. (The dielectric measurements were performed by A.L.Khodakov.)

We desire to thank N.S.Novosil'tsev for his interest in the work.

Scientific Research Physical-Mathematical Institute at
Rostov-on-the-Don State University

References

1. I.N.Beliaev, M.L.Sholokhovich & G.V.Barkova, Zhur.obshch.khim. 1, (5) 1026 (1956). (Trans.J.General Chemistry.)

2. M.L.Sholokhovich, Zhur.neorgan.khim. (Journ. Inorganic Chemistry), No.5, 134 (1958).

3. G.A.Smolenskii, Doklady AN SSSR, 70, 405 (1950).

4. S.Nomura & S.Sawardo, Phys., Japan, 6, 36 (1951).

5. E.G.Fesenko & A.G.Slabchenko, Zhur.tekh.fiz., 27(7), 1288 (1954).

6. M.C.Quarrie, Amer.Ceram.Soc.Bull., 9, 9, 34 (1955).

X-RAY SPECTROSCOPIC INVESTIGATION OF COMPOUNDS WITH THE PEROVSKITE STRUCTURE

- M.A.Blokhin & A.T.Shuvaev

The present work was devoted to an investigation of the K emission and absorption spectra of Ti, the L emission and emission spectra of Zr, the K absorption spectra of Fe and the L absorption spectra of Sr and Ba in $BaTiO_3$, $SrTiO_3$, $SrFeO_3$, $BaZrO_3$ and $PbZrO_3$.

The work was carried out on a long wavelength photographic vacuum x-ray spectrograph with a curved (r = 500 mm) quartz crystal (1010). In recording the emission spectra, the x-ray tube was operated at a voltage of 4 V_o, where V_o is the excitation potential of the corresponding spectrum, and a current of 4-10 ma. The absorption spectra were recorded against the background of the continuous radiation of a tungsten anode operated at 2 V_o and 28-30 ma. We also studied the fluorescence spectrum of Ti in $BaTiO_3$; the fluorescence was excited by the K series of the primary radiation of chromium with the x-ray tube operated at ~35 kv and 30 ma.

The spectra of Zr and Sr were obtained in the first order; those of Ti and Ba in the second order and that of Fe in the fourth. The resolution of the spectrograph in the region of the L_{III} spectra of Ba and the K spectra of Ti was ~4200; the resolution in the region of the L_{III} spectrum of Zr ~18,500.

The K spectra of Ti in $BaTiO_3$, the K absorption spectrum of Fe in $SrFeO_3$ and the L_{III} absorption spectra of Ba and Sr in these compounds are shown in Fig.1. The Ti $K\beta_5$ emission line characterizes the distribution of p-symmetry electrons in the valence band of the crystal lattice; the Ti K absorption spectrum represents the distribution of p and, partially, d states* in the conduction band. The hump on the long wavelength side of the K edge of Ti(Fe) is separated from the principal absorption edge by a gap of 2-3 ev. Thus there form in these compounds two conduction bands, of which the first contains primarily d states, the second p states.

The L_{III} spectra of Ba and Sr are shifted by the energy difference between the K level of Ti(Fe) and the L_{III} level of Ba(Sr). The bright selective L_{III} absorption lines of Ba and Sr coincide in frequency with the weak long wavelength peak in the K absorption spectrum of Ti(Fe). This indicates that in absorption the quadrupole transitions from the K level of Ti(Fe) and the dipole transitions from the L_{III} level** of Ba(Sr) go to a collective d state conduction band.

The L_{III} spectra of Zr and Ba in $BaZrO_3$ and $PbZrO_3$ are shown in Fig.2. The $L\beta_2$ line and the L_{III} selective absorption line characterize the d state distributions** in the valence band and conduction band, respectively. An energy gap of ~2 ev between the bands is clearly evident.

---

*Only one or two 3d states are filled in the titanium ions bound in the enumerated compounds; the number of vacant 3d states is 8-9, i.e., appreciably greater than the number of filled states. The transition probability of d electrons to the 1s level is very low - 13 times smaller than the transition probability of p electrons.[1] Hence the structure associated with 3d states is evinced only in the absorption spectrum in the form of a weak peak on the long wavelength side of the principal K edge of Ti. Further evidence in favor of this interpretation is the fact that this peak, which is present in the absorption spectra of compounds of the iron transition group, weakens and disappears as the 3d shell is filled, i.e., with increasing atomic number.[2]

**As follows from the experimental data of Jönsson[3] and Hicks[4], the transition probability of s electrons to the L_{III} level is 1-2 orders of magnitude lower than the transition probability for d electrons. Hence the L_{III} spectra essentially characterize the distribution of d states.

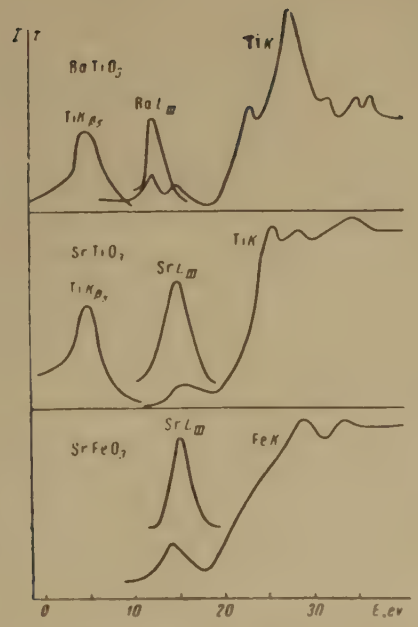

Fig.1. Emission and absorption spectra of ions bound in $BaTiO_3$, $SrTiO_3$ and $SrFeO_3$; the L_{III} absorption spectra of Ba and Sr are shifted by the energy difference between the Ti K (Fe K) and Ba L_{III} (Sr L_{III}) levels.

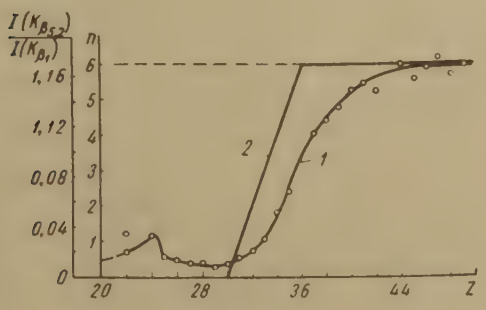

Fig.3.

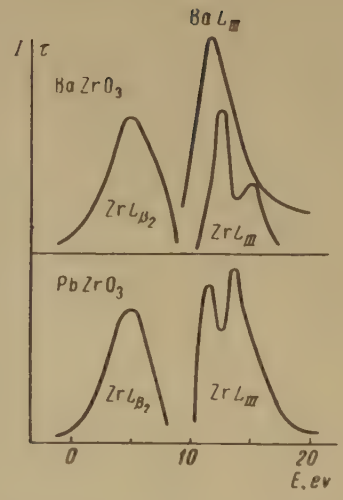

Fig.2. Emission and absorption spectra of Zr in $BaZrO_3$ and $PbZrO_3$ and L_{III} absorption spectrum of Ba in $BaZrO_3$; the L_{III} spectrum of Ba is shifted by the energy difference between the Zr L_{III} and Ba L_{III} levels. The curves for $PbZrO_3$ have been corrected to allow for the width of the L_{III} level of Zr and the apparatus distortion.

In all the investigated spectra of the cations centered in the oxygen octahedra there is evident a line associated with transitions of valence electrons. This indicates that the bonds in these compounds are partially covalent inasmuch as in the case of purely ionic bonds the valence electron cloud is fully localized at the anion and hence the given line could not appear.

For the purpose of rough evaluation of the degree of covalence, we determined the intensity of the $K\beta_5$ line with respect to the $K\beta_1$ line for Ti, both metallic and in $BaTiO_3$. The ratios obtained were 0.020 and 0.035, respectively, i.e., a greater number of p electrons is retained near the Ti ion in $BaTiO_3$ as compared with the metal, which indicates an appreciable degree of covalence of the bonding of Ti with the oxygen in the $BaTiO_3$ lattice.

From the curves of Fig.3, one can find the number of electrons corresponding to a given intensity ratio. Curve 1 shows the variation of the relative intensity $I(K\beta_{5.2})/I(K\beta_1)$ with the atomic number for pure elements in the solid state;*

---

*Curve 1 is plotted on the basis of Meyer's[5] data on the ratio of intensities at the line peaks. Actually, however, the number of p electrons is proportional to the ratio of the integral intensities. Inasmuch as the valence and nearby levels are broadened due to interaction between the atoms in the solid, curve 1 in the $Z < 44$ region lies below the curve for the ratio of integral intensities.

curve 2 gives the Z dependence of the number of 4p electrons in free atoms.

The circle points in Fig.3 represent our experimental data. It will be evident from Fig.3 that there are 1.3 valence p electrons per Ti ion in $BaTiO_3$. In addition the Ti ions have d* and apparently s electrons. Thus the degree of covalence of the Ti bonds in $BaTiO_3$ exceeds 35%.

Previously, one of us[6] investigated the temperature dependence of the height of the conduction band in $BaTiO_3$. It was found that with increasing temperature in approaching the ferroelectric Curie point the conduction band is shifted towards the valence band, i.e., the energy gap narrows. This displacement attains a maximum value of ~0.6 ev at the Curie point; with further increase of temperature above the Curie point the conduction band shifts in the opposite direction, returning to its initial position. It is interesting to note that the activation energy for $BaTiO_3$, as determined from the variation of electric conductivity with temperature,[7] exhibits a similar temperature dependence; at the Curie point the conductivity decreases by exactly 0.6 ev.

Conclusions

1. The valence band in compounds with the perovskite structure is a hybrid one with a large admixture of p states.
2. The formation of a collective d electron conduction band in these compounds has been substantiated experimentally.
3. The conduction band consists primarily of d states with a small admixture of p states.
4. The next band of free states consists primarily of p states with a non-uniform density distribution.
5. The effective charge on the Ti ion in $BaTiO_3$ is not less than 2.7.
6. The energy of the electron states in the conduction band decreases close to the Curie point.

Rostov-on-the-Don State University

References

1. O.Beckman, Arkiv för Fysik, 9, 495 (1955).
2. H.P.Hanson & J.R.Knight, Phys.Rev., 102, 632 (1956).
3. A.Jönsson, Z.Phys., 36, 426 (1926).
4. V.Hicks, Phys.Rev., 36, 1273 (1930); 38, 572 (1931).
5. H.T.Meyer, Wiss. Veröffentlich. aus dem Siemens-Konzern, 7, 108 (1929).
6. M.A.Blokhin, Doklady AN SSSR, 95, 1165 (1954).
7. G.Busch, H.Flury & W.Merz, Helv.phys.acta, 21, 212 (1948).

---

*This is indirectly indicated by the presence of the $L\beta_2$ line of Zr in the spectra of $BaZrO_3$ and $PbZrO_3$. This line is associated with transitions of d valence electrons; the distribution of electrons in these compounds is similar to their distribution in $BaTiO_3$.

INFRARED ABSORPTION SPECTRA OF PEROVSKITE TYPE FERROELECTRIC CRYSTALS

- A.F. Iatsenko

In virtually all current theories of ferroelectricity the primary responsibility for the ferroelectric anomalies in perovskite type crystals is laid on the oxygen octahedron, the central cation being relegated to a subsidiary role. The different theories differ mainly as regards the postulated character of the internal motions of the oxygen octahedron. Investigation of the vibrational spectra of ferroelectric crystals on the basis of the experimental infrared (IR) absorption spectra and Raman spectra can yield valuable information on the atomic arrangements and forces in the crystal lattice.

For investigating the absorption spectra we used an IKS-6 spectrometer for the 0.7 to 25 μ region and a DFS-4 spectrometer for the 0.3 to 0.7 μ region. The latter spectrometer was also used for studying the Raman spectra. The powder specimens for the absorption studies were prepared by the procedure described in Ref.1.

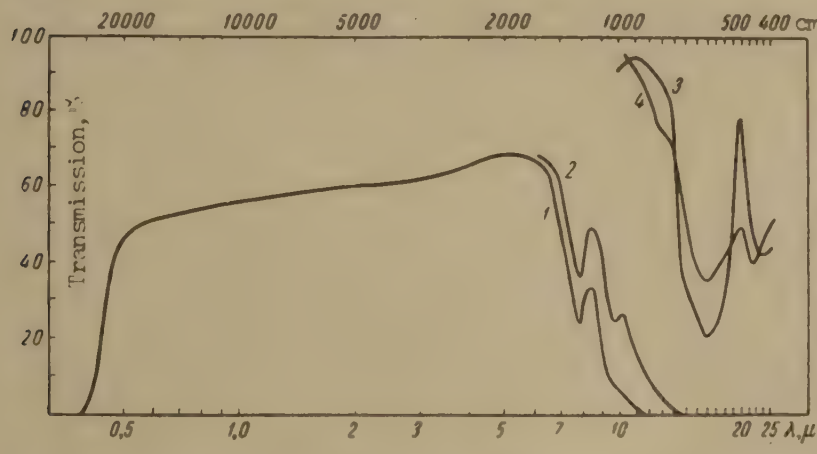

Fig.1. Transmission of barium titanate: 1) single crystal, d = 0.22 mm; 2) single crystal, d = = 0.095 mm, 3) powder, d ≈ 1 micron; 4) finely dispersed nonferroelectric powder, d ≈ 1 micron.

The absorption spectra of $BaTiO_3$ are shown in Fig.1. The single crystals are characterized by continuous absorption in the regions below 0.4 μ and above 10-12 μ and relatively narrow bands at about 8 μ and 10.3 μ. The powder specimens with an effective thickness of 0.5 to 2 microns exhibit strong bands centered at 17.3 and 24.4 μ; the former has a distinct shoulder at about 14.8 μ. At temperatures close to the Curie point and in certain solid solutions, this shoulder is very prominent and often becomes a separate narrow band, disappearing at temperatures above the Curie point. The spectrogram also shows the intrinsic absorption edge, extending from 4000 Å, which is associated with electron transitions from the valence band to the conduction band. In the same figure we show the absorption spectrum obtained for a finely dispersed nonferroelectric specimen of $BaTiO_3$. Noteworthy features are broadening of the ν_1 band and the absence of the shoulder at 14.8 μ. Partially reduced, black $BaTiO_3$ has a spectrum identical with that of the tetragonal modification except that the intrinsic absorption edge extends over the visible region.

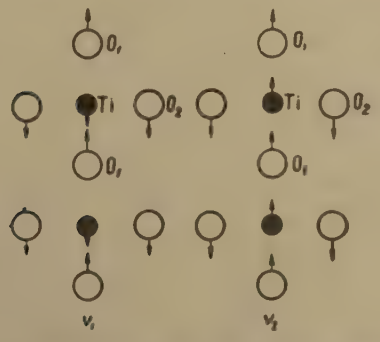

Fig.2. Vibrations of the oxygen octahedra: ν_1- valence (stretching), ν_2- deformation (bending).

We also investigated the IR absorption spectra of a number of other titanates ($CaTiO_3$, $SrTiO_3$ & $PbTiO_3$), zirconates ($SrZrO_3$, $BaZrO_3$ & $PbZrO_3$), stannates ($SrSnO_3$ & $BaSnO_3$) and WO_3. The data on these spectra are summarized in the accompanying table.

Substance	Frequencies			Force constants		Charge	
				10^{-5} CGSE			
	ν_1, cm^{-1}	ν_2, cm^{-1}	$\frac{\Delta\nu_1}{\nu_1}$	k_1	k_2	$\frac{n_1}{e}$	$\frac{n_2}{e}$
$PbTiO_3$ *	575	~420	0,34	1,4	0,76	1,8	1,5
$BaTiO_3$ **	578	~410	0,37	1,1	0,90	1,5	1,9
$SrTiO_3$	620	~420	0,33	1,2	0,65	1,9	2,0
$CaTiO_3$	760 \ 590 /	~430					
$BaTiO_3$ — black***	576	~415					
$BaTiO_3$ — cubic	580	~440	0,42				
$PbZrO_3$ *	593	~380	0,23	1,4	0,54		
$BaZrO_3$	573	~400	0,32				
$SrZrO_3$	584	~400	0,31				
$BaSnO_3$	635	~400	0,21				
$SrSnO_3$	690	435	0,14	1,9	0,74		
WO_3	870	780	0,21	3,3	2,5	1,2	0,88

*The ν_1 band is broadened to the low frequency side.
**The ν_1 band has a shoulder at 675 cm^{-1}.
***Shoulder at 670 cm^{-1}.

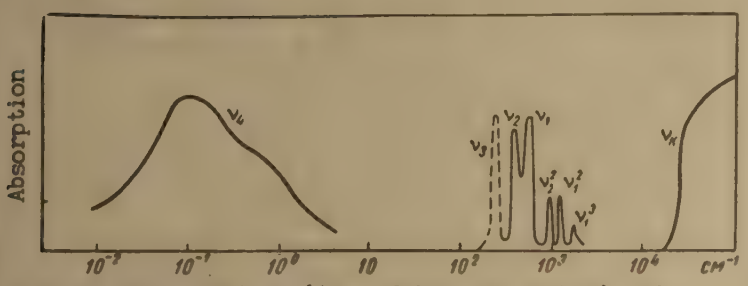

Fig.3. Absorption (in arbitrary units) of ferroelectric perovskite type crystals.

It must be noted that lead zirconate and titanate have an additional band at about 13.5 μ (we have not identified this band but it is certainly not due to impurities); the ν_1 band in the spectra of both these compounds has a shoulder on its low frequency side. Replacement of the light Ti ion by heavier Zr or Sn ions leads to displacement of the spectra to the high frequency side, which indicates appreciable strengthening of the linkage between the central ion and the oxygens.

The infrared vibration spectra of an ideal perovskite lattice should consist of three triply degenerate bands, one of which (40-50 μ)[2] corresponds to oscillations of the Ba ions relative to the TiO_3 groups, while the other two are associated with internal vibrations of the oxygen octahedra (ν_1 is a purely valence vibration; ν_2 is a purely deformation - bending - vibration having a lower frequency than ν_1) (Fig.2). This interpretation is substantiated by the spectrum of WO_3, the lattice of which consists only of oxygen octahedra with W ions at the center. The weak absorption bands in the spectra of single crystals at 8 μ and 10.3 μ may be identified as the first overtones of ν_1 and ν_2.

Full absorption spectrum of perovskite type ($BaTiO_3$) crystals including the microwave region is shown in Fig.3.

We calculated the potential function force constants in the harmonic oscillator approximation for many of the investigated substances (see table). The force constants for $BaTiO_3$ and solid solutions with a Curie point close to room temperature comprise a very small imaginary part. This is in agreement with results obtained by Last[2], although his frequency values differ appreciably from ours. Apparently, the harmonic approximation is not really admissible in this case. Having measured the absolute intensity of the absorption bands, one can determine the dipole charge associated with the valence and deformation vibrations in the

harmonic approximation

$$n = \frac{Q}{e} = \frac{1}{2\pi e\nu}\sqrt{\frac{k\bar{x}}{\pi N}},$$

where Q, ν, k and $\bar{x}$ are, respectively, the dipole charge, the frequency, the force constant and the absolute intensity of the given vibration. The results of our dipole charge evaluations are also listed in the table.

From a comparison of the frequency of the fundamentals and the first overtones one can calculate the mechanical anharmonicity coefficients entering into the expansion of the vibrational energy in powers of the vibrational quantum numbers. For the valence vibrations the relative anharmonicity coefficient is 10% (for $BaTiO_3$), whereas the usually observed anharmonicity of molecular vibrations is of the order of 1% even for the lightest atoms. The large mechanical anharmonicity is also evinced in partial removal of the degeneracy of the valence vibrations (appearance of the shoulder at 14.8 μ on the side of the ν_1 band). It follows from the observed temperature behavior of the shoulder that the mechanical anharmonicity is most pronounced in the vicinity of the Curie point. Comparison of the intensity of the bands of the fundamental ν_1 and its first overtone ($x_{01}/x_{02} \approx 400$) indicates that the magnitude of the electro-optical anharmonicity in the IR region is negligibly small.

We attempted to obtain the Raman spectrum of $BaTiO_3$ in the hope of detecting the valence frequency ν_1. The results were negative, which indicates that the asymmetry of the Ti-O bonds in tetragonal $BaTiO_3$ is insignificant.

It may be of interest to compare our results with the deductions following from some of the current theories of ferroelectricity: a) it follows from Jaynes'[3] theory that there should be an infrared absorption band with $h\nu_0 = 4\ kT_k$ (for $BaTiO_3$, ν_D = 1100 cm^{-1}); this deduction is not substantiated by experiment; b) Slater's[4] theory takes into account only mechanical anharmonicity, yet for wavelengths $\lambda > 1$ cm the electron optical anharmonicity is very appreciable; c) Barrett's[5] relation for the critical temperature $T_{cr} = h\nu/k = 410\ n$ is qualitatively substantiated for the second part of the equality; d) unfortunately the inadequate resolution of our instruments made it impossible to check the predictions of Mason's theory.

Rostov-on-the-Don State University

References

1. A.F.Iatsenko, Zhur.tekh.fiz., 17, 2422 (1957). (Trans. Soviet Physics - Tech. Phys.)
2. J.T.Last, Phys.Rev., 105, 1740 (1957).
3. E.T.Jaynes, Ferroelectricity - Princeton, 1953.
4. J.C.Slater, Phys.Rev., 78, 784 (1950).
5. J.H.Barrett, Phys.Rev., 86, 118 (1952).

ON THE NATURE OF COLOR CENTERS IN BARIUM TITANATE CRYSTALS

- M.S.Kosman & E.V.Bursian

In an earlier communication[1] we reported on observing an effect in $BaTiO_3$ single crystals analogous to coloring in alkali halide crystals (hereinafter AHC). We investigated two types of coloring in crystal specimens prepared by the procedure described in Ref.2: change in the color of the crystals from pale yellow to reddish brown in an oxidizing atmosphere (oxygen) and from pale yellow to bluish gray in a reducing atmosphere (hydrogen or vacuum). Further, it was found that when dc current is passed through a crystal reddish brown color spreads from the anode, grayish blue from the cathode. The wavelength of the absorption band in reddish brown crystals is the same (450-460 mμ) regardless of the method of coloring (oxidizing atmosphere or current).

To emphasize certain similarities with V and F centers in AHC, we shall call the centers responsible for the reddish brown color v centers, and those responsible for the grayish blue, f centers. We note, however, that there are significant differences in the behavior of colored $BaTiO_3$ as compared with AHC. $BaTiO_3$ single crystals are colored much more readily than AHC; v-center coloring can be realized even at room temperature, while at high temperatures there is no need to use high voltages (at 300° a field of 3 v/mm is adequate). The color intensity obtainable is much greater in $BaTiO_3$. No photoeffect in the case of v-coloring is observed. The conductivity of a v-colored crystal is lower than that of a colorless one (whereas in AHC coloring is accompanied by the appearance of a photoeffect and increase of the dark conductance). In the case of rapid deep cooling of colored AHC there occurs "freezing" of the F center concentration, i.e., a higher than equilibrium concentration persists in the cooled crystal. In $BaTiO_3$ the behavior of v centers is different. Thus, if after heating in oxygen, the crystal is cooled gradually over a period of several hours the crystal becomes colored reddish brown. In case of rapid cooling (quenching), however, no v-color develops. If a large crystal (minimum dimension over 1 mm) is cooled quickly, its external parts, which cool more quickly, and, particularly, any chipped-off edges or corners remain uncolored in sharp contrast to the intensely colored central region (Fig.1).

Fig.1. Result of quenching a large $BaTiO_3$ single crystal in oxygen.

According to our rough evaluation, the concentration of color centers in crystals that color well is of the order of 10^{19} cm^{-3}. Such a concentration can hardly affect the structure of the lattice as a whole or noticeably alter the phase transition temperatures, but it is sufficient to produce an appreciable change in conductivity. This in turn should lead to a change in the domain pattern and modification of the pattern dynamics in an electric field. Accordingly, we assumed that coloring should result in a change in the shape of the dielectric hysteresis loop.

Experimental verification of this assumption showed the following. Bleaching of the crystals in a reducing atmosphere (studies of the absorption spectra indicate that chemical reduction is not involved) leads to an appreciable increase of the electric conductivity (the degree of increase is strongly dependent on the cooling conditions). The conductivity of bleached crystals is virtually independent of the temperature in the range from ~20° to 200°C (Fig.2, curve A). At higher temperatures or in stronger fields v-center coloring occurs. In this case the conductivity at first falls off sharply (jump of several orders of magnitude) and

Fig.2. Temperature dependences of the electric conductivity of bleached (A) and v--colored (B) crystals.

then decreases slowly as long as coloring continues. The resistivity at room temperature increases by a factor of 10^4–10^6. At the same time there appears a strong temperature dependence of the conductivity, corresponding to an activation energy of 1.2-1.4 ev (Fig.2, curve B). The phase transition temperature, which varies from 120 to 140° in different specimens, does not change (within ±3°) incident to bleaching or v-center coloring.

Reduction of the crystal begins with appearance of f centers. In the process the conductivity increases greatly. However, the crystal does not lose its ferroelectric properties as evinced by the persistence of domain structure and domain motions in an electric field. Observation of the domain structure and dynamics by means of a polarization microscope is, of course, the only method of detecting ferroelectricity in semiconductors.

If a bleached crystal is connected into a Sawyer-Tower circuit for observing dielectric hysteresis, one observes the following sequence of hysteresis loops (Fig. 2): I - bleached crystal; the oscilloscope trace has nothing in common with a hysteresis loop and indicates only high conductivity and a phase shift; curve II appears immediately after I. Curve III and subsequently IV appear much later, after the crystal has been held in an electric field for an appreciable period. As a result of holding in the field the crystal becomes colored.

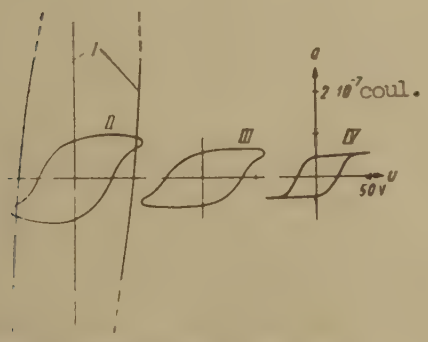

Fig.3. Variation of the hysteresis loops in the process of coloring.

The changes occurring simultaneously with coloring suggest that there is a connection between coloring and aging, although this variation with time obviously does not involve such processes as high voltage polarization, rearrangement of the domain pattern, etc.

X-ray diffraction studies carried out at our request by E.L.Gal'perin showed that the parameters of the $BaTiO_3$ lattice do not change in the process of v-center coloring and bleaching.

On the basis of the experimental data one can propose the following models: a v center is apparently a lattice defect (deficiency of a positive ion) encompassing one or more holes; an f center is an analogous "oxygen" vacancy encompassing one or two electrons. Thus coloring in oxygen amounts to superficial absorption of oxygen atoms; these atoms subsequently transform into ions by appropriation of electrons from neighboring ions in the lattice. This leads to the appearance of the holes necessary for the formation of v centers. Vacant sites of both polarities (Schottky defects) are always present in the crystal lattice. The v-center formation process is hindered by the field induced in the crystal (the crystal is charged positive relative to the surface). At a sufficiently high temperature, this field is liquidated either by diffusion of oxygen ions into the crystal, where they fill the corresponding vacant sites, or by migration of positive ions to the surface, where, as a result, a new lattice layer is formed. Careful density measurements should allow of deciding between these mechanisms.

The migration or spreading of color through the crystal may be explained by the presence within the crystal of a sufficient number of defects, which subsequently trap holes coming from the anode, forming additional new v centers. True,

in view of the neutrality of all parts of the crystal, it must be assumed that initially there is present the same number of positive defects and that there obtains electrolytic conductivity, which makes the movement of defects possible. The displacement of the f cloud through the crystal is due to motion of electrons.

Thus a necessary condition for coloring of $BaTiO_3$ crystals is the presence of defects (vacant sites). In this case from the maximum intensity of coloring (i.e., by measuring the absorption coefficient) one can evaluate the concentration of such defects. This is one of the methods that may be proposed for evaluating the quality of single crystals. Thus, for example, it was found that crystals grown by the Remeika procedure with Fe_2O_3 virtually do not color, which indicates that they are characterized by a high degree of perfection as regards microstructure.

"A.I.Gertsen" Leningrad State Pedagogical Institute

References

1. M.S.Kosman & E.V.Bursian, Doklady AN SSSR, 115, 483 (1957).
2. E.V.Bursian, Uch.zap. (Scientific notes), Leningrad State Pedagogical Institute, 148, 216 (1958).

* * * * * * *

HIGH TEMPERATURE POLYMORPHOUS TRANSFORMATION IN BARIUM TITANATE

- I.A.Trifonov

There is available in the literature information on the dielectric properties,[1] the crystal structure[2] and the methods of preparation[3-6] of nonferroelectric barium titanate; the phase diagrams of this substance have also been obtained.[4,7]

The present work was concerned with the transformation of $BaTiO^3$ from the hexagonal modification to that with the perovskite structure, a process that has hitherto received scant attention from investigators. This transformation is accompanied by changes in a number of structure-sensitive properties, particularly changes in the dielectric constant ϵ. In fact, it is feasible to evaluate the degree of transformation from one crystal modification to another from the change in the magnitude of ϵ.

Curves characterizing the variation of the dielectric constant ϵ as a function of the temperature T for one and the same specimen in different modifications are shown in Fig.1. As a measure of the degree of polymorphous transformation one can conveniently take a quantity connected with the ϵ vs T curve, namely, the difference $\Delta\epsilon = 2_m - \epsilon_n$. Since there is usually present in specimens a mixture of two phases, having different dielectric constants at the given temperature, it is important to establish the functional dependence

$$\epsilon_m = f(\alpha, \epsilon_{mf}, \epsilon_n),$$

where ϵ_n is the dielectric constant of a nonferroelectric specimen, ϵ_m is the dielectric constant at the Curie point of a partially annealed specimen, i.e., the specimen under study, ϵ_{mf} is the dielectric constant at the Curie point of a fully annealed specimen wholly converted to the ferroelectric state and α is the concentration of the ferroelectric phase.

For ϵ_m we can write

$$\epsilon_m = \alpha\epsilon_{mf} + (1 - \alpha)\epsilon_n, \qquad (1)$$

then the concentration α of the ferroelectric phase will be given by

$$\alpha = \frac{\Delta\epsilon}{\epsilon_{mf} - \epsilon_n}$$

In our experiments the transformation of the high temperature modification of $BaTiO_3$ to the modification with the perovskite structure was realized by annealing the crystal. After each anneal, we recorded the variation of ϵ with temperature. The $\epsilon = f(T)$ curves for a sample held for 3 hours successively at 1100, 1150, 1200 and 1250° are shown in Fig.2. One can judge of the appearance of the ferroelectric phase in a given specimen, i.e., after annealing at the given temperature, from the growth of the maximum in the ϵ vs T curve.

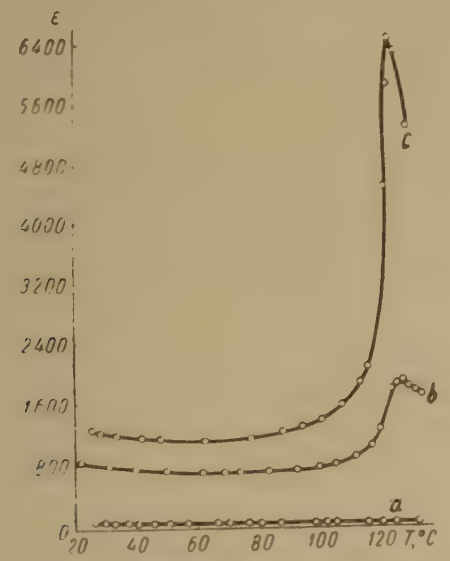

Fig.1. Character of $\epsilon = f(T)$ curves corresponding to different degrees of annealing of a barium titanate specimen: a) before annealing, b) partially annealed, c) after complete annealing.

Our experiments showed that the temperature at which the transformation begins in barium titante lies between 1050 and 1100°. None of the specimens heated at temperature up to 1050° evinced any indication of the beginning of the polymorphous transformation; yet it is reported in the literature[8] that heating of the hexagonal modification of barium titanate at 1050° induces the transformation to the perovskite structure phase.

For specimens with different degrees of development of the polymorphous transformation, the concentration of the ferroelectric phase is a function of the temperature and the annealing time:

$$\alpha = \varphi(T,\tau).$$

In our case, however, the holding time at heat was constant (3 hours); only the annealing temperature was varied.

Differentiating Eq.(1) with respect to temperature, we obtain

$$\frac{d\alpha}{dT} = \frac{1}{\epsilon_{mf} - \epsilon_n}\,\frac{d\Delta\epsilon}{dT} \qquad (2)$$

From the test data one can follow the variation of $\Delta\epsilon = f(T)$; the temperature dependence of α differs from that of $\Delta\epsilon$ only by a constant factor; hence the $\Delta\epsilon = f(T)$ curves characterize the variation of the concentration of the ferroelectric phase with the annealing temperature of the initially hexagonal specimen. The dependence in question is plotted in Fig.3.

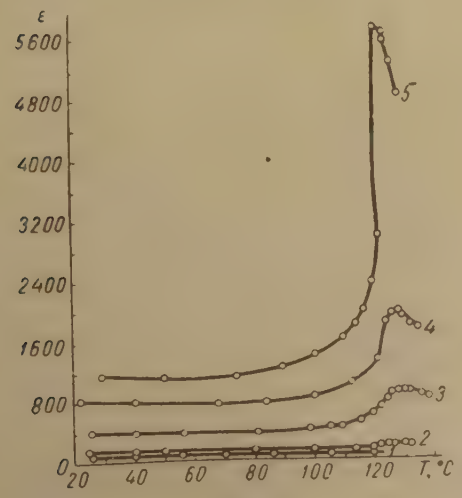

Fig.2.

←Fig.2. $\epsilon = f(T)$ curves corresponding to different phase compositions in a specimen held at different temperatures at 3 hours: 1) before annealing, 2) after heating at 1100°, 3) 1150°, 4) 1200° and 5) 1250°.

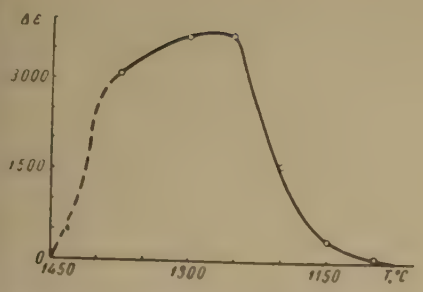

Fig.3. Variation of a quantity ($\Delta\epsilon$) proportional to the concentration of ferroelectric phase in the specimen with the annealing temperature.

According to Trzebiatowski et al[4] the polymorphous transformation point is 1450°; at this temperature both modifications of $BaTiO_3$ are in a state of dynamic equilibrium. The phase composition in the specimen remains constant when it is held at this temperature. Hence in the curve of Fig.3 we have taken $\Delta\epsilon = 0$ at 1450°. The dashed part of the curve indicates the approximate temperature variation of $\Delta\epsilon$ and, consequently, the temperature variation of α in the temperature range from 1450 to 1375°.

The curve characterizing the variation of a quantity (for example, $\Delta\epsilon$) proportional to the concentration of the perovskite structure modification of barium titanate with the temperature of supercooling of the metastable phase (the hexagonal modification at $t < 1450°$) is a typical curve of the dependence of the rate of crystallization of a melt on the degree of supercooling. The similarity of the curves characterizing the variation of the rate of phase transformation with the supercooling temperature in the solid state and in process of solidification indicates that these processes have common traits, namely, formation of crystallization nuclei and their ensuing growth.

Conclusions

1. A distinctive feature of the investigated substance - barium titanate - is that in the process of rearrangement of the crystal lattice it transforms from a nonferroelectric to a ferroelectric state. As a result, some of its structure-sensitive peoperties undergo a considerable change. In analyzing the phase transformation in $BaTiO_3$, we evaluated the degree of transformation from the change in the most structure-sensitive property, namely, the dielectric constant.

2. We determined the character of the variation in the relative concentration of the ferroelectric phase as a function of the heat treatment temperature of the hexagonal modification. The appearance of the $\Delta\epsilon$ vs T curve (Fig.3) indicates that the phase transformation in $BaTiO_3$ is a process involving nucleation.

I desire to express my sincere gratitude to B.M.Vul for valuable advice and N.S.Novosil'tsev for considerate guidance.

Rostov-on-the-Don State University

References

1. B.M.Vul & I.M.Gol'dman, Doklady AN SSSR, 60, 41 (1948).
2. R.D.Burbank & H.T.Evans, Acta crystallogr., 1, 330 (1948).
3. N.S.Novosil'tsev, Dissertation, Moscow State University, 1956.
4. W.Trzebiatowski, M.Drys & J.Benak, Roczniki chemii, 28, 21 (1954).
5. I.N.Beliaev, N.S.Novosil'tsev, A.L.Khodakov & E.G.Fesenko, Doklady AN SSSR, 78, 5 (1951).
6. H.Blattner, B.Matthias & W.Merz, Helv.Phys.acta, 20, 225 (1947).
7. D.E.Rose & R.Roy, J.Amer.Ceram.Soc., 38, 102-113 (1955).
8. C.Frondel, Acta crystallogr., 1, 355 (1948).

NONLINEAR PROPERTIES OF Pb DOPED $BaTiO_3$ SINGLE CRYSTALS AND TRI-GLYCINE SULFATE SINGLE CRYSTALS IN STRONG ELECTRIC FIELDS

- I.S.Zheludev, V.V.Gladkii, L.Z.Rusakov & I.S.Rez

Ferroelectric capacitors are characterized by a nonlinear, hysteresis type variation of charge with the applied field. Assuming that this variation can be represented by an idealized loop of the type shown in Fig.1, one can, according to Mason[1], find the relation between any charge harmonic, the ac and dc field strength and the geometric characteristic of the loop.

Considering the first harmonic, we have the following expressions for the capacitance C_1 and resistance R:

$$C_1 = \frac{q_m}{4\pi E_c}\left[2(\pi - \alpha_1 - \alpha_2 + \alpha_3) + \sin 2\alpha_1 + \sin 2\alpha_2 - \sin 2\alpha_3\right]; \quad (1)$$

$$\frac{1}{R} = \frac{\omega}{\pi E_m^2} S = \frac{2\omega E_c q_m}{\pi \cdot E_m^2 \cdot E_s}\left[E_m + E_s - E_c - E_0\right], \quad (2)$$

where

$$\alpha_1 = \arccos\left[\frac{-E_c + E_s - E_0}{E_m}\right], \quad \alpha_2 = \arccos\left[-\frac{E_m - 2E_c}{E_m}\right],$$

$$\alpha_3 = 2\pi - \arccos\left[\frac{E_c + E_s - E_0}{E_m}\right],$$

S is the area of the loop and the other notation is defined in Fig.1.

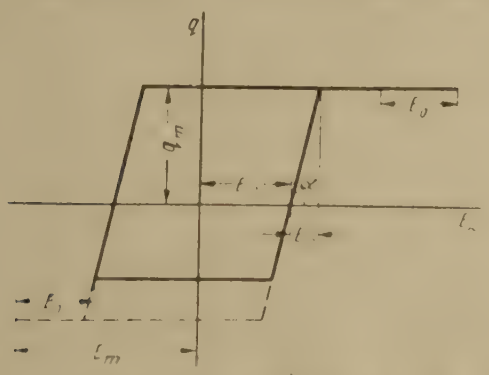

Fig.1. Idealized hysteresis loop: q_m - maximum charge on the capacitor, E_m - crest sinusoidal voltage varying with the frequency , E_c - coercive field strength, E_0 - biasing field strength, and E_s - saturating field strength.

It follows from (1) and (2) that with increasing rectangularity of the loop (i.e., as $E_s \to 0$), both the conductance (1/R) and the susceptance (ωC_1) increase. Hence increasing rectangularity will be accompanied by increase of the first derivatives of 1/R and C_1 with respect to the ac and dc fields, the nonlinearity coefficient $N = (1/C_1)(dC_1/dE_0)$ and the loss tangent tan δ. On the other hand, obviously, tan δ will decrease with decrease of the coercive field E_c. It may be concluded therefore that the best nonlinear material will be one having a maximum rectangularity of the hysteresis loop combined with the lowest coercive field strength.

It may be noted that for the limiting case of a loop in the form of a true rectangle, i.e., with $E_s = 0$ and $E_m = E_c$, the capacitance $C_1 = 0$, $R = \pi E_c/\omega q_m$ and tan $\delta = \infty$.

Thus if there were a material with such an ideal rectangular loop it would behave as a pure resistance.

In view of the above considerations, for the purposes of our study we chose materials characterized by the most nearly rectangular hysteresis loops (Fig.2), namely, a) $BaTiO_3$ single crystals with different amounts of $PbTiO_3$ and b) triglycine sulfate $[(NH_2CH_2COOH)_3 \cdot H_2SO_4]$ single crystals.

In all we investigated five lots of $BaTiO_3$ single crystals with different lead contents. The maximum nonlinearity was exhibited by the specimens containing about 1% $PbTiO_3$ (E_c = 800 v/cm; Curie point ~120°C). Below we give the measurement results only for crystals of this batch.

a b

Fig.2. Hysteresis loops recorded at room temperature: a) $BaTiO_3$ (E_c = 800 v/cm, $P_S = 26 \cdot 10^{-3}$ coulomb/cm^2), b) tri-glycine sulfate (E_c = 300 v/cm^2, $P_S = 2 \cdot 10^{-3}$ coulomb/cm^2).

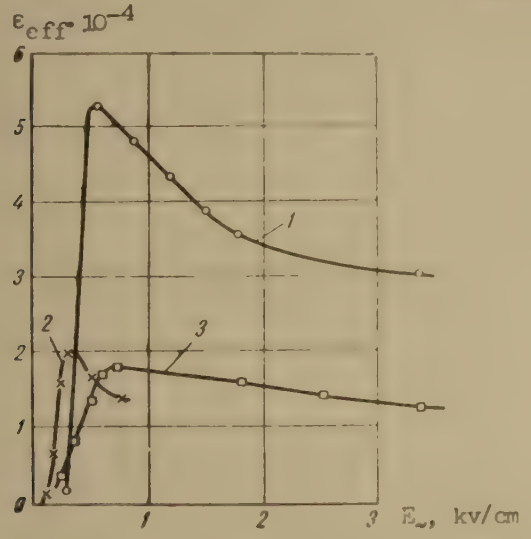

Fig.3. Variation of effective dielectric constant ϵ_{eff} with the ac field E' for 1) $BaTiO_3$, 2) tri-glycine sulfate and 3) Varikond VK-1.

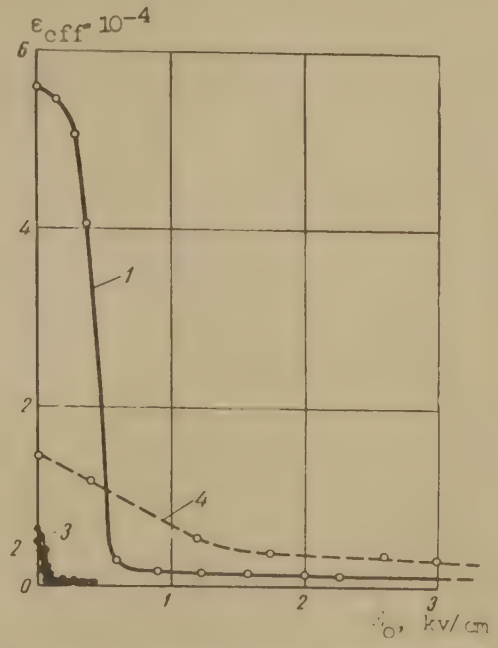

Fig.4. Variation of the dielectric constant ϵ_{eff} with the biasing dc field E_c for 1) $BaTiO_3$, 2) tri-glycine sulfate, 3) Rochelle salt and 4) Varikond VK-1.

The coercive field strength in tri-glycine sulfate depends on the amplitude of the voltage on the crystal and varies in the range from 220 to 600 v/cm; the Curie temperature is 40°C. We carried out measurements of the effective capacitance C_{eff} (i.e., actually ϵ_{eff}) and the first harmonic capacitance C_1 (i.e., ϵ_1) as a function of the ac and dc fields. C_{eff} was determined according to Ohm's law by means of a crystal-resistance circuit; C_1 was measured on an MPP-300 impedance bridge, using a selective indicator in the bridge diagonal. All measurements were performed at room temperature.

The curves for the variation of the dielectric constant with the ac and biasing dc field strengths for $BaTiO_3$ and tri-glycine sulfate are shown in Figs.3 & 4. For purposes of comparison we also give the corresponding data for Varikond VK-1 (Ref.2) and (in Fig.4) Rochelle salt.

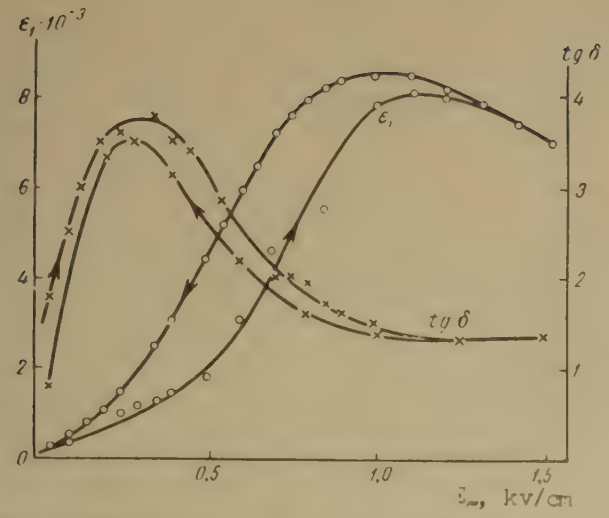

Fig.5. Variation of ϵ_1 and tan δ of tri-glycine sulfate with the ac field $E_\sim$ as $E_\sim$ is increased and decreased ($E_0 = 0$).

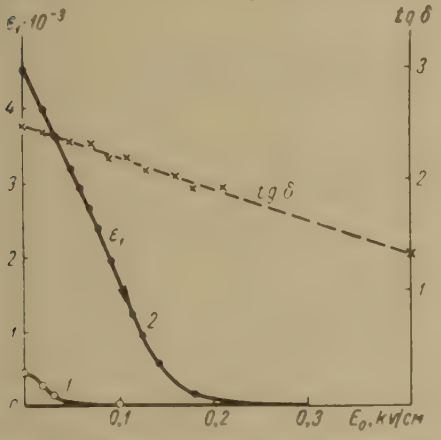

Fig.6. Variation of ϵ_1 and tan δ of tri-glycine sulfate with the dc biasing field E_0 as E_0 is increased and decreased: 1) $E_\sim$ = 100 v/cm and 2) $E_\sim$ = 500 v/cm.

It will be evident that the slopes of the ϵ vs E_0 curves for $BaTiO_3$ crystals, tri-glycine sulfate and Rochelle salt are nearly the same, but that the latter two substances are characterized by consistently lower values of ϵ in the entire range of E_0 values. Inasmuch as the dielectric constant appears in the denominator of the expression for the nonlinearity coefficient N, the substances fall into the following series as regards decreasing values of N: 1) tri-glycine sulfate and Rochelle salt - $N_{max} \approx 80$, 2) $BaTiO_3$ - $N_{max} \approx 30$ and 3) Varikond VK-1 - $N_{max} \approx 2$.

The dielectric loss tangent with zero biasing field has a maximum near $E_m = E_c$; for tri-glycine sulfate $\tan \delta_{max} \approx 3.8$, while for $BaTiO_3$ $\tan \delta_{max} \approx 1.2$. In a dc field ($E_0 \neq 0$), tan δ decreases with increasing E_0 and drops to a very low value in strong fields (~0.05 for both $BaTiO_3$ and tri-glycine sulfate). Obviously, with increasing E_0 and decreasing tan δ, the nonlinearity coefficient N also decreases (going to zero at the limit).

The curves characterizing the variation of ϵ_1 as a function of $E_\sim$ and E_0 recorded for tri-glycine sulfate with increase and decrease of the ac and dc fields are shown in Figs.5 & 6. It will be seen that the "forward" and "reverse" curves do not coincide.

It will be seen from Fig.6, which shows the variation of ϵ_1 with E_0 for two values of $E_\sim$, that at $E_\sim$ = 100 v/cm a dc field of 250 v/cm fully "saturates" the crystal. The value of ϵ measured after removal of the biasing field does not change after the crystal is held for a considerable time in a 100 v/cm ac field or stored in zero field at room temperature for 24 hours.

With increasing ac field strength, the divergence between the "forward" and "reverse" ϵ vs E_0 curves naturally decreases, but it remains noticeable even in strong fields. The divergence between the ϵ curves is smaller for $BaTiO_3$ single crystals and persists only up to E = 500 v/cm.

Conclusions

1. Investigations of tri-glycine sulfate and $BaTiO_3$ single crystals in a strong electric field ($E_m > E_c$) showed that these materials are characterized by a high degree of nonlinearity (for tri-glycine sulfate - $N \approx 80$, for $BaTiO_3$ - $N \approx 30$) and high values of the dielectric loss tangent (for tri-glycine sulfate $\tan \delta_{max} = 3.8$; for $BaTiO_3$ $\tan \delta_{max} = 1.2$).

2. For tri-glycine sulfate crystals we observed a substantial divergence between the ϵ vs field (both ac and dc) curves recorded in increasing and decreasing fields. The appreciable difference between the ϵ curves for tri-glycine sulfate recorded in an increasing and decreasing dc biasing field is evidence of the good electric "memory" of this substance.

Institute of Crystallography,
Academy of Sciences of the USSR &
Central Scientific Research Laboratory for Piezoelectric Materials,
Committee on Radio Electronics, Soviet of Ministers of the USSR

References

1. W.P.Mason & R.F.Wick, Proc. IRE, 42, 1606 (1954).
2. T.N.Verbitskaia, Izv.AN SSSR, Ser.fiz., 20, 185 (1956). (Trans.Bulletin, 20, No.2, 169.)

* * * * *

INDIVIDUAL CHARACTERISTICS OF DOMAINS IN ROCHELLE SALT

- V.L. Indenbom & M.A.Chernysheva

Polarization in ferroelectric materials is a complex process which is accompanied not only by growth of some domains at the expense of others, but also by changes in the polarization of individual domains. For example, if initially there are two domains of equal thickness with antiparallel polarizations, upon the application of an external field (or a mechanical stress field) the absolute magnitude of the polarization will increase in the domain that grows at the expense of its neighbor and decrease in the shrinking domain.

This "individual behavior" of the domains greatly hampers comparison of theory with experiment. Both the thermodynamic and the molecular theories of ferroelectricity operate with quantities pertaining to single crystals, whereas electrical and mechanical measurements (for example, measurements of the spontaneous polarization or deformation) are ordinarily performed on multiple domain specimens in which there occur simultaneously rearrangements within the domains and uncontrolled movements of the domain walls.

There can be little doubt that for rigorous verification of present theories and their further development it would be expedient to have experimental data characterizing individual domains. Even qualitative observation of domain behavior brings to light a number of facts conflicting with the common assumption that the domain structure of ferroelectrics is determined by the energy balance between the surface field and the domain walls. Thus, for example, observation shows that domains in ferroelectrics do not disappear when the specimen is shorted, although it would seem that some investigators regard this as axiomatic.

One of us (Chernysheva[1]) noted in a report presented at the First Conference on Ferroelectricity that the readily measurable angle of rotation of the optical indicatrix of domains can serve as an asymmetry parameter and has certain advantages as such over the domain polarization, which is commonly used in the theory of ferroelectricity, or the spontaneous deformation, which is found to be more convenient in the general theory of phase transitions. Quantitative analysis[2] showed that in Rochelle salt the optical indicatrix rotates about the ferroelectric

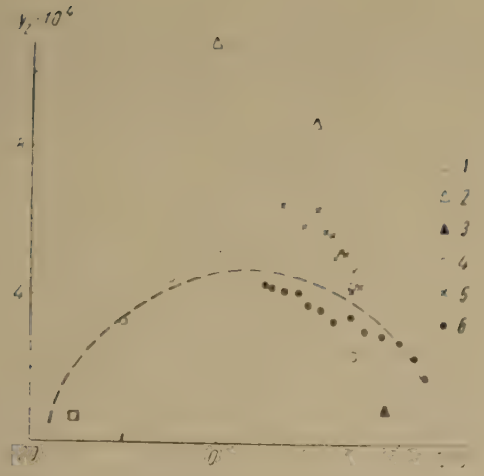

Fig.1. Temperature variation of the monoclinicity parameter of Rochelle salt crystals according to the data of different authors. All the data has been converted to values of the spontaneous deformation y_z: 1) x-ray measurements of the monoclinicity angle,[3] 2) direct measurement of the angle between the Y and Z faces[4], 3) calculated from the residual strain[5], 4) calculated from the spontaneous polarization[4], 5) calculated as the results of the first series of optical measurements shown in Fig.7 of Ref.2, 6) calculated from the results of the ninth series of measurements in Ref.2. The dashed line represents the averaged values from the optical measurements given in Fig.8 of Ref.2.

axis by an angle 30 times greater than the twinning angle which is virtually equal to the spontaneous deformation y_z. At a temperature of about 18° these angles are about half a degree and one minute, respectively. This explains the advantages of the optical method (viewing the specimen through crossed polaroids or Nicols) for measuring the polarization and deformation of individual domains. The results of optical observations can be reduced on the basis of the known relationship between the coefficients of the optical indicatrix, deformation and polarization.[2] The consistence of the diverse data available on the temperature dependence of the monoclinicity parameter of Rochelle salt is illustrated in the diagram of Fig.1 (reproduced from Ref. 2 with additional supplementary material).

Apparently, the spontaneous polarization and deformation of Rochelle salt crystals depend on the history of the specimen and decrease through successive cycles of measurement. In other words, the aging effect may be explained not only by retardation of wall movements by also by "volume aging" of each domain. Further investigation of this effect is essential not only in connection with practical problems but also from the standpoint of theory, inasmuch as investigation of the temperature variation of the monoclinicity parameter, as we showed elsewhere[6], makes it possible to construct the thermodynamic potential of the ferroelectric.

We also made an attempt at direct measurement of the spontaneous deformation of domains in Rochelle salt. As has been shown by Vitovskii[7], Rochelle salt crystals can be cleaved in the c plane. It is logical to assume that if a crystal is fractured at a temperature in the ferroelectric region there should be observable on the cleavage face a twin topography with faces corresponding to the ends of individual domains and inclined relative to each other at an angle equal to twice the twinning angle. And in fact we were able to detect on the surface of crystals cleaved along the c plane a topography similar to that expected. With oblique illumination we could readily discern a roof-like relief (Fig.2,a). The roof ridges can be distinguished from the valleys either by varying the focusing of the microscope or by drawing a sharp point over the surface. In Fig.2,b one can see where the scratching point hit the ridges and passed harmlessly over the valleys. The direction of the ridges was in all cases consistent with the orientation of the domains (the c domains intersect the c plane along the *a* axis).

Interferometric studies of cleavage faces show that the "roofs", as might be expected, have a low pitch (flat slope): as may be seen in Fig.3, the interference bands remain rectilinear over the extent of each domain and change direction sharply in passing over a domain wall. Qualitative analysis of the interferometric

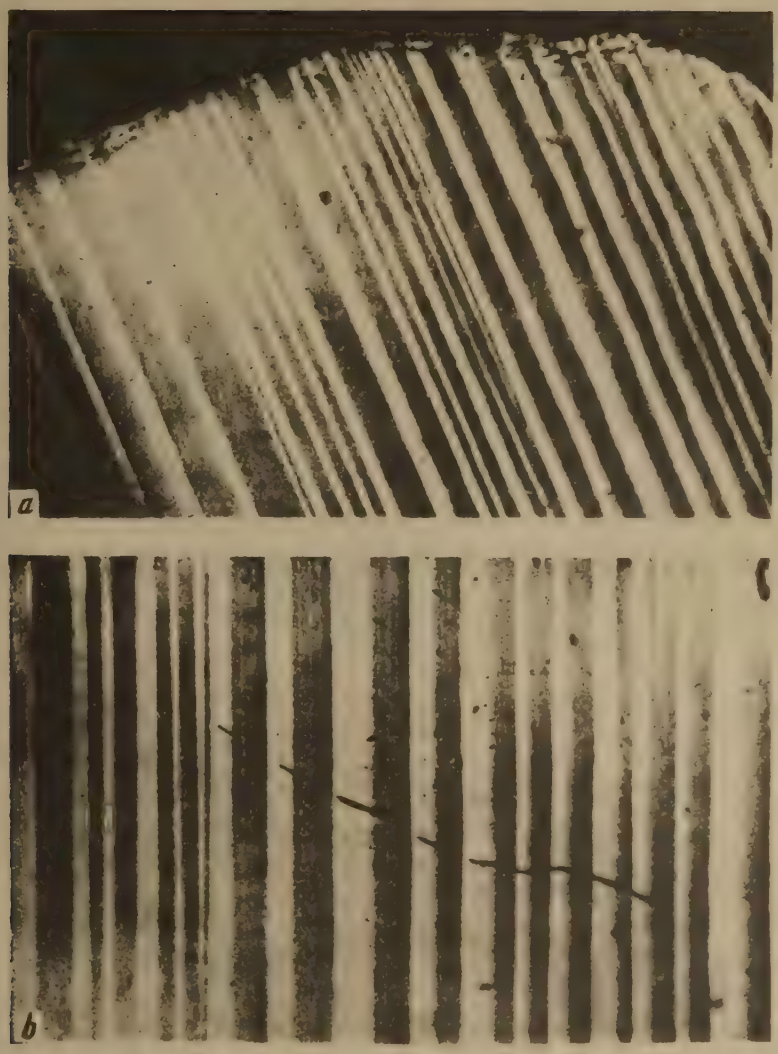

Fig.2. Cleavage face of a Rochelle salt crystal in oblique illumination: a) twin topography at the edge of the specimen; splitting of some of the domains is evident; b) roof-like topography; the microscope is focused on the "valleys", hence the "ridges" are less clear; the fine structure on the slopes of some of the roofs is clearly discernible. Dark trail at center - scratch made by needle point hitting the roof "ridges".

data, however, led to an unexpected result: the angles between neighboring "roof sections" proved to be of the order of 40' instead of the expected 2'. It follows therefrom that either the spontaneous deformation (and polarization) of Rochelle salt is an order of magnitude greater than assumed or that the cleavage planes in the domains do not coincide with the former c plane of the orthorhombic crystal. In the latter case, however, it is not clear why the cleavage plane is a plane with a larger indices.

We refrain from further discussion of the above mentioned effect pending accumulation of more detailed experimental data, but we would like to describe a number of other interesting effects observed in investigating cleavage faces. It is known that at the intersection of a crack with a screw dislocation the sides of the crack are found to be at different elevations and a step equal in height to the Burger dislocation vector develops on the cleavage face. If the crack crosses a block boundary, consisting of a dislocation nucleus (or net), there appears a series of steps - cleavage echelons (Fig.4) - which further reunite into microscopic steps. As a result there form characteristic tree-like patterns.

Typical tree-like patterns observed in our experiments are reproduced in Fig.5. By varying the angle of illumination we could verify that these figures actually correspond to block boundaries. This is discernible in Fig.5,b in which the disorientation of the blocks can clearly be seen owing to differences in illumination. In the same photograph there is evident an interesting correlation between the domain pattern and the beginnings of the cleavage echelons, corresponding to screw dislocations. It may be assumed that the fine structure of the domains

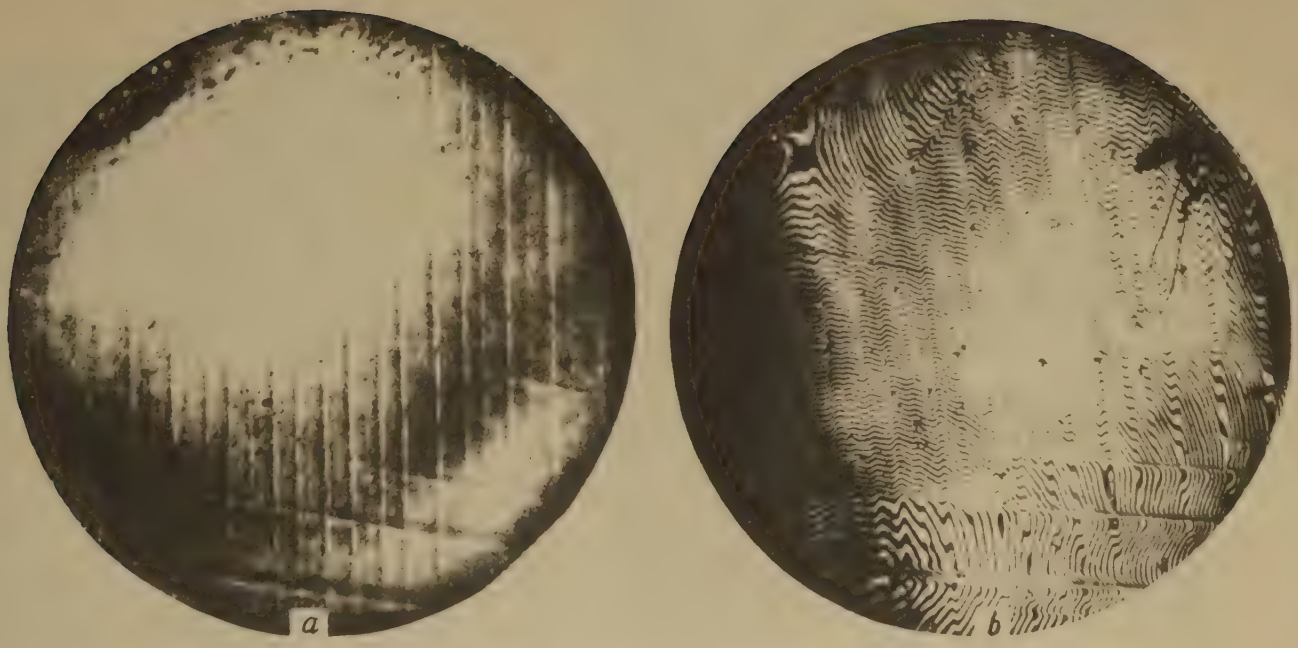

Fig.3. Interferograms of cleavage surface of Rochelle salt crystal: a) control photograph in reflected light; one can see the domain walls (vertical lines) and the cleavage face echelons (lower right); b) interference pattern of the same section of the crystal surface (light from mercury tube, λ = 546 mμ; distance between bands = $\lambda/2$). There are breaks in the interference bands at the domain walls and a distinct shift in the bands at the cleavage echelons.

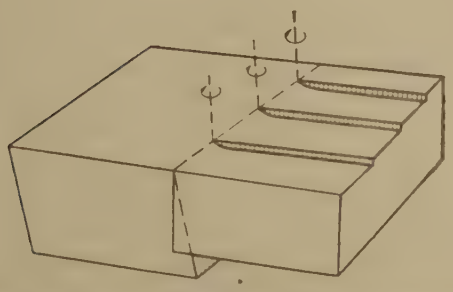

Fig.4. Formation of cleavage echelons at screw dislocations. The series of screw dislocations corresponds to the boundary of blocks rotated relative to each other about an axis perpendicular to the boundary (torsion boundary).

(Fig. 2,b and Fig.3) is connected with individual dislocations. The relation between domain structure and dislocations has been discussed earlier, independently by us[9] and Nakamura[10]. In particular, screw dislocations parallel to the c axis yield a stress field with a nonzero τ_{yz} component, which determines the character of distortions of the twin pattern. Owing to this effect, dislocations can interact with domain walls, influence the coercive force of the ferroelectric, determine the course of restoration of the domain structure after removal of the external field, etc.

Inasmuch as in investigating the fine structure of cleavage faces, one can establish a correlation between the domain pattern and the distribution of dislocations, such studies may prove to be very valuable in investigating other structure-sensitive properties of ferroelectrics. It is of particular interest to bring out the possible relation between dislocations and the magnitude of the coercive force and hence the "memory" attributes of ferroelectrics.

Institute of Crystallography,
Academy of Sciences of the USSR

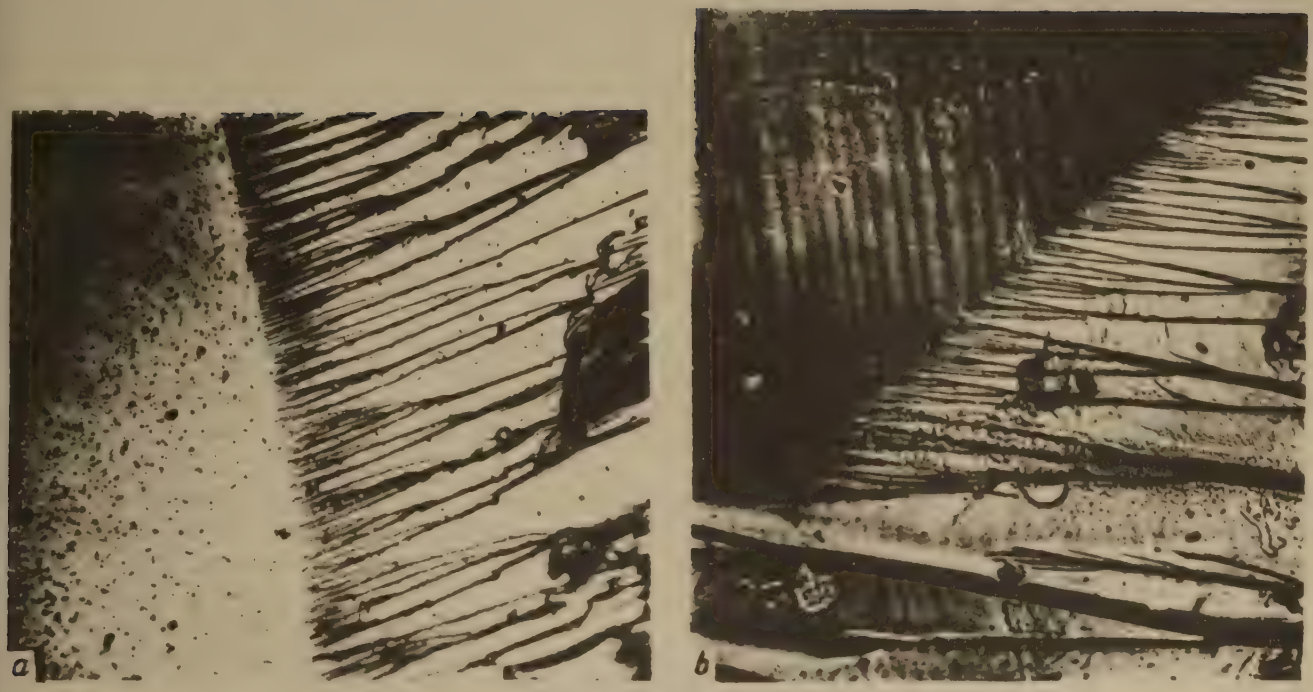

Fig.5. Tree-like cleavage echelon patterns appearing at the boundary of disoriented blocks: a) the beginning of each echelon marks the point of emergence of a screw dislocation to the surface; b) correlation between domain structure and dislocations.

References

1. M.A.Chernysheva, Izv. AN SSSR, Ser.fiz., 21, 289 (1957). (Trans.Bulletin 21, No.2, 293.)

2. V.L. Indenbom & M.A.Chernysheva, Kristallografiia, 2, 526 (1957). (Trans. Soviet Physics - Crystallography.)

3. A.R.Ubbelohde & I.Woodward, Proc.Roy.Soc., 185, 448 (1946).

4. H.Mueller, Phys.Rev., 57, 829, Ibid., 58, 565 (1940).

5. W.G.Cady, Piezoelectricity, N.Y., 1946. (Cited in Russian trans., 1948.)

6. V.L. Indenbom & M.A.Chernysheva, Zhur.eksp.i teor.fiz., 32, 697 (1957). (Trans.Soviet Physics - JETP.)

7. B.V.Vitovskii, Kristally segnetovoi soli (Rochelle salt crystals) Dissertation, Inst.of Crystallography, USSR, Ac.of Sci., 1948.

8. P.B.Hirsch, Progress in Metal Physics, 6, 236 (1956).

9. V.L. Indenbom & M.A.Chernysheva, Doklady AN SSSR, 111, 596 (1956). (Trans. Soviet Physics - Doklady.)

10. T.Nakamura, J.Phys.Soc., Japan, 11, 467 (1956).

SOME RESULTS OF A SEARCH FOR NEW PIEZOELECTRIC MATERIALS

- I. S. Rez

The purpose of the present work, in addition to discovery of new piezoelectrics and investigation of their electrophysical and physicochemical characteristics, was to establish a criterion that would be of help in finding new piezoelectric materials.

There have been several attempts at formulating such a criterion. One of the earliest is the indication given by Wooster[1] that piezoelectric substances are characterized by the presence of acentric atomic structures. The validity of this general categorizing observation was tested as regards inorganic compounds by Zerfoss & Johnston[2]. On the basis of experimental data for more than 400 substances, they established that piezoelectric structures, as a rule, contain asymmetric radicals and that when radicals of this type surround metal ions, the general asymmetry of the structure is enhanced.

In 1952 Koptsik[3] on the basis of extensive statistical material proved the validity of the refined geometric criterion according to which one may "with good probability expect a dielectric crystal to exhibit piezoelectric behavior if as regards its symmetry it belongs to one of the favorable space groups."

Further work of Koptsik and his co-workers on his newly discovered piezoelectric materials substantiated the general validity of this criterion. Unfortunately, the possibility of utilizing this crystallo-physical criterion for purposes of prediction in the search for new piezoelectrics is complicated by the necessity of first having to determine the space group, which is a laborious and not always precise operation particularly as regards determining the acentricity.

The present writer formulated the genetic search principle: it is expedient to seek for new piezoelectrics among families of substances at least one member of which exhibits a pronounced piezoeffect. In such exploratory research, particular attention should be given to investigating the influence of different modifications of the type structure, particularly as regards enhancement of its asymmetry, increase of the molecular dipole moment, elimination of antiparallel packing of structural dipoles, reduction of the packing density and increase of the stresses in the structure due to deformation of valence angles and long bonds. Here the availability of x-ray diffraction data is no longer a limiting factor, which greatly enlarges the number of substances entering into the scope of the search.

The above argument is to a large extent based on the concept of homologous isomorphism introduced by Kitaigorodskii[4] for series of organic compounds, the members of which, having geometrically similar molecules, as a rule form exceptionally similar packings. As has been shown in our experimental work[5], these concepts in a number of cases also hold for complex and organic compounds. Indirect substantiation of the views outlined above was obtained in analysis of the data of Mason-Holden[6] and examination of the distribution of acentric compounds according to types and space group as classified by Donnay & Nowacki[7] and Koptsik[9]. Accordingly, we carried out a selection of substances for testing for piezoactivity: to complete

the picture in some cares we deliberately chose, for control purposes, centrosymmetric structures, which naturally reduced the "yield" of piezoelectrics with respect to the total number of tested substances. A total of 676 substances, most in powder form, were tested for piezoelectric activity in the TsNILP (Central Scientific Research Laboratory for Piezoelectrics) in 1955-1957. The tests were carried out by means of the PT-2 piezotester described elsewhere.

A list of the 363 compounds exhibiting piezoelectric behavior and a description of the test procedure are given in Ref.5. The results of the investigations are summarized in Tables 1 and 2, which show the distribution of the tested and active compounds among the classes of inorganic, complex and organic substances.

Table 1

Distribution according to type of compound of inorganic and complex substances exhibiting piezoactivity

No.	Type compound	Total number tested	Activity detected			
			strong	weak	total	%
1	AX	11	4	3	7	64
2	AX_2	8	—	3	3	37
	$AX_2 \cdot AX$	3	—	—	—	—
3	AX_3, A_2X_5, A_2X_3	9	2	2	4	44
4	With complex AX_3 anion					
	a) plane triangle	13	—	3	3	23
	b) pyramidal form	18	4	7	11	61
5	With complex AX_4 anion	28	2	8	10	36
6	Complex sulfocyanides					
	a) A $[Hg(CNS)_4]$	5	2	3	5	100
	b) A $[Co(CNS)_4]$	4	1	2	3	75
	c) A $[Zn(CNS)_4]$	3	1	—	1	33
	d) A $[CNS]_2 \cdot n$ Py	6	2	3	5	84
	e) A $[CNS]_y \cdot B_x$	6	—	2	2	33
7	Other complexes including					
	a) dimethyl glyoximates	8	6	—	6	75
	b) Pt & Pd complexes	16	7	2	9	56
	c) other complexes	9	2	2	4	44
8	Heteropoly acids & their salts	13	6	4	10	78
	Totals	160	39	44	83	52

Inorganic and Complex Compounds

For convenience of analysis the tested inorganic and complex compounds have been divided into eight basic types with several subtypes (Table 2).

Noteworthy is the exceptionally high "yield" of piezoelectrics, i.e., 52% of the total number of specimens tested exhibited some degree of piezoelectric activity as compared with 17% of acentric structure substances and 6.2% of the substances with a structure favorable to the appearance of the piezoelectric effect of the total number of inorganic compounds investigated by Donnay & Nowacki and Koptsik, respectively.

The following general conclusions may be drawn on the basis of a critical examination of the test data for inorganic compounds:

Table 2

Distribution according to type of compound of organic substances exhibiting piezoactivity

No.	Type compound	Total number tested	Activity detected			
			strong	weak	total	%
1	Amines	90	19	27	46	51
2	Amines salts	48	4	18	22	46
3	Amines acids	32	1	13	20	63
4	Guanadine compounds	14	4	7	11	79
5	Alkaloids	8	6	2	8	100
6	Azo compounds	9	1	4	5	55
7	Carbonyl compounds					
	a) Containing CO group (excluding acids & their salts)	15	6	3	9	60
	b) esters	6	—	2	2	33
	c) oxalates	5	1	2	3	60
	d) phthalates	6	1	2	3	50
	e) other acids & their salts	36	2	8	10	29
8	Polynuclear hydrocarbons					
	a) naphthalene derivatives	12	2	3	5	42
	b) anthraquinone	15	1	8	9	60
	c) Other polynucleates	6	1	1	2	33
9	Nitro compounds	50	11	16	27	54
10	Nitroso compounds	7	1	5	6	86
11	Hydroxy compounds	22	5	8	13	59
12	Hydroxy acids & their salts					
	a) citrates	6	—	2	2	33
	b) tartrates	8	1	4	5	63
	c) lactates	2	2	—	2	100
	d) other hydroxy acids	7	—	2	2	28
13	Salicylic acid derivatives	14	5	6	11	79
14	Sugars & derivatives	14	2	6	8	67
15	Triphenylmethane compounds	21	3	12	15	71
16	Other compounds, including					
	a) oximes	8	4	3	7	87
	b) others	55	5	22	27	49
	Totals.....	516	94	186	280	54

1) Most compounds exhibiting a piezoelectric effect apparently contain readily deformable atomic structures: pyramids, tetrahedra, deformed octahedra or combinations thereof. Substances with relatively rigid atomic structures, such as plane triangles and linear chains, generally exhibit little or no piezoelectric activity.

2) Substances exhibiting a piezoeffect are for the most part compounds with predominantly covalent bonds.

3) In the case of isomorphic substitution, the piezoeffect associated with the skeletal structure is retained, increasing or decreasing depending on the properties of the substituent atom or radical.

Organic Compounds

In analyzing the data of Table 2, one cannot but note that despite the wider range of potentially piezoactive compounds tested, as compared with the list given by Mason-Holden[6], in addition to amines and their derivatives, hydroxy and nitro compounds, our list contains a number of new types of organic substances which give a high "yield" of piezoelectrics.

One might formulate the following "guiding principle" for seeking organic piezoelectrics: they should be searched for among biologically active substances, emphasizing purposeful selection of substituents aimed, on the one hand, at labilizing their readily deformable structures and, on the other hand, at controlling their physical properties to satisfy practical engineering requirements.

I take this occasion to reiterate the view expressed at the Second All-Union Conference on Piezoelectricity in 1955 regarding the importance of systematic research on synthesis of piezoelectric electret-plastics of isotactic (stereographically regular) polymers with polar side chains.

It may not be out of place here to compare the overall results of the search for new piezoelectrics at the TsNILP with the results of the Koptsik group[9] at Moscow State University, who investigated series of substances at random, i.e., without preselection.

Table 3

Comparison of the results of testing substances for piezoelectric activity at the TsNILP and Moscow State University

Type compound	Total number tested	Activity detected					
		strong	%	weak	%	total	%
A. Central S.-R. Lab. for Piezoelectrics Tests							
Inorganic and complex compounds	160	39	24	44	28	83	52
Organic compounds including guanidine compounds (complex)	516	94	18	186	36	280	54
Totals.....	676	133	20	230	33.5	363	53.5
B. Moscow State University Tests							
Inorganic, organic and complex compounds	1200	37	3.1	257	21.4	294	24.5

The evident difference in the "yields" of piezoelectrics (53.5% as against 24.5%) may be taken as evidence of the worth of the genetic selection principle outlined above.

I desire to express my sincere gratitude to my colleagues A.S. Sonin, E.E.Tsepelevich-Volynets, A.A.Filimonov and L.V.Samsonova for active assistance in the work and discussion of results and L.Z.Rusakov and I.S.Zheludev for much valuable advice.

TsNILP of the Committee on Radioelectronics
under the Soviet of Ministers of the USSR

References

1. W.A.Wooster, Crystallophysics, p.27, Cambridge, 1938.
2. S.Zerfoss & L.Johnston, Amer. mineralogist, 34, 61 (1949).
3. V.A.Koptsik, Issledovanie elektricheskikh i uprugikh svoistv kristallov rezortsina (Investigation of the electric and elastic properties of resorcin crystals), Thesis, Moscow State University, 1952; Izv.AN SSSR, Ser.fiz., 20, 219 (1956). (Trans. Bulletin, 20, No.2, 201.)

4. A.I.Kitaigorodskii, Organicheskaia kristallokhimiia (Organic Crystallochemistry), p.241, M.-L., 1955.

5. I.S.Rez, A.S.Sonin, E.E.Tsepelevich & A.A.Filimonov, Trudy (Proceedings) TsNILP, No.3 (1959).

6. W.P.Mason, Piezoelectric crystals and their application to ultrasonics, N.Y., 1950. (Cited in Russian trans., M., 1952.)

7. I.D.H.Donnay & W.Nowacki, Crystal Data, 60. Geolog. Soc. America Memoir, 1954.

8. I.S.Rez, Izv.AN SSSR, Ser.fiz., 21, 466 (1957). (Trans. Bulletin, 21, No.3, 463.)

9. V.A.Kopt sik, A.A.Voronkov & K.A.Minaeva, Issledovanie novykh p'ezoelektricheskikh kristallov na malykh obraztsakh (Investigation of new piezoelectric crystals using small specimens) Vestnik, Moscow State University, Natural Science Series, No.6, 1958.

INFLUENCE OF DIFFERENT FACTORS ON THE CURIE TEMPERATURE OF FERROELECTRICS WITH THE PEROVSKITE STRUCTURE

- Iu.N.Venevtsev, G.S.Zhdanov & S.P.Solov'ev

Introduction

The question of the Curie point T_c in ferroelectric substances with the perovskite structure has been repeatedly treated over the years by many investigators.[1-11]

Despite the wealth of experimental data available on ferroelectrics with the perovskite structure, there is no unanimity of opinion among different authors[1-7] on the question of the Curie temperature. In fact, Shirane, Jona & Pepinsky[12] are of the opinion that the great scope of the experimental material has operated to complicate the situation. This is explained by the fact that even in the case of the most suitable subjects of investigation - solid solutions - various replacement cations differ as regards a number of their characteristics (polarizability, charges, radii, etc.) so that it is difficult to trace and identify the influence of these individual characteristics of the cations on T_c.

The conclusions arrived at in Refs.1-7 are for the most part based on the assumption that the "ferroactive" cations in the various ABO_3 type ferroelectric and antiferroelectric substances under consideration are type B cations. Actually, however, the B cations are the ferroactive ones only in some substances, whereas in others the ferroelectricity must be attributed to the A cations.[8,9,13] Hence, as we pointed out earlier[10], the results of Refs.1-7 are in need of re-examination and revision.

The classification of ferro- and antiferroelectrics with the perovskite structure according to the type of ferroactive cation (A or B) proposed by us[8,9,13] should facilitate discussion of the question of the Curie temperature. Such a re-examination of the question is the purpose of the present paper.

Re-examination of the Question

Ferroelectrics with the perovskite structure are compounds in which the character of the bonds is predominantly ionic.[3,8,12,13] Hence, to start, we can attempt to interpret the experimental facts and, in particular, to explain why one compound has a higher Curie point than another on the basis solely of such ionic characteristics as the polarizability (α), the charges (e) and the ionic radii (R).

In Table 1 we list a number of ABO_3 compounds with the perovskite structure which are now definitely known to possess ferroelectric or antiferroelectric properties and give their Curie points. The compounds are grouped according to the type of ferroactive cation (A or B) and are arranged in order of decreasing values of the geometric factor t.

We recall that under the ferroactive ion we understand the ion that has "room" in the unit cell of the cubic modification.[8,10,13] Depending on which cations (A or B) have "room", i.e., are loosely held, the unit cells of the compounds in question undergo various characteristic distortions (tetragonal, monoclinic or rhombohedral) in different sequences with variation of temperature.[13] From this it may be concluded that the polar rearrangements of the unit cells (including the transition at the Curie point) of ferro- and antiferroelectric compounds are determined primarily by the energy state of the cations that have "room" in the cell, i.e., by the energy state of the ferroactive cations.[8,10] The coordination numbers of the cations (A and B) in the perovskite type lattice are different. Hence for this reason alone the energy states of the A and B cations can differ. This circumstance must be borne in mind in attempting to explain the difference in Curie temperatures for two ferroelectrics with ferroactive cations of different types (A or B).

Table 1

Ferroelectric and antiferroelectric compounds with the perovskite structure

Type of compound	Ferroactive cation	ABO_3	t *	T_c, °K
Ferroelectric	B	$BaTiO_3$	1,03	393
		$KNbO_3$	1,00	692
	A	$KTaO_3$	1,00	13
		$PbTiO_3$	0,98	763
Antiferroelectric	A	$PbHfO_3$	0,92	488
		$PbZrO_3$	0,90	508
		$NaNbO_3$	0,86	633

* $t = \frac{R_{A(C.\#12)} + R_O}{\sqrt{2}\,(R_B + R_O)}$, $R_O = 1.36$ Å.

Theoretical Evaluation of the Influence of Some Cation Parameters on the Curie Temperature

According to Kittel[14], the Curie temperature of a ferroelectric can be approximately determined by evaluating the interaction energy of the dipoles with the internal field acting thereon. From our point of view such theoretical evaluation of the Curie point will be more effective if we consider the interaction energy not of all the dipoles but only of those connected with the ferroactive cation (A or B) at temperatures close to the Curie point. In other words, our problem can be reduced to analysis of how the products P_AE_A and P_BE_B depend on different factors (here P_A and P_B are on the electronic dipole moments associated with the A and B cations, respectively; E_A and E_B are the internal fields acting on these cations). Hence we can follow the variation of the Curie point of ferroelectrics with ferroactive type B cations by determining the variation of P_BE_B (or in the case of substances with ferroactive A ions, by determining the variation of P_AE_A). An increase of the product would indicate an increase of the Curie temperature and vice versa.

In Ref.15 we investigated the character of the variation of the internal fields and electronic dipole moments as functions of the polarizabilities, charges and radii of the cations for the case of the tetragonal modification of the ferroelectrics under study. It is known, however, that in some ferroelectrics the phase appearing immediately below the Curie point is not the tetragonal modification but the rhombohedral, or in the case of antiferroelectrics the pseudomonoclinic (orthorhombic).

Nevertheless, the results obtained in Ref.15 can also justifiably be used for investigating the variation of the products P_AE_A and P_BE_B in cases when the pseudomonoclinic or rhombohedral modification obtains below the Curie point. The fact is that calculations[16] of the fields in the pseudomonoclinic modification of $BaTiO_3$ showed that in this modification, as in the tetragonal one, the strongest field acts on the titanium ion, the weakest on the barium ion; in other words, the qualitative relationships between the fields acting on the A and B ions in different modifications of the same compound persist. In addition, in Ref.15 it was established that the character of these relationships remains the same for different ferroelectrics having the same modification. True, the ferroelectric and antiferroelectric pseudomonoclinic modifications differ as regards their nature[8,9,13] but in this case apparently, too, there is reason to assume that the qualitative

relationships between the fields acting on the A and B ions in the modifications are the same.

Our analysis[9] of the products $P_A E_A$ and $P_B E_B$ showed the following. The Curie temperature of the compounds under study, both those with $t > 1$ and those with $t < 1$ must be the higher, the smaller the lattice period, the greater the polarization and the higher the charge of the ferroactive cation. In addition, it was concluded that the Curie temperature of ferroelectrics with $t > 1$ and $t < 1$ is weakly dependent on the polarizability of the nonferroactive cation.

It must be emphasized that the above deductions regarding the character of the influence of different cation parameters on the Curie temperature are predicated on the assumption that the difference Δ between the size of the "void" (i.e., space in the unit cell) occupied by the ferroactive cation and the radius of this cation remains constant in all cases. Actually this is not always the fact. But there is reason to assume that variation in the geometric conditions for displacement of the ferroactive cations plays a secondary role in determining the Curie point in ferroelectrics for which $t = 1.00 \pm 0.03$. From the results obtained in Ref. 15 it may be inferred that in compounds with $t = 1.00 \pm 0.03$ the internal fields change less with variation (within reasonable limits) of the magnitudes of the displacements of the A or B cation than with variation (within equal ranges) of the charges and polarizabilities of the cations and of the lattice period. In connection with the fact that, as has been shown above, the Curie point depends substantially on the internal fields, it is natural to attribute only a secondary role to the variation of Δ in explaining the difference in Curie points of ferroelectrics with $t = 1.00 \pm 0.03$. It must be emphasized, however, that this inference is valid only when other factors, in addition to Δ, change significantly. This deduction will apparently not be valid when t closely approaches unity. In this case, obviously, small changes in Δ may be significant. It may therefore be assumed that one of the necessary conditions for spontaneous displacement of the ferroactive cations at the Curie point is the requirement that Δ must exceed a certain critical value Δ_{cr} for the given compound and the given conditions. Hence if under certain conditions Δ for a given ferroelectric beomces smaller than Δ_{cr}, ferroelectricity should not be evinced.

In view of what has been said above one can understand the behavior of the Curie point in barium titanate under hydrostatic pressure. According to Merz[17], T_c of this compound decreases (to a certain value) with increasing pressure. Under hydrostatic pressure the lattice period and Δ in the cubic modification of $BaTiO_3$ decrease. Theoretically the first factor acts to increase the Curie temperature. The second factor has the opposite effect; whereas in the absence of pressure at 120° Δ is greater than Δ_{cr}, under pressure this situation will obtain only at lower temperatures. In view of the fact that the Curie temperature of $BaTiO_3$ is reduced under pressure, it may be inferred that the influence of the second factor (Δ) on the Curie point is stronger than that of the first factor (the lattice constant a).

In the specific case of $BaTiO_3$, decrease of the lattice period under pressure was accompanied by decrease in the size of the "void" occupied by the ferroactive cations and, consequently, by decrease of Δ. Examination of the data for other compounds shows that this is not always the case. In the case of $PbTiO_3$-$SrTiO_3$ solid solutions (the values of t for $PbTiO_3$ and $SrTiO_3$ are 0.98 and 0.96, respectively), with replacement of the lead by strontium the lattice period is also reduced, but the relative size of the "voids" occupied by the type A (Pb and Sr) cations increases, i.e., the mean value of Δ increases.

In cases when t differs from unity by more than 0.03, the influence of Δ on the Curie temperature must be taken into account together with the effect of polarization, the charges and the lattice constant. In this connection, the results obtained in Ref.15 indicate that increase of Δ should raise the Curie temperature.

Analysis of Experimental Data

A. Influence of polarizability of A type cations on T_c of compounds with t < 1

To evaluate the influence of polarizability of A type cations on the Curie point in compounds with t < 1 we can refer to the data on lead and strontium titanates. The values of t, the lattice constant a in the cubic modification, the Curie point T_c and the polarizabilities α and radii R of the A and B cations for these two titanates as well as for $PbTiO_3$, which we shall discuss later, are listed in Table 2.

Table 2

Factors influencing the Curie temperature of titanates

ABO_3	$\alpha_A \cdot 10^{24}$, cm^3	$\alpha_B \cdot 10^{24}$, cm^3	R_A, Å	R_B, Å	a, Å	t	T_C, °K
$SrTiO_3$	1,42	0,19	1,20	0,64	$3,90_{18}$°C	0,96	-
$PbTiO_3$	4,34	0,19	1,26	0,64	$3,96_{500}$°C	0,98	763
$PbZrO_3$	4,34	0,80	1,26	0,82	$4,15_{23}$°C	0,90	508

Notes: The electronic polarizabilities for Ti^{4+} and O^{2-} are taken from Ref. 18, the polarizability values for Pb^{2+} and Sr^{2+} are taken from Ref. 19; the ionic radii are taken from Ref. 20; the lattice constants at the indicated temperatures are taken from Refs. 7 & 21-24.

We have included $SrTiO_3$ in this table together with the ferroelectric $PbTiO_3$ and the antiferroelectric $PbZrO_3$ despite the fact that $SrTiO_3$ may be only an induced ferroelectric under certain conditions.[25] We grouped it with the other titanates because like them it has a high dielectric constant. According to Linz[26] the dielectric constant of $SrTiO_3$ at 113°K is 815.

Let us first consider $PbTiO_3$ and $SrTiO_3$. The Curie temperature of $PbTiO_3$ is 763°K. Ferroelectricity in $SrTiO_3$ can be induced only below 90°K. Thus insofar as it is meaningful to speak of the ferroelectric properties of $SrTiO_3$, it must be noted that they are evinced at a much lower temperature than in $PbTiO_3$. What can we deduce from this experimental fact? $PbTiO_3$ and $SrTiO_3$ have identical B type ions (Ti) and different A type ions (Pb and Sr), having different radii, different polarizabilities and different electronic structures. However, the difference in structure amounts essentially to a difference of ionic characteristics, the influence of which on the ferroelectric attributes is undoubtedly secondary; hence we will disregard this factor. Thus we assume that the difference between the Curie temperatures of $PbTiO_3$ and $SrTiO_3$ is connected primarily with the difference in radii and polarizabilities of the Pb and Sr ions. According to the data of Table 3, the polarizability of the Pb ion is 3 times greater than that of the Sr ion. The radius of the Sr ion is slightly smaller than the radius of Pb. However, instead of comparing the ionic radii directly it is more expedient to compare the lattice periods (a) of $PbTiO_3$ and $SrTiO_3$ in the cubic modifications, for precisely these periods, rather than the radii of the individual ions, serve as a measure of the interatomic distances which, according to our argument, together with the charges and polarizabilities, determine the interionic interaction in the respective lattices. Why then does spontaneous polarization appear in $PbTiO_3$ at 763°K, while in $SrTiO_3$ it can be induced only below 90°K? Let us compare the lattices of both compounds at, say, 773°K, i.e., at a temperature slightly above the Curie point of $PbTiO_3$. At this temperature the period of the $PbTiO_3$ lattice a = 3.96 Å.[22,23] The period of the $SrTiO_3$ lattice at room temperature[21] is 3.90 Å, while at 773°K it increases to 3.92 Å, inasmuch as according to our measurements the linear expansion coefficient of $SrTiO_3$ is $1 \cdot 10^{-5}$ degree^{-1}.

Thus at 773°K $PbTiO_3$ and $SrTiO_3$ differ in that the lattice period of $PbTiO_3$ is 0.04 Å greater than the period of $SrTiO_3$ and, in addition, in that the polarizability of the respective type A ions (Pb and Sr) differ by a factor of 3.

The difference between the lattice periods of $PbTiO_3$ and $SrTiO_3$ is not large, not only compared with the interatomic distances in these compounds (~2 Å) but also compared with the differences between lattice periods that can obtain in compounds of this class. For example, the difference between the lattice periods of $PbTiO_3$ and $PbZrO_3$ (see Table 2) at 773°K is 0.20 Å (the linear expansion coefficient of the $PbZrO_3$ lattice in the cubic modification is $\sim 1 \cdot 10^{-5}$ degree^{-1}). Hence it is doubtful that the difference between the lattice periods of $PbTiO_3$ and $SrTiO_3$ alone can explain the great difference between the Curie points of these compounds. It must be concluded, therefore, that the great difference between the Curie points is due primarily to the three-fold difference between the polarizabilities of the Pb and Sr ions.

Thus from the fact that the Curie temperature of $PbTiO_3$ is appreciably higher than that of $SrTiO_3$, we can conclude that in the case of compounds with $t < 1$ the Curie temperature is the higher, the higher the polarizability of the ferroactive type A cation. This deduction is consistent with the theoretical analysis given above and was formulated by us earlier[8,9] as well as by Sawaguchi[7].

B. Influence of the lattice period and polarizability of the B type cations on T_c of compounds with $t < 1$

Now let us turn to $PbTiO_3$ and $PbZrO_3$ (Table 2). The temperature of the titanate (763°K) is appreciably higher than the Curie temperature of the zirconate (508°K). In these two compounds the ferroactive type A ions are identical (Pb), while the type B ions differ as regards both their radii (0.64 and 0.82 Å, respectively) and their polarizabilities ($0.19 \cdot 10^{-24}$ and $0.80 \cdot 10^{-24}$ C/cm^2). Before attempting to evaluate the influence of the difference in polarizabilities of the B ions and of the lattice periods on the Curie temperatures of $PbTiO_3$ and $PbZrO_3$, we note that in this case, in addition to the indicated factors presumably influencing T_c, one must also take into account the difference as regards the possibilities for displacement of the ferroactive Pb cations in the cubic modifications of $PbTiO_3$ and $PbZrO_3$. The Pb ions are loosely held in both lattices, but in $Pb\text{-}ZrO_3$ the "voids" occupied by the Pb ions are appreciably greater than in $PbZrO_3$, i.e., Δ for $PbZrO_3$ is larger than for $PbTiO_3$.

Thus, in the case of the two compounds in question there are appreciable difference as regards Δ, ω and α_B, hence the lower Curie point in $PbZrO_3$ as compared with $PbTiO_3$ may be explained by the depressing influence of either the larger lattice period or of the higher polarizability of the B type ion or again by the "joint depressing" effect of both these factors.

This deduction is not in conflict with the results of our theoretical evaluation according to which increase of the lattice period should reduce the Curie temperature, while the influence of the polarizability of the B cation should be relatively minor. In other words, our inference from the experimental data is not in conflict with the results of our theoretical analysis.

Let us now take up some other experimental factors and see which of them must be taken into account as influential in determining the Curie point.

C. Curie temperature of $Ba(Ti,Zr)O_3$ solid solutions

There is experimental evidence that the Curie point of $Ba(Ti,Zr)O_3$ solid solutions decreases with increasing $BaZrO_3$ content. In attempting to explain this fact we must take into account not only the increase in the mean polarizability of the

B type cations and the growth of the lattice period with increasing $BaZrO_3$ concentration, but also the fact that the Zr ions are "crowded", i.e., tightly held, in the lattice of these solid solutions (according to evaluations[8,9,13,21] $t < 1$ for $BaZrO_3$). In pure $BaTiO_3$ the Ti cations have "room" and hence are ferroactive. It follows that upon the introduction of zirconium to replace the titanium in the BaTiO the number of ferroactive type B cations decreases. Decrease in the number of ferroactive ions in the lattice must obviously hinder polar arrangement of the lattice. In other words, this "squeezing" of the cations, resulting in reduction in the number of ferroactive ions, is an additional factor acting to depress the Curie temperature. The decrease in Curie temperature observed in this case indicates that increase in the period of the lattice and increase in the number of nonferroactive cations together shift the Curie point to the side of lower temperatures more strongly than the increase in the mean polarizability of the B type ions displaces T_C to the side of higher temperatures.

D. $(Ba,Pb)TiO_3$ and $(Ba,Sr)TiO_3$ solid solutions

In the case of $(Ba,Pb)TiO_3$ solid solutions, their components, $BaTiO_3$ and $PbTiO_3$, have ferroactive cations of different types (B and A, respectively). If we reason on the basis of an averaged radius of the A cation ($\bar{R}_A = x \cdot R_{A_I} + (1 - x)R_{A_{II}}$), we might conclude that at a certain proportion of the components (when $\bar{t} = 1$), neither the B nor the A cations will have any room for displacement. Actually, however, in view of the statistical distribution of the A_I and A_{II} cations and owing to inhomogeneity of the atomic spacings in all solid solutions, the Ti cations in some cells and the Pb cations in others will still have the geometric possibility for displacement. Further, increase in the number of ferroactive Ti ions is accompanied by increase in the number of ferroactive Pb ions. As a result, ferroelectric properties are evinced in $(Ba,Pb)TiO_3$ solid solutions in the full range of formation of such solutions, and in view of the fact that the Curie temperature of pure $PbTiO_3$ is higher than that of $BaTiO_3$, the Curie temperature of $(Ba,Pb)TiO_3$ solid solutions increases with increasing $PbTiO_3$ content.

The components of $(Ba,Sr)TiO_3$ solid solutions, like $BaTiO_3$ and $PbTiO_3$ in the preceding case, have values of the factor t greater and smaller than unity, respectively. In contrast to $PbTiO_3$, however, the ferroelectric properties of $SrTiO_3$ as already noted, are evinced (if at all) only in the region of low temperatures. Hence the addition of $SrTiO_3$ to $BaTiO_3$ leads to reduction of the Curie temperature.

The above analyses of the behavior of $(Ba,Pb)TiO_3$ and $(Ba,Sr)TiO_3$ solid solutions show that some properties of ferro- and antiferroelectric solid solutions cannot be understood if one operates only with statistically averaged quantities; one must take into account the inhomogeneities of atomic scale that actually exist in solid solutions.[8]

Conclusions

In this report we have attempted to give a qualitative explanation of the difference between the Curie points of different ferroelectrics with the perovskite structure, operating only with such ionic characteristics as the polarizability, charges and radii, and not taking into account the degree of covalence of the bonds in these compounds. We did this by approximate theoretical evaluation for which purpose we utilized earlier results[15,16] of our investigations of the influence of different cation parameters on the internal fields in ferroelectric substances with the perovskite structure. The deductions arrived at through theoretical analysis are not in conflict with the still scanty pertinent experimental data. It is hoped that as new data become available it will be possible to verify

the other results of our theoretical analysis.

"L.Ia.Karpov" Physical-Chemical Institute

References

1. G.A.Smolenskii, Zhur.tekh.fiz., 20, 137 (1950); Doklady AN SSSR, 70, 405 (1950); Dissertation, Phys. Institute, Ac. of Sci., 1954; Izv. AN SSSR, Ser.fiz., 20, 163 (1956) (Trans.Bulletin, 20, No.2, 149); Usp.fiz.nauk, 62, 41 (1957); Izv. AN SSSR, Ser.fiz., 21, 233 (1957) (Trans.Bulletin, 21, No.2, 235); Zhur.tekh.fiz., 27, 1778 (1957) (Trans.Soviet Phys. - J.Tech.Phys.)
2. G.A.Smolenskii & V.Kh.Kozlovskii, Zhur.tekh.fiz., 23, No.3, 445 (1953).
3. H.D.Megaw, Acta Crystallogr., 5, 739 (1952); Ibid., 7, 187 (1954).
4. P.Vousden, Acta Crystallogr., 4, 373 (1951).
5. A.von Hippel, Z.Phys., 133, 158 (1952); Revs.Mod.Phys., 22, 221 (1950).
6. E.T.Jaynes, Ferroelectricity, p.29.-Princeton, 1953.
7. E.Sawaguchi, J.Phys.Soc.Japan, 8, 615 (1953).
8. Iu.N.Venevtsev, Dissertation, MIFI, 1955.
9. Iu.N.Venevtsev & G.S.Zhdanov, Izv.AN SSSR, Ser.fiz., 20, 178 (1956). (Trans.Bulletin 20, No.2, 161.); Abstracts of reports presented at the First Conference on Ferroelectricity, L., 1956; Abstracts of reports presented at the Second Conference on Crystallochemistry, M., 1957.
10. Iu.N.Venevtsev, G.S.Zhdanov & T.N.Shendrik, Kristallografiia, 1, 657 (1956).
11. Iu.N.Venevtsev, A.N.Kapyshev & Iu.V.Shumov, ibid., 2, 233 (1957) (Trans. Soviet Physics - Crystallography.)
12. G.Shirane, F.Jona & R.Pepinsky, Proc.IRE,43, 1738 (1955).
13. Iu.N.Venevtsev & G.S.Zhdanov, Izv.AN SSSR, Ser.fiz., 21, 275 (1957). (Trans. Bulletin, 21, No.2, 277.); Kristallografiia, 3, No.6 (1958). (Trans.Soviet Physics - Crystallography.)
14. C.Kittel, Introduction to Solid State Physics, N.Y., 1953 (Cited in Russ. trans., 1957.)
15. Iu.N.Venevtsev, G.S.Zhdanov, S.P.Solov'ev & Iu.A.Zubov, Kristallografiia, 3, 473 (1958) (Trans.Soviet Physics - Crystallography.)
16. G.S.Zhdanov, S.P.Solov'ev, Iu.N.Venevtsev & V.V.Ivanova, Kristallografiia, 473, No.2 (1959). (Trans.Soviet Physics - Crystallography.)
17. W.Merz, Proc.Amer.Phys.Soc., 25, 36 (1950); Phys.Rev., 78, 52 (1950).
18. J.C.Slater, Phys.Rev., 78, 748 (1950).
19. G.I.Skanavi, Fizika dielektrikov (Physics of Dielectrics), M.-L., 1949.
20. G.B.Bokii, Vvedenie v kristallokhimiiu (Introduction to crystallochemistry), MGU, M., 1954.
21. H.D.Megaw, Proc.Phys.Soc., 58, 133 (1946).
22. G.Shirane & S.Hoshino, J.Phys.Soc., Japan, 6, 265 (1951).
23. G.Shirane, J.Phys.Soc.Japan, 7, 110 (1952).
24. E.Sawaguchi, J.Phys.Soc.Japan, 7, 110 (1952).
25. H.Gränicher, Helv.phys.acta, 29, 219 (1956).
26. A.Linz, Phys.Rev., 91, 753 (1953).

CRYSTAL STRUCTURE OF THE $BaTiO_3$-$LaAlO_3$ SYSTEM

- I.G. Ismailzade

The structure of solid solutions of barium titanate with compounds of the ABO_3 type wherein the A and B cations have the same valences as Ba and Ti, respectively, have been investigated by a number of authors.[1-4]

The structure of solid solutions of $BaTiO_3$ with ABO_3 type compounds in which the Ba & A and Ti & B ions have different valences is also of interest. Such solid solutions are formed, for example, in the barium titanate-lanthanum aluminate system, which was the subject of the present investigation. The specimens were synthesized and their electric properties measured by Smolenskii, Agranovskaia & Sholokhova. They found that the solid solutions of this system containing less than 16 mole percent $LaAlO_3$ have ferroelectric properties. The addition of lanthanum aluminate to barium titanate sharply reduces the Curie point and the value of the peak dielectric constant.

We investigated the structures of all the $BaTiO_3$-$LaAlO_3$ specimens both by the conventional photographic procedure of recording the diffraction maxima and by the ionization procedure on an URS-50-I x-ray diffractometer. The patterns were recorded using filtered copper radiation (λ = 1.5418 Å). The parameters of the unit cells were determined with reference to the 233 and 332 diffraction maxima.

In all we studied 11 specimens ranging from pure $BaTiO_3$ to pure $LaAlO_3$; in addition to those listed in the table we investigated a specimen containing 50 mole percent of each component. We found that in the rage of $LaAlO_3$ concentrations from 0 to 25 mole percent there form solid solutions crystallizing with the perovskite structure. At 50 mole percent $LaAlO_3$ a heterogeneous mixture is formed.

The lattice constants are listed in the accompanying table.

Sample No.	Content, mole %		a, Å	c, Å	c/a	r, Å³	Curie point, °C
	$BaTiO_3$	$LaAlO_3$					
1	100,0	—	3,9956	4,0352	1,0100	64,42	+120
2	99,0	1,0	3,9951	4,0345	1,0098	64,39	+87
3	97,5	2,5	3,9949	4,0293	1,0086	64,30	+46
4	95,0	5,0	4,0050	—	1,0000	64,24	—14
5	92,5	7,5	4,0011	—	1,0000	64,05	—85
6	90,0	10,0	3,9984	—	1,0000	63,92	—133
7	87,5	12,5	3,9950	—	1,0000	63,76	—
8	85,0	15,0	3,9906	—	1,0000	63,55	—
9	75,0	25,0	3,9800	—	1,0000	63,04	—
10	—	100,0	3,7950	—	1,000	54,65	—

The lattice constants a and c decrease with increasing $LaAlO_3$ content. At 95% $BaTiO_3$ + 5% $LaAlO_3$ the two constants become equal, i.e., the lattice transforms from tetragonal to cubic symmetry.

This inference is consistent with the results of electric measurements for all the investigated specimens. The Curie points of the 99% $BaTiO_3$ + 1% $LaAlO_3$ and 97.5% $BaTiO_3$ + 2.5% $LaAlO_3$ solid solutions are 87° and 46°C, respectively; hence at room temperature they are in the ferroelectric phase and have the tetragonal perovskite type structure. For the 95% $BaTiO_3$ + 5% $LaAlO_3$ solid solution T_c = -14°C; consequently, at room temperature it is paraelectric and must have a cubic lattice. The decrease of the cell parameters is due to the fact that the ionic radii of La^{3+} (1.04 Å) and Al^{3+} (0.57 Å) are small compared with those of Ba^{2+} (1.38 Å) and Ti^{4+} (0.64 Å). Earlier investigators[6,7] attributed a cubic perovskite type structure to lanthanum aluminate with = 3.78 Å. However, as Geller & Bala[5] point out, optical and careful x-ray diffraction studies indicate that the structure consists of rhombohedral cells: a = 5.357 A, α = 60° 6', V = 108.90 A^3

and N = 2. The structure of $LaAlO_3$ has been described as pseudocubic with a = = 3.790 Å and $\alpha = 90^{\circ}\ 5'$, i.e., there obtains minor distortion of the cubic lattice. We obtained a value of $a = 3.795 \pm 0.001$ Å.

Is the $LaAlO_3$ lattice favorable for the occurrence of ferroelectricity? Taking the ionic radii to be La^{3+} = 1.04 Å, Al^{3+} = 0.57 Å and O^{2-} = 1.36 Å, we find that the tolerance factor t = 0.87, i.e., that the geometric conditions allow $LaAlO_3$ to crystallize in the perovskite structure. However, in this case the conditions necessary for the rise of spontaneous polarization are not fulfilled. For the occurrence of ferroelectricity in the crystal, in addition to the necessary geometric conditions ($R_A/R_O \gtrsim 1.0$; and $t \approx 1.05$) an important consideration is the character of the chemical bonds between the central B ions and the oxygens. G.A. Smolenskii is of the opinion that the bonds between the B and O ions are not purely ionic; actually some of the s and d electrons are shared.[8] Assuming with Megaw[9] that the d electrons play a substantial role in the formation of homopolar bonds, we conclude that owing to the fact that there are no d electrons in the electron cloud of the Al atom and in view of the smallness of the tolerance factor t of $LaAlO_3$, this compound should not be ferroelectric. Actually, so far as we know, ferroelectricity has not been observed in $LaAlO_3$.

I desire to express my deep gratitude to G.A.Smolenskii for supplying the specimens and for valuable advice.

Petroleum Institute,
Azerbaidzhan SSR Academy of Sciences

References

1. G.Shirane, S.Hoshino & K.Suzuki, J.Phys.Soc., Japan, 5, 453 (1950).
2. I.G.Ismailzade, Doklady AN SSSR, 2, 527 (1955).
3. W.Coffen, J.Amer.Ceram.Soc., 10, 480 (1954).
4. R.H.Dungan, D.F.Kane & L.R.Bikford, J.Amer.Ceram.Soc., 35, 318 (1952).
5. S.Geller & V.B.Bala, Acta Crystallogr., 9, 1019 (1956).
6. B.F.Ormont, Struktury neorganicheskikh veshchestv (Structures of inorganic substances), p.661, m., 1050.
7. Náray-Szabó, Structure Reports, 11, 455 (1947-1948).
8. G.A.Smolenskii, Izv.AN SSSR, Ser.fiz., 20, 163 (1956) (Trans.Bulletin 20, No.2, 149.)
9. H.D.Megaw, Acta crystallogr., 5, 739 (1952); Ibid., 7, 187 (1954).

CRYSTAL STRUCTURE OF THE NIOBATES AND THE TANTALATES OF BIVALENT METALS AND THEIR SOLID SOLUTIONS

- I.G.Ismailzade

The discovery in 1952-3 of ferroelectricity in cadmium pyroniobate, $Cd_2Nb_2O_7$, stimulated structural investigations of a number of compounds of the $A_2B_2O_7$ type. It was established[1-2] that $Cd_2Nb_2O_7$ is a new type of ferroelectric crystallizing in a cubic lattice of the pyrochlore type.

In addition to pyroniobates, $A_2Nb_2O_7$, and pyrotantalates, $A_2Ta_2O_7$, metaniobates, ANb_2O_6, and metatantalates, ATa_2O_6, are also of considerable interest; among the latter $PbNb_2O_6$ and $PbTa_2O_6$ are ferroelectric.[5,6] Until now, however, the electric and structural properties of these interesting compounds have not been adequately studied. Only in the recently published work of Smolenskii, Isupov & Agranovskaia[7] do we have the first result of electric measurements on the pyro- and metaniobates and tantalates of some bivalent metals. In particular, Smolenskii et al established that strontium pyrotantalate, $Sr_2Ta_2O_7$, is a new ferroelectric with a transition temperature of about 80°C.

Below we give the preliminary results of a structural investigation of this extensive series of compounds and some of their solid solutions. All the samples were synthesized in the laboratory of G.A.Smolenskii. The preparation procedure is described in Ref.7.

The x-ray diffraction studies were carried out on polycrystalline specimens at room temperature (20-30°) using either the conventional powder procedure or ionization detection by means of an URS-50-I x-ray diffractometer. As a rule the lattice periods were determined from the diffractometer data.

The results for AB_2O_6 type compounds together with the data from the literature on some of them are listed in Table 1. We note the great similarity in patterns for orthorhombic $PbNb_2O_6$, on the one hand, and $PbTa_2O_6$, $SrTa_2O_6$ and $BaTa_2O_6$, on the other hand. Apparently, these compounds are isostructural.

The results of structural investigation of compounds of the $A_2B_2O_7$ type are listed in Table 2. The diffraction lines of ferroelectric $Sr_2Ta_2O_7$ are consistent with the tetragonal system: a = 10.628 Å and c = 10.908 Å. Comparison of the unit cells of $Cd_2Ta_2O_7$ and $Sr_2Ta_2O_7$ suggests that the lattice of the latter is a tetragonally distorted pyrochlore lattice.

The studies of Jona, Shirane & Pepinsky[4] showed that replacement of Cd and Nb atoms in cadmium pyroniobate by other atoms (Cd^{2+} by Pb^{2+} and Ca^{2+}; Nb^{5+} by Ta^{5+}) leads to depression of the Curie point. In order to study the influence of ionic replacement in strontium pyrotantalate, Smolenskii & Isupov investigated the electric properties of the $Sr_2Ta_2O_7$—$Sr_2Nb_2O_7$, $Sr_2Ta_2O_7$—$Ba_2Ta_2O_7$ and $Sr_2Ta_2O_7$—$Ca_2Ta_2O_7$ systems.[10,11] We carried out a structural investigation of these systems. (All percentages below are molar.)

1. $Sr_2Ta_2O_7$—$Sr_2Nb_2O_7$ (5, 10 and 20% $Sr_2Nb_2O_7$). Solid solutions with the structure of $Sr_2Ta_2O_7$ are formed in the investigated range of concentrations.

2. $Sr_2Ta_2O_7$—$Ca_2Ta_2O_7$ (20, 40, 60 & 80% $Ca_2Ta_2O_7$). A continuous series of solid solutions with the structure of $Sr_2Ta_2O_7$ is formed in the investigated range.

Table 1

Results of structural investigations of compounds of the AB_2O_6 type

Compound	Structure	Compound	Structure
$BeNb_2O_6$	Not found	$BeTa_2O_6$	Complex
$MgNb_2O_6$	Columbite $a = 5.01$; $b = 14.18$ Å; $c = 5.66$ Å (Ref.4)	$MgTa_2O_6$	Tetragonal $a = 4.70$ Å; $c = 9.18$ Å (Ref.4)
$ZnNb_2O_6$	Columbite $a = 5.036$ Å; $b = 14.18$ Å; $c = 5.715$ Å (4)	$ZnTa_2O_6$	Columbite $a = 5.038$ Å; $b = 14.08$ Å; $c = 5.682$ Å
$CdNb_2O_6$	Columbite $a = 5.85$ Å; $b = 14.8$ Å; $c = 5.15$ Å (4,8)	$CdTa_2O_6$	Columbite $a = 5.84$ Å; $b = 14.82$ Å; $c = 5.12$ Å
$CaNb_2O_6$	Complex	$CaTa_2O_6$	Complex
$SrNb_2O_6$	Complex	$SrTa_2O_6$	Complex (orthorhombic)
$BaNb_2O_6$	Complex	$BaTa_2O_6$	Complex (orthorhombic)
$PbNb_2O_6$	1. Rhombohedral $a = 6.206$ Å $\alpha = 58°18'$ (Ref.9) 2. Orthorhombic $a = 17.51$ Å; $b = 17.81$ Å; $c = 7.73$ Å $N = 20$ (Ref.8)	$PbTa_2O_6$	Complex (orthorhombic)

Table 2

Results of structural investigations of compounds of the $A_2B_2O_7$ type

Compound	Structure	Compound	Structure
$Be_2Nb_2O_7$	Not found	$Be_2Ta_2O_7$	Not found
$Mg_2Nb_2O_7$	Complex	$Mg_2Ta_2O_7$	Complex
$Zn_2Nb_2O_7$	Complex	$Zn_2Ta_2O_7$	Complex
$Cd_2Nb_2O_7$	Cubic (pyrochlore) $a = 10.372$ Å (Ref.4)	$Cd_2Ta_2O_7$	Cubic (pyrochlore) $a = 10.376$ Å (Ref.4)
$Ca_2Nb_2O_7$	Complex	$Ca_2Ta_2O_7$	Cubic (pyrochlore)(distorted) $a = 10.420$ Å
$Sr_2Nb_2O_7$	Complex	$Sr_2Ta_2O_7$	Tetragonal $a = 10.628$ Å; $c = 10.908$ Å
$Ba_2Nb_2O_7$	Tetragonal $a = 10.928$ Å; $c = 11.160$ Å	$Ba_2Ta_2O_7$	Tetragonal $a = 10.940$ Å; $c = 11.168$ Å
$Pb_2Nb_2O_7$	Cubic (pyrochlore), Rhombohedral distortion $a = 10.675$ Å; $\alpha = 88°51'$ (Ref.4)	$Pb_2Ta_2O_7$	Cubic (pyrochlore) Rhombohedral distortion $a = 10.700$ Å; $\alpha = 88°25'$ (Ref.4)

3. $Sr_2Ta_2O_7$—$Ba_2Ta_2O_7$ (6, 9, 12, 20, 40, 60 & 80% $Ba_2Ta_2O_7$). Solid solutions with the structure of $Sr_2Ta_2O_7$ are formed at $Ba_2Ta_2O_7$ concentrations of 6, 9 and 20%. At 40% $Ba_2Ta_2O_7$, there appears a new phase, the structure of which has not yet been established. At 60 and 80% of $Ba_2Ta_2O_7$, there are formed solid solutions with the structure of $Ba_2Ta_2O_7$.

4. $Cd_2Nb_2O_7$—$Cd_2Ti_2O_6$. In the interval of $Cd_2Ti_2O_6$ concentrations from 5 to 20% there are formed substitutional solid solutions (with deficiencies) with the structure of $Cd_2Nb_2O_7$. The lattice parameters decrease with increasing $Cd_2Ti_2O_6$ content; this is presumably due not only to the smaller radius of the Ti^{4+} ion as compared with the Nb^{5+} ion (the difference is small and amounts only to ~0.02 Å) but also to the formation of vacancies in the oxygen ion sublattice.

We also investigated the structures of the $Cd_2Nb_2O_7$—$Na_2Nb_2O_6$ (5, 10, 20, 30, 40 & 50% $Na_2Nb_2O_6$) and $Cd_2Nb_2O_7$—$Mg_2Nb_2O_7$ (5, 10 & 15% $Mg_2Nb_2O_7$) systems. In the former system the solubility of the

second component is of the order of 15-20%. In the latter system the solubility of $Mg_2Nb_2O_7$ does not exceed 2-3%.

Before concluding I would like to say a few words regarding the nature of ferroelectricity in strontium pyrotantalate. In the case of $Cd_2Nb_2O_7$ partial replacement of the Cd^{2+} by larger ions (Ca^{2+} or Pb^{2+}) results in a reduction of the Curie temperature. The same thing occurs when Nb^{5+} is replaced by Ta^{5+}. In $Sr_2Ta_2O_7$ replacement of the Sr^{2+} ions by larger radius ions (Ba^{2+}) leads to depression of the Curie point, while replacement of Ta^{5+} by Nb^{5+} ions greatly raises the Curie point. Consequently, in both ferroelectrics similar ionic replacements give rise to changes in the Curie point in the same direction; hence it may be inferred that the nature of ferroelectricity in $Sr_2Ta_2O_7$ and $Cd_2Nb_2O_7$ is the same.

$Cd_2Ta_2O_7$ is also of interest. Despite the fact that it is isostructural with $Cd_2Nb_2O_7$, ferroelectricity in it has not been detected. This may presumably be explained by its having a very low Curie point due to the presence of the Ta^{5+} ion in the pyrochlore structure.

I desire to express my gratitude to G.A.Smolenskii and V.A.Isupov for helpful discussions.

Petroleum Institute of the
Academy of the Azerbaydzhan SSR

References

1. W.R.Cook & H.Jaffe, Phys.Rev., 88, 1426 (1952).
2. W.R.Cook & H.Jaffe, Phys.Rev., 89, 1297 (1953).
3. G.Shirane & R.Pepinsky, Phys.Rev., 92, 504 (1953).
4. F.Jona, G.Shirane & R.Pepinsky, Phys.Rev., 98, 903 (1955).
5. G.Goodman, J.Amer.Ceram.Soc., 30, 368 (1953).
6. G.A.Smolenskii & A.I.Agranovskaia, Doklady AN SSSR, 97, 237 (1954).
7. G.S.Smolenskii, V.A.Isupov & A.I.Agranovskaia, Doklady AN SSSR, 108, 232 (1956).
8. M.H.Francombe, Acta crystallogr., 9, 683 (1956).
9. B.Lewis & E.A.D.White, Acta crystallogr., 8, 849 (1955).
10. G.A.Smolenskii, V.A.Isupov & A.I.Agranovskaia, Doklady AN SSSR, 113, 803 (1957).
11. V.A.Isupov, Izv.AN SSSR,Ser.fiz., 21, 402 (1957). (Trans. Bulletin, 21, No.3, 404.)

PROPERTIES OF SOLID SOLUTIONS OF BARIUM AND LEAD TITANATES AND FERRATES

- O.I.Prokopalo & E.G.Fesenko

The ferroelectric properties of $BaTiO_3$ and $PbTiO_3$ can be modified significantly by isomorphic replacement of the Ti or metal (Ba or Pb) ions by other ions of approximately the same radius and forming similar chemical bonds. In all the hitherto investigated cases, however, replacement of ions in $BaTiO_3$ did not result in alteration of the perovskite structure characteristic of this substance.

Successful synthesis of hexagonal and tetragonal barium ferrate[1], cubic strontium ferrate and barium ferrate[2] and tetragonal lead ferrate[3] made it feasible to prepare and investigate new solid solutions based on $BaTiO_3$ and $PbTiO_3$ in which part of the Ti ions are replaced by Fe ions. In the present report we give some of the results of our work with $Ba(Ti,Fe)O_3$ and $Pb(Ti,Fe)O_3$ solid solutions. We found that replacement of about 1.5% of the Ti ions with Fe in $BaTiO_3$ results in structural changes, whereas replacement of up to 60% of the Ti ions in $PbTiO_3$ with Fe leads only to changes in the lattice parameters.

$Ba(Ti,Fe)O_3$ Solid Solutions

The barium ferrate was obtained by sintering a stoichiometric mixture of $BaCO_3$ and Fe_2O_3 in an oxygen atmosphere. Tests showed that the modification evinced at room temperature is determined by the highest sintering temperature: at temperatures up to 900° there is obtained the cubic modification, at about 1100° the tetragonal and at temperatures above 1100° the hexagonal.

The influence of sintering temperature on the structure of barium ferrate is similar to that for barium titanate. Thus cubic $BaTiO_3$ obtained from $Ba(OH)_2 \cdot 8H_2O$ + + TiO_2 by roasting at temperatures up to 800°,[4] becomes tetragonal at room temperature, the degree of tetragonality rising with sintering temperature. The transition to the hexagonal modification occurs at about 1450°, but this modification is "fixed" only by quenching.[5]

The availability of different modifications of $BaFeO_3$ and $BaTiO_3$ enabled us to use different pairs of initial components for preparing the solid solutions; specifically, we used cubic $BaTiO_3$ & cubic $BaFeO_3$, cubic $BaTiO_3$ & hexagonal $BaFeO_3$ and tetragonal $BaTiO_3$ & hexagonal $BeFeO_3$.

The solid solution specimens were prepared by the procedure described earlier.[6] We note that in the case of the first two components, the formation of solid solutions is favored by the fine dispersion characteristic of the cubic modifications of $BaTiO_3$ and $BaFeO_3$. X-ray diffraction studies showed that in solid solutions prepared from the first pair of components the tetragonality decreases with increasing $BaFeO_3$ content up to 3%, at which point the structure becomes hexagonal.

The temperature dependences of the dielectric constant obtained for these specimens are shown in Fig.1. The measurements were performed in a 100 v/cm field at a frequency of $5 \cdot 10^5$ cps. Similar results were obtained in measuring ϵ at 50 cps, except that in this case higher values of ϵ were obtained for the samples with 3 and 5% $BaFeO_3$. The increased values are probably due to relaxation polarization.

In the case of the second pair of components - cubic $BaTiO_3$ & hexagonal $BaFeO_3$ - the hexagonal phase particles act as nuclei in the process of sintering. Transition to the hexagonal modification occurs at a relatively low (~0.5%) $BaFeO_3$ content. The temperature dependences of ϵ for a number of samples from this series are shown in Fig.2; the formation of the hexagonal phase is evinced in the temperature behavior of the dielectric constant and its value at the Curie point.

The above observations apply equally to the third pair of components - tetragonal $BaTiO_3$ & hexagonal $BaFeO_3$ - with the difference, however, that whereas the dimensions of the individual crystals in cubic $BaTiO_3$ are of the order of fractions of a micron, in the tetragonal form they exceed 10 microns.

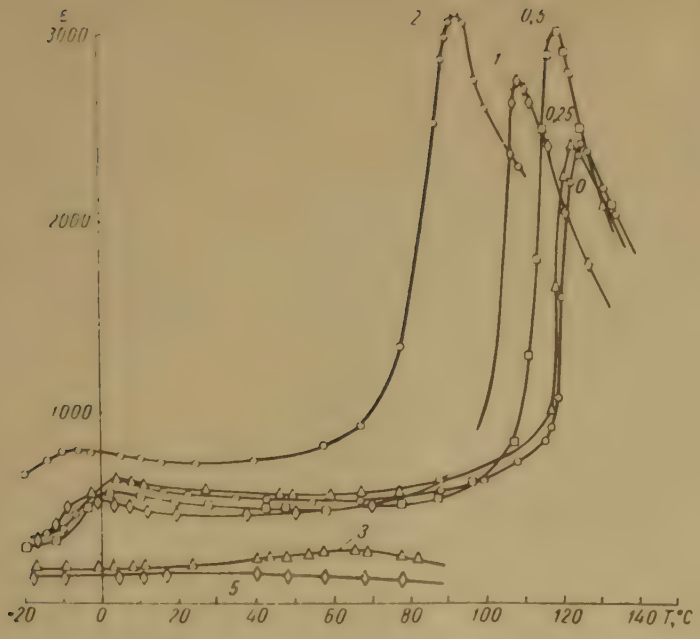

Fig.1. Temperature dependence of the dielectric constant ε of $Ba(Ti,Fe)O_3$ solid solutions with different ferrate concentrations (indicated in percent at the curves). Specimens prepared of cubic $BaTiO_3$ + cubic $BaFeO_3$.

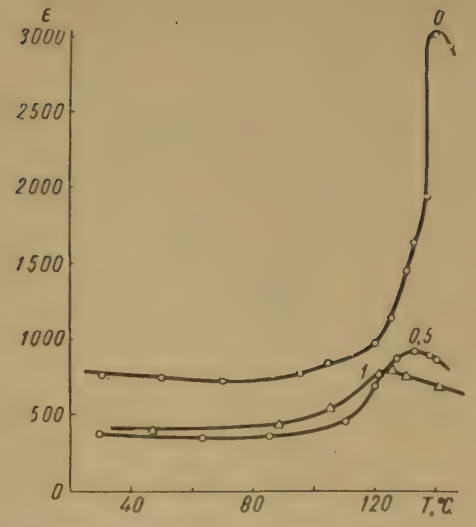

Fig.2. Same as Fig.1 but for second batch of specimens prepared of cubic $BaTiO_3$ + hexagonal $BaFeO_3$.

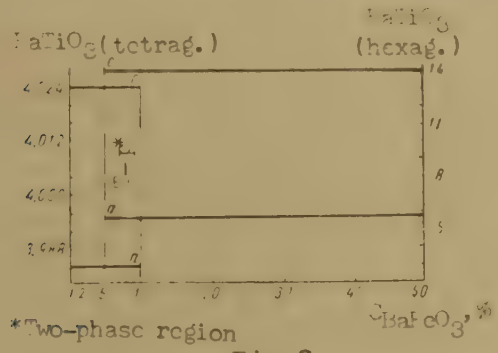

Fig.3

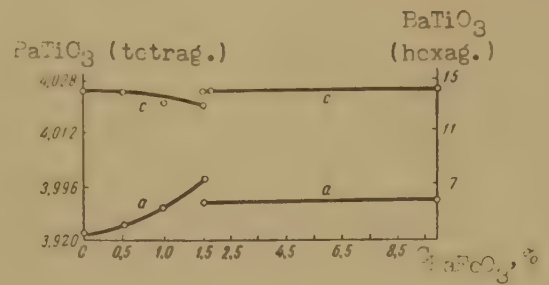

Fig.4

Fig.3. Variation of the lattice parameters of $Ba(Ti,Fe)O_3$ solid solutions with the $BaFeO_3$ content with sintering at 1380°.

Fig.4. Same as Fig.3 but for a sintering temperature of 1500°.

The specimens prepared of the third pair of components were roasted at 1380°. The results of x-ray studies (sensitivity 5%) are shown in Fig.3. It will be evident that at this sintering temperature no solid solutions in the range of $BaFeO_3$ contents up to 10% are formed. At higher concentrations of $BaFeO_3$ there form solid solutions with hexagonal structure.

Roasting of the same samples at 1500° results in broadening of the region of existence of the hexagonal modification down to a $BaFeO_3$ content of 1.5% (Fig.4). The dielectric data for this series of specimens are shown in Fig.5. It is noteworthy that the hexagonal modification is obtained without quenching, i.e., like the perovskite modification, exists at room temperatures.

Thus our experiments showed that barium titanate and barium ferrate form solid solutions which differ from those known hitherto in that with increase in the

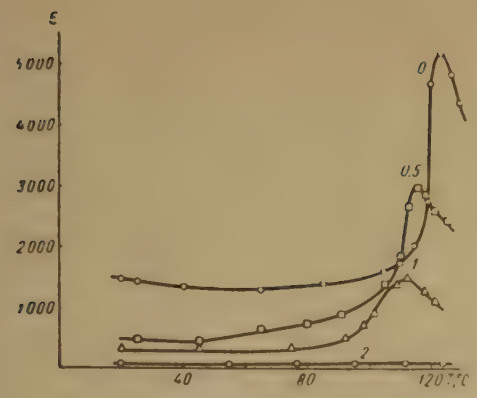

Fig.5

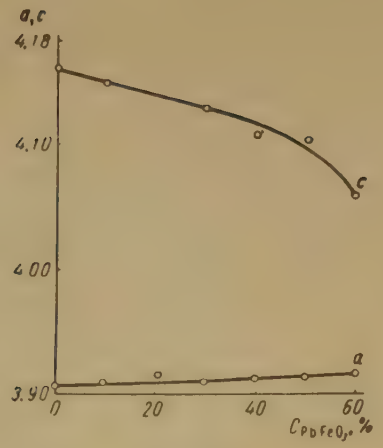

Fig.6

Fig.5. Same as Fig.1 but for specimens prepared from tetragonal $BaTiO_3$ + hexagonal $BaFeO_3$.

Fig.6. Variation of the lattice parameters of $Pb(Ti,Fe)O_3$ solid solutions with the $PbFeO_3$ content.

barium ferrate content above a certain relatively low value the monotonic variation in tetragonality and shift of the Curie point usually observed for such solid solutions is replaced by a sudden transition to the hexagonal modification. The barium ferrate content at which this abrupt transition to the hexagonal phase occurs depends greatly on the preparation procedure.

$Pb(Ti,Fe)O_3$ solid solutions

The initial components in preparing the $Pb(Ti,Fe)O_3$ solid solutions were lead ferrate, prepared by the procedure described in Ref.3, and lead titanate. The solid solutions were synthesized by heating at about 1000° in air.

X-ray diffraction studies showed (Fig.6) that $PbTiO_3$ and $PbFeO_3$ form a series of solid solutions, the tetragonality of which decreases with increasing ferrate content.

Electric measurements revealed that with increasing lead ferrate content both the dielectric constant and the loss tangent decrease, while the activation energy exhibits a tendency to saturation. This can be understood if we assume that the majority carriers in lead titanate are electrons and that the Fe ions in $PbFeO_3$ can go over into the trivalent state, which is a stable one. Then increase in the number of iron ions, which are traps for the conduction electrons even at a relatively low iron content, results in decrease of the through current and leads to the observed effect.

Scientific Research Physical-Mathematical Institute,
Rostov-on-the-Don State University

References

1. W.W.Malinofsky & H.Kedesdy, J.Amer.Chem.Soc., 76, 3090 (1954).
2. L.Harry & J.Vakel, Acta crystallogr., 8, 394 (1954).
3. E.G.Fesenko & O.I.Prokopalo, Kristallografiia, 1, 520 (1956).
4. M.C.Harwood & H.A.Klassens, Nature, 165, 73 (1950).
5. W.Frzebiatowsky, M.Drys & J.Benak, Roczniki chemii, 28, 21 (1954).
6. E.G.Fesenko & O.I.Prokopalo, Kristallografiia, 1, 703 (1956).

ANTIFERROELECTRIC AND FERROELECTRIC PROPERTIES OF SOME SODIUM NIOBATE SOLID SOLUTIONS

- N.N.Krainik

From the standpoint of the theory of antiferroelectricity it is of evident interest to clarify the role of distortions of the crystal lattice due to discrepancies between the actual size of the ions and the ideal size for the given lattice, to evaluate the influence of the nature of the chemical bonds between the ions and to determine what factors effect the relative stability of the ferro- and antiferroelectric phases. Hence the practical and theoretical importance of investigating solid solutions based on antiferroelectric substances. In view of this we undertook the synthesis and investigation of the following systems of solid solutions based on the antiferroelectric, sodium niobate: $NaNbO_3 + LiNbO_3$, $NaNbO_3 + CaNb_2O_6$ and $NaNbO_3 + CaTiO_3$.

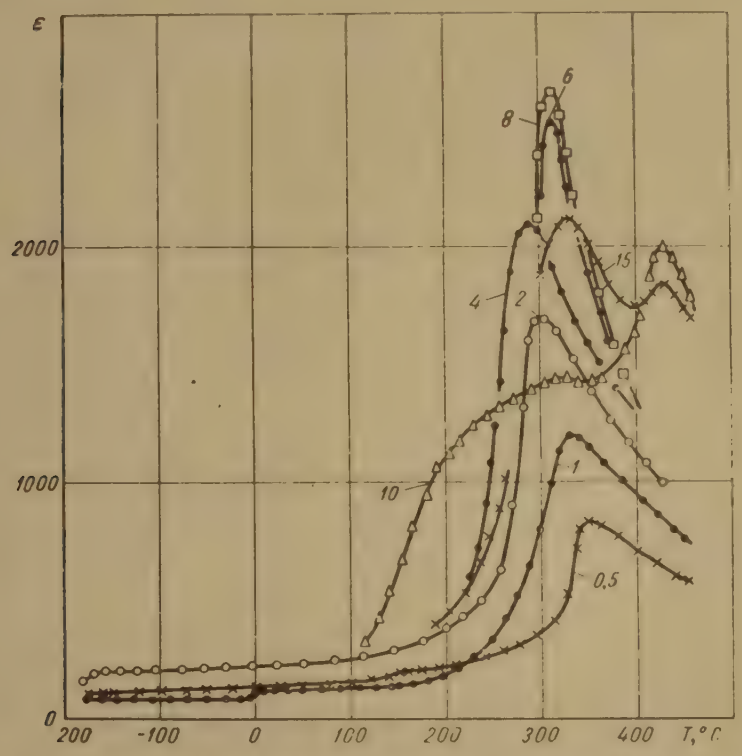

Fig.1. Temperature dependence of the dielectric constant ε of $NaNbO_3$-$LiNbO_3$ solid solution specimens. The figures at the curves indicate the $LiNbO_3$ content in mole percent.

The specimens were prepared by the usual ceramic technique from previously synthesized components: $NaNbO_3$, $LiNbO_3$, $CaNb_2O_6$ and $CaTiO_3$. The heating temperature and holding times at maximum temperature were: $NaNbO_3$ - 1050° (3 hr), $LiNbO_3$ - 800° (1 hr), $CaNb_2O_6$ - 1280° (2 hr), $CaTiO_3$ - 1360° (2 hr); $(100-n)\,NaNbO_3 + nLiNbO_3$ (n = 0.5-15%) - 1370-1250° (1 hr); $(100-n)NaNbO_3 + nCa_{0.5}NbO_3$ (n = 2.5-30%) - 1370-1350° (1 hr) and $(100-n)NaNbO_3 + nCaTiO_3$ (n = 2.5-20%) - 1370-1350° (1 hr).

The temperature dependences of ε for a number of specimens in the $NaNbO_3$-$LiNbO_3$ system as determined at a frequency of 500 kc, are shown in Fig.1. Two phase transitions occur in this system; the temperatures of both decrease with increasing LiNbO3 content up to 2 mole percent. At an $LiNbO_3$ content of 10 and 15 mole percent there is observed an additional maximum of the dielectric constant. An additional ε maximum was also observed for some not fully sintered specimens with 6 and 8% $LiNbO_3$, but this disappeared after heating of the specimens above 450°, whereas in the case of the 10 and 15% $LiNbO_3$ specimens this ε maximum persists after heating. We did not specifically investigate the causes of this additional maximum.

The tentative phase transition diagram for the system is shown in Fig.2,a. Apparently solid solutions are formed up to an $LiNbO_3$ content of 2 mole percent, i.e., the region IV in the diagram is the region of heterogeneous mixtures.

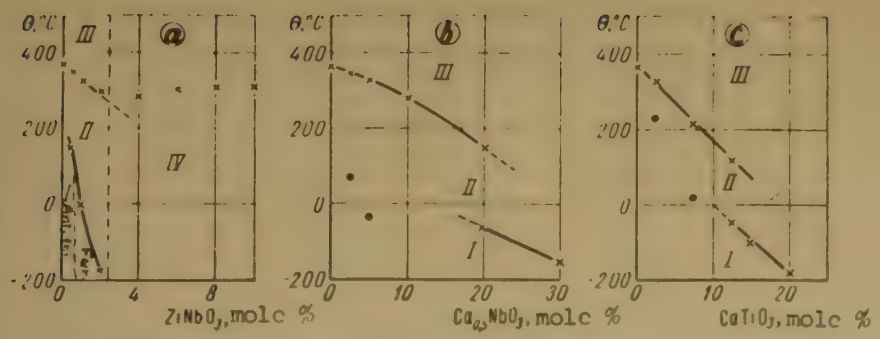

Fig.2. Approximate phase transition diagrams for the systems: a) $NaNbO_3$-$LiNbO_3$, b) $NaNbO_3$-$Ca_{0.5}NbO_3$, c) $NaNbO_3$-$CaTiO_3$.

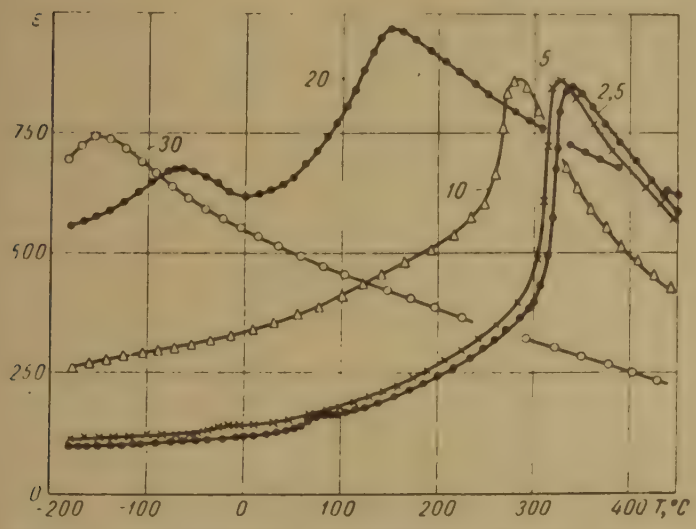

Fig.3. Temperature dependence of the dielectric constant ε of $NaNbO_3$-$Ca_{0.5}NbO_3$ solid solution specimens. The figures at the curves indicate the $Ca_{0.5}NbO_3$ content in mole percent.

Maxima appear in the tan δ vs temperature curves at temperatures somewhat below those of the phase transitions; the tan δ curves exhibit a minima at the Curie points.

Investigation of the field dependence of the dielectric polarization of the $NaNbO_3$-$LiNbO_3$ solid solutions carried out in the range from -196 to +200°C showed that phase II (Fig.2,a) is ferroelectric. The coercive force increases rapidly with decreasing temperature. Hence the spontaneous polarization could be evaluated only approximately: at +180° the spontaneous polarization was not less than $14 \cdot 10^{-6}$ coulomb/cm^2 in samples with 0.5% $LiNbO_3$, $11 \cdot 10^{-6}$ coulomb/cm^2 in samples with 2% and $9 \cdot 10^{-6}$ coulomb/cm^2 in samples with 4%.

In the temperature interval corresponding to phase I (Fig.2,a) no hysteresis loop was observed for the samples with 0.5% $LiNbO_3$ (E = 31 kv/cm^2). In the case of the sample with 1% $LiNbO_3$, however, hysteresis loops with a large coercive force were observed in the region of phase I close to the transition to phase II. The spontaneous polarization was not less than $6 \cdot 10^{-6}$ coulomb/cm^2.

The temperature dependences of ε for a number of specimens of the $NaNbO_3$-$CaNb_2O_6$ and $NaNbO_3$-$CaTiO_3$ systems, measured at a frequency of 500 kc, are shown in Figs.3 & 4. In the range of low concentrations of the second component there is observed a phase transition, the temperature of which shifts to the side of lower temperatures with increased concentration of the second component. At $Ca_{0.5}NbO_3$ and $CaTiO_3$ concentrations above 20 mole percent and 10 mole percent, respectively, there apparently appears a new (second) phase transition, the temperature of which also goes down with increasing concentration of the second component. In addition, in specimens containing less than 20 and 10% $Ca_{0.5}NbO_3$ and $CaTiO_3$, respectively, small humps appear in the ε vs T curves; possibly these humps are associated with phase transitions.

The approximate phase transition diagrams for these systems are shown in Figs. 2,b and c. The temperatures corresponding to the humps in the ε curves are indicated by dots in the phase diagrams. No hysteresis loops in a field of 36 kv/cm were observed in the temperature range corresponding to phase II (Fig.2,b & c). Distinct hysteresis loops were observed, however, in the temperature interval corresponding to phase I. The magnitude of the spontaneous polarization in the given

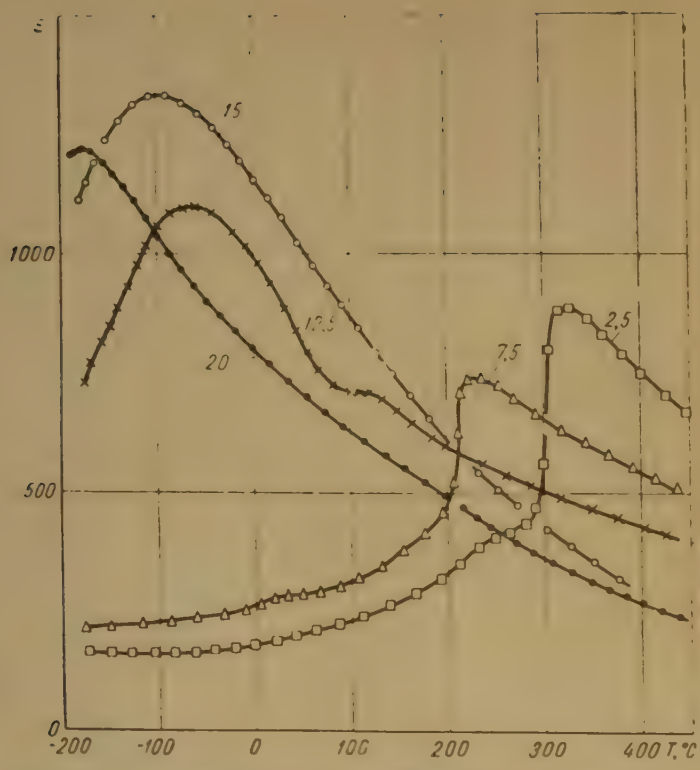

Fig.4. Temperature dependence of the dielectric constant ε of $NaNbO_3$-$CaTiO_3$ solid solution specimens. The figures at the curves indicate the $CaTiO_3$ content in mole percent.

phase is appreciably lower than in the ferroelectric phases I and II (Fig.2,a) in the $NaNbO_3$-$LiNbO_3$ system; for example, spontaneous polarization in the sample with 12.5% $CaTiO_3$ at -170° was $2.3 \cdot 10^{-6}$ coulomb/$/cm^2$; the coercive force was 3.4 kv/cm.

On the basis of the dielectric data obtained for the $NaNbO_3$-$LiNbO_3$ solid solution it may be hypothesized that these solid solutions are similar to solid solutions of $NaNbO_3$ with $KNbO_3$, $PbNb_2O_6$ and $CdNb_2O_6$.[1,2] If this is the case, it follows from the phase diagram (Fig.2,a) that phase I is orthorhombic. Phase II is apparently pseudotetragonal. At $LiNbO_3$ concentrations appreciably exceeding 0.5% dielectric hysteresis loops appear in phase I; however, no anomalies corresponding to a transition to the ferroelectric phase are observed in the $\epsilon = f(T)$ curves for samples representative of the orthorhombic phase.

It follows from the phase diagrams for the $NaNbO_3$-$CaNb_2O_6$ and $NaNbO_3$-$CaTiO_3$ systems (Fig.2,b & c) that phase II is characterized by orthorhombic symmetry (like pure $NaNbO_3$) and apparently is antiferroelectric. Phase I has ferroelectric properties. Possibly this phase is ferrielectric, i.e., in addition to antiparallel displacements of the Nb ions[3] and apparently the O ions, there also occur parallel displacements. Properties of these solid solutions are similar to those of $NaNbO_3$-$NaTaO_3$ solid solutions.[4,5]

In the investigated sodium niobate solid solutions there should also occur[1,6,7] high temperature phase transitions caused by "crumpling" of the crystal structure owing to the small diameter of the corner ions*; we were not, however, able to extend the study of the dielectric properties of our specimens into the range of high temperatures owing to the great increase in their conductivity. The structure of $NaNbO_3$ and its solid solutions below the Curie temperature is distorted owing both to the appearance of ferro- and antiferroelectricity and the contraction or "crumpling" of the crystal structure.

With increase in the size of the corner ion, the "crumpling" decreases (solid solutions of $NaNbO_3$ with $KNbO_3$ and $PbNb_2O_6$) and the superstructure lines associated with this "crumpling" of the crystal structure gradually disappear.[1] It must be noted however that the rise of ferroelectricity does not lead to liquidation of superstructure and, vice versa, disappearance of superstructure does not have an appreciably effect on ferroelectric properties. The character of the deformation connected with small size of the corner ion, in general, differs from the character of deformation due to appearance of ferro- and antiferroelectricity and in some cases one can distinguish between these deformations. This does not neces-

---

*Here and below by the "corner" ion in the lattice of ABO_3 type compounds we understand the A ion; the "central" ion is the B ion.

sarily mean, however, that the "crumpling" deformation has no effect on the deformation associated with the rise of ferro- or antiferroelectricity.

In the light of the experimental data on the $NaNbO_3$ base solid solutions, it would appear that one can divide these solid solutions into two groups according to their dielectric properties. The first group comprises solid solutions of $NaNbO_3$ with $KNbO_3$, $PbNb_2O_6$, $CdNb_2O_6$ and $LiNbO_3$ in which ferroelectric pseudotetragonal and orthorhombic phases appear as the content of the second component is increased. The second group consists of solutions of $NaNbO_3$ with $NaTaO_3$, $CaNb_2O_6$ and $CaTiO_3$ in which a new, apparently, ferrielectric phase develops at a certain concentration of the second component.

It must be emphasized that the solid solutions cannot be assigned to one group or the other solely on the basis of geometric factors. Thus in solid solutions of $NaNbO_3$ with $KNbO_3$ and $PbNb_2O_6$ the dimensions of the unit cell increase with increasing concentration of the second component, while in solid solutions with $CdNb_2O_6$ and, apparently, $LiNbO_3$, the dimensions decrease; nevertheless, these solid solutions belong in the same group.

According to preliminary x-ray diffraction data, the dimensions of the unit cell in $NaNbO_3$-$CaTiO_3$ solid solutions decrease slightly with increasing $CaTiO_3$ content.

In solid solutions of $NaNbO_3$ with $PbNb_2O_6$, $CdNb_2O_6$ and $KNbO_3$ the electronic polarizability of the corner ions increases with increase of the second component. If we assume that increase in the degree of covalence of the cation-anion bonds can increase the dipole moment, in the case of solid solutions of $NaNbO_3$ with $PbNb_2O_6$, $CdNb_2O_6$ and $LiNbO_3$ one can expect to observe an increase of the dipole moment owing to increase of the dipole moments of the corner ions and the oxygen ions as compared with the central dipole moment and also due to increase in the degree of covalence of the bonds between the corner ions and the oxygens. This, apparently, makes the ferroelectric arrangement of ionic displacements more advantageous from the standpoint of the electrostatic energy of the crystal lattice.[8-9] At present the appearance of a ferroelectric component in the ionic displacements in the low temperature phase of solid solutions of $NaNbO_3$ with $NaTaO_6$, $CaNb_2O_6$ and $CaTiO_3$ remains unexplained.

I desire to express my deep gratitude to G.A.Smolenskii for his constant interest in the work and to A.I.Agranovskaia for assistance in preparing the specimens.

Semiconductor Institute,
Academy of Sciences of the USSR

References

1. M.H.Francombe & B.Lewis, Jour.Electronics, 2, 387 (1957).
2. G.Shirane, R.Newham & R.Pepinsky, Phys.Rev., 96, 581 (1954).
3. P.Vousden, Acta crystallogr., 4, 545 (1951).
4. V.A.Isupov, Izv.AN SSSR, Ser.fiz., 21, 402 (1957). (Trans.Bulletin 21, No.3, 404.)
5. V.A.Isupov, Present issue of the Bulletin, p.1497.
6. L.E.Cross & B.J.Nickolson, Phils.Mag., 46, 212 (1955).
7. M.H.Francombe, Acta crystallogr., 9, 256 (1956).
8. N.N.Krainik, Izv.AN SSSR, Ser.fiz., 21, 411 (1957). (Trans.Bulletin 21, No.3, 412.)
9. N.N.Krainik, Zhur.tekh.fiz., 28, 553 (1958). (Trans.Soviet Phys. - Tech. Phys.)
10. J.A.Sauer, Phys.Rev., 57, 142 (1940).

FERROELECTRIC CERAMICS WITH A HIGH CURIE TEMPERATURE

- A.M.Cherepanov, S.V.Bogdanov & R.Ia.Razbash

There are a number of reports[1-7] in the literature concerning the $BaTiO_3$—$PbTiO_3$ system; in most of these reports, however, there is little or no information on the preparation of the investigated specimens, or where such information is given, the described procedure differs substantially from that used by us.

Our experiments showed that in firing in an ordinary furnace atmosphere one can only obtain solid solution specimens with a $PbTiO_3$ content not exceeding 15 mole percent; speciments having this composition can be obtained only if the initial batch is proportioned to contain at least 20 mole percent $PbTiO_3$.

Our research problem was to find a procedure for firing lead-containing compositions that would minimize volatilization of the PbO. The developed procedure yields satisfactory results not only for the $BaTiO_3$—$PbTiO_3$ system but also for all other lead-containing systems.

Under our procedure for both the preliminary and final firings the samples are set in chamotte or suitable saggers on a layer of technical alumina (Al_2O_3) at least 5 mm thick (to prevent reaction of the samples with the sagger material) and then covered with more alumina so that there is a depth of 8-10 mm clay in the case of samples having an area of up to 10 cm^2. In the case of individual samples having a larger area, the depth of covering should be somewhat greater.

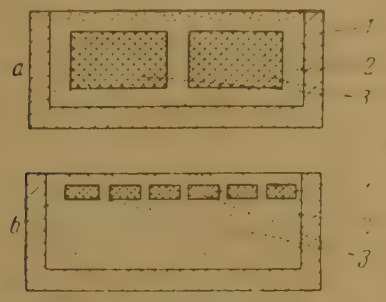

Fig.1. Arrangement for preliminary (a) and final (b) firings 1) chamotte sagger, 2) alumina, 3) samples.

The firing temperatures must be determined experimentally for each given composition; in general the optimum firing temperature depends on a number of factors: the proportion of initial components, their degree of purity, grain size, etc. The final firing temperatures determined for $BaTiO_3$—$PbTiO_3$ specimens made up of pure initial components ranged from 1350° for $PbTiO_3$ and 1450° for $BaTiO_3$.

The proposed firing procedure for lead-containing ceramics is simple and makes it possible to obtain $BaTiO_3$—$PbTiO_3$ solid solutions containing 50% or even more $PbTiO_3$. It should be borne in mind, however, that with a high $PbTiO_3$ content some of the lead compound is still volatilized; hence it should be introduced with some excess into the initial batch. The additional amount of lead compound necessary depends on the firing conditions but in the case of properly controlled heating it does not exceed a few mole percent.

The suggested arrangement for preliminary and final firings are diagrammed in Fig.1. It was found on the basis of chemical analyses and temperature vs inductive capacitance measurements that the evaporation of lead oxide in firing by the described procedure is relatively small. Water absorption of sintered specimens generally did not exceed 1%. The specific gravity of samples fired in the above manner varied from 6.03 for specimens having the composition 95% $BaTiO_3$ + 5% $PbTiO_3$ to 6.88 for 50% $BaTiO_3$ + 50% $PbTiO_3$.

We have successfully used the described procedure during the past five years for preparing different lead-containing ceramics.

Fig.2 shows the variation of the dielectric constant at room temperature with the $PbTiO_3$ concentration of specimens prepared by the described procedure. The temperature dependence of ε for different solid solutions is shown in Fig.3. It is interesting to note that although the absolute value of ε at the Curie point decreases with increasing $PbTiO_3$ content, the ratio of ε at the Curie point to ε_{min} at first increases and only begins to fall off above a certain $PbTiO_3$ content. The variation of the Curie temperature of (Ba,Pb) TiO_3 solid solutions as a function of the $PbTiO_3$ content is shown in Fig.4. It will be seen that the variation is linear up to 50% $PbTiO_3$ (the highest $PbTiO_3$ content in the investigated specimens). Extrapolation of this curve to 100% $PbTiO_3$ gives a Curie temperature of ~490° for pure lead titanate; this is close to the value given in the literature for this compound. The values of the Curie-Weiss constant remain virtually constant with increase of the $PbTiO_3$ concentration both below ($C = 1.5\text{-}1.9 \cdot 10^4$) and above the Curie point ($C = 10.5\text{-}16.5 \cdot 10^4$). It will be noted that below the Curie point C is appreciably smaller than above the Curie point.

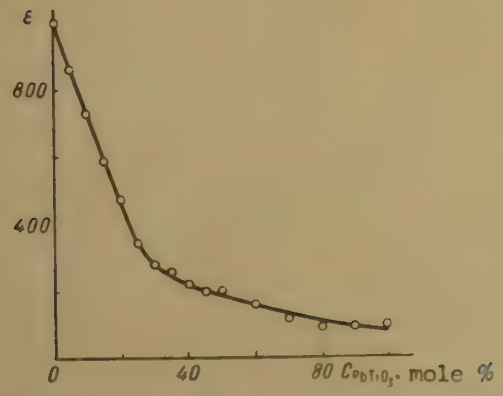

Fig.2. Variation of the dielectric constant of $BaTiO_3$—$PbTiO_3$ solid solutions at room temperature as a function of the $PbTiO_3$ concentration.

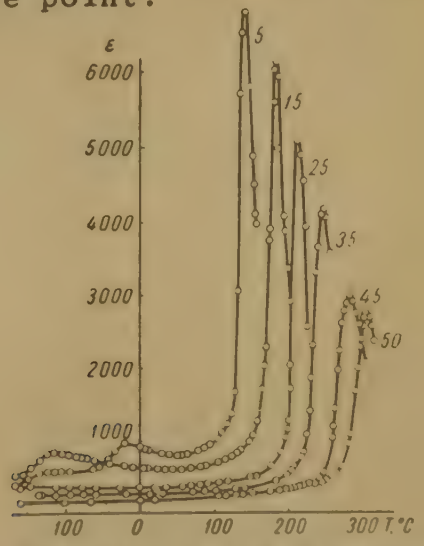

Fig.3. Variation of the dielectric constant with temperature for different $PbTiO_3$ concentrations (indicated in mole percent at the curves).

All the solid solutions in the $BaTiO_3$--$PbTiO_3$ system have approximately the same volume resistivity: ~10^{12} ohm·cm at room temperature (20°) and ~10^8 ohm·cm at 200°. The volume resistivity at 20° appears to be virtually independent of the electric field strength (up to ~8 kv/cm).

The piezoelectric properties of (Ba,Pb)TiO_3 solid solutions are, naturally, of practical interest. The values of the piezoelectric coefficient of different solid solutions measured by the static method at room temperature 5 days after polarization are listed in the accompanying table. It will be evident from the table that polarization of these solid solutions at elevated temperatures tends to increase the value of the piezoelectric coefficient as compared with polarization at room temperature (even though the polarizing field at 110-120°C was only 15 kv/cm as against 25 kv/cm at room

temperature). A similar effect was observed for barium titanate by Bogdanov et al[8].

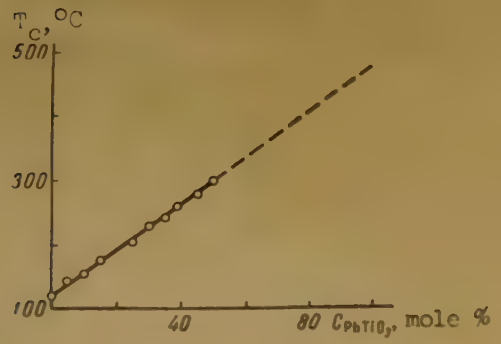

Fig.4. Variation of the Curie temperature with the $PbTiO_3$ concentration in $BaTiO_3$—$PbTiO_3$ solid solution.

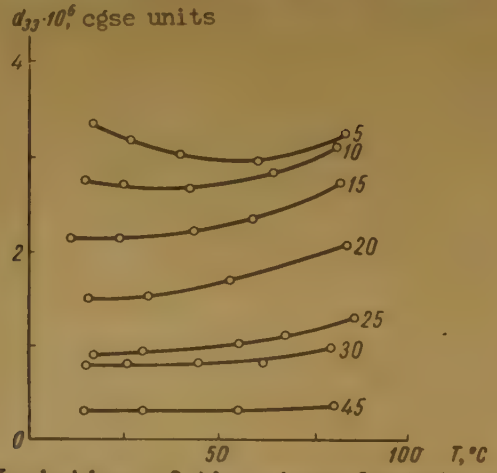

Fig.5. Variation of the piezoelectric coefficient d_{33} as a function of the temperature for different $PbTiO_3$ concentrations (indicated in mole percent at the curves).

The temperature dependences of d_{33} of different solid solutions in the range from 15 to 90° are shown in Fig.5. It will be seen that, except for the 95% $BaTiO_3$ + 5% $PbTiO_3$ composition, the piezoelectric coefficient of the solid solutions tends to increase with temperature. With increasing $PbTiO_3$ concentration the temperature dependence of d_{33} becomes weaker and finally for the 55% $BaTiO_3$ + 45% $PbTiO_3$ solid solution the coefficient is virtually temperature independent.

From the engineering standpoint it would appear most expedient to use compositions containing 10-15 mole percent $PbTiO_3$ since these combine a fairly high value of d_{33} and a high Curie temperature with a weak temperature dependence of d_{33}. Naturally, where the solid solution must be used at elevated temperatures and under conditions where the magnitude of the piezoelectric coefficient is unimportant, it is advisable to use compositions with a high $PbTiO_3$ content.

$PbTiO_3$, mole %	Piezoelectric d_{33} cgse units			
	T = 20° C		T = 110—120° C	
	E = 25 kv/cm		E = 15 kv/cm	
5	3.5		2.85	3.7
10	2.7		1.8	3.35
15	2.3		1.5	2.40
20	1.65		1.27	1.9
25	1.4		1.5	—
30	1.5		1.05	—
35	1.44		1.26	—
40	1.2		0.97	—
45	0.9		0.75	—
50	0.57		0.4	—

We desire to express our gratitude to B.M.Vul for his constant interest in the work and valuable advice.

P.N.Lebedev Physical Institute
Academy of Sciences of the USSR

References

1. S.Nomura & S.Sawada, J.Phys.Soc., Japan, 6, 36 (1951).
2. J.Shirane & K.Suzuki, J.Phys.Soc., Japan, 6, 274 (1951).
3. N.A.Roi, Akust.zhur. (Acoustics Journal), 2, 62 (1956).
4. I.E.Myl'nikova, Izv.AN SSSR,Ser.fiz., 21, 423 (1957). (Trans. Bulletin, 21, No.3, 423.)
5. G.A.Smolenskii, Zhur.tekh.fiz., 20,137 (1951); Doklady AN SSSR, 5, 985 (1952).
6. S.Roberts, J.Amer.Ceram.Soc., 38, 63 (1951).
7. B.Jaffe, R.S.Marzullo & R.S.Roth, J.Res.NBS, 55, No.5, 239 (1955).
8. S.V.Bogdanov, B.M.Vul & R.Ia.Razbash, Zhur.tekh.fiz., 26, 958 (1956).

DIELECTRIC PROPERTIES OF SOLID SOLUTIONS OF THE TERNARY SYSTEM $BaTiO_3$-$PbTiO_3$-$BaSnO_3$

- S.V.Bogdanov, G.M.Kovalenko, R.Ia.Razbash & A.I.Cherepanov

Solid solutions of the $BaTiO_3$-$PbTiO_3$ and $BaTiO_3$-$BaSnO_3$ systems have been rather exhaustively studied.[1-12] Hence we felt it would be of interest to investigate the dielectric properties of polycrystalline solid solutions of the ternary system: $BaTiO_3$-$PbTiO_3$-$BaSnO_3$.

We measured some of the dielectric properties of samples having the following compositions:

95% $BaTiO_3$ + 5% $PbTiO_3$ + n $BaSnO_3$,
90% $BaTiO_3$ + 10% $PbTiO_3$ + n $BaSnO_3$,
85% $BaTiO_3$ + 15% $PbTiO_3$ + n $BaSnO_3$,
80% $BaTiO_3$ + 20% $PbTiO_3$ + n $BaSnO_3$,
75% $BaTiO_3$ + 25% $PbTiO_3$ + n $BaSnO_3$,

where n, the $BaSnO_3$ content, was 2.5, 5, 10 or 15% with respect to the total amount of $BaTiO_3$ + $PbTiO_3$, taken as 100%. The indicated percentages pertain to the composition of the initial batch and are all in mole percent. The initial materials used in preparing the samples were $BaCO_3$, $PbCO_3$, TiO_2 and SnO_2.

Experimental Results

As was expected, the Curie temperature of the investigated solid solutions increases with increasing $PbTiO_3$ content (with the $BaSnO_3$ content constant) and decreased with increasing $BaSnO_3$ content ($PbTiO_3$ content constant). The variation of the Curie point with the composition of the investigated solid solutions is shown in Fig.1. In the first approximation the dependence can be described by the empirical formula

$$T_c = [120 + am - bn]^\circ C, \qquad (1)$$

where m is the $PbTiO_3$ content, n is the $BaSnO_3$ content and $a \approx 3.8$ and $b \approx 5.4$ are empirical coefficients.

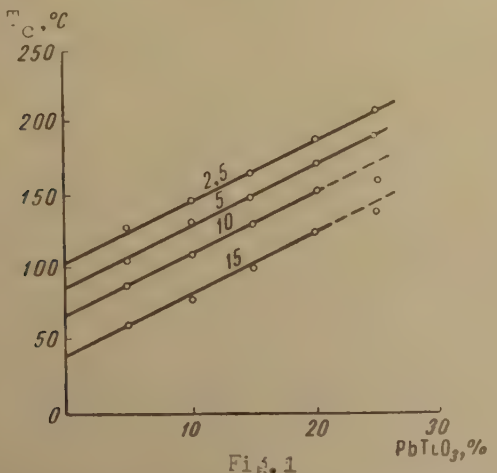

Fig.1

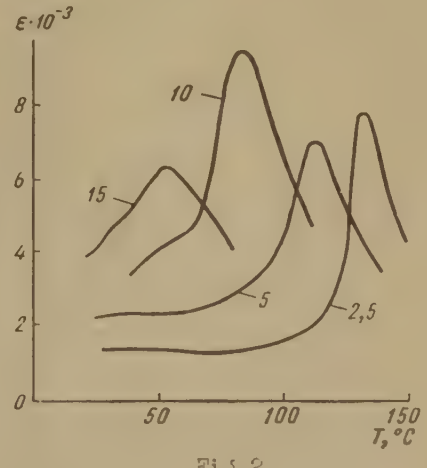

Fig.2

Fig.1. Variation of the Curie temperature with the composition of the $BaTiO_3$-$PbTiO_3$-$BaSnO_3$ samples (figures at curves - mole percent $BaSnO_3$).

Fig.2. Temperature dependences of the dielectric constant of 95% $BaTiO_3$ + 5% $PbTiO_3$ + n $BaSnO_3$ solid solutions (values of n given at the curves).

Spontaneous polarization P_s, residual polarization P_{res} and coercive force E_c of solid solutions of the $BaTiO_3$-$PbTiO_3$-$BaSnO_3$ system

Composition (values in mole %)	$P_s \cdot 10^{-5}$ coul/cm^2	$P_{res} \cdot 10^{-5}$ coul/cm^2	E_c, kv/cm
$BaTiO_3$	5,0	4,2	2,3
$95BaTiO_3 + 5PbTiO_3 + 2,5BaSnO_3$	~5,6	5,6	3,0
$95BaTiO_3 + 5PbTiO_3 + 5BaSnO_3$	6,6	6,0	2,0
$95BaTiO_3 + 5PbTiO_3 + 10BaSnO_3$	5,7	3,0	1,2
$95BaTiO_3 + 5PbTiO_3 + 15BaSnO_3$	4,0	1,3	0,8
$90BaTiO_3 + 10PbTiO_3 + 2,5BaSnO_3$	6,2	6,0	3,7
$90BaTiO_3 + 10PbTiO_3 + 5BaSnO_3$	~6,8	6,8	2,8
$90BaTiO_3 + 10PbTiO_3 + 10BaSnO_3$	5,4	4,0	1,5
$90BaTiO_3 + 10PbTiO_3 + 10BaSnO_3$	3,7	2,3	0,9
$85BaTiO_3 + 15PbTiO_3 + 2,5BaSnO_3$	~7,6	7,6	4,5
$85BaTiO_3 + 15PbTiO_3 + 5BaSnO_3$	~7,2	7,2	4,0
$85BaTiO_3 + 15PbTiO_3 + 10BaSnO_3$	5,0	4,0	1,9
$85BaTiO_3 + 15PbTiO_3 + 15BaSnO_3$	3,8	2,0	1,1
$80BaTiO_3 + 20PbTiO_3 + 2,5BaSnO_3$	~10	10	7,0
$80BaTiO_3 + 20PbTiO_3 + 5BaSnO_3$	~10	10	6,0
$80BaTiO_3 + 20PbTiO_3 + 10BaSnO_3$	8,7	8,0	5,4
$80BaTiO_3 + 20PbTiO_3 + 15BaSnO_3$	7,3	6,0	3,5
$75BaTiO_3 + 25PbTiO_3 + 2,5BaSnO_3$	~7,6	7,6	7,0
$75BaTiO_3 + 25PbTiO_3 + 5BaSnO_3$	7,5	6,6	7,2
$75BaTiO_3 + 25PbTiO_3 + 10BaSnO_3$	7,2	6,0	6,0
$75BaTiO_3 + 25PbTiO_3 + 15BaSnO_3$	6,6	5,0	5,0

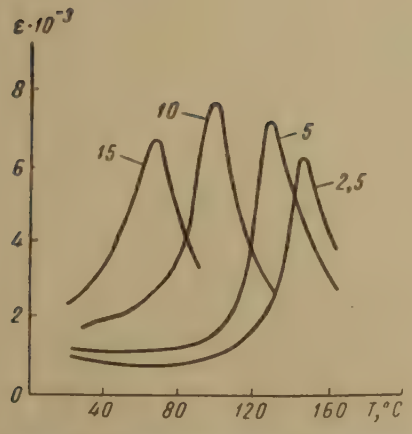

Fig.3. Temperature dependences of the dielectric constant of 90% $BaTiO_3$ + 10% $PbTiO_3$ + n $BaSnO_3$ solid solutions (values of n given at the curves).

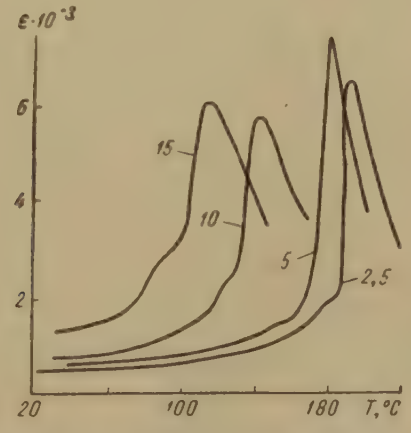

Fig.4. Temperature dependence of the dielectric constant of 80% $BaTiO_3$ + 20% $PbTiO_3$ + n $BaSnO_3$ solid solutions (values of n given at the curves).

In other words, in the first approximation the effects of $PbTiO_3$ and $BaSnO_3$ may be regarded as additive. At appreciable concentrations of $PbTiO_3$ (20-25%) and $BaSnO_3$ (10-15%), however, there is observed a noticeable deviation from this regularity: the Curie point proves to be higher than given by Eq.(1).

The temperature dependences of the dielectric constant for some of the investigated compositions are given in Figs.2, 3 & 4.

The values of the spontaneous polarization, residual polarization, and coercive field of the investigated solid solution specimens, measured by the oscillographic procedure at a frequency of 50 cps and room temperature, are listed in the accompanying table.

The nonlinearity of the permittivity of the investigated specimens was evaluated from the dc electric field dependence of their reversible dielectric constant. The variation of the reversible dielectric constant at room temperature with the electric field strength for some solid solutions containing 15% $BaSnO_3$ is shown

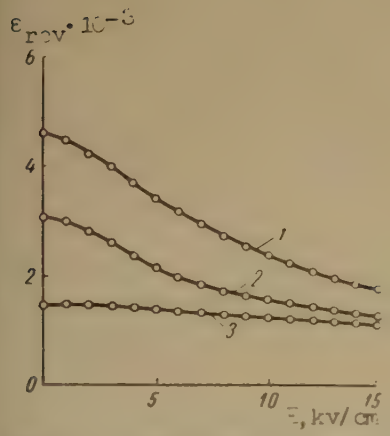

Fig.5. Variation of the reversible dielectric constant as a function of the dc field at room temperature for some solid solutions ($E_{=} \approx 2.5$ to 15 kv/cm, $E_{\sim} \approx 20$ v/cm): 1) 95% $BaTiO_3$ + 5% $PbTiO_3$ + 15% $BaSnO_3$, 2) 90% $BaTiO_3$ + 10% $PbTiO_3$ + 15% $BaSnO_3$, 3) 80% $BaTiO_3$ + 20% $PbTiO_3$ + 15% $BaSnO_3$.

in Fig.5. The nonlinearity $(\Delta\epsilon/\epsilon)(1/E)$ (with $E_{=} \approx 2.5$ kv/cm) proved to be greatest ($\sim 10^{-4}$ cm/v) in the case of the 90% $BaTiO_3$ + 10% $PbTiO_3$ + 15% $BaSnO_3$ solid solution.

Polarized samples of all the investigated solid solutions exhibited piezoelectric activity. The most interesting proved to be compositions with 5% $PbTiO_3$ and 5 and 10% $BaSnO_3$, in which the piezoelectric coefficient d_{33} (measured by the static procedure with $\sigma_{33} \approx 13$ kg/cm^2) approached 10^{-5} cgse units, i.e., was 1.5-2 times greater than in pure $BaTiO_3$.

Discussion

It will be evident from the experimental data that where $BaTiO_3$-$PbTiO_3$-$BaSnO_3$ solid solutions are concerned, the effects of $PbTiO_3$ and $BaSnO_3$ in the range of low concentrations of these compounds are additive in the first approximation. Additivity no longer obtains, however, when the $PbTiO_3$ content begins to exceed 20%. The observed deviations may be explained, first, by the fact that with an appreciable content of $PbCO_3$ in the initial batch there may occur appreciable volatilization of the lead, leading to a decrease of the actual $PbCO_3$ content (as compared with the assumed content based on the batch composition), and, second, by the possibility that in the process of synthesis, in addition to $PbTiO_3$, there is formed some other lead compound. Such a compound, for example, may be one described by the formula "$PbSnO_3$" (see Venevtsev et al[13-15]), the influence of which on the dielectric properties of the solid solutions should be more or less equivalent to that of $BaSnO_3$.[6] It may be assumed that the amount of "$PbSnO_3$" formed is proportional to the content of $PbCO_3$ and SnO_2 in the initial batch, i.e., that in the case of a small amount of either of these components in the initial batch, the quantity of "$PbSnO_3$" forming will be small, its influence minor and the deviation from additivity insignificant.

In the case of compositions containing 5 and 10% $PbTiO_3$, the addition of 5% $BaSnO_3$ leads to an increase of the spontaneous and residual polarizations as compared with other solid solutions with the same $PbTiO_3$ content. This effect can be explained if we recall that the spontaneous polarization of polycrystalline specimens depends on two factors: first, on the magnitude of the spontaneous polarization of the individual domains or microcrystals comprising the polycrystalline specimen and, second, on the degree of its orientation by the electric field. Increase of the $BaSnO_3$ content in the solid solutions, on the one hand, leads to decrease of the spontaneous polarization of the individual domains, and, on the other hand, reducing the volume electrostriction of the domains, facilitates orientation of the polarization vectors by the electric field (the number of 90° orientations increases). In the indicated low range of $BaSnO_3$ concentrations, the second effect probably predominates. Further increase of the $BaSnO_3$ content leads to such a decrease of the spontaneous polarization of the individual domains that this effect begins to predominate and hence the resultant polarization of the poly-crystalline specimen decreases.

Specimens of 95% $BaTiO_3$ + 5% $PbTiO_3$ + 2.5% $BaSnO_3$, 95% $BaTiO_3$ + 5% $PbTiO_3$ + + 5% $BaSnO_3$ and 90% $BaTiO_3$ + 10% $PbTiO_3$ + 5% $BaSnO_3$ exhibit somewhat higher values of spontaneous and residual polarization than pure $BaTiO_3$, with virtually the same coercive force. Specimens of these compositions also yield a well formed hysteresis loop with satisfactory rectilinearity at relatively low values of the external field (6, 5 and 5.6 kv/cm, respectively).

"P.N.Lebedev" Physical Institute,
Academy of Sciences of the USSR

References

1. F.H.Jonker & J.H.van Santen, Chem.Weekblad, 43, 672 (1947).
2. G.A.Smolenskii, Zhur.tekh.fiz., 20, 137 (1950).
3. G.Shirane & K.Suzuki, J.Phys.Soc.Japan, 6, 274 (1951).
4. K.Suzuki, J.Phys.Soc.Japan, 6, 340 (1951).
5. N.A.Roi, Akust.zhur. (Acoustics Journal), 2, 62 (1956).
6. I.E.Myl'nikova, Izv.AN SSSR, Ser.fiz., 21, 423 (1957). (Trans.Bulletin 21, No.3, 423.)
7. G.A.Smolenskii, M.A.Karamyshev & K.I.Rozgachev, Doklady AN SSSR, 79, 53 (1951).
8. R.H.Dungan, D.F.Kane & L.R.Bickford, J.Amer.Ceram.Soc., 35, 318 (1952).
9. G.A.Smolenskii & V.A.Isupov, Doklady AN SSSR, 96, 53 (1954).
10. G.A.Smolenskii & V.A.Isupov, Zhur.tekh.fiz., 24, 1375 (1954).
11. G.A.Smolenskii & V.A.Isupov, Zhur.neorgan.khimii (Journal of Inorganic Chemistry) 1, 1402 (1956).
12. V.A.Bokov, Zhur.tekh.fiz., 27, 1784 (1957). (Trans.Soviet Phys.-Tech.Phys.)
13. Iu.N.Venevtsev & G.S.Zhdanov, Izv.AN SSSR, Ser.fiz., 20, 178 (1956). (Trans. Bulletin 20, No.2, 161.)
14. Iu.N.Venevtsev & G.S.Zhdanov, Zhur.fiz.khimii, 30, 1324 (1956).
15. Iu.N.Venevtsev, G.S.Zhdanov & T.N.Shendrik, Kristallografiia, 1, 657 (1956).

PHASE TRANSITIONS IN SOLID SOLUTIONS OF SODIUM TANTALATE IN SODIUM NIOBATE

- V.A. Isupov

Formerly it was generally held that sodium niobate is antiferroelectric. Recently, however, Cross & Nicholson[1,2] advanced the hypothesis that there occur both antiparallel and parallel ionic displacements in the unit cells of sodium niobate at low temperatures. They termed this state "ferrielectric". So far there is no x-ray evidence for the existence of the ferrielectric state of $NaNbO_3$.

There is also a lack of reliable information in the literature on the nature of the high temperature phase transitions in $NaNbO_3$ at ~500 and ~640°.[3,4] The dielectric constant of $NaNbO_3$ single crystals goes through a sharp high maximum at 320-350° (Fig.1). At 468-518° there is a discontinuity in the ϵ curve, while at 638° there is not even a jump in ϵ, although there is a sudden change of TKϵ. In $(Na,K)NbO_3$ solid solutions the high temperature transitions are shifted to lower temperatures as the Na ions are replaced by K ions.[3]

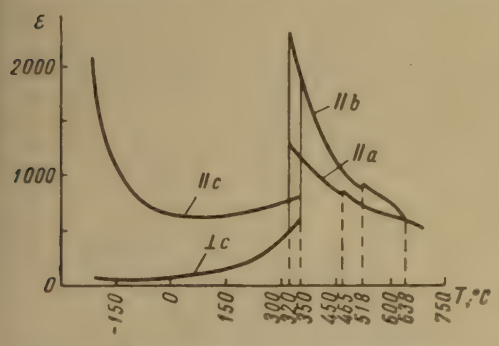

Fig.1. Temperature dependence of the dielectric constant of sodium niobate (after Cross & Nicholson[1]).

In view of the above considerations, we suggested in our report[5] presented at the First Conference on Ferroelectricity that the Curie point of sodium niobate corresponds to the 360° transition and that the high temperature transitions are not associated with ferro- or antiferroelectricity but are similar to the phase transitions in the $(Ca,Sr)TiO_3$ system[6-8] and are due to the small radius of the Na ion. Krainik[9] concurred in this view in his report to the Conference.

Francombe & Lewis[10] arrived at similar conclusions: they showed that the high temperature transitions in the $NaNbO_3$-$KNbO_3$, $NaNbO_3$-$CdNb_2O_6$ and $NaNbO_3$-$PbNb_2O_6$ systems occur when the lattice parameters, varying with temperature, attain a certain value, which is roughly the same for all the compositions of the solid solutions studied by these authors. Below this temperature the -C-Nb-O- chains become zigzag and there occurs "crumpling" of the structure. Francombe & Lewis called such transitions "crumpling transitions". We shall use this term.

In the present work we investigated the phase transitions in the $NaNbO_3$-$NaTaO_3$ system by studying the temperature dependence of the dielectric polarization. It is known that phase transitions occur in $NaTaO_3$ at 630, 580 and 480°.

The solid solution samples were prepared by the usual ceramic procedure from previously synthesized $NaNbO_3$ and $NaTaO_3$. The sintering temperatures were 1280 to 1480° (the holding time at peak temperature was 1 hour).

Below, for the sake of brevity, we shall designate the $NaTaO_3$ content of the investigated solid solutions through x.

Measurements of the dielectric constant at a frequency of 500 kc showed that the dielectric constant of $NaNbO_3$ passes through a maximum at a temperature of 365°. In addition, for all the $NaNbO_3$ samples, we obtained small humps in the ϵ vs T curves at 30-60° and -170°. Similar humps were noted in the ϵ curves for some of the solid solutions. It will be evident from Fig.2 that with increasing x the temperature of the ϵ maximum corresponding to the antiferroelectric transition decreases and the peak itself becomes flatter and lower. At x = 0.75, however, the ϵ peak is sharp and high.

The dielectric constant of $NaTaO_3$ increases only slightly with cooling.

The temperature dependence of the thermal volumetric expansion coefficient of $NaTaO_3$ exhibits no anomalies in the temperature range from -180 to +510°.

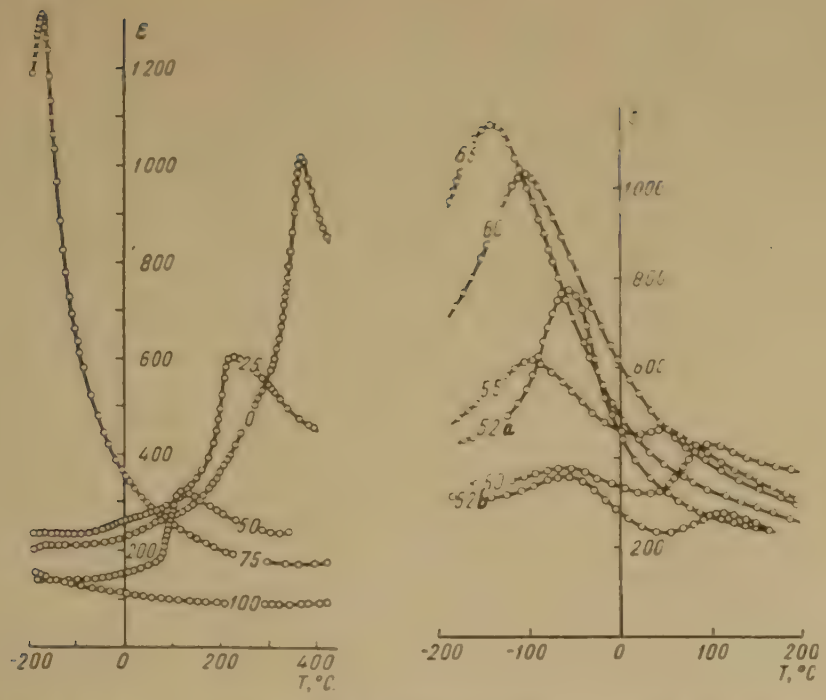

Fig.2.& 3. Temperature dependences of the dielectric constant ϵ of polycrystalline specimens of $Na(Nb,Ta)O_3$ solid solutions measured at 500 kc. The figures at the curves indicate the $NaTaO_3$ content in mole percent.

For one of the samples with x = 0.5 and all the samples with x = 0.55, two maxima appeared in the ϵ vs T curve (Fig.3). At x = 0.6 again only one maximum appears. Thus with increase of x the first ϵ maximum decreases and disappears in the interval $0.5 < x < 0.6$; a second maximum appears in this interval and increases in size with increasing x. The properties of samples with x in the range from 0.5 to 0.6 are greatly dependent on the preparation procedure: for example, samples a and b both with x = 0.52 but sintered at 1400 and 1440° exhibit sharply different variations of ϵ with temperature.

Investigation of P = ƒ(E) showed that none of the samples yielded hysteresis loops at 20°with an 18 kv/cm field. On the other hand, at -196° all the investigated compositions except $NaTaO_3$ yielded dielectric hysteresis loops with $E \approx 40$ kv/cm. In the solid solutions with $x > 0.5$ hysteresis loops were observed only at temperatures lower than that of the second ϵ maximum (the low temperature ϵ peak). The spontaneous polarization of solid solutions with x between 0.52 and 0.65 at -170° varied from 1.45 to 1.8 microcoulomb/cm^2.

On the basis of our dielectric polarization measurements and the data in the literature we constructed the approximate phase diagram for the system shown in Fig.4. In this diagram we have also plotted the points (□ and ×) corresponding to the above mentioned humps in the ϵ vs T curves for the different specimens.

Before turning to a discussion of the experimental results, a few further remarks regarding the "crumpling transitions" are indicated. We believe that the ferro-,

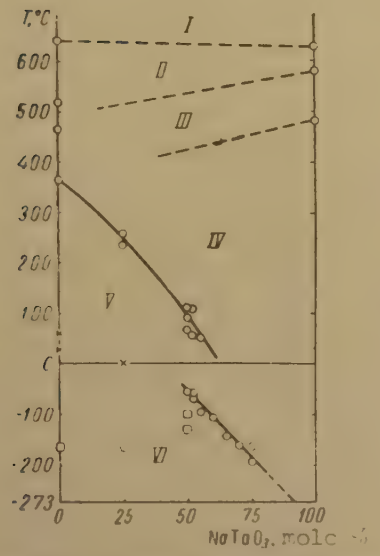

Fig.4. Approximate phase diagram for the $Na(Nb,Ta)O_3$ solid solution system constructed on the basis of our dielectric measurements and the data in the literature: I - paraelectric state (cubic symmetry), II - Q-electric state (tetragonal symmetry), III - Q-electric state (pseudotetragonal (orthorhombic) symmetry), IV - quasiferrielectric state (orthorhombic symmetry), V - antiferroelectric state (orthorhombic symmetry), IV - ferrielectric state.

antiferro- and ferrielectric transitions (let us call these S-electric) are caused by dipole-dipole interaction forces, while crumpling phase transitions are caused by short-range forces. Apparently, it must be assumed that as a result of crumpling phase transitions there may form structures in which 1) the moments of neighboring unit cells are arranged antiparallel and compensate each other, 2) the moments of the unit cells are parallel or 3) the moments of the cells have both parallel and antiparallel components. Let us call these three states quasiantiferroelectric, quasiferroelectric and quasiferrielectric states, respectively (hereinafter we shall refer to them as Q-electric). In contrast to S-electric transitions, the Q--electric phase transitions are not accompanied by sharp and high maxima of the dielectric constant, but can be evinced by discontinuities, i.e., abrupt changes in ϵ or $TK\epsilon$. Crumpling transitions in $(A,A')BO_3$ type solid solutions are characterized by an increase of the transition temperature as the larger A ions are successively replaced by smaller A' ions.

The high temperature cubic→tetragonal phase transitions occur at virtually the same temperature in sodium niobate and sodium tantalate. In contrast, there is an appreciable difference between the Curie points of potassium (or lead) niobate and tantalate. Hence the minor difference between the phase transition temperatures in sodium niobate and tantalate (in view of the almost equal ionic radii of niobium and tantalum) is explained on the assumption that these transitions are essentially crumpling transitions. The same thing may be said of the tetragonal→ →pseudotetragonal (orthorhombic) transition observed in sodium niobate and tantalate at 500 and 580°, respectively, and regarding the transition at 480° in $NaTaO_3$.

Inasmuch as there obtain both antiparallel and parallel ionic displacements in sodium tantalate at room temperature[11], it may be inferred that $NaTaO_3$ is quasiferrielectric below 480°.

It follows from the phase diagram that $NaTaO_3$ can be antiferroelectric only at low temperatures if at all.

The fact that dielectric hysteresis loops were observed for all the investigated compositions (including $NaNbO_3$, but excepting $NaTaO_3$) at -190° gives reason to infer that there is present in all the solid solutions (and $NaNbO_3$) a spontaneously polarized phase, possibly, a ferrielectric one (this is consistent with the deductions of Cross & Nicholson).

The disappearance of the dielectric constant maximum, corresponding to the antiferroelectric transition, and the growth of the low temperature ϵ maximum can be explained by the existence of a narrow insolubility interval at $0.5 < x < 0.6$ or by the presence of defect structure resulting from an insufficiently high sintering temperature. (Novosil'tsev & Khodakov[12] explain the absence of the ϵ maximum at 120° in the curves for barium titanate crystals grown at relatively low temperatures by the presence of defect structure.) It must be admitted, however, that both explanations appear doubtful: the existence of an insolubility interval is little probable, while the analogous disappearance of the antiferroelectric ϵ maximum and the "genesis" of a ferrielectric maximum in $NaNbO_3$-$CaNb_2O_6$ and $NaNbO_3$--$CaTiO_3$ solid solutions, observed by Krainik[13] makes the second explanation highly questionable, inasmuch as the components of both these systems are more readily fusible, so that the sintering temperature used in preparing the specimens cannot be considered insufficiently high (i.e., it is not probable that a defect structure is formed under the given preparation conditions).

I take this opportunity to thank G.A.Smolenskii for his guidance and A.I.Agranovskaia for assistance in preparing the samples.

Semiconductor Institute
Academy of Sciences of the USSR

References

1. L.E.Cross & B.J.Nicholson, Phil.Mag., 46, No.376, 453 (1955).
2. L.E.Cross, Phil.Mag., 1, No.1, 76 (1956).
3. G.Shirane, R.Newnham & R.Pepinsky, Phys.Rev., 96, 531 (1954).
4. M.H.Francombe, Acta Crystallogr., 9, 256 (1956).
5. V.A.Isupov, Izv.AN SSSR, Ser.fiz., 21, 402 (1957). (Trans.Bulletin 21, No.3, 404.)
6. H.Gränicher & O.Jakits, Nuovo Cimento, No.3, 480 (1954).
7. J.McQuarri, Amer.Cer.Soc., 38, 444 (1955).
8. G.A.Smolenskii, V.A.Isupov, A.I.Agranovskaia & E.D.Sholokova, Zhur.tekh. fiz., 27, 2528 (1957). (Soviet Physics - Tech.Physics).
9. N.N.Krainik, Izv.AN SSSR, Ser.fiz., 21, 422 (1957). (Trans.Bulletin 21, No.3, 412.)
10. M.H.Francombe & B.Lewis, Electronics Jour., 2, 387 (1957).
11. H.F.Kay & J.L.Miles, Acta Crystallogr., 10, 213 (1957).
12. N.S.Novosil'tsev & A.L.Khodakov, Doklady AN SSSR, 85, 1263 (1952).
13. N.I.Krainik, Present issue of the Bulletin, p.1486.

INFLUENCE OF Fe_2O_3, SrO, SnO_2, ZrO_2 AND $BaSnO_3$ IMPURITIES ON THE DIELECTRIC HYSTERESIS LOOPS OF POLYCRYSTALLINE $BaTiO_3$ AND $BaTiO_3$-$PbTiO_3$ SOLID SOLUTIONS

- G.M.Kovalenko, S.V.Bogdanov & A.M.Cherepanov

The purpose of the present study was to determine the influence of certain impurities on the parameters of the dielectric hysteresis loops of both polycrystalline $BaTiO_3$ and a number of solid solutions of $BaTiO_3$ with $PbTiO_3$. It is known that even small amounts of extraneous substances can substantially alter the properties of ferroelectric materials.[1-7]

By way of host materials we used barium titanate and six of its solid solutions with lead titanate. By way of additives we used Fe_2O_3, SrO, SnO_2 and ZrO_2 in amounts of up to 3% by weight relative to the host material. The SnO_2 was introduced both in the form of the oxide and in the form of barium stannate. In the latter case the amounts of $BaSnO_3$ added were 2.5 and 5 mole percent in excess of the basic composition. The data on the 47 investigated compositions are listed in Table 1.

Table 1

Composition of investigated substances

Group No.	Host, mole %		Impurities, % by weight over 100			
	$BaTiO_3$	$PbTiO_3$	Fe_2O_3	SrO	SnO_2	ZrO_2
1	100	0	0.1 —	1; 2; 3	—	— —
2	95	5	— —	2; 3 —	— 2; 3	— 2; 3
3	90	10	0.1; 0.2 — —	2; 3 — —	— 2; 3 —	— 2; 3
4	85	15	— — —	2; 3 — —	— 2; 3 —	— 2; 3
5	80	20	0.1; 0.2 — —	— 2; 3 —	— 2; 3 —	— 2; 3
6	75	25	— — —	3 — —	— 1; 2; 3 —	— 2; 3
7	70	30	— —	1 —	— 1	— —

The procedure employed in preparing the specimens differed little from the conventional procedure commonly used in preparing barium titanate. In sintering the lead-containing specimens appropriate measures were taken to minimize volatilization of the lead oxide. The sintering temperature for some of the compositions, particularly those with $BaSnO_3$, was as high as 1550°.

We recorded the dielectric hysteresis loops for all the samples at room temperature (20°) and from these by straight-forward calculations determined the basic loop parameters, namely, the spontaneous polarization P_s, the residual polarization P_o, the coercive force E_c and the rectangularity ratio P_o/P_{max}. The results are shown in Table 2. Among the investigated compositions there are several for which the characteristics of the dielectric hysteresis loop differ appreciably from the corresponding characteristics for the initial host material. The data for several

Table 2

Variation of the spontaneous (P_S) and residual (P_O) polarization, the coercive force (E_C) and the rectangularity factor of the dielectric hysteresis loop (P_O/P_{max}) with the content of Fe_2O_3, SrO, SnO_2 and ZrO_2 impurities

Host material	Hysteresis loop parameters	Parameters in host material	Impurities, % wt.								
			Fe_2O_3		SrO			SnO_2		ZrO_2	
			0,1	0,2	1,0	2,0	3,0	2,0	3,0	2,0	3,0
$BaTiO_3$	$P_S \cdot 10^6$ coul/cm^2	5,0	5,0	--	6,8	4,0	2,2	—	—	—	—
	$P_O \cdot 10^6$ " "	4,2	4,0	—	6,0	3,0	1,8	—	—	—	—
	E_C, kv/cm	2,3	1,9	—	1,6	1,7	1,4	—	—	—	—
	P_O/P_{max}	0,50	0,70	--	0,65	0,50	0,50	—	—	—	—
95% $BaTiO_3$+ +5% $PbTiO_3$	$P_S \cdot 10^6$ coul/cm^2	10,0	--	--	—	6,8	5,3	6,9	6,0	5,7	5,7
	$P_O \cdot 10^6$ " "	9,0	--	--	--	6,0	4,3	6,3	5,6	5,0	5,0
	E_C, kv/cm	2,8	--	--	--	1,6	1,8	2,7	1,8	2,7	1,4
	P_O/P_{max}	0,76	--	--	—	0,75	0,60	0,70	0,73	0,65	0,70
90% $BaTiO_3$+ +10% $PbTiO_3$	$P_S \cdot 10^6$ coul/cm^2	5,4	7,4	6,0	--	9,0	6,7	8,3	4,8	8,0	6,1
	$P_O \cdot 10^6$ " "	5,0	6,5	5,4	--	7,0	5,6	7,7	4,4	6,7	5,6
	E_C, kv/cm	3,6	3,7	3,1	--	1,6	1,5	3,5	3,7	3,7	3,7
	P_O/P_{max}	0,77	0,75	0,77	--	0,65	0,63	0,73	0,70	0,72	0,75
85% $BaTiO_3$+ +15% $PbTiO_3$	$P_S \cdot 10^6$ coul/cm^2	9,2	—	—	—	6,8	6,2	8,0	7,0	8,5	7,0
	$P_O \cdot 10^6$ " "	9,0	—	—	—	6,2	4,9	7,7	6,8	7,8	6,2
	E_C, kv/cm	8,1	—	—	—	2,4	2,4	4,5	4,3	6,2	4,7
	P_O/P_{max}	0,80	—	—	—	0,74	0,56	0,79	0,83	0,81	0,70
80% $BaTiO_3$+ +20% $PbTiO_3$	$P_S \cdot 10^6$ coul/cm^2	7,6	10,3	9,6	--	8,6	7,3	8,0	5,8	6,0	5,8
	$P_O \cdot 10^6$ " "	7,0	8,4	8,0	—	7,4	5,8	7,0	4,4	5,5	5,3
	E_C, kv/cm	10,0	7,4	8,8	—	4,2	2,5	7,2	2,4	7,0	6,8
	P_O/P_{max}	0,83	0,78	0,87	--	0,74	0,67	0,74	0,53	0,74	0,68
75% $BaTiO_3$+ +25% $PbTiO_3$	$P_S \cdot 10^6$ coul/cm^2	7,0	--	-		6,7	8,6	7,3	8,8	8,7	
	$P_O \cdot 10^6$ " "	6,8	--	-		6,5	8,3	6,8	8,6	7,6	
	E_C, kv/cm	9,0	—			3,2	7,0	7,6	9,0	9,2	
	P_O/P_{max}	0,90	—	—	--	—	0,80	0,78	0,75	0,86	0,74
70% $BaTiO_3$+ +30% $PbTiO_3$	$P_S \cdot 10^6$ coul/cm^2	10,7	—	-	7,6	--	--	8,0	—	—	—
	$P_O \cdot 10^6$ " "	10,0	—	—	7,2	—	--	7,6	--	--	—
	E_C, kv/cm	12,0	—	—	10,0	--	--	10,0	--	--	—
	P_O/P_{max}	0,80	—	—	0,80	--	—	0,80	—	--	—

Table 3

Influence of SrO and $BaSnO_3$ on the hysteresis loop parameters and the electric field strength necessary for obtaining saturation loops

Host material		Impurities wt over 100%		Hysteresis loop parameters and saturation field				
$BaTiO_3$	$PbTiO_3$	SrO	$BaSnO_3$	$P_s \cdot 10^6$ coul/cm^2	$P_o \cdot 10^6$ coul/cm^2	E_c	P_o/P_{max}	E
95	5	0	0	10,0	9,0	3,0	0,76	8,0
95	5	0	2,5	5,6	5,0	2,8	0,82	6,0
95	5	0	5,0	6,6	6,0	2,0	0,83	5,0
90	10	0	0	5,4	5,0	7,4	0,77	16,0
90	10	0	5,0	6,8	6,2	2,8	0,85	5,6
75	25	0	0	7,0	6,8	9,0	0,90	18,0
75	25	3	0	6,7	6,5	3,2	0,80	7,6

such compositions are given in Table 3 (the listed values are the averages for 3-4 measurements on samples from different batches). Analysis of the experimental data shows that the addition of impurities is an effective means for modifying the hysteresis loop parameters. For example, the addition of 3% SrO to 75% $BaTiO_3$ + 25 % $PbTiO_3$ has virtually no effect on the values of P_s, P_o and P_o/P_{max} of the initial solid solution, but at the same time reduces the coercive force to almost 1/3 its initial value and more than halves the electric field strength necessary for saturation.

In discussing the mechanism whereby the impurities influence the hysteresis loop parameters it may be argued that the introduced impurities a) act as a flux improving the sintering and enhancing the density of the specimen, b) enter into the crystal lattice and "loosen" it to some extent, c) form new chemical compounds with the other components or, d) by their presence in some way facilitate growth of the crystals in the polycrystalline specimens (as Remeika[1] suggests with respect to Fe_2O_3 in the case of single crystals).

In her report to the Conference, Verbitskaia described the influence of small amounts of impurities on the dielectric properties of ferroelectric substances, in particular, on the dielectric constant and tan δ. She stated that impurities even in the amount of only 0.1% can significantly alter the dielectric properties of the host material. Although she infers that when present in large amounts impurities may form new chemical compounds, Verbitskaia is of the opinion that the impurities act primarily as fluxes improving the sintering.

There is no reason a priori to exclude the possibility of any (or all) of the above effects. It must be noted, however, that although improvement of sintering (flux effect) should lead to increase of P_s and P_o, it can hardly substantially decrease the coercive force. Yet in all the experimental cases where any substantial effect was observed, we found an appreciable decrease of the coercive force sometimes by a factor of almost 3. This shows, at any rate, that impurities do not serve merely as a flux. Unfortunately, until further data are available, it does not appear feasible to give a more detailed analysis of the mechanism involved in the influence of impurities on the dielectric properties of the ferroelectrics.

Conclusions

1. Our experiments showed that the addition of small amounts of Fe_2O_3, SrO, SnO_2, ZrO_2 or $BaSnO_3$ can serve as an effective means of modifying the basic characteristics of the dielectric hysteresis loops of both $BaTiO_3$-$PbTiO_3$ solid solutions.

2. In individual cases the impurities appreciably lower the coercive force E_c and the electric field strength necessary for obtaining saturation without noticeably altering the high initial values of P_s, P_o and the rectangularity factor P_o/P_{max} of the ferroelectric material.

"P.N.Lebedev" Physical Institute,
Academy of Sciences of the USSR

References

1. I.P.Remeika, J.Amer.Chem.Soc., 76, 940 (1954).
2. A.Nishioka, K.Sekikava & M.Owaki, J.Phys.Soc.Japan, 11, 180 (1956).
3. W.W.Coffeen, Trans.Amer.Inst.El.Engr., 72, Part I. 704 (1953).
4. F.T.Rogers, J.Amer.Cer.Soc., 35, 16 (1952).
5. B.Jaffe, R.Roth & S.Marzullo, J.of Research, N.B.Standards, 55, 239 (1955).
6. K.W.Plessner & R.West, J.Electronics and Control, 4, 51 (1958).
7. T.Sakudo, J.Phys.Soc.Japan, 12, 1050 (1957).

NONLINEAR PROPERTIES OF SOME (Ba,Sr)(Ti,Sn)O_3 SOLID SOLUTIONS

- A. I. Medovoi

Investigation of the ferroelectric properties of solid solutions based on barium titanate is of both practical and theoretical interest, inasmuch as such investigations can lead to a better understanding of ferroelectricity. Until now, such investigations have been largely restricted to binary systems. The first to study multiple component systems in the USSR was Myl'nikova[1] who worked with (Ba, Pb)(Ti,Sn)O_3 solid solutions.

In the present work we investigated the (Ba,Sr)(Ti,Sn)O_3 system. We chose this system in view of the possibility of obtaining ceramics with a high dielectric constant and pronounced nonlinear properties.

The specimens were prepared by the usual ceramic technique. The values of ϵ and tan δ were measured on a MKE-2 type bridge at a frequency of 10^4 cps. In these measurements the maximum voltage on the samples did not exceed 4-6 v. The dielectric constant in high electric fields was evaluated from the capacitance which was calculated on the basis of the effective current. Losses were not taken into account.

1. Temperature dependences of ϵ and tan δ in weak fields

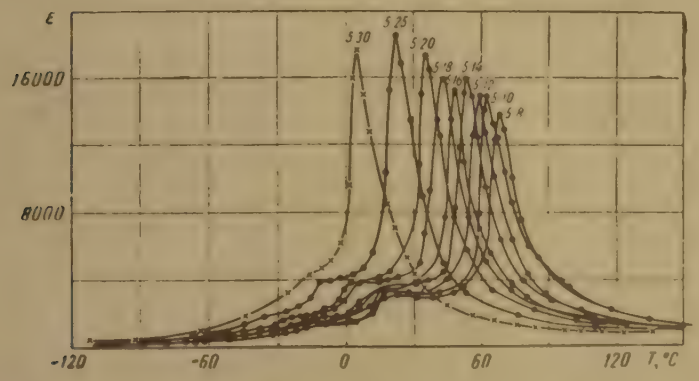

Fig.1. Temperature dependences of the dielectric constant ϵ for a number of solid solutions of the (Ba,Sr)(Ti,Sn)O_3 system. The figures at the curves indicate the respective percentages of $BaSnO_3$ and $SrTiO_3$.

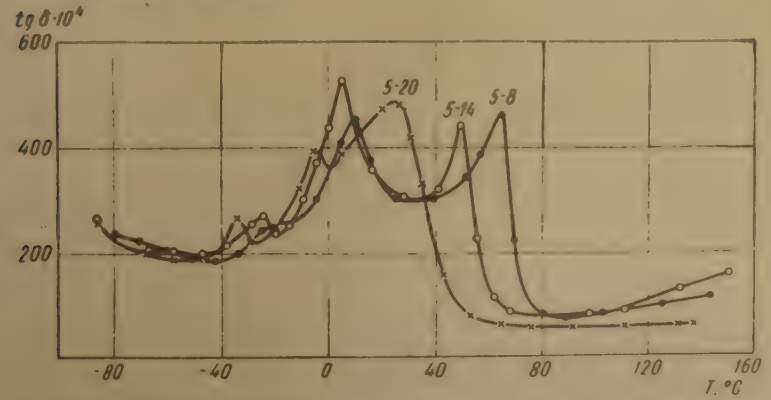

Fig.2. Temperature dependence of tan δ in weak fields.

The measurements were carried out on specimens containing up to 30% strontium titanate. The temperature dependences of ϵ and tan δ in weak electric fields are shown in Figs.1 & 2, respectively.

It will be evident from Fig.1 that there is a range of compositions in which the values of ϵ in the region of the Curie temperature are exceptionally high (i.e., higher than those of other solid solutions). All the ϵ vs T curves have maxima and humps which correspond to phase transitions. As the $SrTiO_3$ content of the specimens is increased, the ϵ maxima and humps shift to lower temperatures. The low temperature phase transitions are more clearly evinced in the tan δ vs temperature curves (Fig.2). There is evident a general rise of tan δ in the region of low temperatures. This is in agreement with the work of Blunt & Love[2] who found that tan δ of polycrystalline $BaTiO_3$ and its solid solutions with $SrTiO_3$ goes through a maximum in the rhombohedral modification. The observed temperature depend-

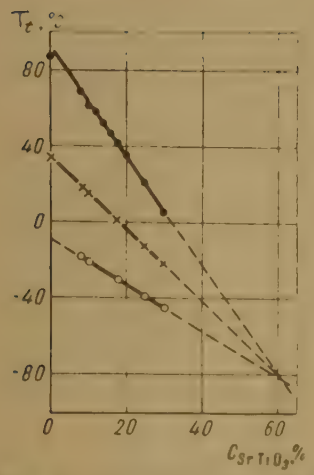

Fig.3. Variation of the phase transition temperatures with the $SrTiO_3$ content in $BaTiO_3$ solid solutions containing 5% $BaSnO_3$.

ence of tan δ in weak fields is consistent with the concepts developed by Bokov.[3]

We used the transition temperature values deduced from the ϵ and tan δ curves to plot the variation of the phase transition temperatures as a function of the $SrTiO_3$ content in a series of solid solutions containing 5% $BaSnO_3$. It will be seen from Fig.3 that the phase transition points fit three straight lines. Extended on the basis of the temperature dependences of ϵ and tan δ these lines intersect at a common point. It follows that an $SrTiO_3$ content $\geqslant 60\%$ there can occur only one phase transition, i.e., a direct cubic→rhombohedral transition. Obviously, the compositions corresponding to the region of approach and intersection of the phase transition lines are characterized by the highest values of ϵ.

A comparison of our data (Fig.1) with the data of Smolenskii & Isupov[4] for the $Ba(Ti,Sn)O_3$ system shows that our solid solutions have sharper ϵ peaks in the region of the Curie point and appreciably higher values of ϵ_{max}.

2. $\epsilon = f(T)$ in strong electric fields

Fig.4 shows the temperature dependences of ϵ at different values of the ac field for a specimen containing 5% $BaSnO_3$ and 12% $SrTiO_3$. Similar curves were obtained for the other investigated solid solutions. It will be seen that ϵ at first increases and then decreases with increase of $E_{\sim}$. The field value at which the maximum value of ϵ is observed depends on the temperature.

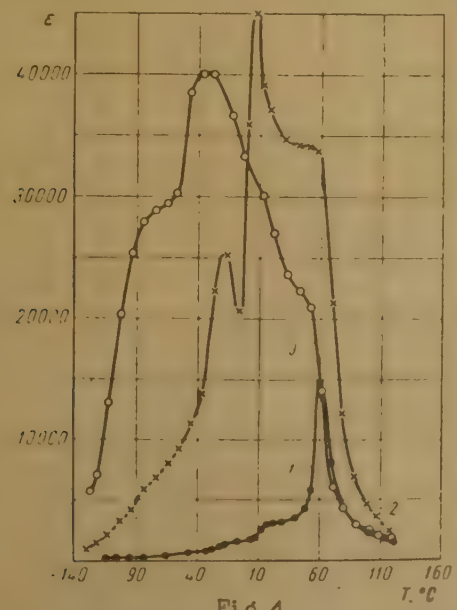

Fig.4

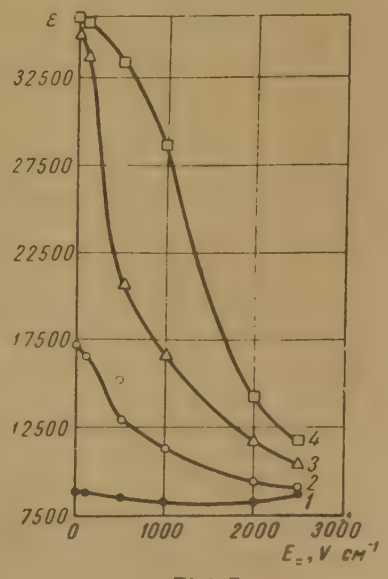

Fig.5

Fig.4. Temperature dependences of ϵ at different values of $E_{\sim}$ for a specimen having the composition 83% $BaTiO_3$ + 5% $BaSnO_3$ + 12% $SrTiO_3$: 1) $E_{\sim}$ = 60 v/cm, 2) 1250 v/cm and 3) 2000 v/cm.

Fig.5. Variation of ϵ with the biasing field at different values of $E_{\sim}$ for a specimen consisting of 87% $BaTiO_3$ + 5% $BaSnO_3$ + 8% $SrTiO_3$: 1) $E_{\sim}$ = = 1000 v/cm, 2) 500 v/cm, 3) 1000 v/cm, 4) 2000 v/cm.

When the ac field is increased to about 1000 v/cm there appear sharp ϵ peaks in the region of the phase transitions; these are connected with increase of the orientational polarization incident to transitions to phases of lower symmetry. With further increase of the field strength these peaks are smoothed out because the number of domains oriented by this field becomes less dependent on the temperature. Naturally, the electric field strength at which ϵ attains the highest value differs for different phase transitions.

3. $\epsilon = f(E_{=})$ at room temperature

We measured the variation of ϵ as a function of the biasing dc field for a series of samples containing up to 25 mole percent strontium titanate. The biasing field dependences of ϵ in different ac fields for the solid solution containing 5% $BaSnO_3$ and 8% $SrTiO_3$ are shown in Fig.5; similar dependences were obtained for the other investigated solid solutions.

It will be obvious from Fig.5 that there is a certain ac field value at which ϵ exhibits the strongest variation with $E_{=}$. Similar dependences were first obtained for some $Ba(Ti,Sn)O_3$ solid solutions by Verbitskaia[5].

The electric nonlinearity coefficient can readily be computed from the slope of the ϵ curves. Calculations and experiments show that the nonlinear properties of the solid solutions in the investigated series are very similar. Hence through appropriate choice of the solid solution composition one can design capacitors having high capacitance values characterized by a weak temperature dependence.

I desire to express my deep gratitude to Dr. G.A.Smolenskii for his interest in the work and discussion of the results.

References

1. I.E.Myl'nikova, Izv.AN SSSR, Ser.fiz., 21, 423 (1957). (Trans.Bulletin 21, No.3, 423.)
2. R.F.Blunt & W.F.Love, Phys.Rev., 76, 1202 (1949).
3. V.A.Bokov, Zhur.tekh.fiz., 27, 1784 (1957). (Trans.Sov.Phys. - Tech.Phys.)
4. G.A.Smolenskii & V.A.Isupov, Zhur.tekh.fiz., 8, 1376 (1954).
5. T.N.Verbitskaia, Doklady AN SSSR, 100, 29 (1955).

LOW TEMPERATURE POLARIZATION OF BARIUM TITANATE CERAMICS

- L.A.Shuvalov, M.M.Kachkacheva, L.Z.Rusakov & I.S.Zheludev

Ferroelectric ceramics acquire piezoelectric properties only as a result of polarization in a strong dc field. The process of polarization consists of rotation through a certain angle of the spontaneous polarization vectors (the Z axes) of the domains comprising the crystal grains of the ceramic. As a result the directions of the Z axes are distributed within a certain angle θ about the direction of the polarizing field E. The limiting values of the distribution angle (θ_{lim}) are also fixed[1]. Commonly "hot polarization" is employed, i.e., the field is applied to a specimen heated to a temperature close to the Curie point. "Cold polarization" (at room temperature) requires a stronger field and more time and, as a rule, leads to lower values of the piezoelectric coefficients.

We carried out a series of experiments on polarization of $BaTiO_3$ ceramic in the orthorhombic phase; we term such polarization "low temperature polarization". These experiments were undertaken in connection with our earlier hypothesis regarding the possibility of obtaining by means of such polarization in relatively moderate fields enhanced values of the piezoelectric coefficients in the orthorhombic and tetragonal forms of the ceramic. Our reasoning is based on the following premises which follow from Ref.1:

I. There are fundamentally only two ways of increasing the piezoelectric coefficients of the ceramic without altering the properties and structure of the individual grains and grain boundaries:

1) One can try in the process of polarization to realize rotations of the domains through the smallest feasible angles; this will reduce the angle θ_{lim} (angle of spread of the domain Z axes) and the smaller this angle, the higher the values of the piezoelectric coefficients[1]. To this end one must use the strongest possible polarizing field, extend the polarization time, etc.

2) Within a given range of allowable domain rotation angles (i.e., with θ_{lim} = const.) one must try to obtain the most favorable inhomogeneity in the distribution of domain orientations, that is, try to increase the distribution density close to the Z axis of the ceramic specimen. This inhomogeneous distribution can be realized, for example, in the following manner.

Assume that the "hot polarized" specimen is transformed from the tetragonal to the orthorhombic phase. Incident to the transition the angle θ is increased by 45° (owing to spontaneous rotation of the domain Z axes through 45°), and the relative and absolute magnitudes of the piezoelectric coefficients of the ceramic will decrease. If the specimen is now brought back to the tetragonal modification by warming in zero field the domains will rotate in the opposite sense and the specimen will return virtually to the initial state. If, however, while the specimen is in the orthorhombic phase we apply a polarizing field oriented in the same direction as the initial polarizing field, the Z axis distribution angle will be reduced from θ to θ_{lim} owing to rotation of the domains whose Z axes are outside the angle θ_{lim}. Now after return to the tetragonal phase the specimen will have higher values of the piezoelectric coefficients than initially, owing to advantageous inhomogeneity of the angular distribution of domains [the distribution density will decrease in the solid angle from θ_{lim} to (θ_{lim} - 45°) and increase in the angle from 0° to (θ_{lim} - 45°)].

II. In addition to the 90 and 180° switching that occurs in the tetragonal modification, in the orthorhombic phase there can also be realized domain rotations through 60°. Hence θ_{lim} in the orthorhombic modification is smaller than in the tetragonal one (45° instead of ~56°); consequently, in the orthorhombic phase there can be realized a higher relative value of the piezoelectric coefficients. However, in transition of the ceramic polarized in the orthorhombic phase

from this phase to the tetragonal one, the piezoelectric coefficients decrease owing to increase of the angle θ because of spontaneous rotation of the domains. Hence the values of the coefficients in the tetragonal phase end up by being smaller than in the case of direct polarization in this phase because θ proves to be greater than θ_{lim}. Now, however, if we polarize the ceramic in the orthorhombic phase and then transform it to the tetragonal phase without removing the polarizing field, owing to enhanced mobility of the domains close to the transition point, we can expect the field to hinder increase of θ above θ_{lim} for the tetragonal phase and we therefore should obtain a more advantageous inhomogeneity of the angular distribution of domains.

III. Although in any particular ferroelectric phase the mobility of the domains decreases with decreasing temperature, in the immediate vicinity of a transition to a lower temperature phase the mobility abruptly increases. This is substantiated by the work of Wieder[2] who observed a sharp decrease of the coercive force in c-domain crystals of $BaTiO_3$ incident to the tetragonal→orthorhombic transition. The experiments of Bokov[3,4] carried out on ceramic also indicated a decrease of the activation energy for the rotation of domains at the tetragonal→orthorhombic transition.

Thus in the orthorhombic phase close to the transition point from the tetragonal one, there are realized favorable conditions for polarization of the ceramic and hence one can expect effective polarization to occur in relatively weak fields.

Experiments and Results

Accordingly, we undertook a series of experiments on polarization and repolarization of $BaTiO_3$ ceramic at temperatures below the transition point to the orthorhombic phase.

We used ceramic disks 36 mm in diameter and 1 mm thick prepared by the conventional procedure. The electrodes were fired on. The specimens were initially polarized at 115° for 1 hour in a 6 kv/cm field and then cooled in the field. The degree of polarization was evaluated on the basis of the piezoelectric coefficient d_{31} which was measured by the resonance-antiresonance procedure[5]. Repeated hot polarization in stronger fields and for longer periods yielded no significant increase in d_{31}; hence it may be assumed that the specimens had the highest value of d_{31} attainable by hot polarization. After polarization the specimens were stored for 10 days; after which the values of d_{31} were measured at 28°C. These were taken as the initial values of the coefficient.

Low temperature repolarization

The repolarization was carried out at 0° (i.e., 5-7° below the tetragonal→→orthorhombic transition point) in a 1 kv/mm field for 1 hour. Then the specimens were heated to the initial temperature (28°) and after a brief aging period the value of d_{31} was again measured. In an alternate procedure the specimens were repolarized with heating in the field to a temperature above the phase transition point. The results of both series of experiments are shown in Table 1. Both repolarization procedures yielded an increase of d_{31}, but in the case of heating in the field, the results, in accord with the considerations set forth above (Section II) proved to be more stable and the increase in d_{31} amounted to 15% on the average.

It is known that the variation of the coercive force at the "boundary" between the tetragonal and orthorhombic modifications is characterized by temperature hysteresis.[2] Hence we carried out experiments on repolarization of the specimens at -15°C, i.e., well below the temperature of the coercive force discontinuity. After application of the polarizing field, we measured the piezoelectric coefficient every

Table 1

Sample No.	d_{31} at 20° (10⁻⁶ esu)		Increase, %	Sample No.	d_{31} at 20° (10⁻⁶ esu)		Increase, %
	Initial	After repolar.			Initial	After repolar.	
	Repolarization at 0°; warming in 2 kv/mm field				Repolarization at 0°; warming in 1 kv/mm field		
15	$1.36 \cdot 10^{-6}$	$1.42 \cdot 10^{-6}$	4	24	$1.30 \cdot 10^{-6}$	$1.53 \cdot 10^{-6}$	17.5
16	1.38	1.50	9	25	1.29	1.47	14
17	1.34	1.56	16	26	1.36	1.53	12.5
18	1.24	1.46	16	27	1.42	1.57	11
19	1.19	1.40	18	28	1.38	1.57	14
20	1.28	1.32	3	29	1.38	1.58	14.5
21	1.25	1.30	4	30	1.36	1.61	18.5

Table 2

Sample No.	Initial value of d_{31}, esu units		Repolarization at -15°; values of d_{31} in esu units			d_{31} at 20° after warming in field	Increase, %
	at 20°	at -15°	after 0.5 hr	after 1.0 hr	after 1.5 hr		
36	$1.33 \cdot 10^{-6}$	$1.18 \cdot 10^{-6}$	$1.39 \cdot 10^{-6}$	$1.43 \cdot 10^{-6}$	$1.46 \cdot 10^{-6}$	$1.60 \cdot 10^{-6}$	20
37	1.31	1.10	1.43	1.42	1.4	1.49	14
40	1.21	1.07	1.34	1.35	1.36	1.49	23
41	1.20	1.01	1.33	1.28	1.35	1.32	10

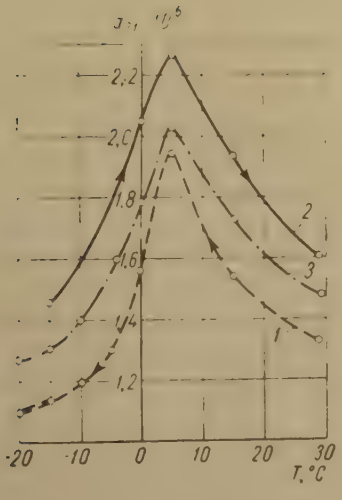

Temperature dependences of d_{31}: 1) before repolarization, 2) after repolarization and 3) after aging for 3 months.

Table 3

Sample No.	d_{31} at 20° (10⁻⁶ esu)		Increase, %
	Not polariz.	After repolariz. at -15° in 1 kv/mm field	
8	$1.32 \cdot 10^{-6}$	$1.45 \cdot 10^{-6}$	10
9	1.34	1.65	23
10	1.33	1.48	11
11	1.32	1.37	4
12	1.31	1.55	18

half hour in order to determine the optimum polarization time. The results are shown in Table 2, from which it may be seen that polarization times in excess of 1.5 hours lead to no further increase of the coefficient. Comparison of the values in Tables 1 & 2 shows that on the average the increase in d_{31} with repolarization at -15°C is no greater than with repolarization at 0°, although individual samples do exhibit a greater increment in d_{31}. Typical temperature dependences of the piezoelectric coefficient before and after repolarization are shown in the accompanying figure.

Low temperature polarization

A number of samples after measurement of d_{31} were depolarized by heating to 200°. These samples were then subjected to low temperature polarization in the orthorhombic phase at 0° in a 1 kv/mm field for 1.5 hours and with heating in the field to ~15°. The results are shown in Table 3. It will be seen that after transition of the ceramic polarized

in the orthorhombic phase to the tetragonal modification in the field the resultant coefficient, far from being lower as in the case of hot polarization (as was the case in heating in zero field) is actually appreciably higher.

Aging

It is known that aging of $BaTiO_3$ ceramic is largely connected with return of domains that have been switched 90° to their original position. Hence we could expect to observe enhanced aging of our specimen. Actually, the decrease of d_{31} with aging was noticeable, particularly in the case of specimens with a large increment in d_{31}. For most samples, however, even after 3 months aging, the value of d_{31} was on the average 10% higher than initially, i.e., before low temperature repolarization (see figure).

A number of the polarized and repolarized samples were subjected to several successive cycles of cooling and heating through the transition point. The values of d_{31} changed very little.

Conclusions

1. Low temperature repolarization in the orthorhombic phase leads to an increase of the piezoelectric coefficient of the ceramic in the tetragonal phase. Repolarization with warming in the field yields an increment of d_{31} averaging 15%. Despite appreciable decrease of the coefficient during aging the final value of d_{31} remains approximately 10% higher than the initial one.

2. Heating in the polarizing field after polarization in the orthorhombic modification hinders decrease of d_{31} upon transition to the tetragonal phase.

3. Polarization in the orthorhombic phase with subsequent heating in the field requires a lower field strength than polarization at room temperatures and yields values of d_{31} equal to or in some cases noticeably higher than obtained with hot polarization. Hence it may be expedient to employ low temperature polarization particularly in cases when hot polarization is inapplicable (for example, owing to high conductivity near the Curie point).

We take this opportunity to thank V.G.Zatevakhina who participated in the experiments.

Institute of Crystallography,
Academy of Sciences of the USSR &
Central Scientific Research Piezoelectric Laboratory,
Committee on Radio Electronics,
Soviet of Ministers of the USSR

References

1. L.A.Shuvalov, Kristallografiia, 2, 119 (1957) (Trans.Soviet Physics - Crystallography.)
2. H.H.Wieder, J.Appl.Phys., 26, 1479 (1955).
3. V.A.Bokov, Zhur.tekh.fiz., 27, 1784 (1955).
4. V.A.Bokov, Ibid., 28, 86 (1958). (Trans.Soviet Physics - Tech.Phys.)
5. L.A.Shuvalov, Kristallografiia, 3, 106 (1958). (Trans.Soviet Physics - Crystallography.)

ON OBTAINING PIEZOELECTRIC CERAMICS FOR HIGH TEMPERATURE APPLICATIONS

- I.S.Rez, E.G.Smazhevskaia & M.M.Kachkacheva

In connection with technological developments the upper bound of the operating temperature range specified for electromechanical ceramic transducers is being extended upward. Transducers made of barium titanate are capable of stable operation only up to a temperature of about 70°, the Curie point of this material being ~120° (Ref.1). It is therefore desirable to search for and investigate piezoceramic materials with higher Curie temperatures.

In view of this we undertook the preparation and investigation of the following substances:

a) $(Ba,Ca)TiO_3$, $(Ba,Pb)TiO_3$ and $(Ba,Ca,Pb)TiO_3$ solid solutions;
b) $Pb(Ti,Zr)O_3$ solid solutions, and
c) lead niobate and solid solutions containing it.

A summary of our results follows.

A. Investigation of the behavior of barium titanate piezoceramics at elevated temperatures with auxiliary polarization showed that these materials could be used up to ~100° with a polarizing voltage of the order of 6 kv/cm (see Fig.1).

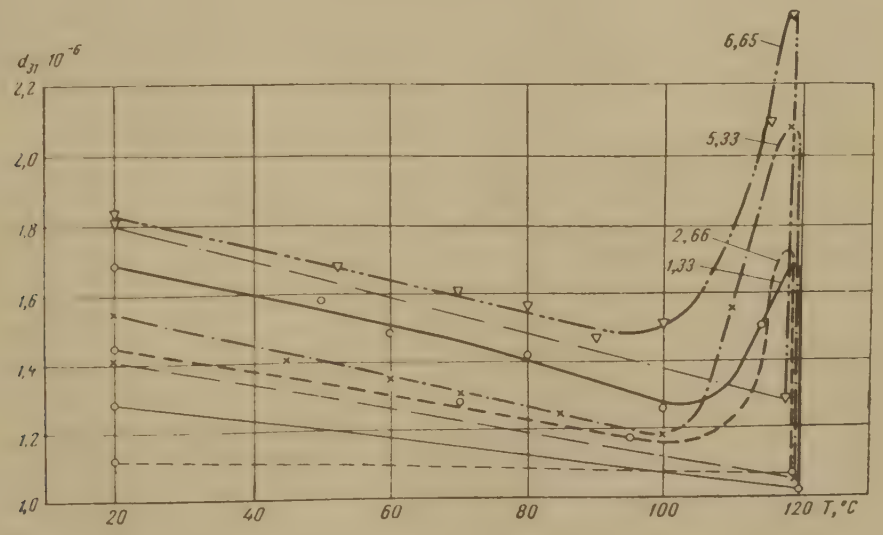

Fig.1. Variation of the piezoelectric coefficient d_{31} with the temperature for different auxiliary polarization potentials (indicated in kv/cm at the curves).

B. Some results of our studies of $(Ba,Ca)TiO_3$, $(Ba,Pb)TiO_3$ and $(Ba,Ca,Pb)TiO_3$ solid solutions are summarized in Figs. 3 & 4. The experimental data indicate that it should be feasible to use piezoceramics of this type without auxiliary polarization up to temperatures of 95 to 200° (the latter figure applies to $(Ba,Pb)TiO_3$); with auxiliary polarization, the effective operating temperature range can probably be extended.

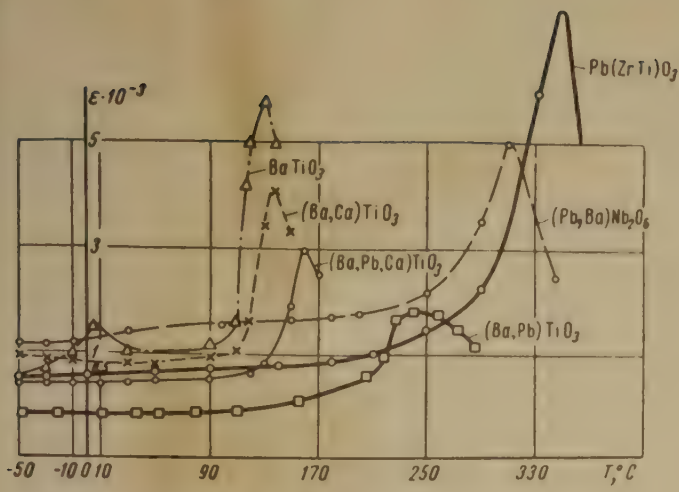

Fig.2. Variation of ε with temperature for different compositions.

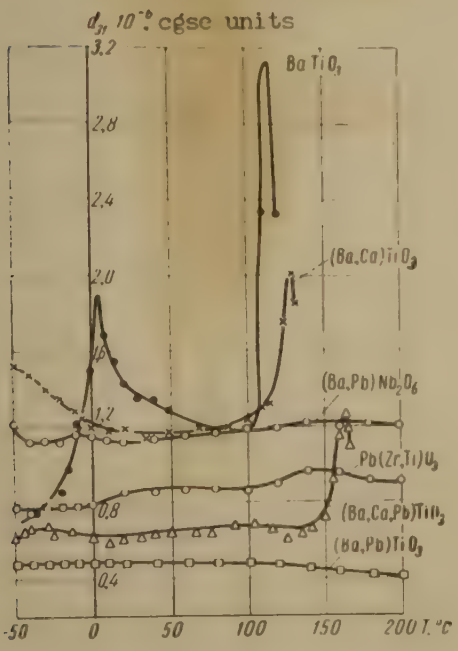

Fig.3. Variation of d_{31} with temperature for different ceramics.

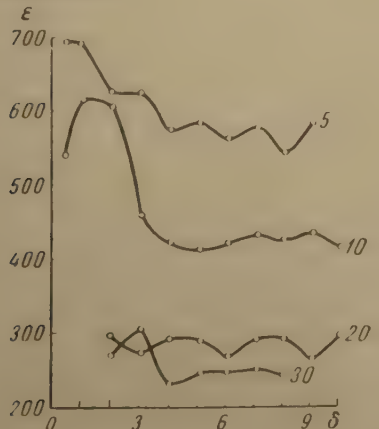

In investigating $(Ba,Pb)TiO_3$ and $(Ba,Ca,Pb)TiO_3$ solid solutions it became apparent that owing to thermal dissociation an appreciable part of the PbO is volatilized during the heating; this results in highly inhomogeneous distribution of the PbO through the thickness of the final ceramic (see Fig.4 which shows the variation of the dielectric constant of samples having an initial composition of 95 to 70% $BaTiO_3$ and 5 to 30% $PbTiO_3$ as successive layers are ground off). Partial evaporation of PbO from such materials has also been noted in the work of Myl'nikova and Valeev[2].

C. Samples of ceramic having the initial composition $Pb(Zr_{0.55}Ti_{0.45})O_3$ (Ref. 3) were obtained with a large scatter of ε, d_{31} and T_C owing to uneven volatilization of PbO. The average characteristics of investigated samples are shown in Figs. 2 & 3.

D. According to the data in the literature,[4] the ferroelectric material with with the highest Curie point (570°) is lead metaniobate - $PbNb_2O_6$. Since we could find no published data on the conditions of formation of $PbNb_2O_6$, a comprehensive thermographic investigation of this reaction was undertaken in the laboratory of Kh.S.Valeev at the GIEKI (State Electric Ceramics Research Institute); after thermographic investigation of pure PbO and Nb_2O_5, the synthesis and sintering of $PbNb_2O_6$ were studied (the respective thermograms are shown in Figs. 5 & 6).

The following designations are used in the thermograms: A - temperature of the standard sample, B - differential temperature, C - variation in the dimension of the sample and D - variation in the weight of the sample.

Sintered $PbNb_2O_6$ samples were polarized in hot silicone oil (liquid No.5).

Fig.4. Variation of ε over the thickness δ of $(BaPb)TiO_3$ samples, i.e., as successive layers are ground off. (The figures at the curve give the mole percent content of $PbTiO_3$).

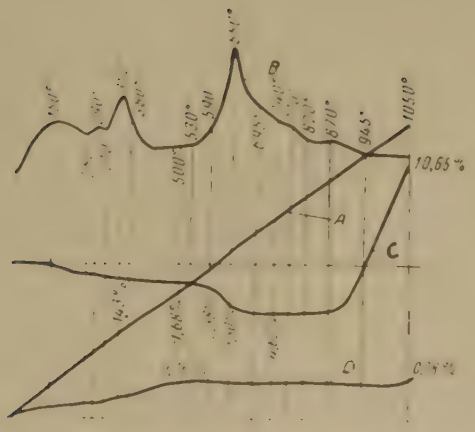

Fig.5. $PbNb_2O_6$ synthesis thermogram.

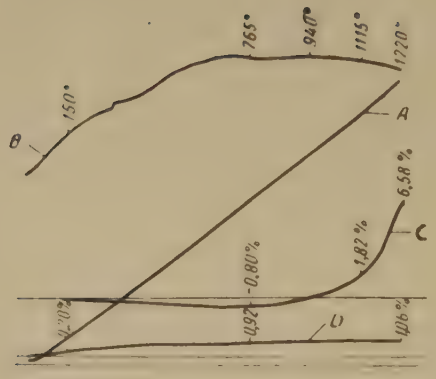

Fig.6. $PbNb_2O_6$ sintering thermogram.

The maximum field gradient at 200°C was 12 kv/cm. The initial thermo-dielectrograms showed a characteristic ε peak at T_C = 570°C. In attempts to record repeat ε vs temperature curves, it was found that the samples cannot withstand reheating above the Curie temperature, i.e., upon reheating apparently undergo a transition to the paraelectric state. A similar observation was made by Francomb[5]. We were unable to detect any piezoelectric activity in pure lead niobate.

In view of the above results, it was clearly desirable to prepare and investigate lead niobate-base solid solutions. Recommendations as regards the range of test compositions for lead niobate piezoelectric ceramics were made by G.A.Smolenskii and V.A.Isupov. Among the compositions investigated so far, the best properties are exhibited by $(Pb_{0.6}Ba_{0.4})Nb_2O_6$; the temperature dependences of ε and d_{31} for this ceramic are shown in Figs. 2 & 3. Of particular interest is the retention of rather high values (to $1.3 \cdot 10^{-6}$) of the piezoelectric coefficient d_{31} up to 200°, the Curie temperature of the materials being ~250°C.

Conclusions

The principal results of our experimental studies are summarized in the table below.

Investigated composition (molar proportions)	T_C, °C	ε	$d_{31} \cdot 10^{-6}$, cgse units	$\frac{d_{31}}{\varepsilon} \cdot 10^{-6}$
$BaTiO_3$	130	1280	1.50	1.17
$(Ba_{0.89}Ca_{0.11})TiO_3$	130	670	0.95	1.41
$(Ba_{0.78}Ca_{0.13}Pb_{0.09})TiO_3$	150	450	0.50	1.11
$(Ba_{0.8}Pb_{0.2})TiO_3$	250	220	0.40	1.82
$(Pb_{0.6}Ba_{0.4})Nb_2O_6$	280	1250	1.30	1.04
$Pb(Zr_{0.55}Ti_{0.45})O_3$	250	600	1.10	1.82

Analysis of the cited data shows that the most promising piezoceramics for high temperature electromechanical transducers are lead niobate-base solid solutions; next in order of desirability are lead zirconate-titanate solid solutions, the preparation of these, however, is technologically more difficult. Barium-calcium

titanate and barium-calcium-lead titanate solid solutions can be used up to temperatures of 120-130° with auxiliary polarization. Barium-lead titanate solutions, apparently, do not hold great promise unless means can be discovered for enhancing the homogeneity of the material and enhancing the low dielectric strength of these ceramics at polarization temperatures through appropriate modification of the composition, i.e., modifications aimed at reducing the conduction losses which hinder piezoelectric excitation of electromechanical transducers of this material.

In conclusion we desire to acknowledge our indebtedness to L.Z. Rusakov for valuable advice and to staff members of the TsNILP L.B. Germaize, A.P.Ermakova, A.V.Konstantinov, N.A.Podol'ner, V.A.Rovnitskii and A.A.Filimonov for their assistance in the work.

TsNILP (Central Scientific Research Laboratory
for Piezoelectrics) of the Committee on Radioelectronics
under the Soviet Ministers of the USSR

References

1. W.P.Mason, Piezoelectric Crystals and their Application to Ultrasonics, N.Y., 1950. (Cited in Russian trans., M., 1952.)
2. N.E.Myl'nikova, Dissertation, IKhS AN SSSR, L., 1955; Kh.S.Valeev et al, Trudy (Proceedings) GIEKI (State Electric Ceramics Research Institute) No.2, 1957.
3. B.Jaffee, R.S.Roth & S.Marzullo, J.Appl.Phys., No.25, 809 (1954).
4. G.J.Goodman, Amer.Ceramic Soc., No.36, 368 (1953).
5. M.H.Francomb, Acta crystallogr., 9, 256 (1956).

METHOD OF MEASURING THE DIELECTRIC CONSTANT AND LOSS TANGENT OF FERROELECTRICS IN HOMOGENEOUS SUPERHIGH FREQUENCY FIELDS (3000 Mc)

- I.V. Ivanov & V.M. Petrov

Investigation of the dielectric characteristics of ferroelectric substances at superhigh frequencies (s.h.f) imposes certain rather rigid requirements on the measurement procedure. In measuring the ac and dc field dependences of ϵ it is essential to make sure that the fields are uniform over the volume of the specimen, for otherwise, if there is an appreciable field dependence, the values of ϵ at different points in the specimen will be different. In the procedures[1-5] employed hitherto for measuring ϵ and tan δ of ferroelectrics the dimensions of the specimens were comparable with the wavelength in the dielectric and hence, obviously, the amplitude of the s.h.f. field varied over the volume of the specimen. Furthermore in these procedures it was difficult or impossible to apply a uniform dc field to the specimen.

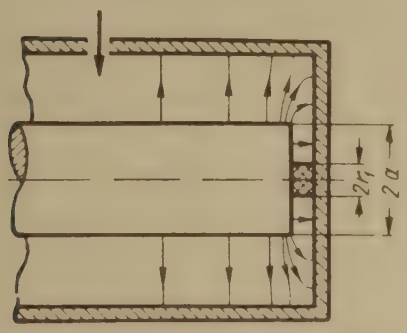

Fig.1 Measuring arrangement.

The difficulties involved in applying homogeneous fields can be overcome by using a coaxial measuring line with the capacitor at the load end (one possible set-up of this type is described in Ref.6). The ferroelectric specimen in the form of a small cylinder is mounted in the plane capacitor formed by the end of the inner conductor and the cap of the outer conductor (Fig.1). In this case the measurements reduce to determining the input impedance of the capacitor. Whereas at microwave frequencies and for dielectrics with a low value of ϵ (as in the case described by Brandt[6]) the input impedance is calculated by means of the static formula for a plane capacitor, for dielectrics with a high value of ϵ the impedance at s.h.f. can differ greatly from the static value, inasmuch as the effective dimensions of the capacitor in this case are comparable with the wavelength.

Calculations show the condition for homogeneity of the s.h.f. field imposes the following requirements as regards the dimensions of the specimen:

$$d < \lambda / 2\sqrt{\varepsilon} \quad \text{and} \quad r_1 \leqslant 0.45 / k\sqrt{\varepsilon}, \tag{1}$$

where $k = 2\pi/\lambda$, d is the height and r_1 is the radius of the specimen (see Fig.1). When the requirements (1) are fulfilled, the field at the periphery of the specimen differs from its value at the center by less than 5%. The input impedance of the capacitor is primarily capacitive and the s.h.f. capacitance can be approximated (to within 5%) by

$$C = \frac{C_0 + \beta C_x}{1 - \alpha}. \tag{2}$$

Here the coefficient

$$\alpha = \varepsilon \frac{\pi}{4} k^2 r_1^2 [N_0(kr_2) - N_0(kr_1)] \tag{3}$$

is less than 0.25 if (1) is satisfied, and the coefficient

$$\beta = \frac{\pi}{4} kr_2 \left[N_1(kr_2) + \frac{1}{2} kr_2 N_0(kr_1) \right]$$

is close to unity; $C_x = \varepsilon r_1^2 / 3.6d$ μμf is the static capacitance of the specimen and $C_0 = r_2^2 / 3.6d$ μμf is the capacitance of the capacitor without the dielectric. The

effective capacitor radius r_2, which taking into account the edge effect is somewhat greater than the radius a of the inner conductor, is determined from measurement of the no-dielectric capacitance C_0 by means of the measuring line.

With increasing radius of the specimen the s.h.f. capacitance C of the capacitor deviates increasingly from the static value. At $r_1 \approx 0.85/k\sqrt{\varepsilon}$, for a = 3.5 mm, C becomes infinite and at still higher values of r_1 the input impedance becomes inductive.

Substituting the complex dielectric constant $\varepsilon(1 - j\tan\delta)$ for ϵ in (2), we express the active component of the impedance in terms of ϵ and tan δ. Thus we obtain the following expressions for the conductance and reactance of the capacitor:

$$G = \frac{\omega(C - C_0)}{1 - \alpha} \tan\delta \text{ and } B = j\omega C \qquad (3)$$

(with tan $\delta \leqslant 0.3$ the loss in the dielectric has virtually no effect on the reactance). Having measured the standing-wave ratio and determined the position of the minimum relative to the minimum with the capacitor short-circuited, we find G and B from the circular diagrams. Further from the appropriate curve (for the given specimen radius) characterizing the variation of C with ϵ (Fig.2), we find ϵ and then calculate tan δ by means of (3).

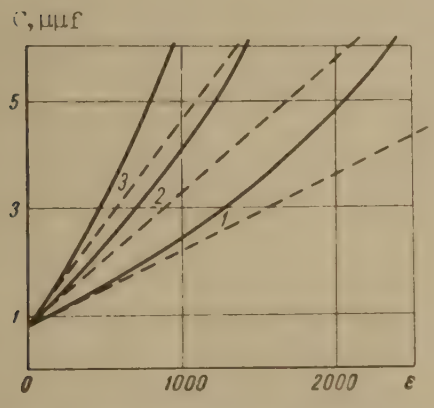

Fig.2 Variation of the s.h.f. capacitance C of the capacitor with ϵ for λ = 10 cm, d = 0.45 mm and r_2 = 3.7 mm: 1) r_1 = 0.15 mm, 2) r_1 = 0.20 mm, 3) r_1 = 0.25 mm. The dashed lines are the corresponding static dependences.

Appreciable losses in ferroelectrics at s.h.f. lead to intense nonuniform heating of the specimen in strong fields. Hence for measurement purposes one must use a pulse generator with a low duty factor. The heat conduction equation yields the following expression for the maximum temperature differential between the center and the end faces of the specimen, which are assumed to be in thermal contact with massive metallic electrodes:

$$\Delta T \quad \frac{\varepsilon \tan\delta \omega E_{\sim}^2 \tau}{14.4\pi \cdot 10^{12} c\sigma (1 - e^{-1/F\tau_0})}. \qquad (4)$$

Here $E_{\sim}$ is the amplitude of the pulse field, τ is the pulse duration and F is the pulse repetition rate, c is the specific heat and σ is the density of the ferroelectric, τ_0 is the temperature rise time at the center of the specimen and is equal to $c\sigma d^2/8\lambda_0$, where λ_0 is the heat transfer coefficient. With τ = 1 μsec, F = 10 pulses/sec and d = 0.5 mm, one can use fields up to 15 kv/cm for barium titanate at λ = 10 cm; the maximum temperature differential in this case is 10°.

The design of the measuring capacitor is shown in Fig.3. The cylindrical specimen with silvered faces is clamped between the piston 1 and the end face of the inner conductor 2 of the coaxial line. The piston, which can be moved by means of the micrometer screw 4 and locked in any desired position by clamp 3, makes it possible to short circuit the capacitor 5 or to obtain the air (no-dielectric) capacitance necessary for determining r_2. The measuring capacitor is connected to the IKL-10M coaxial line by means of the standard plug 6. The dc voltage can be supplied through a slit in the line wall by means of a fine wire connected to the inner conductor (appropriate provision must be made to protect the pulse generator). With this arrangement the dc field on the specimen will also be homogeneous.

The maximum error in measuring ϵ by the described procedure is 10%; the error for tan δ is 15-20%. With specimen radii greater than specified by (1), the accu-

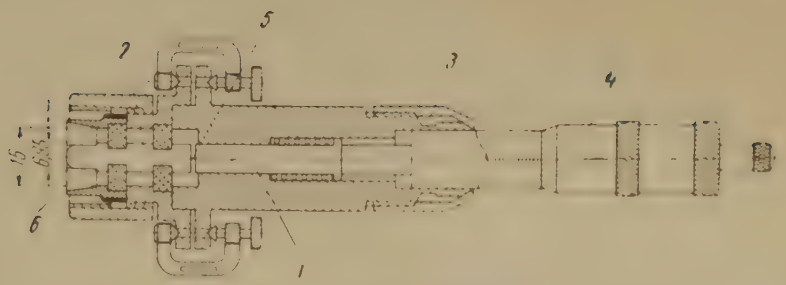

Fig.3. Design of the measuring capacitor.

racy of measurement falls off greatly. In the case of low loss (tan $\delta \lesssim 0.01$) dielectrics, the relative accuracy in determining tan δ will obviously be low.

The described procedure is satisfactory for recording the reversible ϵ and tan δ characteristics of ferroelectrics at superhigh frequencies; with it both the dc and ac field are uniform over the volume of the specimen. If a section of suitable cable is used to couple the measuring capacitor to the coaxial line, the capacitor can be mounted in a thermostat and one can determine the temperature dependences of ϵ and tan δ.

Control measurements were carried out by means of the described set-up on specimens of barium titanate and Varikond VK-1. The results obtained agree with the data in the literature.

We desire to thank T.N.Verbitskaia for discussion of the experimental results and for makihg available the ceramic specimens.

Department of Physics (Theory of Vibrations Section)
Moscow State University

References

1. J.G.Powles, Nature, 162, 614 (1948).
2. H.Iwayanagi, J.Phys.Soc. Japan, 8, 525 (1953).
3. L.Davis & L.Rubin, J. Appl. Phys., 24, 1194 (1953).
4. S.V.Bogdanov, Thesis, USSR Ac. of Sci., M., 1950.
5. A.F.Iatsenko, Thesis, Rostov State University, 1953.
6. A.A.Brandt, PTE (Instr. & Exper. Techniques), No.5, 63 (1957).

OSCILLOGRAPHIC PROCEDURE FOR INVESTIGATING THE INSTANTANEOUS PARAMETERS OF NONLINEAR CAPACITORS

- A.L. Khodakov

1. The dielectric hysteresis loops $q = f(u)$ for ferroelectric capacitors, where q is the charge on the capacitor plate and $u = u_0 \sin \omega t$ is the applied voltage, are usually obtained by means of the Sawyer-Tower[1] circuit.

Let

$$q_1 = -f(u) \tag{1}$$

be the equation describing the lower (ascending) branch of the hysteresis loop. Then for nonpolarized specimens the equation for the upper (descending) branch will be

$$q_2 = -f(-u). \tag{2}$$

If we replace the standard capacitance C_s in the circuit by a standard resistance $R_s = 1/G_s$ (Fig.1), instead of the usual hysteresis loop (charge loop), we will obtain on the oscillograph screen so-called "current loops"[2]. The corresponding values of the current through the ferroelectric capacitor will be described by

$$i_1 = \omega f'(u) \sqrt{u_0^2 - u^2}; \tag{3}$$

$$i_2 = -\omega f'(u) \sqrt{u_0^2 - u^2}. \tag{4}$$

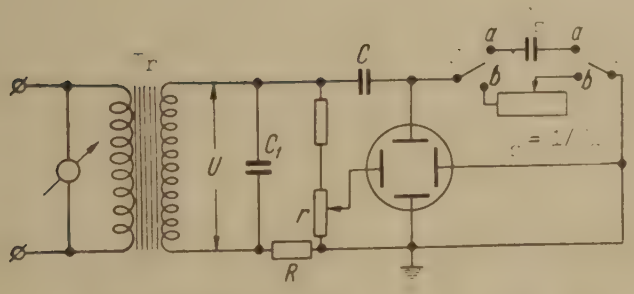

Fig.1. Circuit for obtaining hysteresis loops and current loops: Tr - high voltage transformer, C - capacitor under study, C_s - standard capacitor, R_s - standard resistance, S - switches, r - variable resistance and R - resistor (for applying additional voltage).

In measurements on a high voltage bridge with a resonance indicator, the bridge is balanced through compensation of the first current harmonic. Hence expanding the expression for the current i in a Fourier series and limiting the expansion to the first harmonic, we obtain

$$i = G_m(u_0)\, u_0 \sin \omega t - \omega C_m(u_0)\, u_0 \cos \omega t, \tag{5}$$

where

$$\left.\begin{aligned} G_m(u_0) &= \frac{\omega}{\pi u_0^2} \int_{-u_0}^{u_0} \{f'(u) + f'(-u)\}\, u\, du \\ \text{and} \quad C_m(u_0) &= \frac{1}{\pi u_0^2} \int_{-u_0}^{u_0} \{f'(u) + f'(-u)\} \sqrt{u_0^2 - u^2}\, du \end{aligned}\right\} \tag{6}$$

are the values of the equivalent conductance and capacitance, respectively, obtained in the bridge measurements (when the amplitude of the applied sinusoidal voltage is u_0). From the areas of the current loop $S = \oint i\, du$ and the charging loop

$S_q = \int q du$, as they appear on the oscillograph, we can determine

$$C_m(u_0) = \frac{S_i}{\pi u_0^2 \omega} \tag{7}$$

$$G(u_0) = \frac{Sq}{\pi u_0^2 \frac{1}{\omega}}, \tag{8}$$

as well as

$$\tan\delta = \frac{G_m}{\omega C_m} = \frac{Sq}{\pi C_m u_0^2}, \tag{9}$$

where δ is the dielectric loss angle measured by means of the bridge.

Thus from the oscillograms we can determine the capacitance and tan δ, equivalent to those obtained by measurements on a bridge.

2. Let us now consider the case of a nonlinear capacitor without hysteresis, i.e., a capacitor in which the capacitance and dielectric losses depend unambiguously on the instantaneous value of the voltage. This condition is satisfied, for example, by capacitors with organic dielectrics in high fields, and possibly, by nonlinear capacitors containing dielectrics in which thermal ionic polarization predominates. When a sinusoidal voltage $u = u_0 \sin \omega t$ is applied to the plates of such a capacitor, its instantaneous parameters will depend on u, i.e., $C = C(u)$ and $G = G(u)$. The current through the capacitor will be

$$\left.\begin{aligned} i_1 &= G(u)\,u + \omega C(u)\sqrt{u_0^2 - u^2} \\ \text{and} \\ i_2 &= G(u)\,u - \omega C(u)\sqrt{u_0^2 - u^2} \end{aligned}\right| \begin{aligned} &\text{from 0 to T/2} \\ &\\ &\text{from T/2 to T.} \end{aligned} \tag{10}$$

Thus one can determine the differential parameters $C(u)$ and $G(u)$ from the experimentally observed current loop.

Integrating (10) and invoking the mean value theorem, we obtain the following equations for the two branches of the "charge loop":

$$\left.\begin{aligned} q_1(u) &= C_0(u)\,u - \frac{1}{\omega} G_0(u)\sqrt{u_0^2 - u^2} \\ \text{and} \\ q_2(u) &= C_0(u)\,u + \frac{1}{\omega} G_0(u)\sqrt{u_0^2 - u^2} \end{aligned}\right| , \tag{11}$$

where

$$G(u) = \frac{dC}{du}\{G_0(u)\,u\}$$

and

$$\left.\begin{aligned} G(u) &= -\frac{d}{du}\left\{C_0(u)\sqrt{u_0^2 - u^2}\right\}\frac{\sqrt{u_0^2 - u^2}}{u} \end{aligned}\right| . \tag{12}$$

$C_0(u)$ corresponds to the normal capacitance of the nonlinear capacitor and $G_0(u)$ is the dielectric loss characteristic. Both these quantities can be determined experimentally from the "charge loop".

The instantaneous parameters of the nonlinear capacitor can be determined by utilizing a compensation circuit. To this end we connect a standard resistance $R_S = 1/G_S$ in parallel with C_S. If our test capacitor is a ferroelectric capacitor, then with $G_S = 0$, an ordinary hysteresis loop will appear on the oscillograph screen. As G_S is increased, there will appear symmetrical intersection points at which the upper branch coincides with the lower one. With increase of G_S these points gradually approach the coordinate origin (Fig.2). In the case of a nonlinear capacitor without hysteresis, there also appear such intersection points of the upper and lower branches of the "charge loop"; these points also gradually move toward the center with increase of G_S. Straightforward calculations show that the following equalities obtain for the compensation points:

Fig.2. Oscillograms illustrating compensation of the "charge loop" of $BaTiO_3$ at different values of G_s equal to: a) 0, 2) $2.6 \cdot 10^{-6}$, c) $3.7 \cdot 10^{-6}$, d) $5.4 \cdot 10^{-6}$ mho/cm.

and

$$\left.\begin{aligned} G(u_R) &= \frac{u_{SC}}{u_R} G_S(u_{SC}) \\ C_N(u_R) &= \frac{u_{SC}}{u_R} C_S \end{aligned}\right\}, \qquad (13)$$

where u_R and u_{SC} are, respectively, the voltages on the investigated and standard capacitors at the compensation points. Fig.2 shows a series of oscillograms with compensation points obtained for a capacitor with $BaTiO_3$. Calculations by means of Eqs.(13) are only of illustrative value, inasmuch as a capacitor with barium titanate has hysteresis and hence the values of $C(u)$ and $G(u)$ at the same voltage u will be different for the two branches of the loop.

3. By analogy with ferromagnets[3], one can determine for each point of the polarization curve $P = f(E)$ (where $E = E_0 \sin \omega t$ is the field strength and P is the polarization) a number of different permittivities, specifically, the differential permittivity

$$\varepsilon = \lim_{\Delta E \to 0} 4\pi \frac{\Delta P}{\Delta E}, \qquad (14)$$

the normal permittivity $\epsilon_N = 4\pi(P/E)$ and the reversible permittivity ϵ_{rev}.

The last is determined as follows: if at some point on the hysteresis loop we apply a negative field increment $(-\Delta E_1)$, there will be a corresponding change in polarization $(-\Delta P_1)$ (smaller in absolute magnitude than ΔP). At the limit $\Delta E_1 \to 0$, we will obtain for the given point on the hysteresis loop

$$\varepsilon_{rev} = 4\pi \lim_{\Delta E_1 \to 0} \frac{\Delta P_1}{\Delta E_1}. \qquad (15)$$

Usually the reversible permittivity is determined at a high frequency with simultaneous application of a biasing dc field. If Gans' rule[4], which holds for a number of ferromagnets, were valid for ferroelectrics, the reversible permittivity, as determined from the hysteresis loops, should depend unambiguously on the value of P and agree (for the same P) with the reversible permittivity measured in a biasing dc field.

Comparison of the two permittivities may help clarify the mechanism of polarization in ferroelectrics. We measured ϵ_{rev} at different points of the hysteresis loop by means of the oscillographic set-up mentioned above (Fig.1). To this end we connected the output of a pulse generator across resistor R. The pulse repetition rate was 50 pulses per sec. The pulse could be "moved" along the hysteresis loop by means of a special phase shifter.

The value of ϵ_{rev} was determined from the slope of the pulse trace (Fig.3). The slope of the tangent at the corresponding points of the loop gave us ϵ. The results of measurement of ϵ_{rev} carried out with reference to the descending branch of the hysteresis loop are shown in Fig.4. The differential permittivity attains

Fig.3. Hysteresis loop with superimposed small voltage pulse.

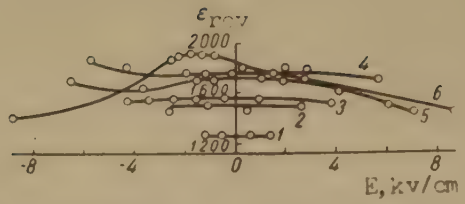

Fig.4. Variation of ϵ_{rev} with the field strength for $BaTiO_3$ at T = 20°. Curves obtained from hysteresis loops with the following values of the peak voltage: 1) 1.4, 2) 2.85, 3) 4.25, 4) 5.65, 5) 7.05 and 6) 9.9 kv/cm.

a maximum value at a field strength equal to the coercive one. The reversible permittivity is appreciably smaller than ϵ and rapidly increases with increasing temperature.

Measurements of the reversible permittivity carried out by us for a number of specimens of $BaTiO_3$ and its solid solutions showed that in general Gans' law does not hold for these substances and the dissipation of energy in partial polarization cycles is low.

Rostov-on-the-Don State University

References

1. S.B.Sawyer & C.N.Tower, Phys. Rev., 35, 269 (1930).
2. A.L.Khodakov, Zhur. tekh. fiz., 26, 51 (1956). (Trans. Soviet Phys. - Tech. Phys.)
3. V.K.Arkad'ev, Elektromagnitnye protsessy v metallakh (Electromagnetic processes in metals), M., 1936.
4. R. Gans, Phys. Rev., 12, 1053 (1911).

FREQUENCY DEPENDENCE OF THE NONLINEARITY OF $BaTiO_3$-$BaSnO_3$ SOLID SOLUTIONS

- A. A. Obukhov

The dielectric constant of ferroelectric substances varies with the strength of the applied ac or dc field. It is known, however, that small variations of a weak high-frequency field do not noticeably alter the dielectric constant of $BaTiO_3$-$BaSnO_3$ solid solutions (Fig.1) Consequently when, in addition to a weak high-frequency field, a strong dc or low-frequency ac field is applied to the investigated specimen its dielectric constant will be determined entirely by the latter field.

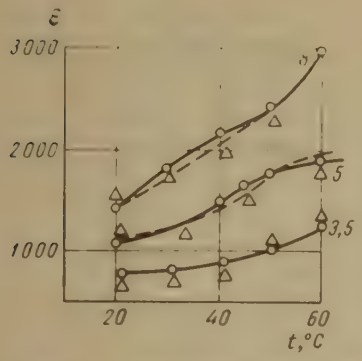

Fig.1. Temperature dependence of the dielectric constant ε for different $BaTiO_3$-$BaSnO_3$ solid solutions at f = = 45 Mc. Dashed curves: $E_\sim$ = 15 v/cm; solid curves: $E_\sim$ = 50 v/cm. Figures at curves - $BaSnO_3$ content in %.

We were guided by the above considerations in undertaking the present investigation of the frequency dependence of the nonlinearity of $BaTiO_3$-$BaSnO_3$ solid solutions. We employed the experimental arrangement diagramed in Fig.2. The capacitor with the investigated ferroelectric specimen was incorporated into the oscillating circuit of the high-frequency oscillator 2. To improve the Q-factor of the circuit a linear capacitor of known value was connected in parallel to the ferroelectric containing capacitor.

In the course of operation of the oscillator, the intensity of the high-frequency field on the specimen-containing capacitor varied but did not exceed 50 v/cm. The frequency (45 Mc) generated by this oscillator was mixed in the nonlinear mixer 3 with the frequency put out by the standard generator 4 and applied to the oscillograph 5. Thus from the oscillograph display, by the zero beat method, we could determine the frequency of the generated oscillations.

Knowing the value of the linear capacitance in the oscillating circuit, the inductance and the frequency of the generated oscillations, we could readily compute the capacitance of the "ferroelectric" capacitor. We compared the capacitance values obtained in this manner with those obtained by direct measurements at the same frequency and field strength in order to revise and correct the assumed inductance and linear capacitance values for the test network.

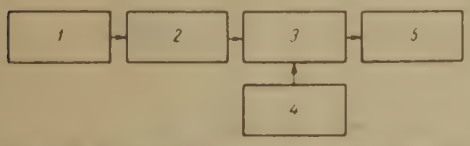

Fig.2 Block diagram of experimental set-up: 1) control voltage source, 2) oscillator with capacitor containing the ferroelectric specimen in the tank, 3) nonlinear mixing unit, 4) standard generator, 5) oscillograph.

Now if a dc field is applied to the "ferroelectric" capacitor, one can readily determine the change in capacitance of the specimen from the change in the oscillator frequency. Instead of a dc biasing frequency, however, we applied a low-frequency "control" field and determined the resultant change in the capacitance of the ferroelectric capacitor from the change in frequency of the generated oscillations.

The measurements were carried out at room temperature, using specimens 0.25-0.3 mm thick. The control field heated the specimens to some extent. The temperature of the specimen was monitored by a miniature thermocouple. It was found that as a result of heating, the temperature of some of the specimens rose 10-15° above room temperature, but in no case did it exceed the Curie point of the material.

As a measure of the nonlinearity we took the ratio $(\epsilon_{max} - \epsilon_{min})/\epsilon_{max} = \Delta\epsilon/\epsilon_{max}$.

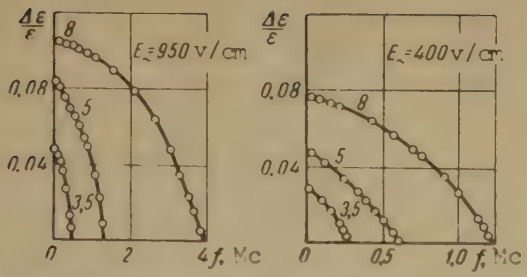

Fig.3. Frequency dependence of the nonlinearity of different $BaTiO_3$-$BaSnO_3$ solid solutions. Fundamental frequency of oscillator 45 Mc. The figures at the curves indicate the $BaSnO_3$ content in percent.

The experimental results are shown in Fig. 3. It will be evident that with increasing control field frequency, the nonlinearity of $BaTiO_3$-$BaSnO_3$ solid solutions decreases, going to zero. The curves of Fig.3 show that the higher the electric field, the higher the frequency at which the nonlinear properties vanish.

It is known from the work of Dungan & Kane[1] that in $BaTiO_3$-$BaSnO_3$ solid solutions the tetragonality of the crystal lattice decreases with increasing $BaSnO_3$ content to 12%. It follows therefore that the nonlinearity of these ferroelectrics rises with decrease of tetragonality. It also follows from our data that the nonlinear properties of ferroelectrics with lower degrees of tetragonality of the crystal lattice vanish at higher frequencies.

The observed decrease of nonlinearity with increasing frequency can be explained by the fact that with increasing frequency of the control field the number of switching domains in the ferroelectric decreases. According to the data of Merz[2] and Little[3], domain motions in $BaTiO_3$ single crystals cease at frequencies above 3-5 Mc regardless of the field strength. Since the structure of $BaTiO_3$-$BaSnO_3$ solid solutions is similar to that of $BaTiO_3$, it may be inferred that the experimentally observed decrease and disappearance of nonlinearity is due to the fact that domains do not have time to reorient with the frequency of the control field.

It must be noted that in addition to nonlinear properties connected with the orientation of the domains there may be nonlinearity due to induced polarization. Nonlinearity of this type, however, is small and probably well within the limit of our experimental error (~1%).

The increase in nonlinearity with decrease of tetragonality of the crystal lattice can probably be explained on the basis of Smolenskii's[4] hypothesis regarding the correlation between the spontaneous deformations and the degree of tetragonality in $BaTiO_3$-$BaSnO_3$ solid solutions.

Conclusions

The results of our experimental work show that the nonlinearity of $BaTiO_3$-$BaSnO_3$ solid solutions depends on the frequency and strength of the applied electric field and also on the degree of tetragonality of the crystal lattice. The nonlinearity of the investigated ferroelectrics goes to zero at frequencies of a few megacycles.

When $BaTiO_3$-$BaSnO_3$ ferroelectrics are employed in electronic equipment for purposes of frequency modulation, the modulating field should not exceed a few megacycles; if this requirement is met the frequency of the controlled field can be of the order of 80 Mc or even higher.

References

1. R.Dungan & I.Kane, J. Amer. Ceram. Soc., 35, 318 (1952).
2. W.Merz, Phys. Rev., 95, 690 (1954).
3. E.Little, Phys. Rev., 98, 978 (1955).
4. G.A.Smolenskii & V.A.Isupov, Zhur.tekh.fiz., 21, 1375 (1954).

FERROELECTRIC CERAMICS WITH DIELECTRIC CONSTANTS UP TO 45,000

- T.N.Verbitskaia & L.M.Aleksandrova

Polycrystalline ferroelectric ceramics with high values of the dielectric constant are extensively used for the fabrication of miniature capacitors and other electronic equipment.

In general the dielectric constant of ferroelectric materials depends on the temperature and the electric field strength.

In evaluating the utility of a given ferroelectric material for specific practical applications, it is essential to know at least three dielectric constant values, namely, the initial constant ϵ_{init}, the Curie point constant ϵ_{θ} and the maximum constant ϵ_{max}. The first two are usually measured in weak fields (~5 v/mm) at room temperature and at the Curie point θ, respectively. The maximum value of the dielectric constant is usually determined from curves characterizing the ac field dependence of ϵ.

In order to obtain high values of the dielectric constant under normal conditions recourse is usually had to materials with a Curie point close to room temperature or to materials with pronounced nonlinear properties. In the former case the value of ϵ can be very appreciable at or slightly above room temperature even in weak fields. A typical example is ferroelectric material T-7500 with a Curie point at about 35-40°. The initial dielectric constant of T-7500 at 20° in a ~5 v/mm field is 4500-5000; the constant at the Curie point is ~7500.

In the case of materials with pronounced nonlinear characteristics, a high value of ϵ is evinced in relatively weak fields owing to rapid increase of ϵ with increasing field strength.

For purposes of illustration, let us compare the nonlinear properties of a number of ferroelectric substances. The initial dielectric constant of barium titanate is ~1700; with increase of the field strength ϵ increases somewhat and attains a maximum value of 8000-10,000 in fields of the order of 600-800 v/mm. The maximum value of ϵ for T-7500 is attained in fields of ~200 v/mm and does not exceed 7500-8000. Thus these two substances are only weakly nonlinear.

The properties of VK-1 ceramic used for production of Varikonds are different. The value of the initial dielectric constant of VK-1 is ~2500. The constant increases rapidly with the field and at 150-200 v/mm becomes 16,000-20,000.

An even more rapid increase of the dielectric constant with field strength is exhibited by the new ferroceramic material designated VK-2. In this ceramic $\epsilon_{init} \approx 2300\text{-}2500$; $\epsilon_{max} \approx 35{,}000\text{-}45{,}000$. This exceptionally high value of ϵ_{max} is attained in relatively weak fields of the order of 100-150 v/mm.

As in the case of many other ferroelectric substances, the weak field values of ϵ obtained vor VK-2 are greatly dependent on the temperature (Fig.1). However, the maximum values of the dielectric constant lie in the range of 35,000 to 46,000 in a wide temperature interval.

VK-2 exhibits pronounced nonlinear properties in an extensive temperature range (Fig.2). The nonlinearity coefficient $K'_{\sim} = \epsilon_{max}/\epsilon_{init}$ is 6 at +40°, 15-18 at 20°, 40 at -10° and 60 at -45°C.

For every ferroelectric material there is a certain optimum field value at which the dielectric constant attains high values in a given temperature interval. In general the higher the dielectric constant, the narrower the high ϵ value temperature interval.

Regardless of the field strength, however, the dielectric constant of $BaTiO_3$ and T-7500 never exceeds 10,000 in the entire temperature range from +60 to -60°C. In contrast, VK-1 in this temperature range can have values of ϵ from 20,000 to 25,000 at optimum values of the field. VK-2 has the highest value of ϵ_{max} of all known ferroelectric ceramics, namely, 45,000.

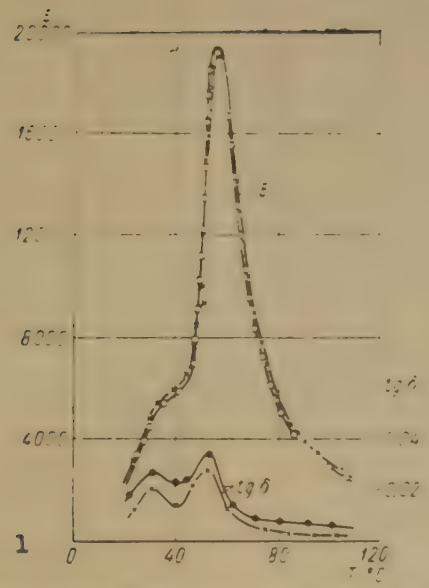

Fig. 1

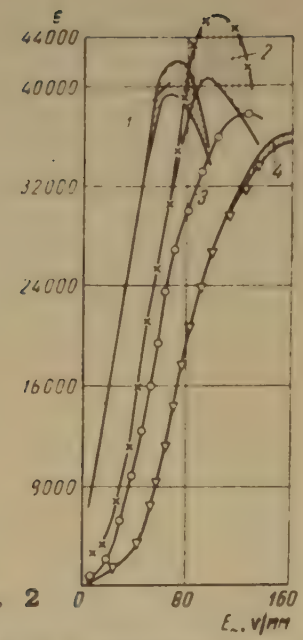

Fig. 2

Fig.1. Temperature dependence of ϵ and tan δ for two VK-2 specimens: f = 1000 cps and $E_{\sim}$ = 3 v/mm.
Fig.2. Variation of ϵ with $E_{\sim}$ at 50 cps for VK-2 at different temperatures: 1) +40°, 2) +20°, 3) -10°, 4) -45°C.

In view of the fact that the slope of the $\epsilon = f(E_{\sim})$ curves for VK-2 does not remain constant, the temperature dependence of ϵ in different electric fields are not represented by a family of similar curves (Fig.3). For most materials, including barium titanate and VK-1, one can establish certain optimum conditions

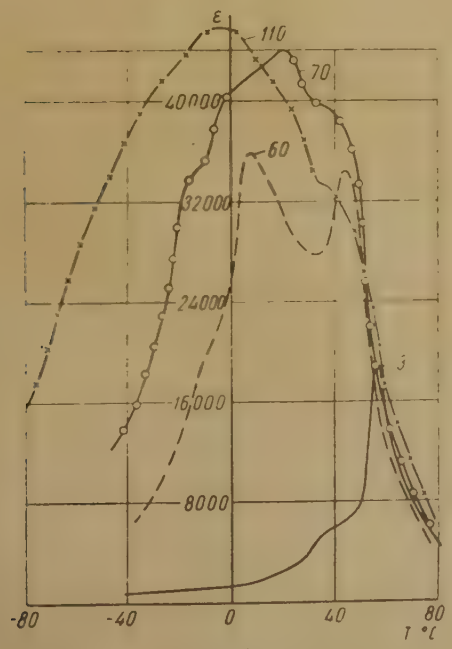

Fig. 3

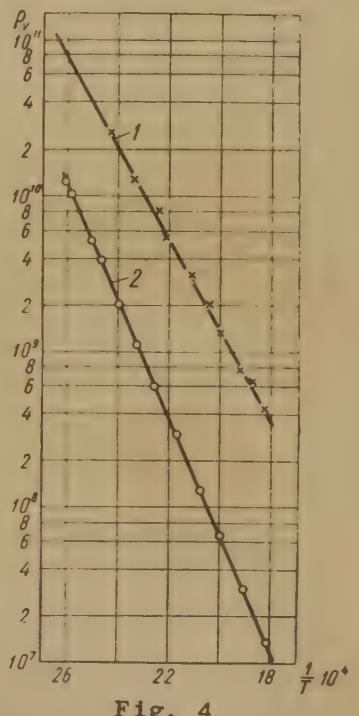

Fig. 4

Fig.3. Temperature dependences of ϵ for VK-2 recorded at different ac field values, as indicated by the figures at the curves.
Fig.4. Temperature dependence of the volume resistivity of VK-2 (1) and $BaTiO_3$ (2) specimens.

under which the dielectric constant remains high over a more or less appreciable temperature range. As will be evident from Fig.3, ϵ for VK-2 remains equal to ~28,000 in the temperature range from 0 to 55° with E = 60 v/mm. In fields of 100-110 v/mm ϵ does not fall below 30,000 in the range from +40 to -50° and stays above 40,000 in the temperature interval from +20 to -30°.

At a given field strength one can attain a very high value of the inductive capacitance for VK-2 in a given temperature range by varying the thickness of the dielectric. For example, an assembly of three parallel connected VK-2 disks about 20 mm in diameter having a total height of ~3 mm has a capacitance of 0.2 μf at E = 100 v. When the Varikonds are prepared in the form of films some 2000 μ thick the dielectric constant attains a value of 45,000 at a voltage of only 20 v.

The high values of nonlinearity and dielectric constant for VK-2 are obtained without sacrifice of other desirable properties. VK-2 ceramic is a good insulator: its volume resistivity in a wide temperature range (100 to 500°) is at least one order of magnitude higher than that of polycrystalline barium titanate (Fig.4).

In view of its pronounced nonlinear and high volume resistivity VK-2 ceramic can be recommended for use not only in ultraminiature capacitors but also for the preparation of new types of Varikonds with even higher nonlinearity coefficients than those obtained hitherto from VK-1. The new types of Varikonds may prove useful for suppressing extra-currents, for pulse shaping and peaking and for dielectric amplifiers as well as many other electronic devices.

DIELECTRIC INVESTIGATION OF FERROELECTRIC CRYSTALS USING MINUTE SAMPLES

- V.A.Koptsik, K.A.Minaeva & B.A.Strukov

In the present report we describe an electronic set-up designed and used by us for recording the temperature dependence of the dielectric constant ϵ and measuring the field dependence of the polarization in the temperature range from -190 to +250°, using small samples. This set-up can also serve for investigating dielectric anomalies in ferroelectrics and thus detecting phase transitions accompanied by changes in ϵ in crystalline substances.

The apparatus utilizes the RC-circuit technique described in the literature[1,2] for obtaining a voltage proportional to the capacitance (provided $1/\omega C \gg R$). The basic electronic circuit is shown in Fig.1. It consists of an audio frequency oscillator, an R_1C_1 network, a cathode follower, a recording type EPP-09 automatic potentiometer, a polarization attachment for determining $P = f(E)$, a second R_5C_2 network, an amplifier for the conduction current and suitable thermostats (the potentiometer and generator are not shown in the diagram).

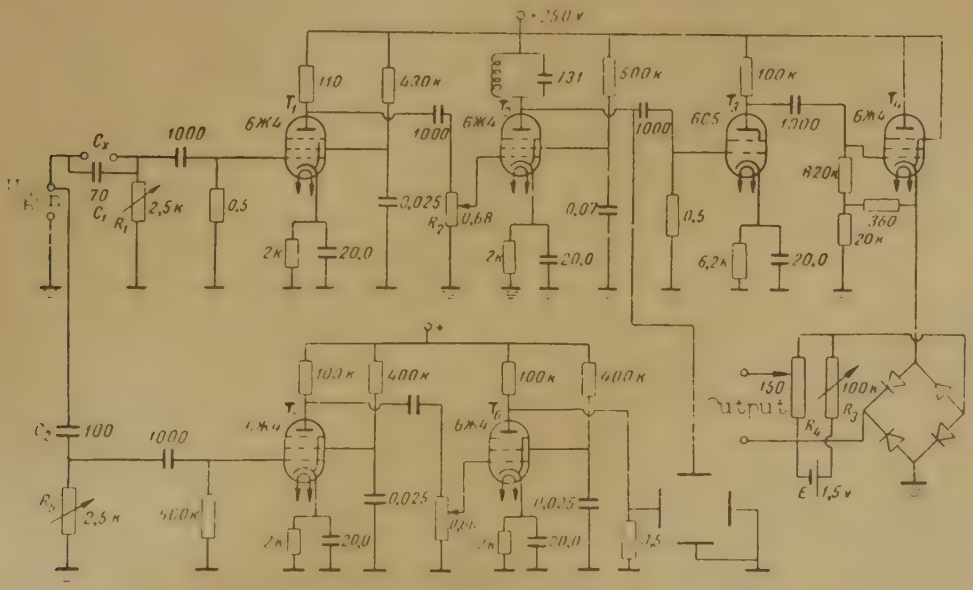

Fig.1. Diagram of the thermodielectrograph (capacitances in the diagram are given in μμf; resistances in kilohms).

The voltage U_{R_1} is amplified by means of a resonance amplifier assembled about the tubes T_1, T_2 and T_3. The second stage of the amplifier has a resonance circuit tuned to 5 kc. The amplification is regulated by the variable resistor R_2. The maximum amplification factor is ~2000. The voltage after the cathode follower (tube T_4) is detected by means of a selenium rectifier and applied (through R_1) to the potentiometer, the displacement of whose carriage is proportional to the complex capacitance. To determine the instant of appearance of conductivity in the crystal the voltage U_{R_1} is compared, by means of an oscillograph, with the voltage taken off the standard R_5C_2 chain with low dielectric loss. To enhance the sensitivity, this voltage is amplified (tubes T_5 & T_6). If the specimen does not conduct the compared voltages are in phase and the beam trace is a straight line, the slope of which varies with the capacitance of the specimen capacitor. When the specimen begins to conduct, the straight line changes to an elipse. This allows of determining the instant of appearance of conductance beginning with 30 megohm. Simultaneously with recording the variation of ϵ as a function of T, the

set-up allows of marking the appearance of spontaneous polarization in the specimen by means of a conventional oscillographic circuit (not shown in Fig.1).

The circuit parameters were selected so that a 1 to 10 μμf change in the capacitance of the test capacitor would produce a full scale displacement of the potentiometer carriage; thus it is feasible to determine absolute changes in capacitance down to 0.1 μμf with an error of 1 to 10% depending on the capacitance value. This choice of circuit parameters makes it possible to detect dielectric anomalies in ferroelectric specimens of very small size (of the order of 0.4 x x 0.4 x 0.1 cm) and to record smooth ϵ vs T curves for linear crystals. Appropriate measures (rigid mounting, short leads and thorough screening) were taken to minimize stray capacitance. By means of resistor R_3, the 10 μμf measurement interval can be shifted up to 150 μμf, which makes it possible to investigate larger capacitance specimens.

A 400 watt wire wound heating coil, supplied from an LATR-1 transformer is used for the high temperature measurements (20-250°C). The specimen is mounted in a small glass tube provided with a low capacitance (~1.5 μμf) spring holder. The heating rate does not exceed 2-3° per min. For the low temperature measurements the specimen is mounted in a sealed Dewar which is immersed to 1/4 its length in liquid nitrogen. The temperature of the specimen is measured by means of two copper-constantan thermocouples connected to an appropriately calibrated millivoltmeter.

The circuit is turned on and adjusted by means of the variable resistors R_1, R_3 and R_4. The linearity of the instrument was checked by substituting standard 1, 3, 7 and 10 μμf capacitors in place of the specimen.

In order to gage the potentialities of the set-up we recorded the ϵ vs T curves for 24 dielectrics. The sample crystal plates measuring 0.4 x 0.4 x 0.1 cm and having an initial capacitance of 1-2 μμf were cut from small single crystals by means of a wire saw. The surfaces were polished by hand on a glass plate with a suitable abrasive in kerosene. Silver foil electrodes were applied to the principal faces. Crystals belonging to polar symmetry classes were investigated in the above room temperature range; the others at both subzero and positive temperatures. We also checked the possibility of working with compressed pellets.

The tests showed that the set-up is capable of giving reasonably accurate ϵ vs T curves. The dielectric constant discontinuity at 120° in polarized barium titanate ceramic was detected using a very small sample (0.1 x 0.1 x 0.1 cm). Similar and fully reproducible results were obtained with equally minute samples of Rochelle salt.

Dielectric anomalies were detected in $(NH_4)_2SO_4$ single crystals at -51°. The ammonium sulfate crystals were grown by evaporation from supersaturated aqueous solutions. The symmetry group of ammonium sulfate crystals at room temperatures is $m \cdot 2 : m$. The usual form of the crystals is defined by the pinacoidal b {010} and c {001} faces and the rhombic prism p {110}, q {011} and q' {021} faces. Upon transition to the ferroelectric phase one of the second order axes (in our case the Z axis) becomes polar and the symmetry of the crystal changes to group $2m$. Dielectric anomalies in ammonium sulfate have been reported by a number of authors[3,4]. We carried out some new, additional measurements.

The temperature dependences of the polarization and coercive field obtained for $(NH_4)_2SO_4$ crystals are shown in Figs.2 & 3. At temperatures of about -60° the spontaneous polarization attains saturation (P_S = 0.11 microcoulomb/cm^2); the coercive field reaches a value of 2 kv/cm. Attempts to attain saturation of polarization at lower temperatures result in fracturing of the crystal along the a (100) and b (010) planes. The polarization curve obtained for $(NH_4)_2SO_4$ is characteristic of ferroelectric materials with hydrogen bonds (for example, KH_2PO_4 and $KNaC_4H_4O_6 \cdot 4H_2O$). At room temperatures the length of the N—H—O bonds in ammonium

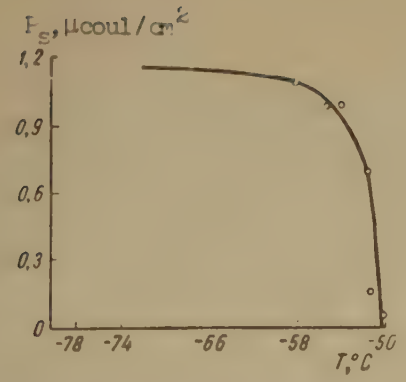

Fig.2. Temperature dependence of polarization in ammonium sulfate crystals.

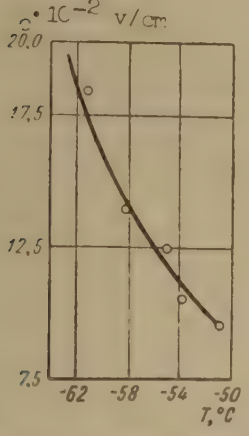

Fig.3. Temperature dependence of the coercive field in ammonium sulfate crystals.

sulfate is 2.86 Å.[5] Deformation incident to the transition to the monoclinic form results in reorientation of the O—N bonds and a nonequivalent change in their lengths; the ferroelectric effect may well be connected with these structural changes.

The temperature dependence of ϵ of ammonium sulfate in the region of high temperatures is characterized by a sharp increase of the conductance near the melting point of the crystals (130°C). By means of the described technique one can also follow the course of other processes connected with changes in the dielectric constant or appearance of conductance.

Attempts to detect ferroelectric anomalies in samples in the form of pellets compressed of Rochelle salt or $BaTiO_3$ powder yielded negative results. The presence of air layers and binder together with the chaotic orientation of the crystal grains in the heterogeneous system completely masked the effect. Apparently tests on small single crystals are less onerous in the long run and yield more dependable results particularly as regards detection of dielectric anomalies.

The described apparatus can be used in searching for new ferroelectric materials and for carrying out preliminary measurements on substances that can readily be obtained in the form of small single crystals. The number of such dielectric substances is very large and it must be emphasized that the difficulties of growing small single crystals have been exaggerated.[6]

Taking advantage of the fact that now the procedure for carrying piezoelectric and ferroelectric tests on minute crystal specimens has been greatly simplified[7,8] one can propose the following program for an extensive search for new ferroelectric materials - see Fig.4.

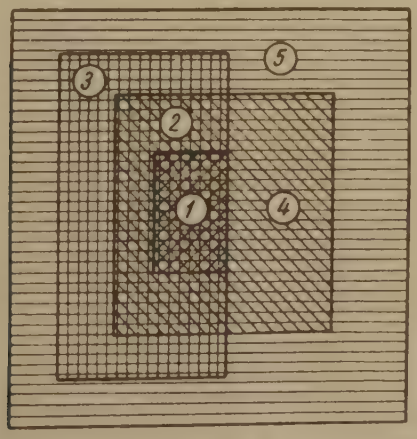

Fig.4. Classification of crystalline dielectrics on the basis of their symmetry and electric properties: 1) ferroelectrics, 2) piezoelectrics with pyrosymmetry and pyroelectrics, 3) piezoelectrics, 4) dielectrics with pyrosymmetry, 5) dielectrics with piezosymmetry, 6) other dielectrics whose symmetry and electric properties are unknown.

The search should be extended "outward" from group 1. Group 2, consisting of piezoelectric crystals with pyroelectric symmetry and pyroelectrics, should be tested first at room temperature for spontaneous polarization (hysteresis loops). Group 3, consisting of piezoelectric crystals, should be investigated at low temperatures for the presence of polarization hysteresis; for detection of ferroelectric phases one should record the temperature dependence of ϵ and thus determine the Curie temperature. Groups 4 and 5, comprising dielectric crystals with pyroelectric and piezoelectric symmetry, and subsequently group 6 (other dielectrics)

should first be tested for presence of a piezoelectric or pyroelectric effect; in the case of positive results they should be classified in Group 3 and treated accordingly.

Obviously, in selecting samples for tests from each group one should bear in mind other factors and considerations that will heighten the probability of finding a new ferroelectric, namely, isomorphism, structural similarity with known ferroelectrics, the character of the particle interaction in the crystal structure, possibility of realizing polymorphous modifications, etc. The available data shows, for instance, that 85% of the substances exhibiting spontaneous polarization (44 pyro- and ferroelectric crystals) belong to the following ten space groups: C_2^2, C_{2t}^{19}, C_{3t}^5, C_{6t}^4, C_3^4, C_{2t}^9, C_6^6, C_{4t}^1, C_{2t}^{20}, C_{3t}^1; these are obviously the groups most "favorable" for pyro- and ferroelectricity. It is found that every one of 120 piezoelectric crystals belonging in one of these space groups exhibits spontaneous polarization. Further accumulation of experimental material may bring to light certain regularities, but it is clear even now that the distribution of ferroelectric crystals over space groups is not uniform, i.e., that some groups are more "favorable" than others. Hence the probability of finding new ferroelectric crystals will be enhanced if we concentrate our search on piezoelectric substances belonging to "favorable" symmetry groups.

Physics Faculty
Moscow State University

References

1. L.Triebwasser, Phs.Rev., 101, 993 (1956).
2. I.S.Rez, Izv.AN SSSR, Ser.fiz., 21, 466 (1957). (Trans.Bulletin 21, No.3, 463.)
3. R.Guillien, Compt.Rend., A, 168, 353 (1932).
4. B.T.Matthias, Phys.Rev., 103, 262 (1956).
5. L.Couture & S.LeMontagner, Compt.Rend., 242, 1084 (1956).
6. A.A.Chumakov & V.A.Koptsik, Kristallografiia, 4, 38 (1959). (Trans. Soviet Phys. - Crystallography.)
7. V.A.Koptsik, Izv.AN SSSR, Ser.fiz., 20, 219 (1956). (Trans. Bulletin 20, No.2, 201.)
8. V.A.Koptsik, K.A.Minaeva, A.A.Voronkov, A.F.Solov'ev, A.N.Izrailenko, E.G.Popkova & G.I.Kozlova, Vestnik, Moscow State University, Ser.math.& phys. No.6, 95 (1958).

Bulletin of the Academy of Sciences of the USSR - Physical Series
Vol.22, No. 12 - December 1959

Transactions of the Second All-Union Conference on Ferroelectricity

TABLE OF CONTENTS

	Page Orig.	Trans.
Contribution to the quantum mechanical theory of ferroelectricity - R.E.Pasynkov	1422	1415
On the electric field dependence of the dielectric constant of ferroelectrics - I.V.Liagini & Ia.I.Geivashovich	1424	1417
Phase trajectory of an oscillating circuit with a ferroelectric - N.S.Novosil'tsev	1427	1420
Contributing to the theory of domain walls in ferroelectrics - V.A.Zhirnov	1431	1424
Aperiodic operation of capacitors containing a ferroelectric - N.F.Shmoilov	1433	1427
Dependence of the ferroelectric properties of perovskite type crystals on the character of the chemical bonds - I.N.Beliaev	1436	1430
On the search for new ferroelectric materials - I.S.Zheludev & A.S.Sonin	1441	1435
Preparation and the dielectric properties of some barium titanate-stannate solid-solution single crystals - A.L.Khodakov & M.L.Sholokhovich	1445	1439
Investigation of the $PbO-BaO-B_2O_3-TiO_2$ system - M.L.Sholokhovich & V.I.Varicheva	1449	1443
X-ray spectroscopic investigation of compounds with the perovskite structure - M.A.Blokhin & A.T.Shuvaev	1453	1447
Infrared absorption spectra of perovskite type ferroelectric crystals - A.F.Iatsenko	1456	1450
On the nature of color centers in barium titanate crystals - M.S.Kosman & E.V.Bursian	1459	1453
High-temperature polymorphous transformation in barium titanate - I.A.Trifonov	1462	1455
Nonlinear properties of Pb doped $BaTiO_3$ single crystals and triglycine sulfate single crystals in strong electric fields - I.S.Zheludev, V.V.Gladkii, L.Z.Rusakov & I.S.Rez	1465	1458
Individual characteristics of domains in Rochelle salt - V.L.Indenbom & M.A.Chernysheva	1469	1461
Some results of a search for new piezoelectric materials - I.S.Rez	1472	1466
Influence of different factors on the Curie temperature of ferroelectrics with the perovskite structure - Iu.N.Venevtsev, G.S.Zhdanov & S.P.Solov'ev	1476	1471
Crystal structure of the $BaTiO_3-LaAlO_3$ system - I.G.Ismailzade	1483	1478
Crystal structure of the niobates and tantalates of bivalent metals and their solid solutions - I.G.Ismailzade	1485	1480
Properties of solid solutions of barium and lead titanates and ferrates - O.I.Prokopalo & E.G.Fesenko	1488	1483
Antiferroelectric and ferroelectric properties of some sodium niobate solid solutions - N.N.Krainik	1492	1486
Ferroelectric ceramics with a high Curie temperature - A.M. Cherepanov, S.V.Bogdanov & R.Ia.Razbash	1497	1490

Dielectric properties of solid solutions of the ternary system $BaTiO_3$-$PbTiO_3$-$BaSnO_3$ - S.V.Bogdanov, G.M.Kovalenko, R.Ia. Razbash & A.I.Cherepanov 1500 1493
Phase transitions in solid solutions of sodium tantalate in sodium niobate - V.A.Isupov 1504 1497
Influence of Fe_2O_3, SrO, SnO_2, ZrO_2 and $BaSnO_3$ impurities on the dielectric hysteresis loops of polycrystalline $BaTiO_3$ and $BaTiO_3$-$PbTiO_3$ solid solutions - G.M.Kovalenko, S.V. Bogdanov & A.M.Cherepanov 1508 1501
Nonlinear properties of some $(Ba,Sr)(Ti,Sn)O_3$ solid solutions - A.I.Medovoi 1512 1505
Low-temperature polarization of barium titanate ceramic - L.A.Shuvalov, M.M.Kachkacheva, L.Z.Rusakov & I.S.Zheludev 1516 1508
On obtaining piezoelectric ceramics for high-temperature applications - I.S.Rez, E.G.Smazhevskaia & M.M.Kachkacheva 1520 1512
Method of measuring the dielectric constant and loss tangent of ferroelectrics in homogeneous superhigh frequency fields (3000 Mc) - I.V.Ivanov & V.M.Petrov 1524 1516
Oscillographic procedure for investigating the instantaneous parameters of nonlinear capacitors - A.L.Khodakov 1527 1519
Frequency dependence of the nonlinearity of $BaTiO_3$-$BaSnO_3$ solid solutions - A.A.Obukhov 1531 1523
Ferroelectric ceramics with dielectric constants up to 45,000 - T.N.Verbitskaia & L.M.Aleksandrova 1534 1525
Dielectric investigation of ferroelectric crystals using minute samples - V.A.Koptsik, K.A.Minaeva & B.A.Strukov 1537 1529

Translated in 1959 by
Columbia Technical Translations
5 Vermont Ave., White Plains, N.Y.

SUMMARY OF THE CONTENTS

of

VOLUME XXII

of the

BULLETIN OF THE ACADEMY OF SCIENCES OF THE USSR

- Physical Series -

SUBJECT SUMMARY - VOLUME 22

Page (Trans)

TRANSACTIONS OF THE FIRST ALL-UNION CONFERENCE ON THE SYNTHESIS AND INVESTIGATION OF SCINTILLATORS FOR DETECTING NUCLEAR RADIATION

Number 1

Technique of growing alkali halide phosphors for scintillation counters - L.M.Shamovskii, L.M.Rodionova & A.S.Glushkova 1
Investigation of scintillators containing boron-organic compounds - A.N.Nikitina, M.D.Galanin, P.M.Aronovich, T.A.Shchegoleva & B.M.Mikhailov 10
Screens for detecting slow neutrons - T.V.Timofeeva & S.P.Khormushko 13
Growth of scintillation crystals by the Kyropoulos procedure - L.M.Beliaev, V.P.Panova, V.A.Perl'shtein, V.V.Chadaeva & I.N.Tsigler 20
On the use of domestic phosphors for scintillation counting (Abstract) - A.N.Pisarevskii & E.D.Terenin 21
Impurity quenching of the photoluminescence of stilbene - A.P.Kilimov & N.P.Shimanskaia 22
Migration and transfer of electron excitation energy in anthracene and naphthalene crystals - I.Ia.Kucherov & A.N.Faidysh 27
Plastic scintillators - I.M.Rozman 34
Scintillation efficiency of carbo- and heterocyclic compounds in plastics - N.A.Adrova, M.M.Koton, Iu.N.Panov & F.S.Florinskii 39
Pulse heights from plastic scintillators with different activators - M.N.Medvedev, E.N.Matveeva & L.Ia.Zhil'tsova 42
Mechanism of energy transfer in plastic scintillators - T.P.Belikova & M.D.Galanin 46
Temperature dependence of the luminescence efficiency of polystyrene plastic scintillators - I.M.Rozman 48
Radiation damage in plastic scintillators - Part II - I.M.Rozman 58
Polystyrene-base plastic scintillators - E.A.Andreeshchev, E.E.Baroni, K.A.Kovyrzina, I.M.Rozman & V.M.Shoniia 64
New photomultipliers - N.S.Khlebnikov 67
Production of photomultipliers and their basic parameters - A.E.Melamid 74
Use of scintillation counters with Type "B" equipment - A.F.Vinogradov 79
The SG-42 field gamma-radiometer - M.M.Sokolov & N.N.Karabanov 84
A scintillation method of checking β-contamination in the presence of a γ-background - G.M.Dikareva 86
Prototype of commercial thermal and fast neutron detectors - V.S.Filonov 89

TRANSACTIONS OF THE EIGHTH ALL-UNION CONFERENCE ON NUCLEAR SPECTROSCOPY

Number 2

Alpha-decay of Cm^{242} - L.N.Kondrat'ev, V.B.Dedov & L.L.Gol'din 97
Decay of Tb^{160} and Ho^{160} and level scheme of Dy^{160} - E.P.Grigor'ev, B.S. Dzhelepov, A.V.Zolotavin, O.E.Kraft, B.Kratsik & L.K.Peker 99
Conversion electron spectrum of a dysprosium fraction - B.S.Dzhelepov, B.K.Preobrazhenskii, I.M.Rogachev & P.A.Tishkin 125

Conversion electron spectra of Gd^{151} and Gd^{153} - N.M.Anton'eva, A.A.Bashilov, G.S.Dzhelepov & B.K.Preobrazhenskii 134
$Nd^{140} \rightarrow Pr^{140} \rightarrow Ce^{140}$ decay series - K.Ia.Gromov, G.S.Dzhelepov, A.G.Dmitriev & B.K.Preobrazhenskii 151
Distinctive features of forbidden β-transitions in deformed nuclei - Z.Bokhnatski 156
Contribution to the theory of internal conversion. Part I.- V.A.Krutov 159
Contribution to the theory of internal conversion. Part II. - V.A.Krutov & K.Müller 168
Gamma-spectrum of La^{140} - V.P.Prikhodtseva & Iu.V.Khol'nov 173
Conversion spectrum of La^{140} - A.A.Bashilov, B.S.Dzhelepov, N.D.Novosil'tseva & L.S.Chervinskaia 176
Precision energy measurements of some lines in the spectra of Ir^{192}, Eu^{152} and Eu^{154} - V.A.Romanov 188
Decay of Rh^{106} - E.P.Grigor'ev, A.V.Zolotavin, I.I.Kuz'min & E.D.Pavlitskaia 191
Twin magnetic lens spectrometer with improved focusing for recording coincidences - V.A.Sergienko 195
Positron spectrum of a dysprosium fraction - B.S.Dzhelepov, O.E.Kraft, B.K.Preobrazhenskii & G.F.Iushkevich 205
High-energy gamma-radiation from Na^{24} - L.V.Gustova, B.S.Dzhelepov, P.F.Ermolov & O.V.Chubinskii 208
Concerning the decay schemes of certain odd-odd nuclei - L.K.Peker 213
On the characteristics of nuclei with small deformation parameters. Properties of Os^{190} - L.K.Peker 224

Number 7

Internal conversion - A review - M.A.Listengarten 755
Conversion electrons from Yb^{169} - K.Ia.Gromov, B.S.Dzhelepov & B.K.Preobrazhenskii 770
Level diagram of Tl^{208} - A.G.Sergeev, E.M.Krisiuk, G.D.Latyshev, V.D.Vorob'ev & T.I.Kol'chinskaia 779
Beta-spectra of the shortlived isotopes Al^{28} and F^{17} - S.S.Vasil'ev & L.Ia.Shavtvalov 782
Conversion electron coincidences in $Tb^{155} \rightarrow Gd^{155}$ decay - B.S.Dzhelepov, B.K.Preobrazhenskii & V.A.Sergienko 785
Coincidences between conversion electrons in the decay of Lu^{173}. Refinement of the $Lu^{173} \rightarrow Yb^{173}$ decay scheme - B.S.Dzhelepov, B.K.Preobrazhenskii & V.A.Sergienko 789
Mass numbers of neutron-deficient terbium isotopes - V.I.Baranovskii, A.N.Murin, V.N.Pokrovskii & I.A.Iutlandov 802
Mass numbers of 52-day gadolinium and 4.3-day europium isotopes - G.M.Gorodinskii, A.N.Murin & V.N.Pokrovskii 805
Mass numbers of neutron-deficient Dy isotopes - A.N.Dobronravova, L.M.Krizhanskii, A.N.Murin & V.N.Pokrovskii 809
New neutron-deficient rare earth isotopes. Lutetium isotope with mass number 167 - P.M.Aron, A.V.Kaliamin, A.N.Murin & V.A.Iakovlev 811
Lutetium isotope with mass number 173 - G.M.Gorodinskii, A.N.Murin, V.N.Pokrovskii & B.K.Preobrazhenskii 812
Relative intensities of γ-transitions in Ho^{160} - E.P.Grigor'ev, B.S.Dzhelepov & A.V.Zolotavin 815
Investigation of the lower excited levels of Th^{230} by observing α-e_K coincidences - A.P.Komar, G.A.Korolev & G.E.Kocharov 818
Investigation of Cs^{134} by the coincidence method - Iu.A.Aleksandrov 821
Radiation from As^{74} - E.P.Grigor'ev, G.S.Dzhelepov, A.V.Zolotavin, V.Ia.Mishin, V.P.Prikhodtseva, Iu.V.Khol'nov & G.E.Shchukin 825
Gamma-spectrum of Lu^{171} - A.I.Lebedev, A.N.Silant'ev & I.A.Iutlandov 833

New data on the relative intensities of the γ-lines of RaC in equilibrium with its decay products - B.S.Dzhelepov, N.N.Zhukovskii, I.F.Uchevatkin & S.A.Shestopalova 835
Determination of the number of photons per disintegration of La^{140} - E.A.Khol'nova 843
Determination of the L/K ratios for Dy^{159} and Er^{159} and evaluation of the $Dy^{159} \rightarrow Tb^{159}$ and $Er^{165} \rightarrow Ho^{165}$ transition energies - O.I.Grigor'ev, B.S. Kuznetsov, N.S.Shimanskaia & I.A.Iutlandov 845
Lifetime of the first excited state of Mg^{24} - N.N.Deliagin & V.S.Shpinel' 855
Concerning Doppler broadening of the lines associated with conversion electrons emitted by recoil nuclei - A.V.Gnedich, L.N.Kriukova, V.V. Murav'eva, V.S.Shpinel' & V.I.Shumshurov 861
Elastic scattering of protons by Si^{28} nuclei. Spin and parity of the 4.31 and 4.73 Mev levels of P^{29} - A.K.Val'ter, I.Ia.Malakhov, P.V.Sorokin & A.Ia.Taranov 865
Toroidal sector type β-spectrometer - S.Salai & D.Bereni 871
Precision measurements of the Co^{60} 1.17 and 1.33 Mev, Hf^{181} 482 kev and Au^{199} 158 and 208 kev γ-lines - M.P.Avotina & O.I.Sumbaev 873
Scattering of longitudinally polarized electrons and positrons by polarized electrons - A.I.Mukhtarov & Iu.S.Perov 876
Bremsstrahlung from a longitudinally polarized electron - B.K.Kerimov & I.M.Nadzhafov 879

Number 8

Gd^{149} conversion electron spectrum - N.M.Anton'eva, A.A.Bashilov, B.S. Dzhelepov & B.K.Preobrazhenskii 889
Gd^{147} and Eu^{147} conversion electron spectra - N.M.Anton'eva, A.A.Bashilov, B.S.Dzhelepov & B.K.Preobrazhenskii 899
Internal conversion coefficients of some nuclear transitions in Eu^{147} and Eu^{149} - V.K.Adamchuk, A.A.Bashilov & B.K.Preobrazhenskii 911
As^{73} conversion electron spectrum - E.P.Grigor'ev, B.S.Dzhelepov, A.V. Zolotavin & V.Ia.Mishin 919
Conversion electron spectrum of the cerium fraction (from the spallation product of Ta) - B.S.Dzhelepov, B.K.Preobrazhenskii, I.M.Rogachev & P.A.Tishkin 923
Conversion electron spectra of some neutron-deficient Ho and Er isotopes - I.S.Dneprovskii & G.M.Kolesov 927
Radiation from Eu^{155} - M.P.Glazunov & B.F.Gulev 932
Coincidences of conversion electrons in $Eu^{147} \rightarrow Sm^{147}$ decay - B.S.Dzhelepov, B.K.Preobrazhenskii & V.A.Sergienko 936
Coincidences of conversion electrons in $Tm^{167} \rightarrow Er^{167}$ decay - B.S.Dzhelepov, B.K.Preobrazhenskii & V.A.Sergienko 940
Tables of functions needed for determining the probability of allowed and forbidden L-capture - I.M.Band, L.N.Zyrianova & Iu.P.Suslov 943
Angular distribution of gamma-rays from positron annihilation in liquid hydrogen and helium - A.S.Basina, K.A.Baskova, B.S.Dzhelepov & M.A. Dolgoborodova 959
Compensation of the Earth's magnetic field - E.M.Krisiuk & G.D.Latyshev 966
Finite size corrections to the Lamb shift - E.V.Teodorovich 975
Accuracy of magnetic field measurements by the nutation method - A.I. Zhernovoi, Iu.S.Egorov & G.D.Latyshev 978
New technique for measuring the spin-lattice relaxation time of liquids - A.I.Zhernovoi & G.D.Latyshev 982
New technique for measuring the spin-spin relaxation time of liquids - A.I.Zhernovoi & G.D.Latyshev 983
Level shifts and the probabilities of corresponding β- and γ-transitions in odd nuclei - V.S.Shpinel' 984

Commercial photomultiplier with improved time resolution and larger output current - A.G.Berkovskii, L.G.Leiteizen & V.G.Pol'skii 990
New data on commercial photomultiplier tubes for scintillation spectrometers - A.G.Berkovskii, I.Ia.Breido, B.M.Glukhovskoi, O.S.Korol'kova, L.G.Leiteizen & E.I.Tarasova 993
Λ-nucleon forces and Λ particle binding energy in hypernuclei - V.A.Filimonov 997

TRANSACTIONS OF THE ALL-UNION CONFERENCE ON THE PHYSICS OF DIELECTRICS

Number 3

Nonferroelectric dielectrics with a high dielectric constant (Abstract) - G.I.Skanavi, Ia.M.Ksendzov, V.A.Trigubenko & V.G.Prokhvatilov 233
Influence of impurities on the electric properties of rutile - Ia.M. Ksendzov 234
Relaxation theory of electric polarization - N.S.Fastov & B.N.Finkel'shtein 246
Polarization and dielectric loss in solid solutions of the first and second kinds (Abstract) - G.A.Smolenskii, V.A.Isupov, A.I.Agranovskaia & E.D.Sholokhova 249
Theory of systems comprising noncentrally interacting particles - A.E.Glauberman 252
Ionic displacement polarization in complex ionic crystals - A.E.Glauberman & I.M.Spitkovskii 258
Thermal ionic polarization and slow processes in solid dielectrics - - V.N.Lozovskii 261
Orientational polarization of dipole gases, solutions and liquids taking into account the internal field - A.A.Borgardt 266
Mechanism of relaxation dielectric loss in crystal hydrates - I.Ts.Liast 274
Structural loss in amorphous dielectrics - V.Kh.Kozlovskii 277
Dielectric loss at high frequencies in Muscovite with inclusions of limonite and biotite - K.A.Vodop'ianov & I.G.Vorozhtsova 282
Dielectric loss at high frequencies in pure and mixed alkali halide crystals - K.A.Vodop'ianov & G.I.Galibina 287
Dielectric constant, dielectric loss and electric conductivity of alkali halide single crystals - B.N.Matsonashvili 294
Dielectric constant of rock salt at high temperatures - M.S.Kosman & N.A.Petrova 308
Dielectric constant of zinc oxide with an admixture of bismuth oxide M.S.Kosman & I.A.Gesse 312
Dielectric constants of bismuthates of some metals - A.M.Kashtanova & G.I.Skanavi 316
Influence of grinding on the dielectric properties of polycrystalline barium titanate - G.M.Kovalenko 318
Dielectric loss and polarization in polymers (Abstract) - G.P.Mikhailov & A.M.Lobanov 320
Theory of dipole moments of polymer molecules (Abstract) - O.B.Ptitsyn, T.M.Birshtein & Iu.A.Sharonov 321
Dielectric loss in crystalline non-polar polymers - S.P.Kabin & G.N. Mikhailov 322
Preparation and properties of new electrets of inorganic dielectrics - A.N.Gubkin & G.I.Skanavi 327
Investigation of the electric and optical properties of electreted polymers - K.V.Filippova 340
On the photoelectret and thermoelectret states in sulfur single crystals - I.S.Zheludev & V.M.Fridkin 348
Multiple component organic electrets - Iu.Ia.Ianson 356

Number 4

Behavior of germanium-type valence crystals in a strong electric field - V.A.Chuenkov 363
Towards derivation of a criterion of electric breakdown of ionic crystals from the kinetic equation - V.A.Chuenkov 369
Polaron theory of breakdown of ionic dielectrics - Iu.I.Gorkun & K.B. Tolpygo 377
Electric strength of polyethylene at high frequencies - S.M.Bragin 389
On certain processes involved in the electric breakdown of solid dielectrics - A.A.Vorob'ev & G.A.Vorob'ev 394
Investigations of breakdown of rock salt containing color centers - A.A.Vorob'ev & G.A.Vorob'ev 399
Temperature dependence of the electric strength of KBr and KCl crystals - E.A.Konorova & L.A.Sorokina 403
Temperature dependence of the electric breakdown strength of ionic crystals - V.D.Kuchin 406
Temperature dependence of the pulse electric strength of certain polycrystalline dielectrics - E.A.Konorova, V.V.Krasnopevtsev & G.I.Skanavi 410
Oscillographic investigation of thermal breakdown of rock salt in DC fields - G.A.Andreev 418
Impulse breakdown of thick layers of ice - A.V.Astafurov 422
On the discharge delay time in ionic crystals - K.K.Sonchik 426
Electric breakdown of a titanium ceramic having a dielectric constant of 80 - I.E.Balygin 429
Some regularities of electric breakdown of liquid dielectrics - I.E.Balygin 435

TRANSACTIONS OF THE EIGHTH CONFERENCE ON CATHODE ELECTRONICS

Number 4

Reflection of electrons and secondary electron emission from some metal surfaces at low primary electron energies - I.M.Bronshtein 442
Investigation of the structure and properties of Ge, Cr and Bi films tapering in thickness in connection with their secondary emission characteristics - N.G.Nakhodkin & A.I.Novosel'skaia 449
Variation of the secondary emission coefficient of KCl with the layer thickness - N.G.Nakhodkin & V.A.Romanovskii 457
Passage of electrons through thin glass films - A.I.Piatnitskii 459
Secondary electron emission of cesium-antimony emitters "from the back" - A.I.Piatnitskii 467

Number 5

Investigation of discrete energy losses of electrons in Mg, MgO, BeO and Ge - N.B.Gornyi 481
Secondary electron emission from alkali halide single crystals at low primary energies - S.A.Fridrikhov & G.N.Goriacheva 491
Secondary emission from thorium oxide activated with barium - B.N.Popov & V.F.Koliverdov 499
Behavior of composite secondary emitters in extended operation - E.G. Kormakova & V.G.Pavlovskaia 509
Some characteristics of new commercial photomultiplier tubes - L.G.Leiteizen, A.G.Berkovskii, B.M.Glukhovskoi, O.S.Korol'kova & E.I.Tarasova 516
Secondary emission from composite emitters in the range of high secondary-emission coefficient values - R.M.Aranovich & A.I.Piatnitskii 521
Some features of the retarding potential curves of surface activated cathodes - V.N.Lepeshinskaia & T.M.Sukova 531
Secondary emission characteristics of magnesium and beryllium alloy cathodes after short-term activation - V.L.Borisov & V.N.Lepeshinskaia 537

Kinetics of charge built-up on a dielectric surface under electron bombardment - I.R.Zakirova & S.A.Fridrikhov 547
Energy distribution of secondary electrons from oxide coated metal surfaces - M.L.Kapitsa 557
Some properties of multialkali photocathodes - A.A.Mostovskii, O.B.Vorob'eva & K.A.Maiskaia 561
Photoelectron emission from some semiconductor and metal cathodes with a reduced work function - P.G.Borziak, V.F.Bibik & O.G.Sarbei 565
Investigation of photocathodes by the radioactive tracer technique - - N.A.Soboleva 575
Field emission patterns of tungsten and molybdenum carbide crystals - A.P.Komar & Iu.N.Talanin 579
Adsorption of zirconium and barium on tungsten and the resultant work function - V.N.Chrednik 592
On the possibility of utilizing bombardment-induced conductance for signal amplification - A.M.Bonch-Bruevich, E.S.Grishin & U.B.Soltamov 602
Optical properties of alkaline earth carbonate layers - I.S.Gorban' 604
Compacted powder cathodes of barium-calcium aluminates and tungstates - A.I.Mel'nikov, A.V.Morozov, B.N.Popov & A.A.Maklakov 610
Electric breakdown of thin layers of alundum - S.N.Koikov & A.N.Tsikin 618
Transient processes in heaters - Iu.K.Shalabutov 623
Design of a vibration-resistant heater with an enhanced service life for high-temperature cathodes - L.A.Timoshin 635
Some technological procedures for reducing cathode-heater leakage current - G.Ia.Pivovarov & Iu.A.Semenov 637

TRANSACTIONS OF THE ELEVENTH ALL-UNION CONFERENCE ON THEORETICAL SPECTROSCOPY

Number 6

Opening address - S.L.Mandel'shtam 645
Forty years development of Soviet spectroscopy - S.E.Frish 648
Optical effects of collective electron oscillations in metals - I.I.Sobel'man & E.L.Feinberg 652
Excitation of spectral lines in the negative glow of a gas discharge - S.E.Frish & I.P.Bogdanova 657
Adiabatic approximation in the quantum theory of atoms - M.G.Veselov & I.B.Bersuker 660
Two-electron model approximation and the so-called anomaly in the spectra of carbon, nitrogen and oxygen - A.P.Jucys, Ia.I.Vizbaraite, V.I.Kavetskis & I.V.Batarunas 663
One-electron wave functions of Tl^+ in certain crystals - M.I.Petrashen' & T.L.Gutman 666
Calculation of one-electron wave functions and oscillator strengths by means of an electronic computer - L.A.Vainshtein 668
Determination of molecular dissociation energies from flame reaction equilibrium studies - L.V.Gurvich & I.V.Veits 670
Dependence of the integral intensity of spectrum lines on the absolute concentration of atoms in an arc discharge - I.V.Dvornikova 674
Determination of the relative oscillator strengths in an arc discharge from the width of the spectrum lines - I.M.Nagibina 678
Isotope shift in the spectra of cerium and zirconium - Iu.P.Dontsov & L.A.Korostyleva 680
Isotope shift in the spectrum of ionized uranium - N.G.Morozova & G.P. Startsev 683
On the accuracy of determination of hyperfine structure constants from optical measurements - N.I.Kaliteevskii, V.I.Perel' & M.P.Chaika 689

On temperature determination from molecular band spectra - L.V.Leskov & L.P.Vasil'eva 693
Motion of ions in plasma - Iu.M.Kagan 699
On the possibility of utilizing spectrum lines as wavelength norms and a length standard - N.R.Batarchukova 704
Observation of anomalous dispersion in short-term processes - A.M.Shukhtin & V.S.Egorov 707
Contribution to the theory of line broadening in plasma - V.I.Kogan 710
Broadening and shift of spectral lines in highly ionized plasma - L.A.Vainshtein, V.G.Koloshnikov, M.A.Mazing, S.L.Mandel'shtam & I.I.Sobel'man 714
Temperature measurement of the glowing vapor cloud in pulse discharges - A.A.Labuda, E.G.Martinkov & I.G.Nekrashevich 716
Measurement of oscillator strengths in atomic spectra - Iu.I.Ostrovskii, N.P.Penkin & L.N.Shabanova 720
Spectroscopic investigation of the state of a gas behind a shock wave - N.N.Sobolev, A.V.Potapov, V.F.Kitaeva, F.S.Faizullov, V.N.Aliamovskii, E.T.Antropov & I.L.Isaev 725
New spectroscopic instruments in the USSR - V.K.Prokof'ev 732
Spectrum of optically dense plasma - H.Bartels 737
Probability of optical transitions in atoms and molecules with a polarizing core - I.B.Bersuker 743
Emission spectrum of the decomposition products of aliphatic hydrocarbons and alcohols in an electrodeless discharge - A.A.Koliubin 747

Number 9

Free electron model calculations of the electric and magnetic properties of complex molecules - M.N.Adamov, M.G.Veselov & T.K.Rebane 1005
Calculation of the absorption spectra of unsaturated hydrocarbon molecules on the basis of the metallic model - L.A.Borovinskii 1009
Theory of vibrational spectra of unsaturated compounds - L.M.Sverdlov, M.G.Borisov, Iu.V.Klochkovskii, E.P.Krainov, V.S.Kukina & N.V.Tarasova 1012
Contribution to the quantum mechanical theory of Raman line intensities - I.I.Sobel'man 1015
Intensities and depolarizations in the Raman spectra of C_6H_6, C_6D_6 and sym. $C_6H_3D_3$ - M.A.Kovner & B.N.Snegirev 1019
Correspondence of the absorption and luminescence bands of complex molecules - B.I.Stepanov 1023
Different forms of concentration quenching and the possibility of distinguishing between them - V.L.Levshin & E.G.Baranova 1027
On the relation between the Kravets integral (area of the absorption band) and the lifetime of the excited state of molecules - M.D.Galanin & Z.A.Chizhikova 1031
Kinetics of impurity quenching of fluorescence in solutions - B.Ia. Svechnikov, V.M.Shirokov, L.A.Kuznetsova & P.I.Kudriashov 1035
Effect of light gases on the electron absorption spectra of aromatic compounds and interaction between the molecules of such compounds - B.S.Neporent 1039
Spectroscopic investigation of inter- and intramolecular interaction of nitro and amino radicals in some benzene derivatives - V.I.Danilova, V.D.Gol'tseva & N.A.Prilezhaeva 1042
Dependence of the spectra of aromatic nitro compounds on the angle of rotation of the nitro group about the C-N bond - P.P.Shorygin & Z.F.Il'icheva 1046

Investigation of vibrational spectra in the region of the valence vibrations of CH - M.M.Sushchinskii 1051
Anharmonicity coefficients and resonance interaction of internal vibrations of the CH group - V.D.Bogdanov & M.M.Sushchinskii 1056
Investigation of the temperature dependence of Raman spectrum line intensities - A.I.Sokolovskaia & R.A.Bazhulin 1057
Raman spectra of some unsaturated cyclic hydrocarbons - V.T.Aleksanian, Kh.E.Sterin, A.A.Mel'nikov & A.F.Plate 1062
Vibrational spectra of some phosphororganic compounds - R.R.Shagidullin 1069
Raman spectrum of vitreous germanium dioxide - V.V.Obukhov-Denisov, N.N.Sobolev & V.P.Cheremisinov 1073
Investigation of the influence of different elements on the structure of silicate glasses by Raman spectroscopy - Ia.S.Bobovich & T.P.Tulub 1076
Spectroscopy of negative radiant energy fluxes - B.I.Stepanov & Ia.S. Khvashchevskaia 1079
Infrared absorption and thermal radiation spectra of some molecular compounds in different states of aggregation - O.V.Fialkovskaia 1083
Infrared reflection spectrum of boron oxide at high temperature - E.P.Markin & N.N.Sobolev 1087
Infrared absorption spectra of molecular compounds with metal halides - A.N.Terenin, V.N.Filimonov & D.S.Bystrov 1089
Towards a clarification of the "hydrogen bond" concept - V.M.Chylanovskii 1092
Investigation of the hydrogen bond in glycols and catechols - V.I.Malyshev & V.N.Murzin 1096
Structure of the OH vibration band in the spectra of crystals containing hydrogen bonds - A.I.Stekhanov 1098
Infrared absorption spectra of organolithium compounds. The intermolecular lithium bond - A.N.Rodionov, D.N.Shigorin, R.V.Talalaeva & K.A.Kocheshkov 1099
Investigation of intermolecular coupling in polyethylene by infrared absorption spectroscopy - I.I.Novak 1103
Influence of temperature and the state of aggregation on the infrared absorption of carbon tetrachloride - M.P.Lisitsa & V.N.Malinko 1106
Changes in the infrared spectrum of ammonia incident to transition from the gaseous to the liquid state - I.V.Demidenkova & L.D.Shcherba 1110
Infrared spectra of salt solutions - E.N.Vasenko, A.P.Cherniavskaia & N.V.Chernaia 1113
Investigation of keto-trans-cis-enol equilibrium by infrared absorption spectroscopy - M.E.Movsesian, M.I.Kabachnik, S.T.Ioffe & K.V.Vapuro 1114
Spectroscopic investigation of the structure of some complex compounds - A.A.Babushkin 1118
Spectroscopic methods of investigating catalytic conversion on metal films - V.M.Griaznov, V.D.Iagodovskii & V.I.Shimulis 1123
Applications of the weak-field free nuclear induction technique in high-resolution radio spectroscopy - A.A.Morozov, A.V.Mel'nikov & F.I.Skripov 1127
Rotational spectrum of water vapor in the 50 to 1500 μ region - N.G.Iaroslavskii & A.E.Stanevich 1131
Determination of the molecular structure of HDSe from its rotational microwave spectrum - V.G.Veselago 1136
Rotational constants of $FH_2C-CH_2Cl^{35}$ molecules - I.A.Mukhtarov 1140

Number 11

Measurement and calculation of the polarization of the emission of helium atoms excited by electron impact - L.A.Vainshtein & G.G.Dolgov 1287
Emission of the negative hydrogen ion - W.Lochte-Holtgreven 1290
Spectroscopic investigation of the rotational mobility of molecules in quasiliquid camphene and tricyclene crystals - Ang Meng Tok, M.F.Vuks & D.S.Nedzvetskii 1294
Phosphorescence spectra of some aromatic acids at liquid air temperature - B.A.Piatnitskii 1296
Determination of the rotational constants of CH_3GeCl_3 from its microwave absorption spectrum (summary) - N.A.Irisova 1299
Method of quasinormal coordinates in crystal optics - V.S.Mashkevich 1300
Spectroscopic investigation of crystals - A.F.Prikhot'ko 1304
Relation between the absorption and dispersion in crystals as evinced in the case of 1,2-benzanthrene - M.S.Brodin & M.S.Soskin 1308
Quantum mechanical description of F-centers in alkali halide crystals - I.V.Abarenkov 1312
Properties and structure of the initial aggregations of F-centers in the process of their colloidal coagulation - A.A.Shatalov 1315
Conditions governing the existence and spectroscopic manifestation of excitons in semiconductors - I.Z.Fisher 1320
Investigation of the role of trapped and free excitons in the luminescence of molecular crystals by polarization methods - N.D.Zhevandrov 1323
Impurity scattering of light in crystals at low temperatures - Iu.E.Perlin 1327
Paramagnetic resonance of impurity centers in ionic crystals - M.F.Deigen 1331
Absorption and luminescence spectra of alkali halide crystals containing impurity ions with isoelectronic shells - M.L.Kats 1337
Spectroscopy of luminescence centers in alkali halide crystal phosphors activated by mercury-like ions - Ch.B.Lushchik & N.E.Lushchik 1341
Fluorescence of pure cadmium sulfide at low temperatures - E.Grillot & M.Bancie-Grillot 1346

TRANSACTIONS OF THE ALL-UNION CONFERENCE ON THE PHYSICS OF MAGNETIC MATERIALS

Number 10

Dynamic constants of magnetically polarized magnetoelastic (Magnetostrictive) and electrically polarized (electrostrictive) media - K.B.Vlasov 1149
Phenomenological theory of ferromagnetism and antiferromagnetism at low temperatures (uniaxial case) - E.A.Turov & Iu.P.Irkhin 1158
Magnetic structure and technical magnetization processes in high-coercivity ferromagnets - Ia.S.Shur 1167
Domain structure dynamics in transformer iron crystals under the influence of stresses - L.V.Kirenskii, M.K.Savchenko & A.M.Rodichev 1171
Changes in the magnetic structure of silicon iron crystals under the influence of elastic stress - V.A.Zaikova & Ia.S.Shur 1177
Magnetic structure of a ferromagnet in the remanence state and changes therein incident to demagnetization by an alternating field - I.E. Startseva & Ia.S.Shur 1183
Temperature stabilization of the magnetic properties of alloys - I.M.Puzei 1188
Magnetic anisotropy and hysteresis loss in rotating magnetic fields in a magnetite single crystal at low temperature - N.N.Narovskaia 1194
Nature of the effect of thermomagnetic treatment in magnetically soft ferromagnets - A.A.Glazer & Ia.S.Shur 1198
Investigation of the kinetics of magnetic domain-orientation in 65% Permalloy - Sh.I.Zusman 1204

Synthesis and magnetic properties of ferrites with a rectangular hysteresis loop - L.I.Rabkin, S.A.Soskin & B.Sh.Epshtein 1210
Kinetics of thermomechanical treatment of ferromagnets - F.N.Dunaev 1217
Grain-orientation in the process of annealing cold-rolled transformer steel - L.V.Mironov 1223
Magnetic analysis of the deformation structure due to cold rolling and recrystallization in pure electrolytic nickel - N.L.Briukhatov, N.A.Grinchar & I.Ia.Ekamasov 1229
Magnetostriction of nickel-iron-molybdenum alloys - I.M.Puzei & B.V. Molotilov 1236
Volume magnetostriction in iron-nickel-molybdenum alloys - I.M.Puzei, B.V.Molotilov & A.I.Rad'kov 1243
Magnetostrictive properties of binary alloys - G.P.D'iakov 1246
Dependence of the sensitivity of magnetostrictive ultrasonic detectors on their magnetic characteristics - Ia.S.Shur, M.G.Luzhinskaia, K.B.Vlasov, O.I.Shiraeva & V.A.Zaikova 1250
Molybdenum induced modifications of the structural transformations in Permalloy - Iu.S.Avraamov, B.G.Livshits & V.B.Osvenskii 1253
Anisotropy of the coercive force in magnetically anisotropic fine-powder specimens - E.V.Shtol'ts, Ia.S.Shur & G.S.Kandaurova 1258
Concerning the temperature dependence of the magnetic properties of high-coercivity alloys - N.A.Baranova & Ia.S.Shur 1263
On the physics of magnetodielectrics - L.I.Rabkin 1266
Magnetic properties of ferrites with a compensation point - K.P.Belov, K.N.Bol'shova, T.A.Elkina & M.A.Zaitseva 1272

TRANSACTIONS OF THE SIXTH CONFERENCE ON LUMINESCENCE (Molecular luminescence)
Number 11

Opening address - A.N.Terenin 1356
Correlation between the luminescence and absorption spectra of complex molecules - B.I.Stepanov 1357
Correlation between the luminescence and absorption spectra of poly-atomic molecules - B.S.Neporent 1362
Relation between the luminescence and absorption spectra of an aqueous solution of fluorescein - M.N.Alentsev & L.A.Pakhomycheva 1367
On the meaning of photoluminescence and scattering - B.I.Stepanov & P.A.Apanasevich 1370
Internal field and spectra of complex molecules in solutions - N.G.Bakhshiev 1377
Temperature dependences of the electronic spectra of some phthalimides - L.G.Pikulik & M.A.Solomakho 1381
Luminescence of powdered materials - Iu.I.Chekalinskaia 1385
Resonance luminescence of matter in finite volumes - A.M.Samson 1389
Dependence of the polarization of phosphorescence of organic materials on the viscosity of the solution - B.Ia.Sveshnikov & P.I.Kudriashov 1393
Variation of the degree of polarization with the fluorescence wavelength - G.P.Gurinovich & A.N.Sevchenko 1397
Polarization of the luminescence of phthalimides - A.M.Sarzhevskii & A.N.Sevchenko 1402
Characteristics of the luminescence of difurylpolyenes - P.F.Nepochatykh 1407

TRANSACTIONS OF THE SECOND ALL-UNION CONFERENCE ON FERROELECTRICITY

Number 12

Contribution to the quantum mechanical theory of ferroelectricity - R.E.Pasynkov 1415
On the electric field dependence of the dielectric constant of ferroelectrics - I.V.Liagini & Ia.I.Geivashovich 1417
Phase trajectory of an oscillating circuit with a ferroelectric - N.S.Novosil'tsev 1420
Contributing to the theory of domain walls in ferroelectrics - V.A.Zhirnov 1424
Aperiodic operation of capacitors containing a ferroelectric - N.F.Shmoilov 1427
Dependence of the ferroelectric properties of perovskite type crystals on the character of the chemical bonds - I.N.Beliaev 1430
On the search for new ferroelectric materials - I.S.Zheludev & A.S.Sonin 1435
Preparation and the dielectric properties of some barium titanate-stannate solid-solution single crystals - A.L.Khodakov & M.L. Sholokhovich 1439
Investigation of the PbO-BaO-B_2O_3-TiO_2 system - M.L.Sholokhovich & V.I.Varicheva 1443
X-ray spectroscopic investigation of compounds with the perovskite structure - M.A.Blokhin & A.T.Shuvaev 1447
Infrared absorption spectra of perovskite type ferroelectric crystals - A.F.Iatsenko 1450
On the nature of color centers in barium titanate crystals - M.S.Kosman & E.V.Bursian 1453
High-temperature polymorphous transformation in barium titanate - I.A.Trifonov 1455
Nonlinear properties of Pb doped $BaTiO_3$ single crystals and tri-glycine sulfate single crystals in strong electric fields - I.S.Zheludev, V.V.Gladkii, L.Z.Rusakov & I.S.Rez 1458
Individual characteristics of domains in Rochelle salt - V.L.Indenbom & M.A.Chernysheva 1461
Some results of a search for new piezoelectric materials - I.S.Rez 1466
Influence of different factors on the Curie temperature of ferroelectrics with the perovskite structure - Iu.N.Venevtsev, G.S. Zhdanov & S.P.Solov'ev 1471
Crystal structure of the $BaTiO_3$-$LaAlO_3$ system - I.G.Ismailzade 1478
Crystal structure of the niobates and tantalates of bivalent metals and their solid solutions - I.G.Ismailzade 1480
Properties of solid solutions of barium and lead titanates and ferrates - O.I.Prokopalo & E.G.Fesenko 1483
Antiferroelectric and ferroelectric properties of some sodium niobate solid solutions - N.N.Krainik 1486
Ferroelectric ceramics with a high Curie temperature - A.M.Cherepanov, S.V.Bogdanov & R.Ia.Razbash 1490
Dielectric properties of solid solutions of the ternary system $BaTiO_3$-$PbTiO_3$-$BaSnO_3$ - S.V.Bogdanov, G.M.Kovalenko, R.Ia.Razbash & A.I.Cherepanov 1493
Phase transitions in solid solutions of sodium tantalate in sodium niobate - V.A.Isupov 1497

Influence of Fe_2O_3, SrO, SnO_2, ZrO_2 and $BaSnO_3$ impurities on the dielectric hysteresis loops of polycrystalline $BaTiO_3$ and $BaTiO_3$-$PbTiO_3$ solid solutions - G.M.Kovalenko, S.V.Bogdanov & A.M.Cherepanov 1501
Nonlinear properties of some (Ba,Sr)(Ti,Sn)O_3 solid solutions - A.I.Medovoi 1505
Low-temperature polarization of barium titanate ceramic - L.A.Shuvalov, M.M.Kachkacheva, L.Z.Rusakov & I.S.Zheludev 1508
On obtaining piezoelectric ceramics for high-temperature applications - I.S.Rez, E.G.Smazhevskaia & M.M.Kachkacheva 1512
Method of measuring the dielectric constant and loss tangent of ferroelectrics in homogeneous superhigh frequency fields (3000 Mc) - I.V.Ivanov & V.M.Petrov 1516
Oscillographic procedure for investigating the instantaneous parameters of nonlinear capacitors - A.L.Khodakov 1519
Frequency dependence of the nonlinearity of $BaTiO_3$-$BaSnO_3$ solid solutions - A.A.Obukhov 1523
Ferroelectric ceramics with dielectric constants up to 45,000 - T.N.Verbitskaia & L.M.Aleksandrova 1525
Dielectric investigation of ferroelectric crystals using minute samples - V.A.Koptsik, K.A.Minaeva & B.A.Strukov 1529

Translated in 1959 by
Columbia Technical Translations
5 Vermont Ave., White Plains, N.Y.

Annual subscriptions $215
Single issues $20

RESUME OF THE CONFERENCE TRANSACTIONS PUBLISHED IN VOLUME 22

of the

Bulletin of the USSR Academy of Sciences

- Physical Series -

	Issue Nos.
Synthesis and investigation of scintillators for detecting nuclear radiation	1
Nuclear spectroscopy	2, 7 & 8
Physics of dielectrics	3 & 4
Cathode electronics	4 & 5
Theoretical spectroscopy	6, 9 & 11
Physics of magnetic materials (to be continued in Vol.23, No. 3)	10
Molecular luminescence (to be continued in Vol.23, No. 1)	11
Ferroelectricity	12

COLUMBIA TECHNICAL TRANSLATIONS
5 VERMONT AVENUE
WHITE PLAINS, N. Y.